

FLORIDA SLAB BEAM BRIDGE WITH ULTRA-HIGH-PERFORMANCE CONCRETE JOINT CONNECTIONS

(Project Nos.: BDV29-977-28 and BDV29-977-65)

Final Report



Principal Investigator

David Garber

Florida International University
10555 W. Flagler St., EC 3606

Miami, FL 33174

Phone: 305-348-4879

Email: dgarber@fiu.edu

Project Manager

Christina Freeman

Florida Department of Transportation
Structures Research Center

2007 E. Paul Dirac Dr.

Tallahassee, FL 32310

Phone: 850-921-7100

Email: Christina.Freeman@dot.state.fl.us

December 2021

DISCLAIMER

The opinions, findings, and conclusions expressed in this publication are those of the author(s) and not necessarily those of the Florida Department of Transportation or the U.S. Department of Transportation.

METRIC CONVERSION TABLE

Approximate Conversions to SI Units

SYMBOL	WHEN YOU KNOW	MULTIPLY BY	TO FIND	SYMBOL
LENGTH				
in	inches	25.4	millimeters	mm
ft	feet	0.305	meters	m
yd	yards	0.914	meters	m
mi	miles	1.61	kilometers	km
AREA				
in²	square inches	645.2	square millimeters	mm ²
ft²	square feet	0.093	square meters	m ²
yd²	square yard	0.836	square meters	m ²
ac	acres	0.405	hectares	ha
mi²	square miles	2.59	square kilometers	km ²
VOLUME				
fl oz	fluid ounces	29.57	milliliters	mL
gal	gallons	3.785	liters	L
ft³	cubic feet	0.028	cubic meters	m ³
yd³	cubic yards	0.765	cubic meters	m ³
NOTE: volumes greater than 1000 L shall be shown in m ³				
MASS				
oz	ounces	28.35	grams	g
lb	pounds	0.454	kilograms	kg
T	short tons (2000 lb)	0.907	megagrams	Mg (or "t")
TEMPERATURE (exact degrees)				
°F	Fahrenheit	5(F-32)/9 or (F-32)/1.8	Celsius	°C
ILLUMINATION				
fc	foot-candles	10.76	lux	lx
fl	foot-Lamberts	3.426	candela/m ²	cd/m ²
FORCE and PRESSURE or STRESS				
kip	1000 pound force	4.45	kilonewtons	kN
lbf	pound force	4.45	newtons	N
lbf/in²	pound force per square	6.89	kilopascals	kPa

Approximate Conversions from SI Units

SYMBOL	WHEN YOU KNOW	MULTIPLY BY	TO FIND	SYMBOL
LENGTH				
mm	millimeters	0.039	inches	in
m	meters	3.28	feet	ft
m	meters	1.09	yards	yd
km	kilometers	0.621	miles	mi
AREA				
mm²	square millimeters	0.0016	square inches	in ²
m²	square meters	10.764	square feet	ft ²
m²	square meters	1.195	square yards	yd ²
ha	hectares	2.47	acres	ac
km²	square kilometers	0.386	square miles	mi ²
VOLUME				
mL	milliliters	0.034	fluid ounces	fl oz
L	liters	0.264	gallons	gal
m³	cubic meters	35.314	cubic feet	ft ³
m³	cubic meters	1.307	cubic yards	yd ³
MASS				
g	grams	0.035	ounces	oz
kg	kilograms	2.202	pounds	lb
Mg (or "t")	megagrams (or "metric ton")	1.103	short tons (2000 lb)	T
TEMPERATURE (exact degrees)				
°C	Celsius	1.8C+32	Fahrenheit	°F
ILLUMINATION				
lx	lux	0.0929	foot-candles	fc
cd/m²	candela/m ²	0.2919	foot-Lamberts	fl
FORCE and PRESSURE or STRESS				
kN	kilonewtons	0.225	1000 pound force	kip
N	newtons	0.225	pound force	lbf
kPa	kilopascals	0.145	pound force per square inch	lbf/in ²

TECHNICAL REPORT DOCUMENTATION PAGE

1. Report No.	2. Government Accession No.	3. Recipient's Catalog No.	
4. Title and Subtitle Florida Slab-Beam Bridge with Ultra-High-Performance Concrete Joint Connections		5. Report Date December 2021	
		6. Performing Organization Code	
7. Author(s) Francisco Chitty and David Garber		8. Performing Organization Report No.	
9. Performing Organization Name and Address Florida International University 11200 SW 8 th Street Miami, FL 33199		10. Work Unit No. (TR AIS)	
		11. Contract or Grant No. BDV29-977-28 and BDV29-977-65	
12. Sponsoring Agency Name and Address Florida Department of Transportation 605 Suwannee Street, MS 30 Tallahassee, FL 32399		13. Type of Report and Period Covered Final Report, March 2016 to December 2021	
		14. Sponsoring Agency Code	
15. Supplementary Notes The small- and large-scale test specimens built by local precasters were tested by research staff at the Marcus H. Ansley Structures Research Center, located at Innovation Park in Tallahassee, Florida.			
16. Abstract The Florida Slab Beam (FSB) is a precast, prestressed, flat-slab beam currently used for off-system, short-span bridges (less than about 65 feet) by the Florida Department of Transportation (FDOT). A modified FSB section and female-to-female joint detail utilizing ultra-high-performance concrete (UHPC) were explored to accelerate construction and improve the performance of the system. Four different joint details with two different section depths were investigated with numerical models and small-scale experimental testing to evaluate the transverse moment capacity and ensure sufficient shear transfer across the joint under strength and fatigue performance. The best performing joint was investigated further with two two-beam and one four-beam large-scale test configurations with service, fatigue, and ultimate strength testing. The impact of leveling the differential camber in one beam was investigated in the four-beam test configuration. The beams in all full-scale systems reached their estimated ultimate flexural strength without any joint debonding or distress. Additionally, no damage was observed in the joint or system for the two-beam and four-beam systems under more than four million cyclic loads. A UHPC simple for dead load, continuous for live load connection was also developed and evaluated using non-linear finite element analysis.			
17. Key Word Florida Slab Beam, Prefabricated Element Connections, Joint Design, Ultra-High-Performance Concrete (UHPC), Accelerated Bridge Construction (ABC), Simple for Dead Load Continuous for Live Load (SDCL)		18. Distribution Statement No restrictions	
19. Security Classif. (of this report) Unclassified	20. Security Classif. (of this page) Unclassified	21. No. of Pages 820	22. Price N/A

ACKNOWLEDGEMENTS

The authors would like to thank the Florida Department of Transportation (FDOT) for providing the funding that made this project possible. Also, the authors would like to recognize the team of engineers and staff at the Marcus H. Ansley Structures Research Center for their efforts on instrumentation and testing of all the Florida Slab-Beam (FSB) specimens throughout the research period – in particular, Steven Eudy, William Potter, Brandon Winter, Paul Tighe, Justin Robertson, Ariana Morales Rapallo, and Sam Adenji.

Special thanks are also due to the project manager, Ms. Christina Freeman, for her support and technical contributions to the project.

Finally, the authors would like to acknowledge Dura-Stress Inc. for the construction of the small-scale FSB specimens, South Eastern Prestressed Concrete Inc. for the construction of the large-scale FSB specimens, and the staff at FDOT's Structural Materials Laboratory for testing the flexural performance of the ultra-high performance concrete (UHPC) samples.

EXECUTIVE SUMMARY

As part of the Florida Department of Transportation (FDOT) interest in developing design guidelines and specifications for the use of ultra-high performance concrete (UHPC) on Florida's transportation projects, a modified Florida Slab Beam (FSB) section with a female-to-female joint detail utilizing UHPC was explored to expedite bridge construction and improve the performance of the system.

Four different FSB details with two section depths (four 12-inch and four 18-inch-thick specimens) were investigated with numerical models and small-scale experimental testing protocols to evaluate the transverse flexural capacity and ensure sufficient shear transfer across the joint under ultimate strength and cyclic testing (with two million cycles). A diamond-shaped shear key (12A2) was determined to be the best performing detail with the largest strength capacity and ductility after cracking, compared to the other joint details that were investigated.

Joint 12A2 was investigated further using two full-scale two-beam test configurations with different load and support conditions. Service and ultimate strength testing was performed on one two-beam system to determine the basic demand and performance of the developed joint before any fatigue loading. Service, fatigue, and ultimate strength testing was performed on the second two-beam test configuration with several different load and support conditions. Over 4.5 million load cycles were applied to this system using two different load and support configurations. No deterioration in the system or joint performance was observed from the fatigue loading. Both systems reached their flexural capacities with no observed joint debonding or distress.

The developed system and joint detail were further evaluated using a full-scale four-beam test configuration with different load and support conditions. One of the beams was designed to have a larger camber than the other three beams by having a different top strand stress. The impact of the camber leveling procedure on the behavior of the four-beam system was investigated. Distribution factors were measured at different points in the testing program to observe any effect of joint deterioration on load distribution. No deterioration in the system or joint performance was observed from the fatigue loading. The four-beam system reached its estimated flexural capacity with no observed joint debonding or distress, outside of a saw cut at one joint boundary used to simulate joint cracking. The camber leveling procedure to account for differential camber in one of the beams led to a 35.1 percent reduction in the cracking load for the beam that was forced down and a 10.2 percent reduction in the cracking load for the other beams in the system; this could affect the design and load rating for the service limit state for systems with differential camber between adjacent beams. Otherwise, the modified FSB system performed well under all joint and system service, fatigue, and strength tests.

A UHPC simple for dead load, continuous for live load (SDCL) connection detail was developed for a two-span continuous superstructure for 12-, 15-, and 18-inch-deep modified FSB sections for their maximum span lengths. The SDCL connection can be designed with non-prestressed strands for the positive moment reinforcement and a combination of high-strength rebar and non-prestressed strands for the negative moment reinforcement.

TABLE OF CONTENTS

Disclaimer	ii
Metric Conversion Table	iii
Technical Report Documentation Page	v
Acknowledgements	vi
Executive Summary	vii
List of Figures	xvii
List of Tables	lii
1. Introduction.....	1
1.1. Background	1
1.2. Objective	1
1.3. Tasks.....	1
1.4. Report Organization	2
2. Literature Review.....	4
2.1. Introduction	4
2.2. Concrete Short-Span Bridge Solutions	4
2.2.1. Adjacent Box Beams.....	4
2.2.2. New England Extreme Tee (NEXT) Beam	9
2.2.3. Poutre-Dalle System and Minnesota Modification.....	13
2.2.4. Inverted-T Prestressed Beams.....	16
2.2.5. Florida Slab Beam.....	19
2.3. Longitudinal and Transverse Joints.....	22
2.3.1. Non-UHPC Joints	23
2.3.2. UHPC Joints.....	27
2.4. Joint Materials	33
2.4.1. Non-UHPC Materials.....	33
2.4.2. UHPC Materials.....	35
2.4.3. UHPC Mixing and Casting Procedure	40
2.5. Other UHPC Bridge Superstructure Applications	42
2.5.1. UHPC Overlays	42
2.5.2. UHPC Members.....	42

3.	Development of FSB Design Standard	44
3.1.	Introduction	44
3.2.	Feasible Span Lengths of Untopped Sections	44
3.3.	Integration of Joint Detail	47
3.4.	Analytical Evaluation of Joint Detail – Methods	51
3.4.1.	Background	51
3.4.2.	Model Geometry	51
3.4.3.	Material Modeling	52
3.4.4.	Loading Protocol.....	54
3.5.	Analytical Evaluation of Joint Detail – Results	55
3.5.1.	Results Summary	55
3.5.2.	Results for Each Analysis Case	57
3.6.	Summary and Conclusions.....	65
4.	Development of The FSB Standard for 75-Foot Single Span.....	66
4.1.	Introduction	66
4.2.	Possible Options for 75-Foot Single Span Length.....	66
4.2.1.	Texas Box Beam.....	66
4.2.2.	NEXT D Beam.....	68
4.2.3.	Pre-Topped Inverted-Tee	70
4.2.4.	Modified Florida Slab Beam.....	72
4.2.5.	Modified Slab Beam	72
4.3.	Comparison of Possible Sections	74
4.4.	Summary and Conclusions.....	76
5.	Small-Scale Joint Static Testing	77
5.1.	Introduction	77
5.2.	Joints Selected for Further Evaluation	77
5.3.	Design of Field-Cast UHPC Connection Details	80
5.4.	Test Matrix	81
5.5.	Specimen Construction	83
5.5.1.	Beam Construction.....	83
5.5.2.	Material Properties.....	85

5.5.3.	Placement of Cast-in-Place Deck.....	93
5.5.4.	Placement of UHPC.....	94
5.5.5.	Observations from Construction.....	96
5.6.	Test Setup.....	106
5.7.	Loading Protocol.....	110
5.8.	Instrumentation Schedule.....	111
5.9.	Numerical Modeling and Estimated Response.....	115
5.10.	Summary of Results.....	115
5.11.	Analysis of Results.....	117
5.11.1.	Method for Determining Absolute Specimen Deflection.....	117
5.11.2.	Method for Determining Cracking Load.....	118
5.11.3.	Performance of Current FSB Joint Detail.....	121
5.11.4.	Performance of 18-inch-deep Specimens.....	123
5.11.5.	Performance of 12-inch-deep Specimens.....	133
5.12.	Conclusions and Recommendations.....	142
5.12.1.	Conclusions.....	142
5.12.2.	Construction and Design Recommendations.....	143
6.	Small-Scale Joint Fatigue Testing.....	145
6.1.	Introduction.....	145
6.2.	Specimens for Fatigue Testing.....	145
6.3.	Fatigue Loading Scheme.....	146
6.3.1.	Assumption for Truck Traffic Number.....	147
6.3.2.	Assumption for Fatigue Load Range.....	147
6.3.3.	Fatigue Load Testing Protocol.....	147
6.3.4.	Selection of After-Cracking Load Range.....	149
6.4.	Data Analysis Procedures.....	151
6.4.1.	Load-Deflection Data.....	151
6.4.2.	Reinforcement Strain Gauge Data.....	153
6.4.3.	Concrete Gauges Data.....	154
6.5.	Accidental Loading Before Fatigue Testing for 12F1-2.....	156
6.6.	Analysis of Results.....	158

6.6.1.	Fatigue Response	158
6.6.2.	Strength Performance after Fatigue Loading.....	163
6.7.	Conclusions and Recommendations.....	167
7.	Full-Scale Experimental Testing (Two-Beam).....	169
7.1.	Introduction	169
7.2.	Test Phases	169
7.3.	Specimen Construction	173
7.3.1.	Beam Construction.....	173
7.3.2.	Material Properties.....	175
7.3.3.	UHPC Joint Construction	180
7.3.4.	Observations from Construction.....	181
7.4.	Loading Configurations and Protocol	185
7.4.1.	Two-Beam Service and Strength Testing (FIU-1/2).....	185
7.4.2.	Two-Beam Fatigue, Service, and Strength Testing (FIU-4/5).....	186
7.5.	Instrumentation Schedule.....	191
7.5.1.	Two-Beam Strength and Service Testing (FIU-1/2).....	192
7.5.2.	Two-Beam Fatigue Service Testing (FIU-4/5).....	195
7.6.	Two-Beam Service and Strength Testing Results (FIU-1/2).....	197
7.6.1.	Summary of Results.....	197
7.6.2.	Service Test Results (FIU-1/2)	197
7.6.3.	Strength Test Results (FIU-1/2).....	204
7.6.4.	Summary.....	212
7.7.	Two-Beam Service and Strength Testing Results (FIU-4/5)	212
7.7.1.	Testing Summary	212
7.7.2.	Fatigue Data Analysis.....	213
7.7.3.	Unrestrained Service Test Results (Stages 1-4, LC 2-4, FC 2-5).....	216
7.7.4.	Restrained Service Test Results (Stages 5-8, FC 2-6)	229
7.7.5.	Rotation Restrained Permit Test Results (Stage 9, FC 2-7).....	242
7.7.6.	Transverse Crack Load Ramp Test Results (Stage 10, FC 2-5cr)	249
7.7.7.	Longitudinal Crack Load Ramps Test Results (Stage 11, FC 2-6cr)	256
7.7.8.	Cracked Restrained Service Test Results (Stage 12-15, FC 2-6cr)	261

7.7.9.	Strength Test Results (Stage 16, LC 2-1)	274
7.8.	Conclusions and Recommendations	283
8.	Full-Scale Experimental Testing (Four-Beam)	285
8.1.	Introduction	285
8.2.	Test Phases	285
8.3.	Specimen Construction	290
8.3.1.	Beam Construction	290
8.3.2.	Differential Camber Construction	290
8.3.3.	Superstructure Construction Procedure	292
8.3.4.	Joints Construction	294
8.3.5.	Material Properties	301
8.3.6.	Observations from Construction	303
8.4.	Loading Configurations and Protocols	308
8.4.1.	Test Setup	308
8.4.2.	Four-Beam Individual Stiffness and Camber leveling Assessments	310
8.4.3.	Four-Beam Fatigue, Service, and Strength Testing	312
8.5.	Instrumentation Schedule	317
8.5.1.	Four-Beam Individual Stiffness and Camber Leveling Instrumentation	319
8.5.2.	Four-Beam Fatigue, Service, and Strength Testing Instrumentation	323
8.6.	Long-Term Monitoring	328
8.6.1.	Camber Measurements	328
8.6.2.	VWG Data	329
8.6.3.	Prestress Losses	333
8.7.	Four-Beam Individual Stiffness and Camber Leveling Results	335
8.7.1.	Summary of Results	335
8.7.2.	Individual Stiffness Results (Stages 1.1 – 1.4; SC 4-1 through SC 4-4)	336
8.7.3.	Camber Leveling Results (Stages 1.5 – 1.6)	338
8.8.	Four-Beam Fatigue and Service Testing Results	347
8.8.1.	Testing Summary	347
8.8.2.	Girder Distribution Factors	348
8.8.3.	Service Test Results (Stages 2, 5, and 8; LC 4-1 through LC 4-4)	352

8.8.4.	Fatigue Test Results	362
8.8.5.	Cracked Service Test Results (Stages 8-9; LC 4-1cr through LC 4-4cr)	378
8.9.	Four-Beam Strength Testing Results	388
8.9.1.	Testing Summary	388
8.9.2.	Strength Test Results (Stage 10, LC 4-5)	388
8.10.	Conclusions and Recommendations	400
9.	Simple for Dead Load and Continuous for Live Load Design Concept for Modified FSB	402
9.1.	Introduction	402
9.1.1.	Background	402
9.1.2.	Construction Sequence.....	403
9.2.	Background on SDCL Connections	405
9.2.1.	AASHTO LRFD Bridge Design Specification.....	407
9.2.2.	FDOT Structure Design Guidelines [102]	410
9.2.3.	Additional Guidance on SDCL Connections	411
9.2.4.	Examples of SDCL Connections	421
9.2.5.	Challenges with SDCL Connections	424
9.3.	Design of SDCL Connection for Modified FSB System	424
9.3.1.	Introduction.....	424
9.3.2.	Preliminary Input and Analysis Assumptions.....	429
9.3.3.	Structural Analysis.....	431
9.3.4.	Cracking Moment for Continuity Diaphragm.....	433
9.3.5.	Design of Positive Moment Reinforcement.....	433
9.3.6.	Design of Negative Moment Reinforcement	440
9.3.7.	Stress Checks in Prestressed Concrete Members.....	443
9.3.8.	Proposed Continuity Diaphragm Design (12-inch)	444
9.3.9.	Additional Depths	444
9.4.	Numerical Evaluation of FSB Joint Detail for Continuity	447
9.4.1.	Loading Configuration and Protocol	447
9.4.2.	Model Geometry	448
9.4.3.	Material Modeling	450
9.4.4.	Loading Protocol and Construction Process	451

9.4.5.	Summary of Results	451
9.4.6.	Conclusions from FEM study	455
9.5.	Summary and Conclusions	456
10.	Summary and Conclusions	457
10.1.	Summary	457
10.2.	Conclusions and Recommendations	458
10.2.1.	Small-Scale Testing Protocol	458
10.2.2.	Large-Scale Testing Protocol	459
10.2.3.	Simple for Dead Load and Continuous for Live Load (SDCL) Recommendations 460	
10.2.4.	Construction and Design Recommendations	461
10.3.	Recommended Future Research	462
	References	463
A.	Construction Drawings	471
A.1.	Construction Plans for Small-Scale Joint Test Specimens	471
A.2.	Construction Procedure for Joints of Small-Scale Specimens	487
A.3.	Construction Plans for Full-Scale Beams	491
B.	Sample Calculations for 75-foot Analyses	493
B.1.	Sample Calculations for Modified FSB for 75-foot Spans Using FDOT Design Program 493	
B.2.	Sample Calculations for TxDOT Type 4B28 for 75-foot Spans Using PGSuper	513
C.	Estimation of Small-Scale Joint Strength	528
C.1.	Material Definition and Analysis Properties	528
C.2.	Estimated Performance of Each Section	531
C.2.1.	18-inch-deep FSB System Detail (FSB-Control)	531
C.2.2.	18-inch-deep FDOT 1 Detail (18F1)	533
C.2.3.	18-inch-deep FDOT 2 Detail (18F2)	535
C.2.4.	18-inch-deep Alternate 1 Detail (18A1)	537
C.2.5.	12-inch-deep FDOT 1 Detail (12F1)	539
C.2.6.	12-inch-deep FDOT 2 Detail (12F2)	541
C.2.7.	12-inch-deep Alternate 1 Detail (12A1)	543

C.2.8.	12-inch-deep Alternate 2 Detail (12A2)	545
D.	Results of Small-Scale Specimens	548
D.1.	Introduction	548
D.2.	Instrumentation Labeling	549
D.3.	Failure Modes	550
D.4.	18-inch Specimens	550
D.4.1.	FSB Control	550
D.4.2.	18F1 (FDOT 1)	559
D.4.3.	18F2 (FDOT 2)	567
D.4.4.	18A1 (Alternate 1)	575
D.5.	12-inch Specimens	582
D.5.1.	12F1 (FDOT 1)	583
D.5.2.	12F2 (FDOT 2)	589
D.5.3.	12A1 (Alternate 1)	596
D.5.4.	12A2 (Alternate 2)	603
E.	Fatigue Testing of Small-Scale Specimens	610
E.1.	Introduction	610
E.2.	Instrumentation Labeling	611
E.3.	Results for 12F1-2	612
E.3.1.	Fatigue Response	613
E.3.2.	Post-Fatigue Static Response	621
E.4.	Results for 12A1-2	622
E.4.1.	Fatigue Response	623
E.4.2.	Post-Fatigue Static Response	631
E.5.	Results for 12A2-2	632
E.5.1.	Fatigue Response	633
E.5.2.	Post-Fatigue Static Response	641
F.	Results of Four-Beam Test Configuration	642
F.1.	Introduction	642
F.2.	Instrumentation Layout for Four-Beam Test Configuration	644
F.3.	Load Stage 1.6 (Surcharge Removal)	654

F.4.	Load Stage 2 – Load Configuration 4-1	660
F.5.	Load Stage 2 – Load Configuration 4-2	666
F.6.	Load Stage 2 – Load Configuration 4-3	672
F.7.	Load Stage 2 – Load Configuration 4-4	678
F.8.	Load Stage 3 and 4	684
F.9.	Load Stage 5 – Load Configuration 4-1	685
F.10.	Load Stage 5 – Load Configuration 4-3	691
F.11.	Load Stage 5 – Load Configuration 4-4	697
F.12.	Load Stage 6 and 7	703
F.13.	Load Stage 8 – Load Configuration 4-1	712
F.14.	Load Stage 8 – Load Configuration 4-2	718
F.15.	Load Stage 8 – Load Configuration 4-3	724
F.16.	Load Stage 8 – Load Configuration 4-4	730
F.17.	Load Stage 9 – Load Configuration 4-1	736
F.18.	Load Stage 9 – Load Configuration 4-2	742
F.19.	Load Stage 9 – Load Configuration 4-3	748
F.20.	Load Stage 9 – Load Configuration 4-4	754
F.21.	Load Stage 10 – Load Configuration 4-5	760

LIST OF FIGURES

Figure 2.1: Three traditionally used prestressed concrete solutions for short-span bridges: (a) box beams, (b) T beams, and (c) slab beams	4
Figure 2.2: Prestressed concrete box beam construction per year [2]	5
Figure 2.3: Typical box beam sections [1]: (a) regular, non-composite section and (b) composite section	6
Figure 2.4: Box beam configurations [2]: (a) adjacent configuration and (b) spread configuration	7
Figure 2.5: Hawk Lake Bridge [5].....	8
Figure 2.6: Shear keys [6]: (a) partial depth shear key and (b) full-depth shear key systems	9
Figure 2.7: High-level railroad platform [7]	9
Figure 2.8: Typical configurations for NEXT beams [8]	10
Figure 2.9: Typical reinforcement for NEXT beams [8]	11
Figure 2.10: Types of joint detail for NEXT D beam [8]	12
Figure 2.11: NEXT beam section at Dailey Precast plant, Shaftsbury, Vermont [7]	12
Figure 2.12: Poutre-Dalle section [9].....	13
Figure 2.13: Construction sequence for Poutre-Dalle System: (a) adjacent placement of beams, (b) installation of joint reinforcement, (c) installation of remaining reinforcement and simultaneous casting of deck and joint [9]	13
Figure 2.14: New type of developed joints [11]: (a) joint between PCSS panels (90-degree hooks) and (b) drop-in reinforced cage.....	14
Figure 2.15: PCSS [11]: (a) typical transverse section of a bridge with PCSS system and (b) typical MnDOT PCSS.....	15
Figure 2.16: Erection of Bridge 04002 located on MN Highway 72 over the Tamarac River near the rural, northern Minnesota town of Waskish [11].....	15
Figure 2.17: (a) 3D FEM representation of an inverted-tee section with straight web and (b) side view FEM representation of an inverted-tee section with straight web [14].....	17
Figure 2.18: (a) Typical composite cross-section and (b) typical reinforcing details [15].....	18
Figure 2.19: Connection detail [15].....	18
Figure 2.20: Phase construction of US-360 bridge [15]	19
Figure 2.21: Florida slab beam superstructure system.....	20
Figure 2.22: Typical FSB section [16].....	21

Figure 2.23: (a) Placement of FSBs adjacent to each other and (b) finished pilot project SR-373 [16].....	21
Figure 2.24: Shear force at joint	22
Figure 2.25: Bending moment at joint	23
Figure 2.26: (a) Most common non-UHPC connection detail (Adapted from Biswas [21]) and (b) most common UHPC connection detail (adapted from Graybeal [22]).....	23
Figure 2.27: Sample joint details for (a) PCSS (Minnesota), (b) inverted-T (Virginia), and (c) Florida slab beam (FSB) (Florida).....	24
Figure 2.28: Transverse joint between precast slabs [21].....	25
Figure 2.29: Two types of mechanical connectors: (a) welded connection detail [23] and (b) grouted HSS pocket connection [24]	26
Figure 2.30: Additional reinforcement required in (a) transverse direction [25] and (b) extending from side of members [26].....	26
Figure 2.31: UHPC joint connection examples adapted from: (a) Royce [27] and (b) Aaleti and Sritharan [28]	27
Figure 2.32: Joint developed by FHWA [29]	28
Figure 2.33: (a) Traditional solution with post-tensioning and (b) UHPC connection solution without post-tensioning [29].....	28
Figure 2.34: (a) Conventional shear key specimen and (b) UHPC shear key specimen [29].....	29
Figure 2.35: Forced cracking [29]	29
Figure 2.36: Sollars Road Bridge cross-section [29].....	30
Figure 2.37: (a) Longitudinal joint detail and (b) shear key dowel detail [29].....	30
Figure 2.38: (a) UHPC connection between precast deck panels as deployed by NYSDOT on CR-47 over Trout Brook, (b) UHPC adjacent box beam connection detail, and (c) combined UHPC deck-level and composite connections as deployed by NYSDOT on I-81 near Syracuse, NY [22].....	31
Figure 2.39: Panel-to-panel and panel-to-girder connection [28].....	31
Figure 2.40: Common panel-to-panel UHPC connection details: (a) waffle deck panel-to-panel connection detail, (b) panel-to-panel headed connection detail, (c) panel-to-panel straight connection detail, and (d) panel-to-panel hairpin reinforcement [28]	32
Figure 2.41: Shear key connection in Wapello County Bridge [28].....	33
Figure 2.42: (a) Compressive UHPC behavior and (b) Tensile UHPC behavior [31]	36
Figure 2.43: General procedure for mixing and casting UHPC [31].....	41
Figure 2.44: Cast-in-place UHPC overlay, immediately (a) before and (b) after placement [31]	42

Figure 2.45: (a) Mars Hill Bridge girder comparison [31] and (b) Pi girder used in Jakway Park Bridge [37].....	43
Figure 3.1: Typical FSB section with 6 to 8-inch CIP composite deck.....	44
Figure 3.2: Difference between (a) depth of longitudinal steel in sections with CIP decks and (b) depth of steel in sections without CIP decks	44
Figure 3.3: Cross-section of bridge composed of 53-inch-wide FSB section (a) with a CIP deck and (b) without a CIP deck used for parametric study.....	45
Figure 3.4: Maximum moment versus span length for topped and untopped FSB sections	46
Figure 3.5: (a) Testing conducted on (b) joint detail between adjacent full-depth precast panels [39].....	47
Figure 3.6: (a) Currently used joint detail for box-beams developed by Graybeal [40] and (b) dimensions of the joint region.....	48
Figure 3.7: (a) Current 12-inch-deep FSB section, (b) proposed modification overlaid on original section, and (c) proposed new 12-inch-deep section with single layer of joint reinforcement	48
Figure 3.8: Construction of bridge with backer rods and CIP UHPC (like current FSB construction procedure).	49
Figure 3.9: Original, transitional, and proposed sections for 12-, 15-, and 18-inch-deep FSB sections with 48-inch widths.....	49
Figure 3.10: 18-inch-deep modified FSB section with (a) one layer and (b) two layers of joint reinforcement	50
Figure 3.11: Proposed options by FDOT engineers: (a) Option 1 and (b) Option 2	51
Figure 3.12: Typical section details for 12-inch deep standard FSB section used for Case 1 modeling: (a) cross-section details [19] and (b) joint details [19].....	51
Figure 3.13: General shape of concrete (a) compression and (b) tension curves	53
Figure 3.14: General shape of stress-strain curve for reinforcement.....	54
Figure 3.15: (a) Loading protocol used by [41] compared to (b) protocol used for analyses	55
Figure 3.16: First three analyses comparing the current connection detail to proposed UHPC connection detail with one and two layers of steel	56
Figure 3.17: Second three analyses comparing the current joint geometry with conventional concrete and UHPC to the modified joint geometry with UHPC.....	56
Figure 3.18: Summary of results for Case 1: (a) cross-section geometry and reinforcement detail, (b) model meshing, (c) load-deflection curve, and (d) crack pattern at failure	58
Figure 3.19: Summary of results for Case 2: (a) cross-section geometry and reinforcement detail, (b) model meshing, (c) load-deflection curve, and (d) crack pattern at failure	59

Figure 3.20: Summary of results for Case 3: (a) cross-section geometry and reinforcement detail, (b) model meshing, (c) load-deflection curve, and (d) crack pattern at failure	60
Figure 3.21: Summary of results for Case 4: (a) cross-section geometry and reinforcement detail, (b) model meshing, (c) load-deflection curve, and (d) crack pattern at failure	61
Figure 3.22: Summary of results for Case 5: (a) cross-section geometry and reinforcement detail, (b) model meshing, (c) load-deflection curve, and (d) crack pattern at failure	62
Figure 3.23: Summary of results for Case 6: (a) cross-section geometry and reinforcement detail, (b) model meshing, (c) load-deflection curve, and (d) crack pattern at failure	63
Figure 3.24: Summary of results for Case 7: (a) cross-section geometry and reinforcement detail, (b) model meshing, (c) load-deflection curve, and (d) crack pattern at failure	64
Figure 3.25: Summary of results for Case 8: (a) cross-section geometry and reinforcement detail, (b) model meshing, (c) load-deflection curve, and (d) crack pattern at failure	65
Figure 4.1: TxDOT Type 4B28 [44].....	67
Figure 4.2: Traditional (a) adjacent and (b) spread configuration for 28-inch deep box beams [44] and (c) adjacent configuration with UHPC connections [29]	68
Figure 4.3: NEXT D beam [8]	69
Figure 4.4: NEXT D beam span lengths [8]	69
Figure 4.5: Deck bulb tee shape compared to adjacent box beam configuration [46].....	70
Figure 4.6: Deck bulb tee span lengths [45]	71
Figure 4.7: (a) PCI deck bulb tee [45], (b) truncated FIB [47], and (c) Florida inverted-T [48].	71
Figure 4.8: Pre-topped FIT	72
Figure 4.9: (a) Original FSB section with currently available depths and (b) modified FSB section required to achieve 75-foot span lengths.....	72
Figure 4.10: (a) Conventional adjacent box beam configuration, (b) proposed modified slab beam section shape, and (c) proposed modified slab beam configuration	73
Figure 4.11: Modified slab beam with (a) bottom and top flanges connected and (b) only top flanges connected.....	74
Figure 4.12: Required section depths and number of 0.6-inch diameter strands to achieve 75-foot span using (a) TxDOT Type 4B20, (b) NEXT D-96, (c) pre-topped Florida inverted-T, (d) modified FSB, and (e) modified slab girder sections	75
Figure 5.1: Proposed joints for experimental testing: (a) FDOT proposed joint detail 1 (“FDOT 1”), (b) FDOT proposed joint detail 2 (“FDOT 2”), and alternate joint detail based on joint developed by Graybeal [55] (“Alternate 1”).....	78
Figure 5.2: Plan view of two beams with joint for proposed testing.....	79
Figure 5.3: Alternate 2 joint detail.....	80

Figure 5.4: Specimen details: (a) current FSB joint detail, (b) proposed FDOT 1 keyway, (c) proposed FDOT 2 keyway, (d) proposed Alternate 1 keyway, and (e) proposed Alternate 2 keyway	82
Figure 5.5: Naming convention for small-scale specimens	83
Figure 5.6: Construction of specimens: (a) specimen form and reinforcement, (b) concrete pour, (c) finished cast, and (d) surface raked finish for FSB control	84
Figure 5.7: (a) Delivery of all slab-beam specimens, (b) beam showing strands, transverse reinforcement and lifting hooks (18-inch FDOT 1 shown)	85
Figure 5.8: UHPC mixing process: (a) weighing of ingredients, (b) dosages preparation, (c) mixing operation of UHPC, and (d) placing operation for the UHPC.....	87
Figure 5.9: UHPC flow test: (a) specimen preparation and (b) spread measurement	89
Figure 5.10: Beam samples for UHPC flexural performance: (a) 4x4x14 in. mold, and (b) broken UHPC beam samples	90
Figure 5.11: Construction of deck and joint in FSB: (a) adjacent FSBs with ¾” spacing, (b) CIP deck form construction, (c) slab and joint reinforcement, and (d) CIP deck pour	93
Figure 5.12: Deck cast for FSB specimens: (a) formwork layout for first testing stage, (b) deck casting operation for first testing stage after rebar placement, (c) alignment layout of broken pieces for second testing stage, and (d) second concrete cast operation	94
Figure 5.13: Casting procedure for UHPC joint: (a) connection detail with plywood block-out and pre-wetting of surfaces to an SSD condition before UHPC placement, (b) mixing operation for the field-cast UHPC, (c) vertical dam used to place the UHPC, and (d) placing operation for the field-cast UHPC	95
Figure 5.14: Casting of UHPC joint for second test: (a) vertical dam layout on broken beams and (b) second testing instance for joint geometry	95
Figure 5.15: (a) Desired interface surface preparation (per FHWA guidelines [39]), (b) heavy sandblast finish provided, (c) joint material separation from Alternate 1 precast section (similar behavior in other specimens), and (d) bond lost between UHPC joint matrix and precast concrete	96
Figure 5.16: Process for exposed aggregate finish: (a) shear-key surface preparation detail, (b) in-form retarder agent, (c) removed shear-key region of the formwork, (d) retarder agent applied to the form wall, (e) block-outs with retarder agent fastened to the formwork, (f) concrete cast after product application, (g) retarded surface after block-outs removal, and (h) pressure washing operation	98
Figure 5.17: Comparison of joint finish: (a) sand-blasted finish and (b) exposed-aggregate finish	99
Figure 5.18: Unnecessary agent application zone (a) before and (b) after joint casting	99

Figure 5.19: (a) FDOT 1 ledge shape, (b) FDOT 2 ledge shape, (c) Alternate 1 ledge shape, and (d) Alternate 2 ledge shape	100
Figure 5.20: (a) FDOT 2 cracked bottom lips and (b) FDOT 2 longitudinal cracks of bottom lips on the underside	101
Figure 5.21: (a) Original FSB shear reinforcement, (b) confinement stirrup, and (c) interface stirrup	101
Figure 5.22: (a) Proposed slab-beam confinement reinforcement (FDOT 1 shown – others similar), (b) confinement stirrup, and (c) Alternate 2 dimension of stirrup loop (two loops needed – others similar)	102
Figure 5.23: (a) Increased steel density and (b) unappropriated confinement spacing and cover	102
Figure 5.24: Transverse rebar misalignment observed in Alternate 2 joint specimen.....	103
Figure 5.25: (a) Large and (b) small clumps collected from dry premix of UHPC.....	104
Figure 5.26: UHPC joint bond comparison: (a) poor bond observed with the faulty UHPC mixture and (b) enhanced bond observed with the adequate UHPC mixture.....	104
Figure 5.27: (a) Chipped keyway border and (b) several damages to the beam border	105
Figure 5.28: (a) Original rebar bent in control FSB and (b) larger rebar bent diameter delivered	106
Figure 5.29: Schematic of testing configuration for small-scale joint testing	106
Figure 5.30: (a) Supports elevation layout, (b) display of support configuration, (c) supports plan layout, and (d) display of supports and testing frame	107
Figure 5.31: (a) Fractured grouted pad due to load block rotation, (b) sliding plates before test, and (c) sliding plates after test	108
Figure 5.32: (a) Testing frame and specimen configuration layout (east view) and (b) display of specimen (control FSB) and testing frame.....	109
Figure 5.33: Bottom wooden frames	109
Figure 5.34: (a) UHPC cast in first testing round, (b) failure obtained from first round, (c) UHPC cast in broken specimen, and (d) failure obtained from second round	110
Figure 5.35: Complete instrumentation schedule (Testing Phase 1)	112
Figure 5.36: Complete instrumentation schedule (Testing Phase 2)	113
Figure 5.37: Actual installed sensors: (a) bottom view with CSGs and CDTs, (b) top view with CSGs, (c) RSG location in UHPC closure, and (d) RSG location in FSB closure.....	114
Figure 5.38: Example of estimated load versus midspan deflection for 18A1	115
Figure 5.39: Example of estimated crack pattern on (a) top and (b) bottom of specimen 18A1115	115

Figure 5.40: Ultimate strength capacity comparison	117
Figure 5.41: Average displacement computation for each sensor group.....	118
Figure 5.42: Actual cracks from visual inspection (12F2-1 shown).....	118
Figure 5.43: Data with cracking loads (18F1-1 shown): (a) load versus deflection plot, (b) load versus rebar strain plot, (c) load versus bottom opening plot, and (d) load versus bottom concrete strain plot	119
Figure 5.44: FSB Control specimen load versus deflection responses with maximum values	121
Figure 5.45: Failure mechanism in FSB-1 and FSB-2: (a) crack develops at vertical leg of hook reinforcement and (b) hinging occurs near load as joint reinforcement pulls out	122
Figure 5.46: (a) Failed FSB Control-1 joint and (b) pull-out cavity in inner confined concrete (dashed line) and longitudinal rebar bend due to bending and pull-out forces (solid lines).....	122
Figure 5.47: Load versus strain in joint reinforcement on the off-load side (south) for FSB-1	123
Figure 5.48: Load versus strain in joint reinforcement on the loaded side (north) for FSB-1...	123
Figure 5.49: 18-inch specimens: load versus deflection experimental static tests with maximum values	124
Figure 5.50: Crack pattern of 18-inch specimens	125
Figure 5.51: Crack pattern of 18-inch specimens (cont.).....	126
Figure 5.52: Typical failure mechanism for proposed 18-inch-deep joint specimens (18F2 is shown): (a) cracking at failure and (b) hinging in the precast section next to the UHPC joint..	127
Figure 5.53: (a) 18F1-1 failed specimen (north), (b) 18F1-2 failed specimen (north), (c) 18F2-1 failed specimen (two broken rebar; north), and (d) 18F2-2 failed specimen (north)	128
Figure 5.54: Load versus strain in joint reinforcement for 18F1-1 on the (a) north and (b) south beams of the joint.....	129
Figure 5.55: Load versus strain in joint reinforcement for 18F2-1 on the (a) north and (b) south beams of the joint.....	130
Figure 5.56: (a) Failed 18A1-1 specimen (loaded beam showed) and (b) UHPC matrix attached to unloaded beam	131
Figure 5.57: 18A1-1 system load versus rebar microstrain in north beam (RSG-8 malfunctioned after 120 kips)	131
Figure 5.58: 18A1 system load versus rebar microstrain in unloaded beam	132
Figure 5.59: 12-inch specimens: experimental static tests with maximum values	133
Figure 5.60: Crack pattern of 12-inch specimens (dashed lines indicate cracks formed in the cyclic stage); *strength test performed after fatigue testing	134

Figure 5.61: Crack pattern of 12-inch specimens (dashed lines indicate cracks formed in the cyclic stage) (cont.); *strength test performed after fatigue testing.....	135
Figure 5.62: First typical failure pattern in 12-inch specimens: (a) cracking at failure and (b) after failure (12F1 is shown).....	136
Figure 5.63: Second typical failure pattern in 12-inch specimens: (a) cracking at failure and (b) after failure (12F1 is shown).....	136
Figure 5.64: Cracking at failure for (a) 12F1-1 and (b) 12F2-1	137
Figure 5.65: 12F1-1 system load versus rebar microstrain in (a) south beam and (b) north beam	138
Figure 5.66: 12F2-1 system load versus rebar microstrain in (a) south beam and (b) north beam	139
Figure 5.67: (a) Failed 12A1-1 specimen and (b) Failed 12A2-1 specimen	140
Figure 5.68: Two hypotheses for cracking at level of joint reinforcement: (a) splitting caused by pull-out of joint reinforcement (12F1 shown) and (b) cracking under reinforcement caused by beam bending (12A2 shown)	140
Figure 5.69: 12A1-1 system load versus rebar microstrain in (a) south beam and (b) north beam (defective rebar responses are not shown)	141
Figure 5.70: 12A2-1 system load versus rebar microstrain in (a) south beam and (b) north beam	142
Figure 6.1: Joint geometries for specimens tested with fatigue loading: (a) 12F1, (b) 12A1, and (c) 12A2	145
Figure 6.2: Refined design footprint for fatigue design [72].....	147
Figure 6.3: Summary of results and recommended design provision [74].....	149
Figure 6.4: Procedure for selecting load range from rebar strain range (for 12F1).....	150
Figure 6.5: Example of load deflection ranges for (a) under-cracking and (b) after-cracking fatigue steps (for 12F1-1).....	151
Figure 6.6: Hypothetical data for normalized stiffness values every 1000 cycles.....	152
Figure 6.7: Average displacement computation for each sensor group.....	152
Figure 6.8: Sample of rebar gauge strains from static test within range of proposed fatigue testing loads; measured rebar strain ranges are highlighted (from 12F1-1)	153
Figure 6.9: Hypothetical strain per applied load versus number of cycles for reinforcement... ..	154
Figure 6.10: Strain in bottom of concrete for 12F1-1 (from static test)	155
Figure 6.11: Strain per applied load (kip) per number of cycles for bottom concrete strains	155

Figure 6.12: Cracking and crack lengths after accidental loading of 12F1-2 before fatigue testing on the (a) west side and (b) east side	156
Figure 6.13: Cracking and crack lengths after accidental loading of 12F1-2 before fatigue testing on the (a) bottom of the west side and (b) bottom of the east side	157
Figure 6.14: Normalized absolute stiffness of system for joints (a) 12F1, (b) 12A1, and (c) 12A2	158
Figure 6.15: Reinforcement strain change per load change versus cyclic load for joint reinforcement at center of specimens for the unloaded (RSG-5) and loaded (RSG-15) side.....	160
Figure 6.16: Concrete strain change per load change versus cyclic load at center of specimens for the unloaded (CSG-2, CSG-3) and loaded (CSG-5) side.....	161
Figure 6.17: Displacement change of crack gauge per load change versus cyclic load at center of specimens (CDT-3).....	162
Figure 6.18: Load-deflection curves for strength and post-fatigue strength tests for joints (a) 12F1, (b) 12A1, and (c) 12A2.....	163
Figure 6.19: Failure crack for ultimate strength testing of 12F1 (a) without any fatigue load applied, 12F1-1 and (b) after fatigue loading, 12F1-2.....	164
Figure 6.20: Failure cracking and mechanism for strength testing of 12F1 (a) without any fatigue load applied, 12F1-1 and (b) after fatigue loading, 12F1-2.....	164
Figure 6.21: Failure crack for ultimate strength testing of 12A1 (a) without any fatigue load applied, 12A1-1 and (b) after fatigue loading, 12A1-2	165
Figure 6.22: Failure cracking and mechanism for strength testing of 12A1 (a) without any fatigue load applied, 12A1-1 and (b) after fatigue loading, 12A1-2	165
Figure 6.23: Failure crack for ultimate strength testing of 12A2 (a) without any fatigue load applied, 12A2-1 and (b) after fatigue loading, 12A2-2	166
Figure 6.24: Failure cracking and mechanism for strength testing of 12A2 (a) without any fatigue load applied, 12A2-1 and (b) after fatigue loading, 12A2-2	167
Figure 7.1: Testing phases for full-scale FSB tests (chapter number in parentheses)	169
Figure 7.2: Phase I (FIU-1 and FIU-2) strength and service test configurations.....	170
Figure 7.3: Schematic of bottom support location.....	172
Figure 7.4: Comparison between (a) simply supported and (b) end moment restrained support conditions.....	173
Figure 7.5: Casting schedule for eight full-size beams for full-scale testing.....	173
Figure 7.6: Construction of reinforcing cage and formwork for full-scale beams: (a) prestressing strand and reinforcement cage constructed, (b) side forms with paste retarding agent, and (c) assembled formwork and reinforcement ready for casting.....	174

Figure 7.7: Casting of concrete for full-scale beams: (a) casting of concrete, (b) float finish on top of beams, and (c) finished beam after casting	174
Figure 7.8: (a) Removal of forms with paste retarding agent on concrete surface, (b) pressure washing away of paste retarding agent and unhydrated cement paste, and (c) exposed aggregate finish after procedure	175
Figure 7.9: (a) Beam release stage and (b) delivery of slab-beam specimens	175
Figure 7.10: UHPC mixing process for two-beam test configurations: (a) mixer working area preparation, (b) mixing operation of UHPC materials, (c) casting operation, and (d) top form closure and weights location	177
Figure 7.11: UHPC flow test: (a) mold removal and (b) spread measurement	178
Figure 7.12: UHPC samples: (a) 4x4x14 in. beam in molds after grinding for dimensional consistency and (b) ten 4x8 in. cylinders for compressive strength	179
Figure 7.13: Casting procedure for UHPC joint: (a) beams alignment with ¾-inch gap and backer rod, (b) connection detail with plywood block-out and top strips for over pour volume, (c) casting operation for the field-cast UHPC, (d) rodding procedure for two encountering pour heads, and (e) top formwork hold using weights	181
Figure 7.14: Joint construction observations: (a) side form segments, (b) side form segments attached, (c) UHPC leakage at joint end, and (d) attachment of bottom plywood strip to stop leakage	182
Figure 7.15: Backer rod detail: (a) 1-inch diameter rod and (b) rod extension through block-out form	183
Figure 7.16: Master Finish HV retarder degrees of penetration: (a) light and (b) medium light	184
Figure 7.17: UHPC grinded surface: (a) surface finish after two days using gas grinder (showing precast abrasion), and (b) surface finish after one day using electric grinder	184
Figure 7.18: HL-93 truck load with full and half rear axle identification (from [77])	185
Figure 7.19: Proposed test setup for Load Configuration 2-4 (a) schematic and (b) plan and elevation views	185
Figure 7.20: Proposed test setup for Configuration 2-1 (a) schematic and (b) plan and elevation views	186
Figure 7.21: Proposed test setup for Configuration 2-5 (a) schematic and (b) plan and elevation views, (c) reverse sinusoidal load protocol for FC 2-5, and (d) static transverse cracking load protocol for FC 2-5cr	187
Figure 7.22: Transverse crack procedure (FC 2-5cr): (a) uniform load application, (b) east side load increment, and (c) cracking occurred at total load of 65 kips	188

Figure 7.23: Proposed test setup for Configuration 2-6 (a) schematic and (b) plan and elevation views, (c) reverse sinusoidal load protocol for FC 2-6, (d) static load protocol for FC 2-6, and (e) static longitudinal cracking load protocol for FC 2-6cr.....	189
Figure 7.24: Longitudinal crack procedure (south view): (a) uniform load application until bearing of the interior supports, (b) continued uniform load increment, and (c) maximum applied load to obtain longitudinal cracking	190
Figure 7.25: Proposed test setup for Configuration 2-7 (a) schematic and (b) plan and elevation views	190
Figure 7.26: End moment restraint detail: (a) south-end view and (b) welded plate detail.....	191
Figure 7.27: Two-beam test with two main sensor regions	191
Figure 7.28: Instrumentation used for full-scale testing: (a) RSGs, (b) CSGs, (c) CDTs, and (d) LDTs	192
Figure 7.29: Two-beam (FIU-1/2) span center sensor location and types.....	193
Figure 7.30: Two-beam (FIU-1/2) support sensor location and types (both supports identical)	194
Figure 7.31: Two-beam (FIU-4/5) span center sensor location and types.....	195
Figure 7.32: Two-beam (FIU-4/5) support sensor location and types (both supports identical)	196
Figure 7.33: Load versus midspan displacement for service load testing with LC 2-4 for FIU-1/2	198
Figure 7.34: Bottom crack pattern at midspan for service load testing with LC 2-4 for FIU-1/2 at: (a) 0 kips, (b) 30 kips, (c) 50 kips, and (d) 68 kips.....	199
Figure 7.35: Crack displacement gauge used across joint	199
Figure 7.36: Load versus average strain across top of joint for service load testing with LC 2-4 for FIU-1/2	200
Figure 7.37: Load versus average strain across bottom of joint for service load testing with LC 2-4 for FIU-1/2	201
Figure 7.38: Expected stresses on top and bottom of specimen from transverse flexure.....	201
Figure 7.39: Load versus transverse concrete strain for service load testing with LC 2-4 for FIU-1/2 for (a) top and (b) bottom of beam in the midspan section of the system	202
Figure 7.40: Load versus strain for service load testing with LC 2-4 for joint reinforcement extending from FIU-1 for the (a) midspan and (b) south sections of the system	203
Figure 7.41: Load versus longitudinal concrete strain for service load testing with LC 2-4 for FIU-1/2 for (a) top and (b) bottom of beam in the midspan section of the system	204
Figure 7.42: Load versus midspan displacement for ultimate strength testing with LC 2-1 for FIU-1/2.....	205

Figure 7.43: Bottom crack pattern at midspan for ultimate strength testing with LC 2-1 for FIU-1/2 at: (a) 0 kips, (b) 60 kips, and (c) 80 kips; blue = new cracks, red = cracks from previous tests	206
Figure 7.44: Load versus average strain across top of joint for ultimate strength testing with LC 2-1 for FIU-1/2.....	206
Figure 7.45: Load versus average strain across bottom of joint for ultimate strength testing with LC 2-1 for FIU-1/2.....	207
Figure 7.46: Load versus transverse concrete strain for ultimate strength testing with LC 2-1 for (a) top and (b) bottom of beam in the midspan section of FIU-1/2	208
Figure 7.47: Load versus strain for ultimate strength testing with LC 2-1 for joint reinforcement extending from FIU-1 for the (a) midspan and (b) south sections of the system	209
Figure 7.48: Crushing of FIU-1/2 concrete at failure for LC 2-1: (a) overview and (b) joint....	210
Figure 7.49: FIU-1/2 joint edge cores: location of cores (a) along length and (b) in cross section, (c) three core samples with bottom lip debonded, and (d) observed debonding crack extending into the precast matrix.....	210
Figure 7.50: Load versus longitudinal concrete strain for ultimate strength testing with LC 2-1 for (a) top and (b) bottom of beam in the midspan section of FIU-1/2	211
Figure 7.51: Summary of testing stages performed on two-beam setup with FIU-4/5.....	212
Figure 7.52: Location of (a) actuators and (b) LDT displacement sensors	214
Figure 7.53: Hypothetical data for normalized stiffness values every 1000 cycles.....	215
Figure 7.54: Hypothetical strain per applied load versus number of cycles for reinforcement. 216	
Figure 7.55: Strain per applied load (kip) per number of cycles for bottom concrete strains ...	216
Figure 7.56: Load versus midspan displacement load testing with Load Configuration 2-4 before (LR 1-1 dashed) and after (LR 4-1 solid) Fatigue Configuration 2-5.....	217
Figure 7.57: Normalized stiffnesses at midspan for west and east actuators and for the average midspan response	218
Figure 7.58: Load versus average strain across top of joint for permit load testing with LC 2-4 for (a) FIU-4/5 (LR 4-1) and (b) FIU-1/2.....	219
Figure 7.59: Load versus average strain across bottom of joint for permit load testing with LC 2-4 for (a) FIU-4/5 (LR 4-1) and (b) FIU-1/2	219
Figure 7.60: Load versus transverse concrete strain for permit load testing with LC 2-4 for FIU 1/2 and FIU 4/5 (LR 4-1) for (a) top and (b) bottom of beam in the midspan section of the system	221
Figure 7.61: Load versus strain for permit load testing with LC 2-4 for joint reinforcement in FIU 4/5 (LR 4-1) and FIU 1/2 for the (a) midspan and (b) south sections of the systems	222

Figure 7.62: Strain change per change in load versus cyclic load for top CDTs in Stage 2/3....	223
Figure 7.63: Strain change per change in load versus cyclic load for bottom CDTs in Stage 2/3	224
Figure 7.64: Strain change of top transverse CSGs per change in load at center of specimen in Stage 2/3.....	225
Figure 7.65: Strain change of bottom transverse CSGs per change in load at center of specimen in Stage 2/3	225
Figure 7.66: Maximum strain of RSGs per applied load versus cyclic load at center of specimen	226
Figure 7.67: Load versus longitudinal concrete strain for permit load testing with LC 2-4 for FIU-4/5 (LR 4-1) and FIU-1/2 for (a) top and (b) bottom of beam in the midspan section of the system	227
Figure 7.68: Strain change of top longitudinal CSGs per change in load versus cyclic load at center of specimen	228
Figure 7.69: Strain change of bottom longitudinal CSGs per change in load versus cyclic load at center of specimen	228
Figure 7.70: Intermediate support detail underneath FIU-5 at center region	229
Figure 7.71: Load per actuator versus time for LR 5-3 and LR 8-1	230
Figure 7.72: Load versus midspan displacement load testing with Load Configuration 2-6 before (LR 5-3 dashed) and after (LR 8-1 solid) Fatigue Configuration 2-6.....	230
Figure 7.73: Normalized stiffnesses at midspan for west and east actuators and average system response for FC 2-5 and FC 2-6.....	232
Figure 7.74: Load versus average strain across top of joint for permit load testing of FIU 4 and FIU 5 with (a) FC 2-5 (LR 4-1) and FC 2-6 (LR 8-1)	233
Figure 7.75: Load versus average strain across bottom of joint for permit load testing of FIU 4 and FIU 5 with (a) LC 2-4 (LR 4-1) and FC 2-6 (LR 8-1)	233
Figure 7.76: Load versus transverse concrete strain for permit load testing of FIU-4/5 with LC 2- 4 (LR 4-1) and FC 2-6 (LR 8-1) for (a) top and (b) bottom of beam in the midspan section of the system	234
Figure 7.77: Load versus strain for permit load testing of FIU-4/5 with LC 2-4 (LR 4-1) and FC 2-6 (LR 8-1) for joint reinforcement extending from FIU-5 for the (a) midspan and (b) south sections of the system	235
Figure 7.78: Strain change of crack gauge per change in applied load versus number of cycles for CDTs on top of joint for FC 2-5 and FC 2-6	236
Figure 7.79: Strain change of crack gauge per change in applied load versus number of cycles for CDTs on the bottom of joint for FC 2-5 and FC 2-6	237

Figure 7.80: Strain change of top transverse CSGs per change in applied load versus number of cycles at center of specimen	238
Figure 7.81: Strain change of bottom transverse CSGs per change in applied load versus number of cycles at center of specimen	238
Figure 7.82: Strain change of RSGs per change in applied load versus number of cycles at center of specimen for FC 2-5 and FC 2-6	239
Figure 7.83: Load versus longitudinal concrete strain for service load testing with LC 2-4 (LR 4-1) and FC 2-6 (LR 8-1) for (a) top and (b) bottom of beam in the midspan section of the system	240
Figure 7.84: Strain change of top longitudinal CSGs per change in applied load versus number of cycles at center of specimens with FC 2-5 and FC 2-6.....	241
Figure 7.85: Strain change of bottom longitudinal CSGs per change in applied load versus number of cycles at center of specimens with FC 2-5 and FC 2-6.....	241
Figure 7.86: Load versus midspan displacement load testing with Load Configuration 2-4 before (LR 1-1 dashed) and after (LR 9-3 solid) Fatigue Configuration 2-7.....	242
Figure 7.87: Load versus midspan displacement load testing with Fatigue Configuration 2-7 – North End response (LR 9-3).....	243
Figure 7.88: Load versus average strain across top of joint in FIU-4/5 system for (a) FC 2-7 (LR 9-3) and (b) LC 2-4 (LR 4-1).....	243
Figure 7.89: Load versus average strain across bottom of joint in FIU-4/5 system for (a) FC 2-7 (LR 9-3) and (b) LC 2-4 (LR 4-1)	244
Figure 7.90: Load versus transverse concrete strain for service load testing with FC 2-7 (LR 9-3) and LC 2-4 (LR 4-1) for (a) top and (b) bottom of beam in the midspan section of the system	245
Figure 7.91: Load versus strain for service load testing with FC 2-7 (LR 9-3) and LC 2-4 (LR 4-1) for joint reinforcement extending from FIU-5 for the (a) midspan and (b) south sections of the system	246
Figure 7.92: Load versus longitudinal concrete strain for service load testing with FC 2-7 (LR 9-3) and LC 2-4 (LR 4-1) for (a) top and (b) bottom of beam in the midspan section of the system	247
Figure 7.93: Load versus longitudinal concrete strain for service load testing with Fatigue Configuration 2-7 for (a) top and (b) bottom of the beam in the south end section of the system (LR 9-3)	248
Figure 7.94: Applied load versus time for Stage 10 testing using loading like FC 2-5.....	249
Figure 7.95: Load versus midspan displacement crack load testing with FC 2-5cr (LR 10-1) ..	250
Figure 7.96: Bottom crack pattern at midspan for transverse cracking load ramp at: (a) 0 kips and (b) 65 kips (LR 10-1)	250

Figure 7.97: Load versus average strain across top of joint for transverse cracking load testing with (a) FC 2-5cr (LR 10-1) and (b) LC 2-4 (LR 4-1).....	251
Figure 7.98: Load versus average strain across bottom of joint for transverse cracking load testing with (a) FC 2-5cr (LR 10-1) and (b) LC 2-4 (LR 4-1).....	252
Figure 7.99: Load versus transverse concrete strain for transverse cracking load testing with FC 2-5cr (LR 10-1) and LC 2-4 (LR 4-1) for (a) top and (b) bottom of beam in the midspan section of the system	253
Figure 7.100: Load versus strain for transverse cracking load testing with FC 2-5cr (LR 10-1) and LC 2-4 (LR 4-1) for joint reinforcement extending from FIU-5 for the (a) midspan and (b) south sections of the system.....	254
Figure 7.101: Load versus longitudinal concrete strain for transverse cracking load testing with FC 2-5cr (LR 10-1) and LC 2-4 (LR 4-1) for (a) top and (b) bottom of beam in the midspan section of the section.....	255
Figure 7.102: Load versus midspan displacement using FC 2-6cr (LR 11-2).....	256
Figure 7.103: Load versus average strain across top of the joint for (a) FC 2-6cr (LR 11-2) and (b) FC 2-6 (LR 8-1).....	257
Figure 7.104: Load versus average strain across bottom of joint for (a) FC 2-6cr (LR 11-2) and (b) FC 2-6 (LR 8-1).....	257
Figure 7.105: Load versus transverse concrete strain for FC 2-6cr (LR 11-2) and FC 2-6 (LR 8-1) for (a) top and (b) bottom of beam in the midspan section of the system	258
Figure 7.106: Load versus strain for joint reinforcement extending from FIU-5 for FC 2-6cr (LR 11-2) and FC 2-6 (LR 8-1) for the (a) midspan and (b) south sections of the system.....	259
Figure 7.107: Load versus longitudinal concrete strain or FC 2-6cr (LR 11-2) and FC 2-6 (LR 8-1) for (a) top and (b) bottom of beam in the midspan section of the section (LR 11-2).....	260
Figure 7.108: Load per actuator versus time for (a) LR 12-1 and (b) LR 15-1 (service load testing before and after FC 2-6cr cyclic loading).....	261
Figure 7.109: Load versus displacement for (a) LR 10-1 and LR 15-1 and (b) LR 12-1 and LR 15-1	262
Figure 7.110: Normalized stiffnesses at midspan for (a) west and (b) east actuator and (c) average midspan response using LDTs for all cyclic loads.....	263
Figure 7.111: Bottom crack pattern at midspan for transverse cracking load ramp: (a) after LR 10-1 and (b) after LR 15-1	264
Figure 7.112: Transverse cracks on FIU-4 exterior bottom lip (after LR 15-1) at: 0 kips (red) and 65 kips (blue)	264
Figure 7.113: Load versus average strain across top of joint for (a) LR 10-1 (FC 2-5cr), (b) LR 12-1 (FC 2-6cr), and (c) LR 15-1 (FC 2-5cr).....	265

Figure 7.114: Load versus average strain across bottom of joint for (a) LR 10-1 (FC 2-5cr), (b) LR 12-1 (FC 2-6cr), and (c) LR 15-1 (FC 2-5cr)	265
Figure 7.115: Load versus transverse concrete strain for LR 10-1, LR 12-1, and LR 15-1 for (a) top and (b) bottom of beam in the midspan section of the system	266
Figure 7.116: Load versus strain for LR 10-1, LR 12-1 and LR 15-1 for joint reinforcement extending from FIU-5 for the (a) midspan and (b) south sections of the system	267
Figure 7.117: Strain change of crack gauge per change in applied load versus number of cycles at center of specimen (top) for all cyclic loading	268
Figure 7.118: Strain change of crack gauge per change in applied load versus number of cycles at center of specimen (bottom) for all cyclic loading	269
Figure 7.119: Strain change of top transverse CSGs per change in applied load versus number of cycles at center of specimen for all cyclic loading	270
Figure 7.120: Strain change of bottom transverse CSGs per change in applied load versus number of cycles at center of specimen for all cyclic loading.....	270
Figure 7.121: Strain change of RSGs per change in applied load versus number of cycles at center of specimen for all cyclic loading	271
Figure 7.122: Load versus longitudinal concrete strain for LR 10-1, LR 12-1 and LR 15-1 for (a) top and (b) bottom of beam in the midspan section of the system (LR 15-1)	272
Figure 7.123: Strain change of top longitudinal CSGs per change in applied load versus number of cycles at center of specimen for all cyclic loading.....	273
Figure 7.124: Strain change of bottom longitudinal CSGs per change in applied load versus number of cycles at center of specimen for all cyclic loading.....	273
Figure 7.125: Load versus midspan displacement for ultimate strength testing with LC 2-1 for FIU 4/5 and FIU 1/2.....	274
Figure 7.126: Bottom crack pattern at midspan for ultimate strength testing with Load Configuration 2-1 at (a) 0 kips, (b) 65 kips, and (c) 90 kips; blue = new cracks, red = cracks from previous tests.....	275
Figure 7.127: Load versus average strain across top of joint for ultimate strength testing with LC 2-1 for (a) FIU-4/5 and (b) FIU-1/2.....	276
Figure 7.128: Load versus average strain across bottom of joint for ultimate strength testing with LC 2-1 for (a) FIU-4/5 and (b) FIU-1/2.....	277
Figure 7.129: Load versus transverse concrete strain for ultimate strength testing with LC 2-1 for (a) top and (b) bottom of beam in the midspan section of FIU-4/5 and FIU-1/2	278
Figure 7.130: Load versus strain for ultimate strength testing with LC 2-1 for joint reinforcement extending from FIU-5 and FIU-2 for the (a) midspan and (b) south sections of the system.....	279

Figure 7.131: Crushing of FIU-5 and FIU-4 concrete at failure for Load Configuration 2-1: (a) overview and (b) crushing of UHPC in joint.....	280
Figure 7.132: FIU-1/2 and FIU4/5 joint edge cores: (a) location along length of cores taken, (b) cross section location, (c) Core #1, (d) Core #2, and (e) Core #3 with cracking highlighted	281
Figure 7.133: Load versus longitudinal concrete strain for ultimate strength testing with LC 2-1 for (a) top and (b) bottom of beam in the midspan section of FIU-4/5 and FIU-1/2.....	282
Figure 8.1: Testing phase III for full-scale FSB tests	285
Figure 8.2: Phase III (FIU-6, FIU-3, FIU-8, and FIU-7) service and strength test configurations	287
Figure 8.3: Phase III (FIU-6, FIU-3, FIU-8, and FIU-7) fatigue test configurations	288
Figure 8.4: Six-beam casting sequence for testing Phase II and Phase III	291
Figure 8.5: Construction of second set of beams: (a) FIU-8, FIU-7, and FIU-6 mild reinforcement and formwork construction, (b) concrete pour of first group of beams, (c) top strand layer de-tension, and (d) observed misalignment of mild reinforcement in second group of beams	291
Figure 8.6: FIU-3 differential camber (a) before and (b) after load block application.....	292
Figure 8.7: FIU-3 camber leveling: (a) load block weights in pounds and placement order (not to scale), (b) west view, and (c) south view.....	294
Figure 8.8: Preparation of UHPC joints: (a) superstructure preparation with load blocks, (b) joints with top strips formwork for over pour volume, and (c) plywood block-outs at joint ends with extended backer rods	295
Figure 8.9: UHPC mixing and placement procedure: (a) premix added to mixer, (b) initial UHPC casting in uncovered joint, (c) rodding procedure for two encountering pour heads, and (d) joints covered with top formwork and weights to finish joint cast.....	296
Figure 8.10: UHPC joint grinding procedure: (a) top formwork removal a day after cast, (b) joint grinding action with electric grinder, (c) joint finish after grinding, and (d) joint surface a day after grinding.....	297
Figure 8.11: UHPC flow test: (a) material pour, (b) mold removal, (c) setting period, and (d) spread measurement.....	299
Figure 8.12: Load blocks removal from FIU-3: (a) load block weights in pounds and removal order (not to scale), (b) block 3 removal, and (c) block 4 removal	300
Figure 8.13: Saw-cut procedure on FIU 6-3 joint: (a) saw cut alignment, (b) saw cut south view, and (c) saw cut north view	300
Figure 8.14: UHPC samples: (a) 4x4x14 in. steel molds for UHPC beams, (b) UHPC beams curing process, (c) 4x8 in. UHPC cylinder preparation and cast, and (d) cylinders for compressive strength.....	302

Figure 8.15: Camber readings from FIU-3, FIU-6, FIU-7, FIU-8 at release and at 447 days (before load blocks placement).....	304
Figure 8.16: FIU-3 joint reinforcement length observations at (a) precast yard and (b) structures lab.....	304
Figure 8.17: Beams sweep: (a) sweep direction and dimensions (not to scale), (b) middle joint region gap, and (c) end joint region gap	305
Figure 8.18: Covered leakage zones at (a) south support and (b) middle region	306
Figure 8.19: Joint construction issue: (a) side form misalignment with chamfered form and (b) bottom ledge geometry after side form removal.....	306
Figure 8.20: Crack patterns observed on (a) FIU-8, (b) FIU-7, and (c) FIU-6 top surfaces	307
Figure 8.21: Load blocks overlapping joint region (a) during UHPC cast, (b) during UHPC grinding, (c) after formwork removal, and (d) during blocks removal.....	308
Figure 8.22: Testing frame and support layout.....	309
Figure 8.23: (a) Bottom steel I-beams, (b) clearance display between specimen and sensors ...	309
Figure 8.24: HS-20 truck load with rear half-axle identification (from [82])	310
Figure 8.25: Load blocks used for surcharge protocol: (a) dimensions, (b) arrangement, and (c) supports	310
Figure 8.26: Test setup for Stiffness Configuration 4-1 through 4-4 (a) schematic and (b) plan and elevation view	311
Figure 8.27: Test setup for Camber Leveling 4-2: (a) schematic and (b) plan and elevation view	312
Figure 8.28: HS-20 truck load with full and half rear axle identification (from [82])	313
Figure 8.29: Test setup for Load Configuration 4-1 through 4-4 (a) schematic and (b) plan and elevation view	313
Figure 8.30: Test setup for Load Configuration 4-1cr through 4-4cr (a) schematic and (b) plan and elevation view	314
Figure 8.31: Test setup for Load Configuration 4-5 (a) schematic and (b) plan and elevation view	315
Figure 8.32: Test setup for Fatigue Configuration 4-6 (a) schematic, (b) plan and elevation view, and (c) reverse sinusoidal load protocol	316
Figure 8.33: Proposed test setup for Fatigue Configuration 4-7 (a) schematic, (b) plan and elevation view	317
Figure 8.34: Four-beam test with two main sensor regions.....	317
Figure 8.35: Instrumentation used for four-beam testing: (a) RSGs, (b) CSGs, (c) CDTs, (d) support LDTs, (e) bottom center LDTs, and (f) VWGs	318

Figure 8.36: (a) high precision altimeter, (b) VWA, and (c) DAQ	319
Figure 8.37: Four-beam stiffness and camber leveling testing instrumentation toward north support.....	320
Figure 8.38: Four-beam stiffness and camber leveling testing instrumentation at midspan	321
Figure 8.39: Four-beam stiffness and camber leveling testing instrumentation toward south support.....	322
Figure 8.40: Four-beam fatigue, service, and strength testing instrumentation at north support (top).....	323
Figure 8.41: Four-beam fatigue, service, and strength testing instrumentation at north support (bottom).....	324
Figure 8.42: Four-beam fatigue, service, and strength testing instrumentation at midspan	325
Figure 8.43: Four-beam fatigue, service, and strength testing instrumentation at south supports (top).....	326
Figure 8.44: Four-beam fatigue, service, and strength testing instrumentation at south supports (bottom).....	327
Figure 8.45: VWG locations at beam midspan: (a) cross section and (b) cut A-A at midspan..	328
Figure 8.46: VWG locations at beam end: (a) cross section and (b) cut A-A near beam end....	328
Figure 8.47: Morning camber readings of FIU specimens	329
Figure 8.48: Strain change over time measured using vibrating wire strain gauges for (a) FIU-3, (b) FIU-6, (c) FIU-7, and (d) FIU-8.....	330
Figure 8.49: Strain across cross-section height at release for (a) FIU-3, (b) FIU-6, (c) FIU-7, and (d) FIU-8.....	331
Figure 8.50: Strain across cross-section height at t = 100 days for (a) FIU-3, (b) FIU-6, (c) FIU-7, and (d) FIU-8	331
Figure 8.51: Strain across cross-section height at t = 525 days for (a) FIU-3, (b) FIU-6, (c) FIU-7, and (d) FIU-8	332
Figure 8.52: Curvature versus time (found using top and bottom strains) for FIU-3, FIU-6, FIU-7, and FIU-8.....	333
Figure 8.53: Determination of strain in prestressing strands with (a) VWG location in cross section and (b) strain profile across section depth	333
Figure 8.54: Prestress loss versus time for FIU-3, FIU-6, FIU-7, and FIU-8.....	334
Figure 8.55: Location of (a) actuators and (b) LDT sensors.....	335
Figure 8.56: Load versus displacement curves for load testing with Stiffness Configuration 4-1 through 4-4 (before joint cast)	337

Figure 8.57: Load versus longitudinal concrete strain load testing with Stiffness Configuration 4-1 through 4-4 (before joint cast)	337
Figure 8.58: Load blocks installation (weight in kips) versus time before joint construction on FIU-3.....	338
Figure 8.59: Load versus absolute center, north, and south displacements load testing with Camber Leveling (before joint cast) on FIU-3	339
Figure 8.60: Load versus longitudinal concrete strain load testing with Camber Leveling 4-2 (before joint cast) on FIU-3	339
Figure 8.61: Moment-curvature responses with and without long-term prestress losses for (a) FIU-3 and (b) FIU-6/7/8	341
Figure 8.62: Estimated strain profile without prestress losses at $M = 0$ kip-ft. for (a) FIU-3 and (b) FIU-6/7/8 from RESPONSE2000	342
Figure 8.63: Estimated strain profile for FIU-3 from RESPONSE2000 with and without long-term prestress losses for (a) release, (b) moment caused by surcharge load, and (c) difference between release and surcharge load state of strain	342
Figure 8.64: Load blocks removal (weight in kips) versus time after joint construction on FIU-3	343
Figure 8.65: Load versus average midspan deflection of each beam during removal of surcharge load (Stage 1.6).....	344
Figure 8.66: Load versus longitudinal strain during surcharge load removal for (a) top CSGs and (b) bottom CSGs, including estimated initial precompression strains.....	345
Figure 8.67: Load versus transverse strain on top of system at midspan measured using CSGs during removal of surcharge load (Stage 1.6).....	346
Figure 8.68: Load versus average strain across joint on top of system at midspan measured using CDTs during removal of surcharge load (Stage 1.6)	346
Figure 8.69: Load versus transverse strain on bottom of system at midspan measured using CSGs during removal of surcharge load (Stage 1.6).....	347
Figure 8.70: Summary of testing stages performed on four-beam setup with FIU-6/3/8/7.....	347
Figure 8.71: Load versus longitudinal strain measured using CSGs on bottom of system at midspan for Stage 2 and (a) LC 4-1, (b) LC 4-2, (c) LC 4-3, and (d) LC 4-4	349
Figure 8.72: Load versus deflection during Stage 2 for (a) LC 4-1, (b) LC 4-2, (c) LC 4-3, and (d) LC 4-4	353
Figure 8.73: Measured girder distribution factors for Stage 2 loading.....	354
Figure 8.74: Load versus longitudinal concrete strain on bottom of system at midspan measured using CSGs for Stage 2 (a) LC 4-1, (b) LC 4-2, (c) LC 4-3, and (d) LC 4-4	355

Figure 8.75: Load versus transverse concrete strain on top of system at midspan measured using CSGs for Stage 2 (a) LC 4-1, (b) LC 4-2, (c) LC 4-3, and (d) LC 4-4.....	357
Figure 8.76: Load versus average transverse strain across top of joint at midspan measured using CDTs for Stage 2 (a) LC 4-1, (b) LC 4-2, (c) LC 4-3, and (d) LC 4-4.....	358
Figure 8.77: Load versus transverse concrete strain on bottom of system at midspan measured using CSGs for Stage 2 (a) LC 4-1, (b) LC 4-2, (c) LC 4-3, and (d) LC 4-4	359
Figure 8.78: Load versus transverse concrete strain on top of system along length of FIU-3 measured using CSGs for Stage 2 LC 4-1, LC 4-2, LC 4-3, and LC 4-4	360
Figure 8.79: Load versus strain for joint reinforcement in Joint 6-3 and Joint 3-8 near midspan for Stage 2 LC 4-1.....	361
Figure 8.80: Load versus midspan displacement for permit load testing Stages 2, 5, and 8 with LC 4-1 through LC 4-4 (Stage 5 LC 4-2 was skipped).....	362
Figure 8.81: Normalized stiffnesses at midspan for system: (a) west side, (b) east side, and (c) average midspan response.....	363
Figure 8.82: Girder distribution factors (GDFi) for LC 4-1, LC 4-2, LC 4-3, and LC 4-4 on Stages 2 through 8 (Stage 5 LC 4-2 was skipped).....	364
Figure 8.83: Load versus bottom longitudinal concrete strain for permit load testing for Stage 2 (a) LC 4-1 and (b) LC 4-4; Stage 5 (c) LC 4-1 and (b) LC 4-4; and Stage 8 (e) LC 4-1 and (f) LC 4-4 (B15 malfunctioned in Stage 8).....	365
Figure 8.84: Load versus bottom longitudinal concrete strain for service load testing for Stage 2 (a) LC 4-2 and (b) LC 4-3; Stage 5 (c) LC 4-3; and Stage 8 (e) LC 4-2 and (f) LC 4-3	366
Figure 8.85: Bottom strain change of longitudinal CSGs per change in load versus number of cycles at center of specimen for FC 4-6 and FC 4-7.....	367
Figure 8.86: Load versus top transverse concrete strain for service load testing for LC 4-1 for (a) Stage 2 CSGs, (b) Stage 2 CDTs, (c) Stage 5 CSGs, (d) Stage 5 CDTs, (e) Stage 8 CSGs, and (f) Stage 8 CDTs	368
Figure 8.87: Load versus bottom transverse concrete strain for service load testing for LC 4-1 for (a) Stage 2 CSGs, (b) Stage 2 CDTs, (c) Stage 5 CSGs, (d) Stage 5 CDTs, (e) Stage 8 CSGs, and (f) Stage 8 CDTs	369
Figure 8.88: Load versus center west rebar strain for service load testing with LC 4-1 for Stage 2, Stage 5, and Stage 8	370
Figure 8.89: Load versus top transverse concrete strain for service load testing for LC 4-3 for (a) Stage 2 CSGs, (b) Stage 2 CDTs, (c) Stage 5 CSGs, (d) Stage 5 CDTs, (e) Stage 8 CSGs, and (f) Stage 8 CDTs	371
Figure 8.90: Load versus bottom transverse concrete strain for service load testing for LC 4-3 for (a) Stage 2 CSGs, (b) Stage 2 CDTs, (c) Stage 5 CSGs, (d) Stage 5 CDTs, (e) Stage 8 CSGs, and (f) Stage 8 CDTs	372

Figure 8.91: Load versus center west rebar strain for service load testing with LC 4-3 for Stage 2, Stage 5, and Stage 8.....	373
Figure 8.92: Top strain change of transverse CSGs and CDTs per change in load versus number of cycles at center of specimen across: (a) Joint 6-3, (b) Joint 3-8, and (c) Joint 8-7	374
Figure 8.93: Bottom strain change of transverse CSGs and CDTs per change in load versus number of cycles at center of specimen across: (a) Joint 6-3, (b) Joint 3-8, and (c) Joint 8-7 ...	375
Figure 8.94: Rebar strain change per change in load versus number of cycles at center west of Joint 6-3, Joint 3-8, and Joint 8-7	376
Figure 8.95: Rebar strain change per change in load versus number of cycles at west of joints south ends for Joint 6-3, Joint 3-8, and Joint 8-7.....	376
Figure 8.96: Load versus midspan displacement for service load testing Stage 8 LC 4-1 through LC 4-4 and Stage 9 LC 4-1cr through LC 4-4cr.....	378
Figure 8.97: Girder Distribution Factors (GDF) for LC 4-1, LC 4-2, LC 4-3, and LC 4-4 on Stages 8 and 9	379
Figure 8.98: Load versus bottom longitudinal concrete strain for service load testing with LC 4-1 and LC 4-4 for (a) Stage 8 and (b) Stage 9 (LC 4-4 B15 malfunctioned in Stage 8)	380
Figure 8.99: Bottom longitudinal behavior when interior beams are loaded for LC 4-2: (a) Stage 8 and (b) Stage 9; and for LC 4-3: (c) Stage 8 and (d) Stage 9	381
Figure 8.100: Load versus top transverse concrete strain for service load testing comparison between CSGs in Stage 8 (a) LC 4-1 and Stage 9 (b) LC 4-1cr, and CDTs in Stage 8 (c) LC 4-1 and Stage 9 (d) LC 4-1cr.....	382
Figure 8.101: Load versus bottom transverse concrete strain for service load testing comparison between CSGs in Stage 8 (a) LC 4-1 and Stage 9 (b) LC 4-1cr, and CDTs in Stage 8 (c) LC 4-1 and Stage 9 (d) LC 4-1cr.....	383
Figure 8.102: Load versus center west rebar strain for service load testing with LC 4-1 for Stage 8 and LC 4-1cr with Stage 9	384
Figure 8.103: Load versus top transverse concrete strain for service load testing comparison between CSGs in Stage 8 (a) LC 4-3 and Stage 9 (b) LC 4-3cr, and CDTs in Stage 8 (c) LC 4-3 and Stage 9 (d) LC 4-3cr.....	385
Figure 8.104: Load versus bottom transverse concrete strain for service load testing comparison between CSGs in Stage 8 (a) LC 4-3 and Stage 9 (b) LC 4-3cr, and CDTs in Stage 8 (c) LC 4-3 and Stage 9 (d) LC 4-3cr (CSG B11 malfunctioned on Stage 8).....	386
Figure 8.105: Load versus center west rebar strain for permit testing with LC 4-3 for Stage 8 and LC 4-3cr with Stage 9.....	387
Figure 8.106: Load versus average midspan deflection for ultimate strength testing with LC 4-5	388

Figure 8.107: Bottom crack pattern at midspan for ultimate strength testing with LC 4-5 for FIU-6/3/8/7 for: (a) Steps 1 through 4 and (b) Step 5	390
Figure 8.108: Photographs from failure (331.4 kips) at (a) first crushing in FIU-7 and (b) crushing of concrete continuing across the width of the superstructure	390
Figure 8.109: Additional photographs after failure of the four-beam system: (a) overview from the north-east, (b) overview from the south-west, (c) FIU-6 at midspan, (d) top of FIU-8 and FIU-3 at midspan, and (e) FIU-7 at midspan.....	391
Figure 8.110: Load versus longitudinal concrete strain for ultimate strength testing with LC 4-5 for (a) top and (b) bottom of beams in the midspan section of FIU-6/3/8/7.....	392
Figure 8.111: Load versus average strain across top of joints for ultimate strength testing with LC 4-5 for FIU-6/3/8/7	394
Figure 8.112: Load versus average strain across top of joints for ultimate strength testing with LC 4-5 for FIU-6/3/8/7	395
Figure 8.113: Load versus transverse concrete strain for ultimate strength testing with LC 4-5 for (a) top and (b) bottom of beams in the midspan section of FIU-6/3/8/7 (B11 and B19 malfunctioned)	396
Figure 8.114: Load versus strain for ultimate strength testing with LC 4-5 for west reinforcement of FIU 6-3, FIU 3-8, and FIU 8-7 joints at midspan section of the system	397
Figure 8.115: Crushing of FIU-6/3/8/7 concrete at failure for LC 4-5: (a) overview and (b) crushing of precast section and UHPC joint (FIU 6-3).....	398
Figure 8.116: South, center, and north core locations on: (a) Joint 6-3, (b) Joint 3-8, and (c) Joint 8-7	398
Figure 8.117: FIU-6/3/8/7 joints edge cores locations and crack patterns: (a) Joint 6-3, (b) Joint 3-8, and (c) Joint 8-7 cores	399
Figure 9.1: Moment diagram and maximum deflections for two-span structures that are: (a) simply-supported and (b) continuous.....	402
Figure 9.2: Construction sequence for SDCL bridge system [95] (modified from Freyermuth [93]).....	404
Figure 9.3: Moments distribution during construction sequence (PCI Bridge Design Manual [45], 2011)	405
Figure 9.4: Moment diagram for multi-span structures being simply supported (black) and continuous (red)	405
Figure 9.5: Traditional SDCL joint detail between adjacent spans	406
Figure 9.6: Four different slab-diaphragm-bent cap configurations used in field (adapted from [96]).....	406
Figure 9.7: Diaphragm reinforcement location (Adapted from PCINER, 1998 [103]).....	412

Figure 9.8: Example continuity connection at pier for precast quad tee section without CIP deck from Robert Moses Causeway Bridge Rehabilitation over Great South Bay [104]	414
Figure 9.9: Example continuity connection at pier for precast inverted-tee beams with CIP deck from Bridge 13004, TH 8 over Center Lake Channel (MN) [104].....	414
Figure 9.10: Example continuity connection at pier for precast box beam without CIP deck from Unquowa Road (CT) [104]	415
Figure 9.11: (a) Sample test setup for Specimen 2 and test results for (b) Specimen 2, (c) Specimen 1, and (d) Specimen 3 from Noppakunwijai et al. [106].....	416
Figure 9.12: (a) Test specimen and (b) summary of results from Graybeal [110]	418
Figure 9.13: (a) Joint details and (b) crack pattern for 30-inch splice at $0.8P_u$ load from Maya and Graybeal [109]	418
Figure 9.14: Details of SDCL connection with UHPC and GFRP by Perry et al. [101].....	419
Figure 9.15: Details for SDCL connection with UHPC between I-beams by Floyd et al. [111]	419
Figure 9.16: Detail for column-to-cap beam and superstructure-to-cap beam connections from Benjumea et al. [113].....	420
Figure 9.17: Positive moment restraint connection details (adapted from Freyermuth [93]).....	421
Figure 9.18: Strand splice devices for continuity (adapted from Tadros et al. [99]).....	422
Figure 9.19: High-strength threaded rod for deck weight continuity (adapted from Ma et al. [100]). Note: units in inches.....	423
Figure 9.20: Lap spliced rebar (or strand) for diaphragm continuity with UHPC joint fill (adapted from Perry et al. [101])	423
Figure 9.21: Previously observed field issues with SDCL connections in prestressed members	424
Figure 9.22: Typical FSB detail at intermediate bents or piers (Adapted from FDOT [19])	425
Figure 9.23: Modified FSB detail without CIP deck at intermediate bents or piers.....	425
Figure 9.24: Splicing of hooked prestressing strands for positive moment reinforcement (based on Floyd et al. [111] and Noppakunwijai et al. [106]).....	426
Figure 9.25: Splicing of high-strength rebar for positive moment reinforcement (based on Floyd et al. [111]).....	427
Figure 9.26: Lap-spliced high-yield rebar for continuity (based on Perry et al., [101]).....	428
Figure 9.27: Non-contact and lap-spliced high-yield rebar for continuity (adapted from Perry et al., [101]).....	428
Figure 9.28: Lap-spliced, hooked strands for continuity (adapted from Freyermuth [93]).....	429
Figure 9.29: Load schematics for (a) Bridge 1 and (b) Bridge 2.....	431

Figure 9.30: Summation of Strength I Moment envelopes for continuous FSB system diaphragm	432
Figure 9.31: Preliminary location of the mild reinforcement for the positive moment design ..	434
Figure 9.32: Additional detailing check for embedment of reinforcement into the girder, based on Miller et al. [98]	437
Figure 9.33: Positive moment connection with 8 #6 mild reinforcement: (a) elevation and (b) ends view	437
Figure 9.34: Required UHPC diaphragm width for straight, non-prestressed strand splice for positive moment reinforcement	438
Figure 9.35: Non-prestressed strand hook details at ends of FSB	438
Figure 9.36: Positive moment connection with non-prestressed bent strands: (a) elevation and (b) ends view	440
Figure 9.37: Preliminary location of high-strength rebar for the negative moment design.....	441
Figure 9.38: Negative moment connection with high-yield reinforcement and non-prestressed hooked strands: (a) elevation and (b) ends view.....	443
Figure 9.39: Diaphragm connection detail for 12-in. thick FSB system: (a) section through diaphragm connection and (b) FSB end region reinforcement detail. Note: units in inches	444
Figure 9.40: Minimum and maximum moments for Strength I for (a) 15-inch-deep FSB with 44-foot spans and (b) 18-inch-deep FSB with 55-foot spans.....	446
Figure 9.41: Load configuration based on (a) FL120 rear axle [124] load and (b) HS20 rear axle wheel patch geometry [82].....	448
Figure 9.42: Two-span bridge model (not to scale): (a) spans length and (b) half span model restraining rotation at midspan.....	449
Figure 9.43: Two-beam and longitudinal joint with diaphragm layout (not to scale): (a) longitudinal joint and negative diaphragm reinforcement, and (b) section cuts with reinforcement distribution at load points (A-A), supports (B-B), and diaphragm (C-C).....	449
Figure 9.44: Load per patch versus deflection response for: (a) north span and (b) south span	452
Figure 9.45: Maximum principal stress maps for (a) FSBs and (b) UHPC materials	453
Figure 9.46: Maximum principal stress maps at cuts made at (a) FSB-to-diaphragm boundary and (b) center diaphragm region.....	454
Figure 9.47: Maximum principal stress maps at (a) joint reinforcement near diaphragm region and (b) diaphragm negative reinforcement	455
Figure 10.1: Proposed joint geometry based on small-scale joint testing and two-beam system tests	457

Figure 10.2: Proposed SDCL connection for modified FSB system: (a) section through diaphragm connection and (b) FSB end region reinforcement detail. Note: units in inches	458
Figure C.1: Simply supported beam with uniform load partially distributed	530
Figure C.2: Estimated load-deflection response for control specimen	531
Figure C.3: (a) Specimen testing layout. (b) Top expected cracking pattern before failure and (c) bottom expected cracking pattern before failure for Control.....	531
Figure C.4: Estimated load-deflection response for 18F1 specimen	533
Figure C.5: (a) Specimen testing layout. (b) Top expected cracking pattern before failure and (c) bottom expected cracking pattern before failure for 18F1.....	534
Figure C.6: Estimated load-deflection response for 18F2 specimen	535
Figure C.7: (a) Specimen testing layout. (b) Top expected cracking pattern before failure and (c) bottom expected cracking pattern before failure for 18F2.....	536
Figure C.8: Estimated load-deflection response for 18A1 specimen	537
Figure C.9: (a) Specimen testing layout. (b) Top expected cracking pattern before failure and (c) bottom expected cracking pattern before failure for 18A1	538
Figure C.10: Estimated load-deflection response for 12F1 specimen	539
Figure C.11: (a) Specimen testing layout. (b) Top expected cracking pattern before failure and (c) bottom expected cracking pattern before failure for 12F1	540
Figure C.12: Estimated load-deflection response for 12F2 specimen	541
Figure C.13: (a) Specimen testing layout. (b) Top expected cracking pattern before failure and (c) bottom expected cracking pattern before failure for 12F2	542
Figure C.14: Estimated load-deflection response for 12A1 specimen	543
Figure C.15: (a) Specimen testing layout. (b) Top expected cracking pattern before failure and (c) bottom expected cracking pattern before failure for 12A1	544
Figure C.16: Estimated load-deflection response for 12A2 specimen	545
Figure C.17: (a) specimen testing layout, (b) top expected cracking pattern before failure, and (c) bottom expected cracking pattern before failure for 12A2.....	546
Figure D.1: Instrumentation labels for gauges.....	549
Figure D.2: FSB-1: (a) transverse joint reinforcement, (b) full joint and deck reinforcement before casting, (c) side view of failure, and (d) top view of failure	551
Figure D.3: (a) Unloaded side of control specimen after failure, (b) Concrete rupture inside caged matrix, (c) Longitudinal rebar bend, and (d) Bond loss of CIP deck.....	552
Figure D.4: FSB-1 response: (a) load versus rebar strain on south side, (b) load versus rebar strain on north side, and (c) load versus central bottom opening	554

Figure D.5: FSB-1 response: (a) load versus bottom concrete strain, (b) cracking load determination based on load versus bottom concrete strain response, and (c) load versus top concrete strain	555
Figure D.6: FSB-2: (a) crack pattern in CIP deck concrete failure, (b) greater crack pattern in CIP deck concrete failure, (c) CIP deck concrete cylinder failure, and (d) exposed joint reinforcement after failure.....	556
Figure D.7: FSB-2 response: (a) load versus rebar strain on south side, (b) load versus rebar strain on north side, and (c) load versus central bottom opening	557
Figure D.8: FSB-2 response: (a) load versus bottom concrete strain, (b) cracking load determination based on load versus bottom concrete strain response, and (c) load versus top concrete strain	558
Figure D.9: 18F1-1: (a) failed specimen and (b) close-up of hinge developing in top corner of precast member next to UHPC joint.....	559
Figure D.10: 18F1-1: (a) south beam with UHPC matrix, (b) poor bond due to unaffected UHPC matrix on south beam, (c) north beam with dent at the top, and (d) poor UHPC bond at the rebar level in north beam.....	560
Figure D.11: 18F1-1 response: (a) load versus rebar strain on north side, (b) load versus rebar strain on south side, and (c) load versus central bottom opening	561
Figure D.12: 18F1-1 response: (a) Load versus bottom concrete strain, (b) cracking load determination based on load versus bottom concrete strain response, and (c) load versus top concrete strain	562
Figure D.13: 18F1-2: (a) fractured joint specimen from west side and (b) bottom view of joint failure from west side.....	563
Figure D.14: 18F1-2 after failure (a) failed south beam from the east side, (b) side of failed joint in south beam, (c) failed north beam, and (d) imprints in failed joint of shear reinforcement from precast section.....	564
Figure D.15: 18F1-2 response: (a) load versus rebar strain on north side, (b) load versus rebar strain on south side, and (c) load versus central bottom opening	565
Figure D.16: 18F1-2 response: (a) load versus bottom concrete strain, (b) cracking load determination based on load versus bottom concrete strain response, and (c) load versus top concrete strain	566
Figure D.17: 18F2-1: (a) failed specimen and (b) possible stress concentration pattern at the top on east side.....	567
Figure D.18: 18F2-1: (a) south beam with unbonded and bonded UHPC matrix, (b) unbonded UHPC matrix showing shrinkage cracks in south beam, (c) north beam showing precast concrete failure, and (d) failed reinforcement in north beam.....	568

Figure D.19: 18F2-1 response: (a) load versus rebar strain on north side, (b) load versus rebar strain on south side, and (c) load versus central bottom opening	569
Figure D.20: 18F2-1 response: (a) load versus bottom concrete strain, (b) cracking load determination based on load versus bottom concrete strain response, and (c) load versus top concrete strain	570
Figure D.21: 18F2-2: (a) possible tension and compression zones and (b) possible compressive stress concentration at the top in west side view	571
Figure D.22: 18F2-2: (a) UHPC matrix from south beam showing better bond and possible linear strain distribution, (b) UHPC matrix from south beam showing better UHPC-to-beam bond, (c) cover spalled from north beam and top dent, and (d) exposed shear reinforcement due to concrete cover removal on north beam	572
Figure D.23: 12F2-2 response: (a) load versus rebar strain on north side, (b) load versus rebar strain on south side, and (c) load versus central bottom opening	573
Figure D.24: 12F2-2 response: (a) load versus bottom concrete strain, (b) cracking load determination based on load versus bottom concrete strain response, and (c) load versus top concrete strain	574
Figure D.25: 18A1-1: (a) failed specimen with complete UHPC matrix detachment, (b) Failure of top lip due to compressive stress concentration from west side.....	575
Figure D.26: 18A1-1: (a) UHPC matrix with lack of bond in south beam, (b) poor bond shown at the top UHPC matrix in south beam, (c) development and fracture of transverse rebar in north beam, and (d) top ledge failure due to high compressive stress accumulation in north beam....	576
Figure D.27: 18A1-1 response: (a) load versus rebar strain on north side, (b) load versus rebar strain on south side, and (c) load versus central bottom opening	577
Figure D.28: 18A1-1 response: (a) load versus bottom concrete strain, (b) cracking load determination based on load versus bottom concrete strain response, and (c) load versus top concrete strain	578
Figure D.29: 18A1-2: (a) failed specimen with probable force distribution and (b) spalling of top lip due to potential shear plane.	579
Figure D.30: 18A1-2 response: (a) load versus rebar strain on north side, (b) load versus rebar strain on south side, and (c) load versus central bottom opening	580
Figure D.31: 18A1-2 response: (a) load versus bottom concrete strain, (b) cracking load determination based on load versus bottom concrete strain response, and (c) load versus top concrete strain	581
Figure D.32: Typical failure in 12-inch-deep specimens with diagonal crack through joint: (a) cracking at failure and (b) after failure	582
Figure D.33: Typical failure in 12-inch-deep specimens with cracking along joint face and at level of reinforcement: (a) cracking at failure and (b) after failure	583

Figure D.34: 12F1-1: (a) failed joint specimen and (b) bottom lip failure	584
Figure D.35: 12F1-1 response: (a) load versus rebar strain on south side, (b) load versus rebar strain on north side, and (c) load versus central bottom opening	585
Figure D.36: 12F1-1 response: (a) load versus bottom concrete strain, (b) cracking load determination based on load versus bottom concrete strain response, and (c) load versus top concrete strain	586
Figure D.37: 12F1-2: (a) failed joint specimen after overload performance, (b) continuous failure line along the UHPC-to-precast boundary, (c) pull-out cone shapes observed in UHPC matrix, and (d) cavity left by UHPC cover detachment	587
Figure D.38: 12F1-2 response: (a) load versus rebar strain on south side, (b) load versus rebar strain on north side, and (c) load versus central bottom opening	588
Figure D.39: Load versus bottom concrete strain response for 12F1-2 response.....	589
Figure D.40: 12F2-1: (a) failed specimen with similar failure cracks to 18F2 and (b) east side failed specimen	590
Figure D.41: 12F2-1 response: (a) load versus rebar strain on south side, (b) load versus rebar strain on north side, and (c) load versus central bottom opening	591
Figure D.42: 12F2-1 response: (a) load versus bottom concrete strain, (b) cracking load determination based on load versus bottom concrete strain response, and (c) load versus top concrete strain	592
Figure D.43: 12F2-2: (a) failed beam – west side, (b) failed joint – east side, (c) concrete failure at the cover region, and (d) extension of concrete crack (load application point shown)	593
Figure D.44: 12F2-2 response: (a) load versus rebar strain on north side, (b) load versus rebar strain on south side, and (c) load versus central bottom opening	594
Figure D.45: 12F2-2 response: (a) load versus bottom concrete strain, and (b) cracking load determination based on load versus bottom concrete strain response	595
Figure D.46: 12A1-1: (a) failure cracks and (b) diagonal crack in UHPC matrix.....	596
Figure D.47: 12A1-1 response: (a) load versus rebar strain on south side, (b) load versus rebar strain on north side, and (c) load versus central bottom opening	598
Figure D.48: 12A1-1 response: (a) Load versus bottom concrete strain, (b) cracking load determination based on load versus bottom concrete strain response, and (c) load versus top concrete strain	599
Figure D.49: 12A1-2: (a) failed specimen with hinge location highlighted, (b) longitudinal cracks observed on top of the specimen, (c) transverse crack at level of reinforcement in precast section, and (d) cracks extending into beam from joint	600
Figure D.50: 12A1-2 response: (a) load versus rebar strain on south side, (b) load versus rebar strain on north side, and (c) load versus central bottom opening	601

Figure D.51: Load versus bottom concrete strain for 12A1-2	602
Figure D.52: 12A2-1: (a) failed specimen and (b) east side joint face showing similar rupture pattern with less amount of cracks.....	604
Figure D.53: 12A2-1 response: (a) load versus rebar strain on south side, (b) load versus rebar strain on north side, and (c) load versus central bottom opening	605
Figure D.54: 12A2-1 response: (a) load versus bottom concrete strain, and (b) cracking load determination based on load versus bottom concrete strain response	606
Figure D.55: 12A2-2: (a) west side failed specimen and (b) east side joint face showing similar rupture pattern with more amount of cracks	607
Figure D.56: 12A2-2 response (a) load versus rebar strain on south side, (b) load versus rebar strain on north side, and (c) load versus central bottom opening	608
Figure D.57: 12A2-2 response: load versus bottom concrete strain (CSG 1 to 3 malfunctioned)	609
Figure E.1: Instrumentation labels for gauges on the specimens.....	611
Figure E.2: Joint details for joint 12F1	612
Figure E.3: Normalized cycle stiffness for 12F1-2.....	613
Figure E.4: High reinforcement strain over force for each cycle for 12F1-2 (1 of 2)	614
Figure E.5: High reinforcement strain over force for each cycle for 12F1-2 (2 of 2)	615
Figure E.6: Reinforcement strain change over force change for each cycle for 12F1-2 (1 of 2)	616
Figure E.7: Reinforcement strain change over force change for each cycle for 12F1-2 (2 of 2)	617
Figure E.8: High concrete strain over force for each cycle for 12F1-2	618
Figure E.9: Concrete strain change over force change for each cycle for 12F1-2.....	619
Figure E.10: Crack gage results for each cycle for 12F1-2	620
Figure E.11: Load versus displacement plot for strength testing of 12F1 (a) without any fatigue load applied, 12F1-1, and (b) after fatigue loading, 12F1-2.....	621
Figure E.12: Joint details for joint 12A1	622
Figure E.13: Normalized cycle stiffness for 12A1-2	623
Figure E.14: High reinforcement strain over force for each cycle for 12A1-2 (1 of 2).....	624
Figure E.15: High reinforcement strain over force for each cycle for 12A1-2 (2 of 2).....	625
Figure E.16: Reinforcement strain change over force change for each cycle for 12A1-2 (1 of 2)	626

Figure E.17: Reinforcement strain change over force change for each cycle for 12A1-2 (2 of 2)	627
Figure E.18: High concrete strain over force for each cycle for 12A1-2	628
Figure E.19: Concrete strain change over force change for each cycle for 12A1-2	629
Figure E.20: Crack gage results for each cycle for 12A1-2	630
Figure E.21: Load versus displacement plot for strength testing of 12A1 (a) without any fatigue load applied, 12A1-1, and (b) after fatigue loading, 12A1-2	631
Figure E.22: Joint details for joint 12A2	632
Figure E.23: Normalized cycle stiffness for 12A2-2	633
Figure E.24: High reinforcement strain over force for each cycle for 12A2-2 (1 of 2)	634
Figure E.25: High reinforcement strain over force for each cycle for 12A2-2 (2 of 2)	635
Figure E.26: Reinforcement strain change over force change for each cycle for 12A2-2 (1 of 2)	636
Figure E.27: Reinforcement strain change over force change for each cycle for 12A2-2 (2 of 2)	637
Figure E.28: High concrete strain over force for each cycle for 12A2-2	638
Figure E.29: Concrete strain change over force change for each cycle for 12A2-2	639
Figure E.30: Crack gage results for each cycle for 12A2-2	640
Figure E.31: Load versus displacement plot for strength testing of 12A2 (a) without any fatigue load applied, 12A2-1, and (b) after fatigue loading, 12A2-2	641
Figure F.1: Load versus displacement measured using LDTs for Load Stage 1.6 (surcharge removal)	654
Figure F.2: Load versus longitudinal strain (measured by CSGs) for Load Stage 1.6 (surcharge removal)	655
Figure F.3: Load versus transverse strain (measured by CSGs) for Load Stage 1.6 (surcharge removal)	656
Figure F.4: Load versus average strain across the joints (measured by CDTs) for Load Stage 1.6 (surcharge removal)	657
Figure F.5: Load versus rebar strain (measured by RSGs) for Load Stage 1.6 (surcharge removal)	658
Figure F.6: Load versus rebar strain (measured by RSGs) for Load Stage 1.6 (surcharge removal) (cont.)	659
Figure F.7: Load versus displacement measured using LDTs for Load Stage 2, LC 4-1	660
Figure F.8: Load versus longitudinal strain (measured by CSGs) for Load Stage 2, LC 4-1	661

Figure F.9: Load versus transverse strain (measured by CSGs) for Load Stage 2, LC 4-1.....	662
Figure F.10: Load versus average strain across the joints (measured by CDTs) for Load Stage 2, LC 4-1	663
Figure F.11: Load versus rebar strain (measured by RSGs) for Load Stage 2, LC 4-1.....	664
Figure F.12: Load versus rebar strain (measured by RSGs) for Load Stage 2, LC 4-1 (cont.) ..	665
Figure F.13: Load versus displacement measured using LDTs for Load Stage 2, LC 4-2.....	666
Figure F.14: Load versus longitudinal strain (measured by CSGs) for Load Stage 2, LC 4-2...	667
Figure F.15: Load versus transverse strain (measured by CSGs) for Load Stage 2, LC 4-2.....	668
Figure F.16: Load versus average strain across the joints (measured by CDTs) for Load Stage 2, LC 4-2	669
Figure F.17: Load versus rebar strain (measured by RSGs) for Load Stage 2, LC 4-2.....	670
Figure F.18: Load versus rebar strain (measured by RSGs) for Load Stage 2, LC 4-2 (cont.) ..	671
Figure F.19: Load versus displacement measured using LDTs for Load Stage 2, LC 4-3.....	672
Figure F.20: Load versus longitudinal strain (measured by CSGs) for Load Stage 2, LC 4-3...	673
Figure F.21: Load versus transverse strain (measured by CSGs) for Load Stage 2, LC 4-3.....	674
Figure F.22: Load versus average strain across the joints (measured by CDTs) for Load Stage 2, LC 4-3	675
Figure F.23: Load versus rebar strain (measured by RSGs) for Load Stage 2, LC 4-3.....	676
Figure F.24: Load versus rebar strain (measured by RSGs) for Load Stage 2, LC 4-3 (cont.) ..	677
Figure F.25: Load versus displacement measured using LDTs for Load Stage 2, LC 4-4.....	678
Figure F.26: Load versus longitudinal strain (measured by CSGs) for Load Stage 2, LC 4-4...	679
Figure F.27: Load versus transverse strain (measured by CSGs) for Load Stage 2, LC 4-4.....	680
Figure F.28: Load versus average strain across the joints (measured by CDTs) for Load Stage 2, LC 4-4	681
Figure F.29: Load versus rebar strain (measured by RSGs) for Load Stage 2, LC 4-4.....	682
Figure F.30: Load versus rebar strain (measured by RSGs) for Load Stage 2, LC 4-4 (cont.) ..	683
Figure F.31: Load versus displacement measured using LDTs for Load Stage 5, LC 4-1.....	685
Figure F.32: Load versus longitudinal strain (measured by CSGs) for Load Stage 5, LC 4-1...	686
Figure F.33: Load versus transverse strain (measured by CSGs) for Load Stage 5, LC 4-1.....	687
Figure F.34: Load versus average strain across the joints (measured by CDTs) for Load Stage 5, LC 4-1	688
Figure F.35: Load versus rebar strain (measured by RSGs) for Load Stage 5, LC 4-1.....	689

Figure F.36: Load versus rebar strain (measured by RSGs) for Load Stage 5, LC 4-1 (cont.) ..	690
Figure F.37: Load versus displacement measured using LDTs for Load Stage 5, LC 4-3.....	691
Figure F.38: Load versus longitudinal strain (measured by CSGs) for Load Stage 5, LC 4-3...	692
Figure F.39: Load versus transverse strain (measured by CSGs) for Load Stage 5, LC 4-3.....	693
Figure F.40: Load versus average strain across the joints (measured by CDTs) for Load Stage 5, LC 4-3	694
Figure F.41: Load versus rebar strain (measured by RSGs) for Load Stage 5, LC 4-3.....	695
Figure F.42: Load versus rebar strain (measured by RSGs) for Load Stage 5, LC 4-3 (cont.) ..	696
Figure F.43: Load versus displacement measured using LDTs for Load Stage 5, LC 4-4.....	697
Figure F.44: Load versus longitudinal strain (measured by CSGs) for Load Stage 5, LC 4-4...	698
Figure F.45: Load versus transverse strain (measured by CSGs) for Load Stage 5, LC 4-4.....	699
Figure F.46: Load versus average strain across the joints (measured by CDTs) for Load Stage 5, LC 4-4	700
Figure F.47: Load versus rebar strain (measured by RSGs) for Load Stage 5, LC 4-4.....	701
Figure F.48: Load versus rebar strain (measured by RSGs) for Load Stage 5, LC 4-4 (cont.) ..	702
Figure F.49: Normalized Stiffness at midspan for west and east actuators and average system response for FC 4-6 and FC 4-7.....	703
Figure F.50: Top concrete strain change per change in load versus number of cycles	704
Figure F.51: Top concrete strain change per change in load versus number of cycles (cont.)...	705
Figure F.52: Bottom concrete strain change per change in load versus number of cycles.....	706
Figure F.53: Bottom concrete strain change per change in load versus number of cycles (cont.)	707
Figure F.54: Top crack gage strain change per change in load versus number of cycles.....	708
Figure F.55: Bottom crack gage strain change per change in load versus number of cycles	708
Figure F.56: Rebar strain change per change in load versus number of cycles for Joint 6-3 reinforcement	709
Figure F.57: Rebar strain change per change in load versus number of cycles for Joint 3-8 reinforcement	710
Figure F.58: Rebar strain change per change in load versus number of cycles for Joint 8-7 reinforcement (RSG-49, RSG-55, and RSG-56 malfunctioned)	711
Figure F.59: Load versus displacement measured using LDTs for Load Stage 8, LC 4-1.....	712
Figure F.60: Load versus longitudinal strain (measured by CSGs) for Load Stage 8, LC 4-1...	713
Figure F.61: Load versus transverse strain (measured by CSGs) for Load Stage 8, LC 4-1.....	714

Figure F.62: Load versus average strain across the joints (measured by CDTs) for Load Stage 8, LC 4-1	715
Figure F.63: Load versus rebar strain (measured by RSGs) for Load Stage 8, LC 4-1	716
Figure F.64: Load versus rebar strain (measured by RSGs) for Load Stage 8, LC 4-1 (cont.) ..	717
Figure F.65: Load versus displacement measured using LDTs for Load Stage 8, LC 4-2.....	718
Figure F.66: Load versus longitudinal strain (measured by CSGs) for Load Stage 8, LC 4-2...	719
Figure F.67: Load versus transverse strain (measured by CSGs) for Load Stage 8, LC 4-2.....	720
Figure F.68: Load versus average strain across the joints (measured by CDTs) for Load Stage 8, LC 4-2	721
Figure F.69: Load versus rebar strain (measured by RSGs) for Load Stage 8, LC 4-2.....	722
Figure F.70: Load versus rebar strain (measured by RSGs) for Load Stage 8, LC 4-2 (cont.) ..	723
Figure F.71: Load versus displacement measured using LDTs for Load Stage 8, LC 4-3.....	724
Figure F.72: Load versus longitudinal strain (measured by CSGs) for Load Stage 8, LC 4-3...	725
Figure F.73: Load versus transverse strain (measured by CSGs) for Load Stage 8, LC 4-3.....	726
Figure F.74: Load versus average strain across the joints (measured by CDTs) for Load Stage 8, LC 4-3	727
Figure F.75: Load versus rebar strain (measured by RSGs) for Load Stage 8, LC 4-3.....	728
Figure F.76: Load versus rebar strain (measured by RSGs) for Load Stage 8, LC 4-3 (cont.) ..	729
Figure F.77: Load versus displacement measured using LDTs for Load Stage 8, LC 4-4.....	730
Figure F.78: Load versus longitudinal strain (measured by CSGs) for Load Stage 8, LC 4-4...	731
Figure F.79: Load versus transverse strain (measured by CSGs) for Load Stage 8, LC 4-4.....	732
Figure F.80: Load versus average strain across the joints (measured by CDTs) for Load Stage 8, LC 4-4	733
Figure F.81: Load versus rebar strain (measured by RSGs) for Load Stage 8, LC 4-4.....	734
Figure F.82: Load versus rebar strain (measured by RSGs) for Load Stage 8, LC 4-4 (cont.) ..	735
Figure F.83: Load versus displacement measured using LDTs for Load Stage 9, LC 4-1.....	736
Figure F.84: Load versus longitudinal strain (measured by CSGs) for Load Stage 9, LC 4-1...	737
Figure F.85: Load versus transverse strain (measured by CSGs) for Load Stage 9, LC 4-1.....	738
Figure F.86: Load versus average strain across the joints (measured by CDTs) for Load Stage 9, LC 4-1	739
Figure F.87: Load versus rebar strain (measured by RSGs) for Load Stage 9, LC 4-1.....	740
Figure F.88: Load versus rebar strain (measured by RSGs) for Load Stage 9, LC 4-1 (cont.) ..	741

Figure F.89: Load versus displacement measured using LDTs for Load Stage 9, LC 4-2.....	742
Figure F.90: Load versus longitudinal strain (measured by CSGs) for Load Stage 9, LC 4-2...	743
Figure F.91: Load versus transverse strain (measured by CSGs) for Load Stage 9, LC 4-2.....	744
Figure F.92: Load versus average strain across the joints (measured by CDTs) for Load Stage 9, LC 4-2	745
Figure F.93: Load versus rebar strain (measured by RSGs) for Load Stage 9, LC 4-2.....	746
Figure F.94: Load versus rebar strain (measured by RSGs) for Load Stage 9, LC 4-2 (cont.) ..	747
Figure F.95: Load versus displacement measured using LDTs for Load Stage 9, LC 4-3.....	748
Figure F.96: Load versus longitudinal strain (measured by CSGs) for Load Stage 9, LC 4-3...	749
Figure F.97: Load versus transverse strain (measured by CSGs) for Load Stage 9, LC 4-3.....	750
Figure F.98: Load versus average strain across the joints (measured by CDTs) for Load Stage 9, LC 4-3	751
Figure F.99: Load versus rebar strain (measured by RSGs) for Load Stage 9, LC 4-3.....	752
Figure F.100: Load versus rebar strain (measured by RSGs) for Load Stage 9, LC 4-3.....	753
Figure F.101: Load versus displacement measured using LDTs for Load Stage 9, LC 4-4.....	754
Figure F.102: Load versus longitudinal strain (measured by CSGs) for Load Stage 9, LC 4-4.	755
Figure F.103: Load versus transverse strain (measured by CSGs) for Load Stage 9, LC 4-4....	756
Figure F.104: Load versus average strain across the joints (measured by CDTs) for Load Stage 9, LC 4-4	757
Figure F.105: Load versus rebar strain (measured by RSGs) for Load Stage 9, LC 4-4.....	758
Figure F.106: Load versus rebar strain (measured by RSGs) for Load Stage 9, LC 4-4 (cont.)	759
Figure F.107: Load versus displacement measured using LDTs for Load Stage 10, LC 4-5.....	760
Figure F.108: Load versus longitudinal strain (measured by CSGs) for Load Stage 10, LC 4-5761	
Figure F.109: Load versus transverse strain (measured by CSGs) for Load Stage 10, LC 4-5..	762
Figure F.110: Load versus average strain across the joints (measured by CDTs) for Load Stage 10, LC 4-5	763
Figure F.111: Load versus rebar strain (measured by RSGs) for Load Stage 10, LC 4-5.....	764
Figure F.112: Load versus rebar strain (measured by RSGs) for Load Stage 10, LC 4-5 (cont.)	765

LIST OF TABLES

Table 2.1: 3 rd generation bridges built in Minnesota [11]	16
Table 2.2: Ultimate load capacity for each specimen [14]	17
Table 2.3: FSB property table (beam widths are from 4' to 5').	20
Table 2.4: Commercial grout materials [30].....	34
Table 2.5: Non-commercial grout materials [30]	35
Table 2.6: Typical composition of UHPC [31].....	36
Table 2.7: Typical field-cast UHPC material properties [22].....	37
Table 2.8: Typical ranges of UHPC non-proprietary mixtures with fine aggregates (not including steel fibers) (based on data from Graybeal [32])	39
Table 2.9: Cost of material per volume of low cost UHPC [32]	39
Table 3.1: Analysis assumptions for parametric study	45
Table 3.2: Maximum span lengths and corresponding flexural capacities for 53-inch-wide FSB topped and un-topped section with 18-inch total section depths	46
Table 3.3: Approximate UHPC volume required and material cost for two-span, 110-foot total length, 84-foot-wide bridge	50
Table 3.4: Material properties for six main analyses in analytical program.....	52
Table 3.5: Summary of concrete material models used.....	53
Table 3.6: Summary of steel properties for all reinforcement used in model.....	53
Table 3.7: Summary of results from initial six analyses.....	57
Table 4.1: TxDOT box beam section properties [44].....	67
Table 4.2: NEXT D beam section properties [8]	70
Table 4.3: Comparison of section properties	75
Table 5.1: Comparison of three joints proposed for testing.....	79
Table 5.2: Guidance for structural design of UHPC connections [39].....	81
Table 5.3: Concrete mixture design for Class VI concrete used in precast sections	85
Table 5.4: Concrete mixture design for Class II concrete used for CIP deck and joint in FSB control specimens.....	86
Table 5.5: Mixture design to repair ledge in 12F2-1	86
Table 5.6: UHPC mixtures for Testing Phase 1 (using JS1212 pre-mix).....	88
Table 5.7: UHPC mixtures for Testing Phase 2 (using JS1000 pre-mix).....	88
Table 5.8: UHPC flow tests	89

Table 5.9: Specified and measured concrete strength for small-scale test specimens.....	91
Table 5.10: Steel material data.....	92
Table 5.11: Loading rate and significant steps (*Sensor removal).....	111
Table 5.12: Summary of predicted and measured results for small-scale testing.....	116
Table 5.13: Summary of measured cracking and maximum loads for each specimen.....	120
Table 6.1: FDOT standards for low volume highways (AADT: annual average daily traffic). 146	
Table 6.2: Fatigue loading scheme	148
Table 6.3: Summary of strength and post-fatigue testing strength results.....	163
Table 7.1: Phase I (FIU-1 and FIU-2) strength and service testing schedule (*remove instrumentation under beam)	170
Table 7.2: Phase II (FIU-4 and FIU-5) service, fatigue, and strength testing schedule.....	171
Table 7.3: UHPC mixtures for Testing Phases 1 and 2 (using JS1000 pre-mix).....	177
Table 7.4: UHPC flow tests	178
Table 7.5: Specified and measured concrete strength for large-scale test specimens	179
Table 7.6: Steel material data.....	180
Table 7.7: Summary of predicted and measured results for large-scale specimen.....	197
Table 7.8: Measured compression strength for precast concrete and UHPC, *age at time of test	197
Table 7.9: Observations during service load testing of FIU-1/2.....	198
Table 7.10: Observations during ultimate strength testing of FIU-1/2.....	205
Table 7.11: Measured compression strength for precast concrete and UHPC, *age at time of test	213
Table 7.12: Observations during ultimate strength testing of FIU-4/5.....	275
Table 8.1: Four-beam flexural stiffness loading and camber leveling schemes.....	286
Table 8.2: Four-beam service, fatigue, and strength loading scheme.....	289
Table 8.3: Summary of beam stiffnesses measurement and joint construction stages	293
Table 8.4: UHPC mixtures for Testing Phase III (using JS1000 pre-mix).....	298
Table 8.5: UHPC flow tests	299
Table 8.6: Saw cut depths at four locations	301
Table 8.7: Specified and measured concrete strength for Testing Phase III specimens.....	302
Table 8.8: Steel material data.....	303
Table 8.9: VWG reading type during life of beams.....	329

Table 8.10: Top and bottom fiber strains and curvature at different times after release	332
Table 8.11: Measured prestress loss at time of last reliable measurement	334
Table 8.12: Estimated prestress loss at time of last measurement based on AASHTO LRFD Refined Estimate Procedure [82]	335
Table 8.13: Summary of maximum deflections, longitudinal bottom strains, and stiffnesses at 20 kips for large-scale specimens	336
Table 8.14: Summary of maximum deflection, longitudinal bottom strain, and surcharge application for FIU-3	336
Table 8.15: Prestress loss estimates per layer for FIU-3 (1 of 2)	340
Table 8.16: Prestress loss estimates per layer for FIU-3 (2 of 2)	340
Table 8.17: Prestress loss estimates per layer for FIU-6, FIU-7, and FIU-8 (1 of 2)	340
Table 8.18: Prestress loss estimates per layer for FIU-6, FIU-7, and FIU-8 (2 of 2)	341
Table 8.19: Measured compression strength for precast concrete, *age at time of test	348
Table 8.20: Measured compression strength for UHPC joints, *age at time of test.....	348
Table 8.21: Distribution factor comparison between top and bottom CSGs for Stage 2 loading.....	349
Table 8.22: Distribution factor comparison between bottom CSGs and beam deflection for Stage 2 loading.....	350
Table 8.23: Summary of GDF_i for all static tests, *loaded beam	351
Table 8.24: Exterior and interior girder distribution factors.....	351
Table 8.25: Measured and estimated total longitudinal strain at 30 kips for Stage 2	356
Table 8.26: Summary of predicted and measured results for four-beam specimen.....	388
Table 8.27: Observations during ultimate strength testing of FIU-3/6/8/7.....	389
Table 8.28: Measured cracking load and associated bottom fiber longitudinal strains	392
Table 8.29: Measured and estimated top fiber longitudinal strains at failure.....	393
Table 9.1: Approximate minimum installation time for decked stringer systems (from Culmo [104]).....	415
Table 9.2: Maximum span lengths for FSB depths.....	429
Table 9.3: QConBridge™ Strength I Moment envelopes for Bridge 1, Bridge 2, and Summation	432
Table 9.4: Summary of inputs for SDCL analyses for all three section depths.....	445
Table 9.5: Positive moment design of SDCL connection for 12-, 15-, and 18-inch-deep modified FSB sections with non-prestressed strands	447

Table 9.6: Negative moment design of SDCL connection for 12-, 15-, and 18-inch-deep modified FSB sections with high-strength rebar and non-prestressed strands.....	447
Table 9.7: Concrete material definitions.....	450
Table 9.8: Prestressing strand material definitions.....	450
Table 9.9: Joint reinforcement definition.....	451
Table C.1: Max. forces and displacements computed.....	528
Table C.2: Concrete definition.....	528
Table C.3: Joint reinforcement definition.....	529
Table D.1: Summary of measured cracking and maximum loads for each specimen.....	548
Table D.2: FSB Control Strength testing summary.....	550
Table D.3: 18F1 Strength testing summary.....	559
Table D.4: 18F2 Strength testing summary.....	567
Table D.5: 18A1 Strength testing summary.....	575
Table D.6: 12F1 Strength testing summary.....	583
Table D.7: 12F2 Strength testing summary.....	589
Table D.8: 12A1 Strength testing summary.....	596
Table D.9: 12A2 Strength testing summary.....	603
Table E.1: Summary of strength and post-fatigue testing strength results.....	610
Table F.1: Four-beam service, fatigue, and strength loading scheme.....	642

1. INTRODUCTION

1.1. BACKGROUND

The Florida Department of Transportation (FDOT) is proactive in the research of new and innovative products, processes, and designs to maximize the efficient use of taxpayer's dollars for Florida's transportation system. One innovation that has received national attention for its exceptional structural properties is ultra-high-performance concrete (UHPC). FDOT has been working on several recent research efforts to develop design guidelines and specifications for the use of UHPC on Florida transportation projects.

A design innovation that was recently released as an FDOT Design Standard is the Florida Slab Beam (FSB). The FSB is a precast, prestressed, flat slab beam that currently requires a cast-in-place (CIP) composite concrete deck topping and longitudinal reinforced concrete joints between beams. The work of this project was aimed at revising the current FSB Design Standard to eliminate the CIP deck and utilize a UHPC longitudinal joint between adjacent beams to create a more durable system that can be more rapidly constructed.

1.2. OBJECTIVE

The primary objective of this research was to develop design details of FDOT's FSB Design Standard utilizing a UHPC longitudinal joint between beams with an asphalt overlay. Several secondary objectives were developed to help achieve the primary objective:

1. Identify previously researched UHPC joint details,
2. Conceptually develop options for UHPC joints between slab beams,
3. Assess the flexural strength and shear demand of the developed joint details using small-scale specimens,
4. Identify the best performing joint detail from the small-scale joint testing,
5. Evaluate the performance of the developed joint detail in two full-scale two-beam test configurations and one four-beam test configuration,
6. Determine the effect of leveling a beam to account for differential camber on the overall system performance, and
7. Develop a preliminary detail for using the simple for dead load and continuous for live load design methodology with the modified FSB Design Standard.

The current FSB Design Standard has three different section depths (12, 15, and 18 inches). The currently available FSB depths only allow for maximum spans of around 60 feet. An additional objective to those listed above was to:

8. Evaluate available cross-section geometries and develop an FSB section for 75-foot span lengths.

1.3. TASKS

These objectives were accomplished through the following research tasks:

1. **Task 1 – Literature Review:** An extensive literature review was conducted on the use of UHPC in bridge joint applications. The emphasis of the literature review was on short-

span bridge solutions, joint options between precast concrete elements, material options for joint applications (including UHPC), and other applications of UHPC in bridge superstructures.

2. **Task 2 – Conceptually and Analytically Develop FSB Design Standards and UHPC Joint Details:** Design of two-lane bridges with different span lengths were conducted to determine the maximum feasible span lengths for bridges utilizing the current FSB Design Standard (with 12-, 15-, and 18-inch depths) with and without CIP decks. Several different longitudinal joint details were developed and evaluated through numerical analyses.
3. **Task 3 – Conceptually and Analytically Develop the FSB Design Standard for a 75-Foot Single Span with UHPC Joints and an Asphalt Overlay:** Two-lane, 75-foot bridge designs were conducted using five different cross section shapes (three from those currently or previously used in practice and two developed in this task). A comparison of these designs was conducted with the section efficiency factor being used as one comparison point.
4. **Task 4 – Small-Scale Joint Testing:** The joints developed in Task 2 and the current FSB joint detail were evaluated using transverse flexural testing of 56-inch-long sections of two adjacent beams with one joint. Ultimate strength and fatigue testing was performed on the specimens with the different joint details.
5. **Task 5 – Full-Scale Specimen Testing (2-Beam Systems):** The best performing joint from Task 4 was used to connect two sets of 30-foot-long modified FSBs. Service, fatigue, and ultimate strength testing was performed with different load and support conditions on these two two-beam test configurations.
6. **Task 6 – Full-Scale Specimen Testing (4-Beam System):** The best performing joint from Task 4 was also evaluated using service, fatigue, and ultimate strength testing on a four-beam system. One of the beams in this system was designed and constructed to have a larger camber than the other three beams to investigate the effect of leveling one beam with differential camber on the behavior of the overall superstructure system.
7. **Task 7 – Simple for Dead Load and Continuous for Live Load (SDCL) Design Concept:** A preliminary SDCL connection detail was developed for use with the modified FSB Design Standard.
8. **Task 8 – Final Report Preparation, Review, and Revision:** A final report was developed to summarize the work and findings from these tasks.

1.4. REPORT ORGANIZATION

This report is divided into eleven chapters and a series of appendices. Chapter 2 presents a complete literature review on precast prestressed short-span bridge sections and joints between precast superstructure elements. The initial development of options for the modified FSB Design Standard is presented in Chapter 3. Chapter 4 presents the development of the FSB Design Standard for 75-foot single span. Chapters 5 and 6 include the results from the small-scale joint experimental investigation. The results from the full-scale testing are presented in Chapter 7 for the two-beam system tests and Chapter 8 for the four-beam system tests. Chapter 9 summarizes the proposed SDCL design detail and a preliminary numerical analysis. Chapter 10 includes a

summary and conclusions of this research and additional topics for further research. Chapter 11 has a list of all the references cited in this report.

2. LITERATURE REVIEW

2.1. INTRODUCTION

Many of the nation's bridges have reached or are nearing the end of their functional design lives and need repair, rehabilitation, or replacement. Most of these bridges have short span lengths (less than 75 feet in length). Prefabricated bridge elements (PBEs) are almost exclusively used in these scenarios to reduce construction times, minimize the impact on the public, and improve durability performance. There are many different short-span bridge options available in the United States and Florida. Each option has its advantages and disadvantages, and each have different requirements for connecting adjacent elements. A review of some of the more commonly used and more recently developed short-span bridge solutions is provided. Following this introduction on short-span bridge solutions is an overview of the various types of longitudinal and transverse joints that have been used to connect adjacent members and a summary of the material types and properties for the materials used in these joints. Ultra-high performance concrete (UHPC) is a commonly used joint material; a brief summary of other UHPC applications is also provided.

2.2. CONCRETE SHORT-SPAN BRIDGE SOLUTIONS

There are several different reinforced and prestressed concrete short-span bridge solutions that are being used across the US. These solutions have traditionally fallen into three different categories: (1) box beams, (2) T beams, and (3) slab beams, as shown in Figure 2.1.

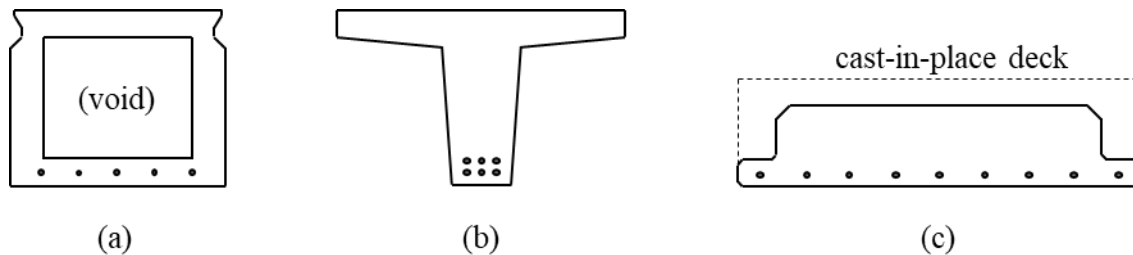


Figure 2.1: Three traditionally used prestressed concrete solutions for short-span bridges: (a) box beams, (b) T beams, and (c) slab beams

Specific cases of these three types of short-span bridge solutions will be introduced and discussed in more detail in the following sections. Although there are many more prefabricated concrete elements in the field, the ones shown are relevant to this research due to their resemblances to the FSB in terms of behavior, technology, and applicability.

2.2.1. Adjacent Box Beams

2.2.1.1. Background

According to Bender and Kriesel [1], the use of box beams began in the late 1940's or early 1950's in the US. Their first introduction is traced back to Pennsylvania and Tennessee, where they were used primarily in short-span applications and were basically voided slabs. Research by the Portland Cement Association (PCA) and several universities was done to verify and improve their strength and durability. This research resulted in sections capable of spanning from 20 to 120 feet. Avendaño et al. [2] created a chart that shows the number of prestressed concrete box

beam bridges built over the last 55 years. The section had a peak of use between 1990 and 1995, when about 16% of all bridges built were box beams. Since its peak, box beam usage has been declining.

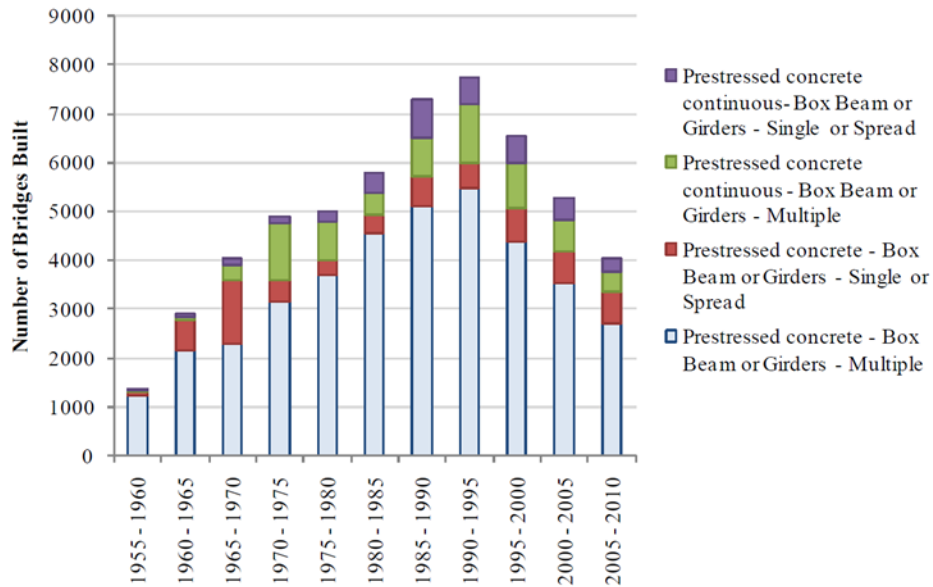


Figure 2.2: Prestressed concrete box beam construction per year [2]

2.2.1.2. Details

According to Bender and Kriesel [1], there are two typical cross-section types for short-span, box beams: (1) regular, non-composite box beams and (2) composite box beams, as shown in Figure 2.3. While dimensions of specific box beam shapes vary from state to state, the general design principles are consistent.

Box beams designed in a regular, non-composite fashion, shown in Figure 2.3 (a), are designed to withstand their share of lane loads and dead loads from the wearing surface without any composite slab cast on top. This type of construction is preferred as it allows for shorter construction times, less field labor, excellent span-to-depth ratios, and good load distribution. Proper detailing of the joint region is extremely important for this type of construction.

Composite box beams, shown in Figure 2.3 (b), are slightly different due to a minimum 4-inch cast-in-place (CIP) deck poured on top of the section. Box beams used in this fashion have protruding stirrups to ensure proper composite action between the precast box beam and the CIP deck. Because the box beams are placed side-by-side, the top of the beams serves as the lower formwork, which allows for quicker construction than spread configurations. The CIP deck will also improve the joint performance between adjacent members.

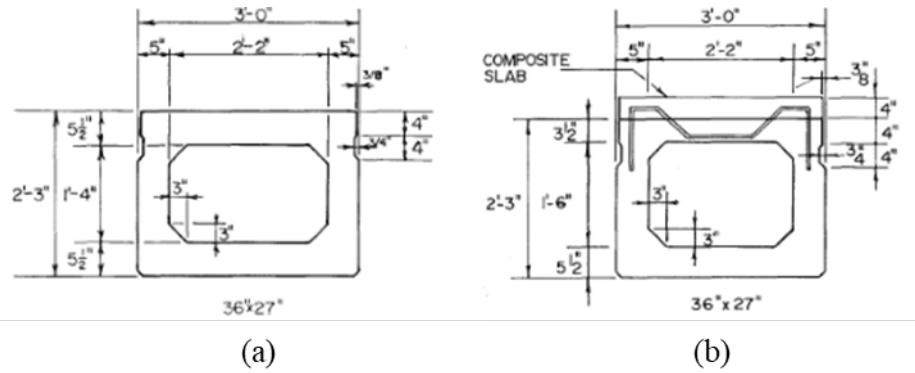


Figure 2.3: Typical box beam sections [1]: (a) regular, non-composite section and (b) composite section

In addition to the variation in section shape, short-span box beams can be used in two basic bridge configurations: (1) adjacent beam and (2) spread beam structures, as shown in Figure 2.4. An adjacent beam configuration is where the box beams are placed immediately next to one another, and no space is left between adjacent members. These adjacent members are connected using longitudinal shear keys and the bonding action of either passive high-strength rods or post-tensioning cables in the transverse direction. In spread beam configurations, the beams are placed several feet apart and driving surface is made of a full-depth, CIP deck and an asphalt overlay in some cases. Because beams in the spread configuration are not immediately adjacent to one another, neither shear keys nor transverse post-tensioning are required. Having spread box beams requires a deeper section than adjacent configurations and also requires additional prestressing strand to handle the additional loads [2].

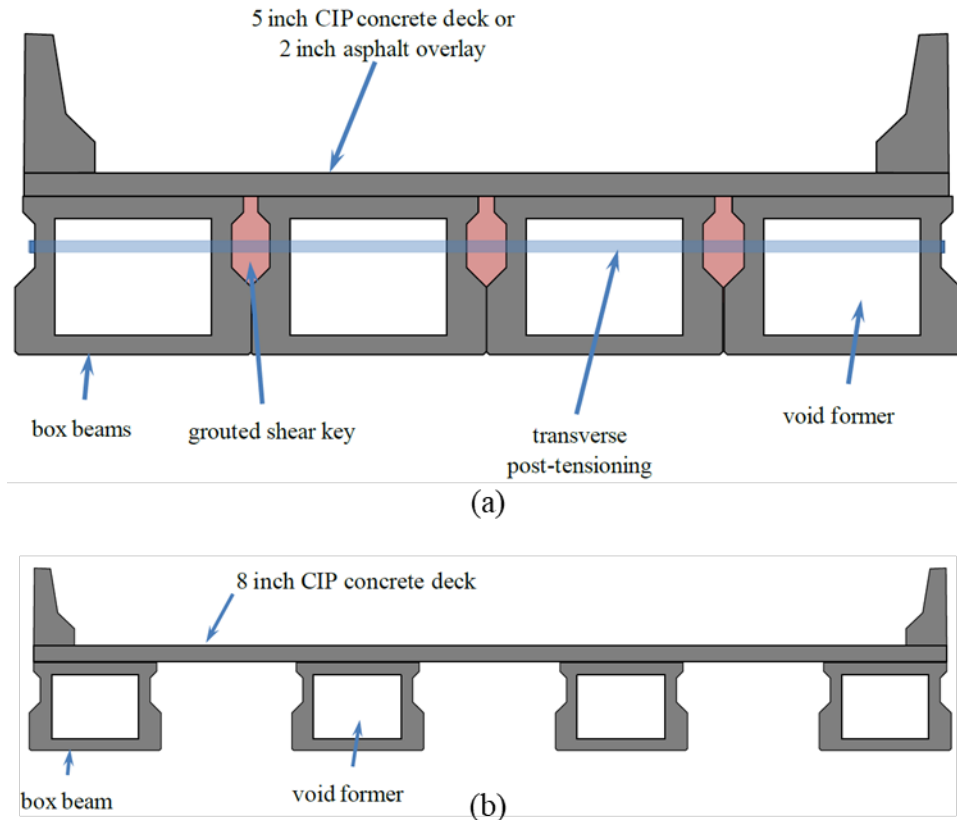


Figure 2.4: Box beam configurations [2]: (a) adjacent configuration and (b) spread configuration

Bender and Kriesel [1], Avendaño et al. [2], Hanna, Morcoux, and Tadros [3], and Corvin [4] provide additional recommendations for the design and detailing of box beams for short-span applications.

2.2.1.3. Current Uses

Box beam bridges are used in many states across the US for many different applications: to carry typical automotive traffic, as pedestrian bridges, as railroad bridges and even in bridge widening applications. A well-known example of an aesthetically pleasing box beam bridge is the Hawk Lake Bridge, located in Ontario, Canada (Figure 2.5). It is located over an existing Canadian Pacific Railway (CPR) rail line and is situated over elevated train tracks, so clearance height was an important part of the design. The single-span bridge (13.8 m wide by 27.2 m long) has 12 side-by-side precast box beams, 11 joints, approach slabs and guardrail curbs. It received in 2010 a PCA Concrete Bridge Award which is a biennial competition that distinguishes quality in design and construction of concrete bridges.



Figure 2.5: Hawk Lake Bridge [5]

2.2.1.4. Challenges

There are a few challenges that the designer must tackle to guarantee the proper behavior of the section. According to Avendaño et al. [2], if the bottom slab of the beam is too flexible, the transfer of forces transversely across the bottom section might be ineffective and the prestressing force placed in the bottom slab might not be transferred appropriately into the webs.

These researchers also highlighted the issue unique to wide beams at both ends when bridges are oriented at a skew angle. If we depict the two webs acting as two simply supported beams, the beam with the shorter span is stiffer and therefore will attract a higher fraction of the load towards the support than the beam with the larger span. The greater the skew angle, the greater the difference in the stiffness between the two webs.

As previously mentioned, challenges also arise with the joint region between adjacent members. Lall, Alampalli, and DiCocco [6] highlight these challenges associated with the shear key geometries implemented in box beams. In the study, field personnel reported that longitudinal cracks were appearing shortly after construction in adjacent box beam bridges of various configurations. This longitudinal cracking can lead to premature spalling and water intrusion. According to a 1990 study [6], 54% of adjacent box beam bridges built between 1985 and 1990 had developed longitudinal cracks over the shear keys. The issue was addressed by suggesting the implementation of full-depth shear keys (see Figure 2.6), full-width bearing pads, higher reinforcement ratio in the concrete deck overlay, and higher transverse post-tensioning forces and two tendons over the depth of the beam at each tendon locations. Cracking between adjacent box beams is still an issue today.

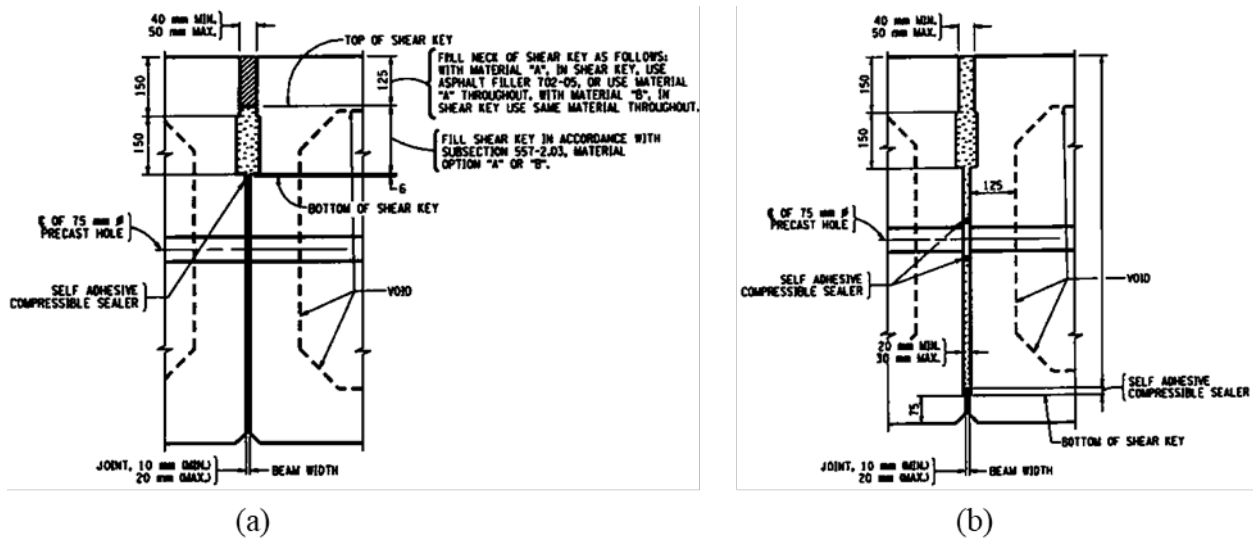


Figure 2.6: Shear keys [6]: (a) partial depth shear key and (b) full-depth shear key systems

Box beams can also have durability concerns related to the construction of the internal void. Box beams are designed to have a void on the interior that is generally constructed using a Styrofoam, stay-in-place form. The Styrofoam form can shift during casting, leaving less interior cover to the prestressing strands and reinforcement. The formed void typically somehow catches water, which has led to accelerated deterioration and corrosion concerns. The issues related to this deterioration are exacerbated as there is no way to easily inspect the inside conditions of a typical box beam.

2.2.2. New England Extreme Tee (NEXT) Beam

2.2.2.1. Background

The New England Extreme Tee (NEXT) beam is another short-span bridge solution implemented as an improvement over box beams. It is basically a modification of a concrete precast section originally developed for high-level railroad platform segment in the northeast (see Figure 2.7).



Figure 2.7: High-level railroad platform [7]

Different parameters were established in the design guidelines of the NEXT beam according to Culmo and Seraderian [7]:

- Bridge spans from 45 to 90 feet
- Section depths vary from 24 to 36 inches
- Widths varies from 8 to 12 feet
- Weight limit of section set to about 120 kip (due to shipment and handling concerns)
- Top flange thickness varies between 4 inches (with CIP deck, avoiding the need for deck forming) and 8 inches (when no CIP deck is used)

2.2.2.2. Details

The Precast/Prestressed Concrete Institute (PCI) Northeast has established three types of NEXT beams, as shown in Figure 2.8 and Figure 2.9. NEXT F beams require a minimum 8-inch-deep CIP concrete deck, but do not require a special longitudinal connection detail. NEXT E beams require only a 4.5-inch-deep CIP deck that includes a closure pour detail to ensure proper connection between adjacent members. The top flange of the NEXT D beam doubles as the wearing surface, so only a closure pour is required to connect adjacent members and create the bridge span. The NEXT D beam is the best solution for Accelerated Bridge Construction (ABC) applications because the only on-sight casting required is a narrow-reinforced closure pour typically made with UHPC or non-shrink grout.

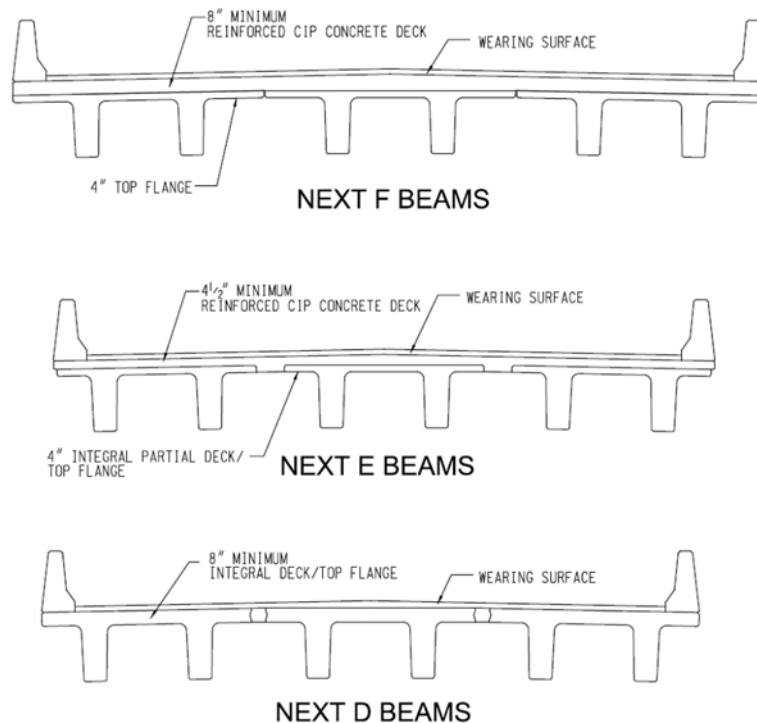


Figure 2.8: Typical configurations for NEXT beams [8]

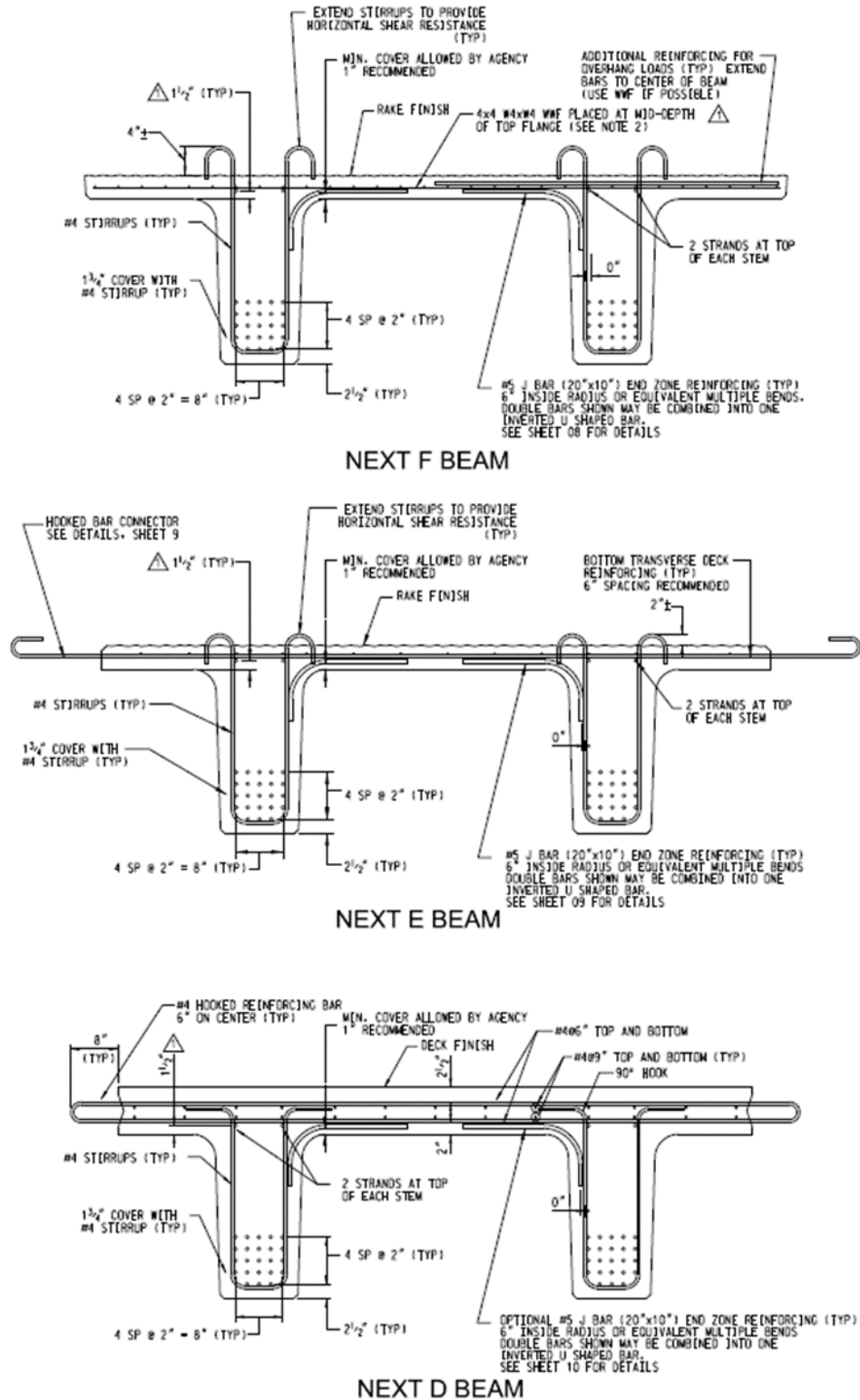


Figure 2.9: Typical reinforcement for NEXT beams [8]

The flange connection for NEXT D beams can be designed in two ways: (1) using hooked bars with non-shrink grout or (2) using straight bars with UHPC, as shown in Figure 2.10. Hooked

bars are not required when using UHPC because using UHPC greatly decreases the development length of reinforcement.

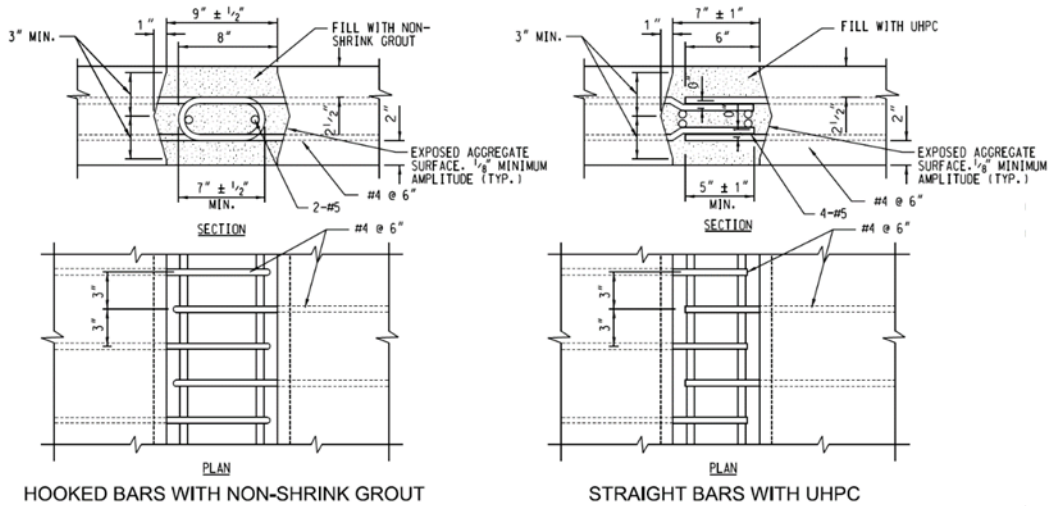


Figure 2.10: Types of joint detail for NEXT D beam [8]

2.2.2.3. Current Uses

The first NEXT beam project was built in 2010 in Maine. As with many short-span bridge solutions, this one was used to completely replace the New Bridge on Route 103 in York, Maine. The Maine DOT had the additional challenges of maintaining the existing profile and navigational clearances, so the bridge section was designed accordingly. A photograph from casting of the NEXT F beams used in this project is shown in Figure 2.11.



Figure 2.11: NEXT beam section at Dailey Precast plant, Shaftsbury, Vermont [7]

2.2.2.4. Challenges

Because the NEXT beam is relatively new (with the first bridge built in 2010), there have not been any long-term issues reported that affect the integrity of the girder. However, PCI Northeast has highlighted in their design guidelines possible difficulties that the designer might encounter. NEXT F beams require more CIP concrete and two layers of deck reinforcing, so there is an increased cost. There is also the possibility of having longitudinal cracks along the inner face of

the stem, especially when there is greater than 20 degrees skew. NEXT E beams requires forming of larger closure pours that can also increase the cost of construction. It is also a possibility to have longitudinal cracking along the inner face of the stem when there is larger than 20 degrees skew. NEXT D beams also require forming of closure pours. Because it is a complete section (i.e., they do not require CIP concrete deck), it is more difficult to accommodate vertical curves. Lastly, this section requires the use of UHPC which can increase the up-front cost of the superstructure but decreases long-term expenses due to future retrofits.

2.2.3. Poutre-Dalle System and Minnesota Modification

2.2.3.1. Background

The Poutre-Dalle (“Beam Slab”) System is a short-span bridge system originally from France that has showed promise in innovation of rapid bridge construction. This beam slab system consists of shallow precast concrete inverted-T beams that are laid down in place one next to the other. They have transverse 180-degree looped bars that ensure the transferring of forces either longitudinally or transversely depending on the configuration (See Figure 2.12).

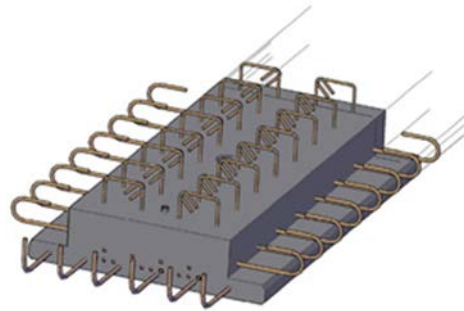


Figure 2.12: Poutre-Dalle section [9]

After they are laid down in parallel, concrete is poured in the inner joints and continued with a top deck all in one single cast. The bottom flanges of the beams are butted up next to each other eliminating the need for formwork. The construction sequence for these members is shown in Figure 2.13.

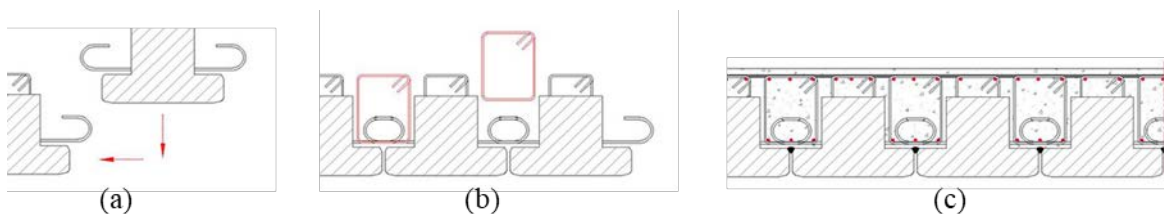


Figure 2.13: Construction sequence for Poutre-Dalle System: (a) adjacent placement of beams, (b) installation of joint reinforcement, (c) installation of remaining reinforcement and simultaneous casting of deck and joint [9]

According to Mercer [10], the system was first introduced in the US when a group of engineers sponsored by the Federal Highway Administration (FHWA) and the American Association of State Highway and Transportation Officials (AASHTO) investigated new technologies on prefabricated bridge systems in France, Japan, and Germany in 2004. This structure came out as

a suitable solution for the rapid replacement of short-span bridges. Captivated with the Poutre-Dalle section, the Minnesota Department of Transportation (MnDOT) was the first to start developing a similar CIP slab span system in 2005.

The study began with a partnership between MnDOT and the University of Minnesota. Mercer [10] states that the team tested a series of connection details to better improve its structural behavior. The major outcome in the study was the modification of the 180-degree hooked bars used in France to 90-degree hooked bars (see Figure 2.14). By this modification, one can now add a pre-tied reinforced cage to better resist shear forces along the joint. This drop-in reinforcement cage serves to control reflective cracks at the joint line. The new section is called Precast Composite Slab Span (PCSS) system by MnDOT.

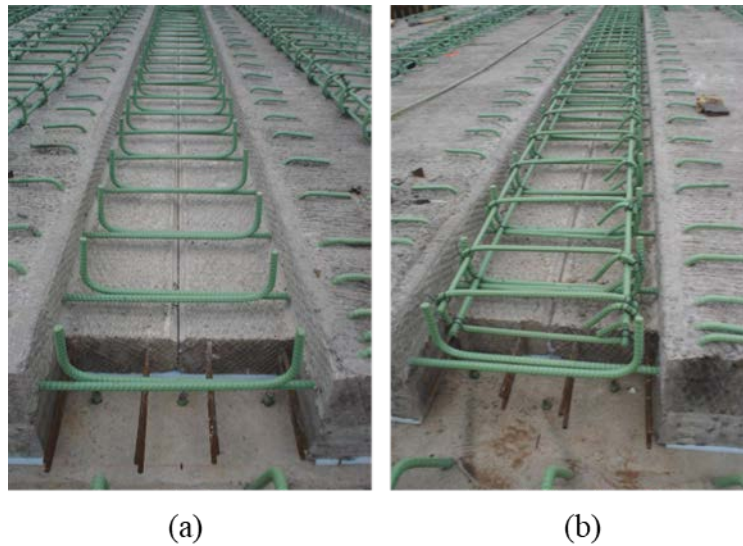


Figure 2.14: New type of developed joints [11]: (a) joint between PCSS panels (90-degree hooks) and (b) drop-in reinforced cage

French et al. [12] and Piccinin and Shultz [13] developed improved details for the PCSS system through experimental testing and field monitoring programs.

2.2.3.2. Details

The new PCSS is a combination of precast, prestressed concrete beams and the traditional concrete slab-span system. A general view of the cross-section developed by MnDOT is shown in Figure 2.15. This section is currently used for short-span bridges ranging from 20 to 65 feet. A roughened concrete surface and 90-degree hooks help to guarantee proper composite action between the girder and deck concrete, as shown in Figure 2.15 (b).

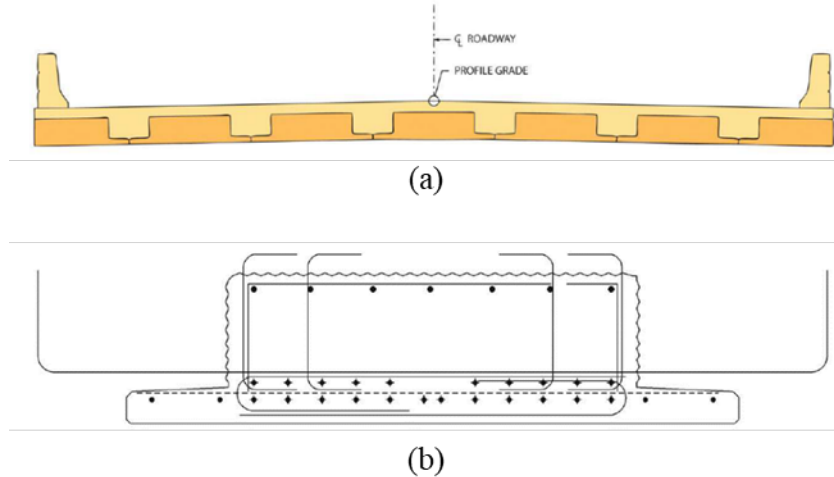


Figure 2.15: PCSS [11]: (a) typical transverse section of a bridge with PCSS system and (b) typical MnDOT PCSS.

2.2.3.3. Current Uses

MnDOT first implemented the described section in two pilot bridge projects over two water crossings. The bridges served as calibration sites so that results of the field and adjustment data from laboratory tests could confirm the system’s durability and verify the first PCSS design assumptions. The bridges are Bridge No. 04002 located on MN Highway 72 over the Tamarac River and Bridge No. 13004 on U.S. Highway 8 over Center Lake Channel. The erection of the bridge is shown in Figure 2.16.



Figure 2.16: Erection of Bridge 04002 located on MN Highway 72 over the Tamarac River near the rural, northern Minnesota town of Waskish [11]

The successful implementation of the section in this first pilot project led to six more PCSS bridges being designed and built in Minnesota. The first group of three bridges or “2nd generation bridges” were built in 2007. By 2009, a group of three more bridges or “3rd generation bridges” were also erected. Some of the main characteristics of the 3rd generation bridges are shown in Table 2.1.

Table 2.1: 3rd generation bridges built in Minnesota [11]

Bridge No., Trunk Highway No., Bridge Name, and Location	6679, T.H. 76 over the South Fork of the Root River, Houston Co.	49007, T.H. 238 over the Swan River, Morrison Co.	49036, T.H. 238 over Pike Creek, Morrison Co.	66004, T.H. 60 over the Cannon River, Rice Co.
Year Built	2007	2009	2009	2009
Total Length	n/a	104'-2"	72'-2"	124'-5"
Width	30'-0"	39'-4"	43'-4"	47'-4"
Span Lengths	19'-0"	34'-1", 34'-10", 34'-1"	23'-5", 24'-2", 23'-5"	40'-5", 40'-10", 40'-5"
f_c Precast and CIP, psi	4000, 4000	6500, 4000	6000, 4000	6000, 4000
Fabricator (PCI-certified producer)	County Materials, Roberts, Wis.	Cretex Concrete Products Maple Grove, Minn.	Cretex Concrete Products Maple Grove, Minn.	Cretex Concrete Products Maple Grove, Minn.
Contractor	MnDOT Bridge Maintenance	Lunda Construction Co., Black River Falls, Wis.	Lunda Construction Co., Black River Falls, Wis.	Minnowa Construction Harmony, Minn.

2.2.3.4. Challenges

There have been several issues reported by the researchers related to the PCSS section. Piccinin and Schultz [13] noted that standardized I-sections might be more economical and practical than PCSS sections for spans longer than 62 feet, which would correspond to a PCSS depth deeper than 25 inches. Further research regarding economic feasibility of the PCSS is needed.

Reflective cracks were observed during the pilot project at two specific locations: along the longitudinal joints and transverse joints at piers. These cracks were determined to be a result of thermal gradient effects [11]. The designers made several improvements to the geometry of the system; this cracking was reduced but not eliminated with these improvements. The University of Minnesota is still monitoring the constructed bridges to better understand the nature of the cracks and their effect on durability.

2.2.4. Inverted-T Prestressed Beams

2.2.4.1. Background

Another inverted-T section for short-to medium-span application is the solution created in Virginia. This inverted-T system was developed with the goal of decreasing reflective cracks along longitudinal joints, which is a big concern associated with such systems. The section has the advantage of a thick CIP topping and the profile is adjusted to reduce stress concentrations. Menkulasi et al. [14] proposed a modification to the straight web shape from the section of Minnesota. They stated that this geometry was creating entrant corners with 90-degree angles, which are a source for crack initiation once the CIP topping is poured.

One of the main design issues tackled in this research was the transverse load distribution. Once the system is fully loaded, a two-way plate bending action takes place. The finite element model developed by the researchers to study the transverse load behavior specifically is shown in Figure 2.17.

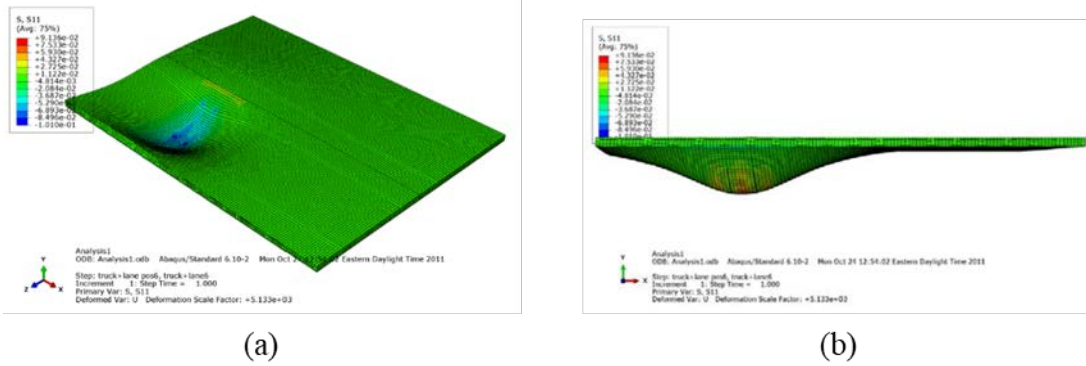



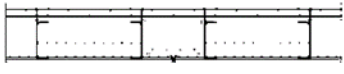
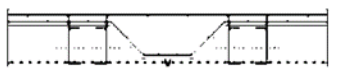
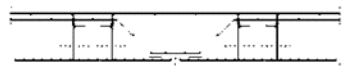
Figure 2.17: (a) 3D FEM representation of an inverted-tee section with straight web and (b) side view FEM representation of an inverted-tee section with straight web [14]

Menkulasi et al. [14] performed an analytical and experimental study to test four specimens with different cross-section configuration:

- Specimen #1 – Straight web with extended bars (like University of Minnesota Section)
- Specimen #2 – Straight web with embedded plate connection
- Specimen #3 – Tapered web with embedded plate connection
- Specimen #4 – tapered web no connection

Each specimen was loaded in increments of 5 kips up to 30 kips, simulating the load that creates transverse flexural stresses. Preliminary results from these tests are shown in Table 2.2.

Table 2.2: Ultimate load capacity for each specimen [14]

Specimen Description	Cracking Load (kips)*	Ratio**	Ultimate Load (kips)
Straight Web with extended bars 	90	2.5	260 Many cracks in all directions
Straight web with embedded plate connection 	100	2.7	225 Fracture of weld at one location and rebar at another
Tapered web with embedded plate connection 	110	3.0	Test stopped at 300 due to capacity of the loading frame.
Tapered web with no connection 	60	1.8	90 (Large Crack Through Precast Section)

The researchers concluded that tapering the webs to reduce straight angles provided necessary integrity between members and deck and prevented cracking due to service loads in the transverse direction. This detail also happened to be the cheapest of the options.

2.2.4.2. Details.

The new section consists of adjacent precast inverted-T beams with tapered webs covered with a CIP topping as shown in Figure 2.18.

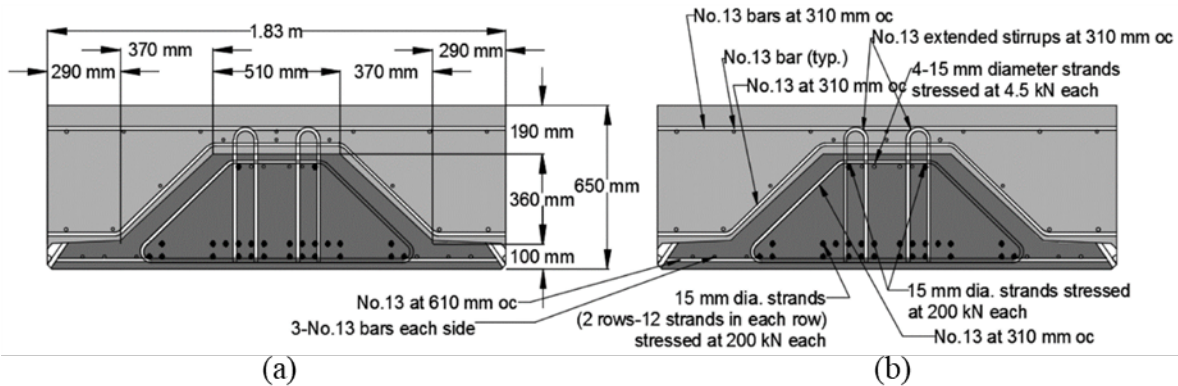


Figure 2.18: (a) Typical composite cross-section and (b) typical reinforcing details [15]

The connection detail between adjacent sections is shown in Figure 2.19. These details are from the first bridge built in Virginia on US 360 near Richmond using the proposed inverted-T beams. The inverted-T beams included discrete embedded steel plates and welded bars.

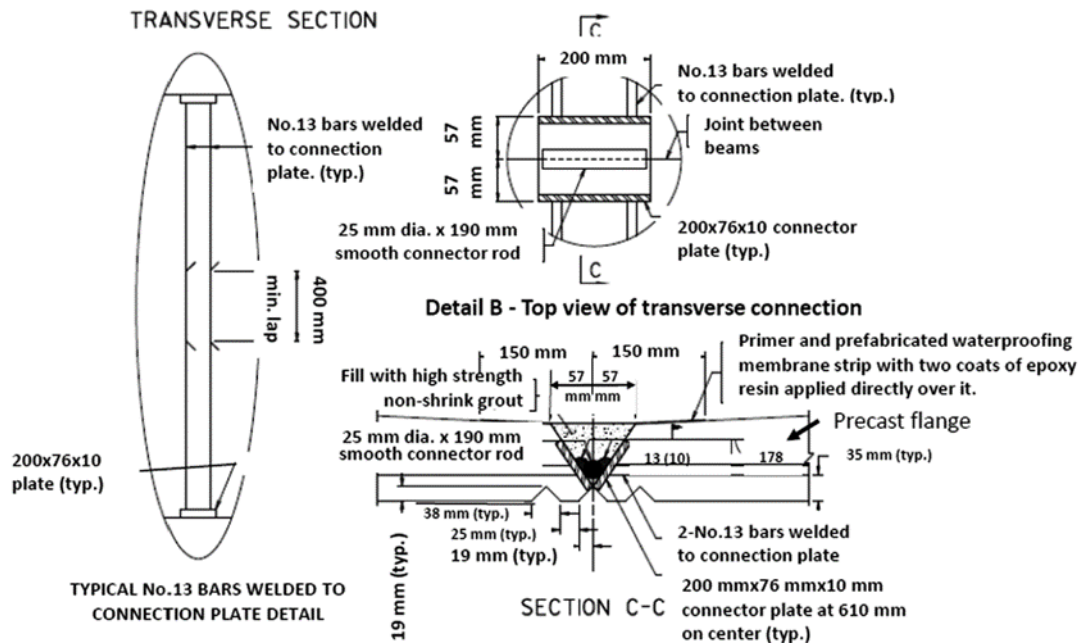


Figure 2.19: Connection detail [15]

2.2.4.3. Current Uses

This section was first implemented in a bridge built in Virginia on US 360 near Richmond. The construction phases of this project are shown in Figure 2.20.

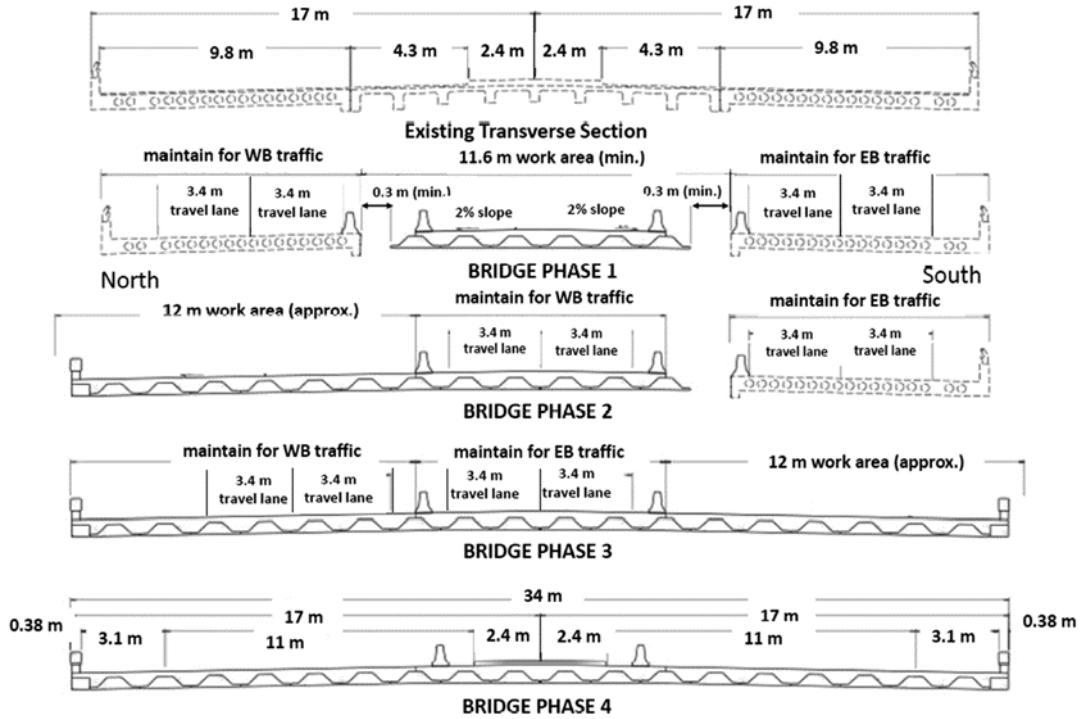


Figure 2.20: Phase construction of US-360 bridge [15]

2.2.4.4. Challenges

Due to the relatively young age of the system, there have not been any challenges reported using this type of section. Menkulasi et al. [14] proposed improvements to the detail by reducing the size and spacing of the transverse reinforcement in the flanges.

2.2.5. Florida Slab Beam

2.2.5.1. Background

The development of the Florida Slab Beam (FSB) has its roots in the Minnesota FCSS. It is also a precast, prestressed, flat slab beam that requires a composite concrete deck topping and longitudinal reinforced concrete joints between beams.

FDOT has worked with precast slab beam units since the late 1940s [16], [17]. The systems have gone through several design modifications, especially to achieve a design that limits cracking in the longitudinal direction. The FSB system has evolved from prestressed slab beam superstructures that were employed by FDOT and used in the mid to late 1950s. On November 9, 1984, FDOT released a memorandum to consultants and precast designers with the sole request of discontinuing the use of the precast prestressed slab units made in that period. The memorandum stated that they had modified this system several times to reduce reflective cracks through the topping at the precast slab interfaces without satisfactory results. A modification was proposed utilizing additional post-tensioning in the transverse direction. These modifications were made in hopes of causing the slab units to act as a monolithic structure and have the proper live load distribution [18].

In January 2006, FDOT introduced another iteration to the FSB system, which was presented in the Developmental Design Standards Indexes D20450 through D20453 and the associated Instructions for Developmental Design Standards as an alternative solution for short-span bridges. After several additional changes to its design, the FSB has been established to be used in off-system bridges with low Average Daily Traffic (ADT) and low Average Daily Truck Traffic (ADTT). In March 2016, the Index D20450 Series Florida Slab Beam was officially presented. The design criteria follows current AASHTO LRFD Bridge Design Specifications, Structure Design Guidelines (SDG), and Structures Detailing Manual (SDM) [19], [20].

2.2.5.2. Details

The FSB superstructure system implemented by FDOT is shown in Figure 2.21. The components of the FSB superstructure are the FSB itself, a CIP reinforced concrete topping, and the railing system.

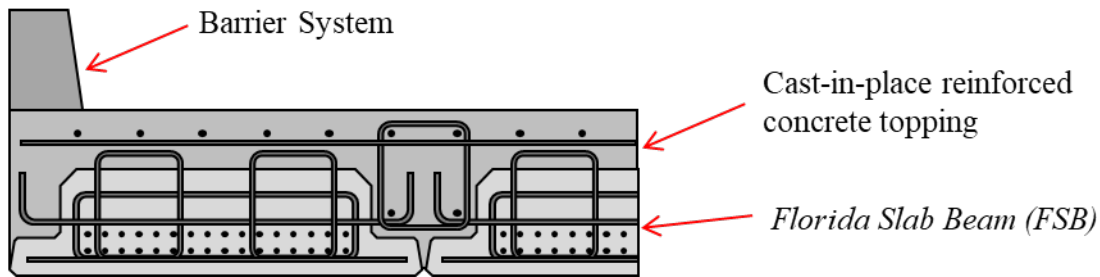


Figure 2.21: Florida slab beam superstructure system

The three different types of FSB members are presented in Table 2.3 with a typical FSB cross section shown in Figure 2.22. Three FSB section depths are currently available: 12-, 15-, and 18-inch depths. Like the Minnesota FCSS, FSBs have square edges with transverse reinforcing bars that protrude from the sides. Unlike the FCSS, however, these reinforcing bars do not extend beyond the edges of the FSB flanges, which facilitates placement. A 2-inch chamfer is used at the top of the precast section to minimize abrupt section changes. This design detail is aimed at eliminating the formation of longitudinal reflective cracks that have traditionally formed at the joint locations.

Table 2.3: FSB property table (beam widths are from 4' to 5').

Index No.	FSB Depth	Span Length
D20451	12"	30 to 50 ft.
D20452	15"	30 to 50 ft.
D20453	18"	30 to 50 ft.

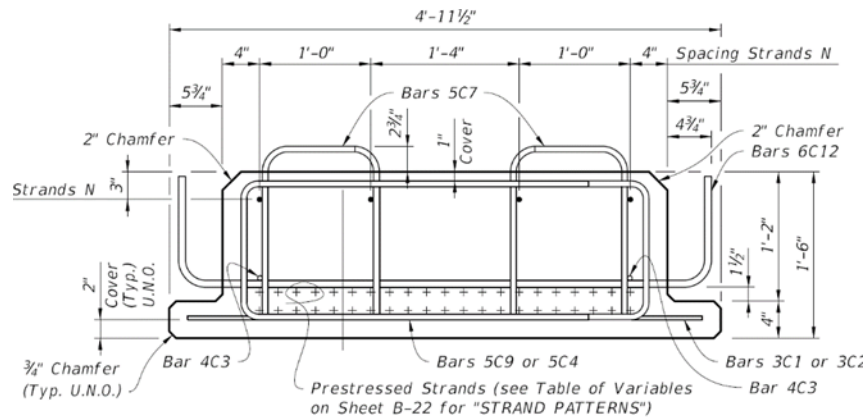


Figure 2.22: Typical FSB section [16]

Cracking can be further reduced by saturating the FSB with water for at least 12 hours prior to casting of the concrete topping, creating a saturated surface condition. FDOT requires the inclusion of a shrinkage-reducing admixture into the concrete mixture for the composite topping [19].

2.2.5.3. Current Uses

The FSB system is intended to be used to replace prestressed slab units [19]. As mentioned before, the FSB superstructure system is currently recommended for off-system bridges with low ADT and ADTT. The pilot project for this system was SR 373 (Orange Avenue) over St. Marks Trail (District Three, Leon County; Tallahassee, Florida). The road closure was for seven weeks, from June 2nd to July 20th of 2014. The designers of this project were the FDOT State Structures Design Office (superstructure and GRS) and George & Associates (roadway, drainage, utilities, and permitting). The placement of the FSB members and the finished bridge are shown in Figure 2.23 (a) and (b), respectively.



Figure 2.23: (a) Placement of FSBs adjacent to each other and (b) finished pilot project SR-373 [16]

As of now, the FSB system is limited to 12-, 15-, and 18-inch beam depths spanning between 30 and 60 feet. There is also a required minimum 6-inch CIP topping made of conventional concrete.

2.2.5.4. Challenges

There were a few lessons learned in the previously mentioned pilot project. The skewness was one hassle for the construction stage. Damage was seen at the corners of the larger length of the members (due to its reduced stiffness). A lower skew angle was recommended for future projects [16]. Additionally, backer rods between the beam joints were improperly sized and resulted in some of the concrete leaking between the adjacent members during casting of the CIP deck. Finally, the manufacturer of the tie bars suggested decreasing the size of the hoop bars in the joint pockets between members to #5 bars (from the #6 bars used in the pilot project). There are no other reported issues, but this may be a result of it only being recently released for use.

2.3. LONGITUDINAL AND TRANSVERSE JOINTS

The increased use of prefabricated bridge elements has caused joints to become a greater area of interest. Joint regions have traditionally been the weakest link in the bridge structure and thus dictate the strength and durability performance of a bridge. Joints must be designed to restrict vertical movement between members and suitably transfer forces due to traffic loads between adjacent members. A joint region (transverse or longitudinal) experiences two types of forces under these traffic loads:

1. **Vertical Shear Forces:** These forces attempt to break the bond between the filling material (grout, epoxy, ultra high-performance concrete, etc.) and the adjacent concrete elements.

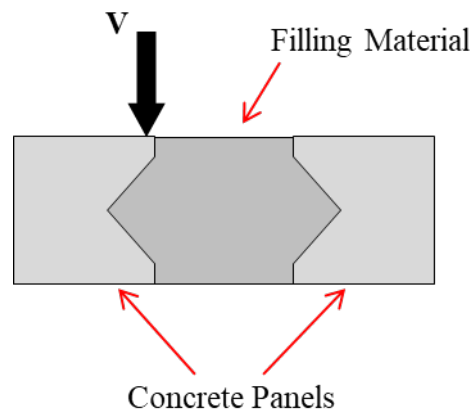


Figure 2.24: Shear force at joint

2. **Bending Moments:** A bending moment that engages compression in the top half of the joint and tension in the bottom half. Some type of reinforcement is required to carry these developed tension stresses in the joint.

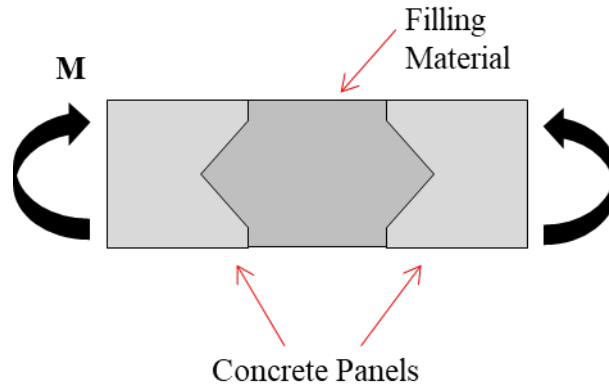


Figure 2.25: Bending moment at joint

Each of the short-span bridge solutions described in §2.2 required the use of some type of transverse or longitudinal joint between members to carry the vertical shear forces and bending moments. This section will introduce some of these typical joint details. The overview will start with non-UHPC connection details (including conventional concrete, grout, transverse post-tensioned, etc.) and move to UHPC connection details. The most common non-UHPC and UHPC connection details are provided in Figure 2.26 (a) and (b), respectively.

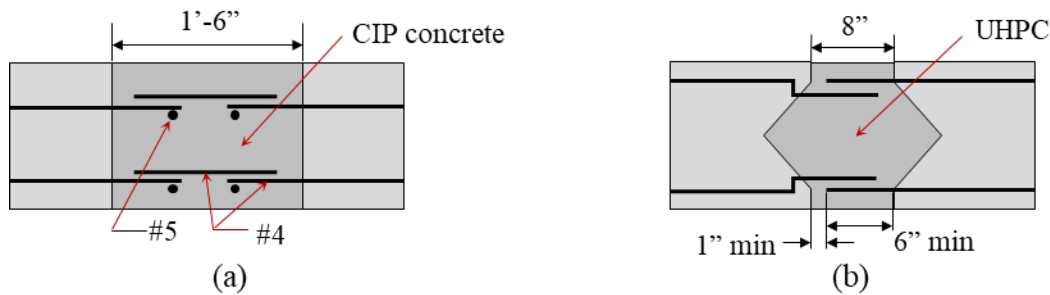


Figure 2.26: (a) Most common non-UHPC connection detail (Adapted from Biswas [21]) and (b) most common UHPC connection detail (adapted from Graybeal [22])

The goal of this summary is not to report on all the types of connections between precast bridge superstructure elements, but to show a sample of the most used details in US bridges. Special attention will be paid to both non-UHPC and UHPC joint details that connect prefabricated elements including full-depth precast concrete deck panels, members with precast full-depth decks (e.g., decked bulb-Ts), adjacent box beams, and other similar details. Other joints (e.g., between columns and bent caps) will not be covered in this section.

2.3.1. Non-UHPC Joints

Prior to UHPC there were several commonly used details utilizing conventional concrete, grout, and even mechanical features like transverse post-tensioning. Some of the more common non-UHPC details will be covered in this section.

2.3.1.1. Non-Post-Tensioned Joint Details

Non-post-tensioned (non-PT) joints were the first put in use in both new and rehabilitated bridges with precast panels primarily due to their low cost and constructability (when compared to similar post-tensioned details). An example of a standard non-PT joint detail is shown in Figure 2.26 (a), from the Pintala Creek Bridge built by the Montgomery County Commission from Alabama in 1973. The detail involved straight #4 reinforcing bars spliced in an 18-inch-wide joint with #5 reinforcing bars placed parallel to the joint providing confinement. The connection region was filled later with CIP concrete.

Later non-PT connection details involved the use of either headed reinforcing bars or hooked bars; these details were primarily used to connect precast panels. The use of headed or hooked reinforcement decreases the development length, which allows for decreased joint widths and overall improvement in the joint region behavior [21].

Non-PT joints are also utilized in the several slab-beam designs that were discussed above (e.g., Poutre-Dalle System, inverted-T beam system used by Virginia DOT, and the Florida Slab Beam). Typically, these sections serve as the formwork for a CIP deck. The CIP deck then serves as both the deck and the agent to join the adjacent beams together. Sample details for the joint regions of three such members are shown in Figure 2.27.

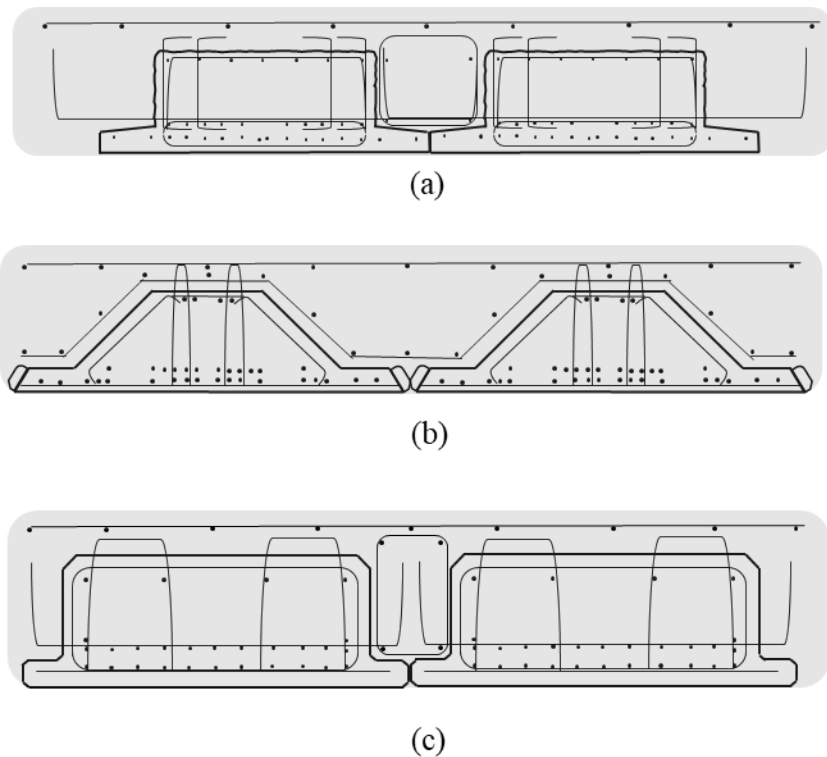


Figure 2.27: Sample joint details for (a) PCSS (Minnesota), (b) inverted-T (Virginia), and (c) Florida slab beam (FSB) (Florida)

2.3.1.2. Post-Tensioned Joint Details

Another popular non-UHPC joint is constructed using transverse post-tensioning. Post-tensioning bridge deck joints helps to have better structural performance and ensures the correct distribution of live loads. Post-tensioning of adjacent members and precast panels has been used since the 1970s. The Big Blue River Bridge over Indiana State Road 140 (near Knightstown, IN) has panels that were transversely pretensioned in the longitudinal direction. Also, the Bean Blossom Creek Bridge on Indiana State Road 37 (near Bloomington, IN) used the same method for the replacement of deteriorating deck panels. These connections have performed well, although there have been partial failures of some of the joints at slab-to-slab interfaces.

Most of the joint details for these post-tensioned joints are like that shown in Figure 2.28, which is from the Amsterdam Interchange Bridge in New York City (built in 1973). Here precast deck panels were conventionally reinforced. The joint was then cast using one part epoxy to two parts of sand to provide a flowable mixture [21].

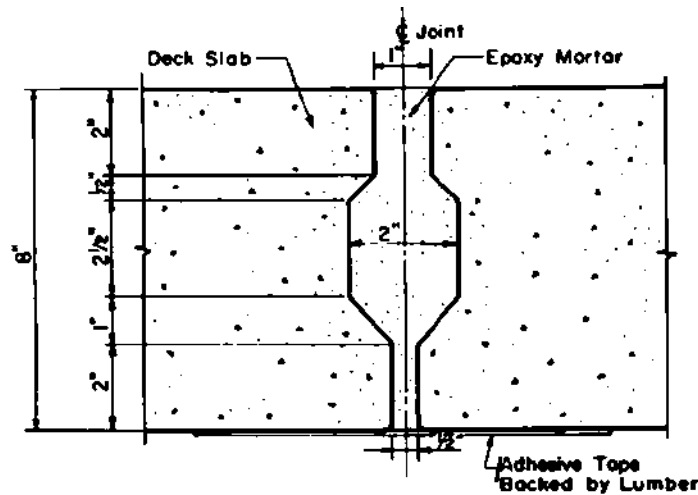


Figure 2.28: Transverse joint between precast slabs [21]

Post-tensioned joints have also been used to connect adjacent box beam superstructures. These systems have typically not performed well, as discussed in §2.2.1.

2.3.1.3. Mechanical Connectors

There are several different types of mechanical connectors that have been designed and implemented. Mechanical connectors are required for carrying tensile loads between the girders because of shrinkage and torsional effects and because of shear due to differential camber between girders. Two examples are shown in Figure 2.29: the Washington DOT's standard mechanical connection detail [23] and the grouted HSS connection detail from NCHRP Report 584 [24].

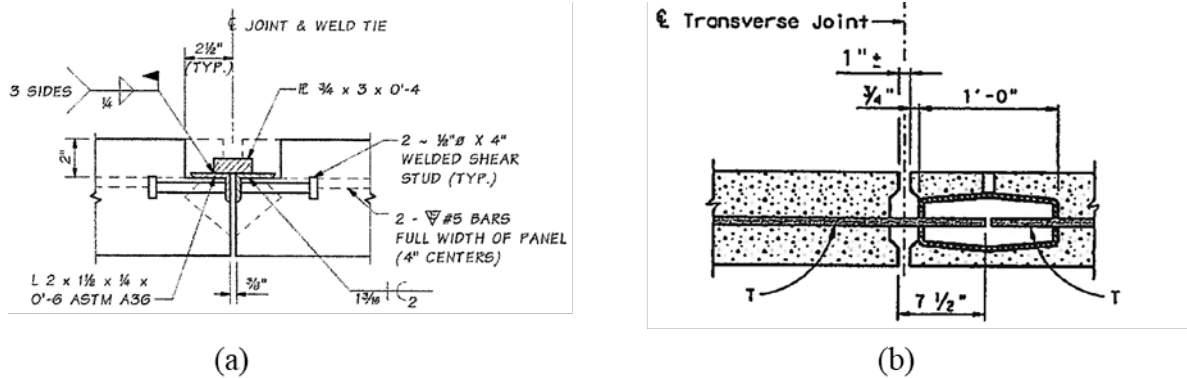


Figure 2.29: Two types of mechanical connectors: (a) welded connection detail [23] and (b) grouted HSS pocket connection [24]

2.3.1.4. Field Performance and Observations

Non-UHPC joints can offer satisfactory performance if they are designed and detailed properly. Most non-PT non-UHPC joint details require large amounts of reinforcement protruding from the precast members. This reinforcement is oftentimes challenging to place, which will result in higher labor costs. Additionally, many of the details described above require the placement of additional reinforcement in the joint, both transverse (to aid in development lengths) and longitudinal (to improve confinement), as shown in Figure 2.30 (a). In some details, reinforcement bars were required to be threaded through 180-degree hooks, as shown in Figure 2.30 (b). Simpler non-UHPC joint details (in terms of reinforcement) require PT, which is also labor intensive.



Figure 2.30: Additional reinforcement required in (a) transverse direction [25] and (b) extending from side of members [26]

Many of these joints do lead to cracking along the joint boundaries. These cracks can lead to water intrusion and affect the long-term performance of the connection detail. This cracking can be exacerbated if there are poor construction practices. One example of this is the Harriman Interchange Ramp (New York) in which the contractor used an epoxy mortar of unsatisfactory quality at some joint locations with evidence of improper proportioning.

2.3.1.5. Summary

There are many different types of non-UHPC joint details that both require and do not require the use of post tensioning. Non-PT joints generally require large amounts of reinforcement both at the precast plant and at the bridge site. These joints also often require inclusion of at least a partial-depth CIP deck included in the deck cast. Post-tensioned, non-UHPC joints are also used in many applications, but require the extra labor costs and constructability issues associated with field post-tensioning.

2.3.2. UHPC Joints

Transverse deck cracking often present in the joints discussed above has led to the development of alternate joint details utilizing higher performance materials (e.g., UHPC). Two such joint details are shown in Figure 2.31.

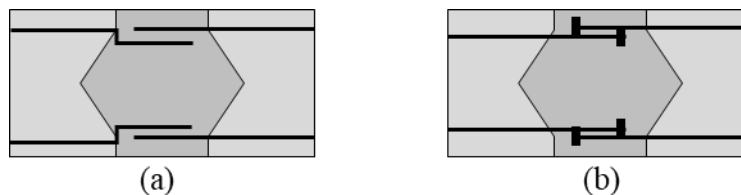


Figure 2.31: UHPC joint connection examples adapted from: (a) Royce [27] and (b) Aaleti and Sritharan [28]

UHPC has been utilized in many different applications since the mid-1990s in Europe. While UHPC is used in many different applications (e.g., overlays, full bridge elements, joints, etc.), the focus of this section will be on uses of UHPC in joints between adjacent elements or precast deck panels. This material has enabled significant simplification in the design of field-cast connections and allowed easy field assembly of prefabricated bridge components.

2.3.2.1. Graybeal [29]

Graybeal et al. [29] developed a joint detail to be used between adjacent box beams, with the objective of enhancing the performance of the longitudinal connection detail. The concept was dependent on the use of UHPC. Details for the developed joint are shown in Figure 2.32.

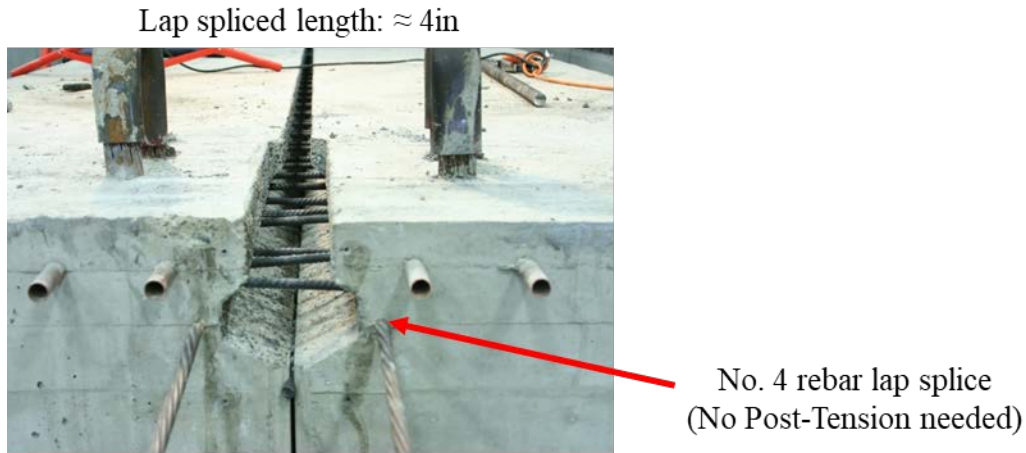


Figure 2.32: Joint developed by FHWA [29]

Before the development of the UHPC connection, there were two primarily used female-to-female connection details used to connect adjacent members, as shown in Figure 2.33 (a). Both options required the use of transverse post-tensioning (as discussed above). Graybeal [29] developed a simpler joint detail using UHPC that required no transverse post-tensioning, shown in Figure 2.33 (b).

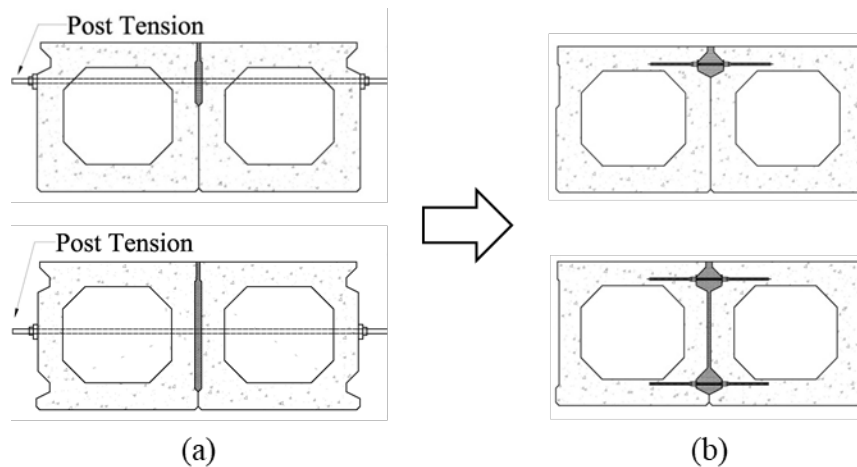


Figure 2.33: (a) Traditional solution with post-tensioning and (b) UHPC connection solution without post-tensioning [29]

These joint details were developed through an extensive experimental program involving both small-scale testing (focused on the joint development) and full-scale testing (focused on the performance of the joint detail in two adjacent girders). Two of the full-scale configurations used in the experimental program are shown in Figure 2.34. The current shear key configuration utilizing conventional grout materials and transverse post-tensioning tendons, shown in Figure 2.34 (a), was used to develop a baseline performance to start as a comparison point for testing. The developed UHPC connection detail, shown in Figure 2.34 (b), required the use of #4 reinforcement extended 5.5 inches into the joint, which provided a 4-inch splice length. The surface was prepared by using a retarding agent on the formwork and then sandblasting the

surface; this created an exposed aggregate finish in the joint and improved the bond performance.



Figure 2.34: (a) Conventional shear key specimen and (b) UHPC shear key specimen [29]

Two different loading protocols were used in the full-scale experimental program: (1) simply supported and (2) simply supported with restrained deflections on one specimen at midspan. Neither of the loading protocols were able to create distress in the connection region for the UHPC connection details. To see the post-cracking behavior of the joint detail, cracking of the joint was caused by placing a transverse load on the girders, as shown in Figure 2.35.

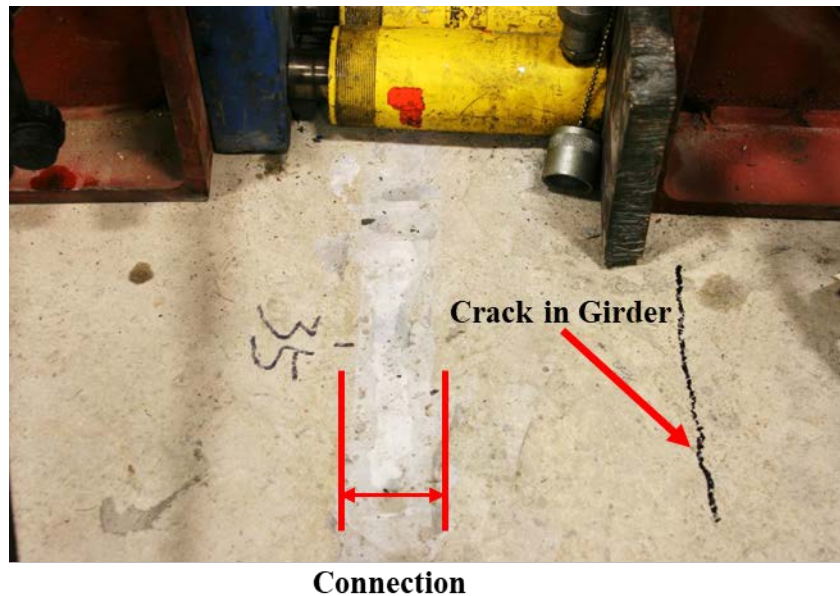


Figure 2.35: Forced cracking [29]

Graybeal [29] found that the transverse PT did not prevent crack propagation after initiation. They found that the UHPC connections, on the other hand, performed well and created a robust joint region.

Because of the positive results of the FHWA testing, several bridges have been constructed using the proposed UHPC joint detail. One example is the Sollars Road Bridge built in Fayette County (Ohio). The Sollars Road Bridge consists of seven adjacent precast, prestressed box beams, shown in Figure 2.36. The bridge was constructed without any transverse post-tensioning and

without any composite deck, relying fully on the UHPC joints for compatibility and load transfer between members. The use of these joints with the prefabricated box beams allowed the construction project to be completed quickly, with construction starting on May 28th and the bridge being opened to traffic on August 13th (both of 2014). Details of the joint region used in this project are shown in Figure 2.37.

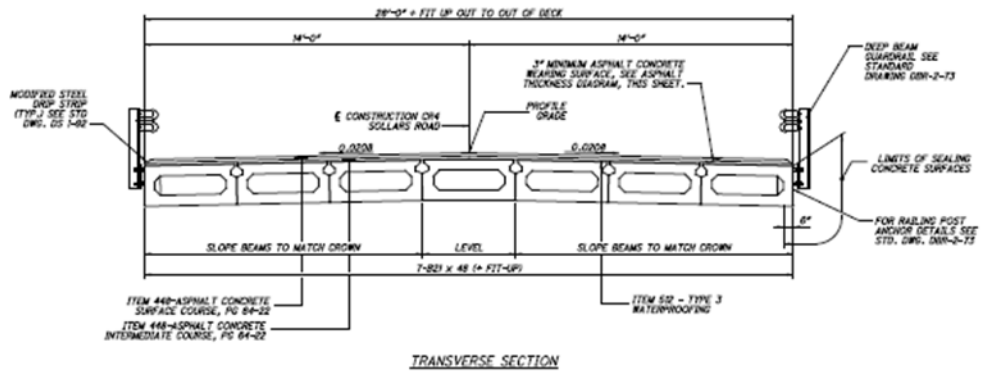


Figure 2.36: Sollars Road Bridge cross-section [29]

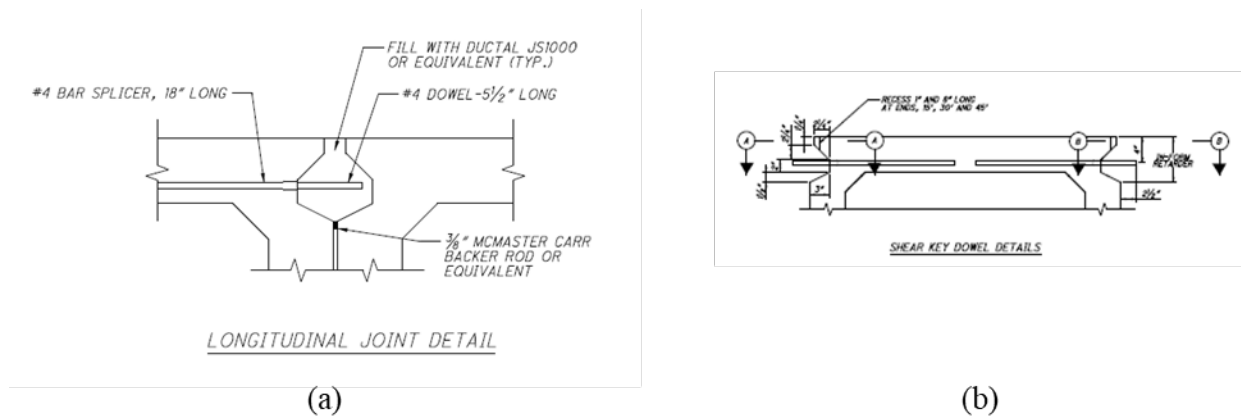


Figure 2.37: (a) Longitudinal joint detail and (b) shear key dowel detail [29]

To facilitate the use of UHPC joints and summarize the results of the work done by the FHWA, Graybeal [22] released a technical note on UHPC bridge connections. The note includes details for several different types of connections as well as the properties of several different available UHPC materials. Some of the developed details are shown in Figure 2.38.

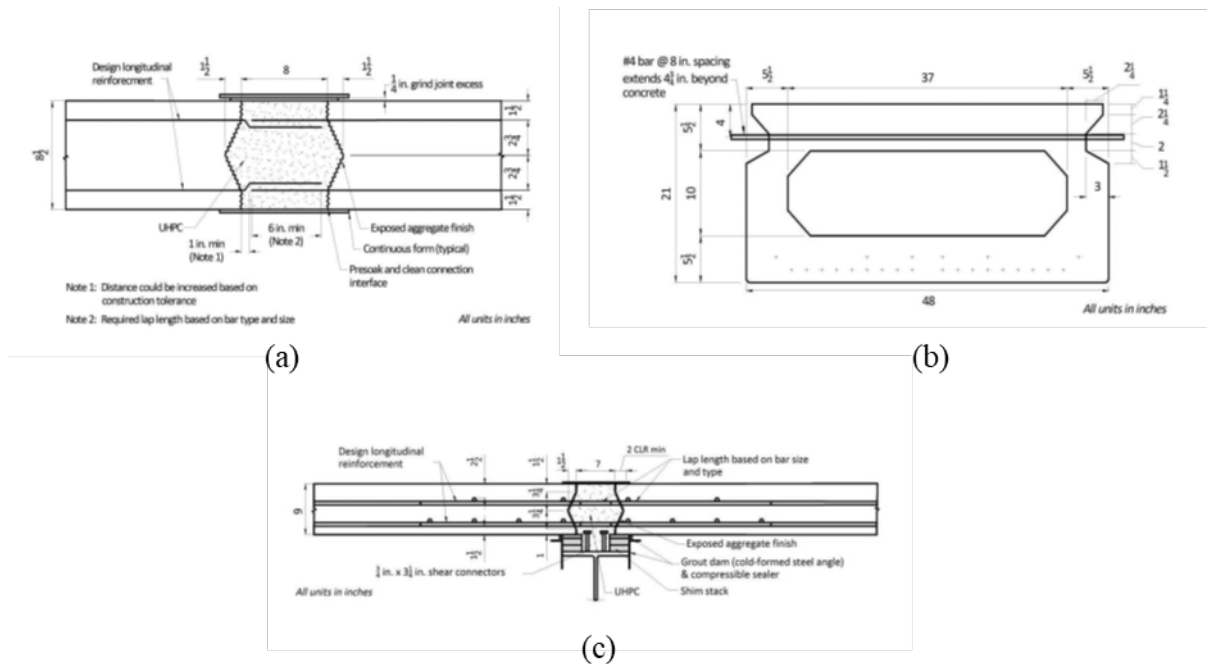


Figure 2.38: (a) UHPC connection between precast deck panels as deployed by NYSDOT on CR-47 over Trout Brook, (b) UHPC adjacent box beam connection detail, and (c) combined UHPC deck-level and composite connections as deployed by NYSDOT on I-81 near Syracuse, NY [22]

2.3.2.2. Aaleti and Sritharan [28]

Another UHPC joint detail recently developed was to connect full-depth, precast, UHPC waffle-deck panels [28]. The details of this joint region are shown in Figure 2.39.

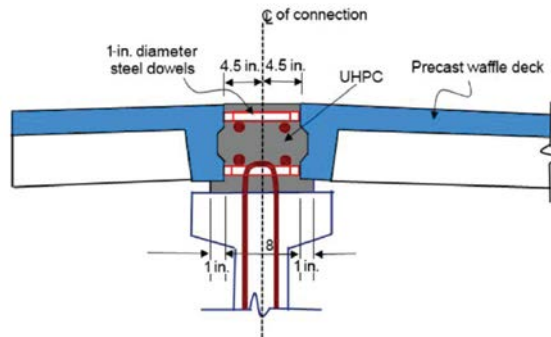


Figure 2.39: Panel-to-panel and panel-to-girder connection [28]

This UHPC joint detail was developed through a full-scale experimental program involving the testing (with service, ultimate, and fatigue loads) of adjacent panels connected using several different UHPC joint details, as shown in Figure 2.40. Two different joint geometries were tested with four different reinforcement details. A joint geometry like that developed by Graybeal et al. [22], introduced above, was used with straight headed reinforcement, hairpin reinforcement, and straight reinforcement. A shallower joint that was self-forming and only used one layer of reinforcement was also tested.

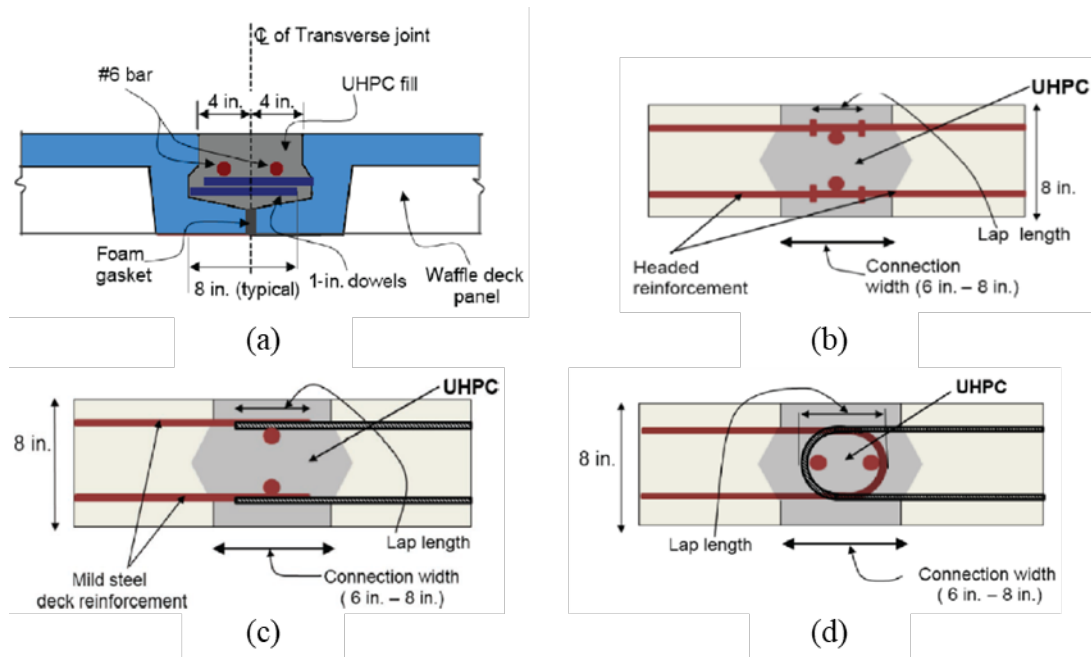


Figure 2.40: Common panel-to-panel UHPC connection details: (a) waffle deck panel-to-panel connection detail, (b) panel-to-panel headed connection detail, (c) panel-to-panel straight connection detail, and (d) panel-to-panel hairpin reinforcement [28]

The results of these tests led to the final joint geometry and reinforcement configuration shown in Figure 2.39. The main feature of this joint are straight dowel bars extending from the panels, shear hooks extending from the girder, longitudinal reinforcement running along the length of the joint, and UHPC to finish the joint.

This UHPC joint detail was used in the Little Cedar Creek Bridge (Wapello County, Iowa) as part of the FHWA Highways for LIFE program. The UHPC joint detail was used in both the transverse and longitudinal directions to connect the waffle slab panels, as shown in Figure 2.41.

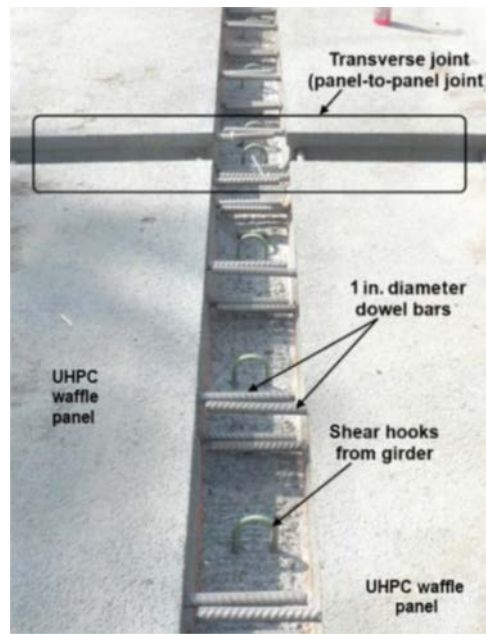


Figure 2.41: Shear key connection in Wapello County Bridge [28]

Other state DOTs have expressed interest in UHPC waffle deck components and the developed joint detail for aging bridge replacements.

2.3.2.3. Field Performance and Observations

The bridge industry is becoming more interested in the use of prefabricated bridge components designed to incorporate UHPC joint details as they both accelerate construction and are thought to improve long-term durability. While there is a fair amount of research on joint details and some durability testing of UHPC materials, the use of UHPC joints in field applications is too recent to be able to gain any true insights on long-term performance. The use of UHPC joints has been shown to ease and accelerate construction, as many of the details require no reinforcement be placed at the construction site.

2.4. JOINT MATERIALS

There are several different types of materials that are utilized in the joint regions described above. Each joint material has its own composition and properties that make it better suited for certain applications. Some of the primary materials that are used in these joints are: conventional concrete, self-consolidating concrete, cementitious grout, and UHPC.

2.4.1. Non-UHPC Materials

Many different non-UHPC materials are used in joint regions: conventional concrete, self-consolidating concrete, and cementitious grout are the primary three. Conventional and self-consolidating concretes are typically used in non-PT connections, with either a wide joint region with large amounts of reinforcement or in situations where the joint is cast with a CIP deck. Conventional and self-consolidating concretes are non-proprietary, although some of their components are proprietary products (e.g., some admixtures or supplementary cementitious materials).

Cementitious grout is the material typically used in the shear pockets of joints with transverse post-tensioning. While conventional and self-consolidating concretes are non-proprietary, grouts are normally proprietary and come in prepackaged bags, and they can be used in these joints for several reasons [30]:

- Relatively high strength at young age
- Minimal shrinkage deformation
- Low permeability
- Increased bonding capabilities with hardened concrete surfaces

The following table, Table 2.4 and Table 2.5, describe some of the commercial and non-commercial grout products.

Table 2.4: Commercial grout materials [30]

Name	Characteristics
<i>SET-45</i>	It is a one-component concrete repair and anchoring material, which sets in 15 minutes approximately. For use in ambient temperatures below 85° F (29° C).
<i>SET-45 Hot Weather (HW)</i>	Same one-component concrete repair and anchoring material with same setting time. For use in ambient temperatures below 85-100°F (29-38°C).
<i>SET GROUT</i>	Natural aggregate non-shrink grout: Portland cement-based product, non-catalyzed, multi-purpose construction grout containing mineral aggregate.
<i>EMACO 2020</i>	It is a methyl methacrylate (MMA), polymer concrete system designed for the protection and rehabilitation of horizontal, formed vertical or overhead concrete surfaces. It consists of three parts denominated A, B, and C, for binder, aggregate and initiator, respectively.
<i>EMACO 2041</i>	Bonding agent for EMACO 2020: It is a one-component, moisture-tolerant acrylic bonding agent applied to concrete or steel prior to the placement of EMACO 2020.

Table 2.5: Non-commercial grout materials [30]

Name	Characteristics
<i>Hydraulic Cement Concrete (HCC)</i>	This mix was used on some bridges built prior 1972. It has a minimum concrete strength of 4,000 psi (27.6 MPa), relatively high slump (about 6 in), and maximum aggregate size of ½ in.
<i>Latex Modified Concrete (LMC)</i>	It consists of a latex emulsion added to an HCC mix. The latex forms a thin film on the aggregate surface, which enhances the bond between the past and the aggregate and results in high compressive strength and less permeable concrete mix.
<i>Type K-Cement Concrete Mix</i>	This concrete mix has a specified concrete strength of 4,000 psi (27.6 MPa), and only cement type K is used in the mix. The concrete has no fly ash, and the maximum aggregate size is 3/8 in. Type K cement is an expansive cement that contains anhydrous calcium aluminate, which being mixed with water forms a paste that during the early hydrating period occurring after setting, increases in volume significantly more than does portland cement paste.

2.4.2. UHPC Materials

UHPC is a cementitious composite material first developed in the 1990s and commercially available in the US since the early 2000s. It is typically acquired from a merchant in three separate components: a pre-bagged cementitious powder, chemical admixtures, and steel fiber reinforcement. Water is the last ingredient added at the construction site. Afterwards, the mixture is placed into the formwork using standard construction equipment.

This material is known for its superior performance such as high compressive strength (above 18 ksi), long-term durability, low permeability, high usable tensile strength, strain hardening response, and low water-to-cement ratio (compared to conventional concrete). The typical composition of UHPC is presented in Table 2.6. Current compressive and tensile behavior are shown in Figure 2.42. Typical field-cast properties are shown in Table 2.7.

Table 2.6: Typical composition of UHPC [31]

Component	Amount	% by Weight
Portland Cement	1200 lb/yd ³	28.5
Silica Fume	390 lb/yd ³	9.3
Fine Sand	1720 lb/yd ³	41.0
Ground Quartz	355 lb/yd ³	8.5
Superplasticizer	51 lb/yd ³	1.2
Water	218 lb/yd ³	5.2
Steel Fibers	263 lb/yd ³	6.3

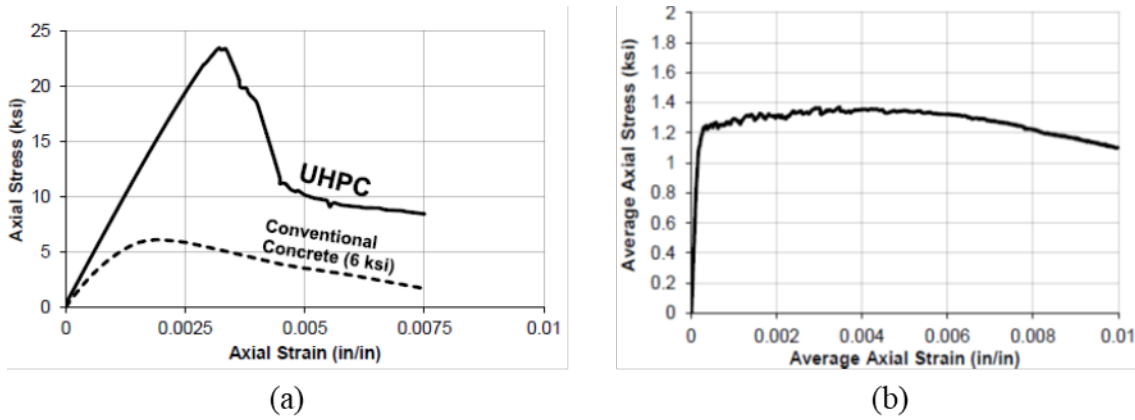


Figure 2.42: (a) Compressive UHPC behavior and (b) Tensile UHPC behavior [31]

Table 2.7: Typical field-cast UHPC material properties [22]

Material Characteristic	Average Result
Density	155 lb/ft ³
Compressive strength (ASTM C39, 28-day)	24 ksi
Modulus of elasticity (ASTM C469, 28 day)	7,000 ksi
Direct tension cracking strength (uniaxial tension with multiple cracking)	1.2 ksi
Split cylinder cracking strength (ASTM C496)	1.3 ksi
Prism flexure cracking strength (ASTM C1018, 12-inch span)	1.3 ksi
Tensile strain capacity before crack localization and fiber debonding	> 0.003
Long-term creep coefficient (ASTM C512; 11.2 ksi load)	0.78
Long-term shrinkage (ASTM C157; initial reading after set)	555 microstrain
Total shrinkage (embedded vibrating wire gauge)	790 microstrain
Coefficient of thermal expansion (AASHTO T259; 0.5-inch depth)	8.2×10^{-6} in./in./°F
Chloride ion penetrability (ASTM C1202, 28-day test)	360 coulombs
Chloride ion permeability (AASHTO T259; 0.5-inch depth)	< 0.10 lb/yd ³
Scaling resistance (ASTM C672)	No scaling
Abrasion resistance (ASTM C944 2x weight; ground surface)	0.026 oz. lost
Freeze-thaw resistance (ASTM C 666A; 600 cycles)	RDM = 99 percent
Alkali-silica reaction (ASTM C1260; tested for 28 days)	Innocuous

2.4.2.1. Proprietary UHPC Materials

There are several commercially available UHPC materials in the US. The following list of proprietary UHPCs have been shown to align with the needs of typical UHPC joint projects [22]:

- BCV[®] (Beton Composite Vicat produced by VICAT)
- BSI[®] (Beton Special Industriel produced by EIFFAGE)

- Cor-tuf[®] (produced by The US Army Corps of Engineers – Engineer Research and Development Center)
- CRC[®] (Compact Reinforced Composite by Hi-Con)
- Densit[®] (produced by Densit Aps)
- Ductal[®] (produced by Lafarge Holcom)

Lafarge Holcom (producer of Ductal[®]) has developed a proprietary UHPC mixture specifically for joint solutions. The product is called Ductal[®] JS1000 and is advertised as a field-cast joint fill solution for precast deck panel bridges. The main components of this Ductal[®] JS1000 mixture are:

- **Premixture:** Silica fume ground quartz, sand, and cement
- **High tensile steel fibers:** 0.2 mm (0.008 in.) diameter x 14 mm (0.5 in.) long (>2000 MPa [290 psi]).
- **Admixture:** High range water reducer (3rd generation of their formulation)
- **Water and/or ice**

These proprietary UHPC materials are expensive but offer more consistent wet and hardened properties than can normally be achieved with locally available materials.

2.4.2.2. *Non-Proprietary UHPC Materials*

Due to the high cost of the proprietary UHPC products and limitations that have been presented with “buy America” contract clauses, many states have conducted research to develop non-proprietary UHPC mixtures. Typical ranges for the mixture proportions for these non-proprietary UHPC mixtures are shown in Table 2.8; these values are the ranges of four different non-proprietary UHPC mixtures summarized by Graybeal [32].

Table 2.8: Typical ranges of UHPC non-proprietary mixtures with fine aggregates (not including steel fibers) (based on data from Graybeal [32])

Component	Typical Range
<i>White Cement (lb/yd³)</i>	1248 to 1311
<i>Silica Fume (lb/yd³)</i>	312 to 328
<i>Fly Ash (lb/yd³)</i>	303 to 318
<i>HRWR (lb/yd³)</i>	45 to 48
<i>Fine Aggregate (lb/yd³)</i>	1871 to 1966
<i>Aggregate-to-cement ratio</i>	1.5
<i>w/cm ratio</i>	0.23 to 0.24
<i>Spread (inch)</i>	10.4 to 12.4
<i>Avg. Compressive Strength at 28 days (ksi)</i>	23.5 to 29.0
<i>Cost (\$/yd³)</i>	472 to 652

Graybeal [32] also investigated the cost of each of the components in the UHPC mixture, as shown in Table 2.9. He found that the steel fibers are by far the most expensive component of the UHPC mixture. The cost of the UHPC mixture is increased by about \$470 per cubic yard when 1.5-percent by volume of fiber reinforcement is added to the mixture.

Table 2.9: Cost of material per volume of low cost UHPC [32]

Material	Cost (\$/yd³)
<i>Portland Cement (II/V)</i>	73.66
<i>Silica Fume</i>	82.57
<i>Fly Ash</i>	7.54
<i>HRWR</i>	103.60
<i>Fine Aggregate</i>	12.82
<i>Fibers (1.5%)</i>	472.39
<i>Total</i>	751.59

2.4.3. UHPC Mixing and Casting Procedure

Mixing of UHPC materials is done slightly different than conventional concrete materials. The full casting procedure is shown in Figure 2.43. One of the main differences regarding mixing is that UHPC requires a large amount of shear energy to mix properly. This means that either a high-shear mixer must be used, or a long mixing time is required. The mixing time and energy required for UHPC is one of the major limitations of the material. After the UHPC is properly mixed, it behaves similarly to a self-consolidating concrete. The UHPC can be placed in one location and allowed to flow down the member and joint. It should be noted that fiber reinforcement will align in the direction of the flow, so care should be taken to ensure that fibers are correctly oriented for the application. Steam curing will improve early age strength, but top forming or moist curing will result in satisfactory behavior for most applications. Finally, the UHPC can be used as the riding surface but requires grinding if it is to be used without an asphalt overlay.

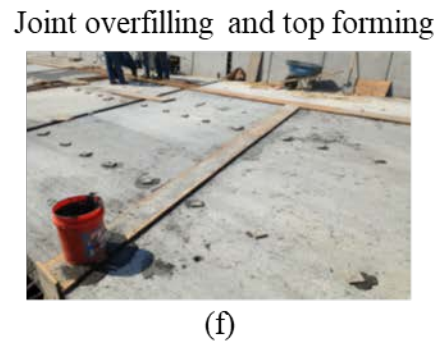
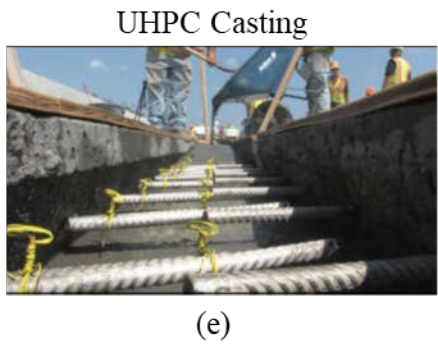
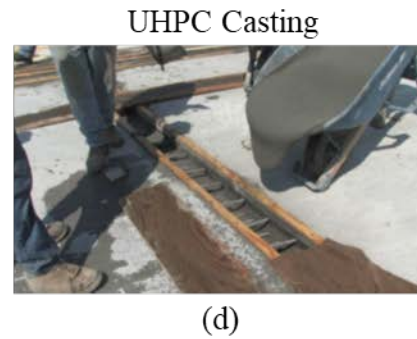
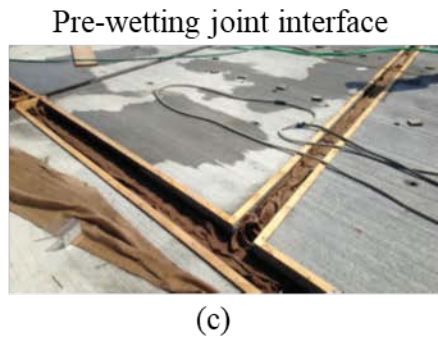
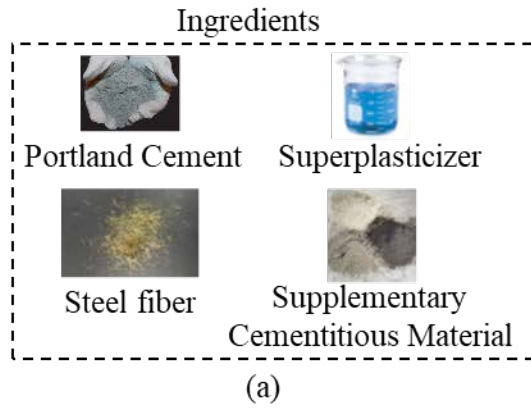


Figure 2.43: General procedure for mixing and casting UHPC [31]

2.5. OTHER UHPC BRIDGE SUPERSTRUCTURE APPLICATIONS

The benefits of UHPC have been extended to other applications in bridge superstructures. Two of these applications (as overlays and full members) will be briefly introduced in this section.

2.5.1. UHPC Overlays

Overlays made of UHPC are being used to rehabilitate decks of aging bridges. One example is the Chillon Viaduct near Lausanne (Switzerland), as shown in Figure 2.44. The deck was replaced with a CIP UHPC overlay in order to improve the durability of the riding surface and protect the existing structure underneath [33].

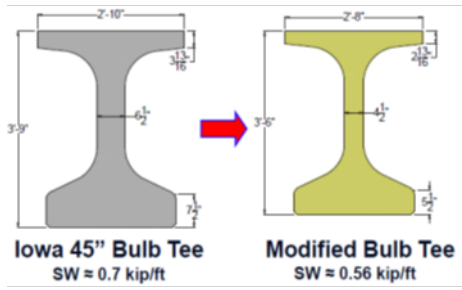


Figure 2.44: Cast-in-place UHPC overlay, immediately (a) before and (b) after placement [31]

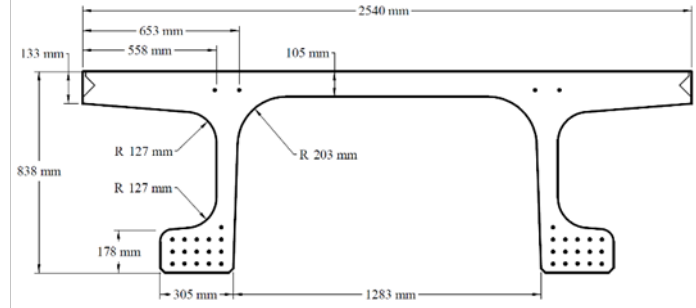
There have been many other research efforts looking into the use of UHPC for overlay applications, but it is not yet being widely used in field applications. There are still some concerns with the integrity of the UHPC with the remaining deck and with how existing corroded reinforcement behaves after being sealed by the material.

2.5.2. UHPC Members

UHPC has also been used in other bridge members such as deck panels ([28], [34]), piles [35], and bridge girders ([31], [36], [37]). The use of UHPC in these members allows for optimized section dimensions and decreased amounts of steel. For example, shear reinforcement in bridge girders has been eliminated in some applications. Two examples of UHPC girder sections are shown in Figure 2.45: The Mars Hill Bridge (Iowa) and the Jakway Park Bridge (Iowa). The use of UHPC in these projects allowed for lighter superstructures, which in turn decreased the loading on the substructure elements.



(a)



(b)

Figure 2.45: (a) Mars Hill Bridge girder comparison [31] and (b) Pi girder used in Jakway Park Bridge [37]

3. DEVELOPMENT OF FSB DESIGN STANDARD

3.1. INTRODUCTION

This chapter summarizes (1) the impact of eliminating the cast-in-place (CIP) deck from the FSB Design Standard on the feasible span lengths and (2) development of UHPC joint details that can be integrated into the FSB Design Standard.

3.2. FEASIBLE SPAN LENGTHS OF UNTOPPED SECTIONS

The FSB detail currently includes an 8-inch CIP composite deck, as shown in Figure 3.1. The CIP deck is used in these sections to connect adjacent members, but also provides additional depth, which adds capacity to the section.

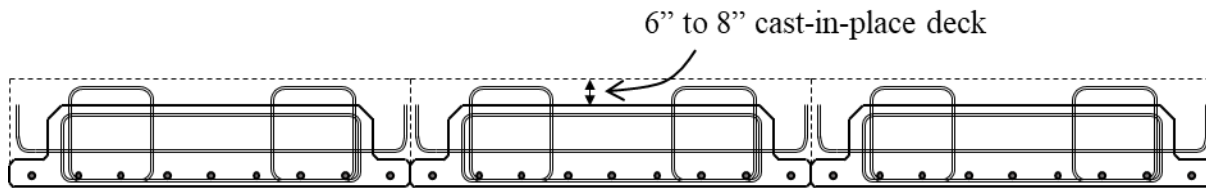


Figure 3.1: Typical FSB section with 6 to 8-inch CIP composite deck

The moment capacity was evaluated for several un-topped sections to determine the maximum allowable span lengths. The un-topped section was compared to the topped FSB section with the aid of a FDOT design sheet developed for standard FDOT bridge sections. The current FSB section was evaluated assuming a CIP deck thickness of 6 inches (topped) and 0 inches (un-topped), as shown in Figure 3.2. The primary effect of not including a CIP composite deck on the section is a decrease in the depth of the primary moment resisting reinforcement, which will decrease the overall moment capacity of the section.

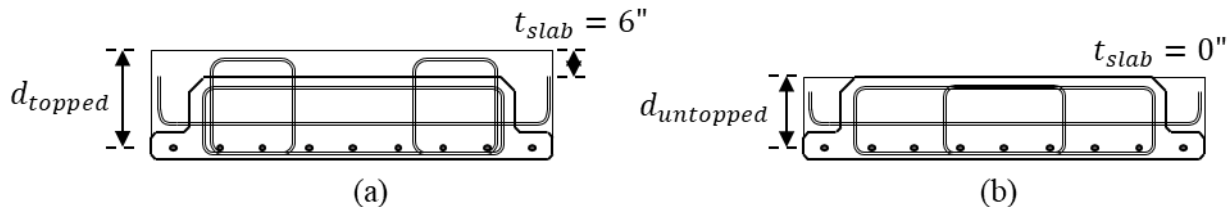


Figure 3.2: Difference between (a) depth of longitudinal steel in sections with CIP decks and (b) depth of steel in sections without CIP decks

The evaluation of the different span lengths for the parametric study was made using a typical two-lane bridge configuration. An FSB section with a 53-inch width was chosen for this bridge configuration with various section heights (12, 15, and 18 inches). All three sections were investigated with spans varying from 30 feet up to their longest possible span length. The horizontal layout of the two-lane typical bridge configuration used in the parametric study is shown in Figure 3.3. The parametric study was completed looking at FSB sections with a 6-inch-thick CIP deck (topped FSB) and without a deck (un-topped FSB).

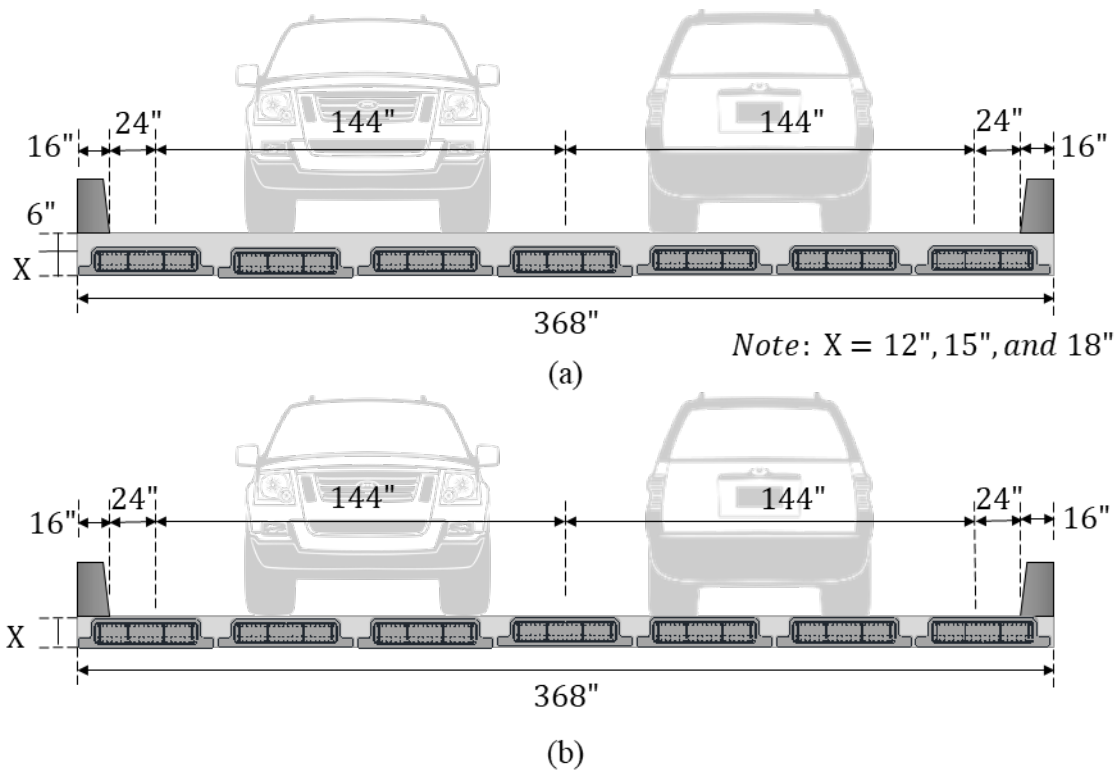


Figure 3.3: Cross-section of bridge composed of 53-inch-wide FSB section (a) with a CIP deck and (b) without a CIP deck used for parametric study

The remaining assumptions for the example bridge are found in Table 3.1.

Table 3.1: Analysis assumptions for parametric study

Assumptions for Parametric Study
• Exterior beam design
• Aggressive corrosive environment
• Beam concrete strength: 6.0 ksi (release) and 8.5 ksi (28 days)
• 0.6-inch diameter low-relaxation strand used
• No debonded or draped strands
• Topped section: 6-inch composite slab with $f'_c = 4$ ksi (28 days)
• Untopped section: 0.00001-inch composite slab with $f'_c = 4$ ksi (28 days) for slab and joint regions

Results from this analysis are summarized in Figure 3.4 and Table 3.2. A comparison between a topped (with a 6-inch CIP deck) and un-topped section that would yield similar total section depths is shown in Table 3.2; both designs would yield a total section depth of 18 inches. The un-topped section would offer both a greater maximum span length and a greater maximum capacity. This is a result of the un-topped section being composed entirely of the precast concrete

material with an ultimate strength of 8.5 ksi, compared to the 4 ksi ultimate compressive strength of the slab concrete.

Table 3.2: Maximum span lengths and corresponding flexural capacities for 53-inch-wide FSB topped and un-topped section with 18-inch total section depths

	Maximum Span Length	Maximum Capacity
FSB 12x53 (with CIP deck)	43 feet	901 k-in.
FSB 18x53 (w/o CIP deck)	55 feet	1,235 k-in

The FSB section with a 6-inch CIP deck has a maximum feasible design length of between 43 feet and 61 feet (depending on whether a 12-, 15-, or 18-inch-deep section is used). This can be compared to the un-topped section, which has a maximum feasible design length of between 32 feet and 55 feet with the same three section depths. Additionally, not including the CIP deck resulted in a decrease in nominal moment capacity of between 28-percent (for the 18-inch-deep section) and 48-percent (for the 12-inch-deep section).

According to the FDOT Structures Design Guidelines (SDG) [38], the camber in precast flat slab superstructures is required to be a minimum of 1/4-inch positive (upward) at the end of construction. This camber requirement controlled the design of the conventional, topped FSB sections. Stress limits controlled the design of the un-topped FSB sections. Other deflections and the ultimate moment capacity were sufficient in all designs.

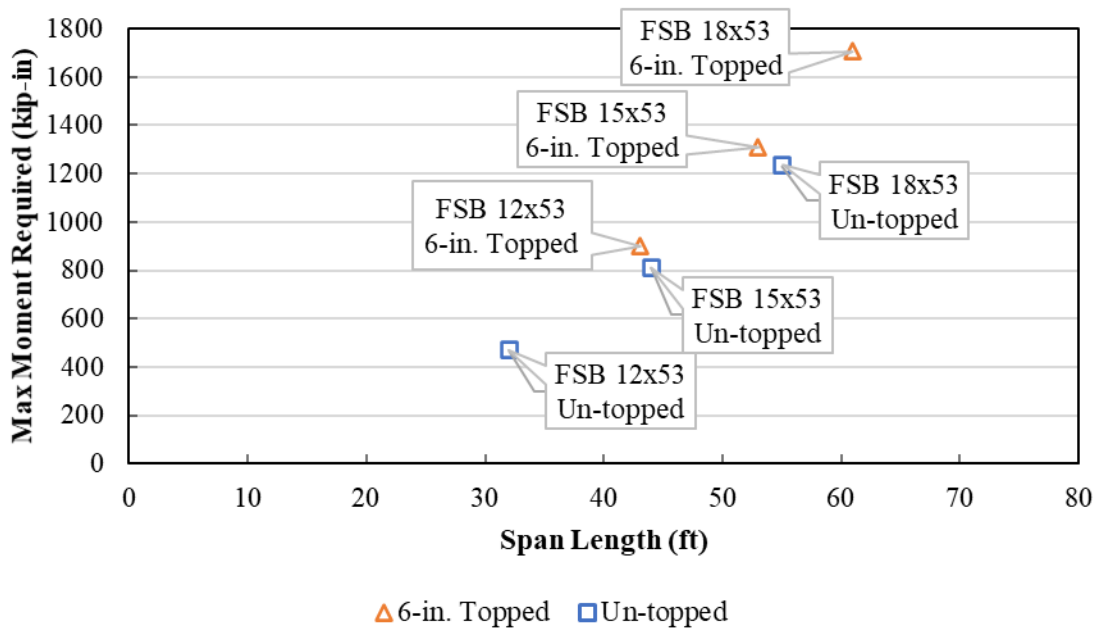


Figure 3.4: Maximum moment versus span length for topped and untopped FSB sections

The currently available depths for the FSB section are only recommended for spans of less than 55 feet if no CIP deck is included. Modifications to the section or use of alternative shapes to achieve longer spans were explored later in Chapter 4.

3.3. INTEGRATION OF JOINT DETAIL

There are several joint details that have been developed through extensive testing on adjacent members and precast, full-depth panels, as discussed in the previous chapter. The two joint details that were considered for integration in the modified FSB section are shown in Figure 3.5 and Figure 3.6. The general shape of the joint detail between box beam girders was used in the modified FSB shape. The two layers of steel used between adjacent full-depth precast deck panels was considered in connection of deeper modified FSB shapes.

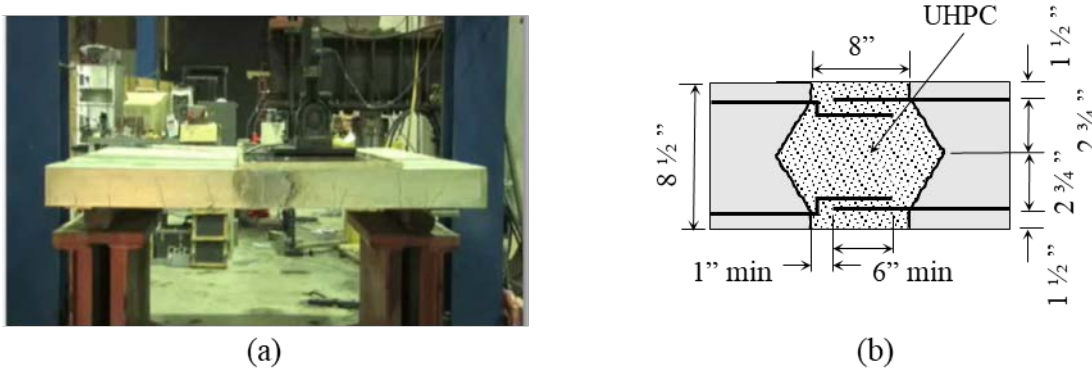


Figure 3.5: (a) Testing conducted on (b) joint detail between adjacent full-depth precast panels [39]

The joint detail between the adjacent box beam girders was used as the starting point for the modified FSB shape; the geometric details of this joint are shown in Figure 3.6. This joint type features one layer of #4 reinforcement that extends 4.75 inches beyond the edge of the concrete and embedded into the precast section 18 inches spaced at 8 inches. These bars are staggered or offset between beams for constructability purposes. A mechanical reinforcement splice connection is used at the precast section boundary to allow for solid formwork to be used without holes. The reinforcement extending into the joint region is installed after the forms are stripped using the mechanical splice.

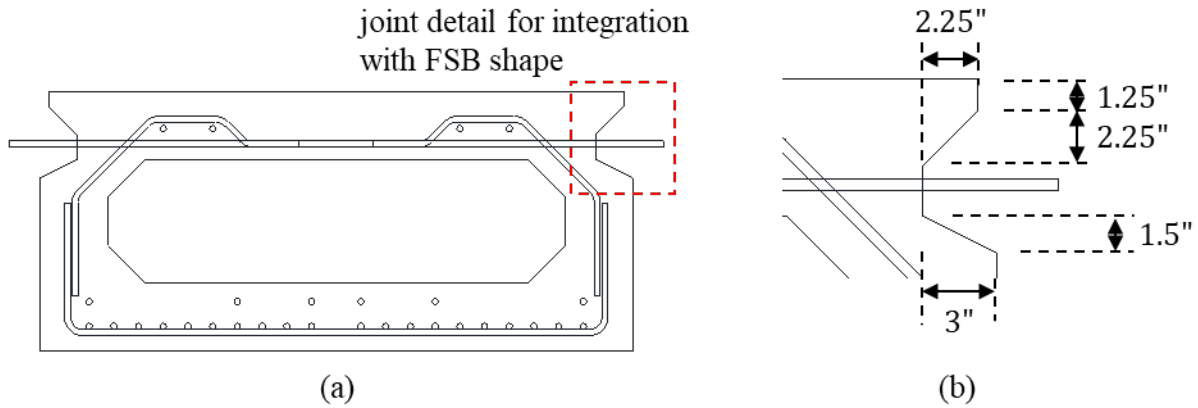


Figure 3.6: (a) Currently used joint detail for box-beams developed by Graybeal [40] and (b) dimensions of the joint region

The initially proposed shape integrates the abovementioned adjacent box beam detail with the current FSB cross section shape, as shown in Figure 3.7. By using the current FSB cross section shape as the starting point, steel formwork may be designed with inserts for both the current and modified FSB section. This would allow precast plants to better accommodate the construction of both designs.

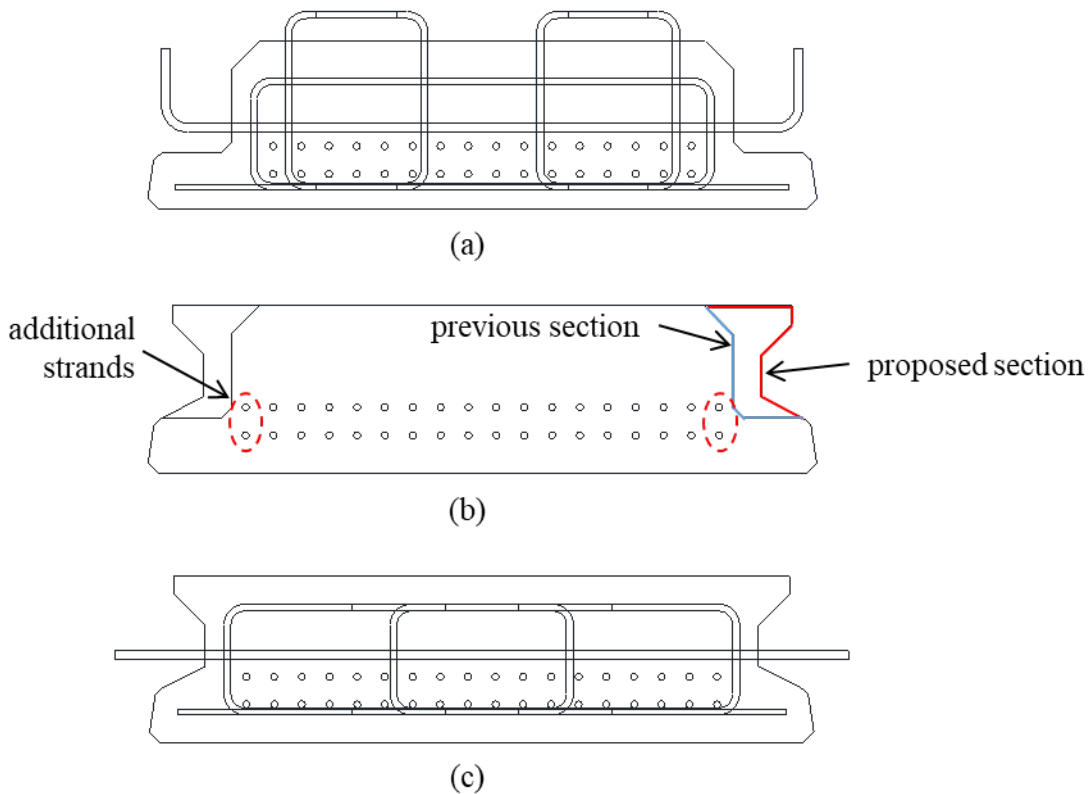


Figure 3.7: (a) Current 12-inch-deep FSB section, (b) proposed modification overlaid on original section, and (c) proposed new 12-inch-deep section with single layer of joint reinforcement

The modified FSB shape will also use the same bottom flange geometry as the current FSB section. Using the same bottom flange geometry will allow for contractors to use a similar construction procedure as has been used on current FSB bridges, as shown in Figure 3.8. Members can be first placed immediately adjacent to each other. Next, backer rods can be placed to seal the bottom of the joint. UHPC can then be cast to fill the joint region and connect adjacent members. An asphalt overlay can then be used to create the driving surface and account for any differential camber between members or overfill of the UHPC joints.

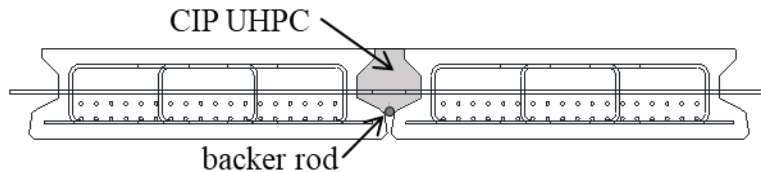


Figure 3.8: Construction of bridge with backer rods and CIP UHPC (like current FSB construction procedure).

The modified section can be used with the same three depths that are currently used for the FSB, as shown in Figure 3.9. The proposed section will use the same top and bottom geometry of the joint with a longer straight portion at mid-depth of the section. Another benefit of the modified section is the potential to add one more column of strands on each side of the section, as shown in Figure 3.7 (b).

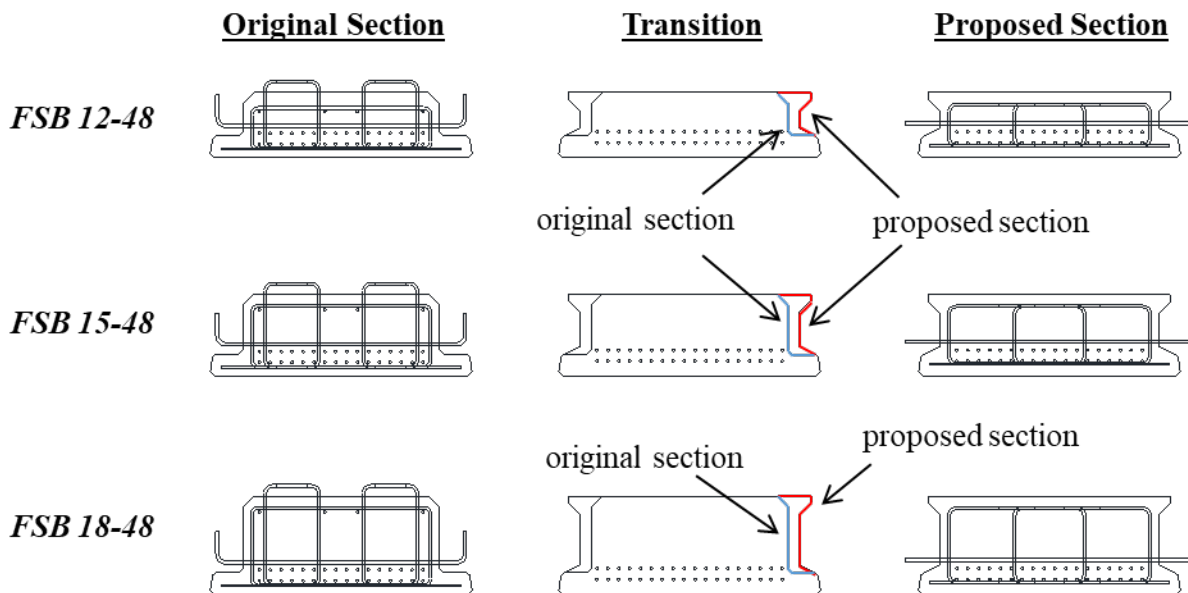


Figure 3.9: Original, transitional, and proposed sections for 12-, 15-, and 18-inch-deep FSB sections with 48-inch widths

One of the aspects of the detail that needs to be further considered is the need for two layers of joint reinforcement in the modified FSB section (as is typically used for adjacent precast deck panels [39]). This additional layer of steel in the joint region is shown next to a single layer of steel in Figure 3.10.

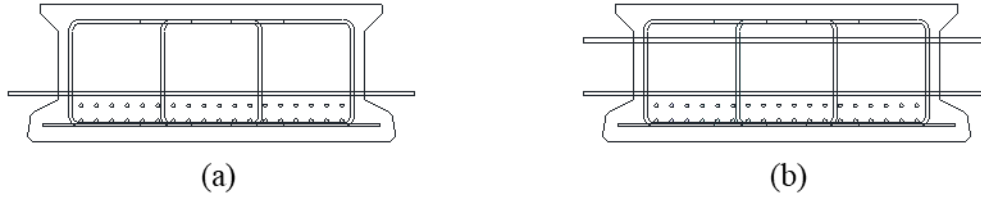


Figure 3.10: 18-inch-deep modified FSB section with (a) one layer and (b) two layers of joint reinforcement

In addition to the benefit of using a joint shape that has already been initially investigated, the modified joint detail will also allow for less UHPC to be used during the final construction and assembly of the bridge. The volume and approximate material cost for a standard two-span bridge with 55-foot-long spans and four lanes of traffic (total width of 84 feet) is shown in Table 3.3. The costs shown in this table are based on a list price for prebagged UHPC (\$2,500 per cubic yard), which is not necessarily the bid price that an owner would observe on a proposal. The actual price that an owner would observe would depend on the volume, the prime contractor markup, and the perceived risk (among other factors). This cost can range from \$3,000 to more than \$8,000 per cubic yard. Using the modified FSB section uses up to 71-percent less material than the current FSB section shape.

Table 3.3: Approximate UHPC volume required and material cost for two-span, 110-foot total length, 84-foot-wide bridge

Section Depth (in.)	Current Joint		Modified Shape		Percent Difference
	Volume (yd ³)	Material Cost (\$)	Volume (yd ³)	Material Cost (\$)	
12	51.0	\$127,500	15.0	\$37,500	71%
15	69.3	\$173,250	24.2	\$60,500	65%
18	87.7	\$219,250	33.4	\$83,500	62%

An additional two joint details were proposed by FDOT engineers, as shown in Figure 3.11, to simplify the joint detail. These joint details are based on the current FSB section with a slightly reduced joint width (Option 1) and with a reduced joint width and ledge depth (Option 2). Option 2 (with its shallower bottom ledge depth) allows for the joint reinforcement to be placed lower in the section, as shown in Figure 3.11.

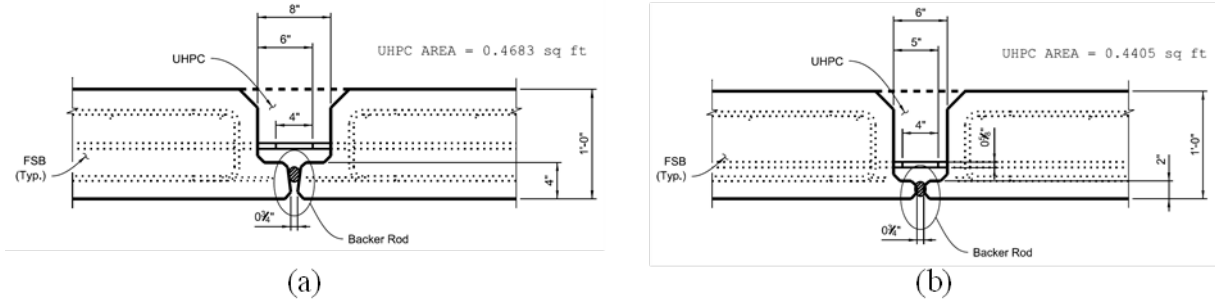


Figure 3.11: Proposed options by FDOT engineers: (a) Option 1 and (b) Option 2

Analyses were performed on these joint details using 12- and 18-inch section depths.

3.4. ANALYTICAL EVALUATION OF JOINT DETAIL – METHODS

3.4.1. Background

The analytical investigation was completed using a finite element modeling (FEM) software specifically tailored for reinforced concrete modeling applications, ATENA. An overview of the model details and the loading protocol selected for these initial models will be the focus of this section.

3.4.2. Model Geometry

Eight different models were created during this initial investigation. The first model (Case 1) created was the existing FSB section with the current joint geometry and reinforcement, as shown in Figure 3.12. The initial model was of a 12-inch-deep standard FSB section with a 53-inch width (FSB 12x53) and a 6-inch-deep CIP deck (giving an overall final section thickness of 18 inches).

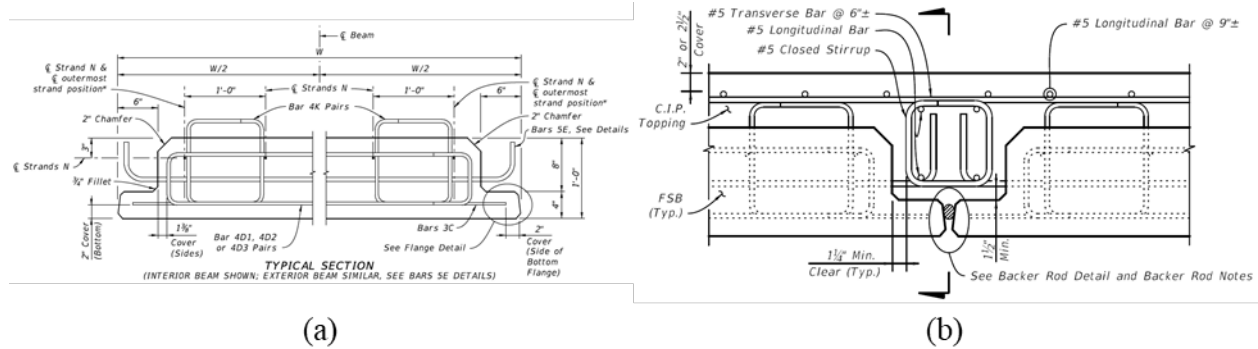


Figure 3.12: Typical section details for 12-inch deep standard FSB section used for Case 1 modeling: (a) cross-section details [19] and (b) joint details [19]

The material details for the model are summarized in Table 3.4. Conventional concrete with an ultimate strength of 8.5 ksi was used for the FSB section in all models. The compressive strength of the concrete was varied depending on if conventional concrete (4 ksi) or UHPC (18.3 ksi) was used.

Table 3.4: Material properties for six main analyses in analytical program

Case #	Type of Section	Section f'_c (ksi)	Joint f'_c (ksi)	Thickness of section (in)	CIP deck
1	FSB 12x53	8.5	4.0	12 (18 composite)	yes (6")
2	Modified FSB 18x53 (1 layer of steel)	8.5	18.3	18	no
3	Modified FSB 18x53 (2 layers of steel)	8.5	18.3	18	no
4	FSB 12x53	8.5	4.0	12	no
5	FSB 12x53	8.5	18.3	12	no
6	Modified FSB 12x53 (1 layer of steel)	8.5	18.3	12	no
7	FDOT – Option 1	8.5	18.3	12	no
8	FDOT – Option 2	8.5	18.3	12	no

The next two models were using the modified joint geometry (based on the box beam joint integration) with one-layer (Case 2) and two-layers (Case 3) of joint reinforcement and UHPC cast in the joint region. These models both had the same section depth as the total composite section of Case 1 (18 inches). The details of these sections are like those shown above in Figure 3.6 through Figure 3.10 above.

The final analyses were on 12-inch-deep FSB sections without CIP decks. Case 4 and Case 5 were both using the current FSB section properties, as shown in Figure 3.12. Case 4 had the current reinforcement detailing, modified to not include any CIP deck, and conventional concrete used in the joint region. Case 5 had the same joint geometry and reinforcement as Case 4 but used UHPC in the joint region. Case 6 was the modified FSB joint detail with one layer of straight reinforcement and UHPC in the joint region. Case 7 and Case 8 were the modified FSB joint detail based on FDOT recommendations with one layer of straight reinforcement and UHPC in the joint region.

Meshing of all the models was generated automatically using the default mesh size.

3.4.3. Material Modeling

The material properties used for modeling the concrete and UHPC in the sections are summarized in Table 3.5. The FSB section and conventional joint were both modeled using a conventional concrete model (CC3DNonLinCementitious2) with the shown ultimate compressive and tensile stresses. The UHPC joint material was modeled using a fiber-reinforced concrete model (CC3DNonLinCementitious2SHCC) with the ultimate compressive and tensile strengths and a fiber content of 2-percent volume shown in Table 3.5.

Table 3.5: Summary of concrete material models used

Material	Base Material Prototype	f'_c (ksi)	f_t (ksi)	E_c (ksi)
FSB Section	CC3DNonLinCementitious2	8.5	0.553	4,350
Conventional Joint	CC3DNonLinCementitious2	4.0	0.319	4,350
UHPC Joint	CC3DNonLinCementitious2SHCC	18.3	0.800	6,200

The general shape of the concrete material curves is shown in Figure 3.13. The concrete compression curve is represented as parabolic to the ultimate compression strength and linear to failure for both the conventional and UHPC materials. The tensile behavior of the conventional and UHPC materials differ, as shown in Figure 3.13 (b). While the tensile strength declines rapidly for the conventional concrete, the fibers in the UHPC material model give the concrete some post cracking strength and ductility.

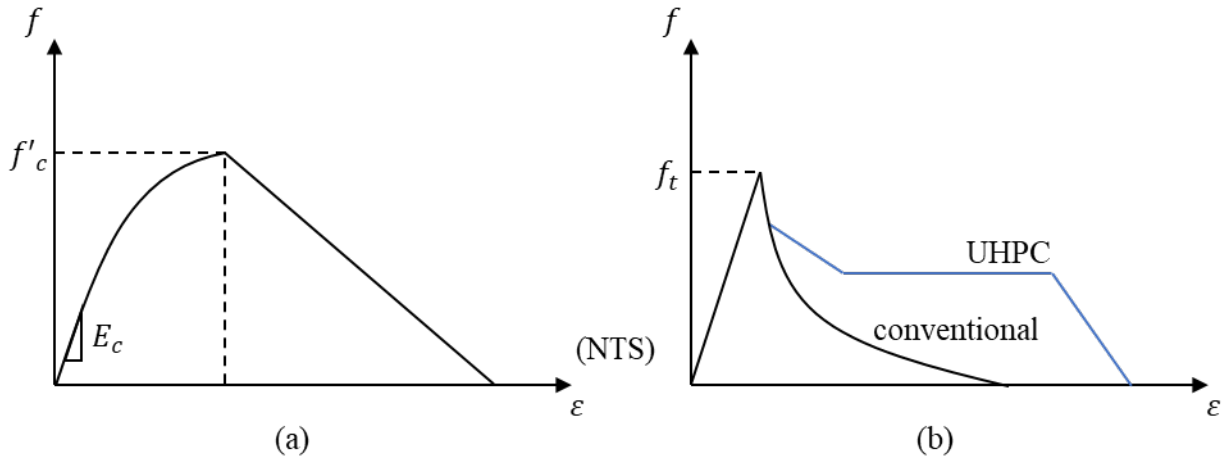


Figure 3.13: General shape of concrete (a) compression and (b) tension curves

The material properties used for modeling the steel reinforcement and prestressing strands in the section are summarized in Table 3.6. All steel was modeled as typical Grade 60 reinforcement. The prestressing strands for these models were modeled the same as the non-prestressed steel reinforcement as the models were looking at the transverse behavior of the section and the joint strength. The modeling of the prestressing strands will be refined in future models.

Table 3.6: Summary of steel properties for all reinforcement used in model

Material	Base Material Prototype	f_y (ksi)	E_s (ksi)
Conventional Reinforcement	CCReinforcement	60	29,000

The stress-strain curve used for modeling of the reinforcement type CCReinforcement is shown in Figure 3.14.

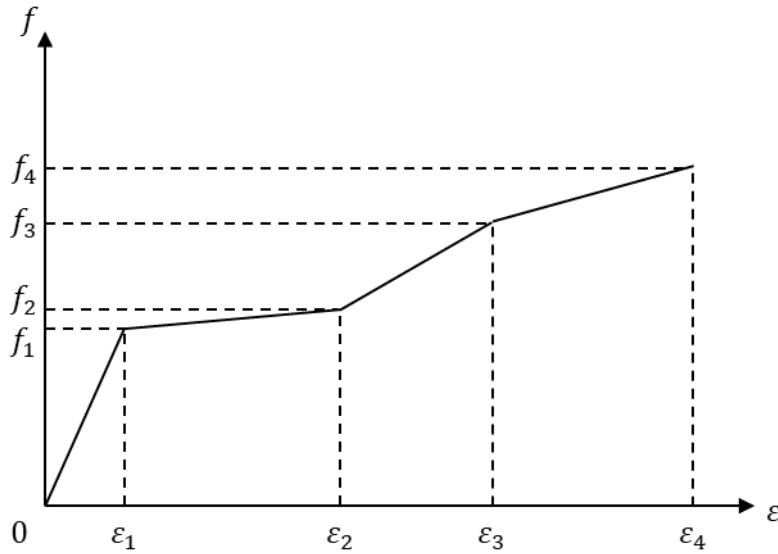


Figure 3.14: General shape of stress-strain curve for reinforcement

These material models for the concrete and steel will be further refined for future modeling efforts.

3.4.4. Loading Protocol

The loading protocol used in the analyses was based on testing performed by Graybeal [41] on adjacent concrete deck panels and also used by other researchers [42]. This loading protocol involves placement of a 20-inch by 10-inch load (equivalent to a wheel loading footprint) immediately adjacent to the joint region. Placement of the load adjacent to (rather than on top of) the joint region places combined bending and axial stresses on the joint.

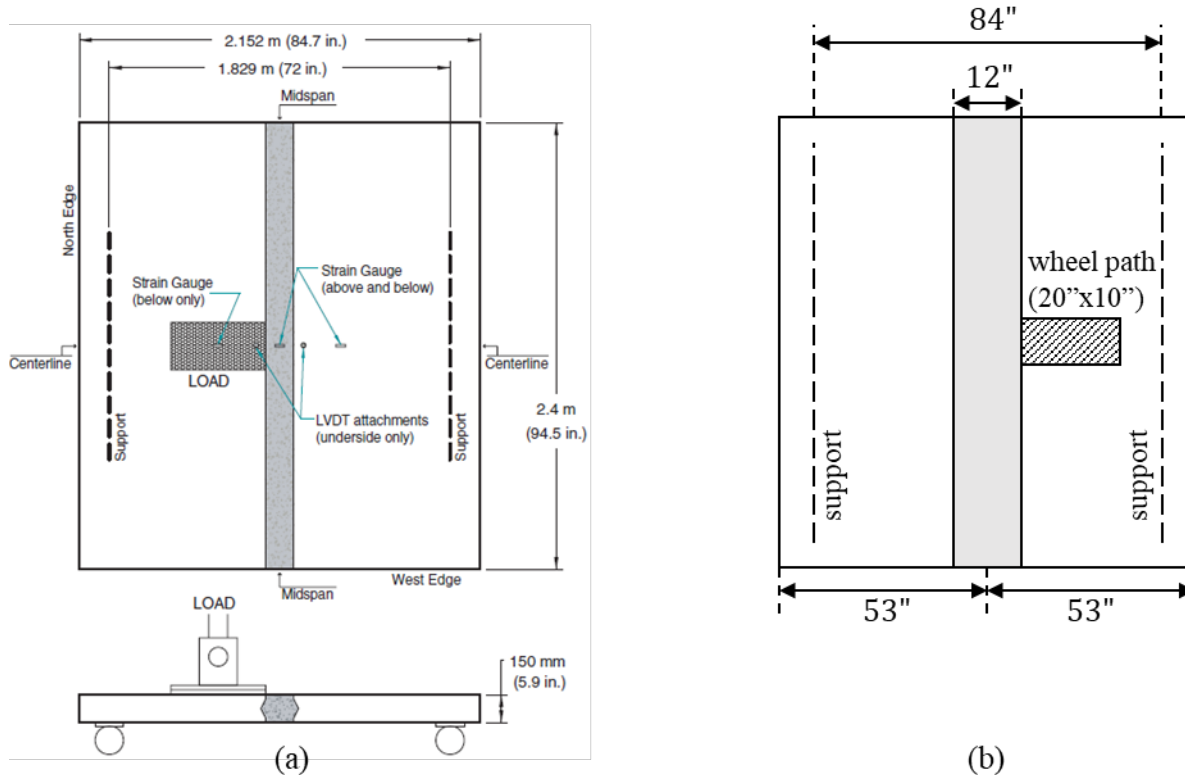


Figure 3.15: (a) Loading protocol used by [41] compared to (b) protocol used for analyses

The load was applied through a deflection-controlled system in 40 equal load steps to failure. The measured applied load at the failure point was then used to compare the joint section capacities.

3.5. ANALYTICAL EVALUATION OF JOINT DETAIL – RESULTS

3.5.1. Results Summary

The eight analyses were split into two sets for comparison: Cases 1 through 3 and Cases 4 through 8. The first three analyses, shown in Figure 3.16, compared the behavior of the current section and joint detail with the proposed section and joint detail with one and two layers of steel. The overall depth of the composite section for Case 1 (18 inches) was kept the same for the section depths of Case 2 and Case 3.

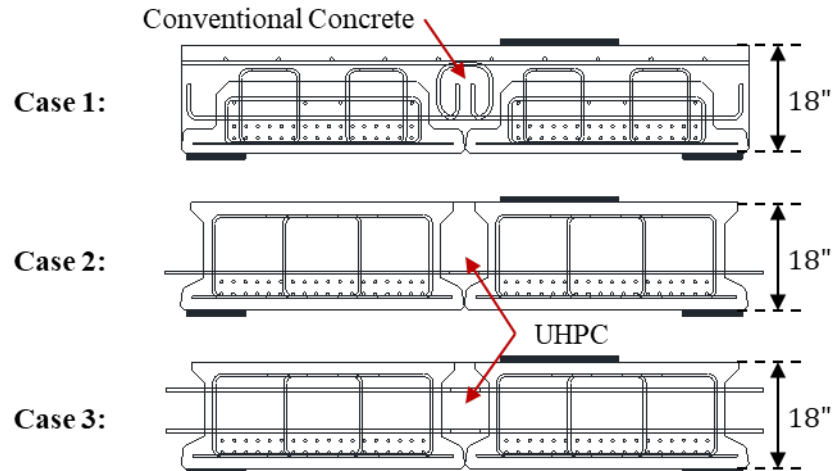


Figure 3.16: First three analyses comparing the current connection detail to proposed UHPC connection detail with one and two layers of steel

The next five cases were to investigate the joint details on shallower sections (12 inches deep), shown in Figure 3.17. These analyses were also used to investigate the behavior of the joint detail if conventional concrete was used with a similar reinforcement pattern to that which is currently used, but without the CIP composite deck.

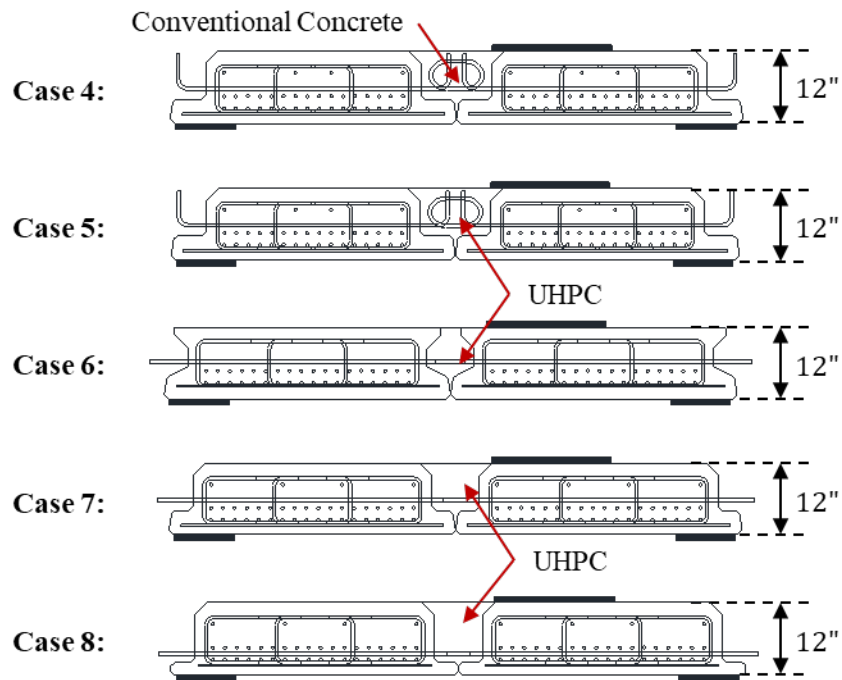


Figure 3.17: Second three analyses comparing the current joint geometry with conventional concrete and UHPC to the modified joint geometry with UHPC

A summary of the analysis results is shown in Table 3.7. The detailed results will be discussed in more detail below but in short, the modified joint region with either one or two layers of steel performs better than the current FSB section and joint detail, as can be seen in the comparison

between Cases 1 through 3. For the shallower section, the modified joint details with UHPC performed as well as the current joint geometry filled with conventional concrete.

Table 3.7: Summary of results from initial six analyses

Case #	Type of Section	Max. Force (kips)	Displacement at Max. Force (in.)
1	FSB 12x53	1,174	0.0868
2	Modified FSB 18x53 (1 layer of steel)	1,377	0.0872
3	Modified FSB 18x53 (2 layers of steel)	1,352	0.0731
4	FSB 12x53 (CC in joint)	753.8	0.0988
5	FSB 12x53 (UHPC in joint)	945.6	0.1128
6	Modified FSB 12x53 (1 layer of steel)	763.0	0.1335
7	FDOT Proposed – Option 1	975.7	0.1512
8	FDOT Proposed – Option 2	845.9	0.0886

3.5.2. Results for Each Analysis Case

A more detailed summary of the results for each of the analyses is presented in the following sections. These results include a load-displacement curve and a crack pattern at failure. In general, the proposed section design and joint detail performed as well or better than the current FSB section and joint detail.

Additionally, in most of the analyses, the crack pattern was more representative of a punching shear failure. For these cases (all but Case 4), the punching shear crack pattern would suggest that the joint region is behaving well and is not controlling the capacity. In Case 4, there is a significant amount of cracking along the joint boundary. This cracking extends the entire way to the end of the members and is more evenly distributed along the length than the other members. This cracking pattern would suggest that the joint detail is controlling the capacity of this section, which shows that the CIP deck is required to have good behavior of the current FSB section and joint details with conventional concrete closure pours.

3.5.2.1. Case 1 – FSB 12x53 with 6-inch CIP Deck

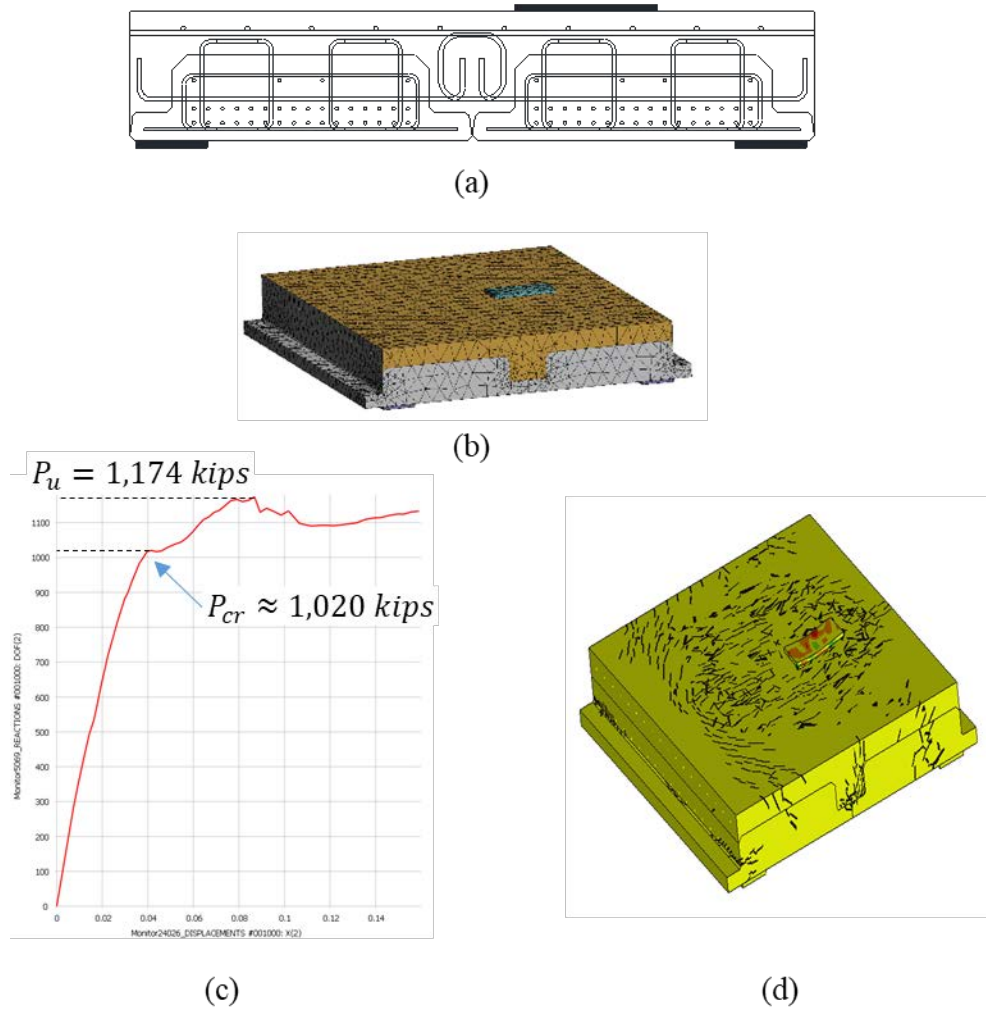


Figure 3.18: Summary of results for Case 1: (a) cross-section geometry and reinforcement detail, (b) model meshing, (c) load-deflection curve, and (d) crack pattern at failure

3.5.2.2. Case 2 – Modified FSB 18x53 with UHPC Joint and Single Reinforcement Layer

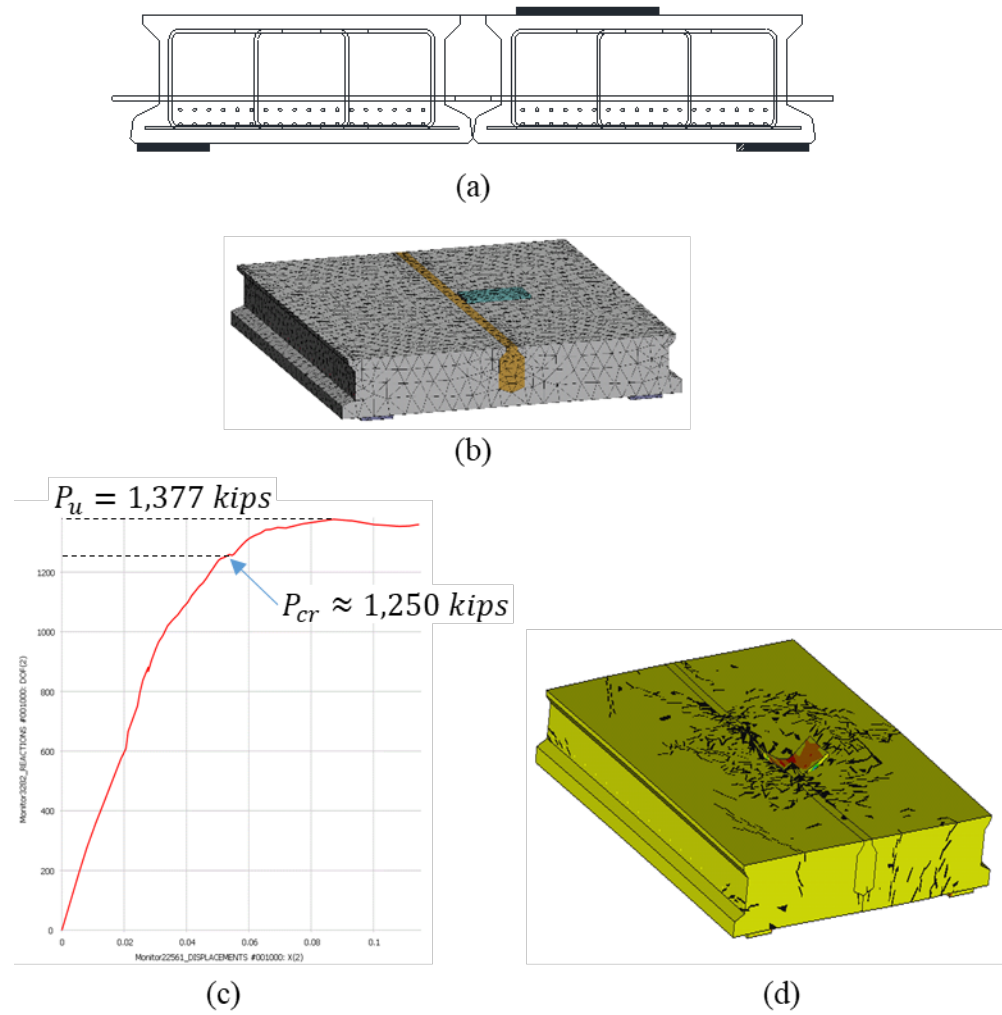


Figure 3.19: Summary of results for Case 2: (a) cross-section geometry and reinforcement detail, (b) model meshing, (c) load-deflection curve, and (d) crack pattern at failure

3.5.2.3. Case 3 – Modified FSB 18x53 with UHPC Joint and Double Reinforcement Layer

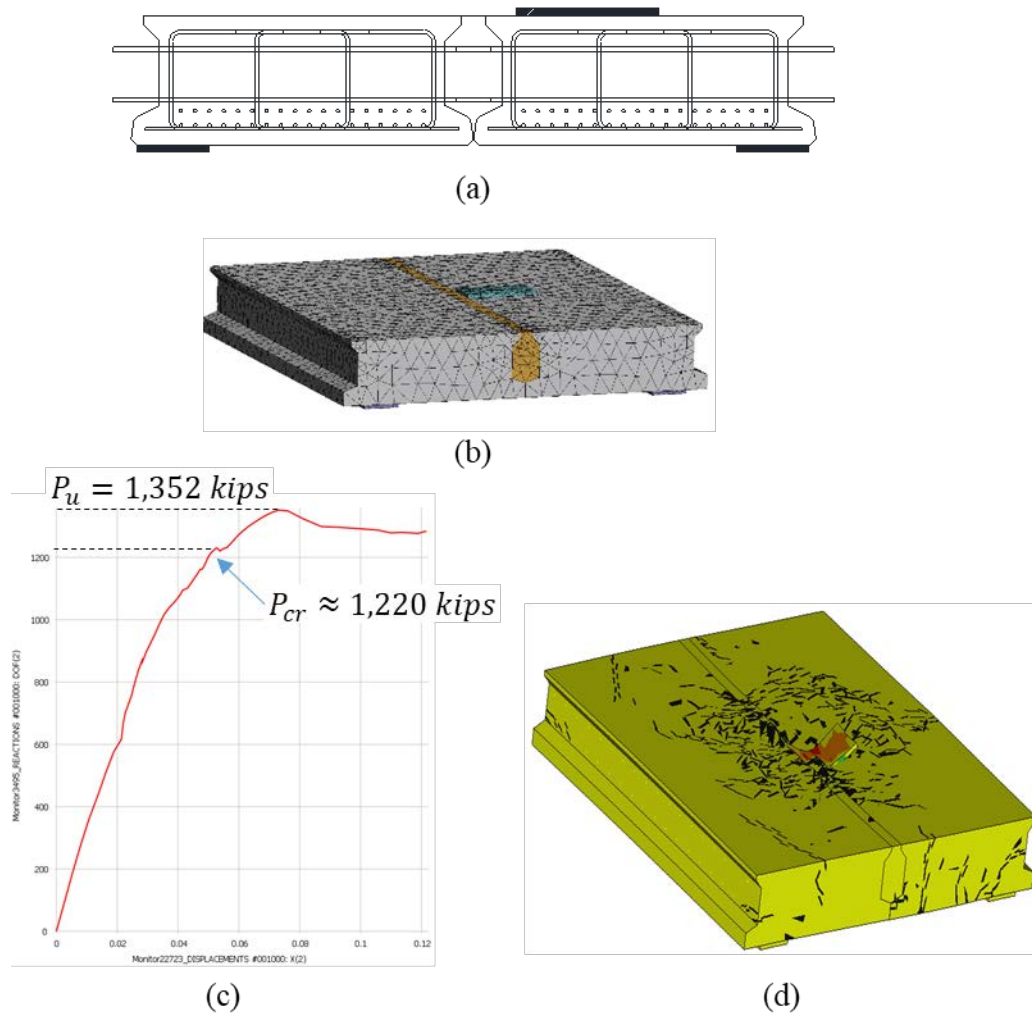


Figure 3.20: Summary of results for Case 3: (a) cross-section geometry and reinforcement detail, (b) model meshing, (c) load-deflection curve, and (d) crack pattern at failure

3.5.2.4. Case 4 – FSB 12x53 with Conventional Concrete Joint and without CIP Deck

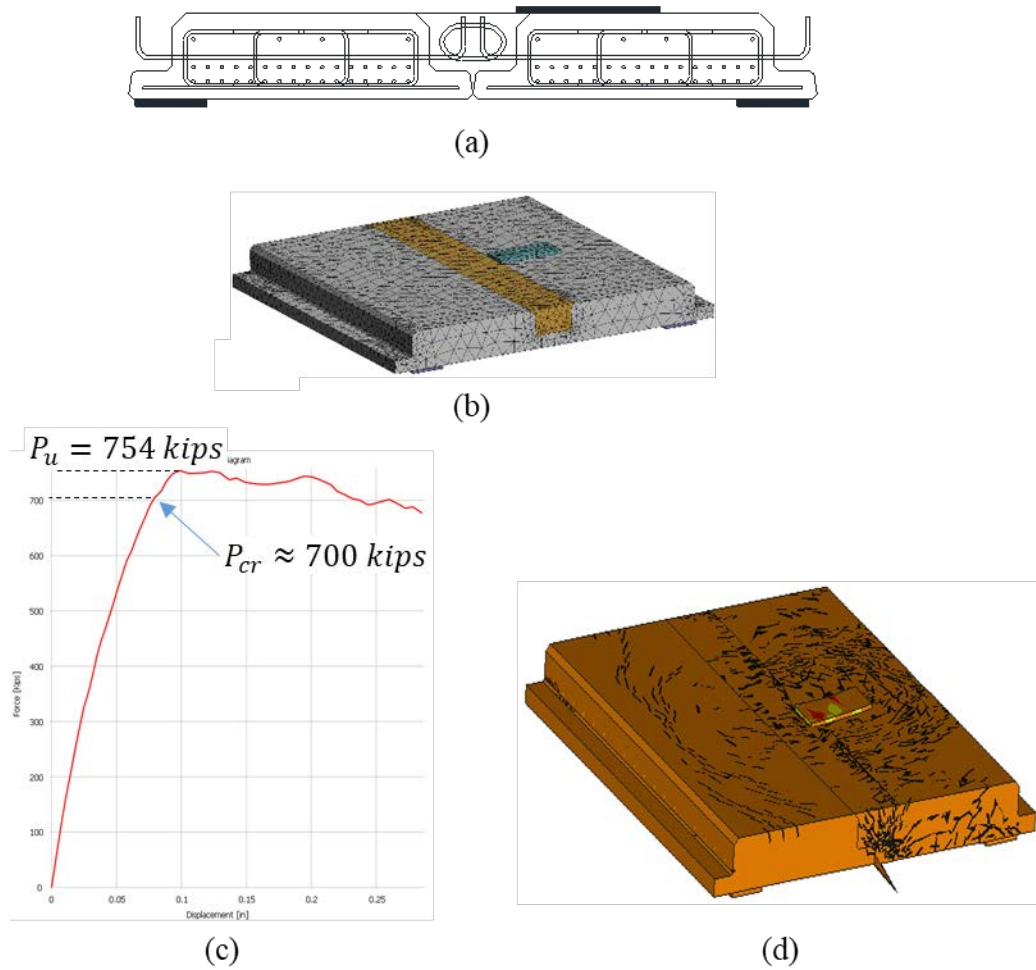


Figure 3.21: Summary of results for Case 4: (a) cross-section geometry and reinforcement detail, (b) model meshing, (c) load-deflection curve, and (d) crack pattern at failure

3.5.2.5. Case 5 – FSB 12x53 with UHPC Joint and without CIP Deck

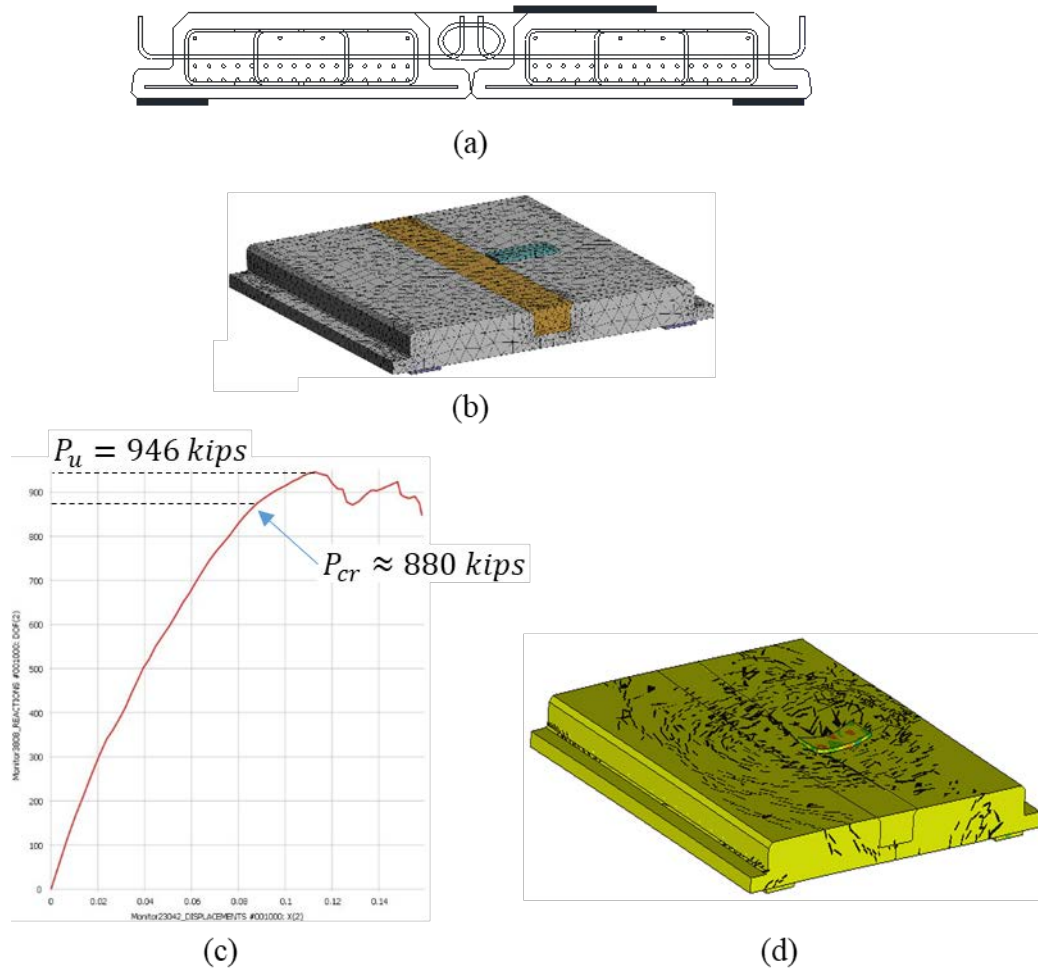


Figure 3.22: Summary of results for Case 5: (a) cross-section geometry and reinforcement detail, (b) model meshing, (c) load-deflection curve, and (d) crack pattern at failure

3.5.2.6. Case 6 – Modified FSB 12x53 with UHPC Joint

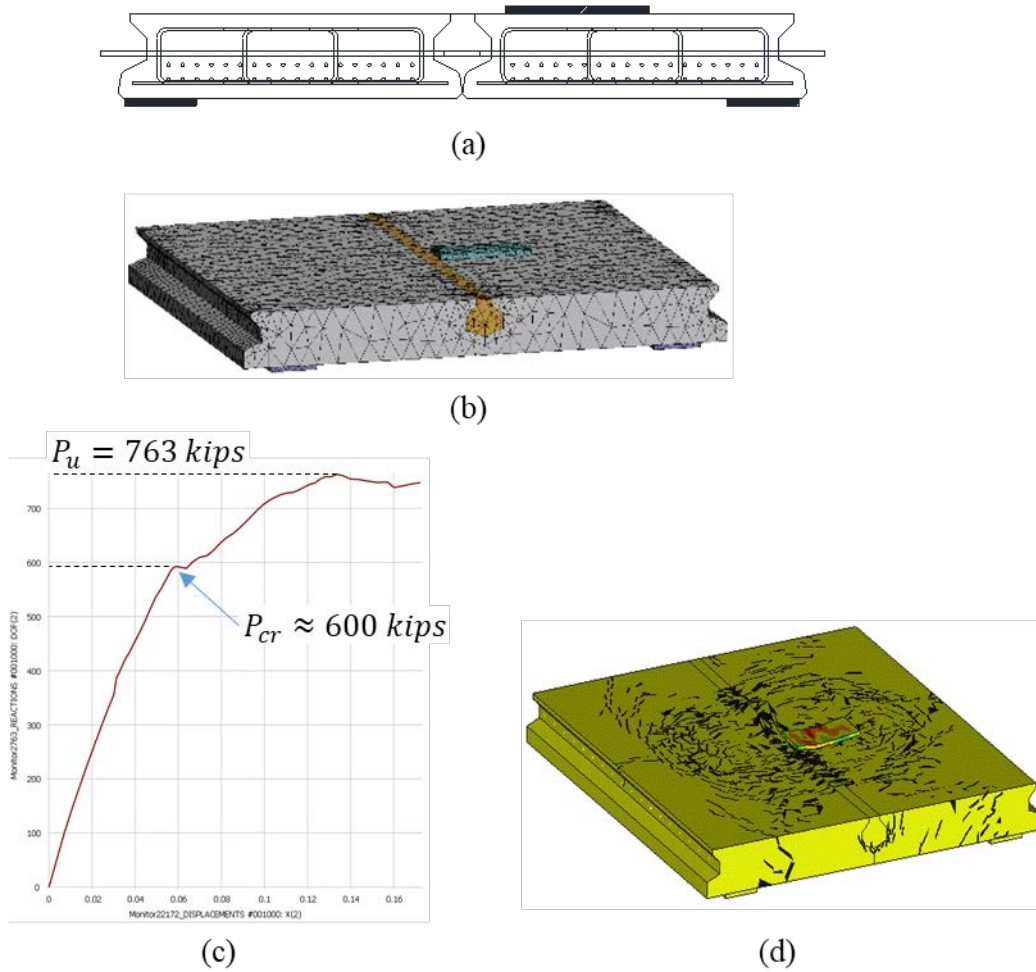


Figure 3.23: Summary of results for Case 6: (a) cross-section geometry and reinforcement detail, (b) model meshing, (c) load-deflection curve, and (d) crack pattern at failure

3.5.2.7. Case 7 – Modified FSB 12x53 with UHPC Joint (FDOT Engineer Option 1)

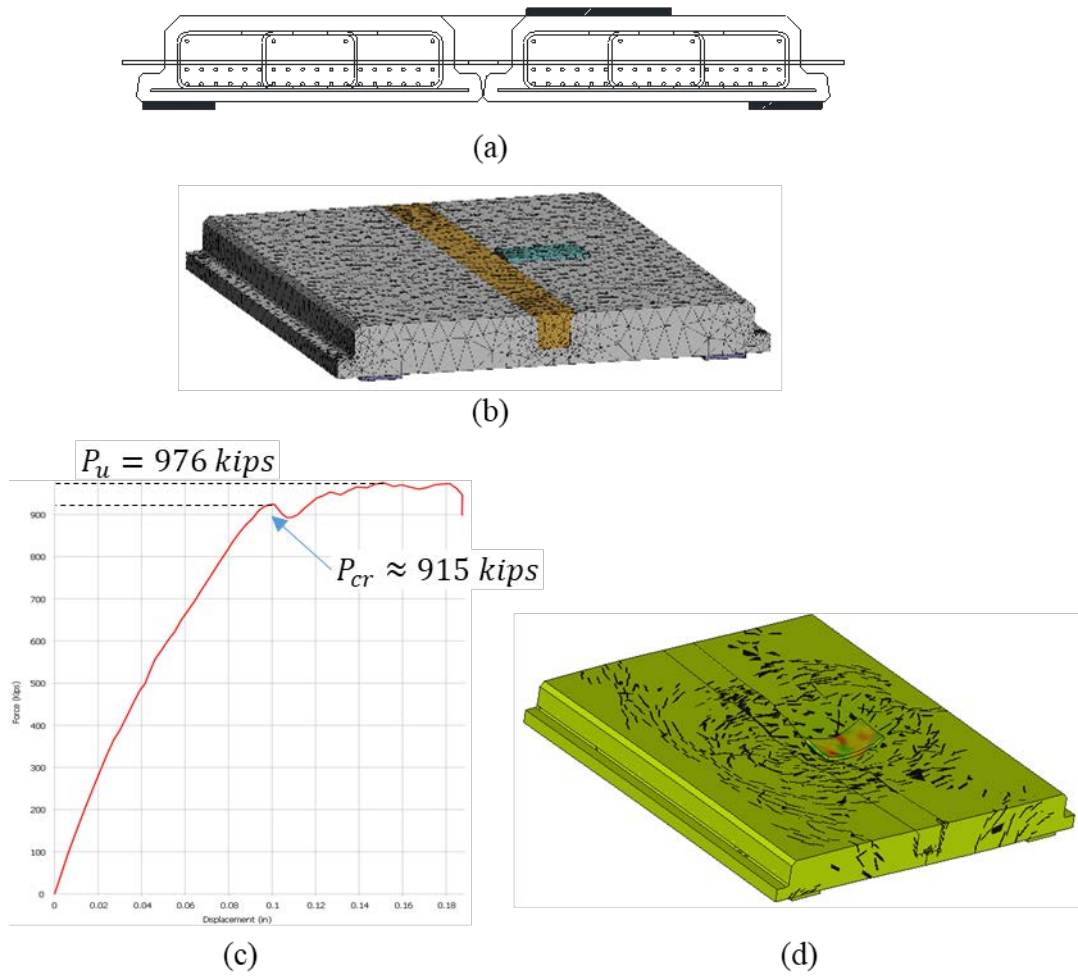


Figure 3.24: Summary of results for Case 7: (a) cross-section geometry and reinforcement detail, (b) model meshing, (c) load-deflection curve, and (d) crack pattern at failure

3.5.2.8. Case 8 – Modified FSB 12x53 with UHPC Joint (FDOT Engineer Option 2)

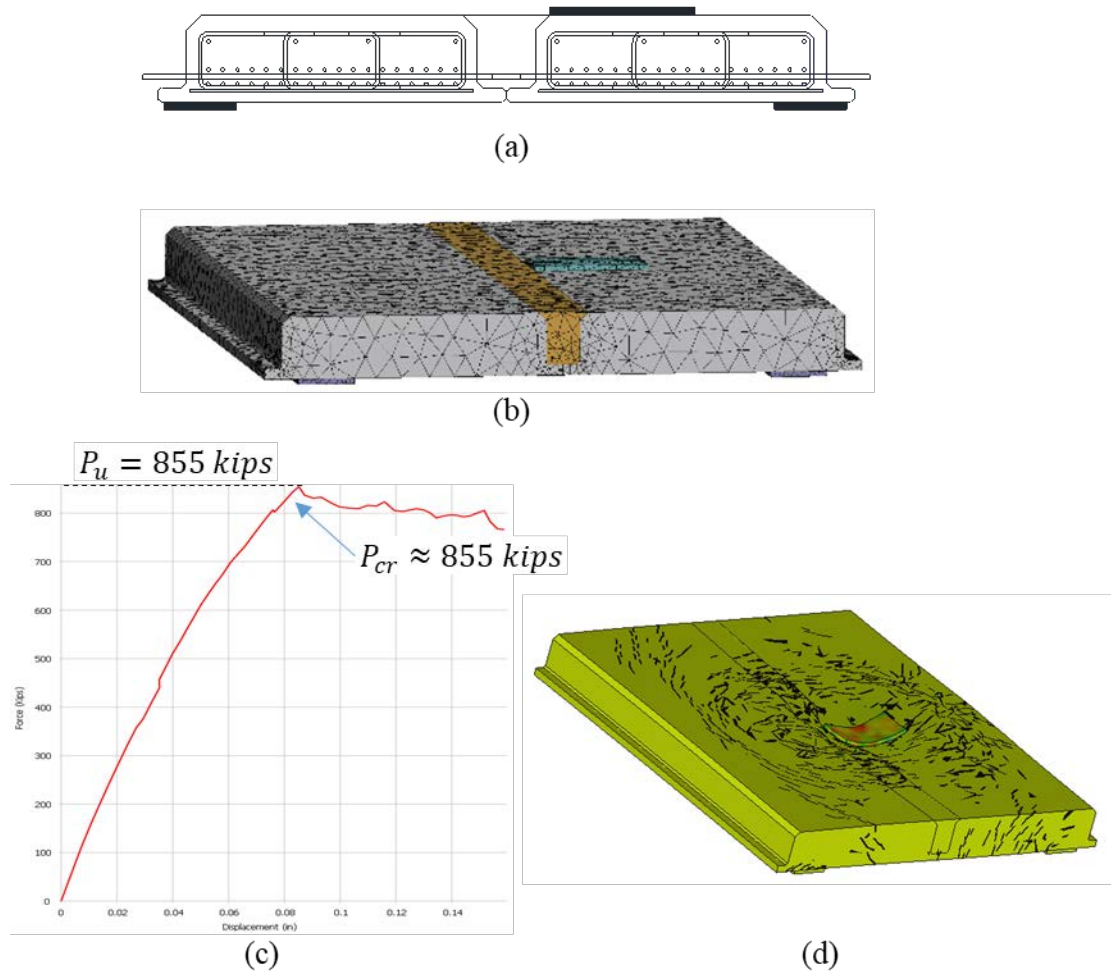


Figure 3.25: Summary of results for Case 8: (a) cross-section geometry and reinforcement detail, (b) model meshing, (c) load-deflection curve, and (d) crack pattern at failure

3.6. SUMMARY AND CONCLUSIONS

A parametric study was first conducted to determine the allowable span lengths for the three different FSB sections without CIP composite decks. The potential maximum allowable span lengths range from 32 feet for the 12-inch-deep FSB section to 55 feet for the 18-inch-deep FSB section. Following the parametric study, previously successful UHPC joint details were integrated into the FSB cross section shape. Two additional details were proposed by FDOT engineers to simplify the joint detail. These joint details were compared to the proposed joint detail and were found to perform well through the FEM results.

The results from this chapter were used to guide the selection of the joints to be evaluated experimentally in Chapter 5.

4. DEVELOPMENT OF THE FSB STANDARD FOR 75-FOOT SINGLE SPAN

4.1. INTRODUCTION

The currently available FSB sections without composite CIP decks have a maximum span length of 55 feet. The focus of this chapter is to investigate the FSB depth and shape required to span 75 feet and compare it to other available and developed options.

4.2. POSSIBLE OPTIONS FOR 75-FOOT SINGLE SPAN LENGTH

Several options are presented in this chapter for sections that can span 75 feet. The presented sections are currently available sections (slightly modified if needed) or proposed alternatives. Currently available sections included in the below comparison are based on the following characteristics:

- **No CIP Deck:** All sections have no CIP deck, which will allow the section to be used for accelerated construction.
- **High Notoriety:** Selected sections are being used heavily in specific regions or nationally.
- **Adaptability for ABC Projects:** Selected sections either already have recommended longitudinal joint details or can implement an available joint detail for use with UHPC.
- **Efficient for Short-Span Bridge:** These sections are tailored for bridge spans between 50 and 120 feet; longer span options were not included.

Based on these criteria, two currently available sections were chosen for the comparisons below: box beam and double tee beam. The Texas Department of Transportation (TxDOT) box beam was chosen as the specific box beam section for analysis due to the availability of free design software, PGSuper [43]. Most box sections have a similar shape to the Texas box beam, so the below analysis is representative of all box beam options. The NEXT beam was selected for the below analysis as it is a popular standardized double tee section. These two sections are compared to a pre-topped inverted tee section, modified depth FSB section, and a modified slab beam section.

4.2.1. Texas Box Beam

Many states currently use precast box beams for short- to long-span bridge applications, as discussed in Chapter 1. One example of a commonly used box beam section is the TxDOT box beam, shown in Figure 4.1.

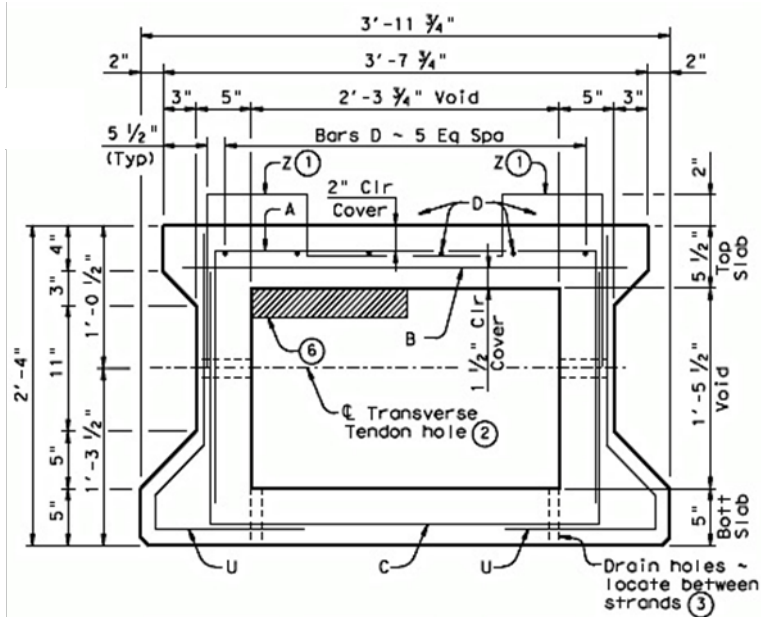


Figure 4.1: TxDOT Type 4B28 [44]

Standard TxDOT box beams come in four different depths (20-inch, 28-inch, 34-inch, and 40-inch), two different widths (4-foot and 5-foot) and are recommended for spans between 30 and 120 feet. The section properties for all the available sections from TxDOT with their recommended maximum span lengths are shown in Table 4.1. The recommended maximum span lengths in this table all are for sections with a 2-inch asphalt overlay.

Table 4.1: TxDOT box beam section properties [44]

Beam Type	y_t (in)	y_b (in)	A_g (in ²)	I_g (in ⁴)	Weight (plf)	Recommended Max Span Length (ft)
4B20	10.19	9.81	591.8	28,086	616	65
5B20	10.12	9.88	717.8	35,234	748	65
4B28	14.38	13.62	678.8	68,745	707	80
5B28	14.26	13.74	804.8	85,370	838	80
4B34	17.92	16.08	798.8	115,655	832	100
5B34	17.72	16.28	924.8	142,161	963	100
4B40	21.63	18.37	943.8	180,159	983	120
5B40	21.36	18.64	1069.8	219,007	1,114	120

These beams can be used in either an adjacent or spread configuration, as shown in Figure 4.2. The adjacent box beam configuration is the one of interest for this study since it allows for accelerated construction with use of UHPC in the longitudinal joints, as shown in Figure 4.2 (c).

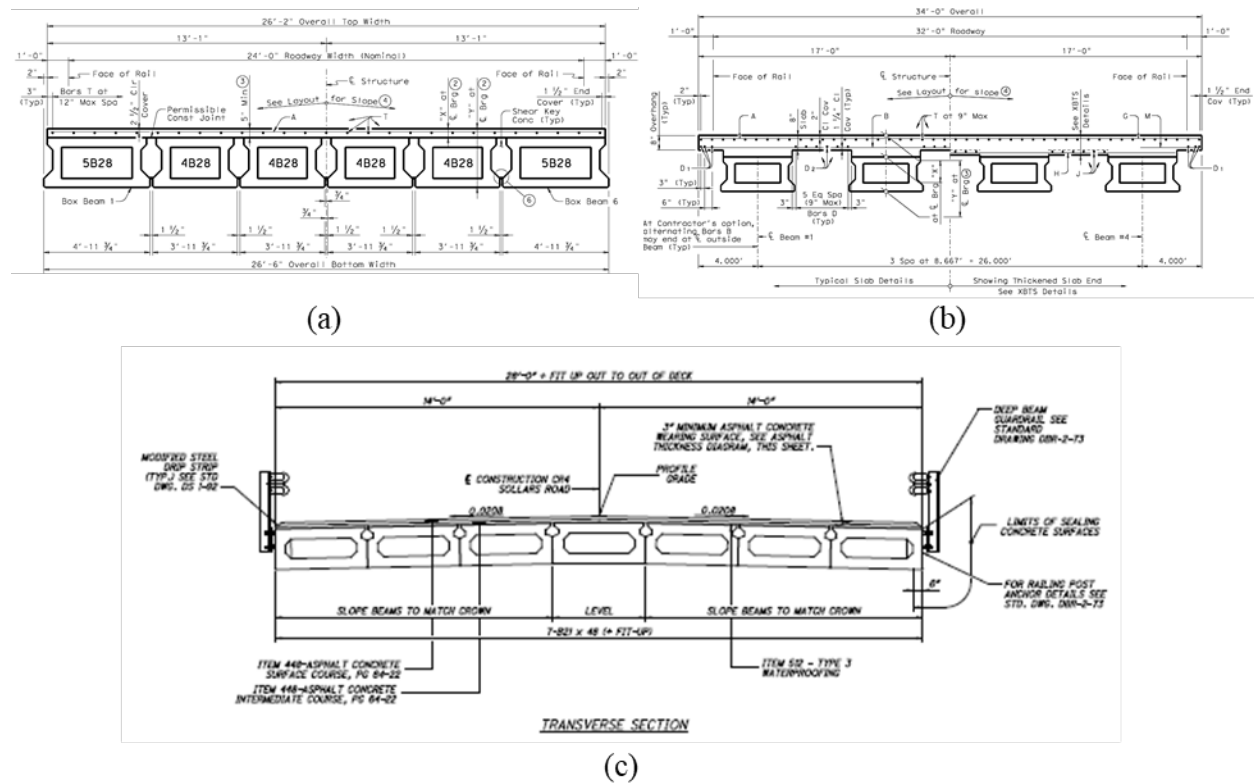


Figure 4.2: Traditional (a) adjacent and (b) spread configuration for 28-inch deep box beams [44] and (c) adjacent configuration with UHPC connections [29]

4.2.2. NEXT D Beam

The NEXT D beam was chosen for the analysis as it is the double tee section that is beginning to be used in practice and is included in the PCI Bridge Design Manual [45]. The NEXT D Beam, shown in Figure 4.3, is the NEXT beam option with the deck cast as part of the girder, which allows for accelerated construction and the potential for UHPC to be used in the longitudinal joints.

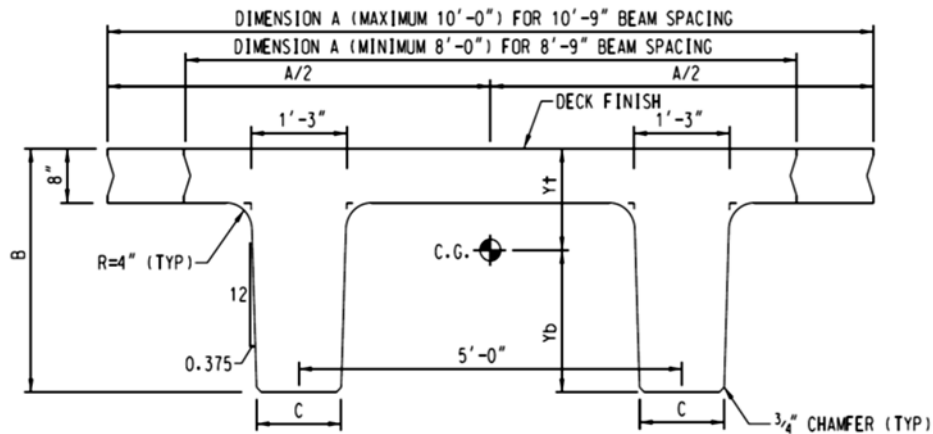


Figure 4.3: NEXT D beam [8]

These beams are available in four different depths (28-inch, 32-inch, 36-inch, and 40-inch), two different widths (96-inch and 120-inch) and are recommended for spans between 20 feet and 80 feet, as shown in Figure 4.4.

Chart NEXT-2
NEXT Type D x 96 Beams

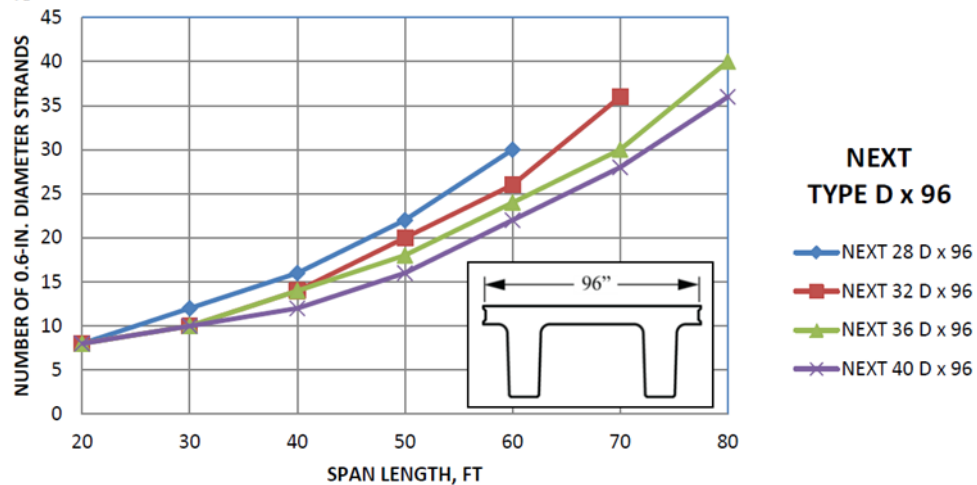


Figure 4.4: NEXT D beam span lengths [8]

The section properties with the recommended maximum span lengths for the NEXT D beam family of sections are shown in Table 4.2.

Table 4.2: NEXT D beam section properties [8]

Beam Type	y_t (in)	y_b (in)	A_g (in ²)	I_g (in ⁴)	Weight (plf)	Recommended Max Span Length (ft)
28 D 96	9.94	18.06	1,346	85,651	1,402	60
28 D 120	9.20	18.80	1,538	92,597	1,602	55
32 D 96	11.43	20.57	1,455	126,111	1,516	70
32 D 120	10.57	21.44	1,647	136,502	1,716	65
36 D 96	12.97	23.03	1,562	176,674	1,627	80
36 D 120	11.99	24.01	1,754	191,453	1,827	75
40 D 96	14.54	25.47	1,666	238,059	1,735	80
40 D 120	13.45	26.55	1,858	258,171	1,935	80

4.2.3. Pre-Topped Inverted-Tee

The decked bulb tee beam is another option for medium to long span bridges. The decked bulb tee shape for medium span bridges is intended to behave like a series of adjacent box beams, as shown in Figure 4.5, while not requiring the difficulties associated with precasting voided sections and allowing for inspection of all sides of the girders and deck.

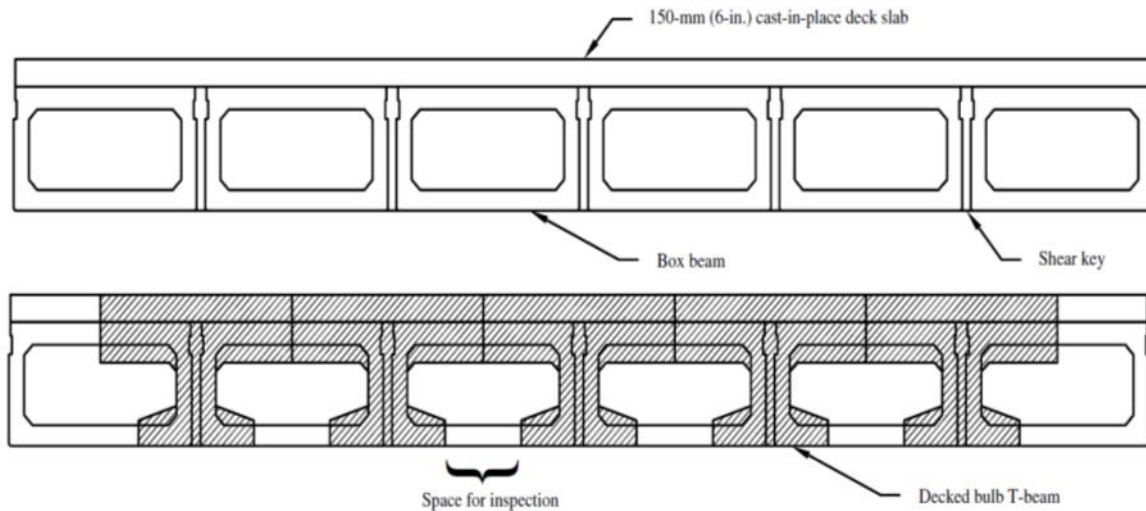


Figure 4.5: Deck bulb tee shape compared to adjacent box beam configuration [46]

PCI provides a deck bulb tee option that is suitable for span lengths between 40 and 170 feet, as shown in Figure 4.6.

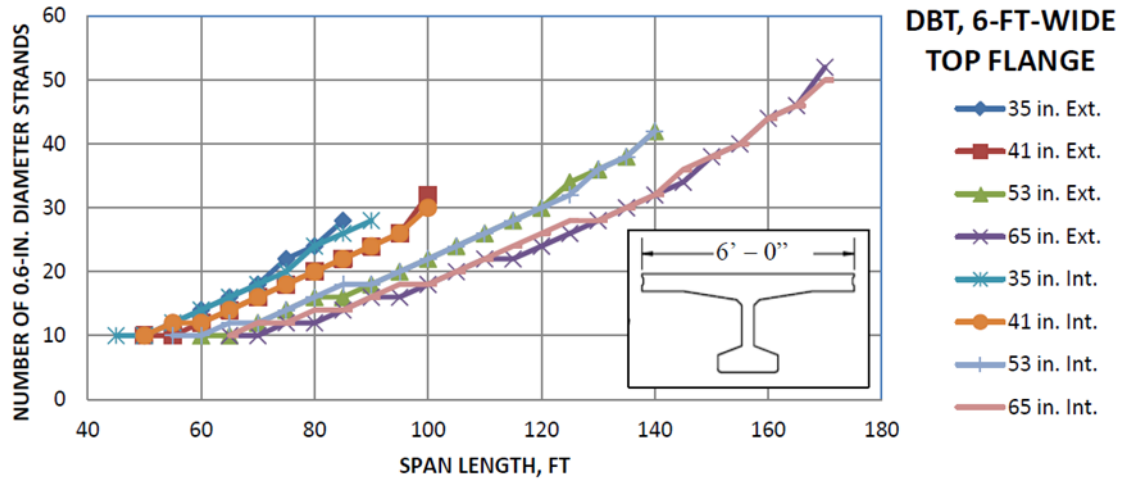


Figure 4.6: Deck bulb tee span lengths [45]

There are two sections that have been used by FDOT or proposed for use that would also work as pre-topped inverted tee or bulb-tee sections: Florida inverted tee and truncated Florida I Beam (FIB). These two sections are shown with the PCI deck bulb tee in Figure 4.7.

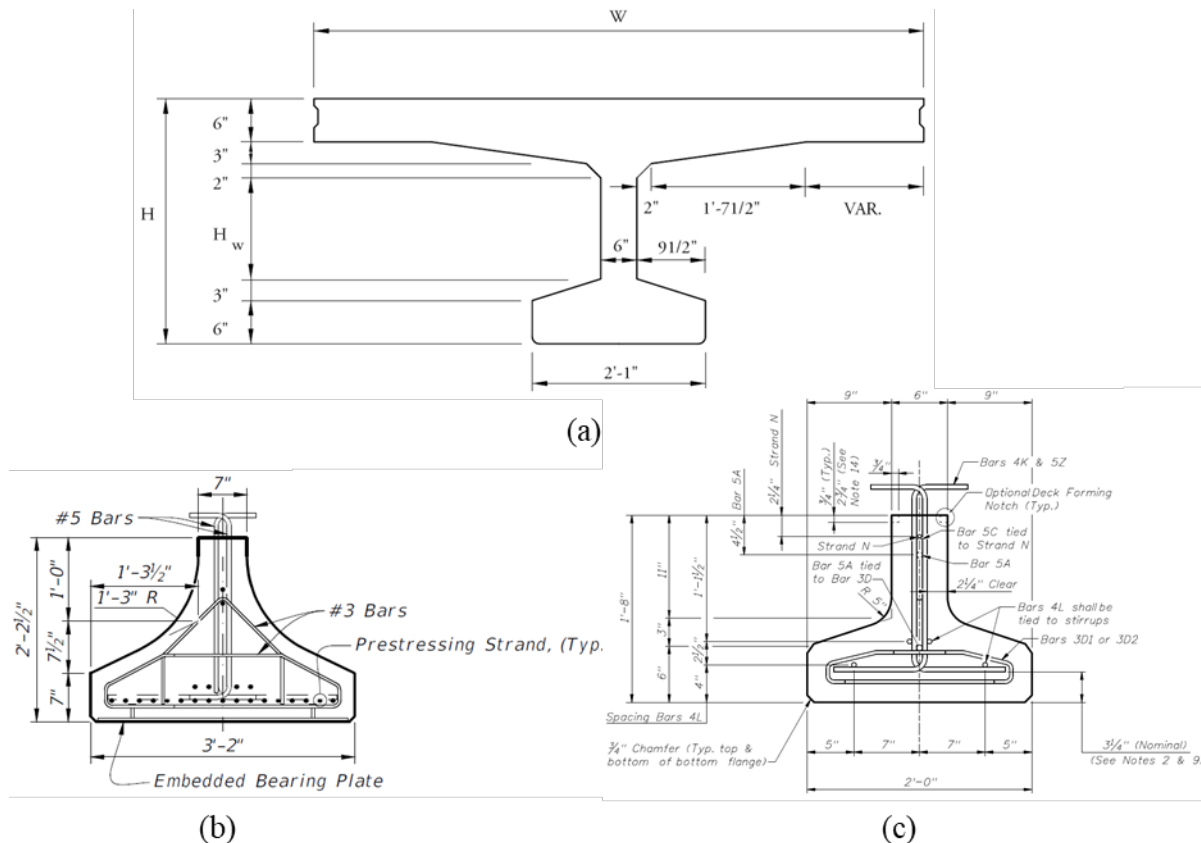


Figure 4.7: (a) PCI deck bulb tee [45], (b) truncated FIB [47], and (c) Florida inverted-T [48]

A pre-topped Florida Inverted-T (FIT) beam was chosen for the below comparison as the FIT section was available for design in the available FDOT design program [49]. A pre-topped FIT

shape is representative of the behavior of the beams in this category. The section and section properties for the chosen pre-topped FIT shape are shown in Figure 4.8.

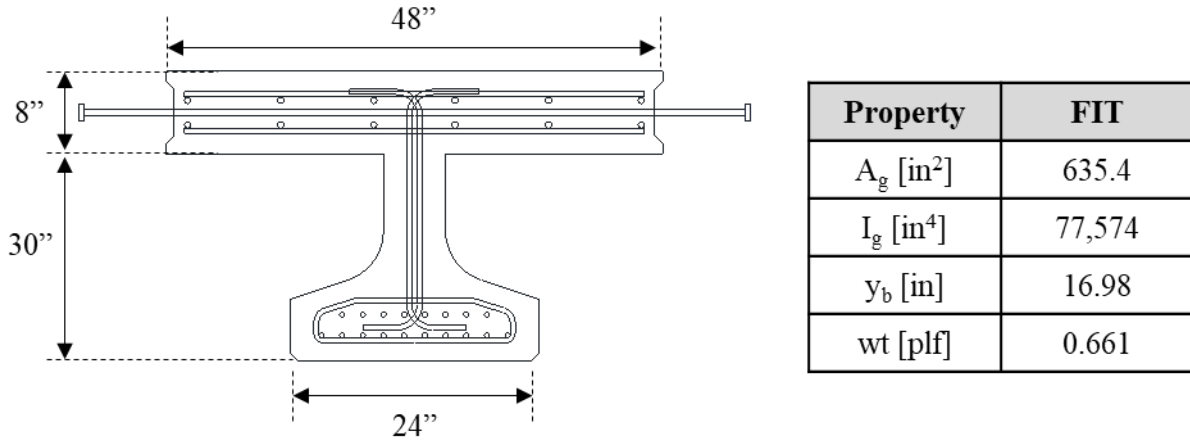


Figure 4.8: Pre-topped FIT

4.2.4. Modified Florida Slab Beam

As described in the previous chapter, the maximum possible span length of the current 18-inch-deep FSB section is 55 feet. To achieve the desired 75-foot span length, the FSB depth would need to be increased to 27-inches, as shown in Figure 4.9. This section was also analyzed using the available FDOT design program [49].

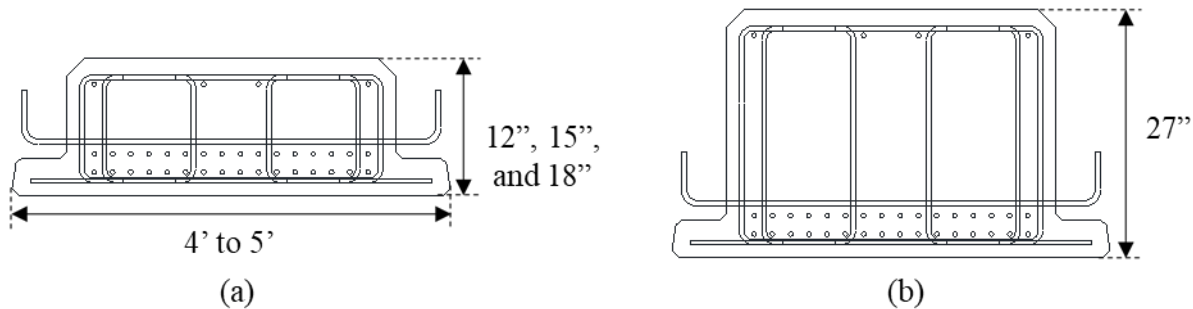


Figure 4.9: (a) Original FSB section with currently available depths and (b) modified FSB section required to achieve 75-foot span lengths

4.2.5. Modified Slab Beam

An additional section was developed for short- to medium-span bridge lengths. Like the decked bulb-tee shape, the design is inspired by a conventional box girder. The main difference between the systems is the change in location of the closure pour and the void in the cross section, as shown in Figure 4.10. The modified slab beam would not require a voided precast section but would use longitudinal closure pours to connect adjacent members.

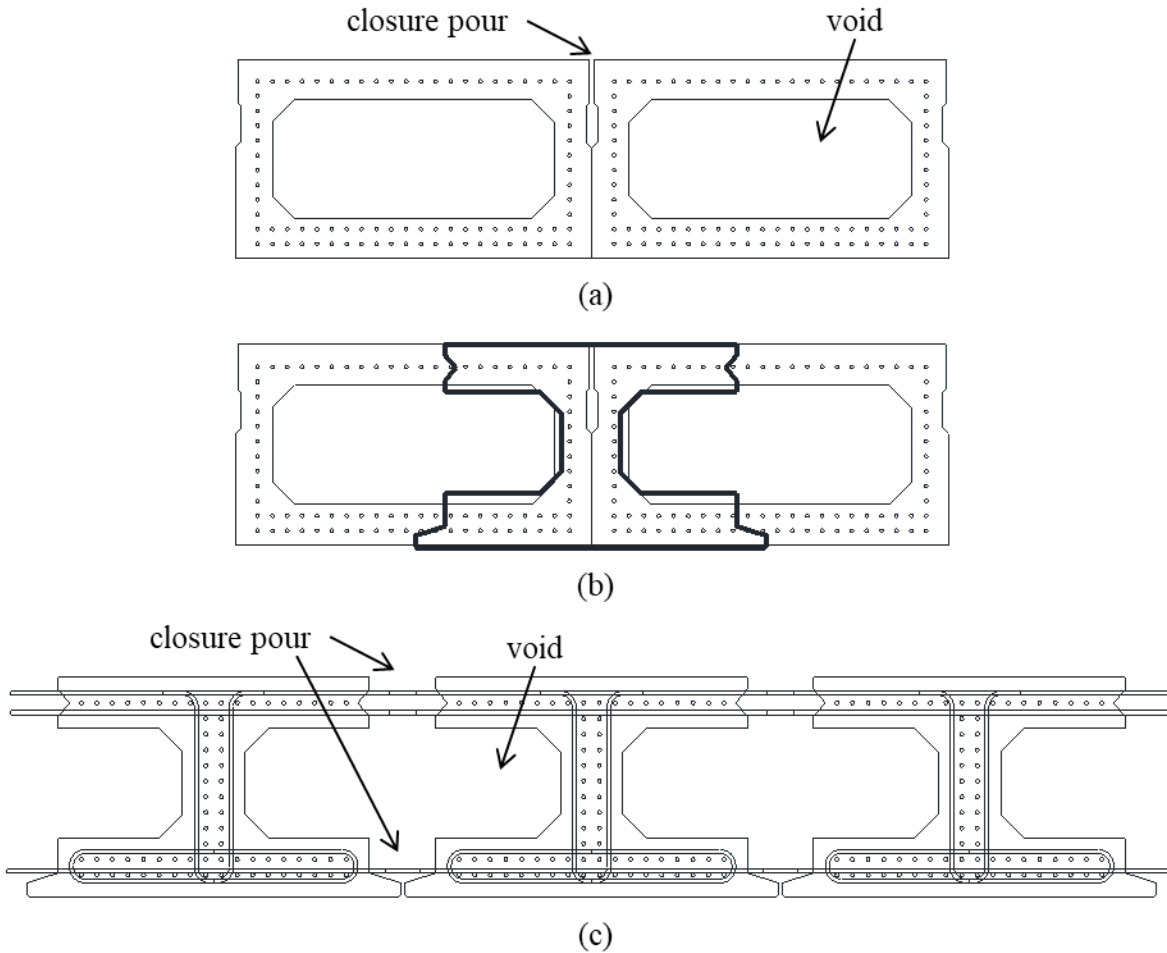


Figure 4.10: (a) Conventional adjacent box beam configuration, (b) proposed modified slab beam section shape, and (c) proposed modified slab beam configuration

The longitudinal closure pours could be used to connect both the top and bottom flanges, as shown in Figure 4.10 (c) and Figure 4.11 (a). Connecting both top and bottom flanges would allow the bridge to perform as a slab beam bridge, which would decrease the demand on each girder and improve overall behavior. The longitudinal closure pours could also be used to only connect the top flanges of the members, as shown in Figure 4.11 (b). Only connecting the top flanges would be easier to construct and result in the bridge behaving like the pre-topped inverted tee beam bridges discussed above.

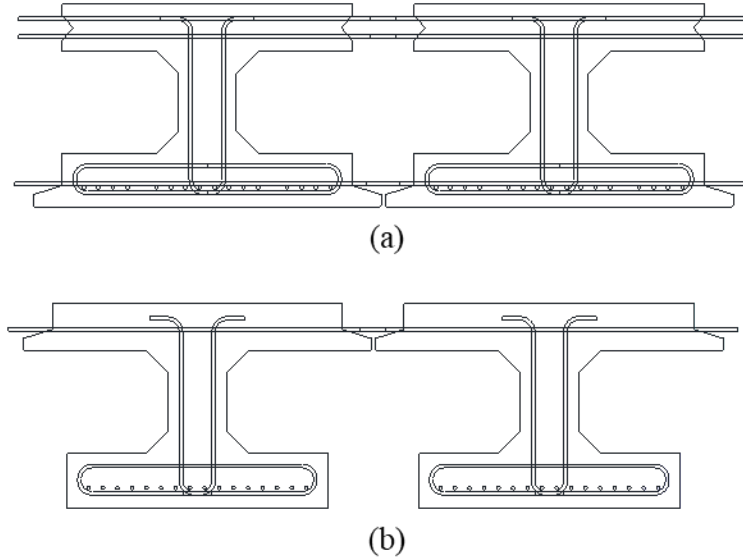


Figure 4.11: Modified slab beam with (a) bottom and top flanges connected and (b) only top flanges connected

The section properties for the preliminary modified slab beam section shape with a 28-inch depth are provided in Table 4.3. Additional details would need to be developed for the end block region, reinforcement, joint region, and other items before the modified section should be used. Development of these details is outside the scope of the preliminary study of this chapter but is recommended for future work.

4.3. COMPARISON OF POSSIBLE SECTIONS

The five sections listed above were used to design a bridge with a 75-foot span length and the same properties described in Chapter 3. The beams were designed using a FDOT Prestress Beam - LRFD [49], PGSuper [43], and UTPstrs (a design tool developed for previous projects conducted by the researchers [50]). The final cross section designs for all the sections are shown in Figure 4.12 and additional details are provided in Table 4.3.

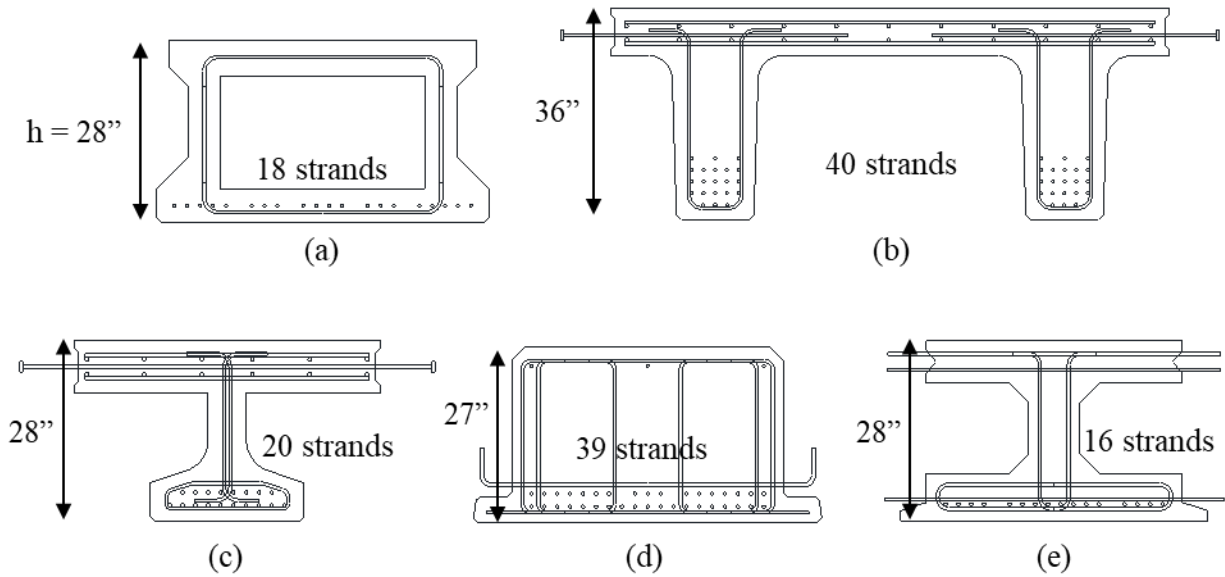


Figure 4.12: Required section depths and number of 0.6-inch diameter strands to achieve 75-foot span using (a) TxDOT Type 4B20, (b) NEXT D-96, (c) pre-topped Florida inverted-T, (d) modified FSB, and (e) modified slab girder sections

The efficiency factor developed by Guyon [51] and discussed by others [52]–[54], shown in Equation 4-1, was used to evaluate these five options.

$$\rho = \frac{I}{Ay_b y_t} = \frac{r^2}{y_b y_t} \quad \text{Equation 4-1}$$

The efficiency factors for all five options are shown in Table 4.3. A larger efficiency factor means that a section is more efficient.

Table 4.3: Comparison of section properties

Section Type:	Texas 4B28	NEXT D 96	Pre-Topped FIT	FSB 27x53	Modified Slab
depth [in]	28	36	28	27	28
width [in]	48	96	48	53	48
0.6" diameter strands for 75' length	18	40	20 (4*)	39 (3**)	16
A _g [in ²]	678.8	1,562	635.4	1,176	703.7
I _{xx} [in ⁴]	68,745	176,674	77,574	74,098	68,525
y _t [in]	14.38	12.97	11.02	13.99	14.73
y _b [in]	13.62	23.03	16.98	13.01	13.27
weight [k/ft]	0.707	1.627	0.661	1.225	0.733
ρ (efficiency)	0.517	0.379	0.652	0.351	0.498

*debonded strands; **top strands

There are several observations that can be made from the above analysis.

1. The solid slab shape required by the FSB 27x53 has the lowest efficiency and thus the largest number of strands.
2. The NEXT D 96 is the second least efficient section. The required section depth is 36 inches, which is at least eight inches deeper than the other sections. The strand pattern in the NEXT D 96 also only allows six strands in the lowest stand layer and then 10 strands in each of the subsequent layers. Because of this layout, most of the strands are not located in their most effective location.
3. The TxDOT Type 4B28 and the proposed modified slab beam have similar properties and efficiency factors and thus have similar designs. Both sections require less stands at similar depth compared to the modified FSB section.
4. The proposed modified slab beam only has 16 strands of a possible 36 bottom flange strand locations. This would suggest that the modified slab beam could be used for longer spans than 75 feet.
5. The pre-topped Florida Inverted-T beam was the most efficient section of the five sections investigated. The narrower bottom flange is only large enough to hold the strands required for the 75-foot span. Having the narrower bottom flange decreases the weight of the section and increases its efficiency.

4.4. SUMMARY AND CONCLUSIONS

The purpose of the work conducted for this chapter was to investigate possible cross section shapes that could be used for 75-foot span lengths. Five different cross sections were investigated to see the section depth and number of strands required to achieve a 75-foot span length. The solid slab required for the FSB section and the thick webs of the NEXT D beam resulted in these two sections being the least efficient of the five investigated. The modified slab beam, pre-topped FIT beam, and box beam all were efficient sections for the 75-foot span, and all are viable options.

5. SMALL-SCALE JOINT STATIC TESTING

5.1. INTRODUCTION

The test matrix, observations from specimen construction, testing plan, and results from the small-scale experimental testing will be summarized in this chapter. The test results include the cracking and ultimate strength of several sections and then the performance of a selected number of joints under fatigue loading.

5.2. JOINTS SELECTED FOR FURTHER EVALUATION

Three joints were initially selected for further evaluation through experimental testing, as shown in Figure 5.1. Since all the joints will be used in solid slab beam bridges, all proposed joints (and corresponding sections) will result in final bridge structures with the same maximum span lengths and load ratings.

Two of the joint details had straight joint sides with no shear keys, as shown in Figure 5.1 (a) and (b); these joint details were developed and proposed by FDOT engineers. The primary differences between these two joint details were the thickness of the bottom flange, presence of reinforcement in the bottom flange, and depth of the joint reinforcement. FDOT 1 had a 4-inch-deep bottom flange with reinforcement extending into the flange. FDOT 2 had a 2-inch-deep flange without reinforcement extending into the ledge; this option allowed the joint reinforcement to be located two inches lower in the joint, which would increase the ultimate flexural strength of the joint. These joints both had square, sharp transitions along the joint border. These shapes were thought to be easier to construct but may lead to stress concentrations at the corners. These joints also had straight sides with only the bottom flange intersecting the joint plane, so an exposed aggregate finish was required to provide sufficient shear transfer.

The location of the joint reinforcement was chosen to ensure that proper cover could be achieved between the bars and the ledge (discussed further in the following section); this allowed UHPC to flow under the bars, which decreases the development length. Both joints had the same width (6 inches), embedment length of reinforcement (5 inches) and splice length (4 inches), and both joints used an exposed aggregate finish on their vertical faces, which was achieved by the precaster prior to delivery to the SRC.

The third joint detail (Alternate 1), shown in Figure 5.1 (c), was a combination of the FSB joint and the adjacent box beam joint tested by Graybeal [55]. The primary benefits of this joint are the gradual transitions at the joint boundary and the inclusion of top and bottom flanges. The shear key ensures sufficient shear transfer between the precast section and the joint by adding interface area for enhanced interface bond. The inclined transitions between flanges and webs decreases stress concentrations that may occur at the sharp transitions. Construction and testing of this joint detail provided a comparison (1) between the shear transfers of a joint with a shear key compared to one relying on aggregate interlock and (2) between a joint with gradual transition between flange and web compared to one with a sharp corner.

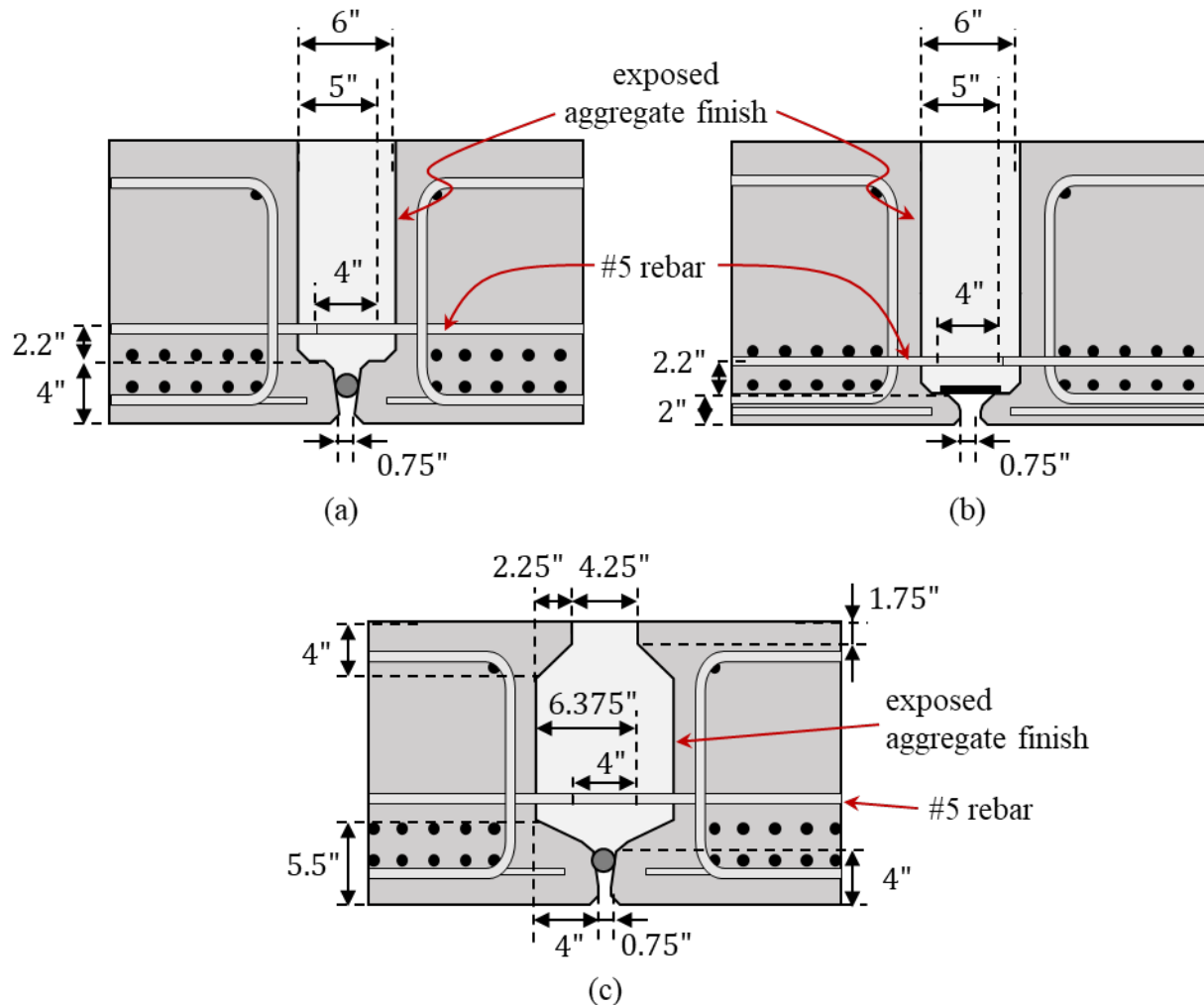
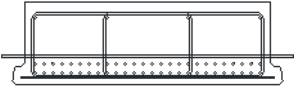
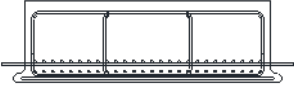
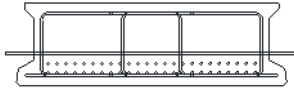


Figure 5.1: Proposed joints for experimental testing: (a) FDOT proposed joint detail 1 ("FDOT 1"), (b) FDOT proposed joint detail 2 ("FDOT 2"), and alternate joint detail based on joint developed by Graybeal [55] ("Alternate 1")

A comparison of the three joints is presented in Table 5.3, showing: cross section, joint area, approximate UHPC cost per foot of joint, embedment length, splice length. The approximate UHPC cost shown in the table is based on a cost of \$2,500 per cubic yard, which is an estimate of the list prices of a prebagged UHPC. Actual bid tabs can range from \$3,000 to more than \$8,000 per cubic yard. All three of the proposed joints have similar properties. The Alternate 1 joint design has a slightly larger area of UHPC and longer embedment length.

Table 5.1: Comparison of three joints proposed for testing

Beam Cross Section	Joint Area (for 18-in. depth) (in ²)	Approx. UHPC Cost (per foot of joint)	Embedment Length (in)	Splice Length (in)
FDOT 1 	84.5 in ²	\$54.30	5 in.	4 in.
FDOT 2 	95.4 in ²	\$61.30	5 in.	4 in.
Alternate 1 	108.4 in ²	\$69.70	6.375 in.	4 in.

All the UHPC joints tested had the joint reinforcement placed at 6 inches on center, as shown in Figure 5.2. Placing the reinforcement bars at 6 inches on center and staggering them between beams created a center-to-center spacing of 3 inches (clear spacing of 2.375 inches). As shown in Table 5.4, the maximum recommended clear spacing is 3 inches, which was satisfied by this layout.

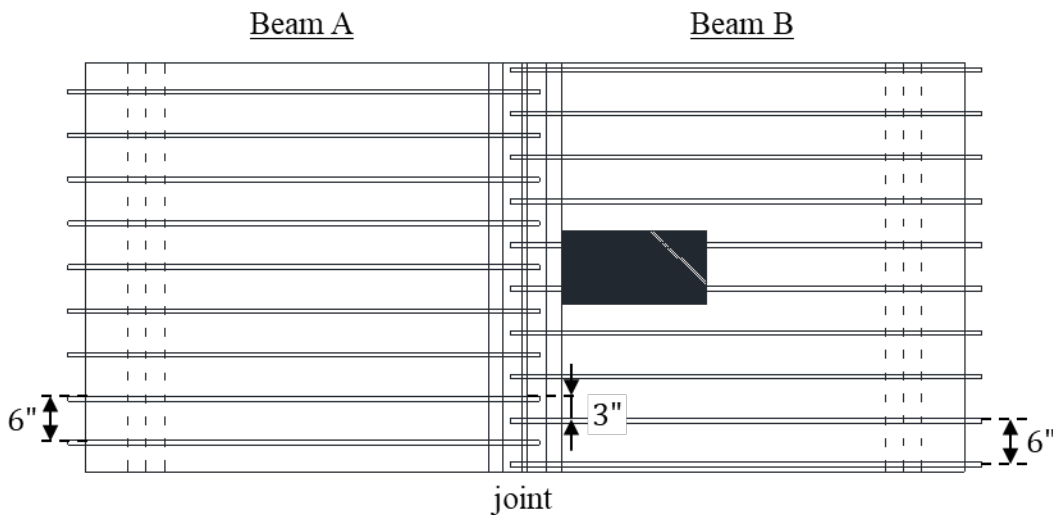


Figure 5.2: Plan view of two beams with joint for proposed testing

A fourth joint detail (Alternate 2) was developed after completing the tests on the three 18-inch and 12-inch joint geometries. Alternate 2 aimed to enhance the Alternate 1 detail by having an increased lever arm length by decreasing the bottom flange thickness and moving the joint rebar further down. This was achieved by decreasing the thickness of the bottom ledge by 1.375 inches, to have 0.75 inches (the minimum cover for this face) between the ledge reinforcement and top of ledge. The joint reinforcement in this new configuration extended 6.375 inches from the beam, which resulted in an increased lap length (of 5.25 inches). Finally, the area of the joint

was decreased by moving the vertical interior face of the joint further out. Moving the interior face out also decreased the stress concentration placed on the top flange. The new joint geometry also will accommodate construction tolerances for beam placement.

During the tests of the 12-inch and 18-inch-deep Alternate 1 specimens, it was observed that the top flanges were failing due to stress concentration in the concrete produced by the actuator plates placed on top of that location. As a result, a single #4 bar layer was placed in the top lip. This joint was named Alternate 2 and is depicted in Figure 5.3.

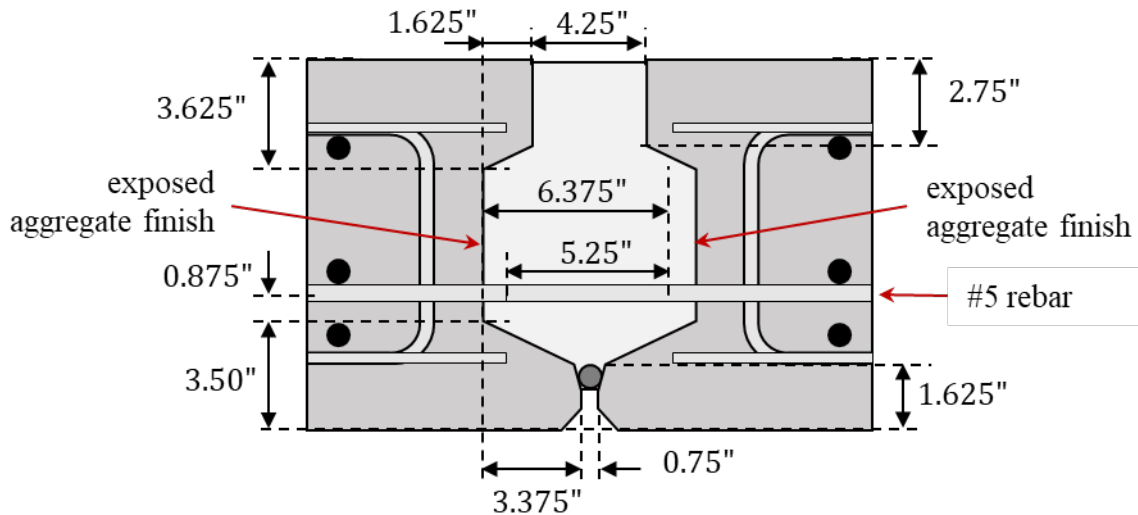


Figure 5.3: Alternate 2 joint detail

5.3. DESIGN OF FIELD-CAST UHPC CONNECTION DETAILS

Although UHPC connections are not yet included in the AASHTO LRFD Bridge Design Specification or Florida DOT Bridge Standards, there is a Guide Specification that was developed from the FHWA [39]. This FHWA publication provides guidance on the design and fabrication of UHPC joints. The relevant recommendations for this research are summarized in this section.

First, the precast concrete surface of the joint region that was bonded to the UHPC was intentionally roughened using an exposed aggregate finish. If the precast concrete surface is not roughened, shear transfer between the joint and precast section will be dependent on protruding reinforcement and shear key details. Roughening the surface will also help to create sufficient bond between the precast concrete and UHPC; this will make any tensile cracking develop in the precast section rather than along the interface. The surface was intentionally roughened to a 0.25-inch amplitude.

The recommended embedment lengths, cover, lap splice length, and spacing between spliced bars are summarized in Table 5.2. These recommendations are based on UHPC with 2-percent (by volume) steel fiber reinforcement and a compressive strength of at least 14 ksi. The 14 ksi compressive strength requirement allows for accelerated construction applications, as UHPC can reach 14 ksi within the first few days after casting [56].

The joint regions proposed for testing all use #5 rebar as the primary joint reinforcement. The calculated recommended values for #5 ($d_b = 0.625$ inches) are shown in Table 5.2 alongside those provided in the FDOT recommended joints. The alternate joint detail has the same provided values other than a longer embedment length of 6.375 inches and a longer lap splice length of 5.25 inches for Alternate 2.

Table 5.2: Guidance for structural design of UHPC connections [39]

Parameter	Formula	Value	Provided
<i>Embedment Length</i>	$l_d = 8d_b$	$8 * 0.625 = 5$ in.	5 in.
<i>Cover</i>	$\geq 3d_b$	$3 * 0.625 = 1.875$ in.	1.875 in.
<i>Lap splice length</i>	$l_s = 0.75l_d$	$0.75 * 5 = 3.75$ in.	4 in.
<i>Maximum clear spacing</i>	l_s	3.75 in.	2.375 in.

Note: If $f_y \leq 100$ ksi and $2d_b \leq \text{minimum cover} \leq 3d_b$ then the embedment length shall be increased by $2d_b$.

5.4. TEST MATRIX

The objective of the small-scale joint testing was to investigate the transverse joint flexural behavior of the current Florida Slab Beam (FSB) and other proposed joint details with UHPC. Eight joint specimens were tested: four 18-inch-thick joints (control joint and three proposed geometries) and four 12-inch-thick joints (four proposed joints) as depicted in Figure 5.4.

The shallowest section that is achievable with the current FSB design is 12 inches. A 6-inch cast-in-place (CIP) composite deck is then cast at the same time as the joint, which would result in a final section depth of 18 inches, as shown in Figure 5.4 (a). Three of the joint types with 18-inch-deep specimens were compared to the 18-inch-deep current FSB design (12-inch precast section and 6-inch deck).

The behavior of four of the proposed joint geometries was evaluated on 12-inch-deep specimens, which is the shallowest section depth for the current FSB Design Standard. The Alternate 2 joint detail was developed after initial testing of the specimens. Only one set of Alternate 2 specimens could be cast (due to budget and time limitations), which is why only a 12-inch-deep specimen was constructed and tested.

All specimens included prestressing strands with minimal stress to keep the strands from sagging. These sets of specimens provided a direct comparison between the joint behavior at 12 and 18 inches.

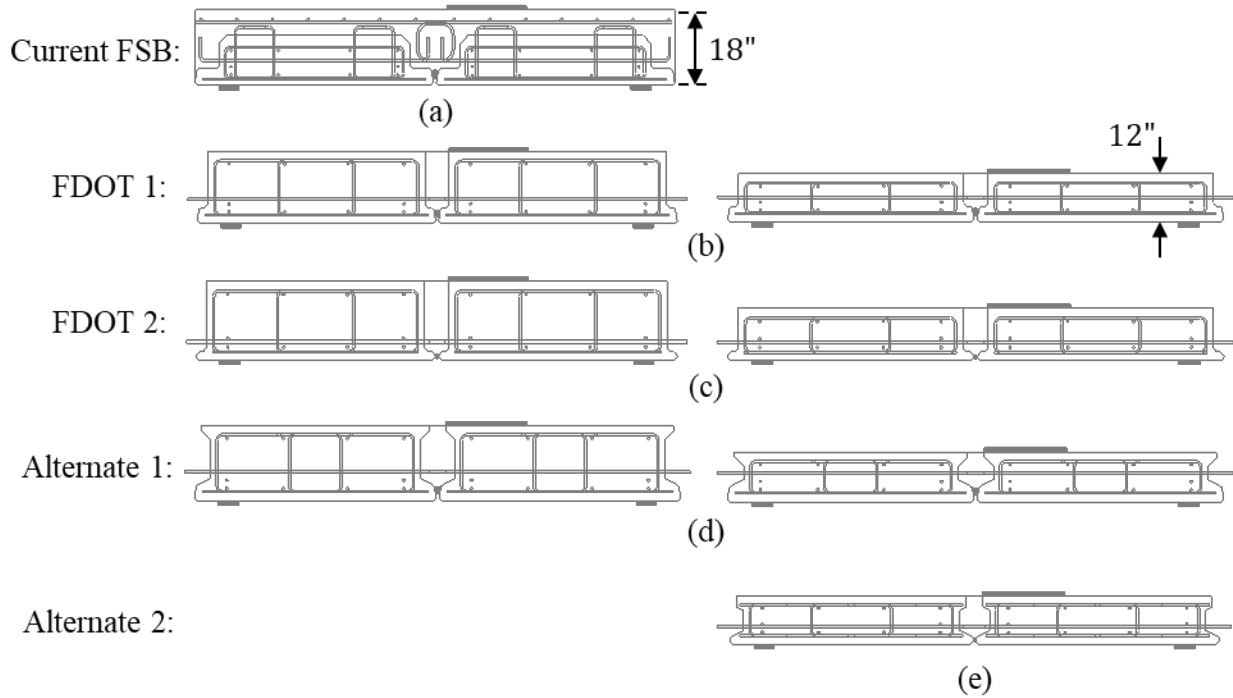


Figure 5.4: Specimen details: (a) current FSB joint detail, (b) proposed FDOT 1 keyway, (c) proposed FDOT 2 keyway, (d) proposed Alternate 1 keyway, and (e) proposed Alternate 2 keyway

The naming convention used for the small-scale test specimens is shown in Figure 5.5. The specimens with the original FSB joint geometry were called “FSB”. The other joints were named based on specimen height (12 or 18 inch) and joint type (F1, F2, A1, A2). The number following the joint name is the test number (1 or 2). As an example, the first test of the 18-inch-deep specimen with the Alternate 1 joint detail was named 18A1-1. This naming convention is used throughout this report.

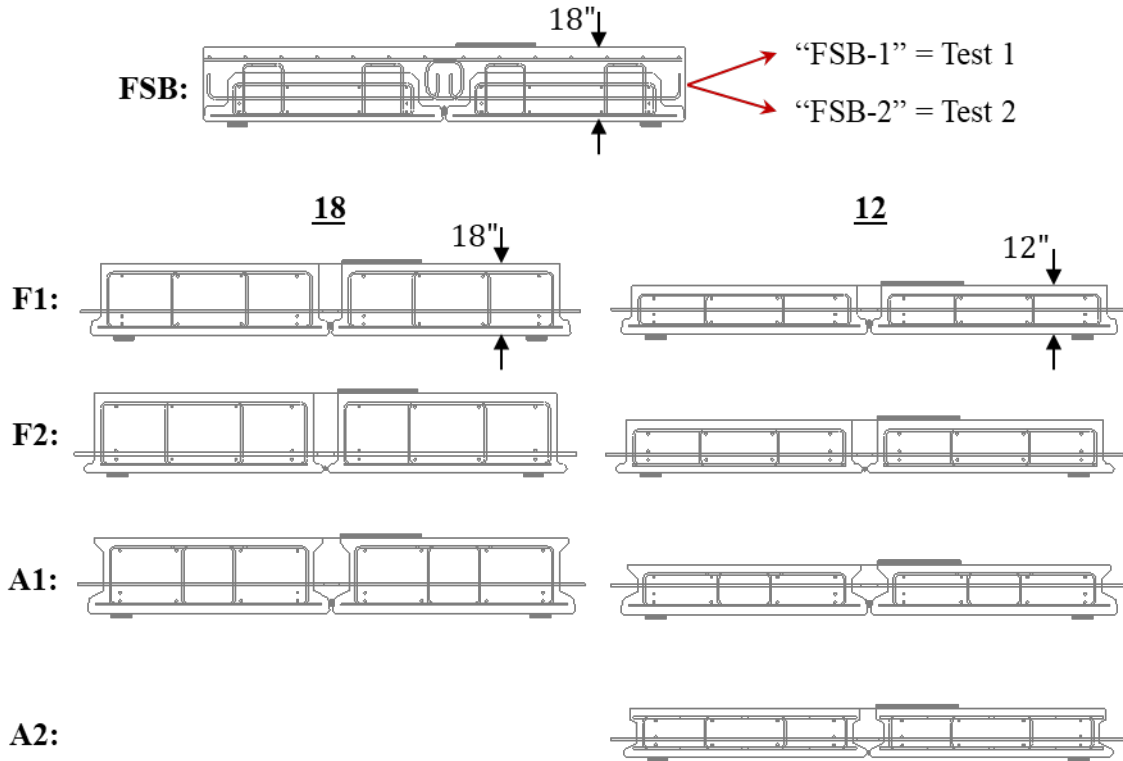


Figure 5.5: Naming convention for small-scale specimens

5.5. SPECIMEN CONSTRUCTION

5.5.1. Beam Construction

Sixteen (16) prestressed slab-beam sections were constructed by a local precaster to assemble the joint specimens, each 56-inch long by 60-inch width. There were two sets of prestressed sections: ten (10) beams of 12-inch thickness and six (6) beams of 18-inch thickness. The steel reinforcement placement and concrete pour are shown in Figure 5.6; this procedure was similar for all the specimens. The control joint specimen (current FSB) consisted of two FSB 12x60 inches and a 6-inch cast-in-place (CIP) deck that was poured once the beams were installed for testing.

The concrete mix specified for all the beams was FDOT Concrete Class VI with a minimum compressive strength at 28 days of 8,500 psi and maximum water/cement ratio of 0.37 lb/lb. The concrete mix used for the control FSB CIP deck was FDOT Concrete Class II (bridge deck) with a minimum compressive strength at 28 days of 4,500 psi and maximum water/cement ratio of 0.44 lb/lb requirements.

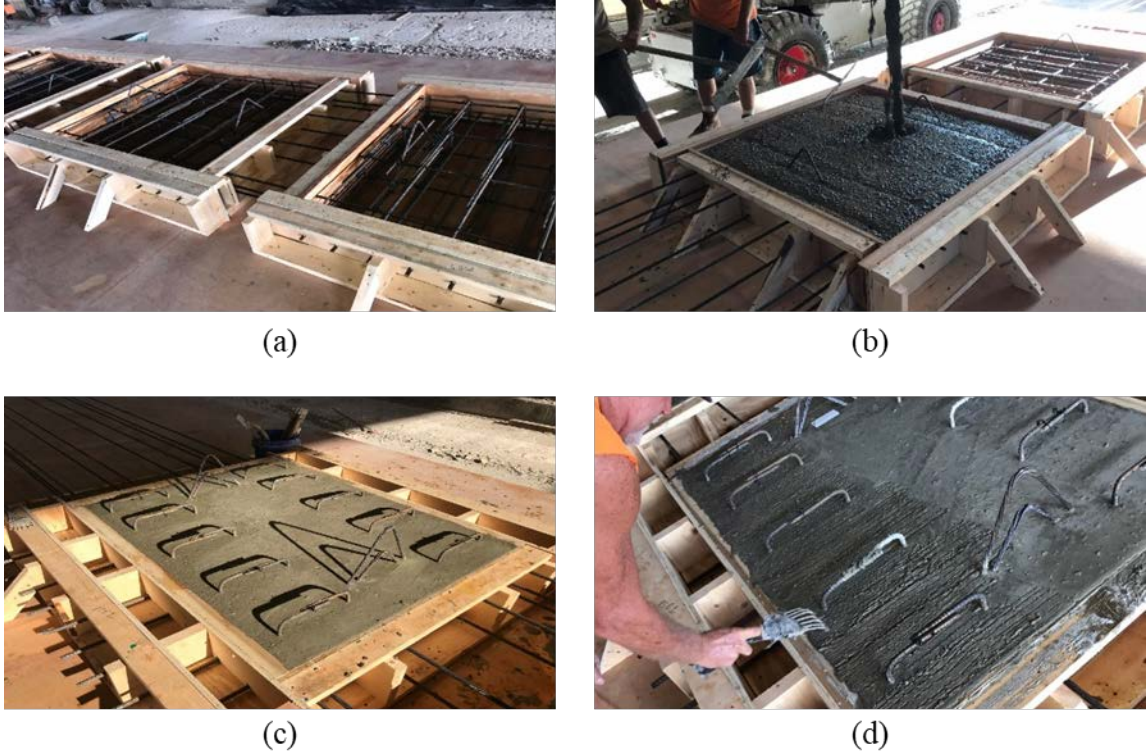


Figure 5.6: Construction of specimens: (a) specimen form and reinforcement, (b) concrete pour, (c) finished cast, and (d) surface raked finish for FSB control

After the concrete was cast in the original FSBs, the top surface was raked to a 0.25-inch amplitude roughness to enhance the bond between the future CIP deck and the beam, as shown in Figure 5.6 (d). The rest of the beams had a smooth float top finish. Interfaces of precast concrete components (i.e., the joint regions) were specified to be intentionally roughened to an exposed aggregate surface finish with 0.25-inch amplitude roughness to ensure sufficient bond between the UHPC and concrete of the precast section. Mild steel (A615) was used for the transverse and shear reinforcement with a yielding strength of at least 60,000 psi. Ten (10) seven-wire prestressing strands were used per beam with ultimate strength of 270 ksi and 0.6-inch diameter. The strands were fully bonded and pre-tensioned to 50 ksi to eliminate sagging of the strands and to simulate some level of prestressing force.

After the beams were built at the precast plant, they were shipped to the FDOT M.H. Ansley Structures Research Center in Tallahassee, as shown in Figure 5.7.



Figure 5.7: (a) Delivery of all slab-beam specimens, (b) beam showing strands, transverse reinforcement and lifting hooks (18-inch FDOT 1 shown)

5.5.2. Material Properties

The relevant material properties for the concrete and reinforcement used to construct the precast sections, CIP deck for the FSB, and joints are presented in this section.

5.5.2.1. Concrete Mixture Designs

The specified mix design for all the precast sections was FDOT Concrete Class VI and for the CIP deck was FDOT Concrete Class II in concordance with FDOT Developmental Specifications [57], [58]. Each precast beam was built by a local precaster using self-consolidating concrete with a target compressive strength at 28 days of 8,500 psi. The measured compressive strength for the concrete used in each of the specimens is shown later in Table 5.9. The mixture design is shown in Table 5.3. The coarse aggregate was product FDOT Code 12 [59] and followed ASTM #67 specification [60] and had a maximum aggregate size of ¾-inch.

Table 5.3: Concrete mixture design for Class VI concrete used in precast sections

Component	Quantity
Cement – Type II	735 lbs.
Fly Ash – Class F	165 lbs.
C12 - #67 Stone	1324 lbs.
F01 – Silica Sand (Concrete)	1270 lbs.
Darex AEA – Admixture for Concrete – Air Entraining	2 fl. oz.
ZYLA 610 – Admixture for Concrete – Type D	36 fl. oz.
ADVA Cast 600 – Admixture for Concrete Type F	50 fl. oz.
Water	36 gallons (300 lbs.)

The concrete used for the CIP deck and joint of the FSB specimens was specified with a target compressive strength at 28 days of 4,500 psi. The concrete mixture design provided by the ready-mix plant is shown in Table 5.4.

Table 5.4: Concrete mixture design for Class II concrete used for CIP deck and joint in FSB control specimens

Component	Quantity
Cement – Type I/II	635 lbs.
Coarse Aggregate	2220 lbs.
Fine Aggregate	1420 lbs.
Fly Ash – Class F	155 lbs.
Darex AEA – Admixture for Concrete – Air Entraining	4 fl. oz.
WRDA64 – Admixture for Concrete	40 fl. oz.
Water	24 gallons

One of the bottom ledges needed to be repaired in the 12F2-1 specimens due to fracture when the beams were being prepared for UHPC casting. A concrete mixture, shown in Table 5.5, was used to repair the ledge and proceed with the UHPC cast.

Table 5.5: Mixture design to repair ledge in 12F2-1

Component	Quantity
Vibropruf-11	50 lbs.
Sand	7 lbs.
Pea Gravel	20 lbs.
River Rock	10 lbs.
Water	8.85 lbs.

The UHPC mixture was specified to be Ductal® JS1000, which is a proprietary UHPC mixture commonly used for field-cast closure pours for prefabricated bridge element connections. This UHPC mixture contains the following components:

- *Premix (dark grey)*: pre-blended cement, sand, ground quartz, and silica fume
- *Liquid Admixture*: high range water reducer
- *Steel fibers*: 0.008 in. diameter x 0.5 in. long; tensile strength > 290 ksi
- *Water and/or ice*: Ice required when batching in warm/hot weather

The procedure for mixing the UHPC is shown in Figure 5.8 and included the following steps:

1. Weigh out each ingredient for mixture
2. Add dry Premix
3. Add ice/water and superplasticizer
4. Mix until fluid (10 to 15 minutes)
5. Add steel fibers
6. Mix 5 minutes, or until complete uniformity

7. Perform flow table test. If mixture is not fluid (below 5 inches), add 5% more water (if temp. $\leq 75^{\circ}\text{F}$) or 5% ice (if temp. $> 75^{\circ}\text{F}$). If too fluid (above 9 inches), add dry material and fiber.
8. Mix additional 5 minutes, or until completely uniform, if additional materials added, otherwise skip to 9
9. Place UHPC and make cylinders

The UHPC component dosages were prepared by weight and measured before mixing began, as shown in Figure 5.8 (a) and (b). The components were mixed in an Imer Mortarman high-shear mixer, shown in Figure 5.8 (c). After mixing, the UHPC was placed in the joints, as shown in Figure 5.8 (d), and used to make cylinders and small beams for materials testing.

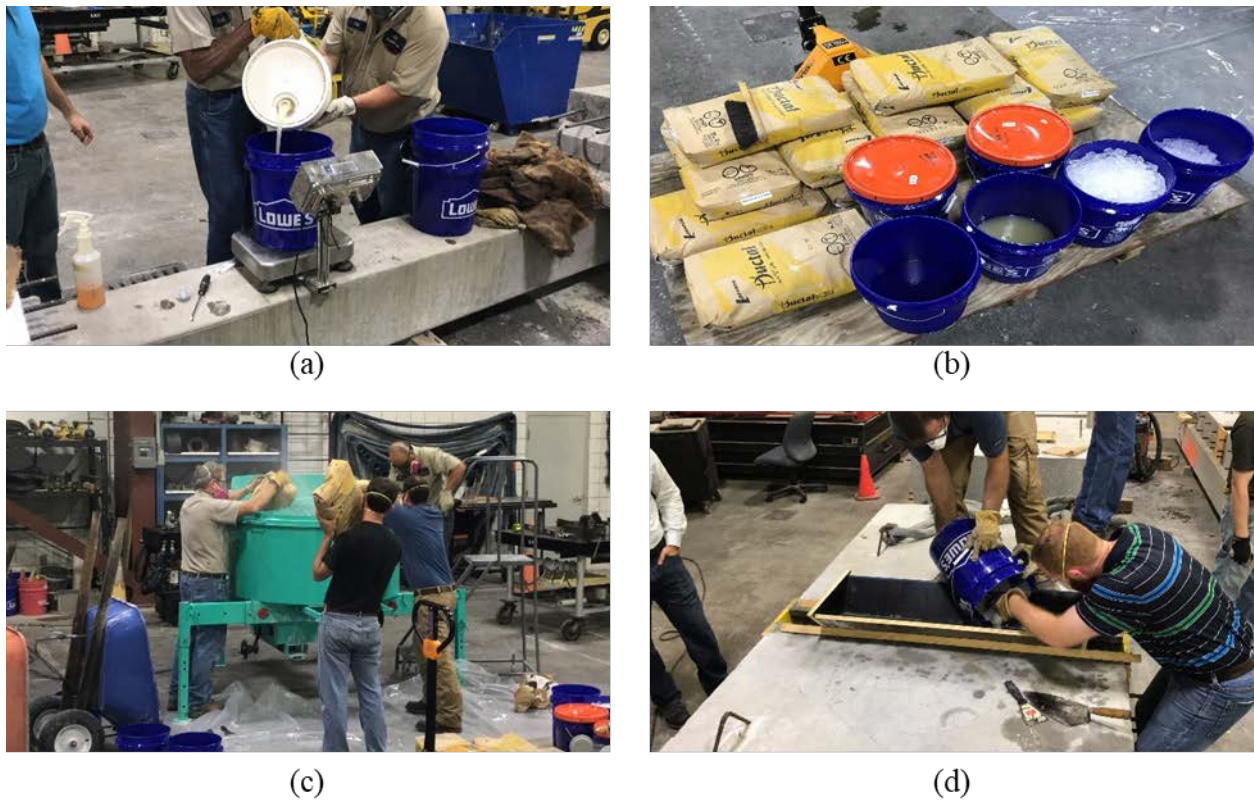


Figure 5.8: UHPC mixing process: (a) weighing of ingredients, (b) dosages preparation, (c) mixing operation of UHPC, and (d) placing operation for the UHPC

Although JS1000 was specified, the pre-mix for JS1212 (a high early strength UHPC) was provided. The mistake was not caught before casting of the first joints, so the first joints were cast using the JS1212 pre-mix with the JS1000 admixtures. This resulted in a UHPC that only had around 30 minutes of working time. The mixture proportions of the UHPC batches prepared with the JS1212 pre-mix and JS1000 admixtures are shown in Table 5.6.

Table 5.6: UHPC mixtures for Testing Phase 1 (using JS1212 pre-mix)

UHPC Batch	Design Mix (Pounds)					Specimen ID	Ambient Temp. (°F)
	Premix	Ice	Water	Admixture	Steel		
1	552.31	27.34	3.04	7.73	39.21	12F2-1	77
2	708.60	31.46	7.86	9.92	50.31	12F1-1, 12A1-1	78
3	600.75	23.23	9.96	8.41	42.65	18F1-1	63
4	605.42	20.16	3.44	8.48	42.98	18F2-1	68
5	655.32	18.35	18.35	9.17	46.53	18A1-1	65

The UHPC used for the second round of tests on each pair of specimens was prepared with the correct JS1000 pre-mix and admixtures. Using the appropriate materials increased the working time to two hours. The mixture proportions of the UHPC batches prepared for this second round of testing are shown in Table 5.7.

Table 5.7: UHPC mixtures for Testing Phase 2 (using JS1000 pre-mix)

UHPC Batch	Design Mix (Pounds)					Specimen ID	Ambient Temp. (°F)
	Premix	Ice	Water	Admixture	Steel		
6	446.60	12.00	12.00	6.25	31.71	12F2-2	53
7	547.04	0.00	26.20	7.66	38.84	18F1-2	57
8	698.04	0.00	32.44	9.77	49.56	18A1-2	48
9	599.48	0.00	28.72	8.39	42.56	18F2-2	48
10	498.86	0.00	23.17	6.98	35.42	12F1-2	63
11	550.78	0.00	25.58	7.71	39.11	12A1-2	70
12	398.16	12.95	5.55	5.57	28.27	12A2-1	78
13	447.64	18.71	2.08	6.27	31.78	12A2-2	85

The rheological properties were measured for each UHPC batch described previously by performing a flow test. A slightly modified version of ASTM C1437 [61] was used per FHWA material tests recommendation [39], as shown in Figure 5.9 (a) and (b). This test consists of a miniaturized version of the spread test used for self-consolidating concrete.

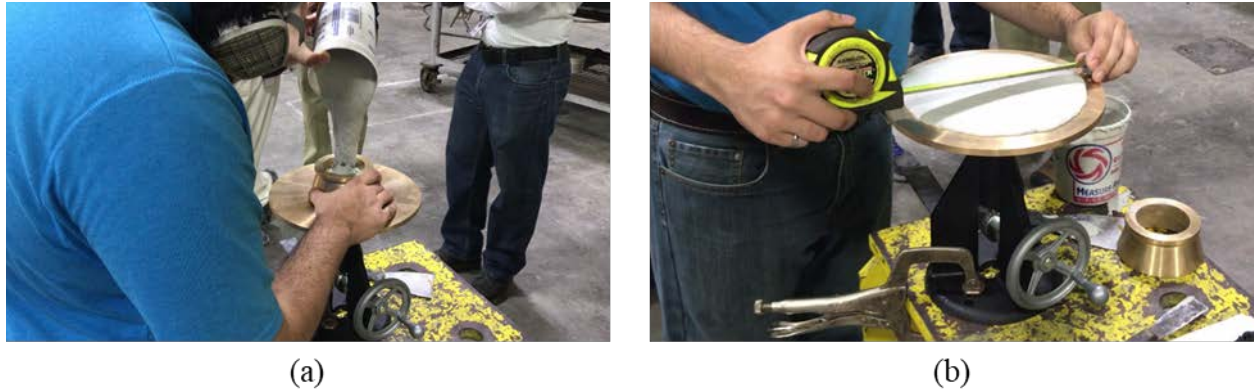


Figure 5.9: UHPC flow test: (a) specimen preparation and (b) spread measurement

The flow tests were conducted immediately after UHPC mixing to assess the mix before placement; results are summarized in Table 5.8. There was a slight difference in temperature and flow between the mixtures using JS1212 pre-mix (batches 1 to 5) and JS1000 pre-mix (batches 6 to 12).

Table 5.8: UHPC flow tests

UHPC Batch	Temperature (°F)	Static Flow (in.)*	Dynamic Flow (in.)*
1	72	7.44	8.38
2	73	8.48	9.19
3	60	7.40	8.03
4	70	7.56	7.98
5	73	7.22	7.81
6	57	8.25	8.94
7	66	8.22	8.81
8	54	8.00	8.50
9	54	8.13	8.69
10	66	8.19	8.75
11	72	8.54	9.13
12	79	8.44	no data
13	81	8.63	9.19

*Average taken from two measurements along different axes of same test sample

5.5.2.2. Hardened Concrete Properties

Compressive strength tests were performed on the cylinder samples taken from each concrete batch of the precast beams, the CIP decks, and the UHPC joints. Five 4-inch by 8-inch concrete cylinders were tested for each precast slab beam and for the FSB deck according to ASTM C39 [62, p. 39]. The average of the five compressive strength values was taken as the measured

strength for every joint during each testing stage. The UHPC compressive strength was measured using 3-inch by 6-inch cylinders prepared and tested based on ASTM C1856 [63] using a similar procedure to ASTM C39 [62, p. 39]; this procedure is described in the FHWA guidelines [39].

Per ASTM C1856 [63], the flexural strength of the UHPC was measured using small-scale beams subjected to third-point loading using ASTM C1609 [64]. Five 4-inch by 4-inch by 14-inch beam samples were cast at the same time the joints were built using metallic molds, shown in Figure 5.10 (a). These beams were tested on the day of joint testing to determine the tensile strength of the UHPC. Some of the fractured beams are shown in Figure 5.10 (b).



(a)



(b)

Figure 5.10: Beam samples for UHPC flexural performance: (a) 4x4x14 in. mold, and (b) broken UHPC beam samples

A summary of all concrete compressive strength and rupture strength properties are shown in Table 5.9.

Table 5.9: Specified and measured concrete strength for small-scale test specimens

Specimen ID	Beam Compression Concrete Strength (f'_c)		Joint Compression Concrete Strength (f'_c)		Joint Rupture Strength (f'_r)
	Specified (ksi)	Measured (ksi)	Specified (ksi)	Measured (ksi)	Measured (ksi)
FSB-1	8.5	12.41	4.5	6.48	N/A
FSB-2	8.5	12.71	4.5	1.37	N/A
18F1-1	8.5	11.87	21.0	24.60	1.80
18F1-2	8.5	11.66	21.0	23.98	1.48
18F2-1	8.5	11.88	21.0	25.48	2.19
18F2-2	8.5	12.21	21.0	24.86	3.04
18A1-1	8.5	11.31	21.0	23.84	2.93
18A1-2	8.5	11.02	21.0	23.27	1.39
12F1-1	8.5	12.40	21.0	23.23	2.10
12F1-2	8.5	12.46	21.0	27.18	1.48
12F2-1	8.5	11.82	21.0	23.94	2.82
12F2-2	8.5	12.47	21.0	24.48	3.04
12A1-1	8.5	12.50	21.0	23.23	2.10
12A1-2	8.5	13.77	21.0	25.94	3.32
12A2-1	8.5	11.17	21.0	24.23	2.67
12A2-2	8.5	12.22	21.0	25.48	1.50

5.5.2.3. Steel Reinforcement Properties

Three sizes of Grade 60 mild steel reinforcement were used to build all the precast specimens: #3, #4, and #5 reinforcement. Six fully bonded pre-tensioned strands were used in the precast section with a small amount of prestressing (50 ksi) to simulate some level of prestressing in the longitudinal direction. The measured properties for the steel reinforcement were provided by the precaster, shown in Table 5.10. The #5 reinforcement was taken from four different lots.

Table 5.10: Steel material data

Description	Yield (psi)	Tensile (psi)
#3 Rebar A615M Gr60	64,400	100,600
#4 Rebar A615M Gr60	70,800	100,200
#5 Rebar A615M Gr60 (a)	66,900	97,400
#5 Rebar A615M Gr60 (a)	65,400	96,600
#5 Rebar A615M Gr60 (a)	66,000	96,300
#5 Rebar A615M Gr60 (a)	66,700	98,200
0.600 7 wire 270 low lax. strand	251,000	275,000

(a) Rebars from four different lots/heats were used

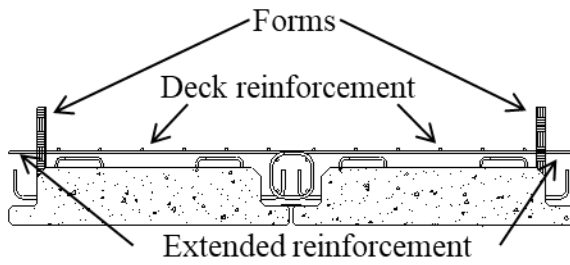
5.5.3. Placement of Cast-in-Place Deck

The construction of the original FSB joint detail was done following the same construction procedure described in the FSB Developmental: FDOT Index D20450 Series Florida Slab Beams [57]. After the two beams were placed side-by-side with a 0.75-inch spacing, formwork was built around the top of the system, and the rebar mat and joint reinforcement cage were placed such that the CIP concrete could be poured. A closed cell polyethylene baker rod was used to seal the bottom gap between the two beams to avoid leakage of the concrete. The FSB joint construction is shown in Figure 5.11.



Figure 5.11: Construction of deck and joint in FSB: (a) adjacent FSBs with $\frac{3}{4}$ " spacing, (b) CIP deck form construction, (c) slab and joint reinforcement, and (d) CIP deck pour

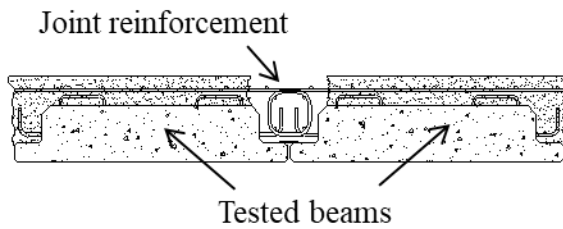
Each slab beam had the same joint geometry on both sides as they were designed to be interior beams in the superstructure. Having the same joint geometry on each side of the beam allowed for two strength tests to be performed per one set of beams, as described in detail in §5.6. Because the control FSB requires a CIP deck, the deck needed to be cast twice to fulfill the two-test requirement. For the first test, the FSB specimens were positioned adjacent to each other, the reinforcement and formwork placed, and the concrete cast, as shown in Figure 5.12 (a) and (b). The forms were placed, and deck reinforcement extended on the outside of the specimens to allow for the second test configuration shown in Figure 5.12 (c). After the beams were tested and rotated for the second phase, another reinforcement joint cage was placed and the top transverse bars in the deck were lapped. Finally, a second concrete cast was performed in the smaller joint-deck region for another testing round as shown in Figure 5.12 (d).



(a)



(b)



(c)



(d)

Figure 5.12: Deck cast for FSB specimens: (a) formwork layout for first testing stage, (b) deck casting operation for first testing stage after rebar placement, (c) alignment layout of broken pieces for second testing stage, and (d) second concrete cast operation

5.5.4. Placement of UHPC

The construction of the UHPC joints followed the same guidelines described in the FHWA publication [39] and shown in Figure 5.13. The beams were placed side by side leaving a $\frac{3}{4}$ -inch gap, and then a plywood panel was placed on each end to enclose the joint for UHPC cast, as shown in Figure 5.13 (a). A vertical dam was built using plywood panels to facilitate the UHPC pour and to avoid any possible material spill, shown in Figure 5.13 (c). All the plywood panels were covered with a waterproof sealer to avoid any water loss of the UHPC mix caused by the wood pores. The UHPC was mixed using an Imer Mortarman vertical shaft mixer, shown in Figure 5.13 (b).

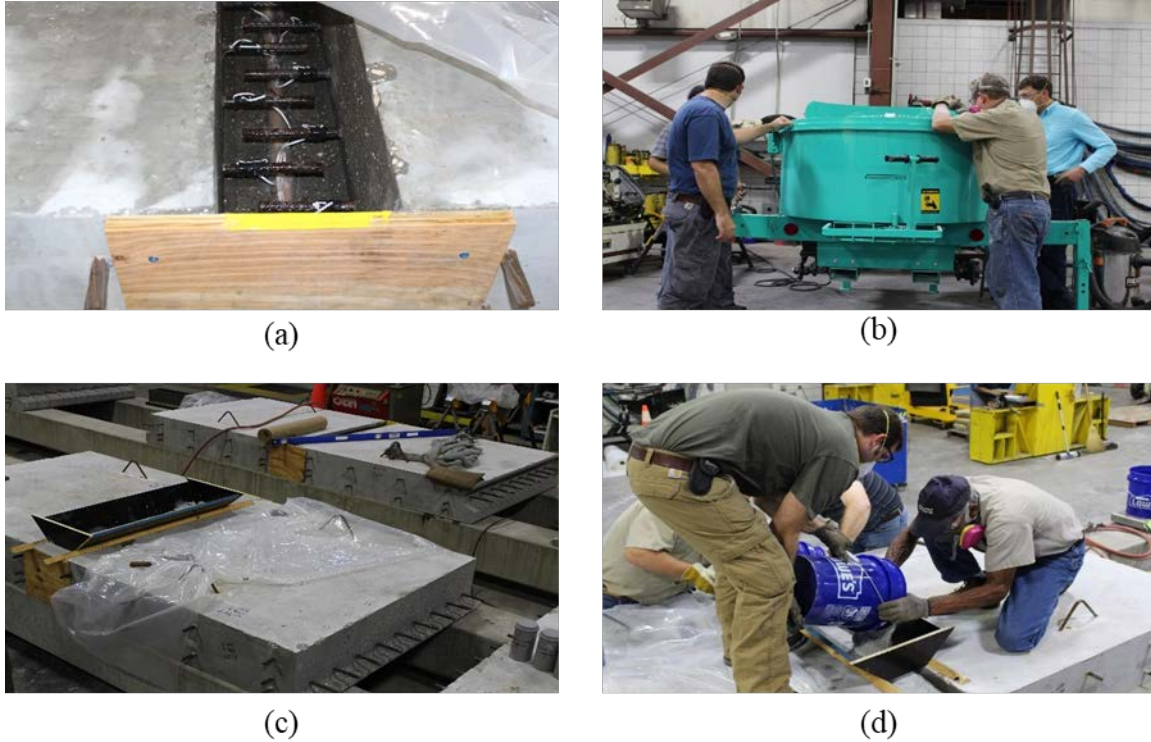


Figure 5.13: Casting procedure for UHPC joint: (a) connection detail with plywood block-out and pre-wetting of surfaces to an SSD condition before UHPC placement, (b) mixing operation for the field-cast UHPC, (c) vertical dam used to place the UHPC, and (d) placing operation for the field-cast UHPC

As described in the previous section, the modified joint geometries were tested twice as well. After the broken specimen were broken or cut apart, they were placed side by side and another UHPC joint was cast using the same vertical dam, shown in Figure 5.14 (a). After the concrete was hardened, the new joint was tested, shown in Figure 5.14 (b).

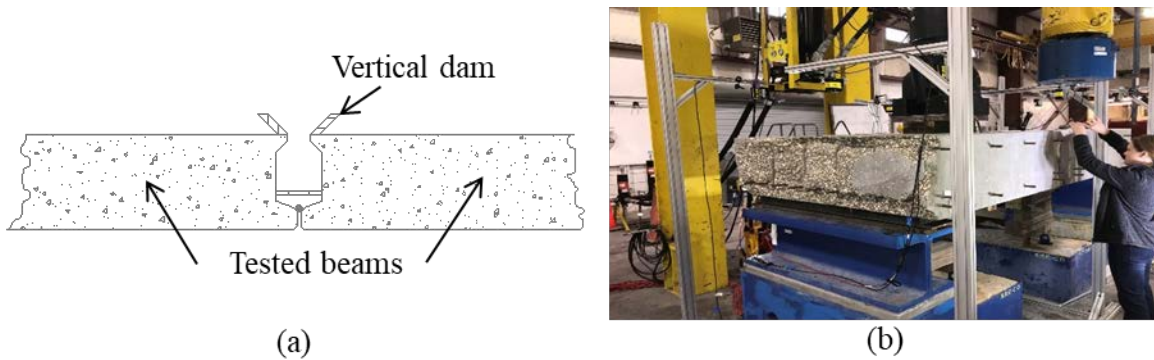


Figure 5.14: Casting of UHPC joint for second test: (a) vertical dam layout on broken beams and (b) second testing instance for joint geometry

5.5.5. Observations from Construction

5.5.5.1. Surface Treatment of Joint Face

According to the FHWA Guidelines [39] for construction of field-cast UHPC connections, interface surface preparation is integral to the bond strength of the UHPC to the precast member. An exposed aggregate finish with at least ¼-inch amplitude showing good macro- and micro-texture is specified to provide extra bonding area between the aggregate in the precast member and the fresh UHPC. The guideline also establishes different bond levels depending on the joint surface treatment: as-cast interface (low), sandblasted interface (intermediate), and exposed aggregate interface (high). The recommended finish is shown in Figure 5.15 (a).

A roughened surface with exposed aggregate was specified to ensure appropriate precast-to-UHPC bond. However, a heavy sandblast finish was provided for the first set of beams cast, including all specimens for the first three joint geometries (FDOT 1, FDOT 2, Alternate 1), as shown in Figure 5.15 (b). The heavy sandblast finish did not create a rough enough surface to properly bond to the UHPC, so there was separation between the joint material (UHPC) and the precast segment during testing, as shown in Figure 5.15 (c) and (d).

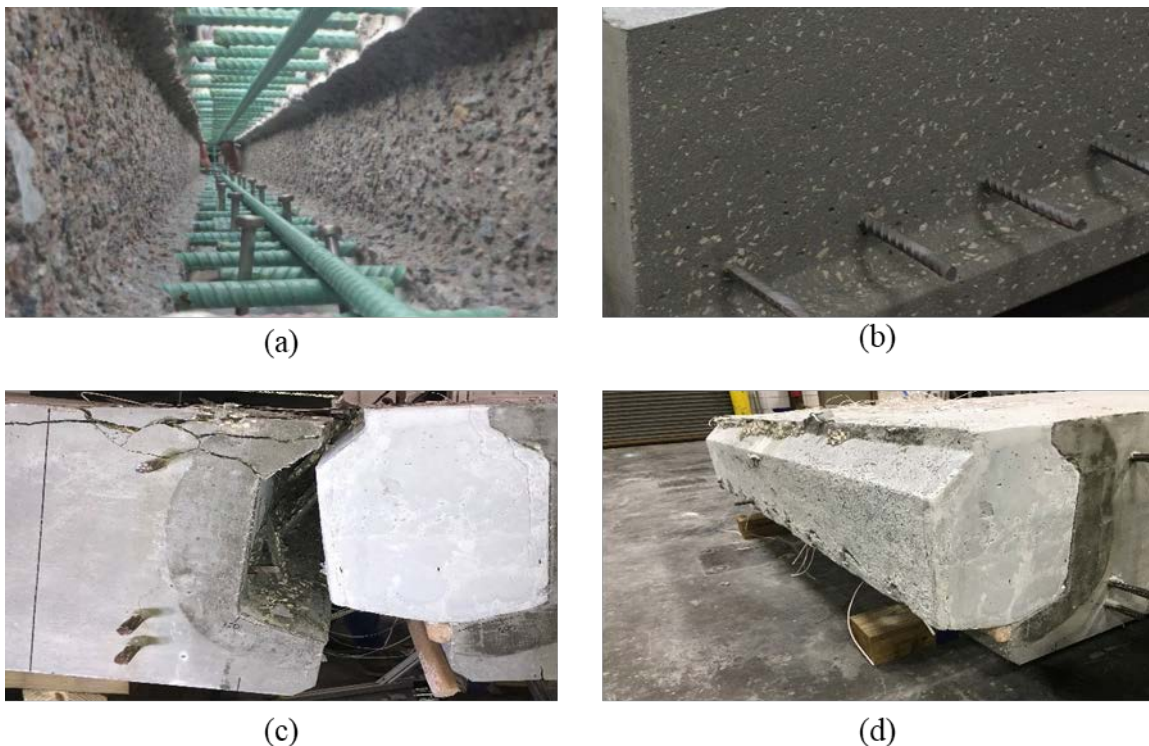


Figure 5.15: (a) Desired interface surface preparation (per FHWA guidelines [39]), (b) heavy sandblast finish provided, (c) joint material separation from Alternate 1 precast section (similar behavior in other specimens), and (d) bond lost between UHPC joint matrix and precast concrete

Although the surface finish of the joint region did not seem to play a role in the ultimate capacity of the connection, it is thought to be a critical factor in the long-term service life of the joint. Insufficient bond can lead to early separation at the interface, which can expose the joint reinforcement to early age pollution penetration (e.g., carbonation and/or chlorides) that might

decrease the transverse capacity and overall performance of the superstructure. An inappropriate UHPC mix design also likely contributed to this poor bond, discussed in §5.5.5.4.

The language for the construction of the joint aggregate exposure was changed in the construction plans of the new geometry (Alternate 2) to describe in detail how to achieve the desired surface finish. Additionally, a mock-up was required to be constructed and approved prior to casting of the specimens.

A set retarding agent was required to be painted on the forms prior to casting to achieve the desired finish. The following additional guidance was provided to the precaster [65]:

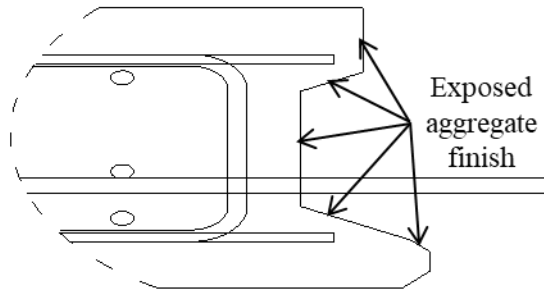
- Form retarders are water activated, so high relative humidity and moisture can decrease agent effectiveness. The set retarding agent should be applied on the same day as casting to minimize this effect.
- A polyurethane clear coat should be applied to wood forms prior to the application of the set retarding agent. This will prevent the set retarding agent from being primarily absorbed by the wood.
- The cement will harden over time, so forms should be removed from joint region and the surface pressure washed within 24 hours after casting.
- Water pressure and distance from joint surface should be adjusted to remove paste without fracturing aggregates.

FDOT also listed three products currently used to achieve the desired aggregate exposures, which were also included in the joint region preparation. These products are:

- BASF: MBT Heat Cote – Lilac [66]
- BASF: Master Finish – Lilac [67]
- Architectural Concrete Chemicals: Altus Series In-Form Retarder – Pink [68]

Note that the color of the set retarding agent symbolizes the magnitude of the exposed aggregate finish achievable with the admixture.

The final Alternate 2 joint surface preparation was achieved using the BASF: Master Finish® - Lilac agent by brushing one coat to the formwork of the keyway geometry approximately 6-8 hours prior to the concrete cast where the exposed aggregate finish was desired. The forms were removed one day after casting, and the surface was pressure washed using constant 3,500 psi water pressure at a controlled distance of application. The process for joint preparation and construction of the Alternate 2 specimens is shown in Figure 5.16.



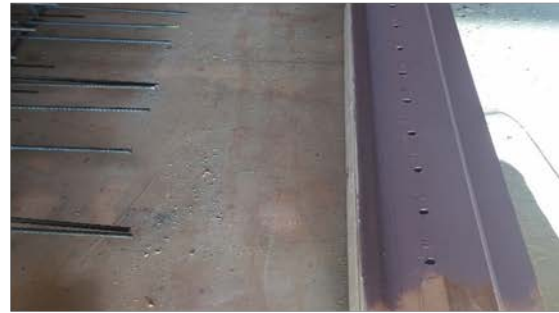
(a)



(b)



(c)



(d)



(e)



(f)



(g)



(h)

Figure 5.16: Process for exposed aggregate finish: (a) shear-key surface preparation detail, (b) in-form retarder agent, (c) removed shear-key region of the formwork, (d) retarder agent applied to the form wall, (e) block-outs with retarder agent fastened to the formwork, (f) concrete cast after product application, (g) retarded surface after block-outs removal, and (h) pressure washing operation

The completed joint finish for the Alternate 2 specimens compared to the finish achieved using sand blasting is shown in Figure 5.17. The procedure used to achieve the joint finish for the Alternate 2 specimens produced a much more roughened surface than the previous procedure, improving the precast concrete-to-UHPC bond.



Figure 5.17: Comparison of joint finish: (a) sand-blasted finish and (b) exposed-aggregate finish

Although the product worked as expected, it was still not enough to achieve a $\frac{1}{4}$ -inch amplitude as the resulted surface was only approximately $\frac{1}{8}$ -inch amplitude. The effect of the type of retarder agent used is directly dependent on the cement content, aggregate size, and environment relative humidity when the formwork brushing process is being performed. A maximum aggregate size of $\frac{3}{4}$ inch was used in the concrete mixture for these beams. Using a maximum coarse aggregate size of $1\frac{1}{4}$ inch is recommended for achieving a $\frac{1}{4}$ -inch amplitude. Additionally, the product application should be limited to the joint surfaces to be in contact with the UHPC. The product was applied to the side and bottom of the bottom flange in the Alternate 2, as shown in Figure 5.18.



Figure 5.18: Unnecessary agent application zone (a) before and (b) after joint casting

5.5.5.2. Size of Bottom Flange and Ledge Thickness

Another issue that was observed during the beam specimen constructions was the thickness of the bottom flange. The bottom flange in these members is used to allow the joint to be self-forming. Different bottom flange geometries were proposed in the design stage of the modified FSB specimens and constructed, as shown in Figure 5.19.

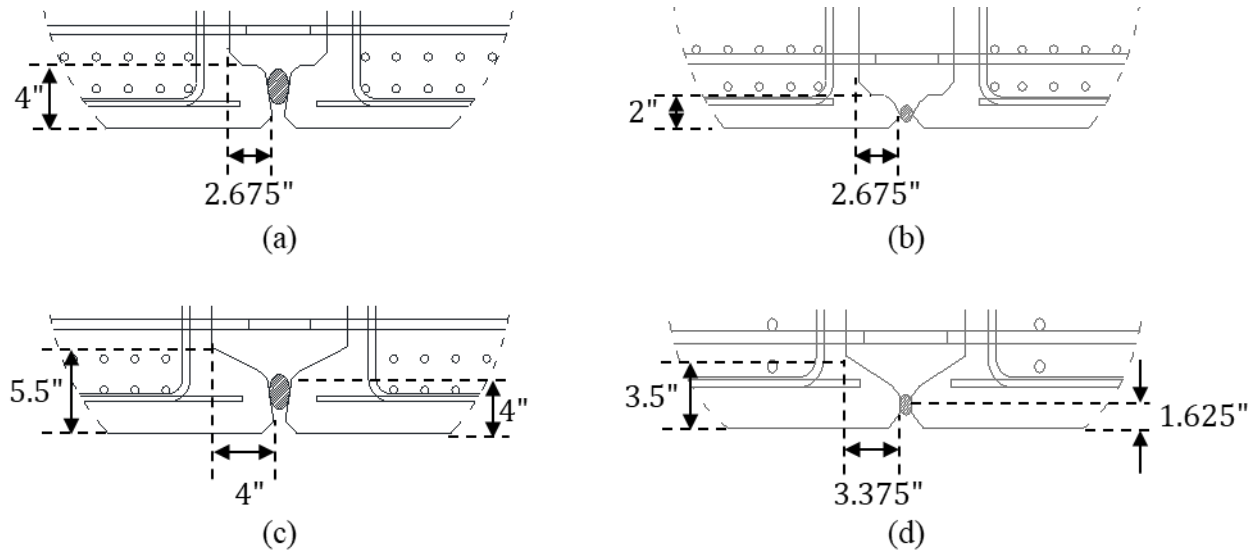


Figure 5.19: (a) FDOT 1 ledge shape, (b) FDOT 2 ledge shape, (c) Alternate 1 ledge shape, and (d) Alternate 2 ledge shape

Thinner bottom ledge depths allowed for greater lever arms for the transverse joint reinforcement. However, thin bottom flanges presented challenges with constructability and stress concentrations during experimental testing. The bottom lip of the FDOT 2 joint geometry was too thin and unreinforced, which led to part of the flange breaking off during construction. These constructability issues occurred on beams only 56 inches long, so these issues would only be magnified for longer beams with larger amounts of prestressing. Additionally, the ledge of the FDOT 2 joint showed cracking during strength testing before reaching the ultimate failure load of the overall connection, as shown in Figure 5.20. These were considered when deciding on the joint details to move forward with for further testing.

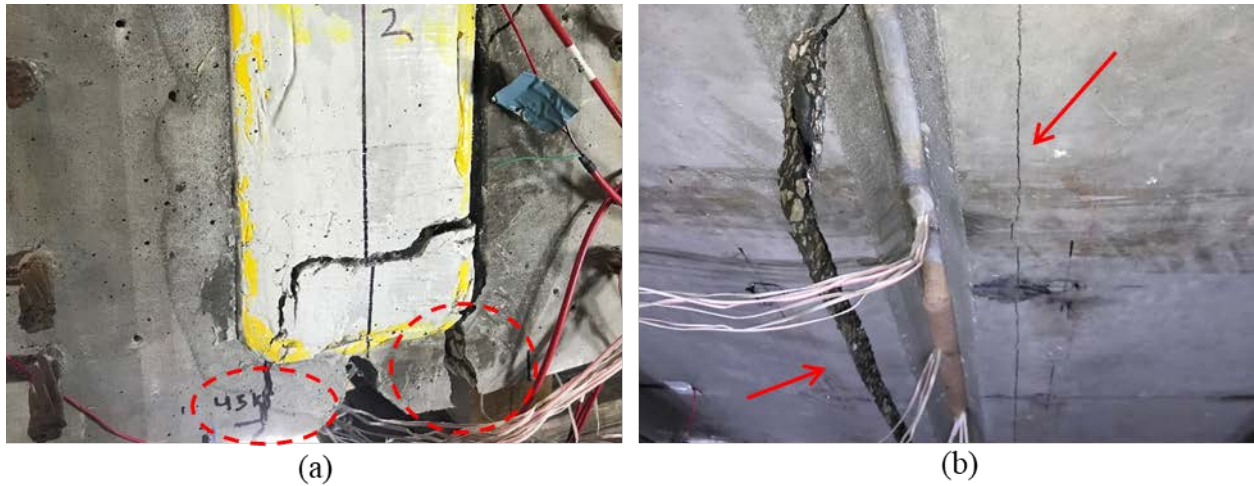


Figure 5.20: (a) FDOT 2 cracked bottom lips and (b) FDOT 2 longitudinal cracks of bottom lips on the underside

5.5.5.3. Reinforcement Detailing

According to the original FSB Developmental specifications [57], a pair of #4 confinement stirrups must be used plus two pairs of #4 interface shear reinforcement, as shown in Figure 5.21. These create at least 4 legs of shear reinforcement within the complete FSB superstructure.

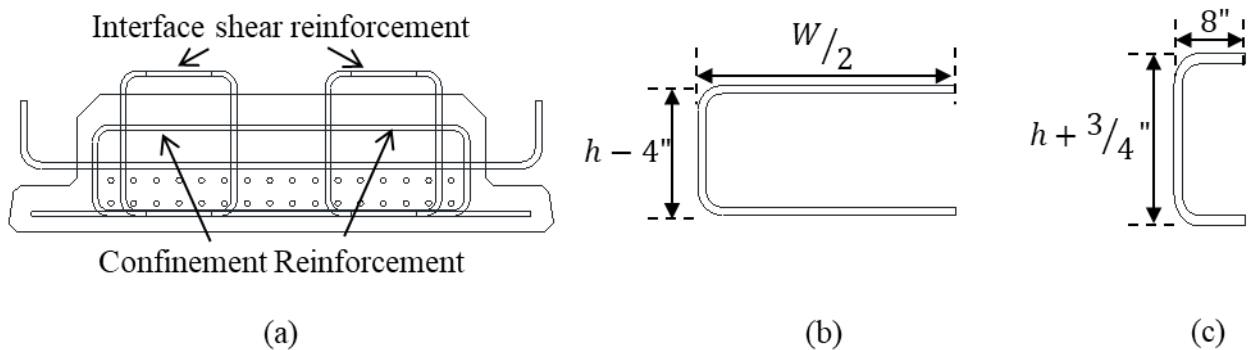


Figure 5.21: (a) Original FSB shear reinforcement, (b) confinement stirrup, and (c) interface stirrup

Because the proposed superstructure system with UHPC joints does not have a CIP deck, the interface shear reinforcement was eliminated. The width of the slab beam though still requires four legs of reinforcement to ensure proper shear strength and withstand bursting stresses from the strands. As a result, the stirrups were shortened to provide four legs using two pairs of bars, as shown in Figure 5.22. Four legs are recommended as several researchers [69]–[71] have shown improved behavior when shear reinforcement is distributed across the width of wide sections.

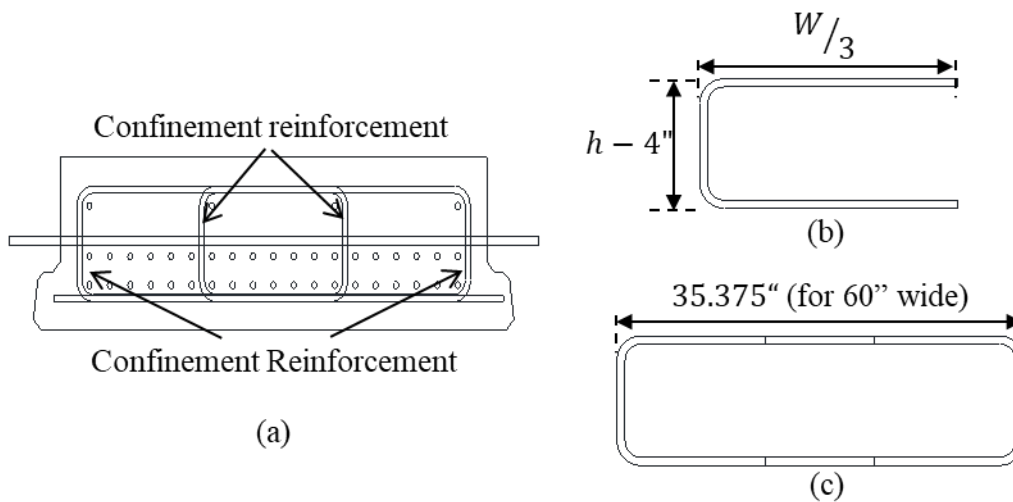


Figure 5.22: (a) Proposed slab-beam confinement reinforcement (FDOT 1 shown – others similar), (b) confinement stirrup, and (c) Alternate 2 dimension of stirrup loop (two loops needed – others similar)

Although this configuration maintained the necessary reinforcement in the new sections, it created an increased steel density of four bars in one single shear plane during construction. This density increased at the end of the specimens as it was difficult to maintain the adequate concrete cover of 2 inches on one side and the specified stirrup spacing on the other side. The bars had to be moved and placed with a slightly shifted angle, as shown in Figure 5.23, to maintain the same location as specified in the production drawings.

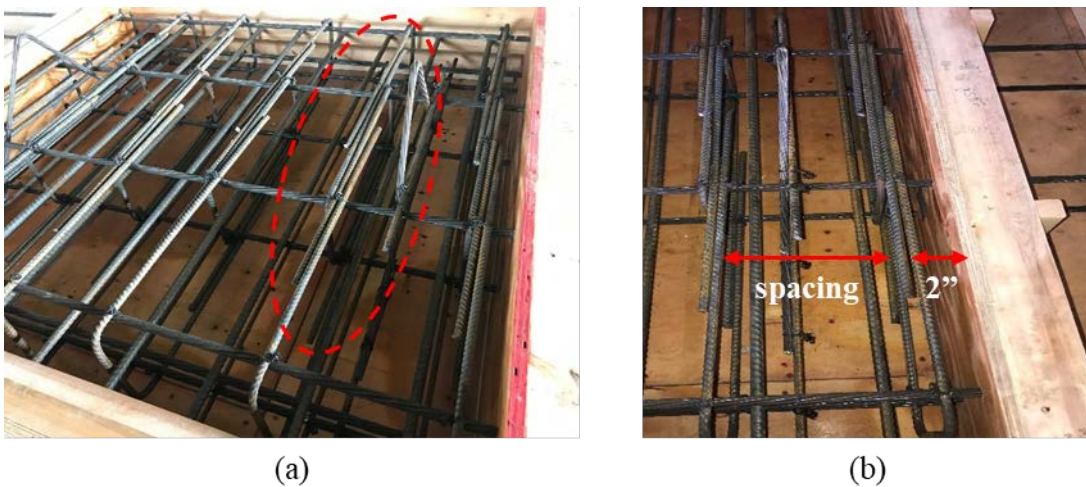


Figure 5.23: (a) Increased steel density and (b) unappropriated confinement spacing and cover

Another concern during the construction of the members was a misalignment of the joint reinforcement. During the placement of the Alternate 2 beams before UHPC cast, it was noticed that one slab beam was roughly 3/16-inch thicker than the other. This difference in thickness meant that the joint reinforcement extending from the two adjacent beams was not in the plane, as shown in Figure 5.24.



Figure 5.24: Transverse rebar misalignment observed in Alternate 2 joint specimen

The 3/16-inch misalignment was higher than the tolerance value specified in the FDOT Structures Design Manual (SDM), Section 25.3 [38], which states a maximum tolerance for dimensions of precast components of $\pm 1/8$ inch. The high tensile strength of the UHPC was thought to still be able to properly develop the reinforcement in the splice, so the decision was made to proceed with the testing. Because this superstructure system will not have a CIP deck to account for large construction misalignments, more restrictive construction tolerances and tolerances for beam camber variability may be required.

5.5.5.4. UHPC Materials

Several hardened clumps of UHPC dry premix were noticed during mixing for the first round of testing. One bag was sampled from the pallet of light grey premix by scooping out the material and sifting it over two layers of screen. Many clumps were found in each scoop of material from the top of the bag, as shown in Figure 5.25 (a). Even though the clumps could be broken up by hand, they were not completely broken up during 20 minutes of mixing with the Imer Mortarman mixer. It was determined that the clumps were in the premix because expired premix was accidentally shipped to the FDOT laboratory.



Figure 5.25: (a) Large and (b) small clumps collected from dry premix of UHPC

The first shipment of UHPC components received were a light grey dry premix and Chryσιο Premia[®] admixture. The light grey premix is used for Ductal[®] JS1212 accelerated mix, which requires a different set of admixtures. The Ductal[®] JS1000 is used with the Chryσιο Premia[®] admixture. The use of the wrong admixture with the wrong premix resulted in a faster setting time and stiffer mix. This likely contributed to the poor bond between precast beam and UHPC observed. The proper dark grey premix was then shipped to the laboratory and used for the second set of joint tests. Using this premix with the appropriate admixture improved flowability and extended the working time for the UHPC mixture. The comparison between the bond of the UHPC to the precast beam for sandblasted finish joints with the first and second UHPC mixtures is shown in Figure 5.26. There was an improved bond with the proper UHPC mixture.



Figure 5.26: UHPC joint bond comparison: (a) poor bond observed with the faulty UHPC mixture and (b) enhanced bond observed with the adequate UHPC mixture

5.5.5.5. *Sharp Edges in Beams*

Beam construction plans were specified with sharp corners at the top of the keyway geometry. Many of these sharp corners were damaged during removal of the forms, as shown in Figure 5.27.

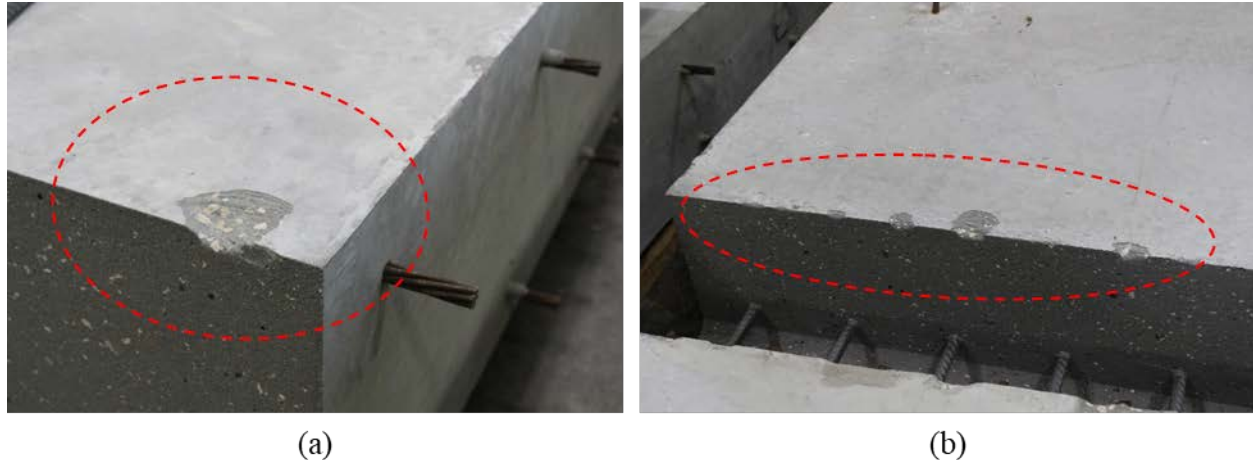


Figure 5.27: (a) Chipped keyway border and (b) several damages to the beam border

Accounting for this damage will be considered when determining the procedure for developing the final riding surface in future phases of this project.

5.5.5.6. *Faulty Rebar Bent in Original FSB Design*

In the original FSB design guidelines [57], a #5 bottom transverse continuity reinforcement with straight bar bend of 90 degrees and typical 2 ½-inch bend diameter is specified for the construction of the joint reinforcement, as shown in Figure 5.28 (a). The currently specified protruding length of the bar is 5 inches, and the height is 6 inches. This reinforcement detail was provided to the precast plant, but the actual bend diameter was much larger than specified in the constructed FSB specimens, as shown in Figure 5.28 (b). The larger bend diameter resulted in the continuity reinforcement not being able to develop, which led to a much lower capacity than expected. These test results and comparison will be discussed in §5.11.

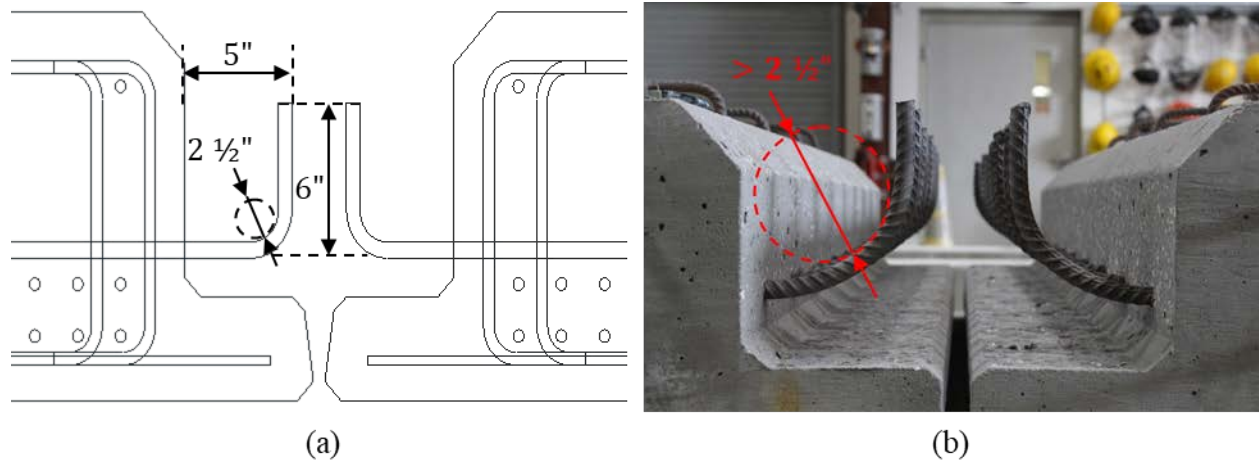


Figure 5.28: (a) Original rebar bent in control FSB and (b) larger rebar bent diameter delivered

5.6. TEST SETUP

The longitudinal performance of each joint specimen was evaluated in a testing frame configuration similar to the previous testing characteristics for longitudinal bridge deck panel-to-panel connections performed by Graybeal [41]. A schematic of the test configuration used for the small-scale joint configuration is shown in Figure 5.29.

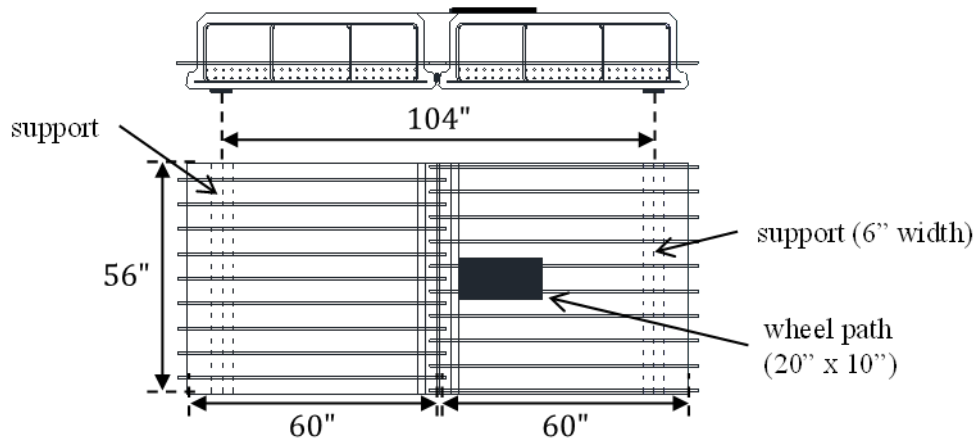
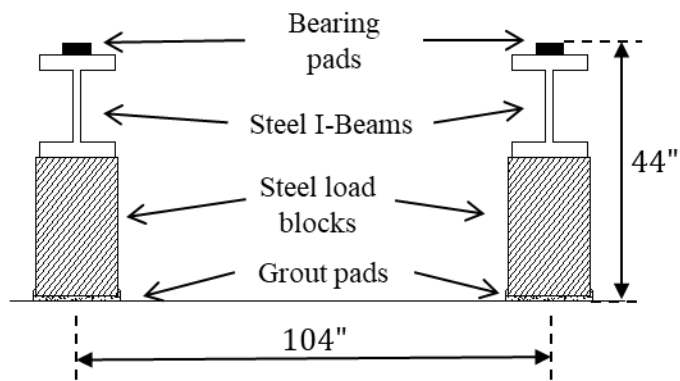


Figure 5.29: Schematic of testing configuration for small-scale joint testing

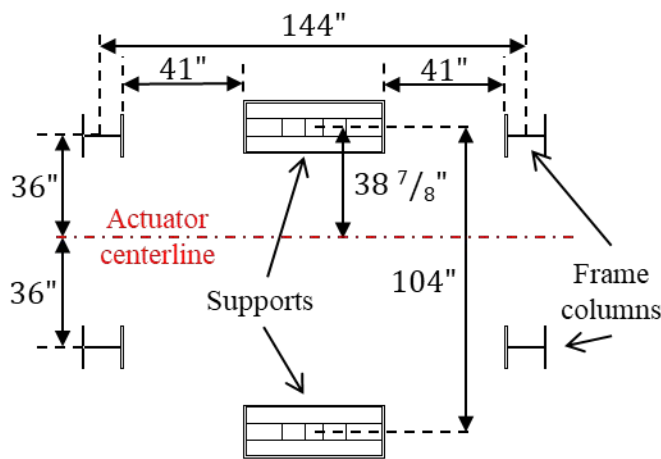
This test setup consisted of two main supports holding the samples in a simply supported configuration with a vertical clearance of 44 inches, as shown in Figure 5.30. The vertical clearance allowed for easy removal of the bottom instrumentation and ensured enough space for documenting crack patterns underneath the beams. The supports were grouted to the strong floor to ensure flatness and avoid undesired movement. The supports consisted of steel load blocks filled with concrete and steel I-beams to ensure enough vertical height.



(a)



(b)



(c)



(d)

Figure 5.30: (a) Supports elevation layout, (b) display of support configuration, (c) supports plan layout, and (d) display of supports and testing frame

Plain 2-inch-thick neoprene bearing pads measuring 48-inch long by 6-inch width were used for the initial test, as shown in Figure 5.30 (b). However, these bearing pads were found to partially restrain the horizontal degree of freedom, which caused undesired rotation and cracking in the grout pad under one of the supports, as shown in Figure 5.31 (a). A modified support was created to allow for horizontal displacement consisting of two sliding plates with a middle Teflon filling and guide rails, as shown in Figure 5.31 (b) and (c). These supports allowed for horizontal displacement and rotation, as shown in Figure 5.31 (c).

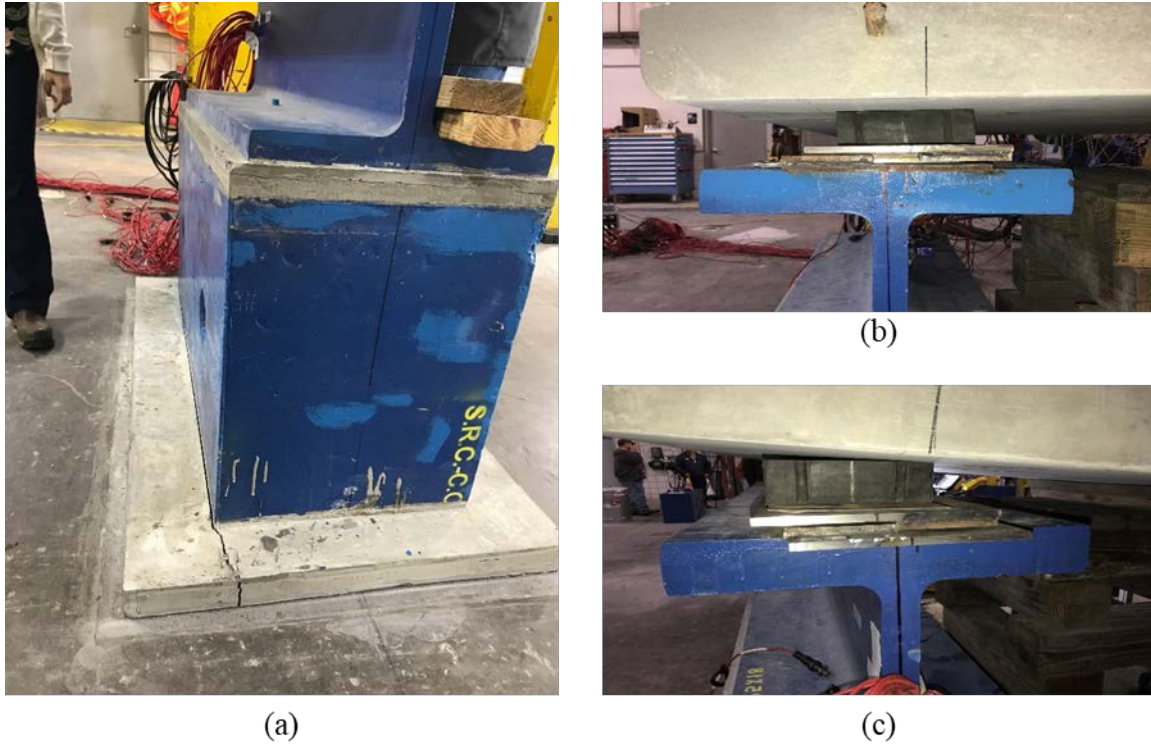
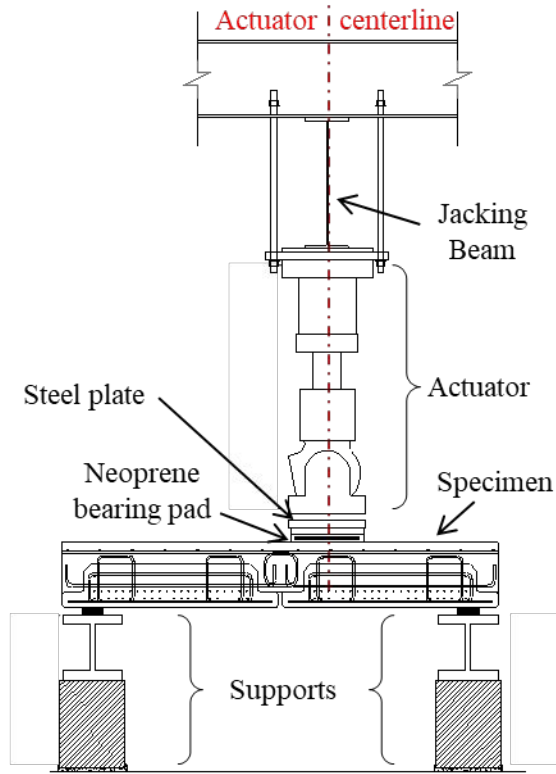


Figure 5.31: (a) Fractured grouted pad due to load block rotation, (b) sliding plates before test, and (c) sliding plates after test

The test setup with one of the FSB specimens ready for testing is shown in Figure 5.32. The simply supported specimens were loaded by a Shore Western hydraulic jack with a 460-kip static and fatigue capacity and an available stroke length of 10 inches. The jack was mounted in a frame with four columns (W14) with a center-to-center dimension of 12 feet longitudinally and 6 feet transversely supporting a double W36x150 jacking beam. The load application point was a steel plate with a 20-inch by 10-inch surface area and 2-inch thickness with a bottom neoprene bearing pad of the same size. The load area is similar to the wheel path of an AASTHO HL-93 truck [72].



(a)



(b)

Figure 5.32: (a) Testing frame and specimen configuration layout (east view) and (b) display of specimen (control FSB) and testing frame

Due to possible excessive deflection or fracture that might occur during the test, two small lumber frames were placed underneath all the specimens as a safety measure, shown in Figure 5.33. Enough clearance was left between the lumber protection and the specimens to ensure adequate deflection until the ultimate capacity was achieved.



Figure 5.33: Bottom wooden frames

As previously stated, two tests were conducted on each set of beams, shown in Figure 5.34. UHPC was cast in the first joint and then tested after 28 days, Figure 5.34 (a) and (b). After

testing, the beams were cut apart or just taken apart if they had broken apart during the first test. The beams were next placed in their second configuration, the UHPC cast in the second joint, and then tested, as shown in Figure 5.34 (c) and (d). A similar procedure was followed for the control FSB with CIP deck described earlier.

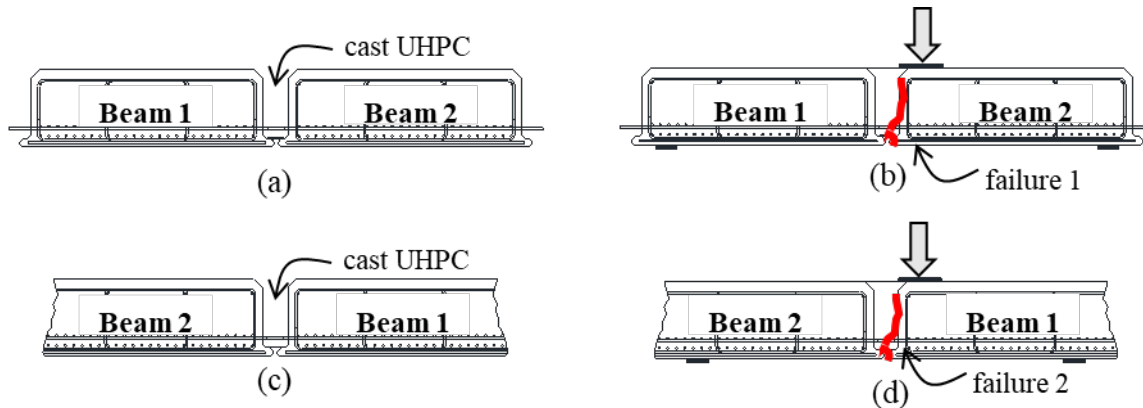


Figure 5.34: (a) UHPC cast in first testing round, (b) failure obtained from first round, (c) UHPC cast in broken specimen, and (d) failure obtained from second round

5.7. LOADING PROTOCOL

The loading protocol consisted of five loading steps, shown in Table 5.11, developed to take pictures and check the progress of cracking. In general, the load was applied at an approximate rate of 0.2 kips/second in two increments (Step 1 and Step 2). Later, the load was applied incrementally until the point of first crack was reached (Step 3). First cracking was detected by:

1. Load versus vertical deflection plot: The plot became non-linear after the first cracking point.
2. Concrete strain versus vertical deflection plot: When cracking occurred within the measurements ranges of the concrete strain gauges (CSG), the plots became non-linear by shifting from the tension side to the compression side of the graph due to tension strength loss on the underside of the specimens.
3. Visual inspections: Visual cracks appeared on both ends of the joint region at the boundary between the two materials and at the bottom fibers of the precast beams.

When first cracking was observed, the following tasks were performed:

- Load at which first cracking was observed was documented
- Cracks were marked and labeled
- Crack lengths were measured and documented
- Pictures were taken of the cracks from different angles

When the first cracking point was observed, the loading was continued until approximately 65 percent of the expected ultimate load calculated by hand (Step 4). At this point, the bottom crack displacement transducers (described in the next section) were removed from underneath the joint. Finally, the specimens were loaded to failure (Step 5).

Table 5.11: Loading rate and significant steps (*Sensor removal)

Joint Specimen	Load Rate	Step 1	Step 2	Step 3	Step 4*	Step 5
FSB-Control	0.2 k/s	10 k	20 k	+ 5 k to cracking	60 k (65% est. capacity)	load to failure
18F1	0.2 k/s	10 k	20 k	+ 5 k to cracking	70 k (65% est. capacity)	load to failure
18F2	0.2 k/s	10 k	20 k	+ 5 k to cracking	80 k (65% est. capacity)	load to failure
18A1	0.2 k/s	10 k	20 k	+ 5 k to cracking	65 k (65% est. capacity)	load to failure
12F1	0.2 k/s	8 k	15 k	+ 10 k to cracking	30 k (65% est. capacity)	load to failure
12F2	0.2 k/s	8 k	15 k	+ 10 k to cracking	45 k (65% est. capacity)	load to failure
12A1	0.2 k/s	8 k	15 k	+ 10 k to cracking	30 k (65% est. capacity)	load to failure
12A2	0.2 k/s	8 k	15 k	+ 10 k to cracking	45 k (65% est. capacity)	load to failure

5.8. INSTRUMENTATION SCHEDULE

Different sensors were placed in each joint specimen to study the flexural behavior during the static testing. Sensors used in the first specimen test are shown in Figure 5.35 and Figure 5.36 for the second test. Four types of gauges were used:

1. Concrete surface gauges (CSG) were placed on the top and on the underside of the beams to measure the concrete strain and were oriented in the flexure direction,
2. Crack displacement transducers (CDT) were attached at the bottom of the specimen to measure the opening distance between the two beams,
3. Rebar strain gauges (RSG) were embedded and attached to the transverse reinforcement to measure strain in the steel, and
4. Laser displacement transducer (LDT) were used to measure the deflections at different locations of the specimens.

The hydraulic jack has a built-in loading cell capable of measuring the load being applied to the joint sample.

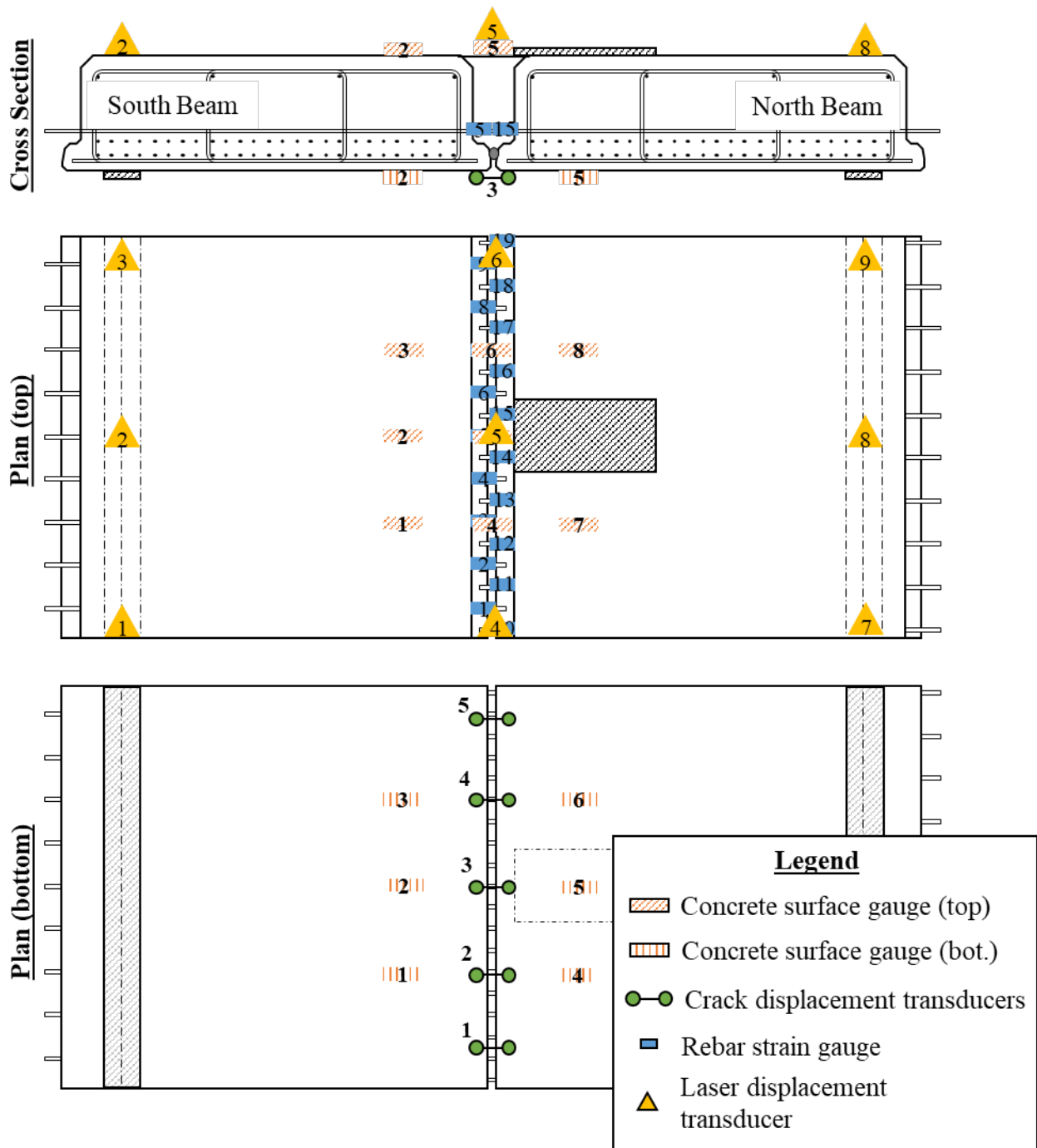


Figure 5.35: Complete instrumentation schedule (Testing Phase 1)

Some of the RSGs, CSGs, and LCOTs were removed from the specimens for Phase 2 of testing, as shown in Figure 5.36.

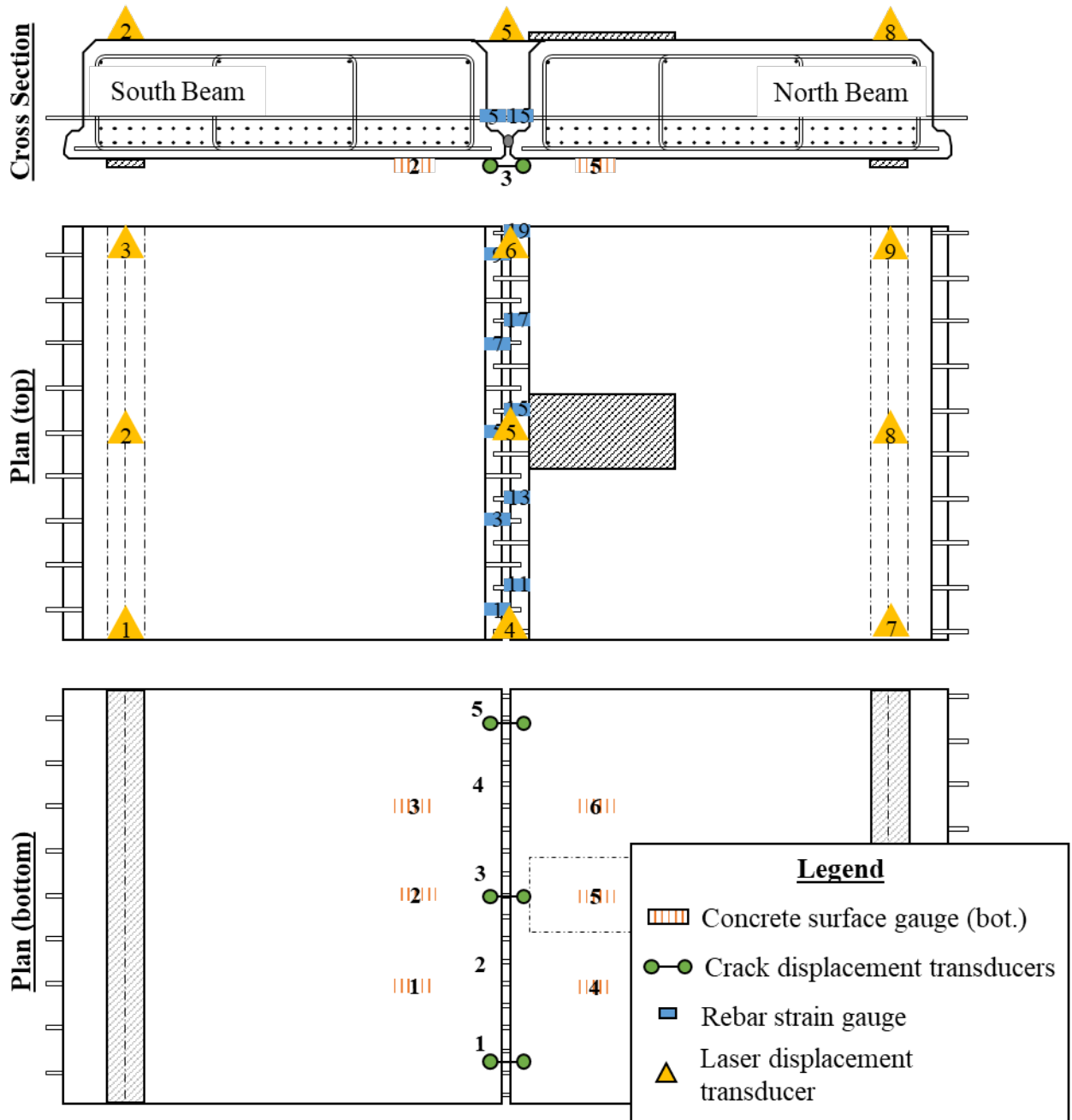


Figure 5.36: Complete instrumentation schedule (Testing Phase 2)

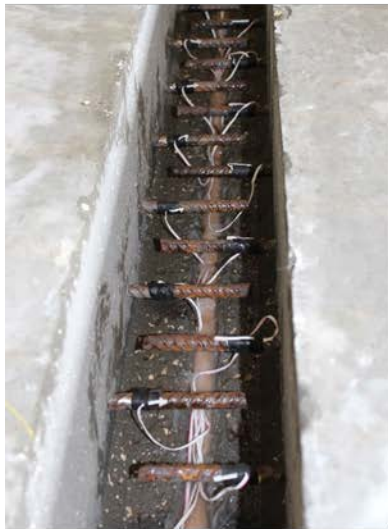
A photograph of the actual sensors installed on one of the specimens is shown in Figure 5.37.



(a)



(b)



(c)



(d)

Figure 5.37: Actual installed sensors: (a) bottom view with CSGs and CDTs, (b) top view with CSGs, (c) RSG location in UHPC closure, and (d) RSG location in FSB closure

5.9. NUMERICAL MODELING AND ESTIMATED RESPONSE

The response of all the small-scale specimens was estimated using ATENA, a non-linear finite element method (FEM) software specially designed for modeling reinforced concrete elements, as described in previous sections. The load versus displacement response (including the cracking and ultimate loads) was obtained for each of the small-scale specimens; an example for 18A1 is shown in Figure 5.38. The expected crack pattern immediately before failure was also obtained from the FEM analyses; an example for 18A1 is shown in Figure 5.39.

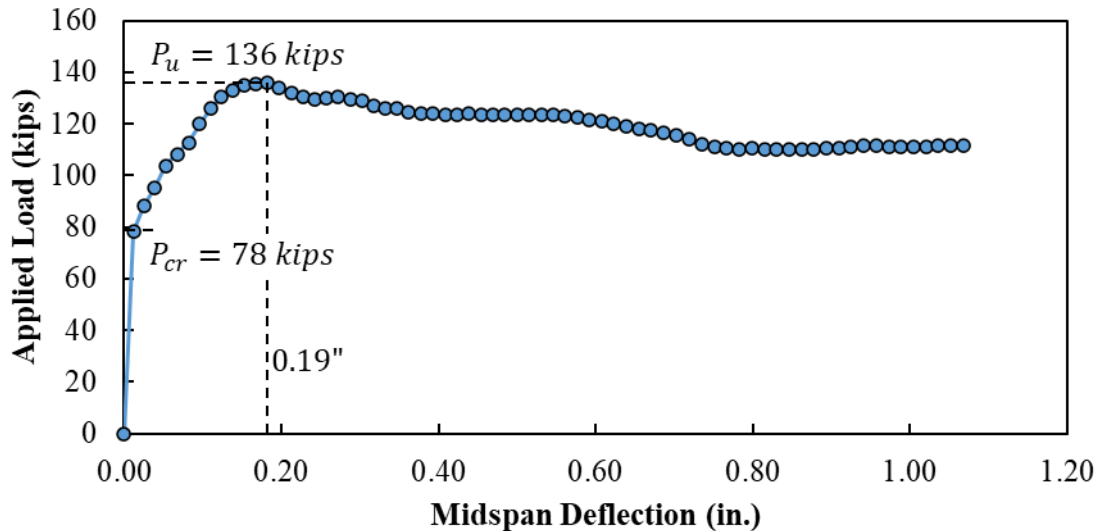


Figure 5.38: Example of estimated load versus midspan deflection for 18A1

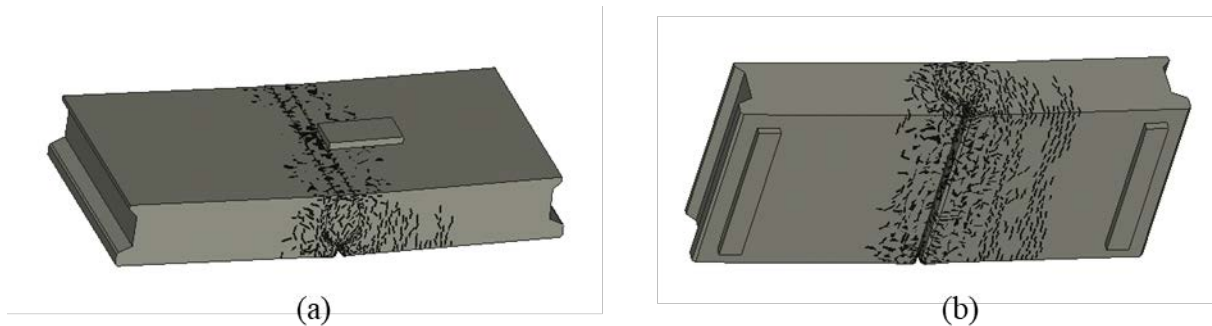


Figure 5.39: Example of estimated crack pattern on (a) top and (b) bottom of specimen 18A1

The failure load was also estimated using simple rectangular stress block assumptions. A summary of all the estimated results is provided in Table 5.12. Calculations and results from the numerical analyses are provided in Appendix C.

5.10. SUMMARY OF RESULTS

A summary of all experimental results is shown in Table 5.12. Results from hand calculations and numerical analyses are provided alongside the results from the two tests for each joint. Static results obtained after fatigue testing are highlighted in the table.

Table 5.12: Summary of predicted and measured results for small-scale testing

Specimen ID	Hand Calculation		Uncalibrated Software Analyses			Experimental Tests		
	P_{cr} (kips)	P_{max} (kips)	P_{cr} (kips)	P_{max} (kips)	Δ at P_{max} (in)	P_{cr} (kips)	P_{max} (kips)	Δ at P_{max} (in)
<i>FSB-1</i>	36.97	88.04	43.85	153.25	-0.48	28.1	63.42	-1.37
<i>FSB-2</i>	36.97	88.04	43.85	153.25	-0.48	22.2	36.43	-0.63
<i>18F1-1</i>	54.34	107.12	80.04	149.84	-0.37	24.3	149.86	-0.52
<i>18F1-2</i>	54.34	107.12	80.04	149.84	-0.37	29.3	149.47	-0.61
<i>18F2-1</i>	54.34	125.58	86.77	169.36	-0.22	24.9	170.21	-0.58
<i>18F2-2</i>	54.34	125.58	86.77	169.36	-0.22	56.9	177.00	-0.72
<i>18A1-1</i>	54.34	100.20	78.13	135.98	-0.19	46.5	154.39	-1.56
<i>18A1-2</i>	54.34	100.20	78.13	135.98	-0.19	26.1	146.06	-1.01
<i>12F1-1</i>	24.60	51.74	25.84	68.87	-0.28	21.3	69.98	-1.36
<i>12F1-2*</i>	24.60	51.74	25.84	68.87	-0.28	--	66.88*	-0.52*
<i>12F2-1</i>	24.60	70.20	33.39	91.90	-0.21	23.5	98.10	-1.32
<i>12F2-2</i>	24.60	70.20	33.39	91.90	-0.21	27.8	99.35	-0.96
<i>12A1-1</i>	24.60	44.82	27.92	49.32	-0.42	22.1	61.04	-1.25
<i>12A1-2*</i>	24.60	44.82	27.92	49.32	-0.42	--	67.53*	-2.22*
<i>12A2-1</i>	24.60	68.47	32.46	104.81	-0.33	22.1	90.91	-1.67
<i>12A2-2*</i>	24.60	68.47	32.46	104.81	-0.33	--	100.46*	-2.05*

* Cyclic testing conducted prior to strength testing for this joint

The cracking loads presented in Table 5.12 were obtained using the concrete surface gauges on the bottom of the specimens. The procedure for obtaining these cracking loads is discussed in §5.11.2.

The ultimate capacity results from each experimental phase and software analysis are all plotted in Figure 5.40. The results from the numerical analyses were in good agreement with the actual capacities measured during the experimental testing. The second testing phase (Test 2) of some of the 12-inch specimens was performed after 2-million cycles of fatigue testing. These results will be discussed in more detail in subsequent sections.

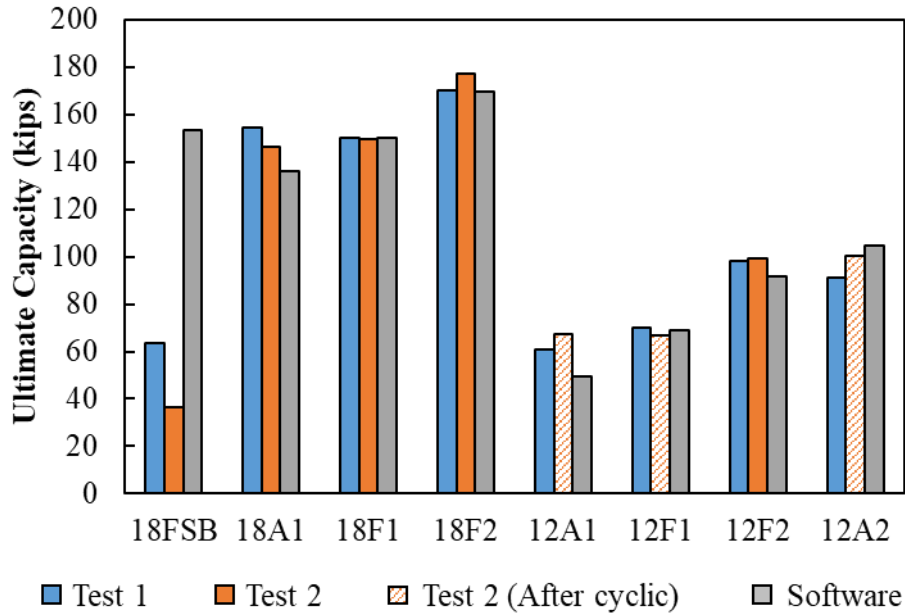


Figure 5.40: Ultimate strength capacity comparison

5.11. ANALYSIS OF RESULTS

The general analysis of results for all the test specimens are described in this section. The load-deflection behavior, cracking load with crack patterns, and reinforcement behavior are analyzed based on the sensor responses and visual observations. Detailed results for all the individual tests are provided in Appendix D and E.

5.11.1. Method for Determining Absolute Specimen Deflection

Nine laser displacement transducers (LDTs) were used to measure the vertical displacement at different locations on top of each specimen: three over each support centerlines and three over the joint matrix centerline. The average of each sensor group was calculated to determine the average deformation at midspan and the end supports, shown in Figure 5.41. Measurements from LDTs were also used to determine if there was any transverse rotation in the specimens during testing (e.g., similar readings in 4, 5, and 6 would mean no transverse rotation).

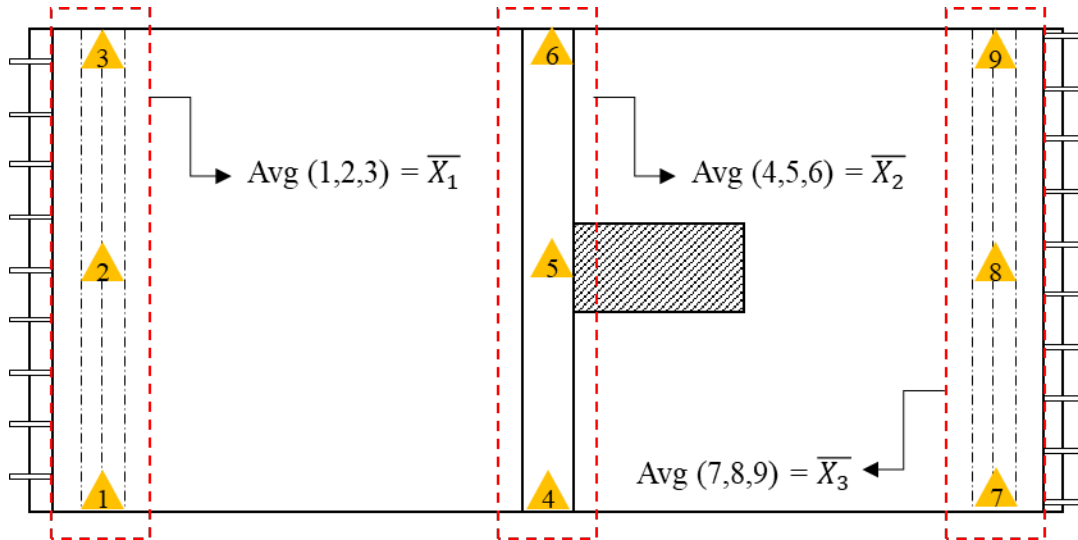


Figure 5.41: Average displacement computation for each sensor group

The absolute specimen deflection (Δ_{mid}) at midspan was calculated by removing the end deflection from the measured midspan deflection, as shown in Equation 5-1. This deflection was used with the measured load to develop the load-deflection behavior for all the joints.

$$\Delta_{mid} = \bar{X}_2 - avg(\bar{X}_1, \bar{X}_3) \quad \text{Equation 5-1}$$

5.11.2. Method for Determining Cracking Load

The cracking load was determined using several different methods:

- *Visual inspection:* An approximate cracking load was obtained through visual inspection during testing. The load at which first cracking appeared was documented and marked, as shown in Figure 5.42. First cracking either occurred in the precast section or at the joint boundary.



Figure 5.42: Actual cracks from visual inspection (12F2-1 shown)

- *Load-deflection plot*: An approximate cracking load was determined using the measured load versus deflection data for each test. Cracking was estimated as the point when there was a substantial slope change in the elastic range as shown in Figure 5.43 (a). This slope change indicated a decrease in specimen stiffness indicating the formation of a crack.
- *Rebar strain gauges (RSG)*: A change in the slope of the load versus rebar strain response was observed at cracking. This is a result of the tensile stress being transferred from the concrete bottommost fiber to the joint reinforcement, as shown in Figure 5.43 (b).
- *Crack displacement transducer (CDT)*: A change in the slope of the load versus bottom opening response was observed when cracking or debonding occurred somewhere in the joint region. A decrease in stiffness signaled first cracking, as shown in Figure 5.43 (c).
- *Concrete strain gauges (CSG)*: The cracking load could also be determined from the load versus bottom concrete strain. The cracking load was taken as the load right before a substantial loss in tensile strain was observed, Figure 5.43 (d).

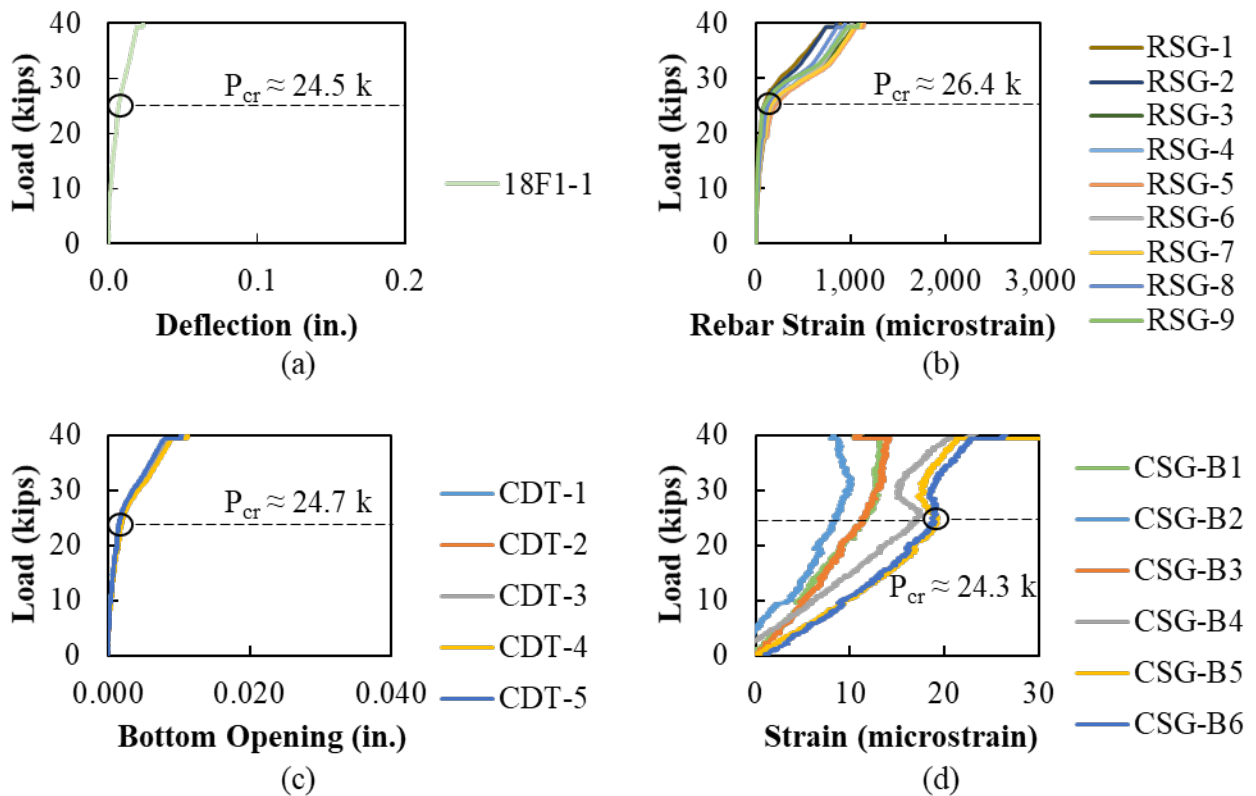


Figure 5.43: Data with cracking loads (18F1-1 shown): (a) load versus deflection plot, (b) load versus rebar strain plot, (c) load versus bottom opening plot, and (d) load versus bottom concrete strain plot

The cracking loads determined using each of these methods for each of the specimens are summarized in Table 5.13. The cracking load was the clearest to determine using the bottom concrete strain gauges, so these values were used as the reported cracking load.

Table 5.13: Summary of measured cracking and maximum loads for each specimen

Specimen ID	Cracking Loads					Reported
	$P_{cr,visual}$ (kips)	$P_{cr,P-\Delta}$ (kips)	$P_{cr,RSG}$ (kips)	$P_{cr,CDT}$ (kips)	$P_{cr,CSG}$ (kips)	P_{cr} (kips)
FSB-1	45	33.3	33.3	34.2	28.1	28.1
FSB-2	10	22.6	23.1	22.3	22.2	22.2
18F1-1	40	24.5	26.4	24.7	24.3	24.3
18F1-2	40	26.7	28.8	28.2	29.3	29.3
18F2-1	60	33.2	40.5	42.5	24.9	24.9
18F2-2	50	51.1	58.6	55.1	56.9	56.9
18A1-1	30	11.7 ^Δ	15.6 ^Δ	15.4 ^Δ	46.5	46.5
18A1-2	40	29.1	38.6	32.2	26.1	26.1
12F1-1	30	20.8	#	#	21.3	21.3
12F1-2*	--	--	--	--	--	--
12F2-1	45	14.8	15.5	16.1	23.5	23.5
12F2-2	15	20.4	23.9	22.4	27.8	27.8
12A1-1	30	13.4	10.6	10.1	22.1	22.1
12A1-2*	--	--	--	--	--	--
12A2-1	25	12.1	12.1	14.1	22.1	22.1
12A2-2*	--	--	--	--	--	--

* cyclic testing conducted prior to strength testing for this joint; members were cracked during the fatigue testing, so no cracking load is reported here

^Δ an initial small drop in stiffness was recorded at a low load; results from CSG were used for cracking load

no immediate change in stiffness could be detected

5.11.3. Performance of Current FSB Joint Detail

The measured load versus displacement response for the FSB control specimens (FSB-1 and FSB-2) compared to the predicted response from numerical modeling is shown in Figure 5.44. The measured initial stiffness was the same as predicted numerically. The experimentally tested specimens had much lower capacities.

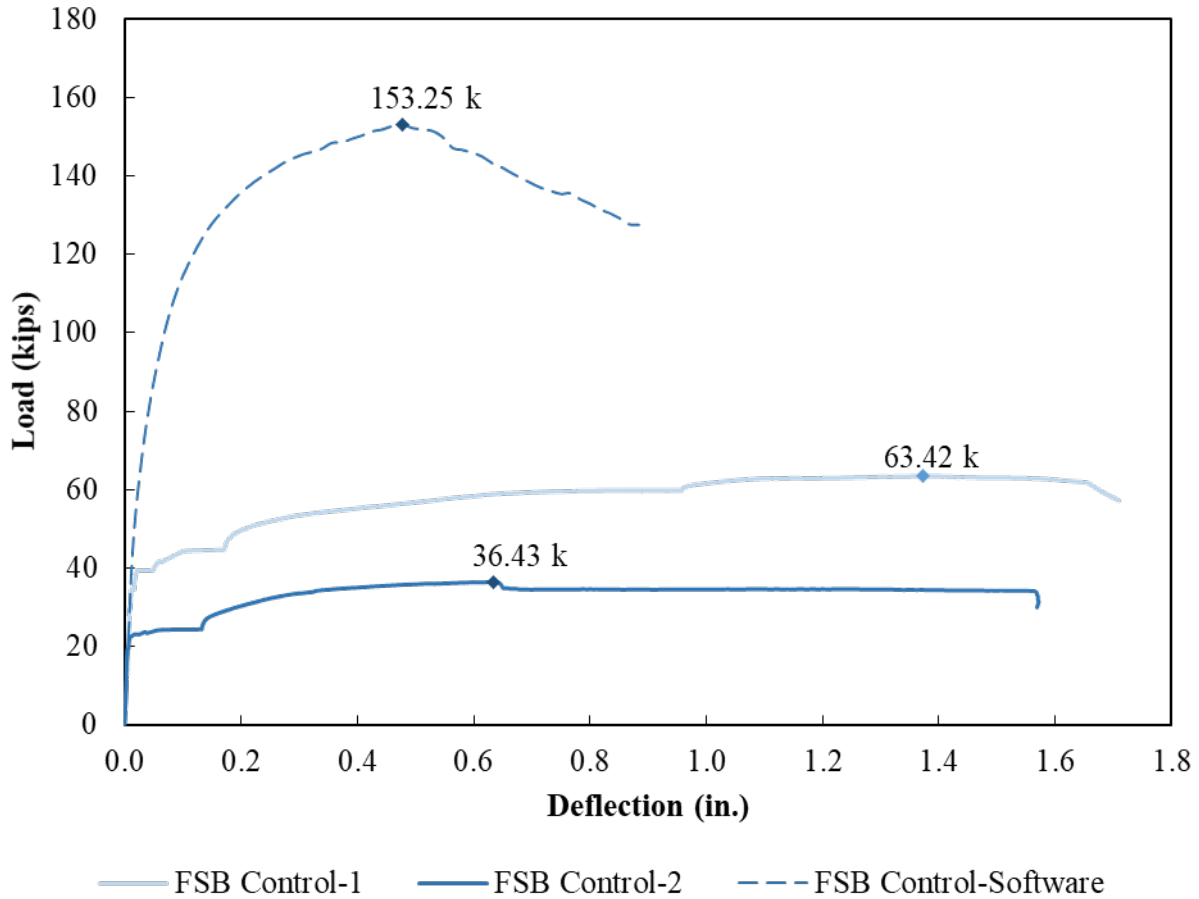


Figure 5.44: FSB Control specimen load versus deflection responses with maximum values

The failure mechanism for the FSB control specimens is shown in Figure 5.45. Both FSB control specimens (FSB-1 and FSB-2) failed due to a development failure of the joint reinforcement, which was the result of the large bend diameter described in §5.5.5.6. In both specimens a crack developed at the location of the vertical leg of the hooked reinforcement, shown in Figure 5.45 (a). This crack then extended to the corner of the load bearing where hinging was observed, shown in Figure 5.45 (b). The second test on the specimen (FSB-2) had a lower failure load than FSB-1 due to the slab and joint concrete having a much lower concrete strength than specified, shown in Table 5.9.

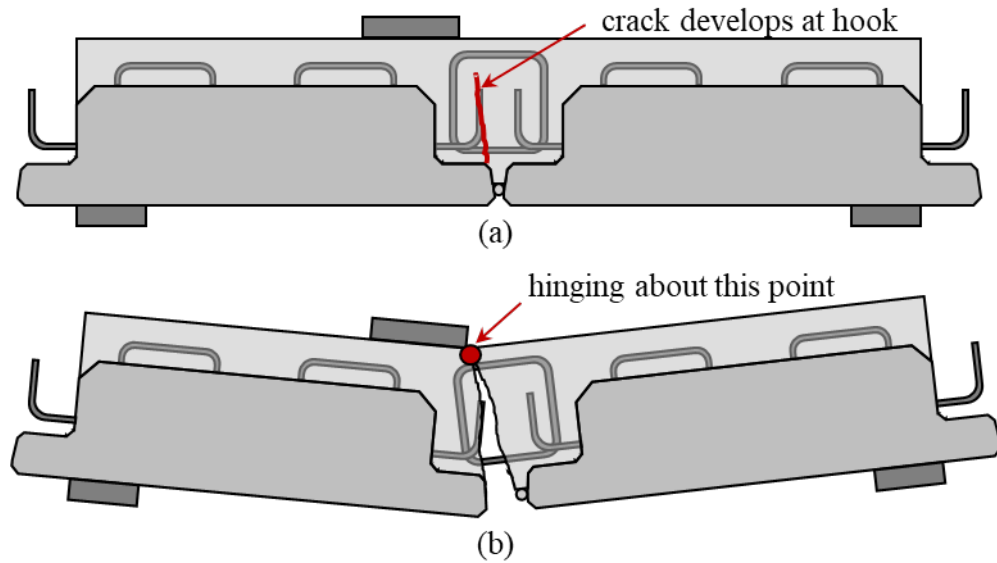


Figure 5.45: Failure mechanism in FSB-1 and FSB-2: (a) crack develops at vertical leg of hook reinforcement and (b) hinging occurs near load as joint reinforcement pulls out

The failed FSB-1 specimen with the joint reinforcement is shown in Figure 5.46 (a). The hooked transverse reinforcement was pulled from the inner concrete confined by the rebar cage in the joint matrix, as shown in Figure 5.46 (b). The bottom longitudinal rebar of the joint cage reinforcement was bent due to the pull-out and bending forces.



Figure 5.46: (a) Failed FSB Control-1 joint and (b) pull-out cavity in inner confined concrete (dashed line) and longitudinal rebar bend due to bending and pull-out forces (solid lines)

None of the transverse reinforcements ruptured in FSB-1, but all bars were engaged, as shown in Figure 5.47 for the south side and Figure 5.48 for the north side. There is a relatively linear response in reinforcement until after cracking occurred. The failure of the joint occurred when the reinforcement pulled out on the north side. The strain gauge response went from positive tension to negative compression at this point.

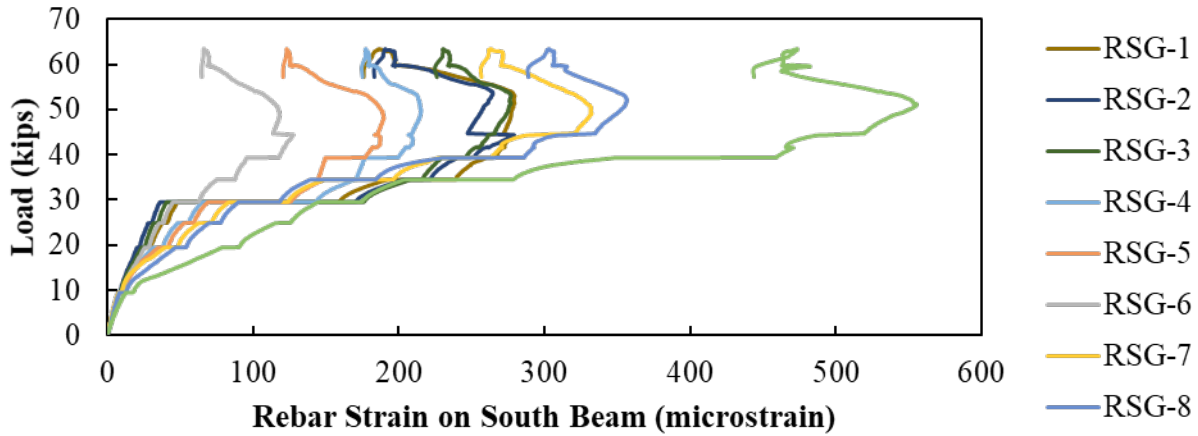


Figure 5.47: Load versus strain in joint reinforcement on the off-load side (south) for FSB-1

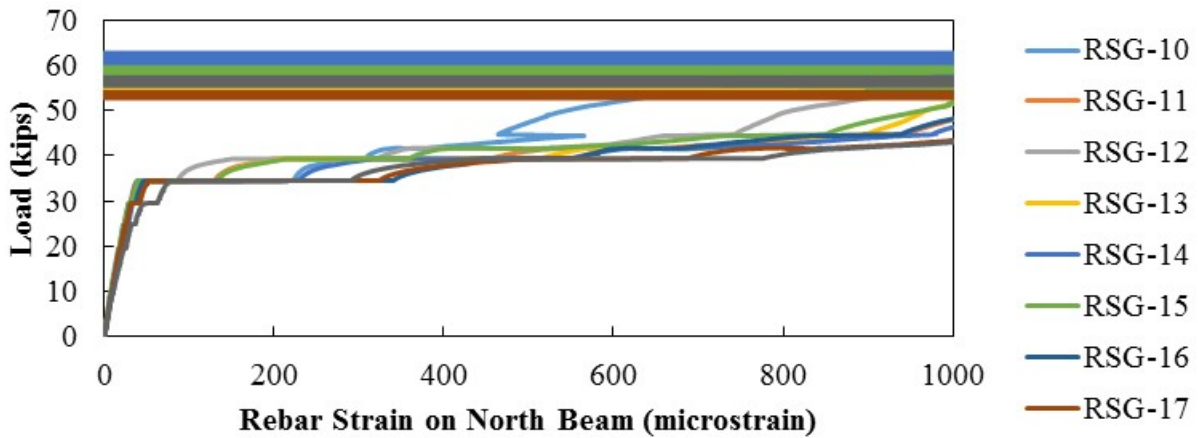


Figure 5.48: Load versus strain in joint reinforcement on the loaded side (north) for FSB-1

The experimental test results were generally within 10 percent of the predicted capacity from the numerical analysis, shown in Table 5.12. For this reason, the estimated FSB joint response from the numerical analysis was used as the point of comparison for the performance of the developed joints.

5.11.4. Performance of 18-inch-deep Specimens

A comparison between all the 18-inch-deep specimens is presented in this section. The measured load versus displacement response for each of the 18-inch-deep specimens is shown in Figure 5.49. The maximum capacity achieved by each specimen is highlighted. The results from the measured and predicted response for the FSB control specimens are also plotted.

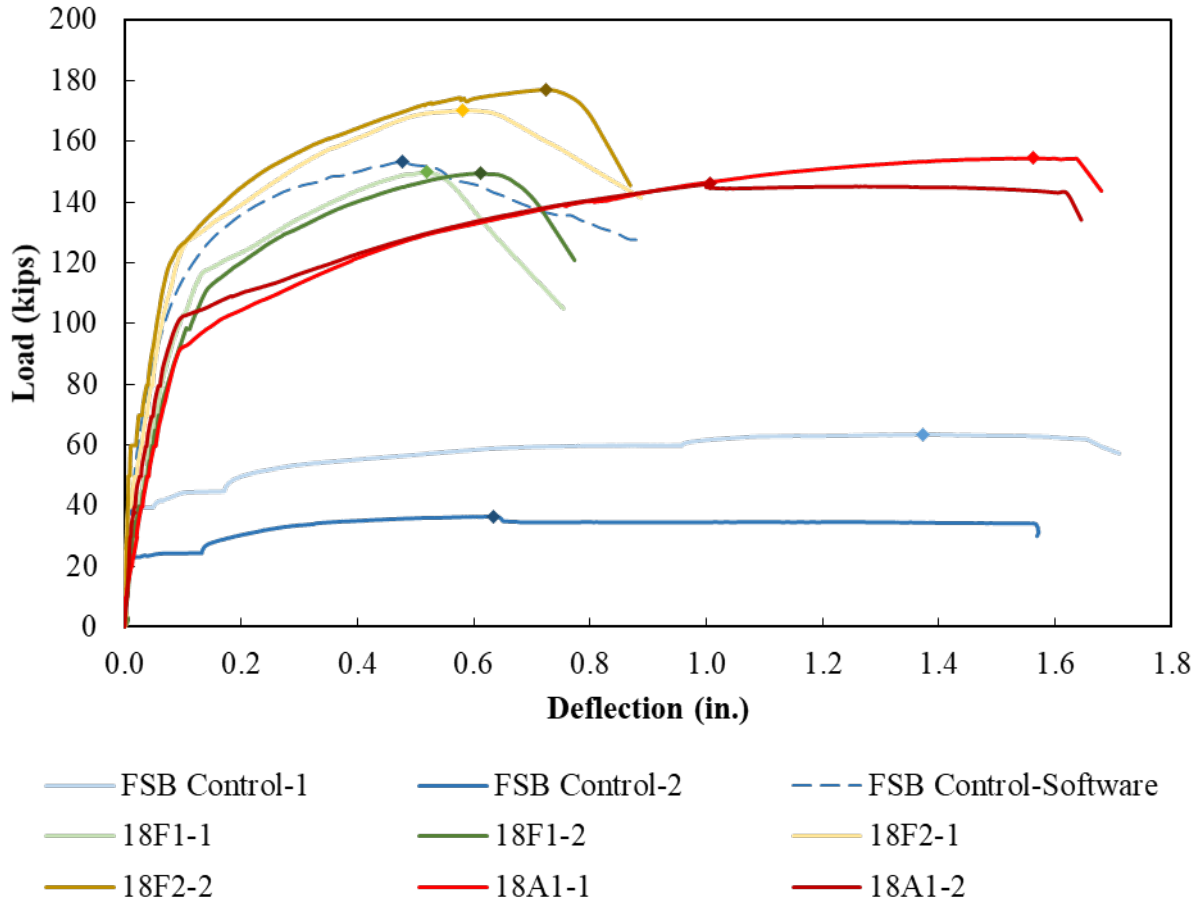


Figure 5.49: 18-inch specimens: load versus deflection experimental static tests with maximum values

Overall, all the developed joint details with UHPC performed similar to or better than the predicted response of the FSB control. The highest capacity was achieved by the 18F2 specimen, with about a 10-percent higher capacity than the FSB control and the other joint details. This higher capacity was a result of an increased lever arm of the joint reinforcement, which translated to enhanced transverse flexural capacity. However, the small ledge depth for 18F2 caused constructability problems, as mentioned in §5.5.5.2. The 18A1 tests had similar capacity to the predicted response of the FSB control specimen and an increased ductility.

5.11.4.1. Serviceability Behavior

The progression of cracking was monitored during testing. The cracking on both sides of the beams when they were first observed and when the bottom CDTs were removed (at fourth loading step: 65% of failure in most cases) is shown in Figure 5.50 and Figure 5.51. Most of the cracking that occurred in the FSB control specimens was in the joint region, likely due to lower tensile concrete strength than the beams. Debonding between the precast beam and UHPC joint occurred in all the UHPC joint specimens, suggesting the bond strength was weaker than the tensile strength of the neighboring concrete.

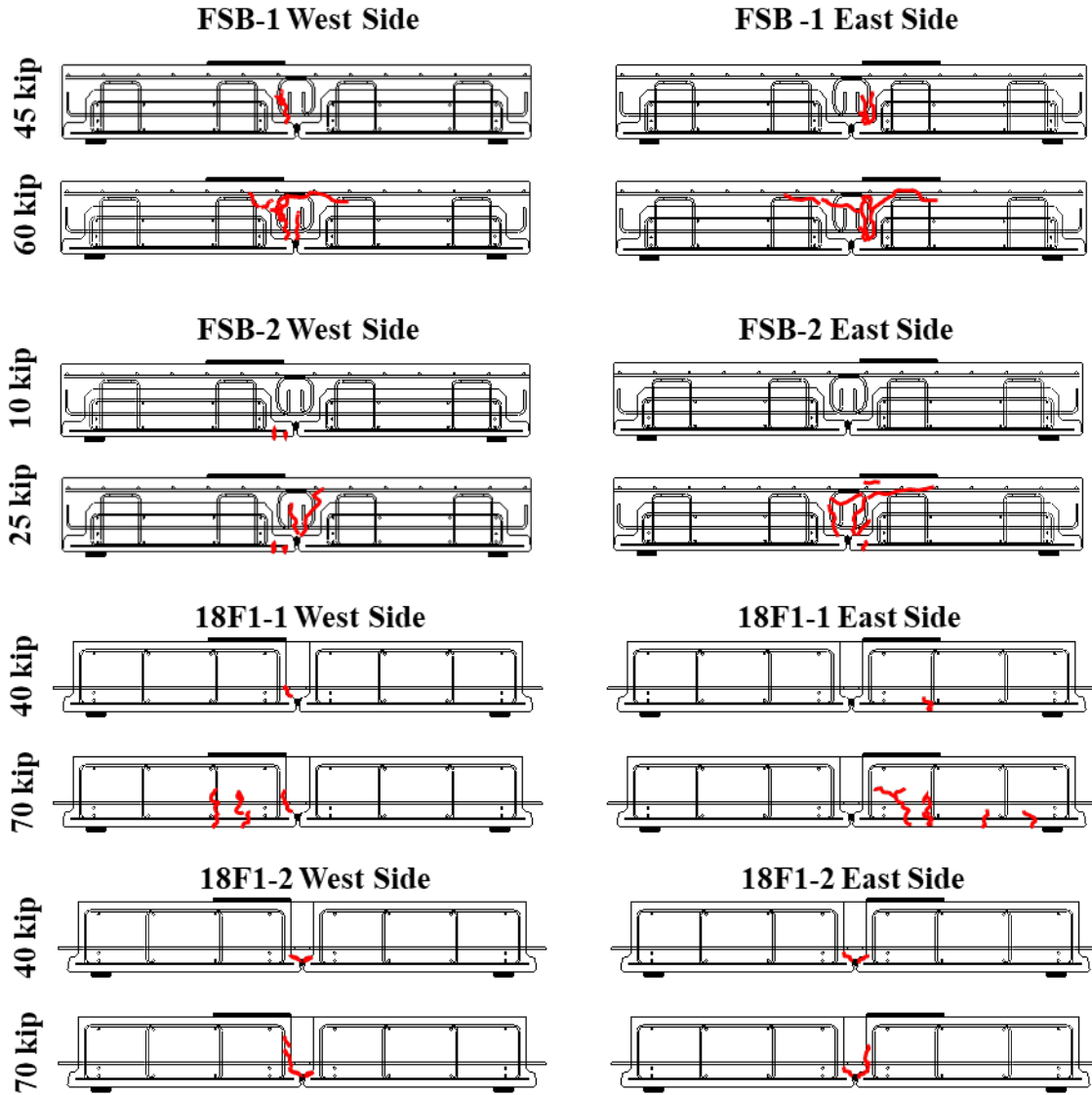


Figure 5.50: Crack pattern of 18-inch specimens

Only minor cracking was observed in the precast portions of specimens 18F2 and 18A1 during both testing stages. This was due to UHPC-to-precast bond loss that occurred before reaching the ultimate capacity of the connection.

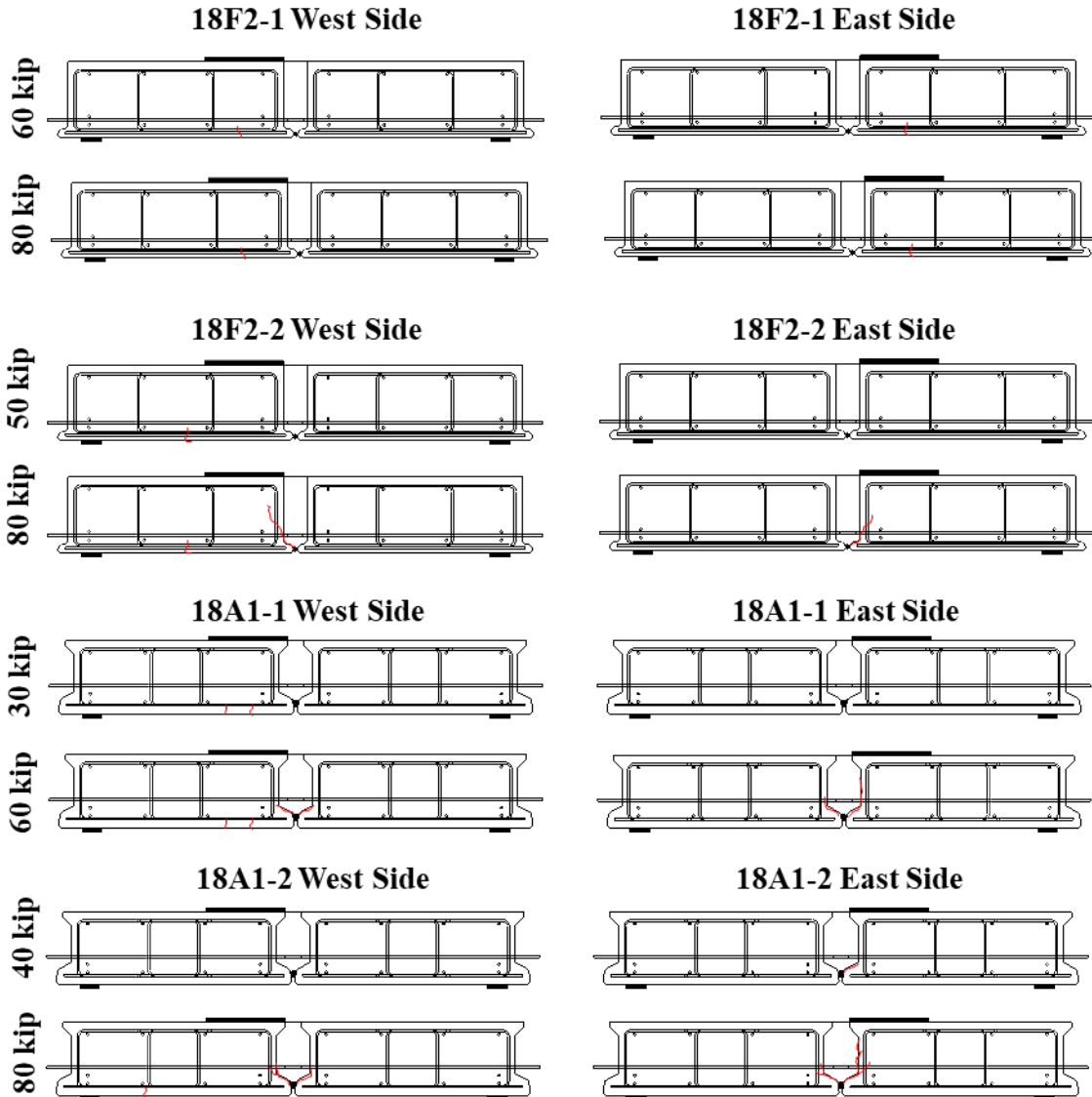


Figure 5.51: Crack pattern of 18-inch specimens (cont.)

5.11.4.2. Ultimate Behavior

The typical failure mechanism observed in the proposed 18-inch joint geometries is shown in Figure 5.52. A crack typically developed either at the joint interface or in the precast concrete if there was sufficient UHPC-to-beam bond, shown in Figure 5.52 (a). This crack would extend the entire height of the joint and then curve into the precast section under the load, where UHPC bond was sufficient. A crack developed in the bottom ledge for the 18F2 joints. Finally, hinging would occur in the precast section under the load next to the UHPC joint producing failure of the specimen either due to pullout (18F1 and 18F2) or rupture of the joint reinforcement (18A1), shown in Figure 5.52 (b).

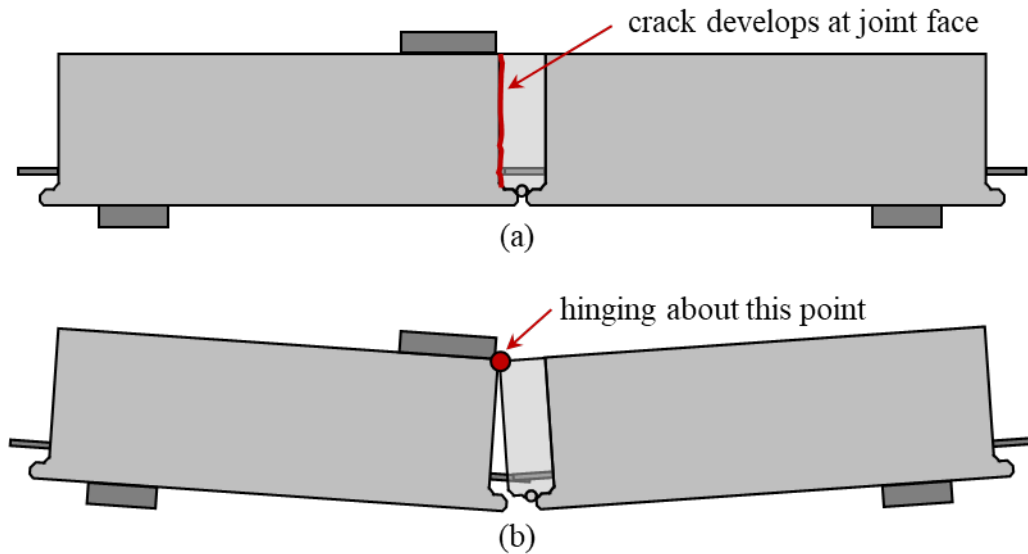


Figure 5.52: Typical failure mechanism for proposed 18-inch-deep joint specimens (18F2 is shown): (a) cracking at failure and (b) hinging in the precast section next to the UHPC joint

A similar pull-out failure was observed in both 18F1 and 18F2 specimens. Cones of UHPC were observed around the joint reinforcement in 18F1, shown in Figure 5.53 (a) and (b). The reinforcement did not fracture, but the formation of these cones in the UHPC caused failure, suggesting a failure of the splice detail. The joint detail in 18F2 had a similar behavior, shown in Figure 5.53 (c) and (d), to 18F1 except there was a fracture of two of the joint reinforcement for this detail. From these two joints, only 18F2 had any joint reinforcement where fracture was observed. The rest of the reinforcement in these specimens yielded but were not able to fracture as the UHPC matrix failed first.

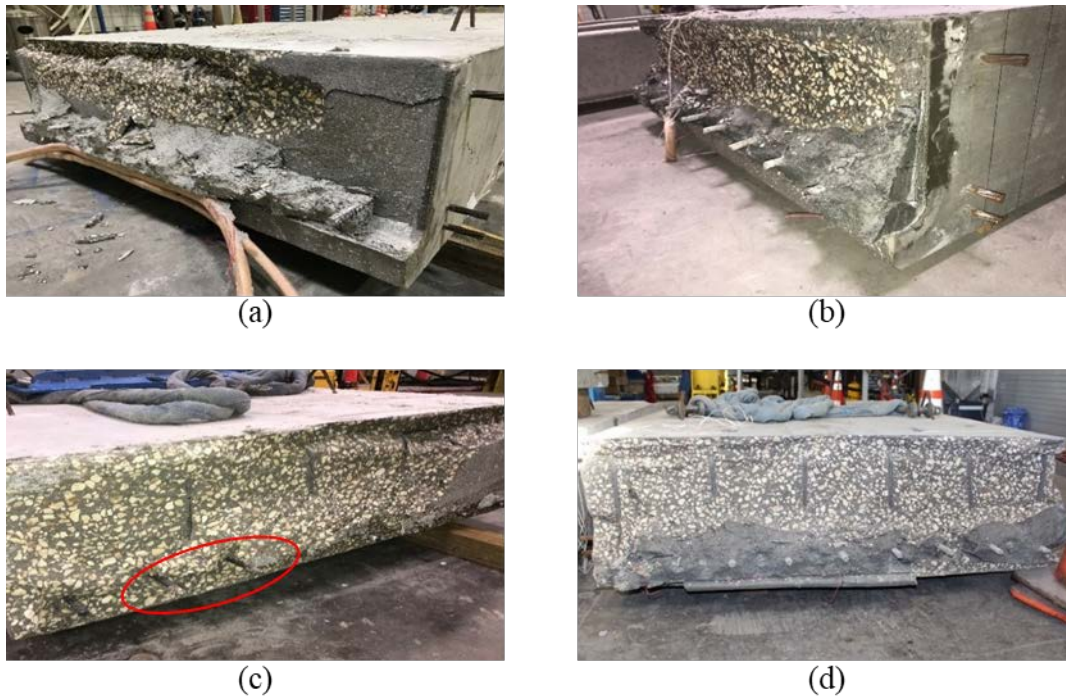
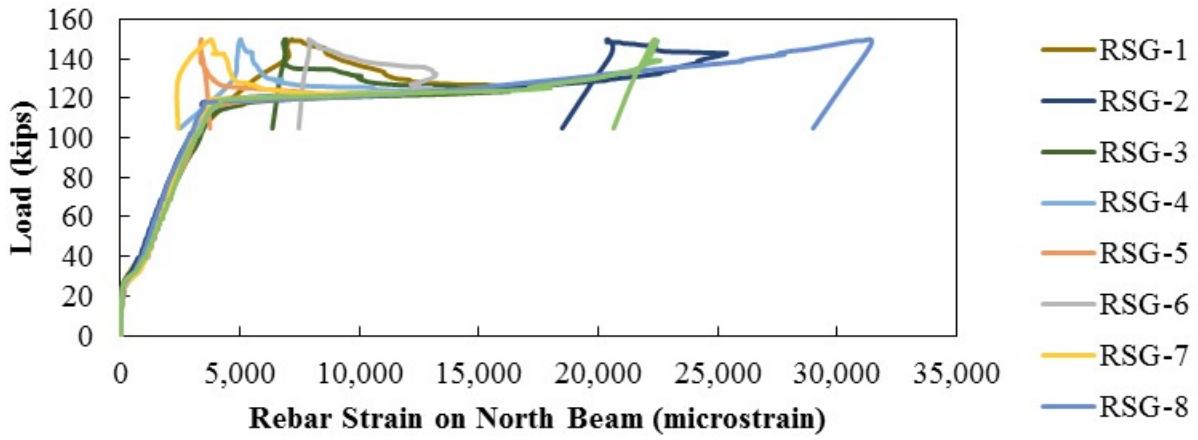


Figure 5.53: (a) 18F1-1 failed specimen (north), (b) 18F1-2 failed specimen (north), (c) 18F2-1 failed specimen (two broken rebar; north), and (d) 18F2-2 failed specimen (north)

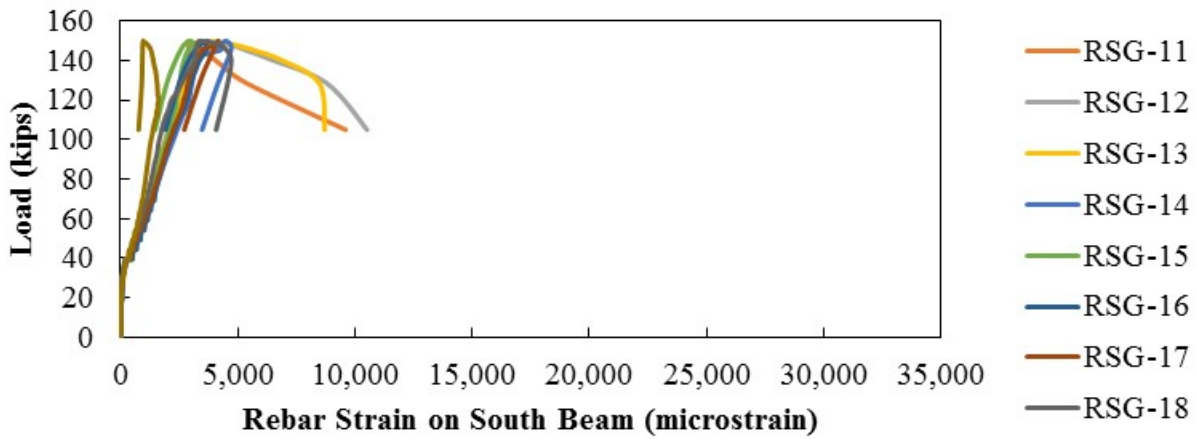
The load versus strain in the joint reinforcement plots are shown in Figure 5.54 for 18F1-1 and in Figure 5.55 for 18F2-1. The reinforcement had two different slopes prior to yielding of the reinforcement: before and after cracking. The yielding of all the reinforcement then occurred at approximately 3,000 microstrain, which would suggest a higher yield strength of the reinforcement than specified. The strain begins to decrease with increasing load at higher loads; this is thought to be a result of the failure in the splice of the joint reinforcement as the UHPC is picking up some of the tensile stresses.

Hinging occurred in the 18F1 and 18F2 specimens, like the mechanism illustrated in Figure 5.52, which meant that there was only one primary failure crack. Because there was one primary failure crack, the reinforcement on the loaded side of the joint increased to higher strains than on the unloaded side of the joint, shown in Figure 5.54 and Figure 5.55.

The strain gauges were placed across the full width of the joint. The strains in the gauges across the joint were comparable, which suggests that all the reinforcement across the width of the joint was equally engaged.



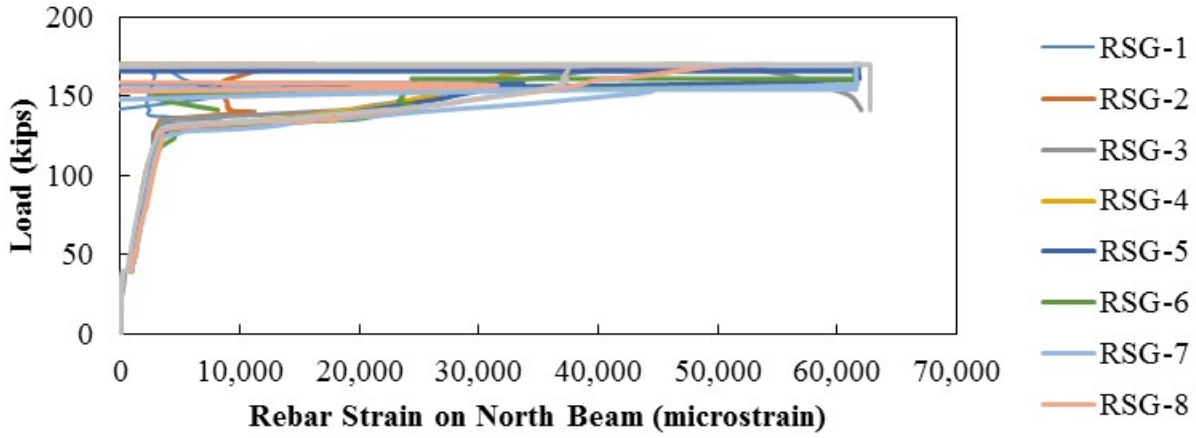
(a)



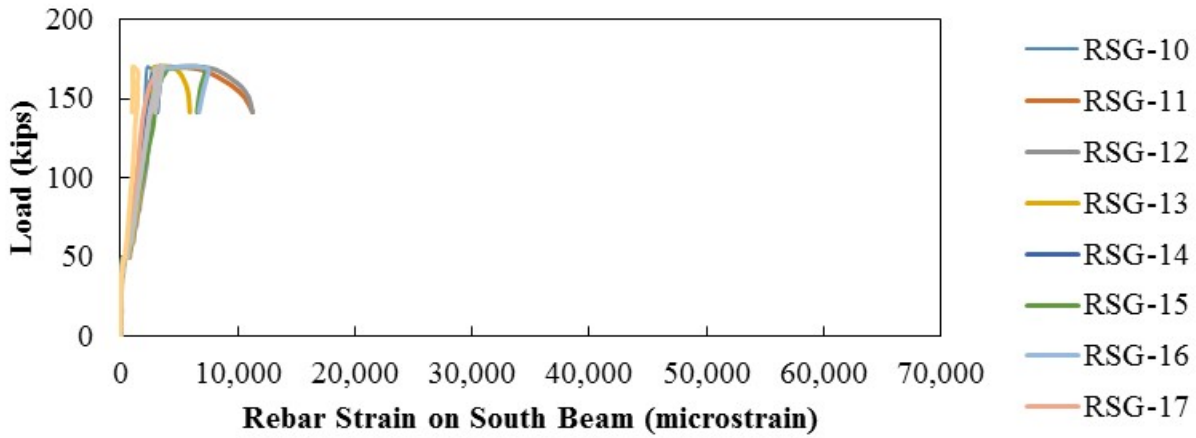
(b)

Figure 5.54: Load versus strain in joint reinforcement for 18F1-1 on the (a) north and (b) south beams of the joint

The 18F2-1 joint reinforcement response is shown in Figure 5.55 (a) for the north side and Figure 5.55 (b) for the south side. The response of this reinforcement was like 18F1-1.



(a)



(b)

Figure 5.55: Load versus strain in joint reinforcement for 18F2-1 on the (a) north and (b) south beams of the joint

The failure plane of the 18A1-1 specimen is shown in Figure 5.56. This joint configuration was the only one in which all the joint reinforcement ruptured, which is likely due to a larger development length provided in the joint. Although its overall capacity was like 18F1 (a result of similar lever arms in the joint reinforcement), its ductility was larger (a product of failure being controlled by the rupture of reinforcement). All reinforcement on the loaded side ruptured at the interface between the precast section and UHPC joint, leaving a bottleneck shape at the tip of each bar as shown in Figure 5.56 (a). Additionally, there were no observed cones in the UHPC, as shown in Figure 5.56 (b).



Figure 5.56: (a) Failed 18A1-1 specimen (loaded beam showed) and (b) UHPC matrix attached to unloaded beam

The 18A1-1 joint reinforcement response for the loaded side is shown in Figure 5.57 and for the unloaded side in Figure 5.58. First cracking was not observed until approximately 30 kips. There was, however, debonding between the precast section and UHPC joint that occurred very early. This early debonding is likely the reason the change in slope in the reinforcement plot occurred at a low load (less than 10 kips). All the reinforcement on both the loaded and unloaded sides yielded. As the load was increased, the strain in the reinforcement on the loaded side of the beam significantly decreased and then remained constant with increasing load. This is likely due to the strain gauges being located adjacent to a point of necking in the reinforcement (where fracture eventually occurred).

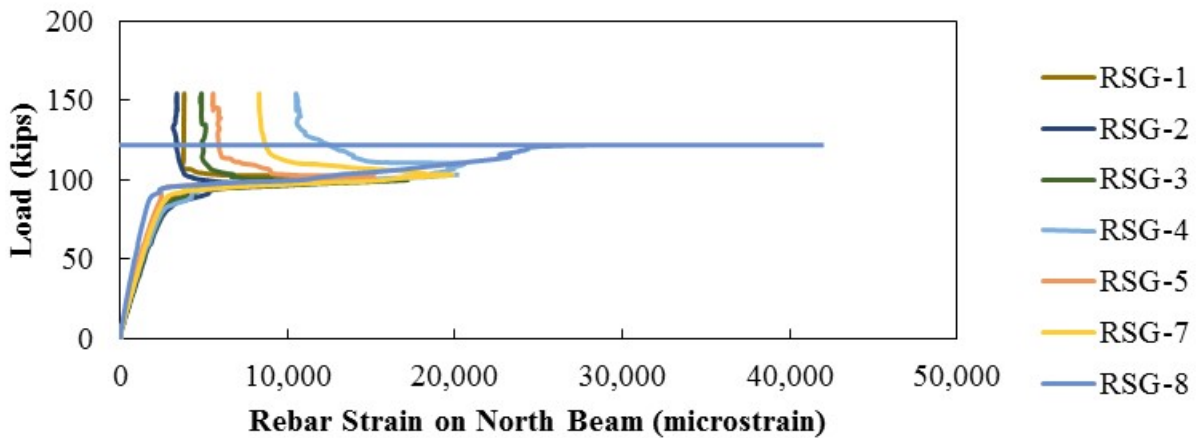


Figure 5.57: 18A1-1 system load versus rebar microstrain in north beam (RSG-8 malfunctioned after 120 kips)

The 18A1-1 joint reinforcement response for the unloaded side is shown in Figure 5.58. This reinforcement yielded and was engaged up until the failure load.

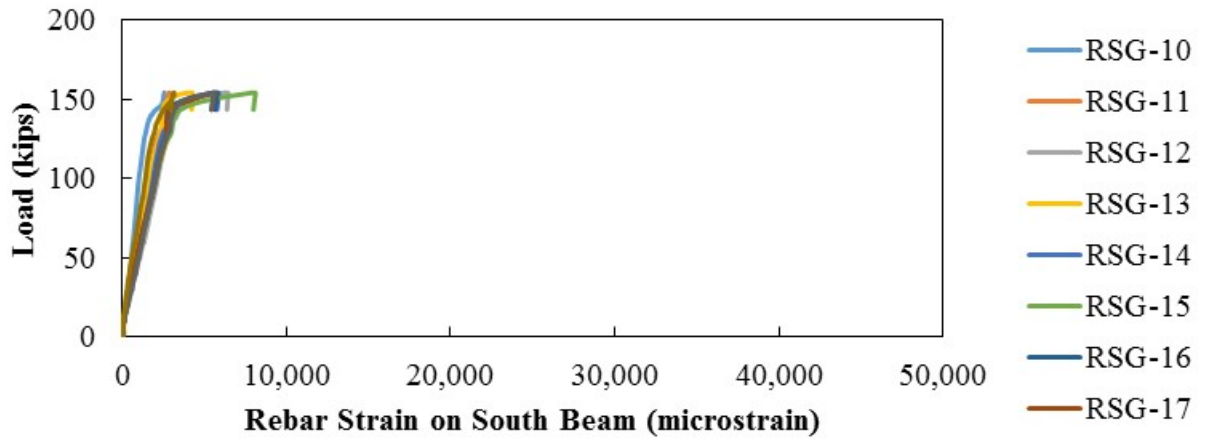


Figure 5.58: 18A1 system load versus rebar microstrain in unloaded beam

A detailed analysis for each of the tests on the 18-inch joints is provided in Appendix D. This analysis includes a discussion on the types of failures, rupture patterns, material performance, and all sensor data.

5.11.5. Performance of 12-inch-deep Specimens

A comparison between all the 12-inch-deep specimens is presented in this section. The measured load versus displacement response for each of the 12-inch-deep specimens is shown in Figure 5.59. The maximum capacity achieved by each specimen is also highlighted. The results for three of the tests was following fatigue testing where over 2 million cyclic loads were applied. A further discussion of the results from the fatigue testing will be presented in subsequent sections.

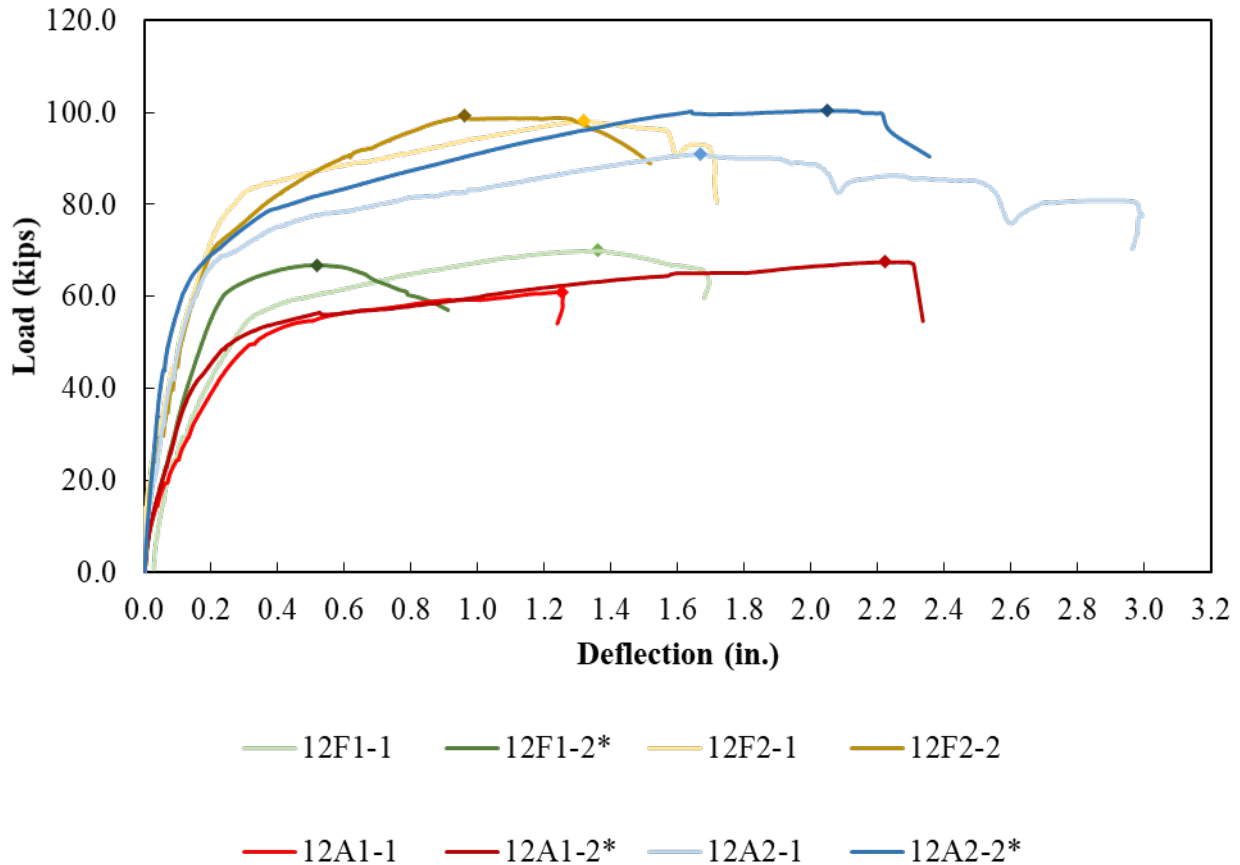


Figure 5.59: 12-inch specimens: experimental static tests with maximum values

As previously mentioned, joints 12F1, 12F2, and 12A1 were first tested. Joints 12F1 and 12A1 exhibited similar performance, with ultimate capacity and deflection at ultimate capacity within 15 percent of each other. The 12F2 joint had significantly higher flexural capacity, due to it having a much larger lever arm for the joint reinforcement. However, the 12F2 joint experienced early rupture of the bottom ledges due to smaller thickness and lack of reinforcement. Also, this thinner ledge was a weak point during casting, transport, and erection and would become more of a challenge for longer and heavier beams.

After the first round of tests was performed on 12F1, 12F2, and 12A1, a new 12-inch-deep joint geometry (12A2) was proposed based on the best characteristics from 12F2 (largest lever arm) and 12A1 (largest rebar embedment length). This joint geometry is described in more detail in

§5.3. Joint 12A2 performed better than the other joints investigated, with a comparable strength to 12F2, increased ductility, and improved constructability.

5.11.5.1. *Serviceability Behavior*

The progression of cracking was monitored during testing. The cracking on both sides of the beams when they were first observed and when the bottom CDTs were removed (at fourth loading step: 65 percent of failure in most cases) are shown in Figure 5.60 and Figure 5.61. Unlike the 18-inch-deep specimens, debonding between the precast section and UHPC joint was only observed in some of the specimens. Cracking at the level of the joint reinforcement was observed in several of the specimens. These cracks accompanied a splitting-type development failure in some of the specimens.

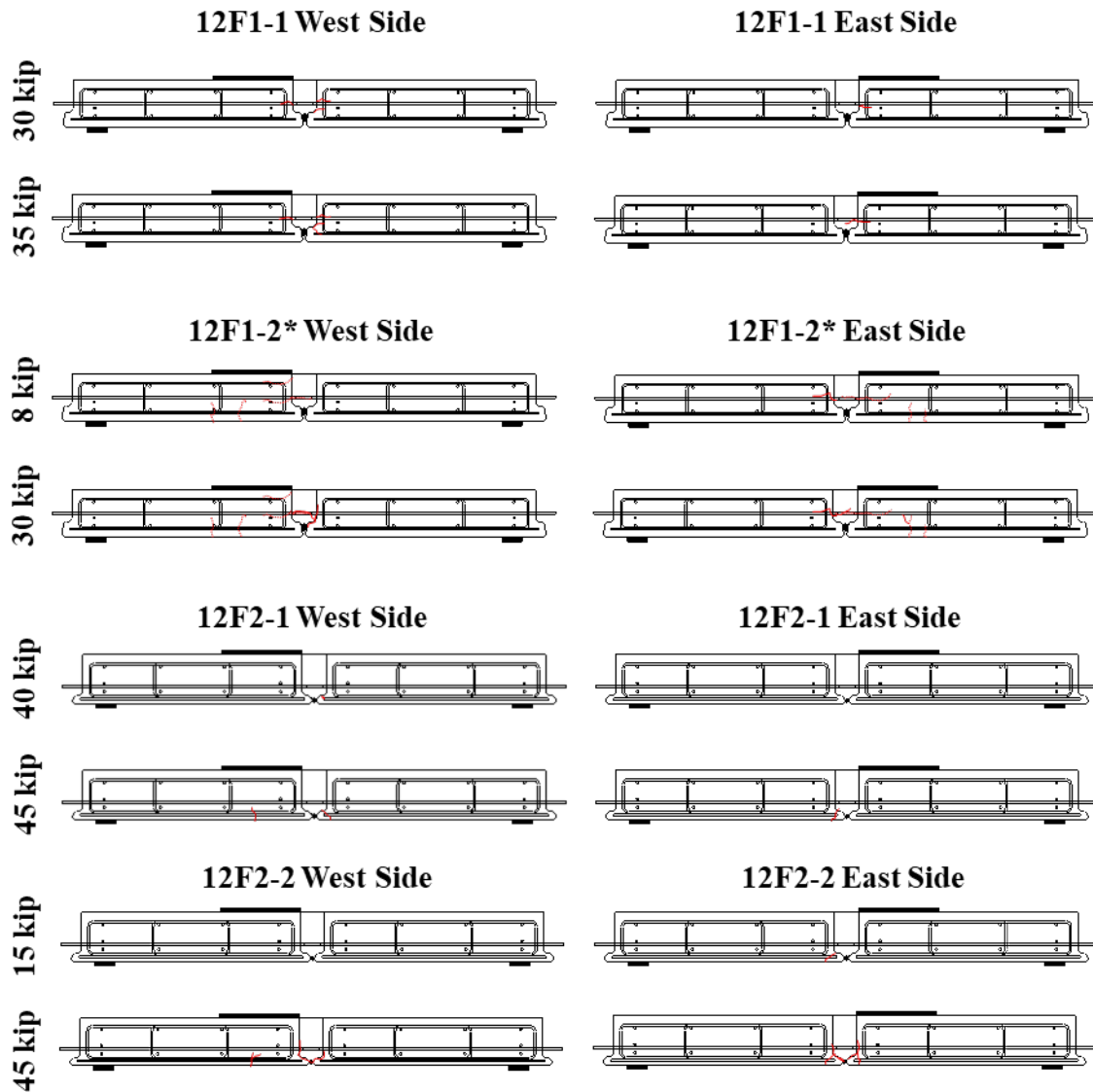


Figure 5.60: Crack pattern of 12-inch specimens (dashed lines indicate cracks formed in the cyclic stage); *strength test performed after fatigue testing

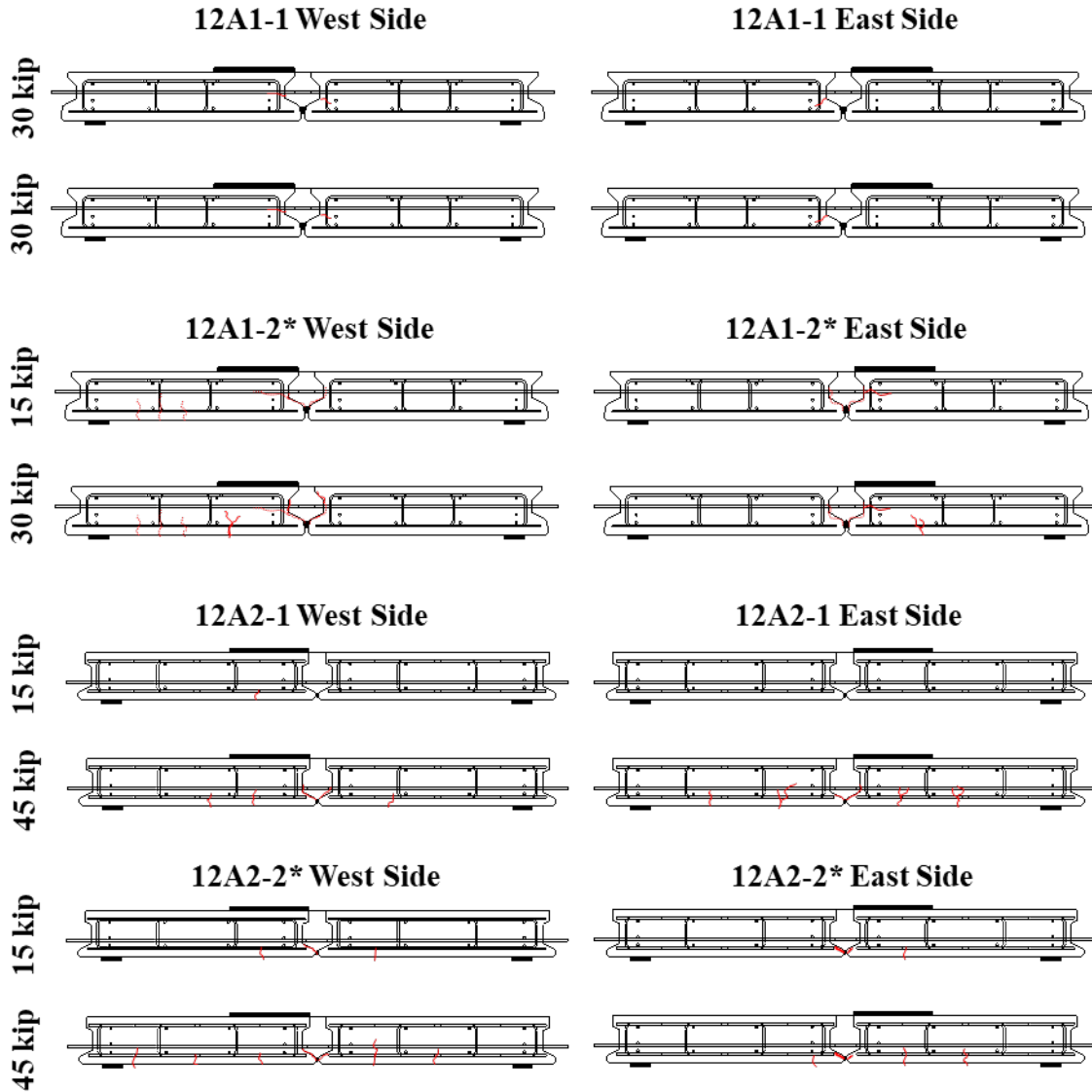


Figure 5.61: Crack pattern of 12-inch specimens (dashed lines indicate cracks formed in the cyclic stage) (cont.); *strength test performed after fatigue testing

5.11.5.2. Ultimate Behavior

There were two typical cracking patterns at failure observed in the 12-inch-deep specimens. The first pattern, observed in 12F1-1 and 12A1-1, began with a diagonal crack formed in the UHPC matrix. This diagonal crack then extended in both directions reaching the top corner of the north beam and the bottom opposite ledge of the south beam, as shown in Figure 5.62 (a). Failure of these specimens happened either by crushing of concrete along the joint interface accompanied by reinforcement fracture or pullout, or by reinforcement pullout prior crushing of the north beam concrete, shown in Figure 5.62 (b).

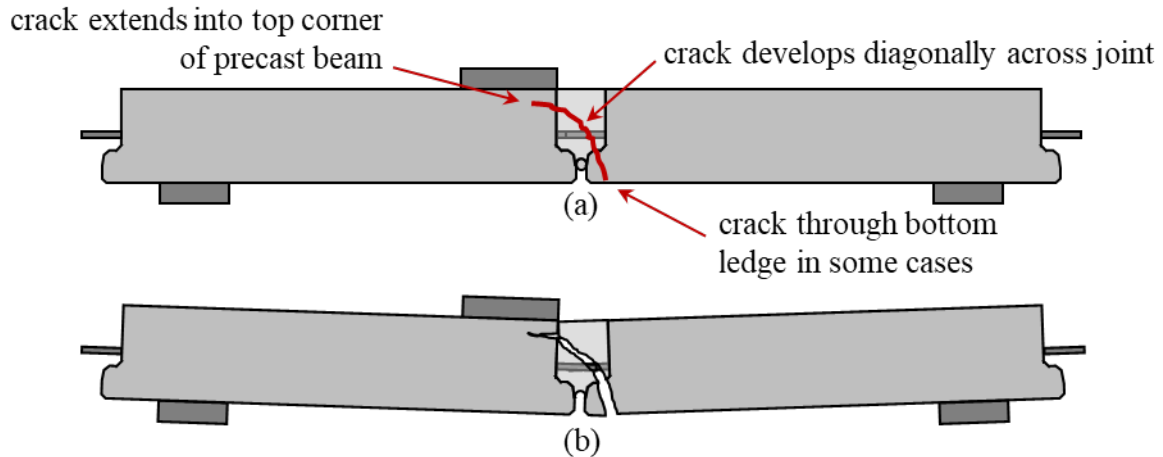


Figure 5.62: First typical failure pattern in 12-inch specimens: (a) cracking at failure and (b) after failure (12F1 is shown)

The second common failure mechanism, observed in 12F2 and 12A2, began with debonding of the UHPC from the precast section or a crack forming parallel to the joint in cases where sufficient bond was achieved, shown in Figure 5.63 (a). A second crack then would form at the level of the joint reinforcement in the joint and in some cases extending into the precast section. Failure would then be triggered by either crushing of the concrete, which was typically accompanied by fracture of the reinforcement, or splitting of the UHPC at the level of the reinforcement triggering a pullout failure.

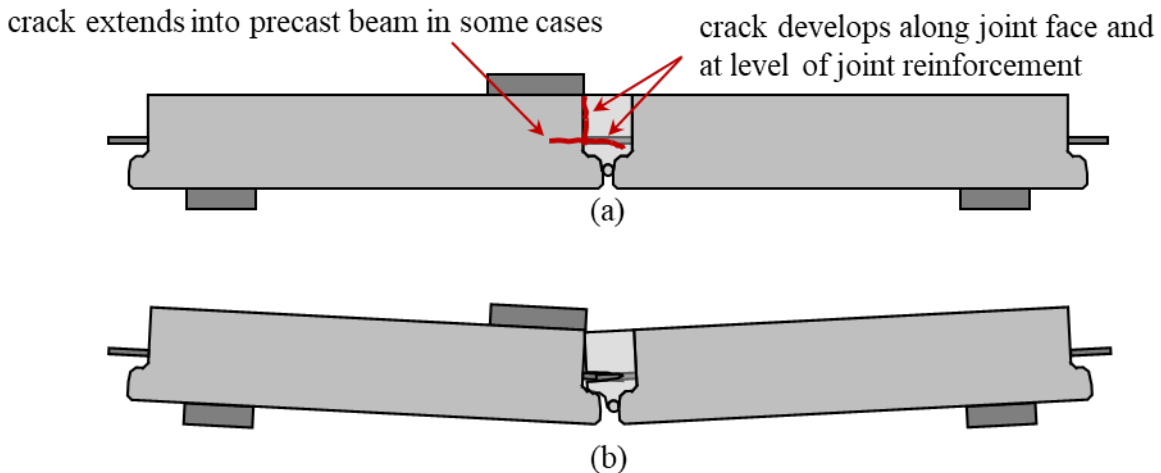


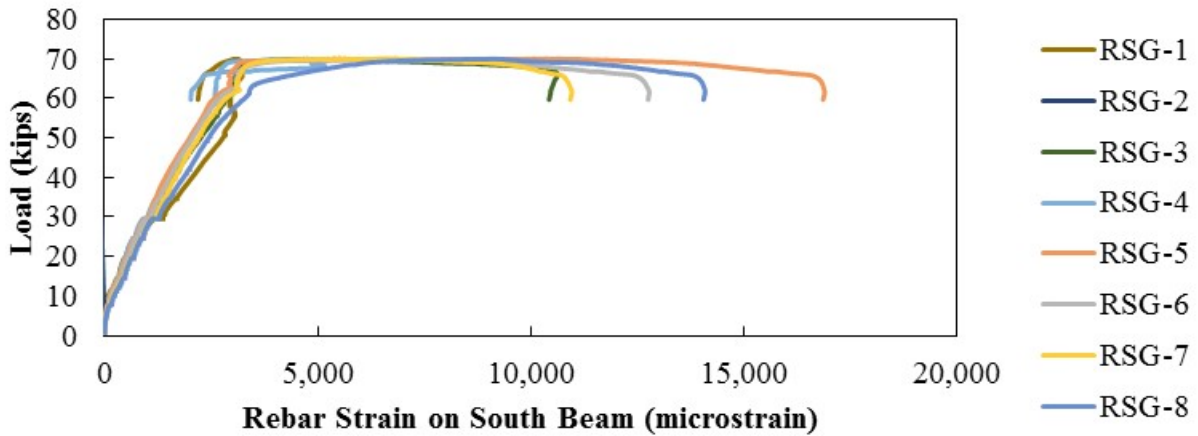
Figure 5.63: Second typical failure pattern in 12-inch specimens: (a) cracking at failure and (b) after failure (12F1 is shown)

The failed 12F1-1 and 12F2-1 specimens are shown in Figure 5.64 (a) and (b), respectively. Diagonal crack patterns were seen on both 12F1 specimens and horizontal splitting cracks on both 12F2 specimens. Hinging behavior was observed in 12F2-1 as the top concrete cover from the north beam ruptured and showed cover spalling.

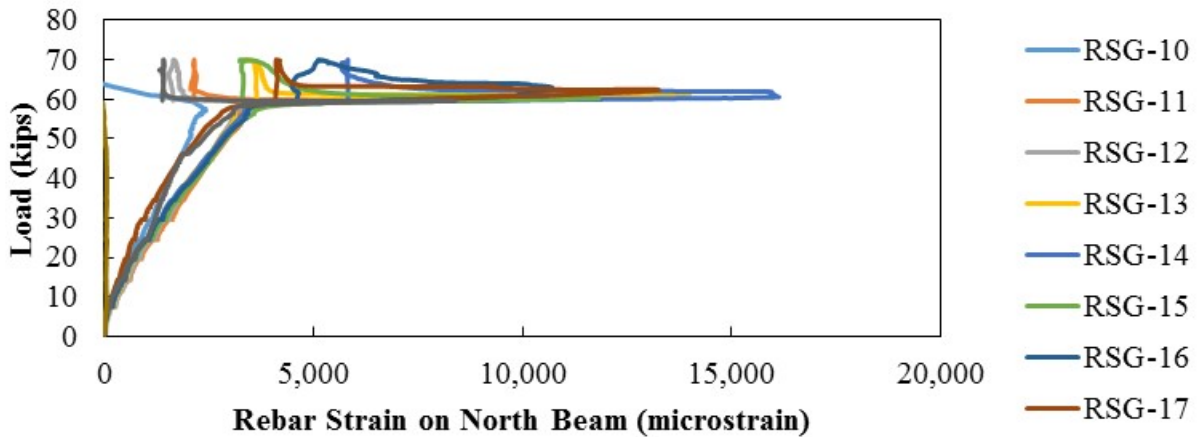


Figure 5.64: Cracking at failure for (a) 12F1-1 and (b) 12F2-1

The 12F1-1 joint reinforcement in the south side is shown in Figure 5.65 (a); all reinforcement was engaged uniformly from 0 kips to 30 kips and showed signs of yielding at approximately 70 kips (failure load). The behavior is similar in the north beam seen on Figure 5.65 (b), but a drop in tensile strain was observed close to the ultimate load for most of the reinforcement indicating a possibly pullout failure. Some reinforcement closer to the joint faces, were not able to develop due to splitting cracks observed at the joint UHPC matrix faces.



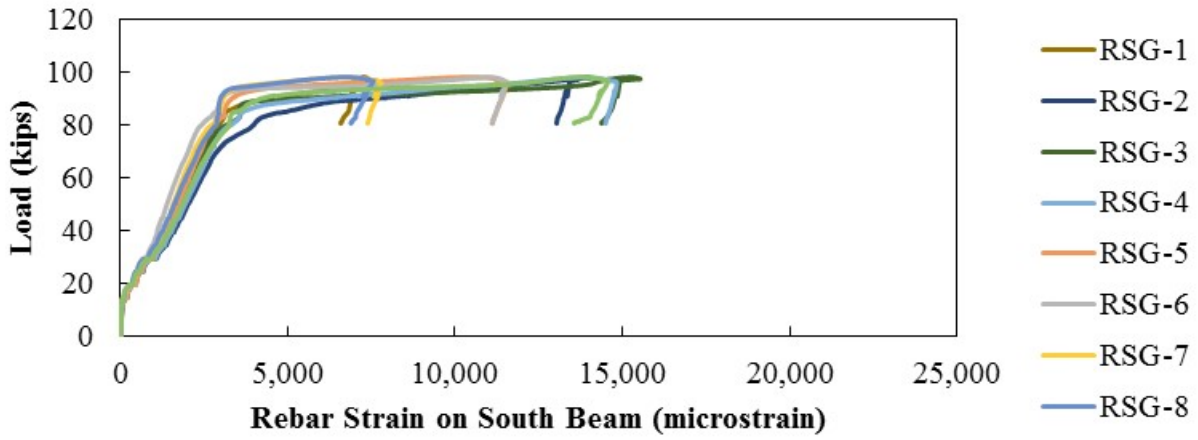
(a)



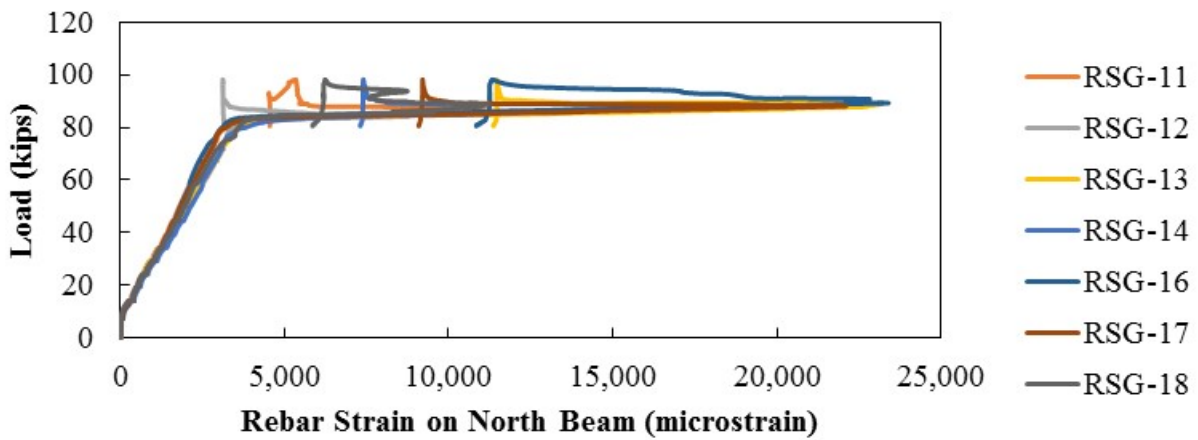
(b)

Figure 5.65: 12F1-1 system load versus rebar microstrain in (a) south beam and (b) north beam

The response observed in joint 12F2-1 reinforcement also reached about 15,000 microstrain as the load level was reaching 100 kips as shown in Figure 5.66 (a). Here, all reinforcement was engaged and a larger response was observed in the reinforcement located closer to the actuator. However, in the north side shown in Figure 5.66 (b), tensile strains larger than 20,000 microstrains were measured in the same central reinforcement. Because these specimens were thinner, cracking was observed at about 20 kips of system load as it can be seen a sharp change in rebar strain slope close to that load level.



(a)



(b)

Figure 5.66: 12F2-1 system load versus rebar microstrain in (a) south beam and (b) north beam

A more ductile behavior was observed in 12A1 and 12A2 specimens due to a larger embedment length of the joint reinforcement. Crushing of the concrete in the compression block under the load caused failure in these specimens, as shown in Figure 5.67 (a) for 12A1-1 and Figure 5.67 (b) for 12A2-1. There was cracking in the 12A1 specimens that extended from the inside corner of the joint to the center for the load point, showing a stress concentration at this point. There is no cracking extending from the inside corner of joint 12A2.



Figure 5.67: (a) Failed 12A1-1 specimen and (b) Failed 12A2-1 specimen

A horizontal crack developed at the level of the joint reinforcement in 12A2-1, shown in Figure 5.67 (b), but no pull-out of the reinforcement was observed. While cracking at the level of the reinforcement caused a splitting type pull-out failure in other specimens, shown in Figure 5.68 (a), the reinforcement level cracking in 12A2-1 extended into the precast section as well and is thought to be caused by bending stresses in the section, shown in Figure 5.68 (b).

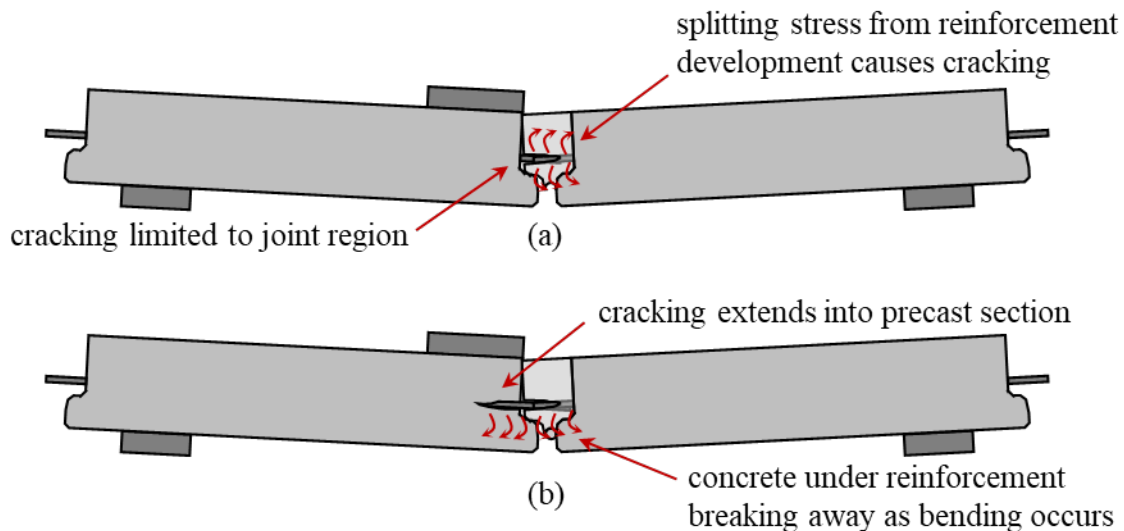
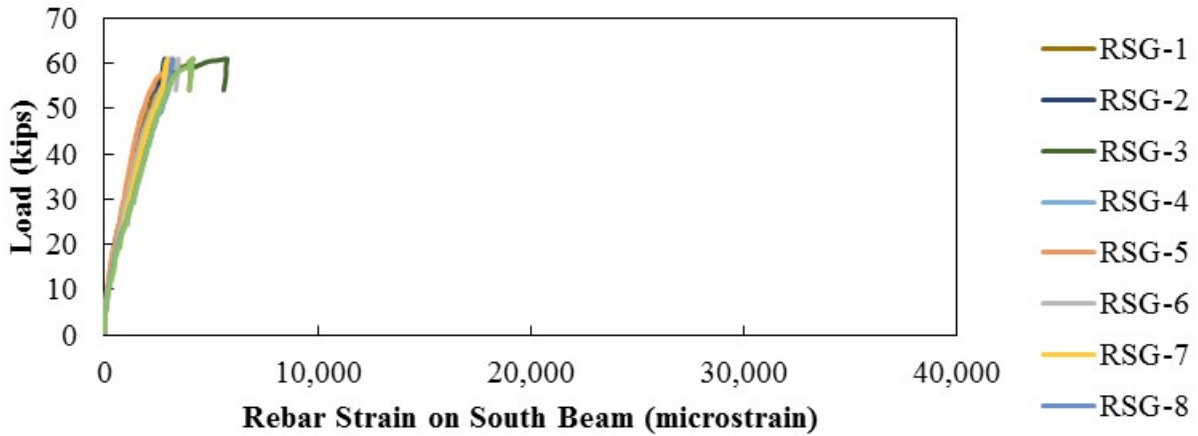


Figure 5.68: Two hypotheses for cracking at level of joint reinforcement: (a) splitting caused by pull-out of joint reinforcement (12F1 shown) and (b) cracking under reinforcement caused by beam bending (12A2 shown)

The load versus reinforcement strain responses for 12A1-1 and 12A2-1 are shown in Figure 5.69 and Figure 5.70, respectively. There was a noticeable difference between the strains in the north and south side of the joint for 12A1-1, suggesting a stress concentration toward the loaded side of the joint and a hinging-type behavior as discussed above. All the reinforcement on the loaded side of the joint yielded, while none of the reinforcement on the unloaded side clearly passed the yield point.



(a)

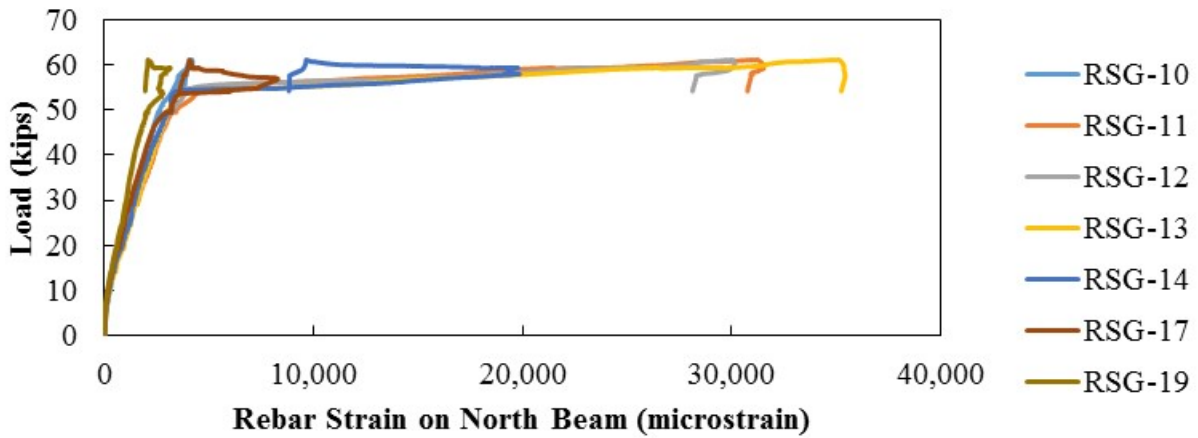
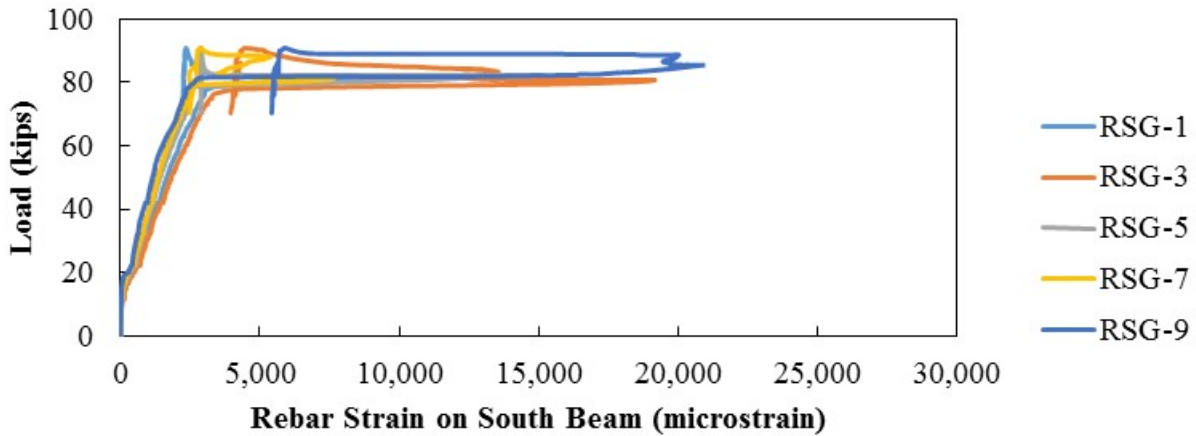
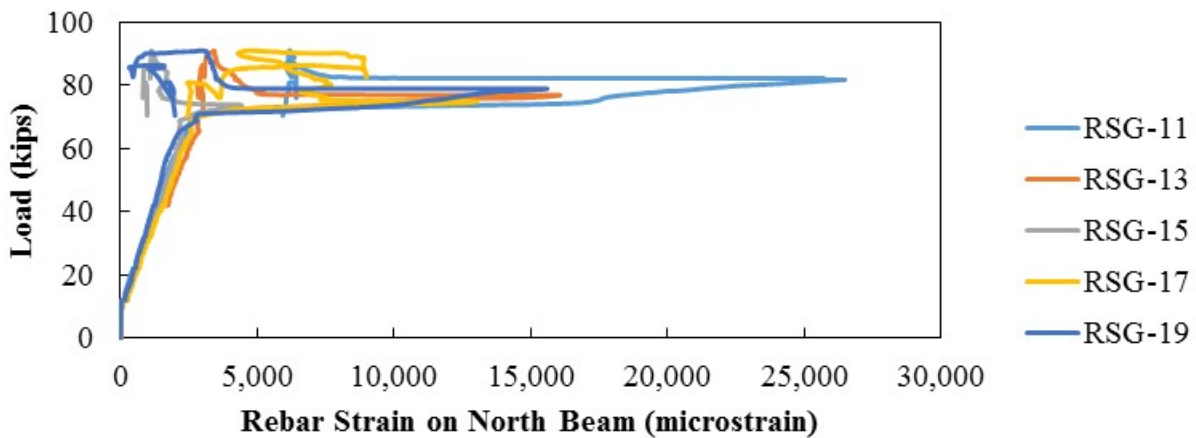


Figure 5.69: 12A1-1 system load versus rebar microstrain in (a) south beam and (b) north beam (defective rebar responses are not shown)

There were similar strains in the reinforcement on both sides of the joint in 12A2-1. This would suggest that there were no stress concentrations or clear hinging at failure of the joint. Joint 12A2-1 had the best ductility likely because strains (and stresses) were better distributed between the reinforcement on both sides of the joint.



(a)



(b)

Figure 5.70: 12A2-1 system load versus rebar microstrain in (a) south beam and (b) north beam

A detailed analysis for each broken 12-inch joint is provided in Appendix D where the types of failures are discussed based on observations on rupture patterns, material performance, and sensor data.

5.12. CONCLUSIONS AND RECOMMENDATIONS

A summary of the conclusions and recommendations made based on the construction and experimental results of the small-scale strength testing is provided in this section.

5.12.1. Conclusions

5.12.1.1. 18-inch Specimen Conclusions

The following conclusions are made based on the construction and experimental results of the 18-inch joint specimens:

- *Issues with FSB control specimens:* The control FSB joint (FSB-1 and FSB-2) did not perform as expected likely due to a larger bend diameter (FSB-1) and the compressive

strength of the deck concrete being much lower than specified (FSB-2). These issues likely caused the development failure of the joint reinforcement prior to yield. The results from the numerical analysis were used as the point of comparison for the developed UHPC joints.

- *Ultimate strength:* Joints 18F1 and 18A1 had similar ultimate capacities to the control FSB (numerical result). Joint 18F2 had a slightly higher capacity because of the larger lever arm of the joint reinforcement.
- *Joint ductility:* Joint 18A1 had the largest ductility among all the joints. This was the only joint where all the joint reinforcement fractured at failure. The joint reinforcement in 18A1 had a larger available development length than in the other joints.
- *Joint finish and debonding:* The sandblasted joint interface preparation was not sufficient to achieve the desired UHPC-to-precast bond. Debonding was observed in all the specimens. A ¼-inch magnitude exposed aggregate finish is required to get satisfactory bond.

Joint 18A1 was the best performing joint of the 18-inch-deep joints and had better performance than the current FSB joint detail.

5.12.1.2. 12-inch Specimen Conclusions

The following conclusions are made based on the experimental testing of the 12-inch joint specimens:

- *Ultimate strength:* The difference in joint reinforcement lever arm had a more pronounced effect on the ultimate strength of the 12-inch-deep specimens. Joint 12F2 and 12A2 had the largest capacities, due to their larger lever arms.
- *Joint ductility:* Joint 12A2 had the largest ductility among all the joints. This joint had the largest available development and splice lengths for the joint reinforcement.
- *Joint finish and debonding:* The 12A2 specimen was constructed with an improved aggregate exposure in the precast joint, compared to the sandblasted joint finish. The surface had an approximate 1/8-inch magnitude exposed aggregate finish and performed better than the other joints.

Joint 12A2 was the best overall performing joint of those tested. Though an 18-inch version of this joint was not experimentally tested, the benefits of this joint over 12A2 will likely translate well to the 18-inch version.

5.12.2. Construction and Design Recommendations

The following design recommendations are made for each case of beam that was tested:

- *Proper bend diameter for current FSB design:* The joint reinforcement must have the correct bend diameter to help with the development of the joint reinforcement. It is recommended that additional testing be done to validate the performance of the current FSB joint detail.
- *Use increased development and splice length of joint reinforcement in UHPC:* Using the currently recommended $8d_b$ embedment length and $0.75l_d$ splice length allowed the

reinforcement to develop its yield strength but resulted in pullout or development causing failure. An increased embedment and splice length resulted in fracture of the reinforcement and crushing of the concrete at failure.

- *Ensure proper surface finish of joint:* An exposed aggregate finish with ¼-inch magnitude is needed to ensure proper bond between the precast member and UHPC joint. Make sure the proper admixtures are used. An aggregate size of 1 ¼ inch may be needed to achieve the ¼-inch magnitude roughness. Casting mock-ups is recommended to ensure the precaster can provide the proper finish. Additionally, the surface should be pre-wetted to an SSD condition immediately before casting of the UHPC.
- *Minimum bottom flange thickness:* The bottom flange of the beam should have an average thickness greater than 2 inches and contain a #3 transverse reinforcing bar. This will prevent the bottom flange from breaking off during casting, transport, or construction of superstructure.
- *Check UHPC materials before casting:* Check that the proper dry pre-mix and compatible admixtures were received. Also check to make sure that the materials are not expired and do not have any large dry clumps.

These design recommendations (with the additional details provided in §5.5.5) were taken into consideration for the full-scale testing portion of this project.

6. SMALL-SCALE JOINT FATIGUE TESTING

6.1. INTRODUCTION

Fatigue testing was performed on three of the 12-inch-deep small-scale specimens: 12F1, 12A1, and 12A2. Approximately 2 million cyclic loads were applied to each joint to test (1) their performance under expected service loads and cycles, (2) if their behavior degraded under increased cyclic loads, and (3) the effect of fatigue loading on the ultimate strength of the joints. The fatigue testing protocol for this project and a summary of the results are presented in this chapter.

6.2. SPECIMENS FOR FATIGUE TESTING

The three best performing joints from the static load testing (12F1, 12A1, and 12A2) were selected for fatigue testing. Details for these three joints are shown in Figure 6.1. These joints were selected based on satisfactory performance from the strength testing and ease of construction compared to the original FSB joint layout.

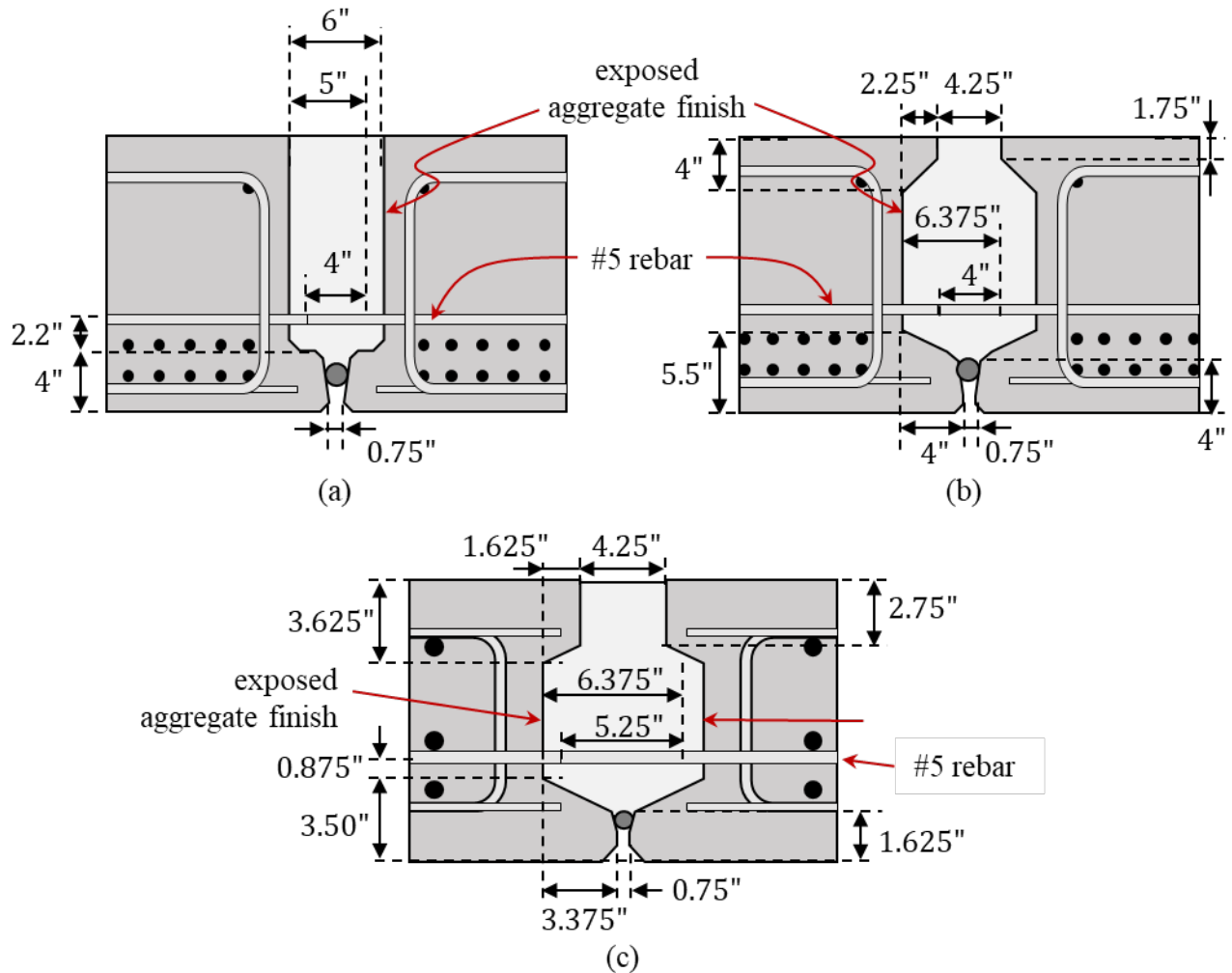


Figure 6.1: Joint geometries for specimens tested with fatigue loading: (a) 12F1, (b) 12A1, and (c) 12A2

As described above, Specimens 12F1 and 12A1 were both cast at the same time using a similar procedure. Specimen 12A2 was cast at a different date using a slightly different procedure. There are a few key points about construction of these specimens that should be mentioned again:

1. The joint interface for 12F1 and 12A1 was finished using sand blasting, which did not noticeably roughen the surface.
2. The finish for the joint interface of 12A2 was achieved using a paste retarder on the formwork and pressure washing of the joint within 24 hours after casting. This procedure led to approximately a 1/8-inch roughened surface.
3. A different UHPC mixture was used for the first static tests of 12F1 and 12A1. The UHPC used for this static testing was less flowable and had a much shorter working time than the UHPC used for the fatigue testing. The second static test used the adequate UHPC (and mix) as fatigue tests of 12F1 and 12A1.
4. The same UHPC mixture was used for the static and fatigue testing of 12A2, which was the same as the mixture used for the fatigue testing of 12F1 and 12A1.

Additional details on the fabrication of these specimens can be found in the previous section.

6.3. FATIGUE LOADING SCHEME

One of the goals of the fatigue testing was to simulate truck traffic loading on the UHPC joint over the expected 100-year service life of the bridge. The fatigue testing was limited to 2 million cycles of load applied and a maximum 2 Hz load rate, due to schedule and laboratory limitations. The FSB section was originally restricted to off-system bridges with a low average daily traffic (ADT) and average daily truck traffic (ADTT) [19]. Off-system projects are bridges not located on the State Highway System (SHS) or the National Highway System (NHS). According to the FDOT Plans Preparation Manual, Volume 1, Glossary of Terms [73], the standards for low volume highways in annual average daily volumes in collector systems are summarized in Table 6.1. These characteristics are the basic values of the fatigue loading scheme definition. Two main assumptions were made in terms of truck traffic number and the range of the fatigue load and are described in the following sections.

Table 6.1: FDOT standards for low volume highways (AADT: annual average daily traffic)

Highway Type	Number of Lanes	Low Volume AADT
Collector - Urban	2-Lane Facility	11,000
Collector - Urban	4-Lane Facility	37,000
Collector - Rural	2-Lane Facility	8,000
Collector - Rural	4-Lane Facility	30,000

6.3.1. Assumption for Truck Traffic Number

The highest AADT was selected from Table 6.1 to ensure the bridge could be used in all locations with 4-lane configurations; the AADT of a 4-lane urban collector is 37,000. FDOT Plans Preparation Manual [73] recommends that the truck traffic be taken as 10 percent of the AADT or the daily count (24-hour count). As a result, the average annual daily truck traffic (AADTT) is 3,700 trucks. This quantity accounts for bidirectional truck traffic, and because the specimen dimension is less than one-lane width (8' – 10 ¾"), the truck numbers must be decreased to unidirectional traffic. The most recent AASHTO LRFD Bridge Design Specifications (§C3.6.1.4.2) [72] states that one direction of traffic carries more than one-half of the bidirectional AADT; thus, designing for 55 percent of the bidirectional AADT is recommended. This factor allows the bidirectional truck traffic number to drop from 3,700 to 2,035 unidirectional truck traffic. Using this AADTT over the 100-year service life give a total of 203,500 trucks passing over the UHPC joint. Note that this does not include traffic growth data for the intended design life, so an assumption will be done to account for any uncertainties.

6.3.2. Assumption for Fatigue Load Range

The type of truck load used in the fatigue testing was the HL-93 as specified in AASHTO LRFD Bridge Design Specifications (§3.6.1.4) [72], the truck footprint is shown in Figure 6.2.

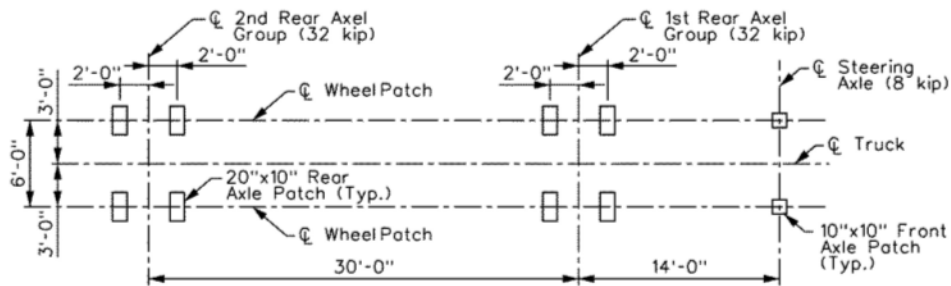


Figure 6.2: Refined design footprint for fatigue design [72]

Each truck has two axle groups of 32 kips and each axle group has four-wheel loads with two of them closely spaced. Because one truck width does not fit entirely in the fatigue specimen width, a half-width truck was used. Therefore, the wheel patch that was used was the same as the strength testing accounting for the largest wheel area and stress. Since each half-width truck has four 20-inch wide by 10-inch-long wheel loads, the number of cycles for a 100-year service life test is four times 203,500 trucks, which is 814,000 cycles. Due to uncertainties of traffic growth previously described, the number of cycles was increased to 900,000 cycles, which translated to about a 10-percent increase. Because the maximum number of cycles permitted is 2,000,000, three different fatigue load ranges were executed, which will be discussed in the following section.

6.3.3. Fatigue Load Testing Protocol

Prior to the start of cyclic loading, the specimens were checked for cracking that may have occurred during fabrication, handling, or installation into test setup. These cracks were marked, photographed, and documented.

The fatigue loading scheme is shown in Table 6.2. The *first load range step* (calibration) was to make sure that sensors were reading correctly, cycled load was stable, and the specimens were behaving as expected for the prescribed load range. Fatigue loading was paused for one day following the calibration stage for the data to be processed. The beams were also visually inspected for cracking or any other damage that occurred; cracking and damage were marked, labeled, photographed, and documented. There were no complications experienced in the calibration stages for these specimens, so the fatigue testing continued with the second step (before cracking performance).

Table 6.2: Fatigue loading scheme

Loading type	Load Range Steps	Lower Limit Load	Upper Limit Load	Frequency	# Cycles	Testing Days
Fatigue	1 - Calibration	2 kip	12.64 kip	2 Hz	200,000	1.15
Fatigue	2 – Before Cracking Performance	2 kip	12.64 kip	2 Hz	900,000	6
Fatigue	3 – After Cracking Performance	19 kip	31 kip	1 Hz	900,000	11
Strength	4 – Overload Performance	0 kip	100 % Failure Load	N/A	N/A	1

The *second load range step* in the fatigue testing was aimed at evaluating the behavior of the joint under the expected fatigue loading and cycles for a 100-year service life. The fatigue load was under the cracking load for these specimens, so the fatigue testing was also used to see if the fatigue loading would cause cracking or debonding between the UHPC and precast system. The range of loading for this second cycle was calculated using Equation 6-1.

$$P = (1 + IM) * P_{wheel} \quad \text{Equation 6-1}$$

$$P = (1 + 0.33) * 8 k = 10.64 kips$$

P was added to the lower limit to calculate the upper limit, as shown in Equation 6-2.

$$P_{upper} = (1 + IM) * P_{wheel} + P_{lower} \quad \text{Equation 6-2}$$

$$P_{upper} = 10.64 k + 2 k = 12.64 kips$$

where:

IM = Dynamic Load Allowance = 0.33 from AASHTO LRFD Bridge Design Specifications (§3.6.2.1) [72]

P_{wheel} = HL-93 rear axle wheel load = 8 kips

P_{lower} = lower cyclic load

P_{upper} = upper cyclic load

The *third load range step* was used to evaluate the effect of cycling from below to above the cracking load on crack growth, bond loss of joint reinforcement, and overall degradation of the system performance. The fatigue load range was selected based on the fatigue stress range in the reinforcement, as discussed above.

After all the fatigue load ranges are applied, the specimens were subjected to static load until failure. The static load test procedure was the same as the other static load tests.

6.3.4. Selection of After-Cracking Load Range

The upper load range was based on the strain and stress ranges in the reinforcing steel. There have been several previous studies investigating the low-cycle and high cycle fatigue strength of reinforcing steel [74], [75]. Since the available cycles for the upper load range was 900,000 cycles, lower and upper loads were selected to cause a stress range in the reinforcement that would have a theoretical fatigue life greater than 1,000,000 cycles. The goal of this fatigue testing was not to fatigue the reinforcement, but to see if the bond between the reinforcement and the UHPC was adversely affected by fatigue loading.

An NCHRP study was conducted by Helgason et al. [74] investigating the fatigue strength of reinforcing bars in concrete. The results from this study are summarized in Figure 6.3. They found that the fatigue strength of the bars was affected by the grade reinforcement, size of bar, stress range (f_r) and low applied stress.

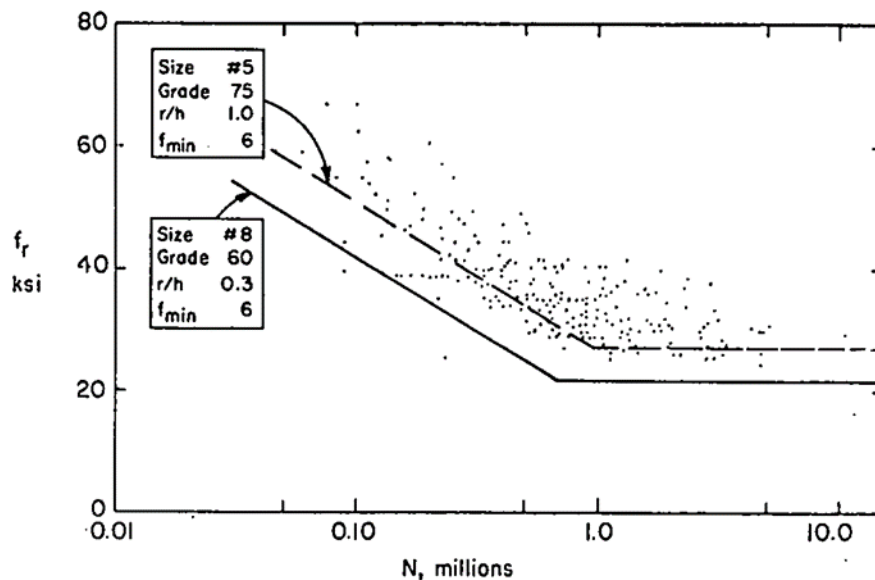


Figure 6.3: Summary of results and recommended design provision [74]

The results from this testing were used to develop a recommended design equation, shown in Equation 6-3.

$$f_r = 21 - 0.33f_{min} + 8(r/h) \quad \text{Equation 6-3}$$

Where:

f_r = stress range (ksi)

f_{min} = corresponding minimum tensile stress (positive) or maximum compressive stress (negative) (ksi)

r/h = ratio of base radius to height of rolled-on deformations (taken as 0.3 if unknown)

Using this expression and looking at the test results, a stress range of 20 ksi in the reinforcement was selected for the after-cracking fatigue loading. This stress range was used to get the load range recommended in the following section.

The fatigue load range was based on an average 20-ksi stress range in the steel, which corresponds to a strain range of 690 microstrain. The load range was selected based on this strain range using the strain versus load response of the reinforcement from the static tests, shown in Figure 6.4. The load range was shifted to ensure that both the visual cracking load and the cracking load from the concrete surface gauges were within the load range. A load range of 19 kips to 31 kips was selected for all the fatigue specimens.

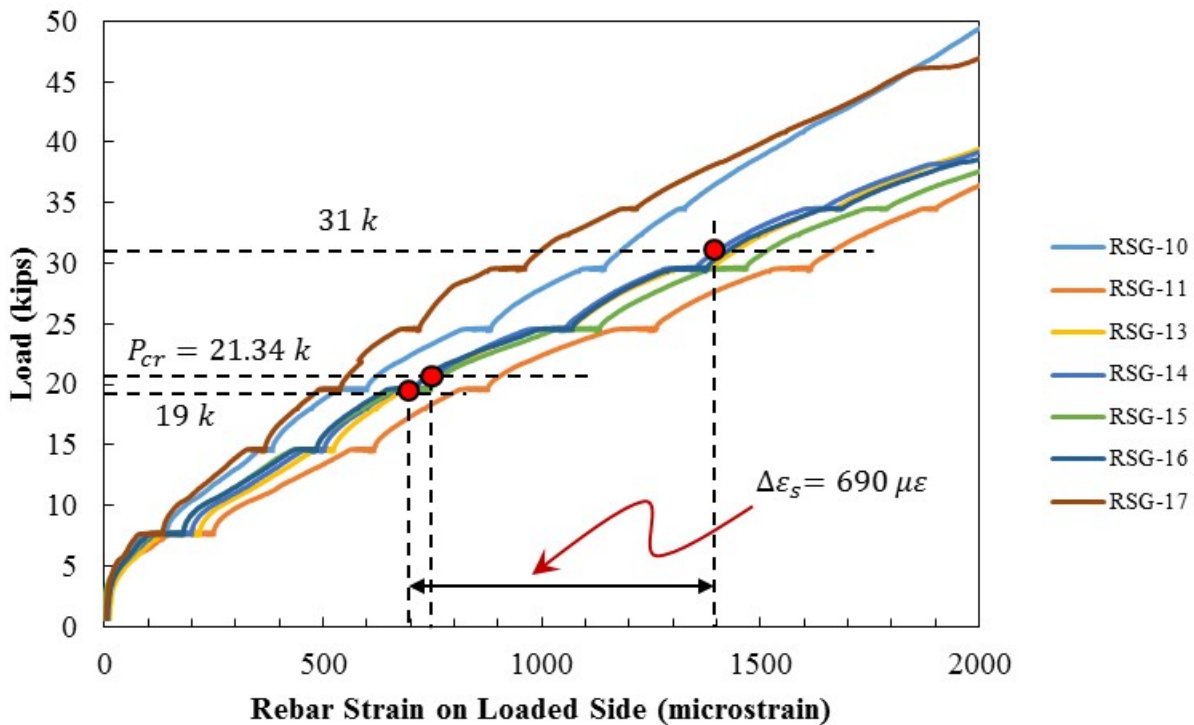


Figure 6.4: Procedure for selecting load range from rebar strain range (for 12F1)

6.4. DATA ANALYSIS PROCEDURES

Vertical displacements were measured by the laser displacement transducers. Strains were measured with the concrete and reinforcement strain gauges. The procedure for processing these measurements is discussed in this section.

6.4.1. Load-Deflection Data

The measured vertical displacements were used with the measured loads to calculate the stiffness of the system during each thousandth cycle, as shown in Figure 6.5 and Equation 6-4. Calculation of these stiffness values only required measurement of the deflection at the lower and upper load values.

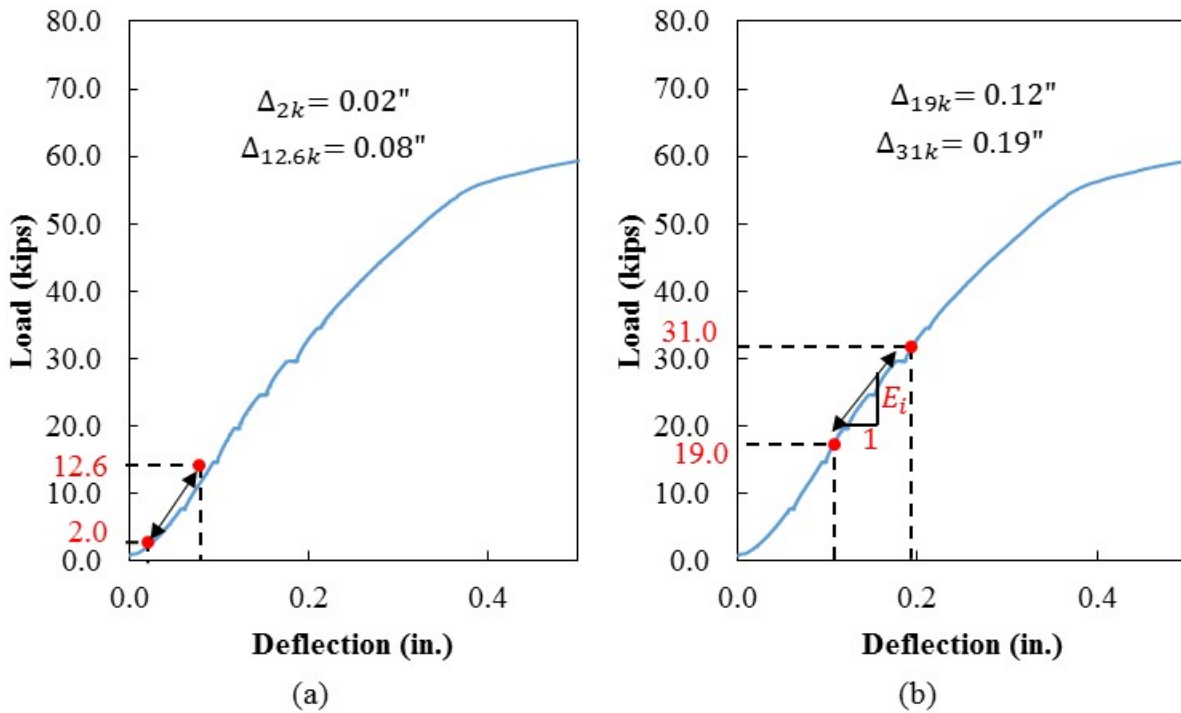


Figure 6.5: Example of load deflection ranges for (a) under-cracking and (b) after-cracking fatigue steps (for 12F1-1)

The equation to calculate the stiffness is shown in Equation 6-4.

$$E_i = \frac{P_{upper} - P_{lower}}{\Delta_{P_{upper}} - \Delta_{P_{lower}}} \quad \text{Equation 6-4}$$

The normalized stiffness was found as the stiffness of the cycle divided by the stiffness of the first cycle, as shown in Equation 6-5. The stiffness was only stored every 1,000 cycles to minimize the amount of data stored over the life of the beam.

$$N_{E_i} = \frac{E_i}{E_0} \quad \text{Equation 6-5}$$

The normalized stiffness was plotted versus the number of cycles for each of the specimens, as shown in Figure 6.6. A drop in the normalized stiffness would reveal strength degradation caused by the cyclic loading. Slight increases and decreases in normalized stiffness not following a general downward trend and not validated by events in any other gauges are not signs of degradation.

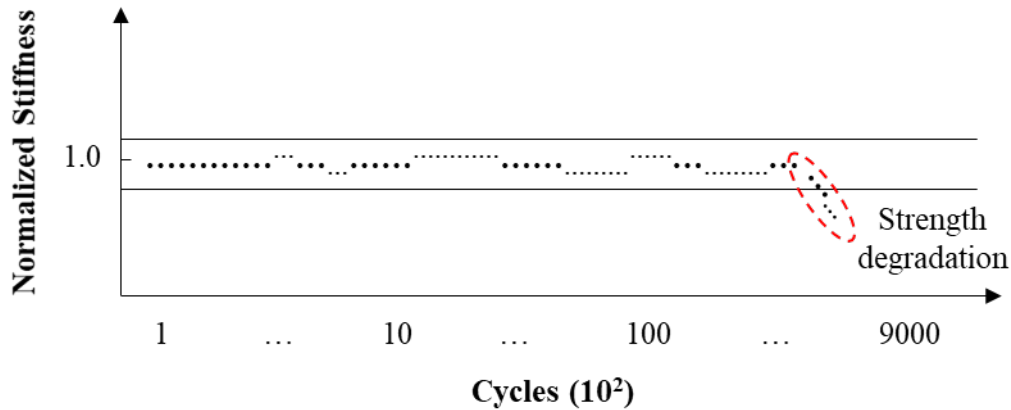


Figure 6.6: Hypothetical data for normalized stiffness values every 1000 cycles

The stiffness was also plotted with the support deflections subtracted from the midspan deflection. For this, the average displacement was found for each of the three laser displacement groups, shown in Figure 6.7. The average maximum and minimum displacement were found for each group for each cycle. There was generally no noticeable difference in displacement between the three gauges in each of the groups, suggesting even displacement over the width of specimens. Because there was no difference across the width, taking the average in the three groups helped to eliminate noise.

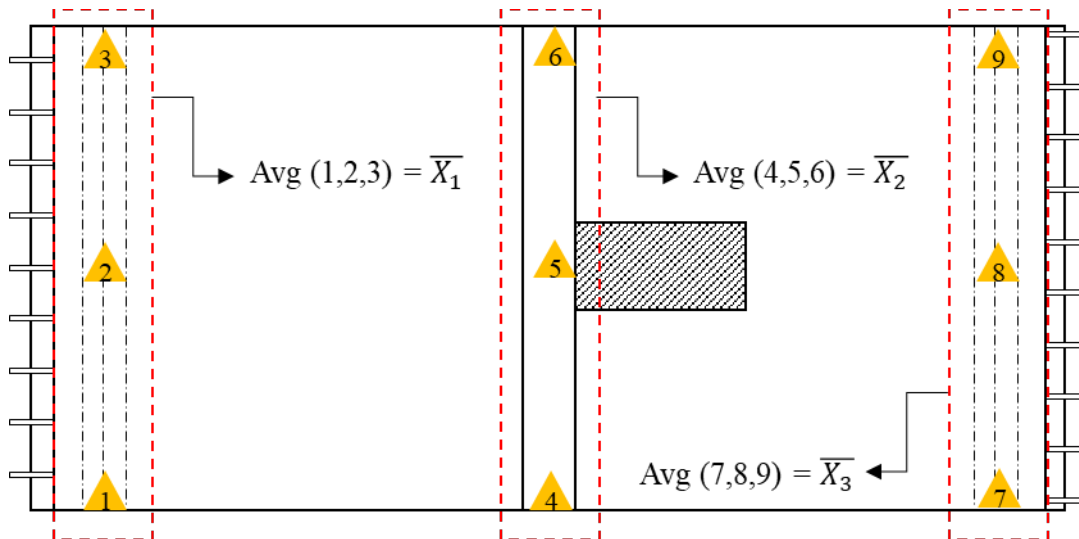


Figure 6.7: Average displacement computation for each sensor group

The absolute specimen deflection (Δ_{mid}) at midspan was calculated by removing the end deflection from the measured midspan deflection, as shown in Equation 6-6.

$$\Delta_{mid} = \overline{X}_2 - avg(\overline{X}_1, \overline{X}_3)$$

Equation 6-6

The absolute stiffness was then found based on this absolute specimen deflection in Equation 6-4. The absolute stiffness was then also used to find the normalized absolute stiffness using Equation 6-5.

6.4.2. Reinforcement Strain Gauge Data

Load versus reinforcement strain for strain gauges on the loaded side of 12F1-1 are shown in Figure 6.8. The range of strains at the selected fatigue loads are highlighted.

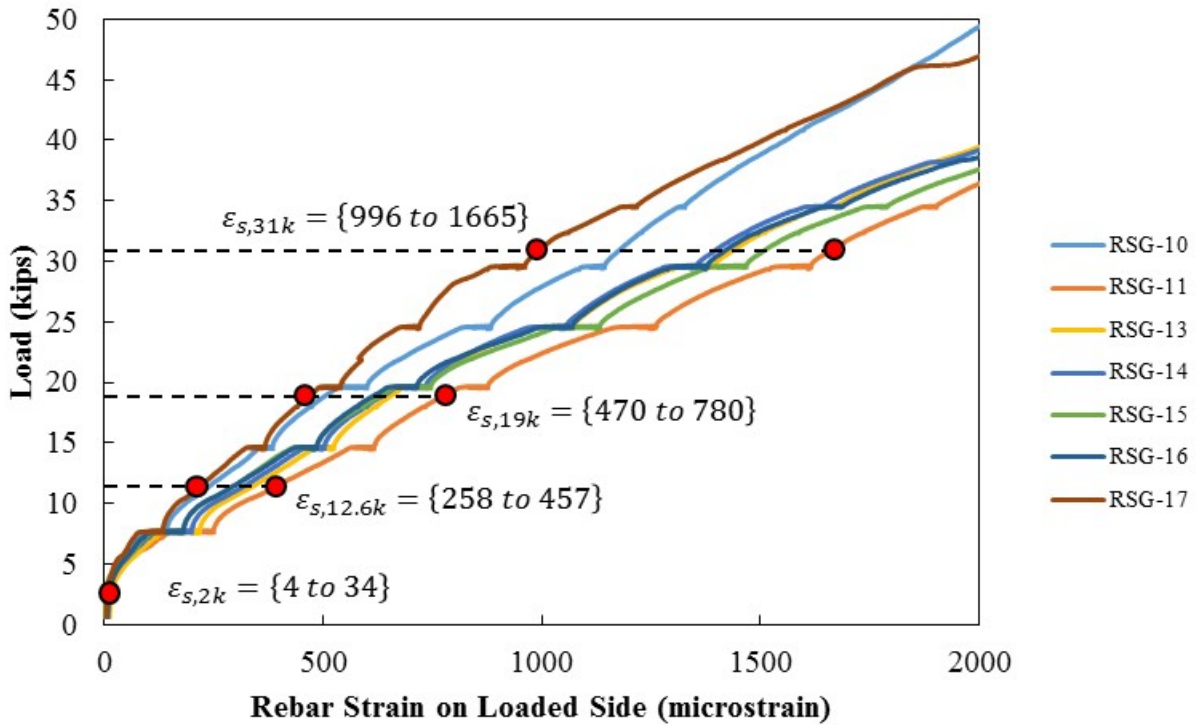


Figure 6.8: Sample of rebar gauge strains from static test within range of proposed fatigue testing loads; measured rebar strain ranges are highlighted (from 12F1-1)

The strains in the reinforcement associated with the lower and upper fatigue loads were recorded every 1,000 cycles. These strains were used to calculate the strain per load for the upper load range (Equation 6-7) and the change in strain per load change (Equation 6-8).

$$N_{\epsilon_{h,i}} = \frac{\epsilon_{upper}}{P_{upper}} \quad \text{Equation 6-7}$$

$$N_{\Delta\epsilon,i} = \frac{\epsilon_{upper} - \epsilon_{lower}}{P_{upper} - P_{lower}} \quad \text{Equation 6-8}$$

where:

ϵ_{upper} = strain measured at upper fatigue load

ϵ_{lower} = strain measured at lower fatigue load

The normalized strains per applied load was then plotted versus the cycle number, as shown in Figure 6.9. Yielding of the reinforcement at the location of the gauge would be indicated by the strain per applied load increasing each cycle. Slip or bond failure would likely be indicated by the strain per applied load decreasing each cycle.

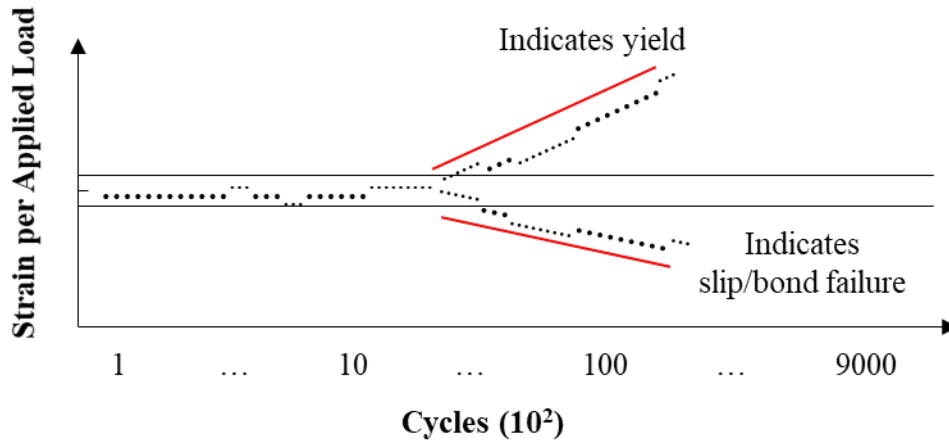


Figure 6.9: Hypothetical strain per applied load versus number of cycles for reinforcement

6.4.3. Concrete Gauges Data

The concrete gauges were monitored like the reinforcement gauges. The concrete strain in the bottom of the concrete found during the static testing of 12F1-1 is shown in Figure 6.10. The strain ranges for the gauges at the specified load ranges are highlighted. The start of the non-linearity in the curves is also highlighted starting at 20 kips in four of the gauges and 30 kips for the final two gauges. These correspond to the first cracking load and the point at which cracking was visually detected, respectively.

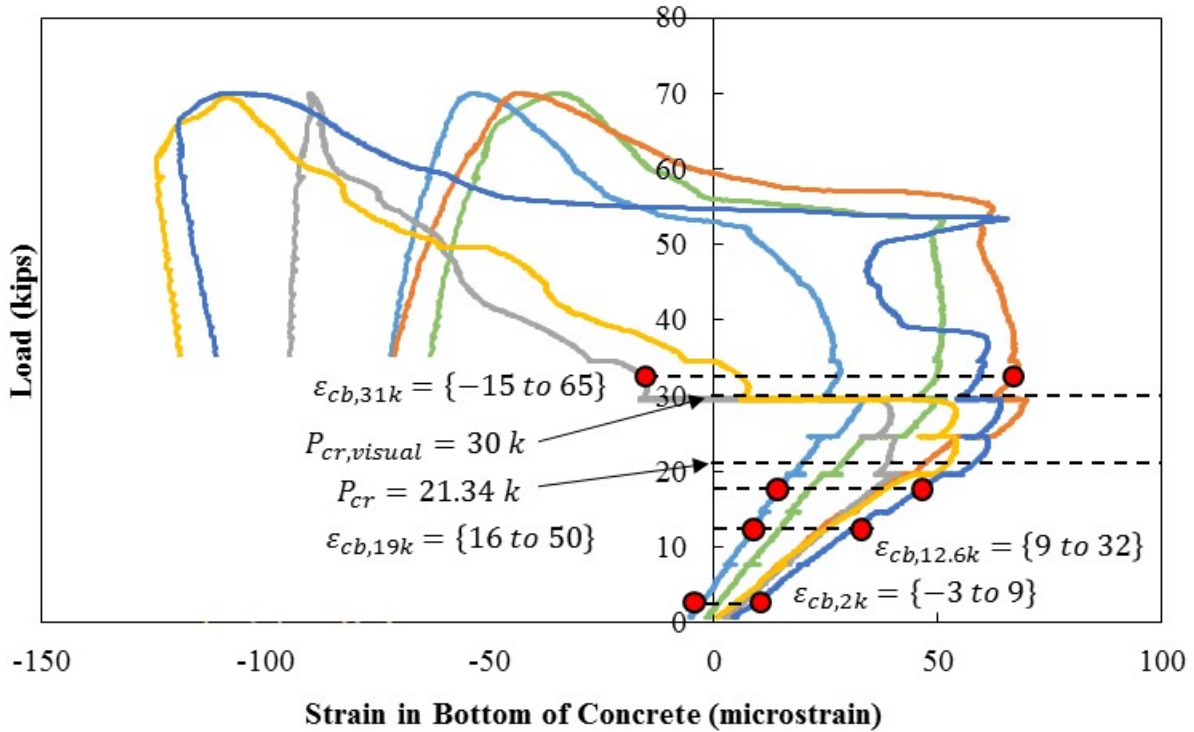


Figure 6.10: Strain in bottom of concrete for 12F1-1 (from static test)

The concrete strain gauge data was normalized the same as the reinforcement data, using Equation 6-7 and Equation 6-8. The strain per applied load versus cycle number was then plotted, shown in Figure 6.11. A drop in the strain per applied load indicates the occurrence of cracking near the location of the gauge.

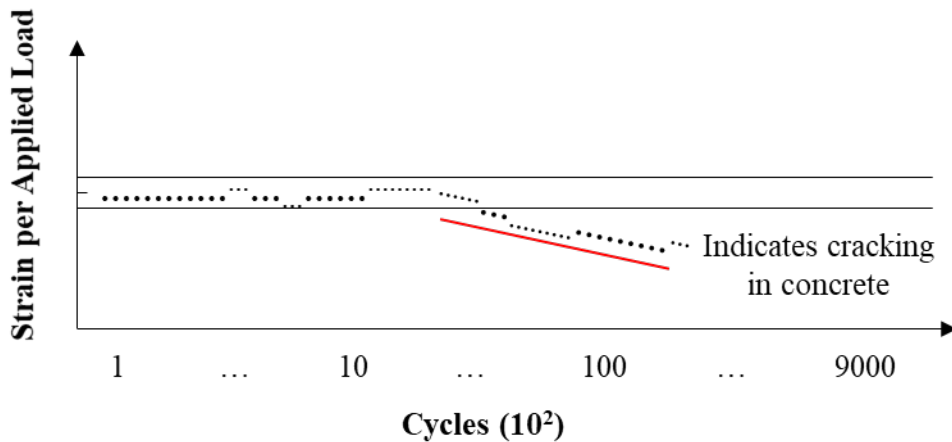


Figure 6.11: Strain per applied load (kip) per number of cycles for bottom concrete strains

Like the stiffness reading, the strain per applied load was only stored every 1,000 cycles to minimize the amount of data stored over the fatigue testing.

6.5. ACCIDENTAL LOADING BEFORE FATIGUE TESTING FOR 12F1-2

The first specimen tested in fatigue (12F1-2) experienced an accidental static load that was applied before the start of the fatigue testing as the specimen was being placed in the test setup. The load was not being measured at the time the accidental loading was applied, so the actual load applied could not be determined.

The accidental load caused cracking in the specimen and the joint region, as shown in Figure 6.12 and Figure 6.13, so it is clear that the load was larger than the cracking load for this specimen (21.3 kips from 12F1-1). Cracking also extended into the joint, which was the crack that eventually led to failure of these specimens. The researchers estimated from the cracking and knowledge of the loading system that the applied load was likely between 40 and 50 kips.

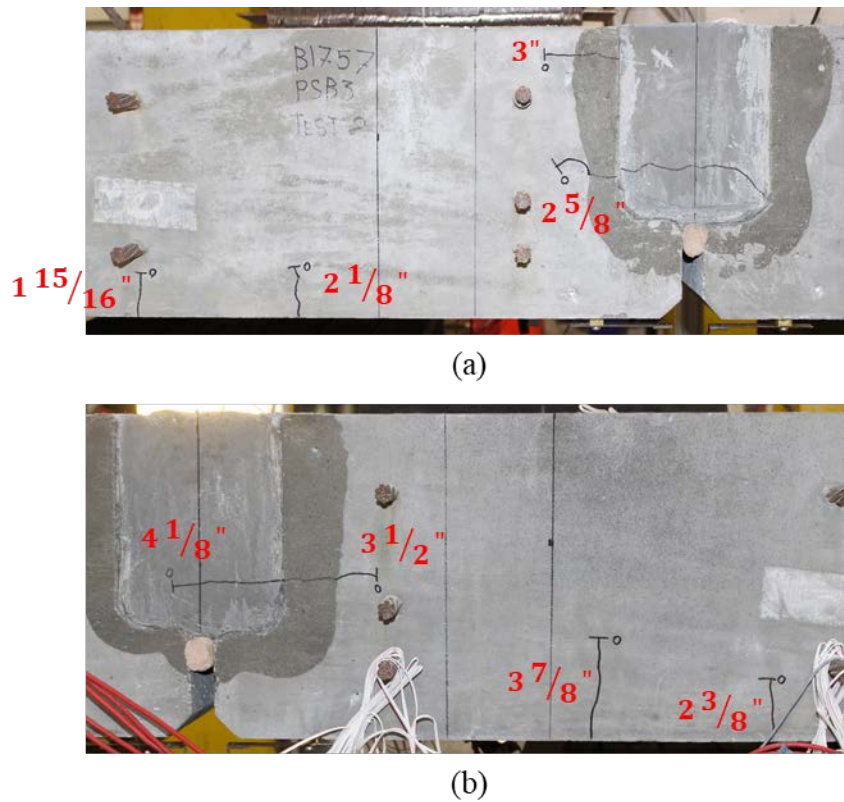


Figure 6.12: Cracking and crack lengths after accidental loading of 12F1-2 before fatigue testing on the (a) west side and (b) east side

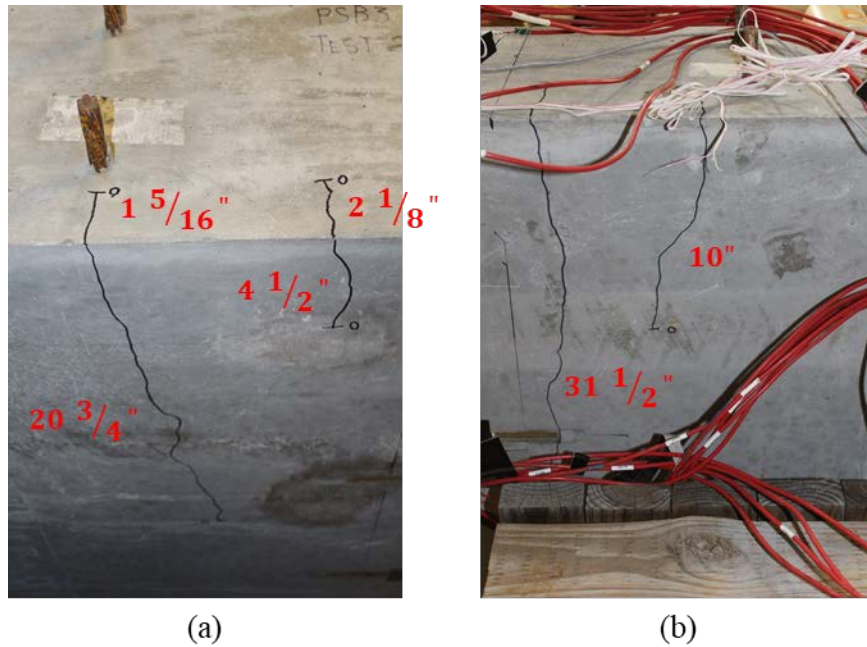


Figure 6.13: Cracking and crack lengths after accidental loading of 12F1-2 before fatigue testing on the (a) bottom of the west side and (b) bottom of the east side

The pre-cracking of 12F1-2 before the fatigue loading impacted the fatigue response of the specimens, primarily in the before cracking fatigue load stage. Some of these effects are discussed in the following sections.

6.6. ANALYSIS OF RESULTS

A summary of the results from the fatigue testing is provided in this section. Complete results for all the gauges in each specimen are provided in Appendix E.

6.6.1. Fatigue Response

6.6.1.1. Overall System Performance

The normalized absolute stiffness for all three of the fatigue specimens is plotted in Figure 6.14. There was no noticeable drop in stiffness in any of the three joints, which would suggest that there was no degradation in strength. There was no change in stiffness in the 12F1 joint between the before and after cracking load ranges because the specimen was cracked before fatigue loading began. The 12A1 and 12A2 joints had drops in stiffness after cracking occurred.

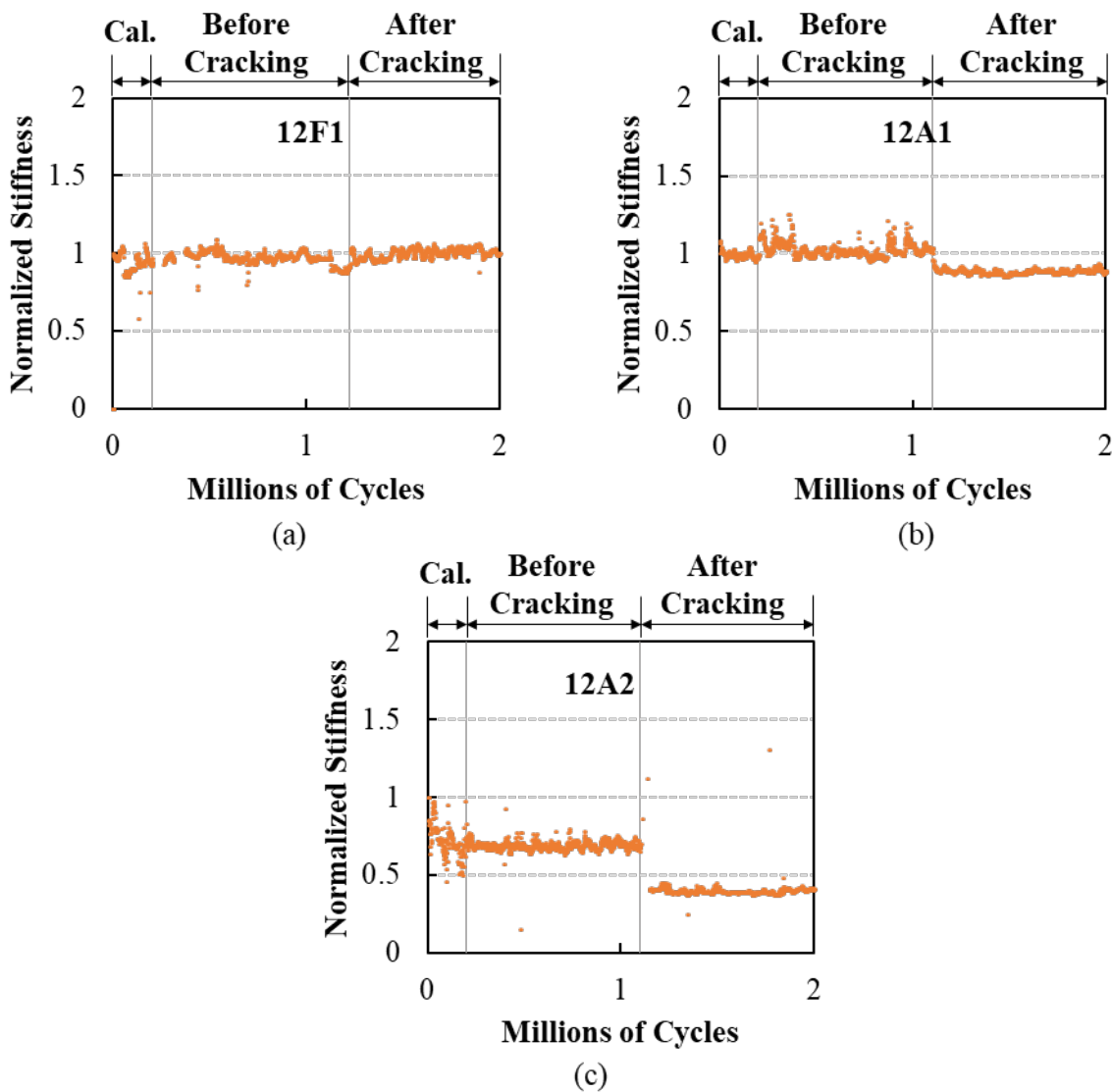


Figure 6.14: Normalized absolute stiffness of system for joints (a) 12F1, (b) 12A1, and (c) 12A2

6.6.1.2. Reinforcement Strain Gauges

The reinforcement strain change per load change for the two strain gauges at the center of the specimens (RSG-5 and RSG-15, see Figure 6.15) is shown for all three of the fatigue specimens in Figure 6.15. There was no significant increase or decrease in the strain change per load change within each of the fatigue loading stages. This would suggest that there were no signs of degradation of the bond of the joint reinforcement or any other deteriorations in the behavior.

The fatigue response is shown next to the measured response from the static testing for all gauges. For the static testing, the measured strain corresponding to the low load of the post-cracking load range would have been measured before cracking occurred. The concrete would have been uncracked at this point for the first fatigue cycle of the post-cracking load range, but the concrete was cracked for all future cycles. This is likely the reason for the large difference between the fatigue and static responses.

6.6.1.3. Concrete Strain Gauges

The concrete strain change per load change for the two concrete surface gauges at the center of the specimens (CSG-B2 and CSG-B5, see Figure 6.16) is shown for all three of the fatigue specimens in Figure 6.16. There was no significant increase or decrease in the strain change per load change within each of the fatigue loading stages. This would suggest that the pre-cracking fatigue loading would not lead to cracking of the specimens and that the post cracking fatigue loading did not cause deterioration of the system performance.

The 12F1-2 specimen was accidentally loaded past cracking before the fatigue load testing began. This is likely the reason there is not a significant difference in behavior between the pre- and post-cracking fatigue loading stages. The difference between the measured static response and fatigue response is likely the same as that explained for the reinforcement strain gauges.

CSG-B2 in 12A2 was not working correctly during the fatigue testing. CSG-B3 data is presented for 12A2 as it is nearby gauge.

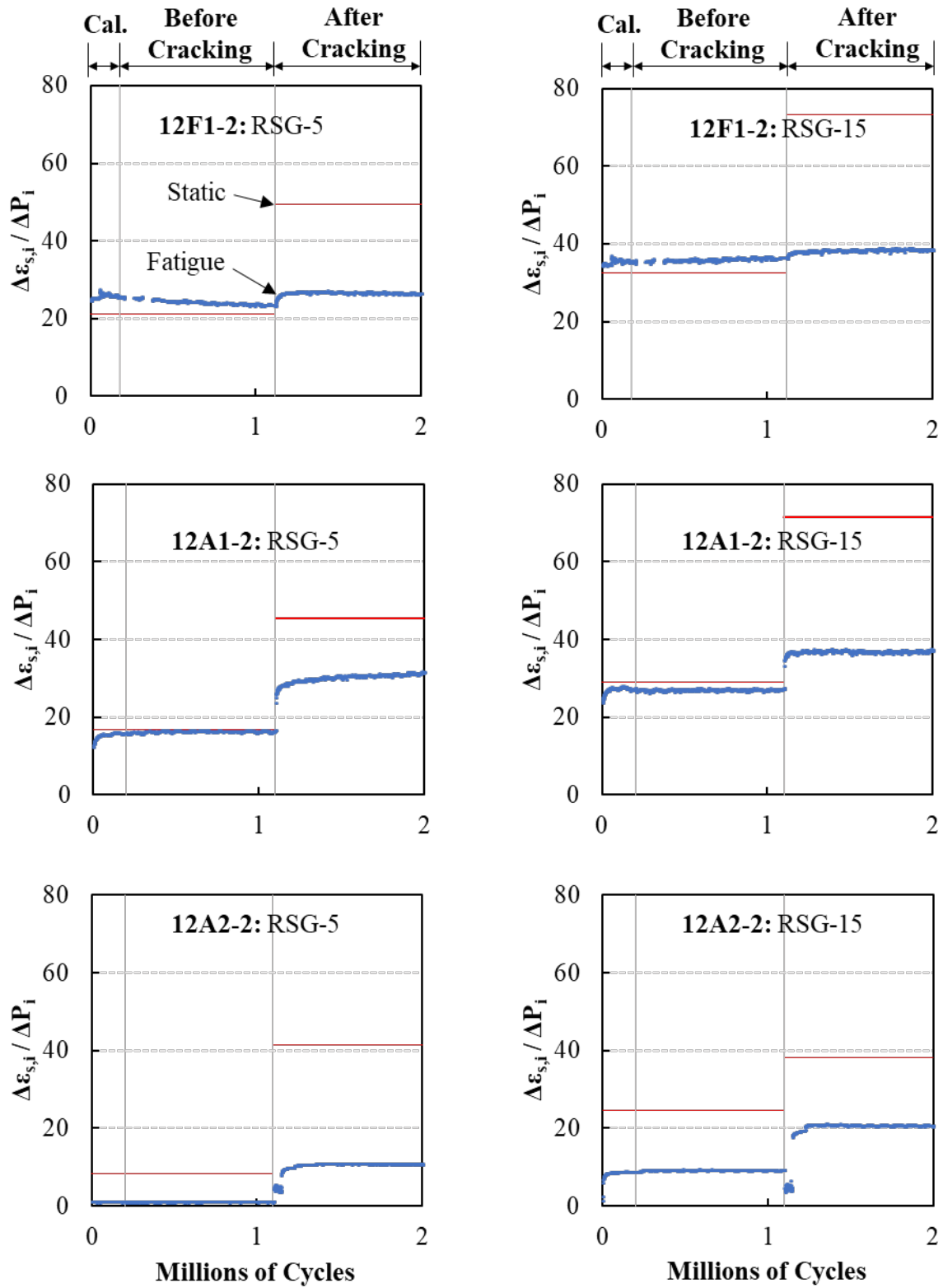


Figure 6.15: Reinforcement strain change per load change versus cyclic load for joint reinforcement at center of specimens for the unloaded (RSG-5) and loaded (RSG-15) side

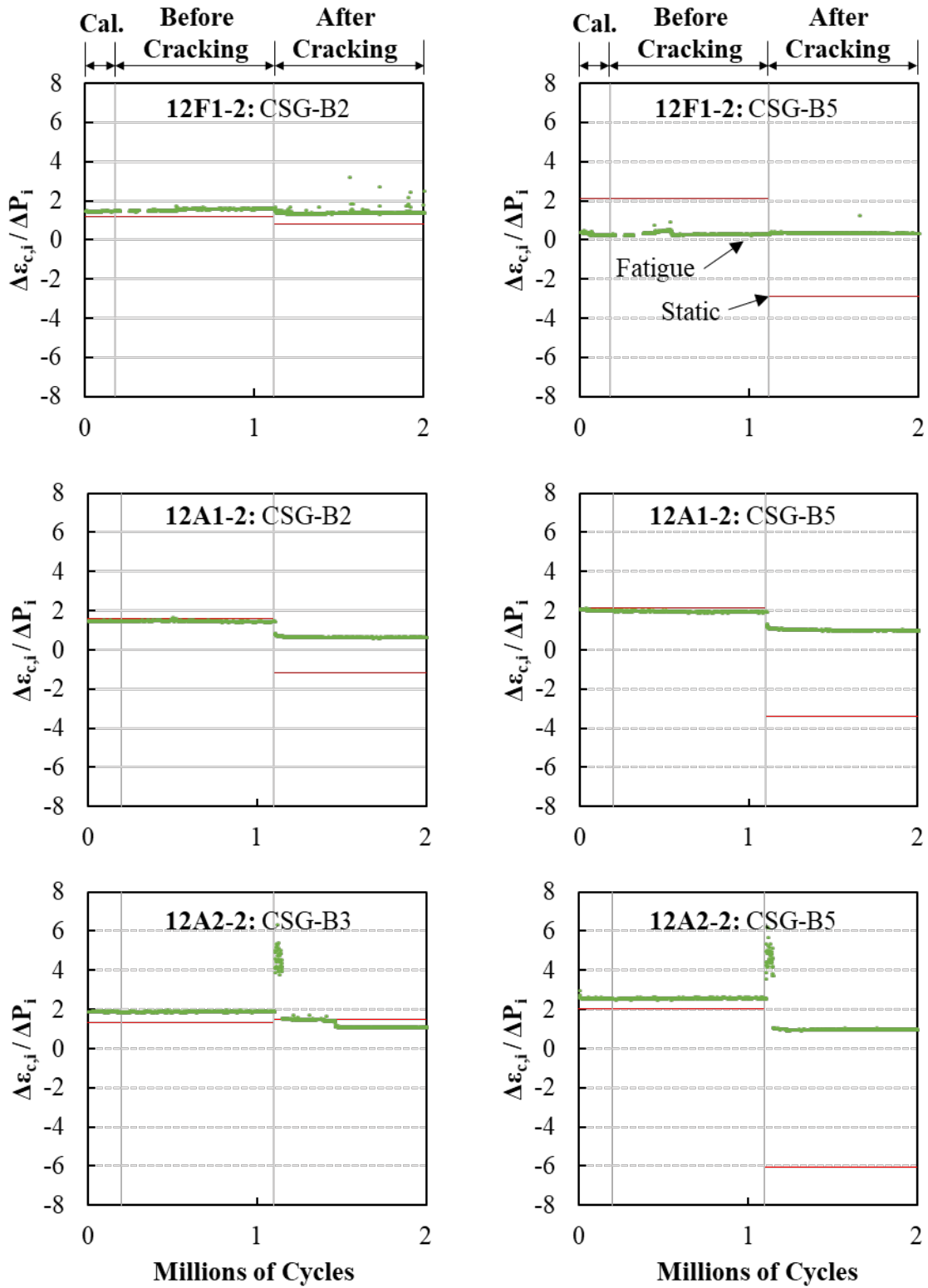


Figure 6.16: Concrete strain change per load change versus cyclic load at center of specimens for the unloaded (CSG-2, CSG-3) and loaded (CSG-5) side

6.6.1.4. Crack Displacement Transducers

The change in bottom joint displacement per load change for the crack displacement gauge at the center of the specimen (CDT-3, see Figure 6.17) is shown for all three fatigue specimens in Figure 6.17. Like the reinforcement and concrete strain gauges, there was no significant increase or decrease in the displacement change per load change within each of the fatigue loading stages. This would suggest that the pre-cracking fatigue loading would not lead to cracking of the specimens and that the post cracking fatigue loading did not cause deterioration of the system performance.

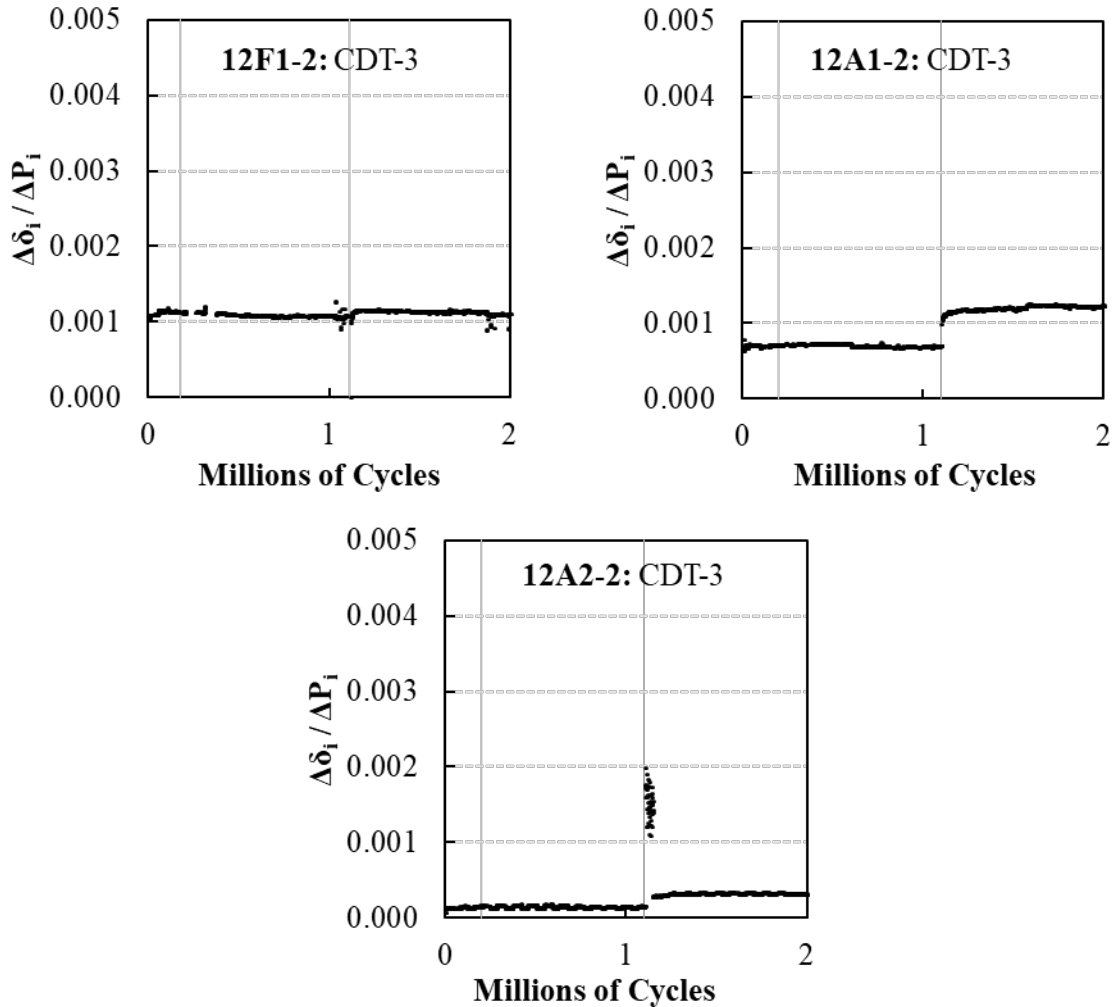


Figure 6.17: Displacement change of crack gauge per load change versus cyclic load at center of specimens (CDT-3)

6.6.2. Strength Performance after Fatigue Loading

The ultimate strength of each joint was measured using static load testing after the conclusion of the fatigue testing. The static load testing was performed in the same way as previously described. The load versus displacement response for the static load testing before and after fatigue loading for the three joints are shown in Figure 6.18.

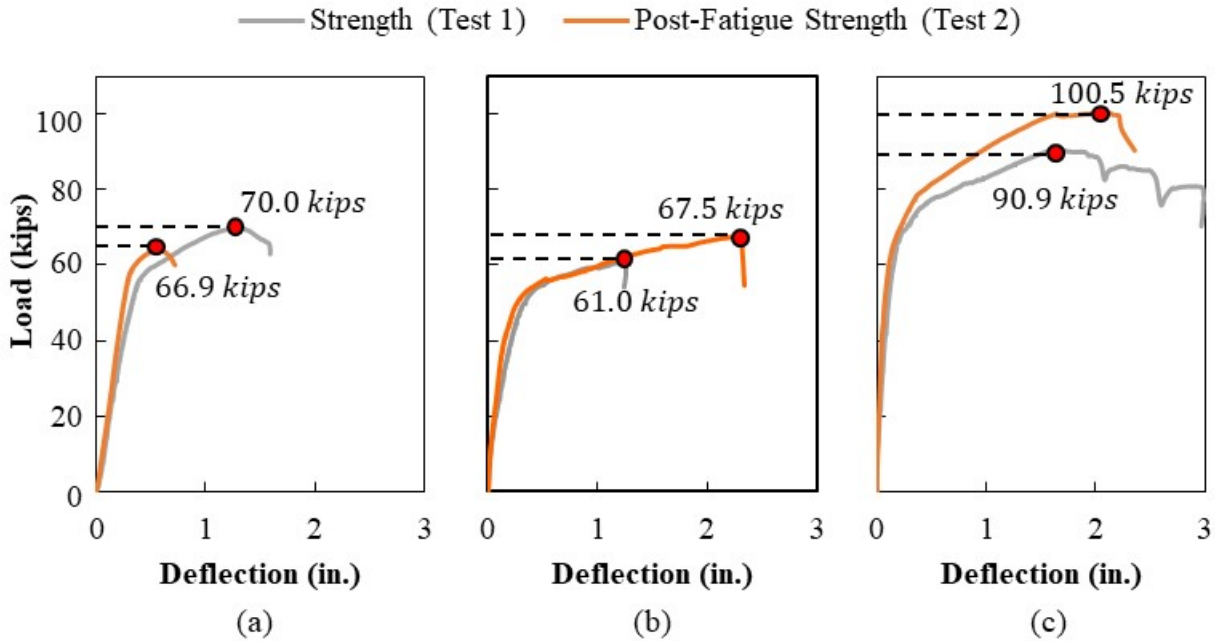


Figure 6.18: Load-deflection curves for strength and post-fatigue strength tests for joints (a) 12F1, (b) 12A1, and (c) 12A2

The ultimate loads for strength and post-fatigue testing strength are also summarized in Table 6.3.

Table 6.3: Summary of strength and post-fatigue testing strength results

Joint	Strength (Test 1)	Post-Fatigue Strength (Test 2)
12F1	70.0 kips	66.9 kips
12A1	61.0 kips	67.5 kips
12A2	90.9 kips	100.5 kips

The strength of 12F1 slightly decreased after the fatigue loading, by about four percent, and the deflection at maximum load increased by about 27 percent. The strength of 12A1 and 12A2 both increased by around 10 percent. The deformation at ultimate also increased around 77 percent for 12A1.

The crack patterns at failure and failure mechanisms for each of the joint types are briefly discussed in the following sections.

6.6.2.1. Failure Mechanisms for 12F1

The failure crack pattern for 12F1 without any fatigue load (12F1-1) and after fatigue loading (12F1-2) is shown in Figure 6.19 and Figure 6.20. Specimen 12F1-1 failed with a crack extending diagonally through the joint region; failure may have been at the splice between the reinforcement. For the specimen tested after fatigue testing (12F1-2), a large crack opened at the location of the joint reinforcement and there was debonding along the joint interface; failure occurred when the reinforcement pulled out of the UHPC in the joint at the location of the joint crack.

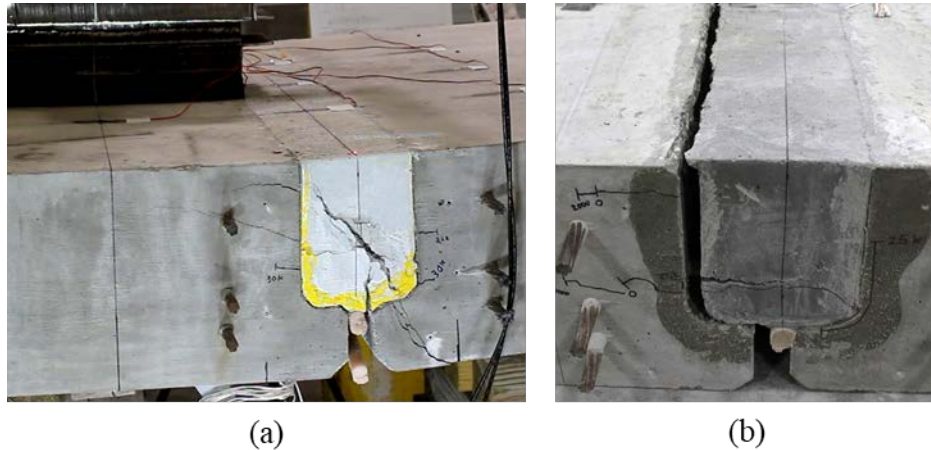


Figure 6.19: Failure crack for ultimate strength testing of 12F1 (a) without any fatigue load applied, 12F1-1 and (b) after fatigue loading, 12F1-2

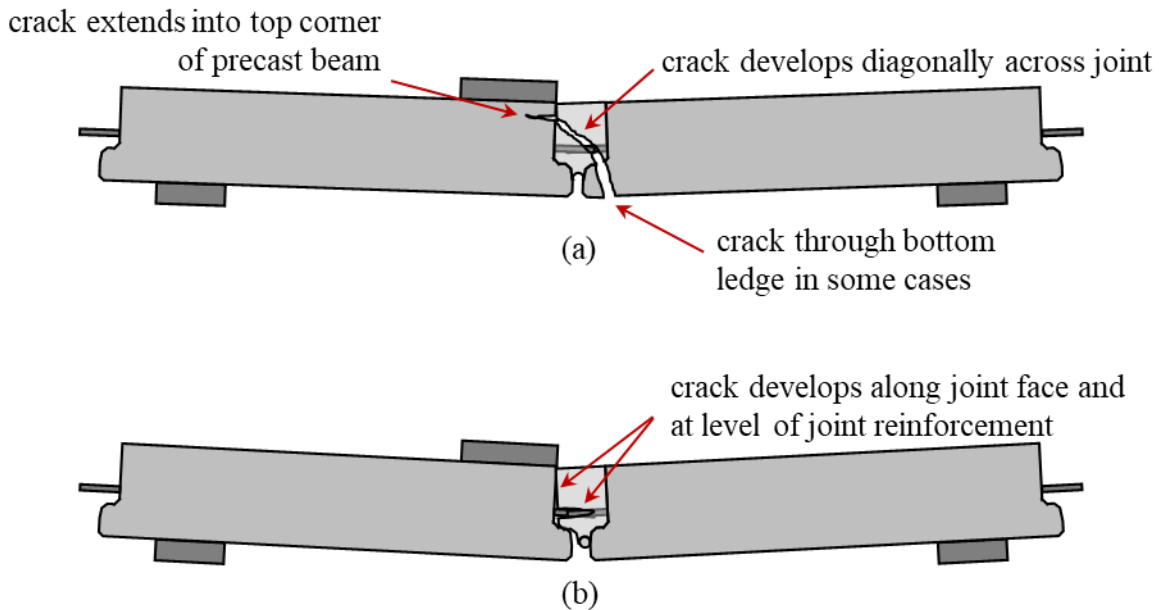


Figure 6.20: Failure cracking and mechanism for strength testing of 12F1 (a) without any fatigue load applied, 12F1-1 and (b) after fatigue loading, 12F1-2

It is not clear whether the fatigue testing caused the different failure mechanism, because different UHPC mixtures were used for the two joints. See §5.3.2 for details and discussion on the different UHPC mixtures.

6.6.2.2. Failure Mechanisms for 12A1

The failure crack pattern for 12A1 without any fatigue load (12A1-1) and after fatigue loading (12A1-2) is shown in Figure 6.21 and Figure 6.22. Specimen 12A1-1 failed with a crack extending diagonally through the joint region; failure may have been at the splice between the reinforcement like 12F1-1. For the specimen tested after fatigue testing (12A1-2), cracking occurred along the boundary of the joint and then extended into the precast section; failure occurred when the concrete in the compression block crushed, and the joint reinforcement fractured.



Figure 6.21: Failure crack for ultimate strength testing of 12A1 (a) without any fatigue load applied, 12A1-1 and (b) after fatigue loading, 12A1-2

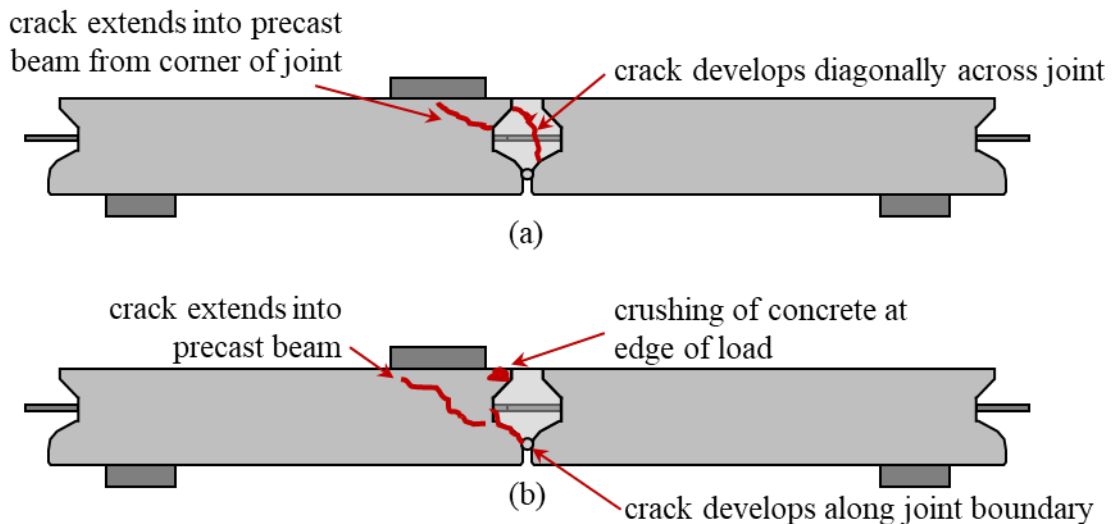


Figure 6.22: Failure cracking and mechanism for strength testing of 12A1 (a) without any fatigue load applied, 12A1-1 and (b) after fatigue loading, 12A1-2

It is not clear whether the fatigue testing caused the different failure mechanism or increase in strength, because different UHPC mixtures were used for the two joints. See §5.3.2 for details and discussion on the different UHPC mixtures.

6.6.2.3. Failure Mechanisms for 12A2

The failure crack pattern for 12A2 without any fatigue load (12A2-1) and after fatigue loading (12A2-2) is shown in Figure 6.23 and Figure 6.24. Both specimens failed due to crushing of the concrete next to the load and the edge of the joint. Additionally, both specimens had large cracking along the joint interface and a moderately sized horizontal crack developing under the load. 12A2-1 developed a crack at the level of the joint reinforcement in the joint and the precast beam. 12A2-2 developed a crack extending from the edge of the bottom lip into the precast beam.



Figure 6.23: Failure crack for ultimate strength testing of 12A2 (a) without any fatigue load applied, 12A2-1 and (b) after fatigue loading, 12A2-2

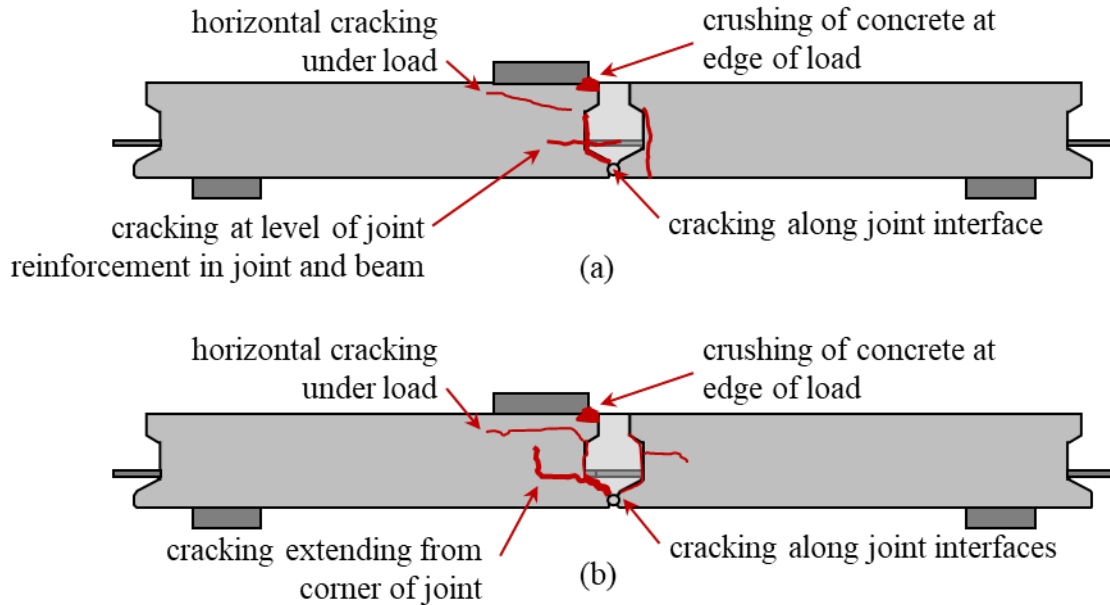


Figure 6.24: Failure cracking and mechanism for strength testing of 12A2 (a) without any fatigue load applied, 12A2-1 and (b) after fatigue loading, 12A2-2

6.7. CONCLUSIONS AND RECOMMENDATIONS

There are several conclusions related to the behavior during the fatigue loading:

- *Before-cracking stage:* The pre-cracking fatigue loading did not cause cracking or show any signs of deterioration in performance for 12A1 and 12A2. Specimen 12F1 was cracked before fatigue loading, so no determination can be made for this joint.
- *After-cracking stage:* The after-cracking fatigue loading did not cause degradation of overall behavior for any of the three joints.

There are several additional conclusions related to the static testing performed after the fatigue loading:

- *Ultimate strength:* There was an increase in the capacity and deflection at ultimate capacity for 12A1 and 12A2 after fatigue loading. There was a slight decrease in the capacity and deflection at ultimate capacity for 12F1 after fatigue loading.
- *Failure mechanisms:* There were different failure mechanisms for 12F1 and 12A1 with and without fatigue loading. The failure mechanism was similar for 12A2 with and without fatigue loading.

Different UHPC mixtures were used for the with- and without-fatigue loading tests for joints 12F1 and 12A1. The UHPC mixture used for the fatigue loaded specimens (12F1-2 and 12A1-2) was better than the UHPC used for the first tests. This may have contributed to the increased capacity of 12A1 after fatigue loading and the different failure mechanisms observed.

Specimen 12F1-2 was also accidentally preloaded past the cracking load while the specimen was being placed into the test setup. It is unclear what effect this accidental preloading had on the behavior of this specimen.

Overall, joints 12A1 and 12A2 performed the best in fatigue and in the post-fatigue static testing. Joint 12A2 is recommended for the future testing as it has a higher flexural strength and better flexural behavior.

7. FULL-SCALE EXPERIMENTAL TESTING (TWO-BEAM)

7.1. INTRODUCTION

The objective of the full-scale experimental testing program was to investigate the behavior of the joint and overall system of the recently developed modified Florida Slab Beam (FSB) with ultra-high-performance concrete (UHPC) joints. The section and joint design for the modified FSB were based on the optimized joint geometry discussed in Chapters 5 and 6. Two two-beam (FIU-1/2 and FIU-4/5) and one four-beam (FIU-6/3/8/7) test configurations were tested using service, fatigue, and ultimate strength tests with several different load and support configurations. This chapter contains a summary of the test phases and load configurations for the full-scale tests, details on specimen construction, the instrumentation schedules, and a summary and discussion of results from testing on both two-beam systems. Discussion for the four-beam test configuration is provided in Chapter 8.

7.2. TEST PHASES

A total of eight (8) 30-foot long, 12-inch-thick FSBs with optimized joint geometry were designed by the researchers and constructed by a local precaster. One set of five beams (FIU-1 through FIU-5) was designed with a prestress configuration per current specifications, with a layer of partially tensioned top strands. The second set of three beams (FIU-6 through FIU-8) had the same strand configuration as the first set of beams except they had fully stressed top strands. Four (4) of the eight (8) beams were used for the testing described in this chapter (two two-beam configurations, Phase I and II). The remaining four (4) beams were used for the four-beam test configuration (Phase III). The beams used in the three phases of the full-scale beam tests are shown in Figure 7.1. Several different loading and support configurations (LC) were used in each phase of testing; these will be described in more detail in later sections.

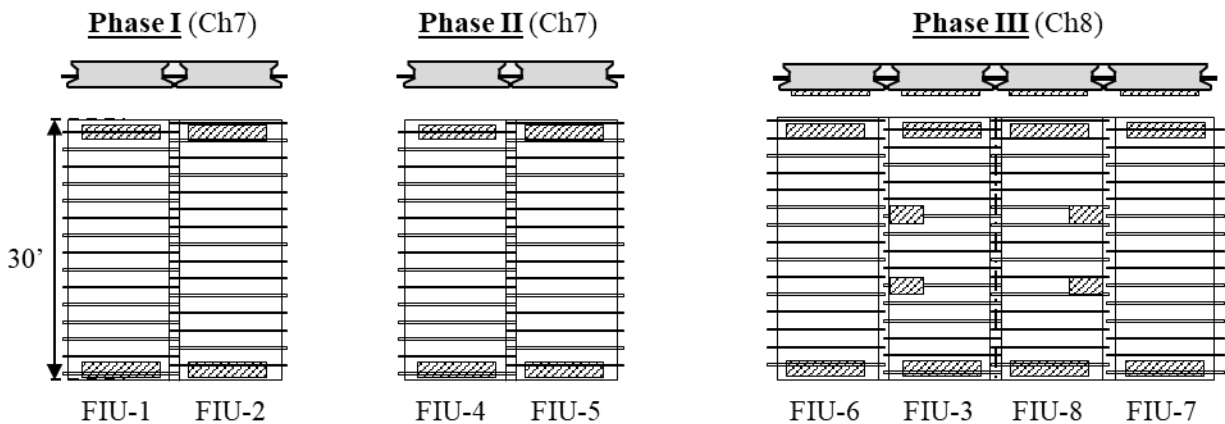


Figure 7.1: Testing phases for full-scale FSB tests (chapter number in parentheses)

The first testing phase (Phase I) was a simply supported, two-beam test configuration with beams FIU-1 and FIU-2. These beams were subjected to service (LC 2-4) and strength (LC 2-1) loading conditions under rear HS-20 half- and full-axle loads, as shown in Figure 7.2. These loading schemes were found to cause the largest joint demand from numerical analyses.

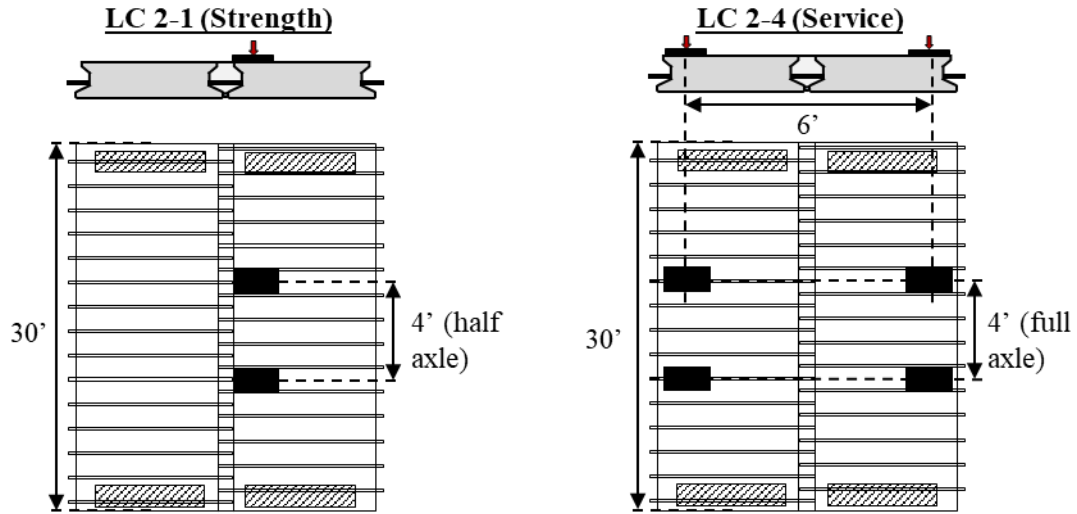


Figure 7.2: Phase I (FIU-1 and FIU-2) strength and service test configurations

The loading rate and testing schedules for the service and strength testing of Phase I are summarized in Table 7.1.

Table 7.1: Phase I (FIU-1 and FIU-2) strength and service testing schedule (*remove instrumentation under beam)

Load Config.	Load Rate	Step 1	Step 2	Step 3	Step 4*	Step 5
LC 2-4 (service)	0.2 k/s	10 k	20 k	+ 10 k to cracking	N/A	N/A
LC 2-1 (ultimate)	0.2 k/s	10 k	20 k	+ 10 k to cracking	120 k (65% est. capacity)	100 % load to failure

The second testing phase (Phase II) was also performed using a two-beam configuration, with FIU-4 and FIU-5. These beams were subjected to a variety of service and fatigue tests before being tested to failure, as summarized in Table 7.2.

Table 7.2: Phase II (FIU-4 and FIU-5) service, fatigue, and strength testing schedule

Stage	Description	Lower Limit Load ^{1,2} (Δ)	Upper Limit Load ^{1,2} (Δ)	Load Conditions	# Cycles	Testing Days
1	Static Elastic FL 120	0 kip (0.00 in.)	30.6 kip (0.74 in.)	Service LC 2-4	5	1
2	Fatigue Calibration	5 kip (0.11 in.)	23.4 kip (0.36 in.)	Fatigue FC 2-5	200,000	2
3	HS20 Truck Load	5 kip (0.11 in.)	23.4 kip (0.36 in.)	Fatigue FC 2-5	1,800,000	11
4	Static Elastic FL 120	0 kip (0.00 in.)	30.6 kip (0.74 in.)	Service LC 2-4	2	1
5	Static Elastic HS20	5 kip ³ (0.11 in.)	23.4 kip ⁴ (0.36 in.)	Service FC 2-6	4	1
6	Fatigue Calibration	5 kip ³ (0.11 in.)	23.4 kip ⁴ (0.36 in.)	Fatigue FC 2-6	200,000	2
7	HS20 Truck Load	5 kip ³ (0.11 in.)	23.4 kip ⁴ (0.36 in.)	Fatigue FC 2-6	1,800,000	11
8	Static Elastic HS20	5 kip ³ (0.11 in.)	23.4 kip ⁴ (0.36 in.)	Service FC 2-6	2	1
9	Static Elastic FL 120	0 kips (0.00 in.)	30.6 kip (0.74 in.)	Service FC 2-7	3	1
10	Transverse Crack Procedure			FC 2-5cr	1	0.25
11	Longitudinal Crack Procedure			FC 2-6cr	2	0.25
12	Static Inelastic FL 120	5 kip ³ (0.11 in.)	35.6 kip ⁴ (0.40 in.)	Service FC 2-6	2	1
13	Fatigue Calibration	5 kip ³ (0.11 in.)	23.4 kip ⁴ (0.36 in.)	Fatigue FC 2-6	200,000	2
14	HS20 Truck Load	5 kip ³ (0.11 in.)	23.4 kip ⁴ (0.36 in.)	Fatigue FC 2-6	500,000	4
15	Static Inelastic FL 120	20 kip (0.11 in.)	45 kip ⁵ (0.45 in.)	Service FC 2-5cr	1	1
16	Ultimate Strength Test			LC 2-1	1	1

¹Loads/displacements listed are for each actuator (not total)

²Acceptable load/displacement range for loading is starting load/displacement $\pm 5\%$.

³Lower load range for FC 2-6 determined from load required to bear against the center supports

⁴Upper load range for FC 2-6 determined from lower load range plus 30.6 kips (service) or 18.4 kips (fatigue)

⁵Upper load range for FC 2-6 determined from maximum actuator capacity (50 kips)

The static loading schemes LC 2-1 and LC 2-4 used in Phase II were the same as those used in Phase I, as shown in Figure 7.2. Three additional fatigue loading schemes were used:

1. **FC 2-5:** This load and support configuration had load points like LC 2-4 with no restraints provided under the system at midspan. Reverse sinusoidal fatigue loading was applied based on HS20 loading for 2,000,000 cycles initially. A similar load configuration was also used to cause transverse cracking in FIU-4 (and not in FIU-5); this configuration is called FC 2-5cr in this chapter.
2. **FC 2-6:** This load and support configuration had similar load and end support points to FC 2-5, but with two additional interior supports provided underneath one of the beams near midspan. A constant load was maintained on the beam with the midspan supports while a sinusoidal fatigue load was applied to the adjacent beam, as shown in Figure 7.3. This configuration included monotonic FL120 loading ramps and 2,000,000 cycles of HS20 loading. A load configuration like FC 2-6 was also used to attempt to cause longitudinal cracking in the joint, called FC 2-6cr in this chapter. An additional 700,000 cycles were applied using FC 2-6 after the transverse and longitudinal cracking service tests.

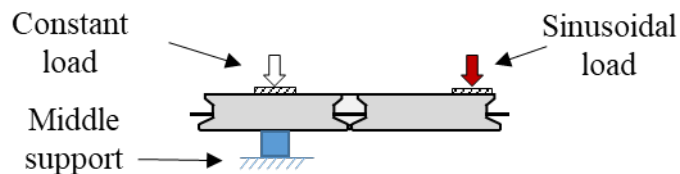


Figure 7.3: Schematic of bottom support location

3. **FC 2-7:** The load points and support conditions on one end of the beam were like LC 2-4. The support on the other end of the beam was shifted toward midspan and a vertical restraint was provided on the end of the beam to simulate the moment restraint provided by an adjacent continuous span, as shown in Figure 7.4. Several monotonic load cycles were performed to see how the joint response would change if the system were used for simple-for-dead-continuous-for-live (SDCL) construction.

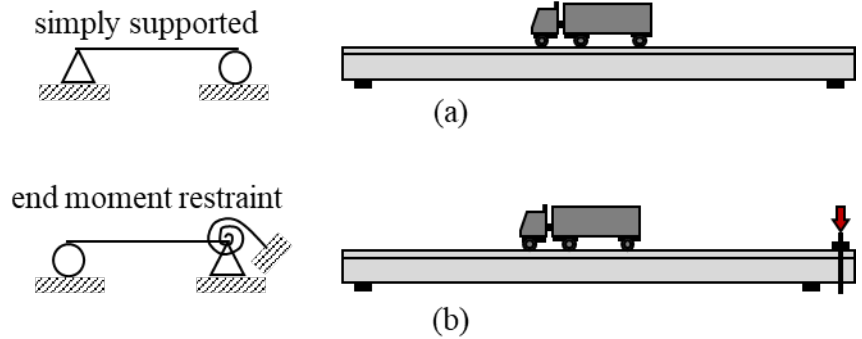


Figure 7.4: Comparison between (a) simply supported and (b) end moment restrained support conditions
Phase III of testing is discussed in Chapter 8.

7.3. SPECIMEN CONSTRUCTION

7.3.1. Beam Construction

Eight (8) prestressed slab beams were constructed by a local precaster to assemble the test specimens, each 30-foot long by 4-foot width. These beams were constructed at two different times. FIU-1 and FIU-2 were constructed first on April 11, 2019 followed by Phase I testing in August 2019. The remaining six (6) beams were then constructed in November 2019 with two different prestressing strand configurations: FIU-3 to FIU-5 had partially stressed top strands and FIU-6 to FIU-8 had fully stressed top strands. The casting dates and strand configurations are shown in Figure 7.5.

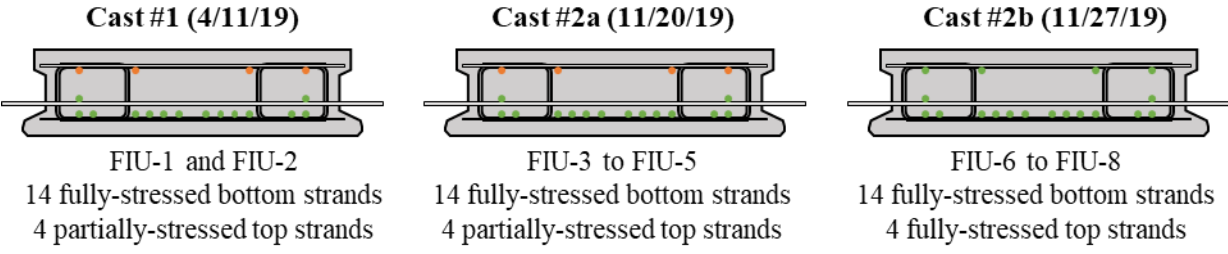


Figure 7.5: Casting schedule for eight full-size beams for full-scale testing

Each beam was built following the developed design specifications and provided in Appendix A. The strands and reinforcement cage were assembled, as shown in Figure 7.6 (a). Mild steel (A615) was used for the transverse and shear reinforcement with a specified yield strength of at least 60,000 psi. Eighteen (18) fully bonded seven-wire prestressing strands were used per beam with an ultimate strength capacity of 270 ksi and 0.6-inch diameter. One set of four beams had fourteen (14) fully prestressed bottom strands to 202.5 ksi and four (4) partially prestressed top strands to 50 ksi. The second set of four beams had fourteen (14) fully prestressed bottom strands and four (4) fully prestressed top strands to 202.5 ksi.

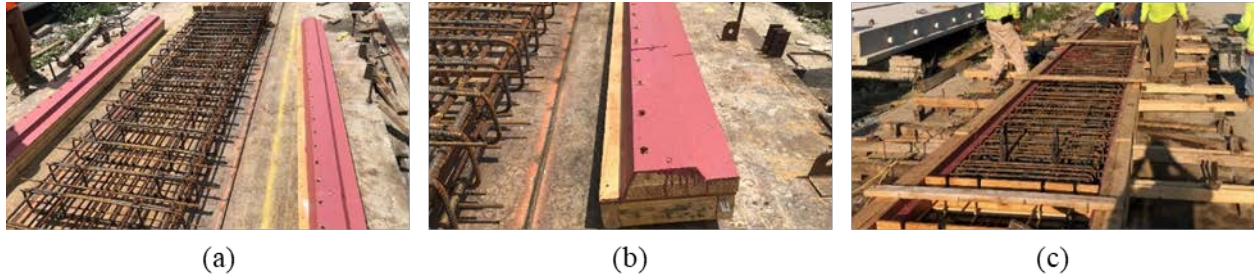


Figure 7.6: Construction of reinforcing cage and formwork for full-scale beams: (a) prestressing strand and reinforcement cage constructed, (b) side forms with paste retarding agent, and (c) assembled formwork and reinforcement ready for casting

Wood formwork was constructed and used for these specimens. A paste retarding agent was painted on the wood forms to achieve a ¼-inch amplitude surface roughness, which has been shown to provide sufficient bond between the UHPC and precast concrete material, see FHWA guidelines on interface surface preparation [39]. To achieve the proper joint surface treatment, a paste retarder, BASF – Mater Finish HV, was specified to be applied during construction. First, a substrate base was applied to each form prior to the application of the set retarding agent to prevent absorption of retarder by the wooden form. Then, the retarder was painter on the forms prior to casting, as shown in Figure 7.6 (a) and (b). The product application was limited to the joint surfaces to be in direct contact with the UHPC, as shown in Figure 7.6 (b), following construction recommendations described in Chapter 5. All side forms were assembled and locked to the steel reinforcement cage 24 hours before concrete pour, as shown in Figure 7.6 (c). Holes with diameters larger than transverse joint rebar were cut in the side forms to avoid difficulties when removing the form after casting.

The concrete was cast after the reinforcement cage and forms were assembled, as shown in Figure 7.7 (a). The top beam surfaces were prepared with a top smooth float finish, as shown in Figure 7.7 (b). Beams were moist cured for at least 24 hours after casting.



Figure 7.7: Casting of concrete for full-scale beams: (a) casting of concrete, (b) float finish on top of beams, and (c) finished beam after casting

The forms were removed approximately 24 hours after casting leaving the retarder attached to the concrete, as shown in Figure 7.8 (d). A pressure washer was used with a constant 3,500 psi water pressure to remove the retarding agent with the unhydrated cement paste, as shown in Figure 7.8 (b). The distance between the pressure washer tip and concrete was varied so just the cement paste and no aggregate was removed. The final exposed aggregate finish after this procedure was

complete is shown in Figure 7.8 (c). The procedure produced a surface roughness approximately equal to the desired ¼-inch amplitude roughness.

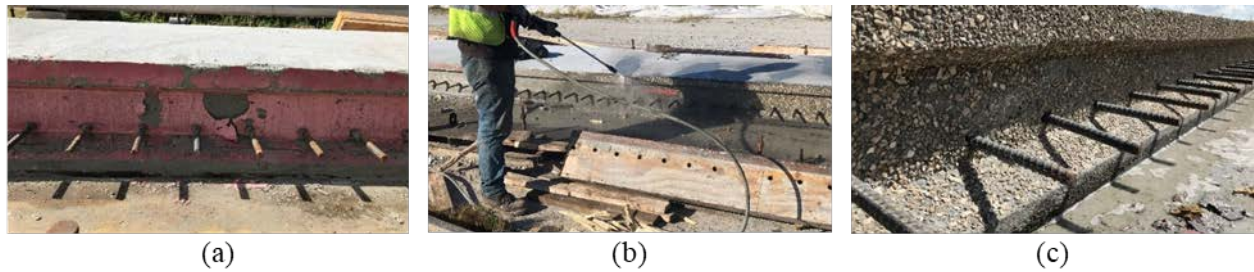


Figure 7.8: (a) Removal of forms with paste retarding agent on concrete surface, (b) pressure washing away of paste retarding agent and unhydrated cement paste, and (c) exposed aggregate finish after procedure

The strands were then released starting at the top row from exterior corner to interior strands; then the middle layers and bottommost layers were released using the same cut pattern, as shown in Figure 7.9 (a). After all the beams were built at the precast plant, they were shipped and delivered to the FDOT M.H. Ansley Structures Research Center in Tallahassee, as shown in Figure 7.9 (b).



Figure 7.9: (a) Beam release stage and (b) delivery of slab-beam specimens

7.3.2. Material Properties

The relevant material properties for the concrete and reinforcement used to construct the precast, prestressed beams and joints are discussed in this section.

7.3.2.1. Concrete Mixture Design

The specified mix design for all the FSB sections was FDOT Concrete Class VI [57], with a minimum compressive strength at 28 days of 8,500 psi and maximum water/cement ratio of 0.37 lb/lb . The measured compressive strength is shown later in Table 7.5.

The UHPC mixture was specified to be Ductal® JS1000, which is a proprietary UHPC mixture commonly used for field-cast closure pours and joint connections for accelerated bridge construction applications. This UHPC mixture contains the same components used in previous small-scale testing protocols described in Chapter 5, containing the following components:

- Premix (dark-grey): pre-blended cement, sand, ground quartz, and silica fume
- Liquid Admixture: high-range water reducer

- Steel fibers: 0.008-inch diameter by 0.5-inch long; tensile strength > 290 ksi
- Water and/or ice: Ice required when batching in warm hot weather

The procedure for mixing the UHPC is shown in Figure 7.10 and included the following steps for the large-scale joint batch:

1. Weigh out each ingredient for mixture
2. Add dry premix
3. Add ice/water and superplasticizer
4. Mix until fluid (10-15 minutes)
5. Add steel fibers
6. Mix five minutes, or until complete uniformity
7. Perform flow table test. If mixture is not fluid (below 5 inches), add 5% more water (if temp. $\leq 75^{\circ}\text{F}$) or 5% ice (if temp. $> 75^{\circ}\text{F}$). If too fluid (above 9 inches), add dry material and fiber
8. Mix additional 5 minutes, or until completely uniform, if additional material added, otherwise skip to step 9
9. Place UHPC and make cylinders and beams for four-point bending test (modulus of rupture)

The UHPC component dosages were prepared by weight and measured before mixing began. The components were then mixed in a Mixer System Horizontal Shaft Mixer, shown in Figure 7.10 (a) and (b). After finishing mixing all components for around 25 minutes, the UHPC was transported in a concrete container and placed in the joint as shown in Figure 7.10 (c). Once the joint was filled with UHPC, it was closed with top formwork using weights, as shown in Figure 7.10 (d). After 24 hours, the joint top formwork was removed, and a grinding operation was performed to even all top surfaces out.

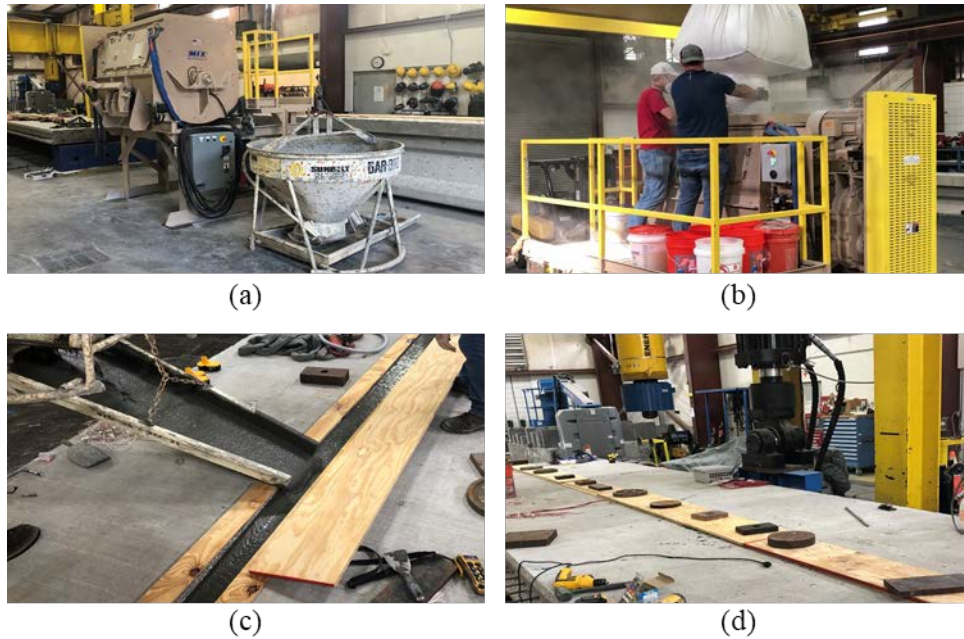


Figure 7.10: UHPC mixing process for two-beam test configurations: (a) mixer working area preparation, (b) mixing operation of UHPC materials, (c) casting operation, and (d) top form closure and weights location

Two JS1000 pre-mix designs were used for each testing phase with same mix proportions. A total volume of 17.02 cubic feet was required for each batch. One bulk bag of dry premix, equivalent to 49 smaller 50-lb. bags, was used, which yielded a total volume of 17.05 cubic feet. The mixture proportions of the UHPC batches prepared with JS1000 admixture are shown in Table 7.3. Additional quantities (about five percent of the quantities used) of premix, ice, water, and steel fibers were set aside to be used if the mix consistency was not correct; the use of these additional materials was not required for any batch.

Table 7.3: UHPC mixtures for Testing Phases 1 and 2 (using JS1000 pre-mix)

UHPC Batch	Design Mix (Pounds)					Specimen ID	Ambient Temp. (°F)
	Premix	Ice	Water	Admixture	Steel		
1	2,460	100.0	14.26	34.44	175.0	FIU-1/2	81
2	2,460	100.0	14.26	34.44	175.0	FIU-4/5	72

The rheological properties were measured for each UHPC batch by performing static and dynamic flow tests. A slightly modified version of ASTM C1437 [76] was used per FHWA material tests recommendation [39], as shown in Figure 7.11 (a) and (b).



Figure 7.11: UHPC flow test: (a) mold removal and (b) spread measurement

The flow tests for each testing phase were conducted immediately after UHPC mixing to determine mix flowabilities before placement; results are summarized in Table 7.4. There was a slight difference in temperature and flow between the mixture of the first batch and the mixture of the second batch.

Table 7.4: UHPC flow tests

UHPC Batch	Temperature (°F)	Static Flow (in.)*	Dynamic Flow (in.)*
1	77.7	8.31	9.25
2	70.1	8.09	8.88

*Average taken from two measurements along perpendicular axes of same test sample

7.3.2.2. Hardened Concrete Properties

Three concrete batches with the same mix proportions were used to construct all eight beams: one batch for FIU-1 and FIU-2, one for FIU-3, FIU-4, and FIU-5, and one for FIU-6, FIU-7, and FIU-8. Compressive strength tests were performed on cylinder samples taken from each concrete batch of the precast beams and the UHPC joints. Ten (10) 4-inch by 8-inch concrete cylinders were tested for each precast slab beam according to ASTM C39 [62, p. 39]: five cylinders at 28 days and five at strength test day. The average of the five compressive strength values was taken as the measured strength for every batch during each testing stage. The UHPC compressive strength was measured using ten 3-inch by 6-inch cylinders prepared and tested based on ASTM C1856 [63] using a similar procedure to ASTM C39 [62, p. 39]: five cylinders at 28 days and five at strength test day; this procedure is described in the FHWA guidelines [39].

Per ASTM C1856 [63], the flexural strength of the UHPC was measured using small-scale beams subjected to four-point loading using ASTM C1609 [64]. Five 4-inch by 4-inch by 14-inch beam samples were cast at the same time the joints were built using metallic molds, and ground for dimensional consistency, as shown in Figure 7.12 (a). These beams were tested on the day of joint testing to determine the tensile strength of the UHPC. Some of the concrete cylinders for one batch are shown in Figure 7.12 (b).



Figure 7.12: UHPC samples: (a) 4x4x14 in. beam in molds after grinding for dimensional consistency and (b) ten 4x8 in. cylinders for compressive strength

A summary of all concrete compressive and modulus of rupture strength properties is shown in Table 7.5. Compressive strengths were measured at 28 days and on the day of ultimate strength testing.

Table 7.5: Specified and measured concrete strength for large-scale test specimens

Specimen ID	Testing Phase	Beam Compression Concrete Strength (f'_c)			Joint Compression Concrete Strength (f'_c)			Joint Rupture Strength (f'_t)
		Target (ksi)	28-day Measured (ksi)	Strength Test Day (ksi)	Target (ksi)	28-day Measured (ksi)	Strength Test Day (ksi)	Measured (ksi)
FIU-1	Phase I	8.5	8.50 ^a	8.74	21.0	22.52	24.31	3.14
FIU-2								
FIU-4	Phase II	8.5	11.28 ^b	12.43	21.0	24.99 ^c	25.93	3.44 ^d
FIU-5								

^a Measured beam compressive strength at 29 days; ^b Measured beam compressive strength at 243 days;

^c Measured joint compressive strength at 36 days; ^d Measured joint tensile strength at 80 days

7.3.2.3. Steel Reinforcement Properties

Four sizes of Grade 60 mild steel reinforcement were used to build all the precast specimens: #3, #4, #5, and #6 reinforcement. Eighteen (18) fully bonded pretensioned strands were used in the precast sections with prestressing forces up to 202.5 ksi. The measured properties for the steel reinforcement were provided by the precaster, shown in Table 7.6.

Table 7.6: Steel material data

Description	Yield (psi)	Tensile (psi)
#3 Rebar A615M Gr60	73,655	108,504
#4 Rebar A615M Gr60	68,043	104,770
#5 Rebar A615M Gr60	67,300	105,500
#6 Rebar A615M Gr60	61,340	101,503
0.600 7 wire 270 low lax. strand	251,000	275,000

7.3.3. UHPC Joint Construction

The construction of the large-scale UHPC joints followed the same guidelines described in the FHWA publication [39] and as shown in Figure 7.13. For each testing stage, the beams were placed side by side leaving a $\frac{3}{4}$ -inch clear gap and filled with a 1-inch backer rod, as shown in Figure 7.13 (a); a transparent silicone was used to fill the gaps between the bottom joint ledges and the backer rod. Plywood squares with painted waterproof sealer were then placed on each end to enclose the joint for UHPC cast, as shown in Figure 7.13 (b). This sealer avoided any water loss from the UHPC mix caused by the wood pores in direct contact. Wooden strips were also placed atop the precast beam ledges aligned with the joint boundary, providing at least a $\frac{1}{4}$ -inch depth for cast overpour purposes, as shown in Figure 7.13 (b). A day before casting the joint, a water seal test was performed by filling the joint volume up with water and leaving it for 24 hours; this also provided a saturated surface dry (SSD) condition for the joint.

The UHPC was mixed using the Mixer System Horizontal Shaft Mixer and cast in the joint starting from one end towards the center, as shown in Figure 7.13 (c). The procedure was then repeated from the other end until the two pour heads were encountered at the middle. A steel rod was gently used making sure the two pour heads mixed, and ensuring the steel fibers crossed the boundary, as shown in Figure 7.13 (d). Plywood formwork was used to cover the top of the joint when the UHPC almost reached the top of the joint, as shown in Figure 7.13 (e). The remaining UHPC was cast through a chimney at one end, increasing the pour height and pressure head to avoid air entrapped inside.



(a)



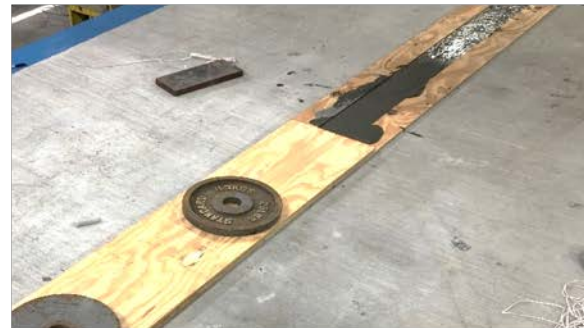
(b)



(c)



(d)



(e)

Figure 7.13: Casting procedure for UHPC joint: (a) beams alignment with $\frac{3}{4}$ -inch gap and backer rod, (b) connection detail with plywood block-out and top strips for over pour volume, (c) casting operation for the field-cast UHPC, (d) rodding procedure for two encountering pour heads, and (e) top formwork hold using weights

7.3.4. Observations from Construction

7.3.4.1. Joint Formwork Quality

The joints were designed to be self-forming with a $\frac{3}{4}$ -inch gap between the bottom flanges sealed with a foam backer rod. The joint geometry of two of the precast beams (FIU-1 and FIU-2) varied slightly along the length of the beams, which led to an inconsistent gap between bottom flanges. This may have been a result of the formwork being built in segments that were then attached together, as shown in Figure 7.14 (a) and (b). As a result, two backer rod layers were used during joint alignment at some regions close to the south end with gaps larger than the $\frac{3}{4}$ -inch specified. The backer rods were installed from the bottom (pushed up into the gap) for FIU-1/2. When the

first UHPC pour started from the south end and the chimney was then used to add extra weight and avoid air voids, the backer rod seal failed and the UHPC started to leak, as shown in Figure 7.14 (c). The pour was immediately stopped, and a bottom plywood board was screwed to the concrete beam underside at the leakage location using Tapcon screws, as shown in Figure 7.14 (d). To avoid any further leakages, the plywood boards were installed along the whole bottom joint gap.

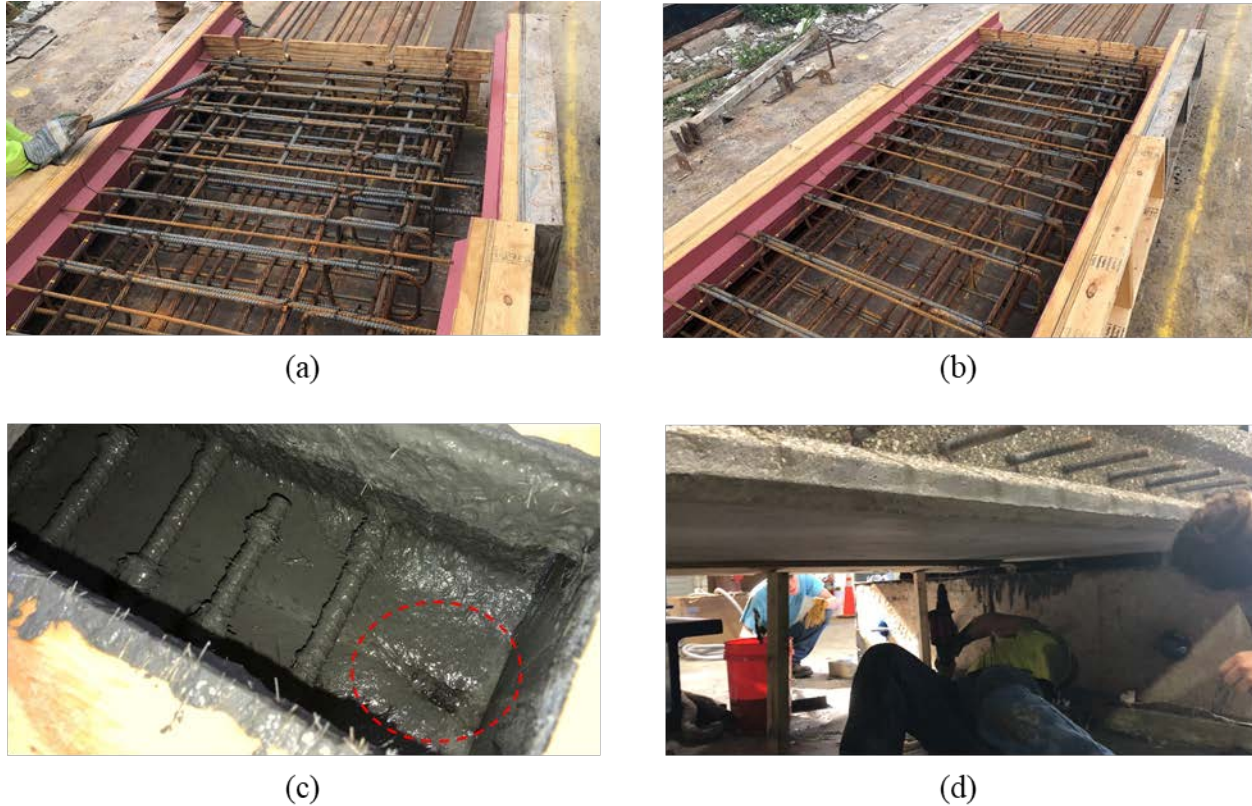


Figure 7.14: Joint construction observations: (a) side form segments, (b) side form segments attached, (c) UHPC leakage at joint end, and (d) attachment of bottom plywood strip to stop leakage

Some of the UHPC that leaked from the joint was recovered by filling up a few buckets and pouring them into the mixer again; this allowed the thixotropic material to remain fluid as the mixer blades were still running while the problem was being fixed. Once the bottom gap was completely covered with plywood boards, a second pour was performed from the north end (opposite side) following the same cast procedure. The chimney was not used this time and the joint volume was successfully filled.

Although the second set of beams (FIU-3 to FIU-8) was built using side form segments too as described in Figure 7.14 (a) and the same size backer rod (1 inch), the UHPC joint construction detail was improved by installing the backer rod from the top down, as shown in Figure 7.15 (a), and extending it outside the block-out joint end, as shown in Figure 7.15 (b). This construction technique helped to avoid any further UHPC leakage in the subsequent joint construction, increasing the joint tightness.



Figure 7.15: Backer rod detail: (a) 1-inch diameter rod and (b) rod extension through block-out form

The use of a larger diameter backer rod (at least $\frac{1}{4}$ -inch larger than joint gap), installing the backer rod from the top down, and extending the backer rod through the joint end form created a watertight seal while allowing for reasonable joint construction tolerances. The precaster used wood forms with holes cut for the joint reinforcement. The use of steel forms and mechanical threaded bars would help expedite construction process, improve joint quality, and avoid joint and reinforcement misalignments during bridge construction.

7.3.4.2. Set Retarding Agent for Joint Surface Treatment

An exposed aggregate finish with at least a $\frac{1}{4}$ -inch surface roughness was specified to ensure appropriate bond between the precast concrete and UHPC in the joint. FDOT currently has three products they recommend for achieving an appropriate exposed aggregate surface condition:

- BASF: MBT Heat Cote – Lilac [66]
- BASF: Master Finish – Lilac [67]
- Architectural Concrete Chemicals: Altus Series In-Form Retarder – Pink [68]

BASF – Master Finish HV Lilac (38) [67] was originally specified for the specimens constructed in this test program, which is used to create a light depth of etch for recommended aggregates ranging from $\frac{1}{4}$ -inch to $\frac{3}{8}$ -inch sizes. The precaster constructed several mockups and found that for their mixes the use of BASF Master Finish HV Lilac resulted in only a $\frac{1}{8}$ -inch amplitude surface roughness, as shown in Figure 7.16 (a). The precaster decided to use a deeper agent penetration (BASF – Master Finish HV Pink (48) [67]) to increase the exposure of the joint material; this product is specified for medium light depth of etch for aggregates ranging from $\frac{3}{8}$ -inch to $\frac{1}{2}$ -inch sizes. The use of this product resulted in the desired $\frac{1}{4}$ -inch roughness, as shown in Figure 7.16 (b).



(a)



(b)

Figure 7.16: Master Finish HV retarder degrees of penetration: (a) light and (b) medium light

Engineers should always specify that the precaster creates mockups using their specific concrete mix and procedure for achieving the exposed aggregate finish. This will help to ensure that the necessary ¼-inch surface roughness is achieved.

7.3.4.3. UHPC Grinding Action

After casting the UHPC joint in the first set of beams (FIU-1 and FIU-2), the overpoured section was difficult to grind using an electric grinder two days after been cast. A gas grinder with a larger grinding area was required, hence it was unavoidable to grind down part of the precast sections, as shown in Figure 7.18 (a). As a result, it was recommended that the grinding to level the joint surface with the precast section should be done no later than one day after casting. After casting the UHPC joint in the second set of beams (FIU-4 and FIU-5), the overpoured section was easily ground down using an electric grinder 24 hours after cast, as shown in Figure 7.18 (b).



(a)



(b)

Figure 7.17: UHPC grinded surface: (a) surface finish after two days using gas grinder (showing precast abrasion), and (b) surface finish after one day using electric grinder

7.4. LOADING CONFIGURATIONS AND PROTOCOL

7.4.1. Two-Beam Service and Strength Testing (FIU-1/2)

Two different load configurations and protocols were used for the first two-beam testing. The first included a full truck axle centered on the beams to maximize the tension on the top of the section; this was called Load Configuration (LC) 2-4. The second configuration had a half truck axle placed immediately next to the joint; this was called LC 2-1. The difference between full axle and half axle is highlighted in Figure 7.19.

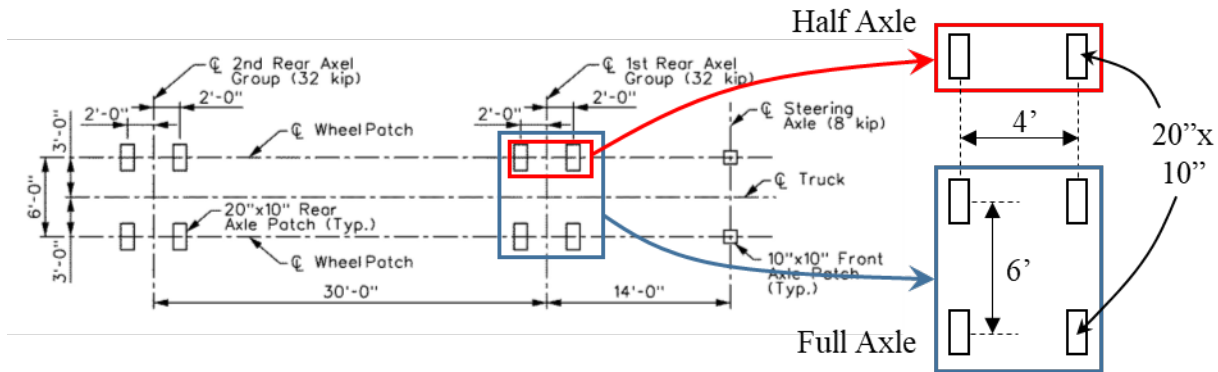


Figure 7.18: HL-93 truck load with full and half rear axle identification (from [77])

Detailed drawings for both configurations are provided separately.

7.4.1.1. Load Configuration 2-4 (Service Loading)

LC 2-4 had a full truck axle with 10-inch by 20-inch wheel patches, as shown in Figure 7.20. The load was applied using one actuator and three spreader beams with the configurations shown in Figure 7.20 (a).

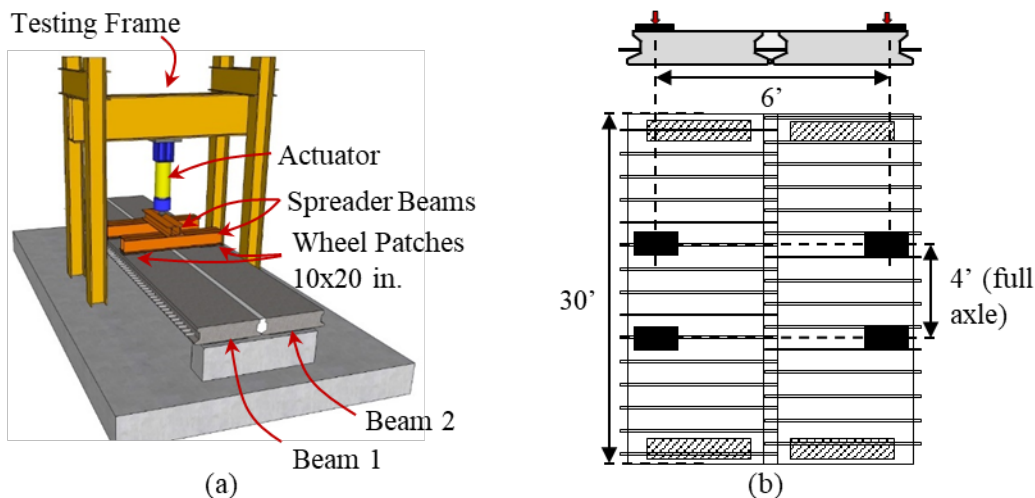


Figure 7.19: Proposed test setup for Load Configuration 2-4 (a) schematic and (b) plan and elevation views

Load was applied using LC 2-4 at a rate of 0.2 kips/second until first cracking was observed, which occurred at approximately 60 kips. First cracking was detected during testing by monitoring:

4. **Load versus vertical deflection plot:** Cracking causes the load versus deflection plot to become non-linear.
5. **Load versus concrete strain plot:** Cracking adjacent to a concrete strain gauge (CSG) results in strain shifting from tension to compression. Cracking through a CSG results in a dramatic increase in tensile strain.

After cracking was observed using the instrumentation readings, the location and extent of cracking was determined through visual inspection.

7.4.1.2. Load Configuration 2-1 (Ultimate Strength)

LC 2-1 had a half truck axle with 10-inch by 20-inch wheel patches, as shown in Figure 7.21. The load was applied using one actuator and one spreader beam with the configurations shown in Figure 7.21 (a). The two-beam specimen was shifted slightly in the load frame before applying load using LC 2-1 to ensure that the hydraulic actuator was centered on the load frame.

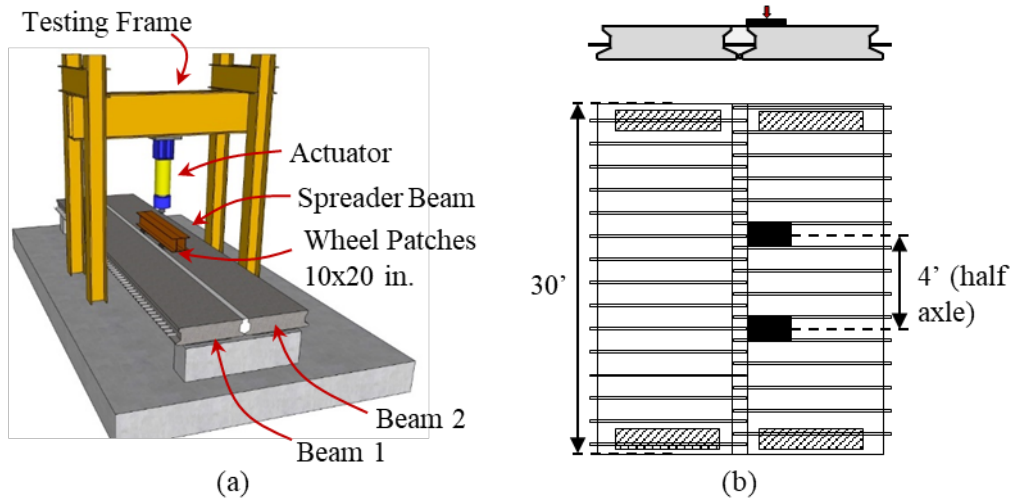


Figure 7.20: Proposed test setup for Configuration 2-1 (a) schematic and (b) plan and elevation views

Load was applied at an approximate rate of 0.2 kips/second. Loading was paused several times to take pictures and monitor the progress of cracking until the load reached 120 kips (about 65% of the estimated capacity). At this point, the crack displacement transducers (CDTs) were removed from underneath the joint and cracks were marked and documented for the last time until after failure. The specimen was then loaded until failure at the same loading rate of 0.2 kips/second.

7.4.2. Two-Beam Fatigue, Service, and Strength Testing (FIU-4/5)

The second two-beam test configuration included three additional fatigue and service load configurations.

7.4.2.1. Fatigue Configuration 2-5 (Fatigue Loading)

The first fatigue configuration (FC) 2-5 included loading positions like LC 2-4 but with a reverse sinusoidal fatigue loading protocol, as shown in Figure 7.22. The same 10-inch by 20-inch wheel patches were used in FC 2-5 as other load configurations. Fatigue loads were applied using two actuators and two spreader beams with the configuration shown in Figure 7.22 (a) and (b) with an alternating 2-Hz sinusoidal wave, as shown in Figure 7.22 (c).

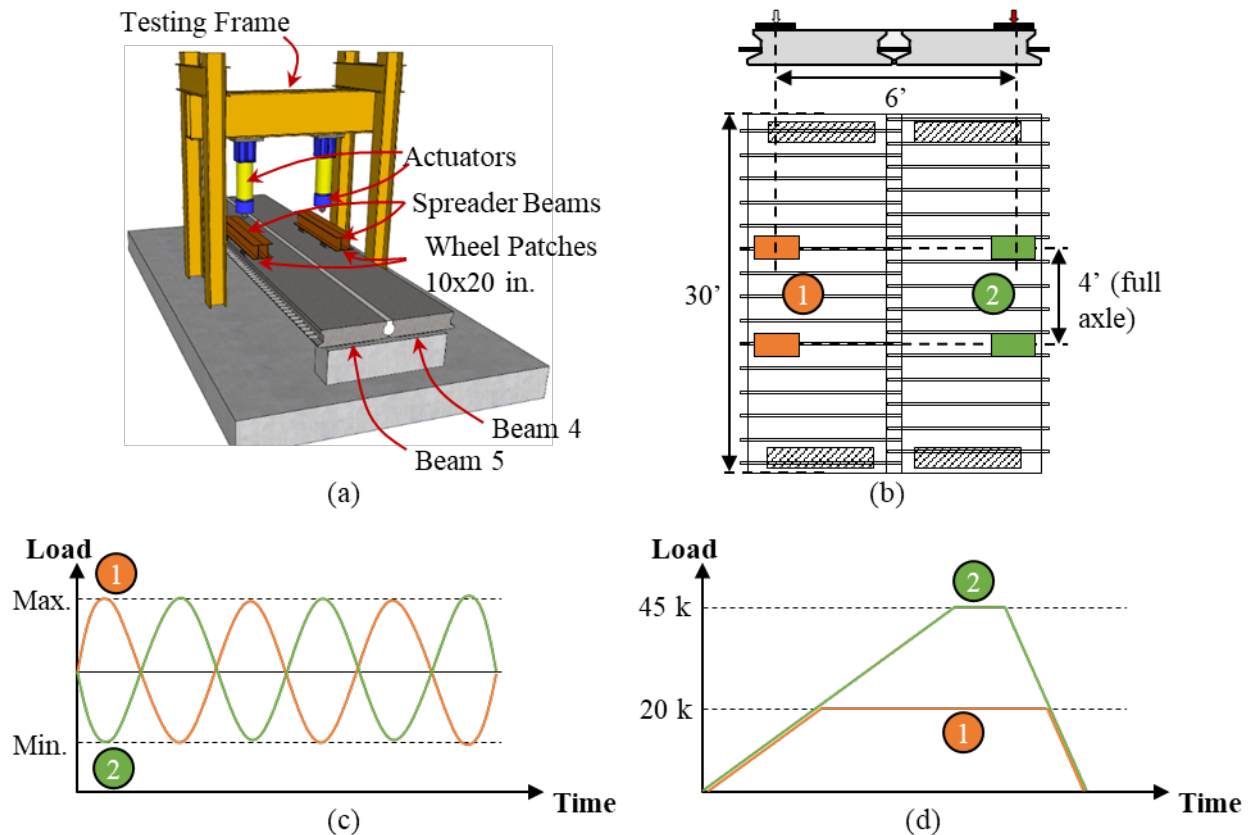


Figure 7.21: Proposed test setup for Configuration 2-5 (a) schematic and (b) plan and elevation views, (c) reverse sinusoidal load protocol for FC 2-5, and (d) static transverse cracking load protocol for FC 2-5cr

The fatigue loading was applied through an applied displacement that corresponded with loads in each actuator of 5 kips (minimum load) and 23.4 kips (maximum load) with a $\pm 5\%$ allowable difference in applied displacement. A total of 2 million cycles were applied using FC 2-5 during Stage 2 and 3, which simulated normal service truck traffic conditions for a 100-year service life. LC 2-4 with a 61.2-kip total load was used to determine the behavior of the system before (Stage 1) and after (Stage 4) fatigue testing with FC 2-5.

A similar load configuration was also used to cause transverse cracking in FIU-4 and not in FIU-5 (Stage 10); this configuration is called FC 2-5cr in this chapter. This configuration consisted of increasing the load in both actuators to 20 kips and then increasing load only in one actuator to 45 kips while the other actuator was held at 20 kips, as shown in Figure 7.22 (d) and Figure 7.23.

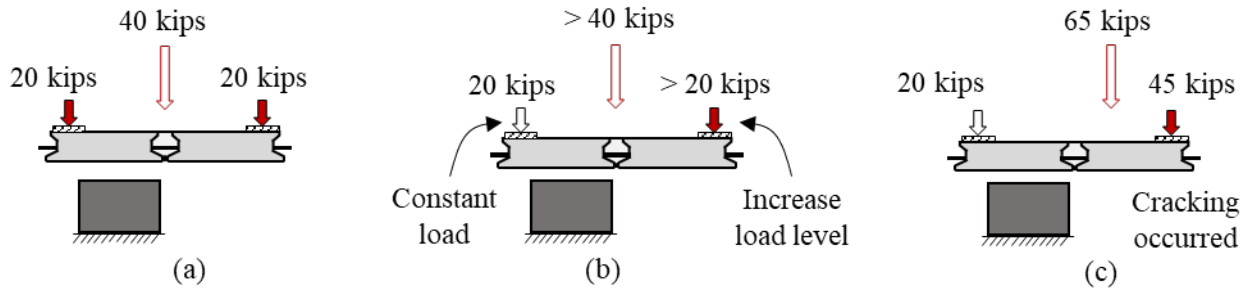


Figure 7.22: Transverse crack procedure (FC 2-5cr): (a) uniform load application, (b) east side load increment, and (c) cracking occurred at total load of 65 kips

7.4.2.2. Fatigue Configuration 2-6 (Restrained Fatigue Loading)

FC 2-6 had a similar load configuration to FC 2-5 but had an additional two intermediate supports underneath one of the beams near midspan, as shown in Figure 7.24 (a) and (b). A constant load of 5 kips was applied on the beam with the midspan restraints while a 2-Hz sinusoidal wave load was applied to the adjacent beam, as shown in Figure 7.24 (c), with a maximum load of 23.4 kips and minimum load of 5 kips. The same 10-inch by 20-inch wheel patches as other load configurations were used in FC 2-6. A total of 2 million cycles were applied using FC 2-6 during Stage 6 and 7.

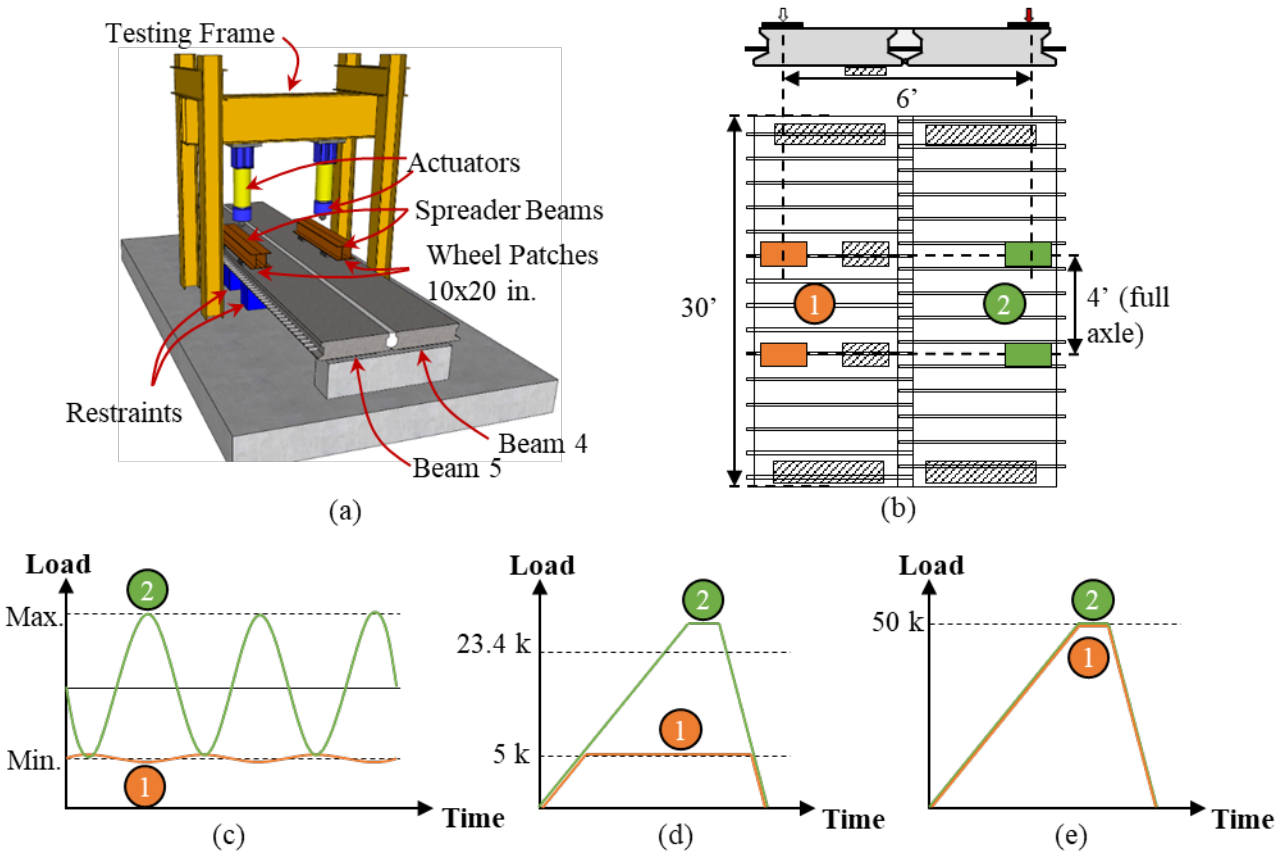


Figure 7.23: Proposed test setup for Configuration 2-6 (a) schematic and (b) plan and elevation views, (c) reverse sinusoidal load protocol for FC 2-6, (d) static load protocol for FC 2-6, and (e) static longitudinal cracking load protocol for FC 2-6cr

Static load testing was performed before (Stage 5) and after (Stage 8) fatigue testing to determine if there was any deterioration in the behavior of the system caused by the fatigue testing. The same support conditions as FC 2-6 were used for the static testing. For static load testing, the load in the actuator in the restrained beam was held constant at 5 kips and the load in the adjacent beam increased to 30.6 kips at a loading rate of 0.2 kips/second, as shown in Figure 7.24 (d).

A test setup like FC 2-6 was also used to try to create a longitudinal crack near the top of the joint (Stage 11); this configuration is called FC 2-6cr in this chapter. The load protocol for this stage consisted of increasing the load in both actuators to 50 kips at the same time and then unloading, as shown in Figure 7.24 (e) and Figure 7.25.

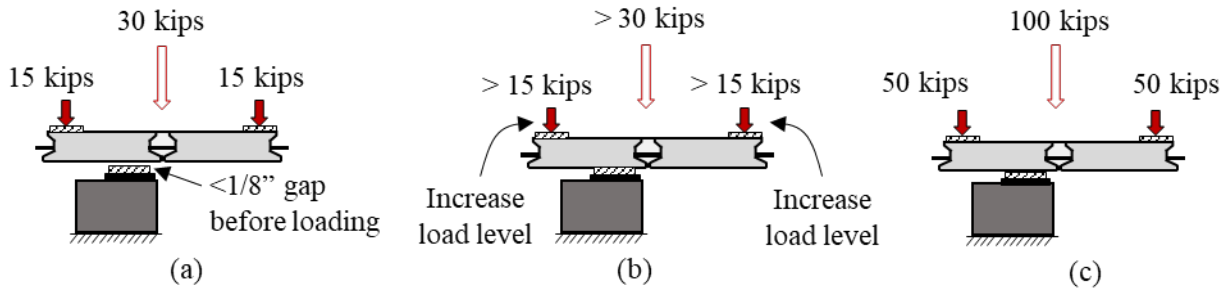


Figure 7.24: Longitudinal crack procedure (south view): (a) uniform load application until bearing of the interior supports, (b) continued uniform load increment, and (c) maximum applied load to obtain longitudinal cracking

An additional 700,000 cycles were applied using FC 2-6 during Stage 13 and 14 after the longitudinal cracking procedure was performed.

7.4.2.3. Fatigue Configuration 2-7 (Continuous Span)

FC 2-7 had the same load configuration as LC 2-4 but with different support conditions. A continuous span was simulated in FC 2-7 by shifting one of the supports toward midspan and providing a vertical restraint at the end of the beam outside the support, as shown in Figure 7.26. This support condition created a moment restraint at one end of the system, which simulated a two-span continuous system. The same 10-inch by 20-inch wheel patches as other load configurations were used in FC 2-7. The load was applied using two actuators and two spreader beams simultaneously with the configuration shown in Figure 7.26 (a). A total load of 61.2 kips was applied at an approximate rate of 0.2 kips/second, simulating a FL120 rear axle load.

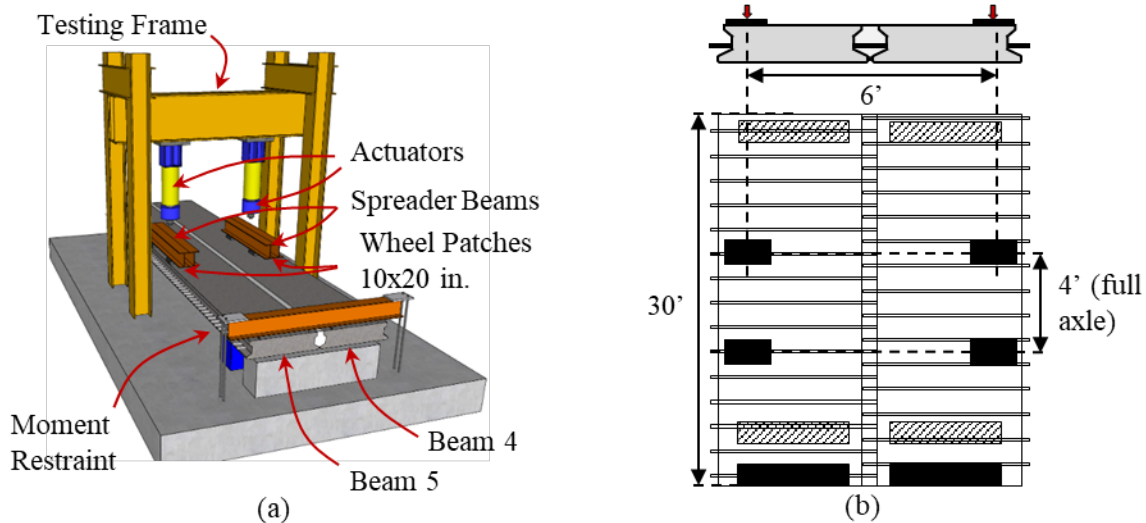


Figure 7.25: Proposed test setup for Configuration 2-7 (a) schematic and (b) plan and elevation views

More details on the continuous support are shown in Figure 7.27. The hold-down system consisted of one beam restraint tied down to the strong floor with threaded rods. Elastomeric bearing pads were placed between the spreader beam and the top of the specimens.



Figure 7.26: End moment restraint detail: (a) south-end view and (b) welded plate detail

7.4.2.4. Load Configuration 2-1 (Post-Fatigue Ultimate Strength)

After all the fatigue and service load testing were complete, the two-beam system with FIU-4 and FIU-5 was tested to failure using the same LC 2-1 load protocol as described in §7.4.1.2. This ultimate load response after all the fatigue testing was compared with the ultimate load response of the system without any fatigue loading (FIU-1/2).

7.5. INSTRUMENTATION SCHEDULE

The instrumentation schedule for the two-beam tests is described in this section. The instrumentation schedules are broken down based on the center span and support regions, as shown in Figure 7.28. Instrumentation was symmetrical about midspan, so the instrumentation in the span center and one support region are shown.

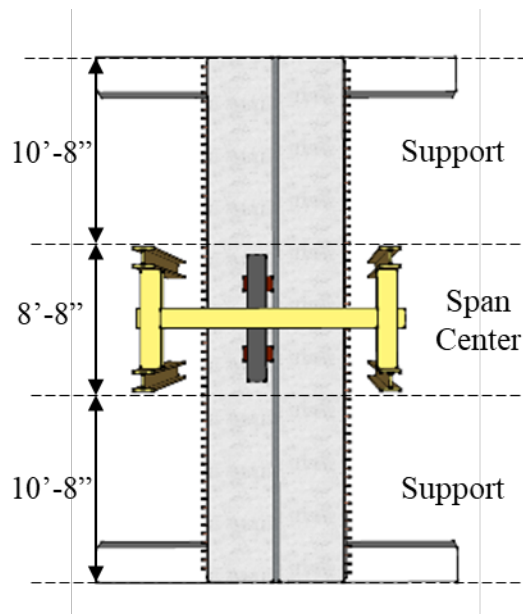


Figure 7.27: Two-beam test with two main sensor regions

Several different types of instrumentation were used in testing of the two-beam systems. Rebar strain gauges (RSGs) were installed on the joint reinforcement extending from each of the precast beams, as shown in Figure 7.29 (a). Concrete surface gauges (CSGs) were installed on the top and bottom of the precast beams in the longitudinal and transverse directions, Figure 7.29 (b). Crack displacement transducers (CDTs) were installed across the joint region along the length of the bottom of the systems, Figure 7.29 (c). Laser displacement transducers (LDTs), Figure 7.29 (d), were placed at five different locations along the length and measured the displacement of the tops of the beams at three locations across the width of the system.

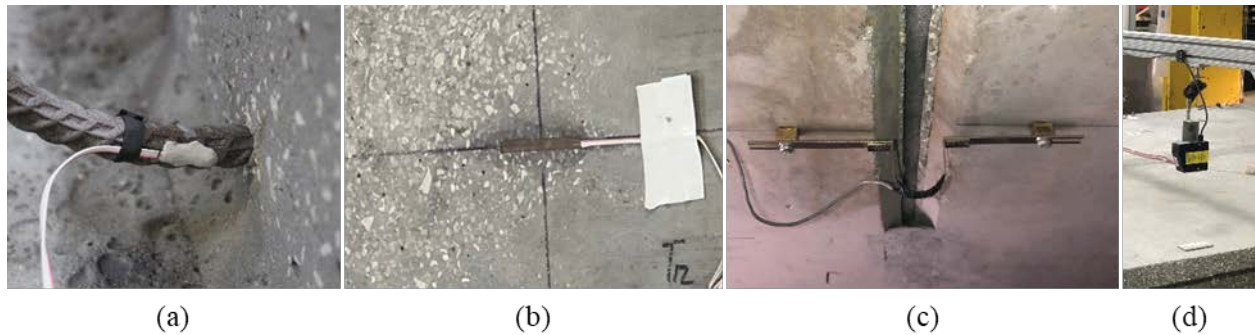


Figure 7.28: Instrumentation used for full-scale testing: (a) RSGs, (b) CSGs, (c) CDTs, and (d) LDTs

7.5.1. Two-Beam Strength and Service Testing (FIU-1/2)

The sensor layout for FIU-1/2 are shown in Figure 7.30 for the center of the span and Figure 7.31 for the support regions.

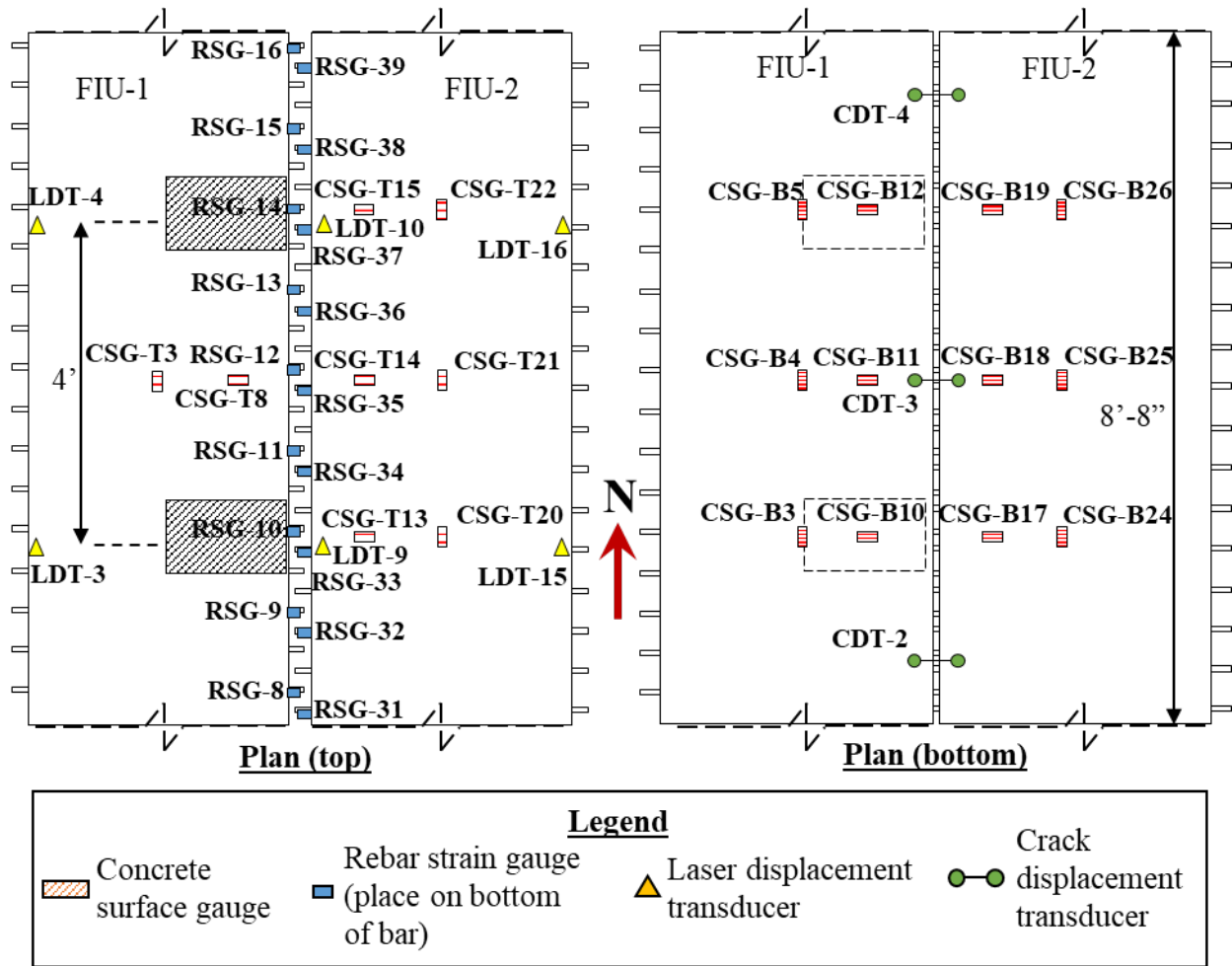


Figure 7.29: Two-beam (FIU-1/2) span center sensor location and types

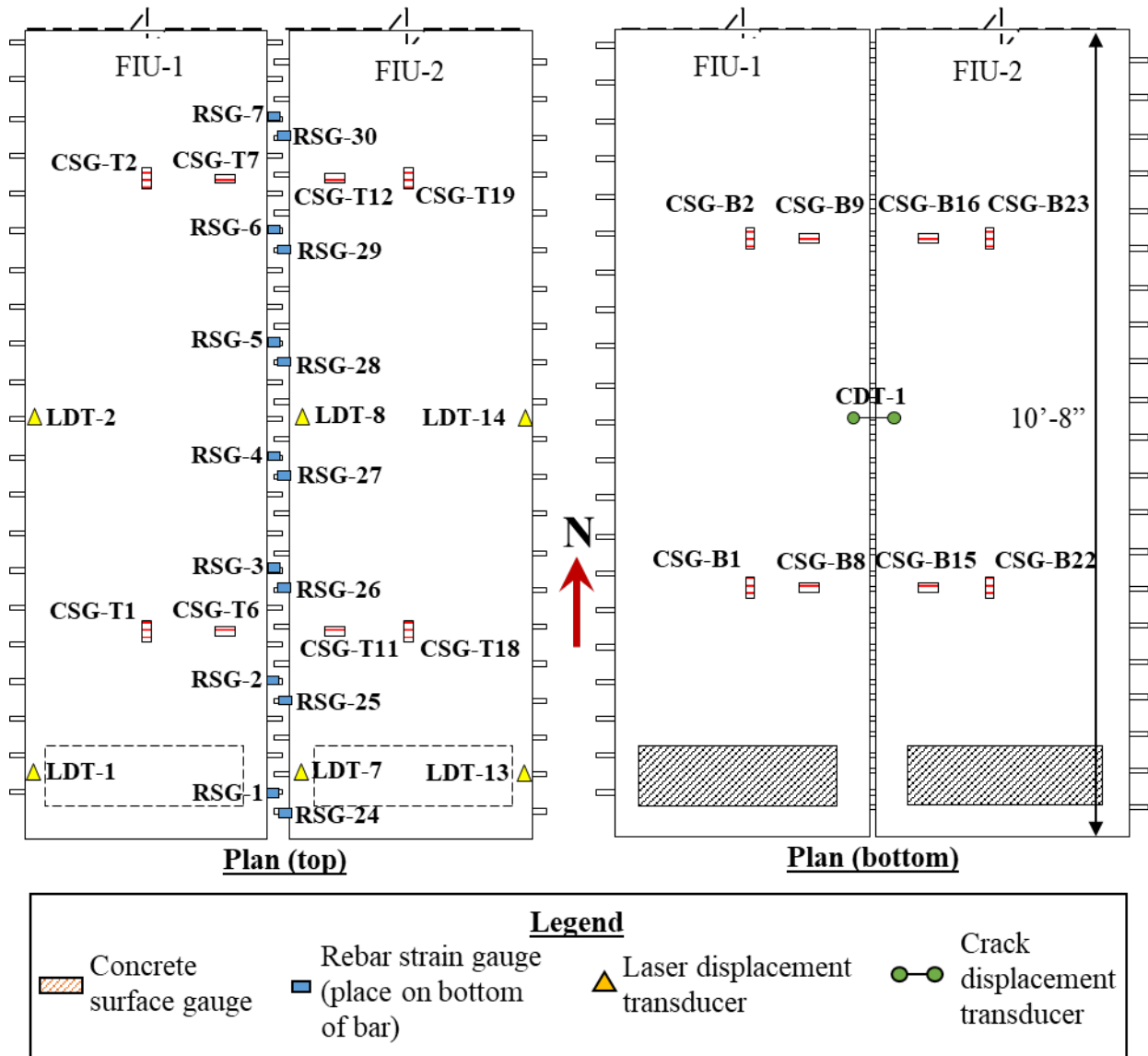


Figure 7.30: Two-beam (FIU-1/2) support sensor location and types (both supports identical)

7.5.2. Two-Beam Fatigue Service Testing (FIU-4/5)

The sensor layout for FIU-4/5 is shown in Figure 7.32 for the center of the span and Figure 7.33 for the support regions. The instrumentation schedule was kept as similar as possible between the two two-beam systems to allow for easier comparisons between the behavior of the two systems.

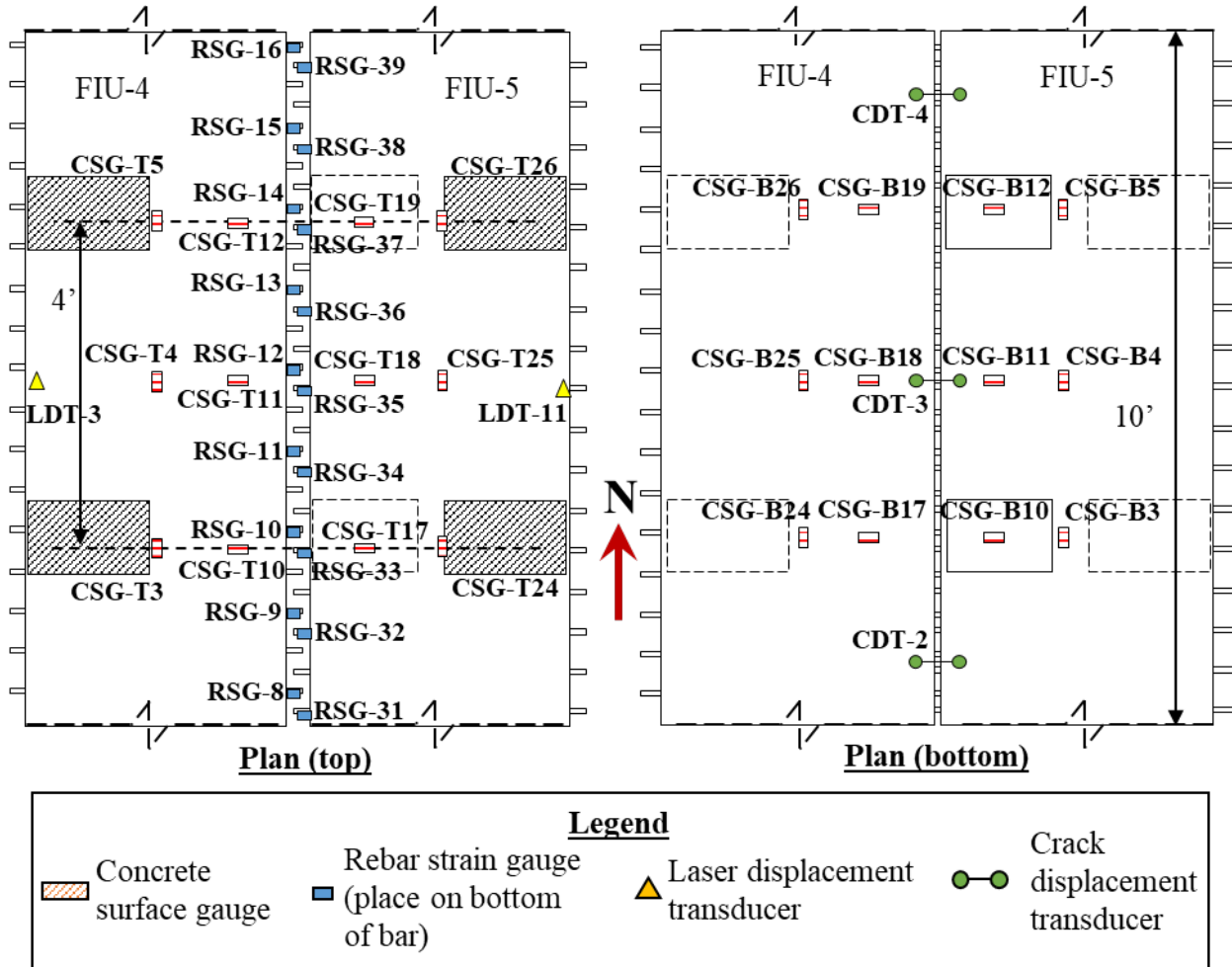


Figure 7.31: Two-beam (FIU-4/5) span center sensor location and types

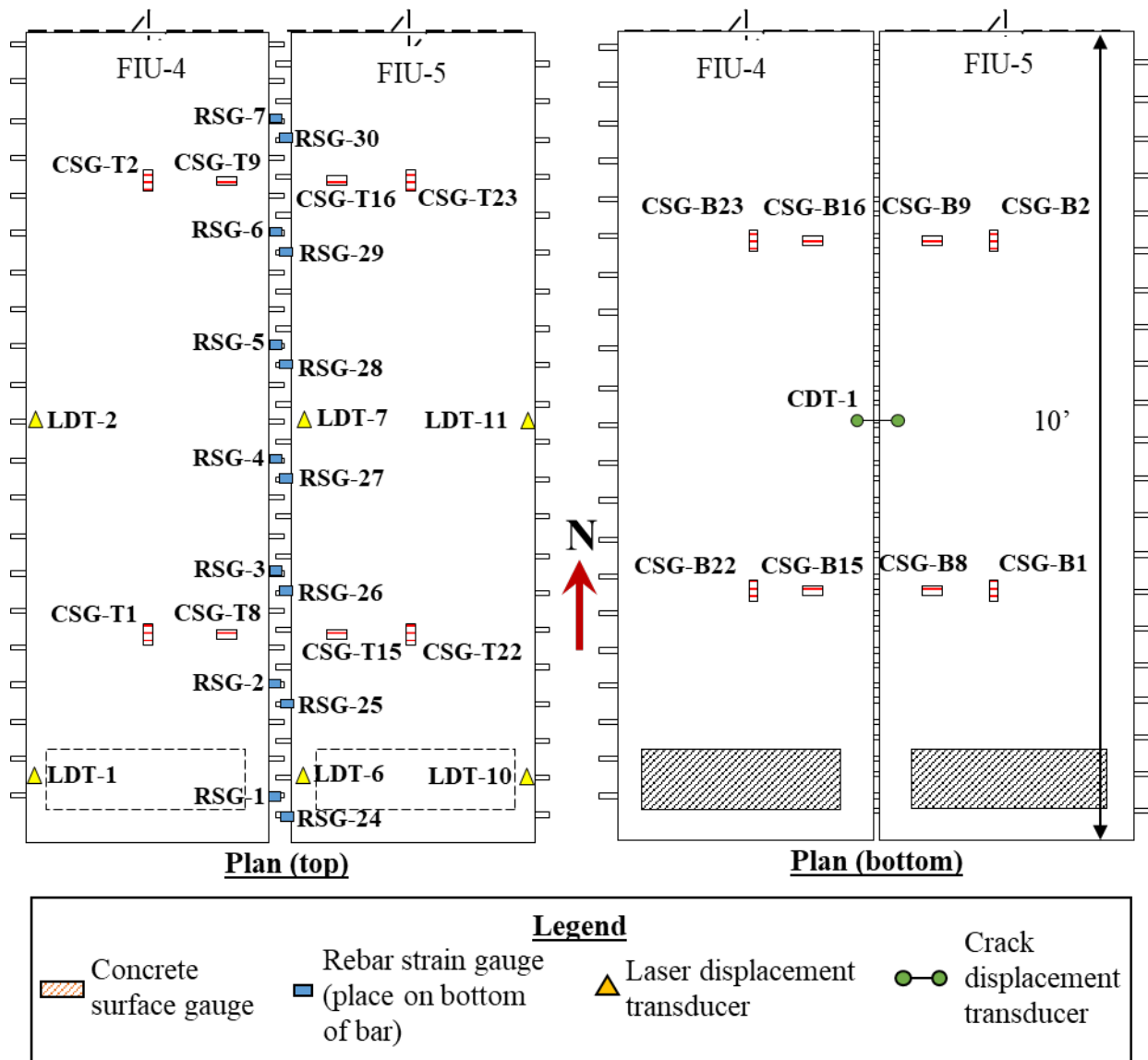


Figure 7.32: Two-beam (FIU-4/5) support sensor location and types (both supports identical)

7.6. TWO-BEAM SERVICE AND STRENGTH TESTING RESULTS (FIU-1/2)

7.6.1. Summary of Results

The two-beam configuration with FIU-1/2 was tested using LC 2-4 for service loading and LC 2-1 for ultimate strength testing of the system. A summary of the predicted and experimental test results is shown in Table 7.7.

Table 7.7: Summary of predicted and measured results for large-scale specimen

Test ID	Hand Calculation		Software Analyses			Experimental Tests		
	P_{cr} (kips)	P_{max} (kips)	P_{cr} (kips)	P_{max} (kips)	Δ at P_{max} (in)	P_{cr}^* (kips)	P_{max} (kips)	Δ at P_{max} (in)
<i>Service</i>	71.2	145.2	64.4	--	--	58.7	--	--
<i>Ultimate</i>	71.2	145.2	--	162.4	3.82	45.0	157.5	6.89

*cracking first occurred during service load testing; the crack reopening load is reported for ultimate strength testing

The measured material properties for the precast concrete and UHPC are shown in Table 7.8.

Table 7.8: Measured compression strength for precast concrete and UHPC, *age at time of test

Precast Concrete		UHPC	
<i>Age (days)</i>	<i>Strength (ksi)</i>	<i>Age (days)</i>	<i>Strength</i>
28	8.50	14	19.23
-	-	28	22.52
112*	8.74	37*	24.31

The modulus of rupture (f_r) was also measured for the UHPC. The average modulus of rupture of the UHPC was 3.14 ksi at 28 days.

7.6.2. Service Test Results (FIU-1/2)

7.6.2.1. Overview

The load versus deflection response for the system under LC 2-4 is shown in Figure 7.34. The deflections shown accounts for the settlement of the supports. There was a minimal differential displacement between the two beams (varying between 1 and 2 percent during testing), which suggests that the load was applied relatively equally on the two beams. The load-deflection behavior began to become non-linear after 60 kips during the first load cycle. This coincided with the cracking load determined based on the concrete strain gauges.

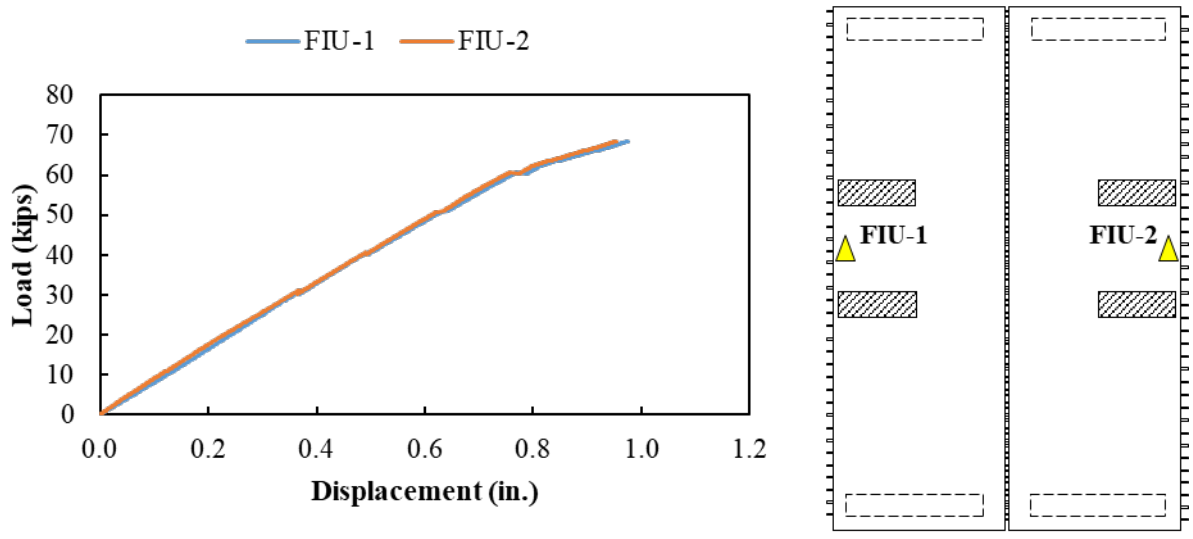


Figure 7.33: Load versus midspan displacement for service load testing with LC 2-4 for FIU-1/2

Observations from the service load testing are summarized by load step in Table 7.9 and observed cracking is shown in Figure 7.35. Several longitudinal shrinkage cracks were noted before testing near midspan in FIU-2. Some narrow longitudinal cracking was observed in the specimens prior to the formation of transverse cracks at 68 kips.

Table 7.9: Observations during service load testing of FIU-1/2

Step	Load Ranges	Observations	Figure
1	0 k	Some longitudinal shrinkage cracks observed on FIU-2 near midspan underneath north load patch	Figure 7.35a
2	10 k – 20 k	No additional cracking observed	-
3	30 k – 60 k	Small longitudinal cracks were observed underneath the specimen	Figure 7.35b Figure 7.35c
4	60 k – 68 k	Transverse cracking observed at midspan underneath specimen at 68 kips; load-deflection curve began to become non-linear in this load range	Figure 7.35d
5	0 k – 68 k	Load was removed and then reapplied to 68 kips	-

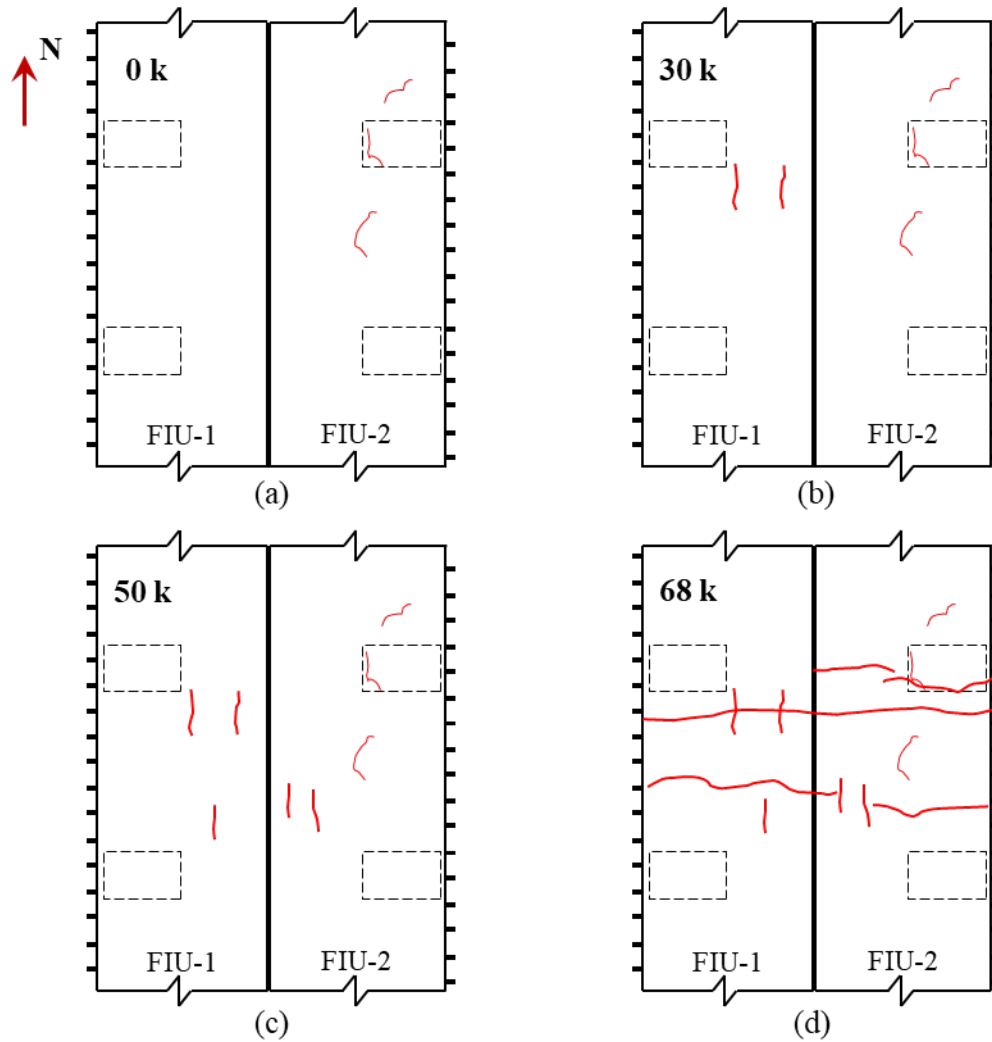


Figure 7.34: Bottom crack pattern at midspan for service load testing with LC 2-4 for FIU-1/2 at: (a) 0 kips, (b) 30 kips, (c) 50 kips, and (d) 68 kips

7.6.2.2. Joint Behavior

Crack displacement gauges (CDTs) were installed crossing the top and bottom of the joint between beams, as shown in Figure 7.36. The ends of the gauge were attached to the precast beam sections (not the joint) to measure any cracking in the joint or debonding of the joint interface.



Figure 7.35: Crack displacement gauge used across joint

The average strain across the joint measured using the CDTs on the top and bottom of the system are shown in Figure 7.37 and Figure 7.38, respectively. The approximate cracking strain of the conventional concrete in the precast section was found using the modulus of elasticity and modulus of rupture equations from §5.4.2.4 and §5.4.2.6 of AASHTO LRFD [78], as shown in Equation 7-1, and included in the figures.

$$\epsilon_t = \frac{f_r}{E_c} = \frac{0.24\sqrt{8.74 \text{ ksi}}}{1,820\sqrt{8.74 \text{ ksi}}} = 132 \times 10^{-6} \quad \text{Equation 7-1}$$

Tension developed across the joint in both the top and the bottom of the system. The average tensile strains at service level loads (32 kips for the full HS-20 truck axle) were much less than the estimated cracking strain for the precast concrete.

The load configuration used for this service load testing was determined through numerical modeling to produce the most transverse tensile stress on the top of the joint. Because the average tensile strain across the top of the joint remained under the estimated cracking strain, it is thought that a top layer of reinforcement to resist tension in the top of the joint is not required.

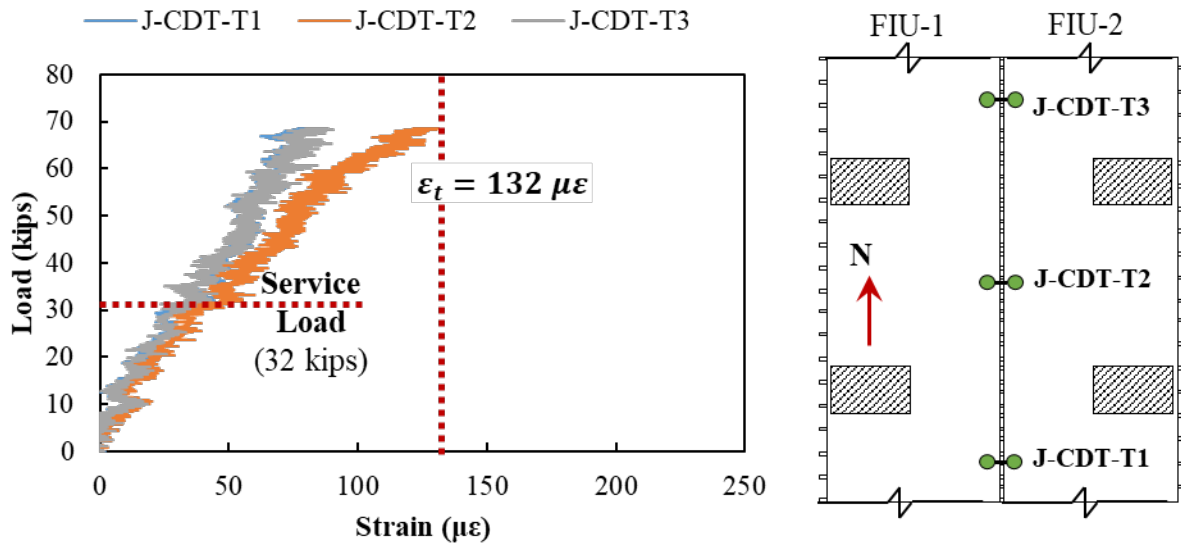


Figure 7.36: Load versus average strain across top of joint for service load testing with LC 2-4 for FIU-1/2

Transverse tension was also measured in the bottom CDTs, see Figure 7.38. The largest joint strains were measured at midspan (J-CDT-T2 and J-CDT-B3) and decreased toward the support. The tensile strains at ultimate were higher than the expected cracking strains, but there were no visual cracks or signs of cracking in the joint reinforcement RSGs, see Figure 7.39.

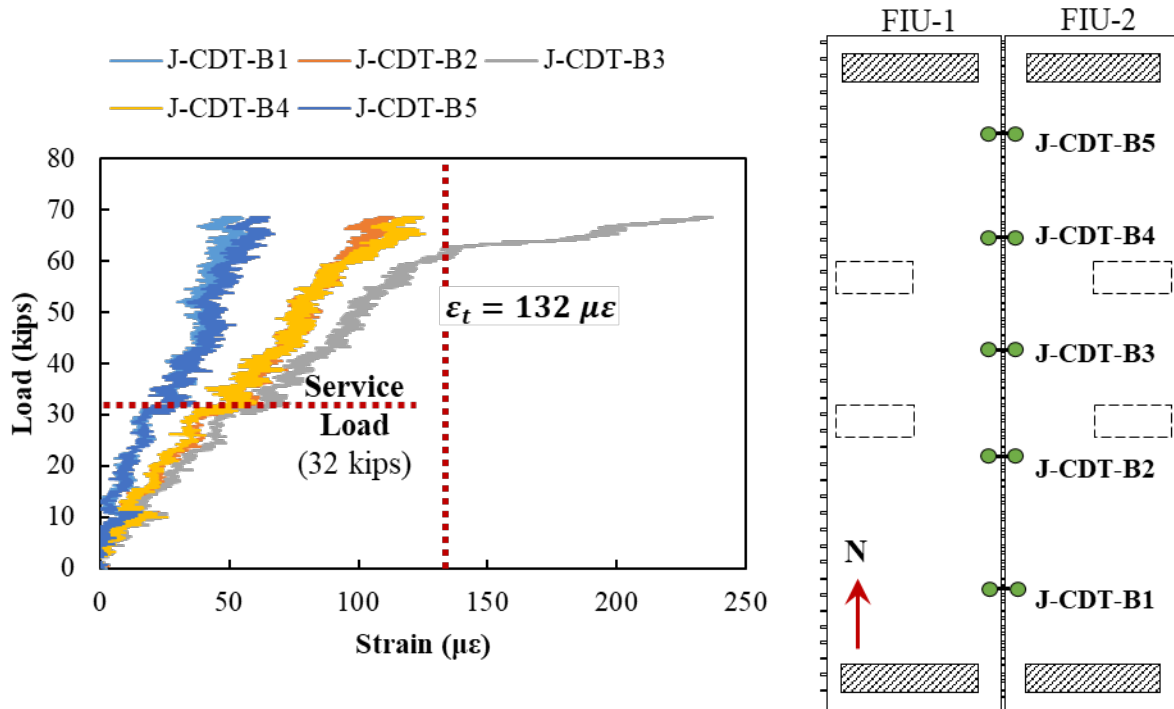


Figure 7.37: Load versus average strain across bottom of joint for service load testing with LC 2-4 for FIU-1/2

Tension in the top of the joint resulted from the transverse bending stresses that developed because the load was applied on the outside edges of the thin slab beam sections, as shown in Figure 7.39. Compression was expected on the bottom of the joint from the transverse bending stresses, which would have also been consistent with the CSG readings. The measured tension in the bottom of the joint may have been due to the polarity being reversed for these gauges.

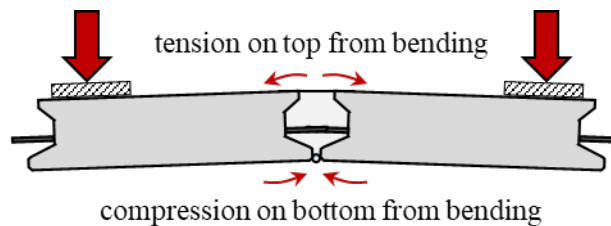


Figure 7.38: Expected stresses on top and bottom of specimen from transverse flexure

The measured response from the transverse concrete strain gauges (CSGs) are shown in Figure 7.40. Transverse tensile strains developed on the top of the section and transverse compression strains on the bottom of the section, consistent with the transverse bending mechanism shown in Figure 7.39 (a). A linear response was observed in the transverse gauges on both the top and bottom of the system. Transverse tensile strains remained below the estimated cracking strain found in Equation 7-1.

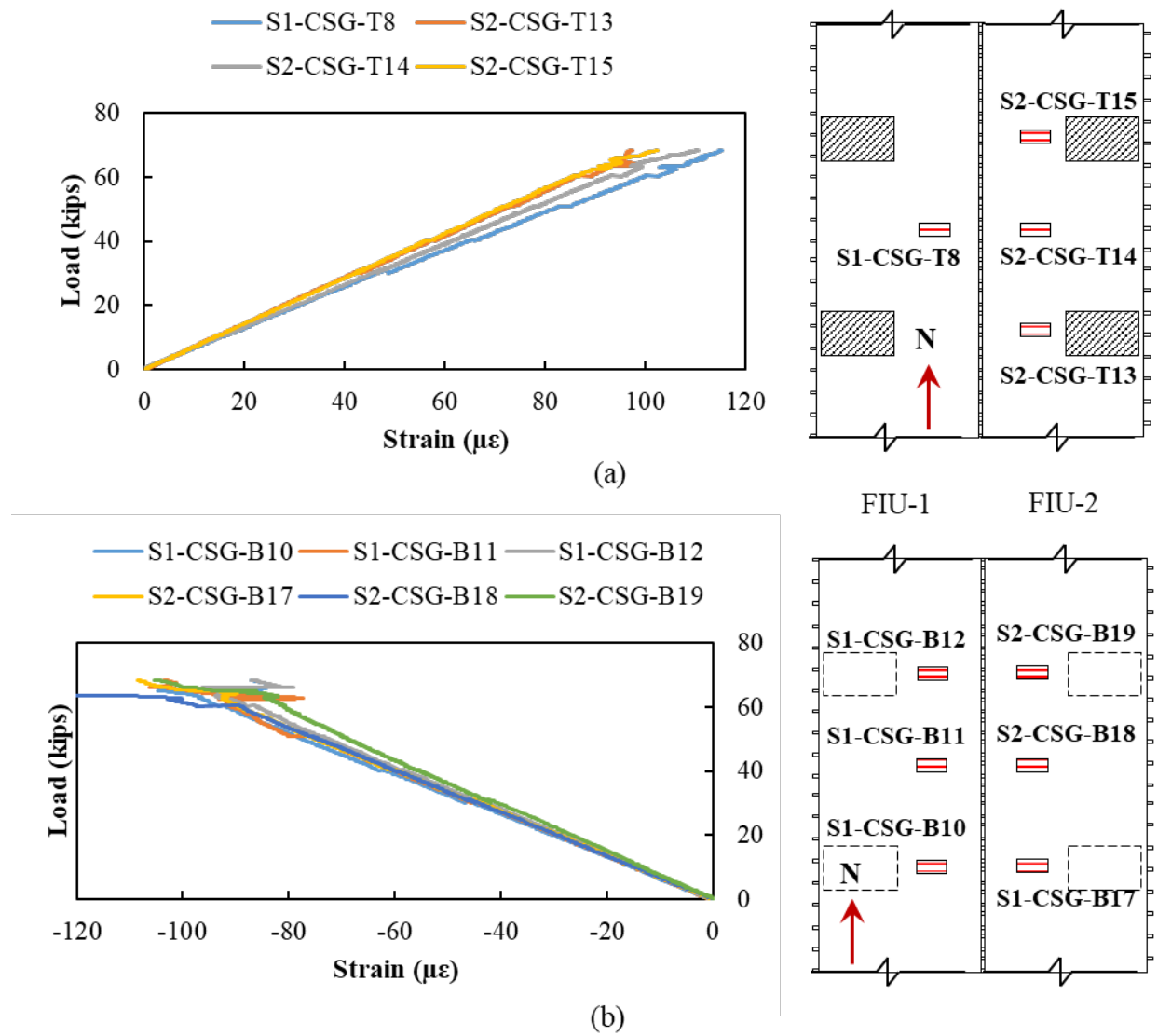


Figure 7.39: Load versus transverse concrete strain for service load testing with LC 2-4 for FIU-1/2 for (a) top and (b) bottom of beam in the midspan section of the system

The measured response for the rebar strain gauges (RSGs) on the joint reinforcement extending from FIU-1 in the midspan and south sections of the system is shown in Figure 7.41. All the joint reinforcement had minor compression strain during testing, which is also consistent with the transverse bending mechanism shown in Figure 7.39 (a). A similar response was measured in the joint reinforcement extending from FIU-2 and joint reinforcement in the north section of the system.

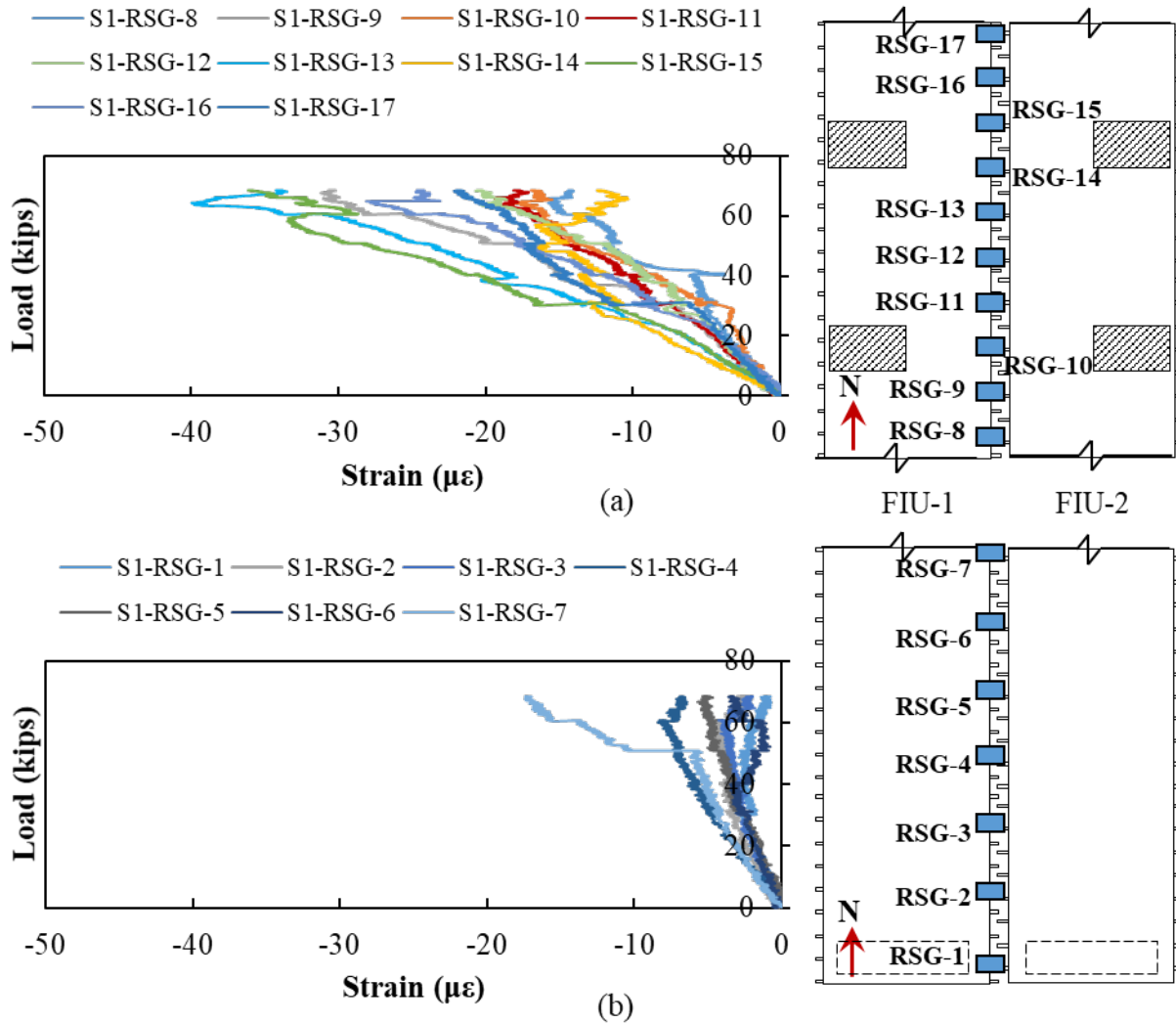


Figure 7.40: Load versus strain for service load testing with LC 2-4 for joint reinforcement extending from FIU-1 for the (a) midspan and (b) south sections of the system

7.6.2.3. Longitudinal Behavior

The measured response from the longitudinal CSGs is shown in Figure 7.42. Longitudinal cracking can be determined using CSGs by looking for a change in slope in the CSGs on the top of the beams or a sharp change in tensile strain in the CSGs on the bottom of the beams. A change in slope of the top gauges occurs between 58 and 60 kips, which was likely a result of transverse cracking in the section.

A sharp change in strain in the bottom gauges either reflects a crack adjacent to the gauge or crack going through the gauge. S1-CSG-B3 and S1-CSG-B4 both have sharp decreases in tensile strain at 58.7 kips, which is a result of a crack developing between these two gauges. This crack continued to open across the bottom of the beam causing a similar sharp decrease in tensile strain in S2-CSG-B24 and S2-CSG-B25 at around 62 kips. S1-CSG-B5 and S2-CSG-B26 both have

sharp increases in tensile strain at an applied load of 64.0 kips, which is a result of an additional crack opening that extended through these gauges. These two cracks observed by the CSGs were confirmed by visual inspection when the loading was held at 68 kips, see Figure 7.35 (d).

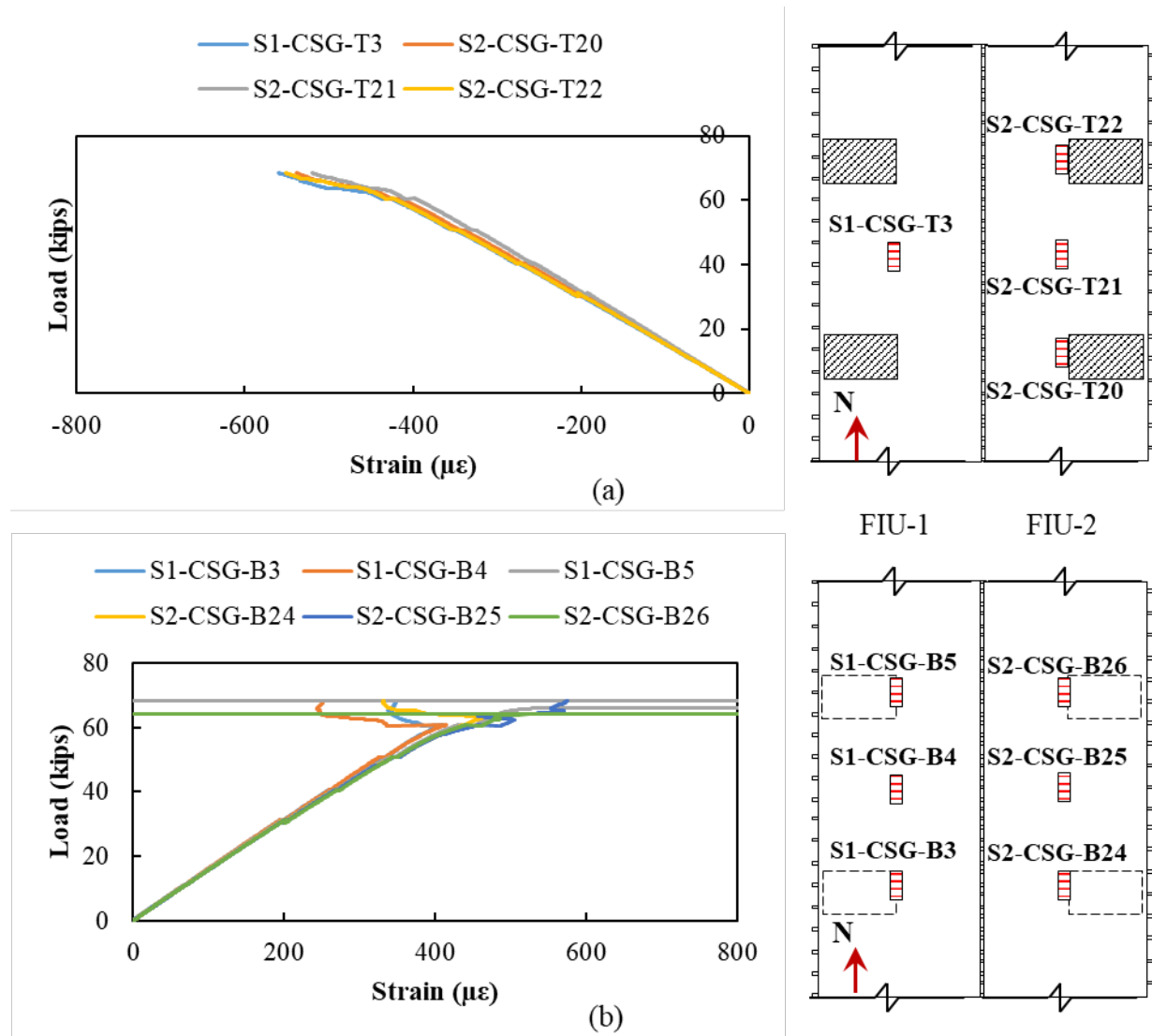


Figure 7.41: Load versus longitudinal concrete strain for service load testing with LC 2-4 for FIU-1/2 for (a) top and (b) bottom of beam in the midspan section of the system

7.6.3. Strength Test Results (FIU-1/2)

7.6.3.1. Overview

The load versus deflection response for the system under LC 2-1 is shown in Figure 7.43. Support settlement is accounted for in the deflection shown. There was a minimal differential displacement between the two beams (with an average of 6 percent difference). There was a 1 to 2 percent differential displacement observed when both beams were loaded (thought to be a result of slight misalignments in the test setup), so only around 4 percent differential displacement was likely a

result of the unsymmetrical loading of LC 2-1. The load-deflection behavior began to become non-linear after 60 kips (like the service load testing).

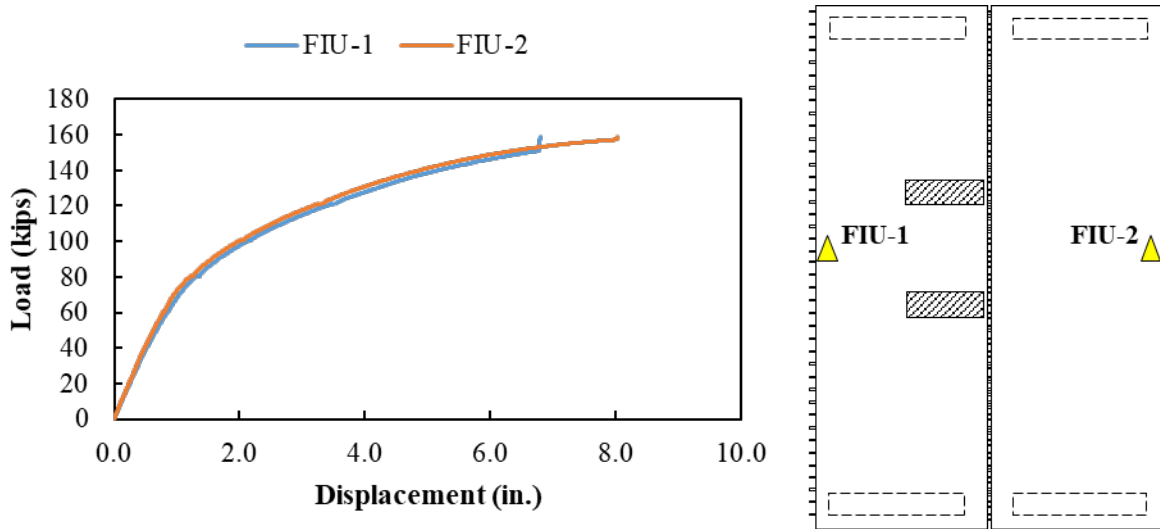


Figure 7.42: Load versus midspan displacement for ultimate strength testing with LC 2-1 for FIU-1/2

Observations from the ultimate strength testing are summarized by load step in Table 7.10 and observed cracking shown in Figure 7.44. Previous cracking was present due to the service load testing; cracks present before ultimate strength testing are shown in red in Figure 7.44. New cracking caused by ultimate strength testing are shown in blue in Figure 7.44. Several additional transverse cracks were observed in the system at 60 kips and 80 kips. Cracks were not visually inspected after 80 kips.

Table 7.10: Observations during ultimate strength testing of FIU-1/2

Step	Load Ranges	Observations	Figure
1	0 k	No crack growth was observed	Figure 7.44a
2	20 k – 40 k	No additional cracks were observed	-
3	40 k – 60 k	New transverse cracks, located at midspan, were observed underneath the specimen at 60 kips in both FIU-1 and FIU-2	Figure 7.44b
4	60 k – 80 k	Transverse cracks seen crossing the whole system at 80 kips	Figure 7.44c
5	Load until failure	Failure load was observed at around 158 kips	-

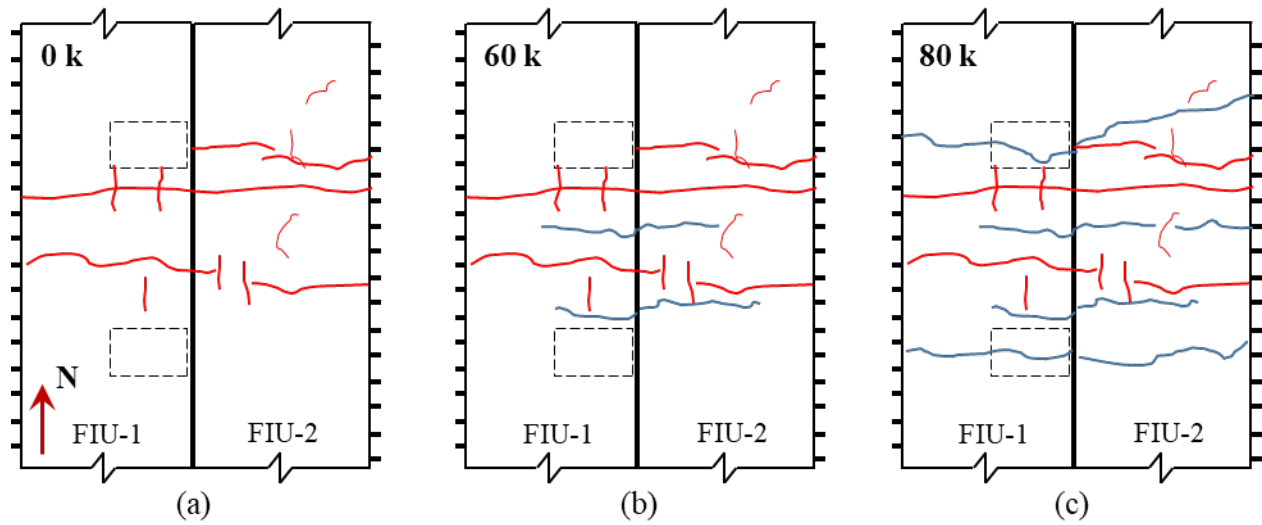


Figure 7.43: Bottom crack pattern at midspan for ultimate strength testing with LC 2-1 for FIU-1/2 at: (a) 0 kips, (b) 60 kips, and (c) 80 kips; blue = new cracks, red = cracks from previous tests

7.6.3.2. Joint Behavior

The average strain across the joint measured using the CDTs on the top and bottom of the system are shown in Figure 7.45 and Figure 7.46, respectively. Tension developed across the top of the joint and compression across the bottom of the joint. The average tensile strain in the top remained under the estimated cracking strain for the precast concrete ($132 \mu\epsilon$) even at the ultimate strength of the prestressed system. CDTs were removed at 80 kips to ensure they were not damaged during testing.

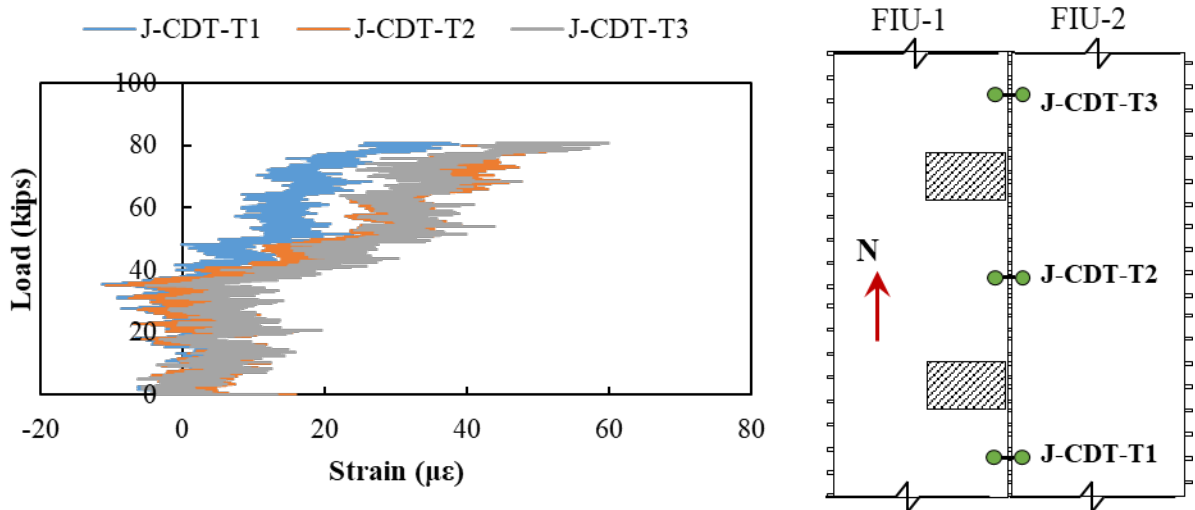


Figure 7.44: Load versus average strain across top of joint for ultimate strength testing with LC 2-1 for FIU-1/2

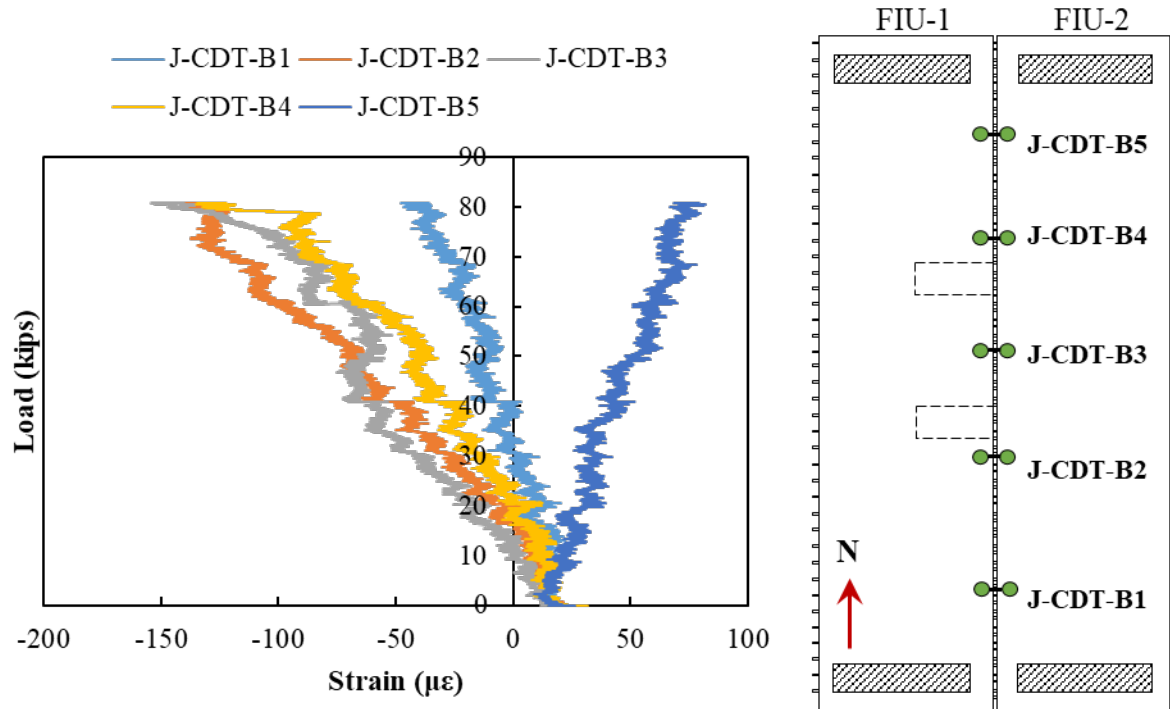


Figure 7.45: Load versus average strain across bottom of joint for ultimate strength testing with LC 2-1 for FIU-1/2

The measured responses from the transverse CSGs are shown in Figure 7.47. Transverse tension developed in the top of the section and transverse compression on the bottom of the section (like the average strain across the joint). The measured transverse tensile strains in the top of FIU-2 did exceed the estimated cracking strain, suggesting that longitudinal cracks were developing in the top of FIU-2, although no visible longitudinal cracking was observed after testing was completed. Additionally, transverse strains in the concrete were like the average transverse strains across the joint (comparing strain values at 80 kips to those shown in Figure 7.45 and Figure 7.46).

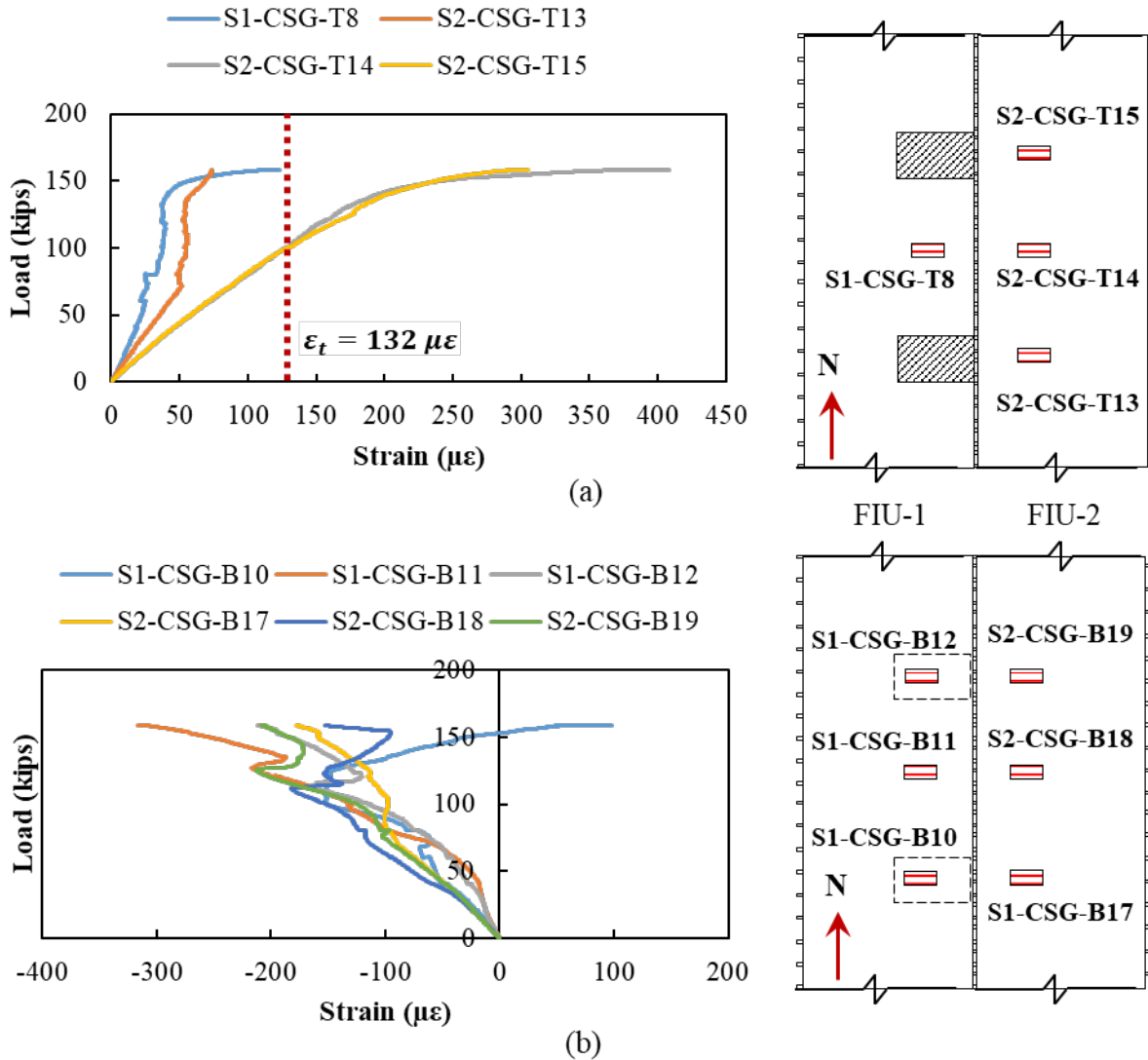


Figure 7.46: Load versus transverse concrete strain for ultimate strength testing with LC 2-1 for (a) top and (b) bottom of beam in the midspan section of FIU-1/2

The measured response for the RSGs on the joint reinforcement extending from FIU-1 in the midspan and south sections of the system is shown in Figure 7.48. Significant tensile strains developed in the joint reinforcement with the reinforcement starting to pick up significant strain between 73 and 87 kips applied load. This jump in strain may suggest that there was cracking developed near the joint or at the joint interface. Large tensile strains were also measured in the joint reinforcement extending from FIU-2 with the reinforcement beginning to pick up significant strains at slightly higher loads (between 85 and 95 kips).

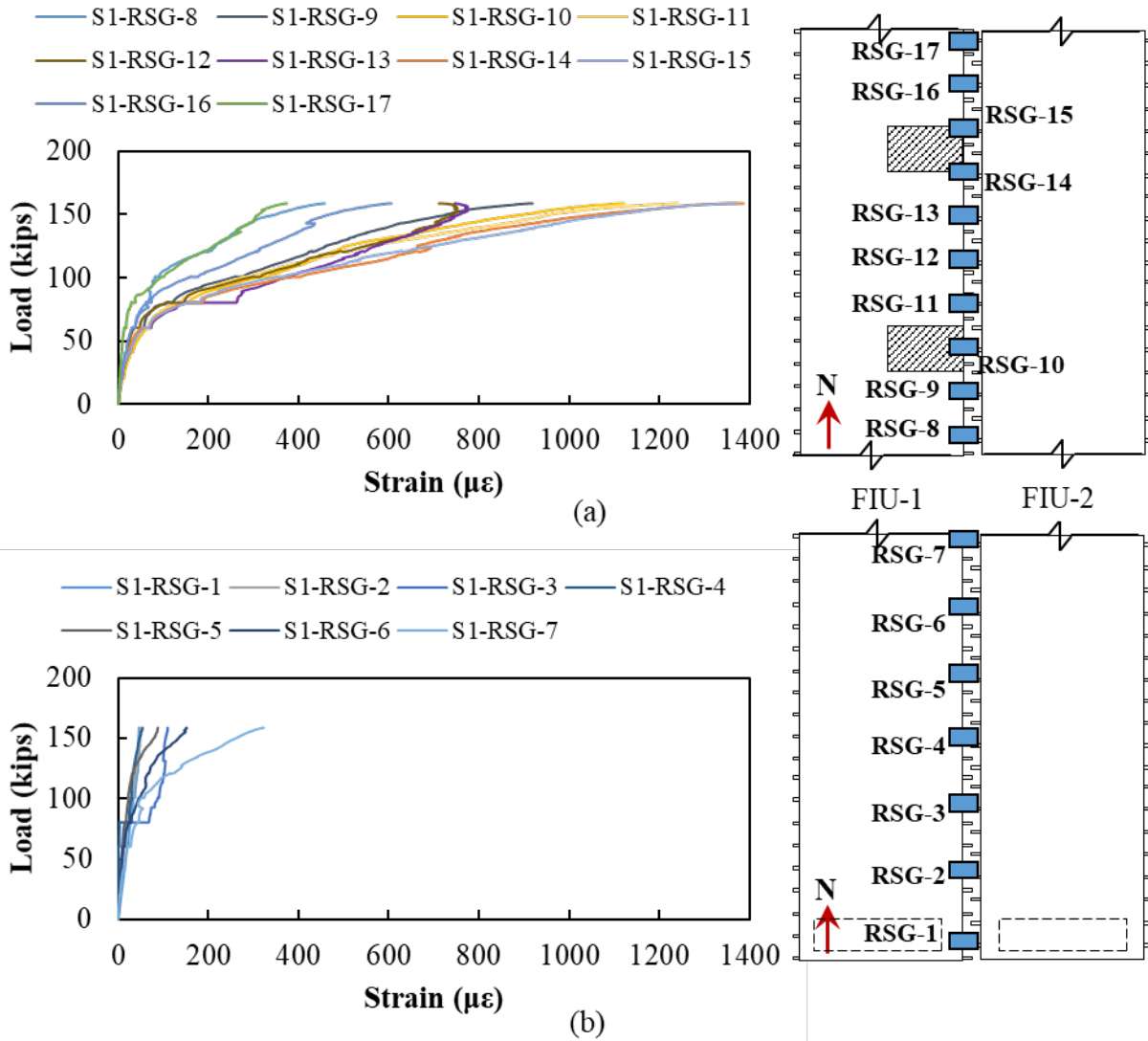


Figure 7.47: Load versus strain for ultimate strength testing with LC 2-1 for joint reinforcement extending from FIU-1 for the (a) midspan and (b) south sections of the system

No joint distress was observed from above the specimen during testing or on top of the specimen after testing. Crushing of the concrete at failure of the system extended across the entire width of the two precast beams and across the UHPC joint, as shown in Figure 7.49.

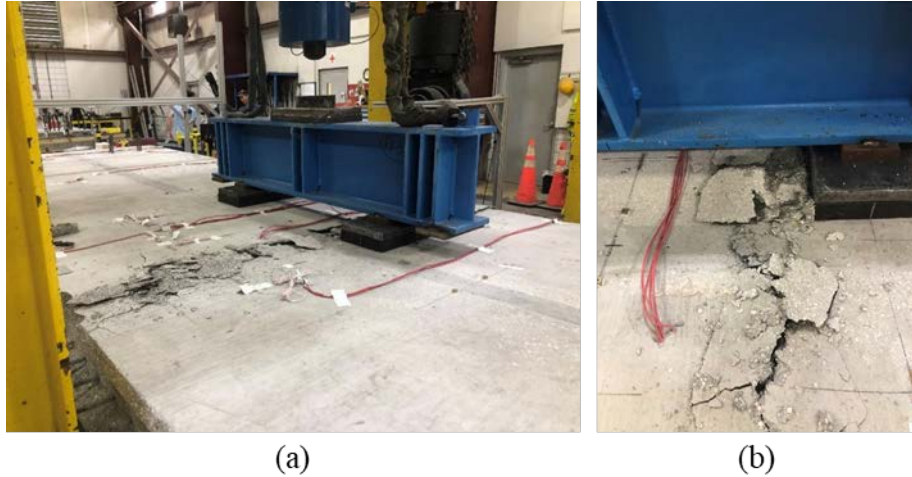


Figure 7.48: Crushing of FIU-1/2 concrete at failure for LC 2-1: (a) overview and (b) joint

Cores of the joint interface were taken after testing at three locations near the load points, as shown in Figure 7.50 (a). There was still good bond observed between the precast concrete and UHPC in joint interface above the bottom flange. A crack was observed along the interface between the top of the bottom flange and the UHPC extending into the precast concrete section, shown in Figure 7.50 (b) and (c).

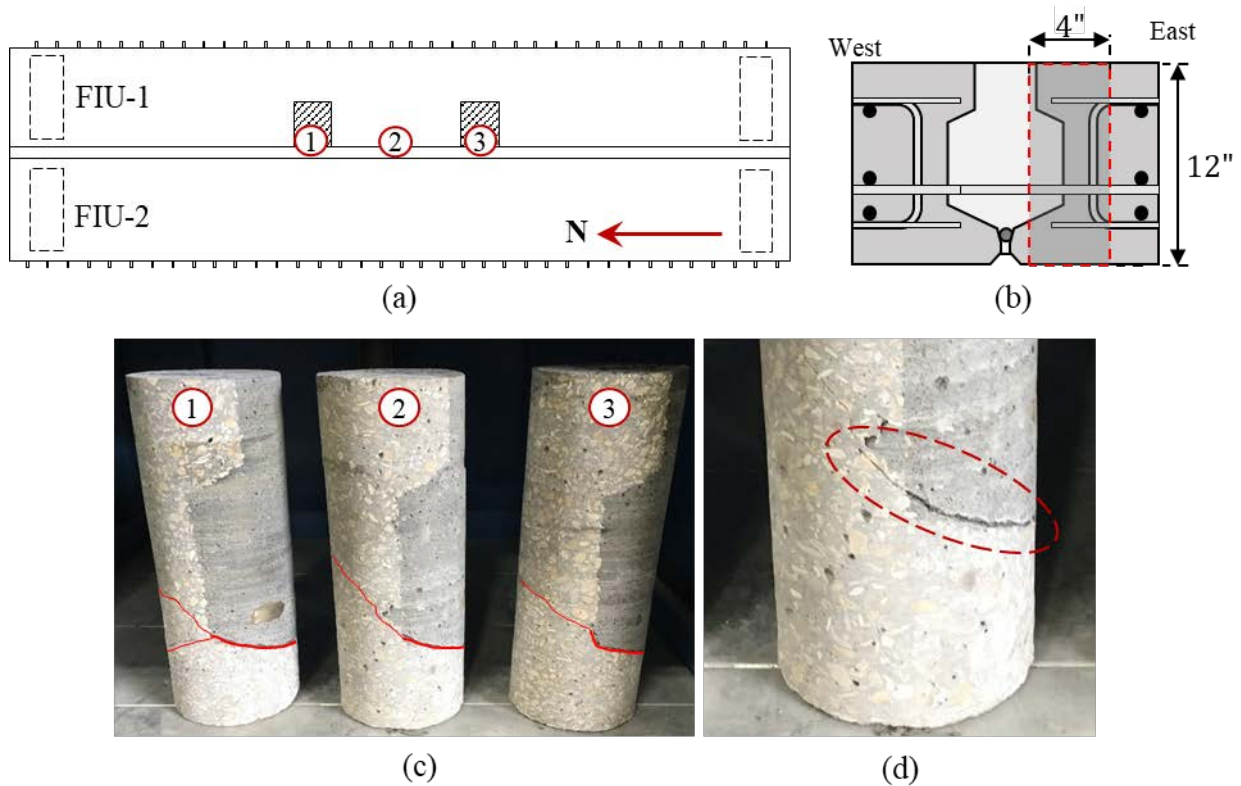


Figure 7.49: FIU-1/2 joint edge cores: location of cores (a) along length and (b) in cross section, (c) three core samples with bottom lip debonded, and (d) observed debonding crack extending into the precast matrix

7.6.3.3. Longitudinal Behavior

The measured response from the longitudinal CSGs are shown in Figure 7.51. The load required to cause reopening of the transverse cracks caused by the service load testing can be determined using the CSGs on the bottom of the beam. Like the initial cracking load, crack reopening can be determined when the slope of the force-strain plot for the CSG becomes nonlinear. The cracks reopened near S1-CSG-B4, S1-CSG-B5, S2-CSG-B24, and S2-CSG-B26 between 35 and 45 kips; this load is lower than the initial cracking load because the concrete has already cracked and has no tensile strength at these crack locations. New cracking was observed through S1-CSG-B3 and S2-CSG-B25 at approximately 70 kips (observed by the spike in tensile strain after this load). Concrete crushing controlled the failure, as shown in Figure 7.49. The concrete strain at failure was approximately 0.003 (compression), which is the value that is typically assumed for the flexural design of reinforced and prestressed concrete members.

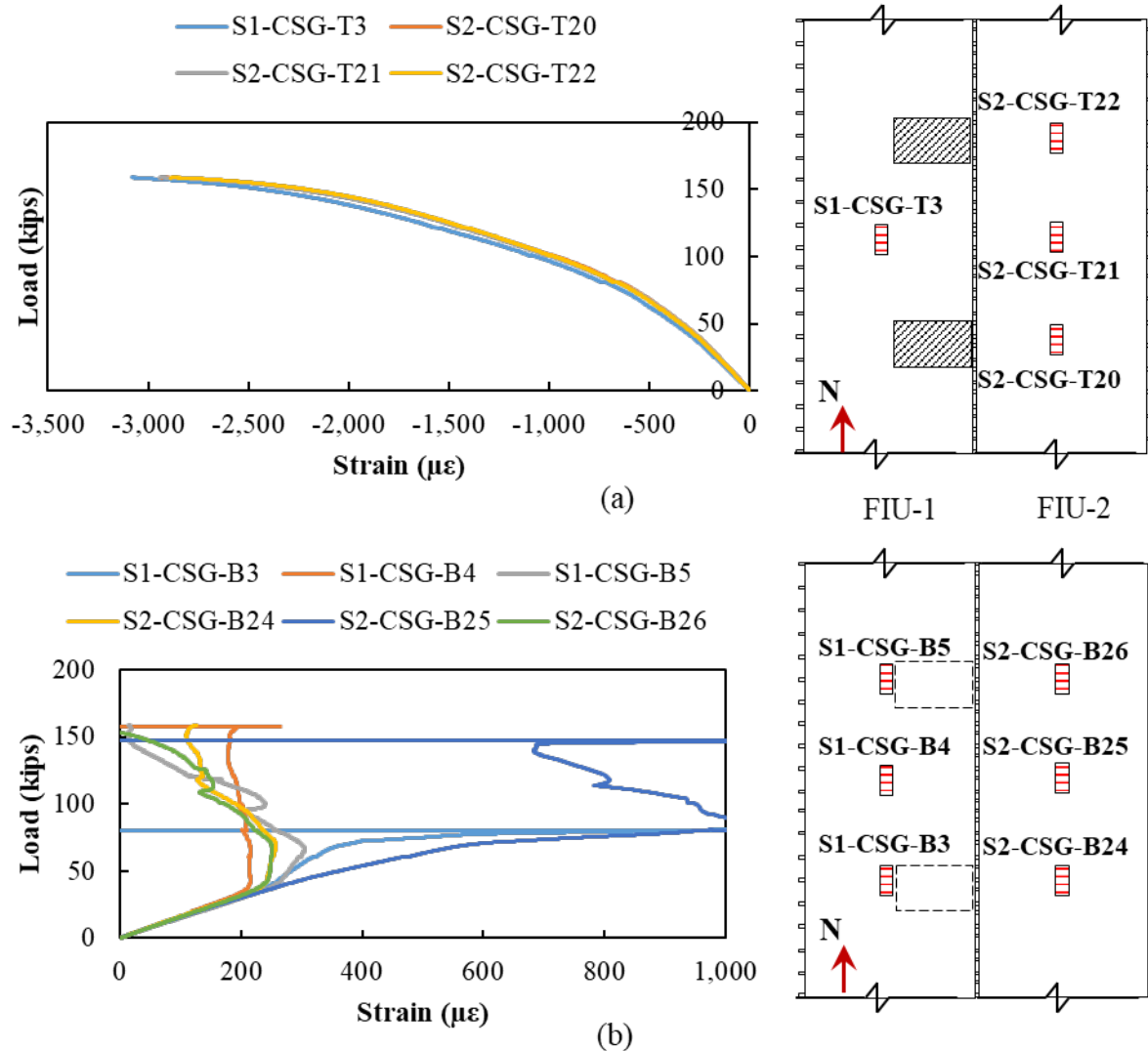


Figure 7.50: Load versus longitudinal concrete strain for ultimate strength testing with LC 2-1 for (a) top and (b) bottom of beam in the midspan section of FIU-1/2

7.6.4. Summary

The following conclusions and observations can be made based on the service load and ultimate strength testing of FIU-1/2:

- The joint performed well during service load and ultimate strength testing. No joint debonding or distress was observed in the joint region at service or ultimate loads. Additionally, the concrete in the compression block crushed across the entire width of the system (including the UHPC joint), which highlighted the quality of the bond between the UHPC and precast concrete.
- The joint successfully transferred the stress between beams. There was only a minor differential displacement between beams when only one beam was loaded. The capacity of the system was greater than the estimated capacity assuming the compression block width equal to the total system width.
- Transverse tension developed across the top of the joint for both loading configurations (2-1 and 2-4). The transverse tension remained well below the estimated cracking strain at service-level loading.

7.7. TWO-BEAM SERVICE AND STRENGTH TESTING RESULTS (FIU-4/5)

7.7.1. Testing Summary

A summary of the 16 different testing stages performed on the two-beam test setup with FIU-4 and FIU-5 is shown in Figure 7.52 and earlier in Table 7.2.

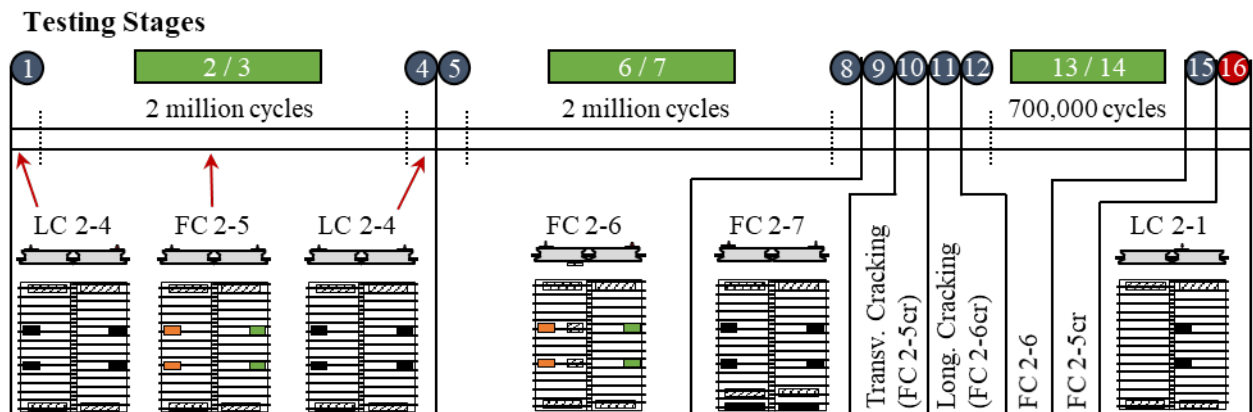


Figure 7.51: Summary of testing stages performed on two-beam setup with FIU-4/5

The results from all testing on FIU-4/5 will be presented in this section organized into the following sections:

1. **Test Stage 1-4:** LC 2-4 and FC 2-5 (fatigue response, static response before and after fatigue loading)
2. **Test Stage 5-8:** FC 2-6 with interior supports (fatigue response, static response before and after fatigue loading)
3. **Test Stage 9:** FC 2-7 with moment restraint at one end (static response)

4. **Test Stage 10:** transverse cracking procedure using loading like FC 2-5cr (static response)
5. **Test Stage 11:** longitudinal cracking procedure using loading like FC 2-6cr (static response)
6. **Test Stage 12-15:** FC 2-6 with interior supports (fatigue response, static response before and after fatigue loading) and FC 2-5cr static test after fatigue testing
7. **Test Stage 16:** ultimate strength test using LC 2-1

Static load testing was performed before and after the fatigue loading stages to determine if there was any change in the response of the system caused by the fatigue loading. There were several static load ramps performed during each of these stages. The static load ramps were named based on the test stage and the number of the ramp during that stage.

Example: 1st load ramp for Stage 4 testing would be: Load Ramp (LR) 4-1

The measured material properties for the precast concrete and UHPC are shown in Table 7.11.

*Table 7.11: Measured compression strength for precast concrete and UHPC, *age at time of test*

Precast Concrete		UHPC	
<i>Age (days)</i>	<i>Strength (ksi)</i>	<i>Age (days)</i>	<i>Strength</i>
243	11.3	36	25.0
295*	12.4	93*	25.9

The modulus of rupture (f_y) was also measured for the UHPC. The average modulus of rupture of the UHPC was 3.44 ksi at 80 days.

7.7.2. Fatigue Data Analysis

The normalization procedures that were used in the small-scale fatigue testing (see Chapter 6) were also used in the full-scale tests. Load was measured throughout testing using load cells and pressure transducers in the east and west actuators, as shown in Figure 7.53 (a). Deflection was measured with the actuators and using laser displacement transducers (LDTs), as shown in Figure 7.53.

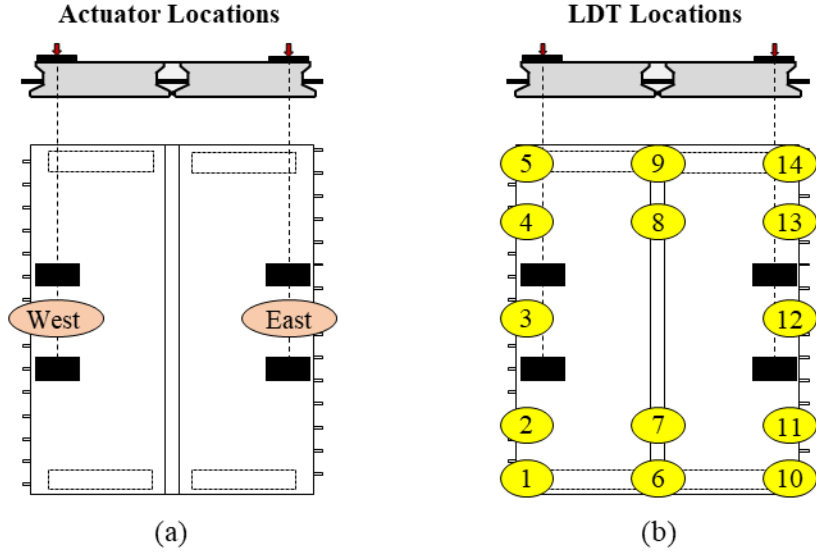


Figure 7.52: Location of (a) actuators and (b) LDT displacement sensors

The stiffness of the system was found based on the maximum and minimum load and deflection for each cycle using the load and deflection measured by the actuators, as shown in Equation 6-4.

$$K_i = \frac{P_{max} - P_{min}}{\delta_{P_{max}} - \delta_{P_{min}}} \quad \text{Equation 7-2}$$

The average system stiffness was also found using the LDT readings. The average load was divided by the average end displacements subtracted from the average midspan displacements, as shown in Equation 7-3 to Equation 7-6. The stiffness was also found for the east and west actuators, where the change in a single actuator load was divided by the average change in displacement for that actuator.

$$\Delta\delta_{1/6/10,i} = Avg\{\Delta\delta_{1,i}, \Delta\delta_{6,i}, \Delta\delta_{10,i}\} \quad \text{Equation 7-3}$$

$$\Delta\delta_i = Avg\{\Delta\delta_{3,i}, \Delta\delta_{12,i}\} - Avg\{\Delta\delta_{1/6/10,i}, \Delta\delta_{5/9/14,i}\} \quad \text{Equation 7-4}$$

$$\Delta P_{west,i} = P_{west,max} - P_{west,min} \quad \text{Equation 7-5}$$

$$K_i = \frac{Avg\{\Delta P_{west,i}, \Delta P_{east,i}\}}{\Delta\delta_i} \quad \text{Equation 7-6}$$

The normalized stiffness was found as the stiffness of the cycle divided by the stiffness of the first cycle of each load configuration, as shown in Equation 6-5. The stiffness was only stored every 1,000 cycles to minimize the amount of data stored over the duration of fatigue testing.

$$N_{K_i} = \frac{K_i}{K_0} \quad \text{Equation 7-7}$$

The normalized stiffness was plotted versus the number of cycles for each of the load points, as shown in Figure 6.6. A drop in the normalized stiffness would reveal strength degradation caused by the cyclic loading. Slight increases and decreases in normalized stiffness not following a general downward trend and not validated by events in any other gauges are not signs of degradation.

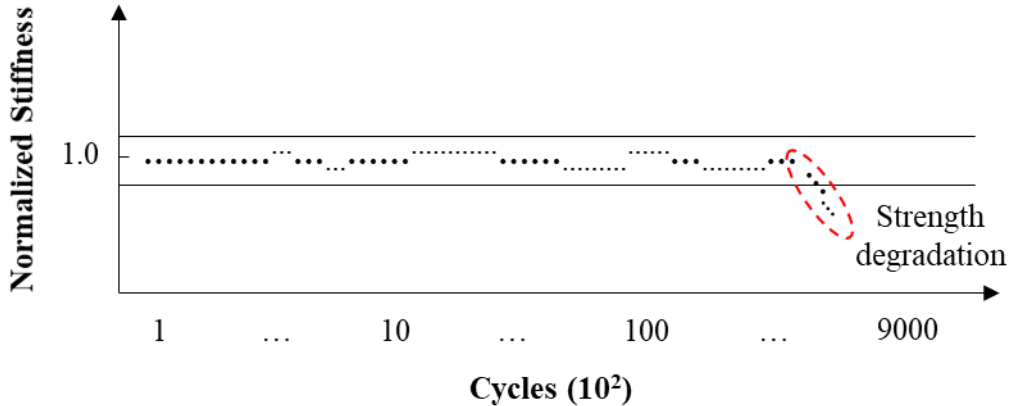


Figure 7.53: Hypothetical data for normalized stiffness values every 1000 cycles

The strains in the reinforcement associated with the lower and upper fatigue loads were recorded every 1,000 cycles. These strains were used to calculate the strain per load for the upper load range (Equation 6-7) and the change in strain per load change (Equation 6-8).

$$N_{\varepsilon_h,i} = \frac{\varepsilon_{max}}{P_{min}} \quad \text{Equation 7-8}$$

$$N_{\Delta\varepsilon,i} = \frac{\varepsilon_{max} - \varepsilon_{min}}{P_{max} - P_{min}} \quad \text{Equation 7-9}$$

where:

ε_{max} = strain measured at upper fatigue load

ε_{min} = strain measured at lower fatigue load

The normalized strain change over change in load always gives a positive value. The type of loading was determined based on the strain at maximum fatigue load and added on the plots to show if the sensor was reading tensile or compressive strains in the system.

The normalized strains per applied load was then plotted versus the cycle number, as shown in Figure 6.9. Yielding of the reinforcement at the location of the gauge would be indicated by the strain per applied load increasing each cycle. Slip or bond failure would likely be indicated by the strain per applied load decreasing each cycle.

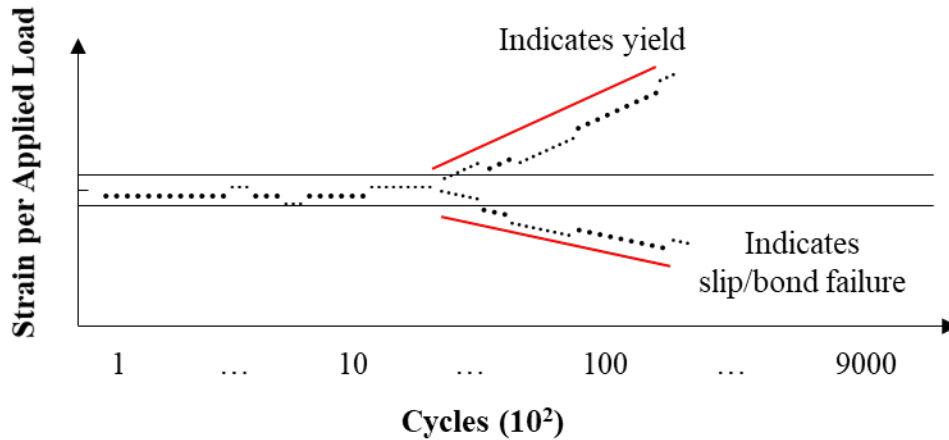


Figure 7.54: Hypothetical strain per applied load versus number of cycles for reinforcement

The concrete strain gauge (CSG) and crack displacement transducer (CDT) data were normalized the same as the reinforcement data, using Equation 6-7 and Equation 6-8. The strain per applied load versus cycle number was then plotted, shown in Figure 6.11. A drop in the strain per applied load indicates the occurrence of cracking near the location of the gauge.

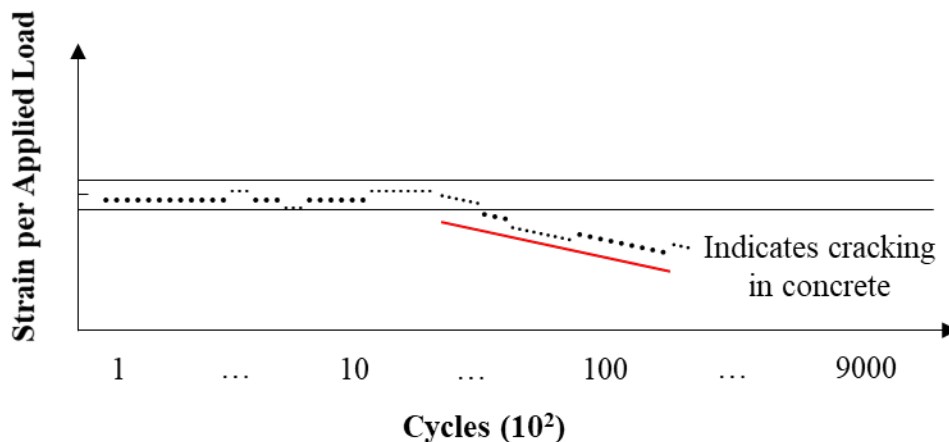


Figure 7.55: Strain per applied load (kip) per number of cycles for bottom concrete strains

Like the stiffness reading, the strain per applied load was only stored every 1,000 cycles to minimize the amount of data stored over the fatigue testing.

7.7.3. Unrestrained Service Test Results (Stages 1-4, LC 2-4, FC 2-5)

7.7.3.1. Overview

The unrestrained service test assessed a simply supported, unstiffened span condition and consisted of four loading stages. Stage 1 simulated five static FL120 rear-axle permit truck load ramps in the elastic range, applied with LC 2-4. Stage 2 and Stage 3 consisted of the application of two million HS20-rear-axle truck cycles applied using FC 2-5. At the end of the fatigue test, two more static FL120 rear-axle permit truck load ramps in the elastic range were applied in Stage 4, using LC 2-4, for a total of seven static ramps. The load versus deflection response for the system under

LC 2-4 before (LR 1-1) and after (LR 4-1) two million cycles of fatigue response is shown in Figure 7.57. The service test results from the two-beam system with FIU-1/2 (see §7.6.2) are used as a comparison in this section for the static test results as this test was also performed with LC 2-4. The deflections shown accounts for the settlement of the supports.

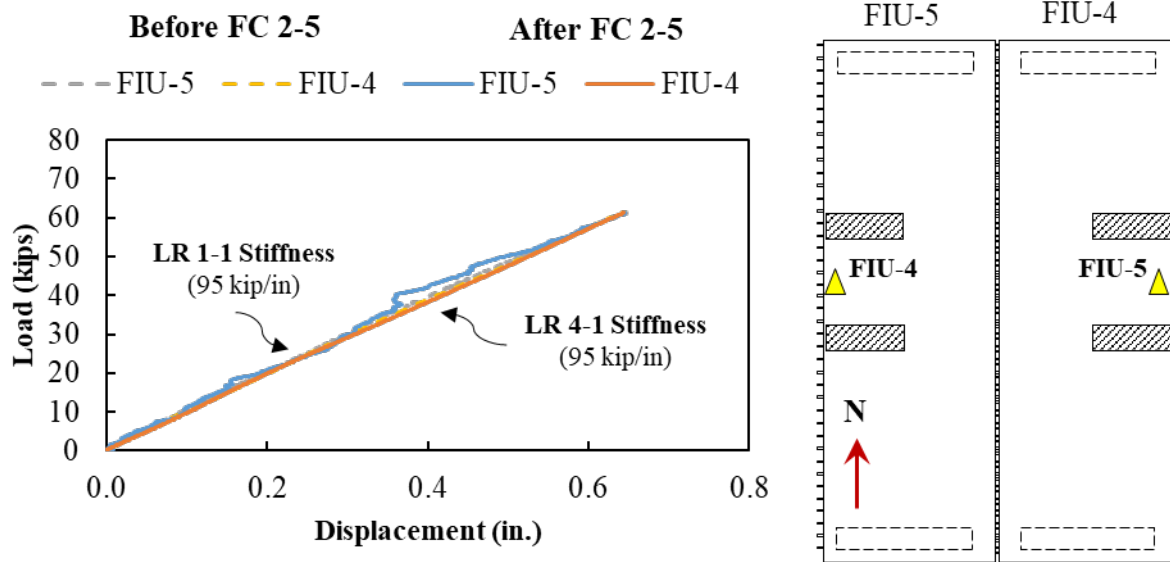


Figure 7.56: Load versus midspan displacement load testing with Load Configuration 2-4 before (LR 1-1 dashed) and after (LR 4-1 solid) Fatigue Configuration 2-5

The load-deflection response remained linear throughout all the service tests. There was a minimal differential deflection between the two beams (varying between one and two percent during testing) in both load ramps before and after fatigue assessment, suggesting that the load was applied relatively equally on the two beams. There was no decrease in system stiffness between the service tests performed before and after cyclic loading; the flexural stiffness obtained from LR 1-1 was 95 kip/in and from LR 4-1 was 95 kip/in. The flexural stiffness of the system was obtained using Equation 7-10.

$$K_{flex} = \frac{\Delta_{load}}{\Delta_{disp}} = \frac{61.4 \text{ kip} - 0.00 \text{ kip}}{0.64 \text{ in.} - 0.00 \text{ in.}} = 95.2 \text{ kip/in} \quad \text{Equation 7-10}$$

The normalized stiffnesses during the cyclic assessment for west and east actuators and the average response of the system are plotted in Figure 7.58. The stiffness was normalized based on the initial stiffness of the system at the beginning of each fatigue test. After two million cycles, there was no noticeable drop in stiffness in any of the two LDTs, which would also suggest that there was no degradation in the overall strength of the two-beam system.

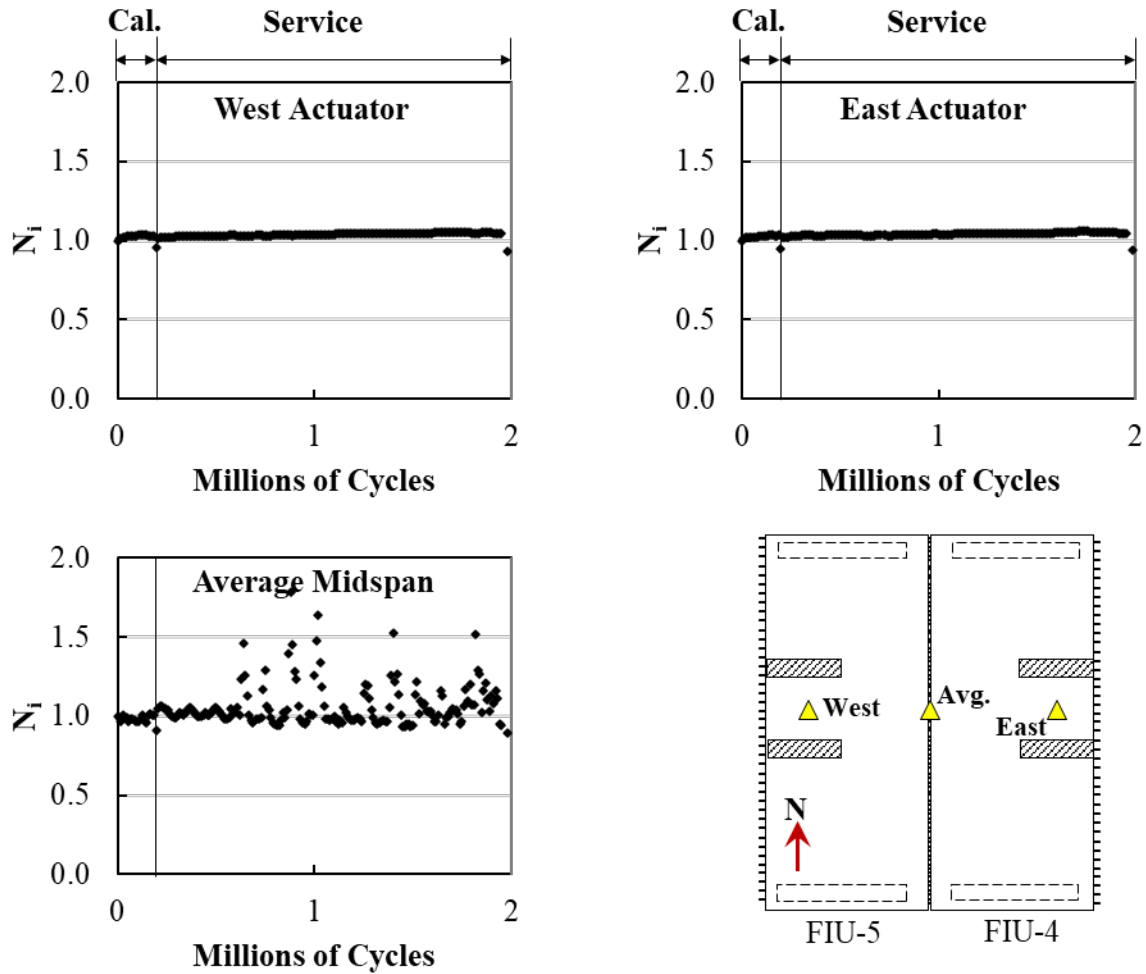


Figure 7.57: Normalized stiffnesses at midspan for west and east actuators and for the average midspan response

7.7.3.2. Joint Behavior

Crack displacement gauges (CDTs) placed across the joint, rebar strain gauges (RSGs) on the joint reinforcement, and concrete strain gauges (CSGs) placed in the transverse direction were used along the length of the system to monitor the performance of the joint during testing. The approximate cracking strain of the conventional concrete in the precast section was found using AASHTO LRFD [78], like FIU-1/2, and is included in figures throughout the FIU-4/5 section.

The load versus average strain responses for the top of the joint measured by the CDTs for FIU-4/5 and FIU-1/2 are shown in Figure 7.59. Transverse strains in the joint remained linear throughout the Stage 1 and 4 service testing of FIU-4/5 with slightly smaller strains than observed during similar testing of FIU-1/2.

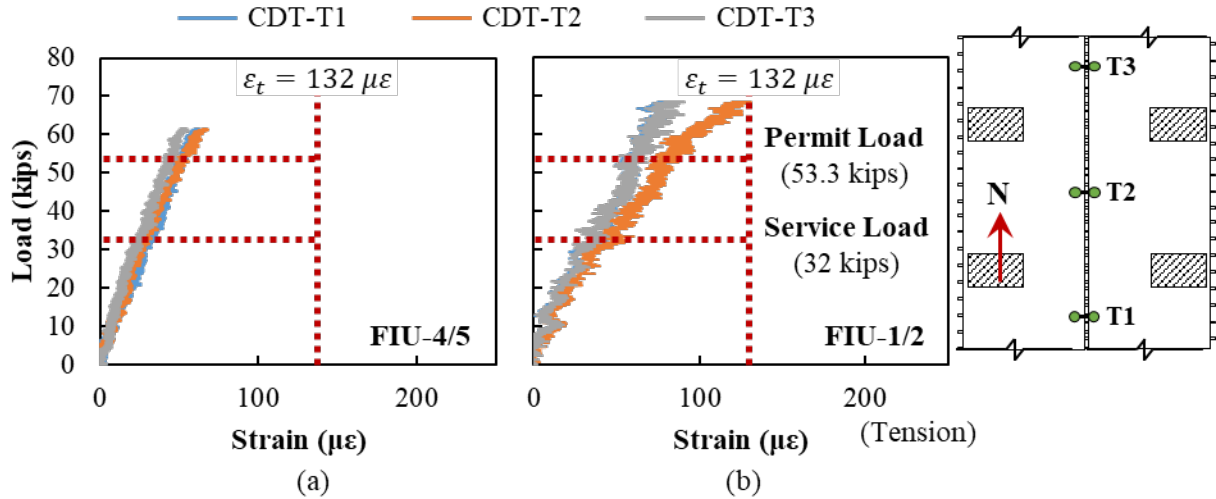


Figure 7.58: Load versus average strain across top of joint for permit load testing with LC 2-4 for (a) FIU-4/5 (LR 4-1) and (b) FIU-1/2

The load versus average strain responses for the bottom of the joint measured by CDTs for FIU-4/5 and FIU-1/2 are shown in Figure 7.60. The joint in FIU-4/5 experienced transverse compression across the bottom of the joint along the length of the system with the largest compressive strain at midspan (CDT-B3), shown in Figure 7.60 (a), which would be consistent with transverse flexural stresses developing (tension on top and compression on bottom). This bottom behavior differs from what was observed in the first service test assessed to FIU-1/2 (see Figure 7.60 (b)), where the bottom CDTs measured tensile strains.

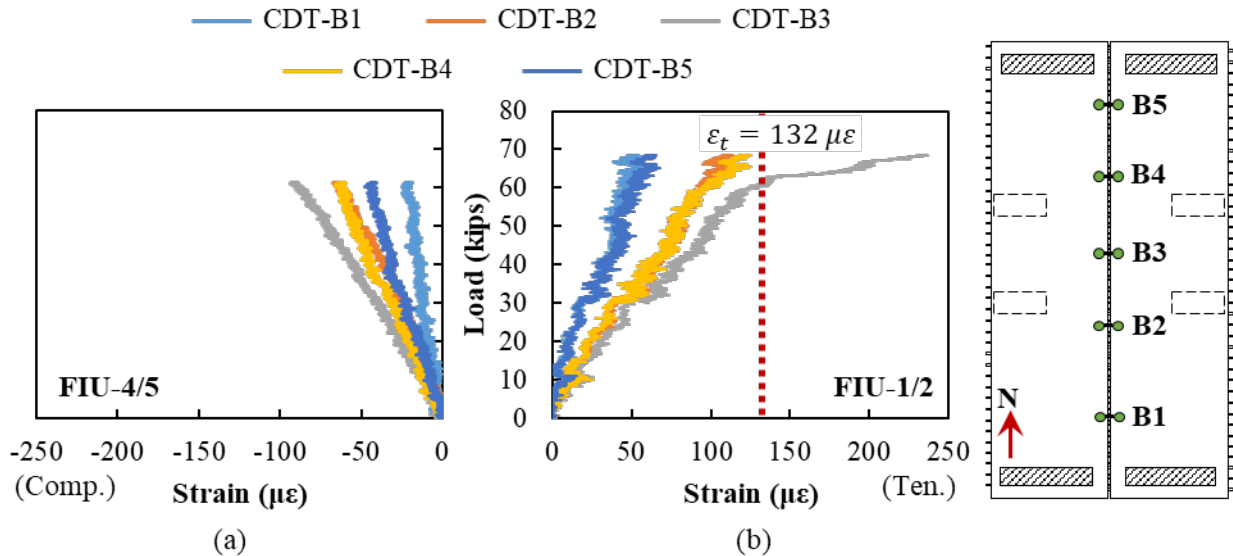


Figure 7.59: Load versus average strain across bottom of joint for permit load testing with LC 2-4 for (a) FIU-4/5 (LR 4-1) and (b) FIU-1/2

The load versus transverse concrete strain responses from LC 2-4 for FIU-4/5 (LR 4-1) and FIU-1/2 are shown in Figure 7.61. Transverse tensile strains developed on the top of the section and transverse compression strains on the bottom of the section for both systems. For FIU-4/5, a linear response was observed in the transverse gauges on the top and bottom of the system with no signs of cracking in the precast section at all load levels. The signs for the CDTs in FIU-4/5 were consistent with the transverse CSGs that were in the precast section. CSG-B18 in FIU-1/2 saw a jump in compression strain at approximately 60 kips; this occurred at the same time as a jump in tension strain occurred in CDT-B3, which may be a sign of some type of cracking developing in the joint at this load. Both systems had similar CSG readings at similar load levels, but the CDT readings (specifically on the bottom of the joint) were completely different. It is unclear why there was a difference in behavior between the two sets of beams, but the results from FIU-4/5 are more understandable as the CDTs and CSGs show transverse compression across the bottom of the width of the specimens.

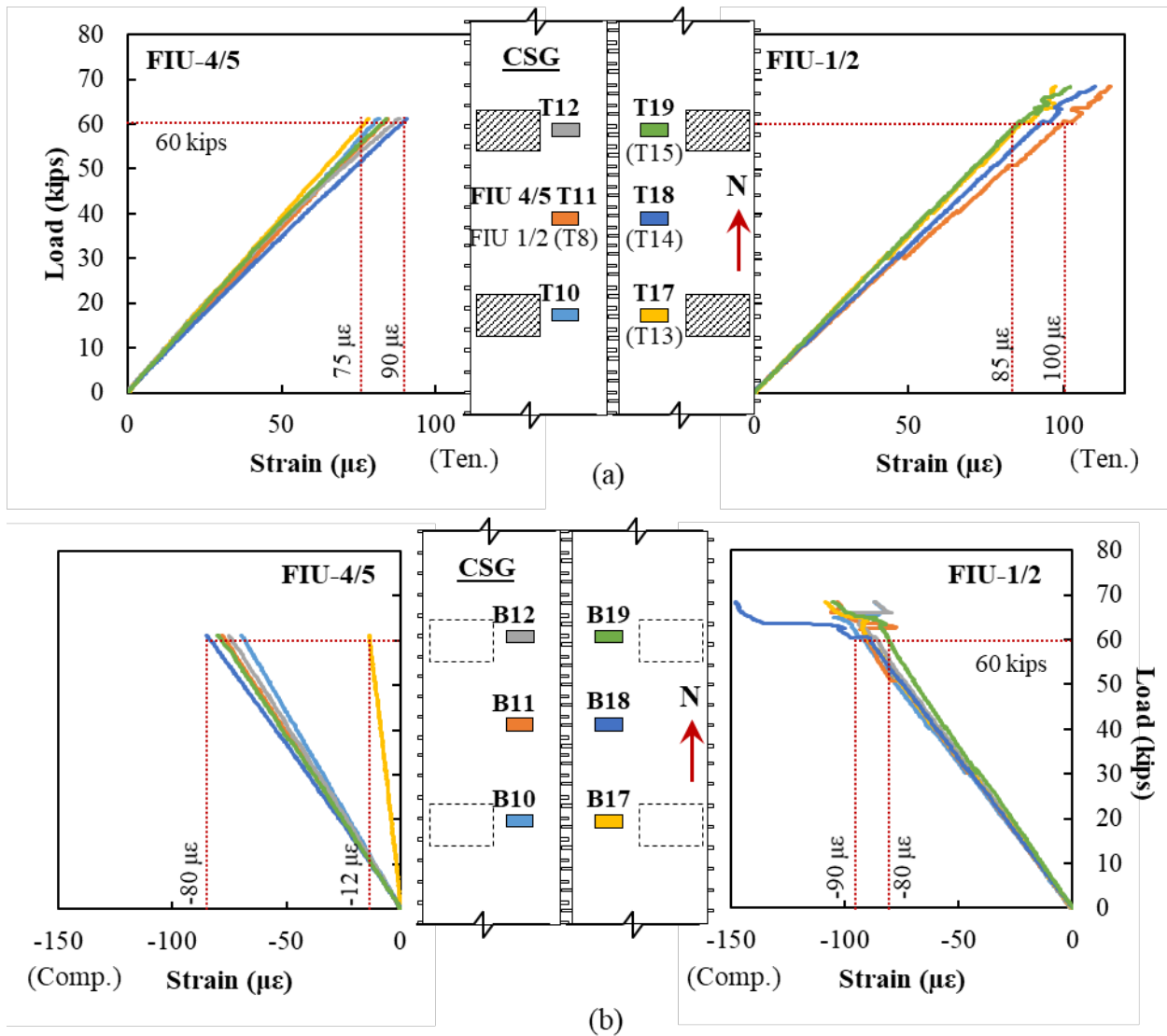


Figure 7.60: Load versus transverse concrete strain for permit load testing with LC 2-4 for FIU 1/2 and FIU 4/5 (LR 4-1) for (a) top and (b) bottom of beam in the midspan section of the system

The measured response during LR 4-1 in FIU-4/5 for the RSGs on the joint reinforcement extending from FIU-5 in the midspan and south sections of the system is shown in Figure 7.62 along with those extending from FIU-1 from testing of FIU-1/2. All joint reinforcement had minor compression strains during testing as the load configuration generated transverse compressive force at the rebar level. The compression strains measured at 60 kips at midspan ranged from below 5 microstrains to about 18 microstrains, as shown in Figure 7.62 (a), opposed to the FIU-1/2 service test strains ranging from 12 to 32 microstrains in compression for the same load level. Some minor tensile strains developed in the reinforcement near the supports in the system with FIU-4/5.

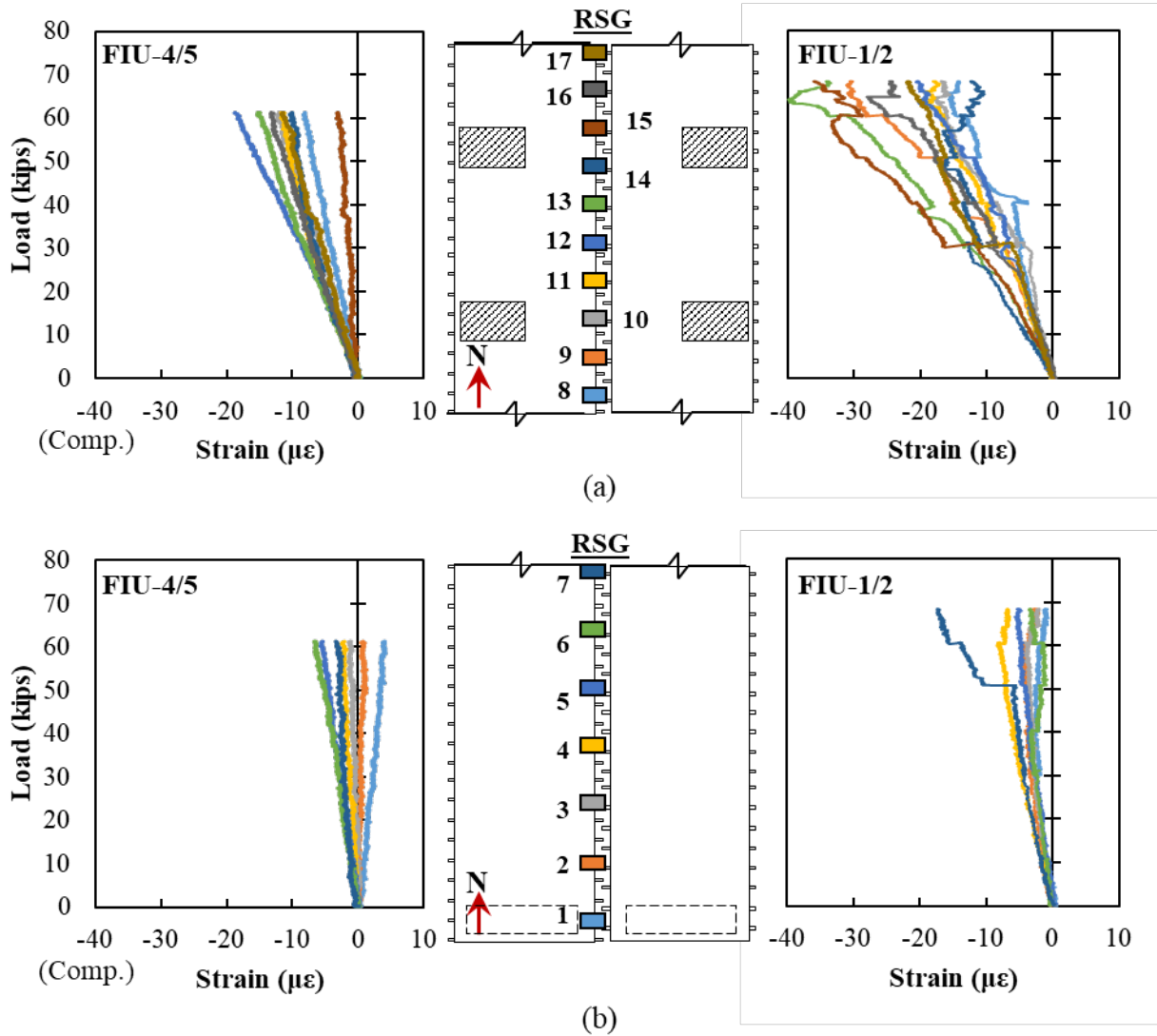


Figure 7.61: Load versus strain for permit load testing with LC 2-4 for joint reinforcement in FIU 4/5 (LR 4-1) and FIU 1/2 for the (a) midspan and (b) south sections of the systems

The strain change per change in load for the CDTs on top of the specimens in the center region are shown in Figure 7.63. After two million load cycles were assessed, the joint showed no signal of debonding or distress along the joint-to-precast boundary region, indicating that under normal service conditions, the joint boundary strength was satisfactory.

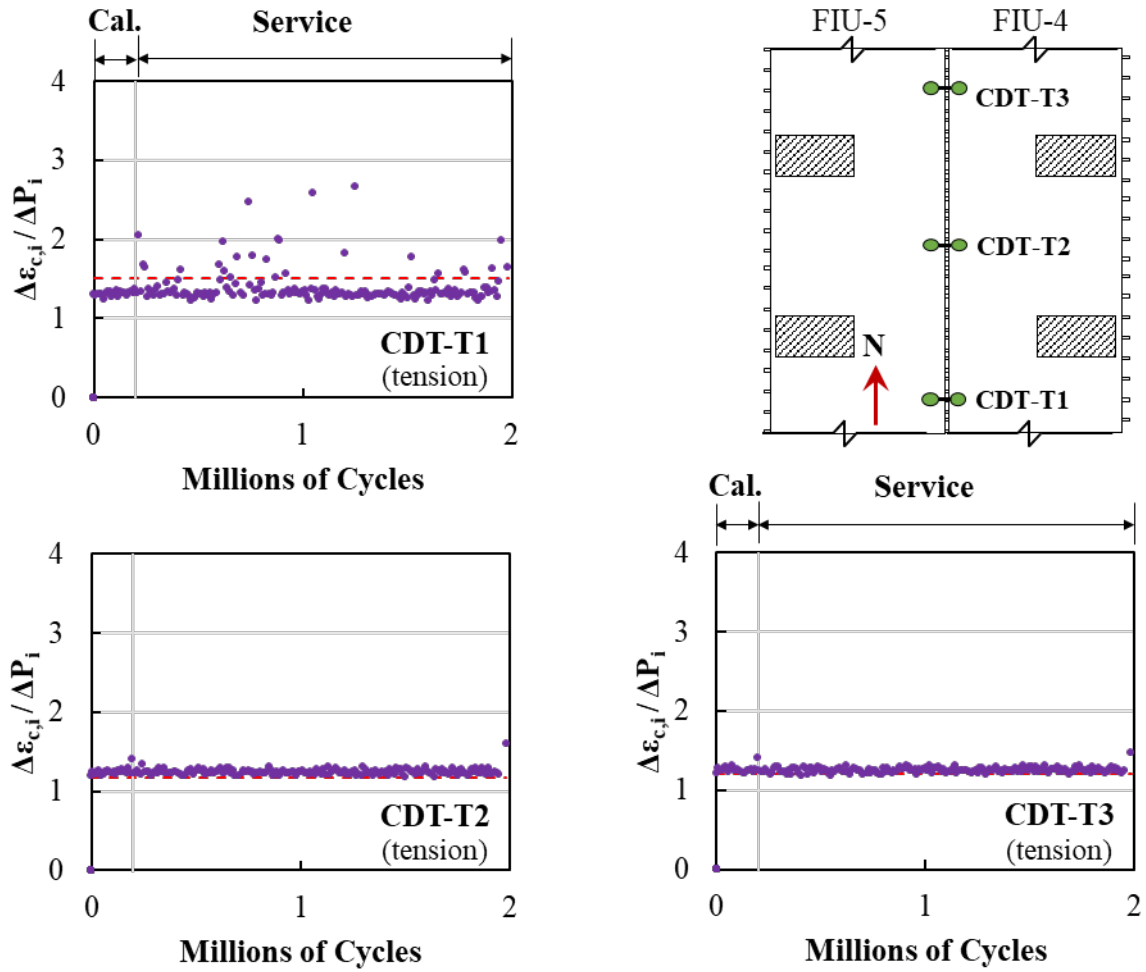


Figure 7.62: Strain change per change in load versus cyclic load for top CDTs in Stage 2/3

The strain change per change in load for CDTs on the bottom of the joint are shown in Figure 7.64. Like the top CDTs, there was no significant increase or decrease in the response of the bottom CDTs.

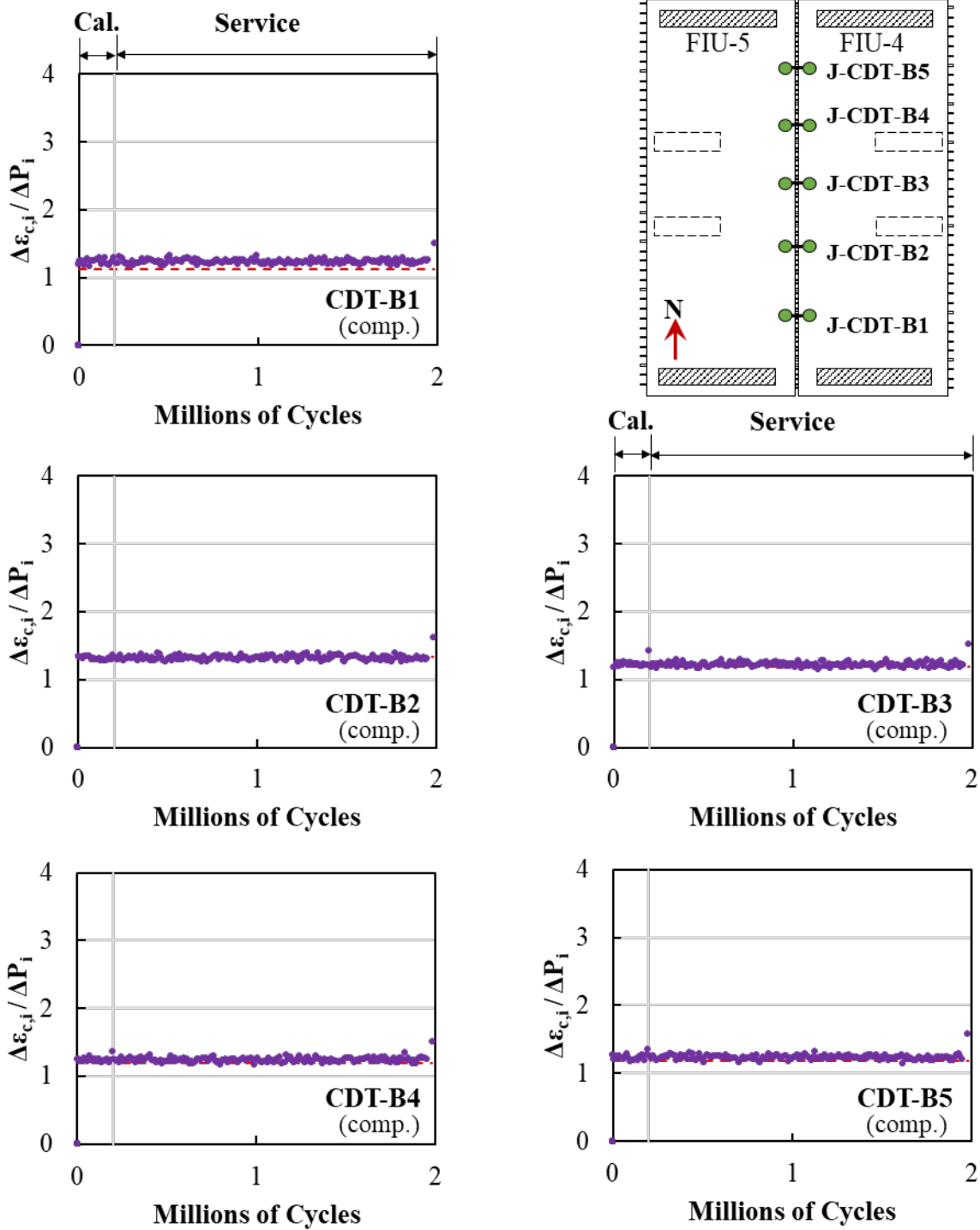


Figure 7.63: Strain change per change in load versus cyclic load for bottom CDTs in Stage 2/3

The measured response from two top transverse concrete strain gauges (CSGs) at midspan are shown in Figure 7.65. The two sensors shown had the largest tensile demand out of the transverse CSGs from this test. There was no significant increase or decrease in their respective strain changes

per maximum applied load. This would suggest that the service fatigue loading would not lead to eventual tensile cracking of the specimen.

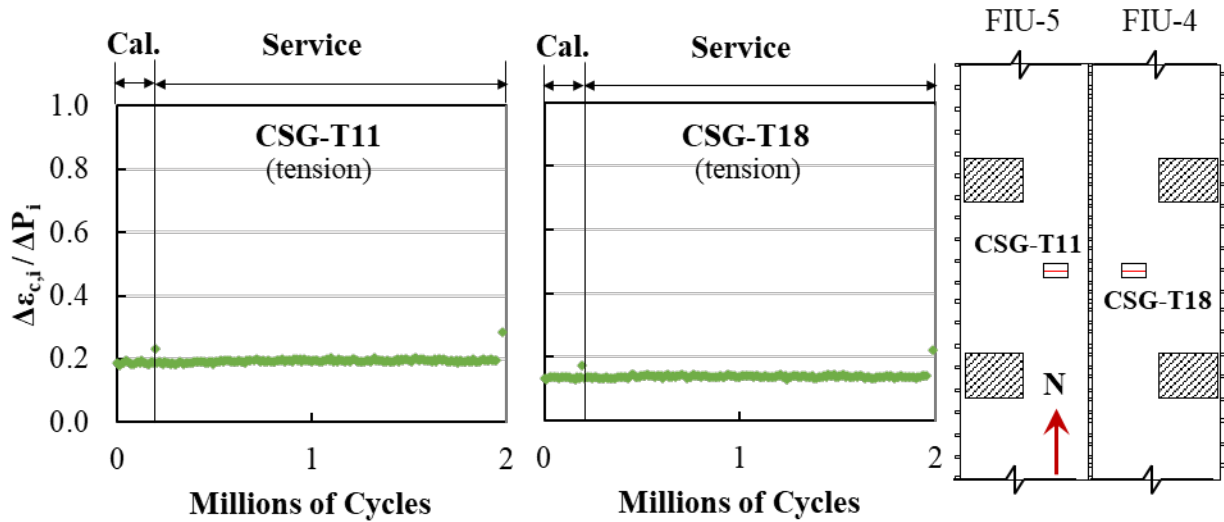


Figure 7.64: Strain change of top transverse CSGs per change in load at center of specimen in Stage 2/3

The measured response from two bottom transverse CSGs are shown in Figure 7.66. There was no apparent change in the response of the transverse CSGs on the bottom of the specimens, suggesting that the behavior was not negatively affected by the fatigue loading during this stage.

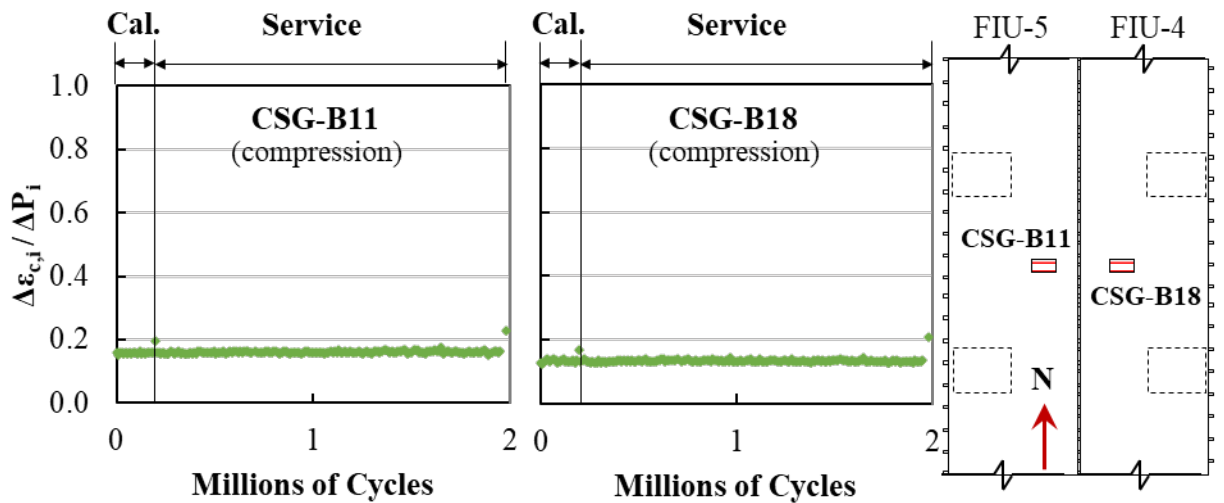


Figure 7.65: Strain change of bottom transverse CSGs per change in load at center of specimen in Stage 2/3

The measured response from three rebar strain gauges (RSGs) located on the west center side is shown in Figure 7.67. The joint reinforcement was not significantly engaged during this service load testing. The fatigue response or the joint reinforcement was like the static response and did not show any change in response during this fatigue loading stage.

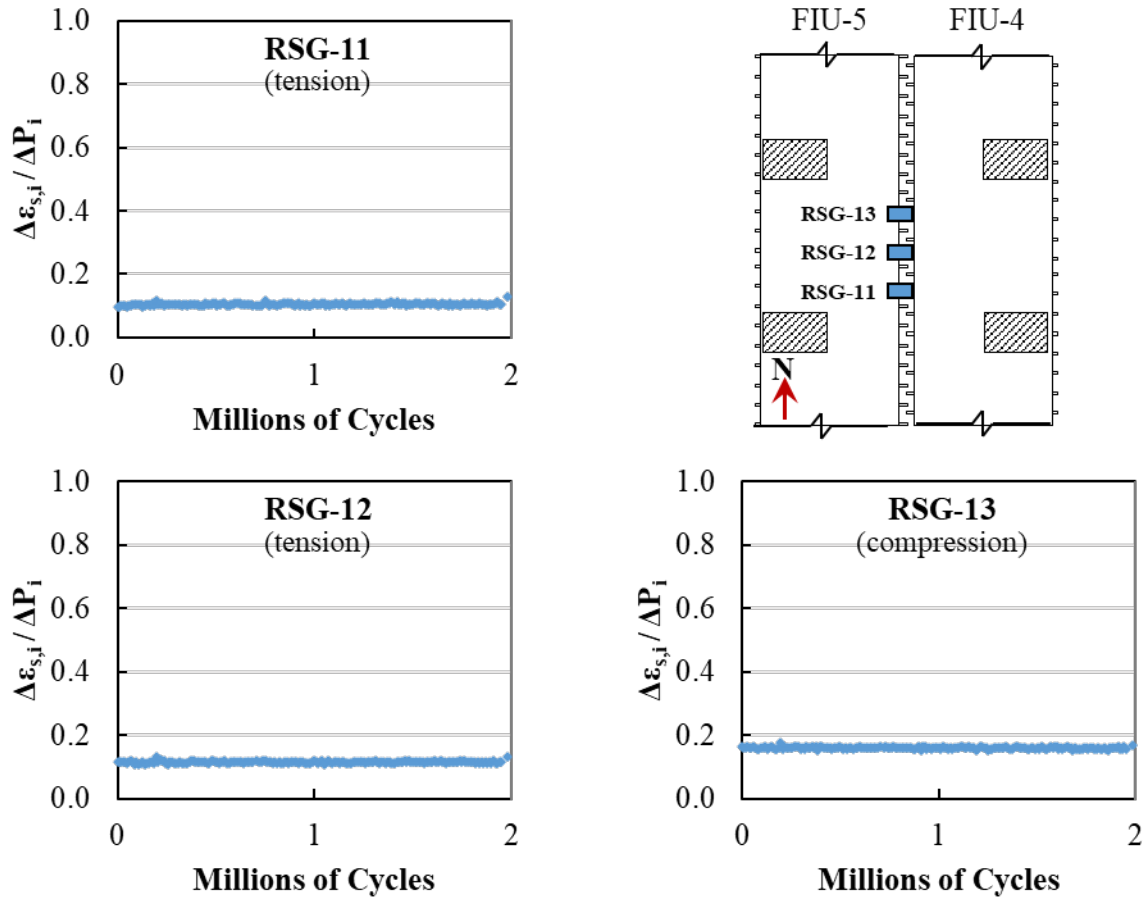


Figure 7.66: Maximum strain of RSGs per applied load versus cyclic load at center of specimen

7.7.3.3. Longitudinal Behavior

The measured responses of the longitudinal CSGs on the top and bottom of the specimens near midspan are shown in Figure 7.68. Longitudinal compressive strains developed on the top of the section and longitudinal tensile strains on the bottom of the section, as shown in Figure 7.68 (a) and Figure 7.68 (b), respectively. A linear response was observed in the longitudinal gauges on both the top and bottom of the system with no signs of change in load-strain slopes at 60 kips. This is like what occurred during testing of FIU-1/2 where there was a linear response to 60 kips; the response in FIU-1/2 then became non-linear after approximately 60 kips due to transverse cracks developing.

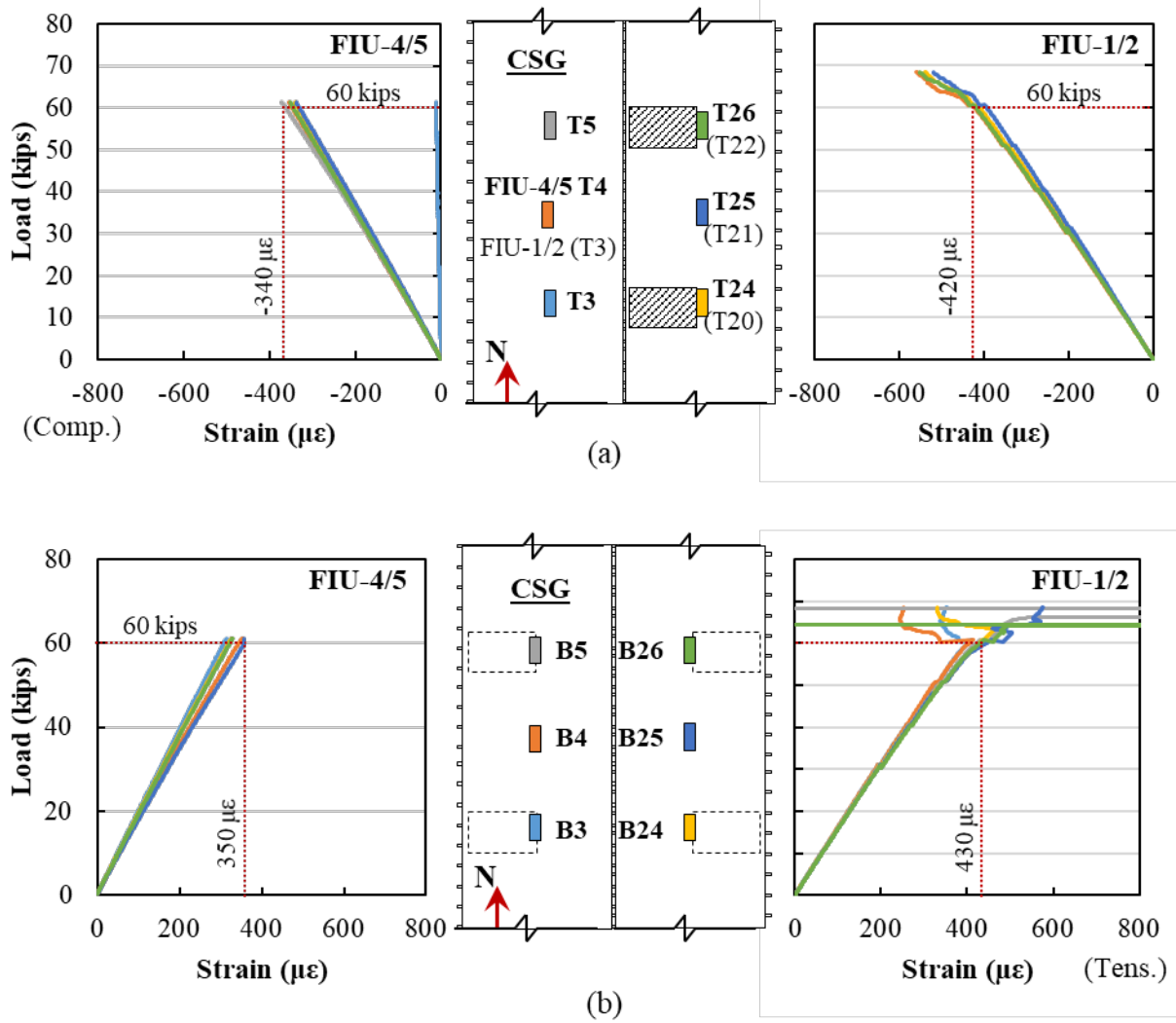


Figure 7.67: Load versus longitudinal concrete strain for permit load testing with LC 2-4 for FIU-4/5 (LR 4-1) and FIU-1/2 for (a) top and (b) bottom of beam in the midspan section of the system

The strain change per change in load for two of the longitudinal CSGs on top of the beams is shown in Figure 7.69. Both gauges were in compression throughout the testing and showed no change in behavior due to the fatigue loading. CSG-T25 had a slightly higher strain change, which is consistent with the slightly higher strain observed in this gauge during the service static load testing.

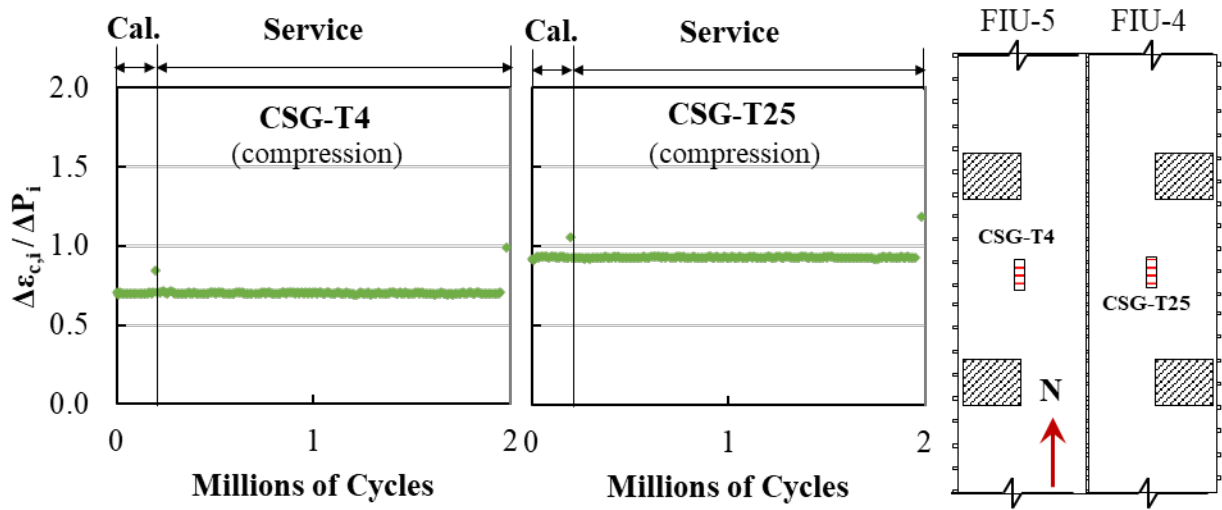


Figure 7.68: Strain change of top longitudinal CSGs per change in load versus cyclic load at center of specimen

The strain change per change in load for two of the longitudinal CSGs on the bottom of the beams is shown in Figure 7.70. Both gauges were in tension throughout the testing and showed no change in behavior due to the fatigue loading. CSG-B25 had a slightly higher strain change, which is consistent with the slightly higher strain observed in this gauge during the service static load testing.

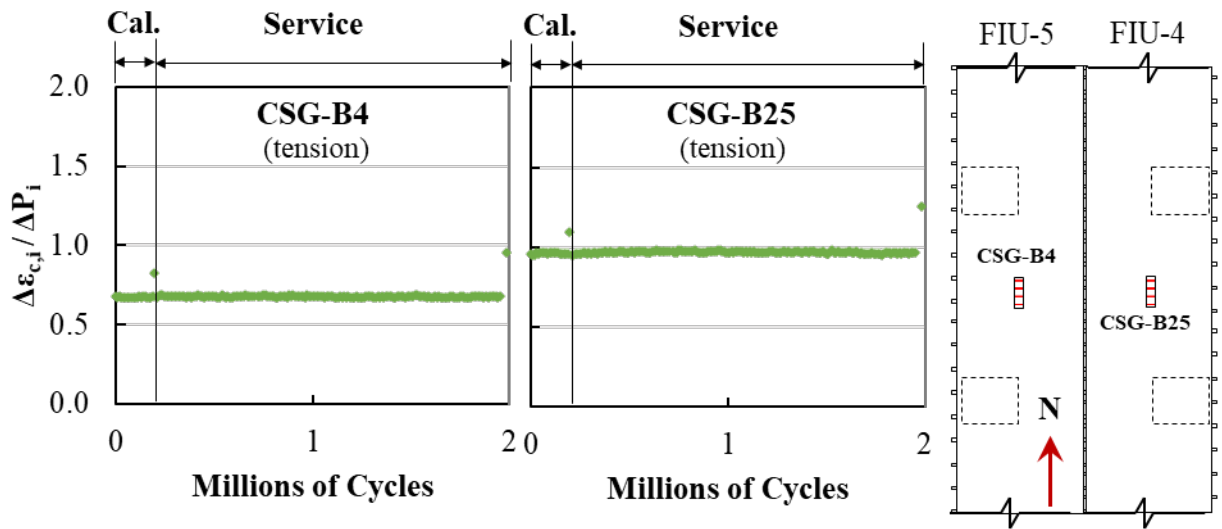


Figure 7.69: Strain change of bottom longitudinal CSGs per change in load versus cyclic load at center of specimen

7.7.3.4. Summary

Service load tests were conducted using LC 2-4 before and after two million cycles of FC 2-5 were applied to the system. There was no observed distress in either concrete or joint reinforcement,

indicating satisfactory performance of the complete precast-joint system under normal service conditions.

There was a difference in transverse behavior of the bottom of the joint between FIU-4/5 and FIU-1/2. Transverse tension was measured across the entire top of the FIU-4/5 system (precast beams and joint) and transverse compression across the entire bottom of the FIU-4/5 system and in the joint reinforcement; this is consistent with flexural stresses developing from transverse bending of the system. FIU-1/2 also showed signs of transverse tension across the entire top of the system, but the bottom of the system experienced transverse compression in the beams and joint reinforcement and tension across the bottom of the joint. The measured response of the bottom CDTs in FIU-4/5 would further suggest that the polarity was reversed in the bottom CDTs for FIU-1/2.

The FIU-4/5 and FIU-1/2 systems showed similar behavior under LC 2-4, other than the bottom CDTs.

7.7.4. Restrained Service Test Results (Stages 5-8, FC 2-6)

7.7.4.1. Overview

The restrained service test assessed a simply supported, stiffened (one beam) span condition (FC 2-6). The intermediate restraint was achieved with two bearing pads on top of two load blocks, as shown in Figure 7.71 (a). Additional shim plates were added between the block and the bearing pads to successfully achieve bearing between the precast section and interior supports during testing, as shown in Figure 7.71 (b).

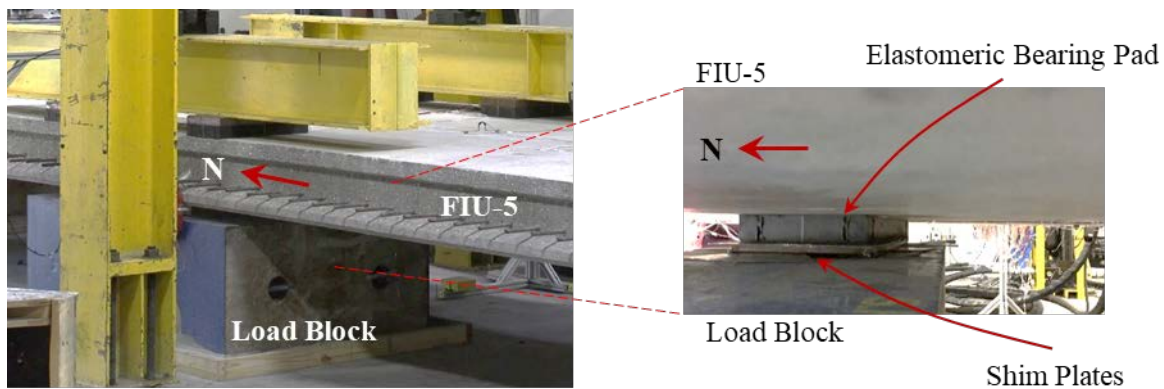


Figure 7.70: Intermediate support detail underneath FIU-5 at center region

Four load stages were performed during the restrained service testing. Stage 5 simulated four static HS-20 rear-axle service load ramps in the elastic range applied with FC 2-6. However, during the first two ramps (LR 5-1 and LR 5-2), the system was not bearing against the intermediate support; this was corrected by adding shim plates. Two additional ramps were assessed (LR 5-3 and LR 5-4) to ensure that the beams were bearing against the center supports during testing, shown in Figure 7.72.

Stage 6 and Stage 7 consisted of the application of two million HS20-rear-axle truck cycles applied using FC 2-6, which applied a cyclic load on the unrestrained beam while maintaining an

approximate 5-kip load on the restrained side. Two additional static HS-20 rear-axle load ramps in the elastic range were applied in Stage 8 (LR 8-1 and LR 8-2), using the same load condition as Stage 5 shown in Figure 7.72.

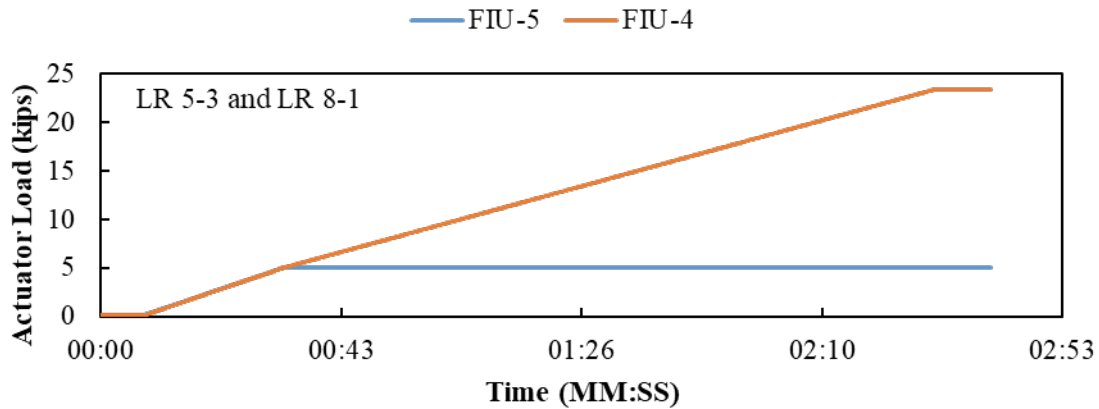


Figure 7.71: Load per actuator versus time for LR 5-3 and LR 8-1

The results from the static testing performed in Stage 4 (LR 4-1 with LC 2-4) are compared with the static response measured using FC 2-6 (LR 8-1) to see the effect of the interior supports on system and joint performance.

The load versus deflection response for the system using FC 2-6 before (LR 5-3) and after (LR 8-1) two million load cycles is shown in Figure 7.73. The deflections shown account for the settlement of the supports.

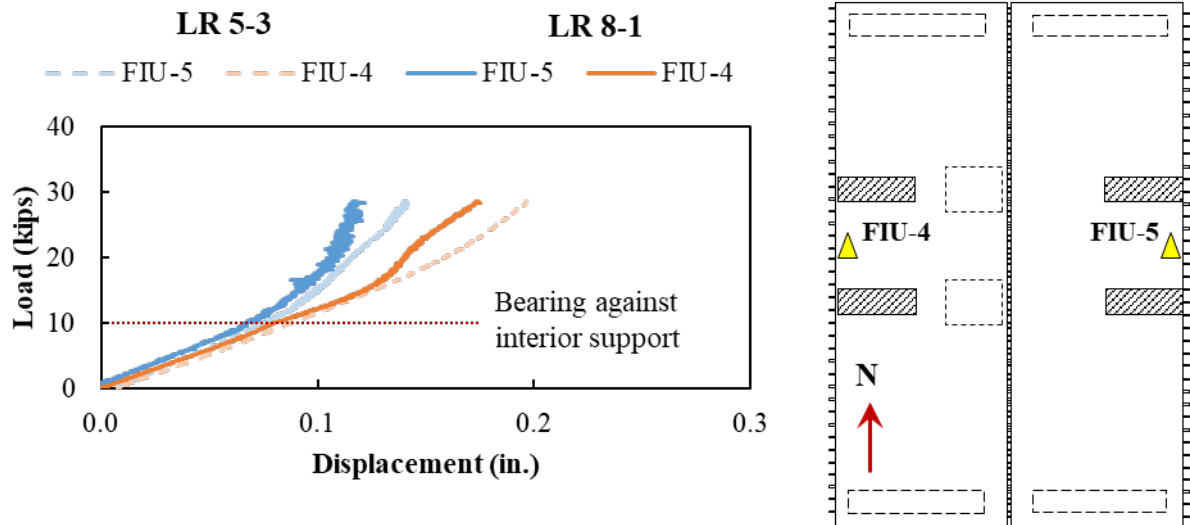


Figure 7.72: Load versus midspan displacement load testing with Load Configuration 2-6 before (LR 5-3 dashed) and after (LR 8-1 solid) Fatigue Configuration 2-6

The system performed similarly before and after fatigue testing from FC 2-6 up until bearing against the interior support (at approximately 10 kips). At this point the system showed a slightly stiffer response after fatigue testing (LR 8-1) compared to before (LR 5-3). This change in behavior

was more likely due to a slight change in load or support conditions since there was no sign of system deterioration in any of the cyclic load response plots.

There was a differential deflection between the two beams as FIU-5 was bearing against the restraints underneath at center region after approximately 10 kips of total applied load and since additional load after 10 kips was applied only to FIU-4. The intermediate support and uneven loading caused a differential deflection between FIU-4 and FIU-5 of about 32 percent before fatigue and 34 percent after fatigue at peak load (28.4 kips).

The normalized stiffnesses during the cyclic assessment for west and east actuators and the average system response are plotted in Figure 7.74. Although FIU-5 was restrained between the intermediate supports and a constant applied load of 5 kips, the movement of the adjacent actuator cycling over FIU-4 from 5 kips to 23.4 kips caused loading fluctuations on the fixed load, ranging from about 4 kips to 5.7 kips. This could be the reason there is more variability in the measured average system response. There was no noticeable drop in stiffness in the actuators or average system response after four million total cycles were applied in the two different fatigue load and support configurations, suggesting there was no degradation in the overall system response caused by the fatigue loading.

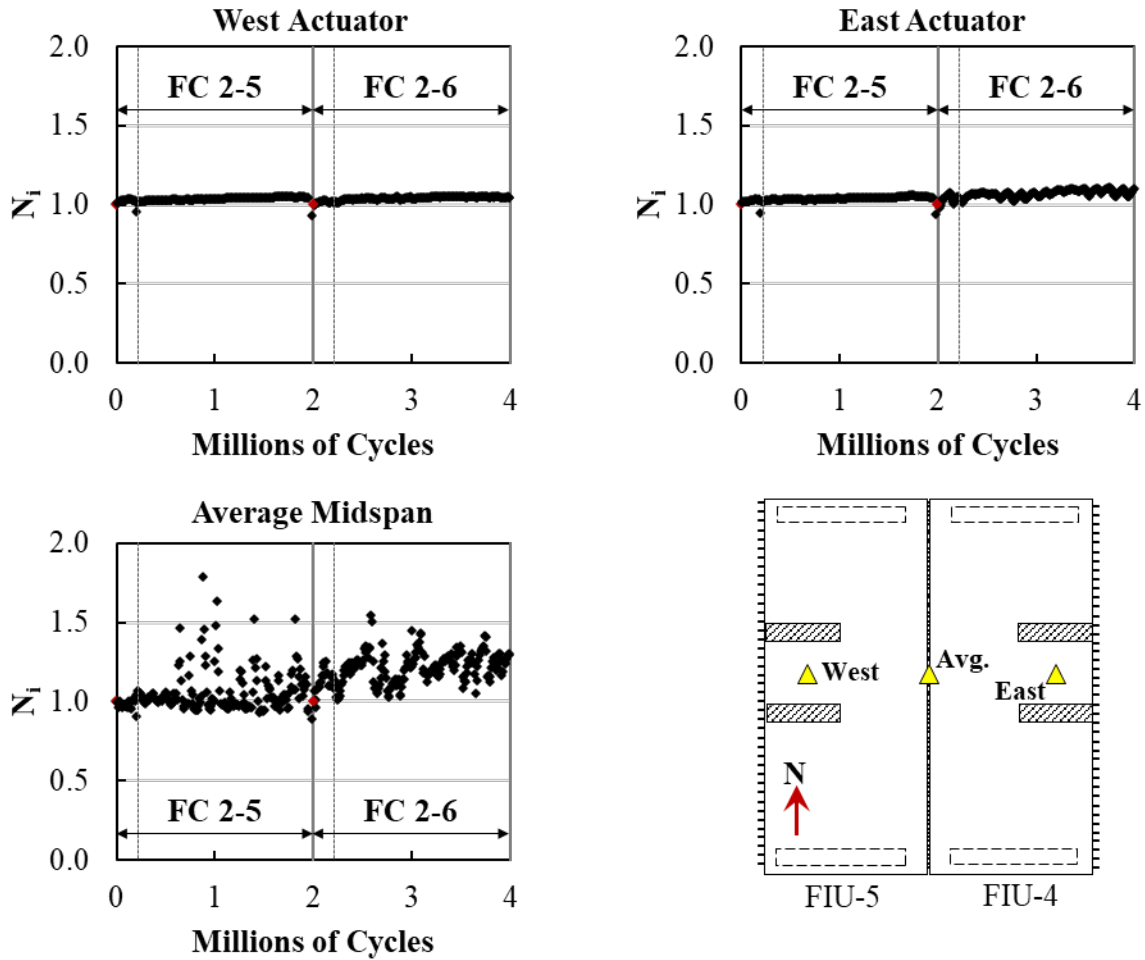


Figure 7.73: Normalized stiffnesses at midspan for west and east actuators and average system response for FC 2-5 and FC 2-6

7.7.4.2. Joint Behavior

The transverse top and bottom strains measured across the joint with CDTs during LC 2-4 and FC 2-6 are shown in Figure 7.75 and Figure 7.76. The top joint strains in FC 2-6 remained linear and in tension during the service load testing and were like those observed in LC 2-4 testing with strains well below the estimated cracking strain.

The transverse strain behavior on the bottom of the joint indicated compression strains at the center region (CDT-B2, CDT-B3, and CDT-B4) and minimal strains at the end regions (CDT-B1 and CDT-B5), as shown in Figure 7.76 (b). The strains in the end regions (CDT-B1 and CDT-B5) were smaller during the restrained test (FC 2-6) than were observed in the unrestrained test (LC 2-4).

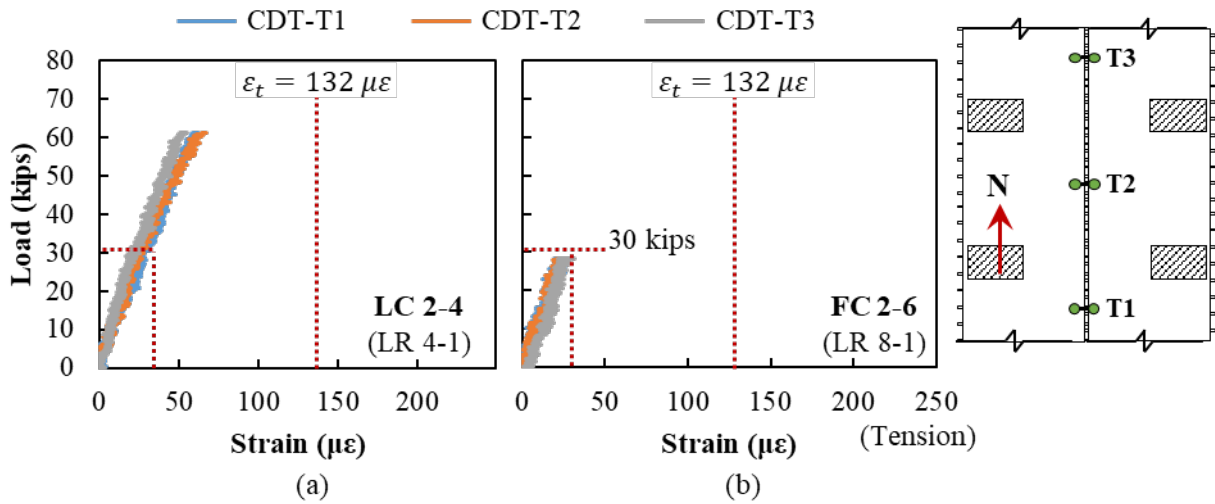


Figure 7.74: Load versus average strain across top of joint for permit load testing of FIU 4 and FIU 5 with (a) FC 2-5 (LR 4-1) and FC 2-6 (LR 8-1)

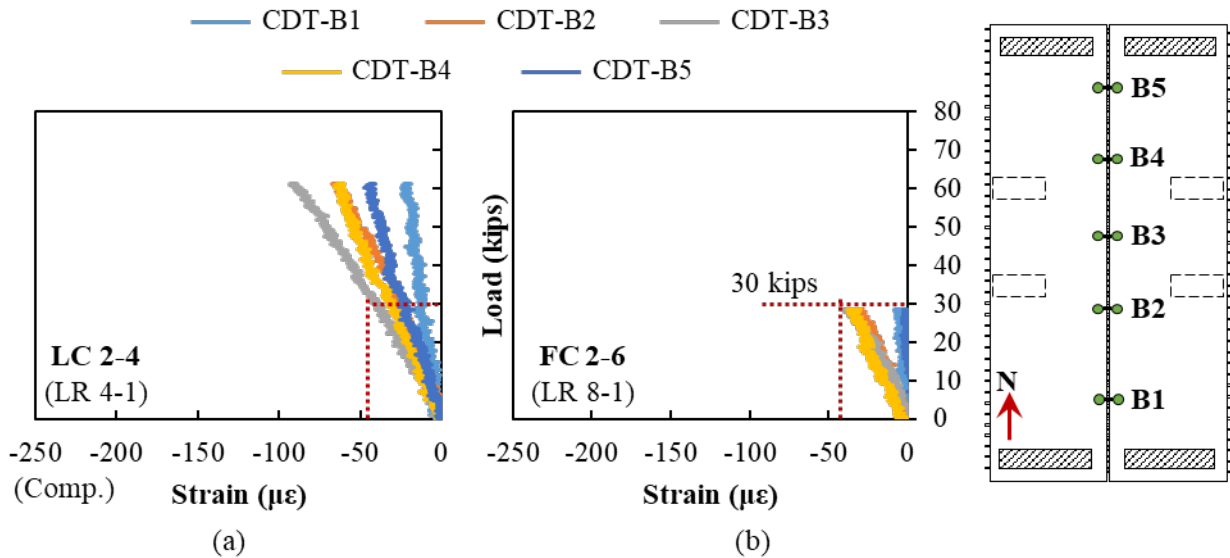


Figure 7.75: Load versus average strain across bottom of joint for permit load testing of FIU 4 and FIU 5 with (a) LC 2-4 (LR 4-1) and FC 2-6 (LR 8-1)

The measured response from the transverse CSGs for LC 2-4 (LR 4-1) and FC 2-6 (LR 8-1) are shown in Figure 7.77. Like the unrestrained test (LC 2-4), transverse tensile strains developed on the top of the section and transverse compression strains on the bottom of the section with FC 2-6. The CSGs on top of the beams responded similar during both load and support configurations up until 10 kips, which was the point when FIU-5 began to engage the intermediate supports for FC 2-6. After FIU-5 began to engage the intermediate supports, the strain in the CSGs in the restrained beam (FIU-5) continued to increase linearly while the strain in the top of the unrestrained beam (FIU-4) had a smaller increase in strain with load. Slightly smaller transverse

tension and compression strains were measured in the restrained service test (FC 2-6) compared to the unrestrained service test (LC 2-4) at similar loads.

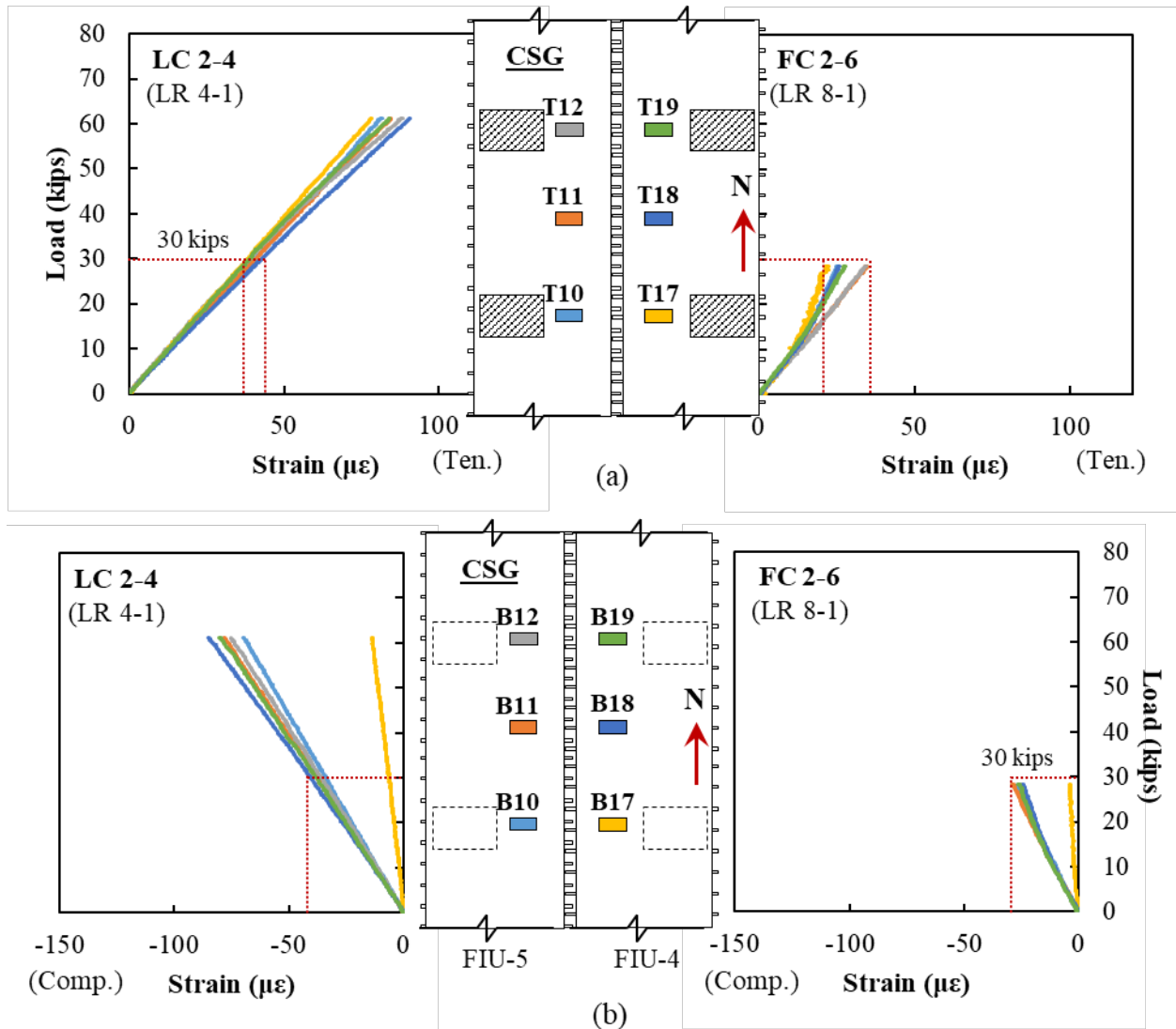


Figure 7.76: Load versus transverse concrete strain for permit load testing of FIU-4/5 with LC 2-4 (LR 4-1) and FC 2-6 (LR 8-1) for (a) top and (b) bottom of beam in the midspan section of the system

The measured response for the RSGs on the joint reinforcement extending from FIU-5 in the midspan and south sections of the system for LC 2-4 and FC 2-6 are shown in Figure 7.78. All joint reinforcement had minimal compression strains during testing as the load configuration generated transverse compressive force at rebar level. There was a similar response in the rebar between LC 2-4 and FC 2-6.

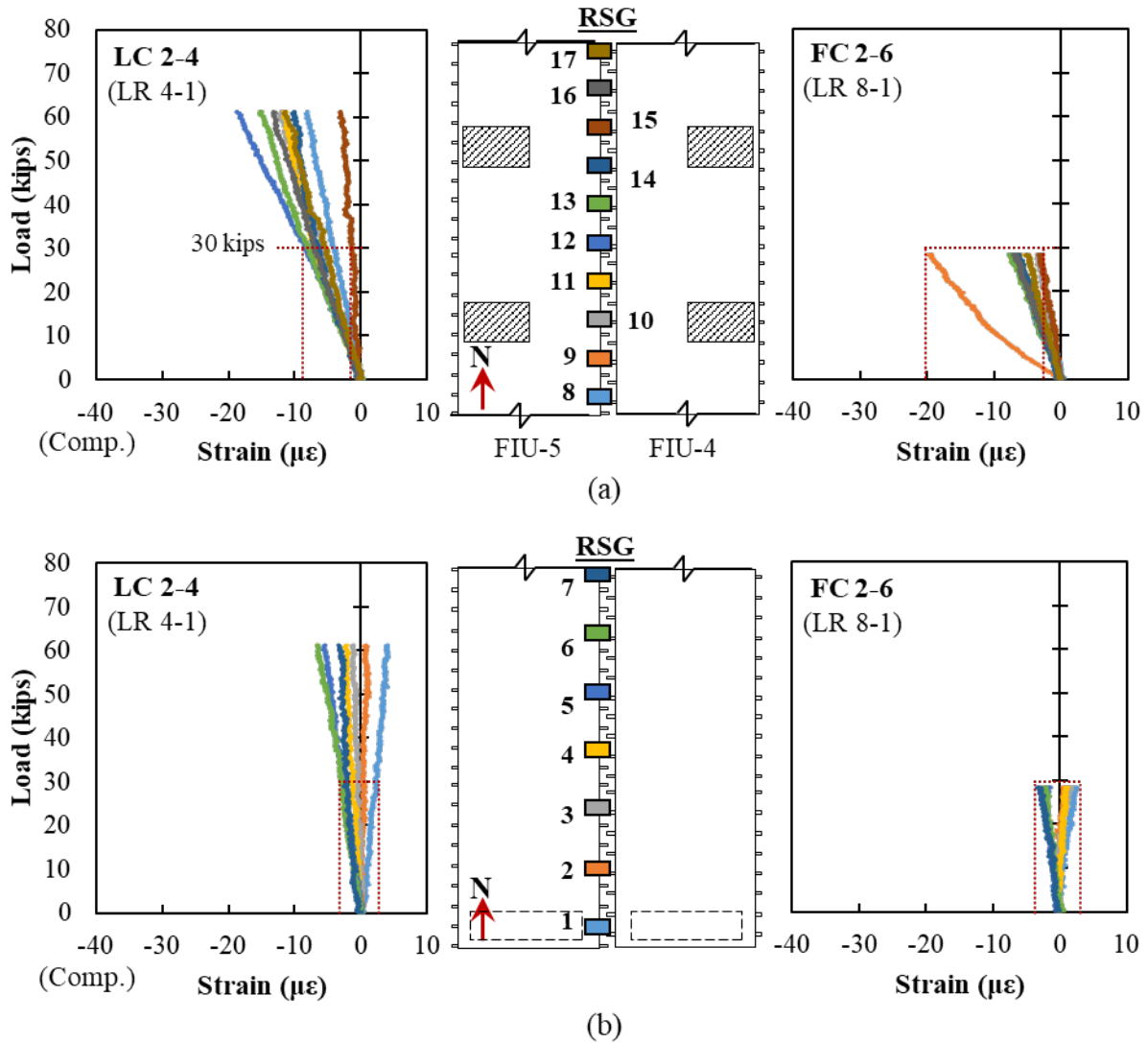


Figure 7.77: Load versus strain for permit load testing of FIU-4/5 with LC 2-4 (LR 4-1) and FC 2-6 (LR 8-1) for joint reinforcement extending from FIU-5 for the (a) midspan and (b) south sections of the system

The fatigue response of the CDTs on the top and bottom of the joint between FIU-4/5 for FC 2-5 and FC 2-6 are shown in Figure 7.79 and Figure 7.80. There was an increase in the strain change per change in applied load for the top and bottom CDTs when the intermediate support was added (FC 2-6) compared to the response with no intermediate supports (FC 2-5). There was no significant increase or decrease in the strain change per maximum applied load within the FC 2-6 fatigue test stage.

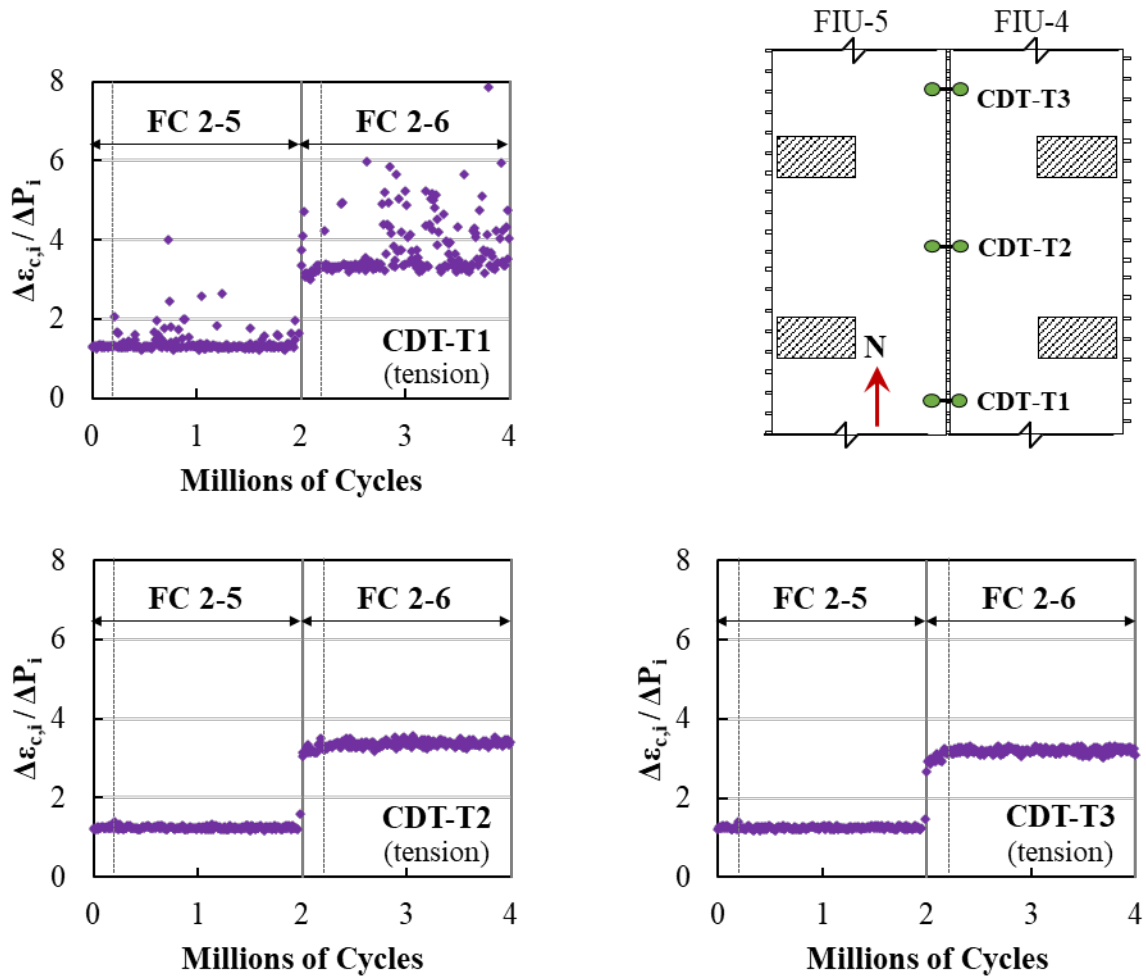


Figure 7.78: Strain change of crack gauge per change in applied load versus number of cycles for CDTs on top of joint for FC 2-5 and FC 2-6

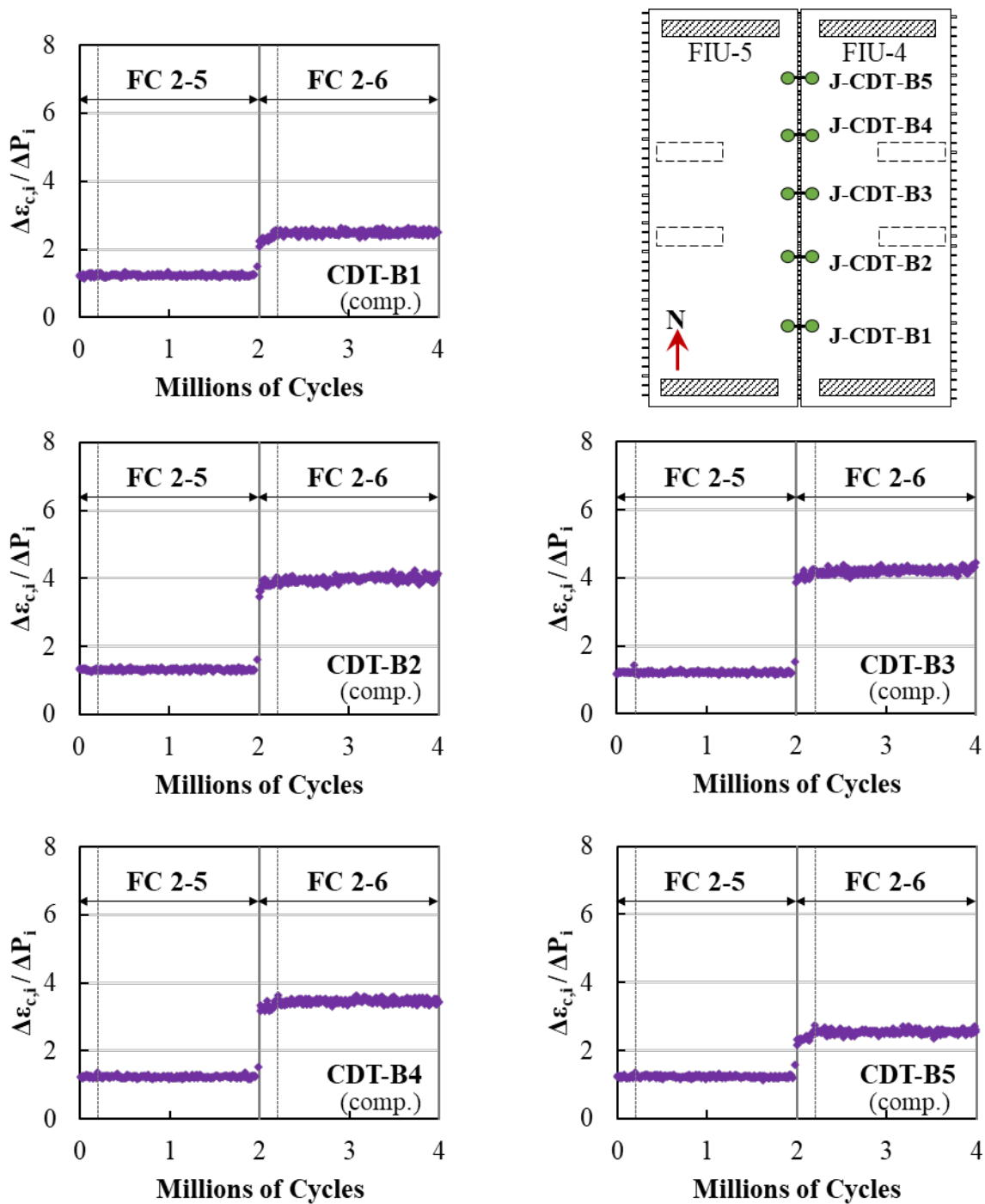


Figure 7.79: Strain change of crack gauge per change in applied load versus number of cycles for CDTs on the bottom of joint for FC 2-5 and FC 2-6

The strain change of two top and two bottom transverse CSGs at midspan over the change in load for FC 2-5 and FC 2-6 are shown in Figure 7.81 and Figure 7.82. The strain change per change in applied load increased when the intermediate supports were added (FC 2-6) compared to the

unrestrained test setup (FC 2-5). There were no significant changes in the cyclic response of these two gauges during FC 2-5 and FC 2-6.

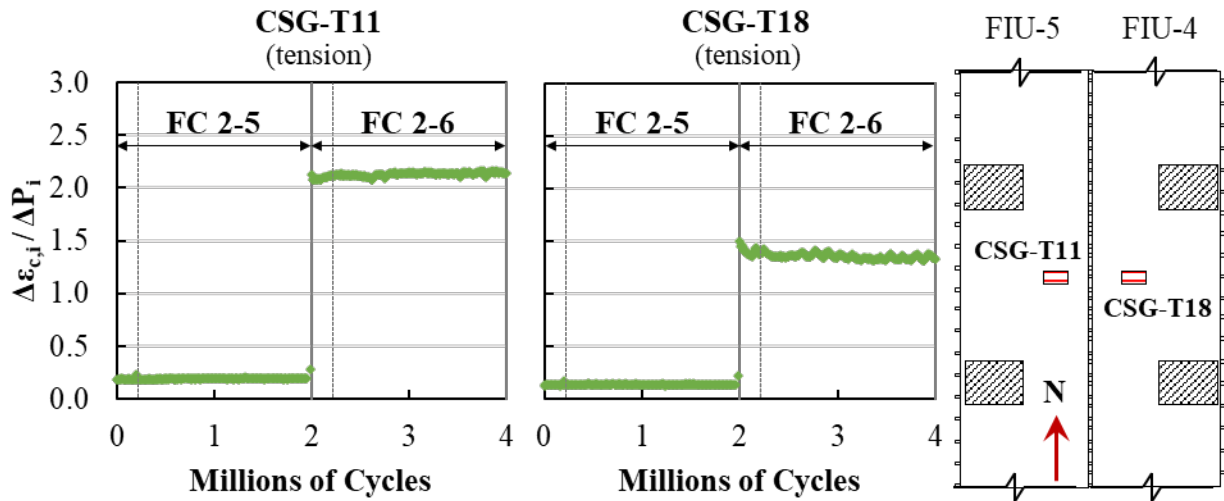


Figure 7.80: Strain change of top transverse CSGs per change in applied load versus number of cycles at center of specimen

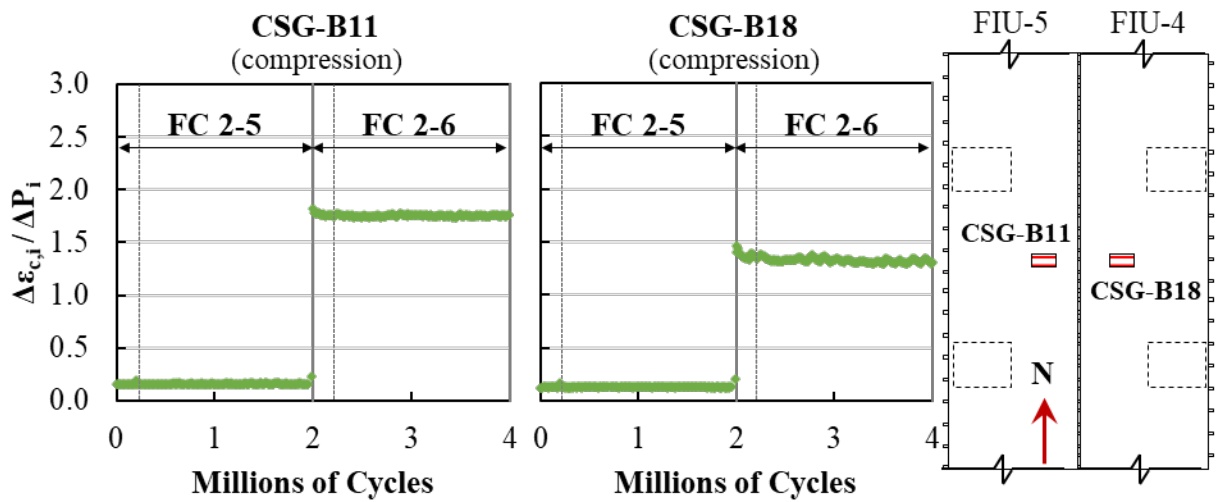


Figure 7.81: Strain change of bottom transverse CSGs per change in applied load versus number of cycles at center of specimen

The measured response from three RSGs located on the west center side is shown in Figure 7.83. There were no signs of deterioration of the bond of the joint reinforcement.

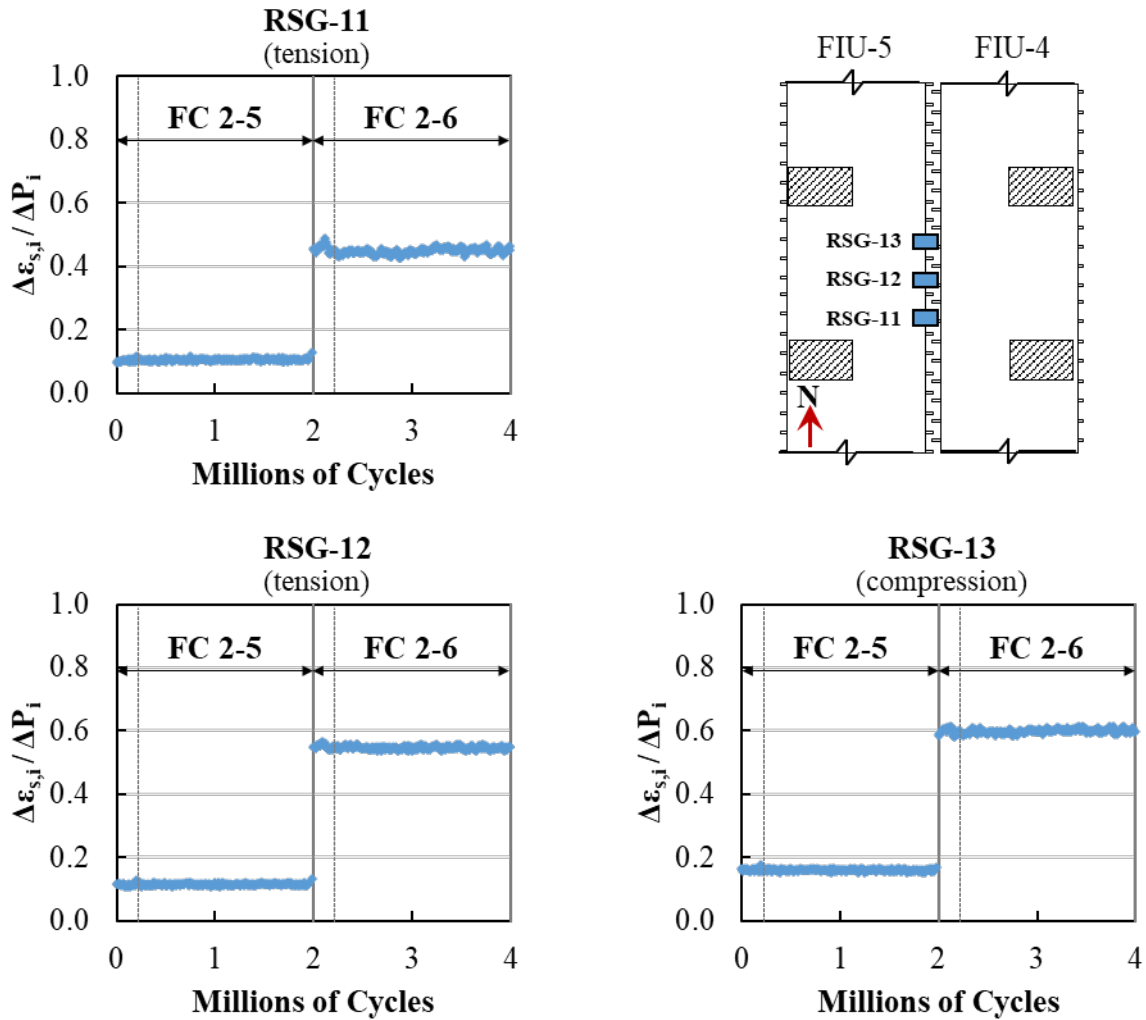


Figure 7.82: Strain change of RSGs per change in applied load versus number of cycles at center of specimen for FC 2-5 and FC 2-6

7.7.4.3. Longitudinal Behavior

The measured responses of the longitudinal CSGs on the top and bottom of FIU-4/5 near midspan under LC 2-4 and FC 2-6 are shown in Figure 7.84. Minimal longitudinal compressive strains developed on the top of the section ranging from 80 to 100 microstrains, and minimal longitudinal tensile strains on the bottom of the section ranging from 65 to 95 microstrains, as shown in Figure 7.84 (a) and Figure 7.84 (b), respectively. There was a noticeable slope change in the load-strain response for FC 2-6 after the system began to engage the intermediate supports (at approximately 10 kips).

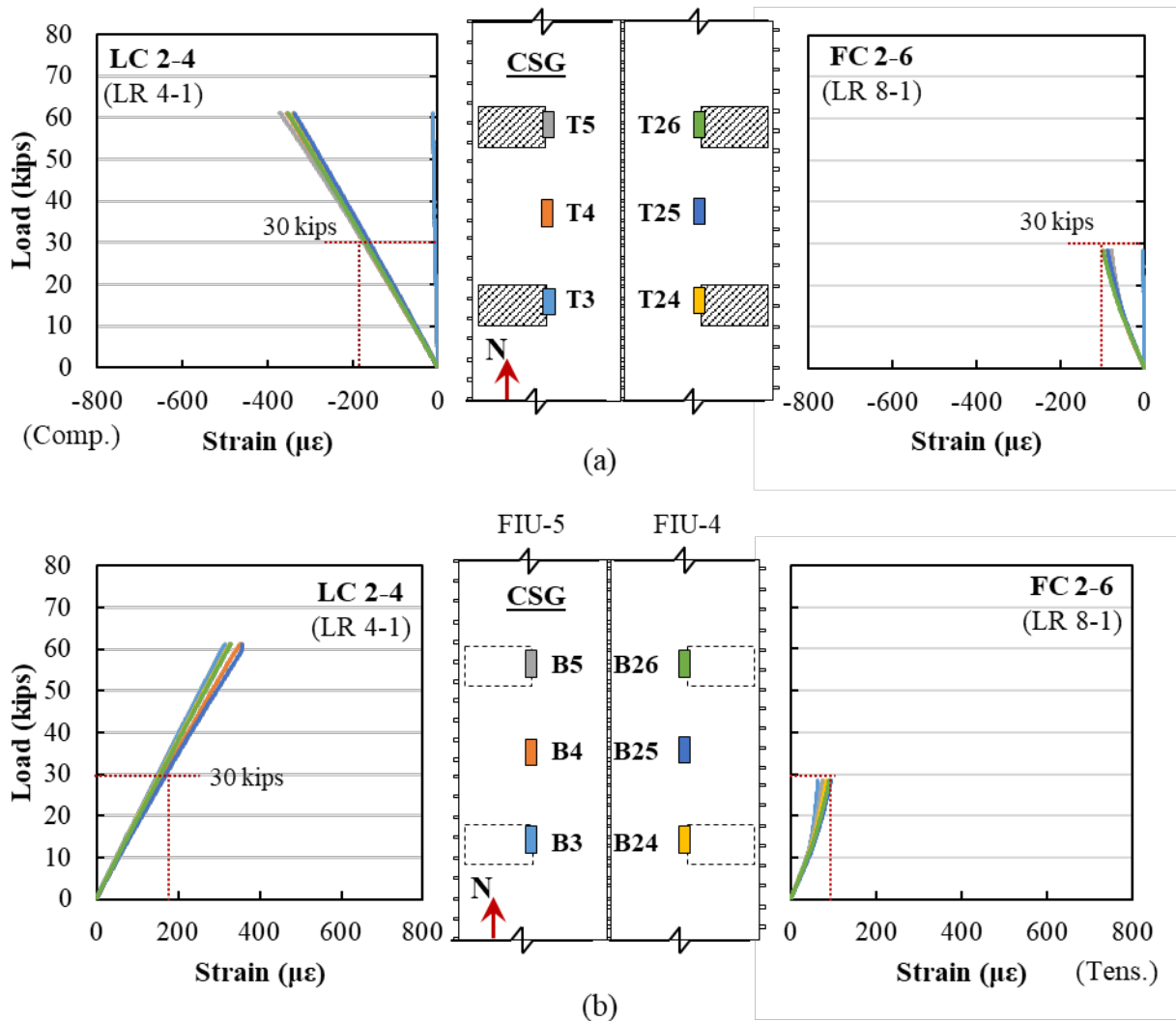


Figure 7.83: Load versus longitudinal concrete strain for service load testing with LC 2-4 (LR 4-1) and FC 2-6 (LR 8-1) for (a) top and (b) bottom of beam in the midspan section of the system

The strain change per change in load for some of the longitudinal CSGs on top and bottom of FIU-4/5 for FC 2-5 and FC 2-6 are shown in Figure 7.85 and Figure 7.86. Compression strains were measured on the top of the specimens and tension on the bottom of the specimens. The strain change per change in applied load was higher with the restrained conditions (FC 2-6) compared to the unrestrained conditions (FC 2-5). There was a slightly decreasing trend in the strain change per applied load for the restrained case (FC 2-6), which may suggest that the service fatigue loading may eventually have led to longitudinal cracking of the specimens. No transverse cracking was observed in the system though after testing.

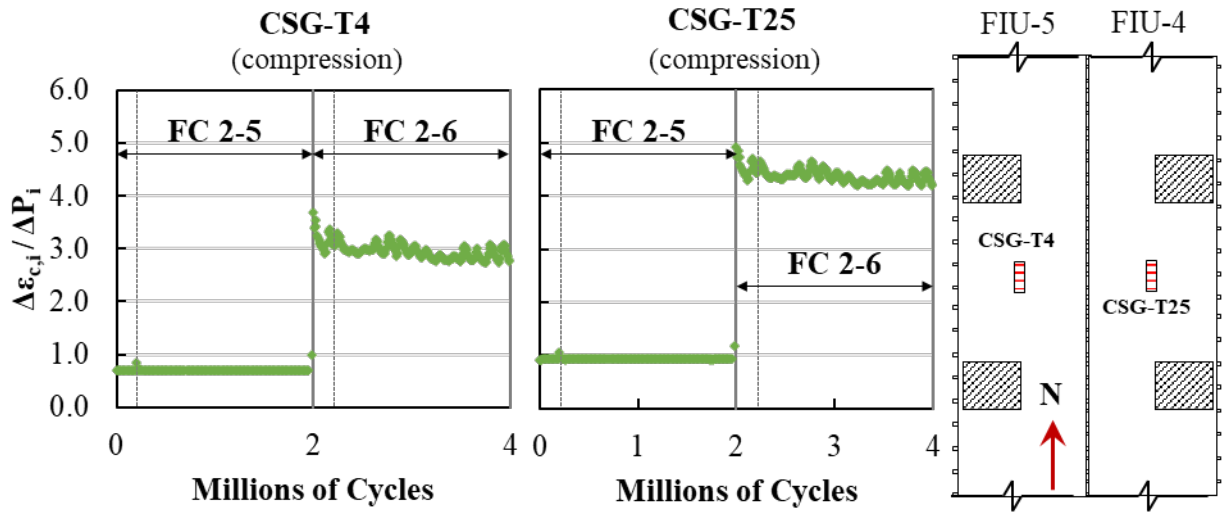


Figure 7.84: Strain change of top longitudinal CSGs per change in applied load versus number of cycles at center of specimens with FC 2-5 and FC 2-6

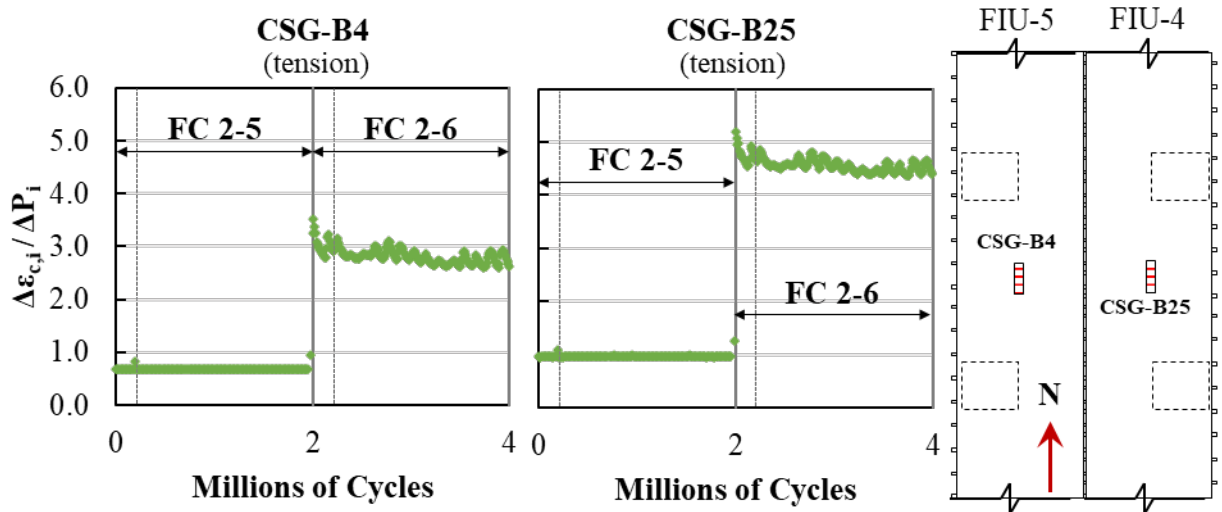


Figure 7.85: Strain change of bottom longitudinal CSGs per change in applied load versus number of cycles at center of specimens with FC 2-5 and FC 2-6

7.7.4.4. Summary

Service load tests were performed before and after two million cycles of FC 2-6 were applied to the system. After the four million total cycles and 13 static FL120 and HS-20 rear-axle service truck load ramps, there was no observed distress in precast concrete, UHPC-to-precast bond, and joint reinforcement responses. The joint and overall system performed well under the restrained service conditions.

The presence of the intermediate supports (FC 2-6) had the following effects on the system response compared to the system response without the intermediate supports (LC 2-4):

- Smaller transverse strains in the precast concrete

- Similar average strains across the top and bottom of the joint
- Similar compression strains in the joint reinforcement
- Smaller longitudinal strains on top and bottom of the precast section

No damage was observed in the joint or precast beams after Stage 5 to 8 testing.

7.7.5. Rotation Restrained Permit Test Results (Stage 9, FC 2-7)

7.7.5.1. Overview

The rotation restrained service test assessed the two-beam system with a moment restraint provided on one end of the system and consisted of one service loading stage with a full rear-axle load (FC 2-7). The moment restraint was provided on the south end to simulate an adjacent continuous span. This stage (Stage 9) simulated three static FL120 rear-axle permit truck load ramps in the elastic range applied with FC 2-7. Tests with a full rear-axle load and simple supports on both ends of the system (LC 2-4) are used as a comparison point for the results from FC 2-7.

The load versus deflection response for the system under FC 2-7 is shown in Figure 7.87. The deflections shown account for the settlement of the supports. The shorter span length and south end rotation restraint led to a stiffer system response with FC 2-7 (144 kip/in) compared to LC 2-4 (95 kip/in), which is equal to a 52 percent increase in the flexural stiffness. There was a minimal differential deflection between the two beams (varying between one and two percent during testing) in all three applied FC 2-7 ramps, suggesting that the load was applied relatively equally on the two beams on each instance.

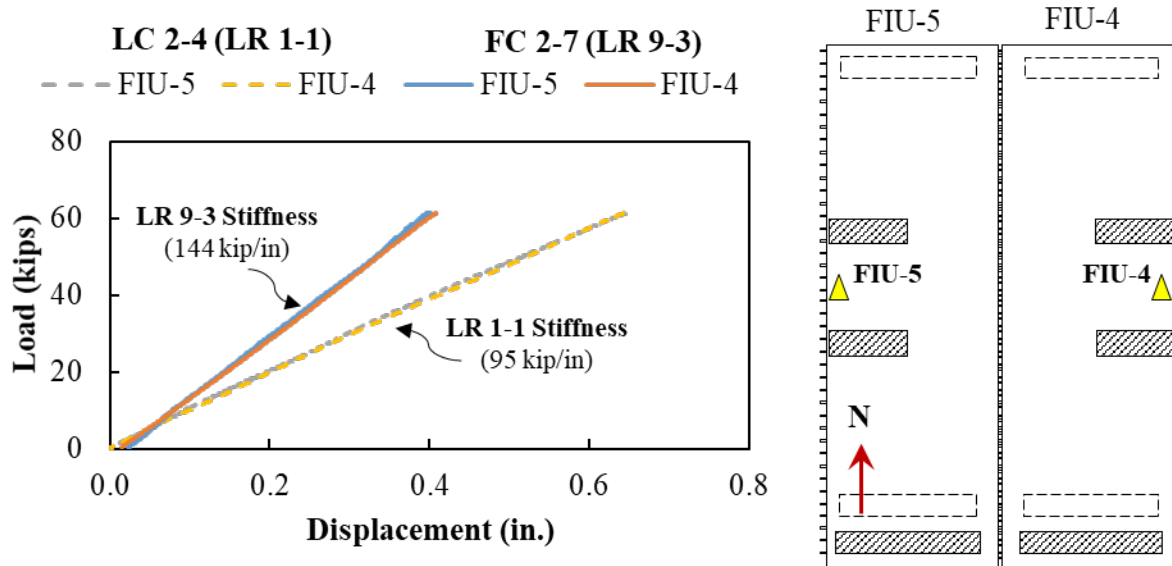


Figure 7.86: Load versus midspan displacement load testing with Load Configuration 2-4 before (LR 1-1 dashed) and after (LR 9-3 solid) Fatigue Configuration 2-7

There was some noise captured in LDT-5, as shown in Figure 7.88, so the settlement in the north support was determined by averaging the readings from LDT-9 and LDT-14.

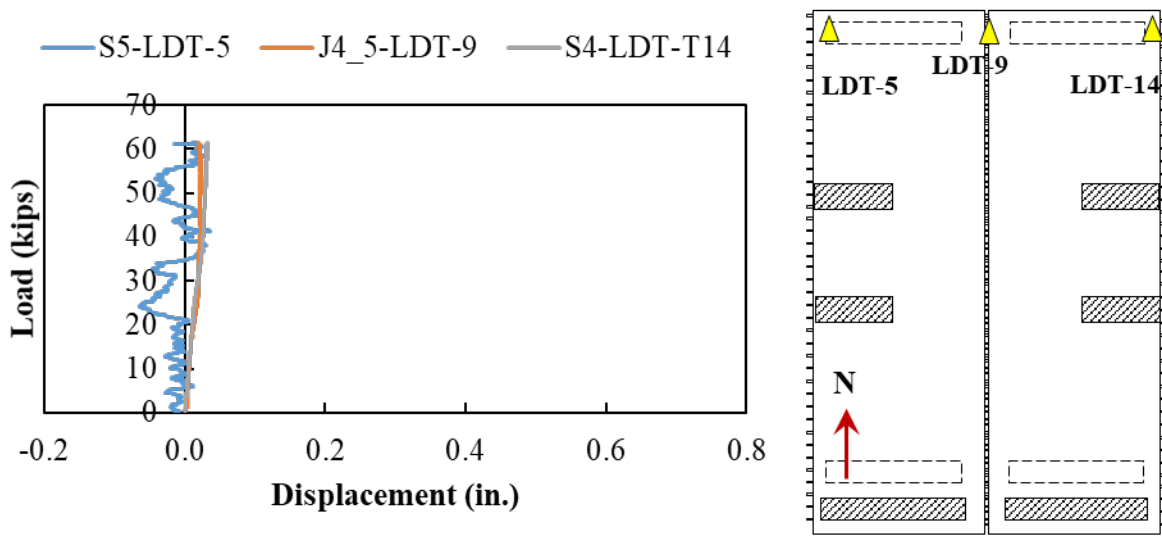


Figure 7.87: Load versus midspan displacement load testing with Fatigue Configuration 2-7 – North End response (LR 9-3)

7.7.5.2. Joint Behavior

The load versus transverse strain response of three CDTs crossing the top of the joint between FIU-4 and FIU-5 for FC 2-7 and LC 2-4 is shown in Figure 7.89. For both load configurations, the average tensile strains at service load level (32 kips for full HS-20 rear truck axle) and permit level loads (53.2 kips for full FL120 rear truck axle) were less than the estimated cracking strain for the precast concrete, with no sign of non-linearities under both load levels. The largest joint strain was measured by CDT-T2 at midspan. There were similar measured tensile strains across the top of the joint for both load configurations.

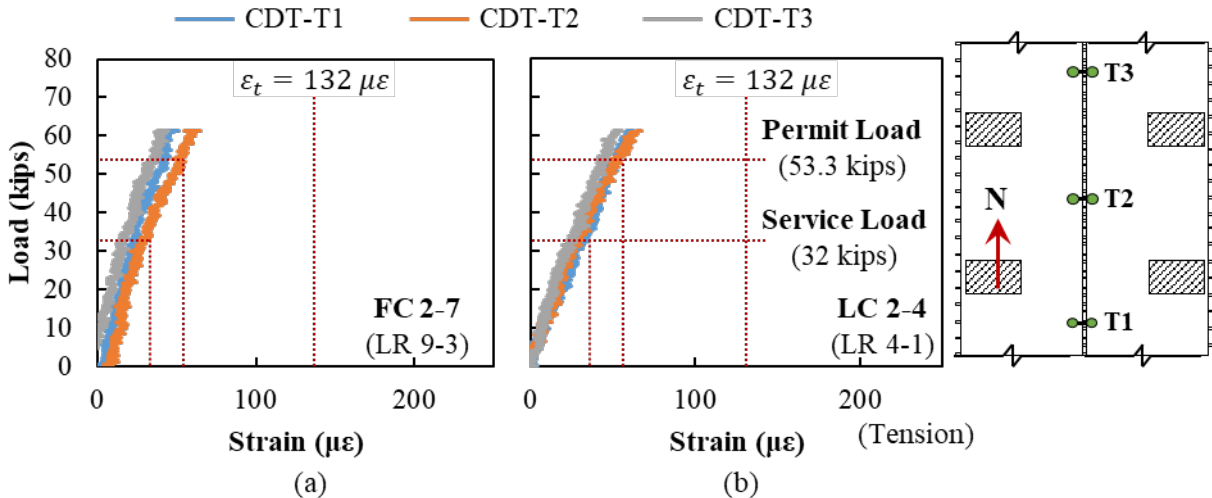


Figure 7.88: Load versus average strain across top of joint in FIU-4/5 system for (a) FC 2-7 (LR 9-3) and (b) LC 2-4 (LR 4-1)

The load versus transverse strain response of five CDTs crossing the bottom of the joint between FIU-4 and FIU-5 for FC 2-7 and LC 2-4 is shown in Figure 7.90. The strain response remained linear throughout testing and reached similar strain levels for both load configurations. The largest joint compressive strain was measured by CDT-B3 at midspan.

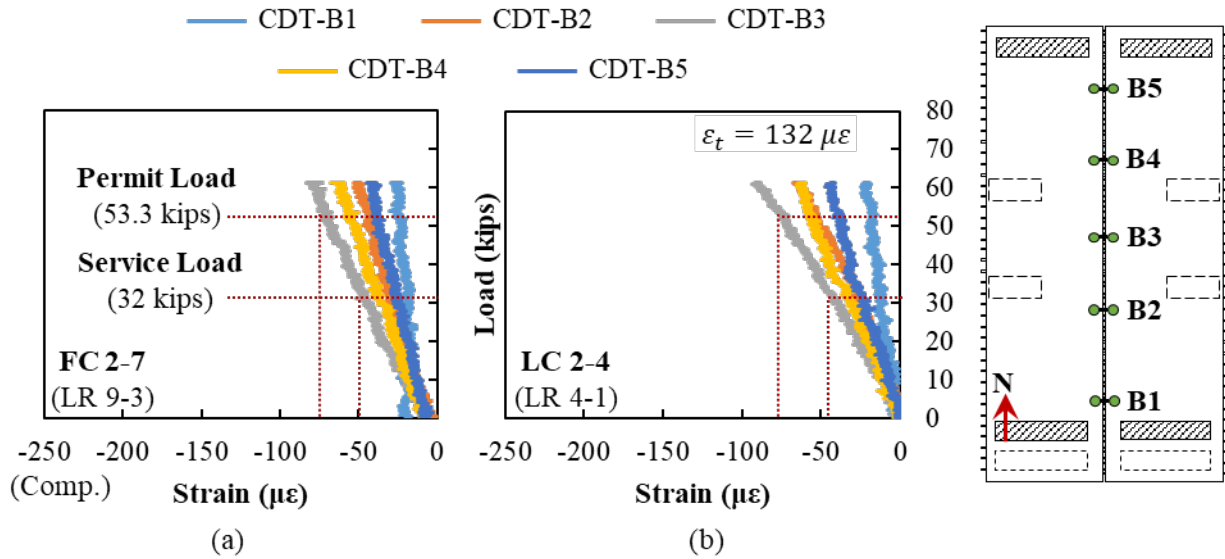


Figure 7.89: Load versus average strain across bottom of joint in FIU-4/5 system for (a) FC 2-7 (LR 9-3) and (b) LC 2-4 (LR 4-1)

The measured response of several transverse concrete strain gauges near midspan of FIU-4/5 for FC 2-7 and LC 2-4 are shown in Figure 7.91. Transverse tensile strains developed on the top of the section and transverse compression strains on the bottom of the section, as shown in Figure 7.91 (a) and Figure 7.91 (b), respectively. A linear response was observed in the transverse gauges on both the top and bottom of the system with no signs of cracking in the precast section at all load levels. The transverse tensile and compression strains in the precast section were smaller with the moment restraint (FC 2-7) compared to results with simple supports (LC 2-4).

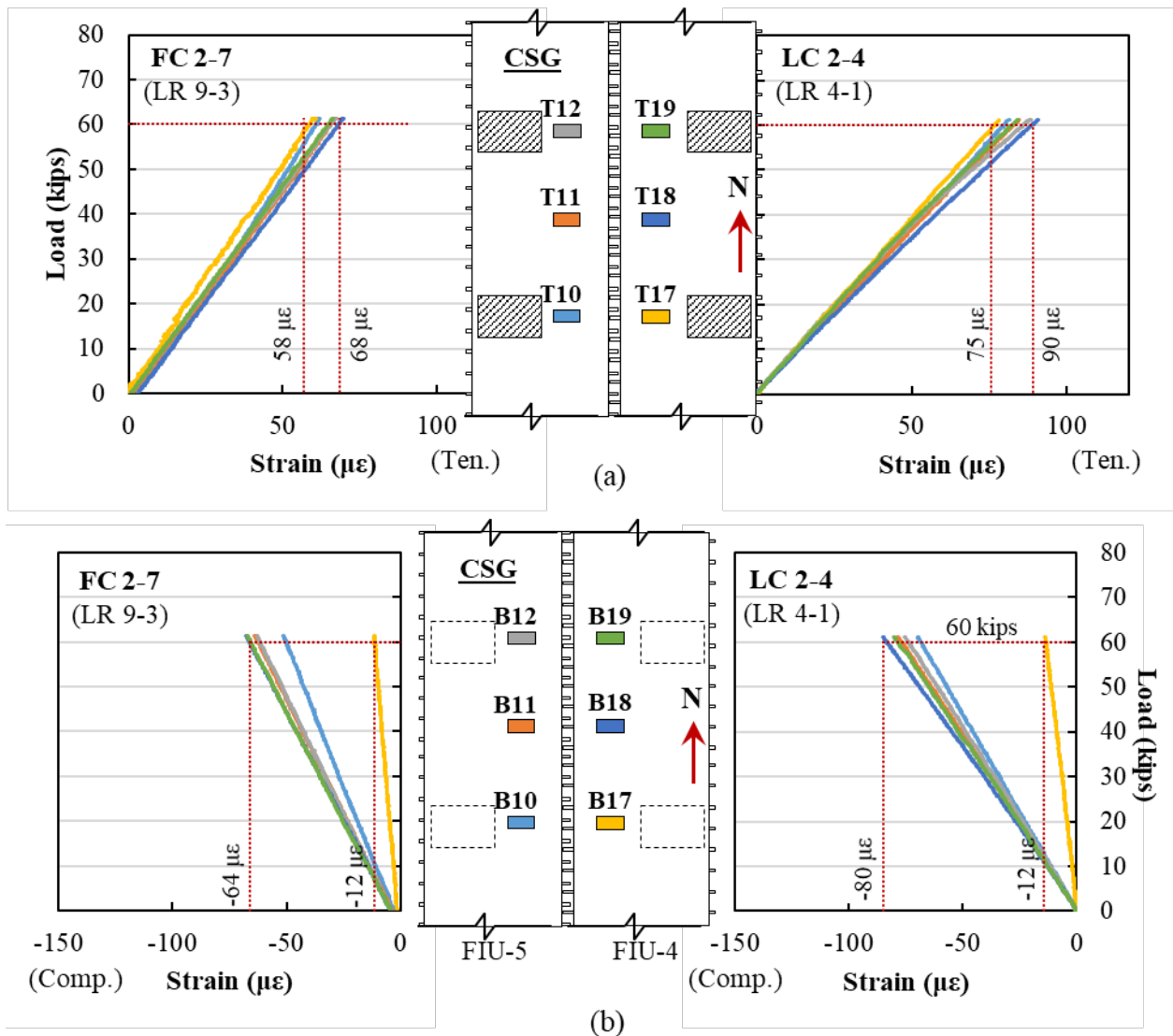


Figure 7.90: Load versus transverse concrete strain for service load testing with FC 2-7 (LR 9-3) and LC 2-4 (LR 4-1) for (a) top and (b) bottom of beam in the midspan section of the system

The measured response for the rebar strain gauges (RSGs) on the joint reinforcement extending from FIU-5 for FC 2-7 (LR 9-3) and LC 2-4 (LR 4-1) is shown in Figure 7.92. All joint reinforcement was engaged at midspan with minor compression strains during testing as the load configuration generated transverse compressive force at rebar level. Minor tension was measured in the reinforcement toward the ends of the beams. A similar response was observed with (FC 2-7) and without (LC 2-4) end moment restraint.

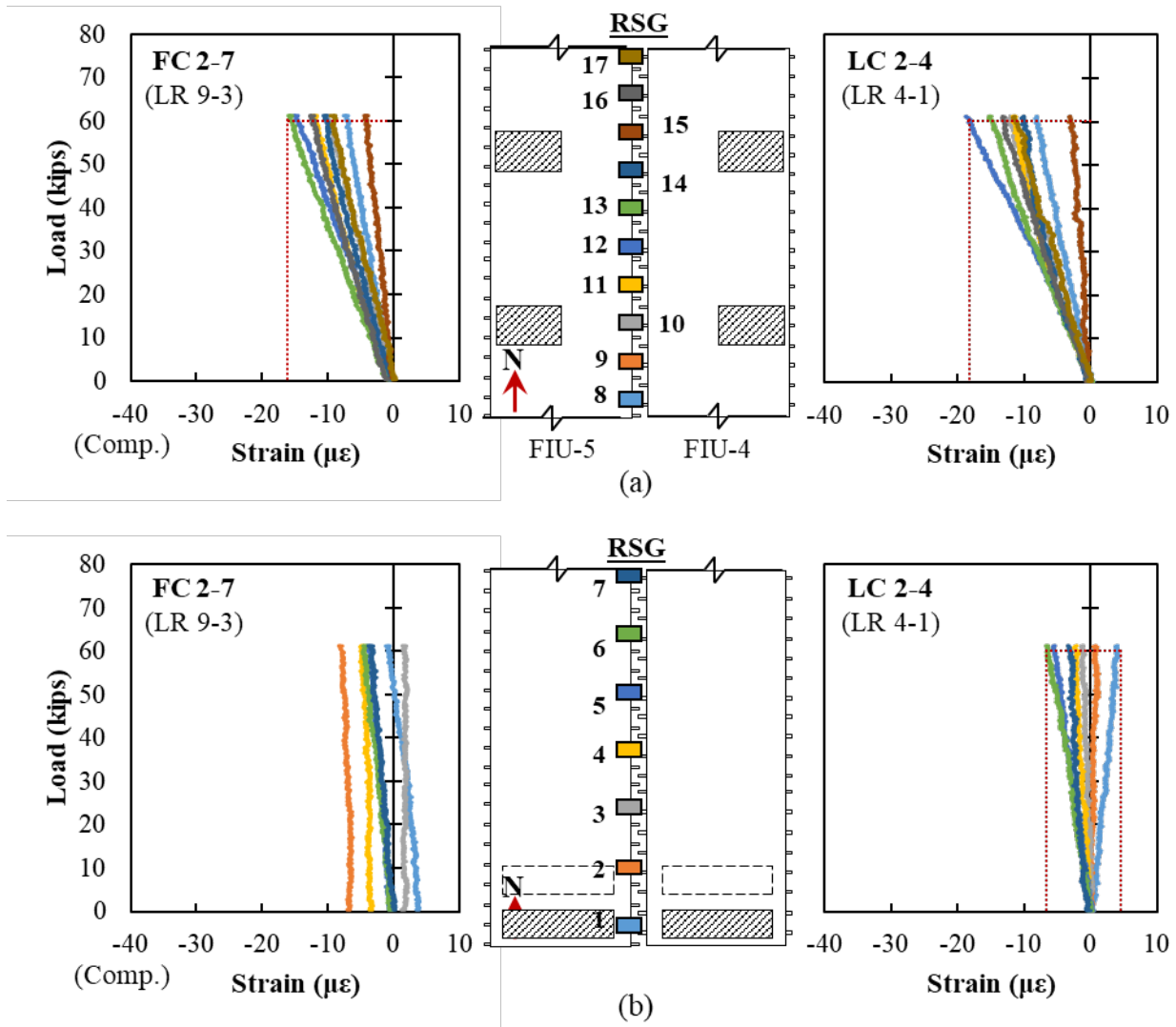


Figure 7.91: Load versus strain for service load testing with FC 2-7 (LR 9-3) and LC 2-4 (LR 4-1) for joint reinforcement extending from FIU-5 for the (a) midspan and (b) south sections of the system

7.7.5.3. Longitudinal Behavior

The measured response from the longitudinal CSGs located at the center region with FC 2-7 (LR 9-3) and LC 2-4 (LR 4-1) are shown in Figure 7.93. Longitudinal compressive strains developed on the top of the section and longitudinal tensile strains on the bottom of the section for both load configurations. The end rotation restraint in FC 2-7 led to reduced longitudinal strains on the top and bottom of the system at midspan (compared to LC 2-4), due to the reduced maximum positive moment when a moment restraint is provided at one support.

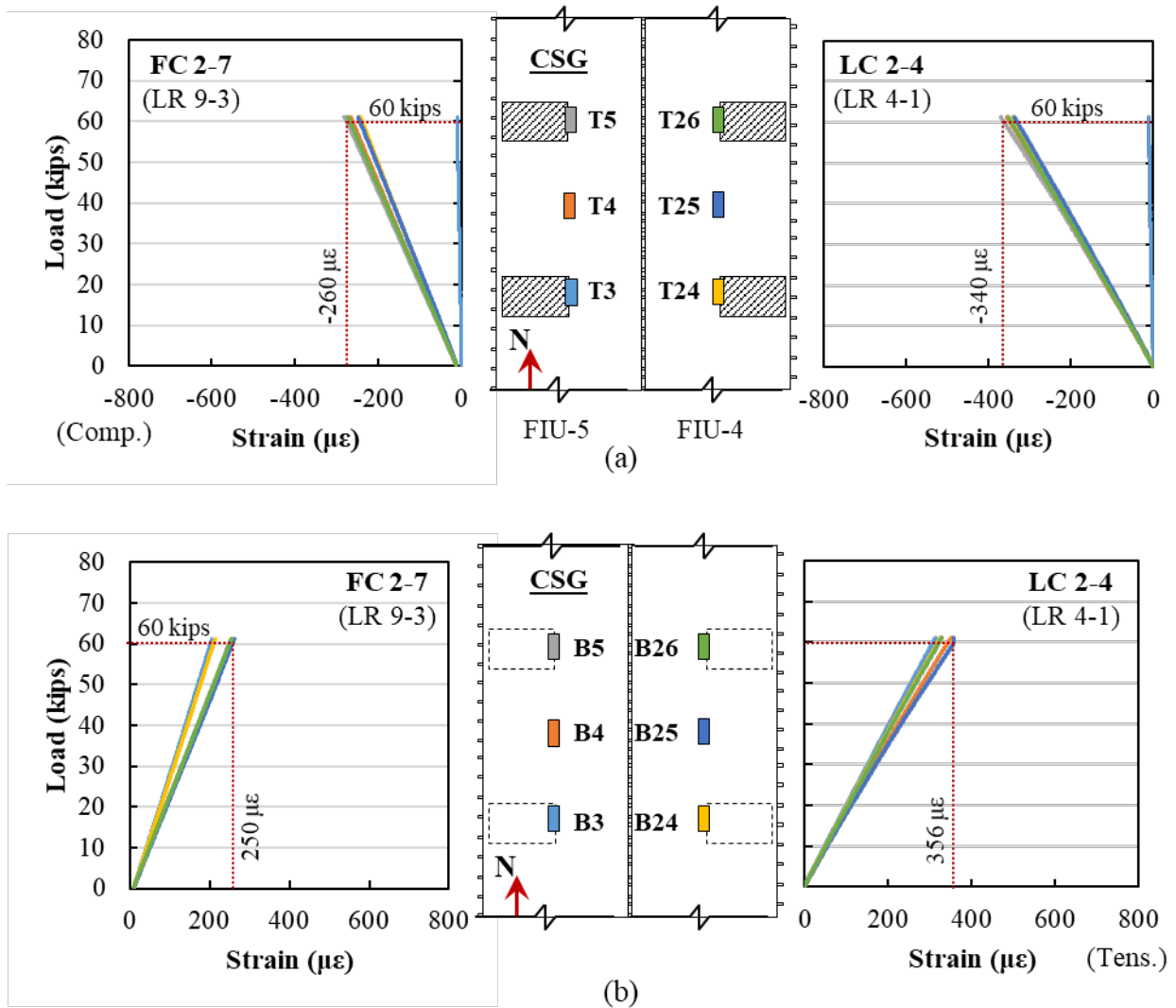


Figure 7.92: Load versus longitudinal concrete strain for service load testing with FC 2-7 (LR 9-3) and LC 2-4 (LR 4-1) for (a) top and (b) bottom of beam in the midspan section of the system

The measured longitudinal concrete strains on top and bottom of FIU-4/5 with (FC 2-7) and without (LC 2-4) the end rotation restraint are shown in Figure 7.94. The end restraint resulted in tension developing on the top and compression on the bottom of the system near the supports, see T1, T22, B1, and B22 for FC 2-7 in Figure 7.94. This response shows that the end rotation restraint caused a negative moment to develop near the support, which is consistent to what would be found in a continuous span structure. These results can be compared to the simple support load configuration (LC 2-4) where compression developed in the top and tension in the bottom of the system, which is consistent with positive moments near the supports.

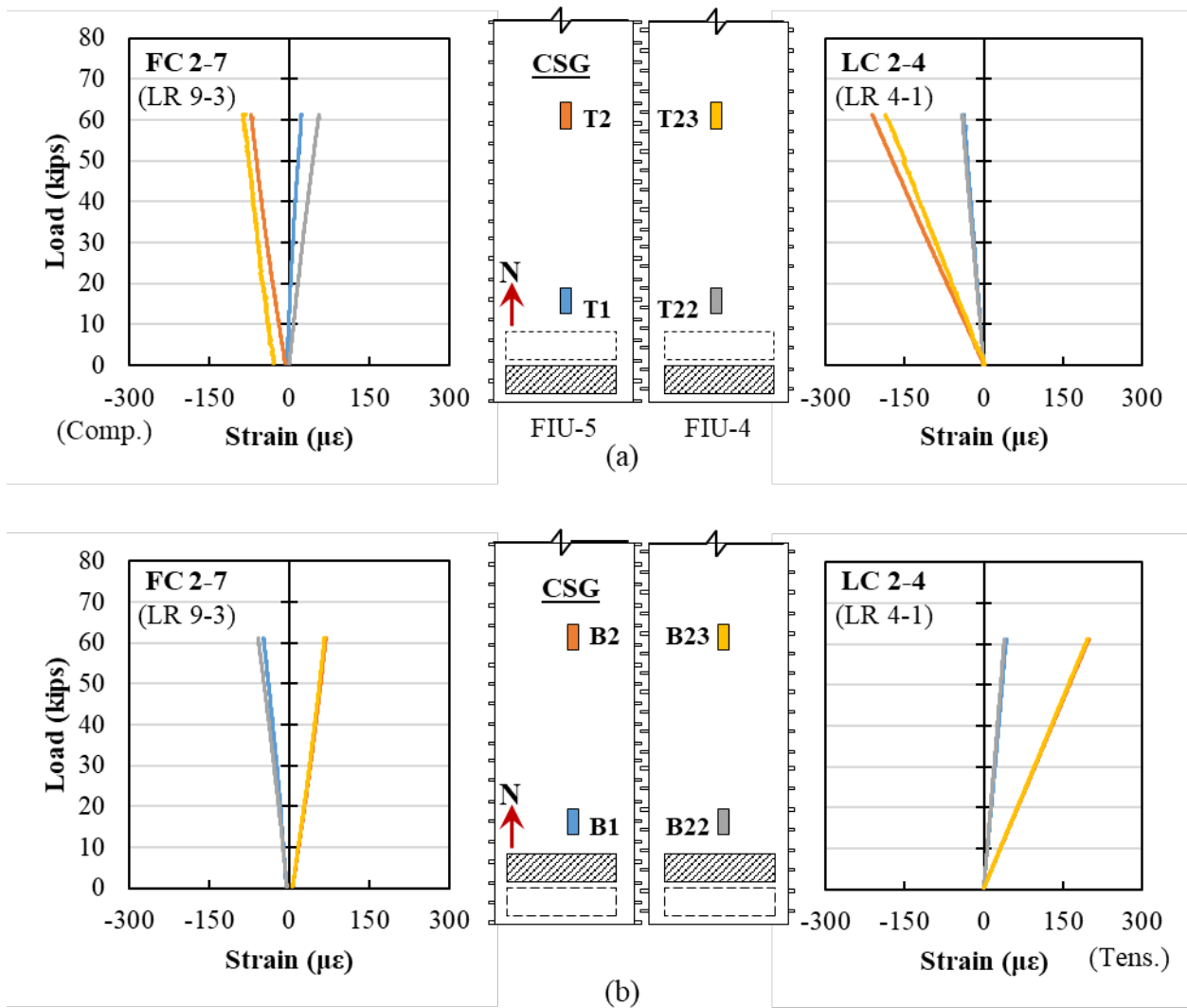


Figure 7.93: Load versus longitudinal concrete strain for service load testing with Fatigue Configuration 2-7 for (a) top and (b) bottom of the beam in the south end section of the system (LR 9-3)

7.7.5.4. Summary

The load configuration with the end moment restrained at one end (FC 2-7) resulted in negative moment developing near the restrained support, evident from the longitudinal CSGs. The joint and system demand on the two-beam configuration with restrained end (FC 2-7) was less than or equal to the simply supported load configuration (LC 2-4). This would suggest that if the joint performs well in a simply supported configuration, it will also perform well if the span were made continuous. There were no signs of distress in the joint or system after the service load testing.

7.7.6. Transverse Crack Load Ramp Test Results (Stage 10, FC 2-5cr)

7.7.6.1. Overview

No degradation in strength was observed during Stages 1 to 9, so additional testing was performed to intentionally damage the system and test the response of the damaged system. The objective of Stage 10 testing was to cause transverse cracking in one of the beams. Causing cracking in only one of the beams would lead to differential stiffness between the two beams, which was thought may increase the demand on the joint.

Cracking in one beam was achieved using load and support conditions like FC 2-5. This load configuration will be called FC 2-5cr in this section. The load was increased in both actuators to 20 kips. Then the load was held constant at 20 kips in the actuator over the west beam (FIU-5) while the load in the actuator over the east beam (FIU-4) was increased to approximately 45 kips, as shown in Figure 7.95. This loading resulted in cracking of FIU-4 while FIU-5 remained uncracked. The total load applied to the system is used in the plots in this section.

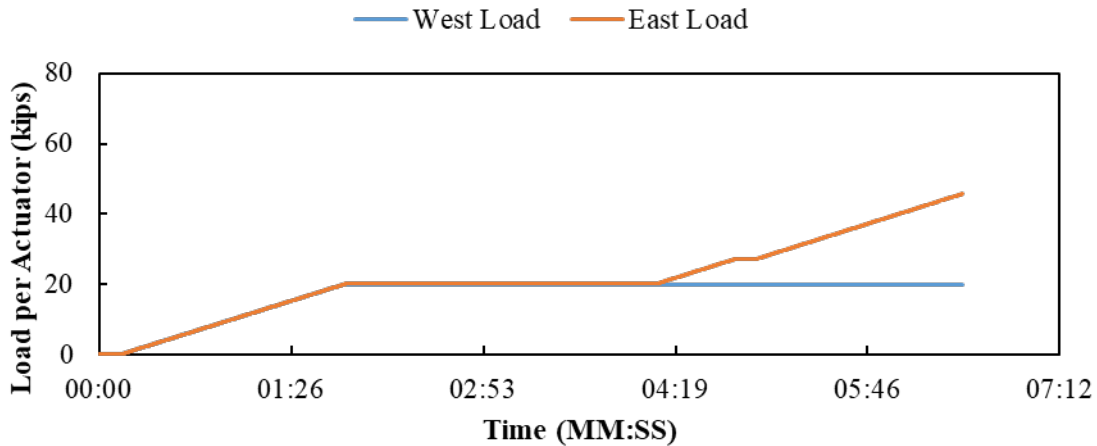


Figure 7.94: Applied load versus time for Stage 10 testing using loading like FC 2-5

The cracked response in Stage 10 (LR 10-1) is compared to the uncracked response from Stage 4 (LR 4-1) in this section.

The total load versus deflection plots for FIU-4/5 are shown in Figure 7.96. The response of FIU-5 remained linear elastic through the entire loading, while FIU-4 began to show a nonlinear response as the load approached the cracking load of approximately 63 kips.

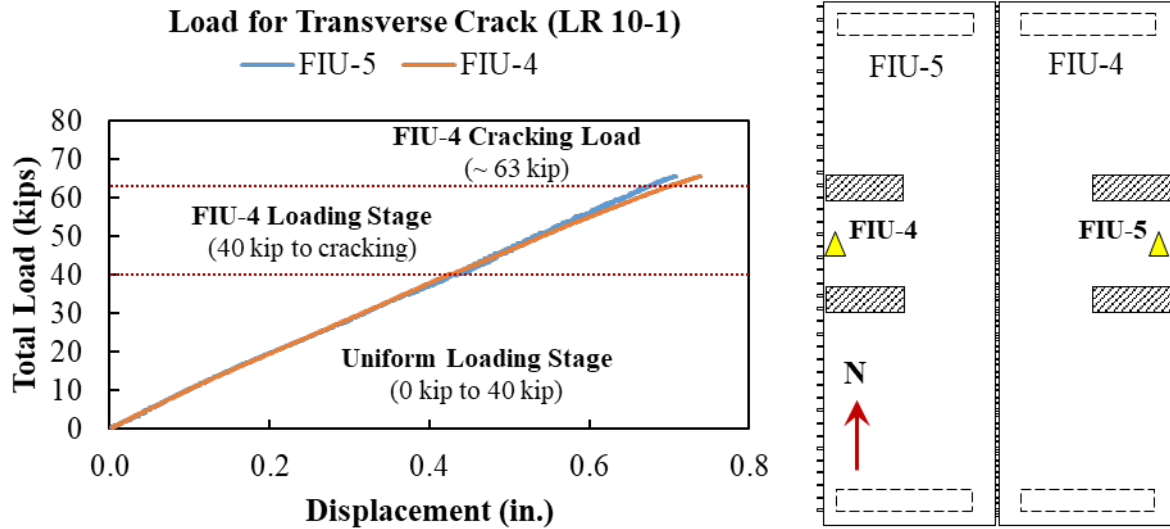


Figure 7.95: Load versus midspan displacement crack load testing with FC 2-5cr (LR 10-1)

The observed crack patterns before and after LR 10-1 (applied with FC 2-5cr) are shown in Figure 7.97. Transverse cracking was first observed in FIU-4 at a load of approximately 63 kips. The load was then held constant at 65 kips while the cracks were marked and measured. Cracks originated from the east side of the beam and grew towards the joint centerline, as shown in Figure 7.97 (b). Two transverse cracks were observed north of CSG-B25 with approximate lengths of 24 and 35 inches. One additional transverse crack was observed just north of CSG-B24 with an approximate length of 24 inches extending from the outside edge of FIU-4. No further cracks were observed in any other region of the specimen.

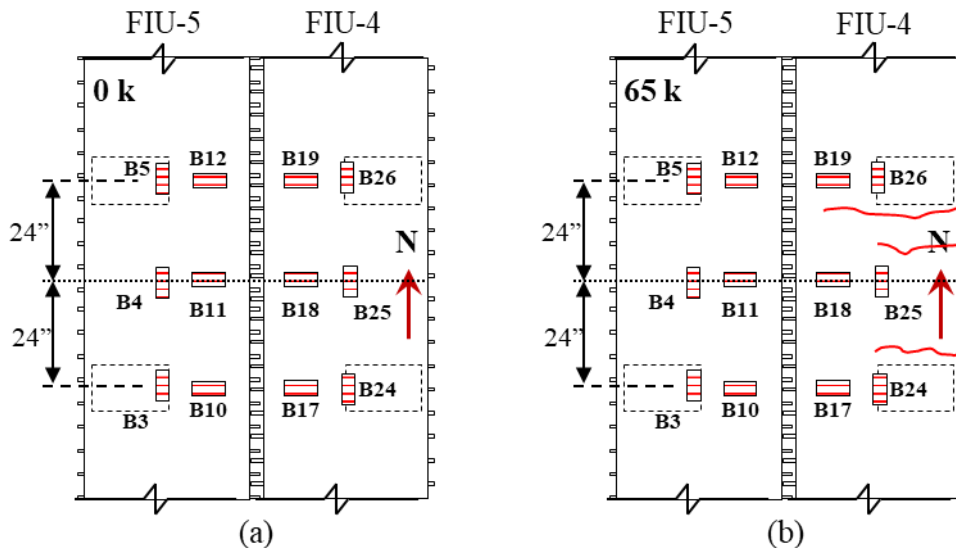


Figure 7.96: Bottom crack pattern at midspan for transverse cracking load ramp at: (a) 0 kips and (b) 65 kips (LR 10-1)

7.7.6.2. Joint Behavior

The average strain across the joint measured using the CDTs on the top and bottom of the system for FC 2-5cr (LR 10-1) and LC 2-4 (LR 4-1) are shown in Figure 7.98 and Figure 7.99, respectively. Tension developed across the top of the joint and compression across the bottom of the joint in both tests. The average tensile strain in the top remained under the estimated cracking strain for the precast concrete ($132 \mu\epsilon$), indicating that there was no distress caused by the loading condition along the joint region. There was no change in behavior after additional load was only applied on one beam (40 kips) or when transverse cracking occurred (63 kips).

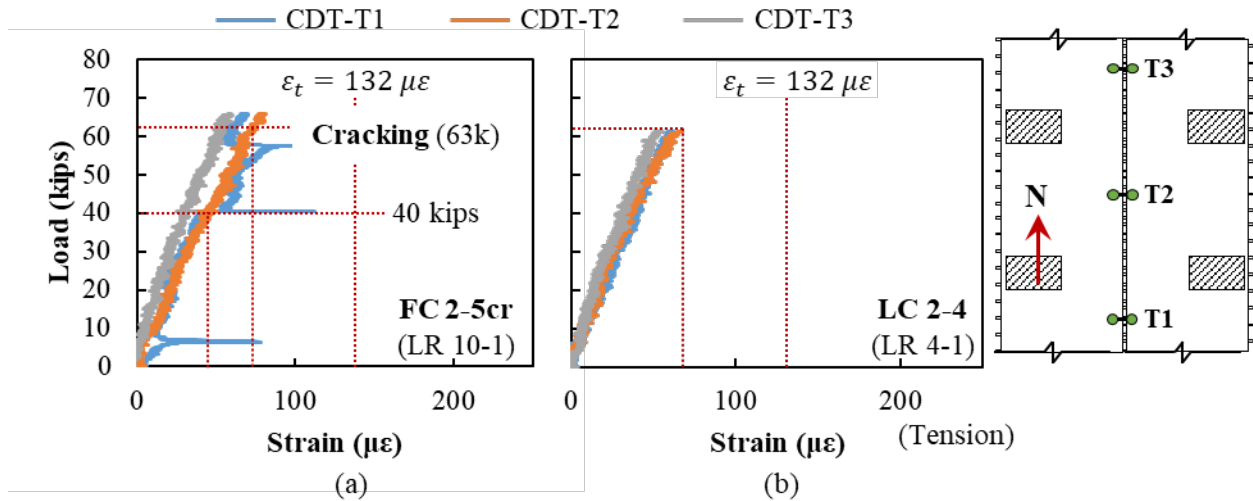


Figure 7.97: Load versus average strain across top of joint for transverse cracking load testing with (a) FC 2-5cr (LR 10-1) and (b) LC 2-4 (LR 4-1)

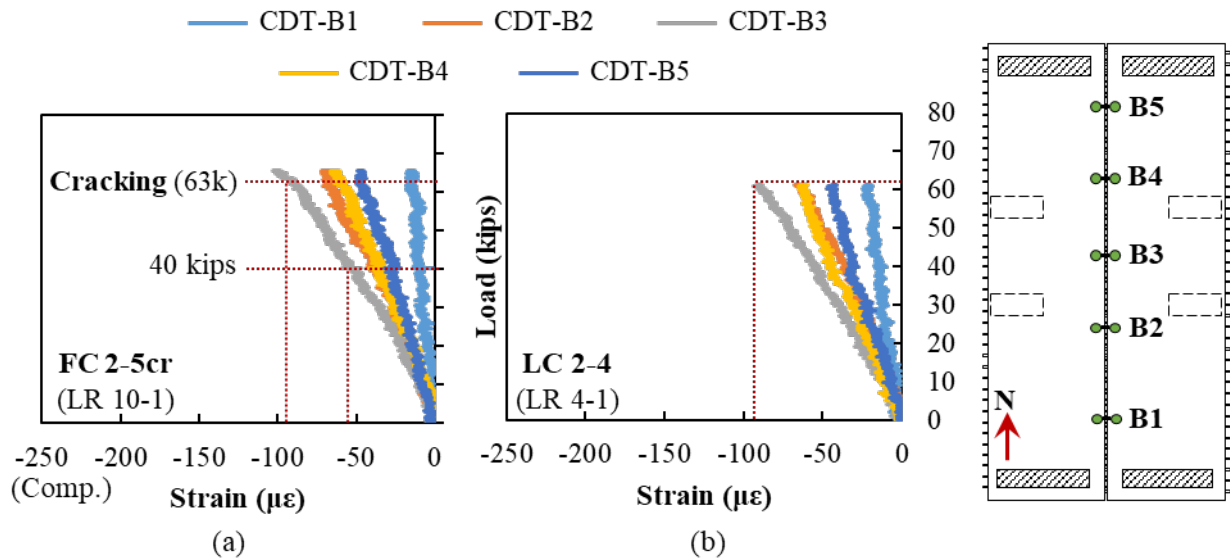


Figure 7.98: Load versus average strain across bottom of joint for transverse cracking load testing with (a) FC 2-5cr (LR 10-1) and (b) LC 2-4 (LR 4-1)

The measured response during LR 10-1 (FC 2-5cr) and LR 2-4 (LC 2-4) from the transverse concrete strain gauges at midspan are shown in Figure 7.100. Transverse tensile strains developed on the top of the section and transverse compression strains on the bottom of the section, as shown in Figure 7.100 (a) and Figure 7.100 (b), respectively. A linear response was observed in the transverse gauges on both the top and bottom of the system with no signs of precast section cracking in the longitudinal direction. There was no change in behavior after additional load was only applied on one beam (40 kips) or when transverse cracking occurred (63 kips).

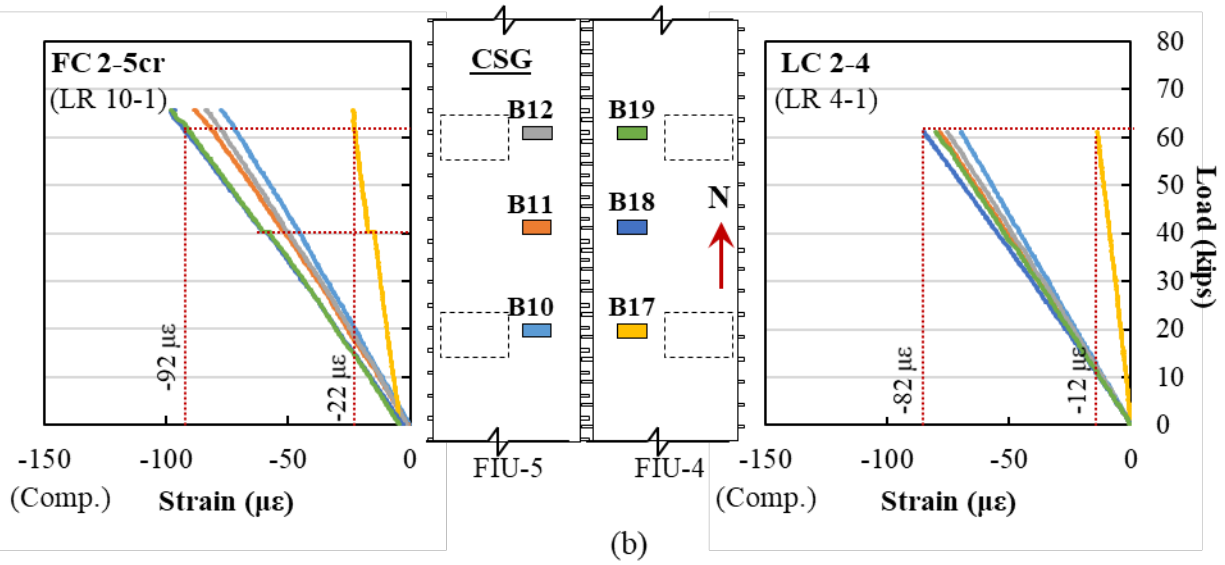
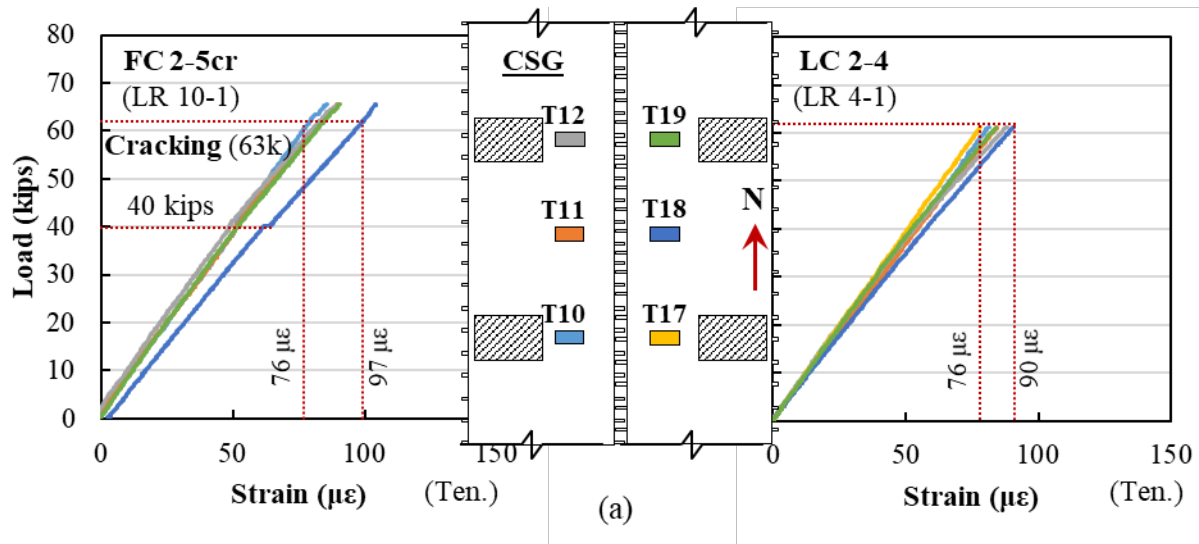


Figure 7.99: Load versus transverse concrete strain for transverse cracking load testing with FC 2-5cr (LR 10-1) and LC 2-4 (LR 4-1) for (a) top and (b) bottom of beam in the midspan section of the system

The measured response during LR 10-1 (FC 2-5cr) and LR 2-4 (LC 2-4) for the RSGs on the joint reinforcement extending from FIU-5 in the midspan and south sections of the system is shown in Figure 7.101. Most of the joint reinforcement had minor compressive strains during testing, other than the four southernmost RSGs which presented minimal tension strains. There was a slight change in slope when cracking occurred in some of the sensors near midspan (e.g., RSG-12 in FC 2-5cr). There was also a slight change in rebar strain when additional load began to only be applied through one actuator (above 40 kips for FC 2-5cr). Similar levels of reinforcement engagement were observed in LR 10-1 and LR 2-4.

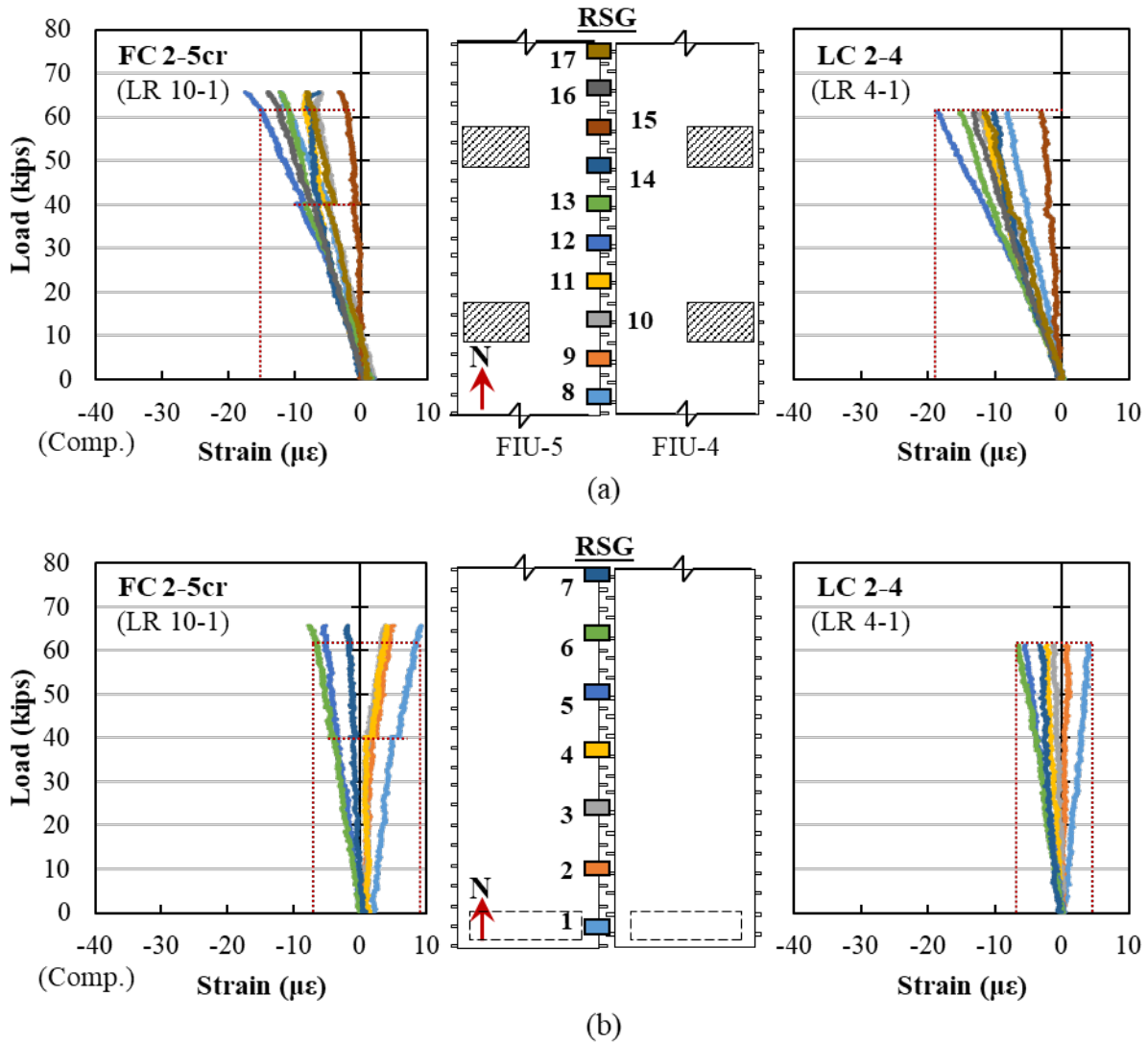


Figure 7.100: Load versus strain for transverse cracking load testing with FC 2-5cr (LR 10-1) and LC 2-4 (LR 4-1) for joint reinforcement extending from FIU-5 for the (a) midspan and (b) south sections of the system

There were no signs of debonding along the joint interface or longitudinal cracking in the precast beams during FC 2-5cr.

7.7.6.3. Longitudinal Behavior

The measured response during LR 10-1 (FC 2-5cr) and LR 4-1 (LC 2-4) from the longitudinal CSGs at midspan are shown in Figure 7.102. A linear response was observed in the CSGs on top of the system with similar levels of compressive strains in LR 10-1 and LR 4-1. The bottom CSGs also measured a linear response during both tests up until the point of cracking in LR 10-1. At cracking, CSG-B24 showed a dramatic increase in strain and CSG-B25 and CSG-B26 showed dramatic decreases in strain. This would indicate a crack going through CSG-B24 and adjacent to CSG-B25 and CSG-B26. The gauges in FIU-5 (CSG-B3, CSG-B4, and CSG-B5) remained linear

elastic during the testing. Strains measured during LR 10-1 were close to those measured in LR 4-1; this would suggest that the beams were close to transverse cracking during LR 4-1 testing.

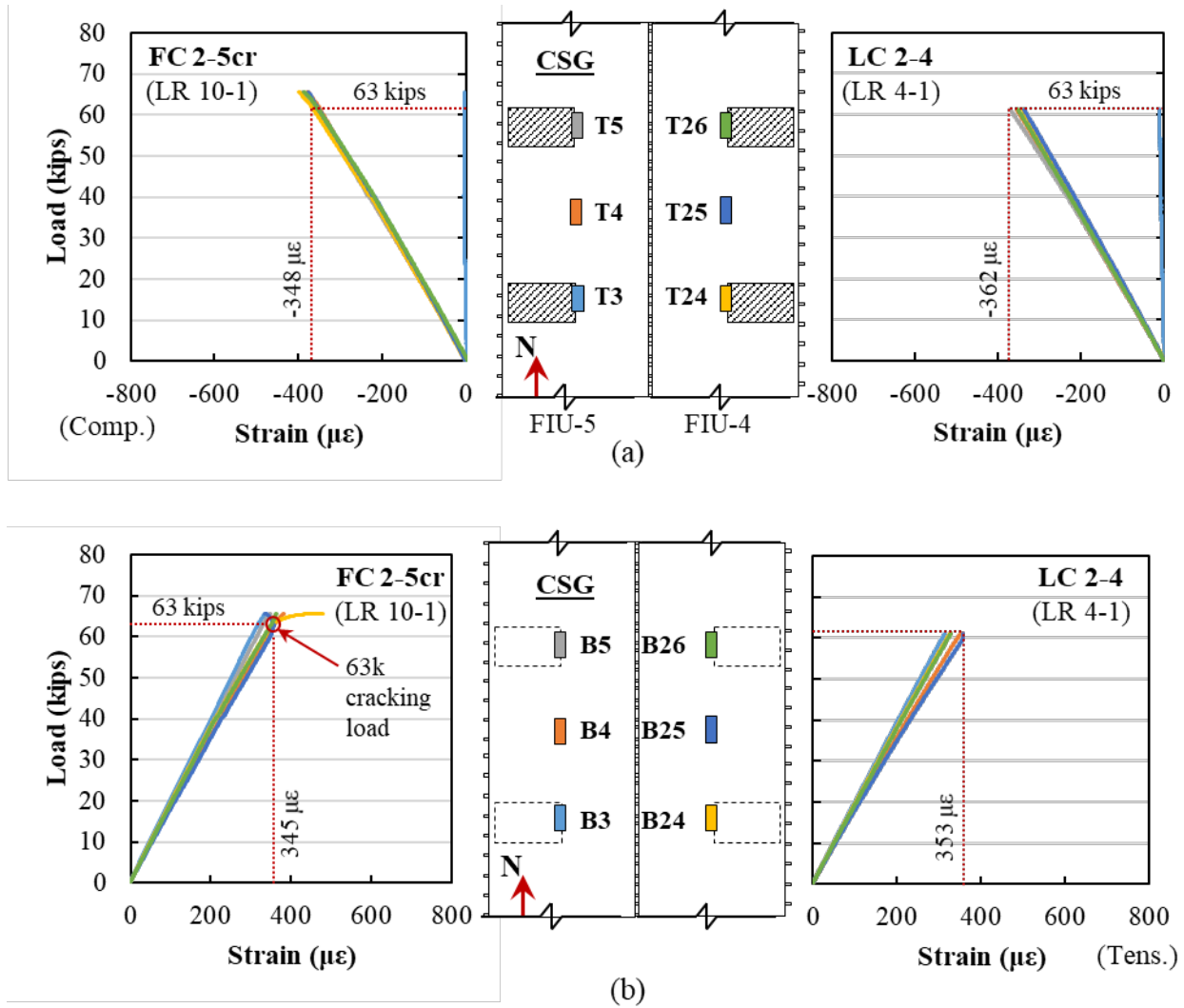


Figure 7.101: Load versus longitudinal concrete strain for transverse cracking load testing with FC 2-5cr (LR 10-1) and LC 2-4 (LR 4-1) for (a) top and (b) bottom of beam in the midspan section of the section

7.7.7. Longitudinal Crack Load Ramps Test Results (Stage 11, FC 2-6cr)

7.7.7.1. Overview

The longitudinal crack procedure detailed in §7.4.2.2 was performed immediately following the transverse crack procedure. For this load protocol, a test setup like FC 2-6 was used (with an interior support); FC 2-6cr will be used in this section to distinguish from earlier testing. Load was added in both actuators at the same time until a total load of 90 kips for LR 11-1 and 100 kips for LR 11-2 was applied to the system (with 45 or 50 kips in each actuator for LR 11-1 and LR 11-2, respectively). The loads shown in this section are the total load applied to the system. Longitudinal cracking was not achieved, but additional load could not be added due to a 50-kip capacity of one of the actuators.

The total load versus displacement for LR 11-2 (using FC 2-6cr) is shown in Figure 7.103. The system response was linear elastic until FIU-5 began to bear against the interior supports. The system stiffness increased after bearing against the interior supports.

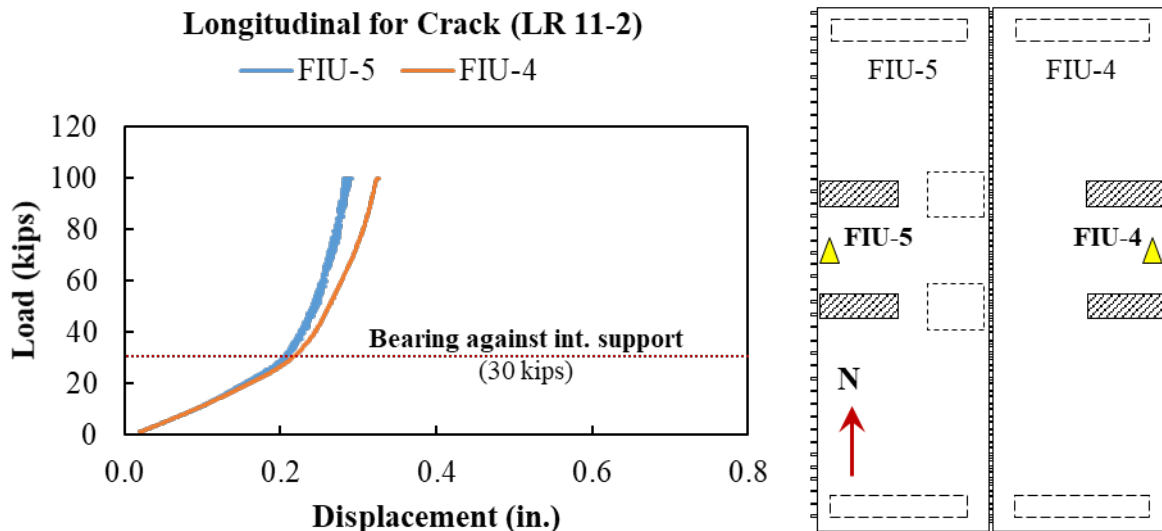


Figure 7.102: Load versus midspan displacement using FC 2-6cr (LR 11-2)

The results in this section will be compared to the service load conducted in Stage 8 using FC 2-6 for some cases. The load was applied differently, and a smaller load applied in FC 2-6.

7.7.7.2. Joint Behavior

The average strains across the joint measured using the CDTs on the top and bottom of the system for FC 2-6cr (11-2) and FC 2-6 (LR 8-1) are shown in Figure 7.104 and Figure 7.105, respectively. Tension developed across the top of the joint and compression across the bottom of the joint. The tensile strains across the joint remained below the estimated cracking strain level for the precast concrete ($132 \mu\epsilon$), reaching approximately $100 \mu\epsilon$ at midspan when the peak load was reached. Slightly higher compression strains across the bottom of the joint were measured for FC 2-6cr compared to FC 2-6 at similar load levels.

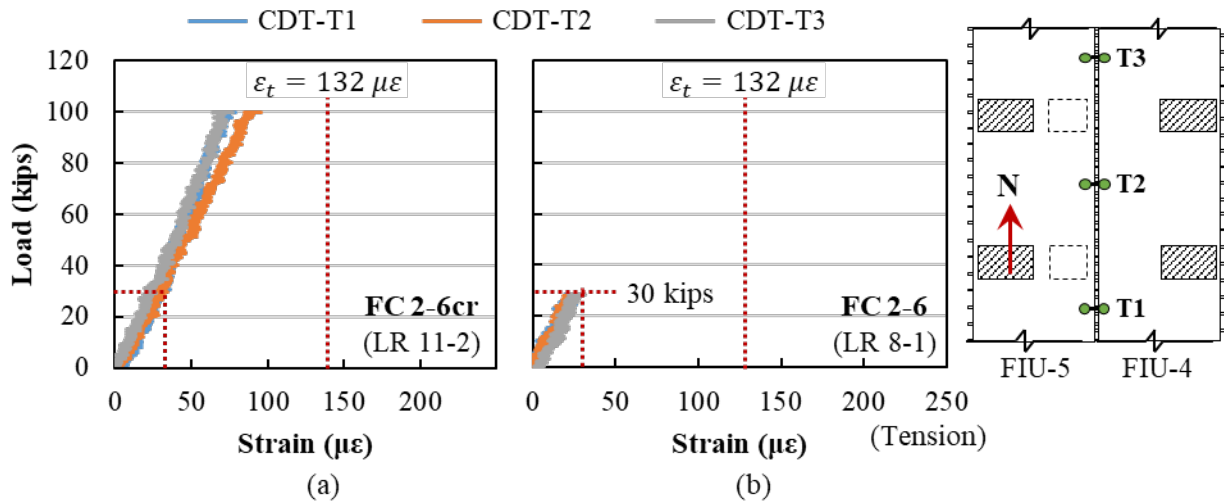


Figure 7.103: Load versus average strain across top of the joint for (a) FC 2-6cr (LR 11-2) and (b) FC 2-6 (LR 8-1)

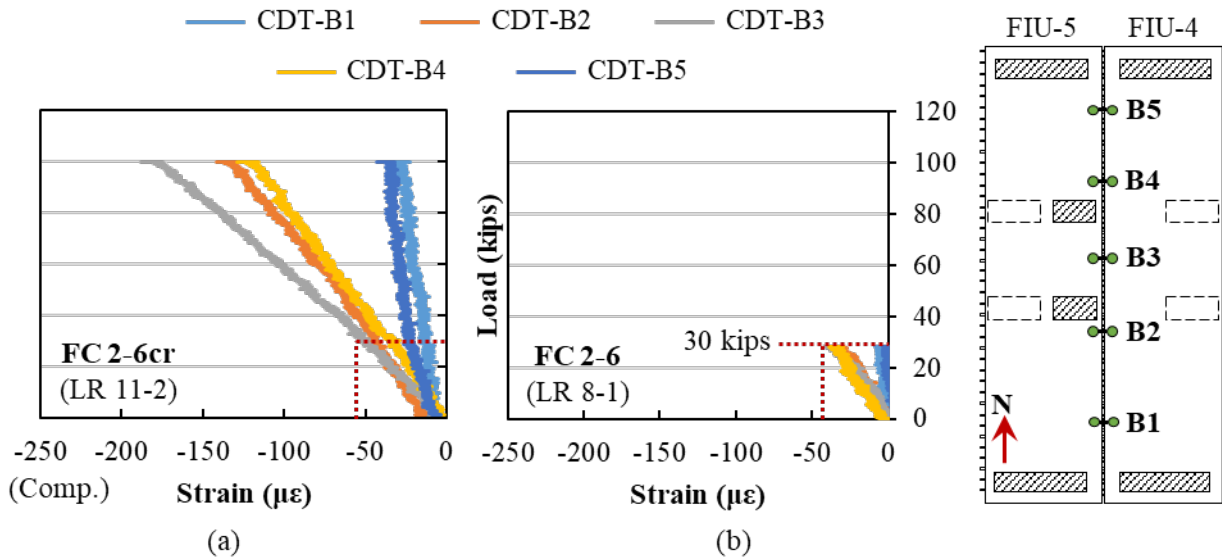


Figure 7.104: Load versus average strain across bottom of joint for (a) FC 2-6cr (LR 11-2) and (b) FC 2-6 (LR 8-1)

The measured response during FC 2-6cr (LR 11-2) and FC 2-6 (8-1) from the transverse CSGs at midspan are shown in Figure 7.106. Transverse tensile strains developed on the top of the section and transverse compression strains on the bottom of the section, as shown in Figure 7.106 (a) and Figure 7.106 (b), respectively. CSG-T10 began to show decreasing tensile strains at approximately 90 kips of total applied load (for FC 2-6cr), which may have been caused by the initiation of longitudinal cracking adjacent to the gauge; however, no cracking was visually observed. Since the joint gauges (CDTs) did not show any signs of cracking, the longitudinal cracking was likely initiating in the precast section.

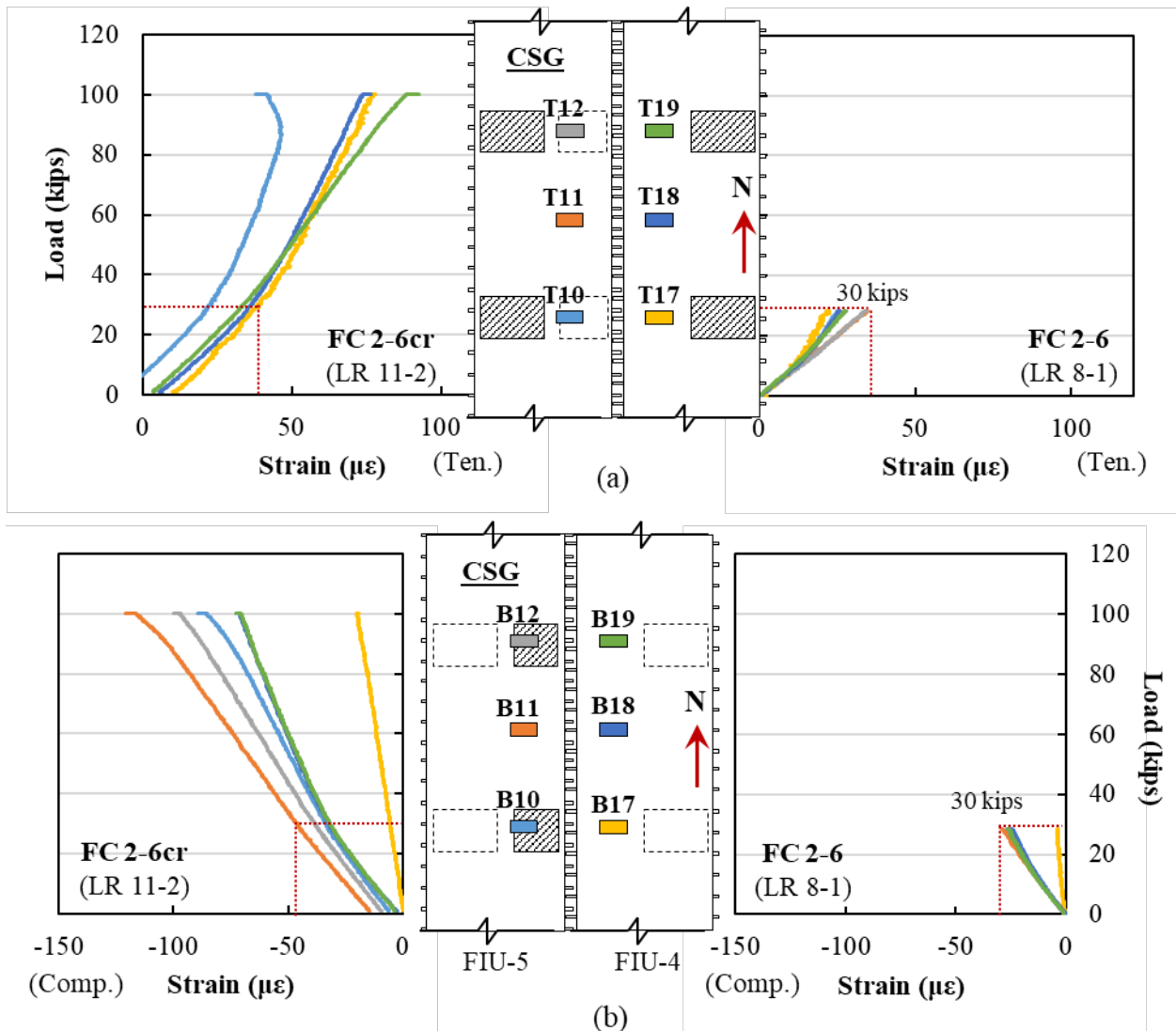


Figure 7.105: Load versus transverse concrete strain for FC 2-6cr (LR 11-2) and FC 2-6 (LR 8-1) for (a) top and (b) bottom of beam in the midspan section of the system

The measured response from the RSGs on the joint reinforcement extending from FIU-5 in the midspan and south sections of the system for FC 2-6cr (LR 11-2) and FC 2-6 (LR 8-1) is shown in Figure 7.107. Most joint reinforcement had only minor compressive strains during the load ramp assessment. However, there were several RSGs near each support that showed minor tensile strains.

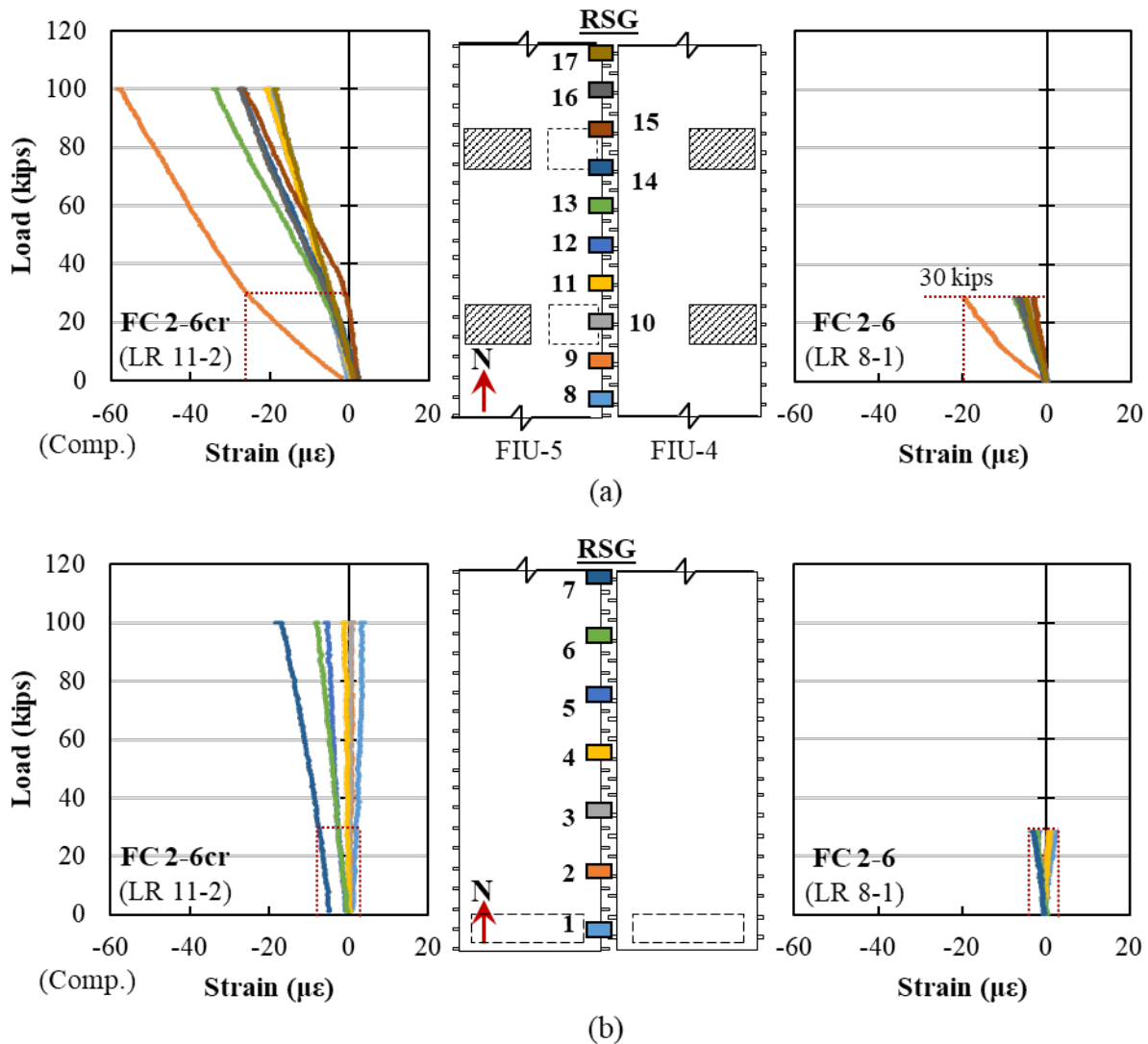


Figure 7.106: Load versus strain for joint reinforcement extending from FIU-5 for FC 2-6cr (LR 11-2) and FC 2-6 (LR 8-1) for the (a) midspan and (b) south sections of the system

There was no visual signs of joint material debonding nor precast cracking in the longitudinal direction. Also, crack growth was not seen in the previously marked transverse cracks.

7.7.7.3. Longitudinal Behavior

The measured response from the longitudinal CSGs at midspan for FC 2-6cr (LR 11-2) and FC 2-6 (LR 8-1) are shown in Figure 7.108. There were no signs of crack growth or new crack formation in the transverse crack that had previously developed on the bottom of FIU-4 at midspan. The effects of FIU-5 bearing against the interior supports can be seen by the change in slope between 20 and 30 kips.

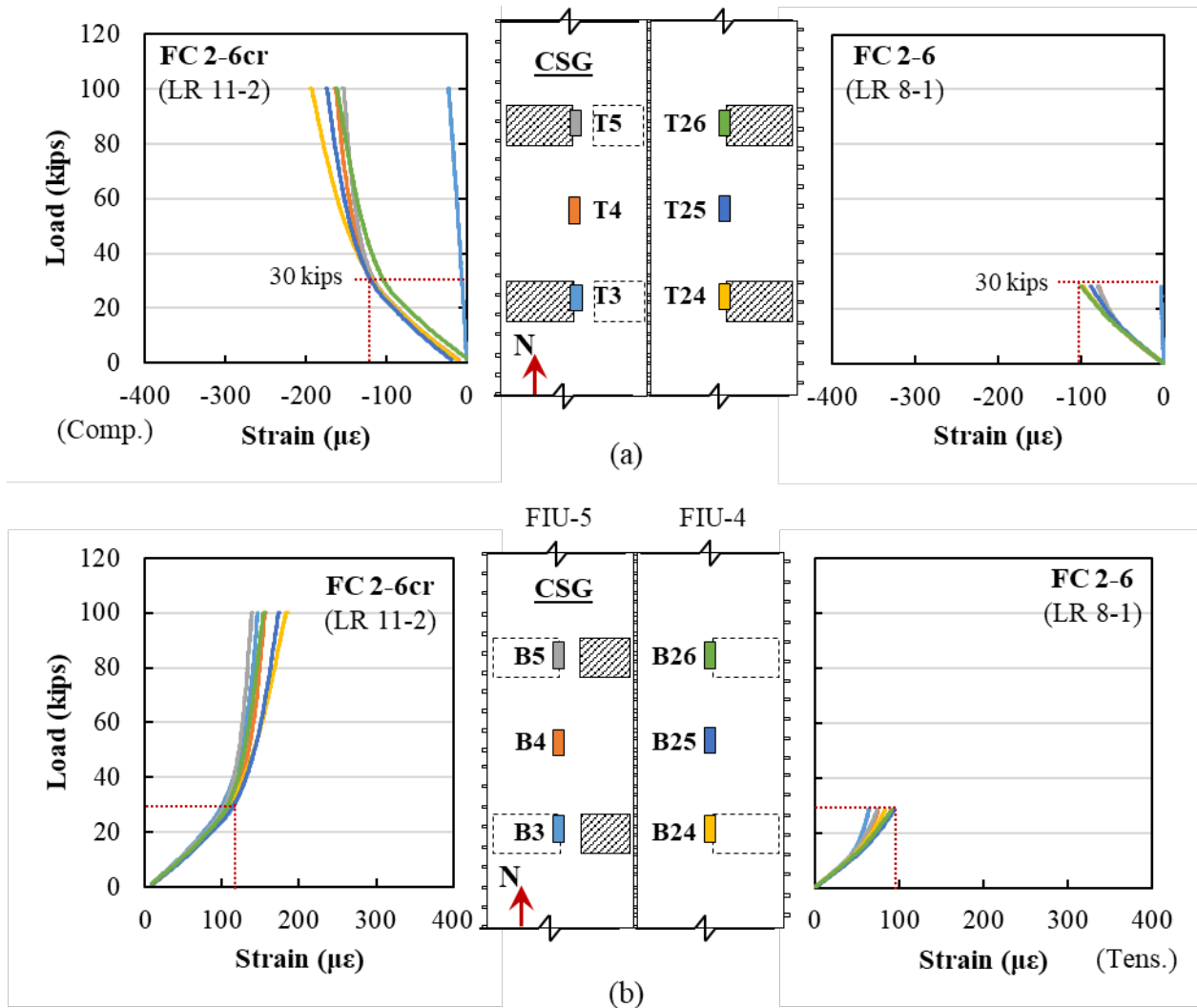


Figure 7.107: Load versus longitudinal concrete strain or FC 2-6cr (LR 11-2) and FC 2-6 (LR 8-1) for (a) top and (b) bottom of beam in the midspan section of the section (LR 11-2)

No longitudinal crack in the precast element or joint material debonding along the joint boundary was observed through the complete load ramp assessment.

7.7.8. Cracked Restrained Service Test Results (Stage 12-15, FC 2-6cr)

7.7.8.1. Overview

Stage 12 to 15 used a similar load protocol to Stage 4 to 8 (FC 2-5 and FC 2-6). Stage 12 involved a service load test with an intermediate support (like FC 2-6). Stages 13 and 14 were fatigue loading stages where 700,000 cycles were applied to the system with the same configuration as FC 2-6. Finally, Stage 15 involved a service load applied to the system with the same configuration and load protocol used in Stage 10 (FC 2-5cr). The applied load per actuator versus time for LR 10-1, LR 12-1, and LR 15-1 are shown in Figure 7.109. The total load applied on the system is used in the plots in this section.

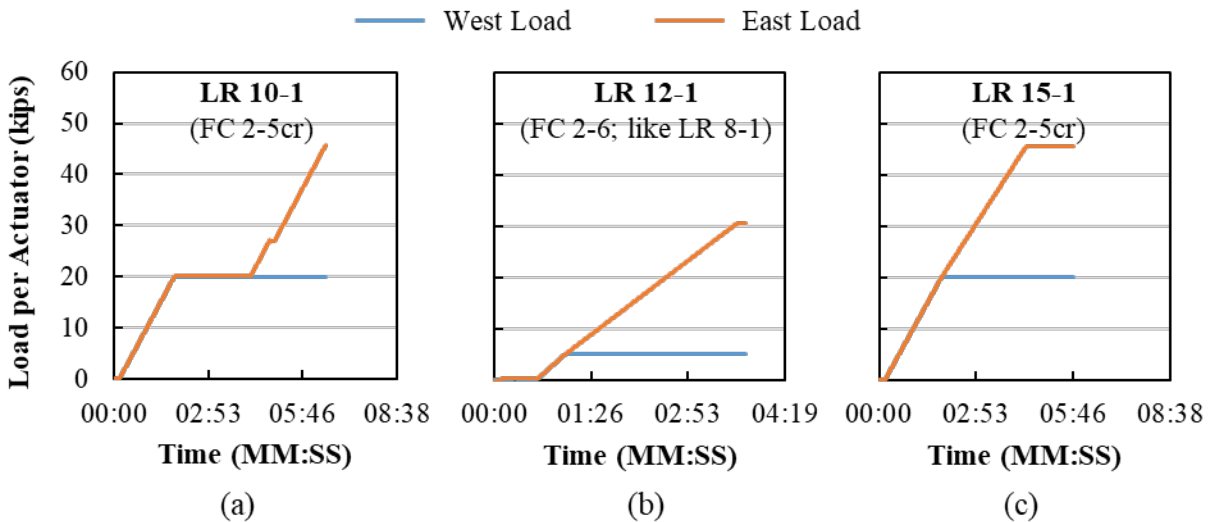


Figure 7.108: Load per actuator versus time for (a) LR 12-1 and (b) LR 15-1 (service load testing before and after FC 2-6cr cyclic loading)

LR 10-1 and LR 15-1 are a comparison of the system response before and after transverse cracking and 700,000 load cycles using FC 2-6. LR 12-1 and LR 15-1 are a comparison of the system response with and without the intermediate supports. These three tests are compared in this section.

The load versus deflection curves for LR 10-1 (FC 2-5cr), LR 12-1 (FC 2-6cr), and LR 15-1 (FC 2-5cr) are shown in Figure 7.110. The overall response of the system did not vary significantly between LR 10-1 and LR 15-1, as shown in Figure 7.110 (a). There is a larger deflection observed in FIU-4, which is a result of the actuator over FIU-4 applying a larger load for FC 2-5cr. The effect of the intermediate supports can be seen in Figure 7.110 (b), where the stiffness of FIU-5 increases when it begins to bear against the intermediate supports.

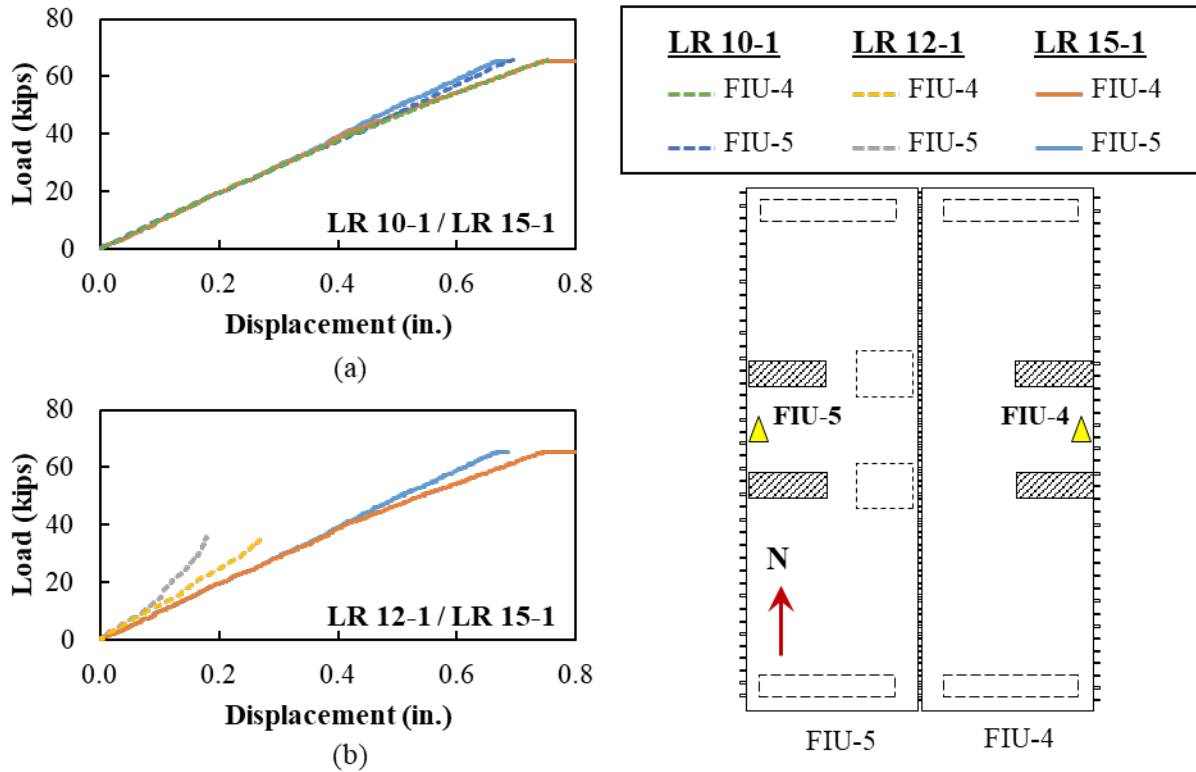


Figure 7.109: Load versus displacement for (a) LR 10-1 and LR 15-1 and (b) LR 12-1 and LR 15-1

The normalized stiffnesses measured by the west and east actuators and the average midspan stiffness are shown in Figure 7.111, all account for measured support settlement. There was not a significant change in normalized stiffness observed in the actuators during Stage 12-15. There was a drop in stiffness of the overall system before and after cracking (from approximately 230 k/in. before to 135 k/in. after cracking). There was a slight increase in normalized stiffness in the overall system response measured by the LDTs, as shown in Figure 7.111 (c).

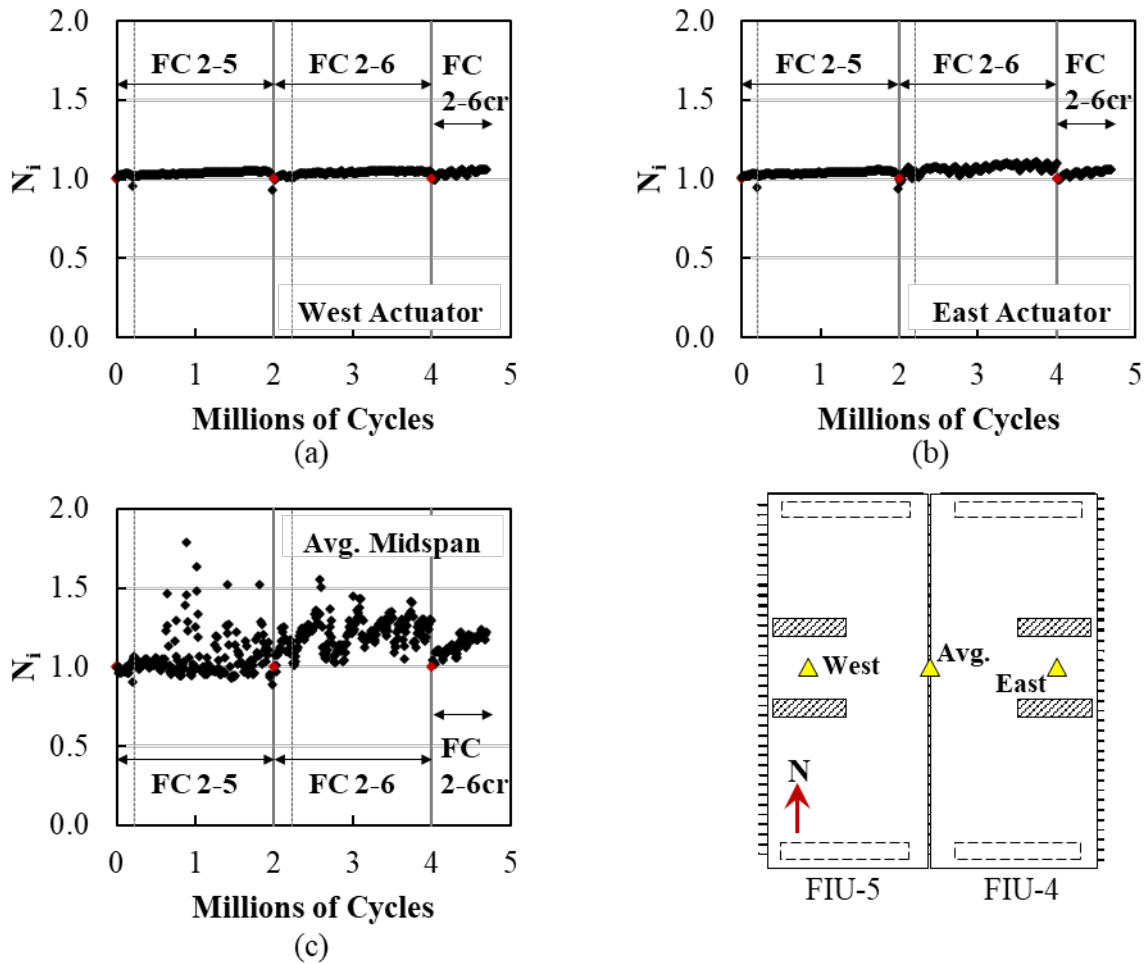


Figure 7.110: Normalized stiffnesses at midspan for (a) west and (b) east actuator and (c) average midspan response using LDTs for all cyclic loads

Crack growth was observed before and after the application of the 700,000 cycles applied (in Stages 13 and 14) and the load application in Stage 15, as shown in Figure 7.112. Two of the three major cracks reported during the transverse crack load ramp test grew by 12 inches at the north of the CSG-B18/CSG-B25 line and 6 inches at the south of the CSG-B18/CSG-B25 line, respectively. Also, two new cracks formed at the south of the sensor line close to the southeast load patch, each of 13 inches and 30 inches respectively, as shown in Figure 7.112 (b). These new cracks extended to the exterior side of FIU-4 and grew through the straight side of the bottom lip, as shown in Figure 7.113.

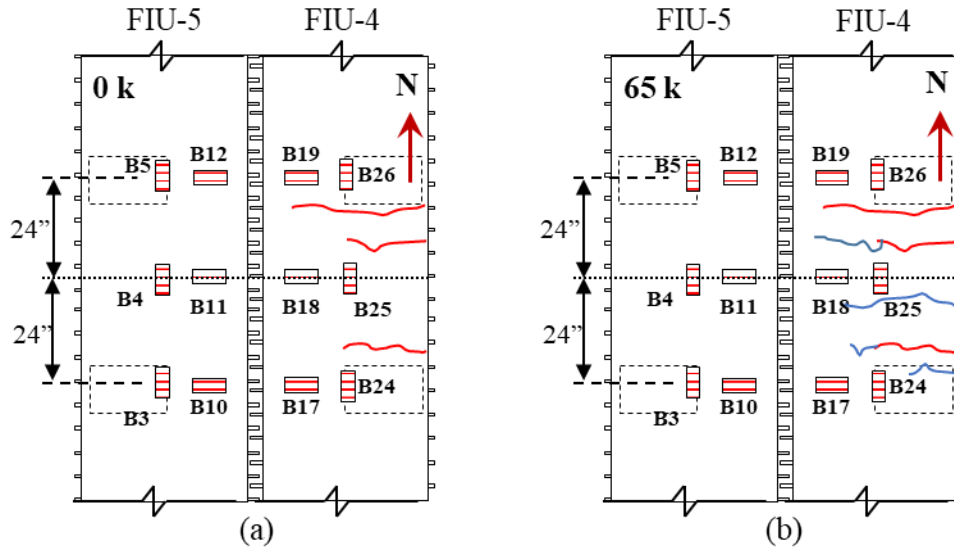


Figure 7.111: Bottom crack pattern at midspan for transverse cracking load ramp: (a) after LR 10-1 and (b) after LR 15-1

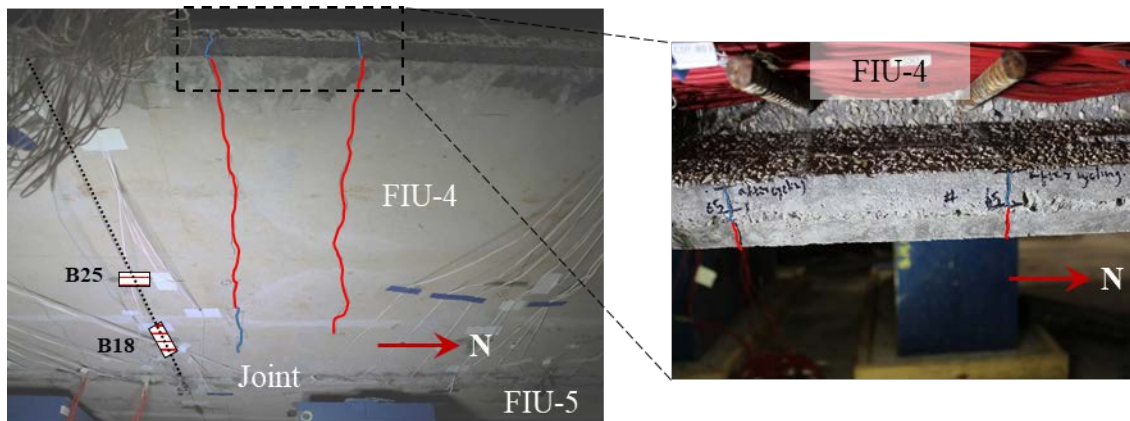


Figure 7.112: Transverse cracks on FIU-4 exterior bottom lip (after LR 15-1) at 0 kips (red) and 65 kips (blue)

7.7.8.2. Joint Behavior

The transverse top and bottom strains measured during LR 10-1, LR 12-1, and LR 15-1 by the CDTs are shown in Figure 7.114 and Figure 7.115. Similar transverse tensile strains across the top of the joint were measured during all three load tests. Tensile strains remained below the theoretical cracking strain. The response remained close to linear elastic for the top CDTs throughout the tests other than noise measured in CDT-T1 during LR 10-1. Similar compressive strains were measured across the bottom of the joint for LR 10-1 and LR 15-1 with slightly higher strains at similar load levels measured for LR 12-1, likely a result of the interior supports. The measured response across the joint would suggest that no distress or cracking occurred in the joint due to the static or fatigue loading.

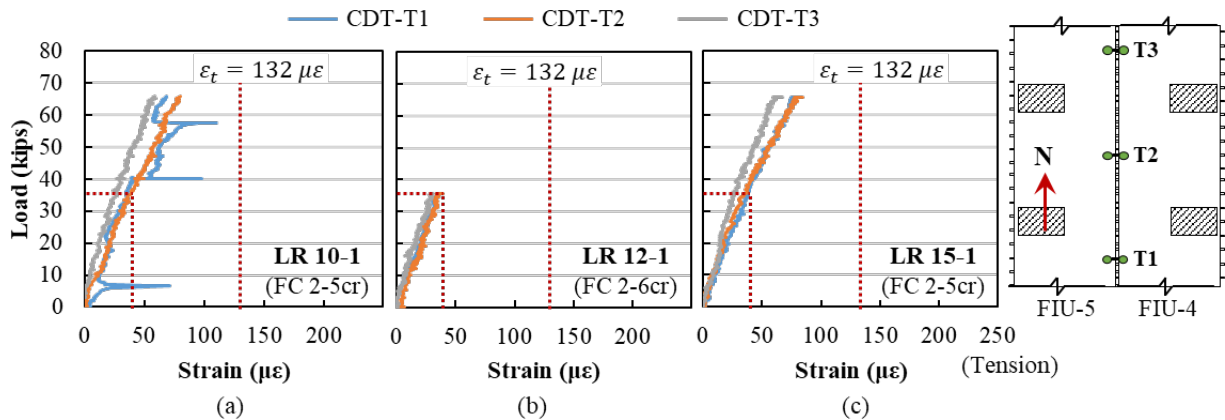


Figure 7.113: Load versus average strain across top of joint for (a) LR 10-1 (FC 2-5cr), (b) LR 12-1 (FC 2-6cr), and (c) LR 15-1 (FC 2-5cr)

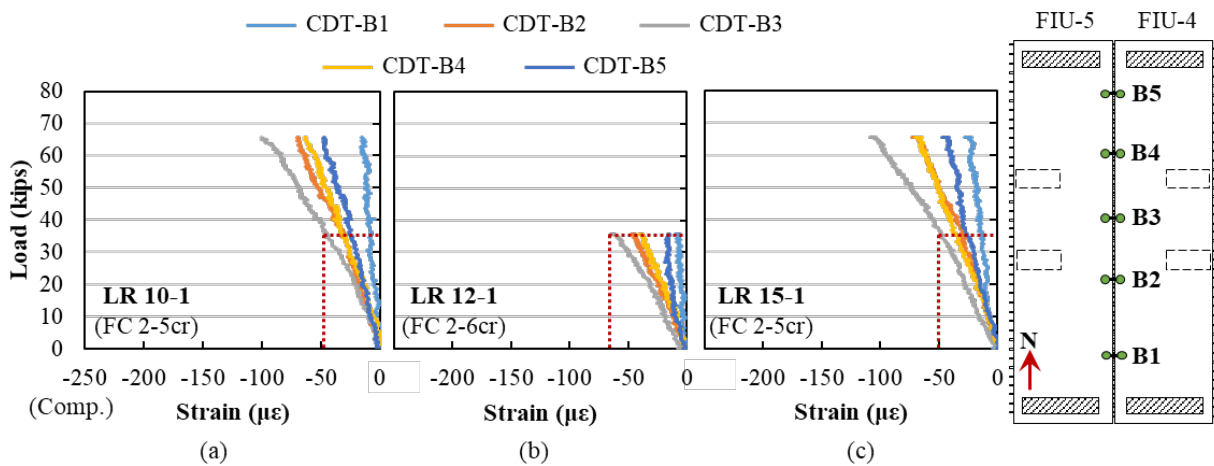


Figure 7.114: Load versus average strain across bottom of joint for (a) LR 10-1 (FC 2-5cr), (b) LR 12-1 (FC 2-6cr), and (c) LR 15-1 (FC 2-5cr)

The response measured during LR 10-1, LR 12-1, and LR 15-1 from the transverse concrete strain gauges at midspan are shown in Figure 7.116. Transverse tensile strains developed on the top of the section and transverse compression strains on the bottom of the section, as shown in Figure 7.116 (a) and Figure 7.116 (b), respectively. A larger top tensile strain at similar load level was measured during LR 12-1 in CSG-T11. The tensile strain in CSG-T11 also increased between LR 10-1 and LR 15-1. No cracking was observed near this gauge and strains are still less than expected cracking strains, but the precast concrete may have been close to cracking near CSG-T11. There was no change in the response of the bottom CSGs between tests, see Figure 7.116 (b).

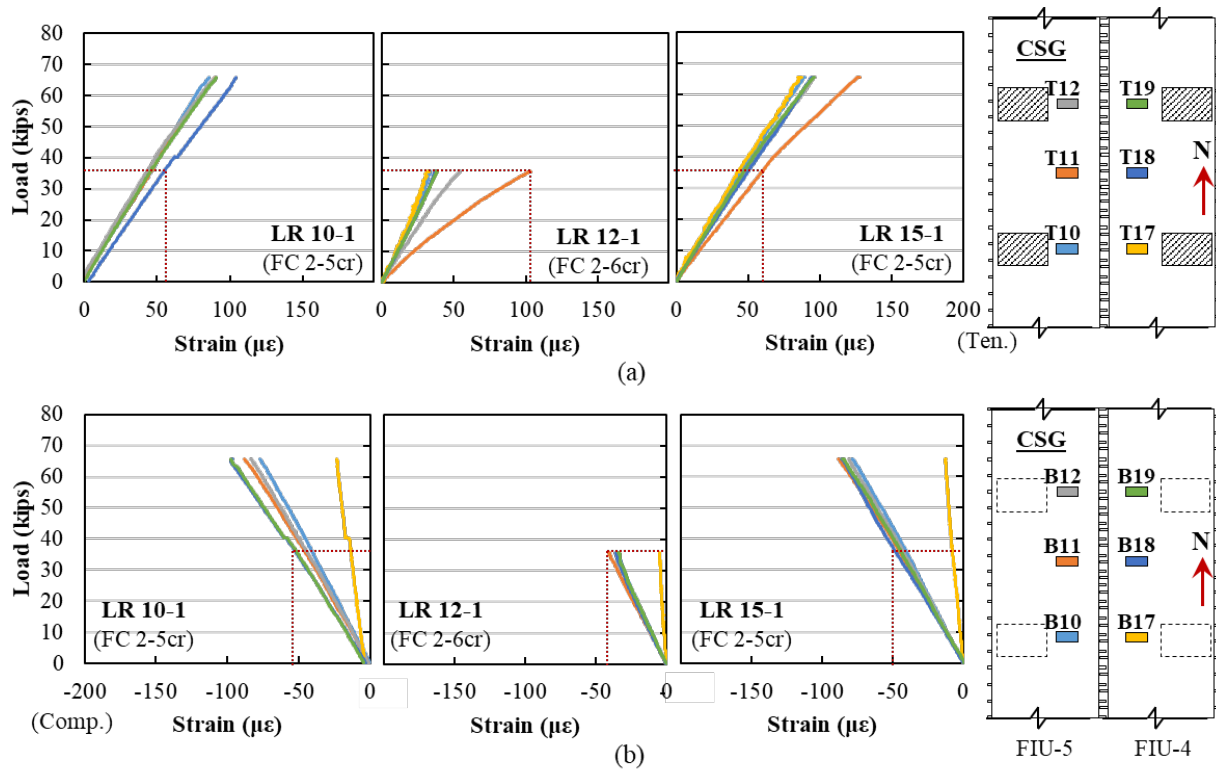


Figure 7.115: Load versus transverse concrete strain for LR 10-1, LR 12-1, and LR 15-1 for (a) top and (b) bottom of beam in the midspan section of the system

The measured response for the RSGs on the joint reinforcement extending from FIU-5 in the midspan and south sections of the system for LR 10-1, LR 12-1, and LR 15-1 are shown in Figure 7.117. All joint reinforcement at midspan had minimal compression strains during the test, as shown in Figure 7.117 (a). RSG-9 had increased strains in LR 12-1 and LR 15-1 compared to LR 10-1. RSG-10, RSG-11, and RSG-12 showed change in response around 40 kips of applied load (when the load on the west beam was held constant and load in east beam was increased). Some RSGs in the end region saw minor tensile strains (RSG-1 through RSG-4) in all loading ramps.

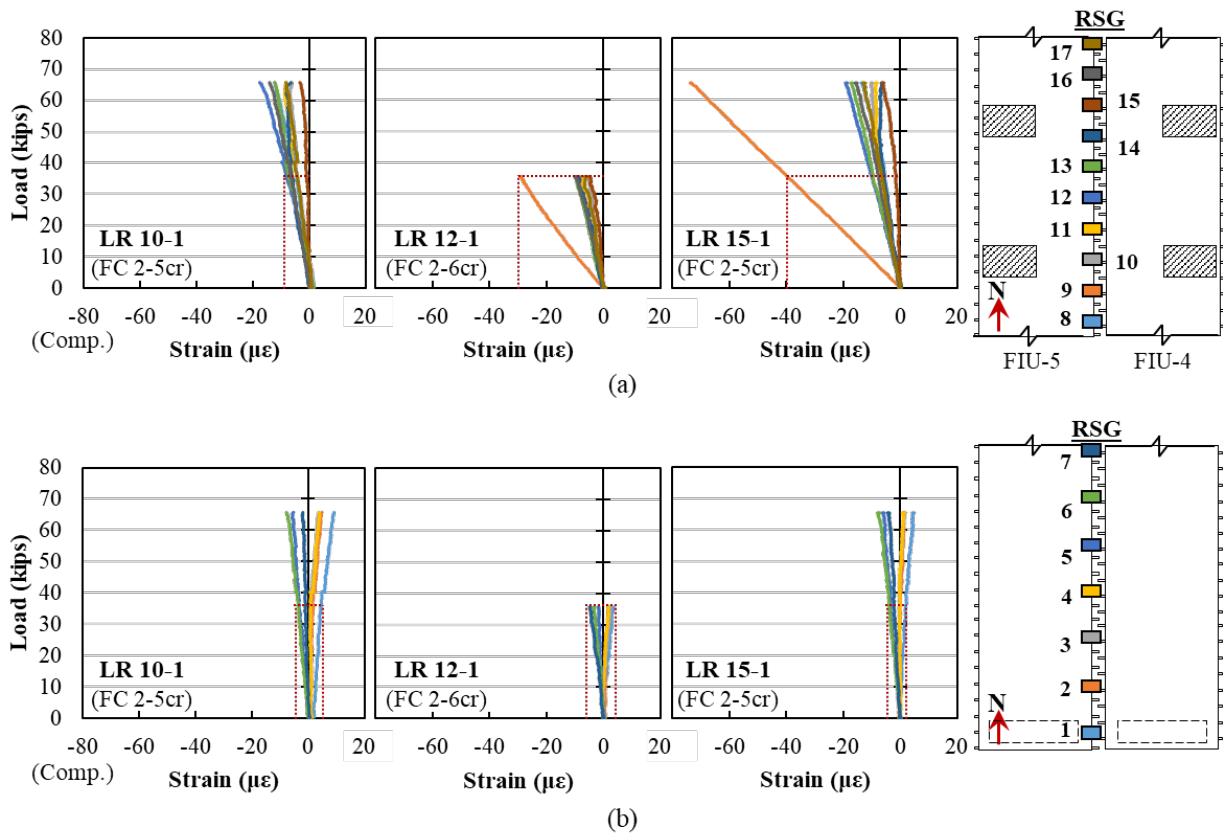


Figure 7.116: Load versus strain for LR 10-1, LR 12-1 and LR 15-1 for joint reinforcement extending from FIU-5 for the (a) midspan and (b) south sections of the system

The strain change per change in applied load for cycles in Stages 13 and 14 for the top and bottom CDTs are shown in Figure 7.118 and Figure 7.119. There was no significant change in the measured response throughout the cyclic loading (outside of the changes caused by different load and support configurations).

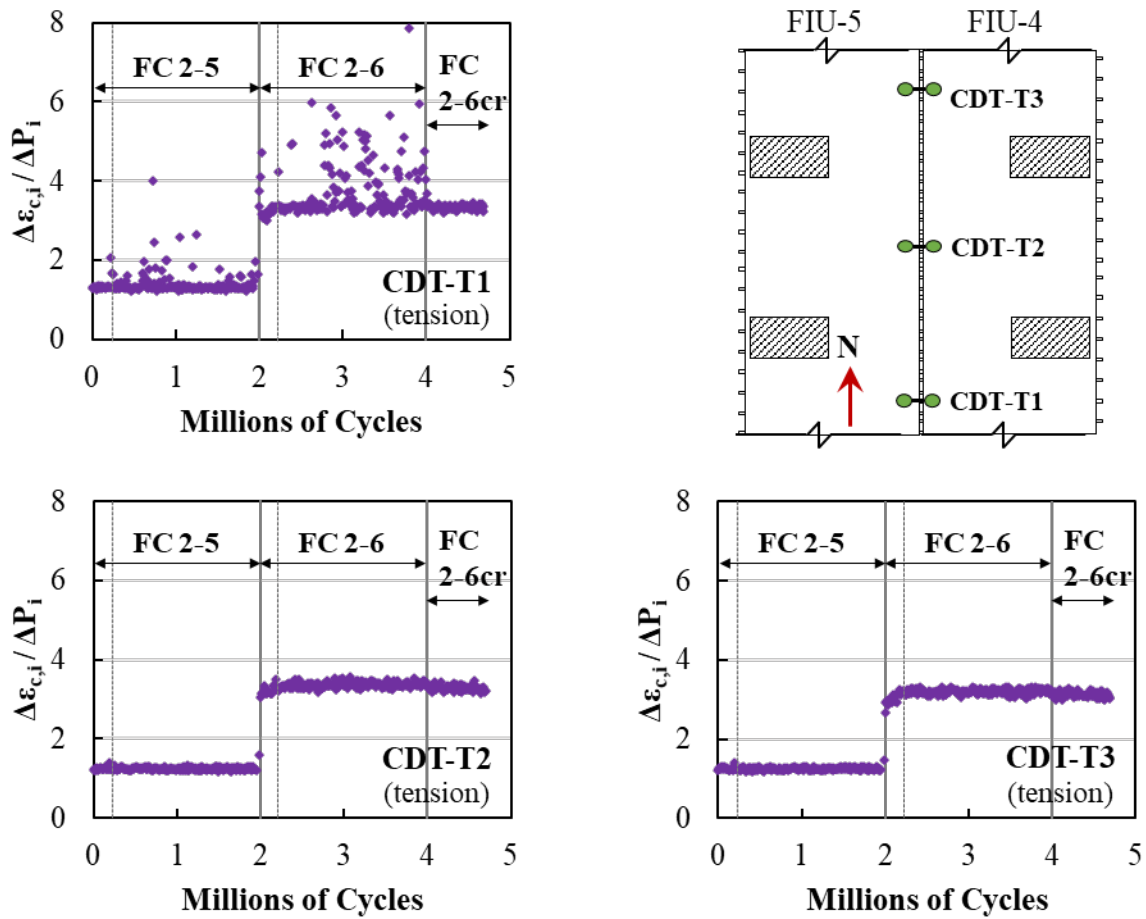


Figure 7.117: Strain change of crack gauge per change in applied load versus number of cycles at center of specimen (top) for all cyclic loading

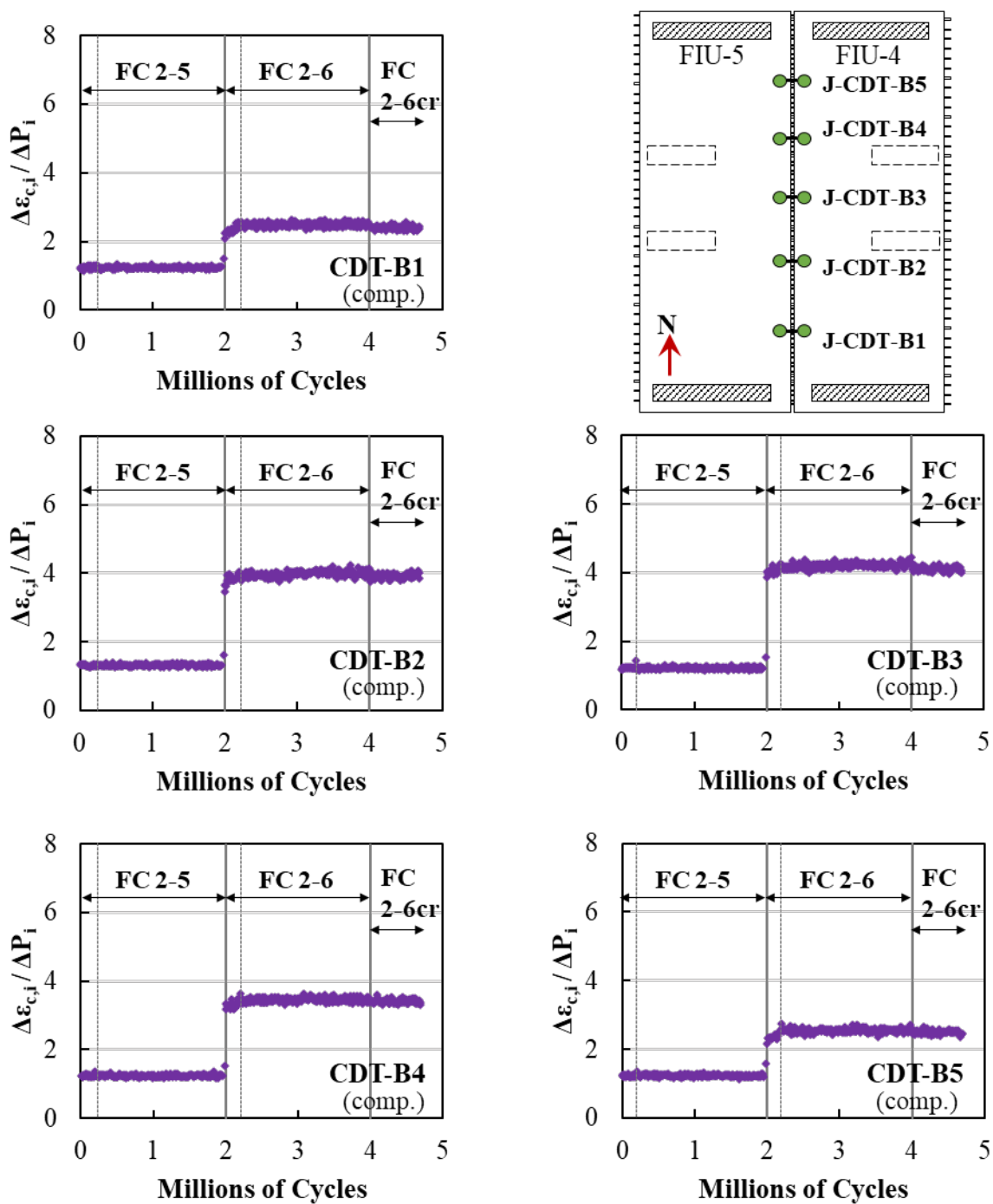


Figure 7.118: Strain change of crack gauge per change in applied load versus number of cycles at center of specimen (bottom) for all cyclic loading

The measured strain change per change in applied load for two top transverse CSGs at midspan are shown in Figure 7.120. There was an increase in strain change per change in applied load for CSG-T11 before and after the transverse and longitudinal cracking load stages. This would suggest that the softer response of FIU-4 led to increased transverse tension in the FIU-5 precast beam,

which is consistent with the observations from the service load tests shown in Figure 7.116. There was minimal change in the transverse response during Stage 13 and 14.

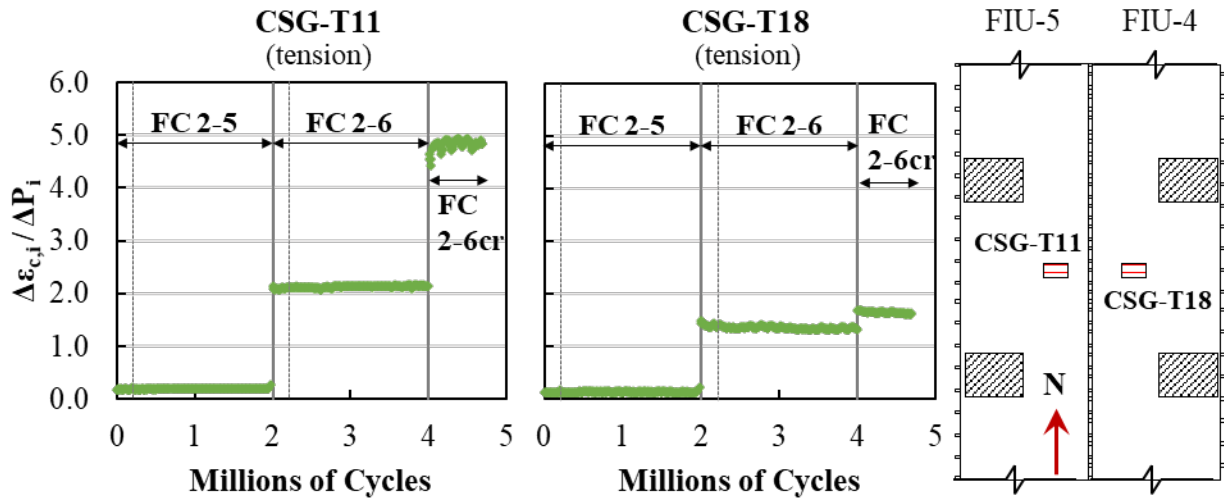


Figure 7.119: Strain change of top transverse CSGs per change in applied load versus number of cycles at center of specimen for all cyclic loading

The measured strain change per change in applied load for two bottom transverse CSGs at midspan are shown in Figure 7.121. A minor change in transverse compression response was observed before and after the transverse and longitudinal cracking load stages with little change between responses within each cyclic load stage.

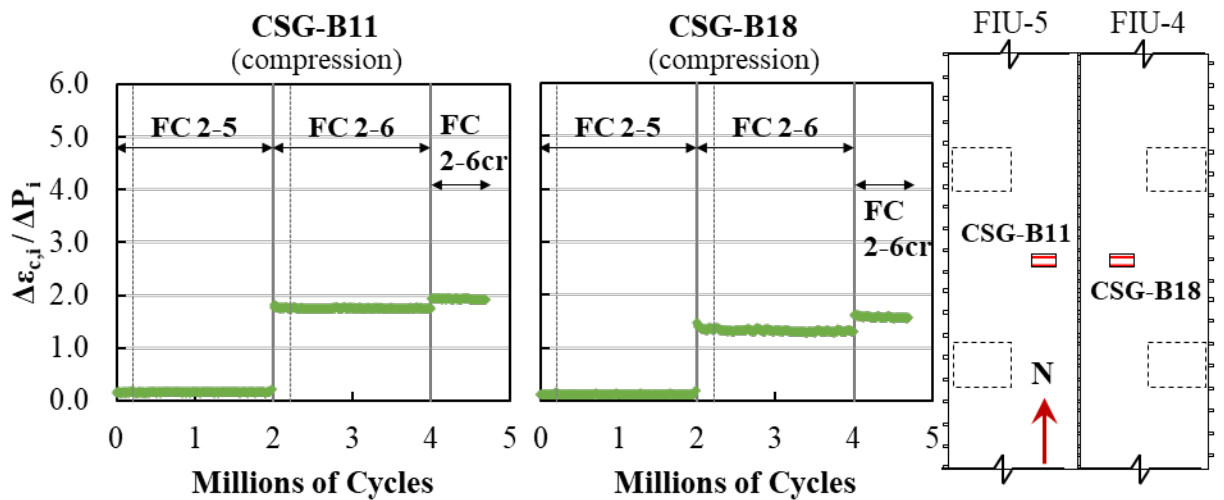


Figure 7.120: Strain change of bottom transverse CSGs per change in applied load versus number of cycles at center of specimen for all cyclic loading

The measured response from three RSGs located on the west center side is shown in Figure 7.122. There was little change in the response in these bars before and after the transverse and longitudinal cracking load stages and within each cyclic load stage.

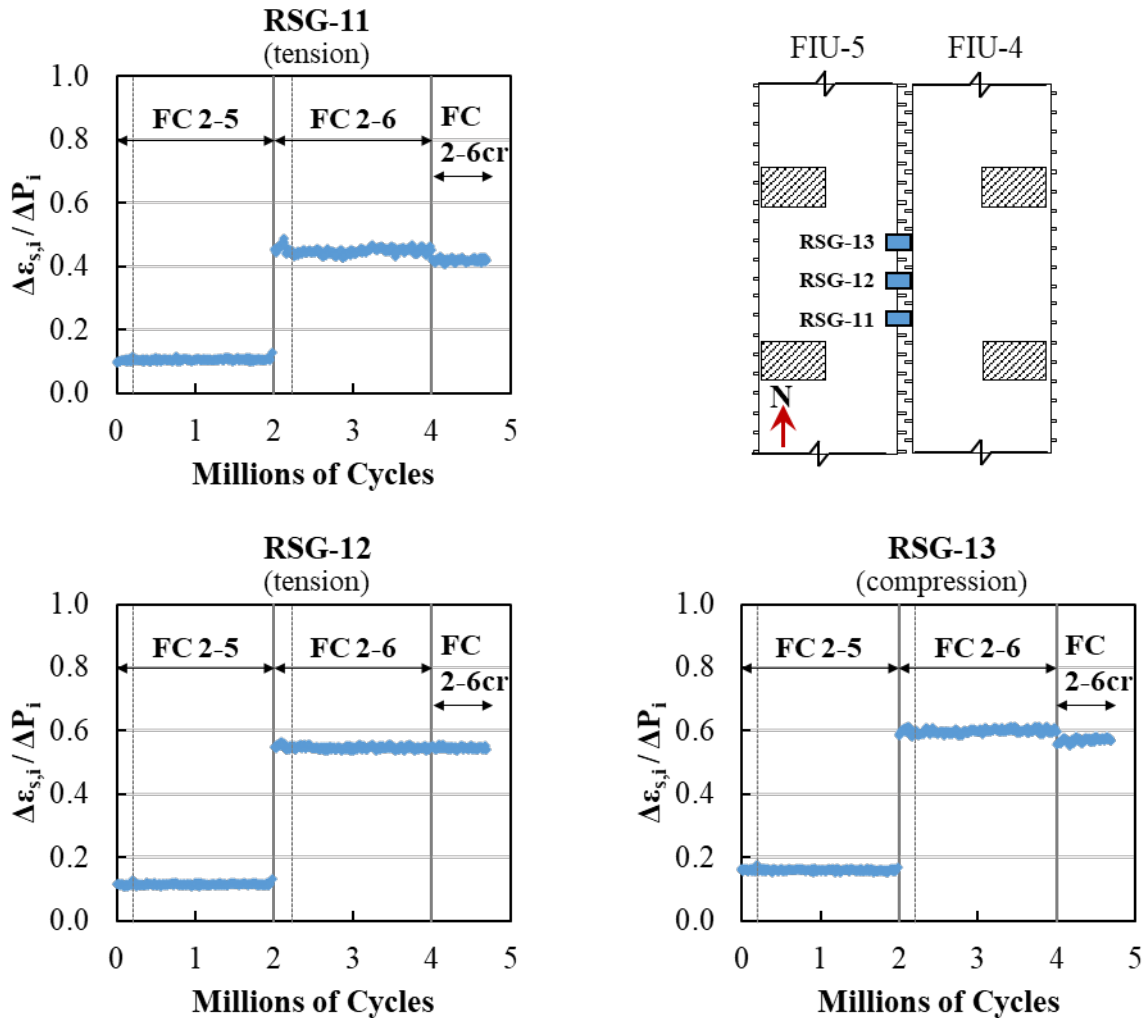


Figure 7.121: Strain change of RSGs per change in applied load versus number of cycles at center of specimen for all cyclic loading

7.7.8.3. Longitudinal Behavior

The measured strain response obtained during LR 10-1, LR 12-1, and LR 15-1 application from the longitudinal CSGs at midspan are shown in Figure 7.123. Similar compression strains were measured on top of system during LR 10-1, LR 12-1, and LR 15-1, as shown in Figure 7.123 (a). Similar response was measured between the two adjacent beams for LR 10-1 and LR 15-1 (without the intermediate supports); slightly higher strains were measured in the unrestrained beam for LR 12-1.

The effect of transverse cracking can be seen for LR 15-1 in Figure 7.123 (b); CSG-B24 began to have a sharp increase in tensile strains and CSG-B25 sharp decrease in tensile strains at approximately 45 kips. This can be compared to the cracking load of approximate 63 kips measured during LR 10-1. The lower load for LR 15-1 is because the beams were already cracked

before testing, so while the tensile strength of the concrete needed to be overcome before cracking in LR 10-1, the cracks began to open as soon as tensile strains developed at the location of the cracks in LR 15-1.

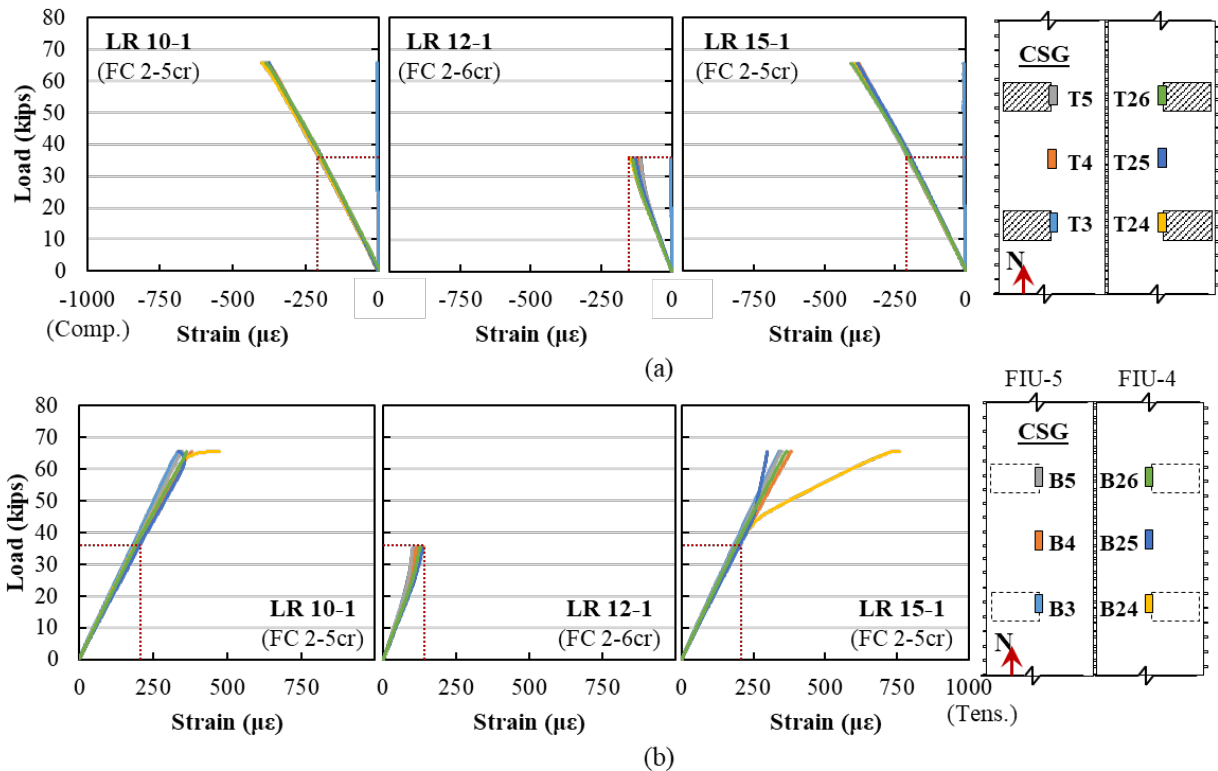


Figure 7.122: Load versus longitudinal concrete strain for LR 10-1, LR 12-1 and LR 15-1 for (a) top and (b) bottom of beam in the midspan section of the system (LR 15-1)

The strain changes per change in applied load versus number of cycles for two longitudinal CSGs in the center region on the top and on the bottom of the system are shown in Figure 7.124 and Figure 7.125, respectively. There was an increase in strain change per applied load before and after the transverse and longitudinal cracking load stages for both the top and bottom of the system. There was also a noticeable decrease in strain change per applied load during the cyclic testing in Stages 13 and 14, suggesting that the transverse cracks were slowly growing during the fatigue testing. This was also confirmed in the visual inspection of the beams, shown in Figure 7.113 above.

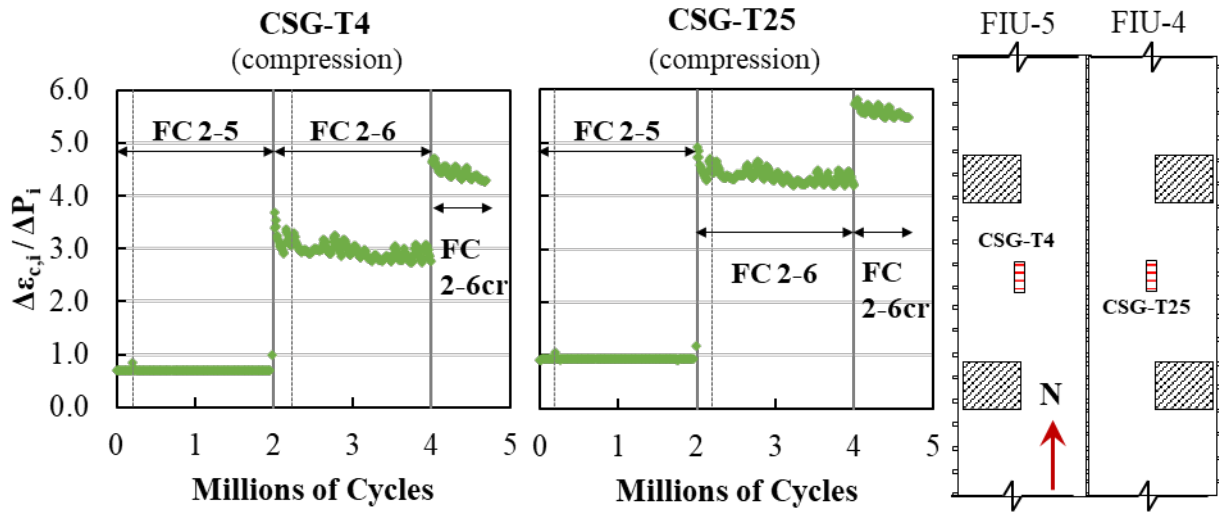


Figure 7.123: Strain change of top longitudinal CSGs per change in applied load versus number of cycles at center of specimen for all cyclic loading

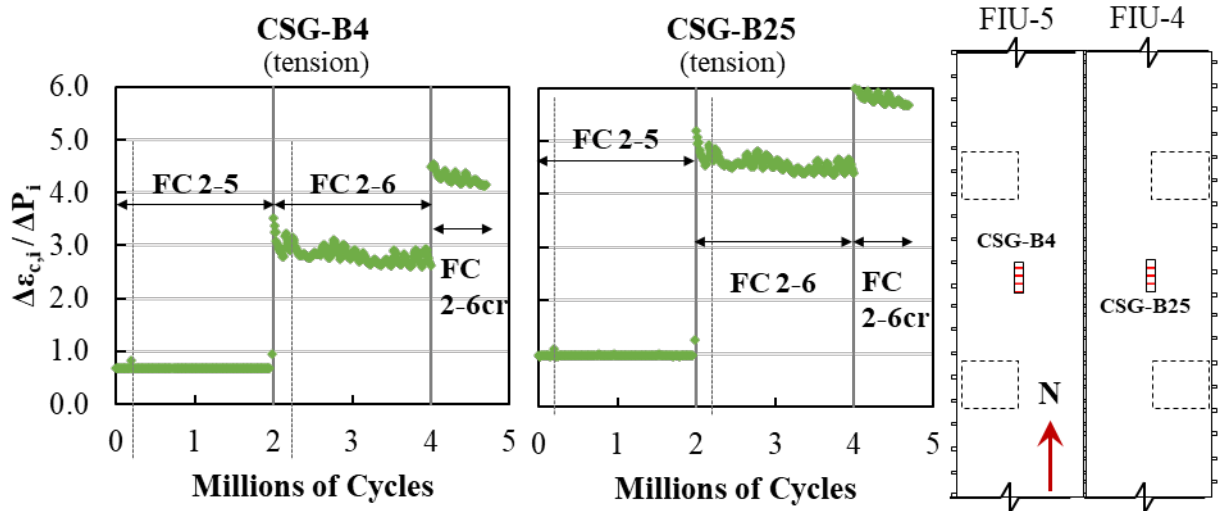


Figure 7.124: Strain change of bottom longitudinal CSGs per change in applied load versus number of cycles at center of specimen for all cyclic loading

7.7.8.4. Summary

The results presented in this section were from the final service and fatigue testing performed on the two-beam system with FIU-4 and FIU-5. Several overall observations from the service and fatigue testing:

1. There was no distress (e.g., cracking or debonding at the joint interface, reinforcement bond) in the joint region during any of the fatigue or static service load testing performed on this two-beam system.

2. Transverse cracking increased the transverse demand on the top of the precast beam when interior supports were provided. The transverse cracking caused decreased stiffness in the unrestrained beam, which led to the increased transverse strains on the top of the restrained precast beam. However, strains remained less than the expected cracking strain and no longitudinal cracks were observed in the top of the beams.
3. After the transverse cracks were created during Stage 11, the fatigue loading caused slow growth of the transverse cracks, observed through the CSG response and visual observation. Fatigue loading prior to Stage 11 would not have likely caused transverse cracks to develop.

7.7.9. Strength Test Results (Stage 16, LC 2-1)

7.7.9.1. Overview

Ultimate strength testing using LC 2-1 was performed on the two-beam system with FIU-4/5 after all the service and fatigue testing was completed. This was the same configuration as the two-beam system with FIU-1/2. Results from these two two-beam system tests will be compared throughout this section to highlight any effects of the fatigue testing on the system response.

The load versus midspan deflection responses for FIU-1/2 and FIU-4/5 ultimate strength tests are shown in Figure 7.126. The supports settlement is accounted for in the deflection shown. Similar ultimate strengths were measured in both systems (159.1 kips for FIU-4/5 and 158.7 kips for FIU 1/2) with a similar load deflection response. The deflection in FIU-4/5 did not increase between approximately 155 kips and failure (159.1 kips); this may have been a result of the change in behavior as hinging in the beam occurred at one of the bearings. Both FIU-1/2 and FIU-4/5 showed a ductile system response with over 6 inches of deflection at the time of failure.

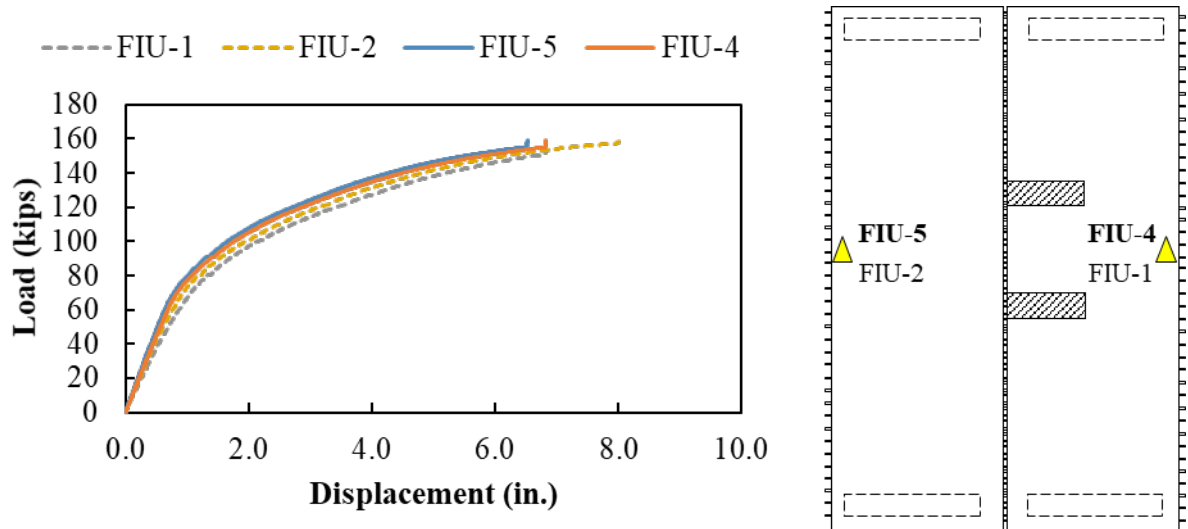


Figure 7.125: Load versus midspan displacement for ultimate strength testing with LC 2-1 for FIU 4/5 and FIU 1/2

Observations from the ultimate strength test are summarized by load step in Table 7.12 and observed crack patterns on the bottom of the specimen in Figure 7.127. Previous cracks were

present due to the crack load ramps and inelastic cyclic assessments; cracks present before ultimate strength testing are marked in red, and cracks caused by ultimate strength testing are shown in blue in Figure 7.127. At 65 kips, some of the previous cracks present in FIU-4 grew and extended into FIU-5; some additional cracks also initiated from the outside edge of FIU-5. At 90 kips, cracking extended across the entire width of the two-beam system. All cracks observed until this point were transverse cracks located near the constant moment region in the midspan of the system. There were no signs of transverse cracking near the supports or longitudinal cracking on top or bottom of the specimens. Cracks were not visually inspected after 90 kips.

Table 7.12: Observations during ultimate strength testing of FIU-4/5

Step	Load Ranges	Observations	Figure
1	0 k	No crack growth was observed	Figure 7.127(a)
2	0 k – 65 k	Crack growth observed on FIU-4. Four transverse cracks developed from the outside of FIU-5.	Figure 7.127(b)
3	65 k – 90 k	Transverse cracks seen crossing the whole system at 90 kips	Figure 7.127(c)
4	Load until failure	Failure was observed at 159.1 kips	-

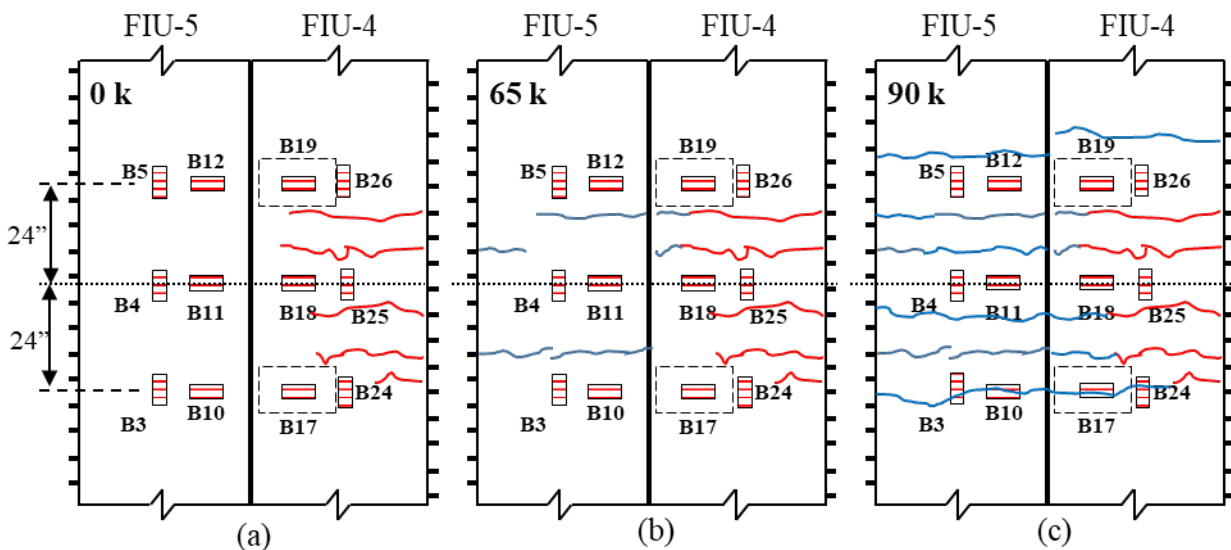


Figure 7.126: Bottom crack pattern at midspan for ultimate strength testing with Load Configuration 2-1 at (a) 0 kips, (b) 65 kips, and (c) 90 kips; blue = new cracks, red = cracks from previous tests

7.7.9.2. Joint Behavior

The average strain across the joint measured using the CDTs on top and bottom of the system are shown in Figure 7.128 and Figure 7.129 for FIU-4/5 and FIU-1/2. The CDTs were removed from the systems before the ultimate capacity was reached, at 80 kips for FIU-1/2 and 90 kips for FIU-4/5. Similar levels of transverse tension developed across the top of the joint for both two-beam tests with levels less than the estimated cracking strain for the precast concrete ($132 \mu\epsilon$).

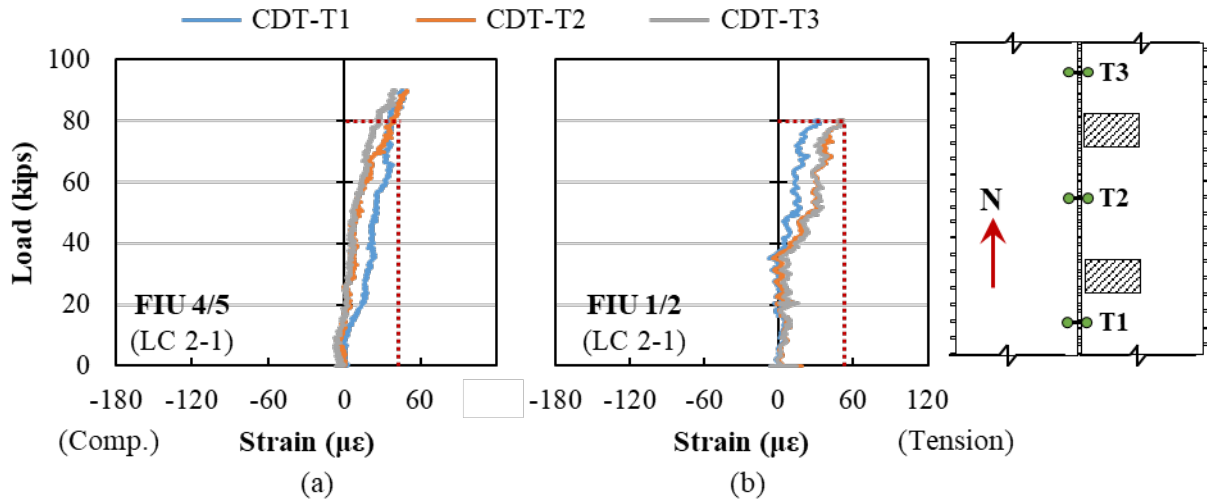


Figure 7.127: Load versus average strain across top of joint for ultimate strength testing with LC 2-1 for (a) FIU-4/5 and (b) FIU-1/2

The strain responses across the bottom of the joint along the length of FIU-4/5 and FIU-1/2 systems are shown in Figure 7.129. Compression strains were measured across the bottom of the FIU-1/2 joint other than the north end of the beam (CDT-B5). Tensile strains were measured in two of the sensors near midspan (CDT-B2 and CDT-B3) for FIU-4/5. The measured tensile strains would suggest that longitudinal cracking may have occurred at approximately 70 kips of total applied, although this was not observed in any of the other transverse strain gauges at this load (e.g., RSGs, CSGs). There was an increase in tensile strains observed in a nearby transverse CSG (CSG-B17) at 90 kips and an observed change in some of the longitudinal CSGs (e.g., CSG-B3, CSG-B25) at this point, see Figure 7.134. These observations may suggest that the change in the CDT response was initially caused by the opening of transverse cracks, but that some longitudinal cracks were developing as the applied load increased.

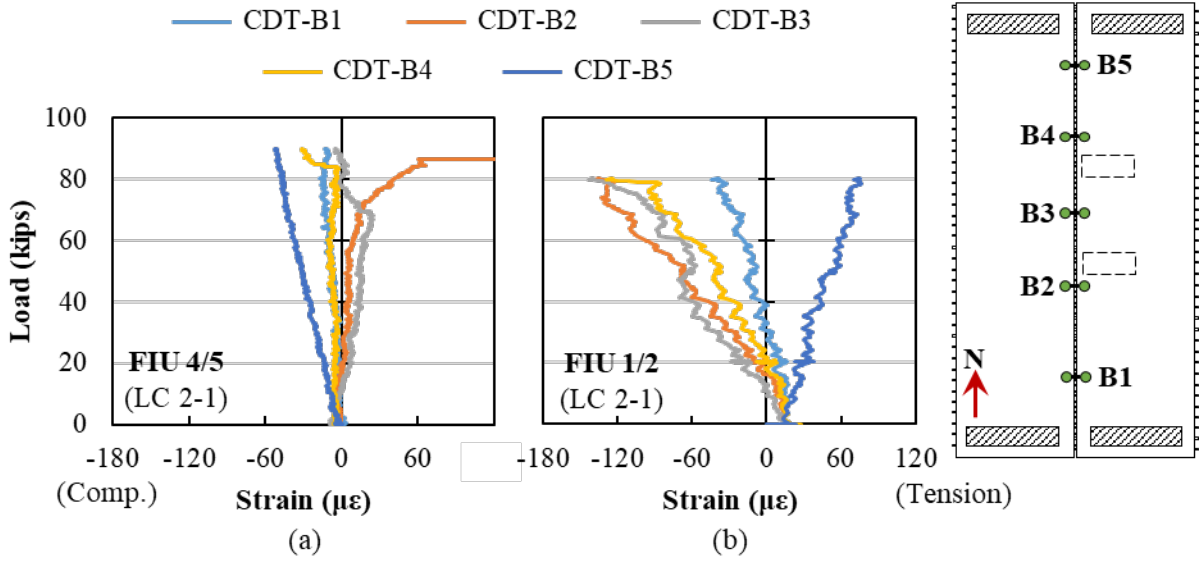


Figure 7.128: Load versus average strain across bottom of joint for ultimate strength testing with LC 2-1 for (a) FIU-4/5 and (b) FIU-1/2

The measured response from the transverse CSGs in the center region are shown in Figure 7.130 for FIU-4/5 and FIU-1/2. Most of the CSGs in both tests showed transverse tension across the top of the joint and transverse compression across the bottom of the joint for both systems. In FIU-4/5, there were possible signs of cracking through CSG-B17 and adjacent to CSG-B10 at approximately 90 kips and through CSG-B11 at approximately 100 kips, which was different than the measured response from FIU-1/2.

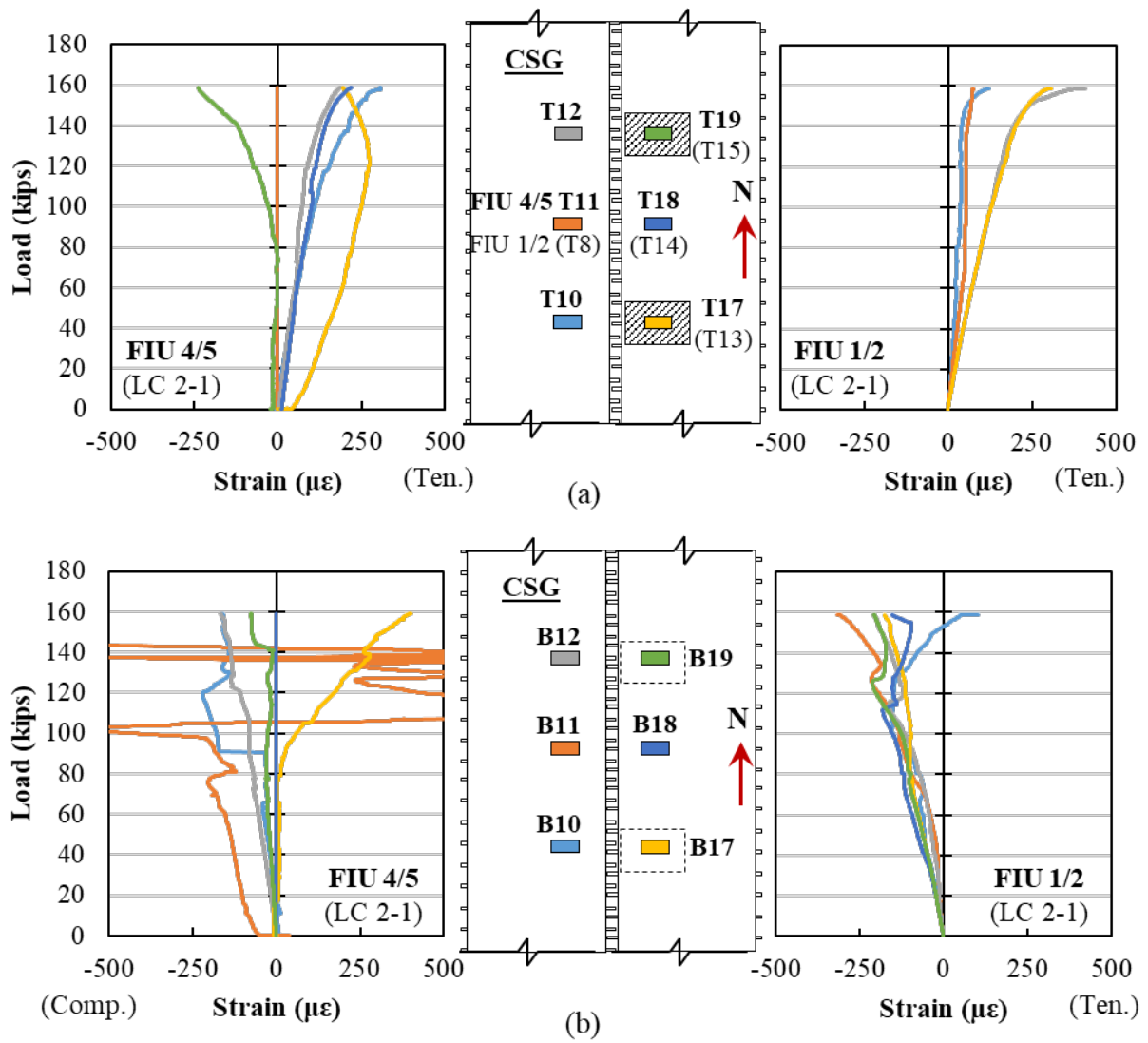


Figure 7.129: Load versus transverse concrete strain for ultimate strength testing with LC 2-1 for (a) top and (b) bottom of beam in the midspan section of FIU-4/5 and FIU-1/2

The measured response for the RSGs on the joint reinforcement extending from the west beam in the midspan and south sections of the system is shown in Figure 7.131 for FIU-4/5 and FIU-1/2. Tensile strains began to develop non-linearly in the joint reinforcement after 75 kips applied load at the center region for both systems, but levels remained below the yield strain of the reinforcement. The reinforcement closest to the load patches had the highest strain levels, with reinforcement strains generally decreasing as the distance from the load patches increased.

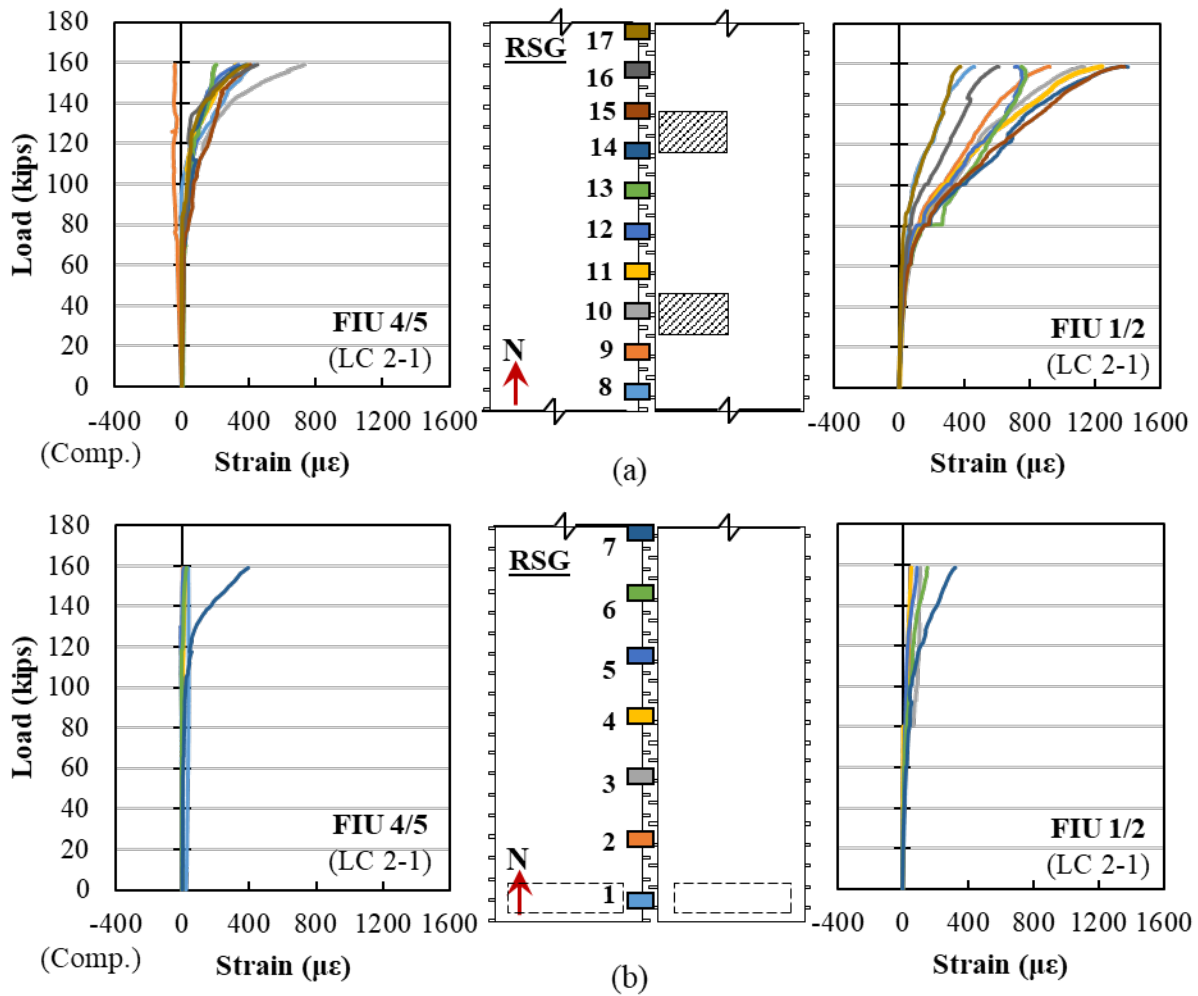


Figure 7.130: Load versus strain for ultimate strength testing with LC 2-1 for joint reinforcement extending from FIU-5 and FIU-2 for the (a) midspan and (b) south sections of the system

Like FIU-1/2 ultimate strength test, no joint distress was observed in FIU-4/5 on the top or bottom of the joint along the length of the system. Failure of both FIU-1/2 and FIU-4/5 was triggered by crushing of the concrete just inside one of the load points, shown in Figure 7.132. The UHPC in the joint region also showed signs of crushing in both systems, which suggests a good bond between the precast beam and the joint.



Figure 7.131: Crushing of FIU-5 and FIU-4 concrete at failure for Load Configuration 2-1: (a) overview and (b) crushing of UHPC in joint

Three cores were taken after testing at the joint interface in the same locations near midspan for FIU-4/5 and FIU-1/2, as shown in Figure 7.133 (a) and (b). The top of some of the cores from FIU-4 broke off while being removed from the beam, see Figure 7.133 (d) and (e); this occurred in FIU-4/5 and not FIU-1/2 because the core from FIU-4/5 did not include any of the UHPC that extended to the top of the joint. There was some minor cracking in most of the cylinders near the interface between the bottom lip of the precast beam and UHPC joint material. This further growth of this crack was likely restrained by the joint reinforcement. There was no debonding or cracking observed along the rest of the joint, which shows good bond between the precast concrete and UHPC and overall good performance of the joint.

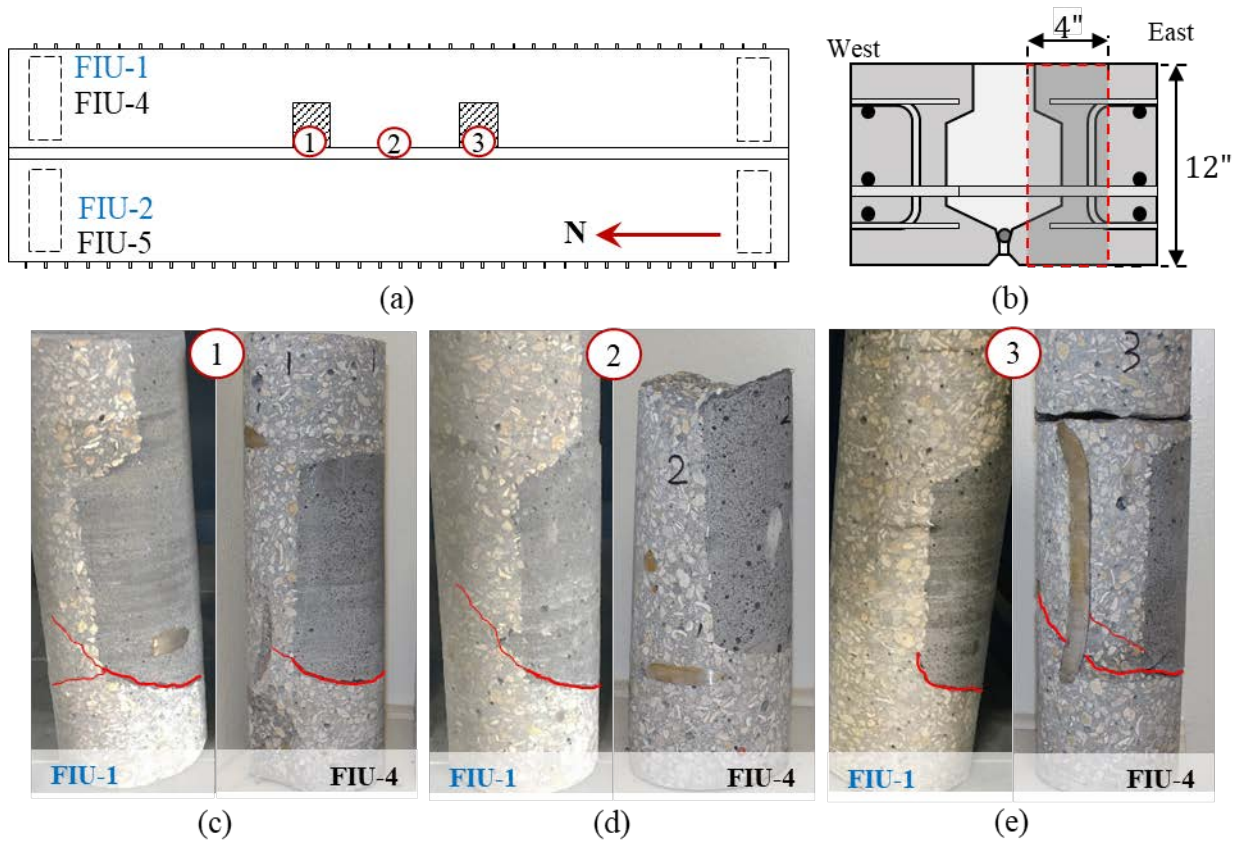


Figure 7.132: FIU-1/2 and FIU4/5 joint edge cores: (a) location along length of cores taken, (b) cross section location, (c) Core #1, (d) Core #2, and (e) Core #3 with cracking highlighted

7.7.9.3. Longitudinal Behavior

The measured response from the longitudinal CSGs at midspan are shown in Figure 7.134 for FIU-4/5 and FIU-1/2. Both systems already had transverse cracking present before the ultimate strength testing. Crack reopening could be observed using the longitudinal CSGs on the bottom of the beams when the load versus strain response became non-linear. This occurred at approximately 45 kips for FIU-4/5 (see CSG-B24) and 40 kips for FIU-1/2 (see all gauges other than CSG-B25). The compressive strains measured on the top of the beams had a parabolic shape in compression up until the crushing of concrete occurred at a strain of approximately 0.003 for both systems. Tensile strain was observed in the top of FIU-4 between the load points (CSG-T25); it is unclear why tensile strain developed at this point.

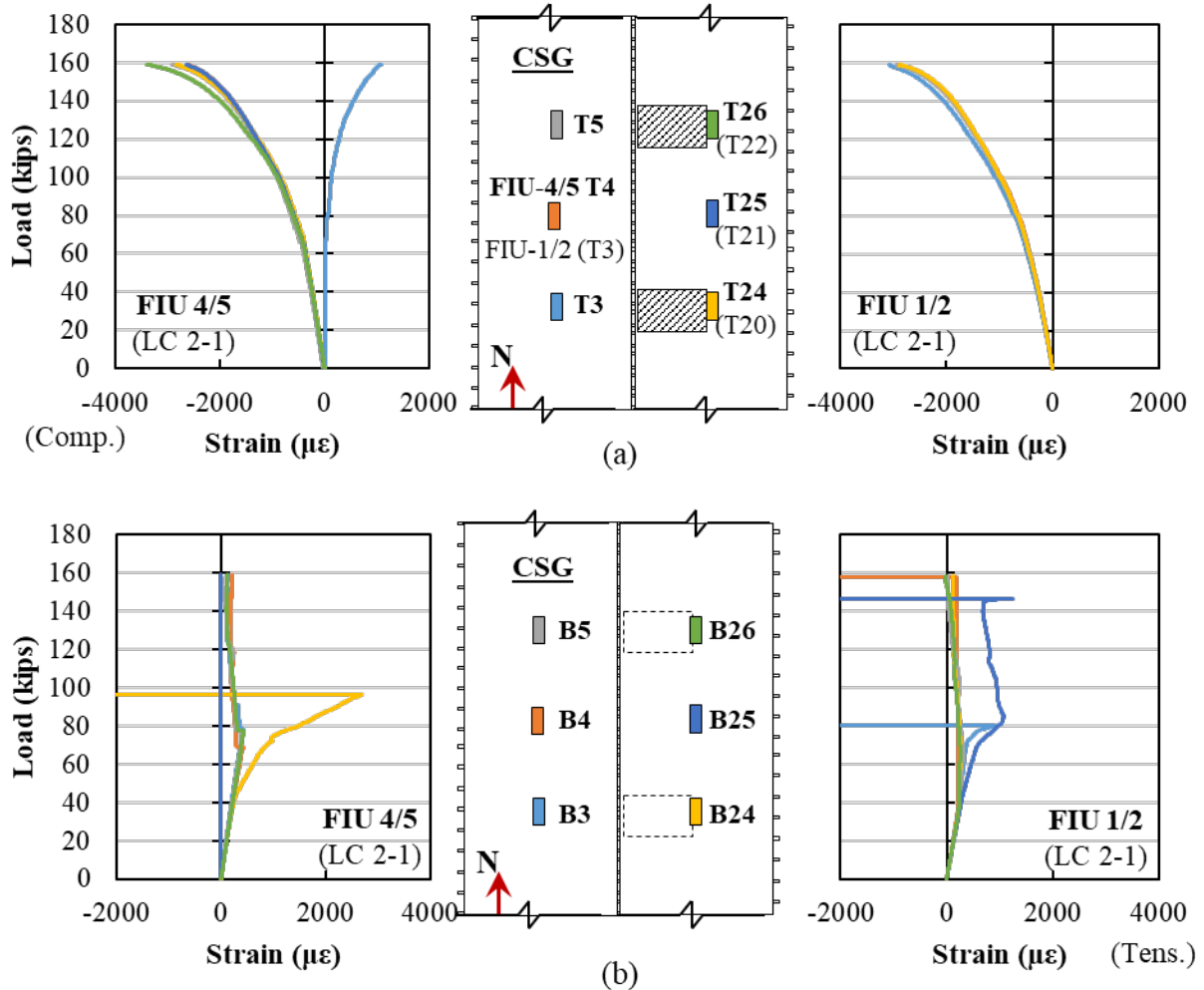


Figure 7.133: Load versus longitudinal concrete strain for ultimate strength testing with LC 2-1 for (a) top and (b) bottom of beam in the midspan section of FIU-4/5 and FIU-1/2

7.7.9.4. Summary

FIU-4/5 had similar performance to FIU-1/2, which shows that the 4.7 million cycles and other service load and cracking tests did not impact the overall system behavior. Both systems showed overall ductile response, effective load transfer between beams, and no damage to the joint at the time of failure. Other observations include:

1. Transverse tension was measured in the top of the beams (CSGs) and across the top of the joint (CDTs) and transverse compression across the bottom of the beams and across the bottom of the joints. This was also observed in the other load and support configurations (LC 2-4, FC 2-5, and FC 2-6). Transverse tension was below the estimated tensile cracking strain for the precast concrete for all service tests but exceeded this strain in the ultimate strength test at high levels of load.

2. Tension was measured in the joint reinforcement with higher tensile strains measured near the load points. The joint reinforcement also appeared to help inhibit the growth of cracks that developed between the top of the bottom lip and UHPC in the joint.
3. Crushing of concrete on the top of the beam occurred across the entire width of the system (including the precast concrete and UHPC joint). This shows the good bond between the UHPC and precast concrete and composite behavior of the system.

7.8. CONCLUSIONS AND RECOMMENDATIONS

Service and ultimate strength testing were performed on one two-beam system (FIU-1/2) and service, fatigue, and ultimate strength testing were performed on a second two-beam system (FIU-4/5). The following conclusions and recommendations can be made based on these two two-beam system tests.

- The joint performed well during service load and ultimate strength testing. No joint debonding or distress was observed in the joint region during any of the service, fatigue, and ultimate load testing. The concrete in the compression block crushed across the entire width of the system (including the UHPC joint), which highlighted the quality of the bond between the UHPC and precast concrete. Additionally, the joint successfully transferred stress between beams; there was only a minor differential displacement between beams when only one beam was loaded.
- FIU-4/5 had similar performance to FIU-1/2 during the ultimate strength testing, which shows that the 4.7 million cycles and other service load and cracking tests did not impact the overall system behavior.
- Transverse tension was measured in the top of the beams (using CSGs) and across the top of the joint (using CDTs) and transverse compression across the bottom of the beams and across the bottom of the joints in all the load and support configurations for FIU-4/5 (LC 2-1, LC 2-4, FC 2-5, FC 2-6, and FC 2-7). Transverse tension was below the estimated tensile cracking strain for the precast concrete for all service tests but exceeded this strain in the ultimate strength test (LC 2-1) at high levels of load (above service levels). Further numerical study should be done on deeper sections (e.g., 15-inch and 18-inch-deep sections) including stresses induced by temperature effects to see if a top layer of reinforcement is needed.
- Transverse cracking of one beam (when the other beam remained uncracked) increased the transverse demand on the top of the adjacent precast beam when interior supports were provided. The transverse cracking caused a decreased stiffness in the unrestrained beam, which led to the increased transverse strains on the top of the restrained precast beam. However, strains remained less than the expected cracking strain and no longitudinal cracks were observed in the top of the beams. This shows that unequal stiffness between adjacent beams can lead to increased demand in the joint.
- Small compression strains ($< 50 \mu\epsilon$) were generally measured in the joint reinforcement for the service and fatigue load configurations (LC 2-4, FC 2-5, FC 2-6, and FC 2-7). Larger tensile strains ($> 300 \mu\epsilon$) were measured during LC 2-1 in the joint reinforcement with the

highest strains measured near the load points. Strains remained under the yield strain for steel. The joint reinforcement also appeared to help inhibit the growth of cracks that developed between the top of the bottom lip and UHPC in the joint.

- There were no signs of bond deterioration between the joint reinforcement and UHPC in the joint during any of the fatigue, service, or strength testing.

These conclusions will be further verified through the four-beam test described in Chapter 8.

8. FULL-SCALE EXPERIMENTAL TESTING (FOUR-BEAM)

8.1. INTRODUCTION

The objective of this testing was to assess the behavior of the joints and superstructure system of the recently developed modified Florida Slab Beam (FSB) with ultra-high-performance concrete (UHPC) joints using a four-beam superstructure system. The section, joint design, and testing protocols for the modified FSBs were based on the optimized joint geometry developed in previous small- and large-scale testing tasks. One four-beam test configuration (FIU-6/3/8/7) was tested using service, fatigue, and ultimate strength tests with several different load and support configurations. This chapter contains a summary of the Phase III test and load configurations used, details on joint construction, the instrumentation schedules, and a summary and discussion of results from testing on the four-beam system.

8.2. TEST PHASES

As described in Chapter 7, a total of eight 30-foot long, 12-inch-thick FSBs with optimized joint geometry were designed by the researchers and constructed by a local precaster. One set of five beams (FIU-1 through FIU-5) was designed with a prestress configuration per current FDOT specifications [57], with a layer of partially tensioned top strands. The second set of three beams (FIU-6 through FIU-8) had the same strand configuration as the first set of beams except they had fully stressed top strands. Four (4) of the eight (8) beams were used for the testing performed previously (two two-beam configurations). The remaining four (4) beams were used in the next phase of testing described in this chapter. The beams used in the third phase of the full-scale beam tests are shown in Figure 7.1. Several different stiffness configurations (SC), loading configurations (LC), and fatigue configurations (FC) were used in this phase of testing; these will be described in more detail in later sections.

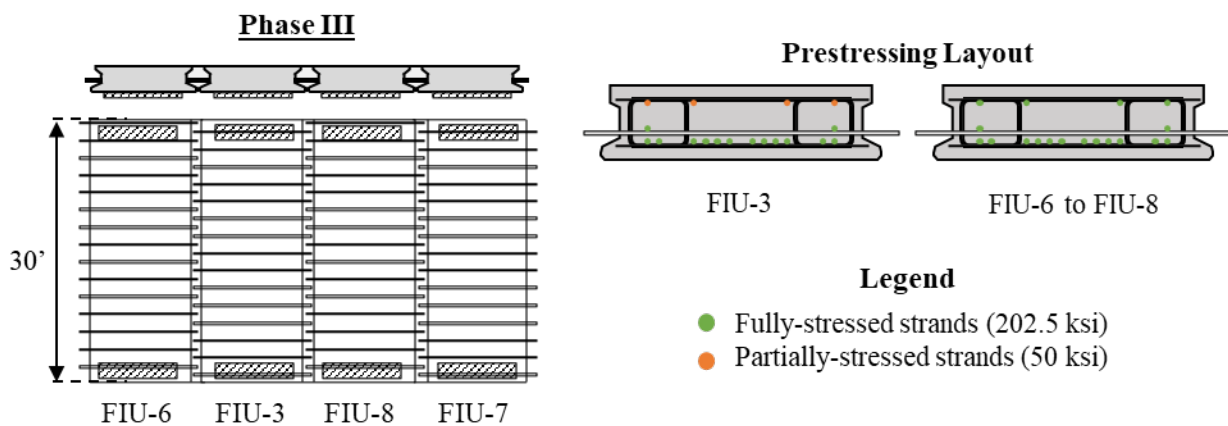


Figure 8.1: Testing phase III for full-scale FSB tests

The third testing phase (Phase III) was a simply supported, four-beam test configuration with beams FIU-6, FIU-3, FIU-8, and FIU-7. These beams were subjected to stiffness (SC 4-1 through SC 4-4) and service (LC 4-1 through LC 4-4) loading conditions under rear HS-20 half axle, as shown in Figure 8.2. FIU-6 through FIU-8 were designed with fully stressed top strands, compared with FIU-3 with partially stressed top strands, which led to a differential camber

between FIU-3 and the adjacent beams. A camber leveling stage (CL 4-2) was performed before construction of the UHPC joints by applying a surcharge load to FIU-3. Once the beams were aligned, the joints were cast, and the surcharge released after the joint material hardened. These stages were designed to measure the locked-in stresses and moment distribution factors caused by the camber leveling action under service conditions. The loading details and testing schedules during the joint construction and camber leveling action during Stage 1 (before and after UHPC joint cast) are shown in Table 8.1.

Table 8.1: Four-beam flexural stiffness loading and camber leveling schemes

Stage	Description	Lower Limit Load ^{(1),(2)} (Δ)	Upper Limit Load ^{(1),(2)} (Δ)	Load Conditions	# Ramps	Testing Days
1.1	FIU-6 Stiffness	0 kip (0.00 in.)	20 kip ⁽³⁾ (0.37 in.)	Service SC 4-1	2	0.5
1.2	FIU-3 Stiffness	0 kip (0.00 in.)	20 kip ⁽³⁾ (0.39 in.)	Service SC 4-2	2	0.5
1.3	FIU-8 Stiffness	0 kip (0.00 in.)	20 kip ⁽³⁾ (0.36 in.)	Service SC 4-3	2	0.5
1.4	FIU-7 Stiffness	0 kip (0.00 in.)	20 kip ⁽³⁾ (0.37 in.)	Service SC 4-4	2	0.5
1.5	FIU-3 Surcharge Application	0 kip (0.00 in.)	19.25 kip ⁽⁴⁾ (0.37 in.)	CL 4-2	1	1
-	UHPC joint pour ⁽⁵⁾	-	-	-	-	-
1.6	FIU-3 Surcharge Removal	19.25 kip ⁽⁴⁾ (0.37 in.)	0 kip (0.00 in.)	CL 4-2	1	1

⁽¹⁾ Loads/displacements listed are for each actuator (not total)

⁽²⁾ Acceptable load/displacement range for loading is starting load/displacement $\pm 5\%$.

⁽³⁾ Two load ramps applied per beam without casting the joints

⁽⁴⁾ Total surcharge generated by heavy weights (10 load blocks)

⁽⁵⁾ UHPC joint pour and grind with surcharge (the beams are joined)

Service (LC 4-1cr through LC4-4cr) and strength (LC 4-5) loading conditions were also investigated with a cracked-joint condition under rear HS-20 half- and full-axle loads, as shown in Figure 8.2. The cracked scenario was simulated by saw-cutting along the length of the UHPC-to-precast boundary region of one exterior joint. These stages were designed to measure the locked-in stresses and moment distribution factors caused by the camber leveling action with a pre-cracked joint under service and strength conditions.

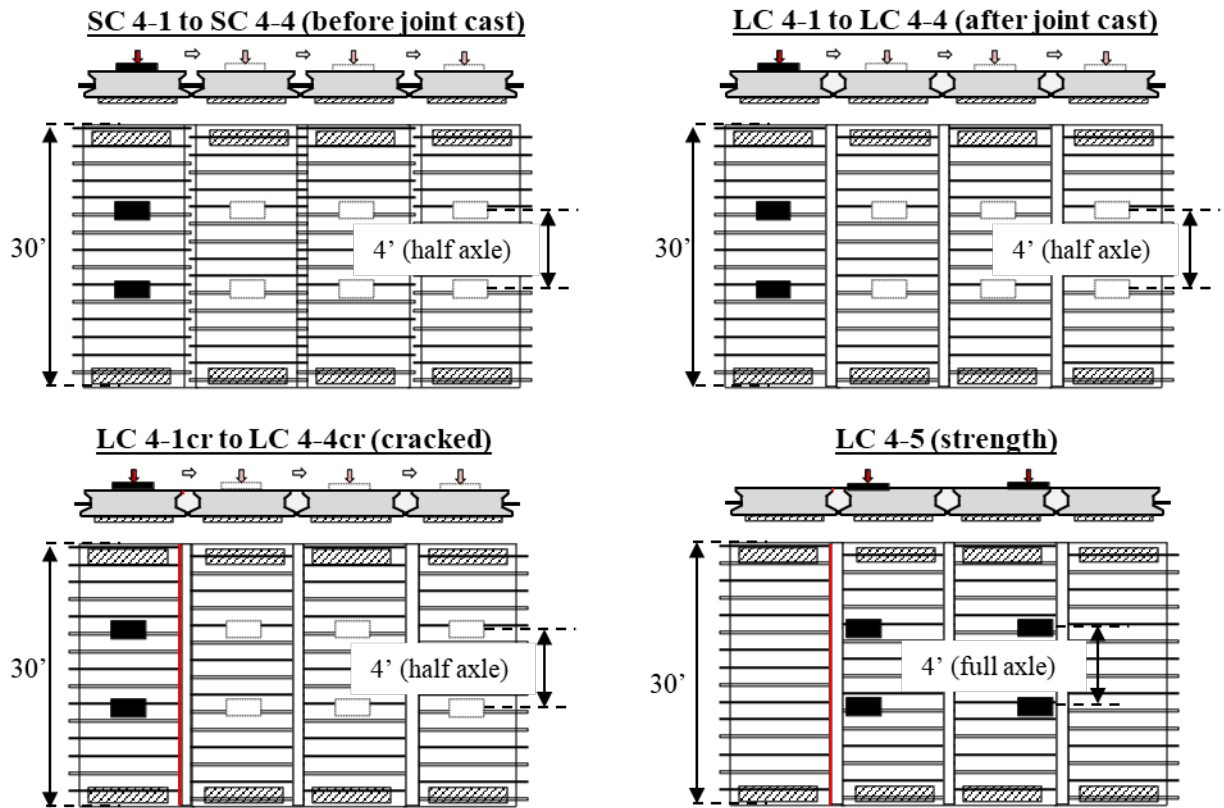


Figure 8.2: Phase III (FIU-6, FIU-3, FIU-8, and FIU-7) service and strength test configurations

Two additional fatigue loading schemes were used, as shown in Figure 8.3:

1. **FC 4-6:** This load configuration had four load points (two points centered at each exterior beam), using two actuators that applied a reverse sinusoidal fatigue loading based on rear HS-20 half axle for 2,000,000 cycles.
2. **FC 4-7:** This load configuration had four load points (load shifted off of specimen centerline at midspan), using two actuators that applied a full HS-20 rear axle fatigue loading for 2,000,000 cycles.

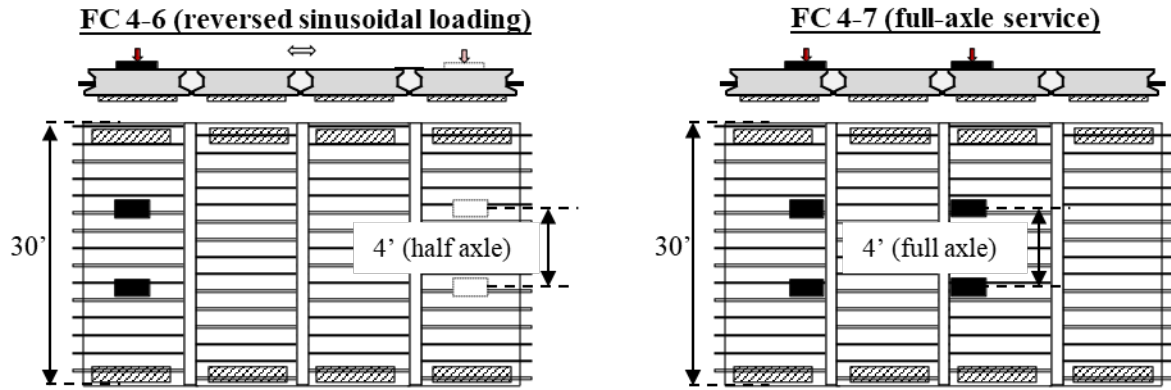


Figure 8.3: Phase III (FIU-6, FIU-3, FIU-8, and FIU-7) fatigue test configurations

The schedule for cyclic testing of the four-beam system including load stages, lower and upper load limits, load conditions, number of cycles and testing days are described in Table 8.2.

Table 8.2: Four-beam service, fatigue, and strength loading scheme

Stage	Description	Lower Limit Load ^{1,2} (Δ)	Upper Limit Load ^{1,2} (Δ)	Load Conditions	# Cycles	Testing Days
1	Stiffness Measured ³					
2	Static Elastic–FL120	0 kip (0.00 in.)	30.6 kip ⁴ (0.00 in.)	Service (LC 4-1 to LC 4-4)	4	4
3	Fatigue Calibration	5 kip (0.00 in.)	23.4 kip ⁵ (0.00 in.)	Fatigue FC 4-6	200,000	2
4	HS20 Truck Load	5 kip (0.00 in.)	23.4 kip ⁵ (0.00 in.)	Service FC 4-6	1,800,000	11
5	Static Elastic–FL120	0 kip (0.00 in.)	30.6 kip ⁴ (0.00 in.)	Service (LC 4-1 to LC 4-4)	4	2
6	Fatigue Calibration	5 kip (0.00 in.)	23.4 kip ⁵ (0.00 in.)	Fatigue FC 4-7	200,000	2
7	HS20 Truck Load	5 kip (0.00 in.)	23.4 kip ⁵ (0.00 in.)	Service FC 4-7	1,800,000	11
8	Static Elastic–FL120	0 kip (0.00 in.)	30.6 kip ⁴ (0.00 in.)	Service (LC 4-1 to LC 4-4)	4	2
	Cracking Procedure ⁶					
9	Static Elastic–FL120	0 kip (0.00 in.)	30.6 kip (0.00 in.)	Service (LC 4-1cr to LC 4-4cr)	4	2
10	Ultimate Strength Test	n/a	n/a	LC 4-5	1	1

¹Loads/displacements listed are for each actuator (not total)

²Acceptable load/displacement range for loading is starting load/displacement $\pm 5\%$.

³Individual Girder Stiffness and Camber Leveling Procedures (see Table 8.1)

⁴One load ramp applied per beam to calculate distribution factors

⁵Upper load range determined from lower load range plus 18.4 kips (fatigue)

⁶Longitudinal crack procedure performed

8.3. SPECIMEN CONSTRUCTION

8.3.1. Beam Construction

A total of eight prestressed slab beams, each 30-foot long by four-foot wide by one-foot thick, were fabricated by a local precast plant. Two beams were constructed for testing Phase I (FIU-1 and FIU-2) in August 2019. Six beams were constructed later in November 2019 for the subsequent testing phases: two beams for testing Phase II (FIU-4 and FIU-5), and four beams for testing Phase III (FIU-3, FIU-6, FIU-7, and FIU-8). Construction specifications such as prestressing layout, reinforcement, and joint construction were covered in detail in Chapter 7.

As previously described in Chapter 7, the specified mix design for all the FSB sections was FDOT Concrete Class VI [57], with a minimum compressive strength at 28 days of 8,500 psi and maximum water/cement ratio of 0.37 lb/lb. The measured compressive strength for the specimens used in testing Phase III is shown later in Table 8.7.

8.3.2. Differential Camber Construction

A differential camber was desired between FIU-3 to FIU-5 and FIU-6 to FIU-8. The differential camber was achieved by modifying the amount of prestressing in the top strands and by modifying the casting procedure. The construction sequence of the six beams was performed in two casting sets, as shown in Figure 8.4, with the main construction steps described below:

1. The first three beams (FIU-6, FIU-7, and FIU-8) were cast on November 20, 2019 with all strands (top four strands and bottom 14 strands) prestressed to 202.5 ksi (43.94 kips per strand). Concrete was cast after all the strands were stressed, mild steel reinforcement installed, and side formwork constructed. One concrete batch was used for FIU-7 and FIU-8, and another concrete batch for FIU-6. Both batches had the same specified mixture design.
2. Six days after casting the first set of three beams (November 26, 2019), the mild reinforcement and side joint forms for the second set of three beams (FIU-3, FIU-4, and FIU-5) was installed around the same strands used for the first set of three beams. The top four strands were then de-tensioned to 0 ksi and then re-tensioned to 50 ksi (10 kips per strand). De-tensioning and re-tensioning of the prestressing strands led to a shift in the mild reinforcement that was tied to the strands. The mild reinforcement was repositioned before casting of the second set of beams. The side joint forms of the first group were removed and the joints pressure washed to achieve the desired exposed aggregate finish.
3. Seven days after casting the first set (November 27, 2019), the second set of beams (FIU-3, FIU-4, and FIU-5) was cast with the top four strands prestressed to 50 ksi (10 kips per strand). The bottom strands (14 strands) remained prestressed to 202.5 ksi (43.94 kips per strand). A third concrete batch was used for FIU-4 and FIU-5, and a fourth concrete batch for FIU-3.
4. Five days after casting the second set of beams (December 2, 2019), all six beams were released. The side forms were also removed this day and the sides of the beams pressure washed to achieve the desired exposed aggregate finish. At release, the FIU-3, FIU-4, and FIU-5 had larger camber (about 0.20 inches of difference) than FIU-6, FIU-7, and FIU-8.

- All six beams were shipped to the structure's laboratory in Tallahassee on December 12, 2019.

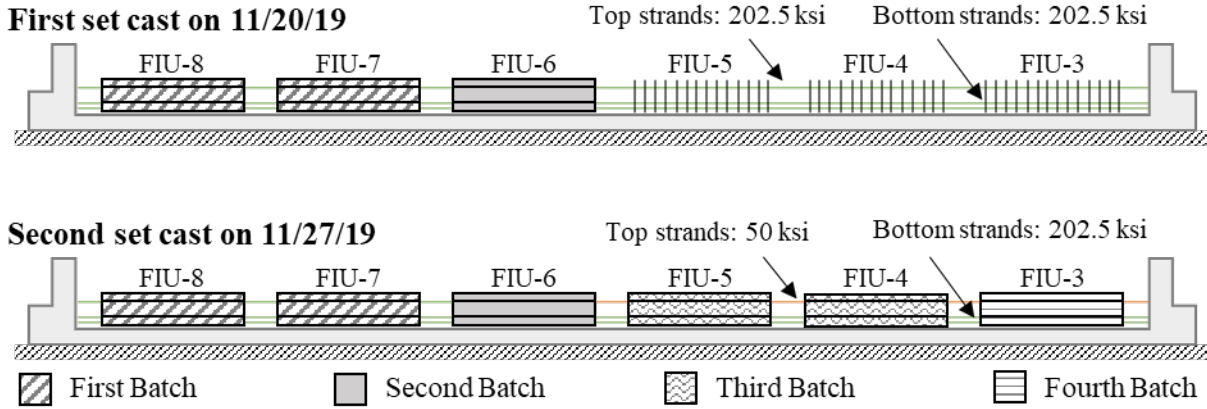


Figure 8.4: Six-beam casting sequence for testing Phase II and Phase III

Some photos of the casting process and shifting of the reinforcement after de-tensioning and re-tensioning the top strands are shown in Figure 8.5.



Figure 8.5: Construction of second set of beams: (a) FIU-8, FIU-7, and FIU-6 mild reinforcement and formwork construction, (b) concrete pour of first group of beams, (c) top strand layer de-tension, and (d) observed misalignment of mild reinforcement in second group of beams

For the Phase III testing described in this chapter, four beams were used: FIU-3, FIU-6, FIU-7, and FIU-8. FIU-4 and FIU-5 were used in the two-beam system test that was previously described.

8.3.3. Superstructure Construction Procedure

The four-beam superstructure beam arrangement was based on having FIU-3, the specimen with the largest camber, as one interior beam. The approximate FIU-3 differential cambers between adjacent beams at midspan, measured before and after load block applications are shown in Figure 8.6. The differential measurements are based on morning camber readings, taken on February 22nd, 2021 before load blocks application, and on April 16th, 2021 after load blocks application. After blocks placement, FIU-3 was 0.375 inches higher than FIU-6 and 0.125 inches lower than FIU-8, which was the final camber measurement before joint construction.

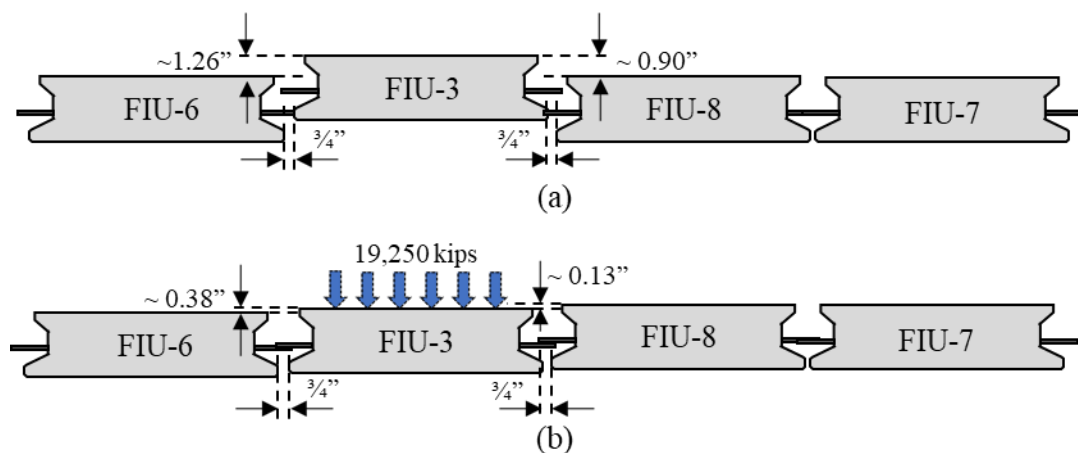
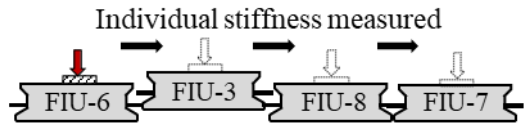

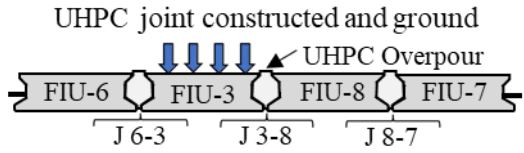
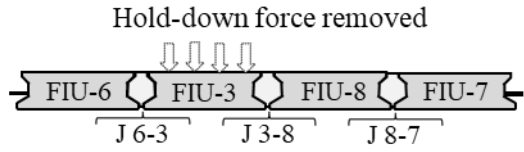
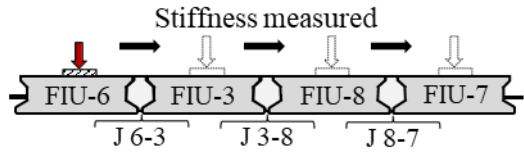


Figure 8.6: FIU-3 differential camber (a) before and (b) after load block application

More details on camber measurements can be found in §8.6.1.

A summary describing the steps taken to measure individual beam stiffnesses before and after joint construction, including the camber leveling procedure, is shown in Table 8.3. Prior to construction of the UHPC joints, each beam was loaded to 20 kips to determine the baseline stiffness of the individual beams (Step 1). Next, a temporary surcharge load to level FIU-3 camber with the adjacent beams was applied (Step 2). The construction of the UHPC joints was then initiated while maintaining the hold-down force during the process (Step 3). After the joints were completely hardened and the instrumentation was installed, the hold-down force was removed (Step 4). Once the surcharge was removed from the fully connected superstructure system, loading of each individual beam (see Table 8.2, Stage 2) was applied to determine the baseline moment distribution factors of the system (Step 5). Detailed drawings of the construction testing scheme were provided separately.

Table 8.3: Summary of beam stiffnesses measurement and joint construction stages

Step	Step Description	Construction Comments	Readings
1	 <p>Individual stiffness measured</p>	Individual girder flexural stiffnesses measured with two HS20 ramps per beam	P- Δ P- ϵ
2	 <p>Hold-down force applied</p>	Sustained load of approx. 20 kips applied holding a differential camber less than 1/4-inch difference	P- Δ P- ϵ
3	 <p>UHPC joint constructed and ground</p>	UHPC cast with overpour and then ground down while maintaining hold-down force	N/A
4	 <p>Hold-down force removed</p>	Hold-down force slowly removed after UHPC in joints hardened	P- Δ P- ϵ
5	 <p>Stiffness measured</p>	Distribution factors measured with two HS20 load ramps per beam	P- Δ P- ϵ

Notation: P- Δ : Load-Deflection Data, P- ϵ : Load-Strain Data

Load blocks were placed on FIU-3 to create a similar deflection to the adjacent beams, as shown in Figure 8.7. A total of 10 load blocks weighing approximately 2 kips each were placed on top of FIU-3 to reduce the differential camber to approximately a 1/4-inch difference between adjacent beams. The resultant hold-down force applied was 19,250 pounds. An approximate one-foot gap was left between the load blocks at midspan to provide sufficient clearance for sensor installation while maximizing the load concentration at midspan.

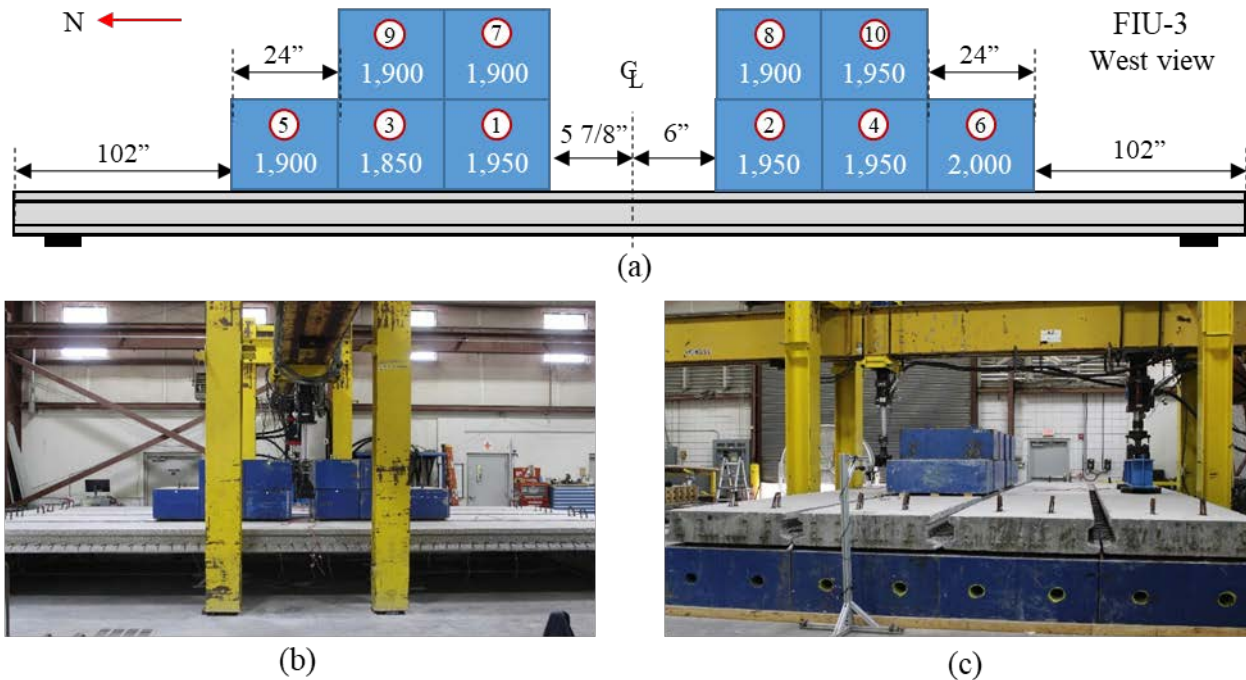


Figure 8.7: FIU-3 camber leveling: (a) load block weights in pounds and placement order (not to scale), (b) west view, and (c) south view

8.3.4. Joints Construction

The relevant four-beam joint system construction steps, including superstructure beams arrangement, beam stiffnesses measurement protocol, camber leveling technique, and UHPC joints construction are discussed in this section. Three joints were constructed at the FDOT structures lab. The joints are identified based on the slab beams they were connecting adjacently: Joint 6-3 for the joint between FIU-6 and FIU-3, Joint 3-8 for the joint between FIU-3 and FIU-8, and Joint 8-7 for the joint between FIU-8 and FIU-7.

8.3.4.1. UHPC Joints Construction

The joints preparation and construction steps followed the same recommended guidelines described in the FHWA publication [39]. The major steps in the UHPC joint preparation are shown in Figure 8.8. The construction of the joints and joint formwork was performed while leaving the load blocks on top of the system, as shown in Figure 8.8 (a). Plywood strips were glued on top of the joint boundary ledges providing approximately 1/4 inch of UHPC above the top of the beams, as shown in Figure 8.8 (b). Plywood end forms with holes for extending the backer rods out were attached to the beams at each joint end providing an enclosure for UHPC cast, as shown in Figure 8.8 (c). Backer rods were then installed in the joint between the beams and extended out of the holes in the end forms. The backer rods were sized 0.5 inch larger than the gap between the bottom ledges to help them remain in place during the casting.

A watertight integrity test was performed once the formwork and baker rods were placed and several days before joint casting. The watertight integrity test was performed by filling the joints with water and monitoring leaking of the water for 15 minutes. Any leakage detected underneath the system was sealed with clear silicone. The joints were cleaned and rewetted on casting day. This process helped to ensure a saturated surface dry (SSD) condition for the joint surfaces before UHPC casting.

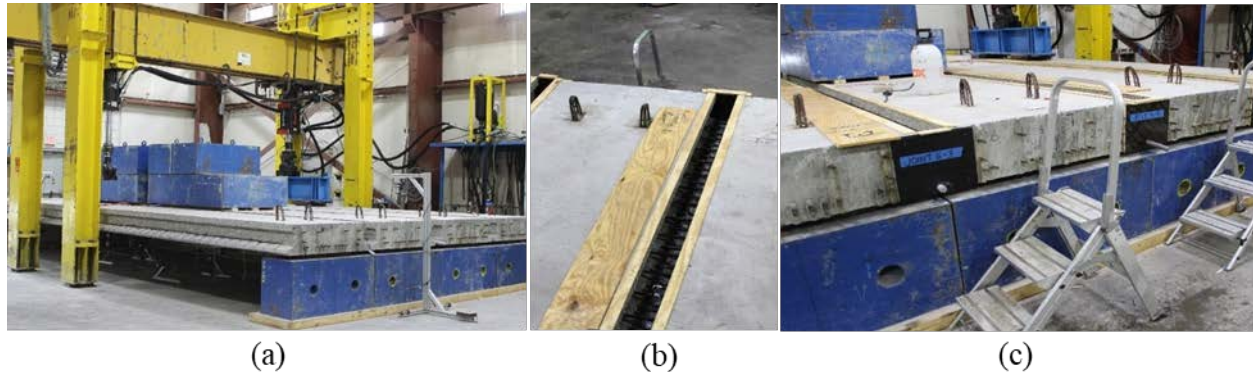


Figure 8.8: Preparation of UHPC joints: (a) superstructure preparation with load blocks, (b) joints with top strips formwork for over pour volume, and (c) plywood block-outs at joint ends with extended backer rods

The UHPC joints were cast using three different batches of UHPC. The UHPC mixture components were mixed in a Mixer System Horizontal Shaft Mixer, shown in Figure 8.9 (a). After finishing mixing all components for around 25 minutes, the UHPC was transported in a concrete hopper attached to an overhead crane and poured in the first joint as shown in Figure 8.9 (b).

The UHPC was placed at one end of the joint and allowed to flow up to the top of the joint at midspan of the beams. UHPC was cast in this position until it almost reached the top of the joint at midspan. At this point, casting was stopped, and top formwork and weights were placed on this half of the joint. The casting position was then moved to the other end of the joint and the process repeated. A steel rod was used to gently mix the region where two UHPC pour heads encountered each other, as shown in Figure 8.9 (c), which helped to ensure steel fibers crossed the boundary. The last UHPC in the joints was cast through a chimney at one end of the joint, which increased the pour height and pressure head to avoid entrapped air inside the joint. The complete joint length was fully covered when the UHPC was cast through the chimney. Joint 6-3 was cast first. This process was repeated for the second joint (Joint 3-8) and subsequently the third joint (Joint 8-7). Once the last joint (Joint 8-7) was cast and covered, the joints were allowed to harden for a period of 24 hours. All three joints were poured the same day with about 30 minutes between pours.



(a)



(b)



(c)



(d)

Figure 8.9: UHPC mixing and placement procedure: (a) premix added to mixer, (b) initial UHPC casting in uncovered joint, (c) rodding procedure for two encountering pour heads, and (d) joints covered with top formwork and weights to finish joint cast

The UHPC joints were prepared for the grinding procedure the day after joint casting. The first step was the removal of the top formwork and side strips, as shown in Figure 8.10 (a). Grinding of the joint was then performed with a Magna-Trap floor grinder starting at one end of the joint and working to the opposite end, as shown in Figure 8.10 (b). A hand-held grinder was used close to the cables from sensors sticking out of the top of the joint and underneath the loading blocks used to apply the surcharge load. A photograph of the joint immediately after the completion of grinding is shown in Figure 8.10 (c). The top of the system was later cleaned and prepared for sensor installation, as shown in Figure 8.10 (d).

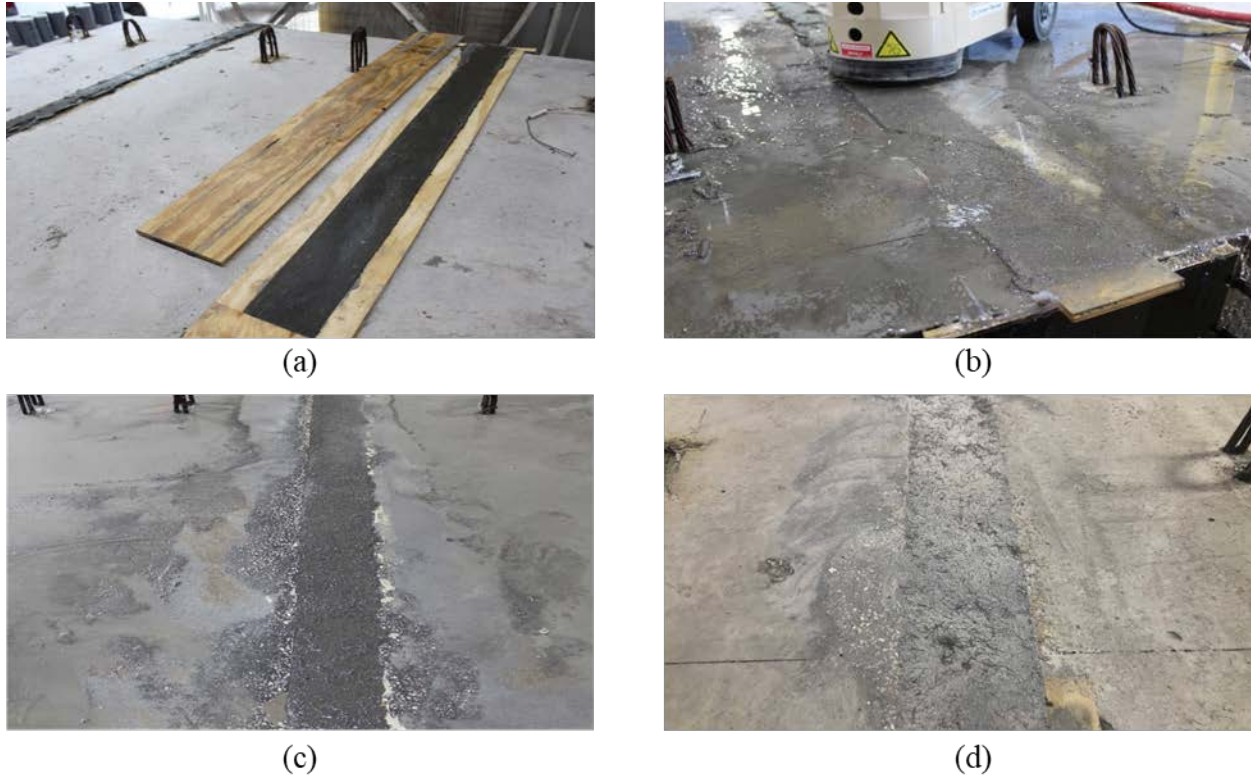


Figure 8.10: UHPC joint grinding procedure: (a) top formwork removal a day after cast, (b) joint grinding action with electric grinder, (c) joint finish after grinding, and (d) joint surface a day after grinding

All instrumentation was installed during the period between the end of joint grinding and the removal of the surcharge load.

8.3.4.2. UHPC Mixture

The UHPC mixtures, specified to be Ductal® JS1000, contains the same components used in previous two-beam testing protocols, containing the following ingredients:

- Premix (dark-grey): pre-blended cement, sand, ground quartz, and silica fume
- Liquid Admixture: high-range water reducer
- Steel fibers: 0.008-inch diameter by 0.5-inch long; tensile strength larger than 290 ksi
- Water and/or ice: Ice required when batching in warm hot weather

The procedure for mixing the UHPC included the following steps for the large-scale joint batches:

1. Weigh out each ingredient for mixture
2. Add dry premix
3. Add ice-water and superplasticizer
4. Mix until fluid (10-15 minutes)
5. Add steel fibers
6. Mix five minutes, or until complete uniformity

7. Perform flow table test. If mixture is not fluid (below 5 inches), add five percent more water (if temp. $\leq 75^{\circ}\text{F}$) or five percent ice (if temp. $> 75^{\circ}\text{F}$). If too fluid (above nine inches of static flow), add more dry material and fiber
8. Mix additional 5 minutes, or until completely uniform, if additional material added, otherwise skip to step 9
9. Place UHPC in the joint and make six cylinders for strength test and three beams for four-point bending test (modulus of rupture)
10. After completing one UHPC joint pour, the mixing process was repeated again from step 2 for subsequent UHPC batches until all three joints were fully cast.

The proportions of the UHPC components were specified by weight and measured before the mixing process began.

One JS1000 pre-mix design was used for all three joints, requiring a volume of 17.02 cubic feet per joint batch, with a total of 51.06 cubic feet of UHPC mixed for all three joints. Each batch required one bulk bag of dry premix, equivalent to 49 smaller 50-lb. bags, which yielded a total volume of 17.05 cubic feet. The mixture proportions of the UHPC batches prepared with JS1000 admixture are shown in Table 8.4. Additional quantities (about five percent of the amounts used) of premix, ice, water, and steel fibers were set aside to be used if the mix consistency was not correct; the use of these additional materials was not required for any batch.

Table 8.4: UHPC mixtures for Testing Phase III (using JS1000 pre-mix)

UHPC Batch	Design Mix (Pounds)					Joint ID	Ambient Temp. ($^{\circ}\text{F}$)
	Premix	Ice	Water	Admixture	Steel		
1	2,460	0.00	114.26	34.44	174.66	Joint 6-3	73
2*	2,460	5.71	108.55	34.44	174.66	Joint 3-8	73
3	2,460	13.86	100.40	34.44	174.66	Joint 8-7	73

*Ice was used in the second UHPC batch, but the specific amount was not recorded. FDOT SRC staff estimated that 5% ice was used based on the temperature of the mixture and past experience.

The rheological properties were measured for each UHPC batch by performing static and dynamic flow tests. A slightly modified version of ASTM C1437 [76] was used per FHWA material tests recommendation [39], which is a miniaturized version of the spread test for self-consolidating concrete. Immediately after mixing each UHPC batch, a small mix portion was poured in the flow mold as shown in Figure 8.11 (a). Once the mold was filled, the mold was gently removed with a twisting action, as shown in Figure 8.11 (b). The initial spread shown in Figure 8.11 (c) was then measured, as shown in Figure 8.11 (d) before the initiation of the table drops for static flow and after the table drops for dynamic flow.

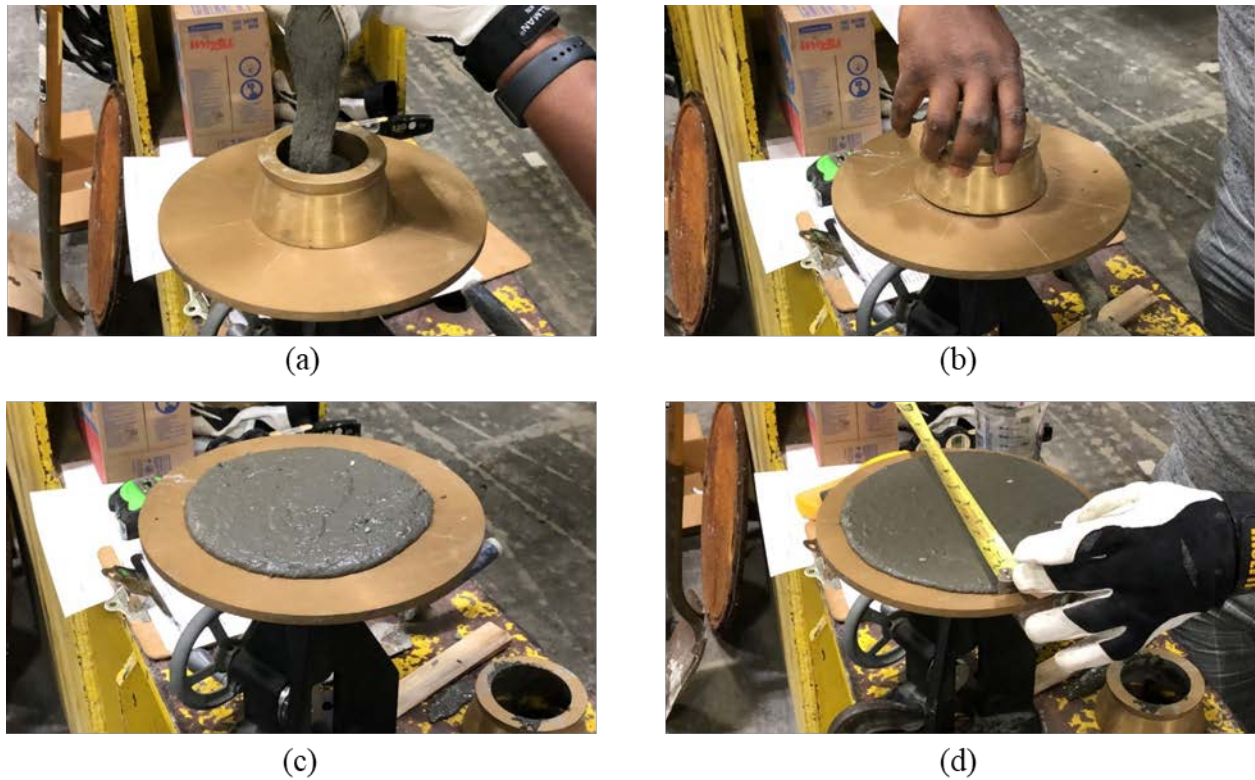


Figure 8.11: UHPC flow test: (a) material pour, (b) mold removal, (c) setting period, and (d) spread measurement

The summary of both flow tests for each UHPC batch are summarized in Table 8.5. There was minimal difference in temperatures and flows between all three mixtures. Also, a slightly higher dynamic flow was reported for the third UHPC batch.

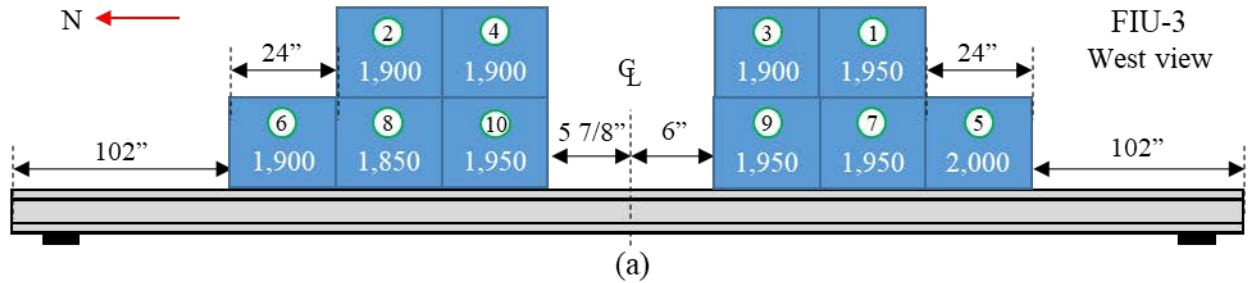
Table 8.5: UHPC flow tests

UHPC Batch	Temperature (°F)	Static Flow (in.)*	Dynamic Flow (in.)*
1	83	8.54	8.56
2	80	8.25	8.69
3	79	8.63	9.28

*Average taken from two measurements along perpendicular axes of same test sample

8.3.4.3. Surcharge Load Removal

The surcharge load was removed from FIU-3 31 days after the casting of the UHPC joints. The load blocks used to apply the surcharge load were removed one at a time from alternating ends of the beam, as shown in Figure 8.12. All debris was cleared from the top of superstructure system after the removal of the load blocks and before the start of service testing.



(b)

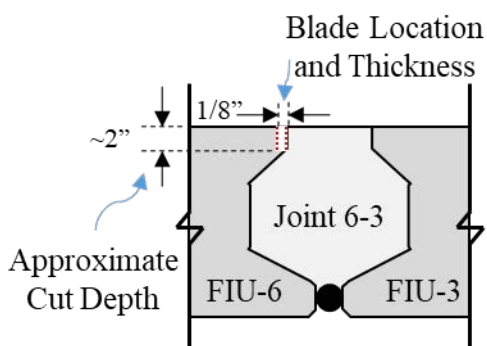


(c)

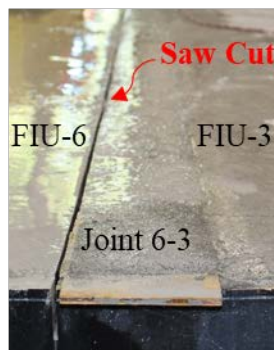
Figure 8.12: Load blocks removal from FIU-3: (a) load block weights in pounds and removal order (not to scale), (b) block 3 removal, and (c) block 4 removal

8.3.4.4. Joint Cracking Procedure

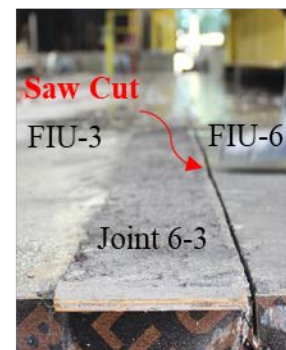
A pre-cracked joint interface was simulated by saw cutting a 2-inch deep cut on the west side of Joint 6-3, as shown in Figure 8.13 (a). The saw-cutting process was performed after finalizing all the fatigue tests (see Table 8.2, Stage 9). One exterior face of the blade was aligned to the side of the UHPC joint such that the cut would be in the precast section. The cut was made from the south end to midspan and then from the north end to midspan. A single continuous cut could not be made because of the actuator interfering with the saw position at midspan.



(a)



(b)



(c)

Figure 8.13: Saw-cut procedure on FIU 6-3 joint: (a) saw cut alignment, (b) saw cut south view, and (c) saw cut north view

The cut depth was measured at four locations along the length of the joint: (a) north end above bearings centerline, (b) 10 feet from north end bearings centerline, (c) 20 feet from north end bearings centerline, and (d) south end above bearings centerline, as shown in Table 8.6. These measurements were taken at three instances of system testing, with no changes reported in between stages.

Table 8.6: Saw cut depths at four locations

Measurement Locations	Saw Cut (in.)	Stage 9 - After LC 4-1cr to LC 4-4cr (in.)
North End (Bearing Centerline)	2.25	2.25
10' from North End	1.75	1.75
20' from North End	1.88	1.75*
South End (Bearing Centerline)	2.06	2.06

**Difference caused by point location of measurement*

8.3.5. Material Properties

8.3.5.1. Hardened Concrete Properties

Three concrete batches with similar mix proportions were used to construct the specimens used in Phase III: one batch for FIU-3, another batch for FIU-6, and another batch for FIU-7 and FIU-8. Compressive strength tests were performed on cylinder samples taken from each concrete batch of the precast beams and the UHPC joints. Ten (10) 4-inch by 8-inch concrete cylinders were tested for each precast slab beam batches following ASTM C39 [62, p. 39]: five cylinders after joint cast and five at strength test day. The average of the five compressive strength values was taken as the measured strength for every batch during each testing time. The UHPC compressive strength was measured using six 3-inch by 6-inch cylinders taken from each joint batch and tested based on ASTM C1856 [63] specifications: three cylinders at 28 days and three at strength test day; this procedure is described in the FHWA guidelines [39]. The average of the three compressive strength values was taken as the measured strength for every batch during each testing time.

The flexural strength properties of each UHPC batch was measured using small-scale beams subjected to four-point bending test as per ASTM C1609 [64]. Three four-inch by four-inch 14-inch beam samples were cast from each UHPC joint batch using metallic molds as shown Figure 7.12 (a) and cured for 24 hours as shown in Figure 7.12 (b). After the curing process, the top part of the beam was ground down for dimensional consistency. These beams were tested at 28 days to determine the tensile strength of the UHPC. The concrete cylinders cast and stored for two UHPC batches are shown in Figure 7.12 (c) and (d), respectively.

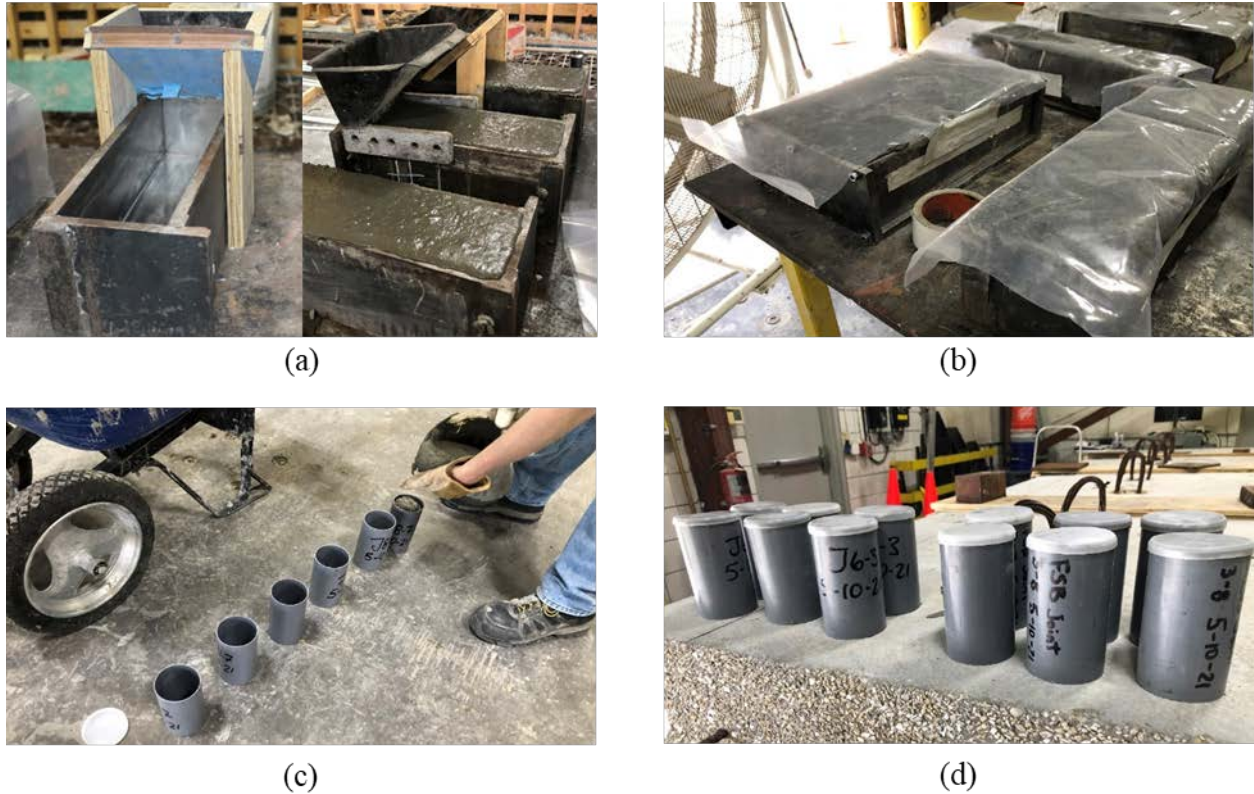


Figure 8.14: UHPC samples: (a) 4x4x14 in. steel molds for UHPC beams, (b) UHPC beams curing process, (c) 4x8 in. UHPC cylinder preparation and cast, and (d) cylinders for compressive strength

A summary of all concrete compressive and tensile strength properties for the beam and joint specimens is shown in Table 7.5. Compressive strengths were measured after joint cast and on the day of ultimate strength testing.

Table 8.7: Specified and measured concrete strength for Testing Phase III specimens

Beam ID	Beam Compressive Concrete Strength (f'_c)			Joint ID	Joint Compressive Concrete Strength (f'_c)			Joint Tensile Strength (f'_t)
	Target (ksi)	After Joint Cast (ksi)	Strength Test Day (ksi)		Target (ksi)	28-day Measured (ksi)	Strength Test Day (ksi)	Measured (ksi)
FIU-3	8.5	11.40 ^a	12.15 ^b	6-3	21.0	23.19	24.08 ^d	2.92 ^c
FIU-6	8.5	11.97 ^a	13.26 ^b	3-8	21.0	24.14	23.28 ^d	3.23 ^c
FIU-7 FIU-8	8.5	11.37 ^a	12.60 ^b	8-7	21.0	22.47	20.89 ^d	3.10 ^c

^a Compressive strength measured at 558 (FIU-3) and 565 (FIU-6, FIU-7, and FIU-8) days, respectively

^b Compressive strength measured at 639 (FIU-3) and 646 (FIU-6, FIU-7, and FIU-8) days, respectively

^c Tensile strength measured at 31 (FIU 6-3), 30 (FIU 3-8), and 32 (FIU 8-7) days, respectively

^d See note in following paragraph

The measured concrete strength for the UHPC on the day of the strength test may be lower than the actual strength. FDOT noticed lower concrete strength at testing compared to 28-day strength for a different research project, which was attributed to a worn-out cylinder grinding disk. There was an additional cylinder for the beam concrete that was tested using the new grinding disk; these results are shown in Table 7.5. However, there were no additional UHPC cylinders, so the strengths shown in Table 7.5 are likely reduced due to the old grinding disk.

8.3.5.2. *Steel Reinforcement Properties*

Four sizes of Grade 60 mild steel reinforcement were used to build all the precast specimens: #3, #4, #5, and #6 reinforcement. Eighteen (18) fully bonded pretensioned strands were used in the precast sections with prestressing forces up to 202.5 ksi. The measured properties for the steel reinforcement were provided by the precaster, shown in Figure 8.8.

Table 8.8: Steel material data

Description	Yield (psi)	Tensile (psi)
#3 Rebar A615M Gr60	73,655	108,504
#4 Rebar A615M Gr60	68,043	104,770
#5 Rebar A615M Gr60	67,300	105,500
#6 Rebar A615M Gr60	61,340	101,503
0.600" 7-wire 270 low lax. strand	251,000	275,000

8.3.6. Observations from Construction

8.3.6.1. *Uneven Camber*

The measured cambers at release and immediately before load block placement are summarized in Figure 8.15. Although FIU-6, FIU-7, and FIU-8 were designed with the same prestressing properties (14 fully-stressed bottom strands and four fully-stressed top strands to 202.5 ksi) and released at the same time, FIU-6 had less camber than FIU-7 and FIU-8, as shown in Figure 8.15. This camber variability was attributed to using a different concrete batch for FIU-6 than FIU-7 and FIU-8.

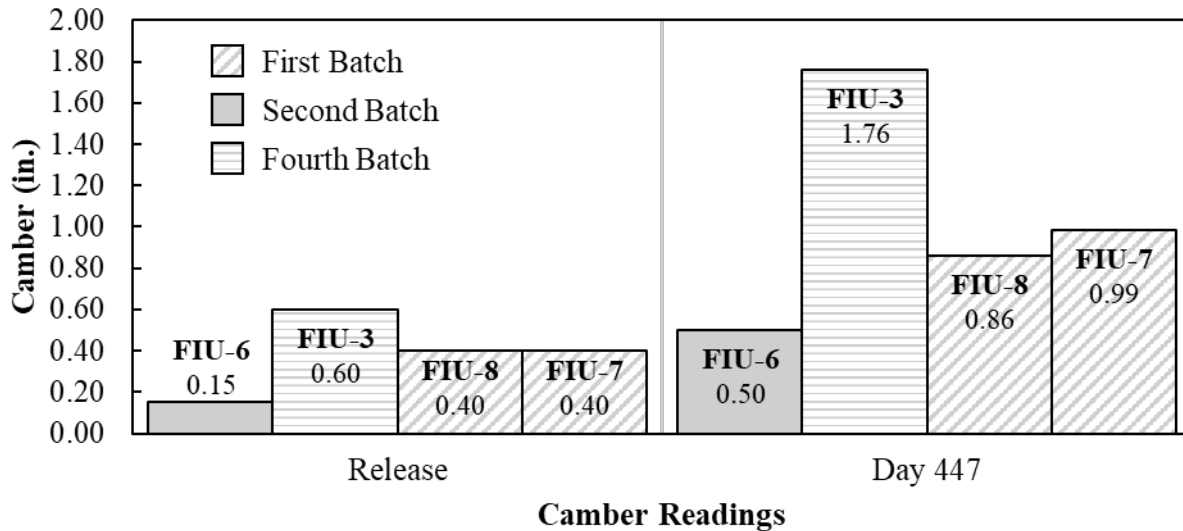


Figure 8.15: Camber readings from FIU-3, FIU-6, FIU-7, FIU-8 at release and at 447 days (before load blocks placement)

8.3.6.2. Irregular Joint Reinforcement Length

A significant variation in the protruding length of the joint reinforcement was observed in FIU-3 after release when the specimens were being prepared for shipment to Tallahassee, as shown in Figure 8.16. The joint reinforcement crosses the entire width of the specimen, so a longer protruding length on one side of the beam coincided with a shorter protruding length on the other side of the beam.

It was decided to trim the extended bars to match the embedment length specifications before placing the beams for joint casting. Joint tolerances allowed for cutting some of the bars by 0.25 to 0.5 inches while still maintaining sufficient development and splice lengths. This construction issue was also observed in the other beams, but the length variations were not as significant as on FIU-3.



Figure 8.16: FIU-3 joint reinforcement length observations at (a) precast yard and (b) structures lab

The variation in the FIU-3 joint reinforcement length was likely due to the construction procedure for these specimens. The reinforcement cage was completely tied, and side forms

installed prior to the de-tensioning and re-tensioning of the strands, which occurred between the casting of FIU-6, FIU-7, and FIU-8 and the casting of FIU-3. When the strands were de-tensioned, the entire cage and some of the formwork shifted. This required the removal and readjustment of some of the side forms and reinforcement. A detailed FSB construction explanation highlighting this issue was presented in the previous large-scale, two-beam testing, see Chapter 7.

8.3.6.3. Longitudinal Form Misalignment

There was misalignment of the form segments along the length of the beam for several of the beam edges, shown in Figure 8.17 (a). This longitudinal misalignment was likely beam sweep, but not a result of prestressing. The misalignment was a result of the side forms not being perfectly lined up during construction, therefore generating an inconsistent gap between bottom flanges. When the interior beams (FIU-3 and FIU-8) were put side by side, their bottom ledges were touching for about 19 inches at the middle joint, as shown in Figure 8.17 (b), with a 1-inch gap at one end and a 0.75-inch gap at the other end as shown in Figure 8.17 (c). However, because the non-contact lap spliced rebar had a minimum spliced length of four inches, maintaining the gap between the beams less than 1.25 inches sufficed for joint construction standards.

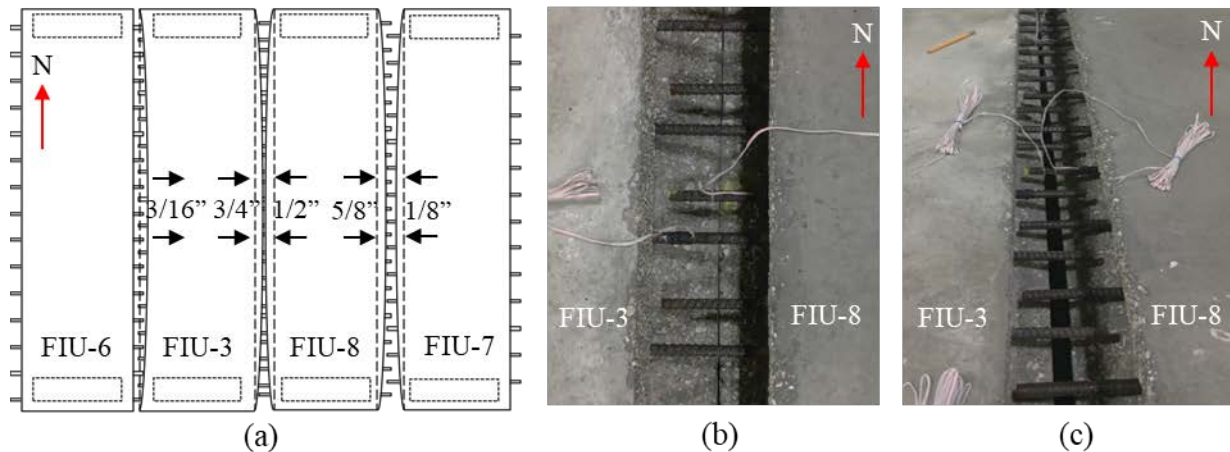


Figure 8.17: Beams sweep: (a) sweep direction and dimensions (not to scale), (b) middle joint region gap, and (c) end joint region gap

The typical recommended tolerance for beam sweep based on PCI MNL-116 [79] is 1/8-inch per 10 feet; therefore, for the 30-foot long FSBs the allowable tolerance is 3/8-inch sweep. FIU-3 and FIU-8 had a sweep larger than this specified tolerance. Care should be taken if side formwork segments (like those used for construction of these beams) are used in the future to ensure the proper longitudinal alignment. Using a single wood or steel form with the addition of mechanical threaded bars as joint reinforcement would likely aid in the final joint construction quality.

Nevertheless, a single backer rod could be used in the joint despite the varying gap between adjacent bottom ledges. An additional clear silicone layer was added from underneath at locations with wider gaps, as shown in Figure 8.18. All joints were watertight other than at some

locations where the sensor cables ran beside the backer rod out the bottom of the joint. No UHPC material leaked during the construction of all the joints.

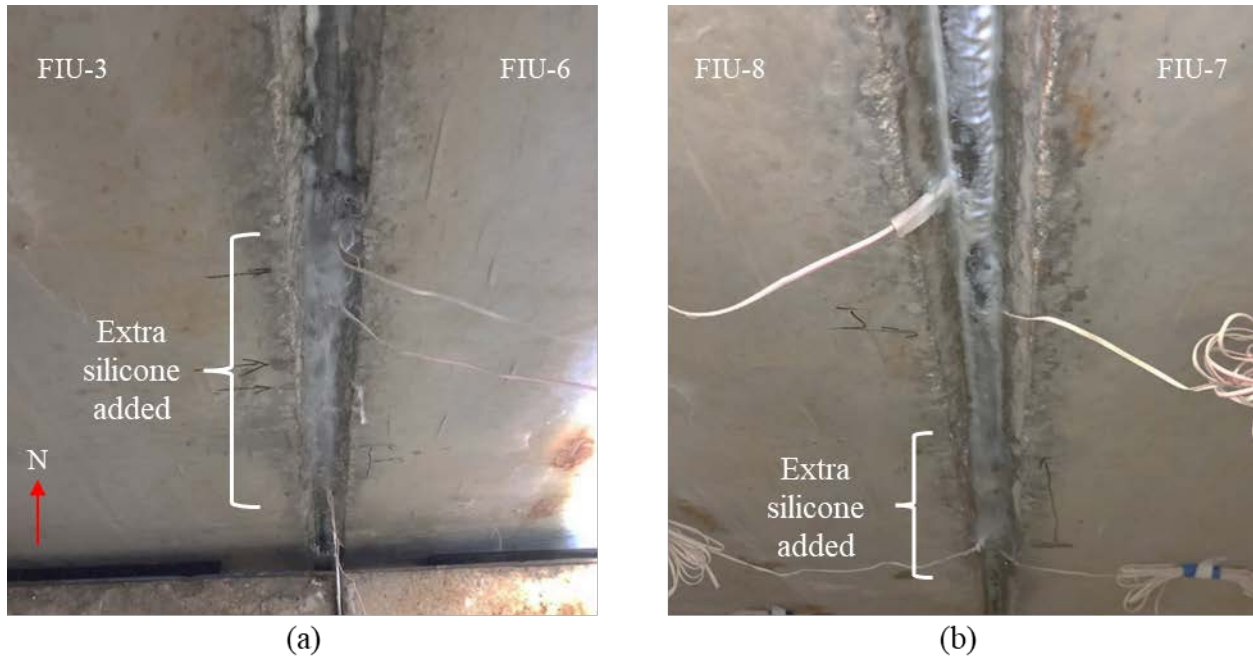


Figure 8.18: Covered leakage zones at (a) south support and (b) middle region

8.3.6.4. Irregular Bottom Ledge Chamfer

Two of the beams built (FIU-3 and FIU-8) had an irregular geometry shape at the chamfered bottom ledge. During the specimen construction, some of the side forms were not installed flush with the bottom chamfered form, as shown in Figure 8.19 (a), which made the bottom ledge wider than it was supposed to be, and therefore some concrete seeped down behind the chamfer on the bottom flange, as shown in Figure 8.19 (b). Once hardened, a cavity in the section underneath the ledge was created, which was chipped off at the lab before joint construction.

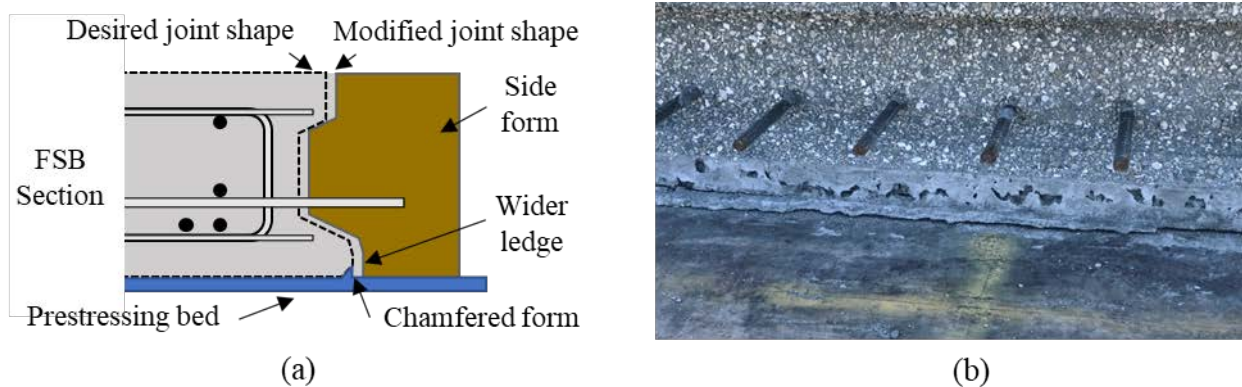


Figure 8.19: Joint construction issue: (a) side form misalignment with chamfered form and (b) bottom ledge geometry after side form removal

8.3.6.5. Concrete Drying Cracks

Several cracks were observed on the top of the beams after finalizing the construction of the first set of fully-prestressed beams (FIU-8, FIU-7, and FIU-6), as shown in Figure 8.20. These shrinkage cracks likely occurred due to the beams not being covered immediately after casting. The second set of beams (FIU-5, FIU-4, and FIU-3) were covered with a plastic cover immediately after casting to help prevent the shrinkage cracking.

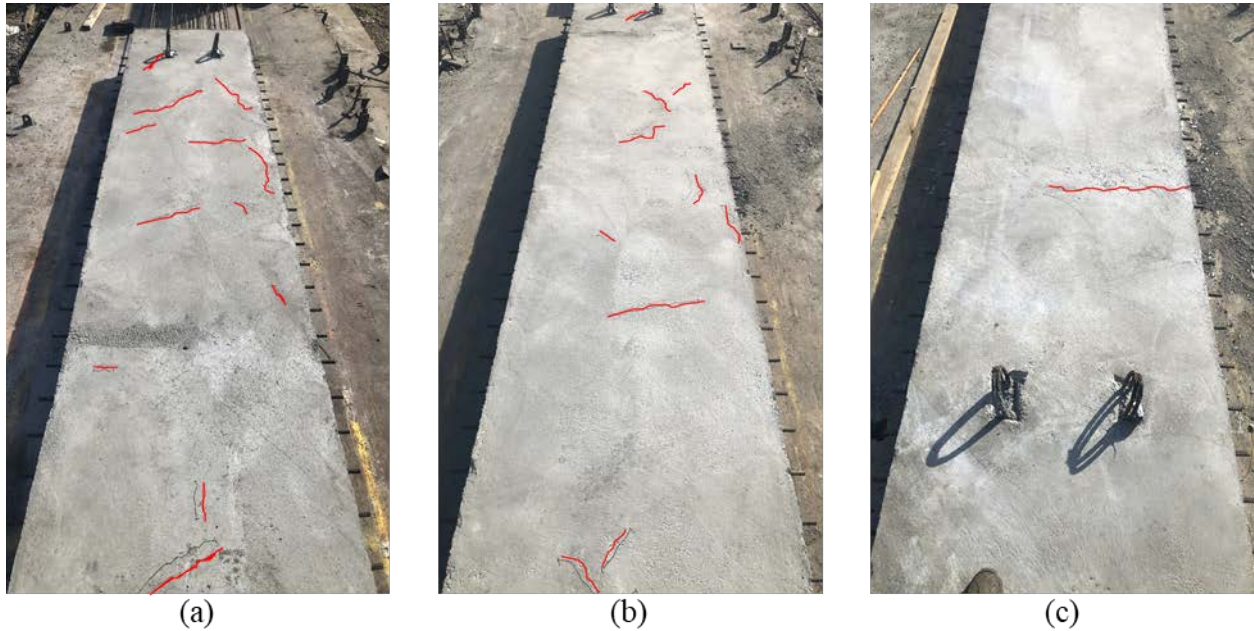


Figure 8.20: Crack patterns observed on (a) FIU-8, (b) FIU-7, and (c) FIU-6 top surfaces

8.3.6.6. Large Load Block Widths

The available load blocks used in the camber leveling stage were wider than FIU-3, creating an approximate one-inch overlap above the adjacent joint regions, as shown in Figure 8.21. This overlap made joint construction and grinding more difficult. The grinding machine could not reach inside the gap, as shown in Figure 8.21 (b), so a hand-held grinder was used to remove the reachable overpoured strip located below the load block. The hand-held grinder with the available clearance around the load blocks could not completely remove the overpoured strip, as shown in Figure 8.21 (c). The strip was not smoothed out in these regions after removing the load blocks 31 days after joint casting; the strip did not interfere with the installation of instrumentation and would have been difficult to remove at this point due to the strength of the UHPC.

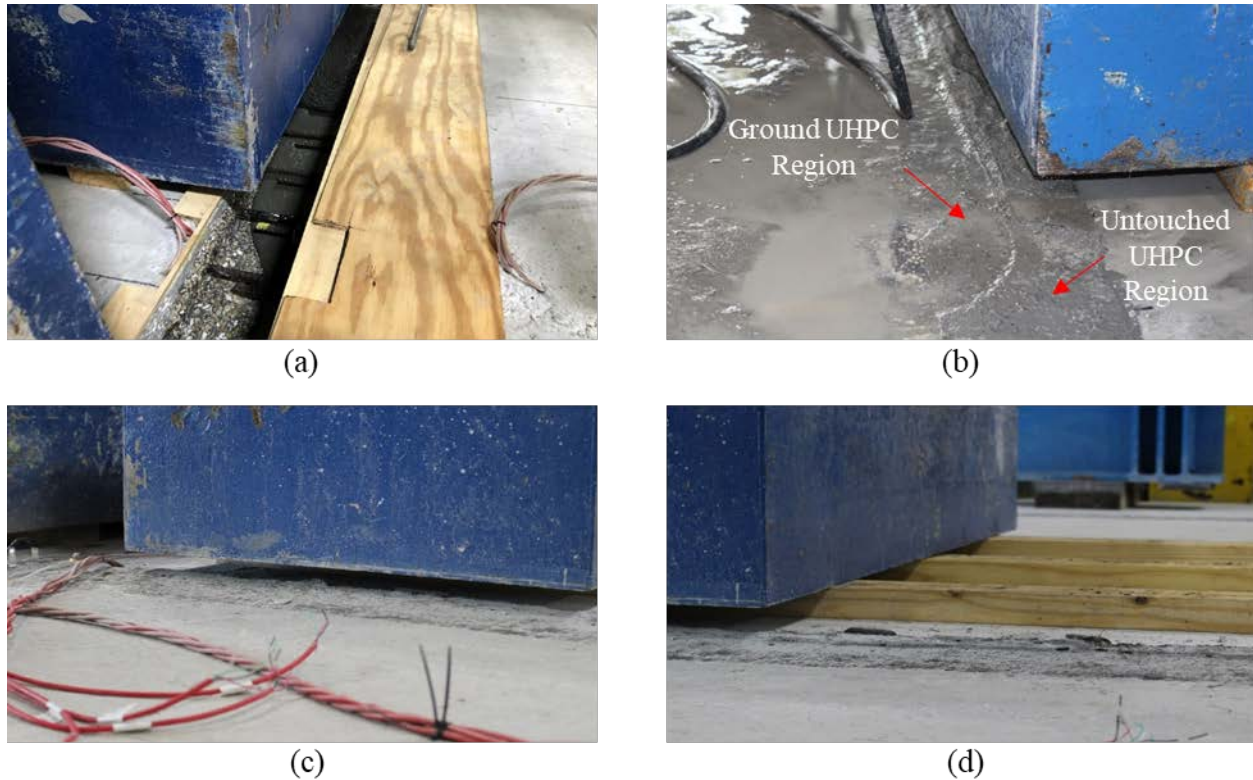


Figure 8.21: Load blocks overlapping joint region (a) during UHPC cast, (b) during UHPC grinding, (c) after formwork removal, and (d) during blocks removal

8.4. LOADING CONFIGURATIONS AND PROTOCOLS

8.4.1. Test Setup

The performance of the four-beam specimen was evaluated following previous testing characteristics for superstructure behavior [46], [80], [81]. The dimensions and testing frame setup are shown in Figure 8.22. Four steel load blocks filled with concrete (48x24x18 inches) were placed at each end of the four-beam system with 32-inch by 8-inch by 2-inch-thick neoprene bearing pads under each beam end providing simple supports at each end. The load blocks provided a minimum vertical clearance of 24 inches, which allowed for easy removal of the bottom instrumentation and ensured enough space for documenting the crack patterns underneath the specimen. The load blocks were grouted to the strong floor to ensure flatness and avoid undesired movement. The span length between the center of the bearings was 28 feet – 11 inches.

Three different actuators were used to complete the loading stages depending on the load configuration. The MTS-55 with a 55-kip capacity and MTS-110 with a 110-kip capacity were used for the service load and fatigue protocols. The Enerpac 800 with an 800-kip capacity was used for the ultimate strength capacity test.

The load frame consisted of four columns (W14) with a center-to-center dimension of 6 feet longitudinally and 18 feet transversely supporting a double W36x150 jacking beam. The

actuators were attached to the jacking beam. The superstructure system was loaded using a set of spreader beams depending on the test setup: double W14x43 (R34), W16x100 (R35), and W18x143 (R31). Each spreader beam distributed the load to two 20-inch by 10-inch steel plates with a 2-inch thickness and neoprene bearing pad of the same size between the steel plates and the beams. The dimensions for the load point were based on the wheel patch of an AASHTO HS20 truck [82].

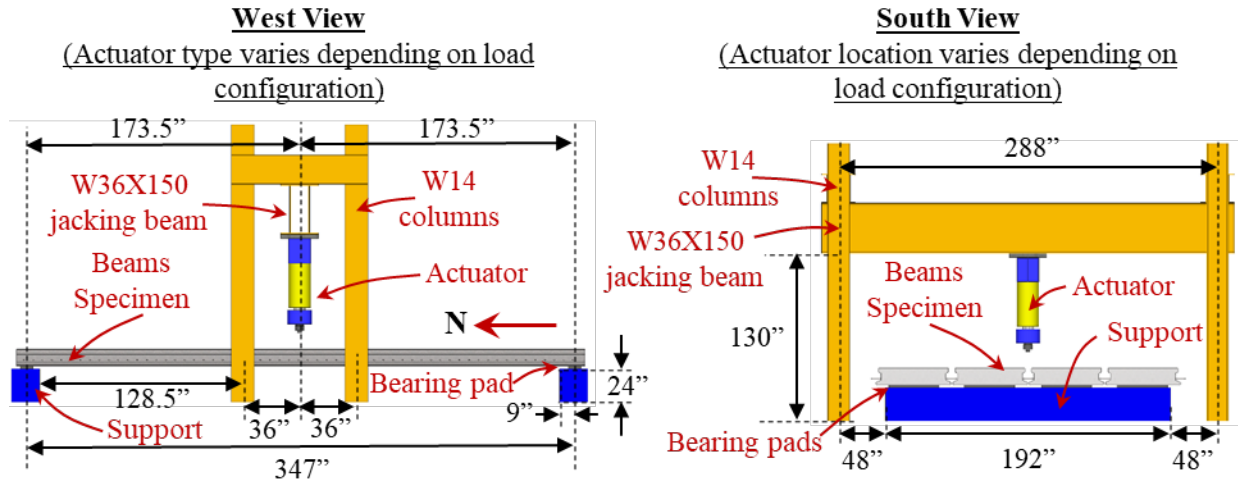


Figure 8.22: Testing frame and support layout

Two small steel I-beams were placed underneath the specimen at midspan as a safety measure in case of sudden failure of the superstructure system, as shown in Figure 8.23 (a). These I-beams helped to protect the sensors that were left underneath the specimen throughout the strength test, as shown in Figure 8.23 (b). Enough clearance was left between the I-beams and the specimens to ensure adequate deflection until system failure.



Figure 8.23: (a) Bottom steel I-beams, (b) clearance display between specimen and sensors

The same test frame and support conditions were used for all service, fatigue, and strength testing phases.

8.4.2. Four-Beam Individual Stiffness and Camber leveling Assessments

Two different load configurations and protocols were first used for the four-beam testing during testing Stage 1. The first included a rear half-axle truck centered at midspan on each beam centerline for measuring flexural stiffness before joint construction; they were called Stiffness Configuration (SC) 4-1 for FIU-6, SC 4-2 for FIU-3, SC 4-3 for FIU-8, and SC 4-4 for FIU-7, respectively. The axle load for the stiffness configuration is based on a rear half-axle HS20 truck, as shown in Figure 8.24.

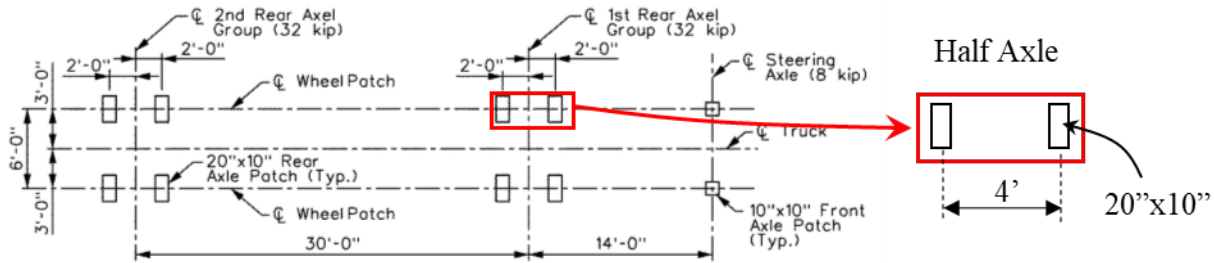


Figure 8.24: HS-20 truck load with rear half-axle identification (from [82])

The second configuration consisted of applying a surcharge load at midspan of FIU-3 for camber leveling proposes during joint construction; Camber Leveling (CL) 4-2. The surcharge load protocol was applied using 10 load blocks, with dimension and weight ranges as shown in Figure 8.25 (a). The load blocks were arranged at midspan of FIU-3 with a pyramidal shape, applying the maximum load per unit area close to the center, as shown in Figure 8.25 (b), and they were supported by three 2 x 4 in. timbers to more evenly distribute the load across the top of FIU-3, as shown in Figure 8.25 (c).

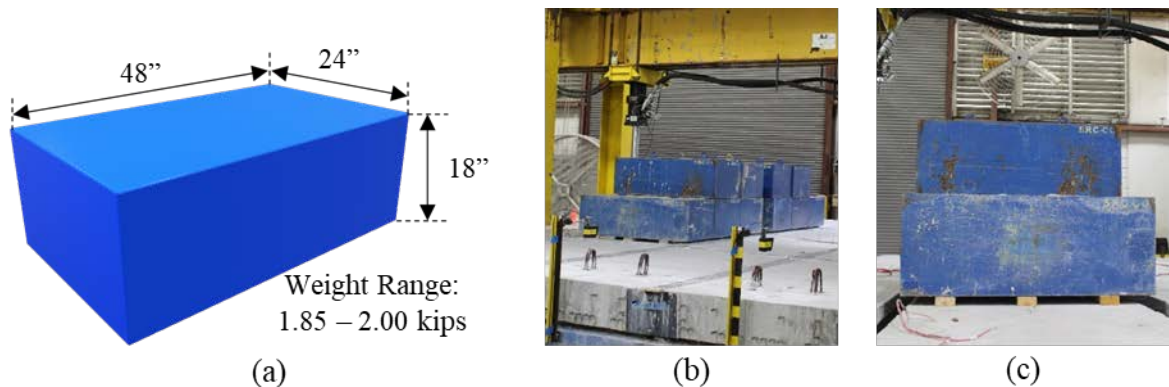


Figure 8.25: Load blocks used for surcharge protocol: (a) dimensions, (b) arrangement, and (c) supports

Detailed drawings for both configurations are provided separately. More details on the individual stiffness and camber leveling protocols are found in §8.3.3.

8.4.2.1. Stiffness Measurement Protocol

The individual beam stiffness was measured before starting the fatigue, service, and strength testing protocols to ensure that the stiffnesses were approximately the same and the future load distribution measurements would not be affected by stiffness variations between beams.

Once all the beams were in position in the testing frame (before the camber leveling protocol), two static load ramps of 20 kips (less than the estimated cracking force of 34.5 kips for each beam) were applied on each beam centerline using one actuator and one spreader beam (R33) oriented longitudinally with two load patches (10-inch by 20-inch wheel patches), as shown in Figure 8.26. The load ramps were applied at a rate of 0.2 kips/second until the upper load limit was reached and then unloaded completely. Also, the load-deflection ($P-\Delta$) and load-strain ($P-\epsilon$) data were monitored by the laser displacement transducers (LDTs) and bottom longitudinal concrete strain gauges (CSGs) for each stiffness configuration case.

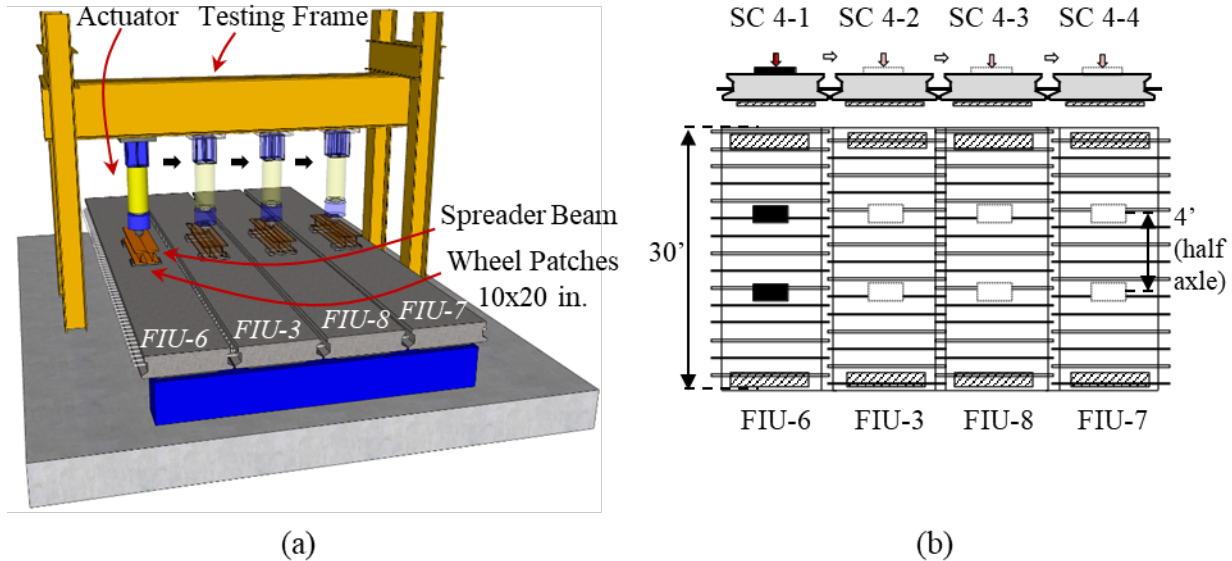


Figure 8.26: Test setup for Stiffness Configuration 4-1 through 4-4 (a) schematic and (b) plan and elevation view

8.4.2.2. Camber Leveling Protocol

After measuring each beam's stiffnesses, a hold-down force was applied on FIU-3 at midspan such that the differential camber in the system was at least equal or less than 0.25-inch difference between adjacent beams. A total of 10 load blocks (24-inch thick by 18-inch wide by 48-inch long) were applied as a hold-down mechanism, as shown in Figure 8.27 (a). Each load block had an approximate weight between 1,850 and 2,000 pounds, for a total surcharge of 19,250 pounds, and they were placed at midspan of FIU-3, as shown in Figure 8.27 (b). Through the loading process of each individual block, the FIU-3 load-deflection ($P-\Delta$) and load-strain ($P-\epsilon$) data were monitored by the laser displacement transducers (LDTs) and a bottom longitudinal concrete strain gauge (CSG).

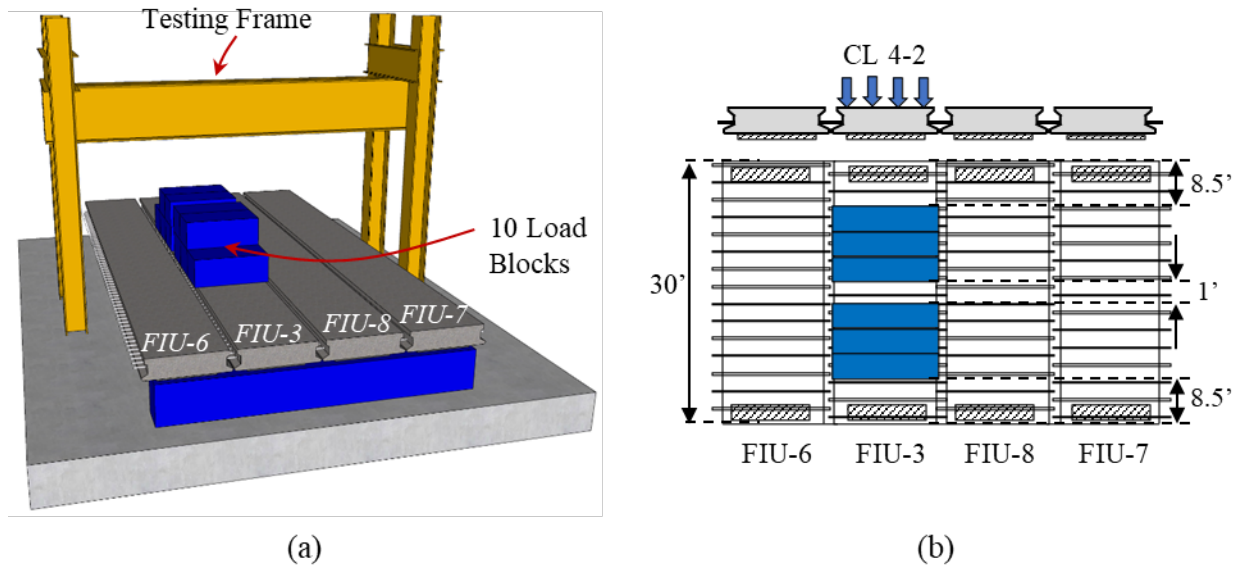


Figure 8.27: Test setup for Camber Leveling 4-2: (a) schematic and (b) plan and elevation view

Once all blocks were placed, the UHPC joint construction was performed maintaining the heavy weights on FIU-3 through the whole process. The surcharge load was removed after the joints were cast, ground down, fully cured (over 28 days), and the rest of the instrumentation was installed. During this process, all specimens load-deflection ($P-\Delta$) and load-strain ($P-\epsilon$) data was monitored. The measured response from this load phase represented the baseline response for the subsequent fatigue, service, and strength tests.

8.4.3. Four-Beam Fatigue, Service, and Strength Testing

Five different load configurations and protocols were used for the second part of the four-beam testing (Stages 2 through 10). The first configuration (service) included a half truck axle centered on each beam centerlines at midspan like the stiffness configurations before casting the joints; these were called Load Configuration (LC) 4-1 through 4-4. A second similar configuration (service) included a half truck axle centered on each beam centerlines at midspan with a cracked-joint condition; these were called LC 4-1cr through LC 4-4cr. A third configuration (strength) had a full truck axle centered at midspan; this was called LC 4-5.

Two additional fatigue load configurations were utilized. The first configuration consisted of a half truck axle centered on each exterior beam at midspan; this was called Fatigue Configuration (FC) 4-6. The second configuration consisted of an off-center, full-axle fatigue load at midspan; this was called FC 4-7. The difference between full axle and half axle is highlighted in Figure 8.28.

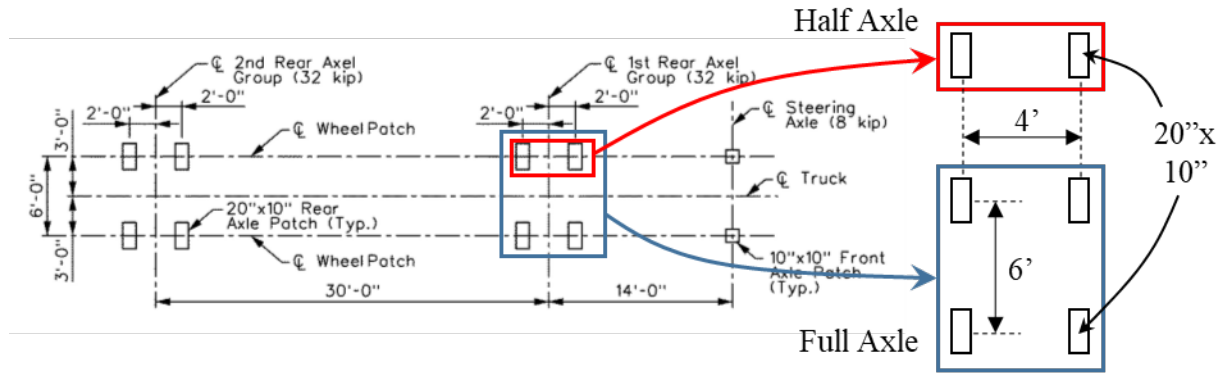


Figure 8.28: HS-20 truck load with full and half rear axle identification (from [82])

Detailed drawings for all configurations are provided separately.

8.4.3.1. Load Configurations 4-1, 4-2, 4-3, and 4-4 (Distribution Factors)

LC 4-1 through LC 4-4 had a half axle with 10-inch by 20-inch wheel patches centered on each beam at midspan, as shown in Figure 8.29. The load was applied using one actuator and one spreader beam (R33) loading one beam at a time.

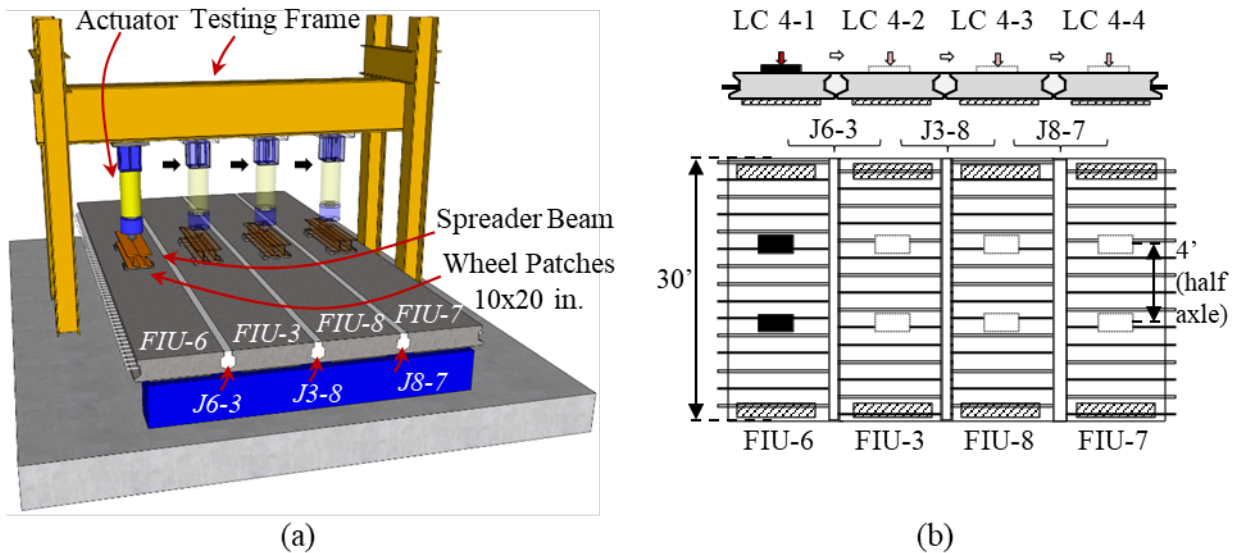


Figure 8.29: Test setup for Load Configuration 4-1 through 4-4 (a) schematic and (b) plan and elevation view

Load was applied using LC 4-1 for FIU-6, LC 4-2 for FIU-3, LC 4-3 for FIU-8, and LC 4-4 for FIU-7 at a rate of 0.2 kips/second until the upper limit load (30.6 kips) was reached, and then unloaded. The load-deflection ($P-\Delta$) and load-strain ($P-\epsilon$) data were measured through the loading process; these load configurations were used to measure girder distribution factors (GDF) and system and joint performance at different stages of testing.

A similar load configuration was also used to measure the GDF and system performance under a cracked condition, as shown in Figure 8.30. The load was applied using one actuator and one

spreader beam (R33) loading one specimen at a time with the configurations shown in Figure 8.30. A joint crack was simulated by saw-cutting along the length of the boundary between the precast section FIU-6 and the Joint 6-3. The cut depth reached at least two inches in the boundary matrix.

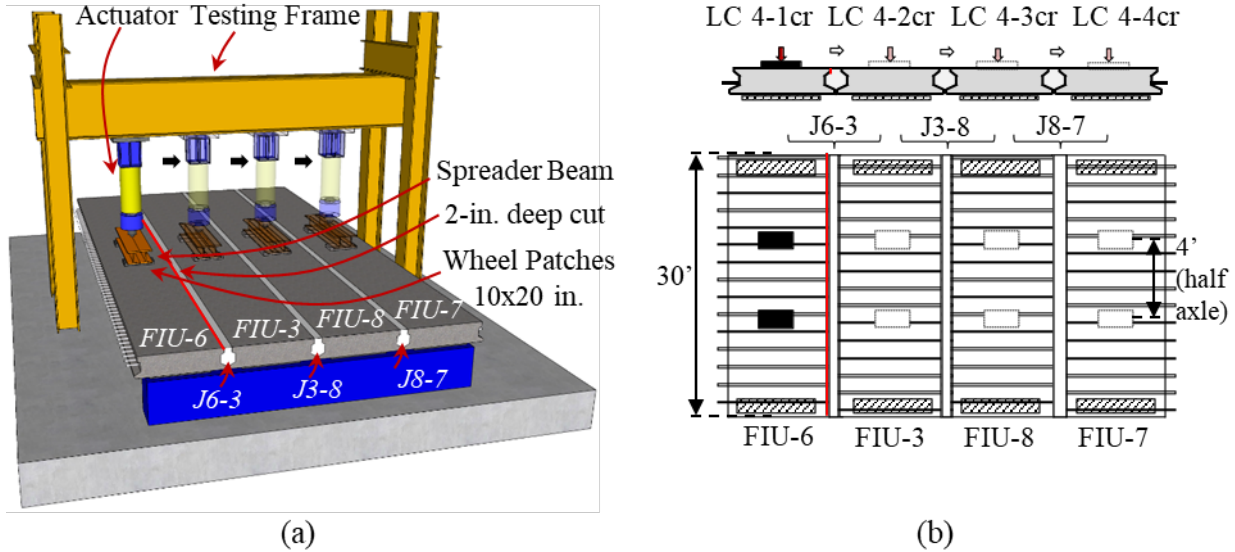


Figure 8.30: Test setup for Load Configuration 4-1cr through 4-4cr (a) schematic and (b) plan and elevation view

Load was also applied using LC 4-1cr for FIU-6, LC 4-2cr for FIU-3, LC 4-3cr for FIU-8, and LC 4-4cr for FIU-7 at a rate of 0.2 kips/second until the upper limit load (30.6 kips) was reached, and then unloaded.

8.4.3.2. Load Configuration 4-5 (Ultimate Strength)

LC 4-5 had a full truck axle with 10-inch by 20-inch wheel patches, as shown in Figure 8.31. The load was applied using one actuator and three spreader beams (two R9 and one R35) with the configuration shown in Figure 8.31 (a).

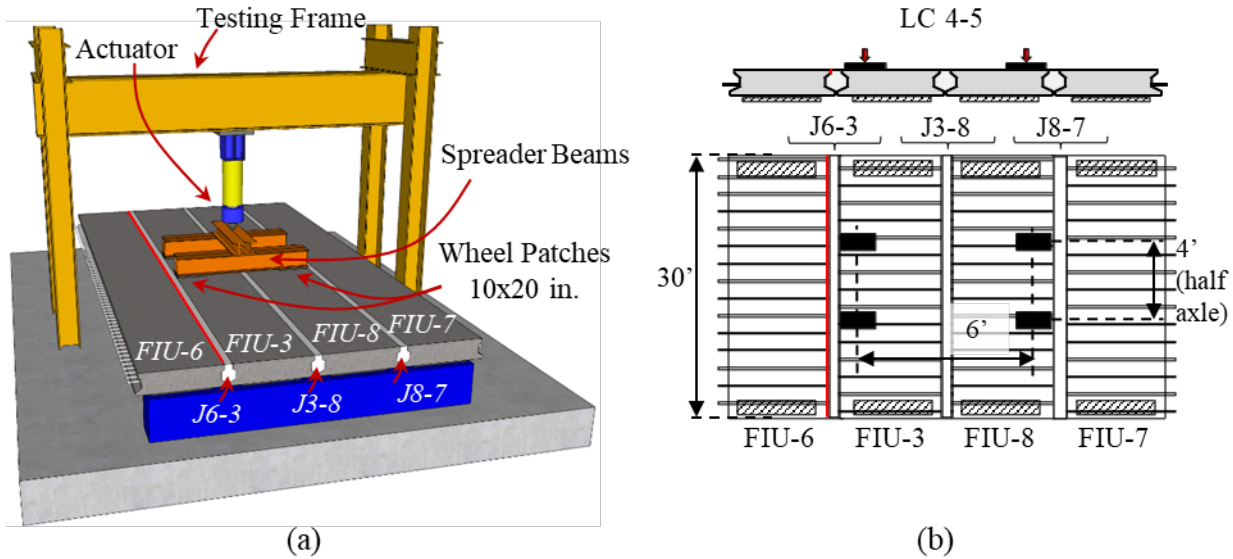


Figure 8.31: Test setup for Load Configuration 4-5 (a) schematic and (b) plan and elevation view

Load was applied at an approximate rate of 0.2 kips/second. Loading was paused five times to take pictures and monitor the progress of cracking until the load reached 150 kips (about 50 percent of the estimated capacity). At this point, all the crack displacement transducers (CDTs) were removed from underneath the joint and cracks were marked and documented for the last time until after failure. The superstructure was then loaded until failure at the same loading rate of 0.2 kips/second.

8.4.3.3. Fatigue Configuration 4-6 (Fatigue Loading)

FC 4-6 had two half truck axles with 10-inch by 20-inch wheel patches and a reverse sinusoidal fatigue loading protocol, as shown in Figure 8.32. Fatigue loads were applied using two actuators and two spreader beams (R34) with the configuration shown in Figure 8.32 (a) and (b) with an alternating 2-Hz sinusoidal wave, as shown in Figure 8.32 (c).

The fatigue loading was applied through an applied displacement that corresponded with loads in each actuator of 5 kips (minimum load) and 23.4 kips (maximum load) with a ± 5 percent allowable difference in applied displacement. A total of two million cycles were applied using FC 4-6 during Stages 3 and 4 which simulated normal service truck traffic conditions for a 100-year service life period. LC 4-1 through LC 4-4 were used to determine the behavior and GDFs of the system before (Stage 2) and after (Stage 5) fatigue testing with FC 4-6.

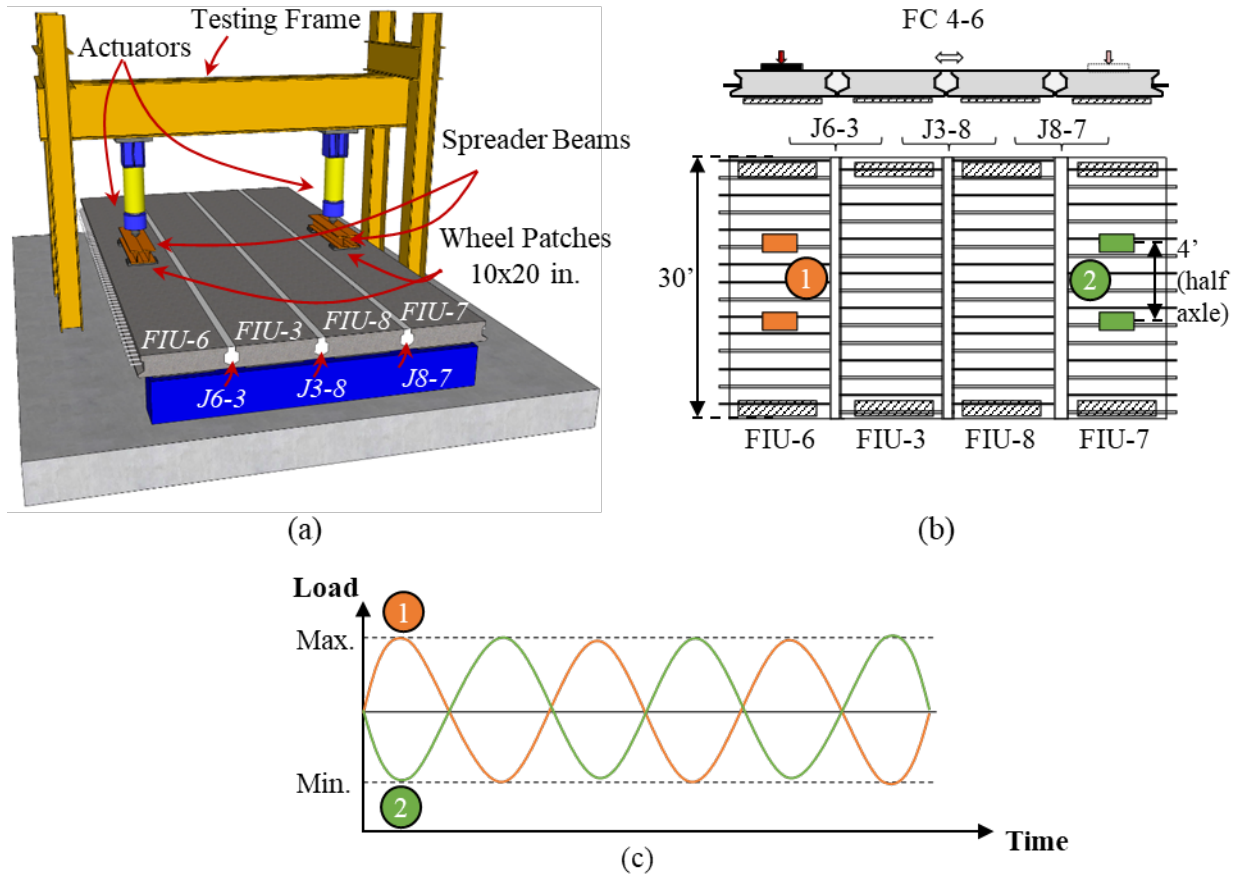


Figure 8.32: Test setup for Fatigue Configuration 4-6 (a) schematic, (b) plan and elevation view, and (c) reverse sinusoidal load protocol

8.4.3.4. Fatigue Configuration 4-7

FC 4-7 had one full truck axle with 10-inch by 20-inch wheel patches off-centered from the middle, as shown in Figure 8.33. Fatigue loads were applied using two actuators and two spreader beams (R34). The fatigue loading was applied through an applied displacement that corresponded with loads in each actuator of 5 kips (minimum load) and 23.4 kips (maximum load) with a ± 5 percent allowable difference in applied displacement. A total of two million cycles were applied using FC 4-7 during Stages 6 and 7 which simulated normal service truck traffic conditions for a 100-year service life period. LC 4-1 through LC 4-4 were used to determine the behavior and GDFs of the system before (Stage 5) and after (Stage 8) fatigue testing with FC 4-7.

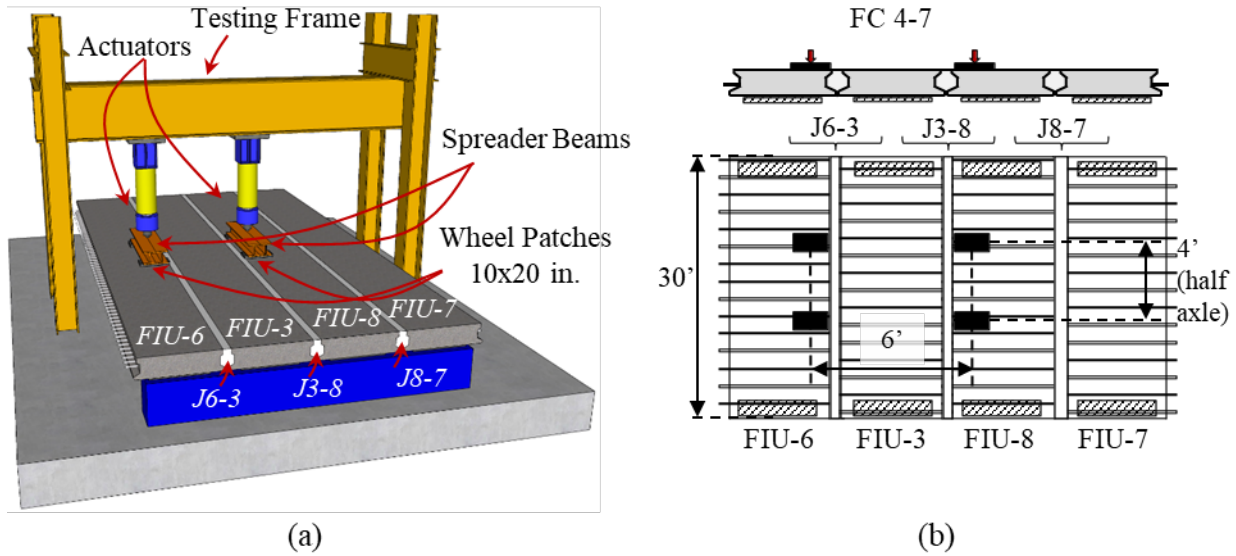


Figure 8.33: Proposed test setup for Fatigue Configuration 4-7 (a) schematic, (b) plan and elevation view

8.5. INSTRUMENTATION SCHEDULE

The instrumentation schedule for the four-beam test is described in this section. The instrumentation schedule is broken down based on the center span and support regions, as shown in Figure 8.34. A detailed set of plans with the complete instrumentation schedule was provided separately.

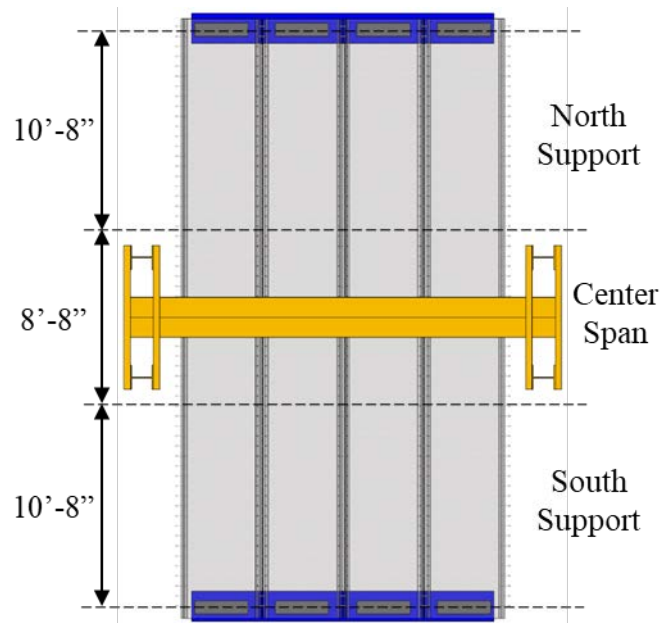


Figure 8.34: Four-beam test with two main sensor regions

Several different types of instrumentation were used in testing of the four-beam system. Rebar strain gauges (RSGs) were installed on the joint reinforcement at critical locations, extending

from each of the precast beams 1 inch from the vertical joint face, as shown in Figure 8.35 (a). Concrete strain gauges (CSGs) were installed on the top and bottom of the precast beams in the longitudinal and transverse directions, as shown in Figure 8.35 (b). Crack displacement transducers (CDTs) were installed across the joint boundary region along the length of the joints, as shown in Figure 8.35 (c). Laser displacement transducer (LDTs) were located at five different locations along the length of the specimen; some LDTs were located on top of the system, Figure 8.35 (d), and some were located on the bottom of the system, Figure 8.35 (e), depending on accessibility. Vibrating wire gauges (VWGs), shown in Figure 8.35 (f), were embedded in the prestressed concrete members at different locations in the cross section and beams.

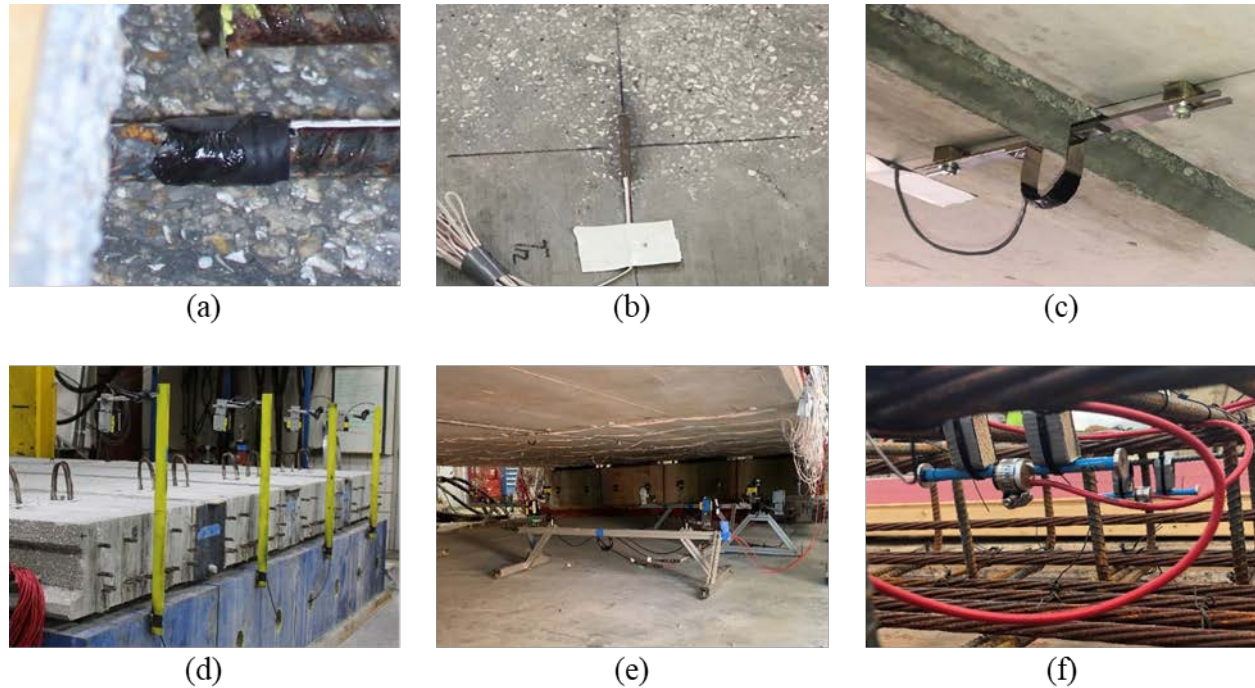


Figure 8.35: Instrumentation used for four-beam testing: (a) RSGs, (b) CSGs, (c) CDTs, (d) support LDTs, (e) bottom center LDTs, and (f) VWGs

Camber readings taken outside and inside the structure's laboratory were measured with a ZIPLEVEL Pro-2000 High Precision Altimeter, as shown in Figure 8.36 (a). VWGs data measurements were taken with a Campbell Scientific Vibrating Wire Analyzer (VWA) reader, as shown in Figure 8.36 (b). Data from sensors during the test were acquired via a Data Acquisition system (DAQ), as shown in Figure 8.36 (c).

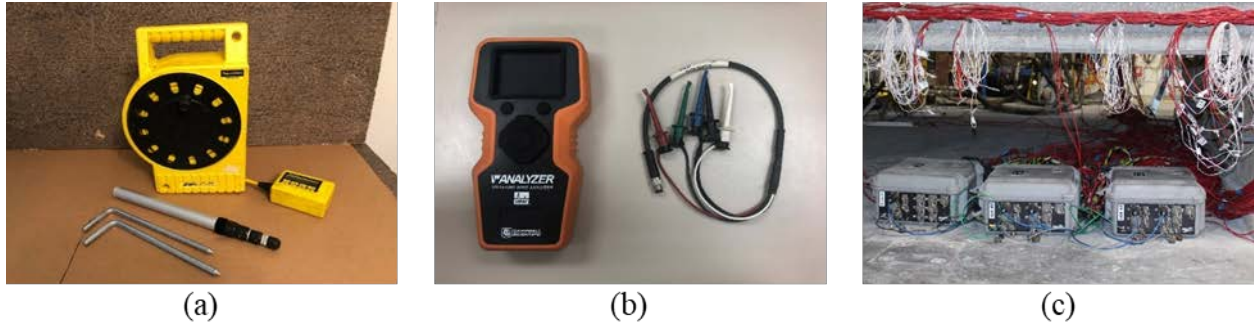


Figure 8.36: (a) high precision altimeter, (b) VWA, and (c) DAQ

8.5.1. Four-Beam Individual Stiffness and Camber Leveling Instrumentation

The instrumentation schedule used for the flexural stiffness ramps and load blocks installation is shown in Figure 8.37 for near the north support, Figure 8.38 for center region and Figure 8.39 for near the south support. For the four-beam superstructure construction with camber leveling test, only bottom longitudinal concrete strain gauges (CSG) and laser displacement transducer (LDT) were used.

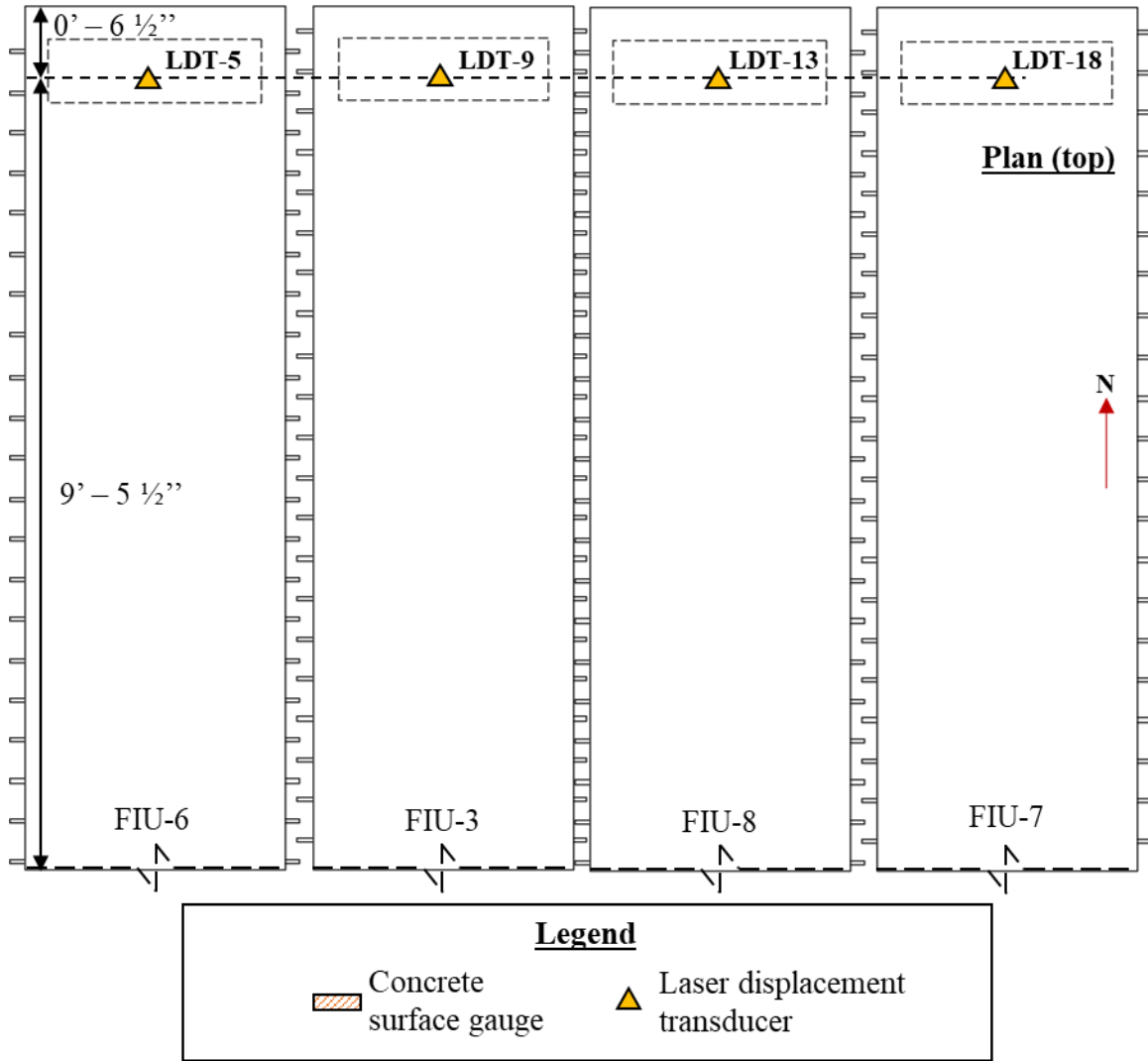


Figure 8.37: Four-beam stiffness and camber leveling testing instrumentation toward north support

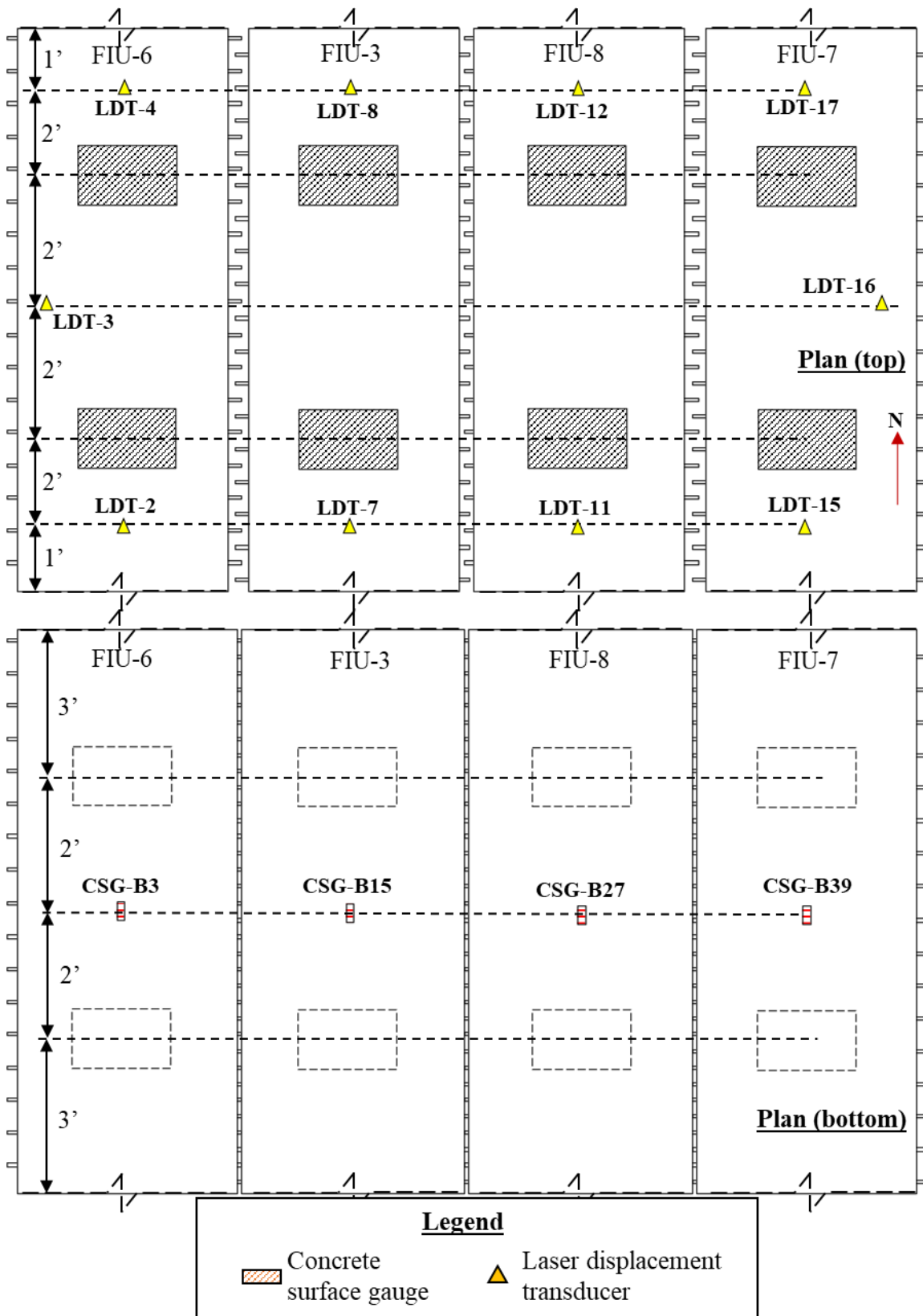


Figure 8.38: Four-beam stiffness and camber leveling testing instrumentation at midspan

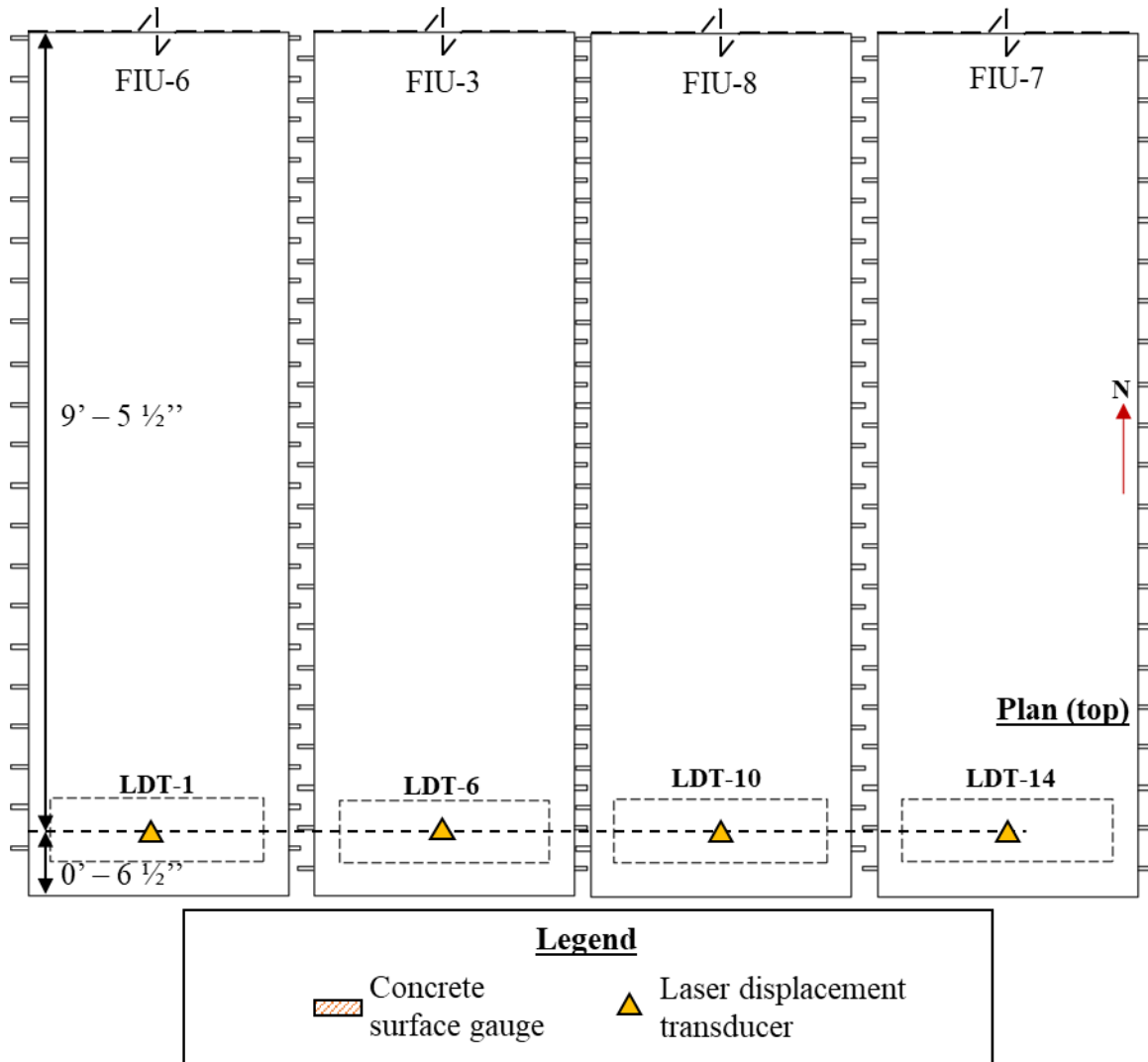


Figure 8.39: Four-beam stiffness and camber leveling testing instrumentation toward south support

8.5.2. Four-Beam Fatigue, Service, and Strength Testing Instrumentation

Once the beam stiffness measurements and camber leveling stages were performed, the complete instrumentation schedule for the subsequent testing stages was installed. The sensor layout for the four-beam configuration is shown in Figure 8.40 and Figure 8.41 for near the north support, Figure 8.42 for the center of the span, Figure 8.43 and Figure 8.44 for near the south support.

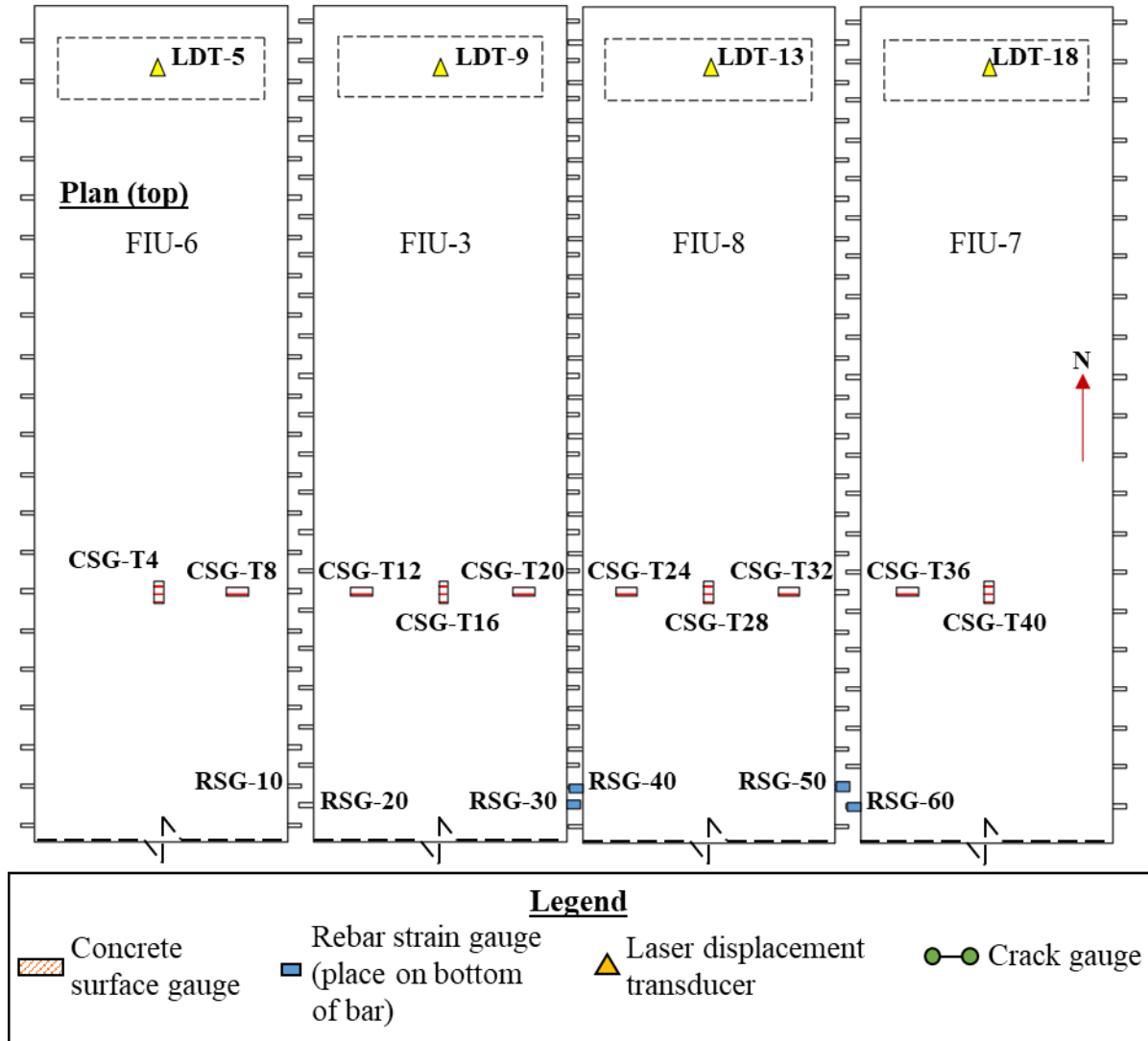


Figure 8.40: Four-beam fatigue, service, and strength testing instrumentation at north support (top)

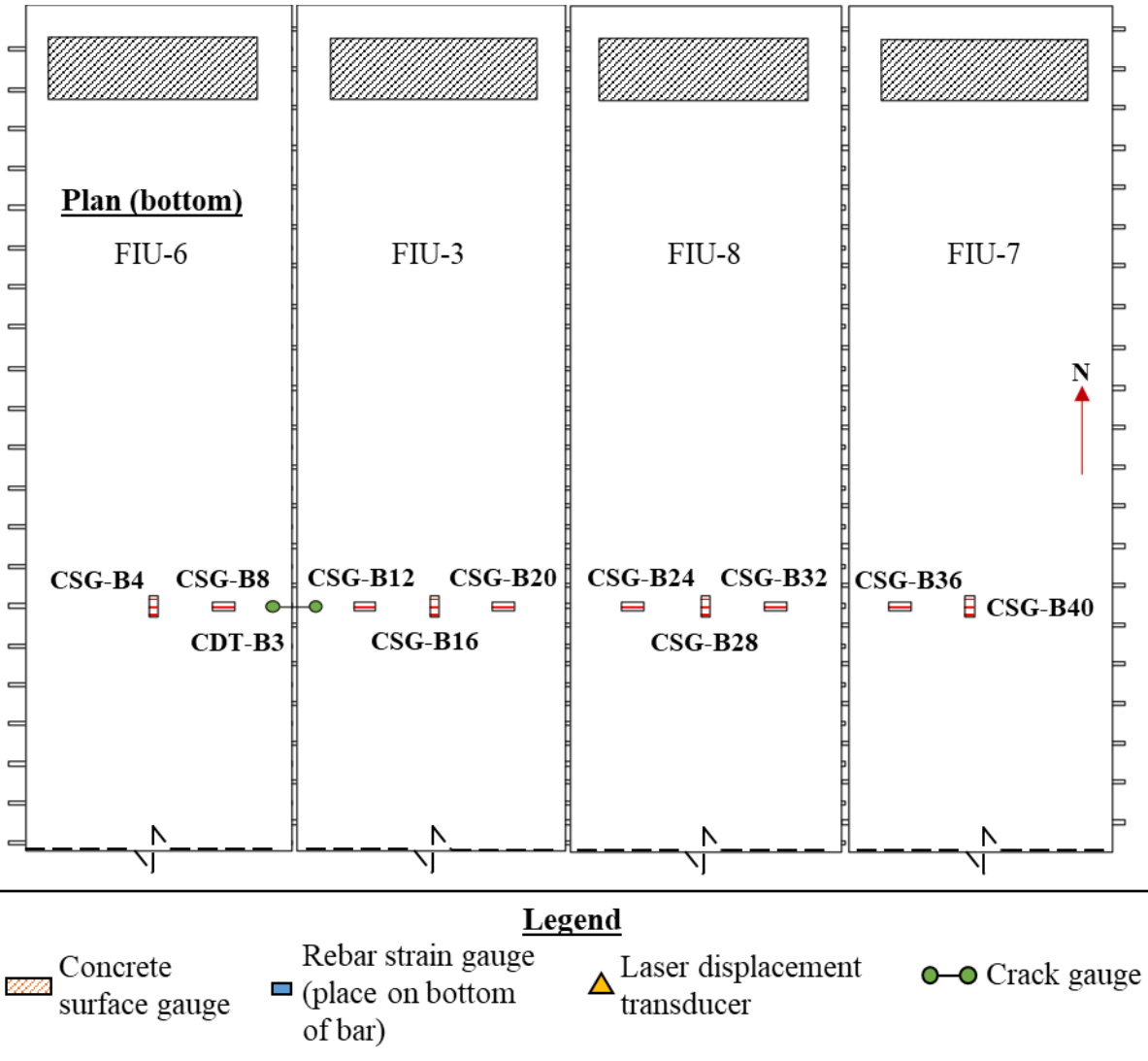


Figure 8.41: Four-beam fatigue, service, and strength testing instrumentation at north support (bottom)

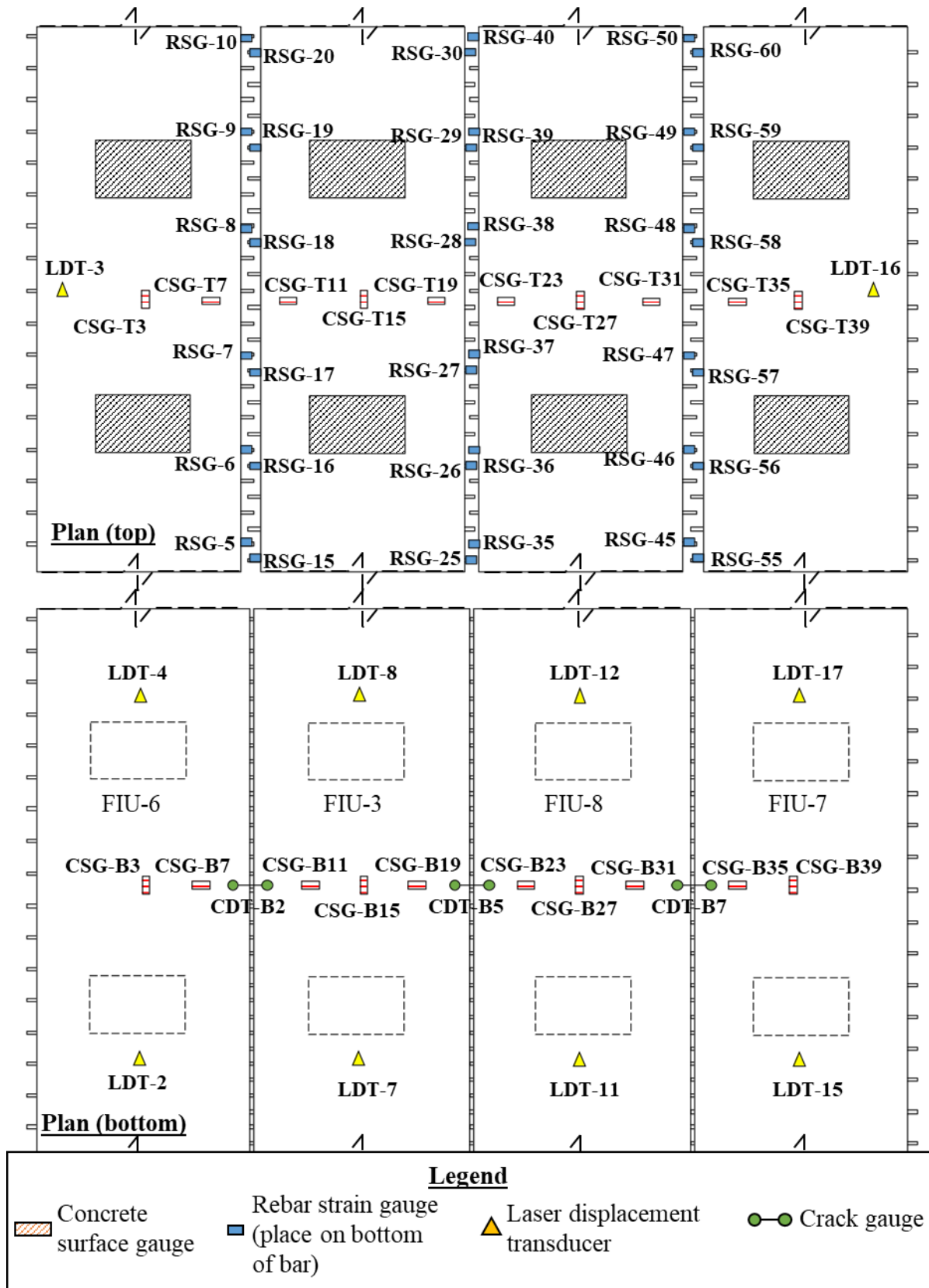


Figure 8.42: Four-beam fatigue, service, and strength testing instrumentation at midspan

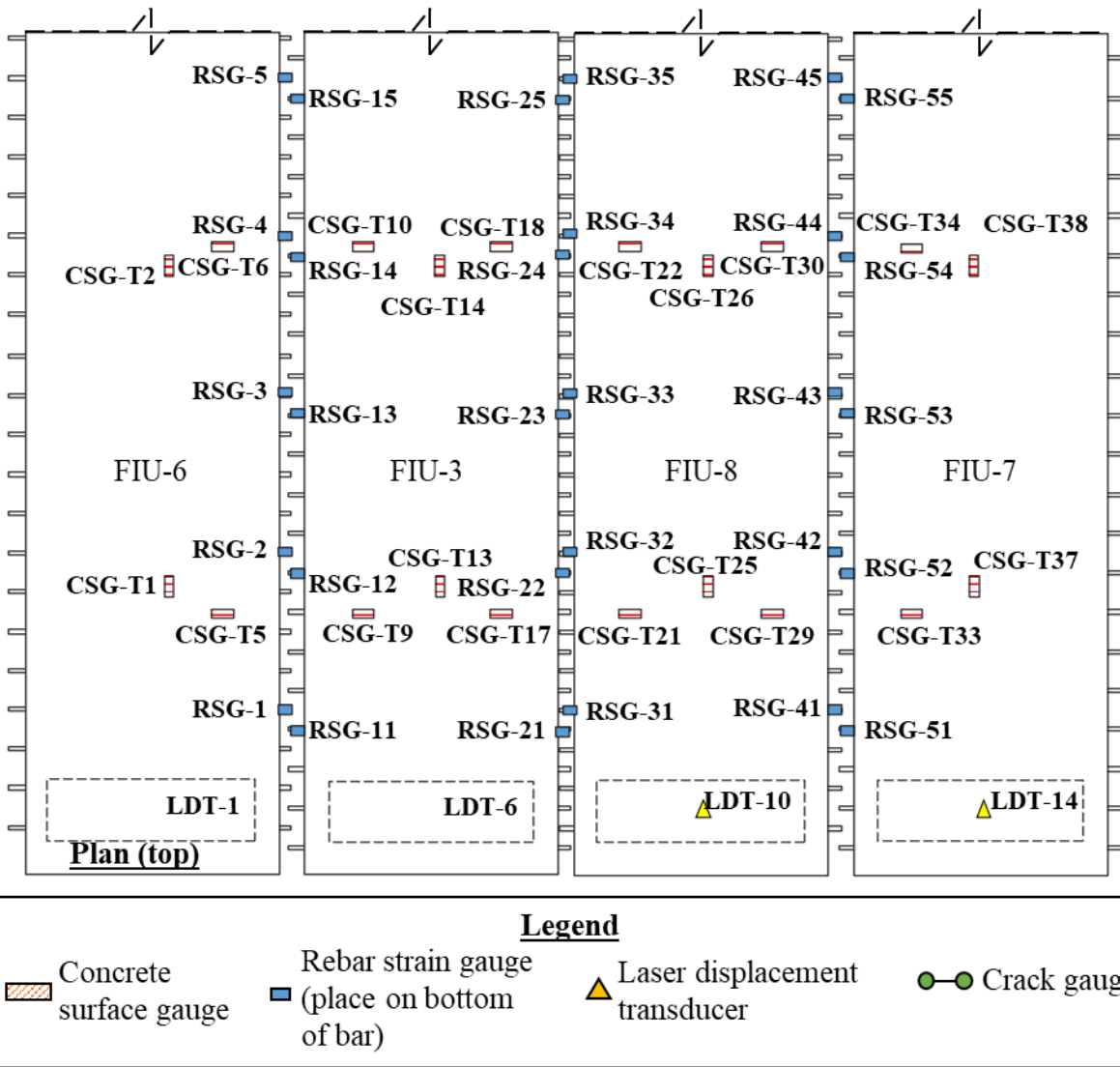


Figure 8.43: Four-beam fatigue, service, and strength testing instrumentation at south supports (top)

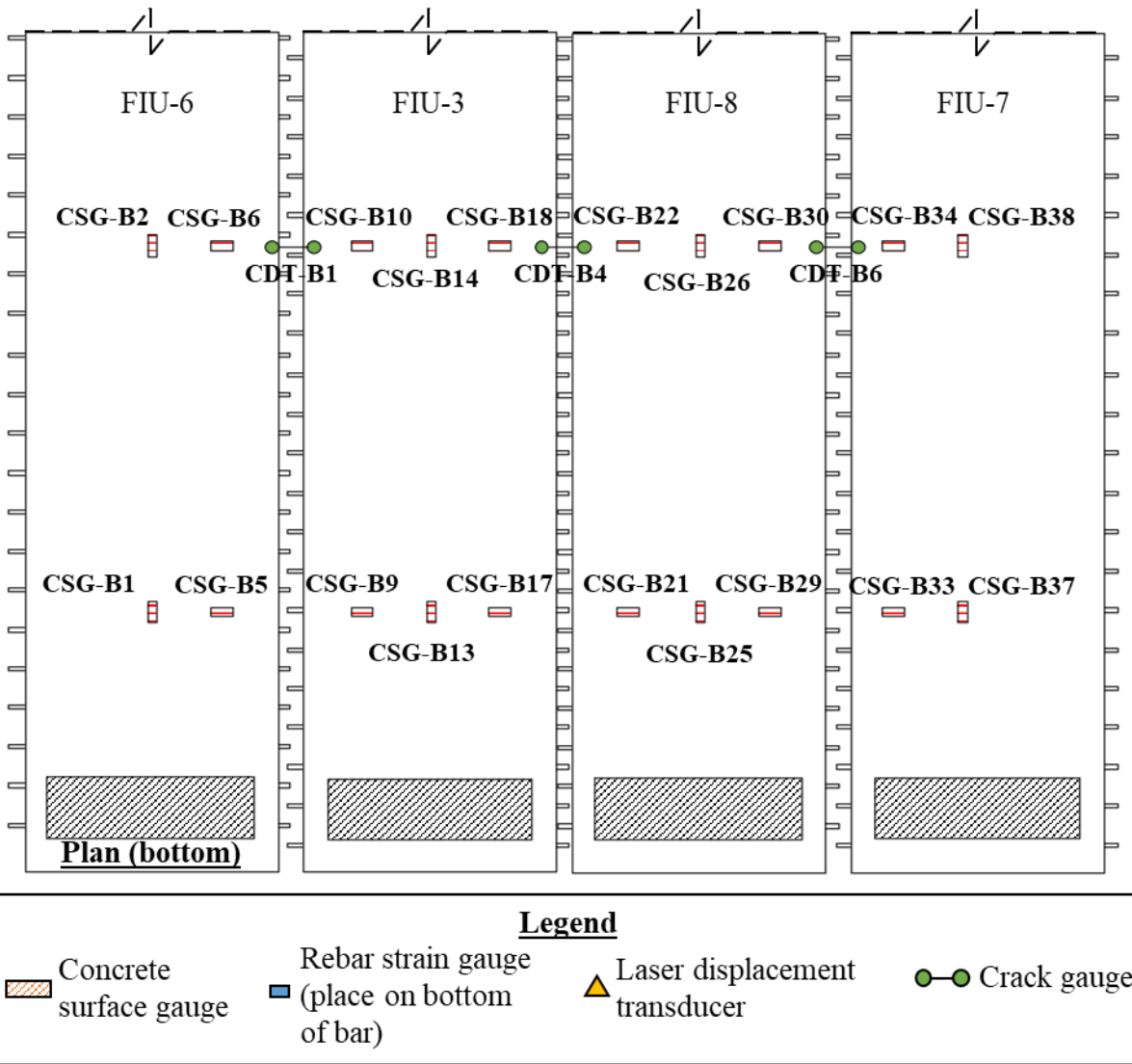


Figure 8.44: Four-beam fatigue, service, and strength testing instrumentation at south supports (bottom)

The VWGs layout for the four-beam Configuration is shown in Figure 8.45 for the center span and Figure 8.46 for the region near the supports.

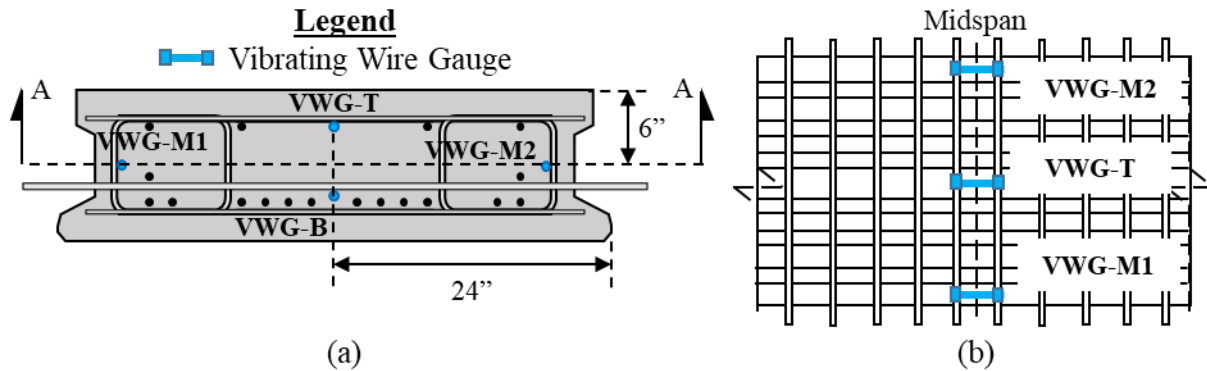


Figure 8.45: VWG locations at beam midspan: (a) cross section and (b) cut A-A at midspan

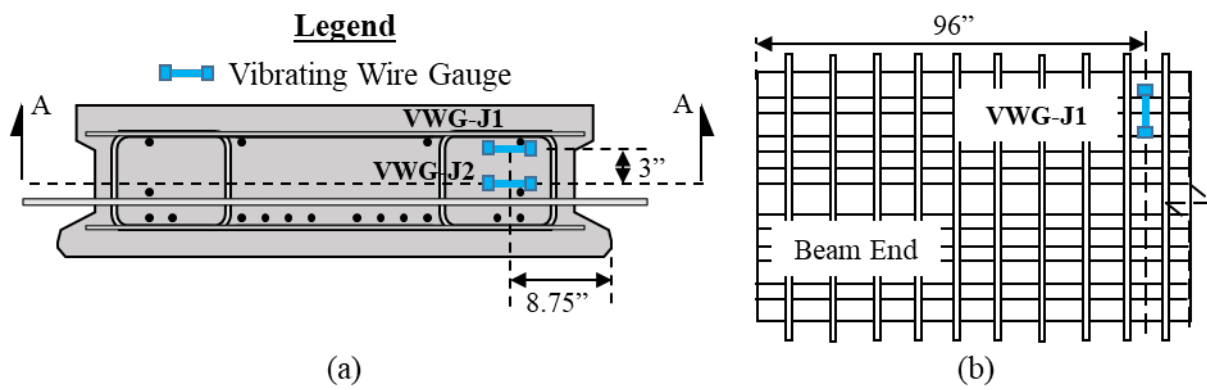


Figure 8.46: VWG locations at beam end: (a) cross section and (b) cut A-A near beam end

8.6. LONG-TERM MONITORING

Camber measurements and vibrating wire gauge (VWG) readings were taken throughout the life of the beams. This section summarizes the camber and VWG results.

8.6.1. Camber Measurements

Camber measurements were taken immediately after release at the precast yard, through the storage time, and during specimen construction in the laboratory for a total of 448 days. The morning camber readings and temperatures from release on December 2nd, 2019 (day 0) to February 22nd, 2021 (day 448) are shown in Figure 8.47. Beam camber readings at the precast yard (release time) were taken using a laser measurement tool aligned with a plumb bob for vertical alignment at midspan of each beam. Beam camber was measured using an altimeter at FDOT SRC.

The largest camber was measured in FIU-3. This beam was designed with four partially-stressed top strands, compared to the four fully-stressed top strands for the other three beams, to encourage a larger camber to develop. The camber for FIU-7 and FIU-8 was similar throughout the life of the beams but was slightly different from the measured camber in FIU-6. FIU-6, FIU-7, and FIU-8. All had the same cross section design, but FIU-6 was cast with a different batch of

concrete than FIU-7 and FIU-8. The same mix design was used for all the beam casts, but there may have been slight variations in the actual concrete properties for FIU-6 that led to the minor difference in camber.

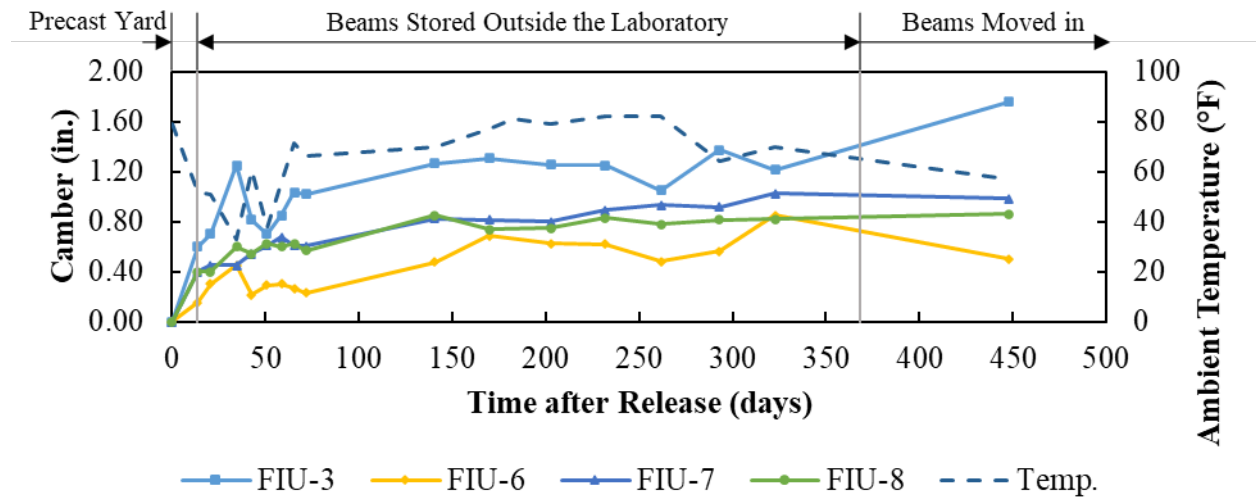


Figure 8.47: Morning camber readings of FIU specimens

The final camber before the placement of the blocks for camber leveling were 1.76 inches for FIU-3, 0.50 inches for FIU-6, 0.86 inches for FIU-8, and 0.99 inches for FIU-7. The beams were aligned based on these final cambers, as described in §8.3, from west to east: FIU-6, FIU-3, FIU-8, FIU-7.

8.6.2. VWG Data

VWG readings were initially taken before and after release at the prestressing plant using a hand reader, as shown in Table 8.9. The beams were then transported to FDOT's SRC between Day 4 and 18. The beams were then attached to a data acquisition system and readings were taken twice per day until Day 118. The readings were then manually taken again after the application of the surcharge load on FIU-3 and before and after joint casting and release and removal of the surcharge load.

Table 8.9: VWG reading type during life of beams

Time	VWG Reading Type
Release to Day 4	Manual
Day 18 to Day 114	Data Acquisition System
Day 525 to Day 556	Manual

The strain change read in the VWGs over time are shown in Figure 8.48. Most of the measured strain changes (around 70 percent) occurred in the first 100 days, which is typical for concrete creep and shrinkage. There was generally a large difference between the readings in M1 and M2, which were located at the same height but on opposite sides of the cross section. This difference shows that there was a variation in strain across the width of the cross section. VWG M2 malfunctioned in FIU-3.

The large change of strain observed in FIU-3 T was likely due to the first reading at Day 525 being taken after the application of the surcharge load. This was the first reading taken since Day 114, so the increase due to time effects and jump due to the loading cannot be differentiated. The reading at Day 525 for the other beams was taken before the application of any external loads, so these readings would be representative of the effect of shrinkage and creep on the measured strains.

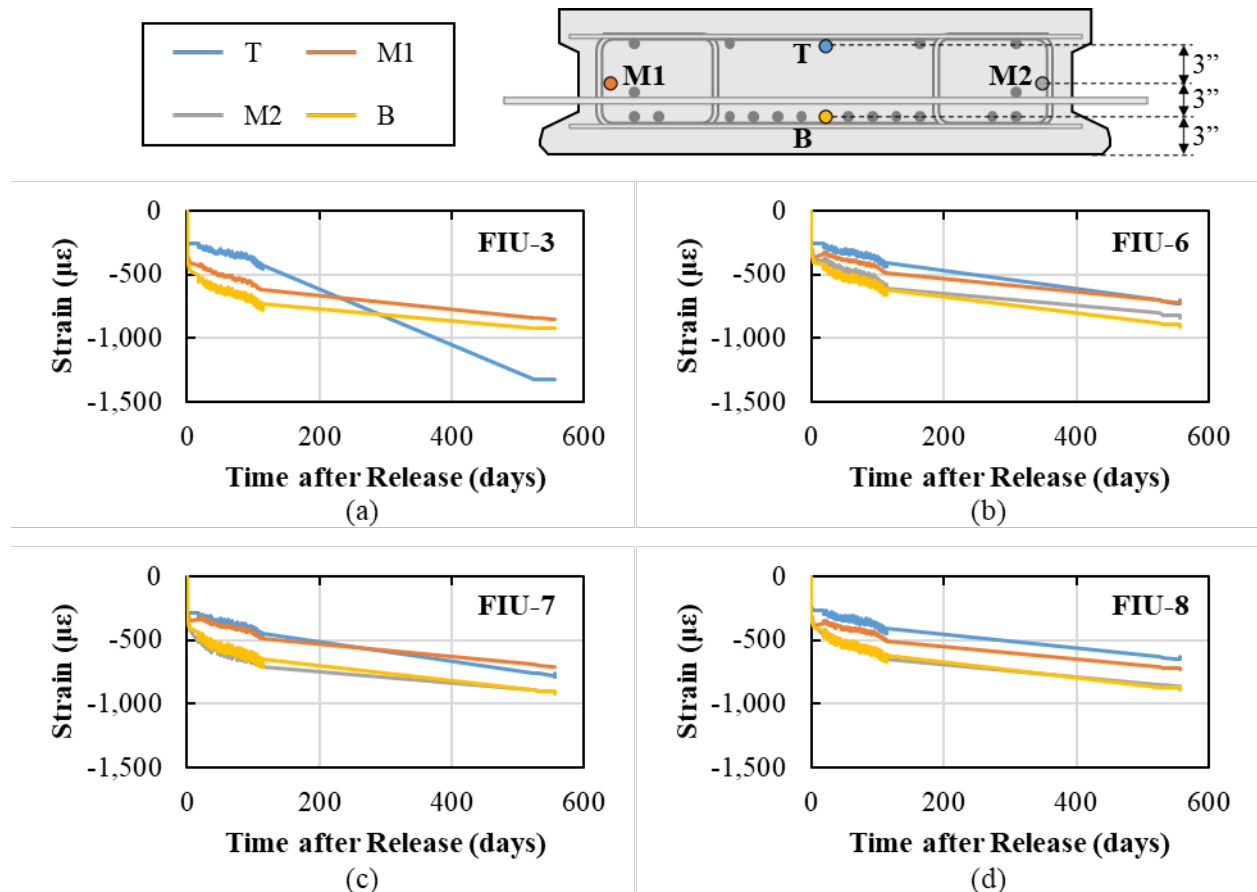


Figure 8.48: Strain change over time measured using vibrating wire strain gauges for (a) FIU-3, (b) FIU-6, (c) FIU-7, and (d) FIU-8

The VWG readings are plotted over the height of the cross section at release in Figure 8.49. The average reading between VWGs M1 and M2 was used for the measured strain at mid-height. The measured strains in the VWGs were used to linearly extrapolate the estimated strains at the top and bottom fibers of the section; these strains are shown in Figure 8.49.

The strain at release is different in FIU-3 than FIU-6, FIU-7, and FIU-8 because FIU-3 had four partially-stressed top strands compared with the four fully-stressed top strands in FIU-6, FIU-7, and FIU-8. These measured strains would have included the effect of the prestressing and the self-weight of the beam (assuming supports are at the ends of the beam). The measured pre-

compression strains in the bottom of the beam at midspan were $-451.5 \mu\epsilon$ for FIU-3 and $-339.9 \mu\epsilon$ average for FIU-6, FIU-7, and FIU-8.

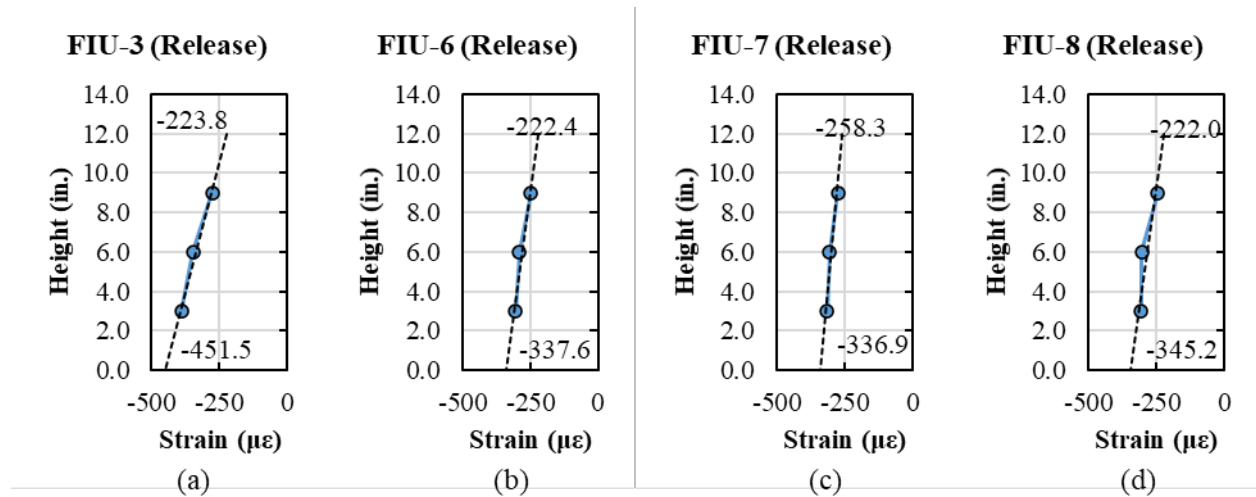


Figure 8.49: Strain across cross-section height at release for (a) FIU-3, (b) FIU-6, (c) FIU-7, and (d) FIU-8

Creep (due to prestressing and self-weight) and shrinkage continued to increase the strains in the cross section over time. The strains across the depth of the cross section, including the extrapolated top and bottom fiber stresses, are shown in Figure 8.50. The bottom fiber strains increased more over time than the top fiber strains due to the larger prestressing force in the bottom of the section.

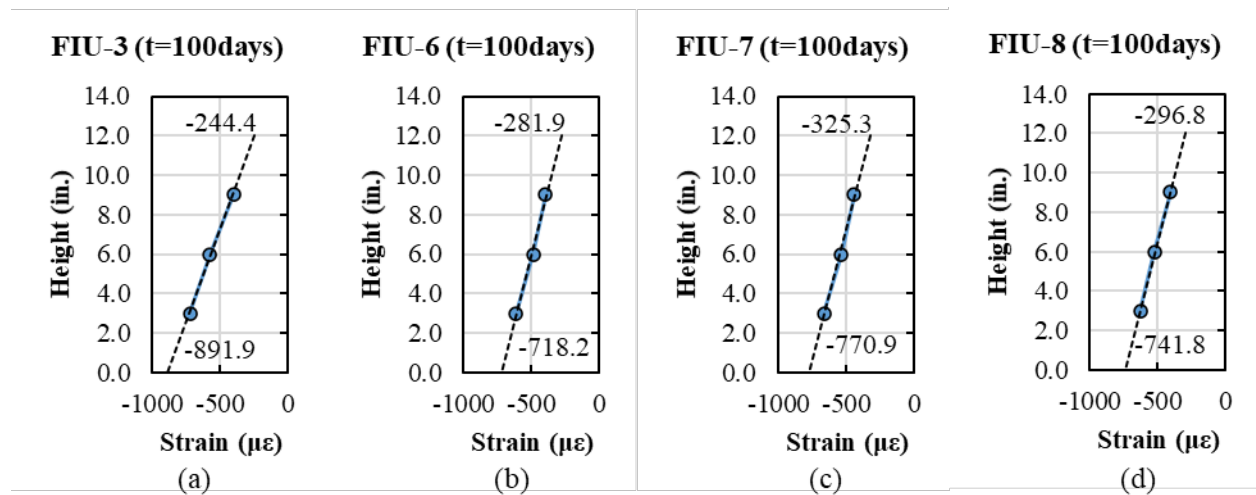


Figure 8.50: Strain across cross-section height at $t = 100$ days for (a) FIU-3, (b) FIU-6, (c) FIU-7, and (d) FIU-8

Another strain reading was taken at 525 days after release, shown in Figure 8.51. The strains continued to increase in FIU-6/7/8 due to creep and shrinkage. The curvature in FIU-3 reversed (higher compression in the top fiber and lower compression in bottom fiber) due to the application of the surcharge load. The strain profile is no longer linear for FIU-3 at $t = 525$ days.

This may have been a result of VWG-M2 malfunctioning in FIU-3. The average of VWG-M1 and VWG-M2 was used to find the average strain at mid-height, but this was not possible for FIU-3.

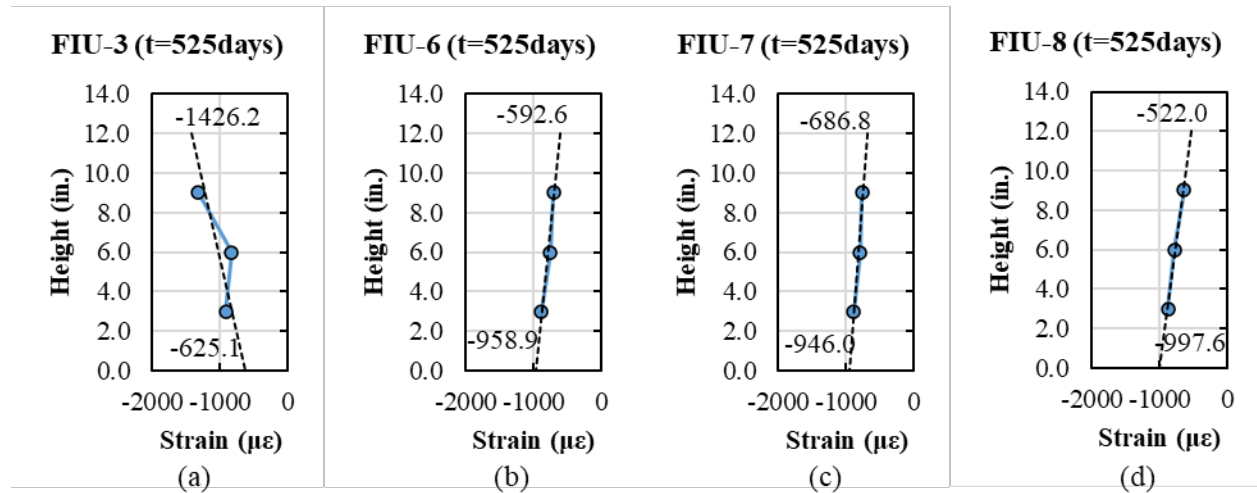


Figure 8.51: Strain across cross-section height at $t = 525$ days for (a) FIU-3, (b) FIU-6, (c) FIU-7, and (d) FIU-8

The strains in FIU-6, FIU-7, and FIU-8 at $t = 525$ days are the measured strains in the section before the installation of the concrete surface gauges. One of the longitudinal surface gauges was already installed in FIU-3 before the application of the surcharge load; the remaining surface gauges were installed after application of the surcharge load.

A summary of the top and bottom fiber strains and associated curvature at several different times is shown in Table 8.10.

Table 8.10: Top and bottom fiber strains and curvature at different times after release

Beam:	FIU-3	FIU-3	FIU-3	FIU-6	FIU-6	FIU-6	FIU-7	FIU-7	FIU-7	FIU-8	FIU-8	FIU-8
Time (days)	ϵ_t ($\mu\epsilon$)	ϵ_b ($\mu\epsilon$)	ϕ ($\times 10^{-6}$ rad/in)	ϵ_t ($\mu\epsilon$)	ϵ_b ($\mu\epsilon$)	ϕ ($\times 10^{-6}$ rad/in)	ϵ_t ($\mu\epsilon$)	ϵ_b ($\mu\epsilon$)	ϕ ($\times 10^{-6}$ rad/in)	ϵ_t ($\mu\epsilon$)	ϵ_b ($\mu\epsilon$)	ϕ ($\times 10^{-6}$ rad/in)
1	-223.8	-451.5	-19.0	-222.4	-337.6	-9.6	-258.3	-336.9	-6.5	-222.0	-345.2	-10.3
50	-187.2	-796.1	-50.7	-227.8	-637.6	-34.2	-271.6	-683.7	-34.3	-248.1	-660.4	-34.4
100	-244.4	-891.9	-54.0	-281.9	-718.2	-36.4	-325.3	-770.9	-37.1	-296.8	-741.8	-37.1
113	-290.0	-899.0	-50.7	-319.6	-730.9	-34.3	-361.2	-768.9	-34.0	-329.5	-744.3	-34.6
525	-1426.2	-625.1	66.8	-592.6	-958.9	-30.5	-686.8	-946.0	-21.6	-522.0	-997.6	-39.6
531	-1428.3	-625.7	66.9	-606.3	-968.1	-30.2	-685.2	-960.1	-22.9	-532.0	-998.4	-38.9
553	-1430.5	-636.4	66.2	-630.3	-965.3	-27.9	-711.5	-953.5	-20.2	-552.6	-996.1	-37.0
555.5	-1431.8	-634.9	66.4	-630.9	-963.7	-27.7	-712.6	-950.9	-19.9	-553.0	-994.0	-36.8
556	-1419.1	-657.5	63.5	-587.7	-1009.9	-35.2	-675.7	-991.5	-26.3	-513.9	-1032.3	-43.2

The curvature plotted versus time is shown in Figure 8.52. The switch in curvature is clear for FIU-3 from negative to positive when the surcharge load is applied. FIU-7 had a slightly decreasing curvature over time compared to the other beams.

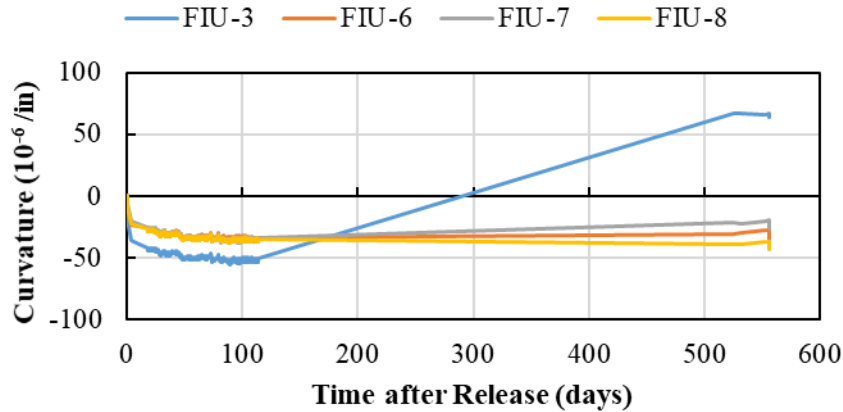


Figure 8.52: Curvature versus time (found using top and bottom strains) for FIU-3, FIU-6, FIU-7, and FIU-8

8.6.3. Prestress Losses

The strains measured using the VWGs were also used to calculate the prestress loss over time. The prestress loss (Δf_p) can be found by determining the strain change at the centroid of the prestressing strands ($\Delta \epsilon_c$), using linear interpolation between the VWGs, and multiplying by the modulus of the prestressing strands (E_p), as shown in Equation 8-1. The relaxation loss of the prestressing strands (Δf_{pRE}) is not measured using VWGs as relaxation does not cause a change in the concrete strain.

$$\Delta f_p = \Delta \epsilon_c \cdot E_p + \Delta f_{pRE} \quad \text{Equation 8-1}$$

The strain at the centroid of the prestressing strands (ϵ_p) can be found assuming a linear strain profile across the depth of the cross section, shown in Figure 8.53. The average strain between outside middle VWGs (M1 and M2) was used in the linear interpolation.

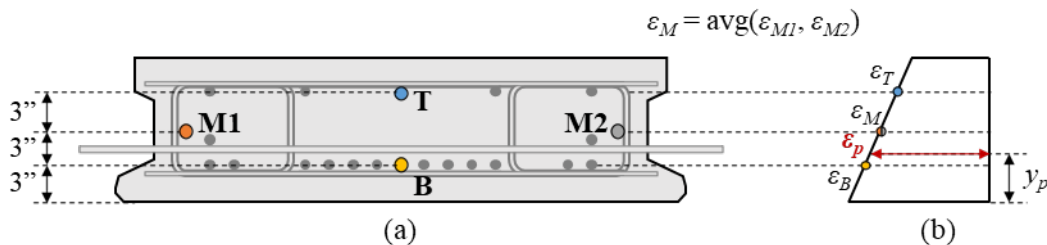


Figure 8.53: Determination of strain in prestressing strands with (a) VWG location in cross section and (b) strain profile across section depth

The prestress loss measured over time is shown in Figure 8.54. The elastic shortening, long-term loss, and total loss are summarized in Table 8.11. The time of the last VWG measurement before any external loads were applied are also summarized in Table 8.11. A VWG measurement was not taken for FIU-3 before the application of the surcharge load for the camber leveling

procedure. For FIU-6, FIU-7, and FIU-8, approximately 55 percent (an average of 8.3 ksi of 15.1 ksi) of the long-term losses occurred by 114 days.

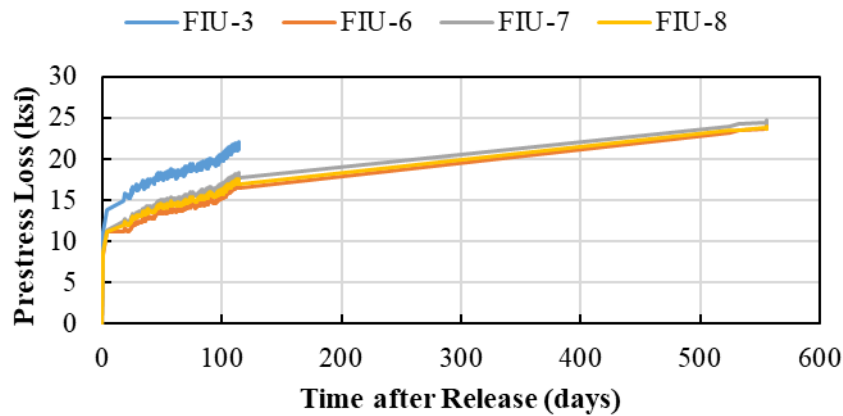


Figure 8.54: Prestress loss versus time for FIU-3, FIU-6, FIU-7, and FIU-8

The measured elastic shortening loss can be seen in Figure 8.54 and Table 8.11. The elastic shortening loss was higher for FIU-3, 11.2 ksi compared to an average of 8.5 ksi for FIU-6, FIU-7, and FIU-8. The higher elastic shortening in FIU-3 was a result of the casting procedure; see §8.3.1 for more details on casting. The release strength and the concrete age at release were less for FIU-3 compared to FIU-6, FIU-7, and FIU-8.

Table 8.11: Measured prestress loss at time of last reliable measurement

Parameter	FIU-3	FIU-6	FIU-7	FIU-8
Release Strength	6.0 ksi	8.5 ksi	8.5 ksi	8.5 ksi
Age at Release	5 days	12 days	12 days	12 days
Elastic Shortening Loss	11.2 ksi	8.4 ksi	8.8 ksi	8.5 ksi
Time at Last Measurement	114 days	525 days	525 days	525 days
Long-Term Loss	10.0 ksi	15.0 ksi	15.4 ksi	14.8 ksi
Total Loss	21.2 ksi	23.4 ksi	24.2 ksi	23.3 ksi

The estimated prestress losses based on the AASHTO LRFD Bridge Design Specification Refined Estimate Procedure [82] are shown in Table 8.12 for final time of 525 days. The measured elastic shortening losses are within 8 percent of the estimated loss for all beams. The long-term loss is within 6.4 percent for FIU-6/7/8. The estimated loss is 124 percent higher than the measured loss for FIU-3 because the last reading was taken at 114 days.

Table 8.12: Estimated prestress loss at time of last measurement based on AASHTO LRFD Refined Estimate Procedure [82]

Type of Loss	FIU-3	FIU-6/7/8
Elastic Shortening Loss	10.3 ksi	7.9 ksi
Long-Term Loss	22.4 ksi	16.1 ksi
Total Loss	32.7 ksi	24.0 ksi

8.7. FOUR-BEAM INDIVIDUAL STIFFNESS AND CAMBER LEVELING RESULTS

8.7.1. Summary of Results

A summary of the individual girder stiffnesses and camber leveling force results during Stage 1 of testing of the four-beam configuration are discussed in this section.

One actuator was used to load each beam individually: MTS-55 for FIU-6, and MTS-110, which was moved sideways, for FIU-3, FIU-8, and FIU-7. This configuration was selected due to ease of setup and placement of the MTS 110 above the beams. The load was measured throughout testing using load cells and pressure transducers in each of the actuators, as shown in Figure 8.55 (a). Deflection of the beams was measured using laser displacement transducers (LDTs), as shown in Figure 8.55 (b).

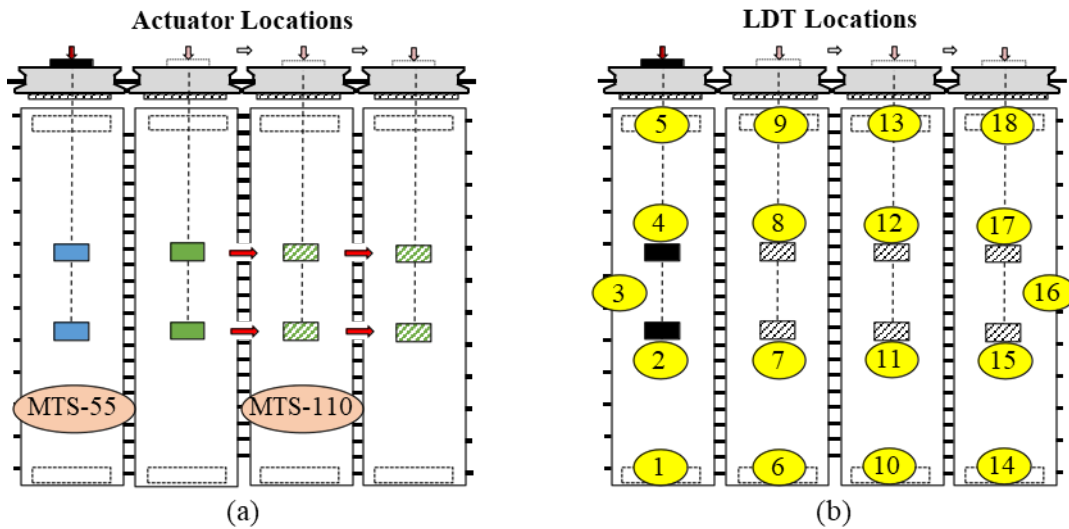


Figure 8.55: Location of (a) actuators and (b) LDT sensors

The absolute displacement was obtained for each beam by removing the average end displacement from the average midspan displacement. An example for FIU-3 is shown in Equation 8-2. This procedure was used to find the beam displacement during all load configurations. The outside midspan displacements, measured using LDT-3 and LDT-16, were also modified by subtracting the average end displacements for FIU-6 and FIU-7, respectively.

$$\Delta_{FIU-3,i} = Avg\{\delta_{7,i}, \delta_{8,i}\} - Avg\{\delta_{6,i}, \delta_{9,i}\} \quad \text{Equation 8-2}$$

The stiffness of each beam was found by taking the change in load from 0 to the service load divided by the change in displacement, as shown in Equation 6-4.

$$K_{flex,i} = \frac{\Delta_{load}}{\Delta_{disp}} = \frac{20 \text{ kip} - 0 \text{ kip}}{\Delta_{20,i} - \Delta_{0,i}} \quad \text{Equation 8-3}$$

The measured maximum deflections, bottom longitudinal concrete strains at midspan, and stiffnesses for each precast specimen at 20 kips of applied load are shown in Table 8.13.

Table 8.13: Summary of maximum deflections, longitudinal bottom strains, and stiffnesses at 20 kips for large-scale specimens

Specimen ID*	Max. Deflection (in.)	Max. Long. Bottom Strain ($\mu\epsilon$)	Flexural Stiffness (kip/in.)
FIU-6	0.37	223.9	53.6
FIU-3	0.39	233.6	51.1
FIU-8	0.36	224.1	55.6
FIU-7	0.37	221.7	54.4

*specimen order is based on beam alignment on superstructure from west (FIU-6) to east (FIU-7)

After measuring the beam individual stiffnesses, the surcharge load was applied. The measured maximum deflection, longitudinal bottom strain, and total surcharge applied to FIU-3 is shown in Table 8.14. During the camber leveling process of FIU-3, a total of ten (10) load blocks were individually added at center region for a total surcharge applied of 19,250 pounds.

Table 8.14: Summary of maximum deflection, longitudinal bottom strain, and surcharge application for FIU-3

Specimen ID	Max. Deflection (in.)	Max. Long. Bottom Strain ($\mu\epsilon$)	Surcharge (kip)*
FIU-3	0.37	213.9	19.25

*total surcharge application utilizing 10 load blocks

A more detailed analysis of the results during the initial stiffness measurements and camber leveling load stages is provided in the following sections.

8.7.2. Individual Stiffness Results (Stages 1.1 – 1.4; SC 4-1 through SC 4-4)

8.7.2.1. Overview

Individual girder stiffness was checked before construction of the joints to ensure that the stiffnesses were approximately the same and that the load distribution measurements (performed during LC tests) would not be affected by stiffness variation between beams.

The load versus deflection responses for each individual beam under SC 4-1 through 4-4 are shown in Figure 8.56. The deflections shown at the center region accounts for the settlement of the supports of each beam. The measured stiffness in FIU-3 (51 kip/in.) was approximately 6.7 percent smaller than the average stiffness of the other three beams (54.7 kip/in.). This is due to

the difference in design between the beams, with FIU-3 having four partially-stressed top strands and FIU-6, FIU-7, and FIU-8 having four fully-stressed top strands.

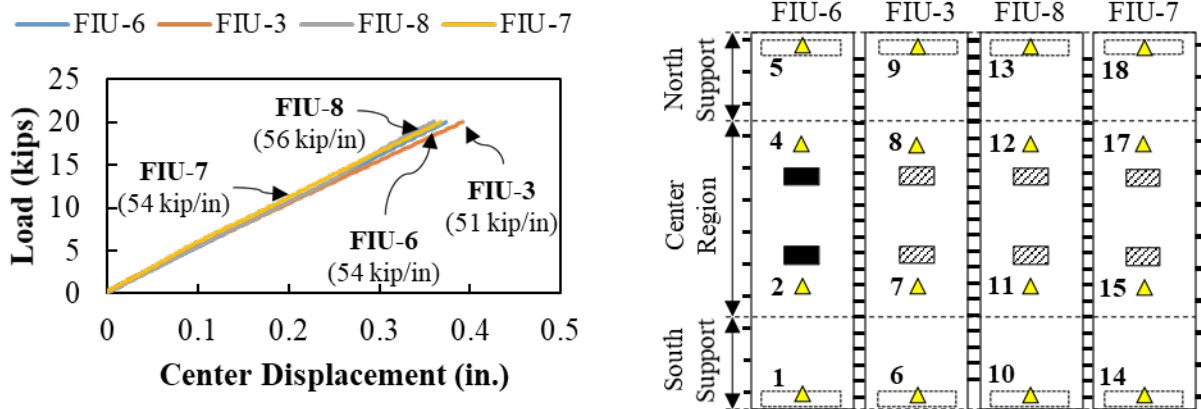


Figure 8.56: Load versus displacement curves for load testing with Stiffness Configuration 4-1 through 4-4 (before joint cast)

The average deflection was measured to be approximately 0.37 in. with no single measurement varying from the average by more than five percent. The specimen with the largest deflection was FIU-3 (0.39 in.) and the one with the lowest deflection was FIU-8 (0.36 in.).

8.7.2.2. Longitudinal Behavior

The load versus bottom concrete longitudinal strain for the system under SC 4-1 through 4-4 is shown in Figure 8.57 for the center region.

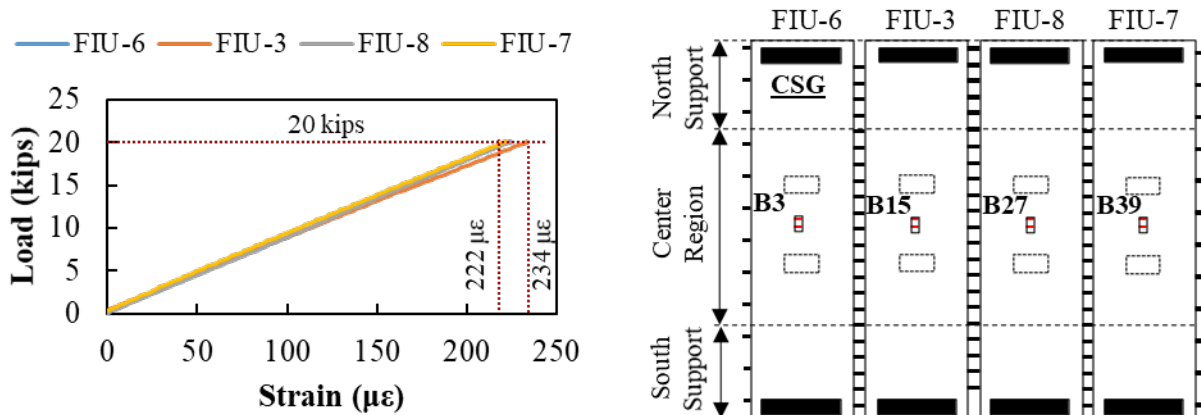


Figure 8.57: Load versus longitudinal concrete strain load testing with Stiffness Configuration 4-1 through 4-4 (before joint cast)

The average bottom longitudinal strain was measured to be approximately 227 $\mu\epsilon$ with no single measurement varying from the average by more than four percent. The specimen with the largest bottom longitudinal strain was FIU-3 (234 $\mu\epsilon$), and the specimen with the lowest bottom longitudinal strain was FIU-7 (222 $\mu\epsilon$).

8.7.3. Camber Leveling Results (Stages 1.5 – 1.6)

8.7.3.1. Application of Surcharge Load (Stage 1.5)

After measuring the individual girder stiffnesses and before joint construction, a surcharge load was applied to FIU-3 to level the additional camber with the adjacent beams. The surcharge load installation consisted of the application of 10 load blocks near midspan of FIU-3 with each block having an average weight of 1.95 kips. The applied load from the load blocks versus time response for FIU-3 is shown in Figure 8.58.

The load blocks were positioned with five just to the north and five just to the south of midspan of FIU-3. The blocks were not placed directly at midspan to allow for the installation of instrumentation (CSG and CDT) after the application of the surcharge load. Load blocks were placed one at a time alternating placement to the north and south of midspan to keep the load balanced on FIU-3; the order of load block placement is shown in Figure 8.58. The placement of the blocks resulted in a total surcharge load of 19.25 kips and took approximately 46 minutes.

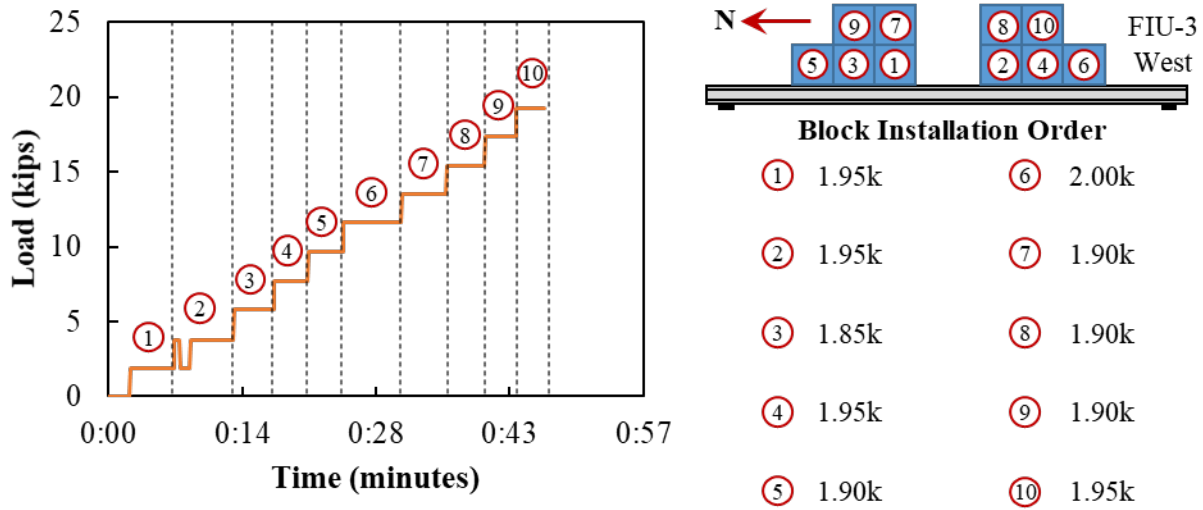


Figure 8.58: Load blocks installation (weight in kips) versus time before joint construction on FIU-3

Deflections were measured along the length of FIU-3 during the surcharge load application procedure, shown in Figure 8.59. The application of the surcharge load resulted in approximately 0.4 inches of deflection in the midspan region, which is the average of LDT-7 and LDT-8 shown in Figure 8.59. This led to an average 0.25-inch difference between the top of FIU-3 and the two adjacent beams, FIU-6 and FIU-8.

The longitudinal strain on the bottom of FIU-3 was measured during the application of the surcharge load, shown in Figure 8.60. A tensile strain of 213 $\mu\epsilon$ was measured using CSG-B15. This longitudinal CSG was installed after strains due to prestressing and time effects occurred.

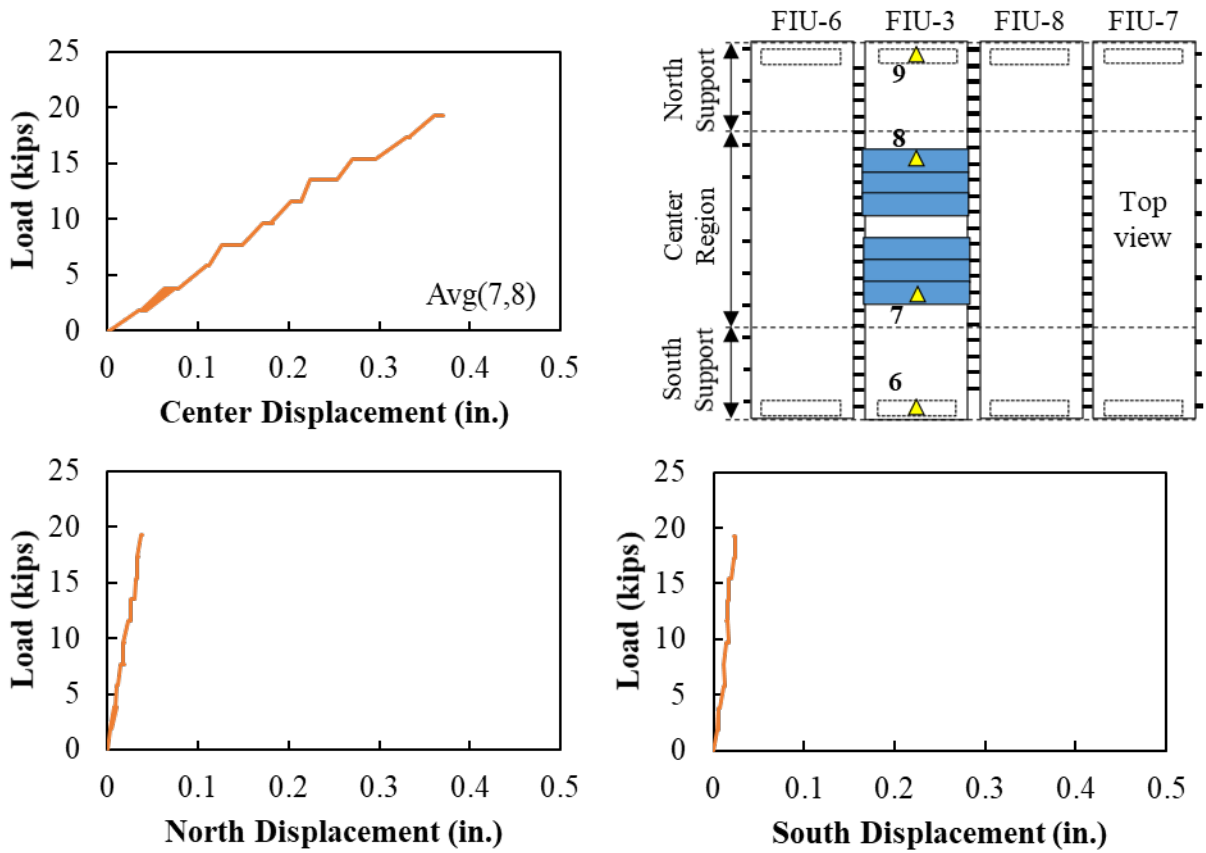


Figure 8.59: Load versus absolute center, north, and south displacements load testing with Camber Leveling (before joint cast) on FIU-3

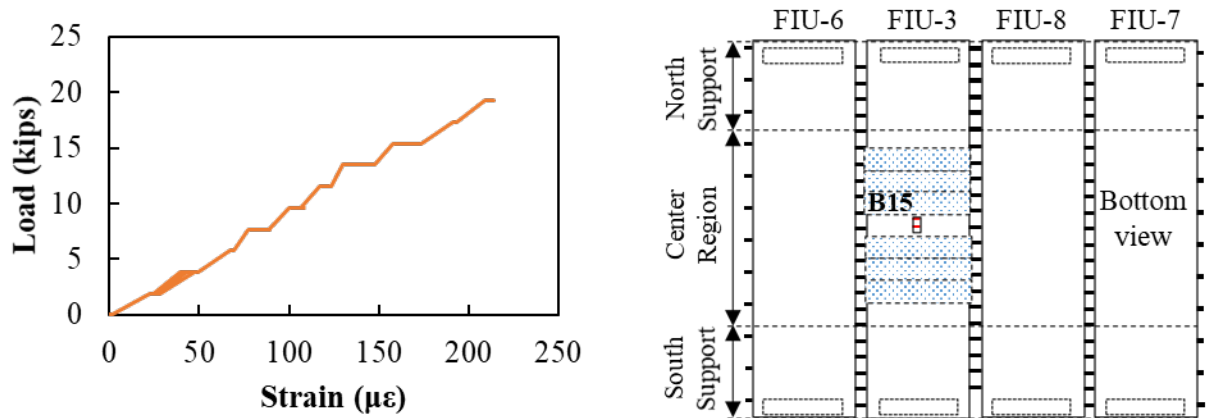


Figure 8.60: Load versus longitudinal concrete strain load testing with Camber Leveling 4-2 (before joint cast) on FIU-3

8.7.3.2. Moment-Curvature Response and Estimation of Precompression Strains

The moment-curvature response was found for FIU-3 with partially stressed top strands and for FIU-6/7/8 with fully stressed top strands using a layered-section analysis software (RESPONSE2000) and the measured concrete strength.

The moment curvature response was determined using a locked-in strain differential without considering any prestress losses ($\Delta\varepsilon_p$) and considering long-term prestress losses ($\Delta\varepsilon_{pLT}$). Long-term losses were calculated using the AASHTO LRFD Bridge Design Specification [82] Refined Estimates of Time-Dependent Losses (§5.9.3.4). Time effects were not considered otherwise in the analysis.

The locked-in strain differential ($\Delta\varepsilon_p$) is defined per layer, so the losses were determined for each layer of prestressing strands. The shrinkage and relaxation losses were assumed to be constant across the depth of the section. The creep losses were calculated for each layer of strands based on a different concrete stress from prestressing (f_{cgp}) at the height of each strand layer. Only long-term losses were removed from the initial jacking stress since elastic shortening is implicitly considered by the analysis software.

A summary of the losses calculated per layer and the final locked in strain considering the long-term losses ($\Delta\varepsilon_{pLT}$) is shown in Table 8.15 through Table 8.18.

Table 8.15: Prestress loss estimates per layer for FIU-3 (1 of 2)

Row	h (in.)	n _{strands}	f _{pj} [ksi]	e _p [in]	f _{cgp} [ksi]	Δf _{pES} [ksi]	Δf _{pSR} [ksi]	Δf _{pCR} [ksi]	Δf _{pR1} [ksi]
1	3.0	12	202.5	2.9	1.856	10.85	8.35	8.43	1.54
2	5.0	2	202.5	0.9	1.567	9.16	8.35	7.12	1.54
3	9.0	4	50.0	-3.1	0.988	5.78	8.35	4.49	1.54

Table 8.16: Prestress loss estimates per layer for FIU-3 (2 of 2)

Row	Δf _{pSD} [ksi]	P _Δ [kips]	Δf _{cd} [ksi]	Δf _{pCD} [ksi]	Δf _{pSS} [ksi]	Δf _{pR2} [ksi]	Δf _{pLT} [ksi]	f _{pj} - Δf _{pLT} [ksi]	Δε _{p,LT}
1	1.78	-71.6	-0.208	1.25	0.00	1.54	22.90	179.6	0.00630
2	1.78	-66.5	-0.148	1.14	0.00	1.54	21.48	181.0	0.00635
3	1.78	-56.2	-0.048	0.85	0.00	1.54	18.57	31.4	0.00110

Table 8.17: Prestress loss estimates per layer for FIU-6, FIU-7, and FIU-8 (1 of 2)

Row	h (in.)	n _{strands}	f _{pj} [ksi]	e _p [in]	f _{cgp} [ksi]	Δf _{pES} [ksi]	Δf _{pSR} [ksi]	Δf _{pCR} [ksi]	Δf _{pR1} [ksi]
1	3.0	12	202.5	2.9	1.582	8.24	6.70	4.58	1.63
2	5.0	2	202.5	0.9	1.494	7.78	6.70	4.33	1.63
3	9.0	4	202.5	-3.1	1.318	6.87	6.70	3.82	1.63

Table 8.18: Prestress loss estimates per layer for FIU-6, FIU-7, and FIU-8 (2 of 2)

Row	Δf_{pSD} [ksi]	P_{Δ} [kips]	Δf_{cd} [ksi]	Δf_{pCD} [ksi]	Δf_{pSS} [ksi]	Δf_{pR2} [ksi]	Δf_{pLT} [ksi]	$f_{pj} - \Delta f_{pLT}$ [ksi]	$\Delta \epsilon_{p,LT}$
1	1.15	-50.4	-0.127	0.58	0.00	1.63	16.27	186.2	0.00653
2	1.15	-49.4	-0.104	0.59	0.00	1.63	16.02	186.5	0.00654
3	1.15	-47.4	-0.061	0.59	0.00	1.63	15.51	187.0	0.00656

The moment-curvature responses for both sections with and without long-term losses are shown in Figure 8.61. The stress in the top strands did not have a significant effect on the maximum moment but did influence the curvature at zero moment and ultimate curvature. The moment-curvature response was not significantly influenced by the inclusion or omission of the long-term losses from the locked-in strain calculation.

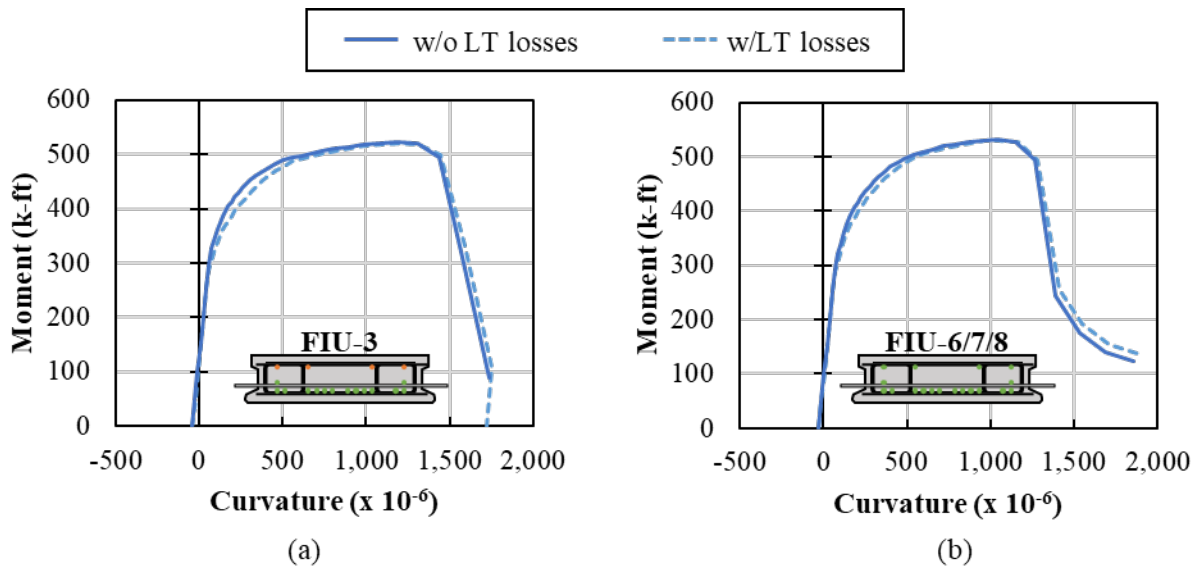


Figure 8.61: Moment-curvature responses with and without long-term prestress losses for (a) FIU-3 and (b) FIU-6/7/8

The strain profile was found for each point on the curve for both sections. The strain profile for the two different sections under zero applied moment with and without long-term prestress losses is shown in Figure 8.62. The strains were not significantly influenced by the inclusion or omission of long-term prestress losses from the locked-in strain differential.

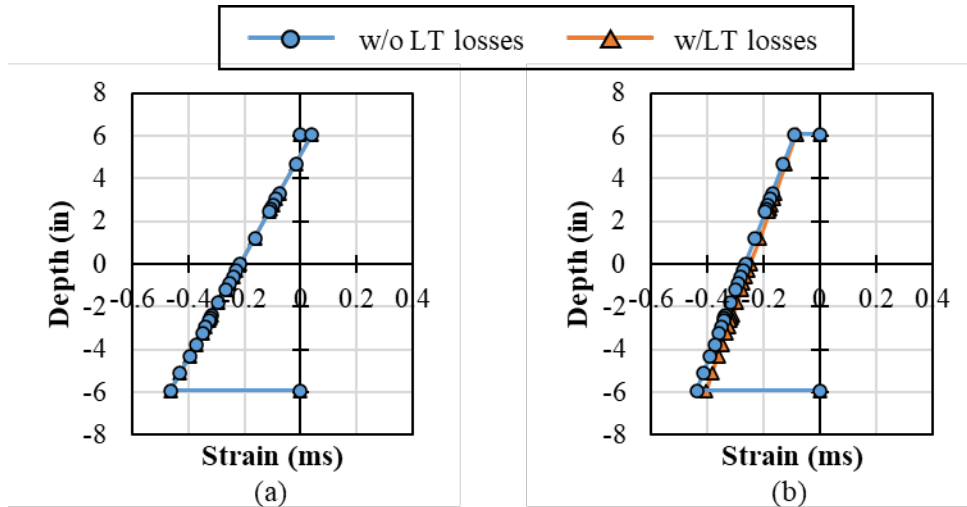


Figure 8.62: Estimated strain profile without prestress losses at $M = 0$ kip-ft. for (a) FIU-3 and (b) FIU-6/7/8 from RESPONSE2000

The strain profile will change with the addition of the surcharge load on the beam. The estimated strain profile with the approximate moment from the surcharge load ($M = 110$ k-ft) is shown in Figure 8.63 (b). The concrete strain gauge (CSG) on the bottom of FIU-3 at midspan (CSG-B15) was installed after release, but before the application of the surcharge load. Therefore, the reading in CSG-B15 would be the difference between the release strain and strain caused by the surcharge moment, shown in Figure 8.63 (c).

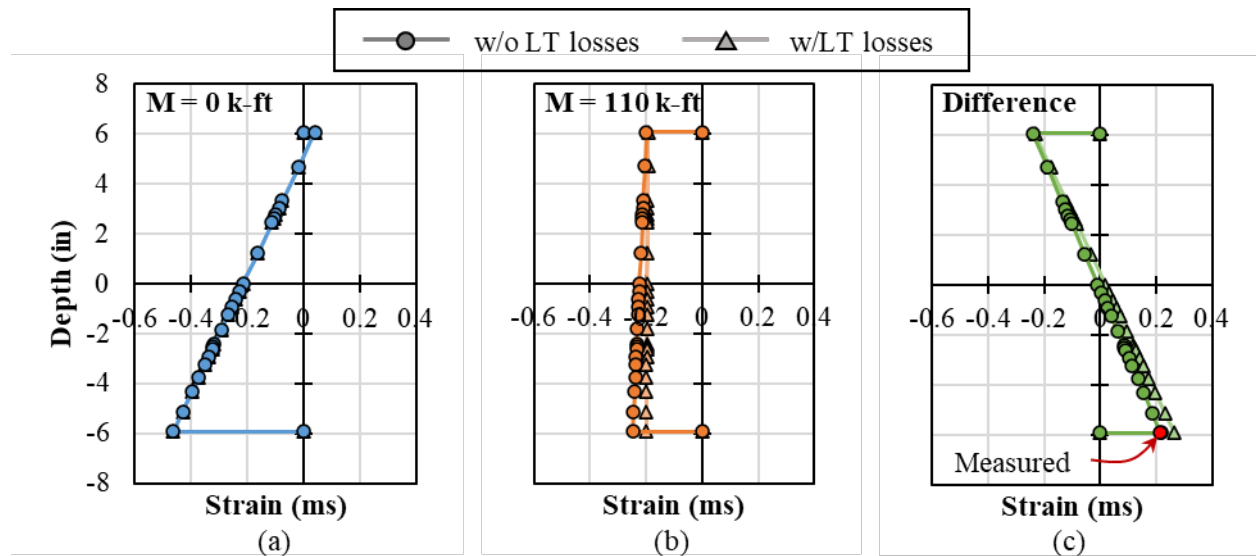


Figure 8.63: Estimated strain profile for FIU-3 from RESPONSE2000 with and without long-term prestress losses for (a) release, (b) moment caused by surcharge load, and (c) difference between release and surcharge load state of strain

While the analysis performed in RESPONSE2000 only approximates the behavior in FIU-3 and FIU-6, FIU-7, and FIU-8, the analysis highlights that there is a precompression in the bottom fiber that must be overcome before cracking occurs. The tension measured in the bottom fiber by

CSG-B15 during the surcharge load application is less than the precompression strains from the prestressing. This simplified analysis did not consider time effects, other than prestress losses in the calculation of the locked-in strain differential.

8.7.3.3. Removal of Surcharge Load (Stage 1.6)

As described in §8.3, the UHPC joints were cast and allowed to harden, and all the instrumentation was installed while the surcharge load remained on FIU-3. After the UHPC hardened and all instrumentation was installed, the surcharge load was removed, shown in Figure 8.64. The 10 load blocks (about 2 kips each) were removed about every 3 minutes during Stage 1.6. The load blocks were removed from alternating sides to help distribute the load along the length of the beam during load removal, i.e., one block was removed from the north side of the beam and then one from the south side of the beam. The removal of all 10 load blocks took approximately 30 minutes.

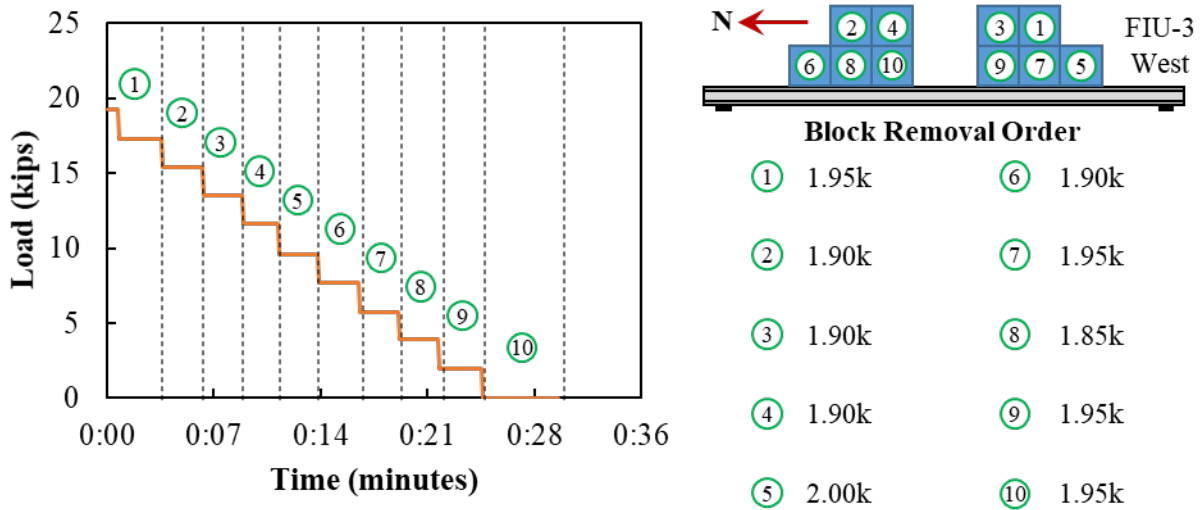


Figure 8.64: Load blocks removal (weight in kips) versus time after joint construction on FIU-3

The load versus average deflections for each beam during the removal of the surcharge load is shown in Figure 8.65. The deflection shown is based on the procedure described above where the average of the end LDTs is subtracted from the average of the midspan LDTs for each beam. The initial deflection in FIU-3 from the surcharge load is included in Figure 8.65. The deflection shown does not include the camber and self-weight deflections for the beams. The deflection of the beams immediately adjacent to FIU-3 were slightly larger than those in FIU-7; showing that the beams adjacent to the beam with differential camber restrain the beam more than other beams.

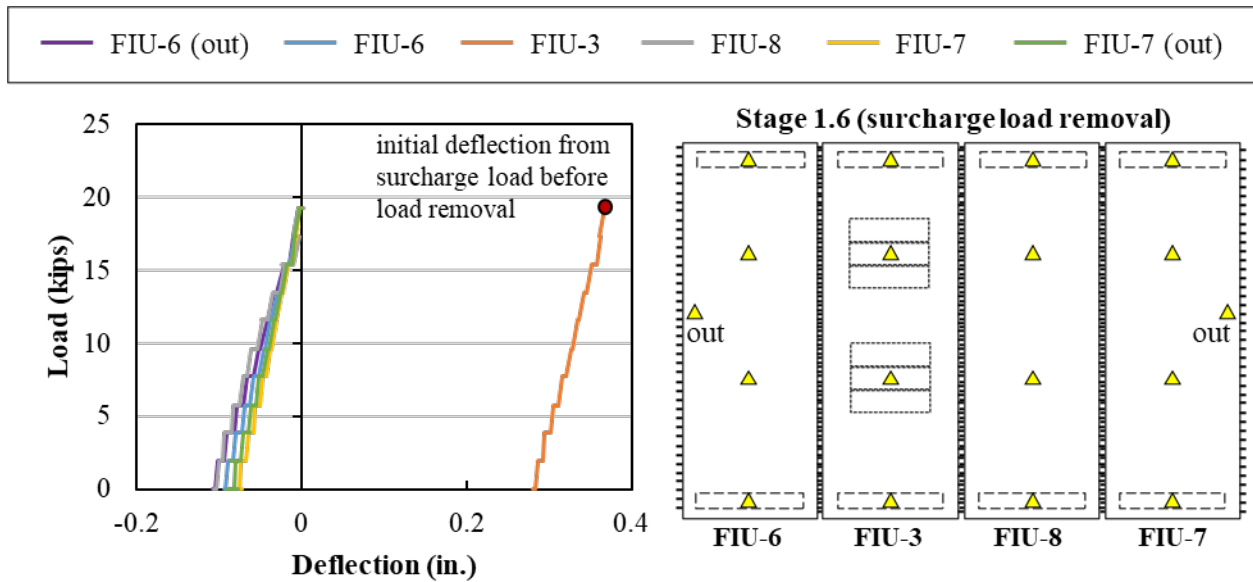


Figure 8.65: Load versus average midspan deflection of each beam during removal of surcharge load (Stage 1.6)

The load versus longitudinal strains during the removal of the surcharge load are shown in Figure 8.66. The estimated initial strain in the section before the removal of the surcharge load is highlighted at 20 kips. Additional tensile stresses occur in the top of the beam and additional compression stresses occur in the bottom of the beam as the surcharge load is removed. The estimated strain in the bottom fiber after the removal of the surcharge load is shown at 0 kips in Figure 8.66. These would be the estimated longitudinal strains locked into the system after prestressing and the removal of the surcharge load. For simplicity, these strains do not consider shrinkage and creep strains that will occur. These shrinkage and creep strains will decrease the effectiveness of the prestressing but will not otherwise influence the concrete stress.

There is a slightly lower compression strain in the top and slightly higher compression strain in the bottom of FIU-6, which shows that FIU-6 is providing slightly more restraint of FIU-3 than the other beams; this is consistent with the deflection measurements. However, the difference is small (about 3 percent), so there is good distribution of the stresses across all three of the restraining beams.

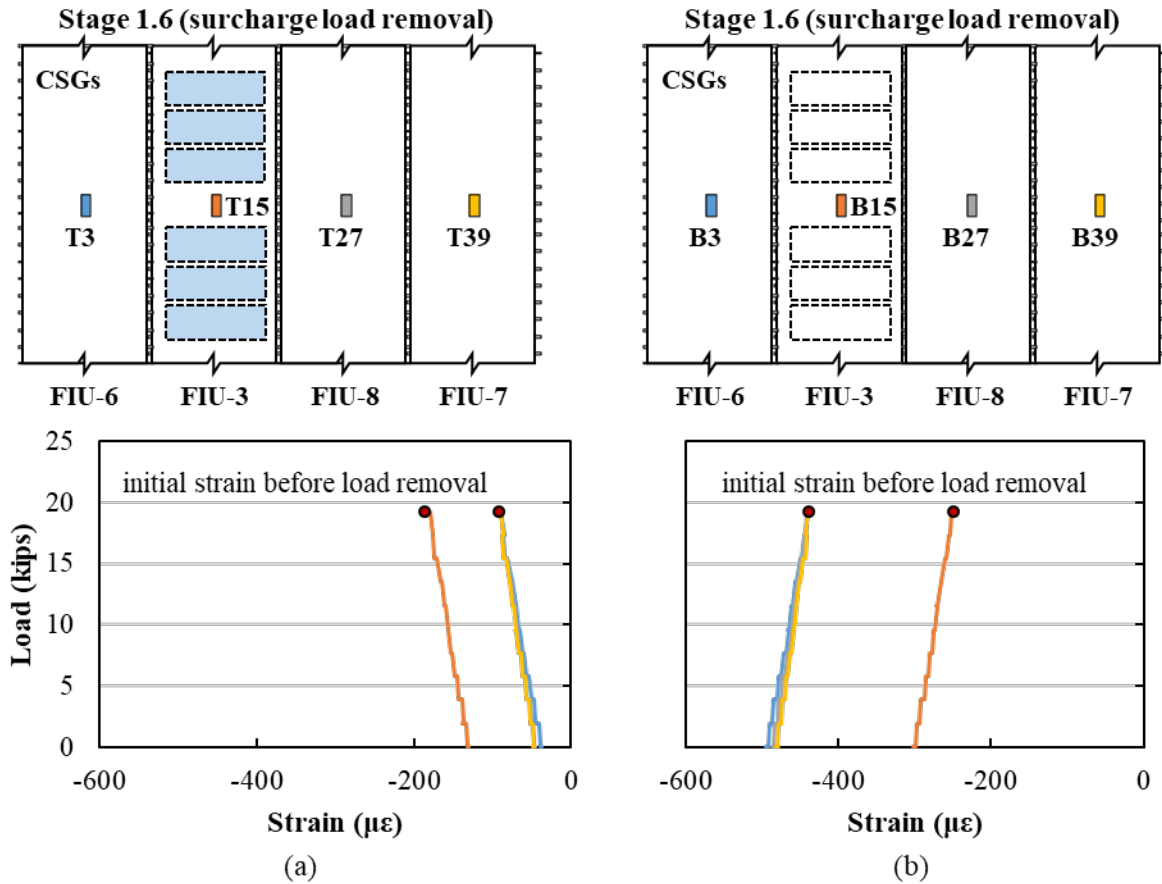


Figure 8.66: Load versus longitudinal strain during surcharge load removal for (a) top CSGs and (b) bottom CSGs, including estimated initial precompression strains

8.7.3.4. Transverse Strains from Removal of Surcharge Load (Stage 1.6)

The transverse strains caused by the removal of the surcharge load are discussed in this section. The maximum transverse strains in the system occurred at midspan, so only the midspan strains are shown. The load versus transverse strain on the top of the system at midspan measured using CSGs and across the joints measured using CDTs are shown in Figure 8.67 and Figure 8.68, respectively. Small transverse tensile strains develop in the top of FIU-3 and across Joint 3-8 as the surcharge load was removed. Small transverse compression strains developed on the top of the other beams and across Joint 6-3 and Joint 8-7.

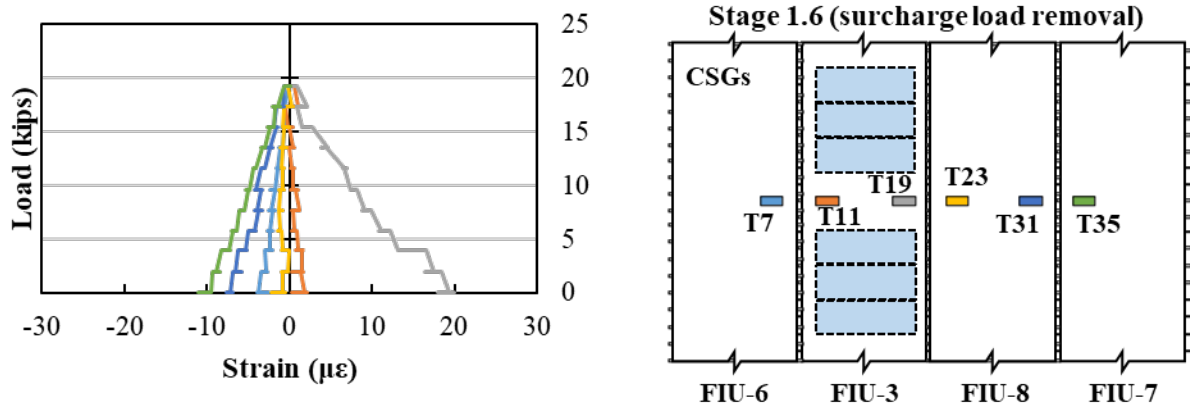


Figure 8.67: Load versus transverse strain on top of system at midspan measured using CSGs during removal of surcharge load (Stage 1.6)

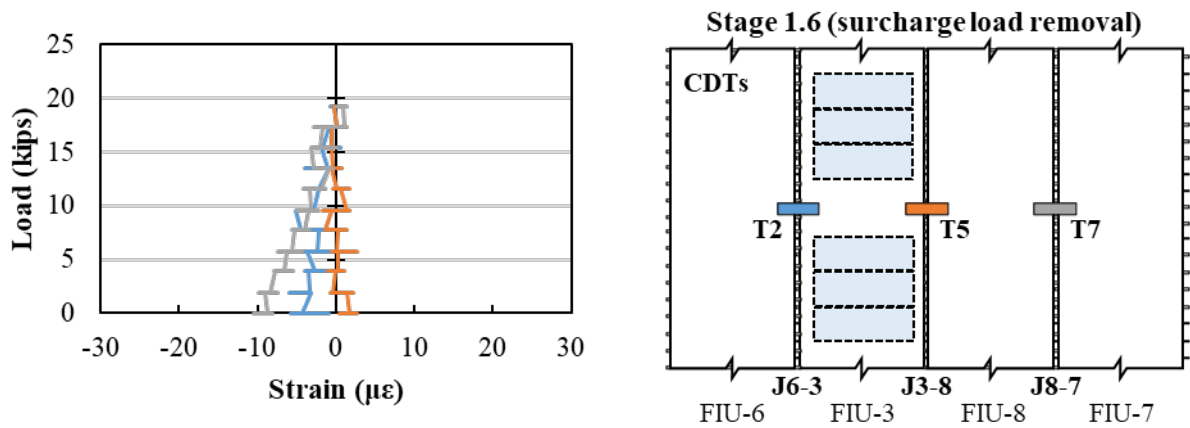


Figure 8.68: Load versus average strain across joint on top of system at midspan measured using CDTs during removal of surcharge load (Stage 1.6)

The load versus transverse strain on the bottom of the system at midspan measured using CSGs is shown in Figure 8.69. The transverse bottom strains are also minor with small compressive strains in FIU-3 and the west side of FIU-8 and small tensile strains in the remainder of the beams.

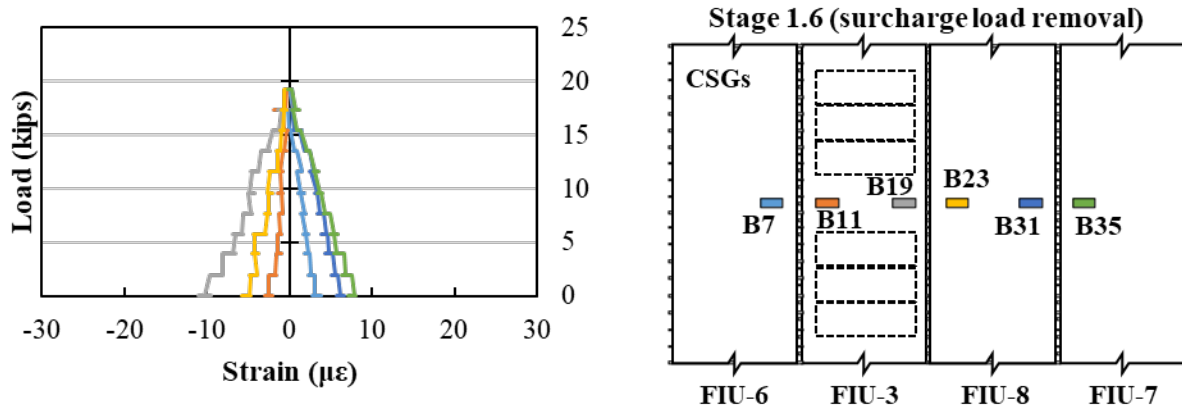


Figure 8.69: Load versus transverse strain on bottom of system at midspan measured using CSGs during removal of surcharge load (Stage 1.6)

Only minor transverse strains developed in the section, suggesting that the camber leveling procedure only had a minor effect on the performance of the joints in the system.

8.8. FOUR-BEAM FATIGUE AND SERVICE TESTING RESULTS

8.8.1. Testing Summary

A summary of the nine different testing stages (stages 2 through 9) performed on the four-beam test setup with FIU-6, FIU-3, FIU-8, and FIU-7 is shown in Figure 8.70 and earlier in Table 8.2.

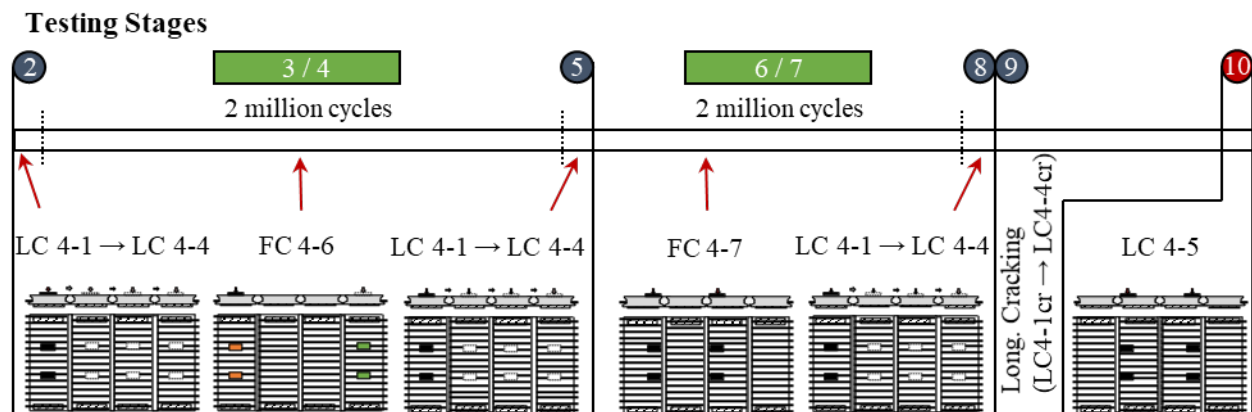


Figure 8.70: Summary of testing stages performed on four-beam setup with FIU-6/3/8/7

The results from all testing on the four-beam system are presented in this section organized into the following sections:

1. Service Test Results: LC 4-1 through LC 4-4 (Stages 2, 5, and 8)
2. Fatigue Test Results: FC 4-6 and FC 4-7 (Stages 3-4, and Stages 6-7)
3. Cracked Service Test Results: LC 4-1cr through LC 4-4cr (Stages 8-9)

The measured material properties for the precast concrete are shown in Table 7.11.

Table 8.19: Measured compression strength for precast concrete, *age at time of test

FIU-3		FIU-6		FIU-7 and FIU-8	
Age (days)	Strength (ksi)	Age (days)	Strength (ksi)	Age (days)	Strength (ksi)
558	11.4	565	12.0	565	11.4
639*	12.2	646*	13.3	646*	12.6

The measured material properties for the UHPC joints are shown in Table 8.20.

Table 8.20: Measured compression strength for UHPC joints, *age at time of test

FIU 6-3		FIU 3-8		FIU 8-7	
Age (days)	Strength (ksi)	Age (days)	Strength (ksi)	Age (days)	Strength (ksi)
28	23.2	28	24.1	28	22.3
109*	24.1	109*	23.3	109*	20.9

The modulus of rupture (f_r) was also measured for the UHPC joints. The average modulus of rupture of the UHPC joints were 2.92 ksi at 31 days for FIU 6-3, 3.23 ksi at 30 days for FIU 3-8, and 3.10 ksi at 32 days for FIU 8-7.

8.8.2. Girder Distribution Factors

Girder distribution factors (GDF) were found for three or four different load configurations (LC) during Stages 2, 5, 8, and 9. GDF can be found based on the longitudinal strain measured on the bottom of each beam at midspan using Equation 8-4 [83]–[92].

$$GDF_i = \frac{\varepsilon_i}{\sum \varepsilon_i} \quad \text{Equation 8-4}$$

The longitudinal strain in each beam was measured using concrete surface gauges (CSGs) B3, B15, B27, and B39, which were at midspan of FIU-6, FIU-3, FIU-8, and FIU-7, respectively. A summary of the measured longitudinal strains on the bottom of the system for Stage 2 loading is shown in Figure 8.71. The strains at the maximum service load (30 kips) were used to find the distribution factors.

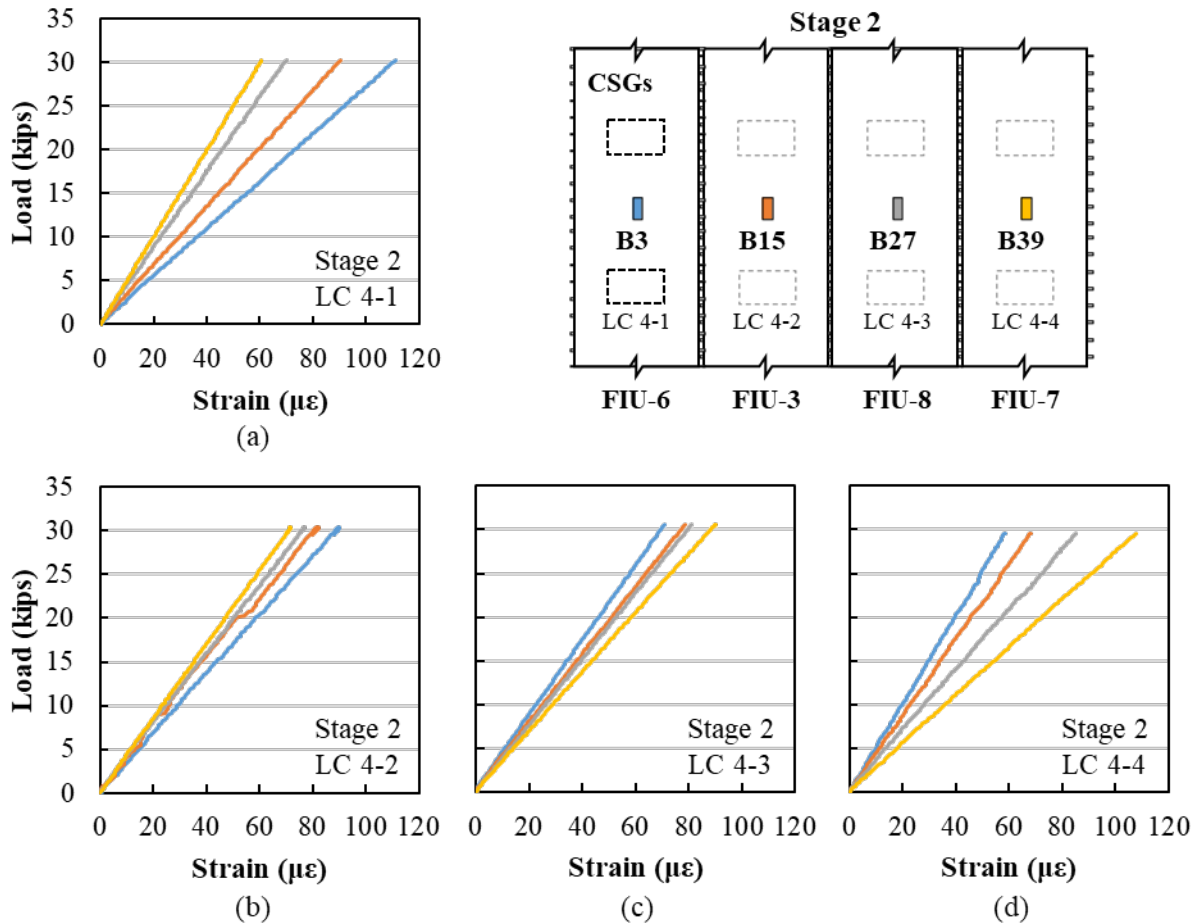


Figure 8.71: Load versus longitudinal strain measured using CSGs on bottom of system at midspan for Stage 2 and (a) LC 4-1, (b) LC 4-2, (c) LC 4-3, and (d) LC 4-4

Several of the longitudinal strain gauges at the midspan of the system (CSG-B15, T3, and T27) malfunctioned during several of the service load tests during Stages 5, 8, and 9 of testing. While the bottom longitudinal CSGs are typically used to find GDF, the top longitudinal CSGs and midspan deflection can also be used to estimate GDF. A comparison between the GDF found using all three measurements is provided in Table 8.21 and Table 8.22.

Table 8.21: Distribution factor comparison between top and bottom CSGs for Stage 2 loading

LC	FIU-6			FIU-3			FIU-8			FIU-7		
	Bot.	Top	% Diff	Bot.	Top	% Diff	Bot.	Top	% Diff	Bot.	Top	% Diff
LC 4-1	0.335	0.335	0.3%	0.272	0.277	1.9%	0.211	0.206	2.2%	0.183	0.181	0.8%
LC 4-2	0.282	0.275	2.6%	0.256	0.264	3.1%	0.239	0.241	0.9%	0.224	0.221	1.4%
LC 4-3	0.222	0.219	1.2%	0.245	0.249	1.4%	0.252	0.254	0.5%	0.281	0.278	0.8%
LC 4-4	0.183	0.182	0.7%	0.213	0.217	1.6%	0.267	0.264	1.0%	0.337	0.338	0.1%
	Average =		1.2%	Average =		2.0%	Average =		1.2%	Average =		0.8%

Overall, there is close agreement between distribution factors found with bottom and top CSGs, with an average difference of 1.3 percent. This close agreement observed during Stage 2 gives confidence to the GDF being determined using the top CSGs when one of the bottom CSGs malfunctioned. There were also some loading stages where there were malfunctioning longitudinal CSGs on the top and bottom of the system.

A comparison between GDF found using the bottom CSGs and beam deflection, found using the procedure described in §8.7, is shown in Table 8.22.

Table 8.22: Distribution factor comparison between bottom CSGs and beam deflection for Stage 2 loading

LC	FIU-6			FIU-3			FIU-8			FIU-7		
	Bot.	Δ	% Diff	Bot.	Δ	% Diff	Bot.	Δ	% Diff	Bot.	Δ	% Diff
LC 4-1	0.335	0.309	7.6%	0.272	0.273	0.2%	0.211	0.236	10.9%	0.183	0.182	0.4%
LC 4-2	0.282	0.271	3.7%	0.256	0.259	1.5%	0.239	0.249	4.1%	0.224	0.220	1.6%
LC 4-3	0.222	0.232	4.5%	0.245	0.244	0.5%	0.252	0.253	0.1%	0.281	0.271	3.4%
LC 4-4	0.183	0.189	3.1%	0.213	0.208	2.6%	0.267	0.283	5.8%	0.337	0.321	4.9%
	Average =		4.7%	Average =		1.2%	Average =		5.2%	Average =		2.6%

There is still generally good agreement between GDF found using bottom longitudinal strain and beam deflection, with an average difference of 3.4 percent. However, the average percent difference is larger for GDF found using beam deflection compared to GDF found using top longitudinal strain, so GDF was only found using beam deflection when there were longitudinal CSGs malfunctioning on both the top and bottom of the system.

A summary of the GDF for all static responses is shown in Table 8.23. The method used to find the GDF is included for each loading ramp. The order of preference for the GDF method was bottom longitudinal CSGs (CSG-B), top longitudinal CSGs (CSG-T), and beam deflection (Δ).

Distribution to exterior girders is higher than distribution to interior girders, even when the interior girders are loaded.

Table 8.23: Summary of GDF_i for all static tests, *loaded beam

Loading Scheme		GDF Method	Girder Distribution Factor			
Stage	Load Configuration		FIU-6	FIU-3	FIU-8	FIU-7
2	LC 4-1	CSG-B	0.335*	0.272	0.211	0.183
	LC 4-2	CSG-B	0.282	0.256*	0.239	0.224
	LC 4-3	CSG-B	0.222	0.245	0.252*	0.281
	LC 4-4	CSG-B	0.183	0.213	0.267	0.337*
3-4	FC 4-6	HS20 Truck Load – 2,000,000 cycles				
5 ^a	LC 4-1	CSG-B	0.335*	0.270	0.212	0.183
	LC 4-3	CSG-T	0.221	0.251	0.251*	0.277
	LC 4-4	CSG-B	0.183	0.216	0.268	0.332*
6-7	FC 4-7	HS20 Truck Load – 2,000,000 cycles				
8	LC 4-1	Δ	0.315*	0.269	0.223	0.193
	LC 4-2	CSG-T	0.282	0.265*	0.229	0.224
	LC 4-3	Δ	0.223	0.240	0.266*	0.271
	LC 4-4	CSG-T	0.178	0.217	0.267	0.337*
9	LC 4-1cr	Δ	0.321*	0.271	0.217	0.190
	LC 4-2cr	Δ	0.273	0.259*	0.239	0.229
	LC 4-3cr	Δ	0.228	0.241	0.262*	0.270
	LC 4-4cr	Δ	0.191	0.221	0.264	0.324*

^aLC 4-2 was not performed during Stage 5.

The maximum distribution for the interior and exterior girders are shown in Table 8.24.

Table 8.24: Exterior and interior girder distribution factors

Method	Exterior GDF	Interior GDF
Maximum Measured	0.337	0.272
AASHTO LRFD	0.383	0.336

GDF were found using the AASHTO LRFD Bridge Design Specification [82] for a typical two-lane superstructure. GDF for interior beams ($g_{interior}$) were also calculated using Equation 8-5 through Equation 8-7 based on AASHTO LRFD BDS Table 4.6.2.2.2b-1 [82] for cross-section type f/g (per Table 4.6.2.2.1-1), and the provisions made by FDOT in the Structural Design Guidelines [38] for slab beam bridges §2.9.A.1.

$$\text{Stiffness Parameter} \quad k = 2.5(N_b)^{-0.2} \geq 1.5 \quad \text{Equation 8-5}$$

$$\text{One Design Lane Loaded} \quad = k \left(\frac{b}{33.3L} \right)^{0.5} \left(\frac{I}{J} \right)^{0.25} \quad \text{Equation 8-6}$$

$$\text{Two or More Design Lanes Loaded} \quad = k \left(\frac{b}{305} \right)^{0.6} \left(\frac{b}{12.0L} \right)^{0.2} \left(\frac{I}{J} \right)^{0.06} \quad \text{Equation 8-7}$$

where:

k = stiffness parameter

N_b = number of beams = 6 beams

L = length of span = 27.75 ft

b = beam width = 48 in.

I = beam inertia = 6,520.79 in⁴

J = polar moment of inertia = 83,256.91 in⁴

For exterior beams ($g_{exterior}$), distribution factor were calculated using Equation 8-8 through Equation 8-10 based on AASTHO LRFD BDS Table 4.6.2.2.2d-1 [82], and the provisions made by FDOT in the Structural Design guidelines [38] for slab beam bridges § 2.9.A.2.

$$\text{Eccentricity - One Design Lane Loaded} \quad = 1.125 + \frac{d_e}{30} \geq 1.0 \quad \text{Equation 8-8}$$

$$\text{Eccentricity - Two or More Design Lanes Loaded} \quad = 1.04 + \frac{d_e}{25} \geq 1.0 \quad \text{Equation 8-9}$$

$$g_{exterior} = e g_{interior} \quad \text{Equation 8-10}$$

Where:

e = eccentricity

d_e = overhang = 0.46 ft

The measured distribution factors were less than the estimated distribution factors.

The distribution factors were also used to compare the behavior of the system in the following sections.

8.8.3. Service Test Results (Stages 2, 5, and 8; LC 4-1 through LC 4-4)

8.8.3.1. Overview

There was little observable difference between the response observed during Loading Stages 2, 5, 8, and 9. The results from Loading Stage 2 are presented and discussed in this section. The

observations made between LC 4-1, LC 4-2, LC 4-3, and LC 4-4 from Loading Stage 2 are also representative of the results during the other loading stages.

The load versus deflection across the width of the four-beam system for all Stage 2 loading configurations are shown in Figure 8.72. As would be expected, loading of FIU-6 (the outermost beam to the west) during LC 4-1 led to the largest deflection of FIU-6, approximately 0.21 inches at 30 kips. A mirrored response was observed when FIU-7 was loaded, with approximately 0.2 inches at the outside of FIU-7 at 30 kips. In general, there was a mirrored displacement response between LC 4-1 and LC 4-4 and LC 4-2 and LC 4.3.

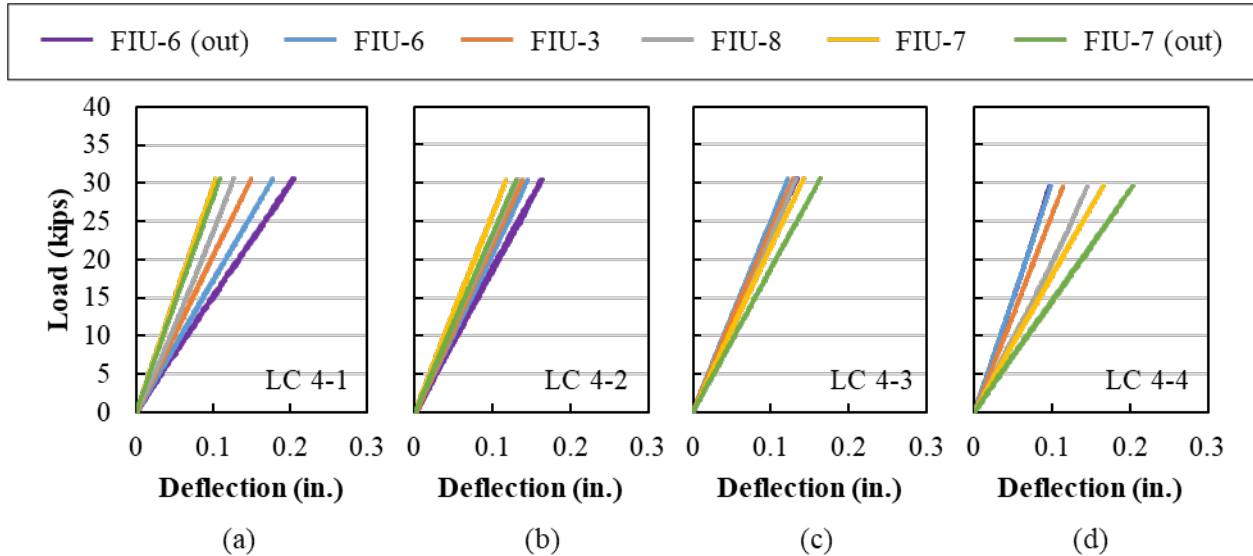


Figure 8.72: Load versus deflection during Stage 2 for (a) LC 4-1, (b) LC 4-2, (c) LC 4-3, and (d) LC 4-4

8.8.3.2. Longitudinal Behavior

The differential camber in FIU-3 did not appear to have any effect on the overall longitudinal service behavior of the four-beam system. The longitudinal response was symmetrical, when comparing LC 4-1 and LC 4-2 to LC 4-4 and LC 4-3. This symmetrical longitudinal behavior can be seen in the girder distribution factors, which are shown in Figure 8.73 and Table 8.23.

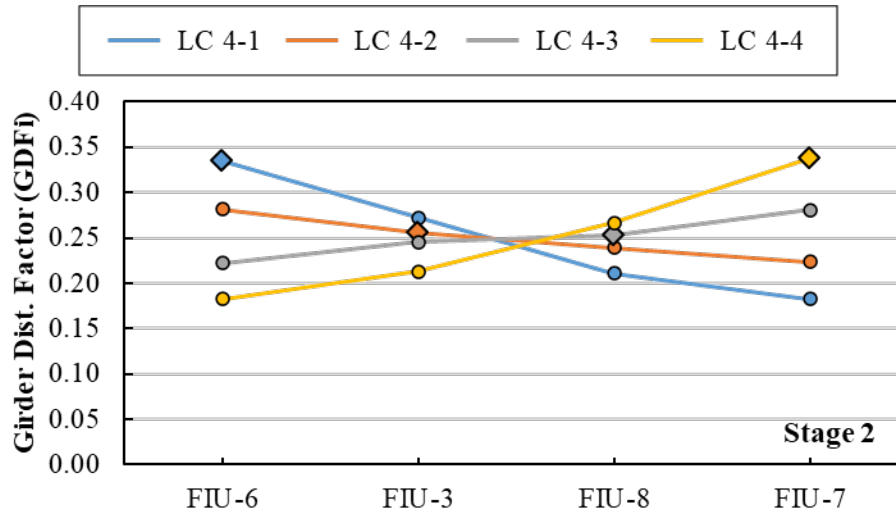
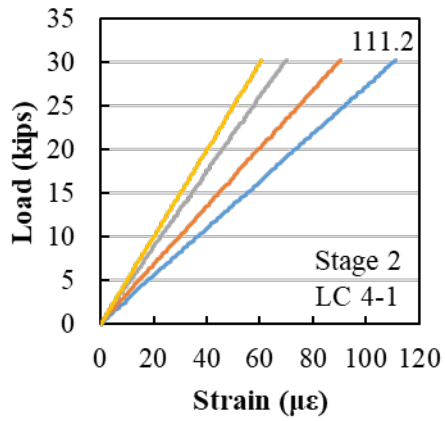
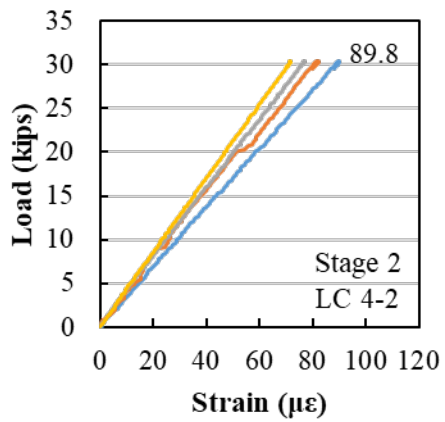
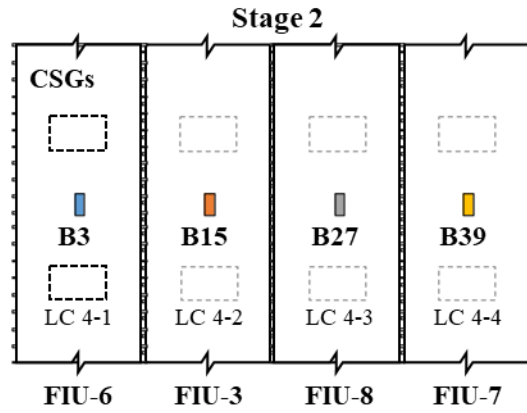


Figure 8.73: Measured girder distribution factors for Stage 2 loading

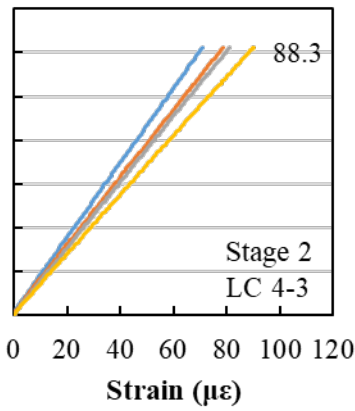
The longitudinal concrete strains on the bottom of the system at midspan of the beams are summarized in Figure 8.74 with the maximum tensile strains highlighted. The estimated strains after the camber leveling procedure and the maximum measured strains from Stage 2 testing are summarized in Table 8.25. The bottom strains in all the beams likely remained in compression throughout all the load configurations during the service load testing.



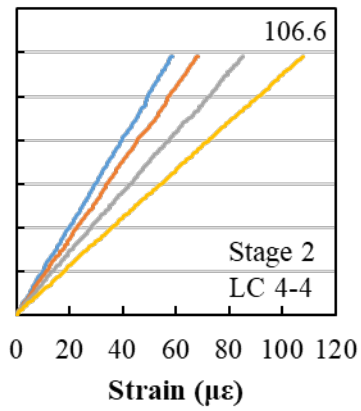
(a)



(b)



(c)



(d)

Figure 8.74: Load versus longitudinal concrete strain on bottom of system at midspan measured using CSGs for Stage 2 (a) LC 4-1, (b) LC 4-2, (c) LC 4-3, and (d) LC 4-4

Table 8.25: Measured and estimated total longitudinal strain at 30 kips for Stage 2

Beam	FIU-6	FIU-3	FIU-8	FIU-7
CSG	B3	B15	B27	B39
Estimated Initial Strain ($\mu\epsilon$)*	-494.7	-301.3	-485.9	-480.8
LC 4-1 ($\mu\epsilon$)	111.2	90.5	70.0	60.7
LC 4-1 – Estimated Total ($\mu\epsilon$)	-383.5	-210.8	-415.8	-420.1
LC 4-2 ($\mu\epsilon$)	88.0	79.9	74.7	69.9
LC 4-2 – Estimated Total ($\mu\epsilon$)	-406.7	-221.4	-411.2	-410.9
LC 4-3 ($\mu\epsilon$)	71.1	78.6	80.9	89.9
LC 4-3 – Estimated Total ($\mu\epsilon$)	-423.6	-222.7	-405.0	-390.9
LC 4-4 ($\mu\epsilon$)	58.5	68.2	85.3	107.9
LC 4-4 – Estimated Total ($\mu\epsilon$)	-436.2	-233.1	-400.6	-372.9

*estimated initial strain from camber leveling procedure discussed in §8.7.3

8.8.3.3. Joints Behavior

The measured load versus transverse concrete strain responses and load versus average strain across the joints on top of the system for Stage 2 load configurations are shown in Figure 8.75 and Figure 8.76, respectively. The load configurations where load was placed on the outside beams (LC 4-1 and LC 4-4) resulted in tension across the width of the four-beam system with maximum tensile strains around 30 $\mu\epsilon$; this was the highest transverse tension measured during LC 4-1 through LC 4-4.

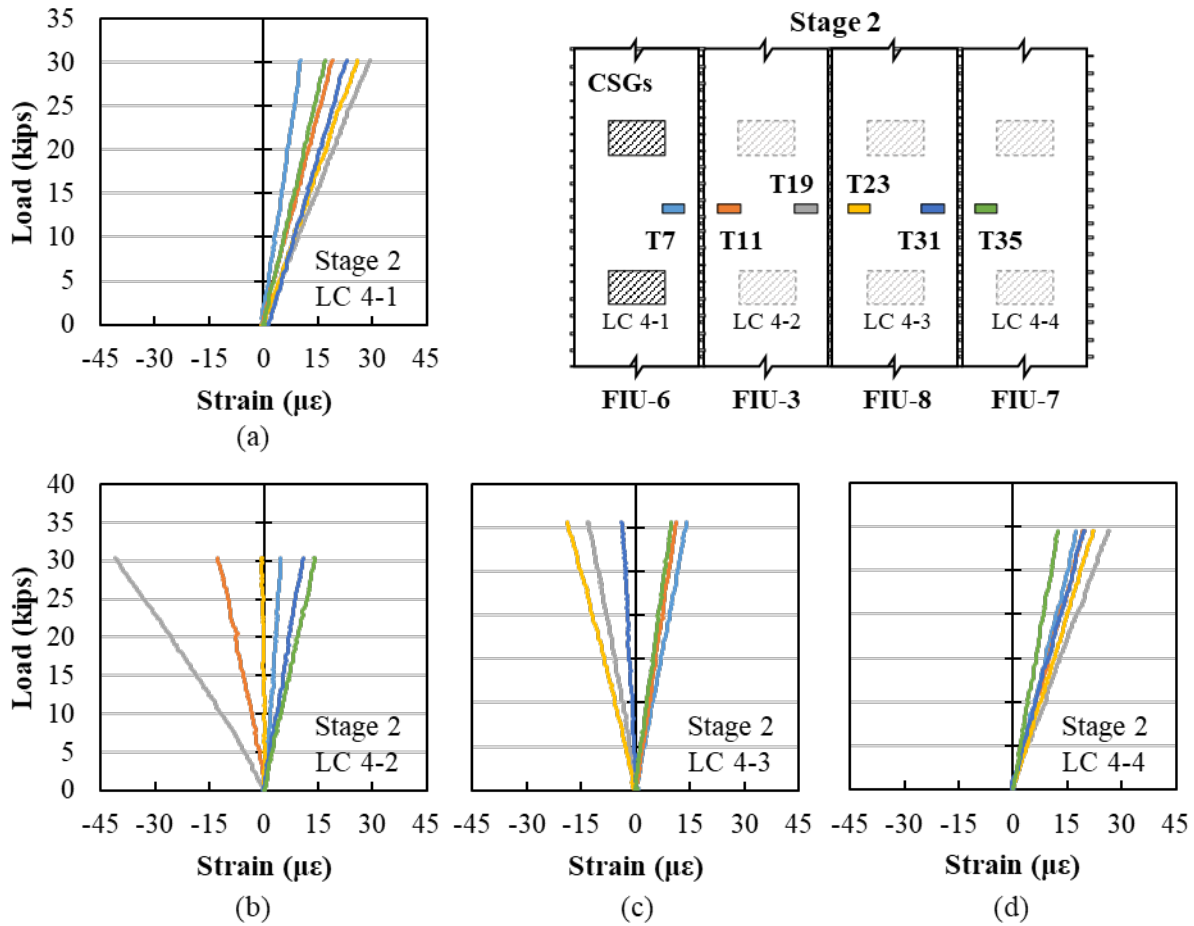


Figure 8.75: Load versus transverse concrete strain on top of system at midspan measured using CSGs for Stage 2 (a) LC 4-1, (b) LC 4-2, (c) LC 4-3, and (d) LC 4-4

Loading of the interior beams resulted in transverse compression on top of the loaded beam, e.g., T11 and T19 are in compression when FIU-3 was loaded in LC 4-2. Small transverse tensile strains developed in the top of the beams on the opposite side of the system, e.g., T31 and T35 developed tension on top when FIU-3 was loaded in LC 4-2. The transverse tension is also observed in the joint opposite the loaded beam, e.g., tension across Joint 8-7 when FIU-3 is loaded and tension across Joint 6-3 when FIU-8 is loaded.

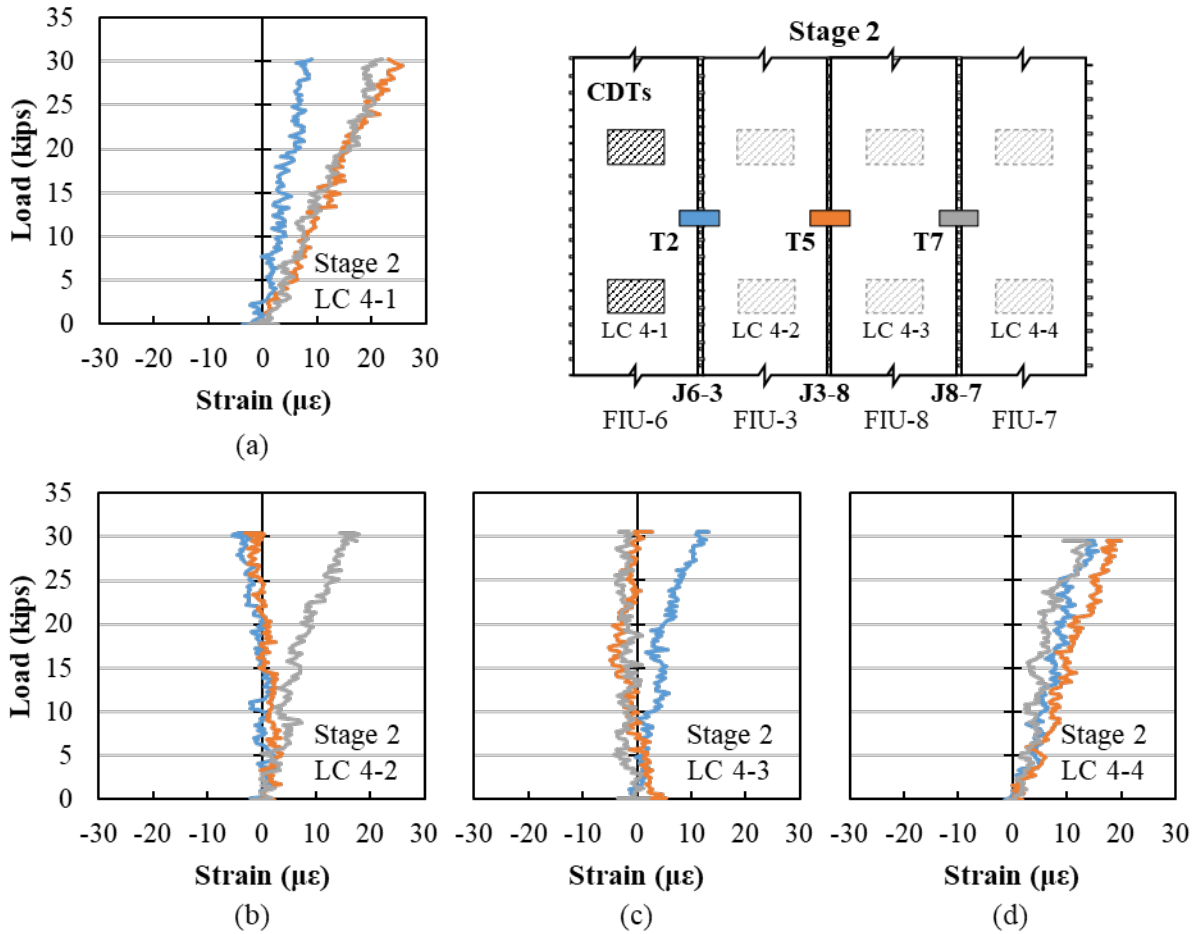


Figure 8.76: Load versus average transverse strain across top of joint at midspan measured using CDTs for Stage 2 (a) LC 4-1, (b) LC 4-2, (c) LC 4-3, and (d) LC 4-4

The measured load versus bottom transverse concrete strain responses across the width of the four-beam system for Stage 2 load configurations are shown in Figure 8.77. The measured strains generally have an opposite magnitude from the transverse concrete strains on top of the system shown in Figure 8.75. The maximum transverse tensile strains develop in CSG-B19 (12.1 $\mu\epsilon$) and CSG-B23 (18.8 $\mu\epsilon$) during loading of the interior beams FIU-3 and FIU-8.

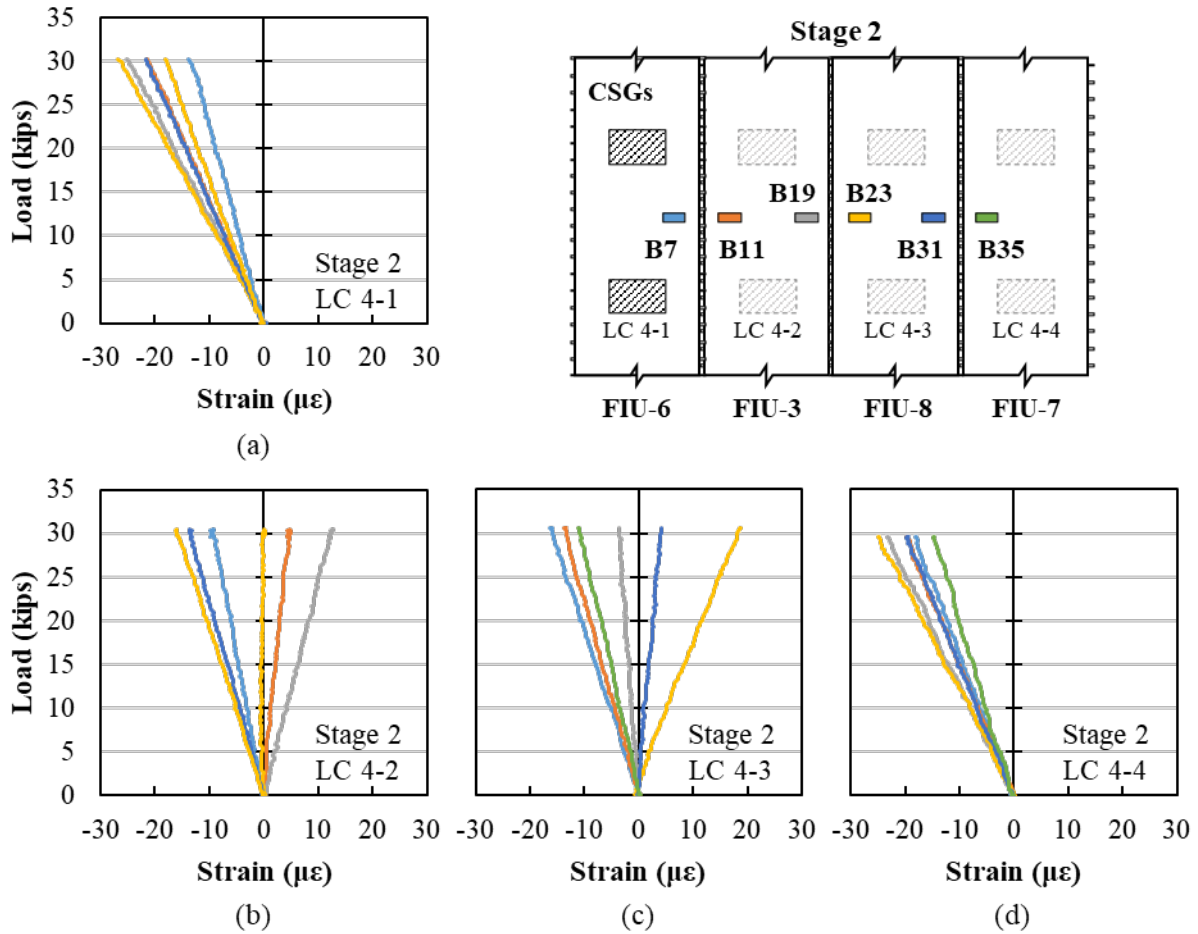


Figure 8.77: Load versus transverse concrete strain on bottom of system at midspan measured using CSGs for Stage 2 (a) LC 4-1, (b) LC 4-2, (c) LC 4-3, and (d) LC 4-4

The measured load versus top transverse concrete strain responses along the length of FIU-3 for Stage 2 load configurations are shown in Figure 8.78. The maximum strains occurred at midspan for all the load configurations; the strains measured in CSG-T11 are highest on the west side of FIU-3 and CSG-T19 highest on the east side of the beam. Small transverse tension develops along the length of FIU-3 for LC 4-1 and LC 4-4 with the highest measured tension near the supports of $18.2 \mu\epsilon$ in CSG-T9 during LC 4-1.

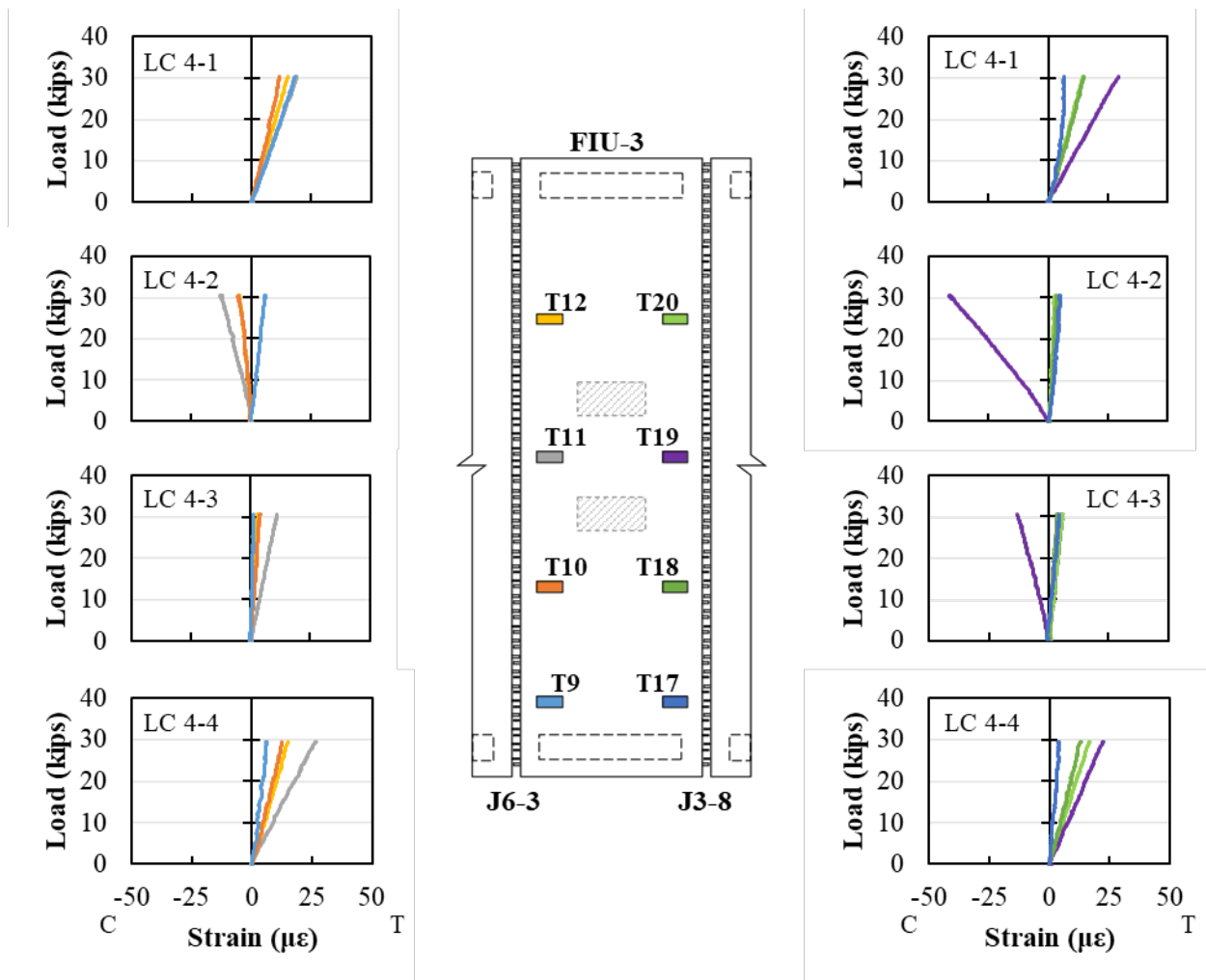


Figure 8.78: Load versus transverse concrete strain on top of system along length of FIU-3 measured using CSGs for Stage 2 LC 4-1, LC 4-2, LC 4-3, and LC 4-4

The load versus joint reinforcement strain responses for some of the joint reinforcement near midspan in Joint 6-3 and Joint 3-8 for Stage 2 LC 4-1 are shown in Figure 8.79. Minimal strains developed in the joint reinforcement during testing, with compression strains in much of the reinforcement. These results were representative of the behavior of the joint reinforcement for all service load testing.

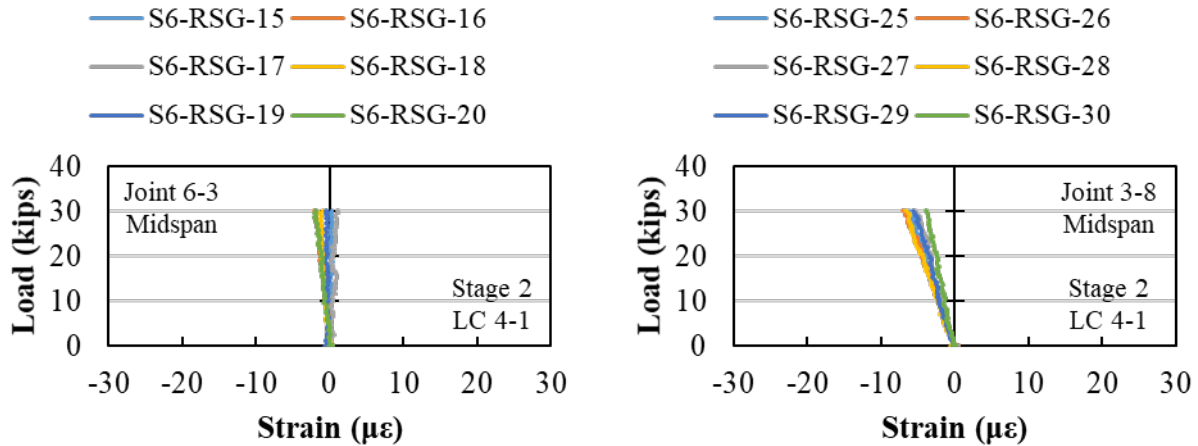


Figure 8.79: Load versus strain for joint reinforcement in Joint 6-3 and Joint 3-8 near midspan for Stage 2 LC 4-1

8.8.3.4. Summary

The following observations can be made based on LC 4-1 through LC 4-4 from Load Stages 2, 5, and 8:

- The camber leveling procedure did not influence the symmetry of the system performance. LC 4-1 and LC 4-4 and LC 4-2 and LC 4-3 had symmetrical system responses about the mid-width of the system.
- Longitudinal tensile strains in the concrete still likely remained in compression in FIU-3 during the service load testing, considering the locked in strains from the camber leveling procedure and the estimated precompression strains from the prestressing.
- All joints performed well during all static load tests. Only minor transverse tension developed in the precast sections and across the joints. The maximum transverse tensile strains were approximately $30 \mu\epsilon$ on top of the system at midspan when the exterior girders were loaded (LC 4-1 and LC 4-4).
- Joint reinforcement remained essentially unengaged during all LC 4-1 through LC 4-4 service load testing, with strains less than $10 \mu\epsilon$ in compression and tension.

Overall, service load testing LC 4-1 through LC 4-4 highlighted the robust performance of the modified FSB cross section with UHPC longitudinal joints.

8.8.4. Fatigue Test Results

8.8.4.1. Overview

The load versus deflection response for the system under LC 4-1 through LC 4-4 for Stages 2, 5, and 8 are shown in Figure 8.80. The deflections shown accounts for the settlement of the supports. On Stage 5, LC 4-2 was not performed as there was no change after two million cycles between the other load configurations.

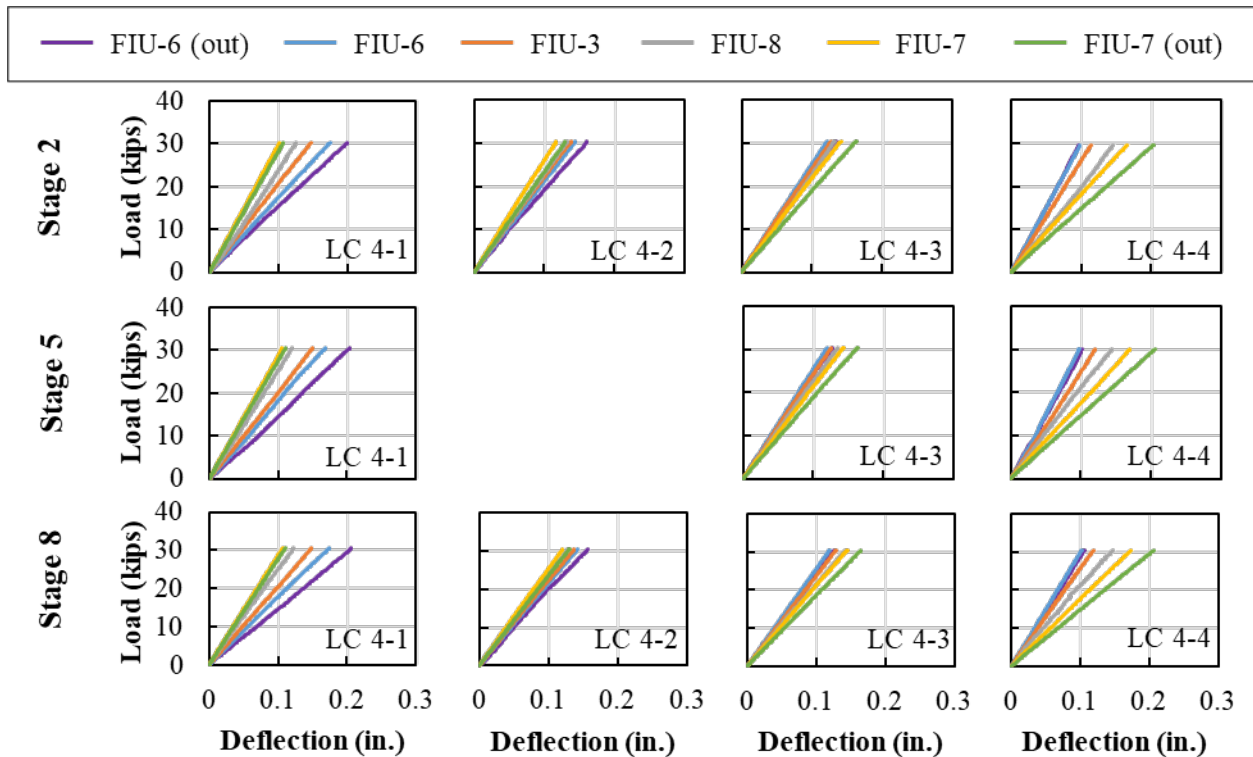


Figure 8.80: Load versus midspan displacement for permit load testing Stages 2, 5, and 8 with LC 4-1 through LC 4-4 (Stage 5 LC 4-2 was skipped)

All beams had the same elastic deflection through all testing stages with no noticeable difference in load versus midspan displacement response caused by the fatigue loading. For LC 4-1 and LC 4-4, FIU-6 and FIU-7 had similar deflection at 30 kips in all stages of 0.2 inches, respectively. The largest interior beam deflections were approximately 0.15 inches for FIU-6 (LC 4-2) and FIU-7 (LC 4-3) respectively. No deflection increase was observed after two million cycles (Stage 5), and after four million cycles (Stage 8) in all load configurations.

The normalized stiffness during the FC 4-6 and FC 4-7 assessments for west and east actuators, and the average midspan superstructure response are shown in Figure 8.81. The stiffness was normalized based on the initial system stiffness at the beginning of each fatigue test. The system stiffness was not impacted by the alternating loading cycles from both actuators on exterior girders (FC 4-6), and after two million cycles, there was no noticeable drop in stiffness in any of the LDTs. Also, the system was not impacted by the rear axle loading off-centered at midspan (FC 4-7); there was no drop in stiffness measured by the LDTs after an additional two million

cycles. This behavior suggests that there was no degradation in the overall superstructure system strength after four million fatigue cycles, and after all 11 load configuration ramps.

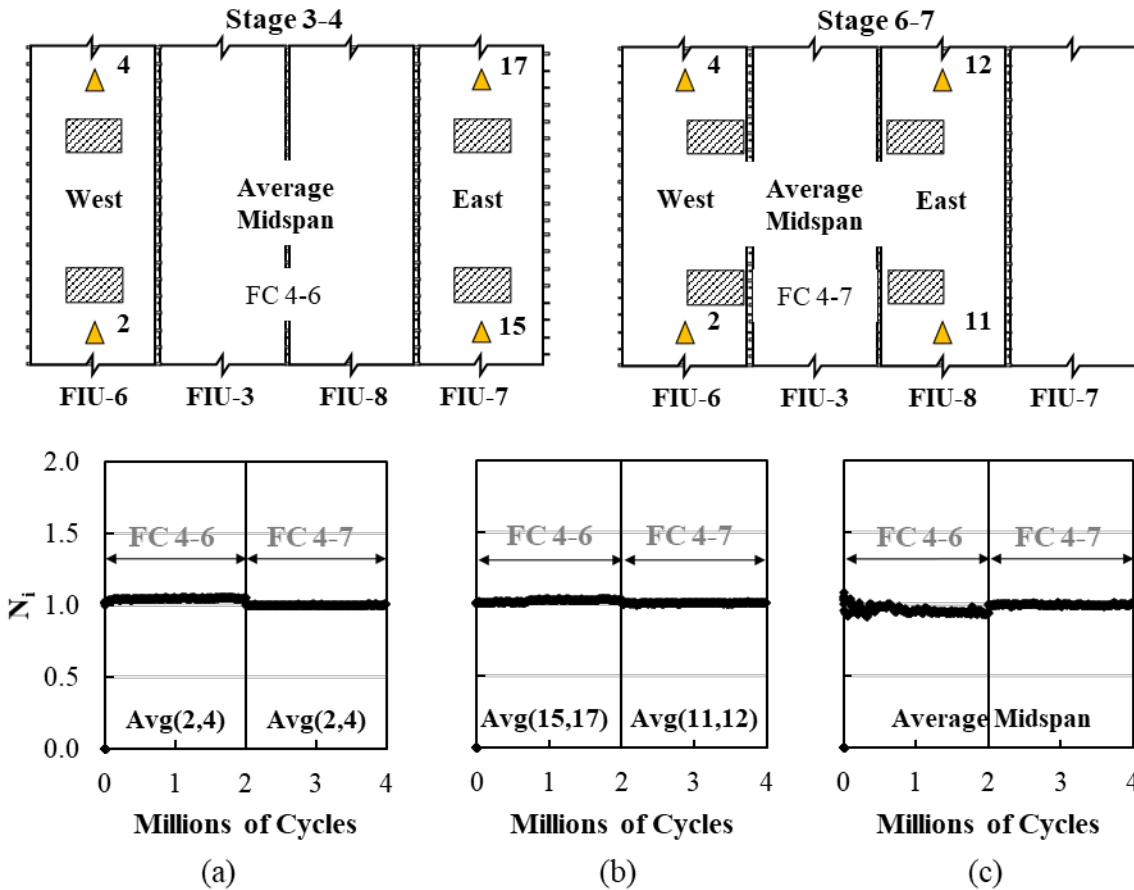


Figure 8.81: Normalized stiffnesses at midspan for system: (a) west side, (b) east side, and (c) average midspan response

8.8.4.2. Longitudinal Behavior

This section summarizes the longitudinal static behavior before and after fatigue cycles during Stages 2, 5, and 8. Also, a discussion of the longitudinal fatigue behavior during Stages 3/4 and 6/7 is presented.

Girder distribution factors (GDF) from LC 4-1, LC 4-2, LC 4-3, and LC 4-4 for Stages 2, 5 and 8 are shown in Figure 8.82. When the exterior beams were loaded (LC 4-1 and LC 4-4), the maximum load percentages received by FIU-6 (LC 4-1) and FIU-7 (LC 4-4) was approximately 34 percent. No noticeable change was observed between Stages 2 and 5 in both load configurations, indicating that the same load distribution was maintained before and after two million fatigue cycles. The same behavior was observed between Stages 5 and 8 after additional two million cycles. However, a slight decrease in the GDF for FIU-6 and slight increase for FIU-8 and FIU-7 was observed between Stages 2 and 8 for LC 4-1 after four million cycles; this difference could be attributed to the variation caused by the GDF calculation method as there was not a noticeable difference in any other instrumentation.

When the interior beams were loaded, the maximum load percentage received by FIU-6 (LC 4-2) and FIU-7 (LC 4-3) was approximately 28 percent. There was an average variability between the three stages of 2.8 percent with a maximum variation for a single beam GDF of 5.6 percent. No noticeable strength decay was observed throughout these load configurations.

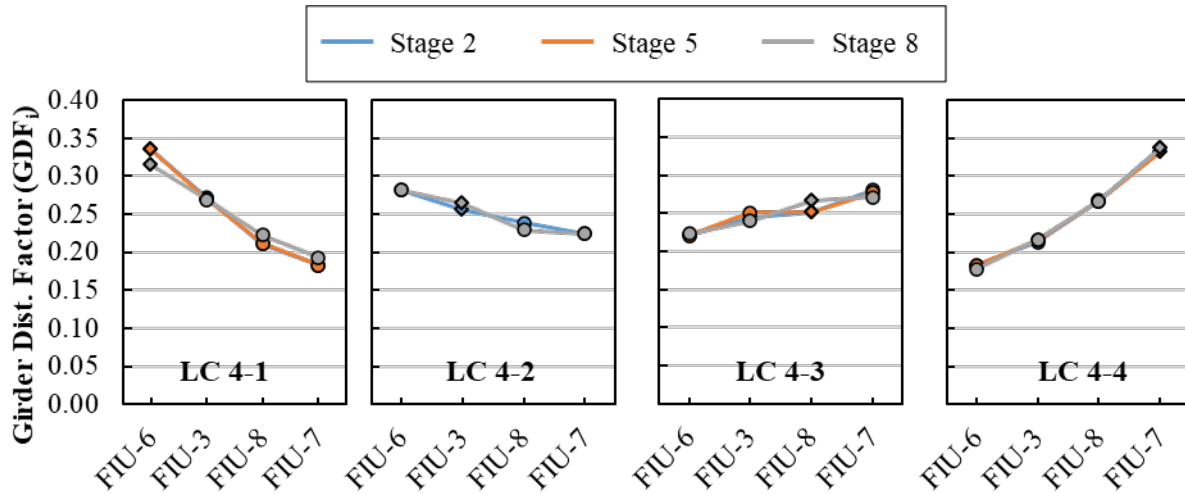


Figure 8.82: Girder distribution factors (GDF_i) for LC 4-1, LC 4-2, LC 4-3, and LC 4-4 on Stages 2 through 8 (Stage 5 LC 4-2 was skipped)

The measured responses of the center longitudinal CSGs at the bottom of the superstructure are shown in Figure 8.83 for LC 4-1 and LC 4-4 during Stages 2, 5 and 8.

Longitudinal tension strains developed at the bottom of the beam sections in all stages, and the initial maximum strains measured at exterior beams were 111 $\mu\epsilon$ on FIU-6 and 108 $\mu\epsilon$ on FIU-7, as shown in Figure 8.83 (a) and (b), respectively. All longitudinal strains showed a linear response with no signs of change in load-strain slopes at 30 kips.

After two million cycles of exterior beams loading (FC 4-6), the maximum strains measured at exterior beams remained the same as shown in Figure 8.83 (c) and (d), with no change in behavior or strength decay. After additional two million cycles of off-centered truck axle (FC 4-7), the maximum strains on exterior beams increased from 111 to 117 $\mu\epsilon$ on FIU-6, and from 108 to 111 $\mu\epsilon$ on FIU-7 as shown in Figure 8.83 (e) and (f), respectively.

After a total of four million fatigue cycles, a linear response was still observed with no signs of change in load-strain slopes at 30 kips, except for CSG-B3 which showed an erratic behavior during Stage 8 LC 4-1 and LC 4-4. However, this did not represent a change in behavior nor system strength decay.

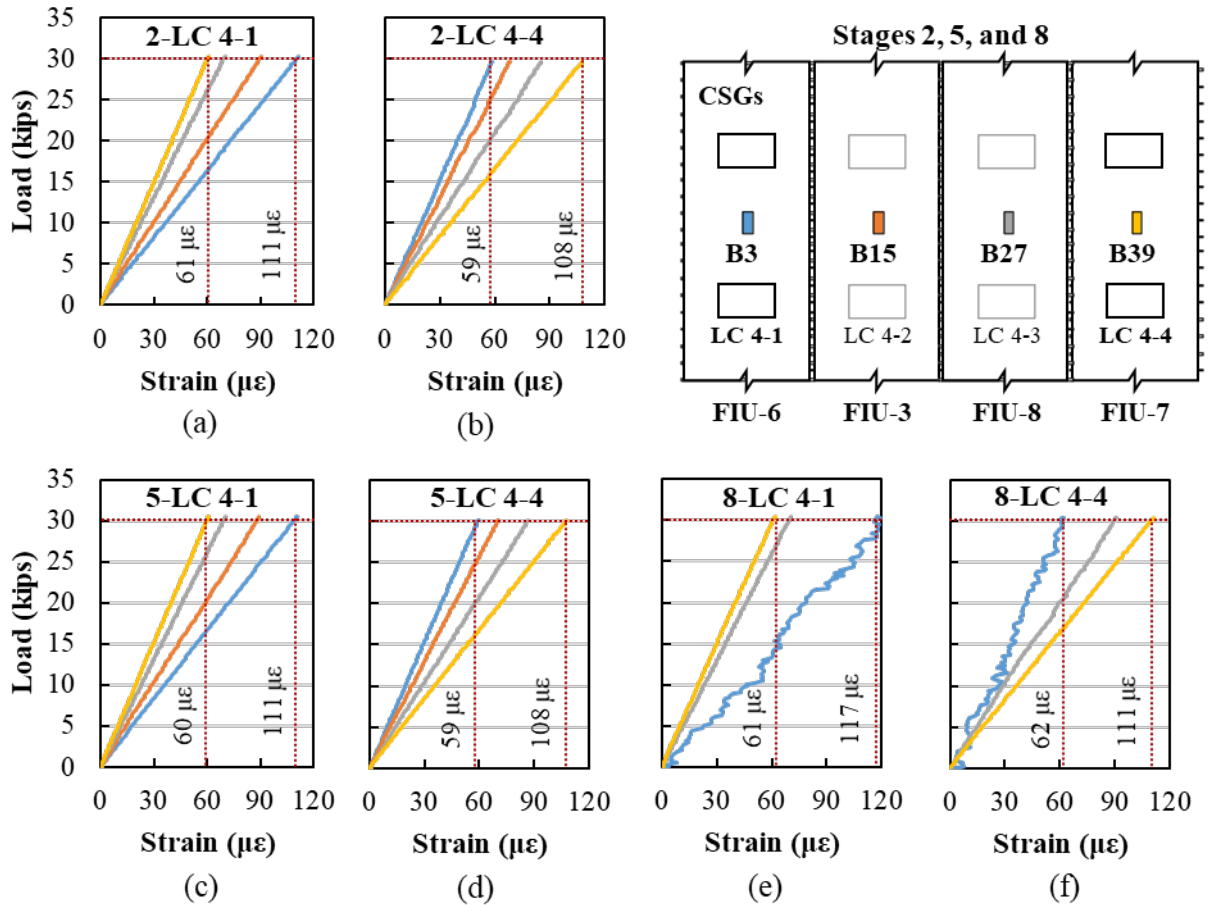


Figure 8.83: Load versus bottom longitudinal concrete strain for permit load testing for Stage 2 (a) LC 4-1 and (b) LC 4-4; Stage 5 (c) LC 4-1 and (b) LC 4-4; and Stage 8 (e) LC 4-1 and (f) LC 4-4 (B15 malfunctioned in Stage 8)

A similar linear response (compression behavior) of the center longitudinal CSGs at the top of the superstructure was measured in LC 4-1 and LC 4-4 during Stages 2 through 8, with no remarkable changes in load-strain pattern.

The measured responses of the center longitudinal CSGs at the bottom of the superstructure are shown in Figure 8.84 for LC 4-2 and LC 4-3 during Stages 2, 5 and 8. Like the behavior when the exterior beams were loaded, longitudinal tension strains developed at the bottom of the section in all beams for all stages, and the maximum strains measured were also on exterior beams: 88 $\mu\epsilon$ on FIU-6 and 90 $\mu\epsilon$ on FIU-7, as shown in Figure 8.84 (a) and (b), respectively. All longitudinal strains showed a linear response with no signs of change in load-strain slopes at 30 kips.

After two million cycles of exterior beams loading (FC 4-6), the maximum strain measured on FIU-7 (LC 4-3) remained the same as the initial response as shown in Figure 8.84 (c), indicating no change in the bottom longitudinal response of interior beams. After an additional two million cycles (FC 4-7), the maximum strain response on FIU-6 (LC 4-2) increased from 88 to 96 $\mu\epsilon$, as shown in Figure 8.84 (d) for Stage 8. However, the maximum strain response on FIU-7 (LC 4-3)

remained the same at 90 $\mu\epsilon$, as shown in Figure 8.84 (e), which suggests that the increase in strain in CSG-B3 was due to the change in behavior of the gauge.

After a total of four million fatigue cycles, the interior beams strain response remained linear with no signs of change in load-strain slopes at 30 kips either.

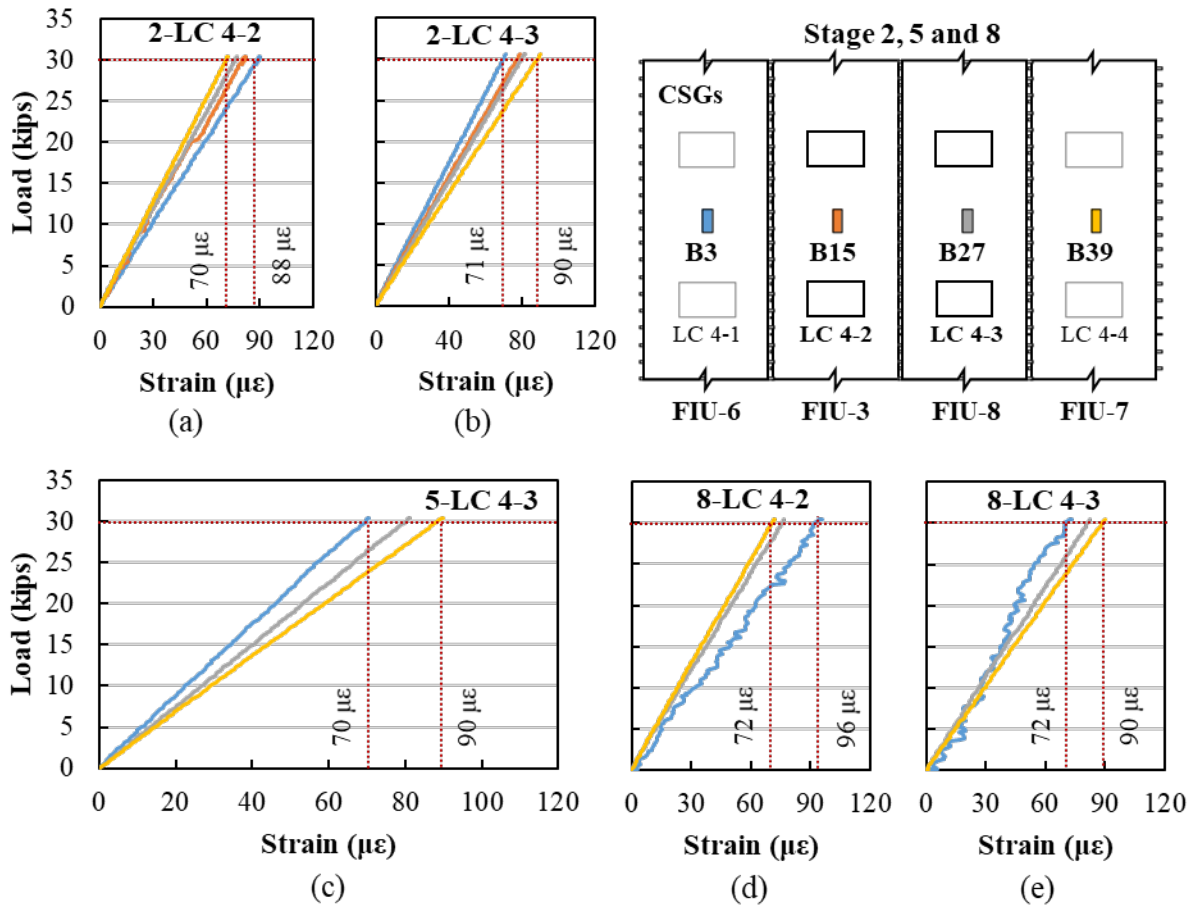


Figure 8.84: Load versus bottom longitudinal concrete strain for service load testing for Stage 2 (a) LC 4-2 and (b) LC 4-3; Stage 5 (c) LC 4-3; and Stage 8 (e) LC 4-2 and (f) LC 4-3

A linear top strain response in compression was observed in LC 4-2 and LC 4-3, with no change in top strain in all Stages 2 through Stage 8.

The longitudinal strain change in load for four longitudinal CSGs at the bottom of the beams during Stages 3/4 (FC 4-6) and Stages 6/7 (FC 4-7) is shown in Figure 8.85. All four gauges were in tension throughout the tests and showed no sign of deterioration in system strength due to fatigue loading. CSG-B3 and CSG-B39 had a slightly higher strain change during FC 4-6 assessment, which is consistent with the higher tension strain observed in these gauges during LC 4-1 and LC 4-4. Also, the same gauges showed higher strain change during FC 4-7 assessment, which is consistent with the higher tension strains observed in these gauges when interior beams were loaded during LC 4-2 and LC 4-3.

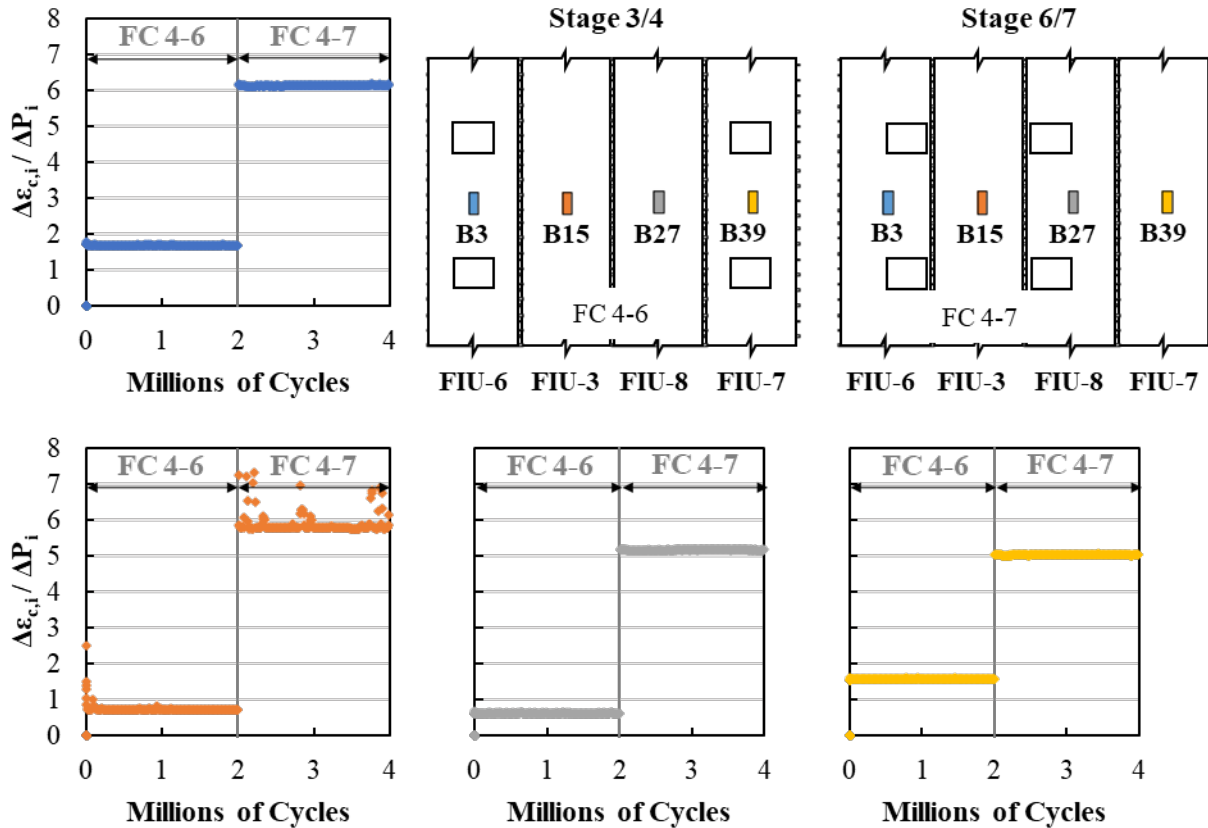


Figure 8.85: Bottom strain change of longitudinal CSGs per change in load versus number of cycles at center of specimen for FC 4-6 and FC 4-7

8.8.4.3. Joints Behavior

This section summarizes the service performance of the joints and transverse strains during Stages 2, 5, and 8 and transverse fatigue behavior during Stages 3/4 and 6/7.

The measured responses of the center transverse CSGs and CDTs at the top of the joints near midspan are shown in Figure 8.86 for LC 4-1 during Stages 2, 5, and 8. When FIU-6 was loaded on LC 4-1, linear transverse tension developed across all the joints near midspan in Stages 2 through 8. Before the cyclic assessment, the initial maximum transverse strain was approximately $30 \mu\epsilon$ in FIU-3 and about $21 \mu\epsilon$ across the Joint 3-8 and Joint 8-7, as shown in Figure 8.86 (a) and (b), respectively. After two million cycles of fatigue assessment (FC 4-6), the strains across the joints were unaltered after performing LC 4-1, as shown in Figure 8.86 (c) and (d), indicating that the joints top transverse behavior was not affected by the cyclic assessment.

After two million additional cycles of fatigue loading (FC 4-7), the strains measured across the joints at midspan were still linear at 30 kips after LC 4-1 as shown in Figure 8.86 (e) and (d) for CSGs and CDTs, respectively. A minimal increase of $1 \mu\epsilon$ was measured in FIU-3 and $2 \mu\epsilon$ across Joint 3-8 region. Nevertheless, the system did not show signs of change in load-strain slopes at 30 kips.

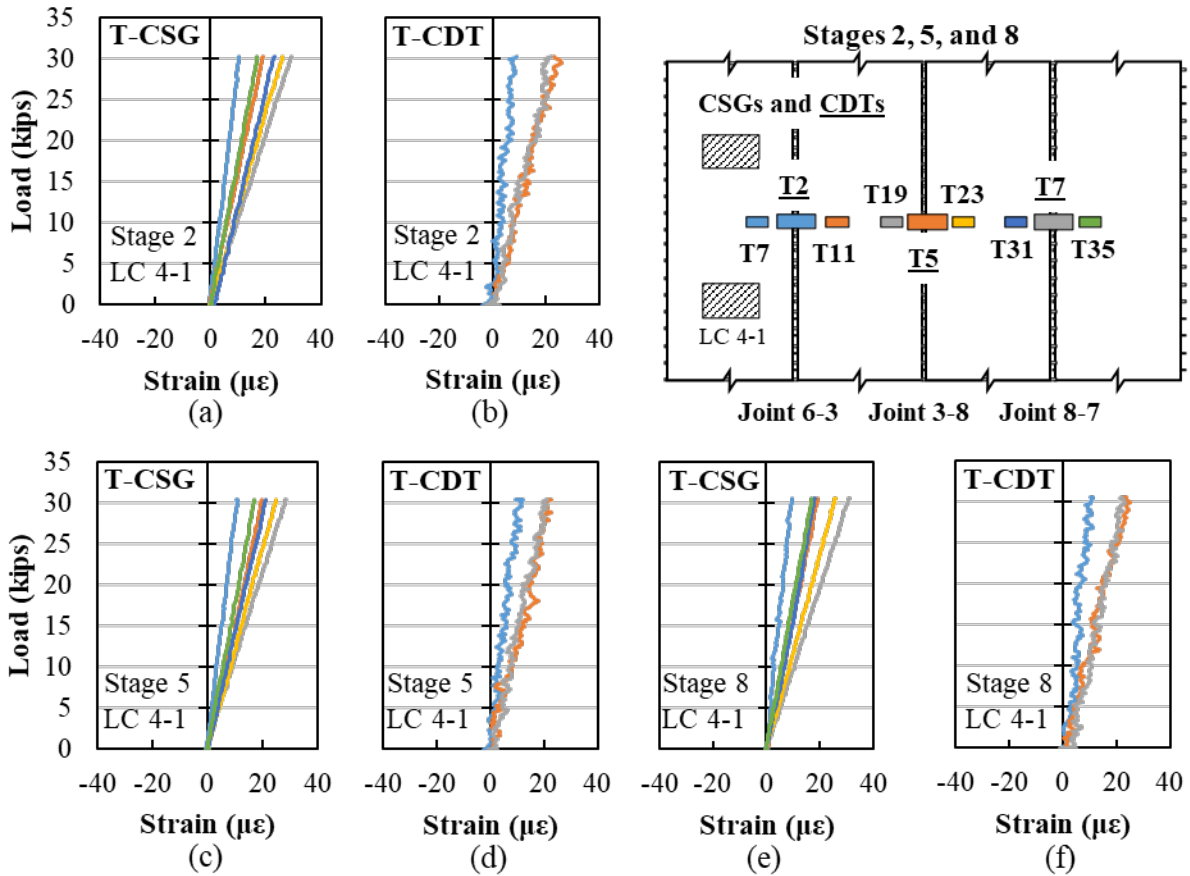


Figure 8.86: Load versus top transverse concrete strain for service load testing for LC 4-1 for (a) Stage 2 CSGs, (b) Stage 2 CDTs, (c) Stage 5 CSGs, (d) Stage 5 CDTs, (e) Stage 8 CSGs, and (f) Stage 8 CDTs

The measured responses of the center transverse CSGs and CDTs at the bottom of the joints near midspan are shown in Figure 8.87 for LC 4-1 during Stages 2, 5, and 8. Similar to the top transverse response, minimal bottom transverse strains in compression were measured across the joints in all stages.

Before the cyclic assessment, the largest bottom transverse strain in compression was measured in FIU-3 and FIU-8 near Joint 3-8 joint, with compressive strains up to $30 \mu\epsilon$ in the precast section as shown in Figure 8.87 (a) and up to $31 \mu\epsilon$ across Joint 8-7 joint. After the first two million cycles, the bottom transverse response remained the same, as shown in Figure 8.87 (c) for the precast region and Figure 8.87 (d) across the joint. The response remained the same after two million additional cycles, as shown in Figure 8.87 (e) for the precast region and Figure 8.87 (f) across the joint, indicating that the bottom transverse response did not change after four million fatigue cycles.

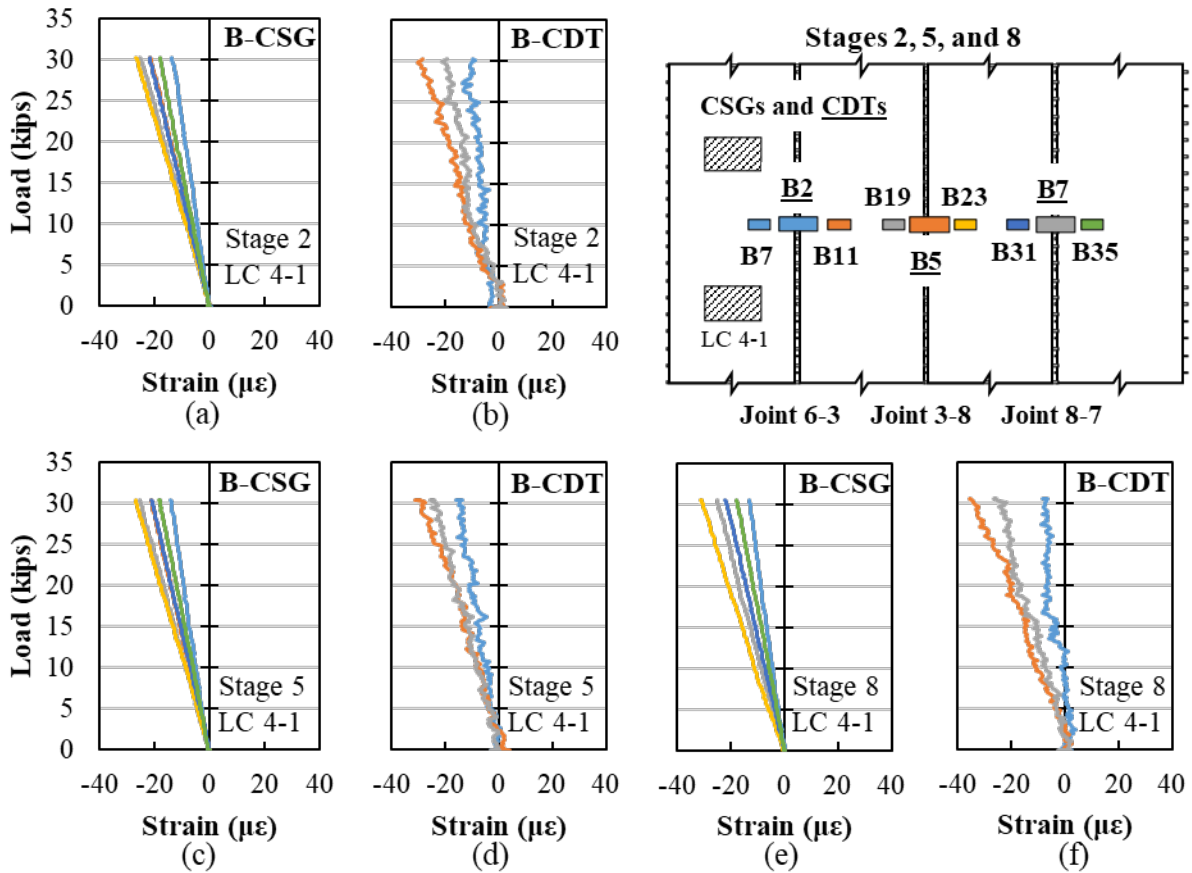


Figure 8.87: Load versus bottom transverse concrete strain for service load testing for LC 4-1 for (a) Stage 2 CSGs, (b) Stage 2 CDTs, (c) Stage 5 CSGs, (d) Stage 5 CDTs, (e) Stage 8 CSGs, and (f) Stage 8 CDTs

The static response before and after fatigue assessment for LC 4-4 was similar to LC 4-1, with no signs of strength decay nor distress across the system.

The load versus rebar strains on the west side of the joints at midspan are shown in Figure 8.88 for LC 4-1 during Stages 2, 5, and 8. At joint rebar level, the strains measured were negligible. Small strain responses were measured on the west side rebar in Joint 6-3 before and after fatigue performance. Minimal compressive strains were measured in Joint 3-8 and Joint 8-7 reinforcement before and after fatigue assessment. The same minimal compressive strains were maintained in those joints throughout all stages, indicating no change in strain behavior at the rebar level after executing the fatigue cycles. The same strain behavior was observed on the east joint side near midspan region.

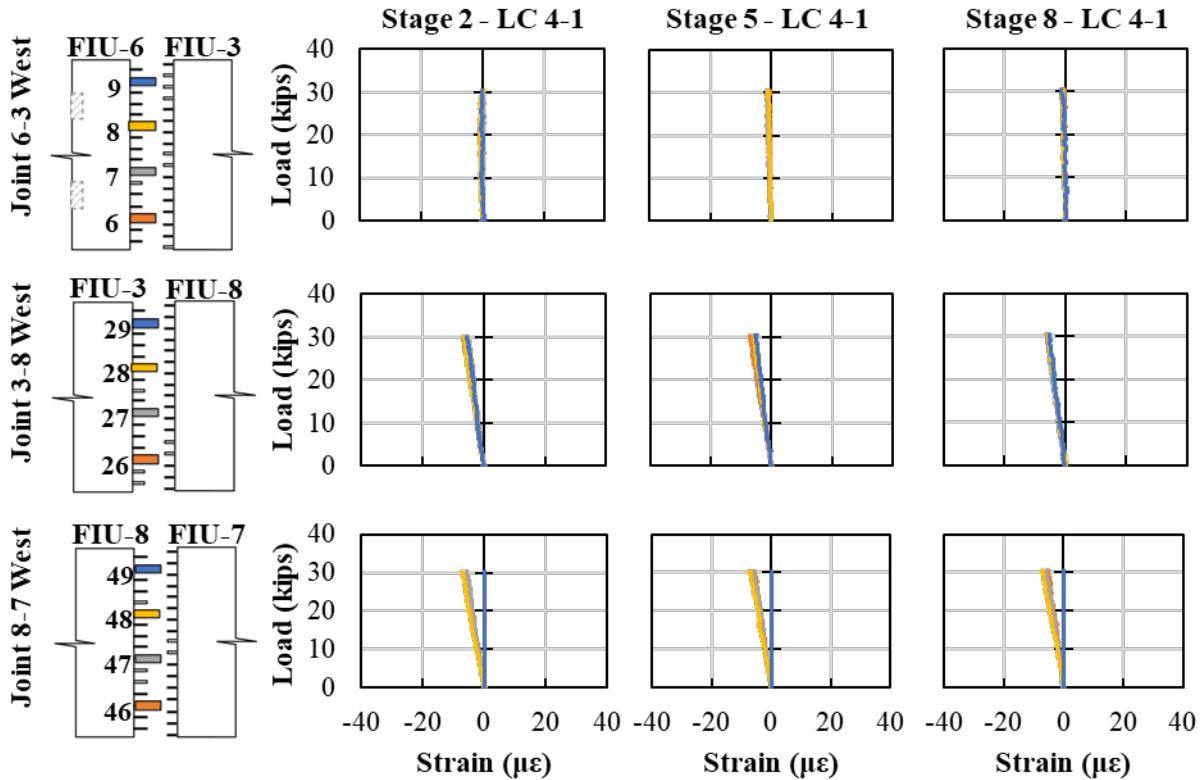


Figure 8.88: Load versus center west rebar strain for service load testing with LC 4-1 for Stage 2, Stage 5, and Stage 8

The measured responses of the center transverse CSGs and CDTs at the top of the joints near midspan are shown in Figure 8.89 for LC 4-3 during Stages 2, 5, and 8. Linear transverse tension and compression developed across all the joints near midspan when FIU-8 was loaded during LC 4-3. Linear compressive strains developed in the precast regions around the load application points in FIU-8 and near Joint 3-8, as shown in Figure 8.89 (a), and small compressive strains developed across Joints 3-8 and 8-7, as shown in Figure 8.89 (b). The same transverse behavior was measured after the first two million cycles, as shown in Figure 8.89 (c), and across the joint regions, as shown in Figure 8.89 (d).

After FC 4-7 tests, the transverse joint behavior remained the same at the precast regions as shown in Figure 8.89 (e) and across the joints as shown in Figure 8.89 (f).

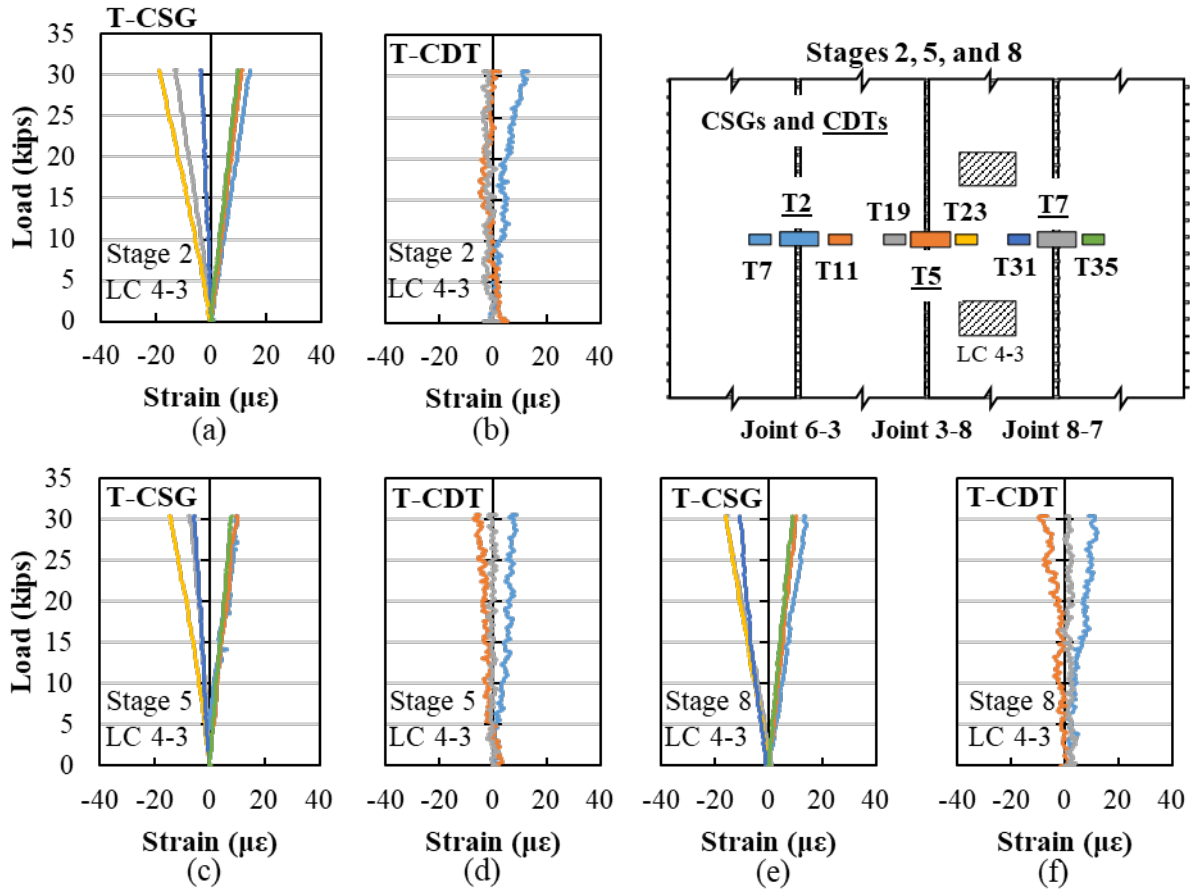


Figure 8.89: Load versus top transverse concrete strain for service load testing for LC 4-3 for (a) Stage 2 CSGs, (b) Stage 2 CDTs, (c) Stage 5 CSGs, (d) Stage 5 CDTs, (e) Stage 8 CSGs, and (f) Stage 8 CDTs

The measured responses of the center transverse CSGs and CDTs at the bottom of the joints near midspan are shown in Figure 8.90 for LC 4-3 during Stages 2, 5, and 8. The transverse strains measured at the bottom of the joints also remained linear before and after the fatigue assessments, with no strength decay at the bottom of the joint regions.

Before and after the first cyclic assessment (FC 4-6), the bottom transverse response was the same as the initial response at the precast section as shown in Figure 8.90 (a), and across the joints as shown in Figure 8.90 (b). The response after two million cycles indicates that the system response remained similar to the original response as shown in Figure 8.90 (c) and (d). After an additional two million cycles, the bottom transverse strains were still unaltered at the precast regions, as shown in Figure 8.90 (e), and across the joint regions, as shown in Figure 8.90 (f).

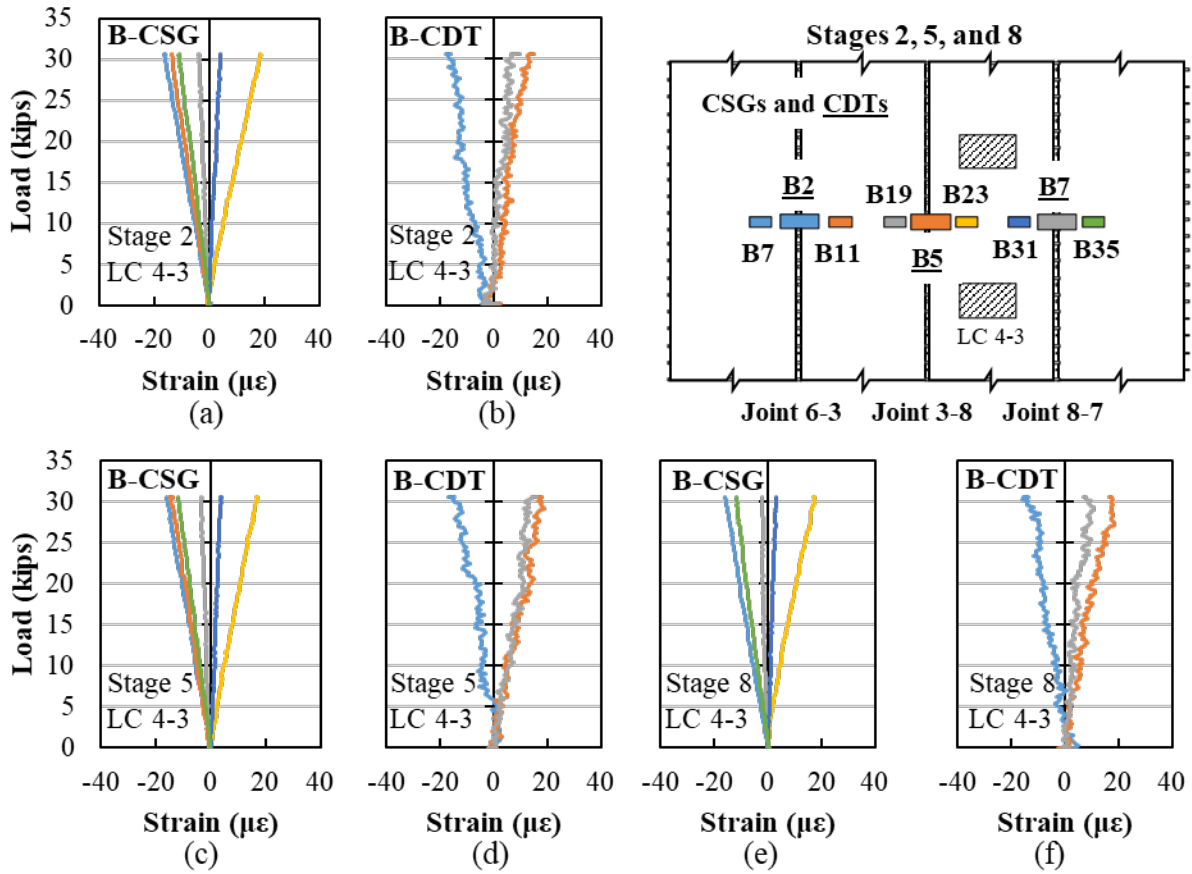


Figure 8.90: Load versus bottom transverse concrete strain for service load testing for LC 4-3 for (a) Stage 2 CSGs, (b) Stage 2 CDTs, (c) Stage 5 CSGs, (d) Stage 5 CDTs, (e) Stage 8 CSGs, and (f) Stage 8 CDTs

The static response before and after fatigue assessment for LC 4-2 was similar to LC 4-3, with no signs of strength decay nor distress across the system.

The load versus rebar strains on the west side of joints at midspan are shown in Figure 8.91 for LC 4-3 during Stages 2, 5, and 8. The measured strains were small in the joint rebar, showing that the rebar was not engaged during this service load testing. Minimal tensile strains were only measured in the Joint 3-8 reinforcement before and after fatigue assessments, with no major strain change per applied load at rebar level. This would indicate that most transverse tension was carried by the concrete to UHPC bond and shear key. A similar behavior was observed on the east joint rebar near midspan and the remaining rebar along the length of the joints.

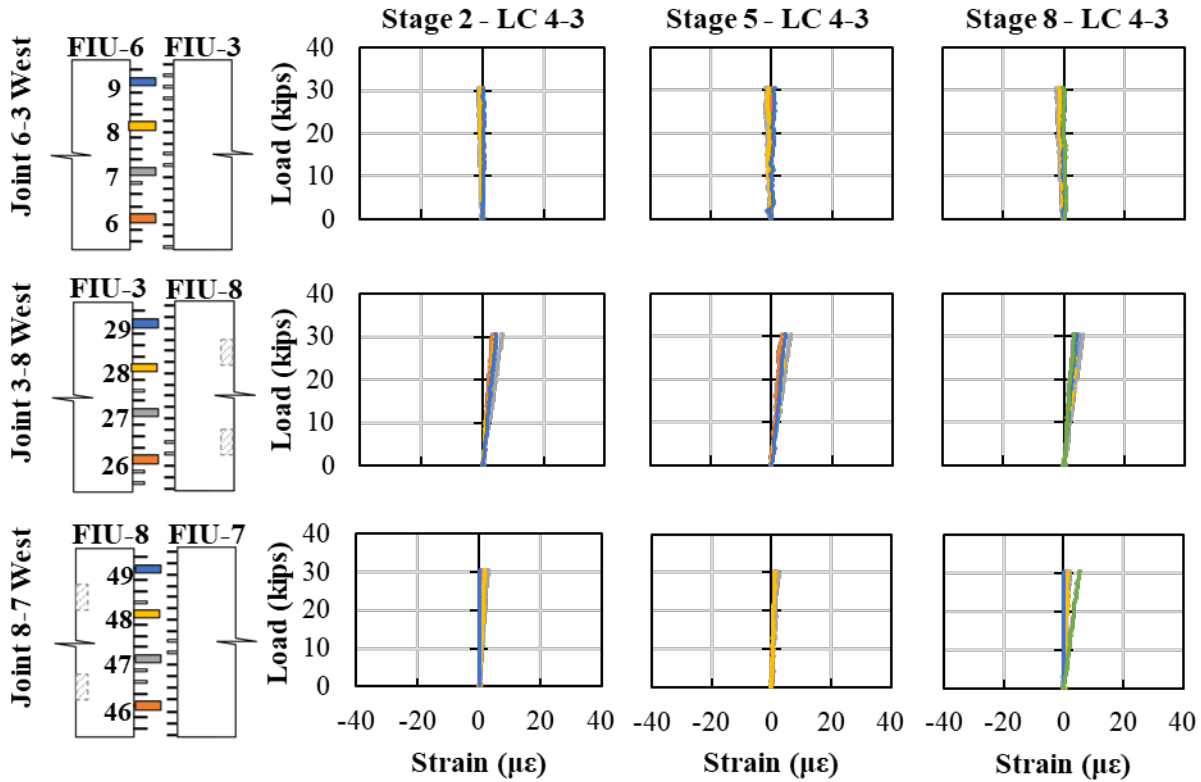


Figure 8.91: Load versus center west rebar strain for service load testing with LC 4-3 for Stage 2, Stage 5, and Stage 8

The transverse strain change per change in load for three regions across the top of the joints is shown in Figure 8.92 during Stages 3/4 and 6/7. All three joint regions had similar transverse responses, with no signs of deterioration in any of the precast nor across the joint regions because the strain changes were very minimal. Only the CDTs had a slightly higher response than the CSGs in all testing stages as shown in Figure 8.92 (a) for Joint 6-3, Figure 8.92 (b) for Joint 3-8, and Figure 8.92 (c) for Joint 8-7. Also, slightly higher strains were observed across the Joint 8-7 region during FC 4-7, indicating that this region had the highest demand when the off-centered axle load was applied. There was some variation in CSG-T19 during the FC 4-7 testing, but this variation was not accompanied by a change in any of the neighboring sensors or in the static response of CSG-T19 during Stage 8 testing. The fatigue response was consistent with the strains observed during the load configuration ramps, and no decay in the behavior was measured.

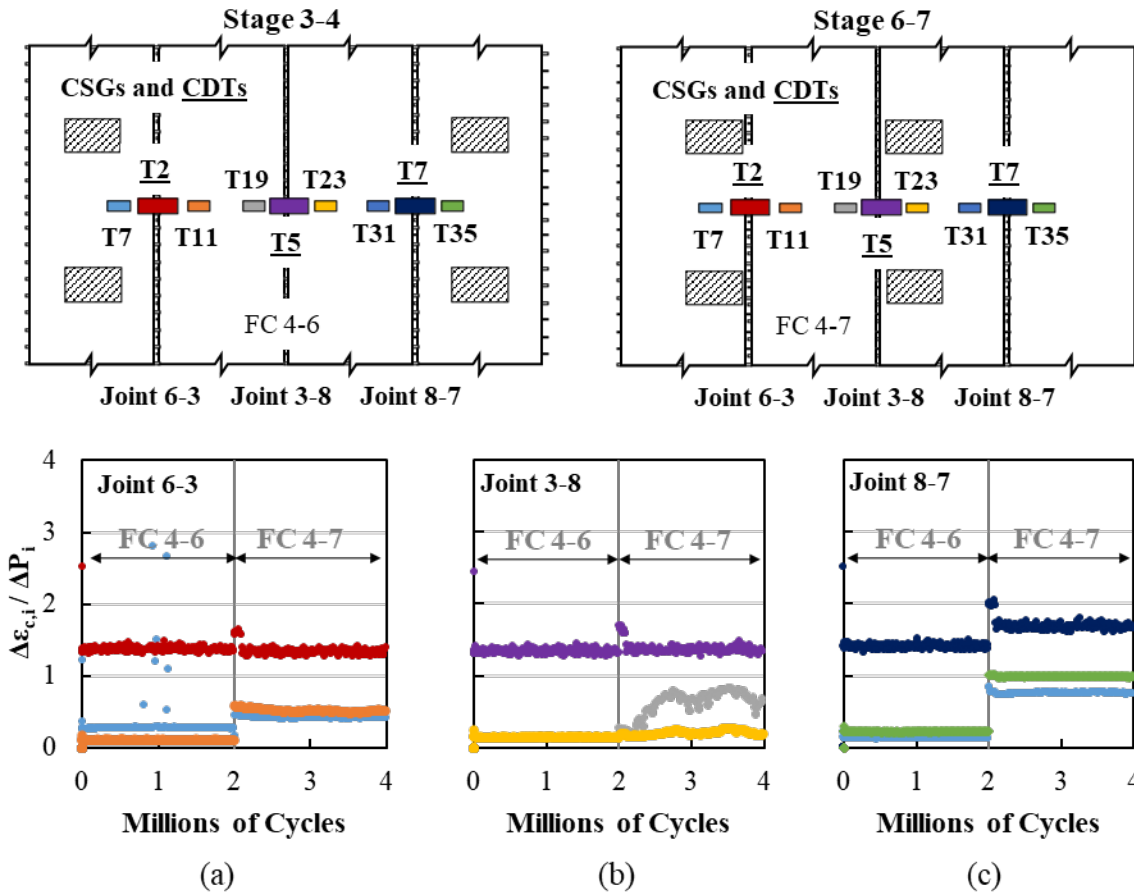


Figure 8.92: Top strain change of transverse CSGs and CDTs per change in load versus number of cycles at center of specimen across: (a) Joint 6-3, (b) Joint 3-8, and (c) Joint 8-7

The transverse strain change per change in load for three regions across the bottom of the joints is shown in Figure 8.93 during Stages 3/4 and 6/7. All three joint regions had similar transverse responses, with no signs of deterioration in any of the precast concrete nor across the joint regions as the strain changes were very minimal. Only the CDTs had a slightly higher response than the CSGs in all testing stages as shown in Figure 8.93 (a) for Joint 6-3, Figure 8.93 (b) for Joint 3-8, and Figure 8.93 (c) for Joint 8-7. Also, slightly higher strains were observed across Joint 8-7 region during FC 4-7, indicating that this region had the highest demand when the off-centered axle load was applied. The fatigue response was also consistent with the strains observed during the load configuration ramps.

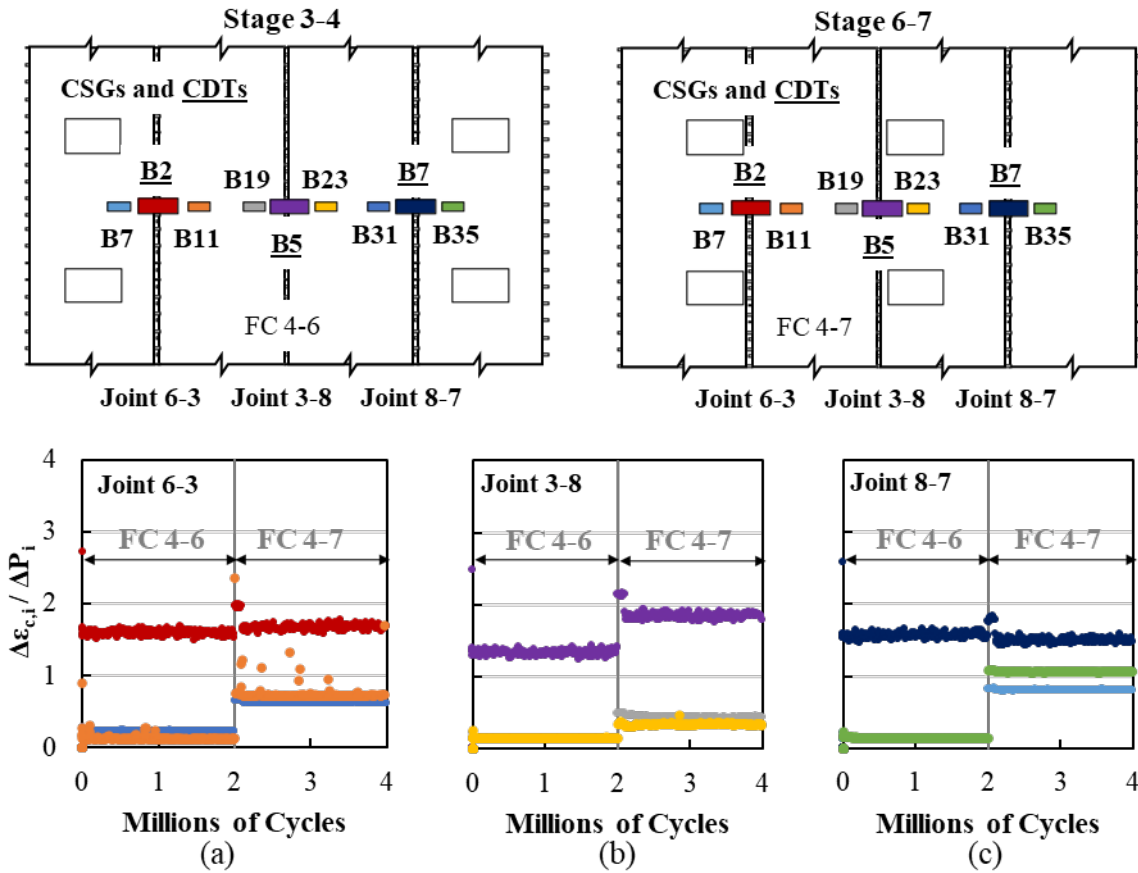


Figure 8.93: Bottom strain change of transverse CSGs and CDTs per change in load versus number of cycles at center of specimen across: (a) Joint 6-3, (b) Joint 3-8, and (c) Joint 8-7

The strain change versus change in load responses for two rebar located at the west side of the joints near midspan are shown in Figure 8.94 during Stages 3/4 and 6/7. Minimal strain changes were measured at midspan of all three joint reinforcement bars, with no major change nor strength decay throughout all four million cycles. In general, the fatigue response was also consistent with the minimal strains measured during the static ramps at the same bars.

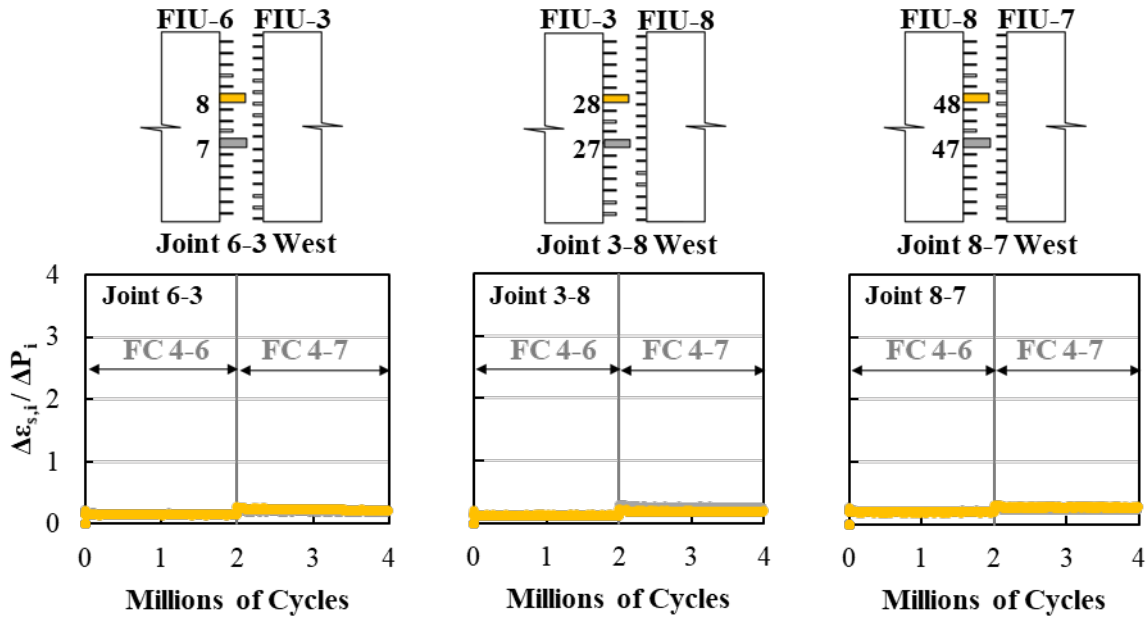


Figure 8.94: Rebar strain change per change in load versus number of cycles at center west of Joint 6-3, Joint 3-8, and Joint 8-7

The strain change versus change in load responses for two rebar located at the west side of joint near the south end of the system are shown in Figure 8.95 during Stages 3/4 and 6/7, with minimal to no strain change measured.

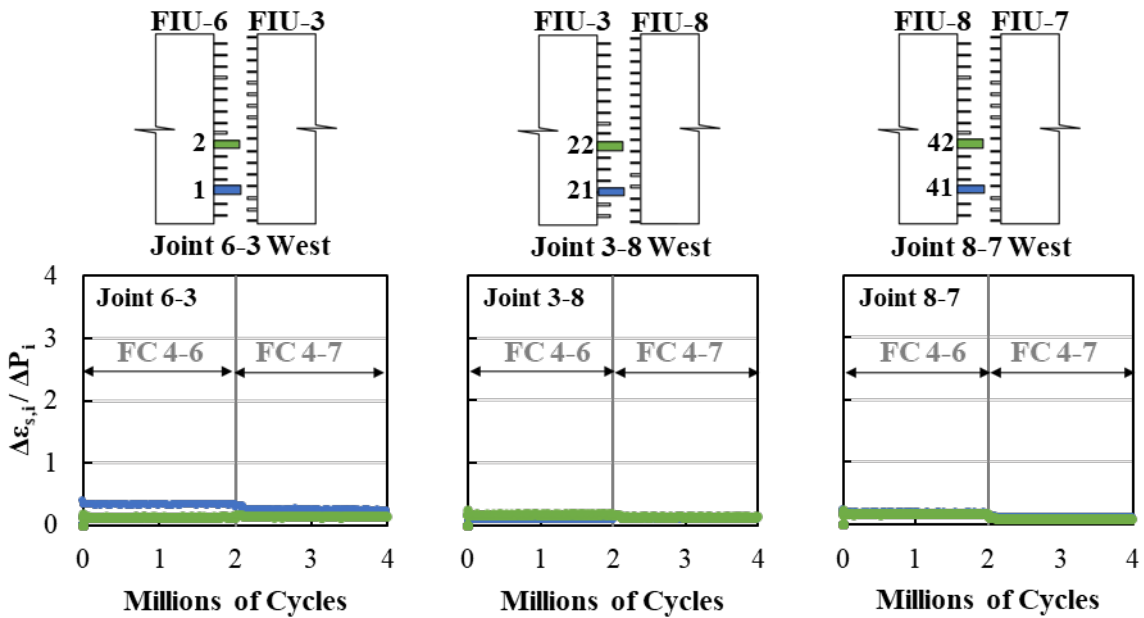


Figure 8.95: Rebar strain change per change in load versus number of cycles at west of joints south ends for Joint 6-3, Joint 3-8, and Joint 8-7

8.8.4.4. *Summary*

The following conclusions and observations can be made based on LC 4-1 through LC 4-4 from Stages 2, 5, and 8:

- All joints performed well during all static load tests before and after fatigue assessment. No debonding nor distress was observed at the precast-to-joint boundary.
- Girder load distribution factors were not altered after fatigue cycles on exterior beams (FC 4-6) and after off-centered rear truck axle (FC 4-7).
- The joints successfully transferred the stress between beams transversely at the top and at the bottom near the midspan region, with the similar strains between precast section and across the joints before and after the fatigue assessment.
- Minimal rebar strain response was measured throughout all testing stages, showing that the joint reinforcement remained unengaged during service testing.

No change in behavior was measured before and after two million fatigue cycles on exterior beams (FC 4-6), and after two million cycles of off-centered rear truck axle load (FC 4-7), which indicates that the system would perform as well as before the cyclic assessment with no signs of precast-to-UHPC joint debonding nor load distribution decay.

8.8.5. Cracked Service Test Results (Stages 8-9; LC 4-1cr through LC 4-4cr)

8.8.5.1. Overview

The joint cracking procedure described in §8.3.4.4 was performed between Stages 8 and 9 to impersonate a crack occurring immediately adjacent to Joint 6-3. The load versus deflection response for the system under LC 4-1 through LC 4-4 for Stage 8 and LC 4-1cr through LC 4-4cr for Stage 9 are shown in Figure 8.96. The deflections shown account for the settlement of the supports. After performing the joint saw cut, no difference in load versus deflection response was observed between load configurations in Stage 8 and Stage 9.

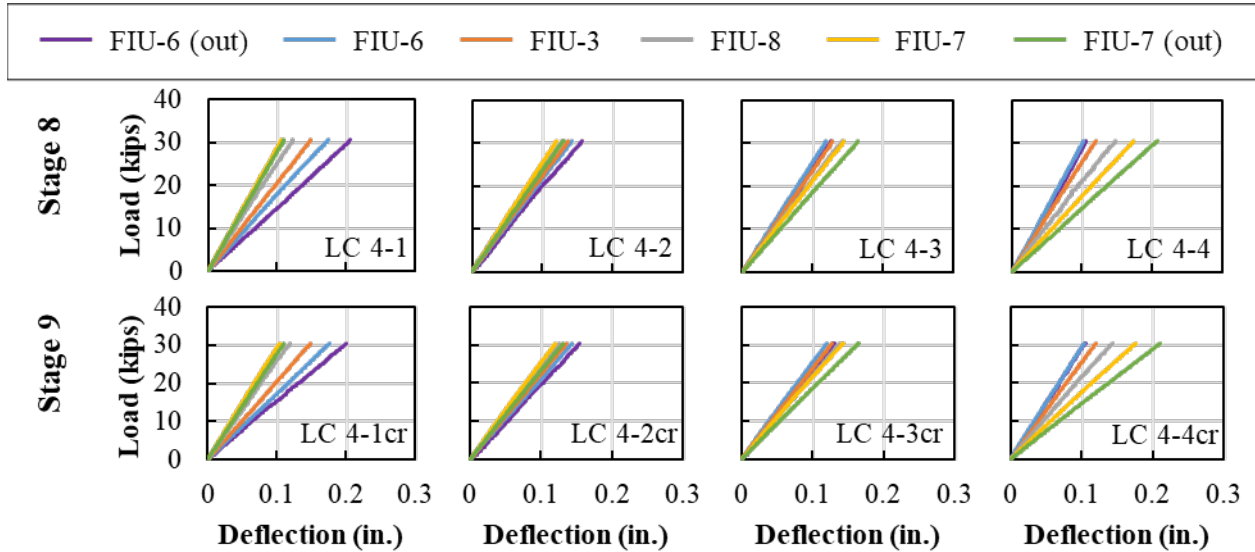


Figure 8.96: Load versus midspan displacement for service load testing Stage 8 LC 4-1 through LC 4-4 and Stage 9 LC 4-1cr through LC 4-4cr

All beams showed elastic deflection behavior through all testing stages. For LC 4-1, LC 4-1cr, LC 4-4, and LC 4-4cr, FIU-6 and FIU-7 had similar deflections at 30 kips in all stages of 0.2 inches. The largest interior beam deflections were approximately 0.15 inches for FIU-6 (LC 4-2 and LC 4-2cr) and FIU-7 (LC 4-3 and LC 4-3cr). No deflection increase was observed after the saw cut procedure in all load configurations for Stage 9.

8.8.5.2. Longitudinal Behavior

This section summarizes the longitudinal static behaviors for Stage 8 and 9 of exterior and interior beams before and after Joint 6-3 longitudinal saw cut.

Girder distribution factors during LC 4-1 through LC 4-4 for Stage 8 and LC 4-1cr through LC 4-4cr for Stage 9, are shown in Figure 8.97. The maximum GDF measured during Stage 8 for FIU-6 was 0.32 and 0.34 for FIU-7 when the exterior beams were loaded. The maximum GDF for FIU-6 was still 0.32 after the joint cut in Stage 9; the GDF for FIU-7 decreased by 6 percent to 0.32. The generally similar behavior indicates that similar load distribution was maintained before and after the joint longitudinal cut when exterior beams were loaded.

Girder distribution factors during LC 4-2 and LC 4-2cr for Stage 8 and LC 4-3 and LC 4-3cr for Stage 9 are also shown in Figure 8.97. The maximum GDFs for FIU-3 and FIU-8 were 0.27 when the interior beams were loaded during Stage 8; the maximum GDF for FIU-6 was 0.28 and for FIU-7 was 0.27 during the same loading.

The maximum GDF in FIU-6 decreased by approximately 3.7 percent for LC 4-2 in Stage 9 after the joint cracking procedure. The GDF in FIU-6 increased slightly for LC 4-3 and LC 4-4, so there was no evidence that the joint cracking led to less load being carried by FIU-6. If the joint cracking affected the load distribution, the GDF for FIU-6 would have increased in LC 4-1 and decreased in the other configurations.

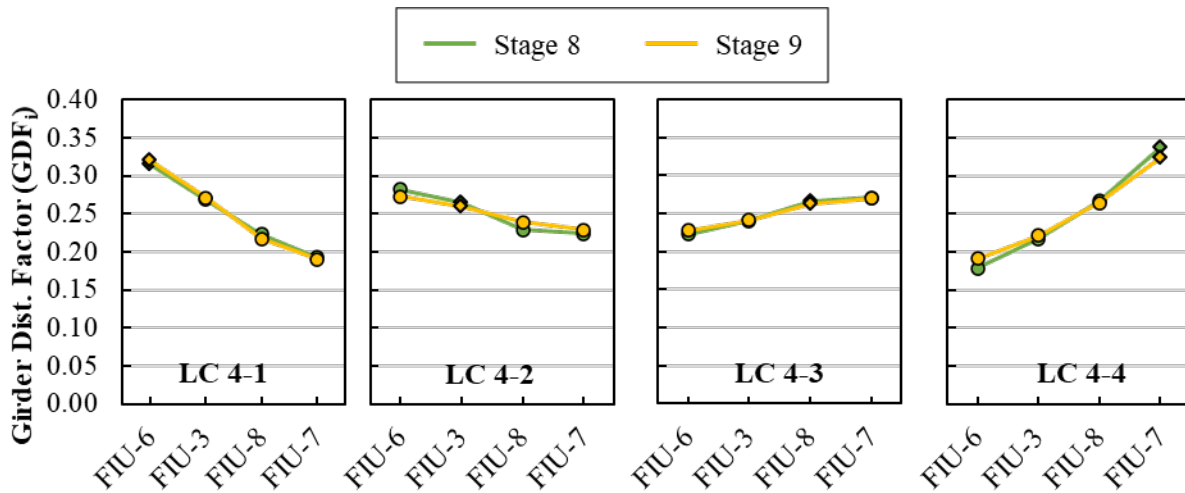


Figure 8.97: Girder Distribution Factors (GDF) for LC 4-1, LC 4-2, LC 4-3, and LC 4-4 on Stages 8 and 9

The measured responses of the center longitudinal CSGs at the bottom of the superstructure are shown in Figure 8.98 for LC 4-1 and LC 4-4 during Stage 8 and LC 4-1cr and LC 4-4cr during Stage 9.

Longitudinal tension strain developed in all sensors at the bottom of the beams before (Stage 8) and after (Stage 9) the joint cut in all load configurations. Similar maximum and minimum longitudinal tensile strains were measured underneath all beams during Stage 8 LC 4-1 as shown in Figure 8.98 (a) and Stage 9 LC 4-1cr as shown Figure 8.98 (b). A similar maximum and minimum strain behavior were measured underneath all beams during Stage 8 LC 4-4 as shown in Figure 8.98 (c) and Stage 9 LC 4-4cr as shown Figure 8.98 (d). This would indicate that no major strain behavior changes were caused by the joint cut of Joint 6-3.

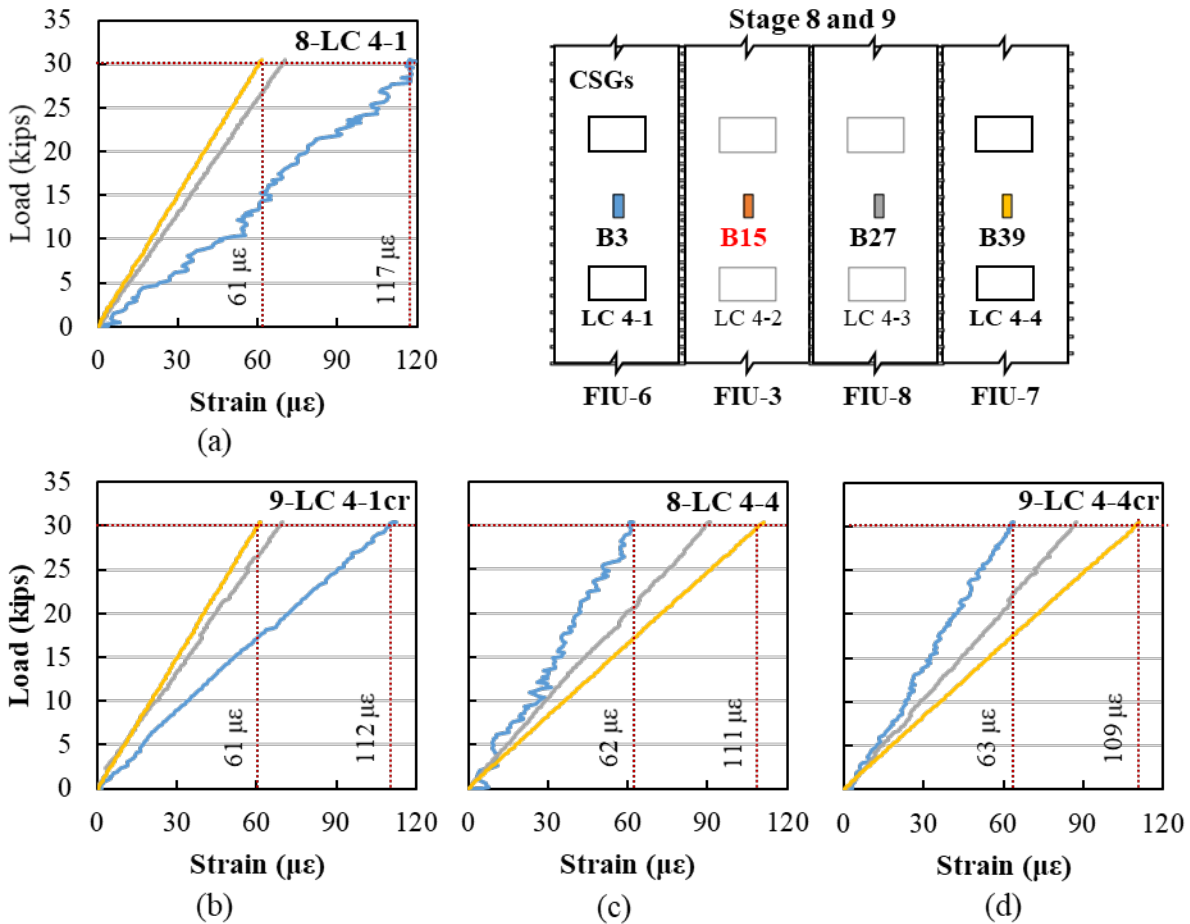


Figure 8.98: Load versus bottom longitudinal concrete strain for service load testing with LC 4-1 and LC 4-4 for (a) Stage 8 and (b) Stage 9 (LC 4-4 B15 malfunctioned in Stage 8)

The same linear response in compression were measured at the center longitudinal top CSGs for the same load configurations in Stages 8 and 9, with no major changes in load-strain pattern.

The measured responses of the center longitudinal CSGs at the bottom of the superstructure are shown in Figure 8.99 for LC 4-2 and LC 4-3 during Stage 8 and LC 4-2cr and LC 4-3cr during Stage 9.

Linear tensile behavior was also measured underneath all beams for all load configurations at 30 kips. Similar maximum and minimum tensile strains were measured in all beams during Stage 8 (LC 4-2) as shown in Figure 8.99 (a) and Stage 9 (LC 4-2cr) as shown in Figure 8.99 (b), with no indication of nonlinearities. The same behavior was observed when FIU-8 was loaded in Stage 8 (LC 4-3) as shown in Figure 8.99 (c) and in Stage 9 (LC 4-3cr) as shown in Figure 8.99 (d), with similar strains after the saw cut. This behavior also indicates that the bottom longitudinal strain behavior did not change after the joint was cut when interior beams were loaded.

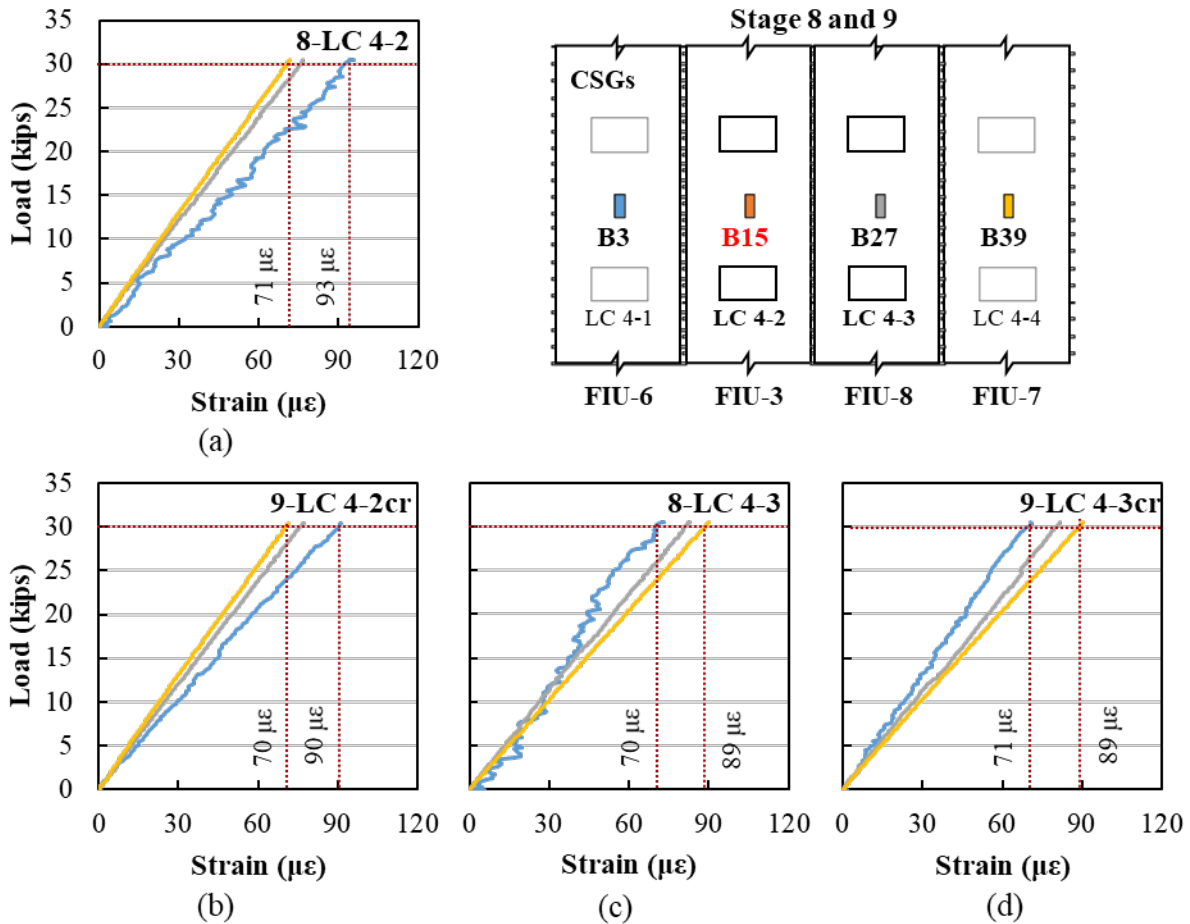


Figure 8.99: Bottom longitudinal behavior when interior beams are loaded for LC 4-2: (a) Stage 8 and (b) Stage 9; and for LC 4-3: (c) Stage 8 and (d) Stage 9

A linear top strain response in compression was also observed in LC 4-2 and LC 4-3 in Stage 8 when compared to LC 4-2cr and LC 4-3in Stage 9 after the joint cut, showing no change in top strain behavior.

8.8.5.3. Joints Behavior

This section summarizes the joints static transverse behavior before and after the joint cut during Stages 8 and 9.

The measured responses of the center transverse CSGs and CDTs at the top of the joints near midspan are shown in Figure 8.100 for LC 4-1 during Stages 8 and 9. The maximum top transverse strain measured at the precast section by the CSGs, with the maximum on FIU-3 (CSG-T19), was about 30 $\mu\epsilon$ before the joint cut at 30 kips as shown in Figure 8.100 (a). After the joint cut in Stage 9, the maximum top transverse strain remained the same as shown in Figure 8.100 (b). However, a slight decrease in transverse strain was observed on FIU 8 (CSG-T31) from 18 $\mu\epsilon$ to approximately 14 $\mu\epsilon$, representing the only small strain change at 30 kips after the joint cut. Nevertheless, this did not represent a major change in top transverse precast behavior.

A similar behavior was measured by the CDTs across the joints before and after the joint as shown in Figure 8.100 (c) and Figure 8.100 (d), respectively. Only a slight decrease of about $3 \mu\epsilon$ was measured across Joint 6-3 by CDT-T2, and a slight increase of $1 \mu\epsilon$ in the other sensors across Joint 3-8 (CDT-T5) and Joint 8-7 (CDT-T7), respectively. This behavior indicates that the top transverse behavior across the joint was also not altered by the joint cut.

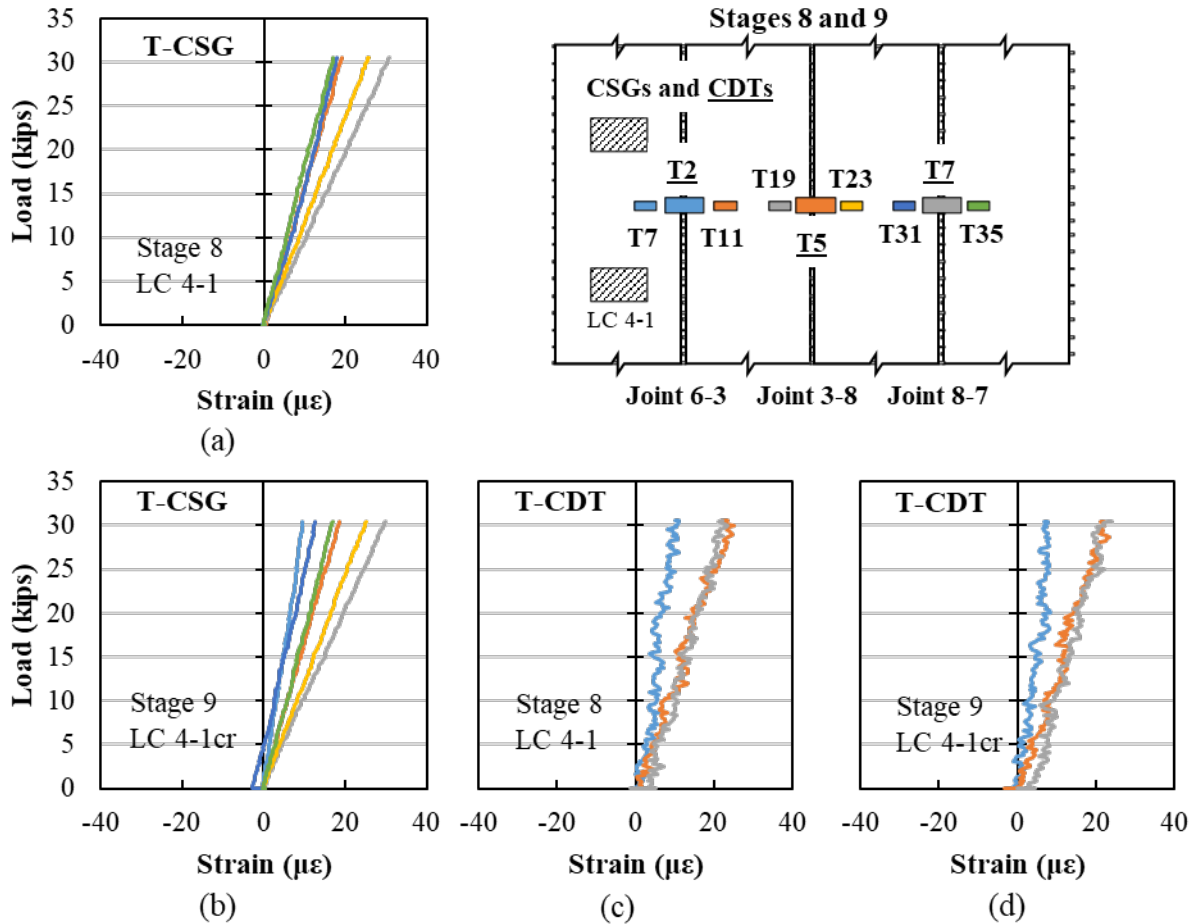


Figure 8.100: Load versus top transverse concrete strain for service load testing comparison between CSGs in Stage 8 (a) LC 4-1 and Stage 9 (b) LC 4-1cr, and CDTs in Stage 8 (c) LC 4-1 and Stage 9 (d) LC 4-1cr

The measured responses of the center transverse CSGs and CDTs at the bottom of the joints near midspan are shown in Figure 8.31 for LC 4-1 during Stages 8 and 9.

A similar behavior to the top transverse strains was observed at the bottom (in compression). The transverse strains remained the same at the bottom of the precast sections near the joints, with the maximum strain measured at FIU-8 by CSG-B23 of about $30 \mu\epsilon$, as shown in Figure 8.31 (a). The same linear behavior and top transverse strains were measured after the joint cut during Stage 9, as shown in Figure 8.31 (b). A similar load-strain response was measured before and after the joint cutting procedure across the joints by the CDTs, as shown in Figure 8.31 (c) and (d). Only a minimal strain variation of $1 \mu\epsilon$ was measured by CDT-B2.

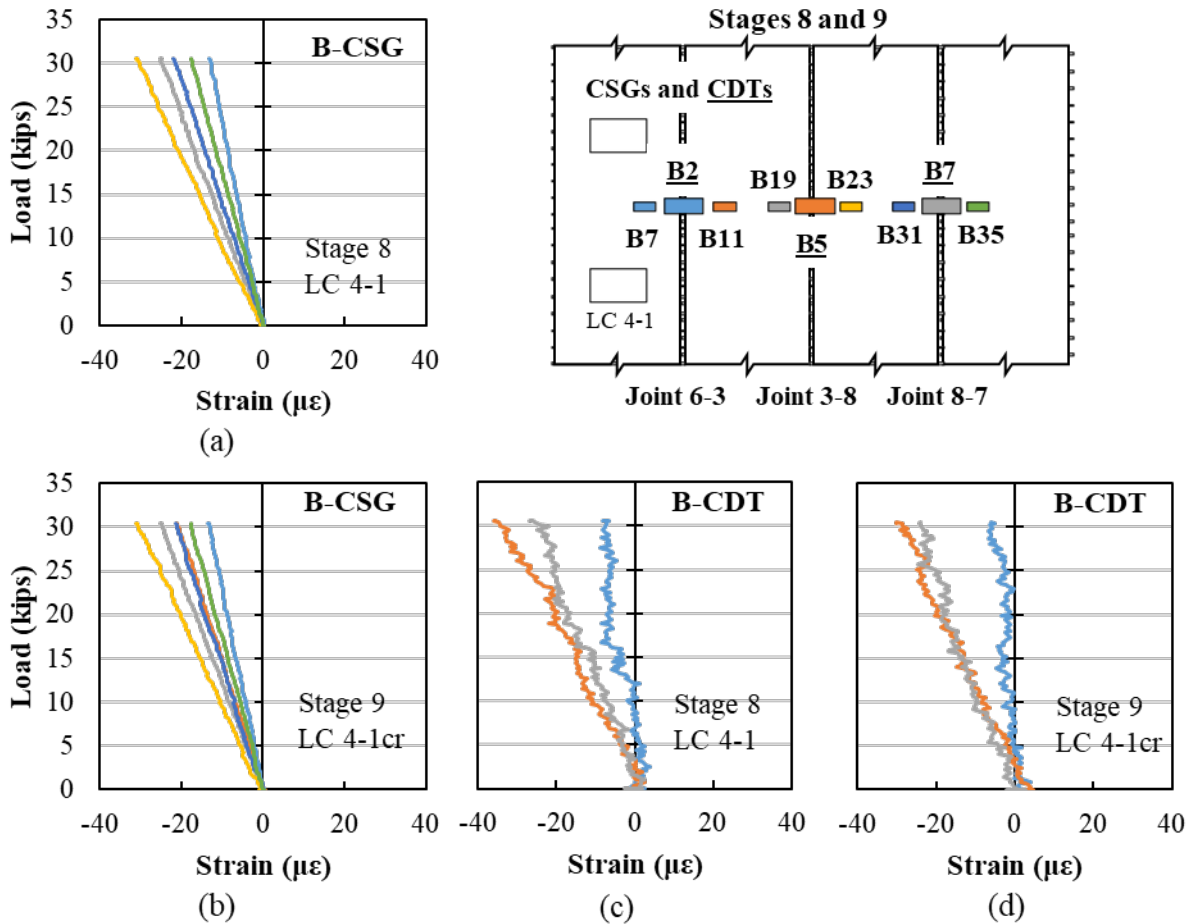


Figure 8.101: Load versus bottom transverse concrete strain for service load testing comparison between CSGs in Stage 8 (a) LC 4-1 and Stage 9 (b) LC 4-1cr, and CDTs in Stage 8 (c) LC 4-1 and Stage 9 (d) LC 4-1cr

The top and bottom static responses before and after the joint cut for LC 4-4 was similar to LC 4-1, with no change in linear behavior nor magnitude across the system.

The load versus rebar strains on the west side of the joints at midspan are shown in Figure 8.102 for LC 4-1 during Stage 8 and LC 4-1cr during Stage 9. Only minor strains were measured in the reinforcement in Joint 6-3 before and after the joint cut. A slight compressive strain response was measured in the reinforcement in Joint 3-8 and Joint 8-7 with 5 and 7 $\mu\epsilon$, respectively, during Stage 8 LC 4-1. This behavior remained the same after the joint cut during Stage 9 LC 4-1cr, indicating that the saw cut in the top of Joint 6-3 did not lead to additional engagement of the joint reinforcement. The same minimal strain response was observed in the joint reinforcement from the east side of the joints near midspan and the additional reinforcement along the length of the joints.

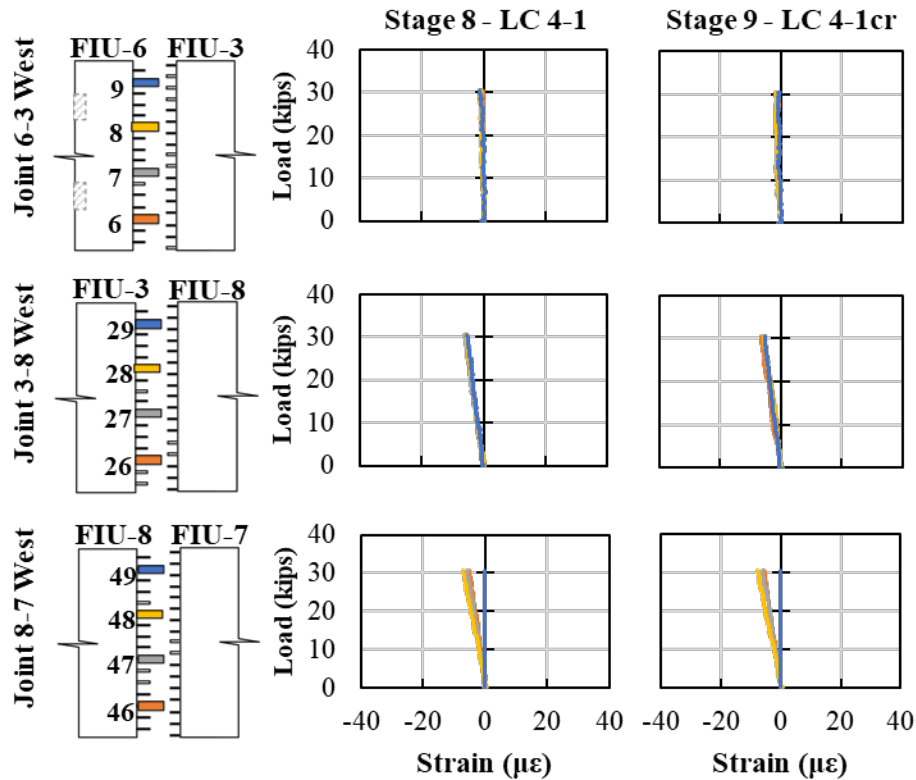


Figure 8.102: Load versus center west rebar strain for service load testing with LC 4-1 for Stage 8 and LC 4-1cr with Stage 9

The measured responses of the center transverse CSGs and CDTs at the top of the joints near midspan are shown in Figure 8.103 for LC 4-3 during Stage 8 and LC 4-3cr during Stage 9. When FIU-8 was loaded before the joint saw cut (Stage 8), compression strains developed on FIU-8 near the adjacent Joint 3-8 (CSG-T23) and Joint 8-7 (CSG-T31), while tension strains developed in the other regions across the width of the system, as shown in Figure 8.103 (a). There was a slight decrease in measured transverse compression strains in FIU-8 after the joint cut (Stage 9), with a decrease of about $5 \mu\epsilon$ near Joint 8-7 (CSG-T31) and $1 \mu\epsilon$ near Joint 3-8 (CSG-T23) as shown in Figure 8.103 (b).

Compression strains were measured across Joint 3-8 and tensile strains across Joint 6-3 and Joint 8-7 by the CDTs during Stage 8, as shown in Figure 8.103 (c). After the joint cut, top tensile strains in Joint 6-3 decreased from $11 \mu\epsilon$ to $6 \mu\epsilon$ in tension at 30 kips. Also, a minimal change in strain was observed after the strain response on top of Joint 8-7 slightly shifted from tension to compression at 30 kips, as shown in Figure 8.103 (d).

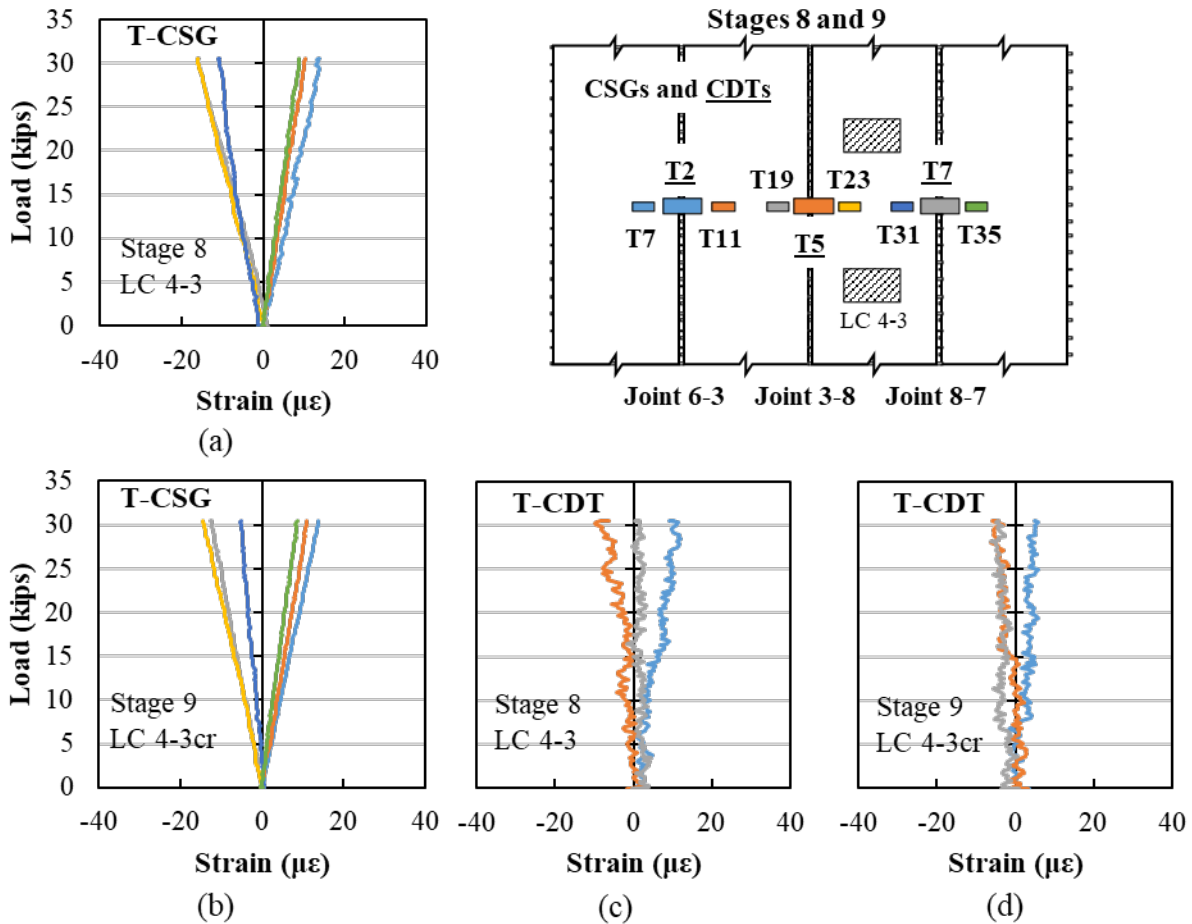


Figure 8.103: Load versus top transverse concrete strain for service load testing comparison between CSGs in Stage 8 (a) LC 4-3 and Stage 9 (b) LC 4-3cr, and CDTs in Stage 8 (c) LC 4-3 and Stage 9 (d) LC 4-3cr

The measured responses of the center transverse CSGs and CDTs at the bottom of the joints near midspan are shown in Figure 8.104 for LC 4-3 during Stage 8 and LC 4-3cr during Stage 9.

Transverse tension strains developed on the bottom precast section of FIU-8 near midspan as shown in Figure 8.104 (a), and transverse compression strains developed on the bottom precast sections of FIU-6, FIU-3, and FIU-7. Only a slight increase of $2 \mu\epsilon$ was measured in CSG-B23 during Stage 9 test, as shown in Figure 8.104 (b), and a minimal strain increase in compression of $1 \mu\epsilon$ measured in the other CSGs at 30 kips; these minimal strain changes did not represent a major change in the behavior of the system after the saw cut procedure.

A similar behavior was measured by the bottom CDTs at 30 kips. Compression strains were measured across Joint 6-3 before the joint cut by CDT-B2, and tensile strains across Joint 3-8 and Joint 8-7 by CDT-B5 and CDT-B7, as shown in Figure 8.104 (c). No noticeable change was observed in the same sensors after the joint cut was performed (Stage 9), as shown in Figure 8.104 (d).

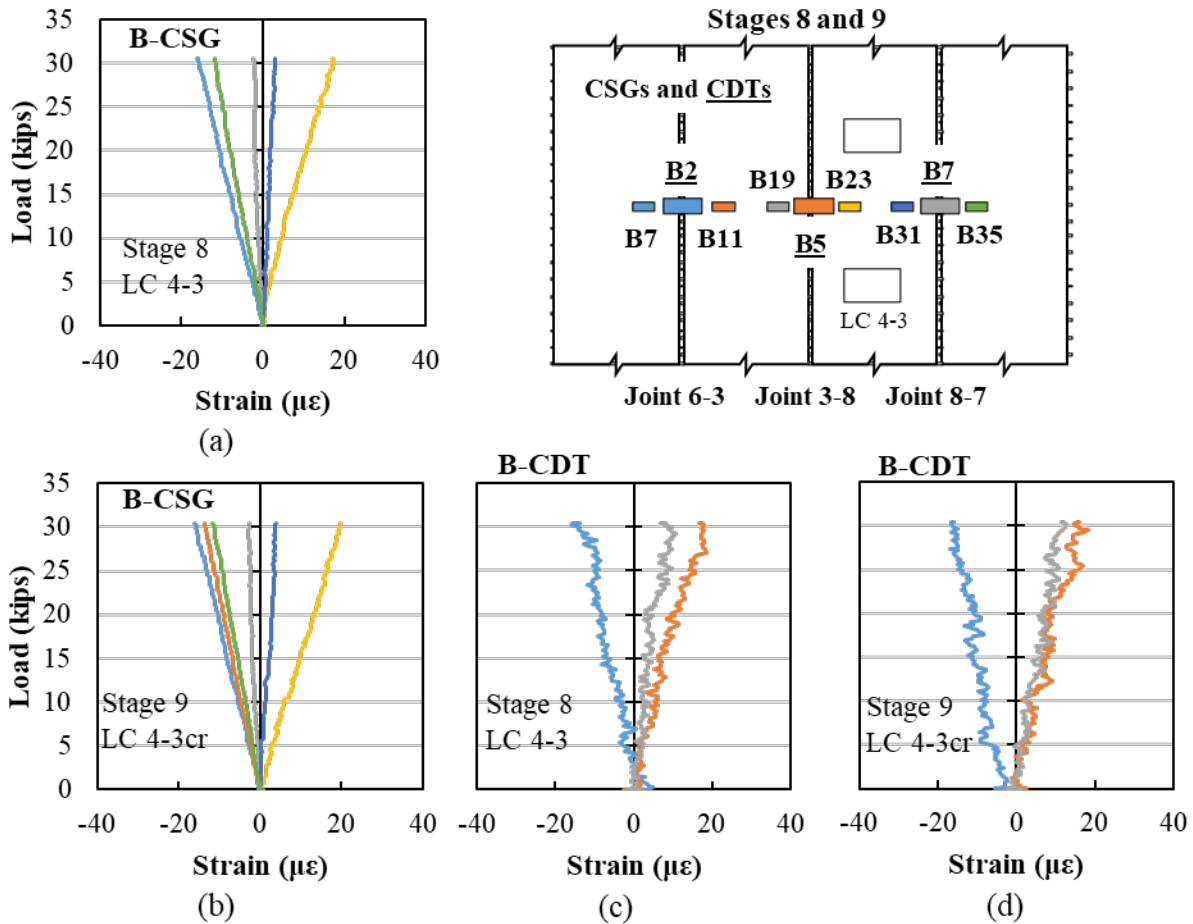


Figure 8.104: Load versus bottom transverse concrete strain for service load testing comparison between CSGs in Stage 8 (a) LC 4-3 and Stage 9 (b) LC 4-3cr, and CDTs in Stage 8 (c) LC 4-3 and Stage 9 (d) LC 4-3cr (CSG B11 malfunctioned on Stage 8)

The static response before joint cutting (LC 4-2 and LC 4-3) were similar to the static response after joint cutting (LC 4-2cr and LC 4-3cr), representing no significant strain change at 30 kips when interior beams were loaded.

The load versus rebar strains on the west side of joints at midspan are shown in Figure 8.105 for LC 4-3 during Stage 8 and LC 4-3cr during Stage 9. Minimal rebar engagement was measured before and after joint cut on Joint 8-7 and Joint 6-3 joints. Minimal tensile strains were measured in Joint 3-8 west side reinforcement, with no changes before and after the joint cut. This would also indicate that most load transfer was still occurring through the concrete-to-UHPC bond and joint shear key. The same minimal strains were observed on the east joint rebar near midspan and the remaining joint reinforcement along the length of the joints.

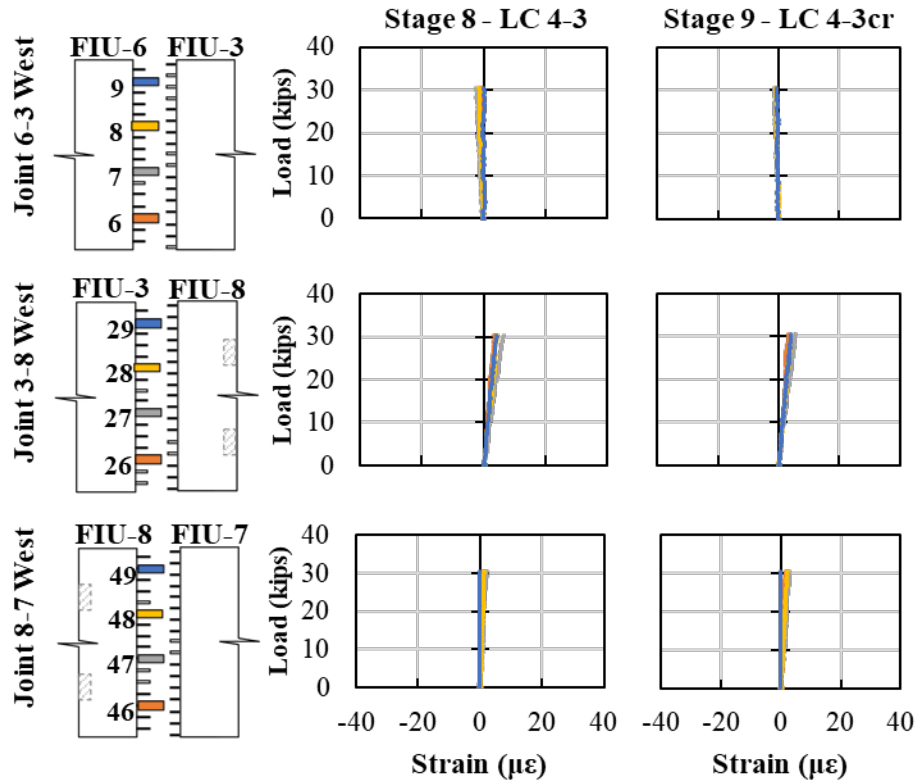


Figure 8.105: Load versus center west rebar strain for permit testing with LC 4-3 for Stage 8 and LC 4-3cr with Stage 9

8.8.5.4. Summary

The following conclusions and observations can be made on Stages 8 and 9 load configuration comparisons:

- Load versus deflection behavior remained the same before and after the joint cut.
- GDF remained similar with no signs of large redistribution of load caused by the joint cut.
- Load versus longitudinal and transverse strains behavior above and below the central superstructure area remained the same before and after the joint cut.
- Rebar strains were minimal before and after the joint cut, indicating that even damage to the top portion of the joint did not lead to engagement of the joint reinforcement.

No significant change in behavior was observed before and after the joint cutting procedure on Joint 6-3, which indicates that the system would perform well even if a longitudinal crack developed along the length of the system next to the joint.

8.9. FOUR-BEAM STRENGTH TESTING RESULTS

8.9.1. Testing Summary

The four-beam configuration with FIU-6/3/8/7 was tested using LC 4-5 for ultimate strength of the system. A summary of the predicted and experimental test results is shown in Table 8.26.

Table 8.26: Summary of predicted and measured results for four-beam specimen

Test ID	Hand Calculation		Software Analyses ¹			Experimental Tests		
	P_{cr} (kips)	P_{max} (kips)	P_{cr} (kips)	P_{max} (kips)	Δ at P_{max} (in)	P_{cr} ² (kips)	P_{max} (kips)	Δ at P_{max} (in)
LC 4-5 (Ultimate)	149.2	297.2	200.0	318.5	--	96.8	331.4	7.30

¹ This analysis had four loading stages: (1) FIU-6/7/8 with fully prestressing pattern and FIU-3 partially prestressed, (2) loading of FIU-3 without UHPC cast, (3) unloading of FIU-3 with UHPC cast, and (4) loading until failure

² First cracking occurred in FIU-3; cracking of the other three beams occurred between 129 kips and 140 kips

8.9.2. Strength Test Results (Stage 10, LC 4-5)

8.9.2.1. Overview

The load versus deflection response for the system under LC 4-5 is shown in Figure 8.106. The deflections shown account for the settlement of the supports. There was a minimal differential displacement between the four beams (about 2 percent), which suggests that the load was distributed relatively equally on the four beams. The overall load-deflection response began to become non-linear after 130 kips, between the first cracking load in FIU-3 (96.8 kips) and in the other three beams (between 129 and 140 kips). The displacement likely exceeded gauge limits for FIU-3, FIU-7, and FIU-8.

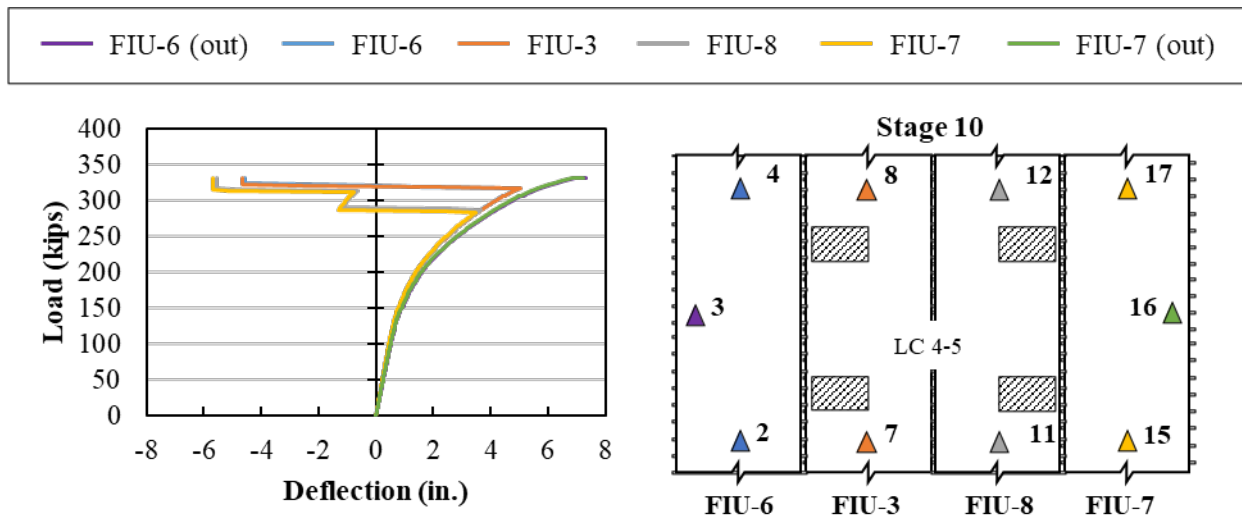


Figure 8.106: Load versus average midspan deflection for ultimate strength testing with LC 4-5

Observations from the service load testing are summarized by load step in Table 8.27 and observed cracking is shown in Figure 8.107. No cracking was visually observed on the top or bottom of the system from Steps 1 through 4, as shown in Figure 8.107 (a). A drop in the longitudinal strain was observed on the bottom of FIU-3 (CSG-B15) at 96.8 kips. Significant changes in the bottom CSGs occurred between 129 and 140 kips for the other three beams (FIU-6, FIU-7, and FIU-8). Cracking was not detected through visual inspection until 150 kips. When the loading was stopped at 150 kips, transverse cracks were visually documented crossing the entire system width underneath, as shown in Figure 8.107 (b). No signs of joint material debonding nor distress was observed during these initial load stops.

Table 8.27: Observations during ultimate strength testing of FIU-3/6/8/7

Step	Load Ranges	Observations	Figure
1	0 k – 30 k	No cracks were observed	Figure 8.107a
2	30 k – 60 k	No cracks were observed.	Figure 8.107a
3	60 k – 90 k	No cracks were observed.	Figure 8.107a
4	90 k – 120 k	No cracks were observed. Longitudinal strains showed signs of cracking on FIU-3 at 96.8 kips (CSG-B15).	Figure 8.107a
5	120 k – 150 k	Transverse cracks were visually observed across the width of the entire system at 150 kips. Longitudinal strains showed signs of cracking between 129 and 140 kips in the bottom CSGs. CDTs were removed from the system at 150 kips.	Figure 8.107b
6	Load until failure	Failure load was observed at 331.4 kips	-

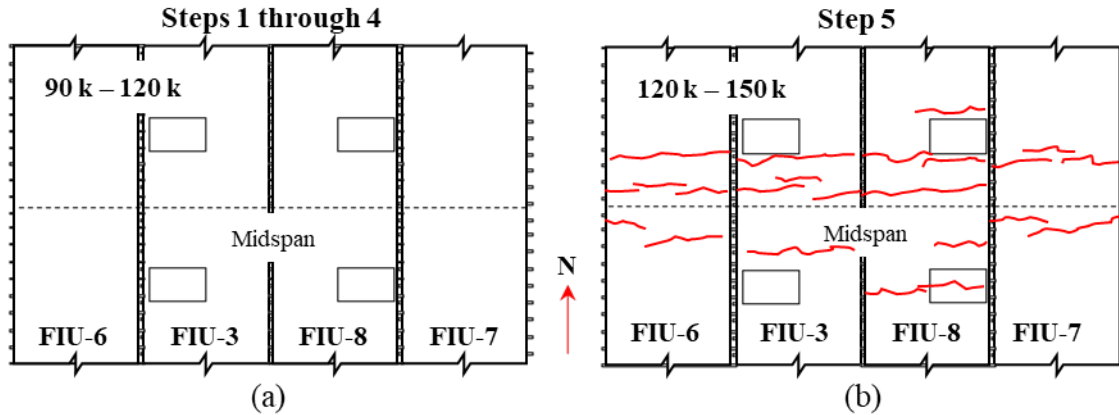


Figure 8.107: Bottom crack pattern at midspan for ultimate strength testing with LC 4-5 for FIU-6/3/8/7 for: (a) Steps 1 through 4 and (b) Step 5

Failure of the four-beam system was caused by crushing of the concrete across the width of the system at a load of 331.4 kips and deflection of 7.30 inches. The crushing of the concrete began on top of FIU-7, shown in Figure 8.108 (a), and then continued across the width of the system, shown in Figure 8.108 (b).

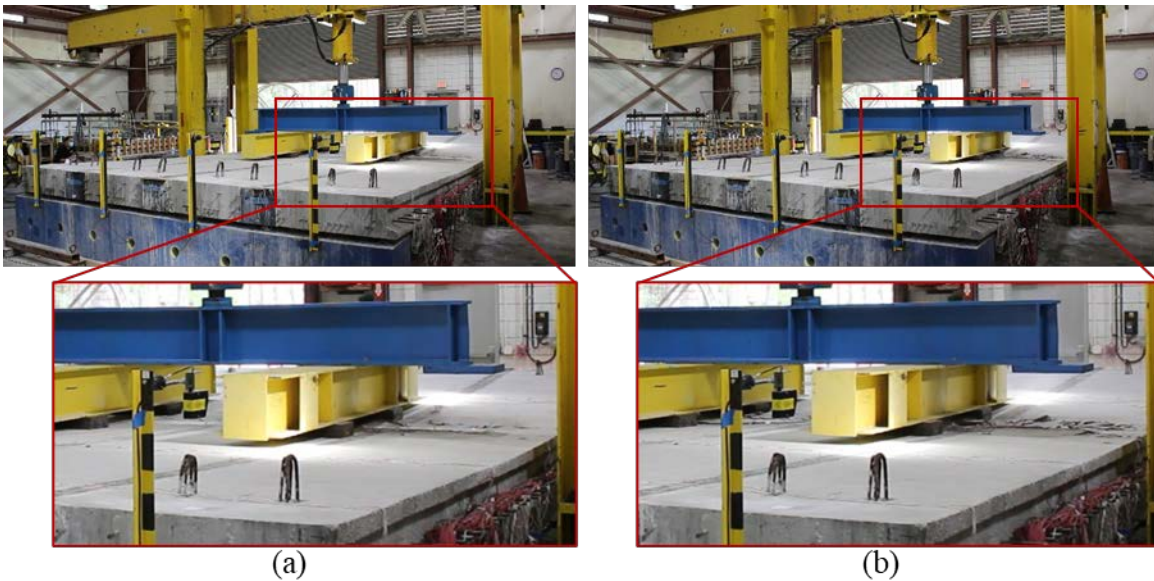


Figure 8.108: Photographs from failure (331.4 kips) at (a) first crushing in FIU-7 and (b) crushing of concrete continuing across the width of the superstructure

Additional photographs of the system after failure are provided in Figure 8.109. Crushing of the concrete primarily occurred in the precast sections, but there were signs of some crushing of the UHPC in the joints.

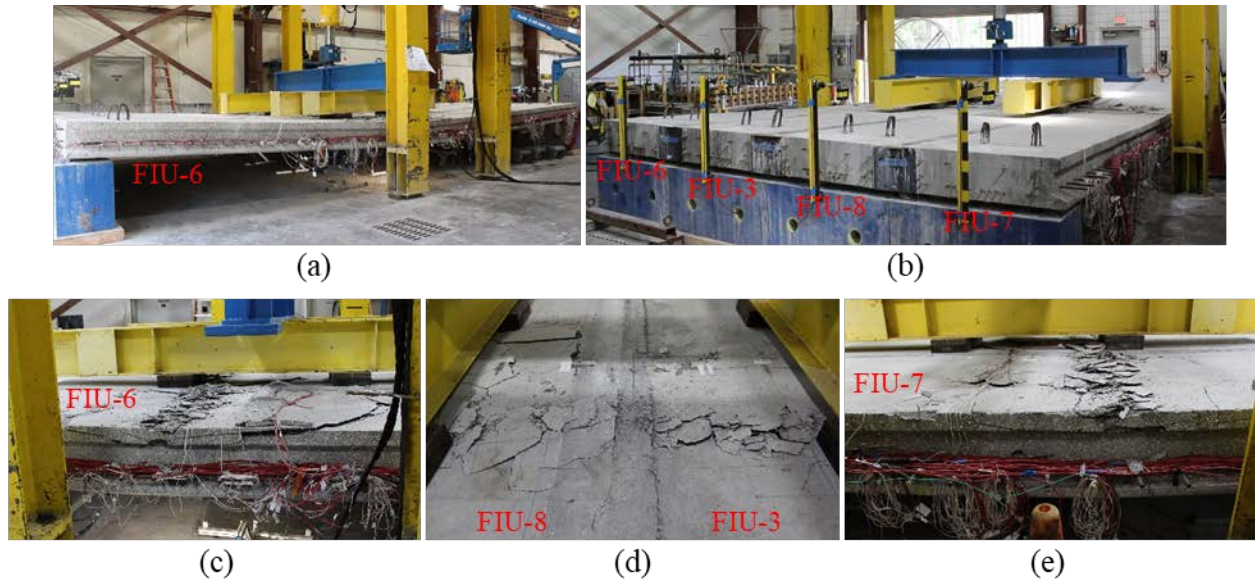


Figure 8.109: Additional photographs after failure of the four-beam system: (a) overview from the north-east, (b) overview from the south-west, (c) FIU-6 at midspan, (d) top of FIU-8 and FIU-3 at midspan, and (e) FIU-7 at midspan

8.9.2.2. Longitudinal Behavior

The measured responses from the longitudinal CSGs are shown in Figure 8.110. The measured longitudinal strains on the bottom of the beams at midspan were used to determine the cracking load for each of the beams. Cracking is signified by a sudden increase or decrease in the measured longitudinal strain; an increase represents a crack extending through the CSG, and a decrease represents a crack extending across the section width adjacent to the CSG. First cracking was observed in FIU-3 (CSG-B15) at 96.8 kips. Cracking of the other beams occurred at a higher load, between 129 and 140 kips. The locked-in stresses in FIU-3 from the camber leveling procedure led to a cracking load that was 27.7 percent less than the average cracking load in the other three beams and 35.1 percent less than the estimated cracking load (149.2 kips). The locked-in stresses also led to the cracking load of the other three beams (FIU-6, FIU-7, and FIU-8) being on average 10.2 percent less than the estimated cracking load (149.2 kips); this is likely due to stresses redistributing to the uncracked beams after cracking in FIU-3 occurs. This could affect the design and load rating for service limit states.

The measured cracking loads and measured and estimated strains at cracking for each beam in the system are summarized in Table 8.28. The measured tensile strains at cracking are much higher than the tensile strength of concrete, which is because the longitudinal CSGs were installed after the precompression strains caused by prestressing occurred. The estimated strains are included in Table 8.28, but the estimate overestimates the initial compressive strains before ultimate testing begins.

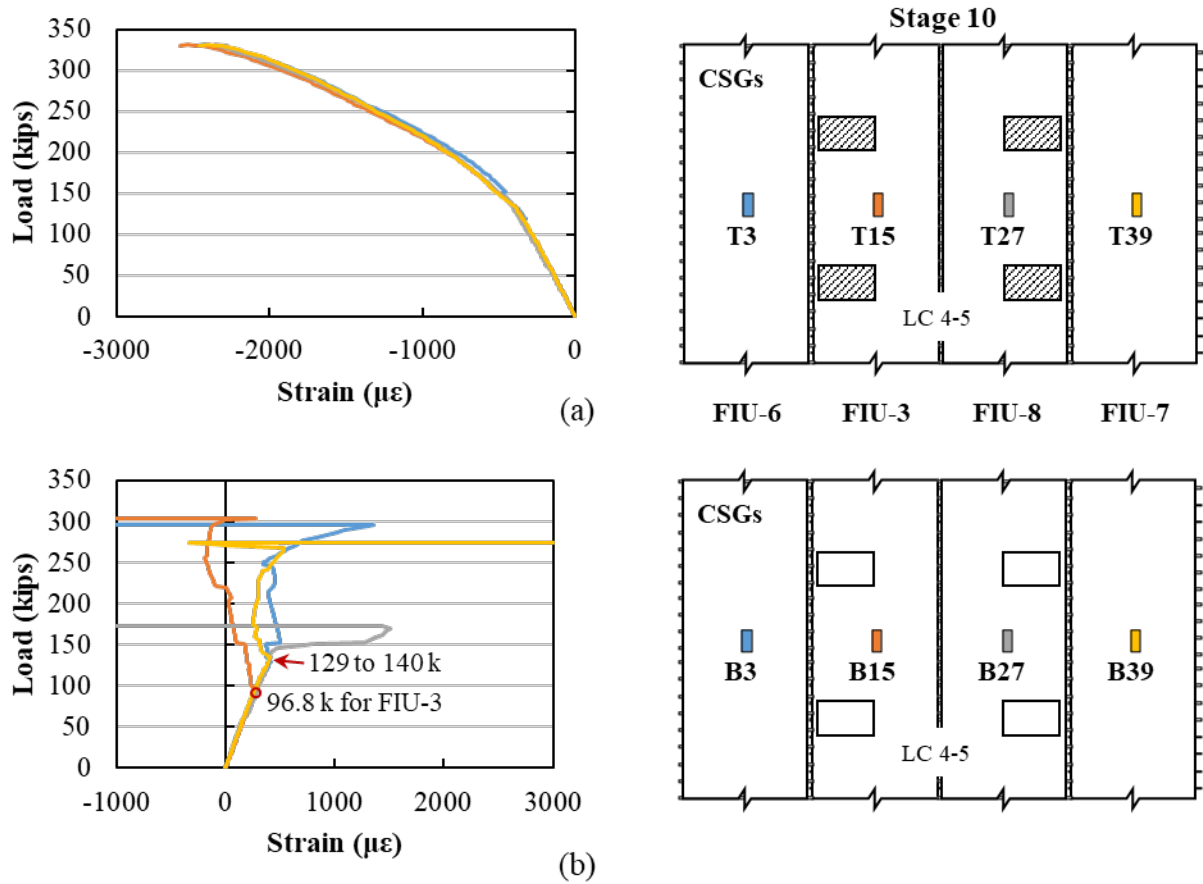


Figure 8.110: Load versus longitudinal concrete strain for ultimate strength testing with LC 4-5 for (a) top and (b) bottom of beams in the midspan section of FIU-6/3/8/7

Table 8.28: Measured cracking load and associated bottom fiber longitudinal strains

Beam	FIU-6	FIU-3	FIU-8	FIU-7
CSG	B3	B15	B27	B39
Estimated Cracking Load ¹	149.2 kips	149.2 kips	149.2 kips	149.2 kips
Measured Cracking Load	129 kips	96.8 kips	140 kips	133 kips
Measured Strain at Cracking (με)	416.8	298.5	416.8	402.4
Estimated Initial Strain (με) ²	-494.7	-301.3	-485.9	-480.8
Estimated Strain at Cracking (με) ³	-77.9	-2.8	-69.1	-78.4

¹ cracking load estimated based on hand calculations for individual beam sections

² estimated initial strain from camber leveling procedure discussed in §8.7.3

³ combination of measured strain and estimated initial strain

Top longitudinal strain remained similar across the width of the superstructure until failure, as shown in Figure 8.110 (a). The top fiber strains at the time of failure are summarized in Table 8.29. The measured top fiber strain was higher in FIU-3 (-2,535 $\mu\epsilon$) than the other three beams (average of -2,394 $\mu\epsilon$) at the time of failure. FIU-3 likely began to behave non-linearly before the other beams, due to the locked in stresses from the camber leveling process, which could have resulted in the 5.9 percent higher compressive strain at ultimate. The failure of the four-beam system was triggered by crushing of the concrete in the top fiber near midspan, so the actual compressive strains were likely higher than those estimated in Table 8.29.

Table 8.29: Measured and estimated top fiber longitudinal strains at failure

Beam	FIU-6	FIU-3	FIU-8	FIU-7
CSG	T3	T15	T27	T39
Measured Strain at Ultimate ($\mu\epsilon$)	-2425	-2535	-2355	-2402
Estimated Initial Strain ($\mu\epsilon$) ¹	-37.4	-131.6	-45.3	-47.4
Estimated Strain at Ultimate ($\mu\epsilon$) ²	-2462	-2667	-2400	-2449

¹ estimated initial strain from camber leveling procedure discussed in §8.7.3

² combination of measured strain and estimated initial strain

8.9.2.3. Joint Behavior

The average strain across the joints measured using the CDTs on the top and bottom of the system are shown in Figure 8.111 and Figure 8.112, respectively. The CDTs were removed from the system at a load of 150 kips to prevent damage of the gauges during testing.

Transverse compression developed across the top of Joint 6-3 along the length of the joint with highest strains of around -48 $\mu\epsilon$ at 150 kips. Small transverse compression strains also developed along the length of Joint 3-8. Small transverse tension strain developed along the length of Joint 8-7 with the highest measured tensile strains at midspan (CDT-T7) of 27 $\mu\epsilon$. The loading was intended to be symmetrical on the system; the unsymmetrical response from the CDTs may have been due to the locked in stresses in FIU-3 from camber leveling.

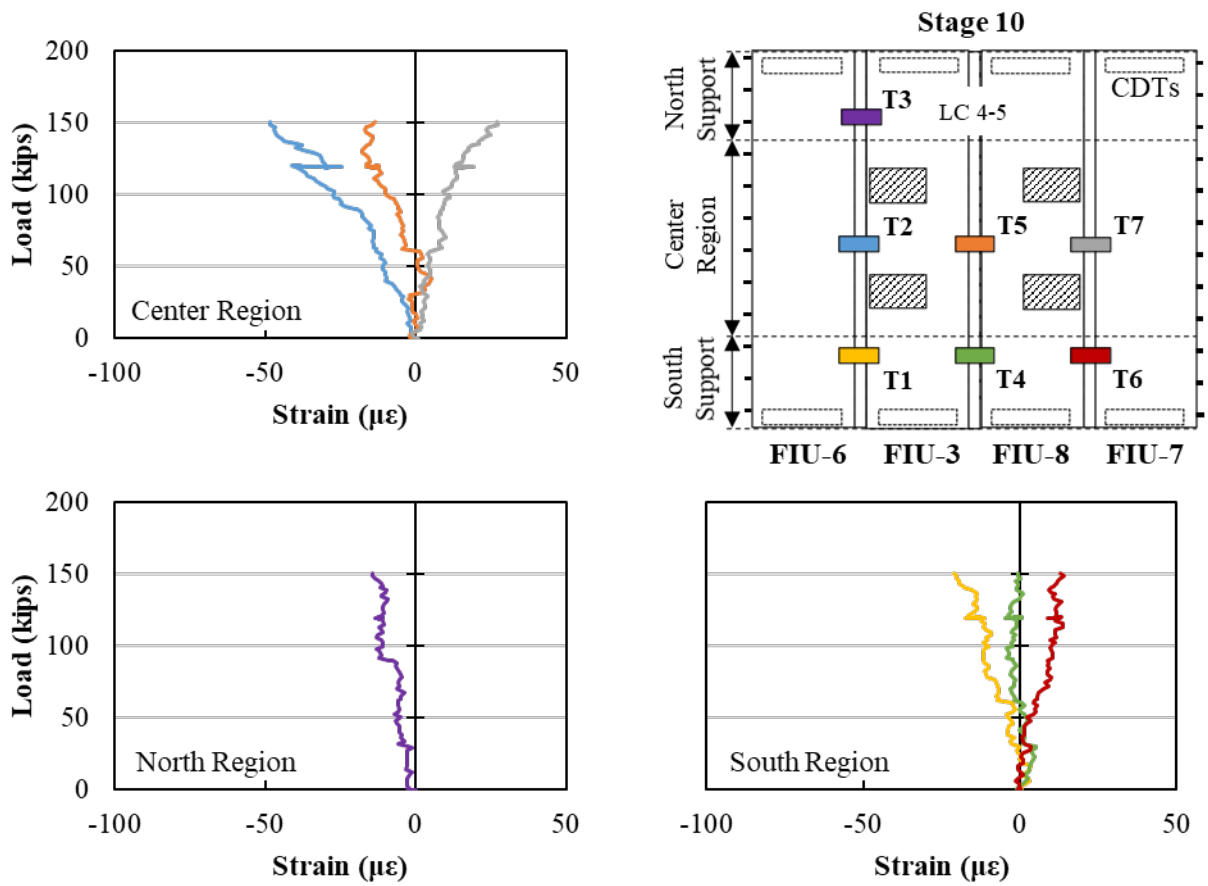


Figure 8.111: Load versus average strain across top of joints for ultimate strength testing with LC 4-5 for FIU-6/3/8/7

Transverse tensile strains developed across the bottom of the joints in the center region, shown in Figure 8.112, with the largest measured tensile strain of 103 $\mu\epsilon$ (CDT-T2) at 150 kips across Joint 6-3. The tensile strains decreased for Joint 3-8 (51.3 $\mu\epsilon$) and Joint 8-7 (10.5 $\mu\epsilon$). This unsymmetrical behavior is similar to top of the joints and may also be due to the locked-in stresses from the camber-leveling procedure.

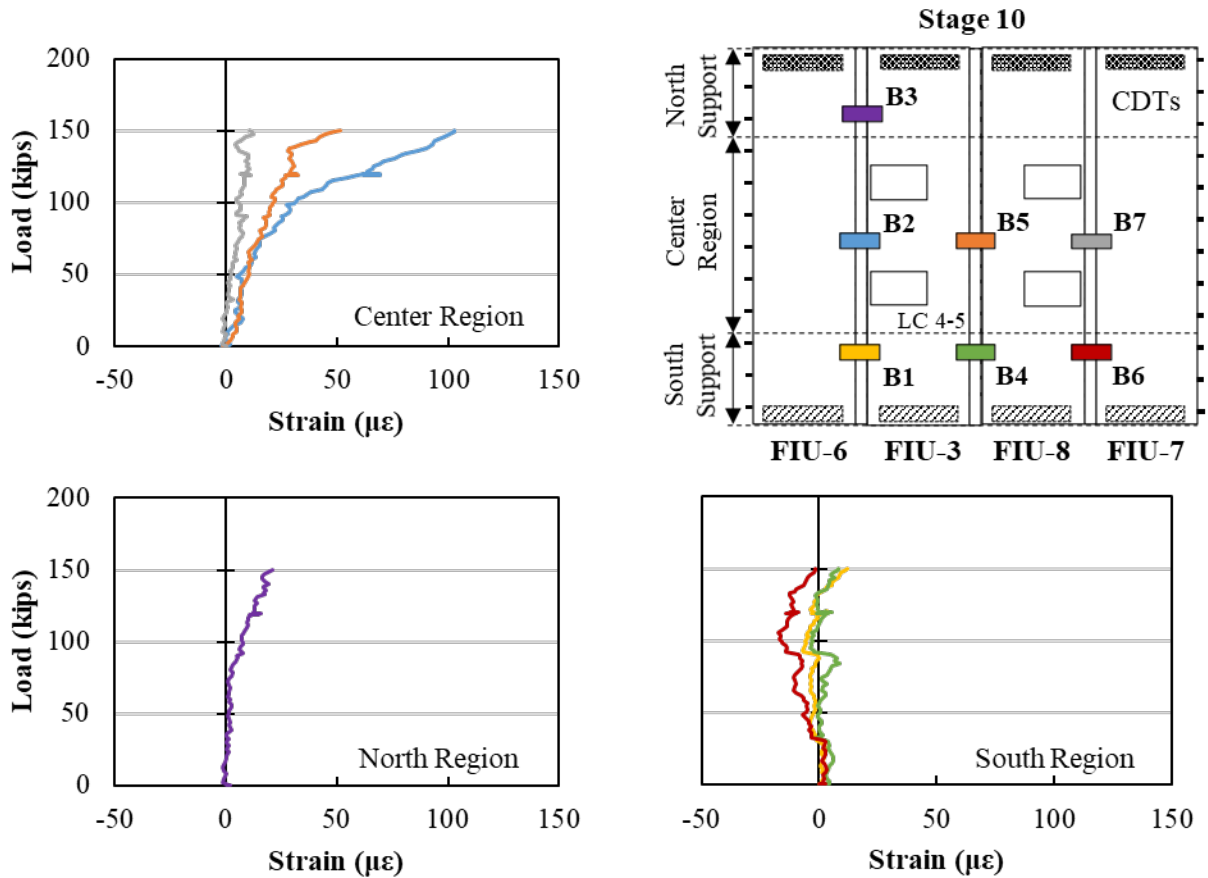


Figure 8.112: Load versus average strain across top of joints for ultimate strength testing with LC 4-5 for FIU-6/3/8/7

The measured responses from the transverse CSGs at the center region near midspan are shown in Figure 8.113. Transverse compression strains developed on the top of FIU-3 (in CSG-T11 and CSG-T19), as shown in Figure 8.113 (a). Transverse tension strains developed across the rest of the width with a maximum transverse tension of $101.6 \mu\epsilon$ at 150 kips in CSG-T35. Transverse tension developed on the bottom of the system near the center, see CSG-B19 and CSG-B23 in Figure 8.113 (b). Transverse compression was measured in the other gauges at midspan on the bottom of the system. The transverse strains measured by many of the CSGs in the system began to decrease in magnitude after approximately 150 kips and continued to decrease as the load approached the failure load of 331.4 kips.

A jump in strain was measured in most of the CSGs at 150 kips. The jump in strains were higher for the gauges on top of the system than on the bottom of the system. The jump in strains were generally minor, less than $10 \mu\epsilon$, but were large for some of the CSGs. The largest jump was negative $3,700 \mu\epsilon$ in CSG-T35. Larger jumps in the strain were filtered out of the data presented in this section.

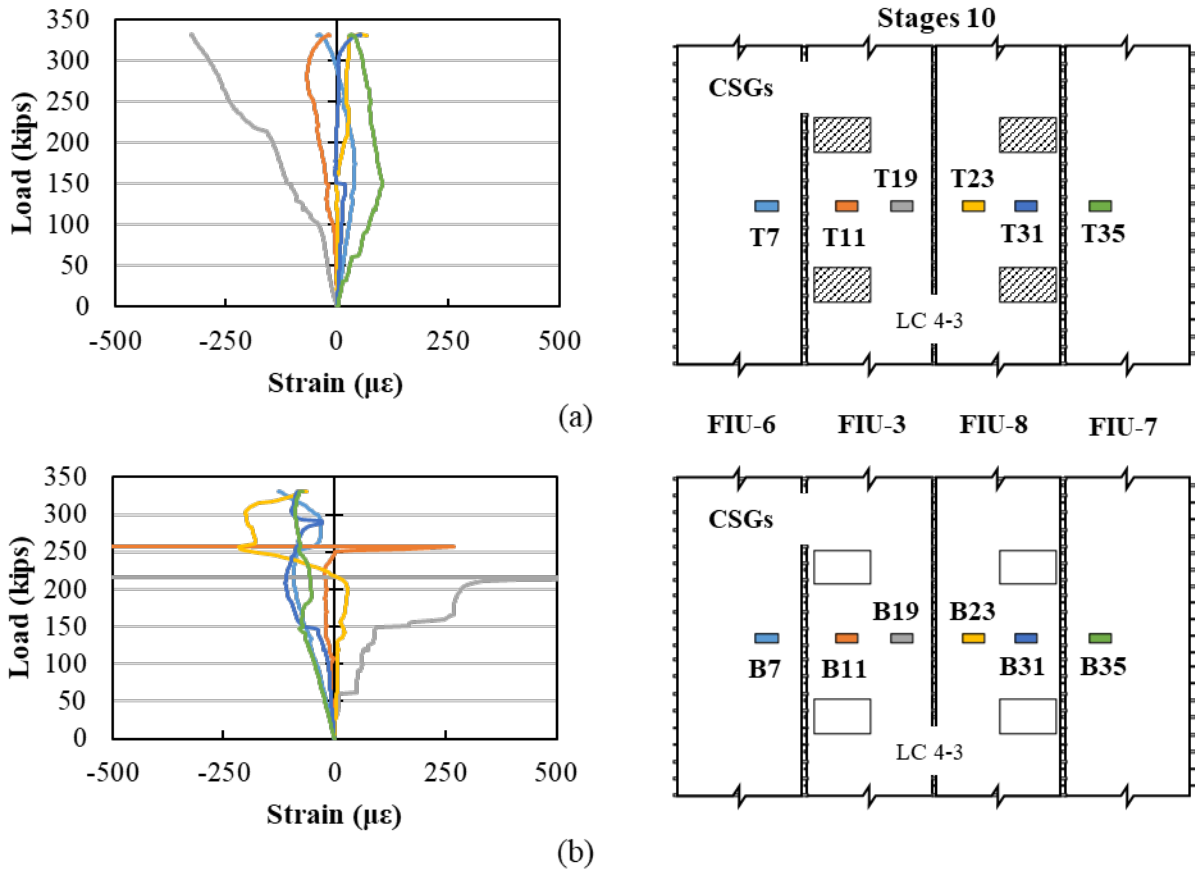


Figure 8.113: Load versus transverse concrete strain for ultimate strength testing with LC 4-5 for (a) top and (b) bottom of beams in the midspan section of FIU-6/3/8/7 (B11 and B19 malfunctioned)

The measured responses for the RSGs on the joint reinforcement extending from the west side of Joint 6-3, Joint 3-8, and Joint 8-7 at the midspan section of the system are shown in Figure 8.114. Large tensile strains developed in the joint reinforcement with the rebar starting to pick up significant strain after approximately 150 kips. This increase in strain may suggest that there was cracking developing at the UHPC-to-precast bond or near the joint matrix. Maximum strains were measured in the middle reinforcement bars in all three joints: 736 $\mu\epsilon$ for Joint 6-3 (RSG-7), 680 $\mu\epsilon$ for Joint 3-8 (RSG-27), and 498 $\mu\epsilon$ for Joint 8-7 (RSG-48). The measured strains remained well below the yield strain for the joint reinforcement bars in all cases.

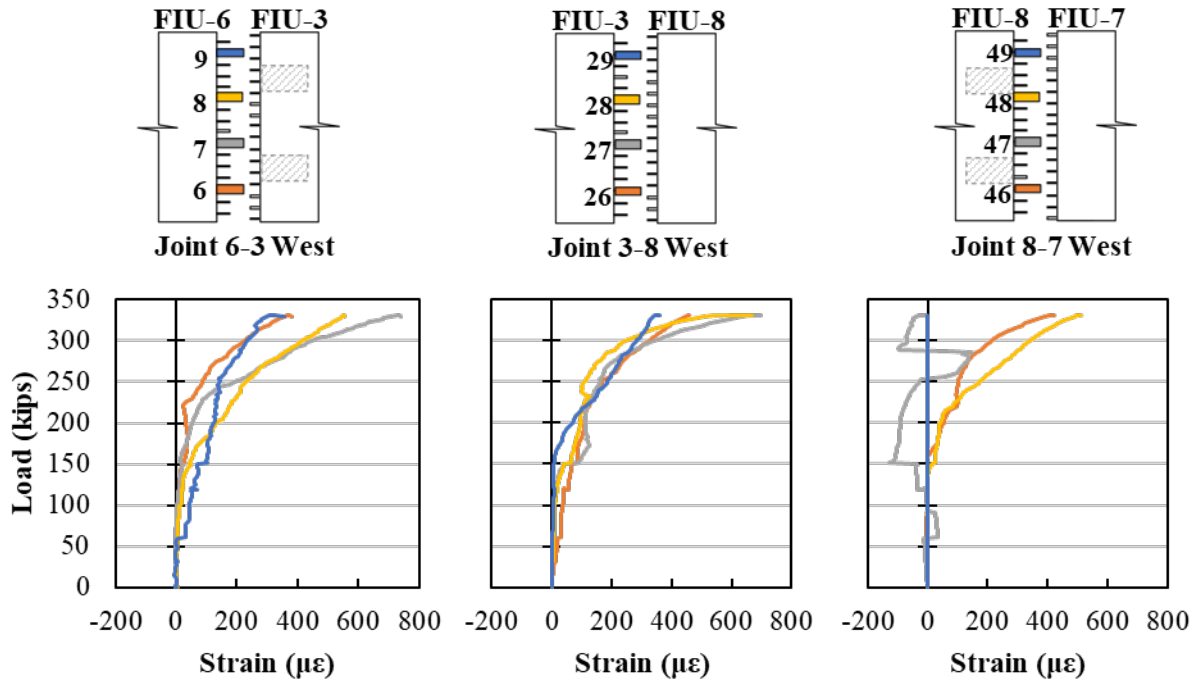


Figure 8.114: Load versus strain for ultimate strength testing with LC 4-5 for west reinforcement of FIU 6-3, FIU 3-8, and FIU 8-7 joints at midspan section of the system

No joint distress or UHPC-to-precast bond rupture was observed from above the specimen during testing or on top of the specimen after testing. Crushing of the concrete at failure of the system extended across the complete width of the four precast beams and primarily across the UHPC joints, as shown in Figure 8.115. The top ledge of the precast concrete crushed on both sides of the superstructure as shown in Figure 8.115 (a) for FIU-6 and Figure 8.115 (b) for FIU-7. In both regions, the crushing of the concrete was located directly above the cracks on the bottom of the system marked earlier in the test, as shown in Figure 8.115 (c) for FIU-6 and Figure 8.115 (d) for FIU-7.

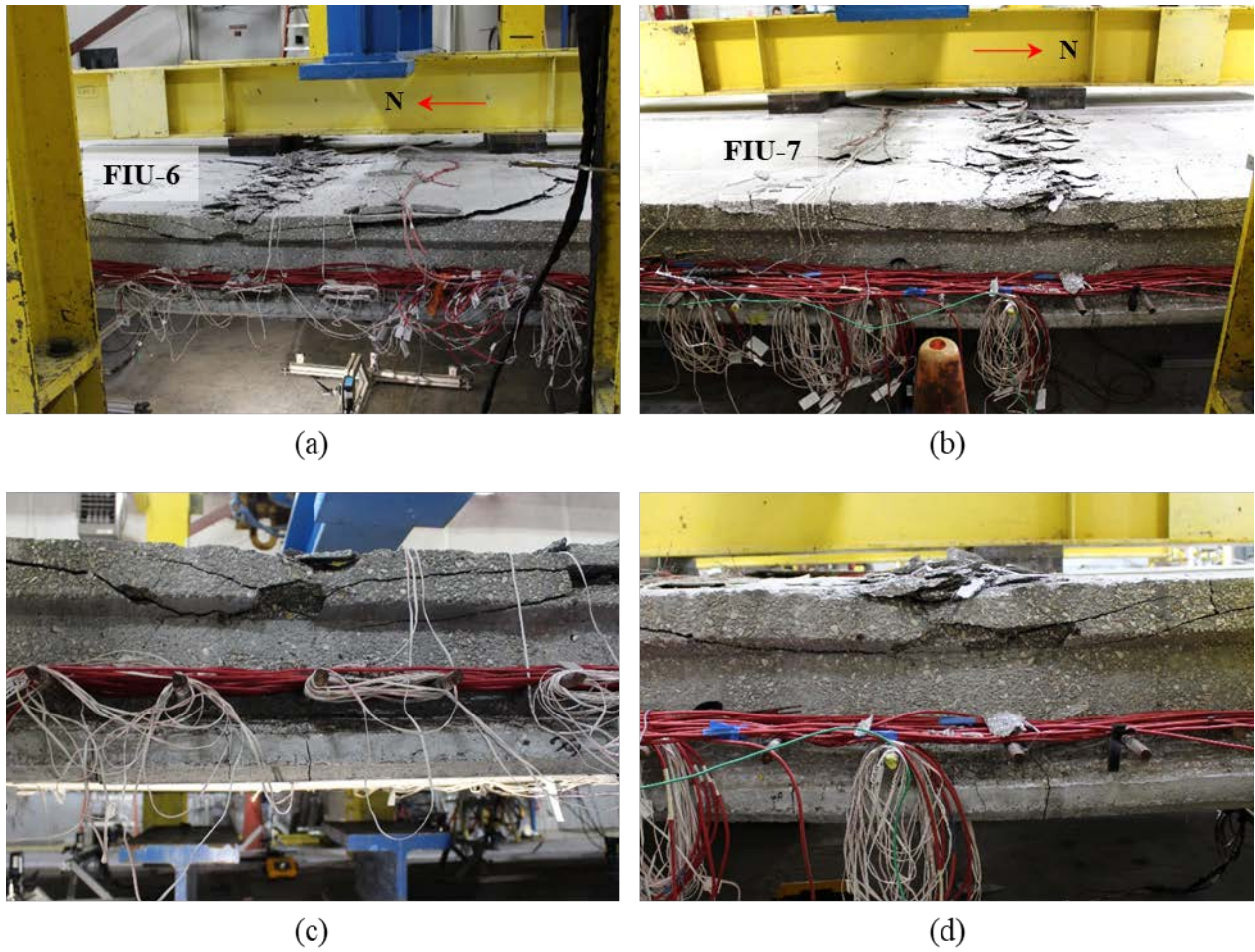


Figure 8.115: Crushing of FIU-6/3/8/7 concrete at failure for LC 4-5: (a) overview and (b) crushing of precast section and UHPC joint (FIU 6-3)

Three concrete cores were taken from the edge of each joint, for a total of nine cores, after the failure of the system, as shown in Figure 8.116. The locations were selected such that the UHPC-to-precast boundary could be seen to locate signs of debonding cracks.

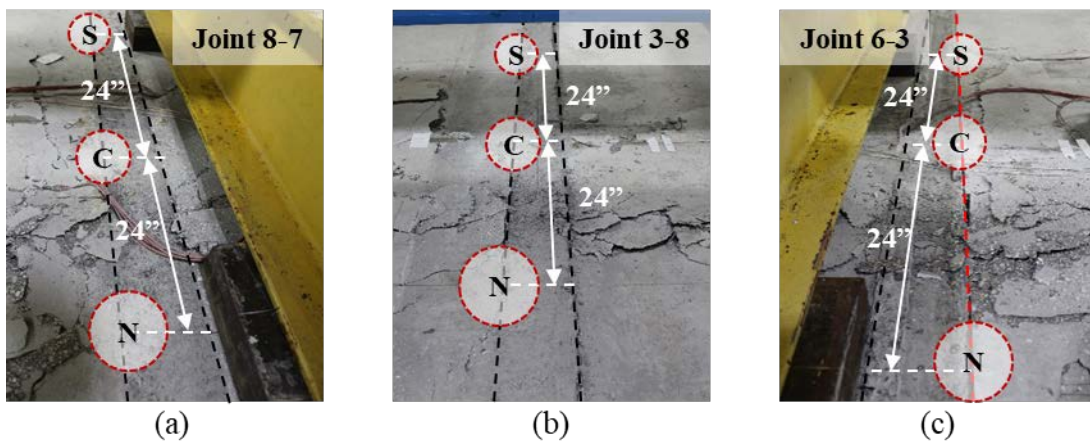


Figure 8.116: South, center, and north core locations on: (a) Joint 6-3, (b) Joint 3-8, and (c) Joint 8-7

The extracted concrete cores at the north, center, and south locations along the length of each joint are shown in Figure 8.117. There was still good bond observed between the precast concrete and UHPC in joint interfaces above the bottom flange. Joint 6-3 showed minor debonding cracks only above the bottom lip at the north location, as shown in Figure 8.117 (a). Also, there were no signs of debonding along the top ledge outside of where the saw cut was performed. Joint 3-8 showed cracks in the center region that developed from the broken bottom ledge at the precast section adjacent to the boundary, and cracks developed in the south region at the top precast section adjacent to the boundary as shown in Figure 8.117 (b). Joint 8-7 was the only joint with signs of cracking in the UHPC matrix, running from the bottom UHPC section up until the joint reinforcement, as shown in Figure 8.117 (c).

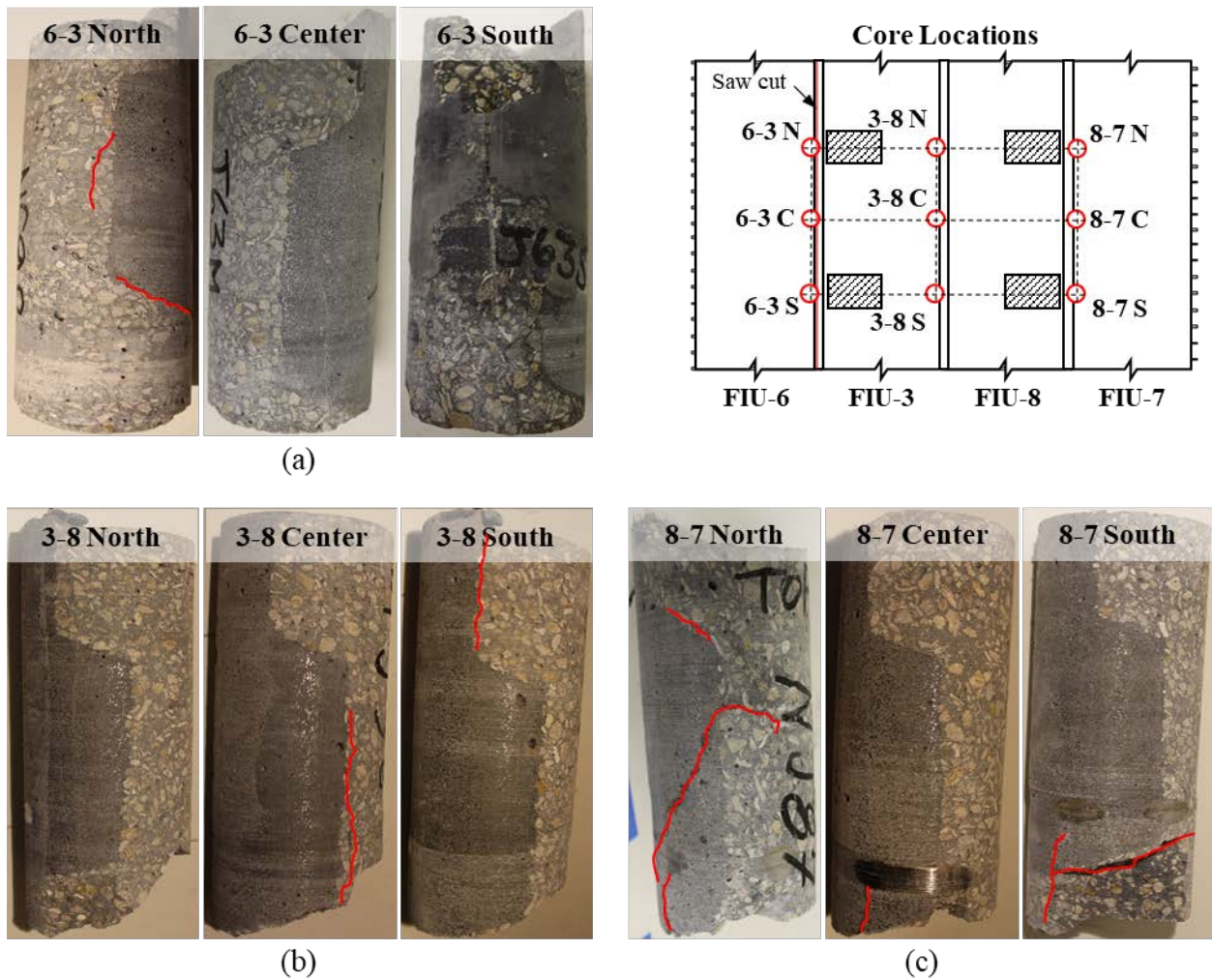


Figure 8.117: FIU-6/3/8/7 joints edge cores locations and crack patterns: (a) Joint 6-3, (b) Joint 3-8, and (c) Joint 8-7 cores

8.9.2.4. Summary

The following conclusions and observations can be made based on the ultimate strength testing of FIU-6/3/8/7:

- The additional stresses in the system from the camber leveling procedure likely did not influence the ultimate strength of the system. The total capacity of the system was estimated accurately and conservatively using conventional compression block approximations and a more detailed nonlinear FEA. The compression block estimate was within 10.3 percent (297.2 kips estimated compared with 331.4 kips measured), and the FEA estimate was within 3.9 percent (318.5 kips estimated compared with 331.4 kips measured).
- The locked-in stresses from the camber leveling procedure decreased the cracking load in all the beams in the system. The measured cracking load in FIU-3 was 27.7 percent less than the cracking load of the other three beams and 35.1 percent less than the estimated cracking load. The average cracking load of the other three beams was 10.2 percent less than the estimated cracking load.
- The joints performed well during ultimate strength testing. No joint debonding or distress was observed in the joint regions at ultimate load.
- The concrete in the compression block of the system crushed across the entire width (primarily including the UHPC joints), which would indicate good bond between the UHPC in the joints and the precast concrete.
- Good load transfer was observed between the beams with only minor differences in deflection of about two percent.

In general, the system behaved well during ultimate strength testing.

8.10. CONCLUSIONS AND RECOMMENDATIONS

Service, fatigue, and ultimate strength testing were performed on a four-beam system (FIU-6/3/8/7). The following conclusions were made based on these four-beam system tests.

- The camber leveling procedure introduced additional longitudinal tensile stresses in the bottom of FIU-3, which led to a lower cracking load for the beam (35.1 percent less than estimated). The load from the cracked FIU-3 redistributed to the other three beams, which led to a lower cracking load for these beams as well (10.2 percent less than estimated). This could affect the design and load rating for service limit states.
- The camber leveling procedure introduced minor transverse strains (less than 20 $\mu\epsilon$ tension and less than 10 $\mu\epsilon$ tension) across the precast sections and joints. These locked-in transverse strains did not lead to any adverse joint behavior during any of the service, fatigue, or ultimate strength testing.
- Girder distribution factors (GDFs) were found using longitudinal strain on the top and bottom of the beams and the midspan deflection. GDFs were not influenced by the differential camber and camber leveling procedure performed on FIU-3; symmetrical behavior of the system was observed during all testing stages. GDFs were less than those estimated using AASHTO LRFD.

- The joints performed well during service load, fatigue, and ultimate strength testing. No joint debonding or distress was observed in the joint regions during any of the service, fatigue, and ultimate load testing. The concrete in the compression block crushed across the entire width of the system (including the UHPC joint). Additionally, the joint successfully transferred stress between beams. There were no signs of bond deterioration between the joint reinforcement and UHPC in the joints during any of the fatigue, service, or strength testing.

The modified FSB system performed well during all the service, fatigue, and ultimate load testing on the four-beam system.

9. SIMPLE FOR DEAD LOAD AND CONTINUOUS FOR LIVE LOAD DESIGN CONCEPT FOR MODIFIED FSB

9.1. INTRODUCTION

The simple for dead load and continuous for live load (SDCL) concept has been used in the bridge industry for the past few decades. SDCL can help to create a more durable structure, by eliminating joints, and can allow for slightly longer spans and smaller deflections, by making adjacent spans continuous.

This chapter includes a background on the SDCL concept, proposed SDCL design integrated with the modified Florida Slab Beam with ultra-high performance concrete (UHPC) joints, and results from numerical analyses on the developed joint design.

9.1.1. Background

Multi-span bridges can be designed and constructed as simple spans for both dead loads and live loads. While designing bridges in such a fashion is simple, it leads to a joint between spans, which can lead to joint leakage and deterioration of the ends of beams and substructure elements. Designing multi-span bridges as simple spans is also not as efficient as designing them as continuous; higher overall moments and increased deflections occur in the simple span case compared to continuous spans, as shown in Figure 9.1 comparing the moment diagrams and maximum deflections for a two-span structure.

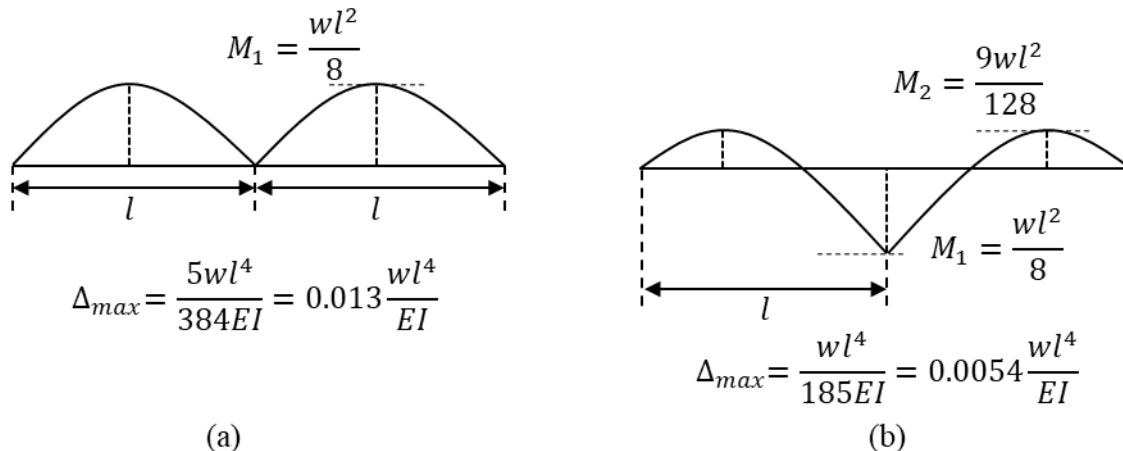


Figure 9.1: Moment diagram and maximum deflections for two-span structures that are: (a) simply-supported and (b) continuous

The region over the support must be designed for negative moment when adjacent spans are made continuous, as shown in Figure 9.1 (b). Negative moment design requires the placement of tensile reinforcement in the top of the superstructure elements. The deck reinforcement in composite members is commonly used as the negative moment reinforcement, but this reinforcement will only make the superstructure behave continuous for loads applied after the deck is cast. This has led to the SDCL concept. In SDCL, non-composite, simply supported beams are designed to support their self-weight and the dead loads from the deck and

construction equipment. Adjacent spans are made continuous during the casting of the deck, so the continuous, composite beams are designed to resist the live loads.

The SDCL concept for prestressed concrete bridges is nearly as old as the US prestressed industry. Freyermuth [93] was an early researcher and designer who saw the advantages of the SDCL concept in 1969. He noticed that designing a continuous structure would (1) eliminate maintenance costs associated with joint leakage between spans, (2) improve the appearance of the structure (as continuous spans would allow for shallower super-structures), (3) improve the efficiency and thus the overall economy of the bridge, and (4) decrease the demand at midspan imposed by traffic loads.

9.1.2. Construction Sequence

According to Nawy [94], there are two different ways to achieve continuity in concrete bridges:

1. *Monolithic Continuity*: All spans are cast and prestressed continuously at the site generally utilizing post-tensioning.
2. *Non-Monolithic Continuity*: Prestressed, precast members are used as simple supported beams and later made continuous at the site by casting the connection over the interior supports. This connection between two adjacent spans includes negative moment reinforcement, such as post-tensioning or mild reinforcement [94].

The construction sequence using the non-monolithic SDCL concept is shown in Figure 9.2. First, girders are placed and properly braced for each span, as shown in Figure 9.2 (a). These girders must have shear studs or extended stirrups to ensure composite behavior with the deck and often have some kind of reinforcement extending from the ends to improve the behavior of the connection between spans. Next, formwork, stay-in-place metal forms, partial-depth panels, or full-depth panels are installed, and all other necessary joint and deck reinforcement is placed, as shown in Figure 9.2 (b). Finally, the bridge deck and the joint region between spans are cast, Figure 9.2 (c). This process allows all future loads to be carried by the continuous, composite members. The most challenging aspect of the design and construction of these systems is the detailing of the joint regions between adjacent spans, which will be discussed further in the future sections.

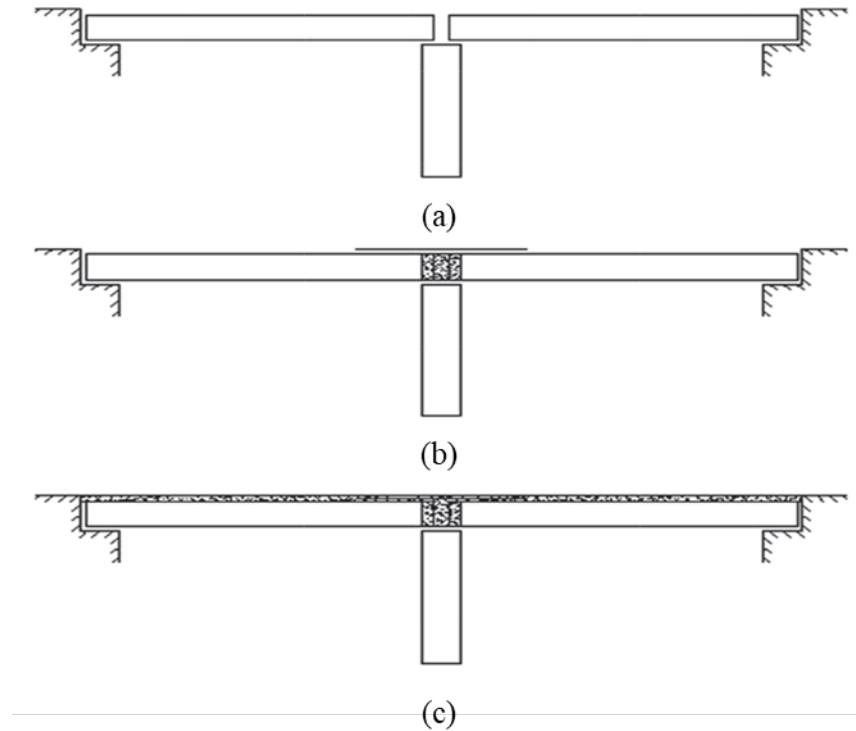


Figure 9.2: Construction sequence for SDCL bridge system [95] (modified from Freyermuth [93])

The distribution of moments before and after continuity is established as shown in Figure 9.3. For prestressed members, when the beams are initially shipped to the site and placed in position, they carry their self-weight and the prestressing force as simply-supported beams, as shown in Figure 9.3 (a). The beam must then carry the weight of the deck and the required construction equipment as a simply-supported beam, as shown in Figure 9.3 (b). The casting and hardening of the deck and joint then make the adjacent spans continuous, which allows all future loads and time effects to be carried by the composite, continuous members as shown in Figure 9.3 (c).

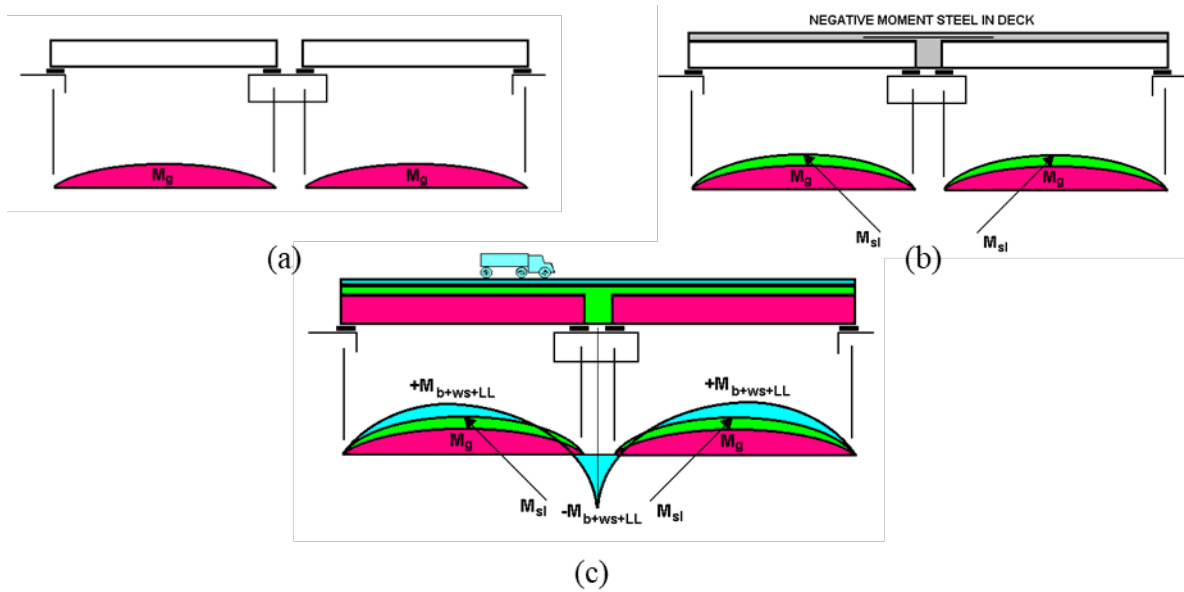


Figure 9.3: Moments distribution during construction sequence (PCI Bridge Design Manual [45], 2011)

Freyermuth [93] described that when bridges are made up of spans with the same length, the maximum live load moments occurs at about 40 percent of the end span length, and 50 percent of the end span lengths in interior beams as shown in Figure 9.4. As a result, it is possible to have separate beam prestressing reinforcement designs for interior spans and exterior spans.

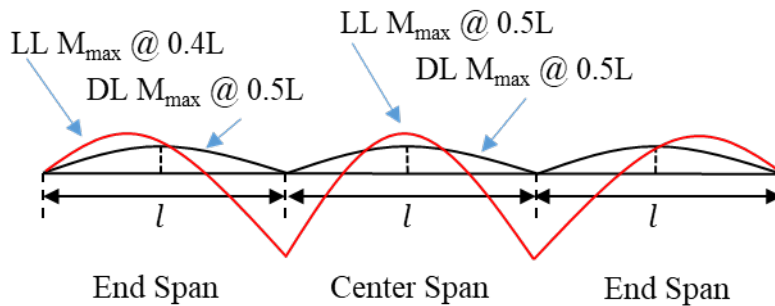


Figure 9.4: Moment diagram for multi-span structures being simply supported (black) and continuous (red)

9.2. BACKGROUND ON SDCL CONNECTIONS

The main challenge in the SDCL philosophy is the design of the connection between adjacent spans over the piers. The connection must be able to withstand the negative moments due to service load, and positive moments due to time dependent stresses such as creep, shrinkage, and temperature variations. The main components of this connection are typically:

1. *Slab*: The reinforcement in the slab will normally carry the tensile stresses from the negative moment over the piers caused by live loads.

2. *Diaphragm*: The diaphragm is used to carry the compression stress in the bottom of the members from the negative moment over the piers.
3. *Spliced Positive Moment Reinforcement*: For prestressed concrete girders, a positive moment will be developed over the piers as a result of creep and shrinkage. The spliced positive moment reinforcement will resist these generated stresses.

These components are highlighted in the typical joint detail shown in Figure 9.5.

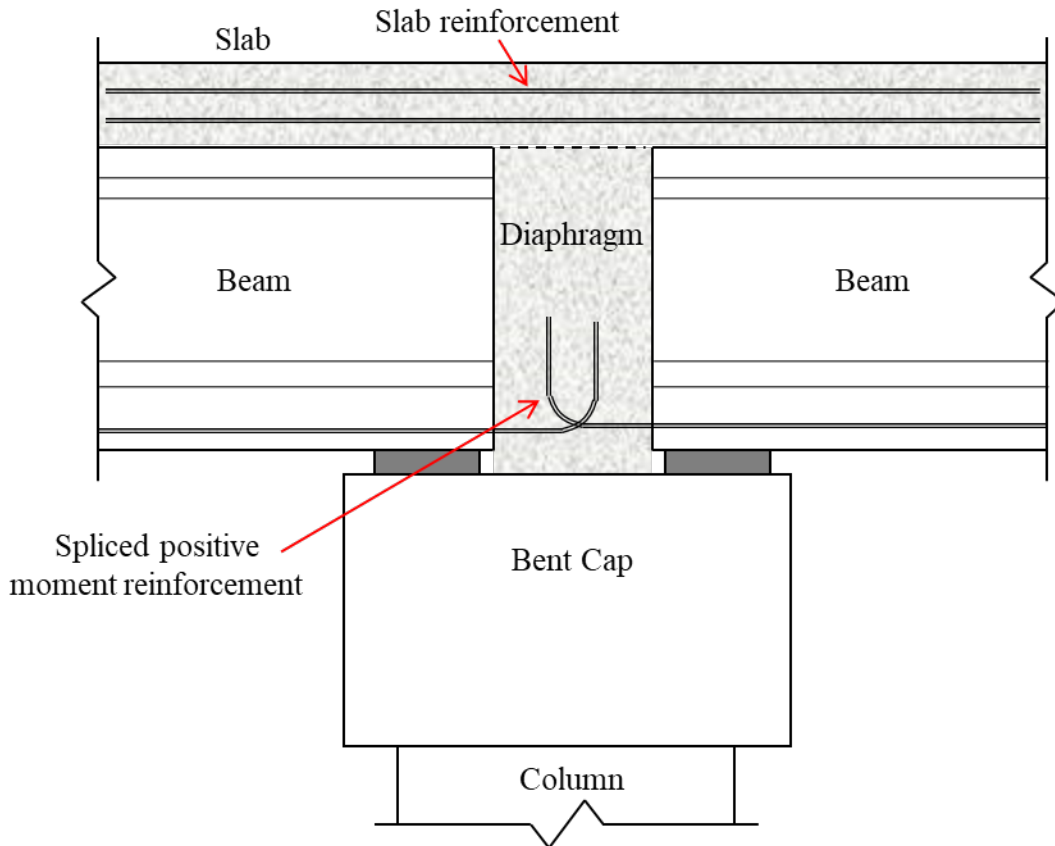


Figure 9.5: Traditional SDCL joint detail between adjacent spans

The shaded portions of Figure 9.5 (slab and diaphragm) are normally cast in place either separately, where the diaphragm is cast first and then the slab or asphalt overlay, or monolithically, where the diaphragm and slab are cast at the same time. The diaphragm can also be precast with the bent cap, as is the case in inverted-T bent caps. These four types of connections are shown in Figure 9.6.

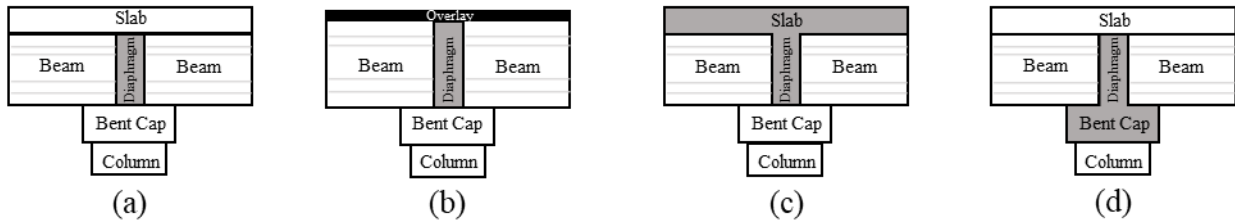


Figure 9.6: Four different slab-diaphragm-bent cap configurations used in field (adapted from [96])

9.2.1. AASHTO LRFD Bridge Design Specification

The AASHTO LRFD Bridge Design Specification [82] has a section covering “Bridges Composed of Simple Span Precast Girders Made Continuous” (§5.12.3.3). This section covers all different aspects of design for SDCL superstructures and connections, some of which will be summarized here.

9.2.1.1. Restraint Moment from Time-Dependent Deformations (§5.12.3.3.2 to §5.12.3.3.4)

Creep, shrinkage, and temperature effects will introduce stresses on the SDCL connection and adjoining precast members. These concrete time effects can be determined based on testing of the concrete materials being used in the project or using the estimation procedures provided in AASHTO LRFD §5.4.2.3. The age of the girder when the superstructure is constructed will affect the stresses generated in the SDCL connection by concrete time effects. Most creep and shrinkage strains occur within the first 90 days after casting (about 60 percent of the creep and 70 percent of the shrinkage of the girder [97]), so the specification has design simplifications that are allowed if the girders are allowed to age for 90 days prior to the construction of the superstructure. According to AASHTO LRFD §5.12.3.3.4, if the girders are allowed to age 90 days, the following simplifications may be made [82]:

- Positive restraint moments caused by girder creep and shrinkage and negative restraint moments at piers caused by deck slab shrinkage may be taken to be zero.
- Computation of restraint moments shall not be required.

A positive moment connection is still required, but with the simplified design check shown in Equation 9.1. This design check was shown by Miller et al. [98] to prevent loss in strength of the connection due to cracking caused by time effects.

$$\phi M_n \geq 1.2M_{cr} \quad \text{Equation 9.1}$$

Where the nominal moment and cracking moment are found based on the positive moment connection details described below.

A minimum of 90 days aging prior to the continuity connection is typically easily achievable, as precast girders typically are cast well in advance and stored at the precast plant prior to superstructure erection. This minimum time for aging can become an issue when girders are damaged during shipping or erection and new girders need to be cast. Miller et al. [98] conducted a survey of practice and found a girder age of 7 days to be a realistic minimum. Using this early of an age girder would result in large positive restrain moments, so they recommend a minimum girder age of at least 28 days [98].

9.2.1.2. Degree of Continuity (§5.12.3.3.5)

The AASHTO LRFD Bridge Design Specification [82] describes two degrees of continuity that can be achieved when designing SDCL bridge spans: full fixity and partial fixity. A full fixity connection allows for design of the superstructure assuming full continuity between adjacent

spans for service and strength limit states. Full fixity can be assumed when either of the following are satisfied:

- Diaphragm design stresses at the bottom including the combination of superimposed permanent loads, settlement, creep, shrinkage, 50 percent of live load, and temperature gradient are compressive, or if
- The precast beams are allowed to age at least 90 days before continuity is established.

If the SDCL diaphragm design does not satisfy either of these requirements, the connection shall be considered partially fixed. Partially fixed connections are designed for continuity for strength limit states only; service limit state would still be designed assuming simple spans.

9.2.1.3. *Design Limit States (§5.12.3.3.6 and §5.12.3.3.7)*

The AASHTO LRFD Bridge Design Specification [82] requires design of SDCL connections and the surrounding region for service limit state and strength limit state. The prestressed, precast girders need to be checked for service and strength limit states. The SDCL connection itself only needs to be checked for strength limit states, since it is not prestressed concrete.

The continuity provided by the SDCL connection can increase the tension in the top of the precast, prestressed member in the negative moment region. For this reason, there are some additional provisions provided for the stress checks in the top of the precast members near the interior supports. Tensile stress limits specified in Table 5.9.2.3.1b-1 for other than segmentally constructed bridges must be checked at the top of the girders near interior supports using Service III load combinations from Table 3.4.1-1. Stresses should be checked after all prestress losses and using f'_c in the stress limit equations. Designers are also allowed to design the top of the precast girders at interior supports as reinforced concrete members at the strength limit state; service limit states would not apply in this case. The cast-in-place (CIP) composite deck slab is not subject to tensile stress limits for the service limit state since it is not a prestressed element.

The continuity diaphragm is not prestressed, so it only needs to be designed for the strength limit state. The reinforcement in the deck resisting the negative moment shall be designed using the strength limit state with provisions for reinforced concrete elements.

9.2.1.4. *Negative Moment Connection (§5.12.3.3.8)*

Reinforcement for negative moment connections is generally provided in the CIP, composite deck made continuous over the diaphragm. The negative moment reinforcement needs to be designed for the strength limit state (not service limit state). The longitudinal reinforcement shall be extended up to the regions of the slab in compression, satisfy §5.10.8.1.2c requirements, and have a staggered termination of the bars.

When a composite CIP deck is not provided, designers have to provide the negative reinforcement developed into the diaphragm from the precast girder itself, also resisting design moments under strength limit state [82]. Several reinforcement options are available for negative moment connection designs: connections utilizing either straight or hooked non-prestressed reinforcement, top prestressing strands, or a combination of the two. Other solutions are also

available such as mechanical reinforcement splices [99], headed rebars [100], or high-yield lap spliced straight rebars or strands [93], [101].

9.2.1.5. Positive Moment Connection (§5.12.3.3.9)

There are three different types of positive moment connections permitted by the AASHTO LRFD Bridge Design Specification [82]:

1. Nonprestressed reinforcement embedded in the precast girders and developed into the continuity diaphragm.
2. Pretensioning strands extended beyond the end of the girder and anchored into the continuity diaphragm. These strands shall not be debonded at the end of the girder.
3. Any connection detail shown by analysis, testing, or approved by the Bridge Owner to provide adequate moment resistance.

A combination of nonprestressed reinforcement and prestressing strands were shown by Miller et al. [98] to also perform well. The face of the girder is the critical section for the development of the positive moment reinforcement.

If the girders are allowed to age 90 days before continuity, then the simplified design check shown in Equation 9.1 may be used. Otherwise, the reinforcement shall be proportioned to resist the larger of the following:

1. Factored positive restraint moment, or
2. $0.6M_{cr}$

The restraint moment can be found as discussed above using the estimation procedures provided in AASHTO LRFD BDS §5.4.2.3. The amount of reinforcement should not exceed $1.2M_{cr}$; a study conducted by Mirmiran et al. [97] determined that a positive moment connection with a capacity greater than $1.2M_{cr}$ provides minimal improvement in the continuity behavior. The cracking moment of the connection (M_{cr}) shall be found using gross composite section properties for the girder and the effective width of the composite deck slab.

Even if a designer requires the girder to be ages 90 days before placement in the field, it can be a good practice for the designer to consider the factored positive restraint moment and $0.6M_{cr}$. The required positive restraint moment may be less than the simplified method in AASHTO LRFD BDS §5.12.3.3.4, which requires the design positive moment to be $1.2M_{cr}$.

When utilizing non-prestressed reinforcement, the designer shall use the yield strength of the reinforcement (providing full development), satisfy §5.10.8, and ensure termination of the reinforcement in staggered pairs [82].

When utilizing prestressing strands extended beyond the girder into the continuity diaphragm, the strands are recommended to project at least 8 inches from the girder face and to be bent into a 90-degree hook or project straight into the continuity diaphragm the development length for the strand found in §5.9.4.3 [82]. The stresses in the strand used for design as a function of the total length of the strand shall not exceed the stress at the service limit state (f_{psl}) when cracked section is assumed, Equation 9.2, and the stress at the strength limit state (f_{pul}), Equation 9.3 [82].

$$f_{psl} = \frac{(l_{dsh} - 8)}{0.228} \quad \text{Equation 9.2}$$

$$f_{pul} = \frac{(l_{dsh} - 8)}{0.163} \quad \text{Equation 9.3}$$

where:

l_{dsh} = total length of extended strand (in.)

f_{psl} = stress in the strand at the service limit state, cracked section shall be assumed (ksi)

f_{pul} = stress in the strand at the strength limit state (ksi)

Additionally, per §C5.12.3.3.10 [82], [98], embedding the precast girder 6 inches into the continuity diaphragm improves the performance of positive moment connections by reducing the stresses in the positive moment reinforcement. However, this is not feasible for slab beam shapes.

These provisions can be used to design the SDCL connection.

9.2.2. FDOT Structure Design Guidelines [102]

The Florida Department of Transportation (FDOT) Structures Design Guidelines (SDG) [102] has additional guidance for the continuity of precast beams in §4.1.7 [102]. Additional requirements for the continuity of precast beams are provided in §4.1.7-C [102]:

1. Beams must be of the same type, depth and spacing for all spans within the main span unit.
2. Full depth continuity diaphragms monolithic with the bridge deck shall be provided.
3. Bottom tension ties between beam ends in adjacent spans over interior supports shall be provided.
4. The reinforcement in the negative moment regions shall be designed to resist effects due to live load, superimposed dead load and temperature.
5. The casting sequence for the deck and diaphragm shall be based on one of the following options:
 - a. Option 1
 - i. Cast the positive moment regions of the deck after the girders have reached a minimum age of 90 days,
 - ii. Cast the continuity diaphragms and the associated negative moment regions of the deck without a construction joint between them after the positive moment regions of the deck have cured for a minimum of 72 hours.
 - b. Option 2
 - i. Cast the deck on one of the end spans of the continuous unit up to the first continuity diaphragm with the pour allowed to proceed in either direction after the beams have reached a minimum age of 90 days,
 - ii. The deck on the second span and the first continuity diaphragm shall be cast without a construction joint between the deck and the diaphragm,
 - iii. Repeat step “ii” for successive spans in the continuous unit.

Current SDG guidelines do not provide design requirements for continuity diaphragms made with UHPC nor continuity of precast beams for live loads without cast-in-place (CIP) decks.

9.2.3. Additional Guidance on SDCL Connections

The requirements for positive and negative moment diaphragm reinforcement from several additional design guidelines and researchers are summarized in this section.

9.2.3.1. PCI New England Technical Committee [103]

The PCI New England Region (PCINER) Technical Committee developed guidelines for simple span members made continuous in multi-span bridges [103]. These guidelines specify that members shall be assumed to act as simple spans for prestressing forces application, dead load, and non-composite dead loads. The design for continuity would carry the superimposed dead loads, live loads, and loading due to time effects. Also, for the positive moment connections, the committee suggested a moment to develop at interior supports equal to $1.2M_{cr}$ (+) of the composite section [103], similar to the AASHTO guidelines [82]. Strand extensions beyond the member ends is recommended to make the positive connection in the diaphragms. Diaphragm ties within six inches of the bottom precast member bulb shall also be assumed to contribute with the positive moment connection if properly engaged with transverse ties [103].

As per the PCINER [103], the diaphragm connection shall be designed by the working stress method with an ultimate strength check, as shown in Equation 9.4 through Equation 9.10 and in Figure 9.7:

Working Stress Design:

$$f_{ps} = \frac{(l_e - 8.25)}{0.228} \leq 150 \text{ ksi, for } L_{pb} \leq 8.25" \quad \text{Equation 9.4}$$

$$f_{ps} = \frac{L_e - L_{pb}}{0.228} + \frac{L_{pb} - 8.25}{0.472} \leq 150 \text{ ksi, for } L_{pb} > 8.25" \quad \text{Equation 9.5}$$

$$A_{ps} = \frac{M - A_s f_y * (j d_{ps} + d - d_{ps})}{f_{ps} j d_{ps}} \quad \text{Equation 9.6}$$

Ultimate Strength Check:

$$f_{pu} = \frac{L_e - 8.25}{0.163} \text{ for } L_{pb} \leq 8.25" \quad \text{Equation 9.7}$$

$$f_{pu} = \frac{L_e - L_{pb}}{0.163} + \frac{L_{pb} - 8.25}{0.337} \text{ for } L_{pb} > 8.25" \quad \text{Equation 9.8}$$

$$a = \frac{A_{ps} f_{pu} + A_s f_y}{0.85 f'_c b} \quad \text{Equation 9.9}$$

$$M_u = 0.9 [A_{ps} f_{pu} (d_{ps} - a/2) + A_s f_y (d - a/2)] \quad \text{Equation 9.10}$$

Reinforcement location:

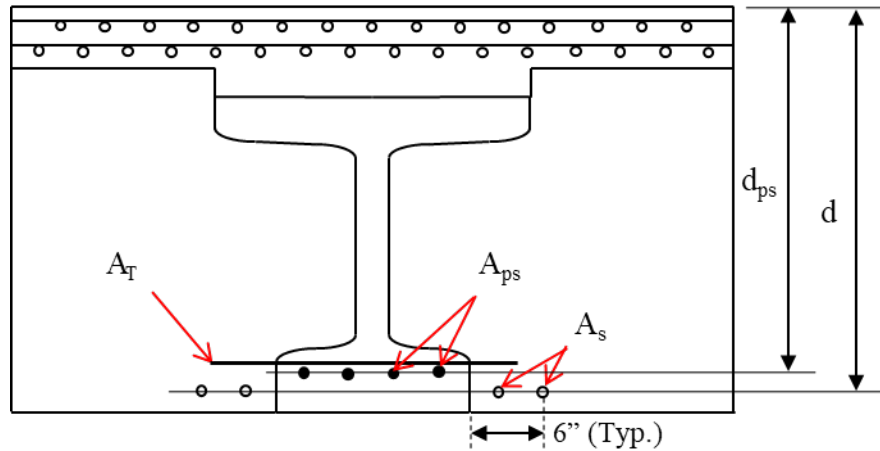


Figure 9.7: Diaphragm reinforcement location (Adapted from PCINER, 1998 [103])

Where:

- a = depth of compression stress block
- b = compression flange width
- d = distance from extreme compressive fiber to the centroid of the diaphragm tie
- d_{ps} = distance from the extreme compression fiber to the centroid of the strand
- f'_c = compressive strength of deck concrete
- f_{ps} = allowable working stress per strand
- f_{pu} = stress of strand at general slip (defined as measurable slip)
- f_y = diaphragm tie yield stress
- jd_{ps} = internal moment arm = $0.94d_{ps}$ (approximates T-Beam with low reinforcement steel percentage)
- A_{ps} = required area of embedded strand
- A_s = area of diaphragm ties within six inches of the bottom bulb
- A_T = area of transverse reinforcement
- L_e = total embedment length of strand
- L_{pb} = prebend length of embedded strand (9 inches)
- M = design moment $\geq 1.2M_{cr}$
- M_u = ultimate moment capacity of connection

For the negative moment reinforcement, the reinforcing steel required shall be provided in the deck (both top and bottom mats of deck slab) and determined by assuming the member to be a rectangular section with a compressive block width equal to the bottom flange width of the member. Lastly, time-dependent effects may be neglected if provisions are made to ensure the concrete members cure for a minimum of 60 days prior the application of additional dead loads [103]. The PCINER recommend if state standards exist, they take precedent over these guidelines and details.

9.2.3.2. *NCHRP Report 519 [98]*

NCHRP Report 519 [98] was one of the most comprehensive studies conducted on SDCL connections and was used to develop the current language provided in the current AASHTO LRFD Bridge Design Specifications [82]. NCHRP Report 519 provided several different detailed design examples on popular girder types in Appendix D; these include: (1) AASHTO Type III girder, (2) PCI BT-72 girder, (3) 51-inch deep spread box girder, and (4) adjacent AASHTO BIII-48 box girder without composite deck. In these design examples, the researchers compared the effect of girder age when continuity is established at girder ages of 7 days, 28 days, and 90 days [98].

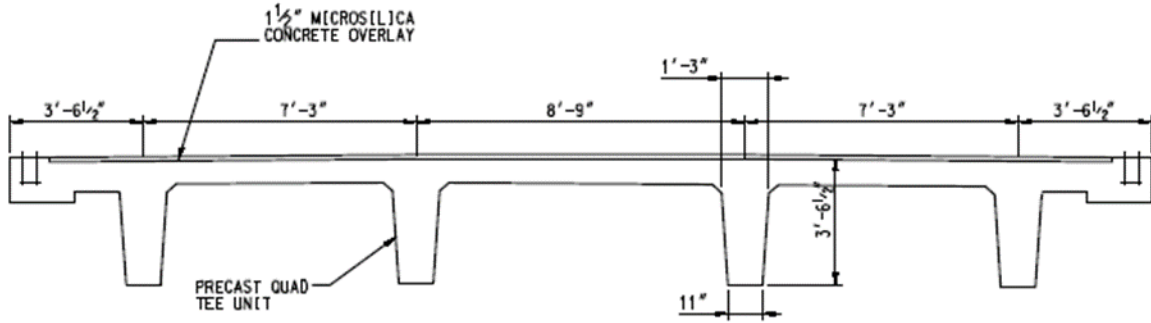
Some important design considerations were:

1. The girder spacing and span length were fixed for each design example,
2. The examples consider only interior girders,
3. Each example provides reinforcement details for the connections at the continuity diaphragm,
4. Constructability is considered in developing the details,
5. Typical design loads are used in the designs, and
6. Conventional materials are used for all designs.

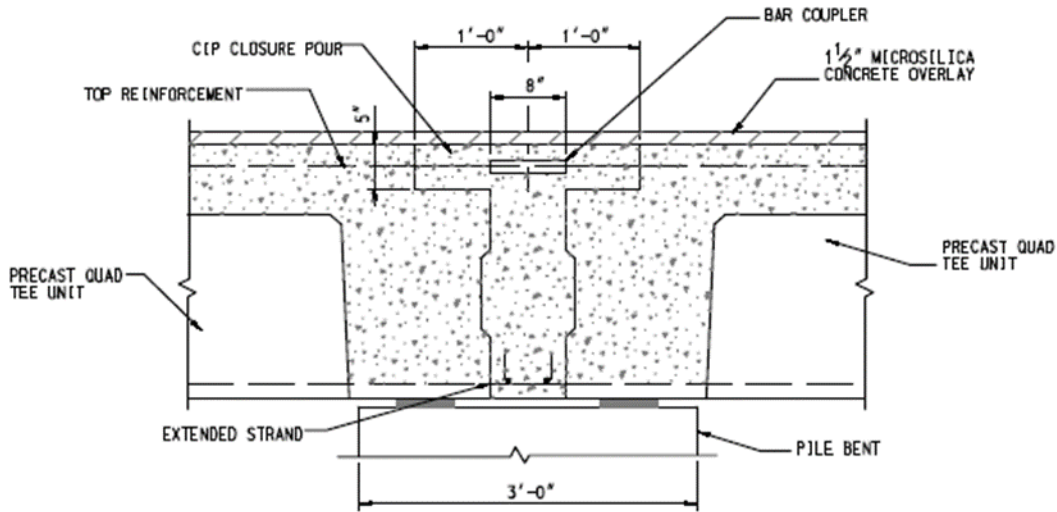
These design considerations and design example procedure were followed to develop the FSB continuity connection.

9.2.3.3. *FHWA Design Guidelines [104]*

FHWA provides guidance related to connection of precast elements in several documents. One of these documents, Connection Details for Prefabricated Bridge Elements and Systems [104], provides specific details on simple span beams made continuous for live loads (§2.3.3). This section references NCHRP Report 322 [105]. Culmo [104] provides a general background on SDCL construction for concrete and steel superstructures and several sample details from completed projects. These sample details include specific information related to background of detail, design characteristics, speed of construction, constructability, cost, durability, inspection access, and future maintenance. The sample details related to SDCL include a continuity connection for a precast quad tee section without CIP deck (Figure 9.8), precast inverted-tee beam with CIP deck (Figure 9.9), and precast box beam without CIP deck (Figure 9.10). A bar coupler or splice sleeve is used to connect the negative moment reinforcement extending from the precast members for the systems without CIP decks.

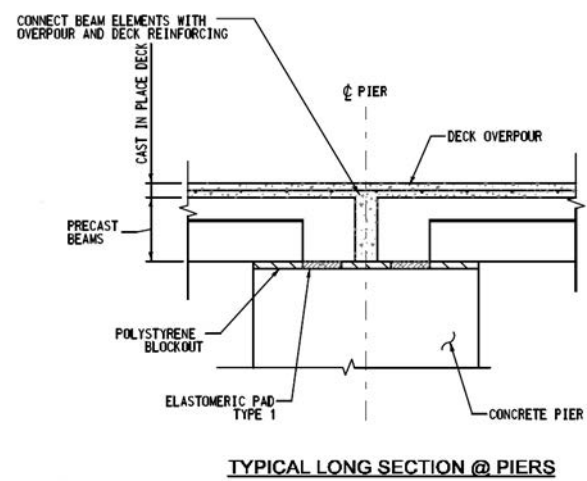


TYPICAL BRIDGE SECTION



CONTINUITY CONNECTION AT PIER

Figure 9.8: Example continuity connection at pier for precast quad tee section without CIP deck from Robert Moses Causeway Bridge Rehabilitation over Great South Bay [104]



(a)



(b)

Figure 9.9: Example continuity connection at pier for precast inverted-tee beams with CIP deck from Bridge 13004, TH 8 over Center Lake Channel (MN) [104]

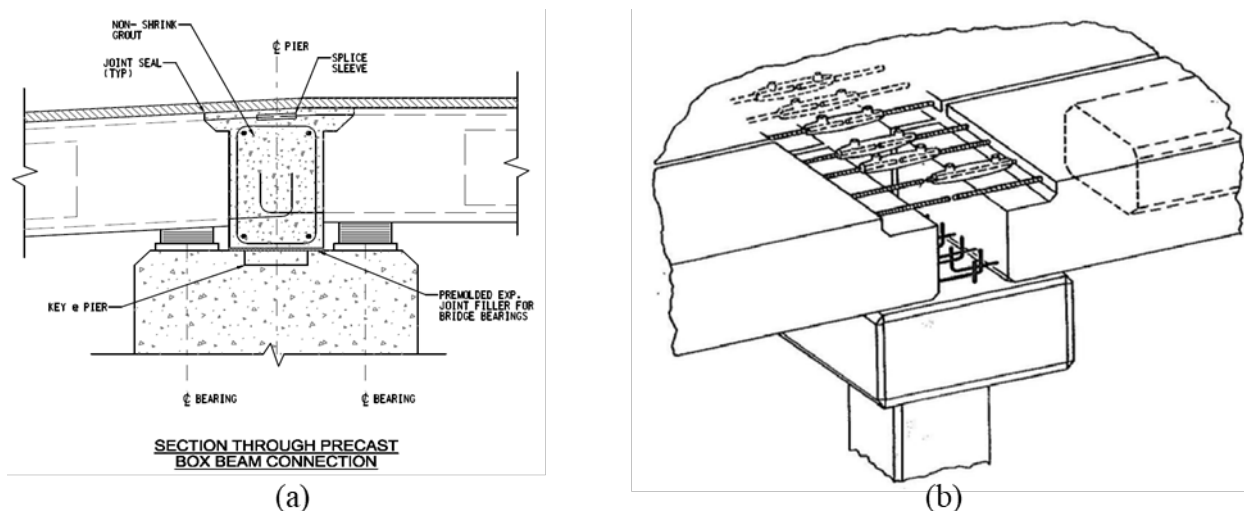


Figure 9.10: Example continuity connection at pier for precast box beam without CIP deck from Unquowa Road (CT) [104]

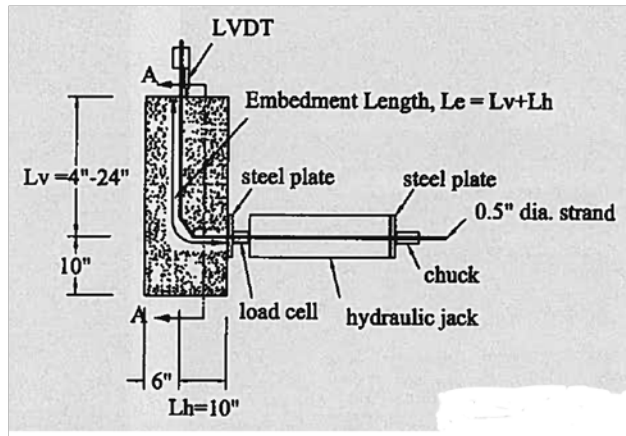
Culmo [104] also provides a table with the minimum installation times for different types of systems; some of these times related to diaphragm construction and SDCL connections for prestressed concrete superstructures are shown in Table 9.1.

Table 9.1: Approximate minimum installation time for decked stringer systems (from Culmo [104])

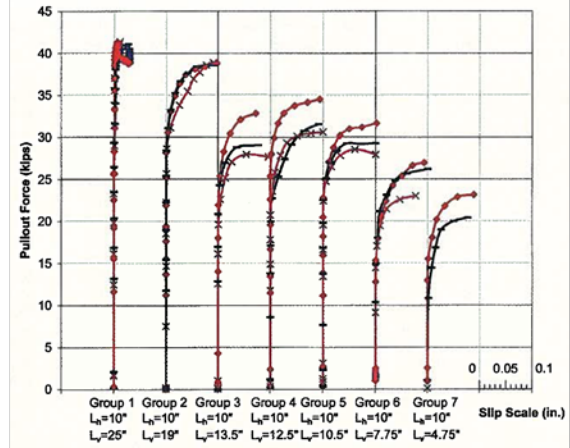
System	Minimum Installation Time*	Comments
Cast-in-place concrete diaphragm on PS beams	2 days	Time includes forming multiple diaphragms and placing of concrete
Precast diaphragms on PS beams	1 day	Multiple diaphragms can be completed in one day
Cast-in-place closure pour splice on PS beams	2 days	Time includes forming multiple splices and placing of concrete
Live load continuity connections on concrete and steel beams	3 days	Time includes forming multiple closure pours and placing of concrete

9.2.3.4. Noppakunwijai et al. [106]

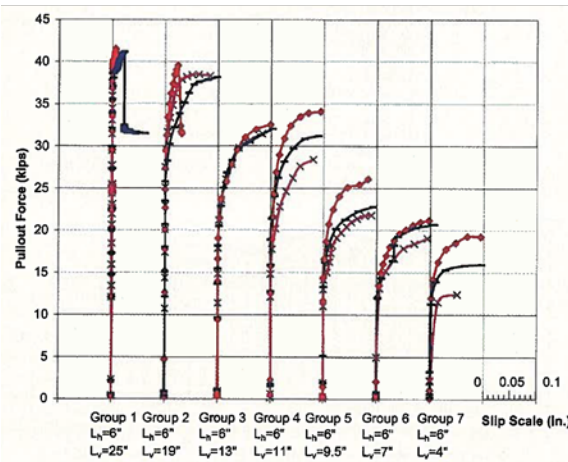
Noppakunwijai et al. [106] conducted a study where 0.5-in. and 0.6-in. diameter strands with different embedment lengths were subjected to pullout failures with a test setup as shown in Figure 9.11 (a). These researchers varied the distance from the end face of the prestressed member (L_h) and the vertical embedment length of the non-prestressed bent strand (L_v). A summary of their results is shown in Figure 9.11.



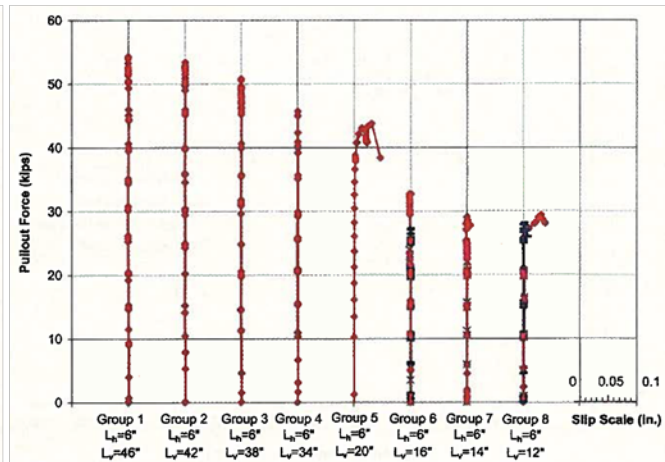
(a)



(b)



(c)



(d)

Figure 9.11: (a) Sample test setup for Specimen 2 and test results for (b) Specimen 2, (c) Specimen 1, and (d) Specimen 3 from Noppakunwijai et al. [106]

Noppakunwijai et al. [106] proposed Equation 9.11 to calculate the developed strand stress for a provided embedment length of non-prestressed bent strand with a fixed horizontal embedment of 6 inches.

$$f_{ps} = 0.017 f_{pu} \frac{L_v}{d_b} \leq 0.8 f_{pu} \quad \text{Equation 9.11}$$

Where:

f_{ps} = developed strand stress (ksi or MPa)

L_v = vertical embedment length of non-prestressed bent strand (in. or mm)

f_{pu} = specified tensile strength of prestressing tendons (ksi or MPa)

d_b = nominal diameter of strand (in. or mm)

They recommend that 80 percent of the specified strand strength ($0.8f_{pu}$) can be assumed when the 0.5- and 0.6-inch diameter strands have total embedment lengths ($L_h + L_v$) of 30 and 36 inches, respectively. They also recommend a minimum total embedment length ($L_h + L_v$) of 16 inches for crack control at service load levels due to positive moments from time effects at the piers. These values and the proposed Equation 9.11 are all based on a concrete strength of 4,000 psi.

Other researchers [107] conducted testing on 0.5-inch diameter strands and had come to similar conclusions to what is currently in AASHTO LRFD [82].

9.2.3.5. *Guidance Related to UHPC*

Ultra-high performance concrete (UHPC) has been used for many different applications, as summarized in earlier tasks of this project. UHPC research relevant to SDCL connections for the modified FSB section relates to the splicing of straight reinforcing bars for the negative moment reinforcement and the splicing of prestressing strands in UHPC for the positive moment reinforcement. The design recommendations provided by Graybeal [108] can be used for the splicing of the conventional reinforcement in the top of the joint used to resist the negative moment; these recommendations have been summarized in earlier tasks.

Splicing of prestressing strands was studied by Maya and Graybeal [109] and Graybeal [110]. Graybeal [110] tested the splicing of straight strands in UHPC, as shown in Figure 9.12 (a). He found that 0.5-inch diameter strands required an embedment length of about 15.7 inches to develop the nominal strand strength (270 ksi) for UHPC with steel fibers; a 0.6-inch diameter strand would require about 23.6 inches to develop 270 ksi. Graybeal [110] did not test any hooked strands.

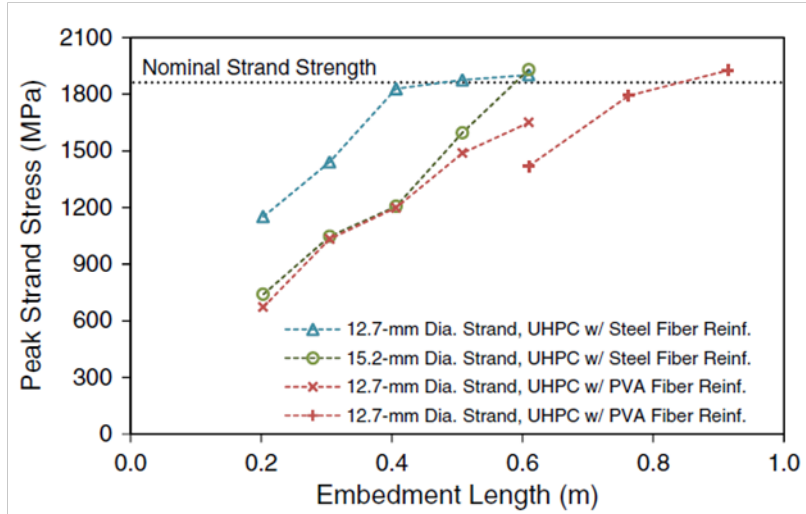
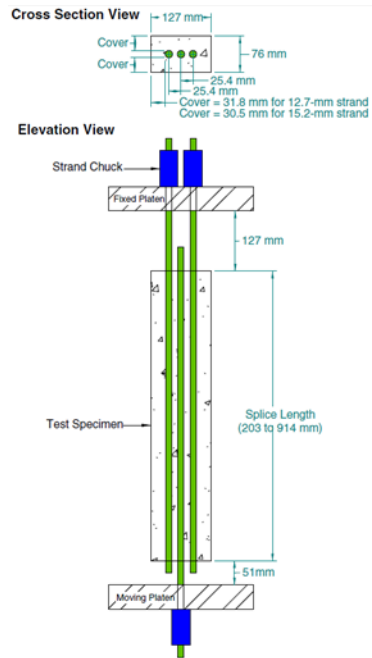


Figure 9.12: (a) Test specimen and (b) summary of results from Graybeal [110]

Maya and Graybeal [109] also tested the splicing of strands in two-beam, box-beam system, as shown in Figure 9.13. Only the positive moment restraint provided by the spliced strands was tested, not the negative moment restraint. Splice lengths of 24 inches (40 times the strand diameter) and 30 inches (50 times the strand diameter) were used for the prestressing strands in two specimens, based on the results from Graybeal [110]. The splices performed well with the 30-inch splice reaching 90 percent of the ultimate flexural capacity estimated for the fully prestressed section.

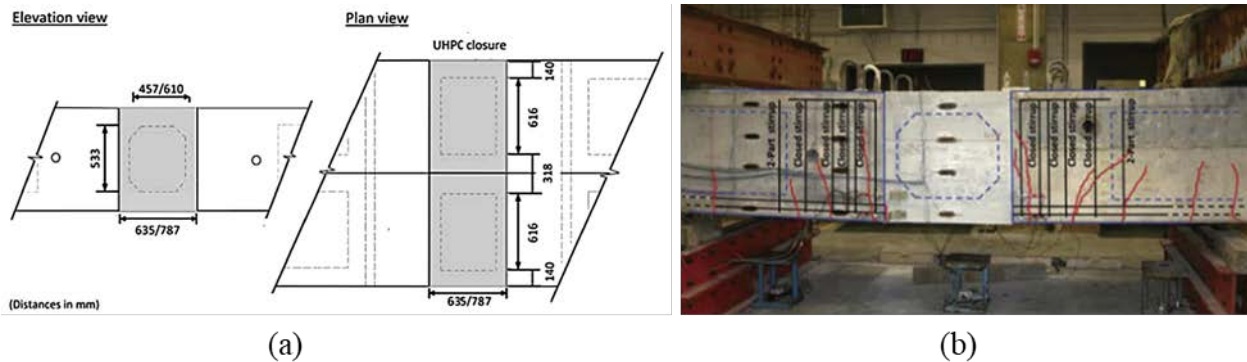


Figure 9.13: (a) Joint details and (b) crack pattern for 30-inch splice at $0.8P_u$ load from Maya and Graybeal [109]

There has been no research on the pullout strength or splice length for non-prestressed hooked strands in UHPC or even high strength concrete.

Several additional researchers and practitioners tested or implemented in the field specific SDCL connections with UHPC. Perry et al. [101] used UHPC to create an SDCL connection between adjacent spans in a three-span box beam bridge. They used glass fiber reinforced polymer (GFRP) extending from the box beams with field placed GFRP bars to create the negative moment connection, shown in Figure 9.14. No positive moment reinforcement or prestressing was spliced in this project.

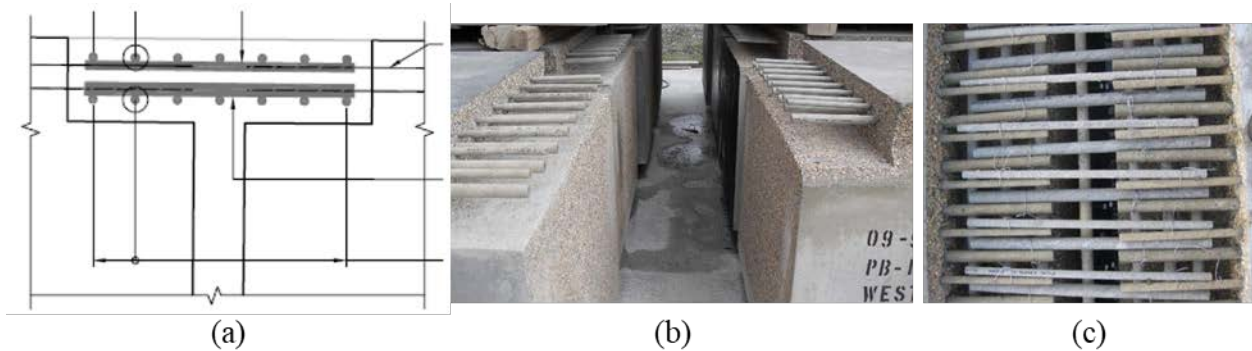


Figure 9.14: Details of SDCL connection with UHPC and GFRP by Perry et al. [101]

A larger research effort by Floyd et al. [111] on UHPC connections and repairs tested six continuity specimens by connecting two precast, prestressed I beams with UHPC joints. Two different connection details were investigated, one for new construction and one for repair of existing structures with continuity connections; both details were designed based on AASHTO LRFD [82] requirements for negative moment and $1.2M_{cr}$ for positive moment. The SDCL connection between the adjacent spans included spliced #5 bars extending from the composite deck in the negative moment region and a combination of hooked prestressing strands and straight #3 bars in the positive moment region, as shown in Figure 9.15. This SDCL joint detail performed well during their strength testing, with the failure occurring outside of the joint region. The retrofit continuity detail was implemented in a field study summarized by Looney et al. [112].

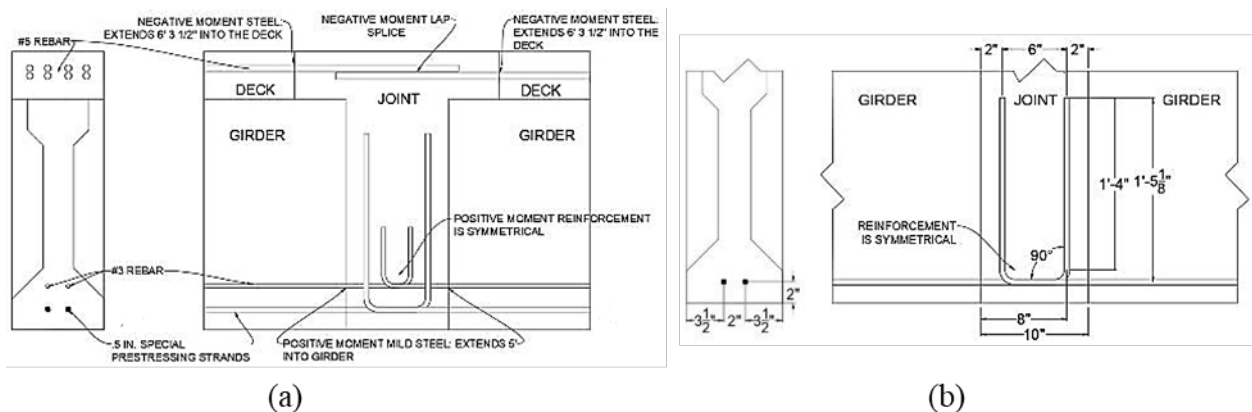


Figure 9.15: Details for SDCL connection with UHPC between I-beams by Floyd et al. [111]

Benjumea et al. [113] constructed a scaled two-span bridge structure with six different ABC connections. One of these connections was a continuity connection between adjacent spans and with the columns and cap, shown in Figure 9.16. This detail included a conventional concrete CIP portion between the precast, prestressed bulb-tee girders and a UHPC top layer to connect the deck panels.

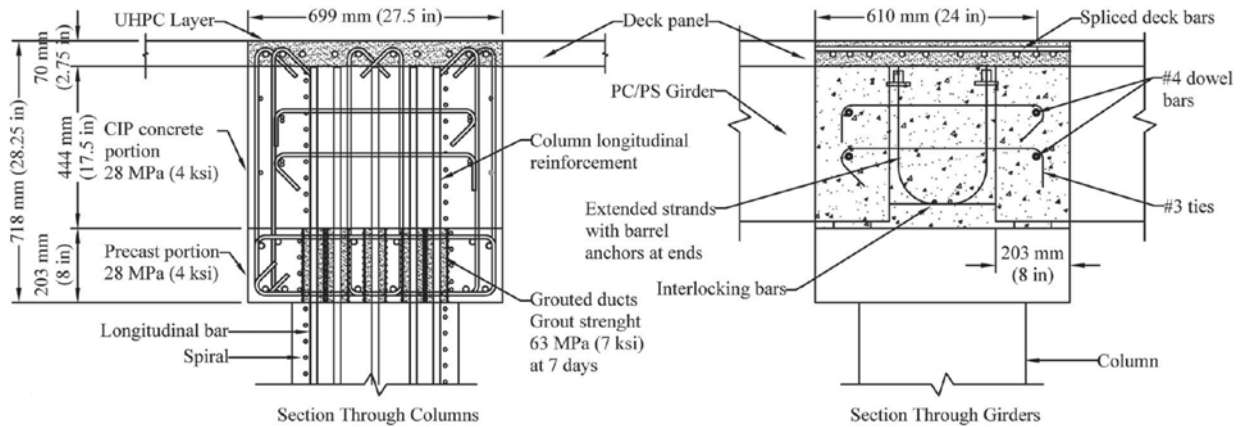


Figure 9.16: Detail for column-to-cap beam and superstructure-to-cap beam connections from Benjumea et al. [113]

Other researchers have investigated related topics including girder repair with UHPC [114], integral abutment connections with UHPC [113], [115], and SDCL connections in steel bridge systems [116].

9.2.4. Examples of SDCL Connections

Many different connection details have been used to achieve continuity between adjacent spans. This section summarizes some of the previously used details that could be implemented for a SDCL connection with the modified FSB system.

The most common positive moment connection is shown in Figure 9.17. This detail consists of the prestressing strands being extended beyond the end of the prestressed section and hooked up in the diaphragm region. Conventional deformed reinforcement can also be used in place of the prestressing strands, but it can be difficult to find space for additional reinforcement in the ends of prestressed beams. There is typically additional field placed transverse reinforcement located at the inside of the bend in the strands or bars to improve the splice behavior and provide reinforcement for the CIP diaphragm. This detail has been used by many researchers [93], [97], [98], [103], [106].

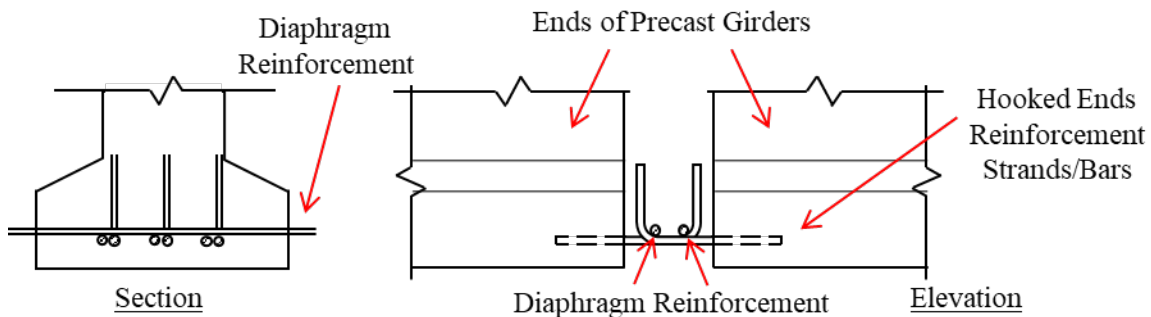


Figure 9.17: Positive moment restraint connection details (adapted from Freyermuth [93])

The negative moment reinforcement to achieve continuity is typically placed in the CIP deck. There have been several different details for providing negative moment reinforcement for superstructures without a CIP deck. Tadros et al. [99] proposed a detail where top prestressing strands are extended from the end of the precast girder and spliced together using a mechanical splice, as shown in Figure 9.18. They proposed using jacking brackets and hydraulic jacks to put tension in the top spliced strands before casing the joint concrete. The jacking system would push the ends of joined members outward to introduce tension into all coupled strands in the diaphragm before casting of the joint. The bolt sleeves shown in Figure 9.18 are to allow for the mounting of the jacking brackets for the hydraulic jacks.

Once the strands were jacked and forms installed, concrete with high early strength and low shrinkage properties was cast and cured in the diaphragm, maintaining the jacking system tensile force levels during this stage. After the concrete reached the required strength, the jacking force was released introducing precompression into the diaphragm. A similar method was successfully implemented in the Tenth Street Pedestrian/Bicycle Overpass project in Lincoln, Nebraska [117].

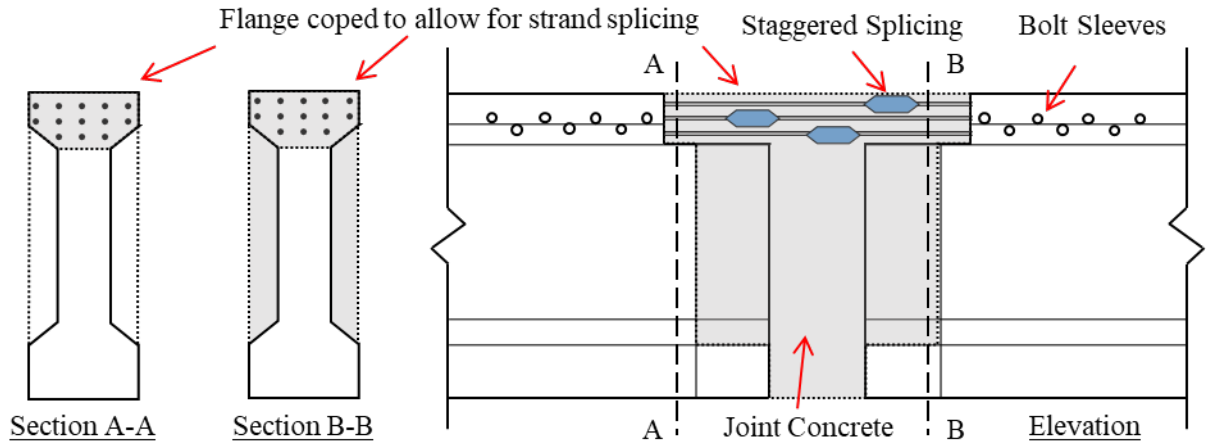


Figure 9.18: Strand splice devices for continuity (adapted from Tadros et al. [99])

Ma et al. [100] developed a negative moment reinforcement connection detail utilizing high strength threaded rods in the top flange of prestressed concrete I beams, as shown in Figure 9.19. Ma et al. [100] tested two different details with 1-inch diameter threaded rods, one with six threaded rods with a yield stress of 92 ksi and the other with four threaded rods with a yield stress of 150 ksi. The threaded rods were cast in the top flange of the prestressed concrete beams offset between the ends of the beams in adjacent spans. The connection was made by bolting the threaded rods on opposite sides of flat plates, as shown in Figure 9.19.

This continuity reinforcement was designed for negative moment due to the weight of deck slab and any other construction load, while additional negative longitudinal reinforcement was placed in the deck region for resistance of superimposed dead and live loads. Although this method still requires negative reinforcement from the deck, the density of negative reinforcement at deck level over the diaphragm is greatly reduced, providing ease of construction. Ma et al. [100] concluded that placing some of the top continuity reinforcement in I-beam top flange can increase the composite action between the girder and the slab and also increase the possible span lengths for a given section by as much as 20 percent.

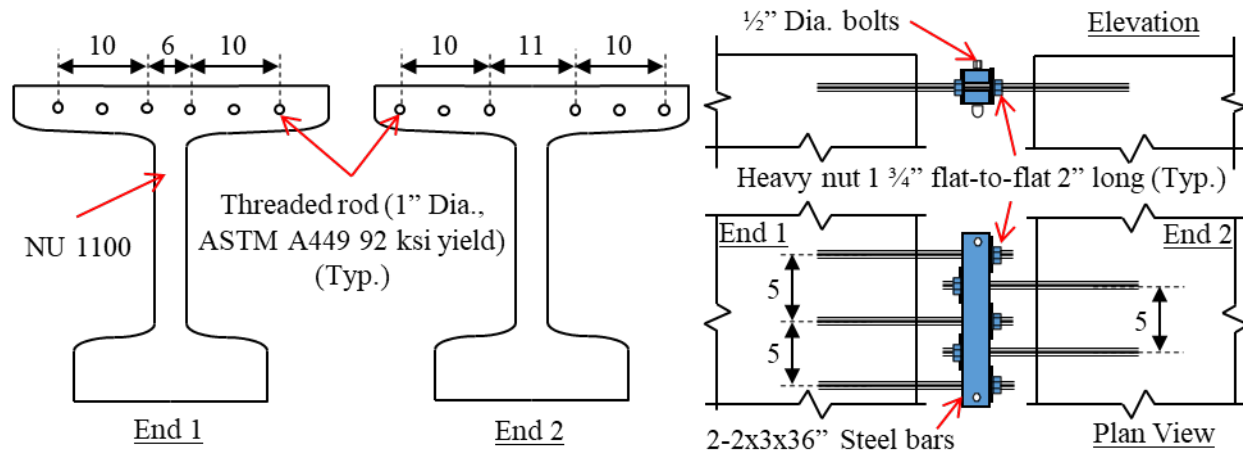


Figure 9.19: High-strength threaded rod for deck weight continuity (adapted from Ma et al. [100]). Note: units in inches

As discussed above, the Ministry of Transportation of Ontario (MTO) implemented the use of UHPC in a three-span, prestressed adjacent box beam bridge with intermediate live-load continuity diaphragm details [101], as shown in Figure 9.20. The beams were designed with high-performance concrete, carbon fiber reinforced polymer (CFRP) for the beam reinforcement, and glass fiber reinforced polymer (GFRP) for the continuity reinforcement in the diaphragms. An exposed-aggregate finish was used on the end of the beam to enhance the bond between the precast sections and the diaphragm fill. The use of UHPC in the diaphragm minimized the connection dimensions while providing less total shrinkage across the joint. Also, the UHPC allowed for shorter rebar development lengths to fully develop the GFRP bars, allowing for an 8-inch wide joint compared to a conventional design of a 24 inch-wide joint [101]. Once the beams were in position on top of the supports, additional GFRP bars were spliced with each box girder end region reinforcement, developing the load from one span to the contiguous, as shown in Figure 9.20.

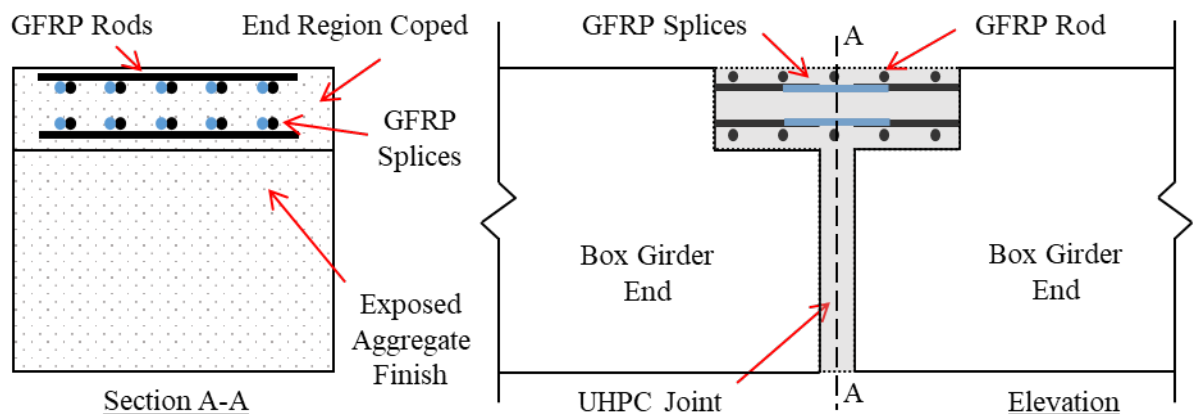


Figure 9.20: Lap spliced rebar (or strand) for diaphragm continuity with UHPC joint fill (adapted from Perry et al. [101])

9.2.5. Challenges with SDCL Connections

There have been several challenges and issues that have arisen with the SDCL concept during the past few decades. Walton and Bradberry [96] developed a historical summary of instances where the SDCL concept was used in precast, prestressed structures in Texas. They observed that cracking and crushing of the concrete often occurred in several locations of the bridge over the piers, as shown in Figure 9.21. They also found that improved efficiency would only lead to about 6-percent less longitudinal reinforcement and a slightly lower concrete strength (compared to a similar simply-supported design). Because of the challenges associated with the joint detailing and not as many perceived benefits, Texas no longer uses the SDCL concept in design.

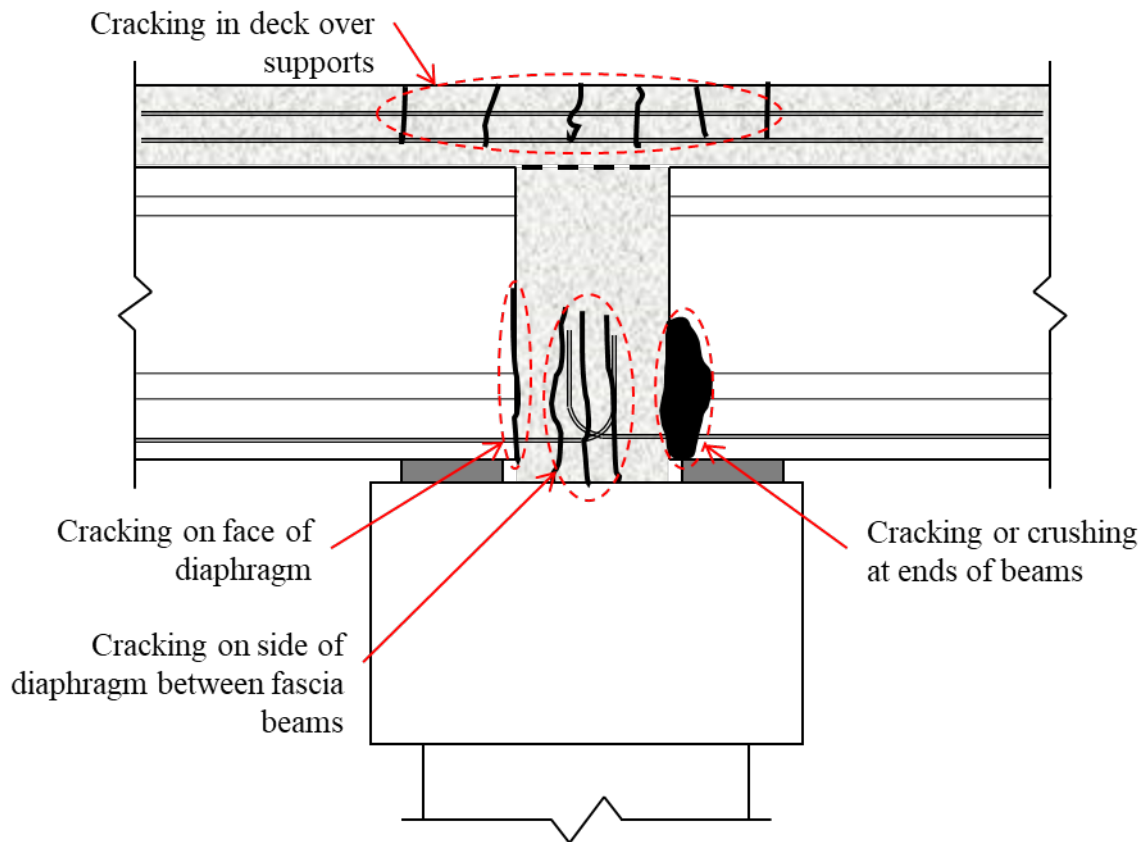


Figure 9.21: Previously observed field issues with SDCL connections in prestressed members

9.3. DESIGN OF SDCL CONNECTION FOR MODIFIED FSB SYSTEM

9.3.1. Introduction

The current FSB joint detail for a typical 12-inch-deep FSB with a 6-inch CIP deck at intermediate bent caps or pier caps along the beam centerline is shown in Figure 9.22. Current FSB superstructures are designed to act as simple spans under both dead load and live load [19] with a typical two-inch thick expansion joint poured with backer rod between inner spans [118]; therefore no continuity of the CIP deck pour nor joint cage with deck reinforcement are provided over the intermediate supports.

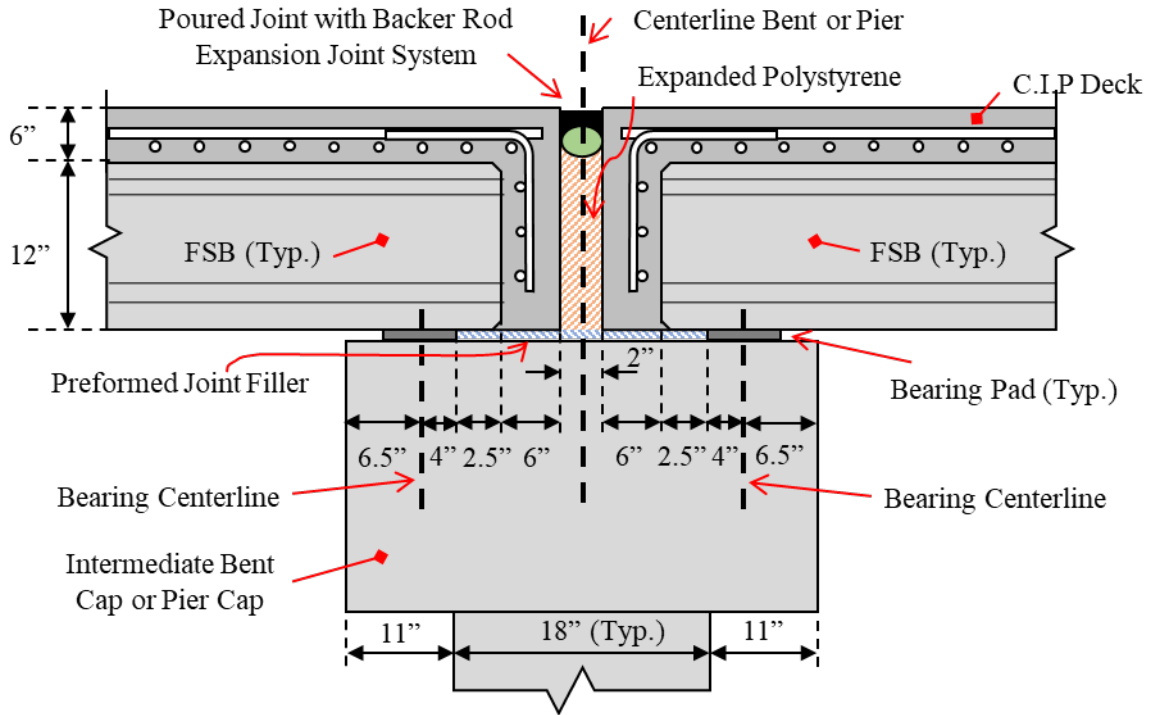


Figure 9.22: Typical FSB detail at intermediate bents or piers (Adapted from FDOT [19])

The modified FSB system with UHPC in the longitudinal joints for accelerated construction does not include a CIP deck [119], hence the 6-inch CIP deck region behind each FSB span end would not be required in the design detail at intermediate supports, as shown in Figure 9.23. Based on the current bearing pad's typical locations and intermediate bent cap or pier cap dimensions, a width between beams of 14 inches would be available for a possible continuity diaphragm detail.

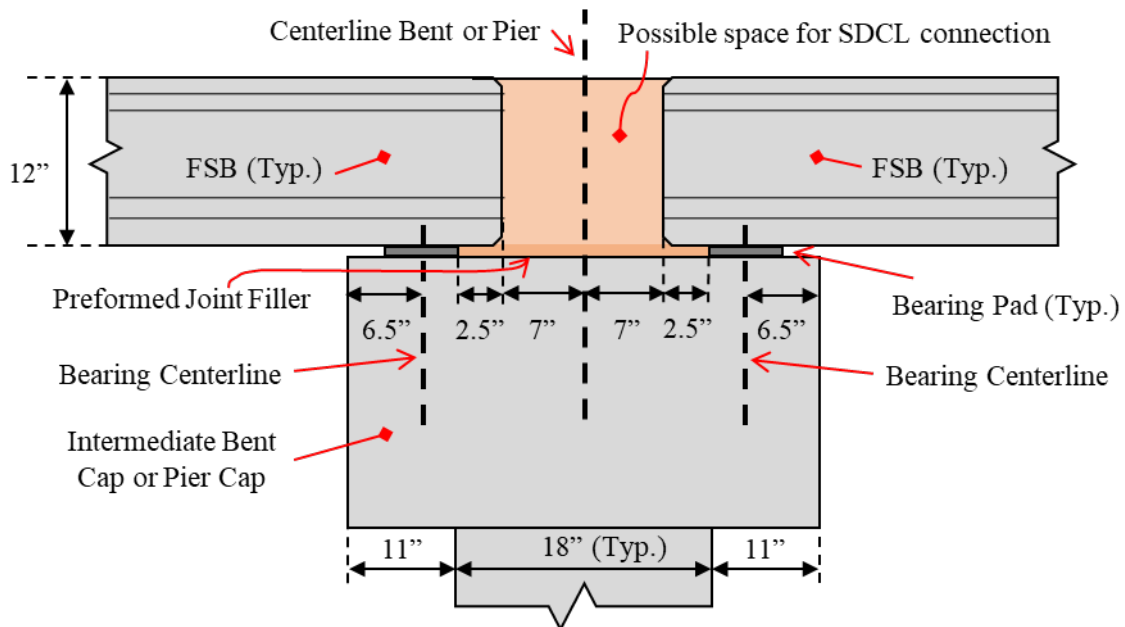


Figure 9.23: Modified FSB detail without CIP deck at intermediate bents or piers

There are several different positive and negative moment connection details based on previous research and practice that could be used for a SDCL connection between adjacent FSB spans. Only possible details utilizing UHPC are shown in this section. Using the same material in the diaphragm region will allow for the joints and diaphragm to be cast at the same time. The reinforcement and details shown are just schematic designs; the reinforcement shown is not based on an actual design. An actual design based on one of these concepts is performed in later sections.

A sample detail for the positive moment reinforcement based on Floyd et al. [111] is shown in Figure 9.24. The prestressing strands in the bottom of the modified FSB section could be spliced in the UHPC with an 8-inch embedment (6-inch splice length) and 90-degree hook. The vertical leg of the hook in the prestressing strand (L_v as defined by Noppakunwijai et al. [106]) would depend on the depth of the section. For a 12-inch-thick FSB, the vertical leg of the hook could be a maximum of 7 inches (based on 12-inch depth, 3-inch distance between bottom and center of prestressing strands, and 2-inch cover between end of strand and top of section).

An additional transverse reinforcing bar can be placed at the inside of the bend radius of the prestressing strands, as highlighted in Figure 9.24. This transverse reinforcement was recommended by Tadros and Jongpitaksseel [120] to improve the development of the hooked strands; they used #5 bars with 0.6-inch diameter prestressing stands.

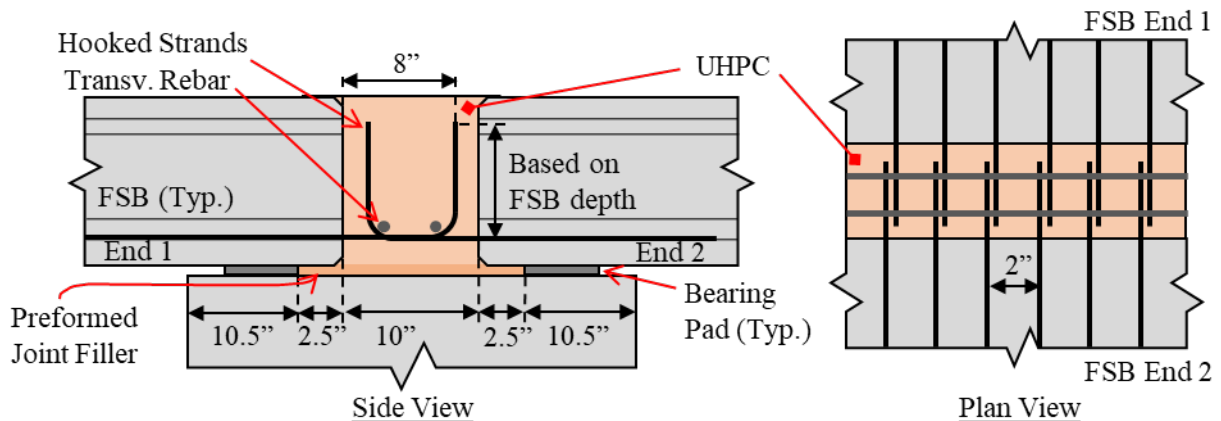


Figure 9.24: Splicing of hooked prestressing strands for positive moment reinforcement (based on Floyd et al. [111] and Noppakunwijai et al. [106])

The stress in the strand using Equation 9.11, from Noppakunwijai et al. [106], would be 53.4 ksi, as shown below. This equation was developed based on 4 ksi concrete, so using this value would be extremely conservative for UHPC.

Equation from Noppakunwijai et al. [106] using 4 ksi concrete

$$f_{ps} = 0.017 f_{pu} \frac{L_v}{d_b} \leq 0.8 f_{pu} \quad \text{Equation 9.11 shown above}$$

$$f_{ps} = 0.017(270 \text{ ksi}) \left(\frac{7''}{0.6''} \right) = 53.4 \text{ ksi} \leq 0.8(270 \text{ ksi}) = 216 \text{ ksi}$$

Specific testing has not been conducted on the development of hooked non-prestressed strands in UHPC. The detail shown below with the additional transverse reinforcing bar is likely to be able to develop the $0.8f_{pu}$ in the strand, but more testing could be done to verify.

An additional option for the positive moment reinforcement is to add high-strength rebar extending from the bottom of the sections to splice for the positive moment reinforcement, as shown in Figure 9.25. The addition of reinforcement in the bottom of the section may be difficult due to the presence of prestressing strand and general congestion of the end regions with the additional splitting and confinement reinforcement. A combination of spliced high-strength rebar and hooked non-prestressed strands in UHPC were used for the positive moment reinforcement by Floyd et al. [111].

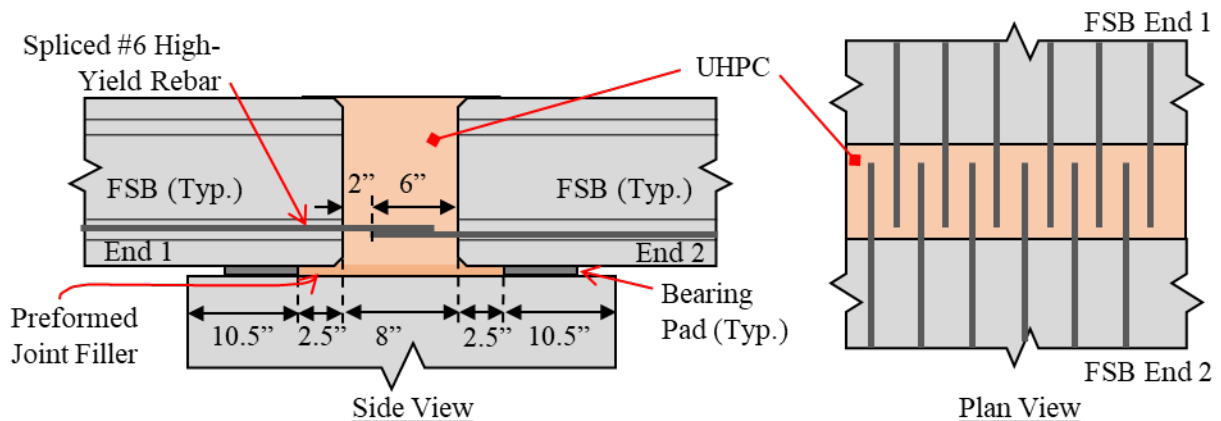


Figure 9.25: Splicing of high-strength rebar for positive moment reinforcement (based on Floyd et al. [111])

Three different preliminary details were developed for splicing of the negative moment reinforcement in the UHPC diaphragm:

1. **Spliced high-strength reinforcement (Figure 9.26):** This detail is based on Perry et al. [101] and would include high-strength rebar extending from the ends of the FSBs in adjacent spans. High-strength rebar is proposed to be used due to the amount of reinforcement needed in the negative moment region and the available space in the end region of the FSB section. The bars extending from the beam ends would be spliced with field placed rebar overlapping extended bars from both beams. The joint would need to be 14 inches wide to accommodate the rebar splices. The rebar extending from the beam ends could be placed at the same location in each beam, since they do not interfere with the rebar extending from the other beam. Perry et al. [101] found that the field-placed rebar led to congestion in the joint region.

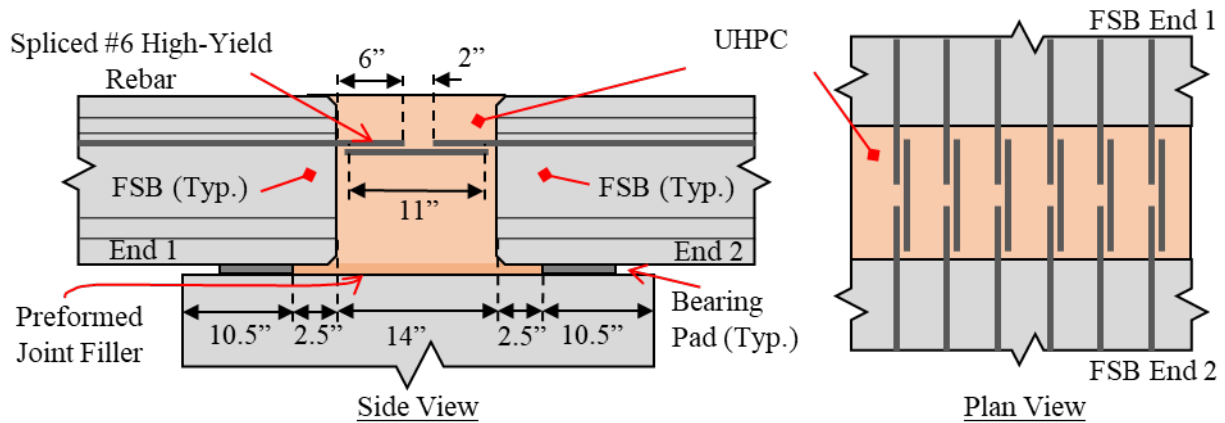


Figure 9.26: Lap-spliced high-yield rebar for continuity (based on Perry et al., [101])

2. **Non-contact lap splice of high-strength rebar (Figure 9.27):** This detail would also involve the splicing of high-strength rebar, but a non-contact lap splice would be used to eliminate the need for field-placed rebar and decrease the congestion in the joint. A non-contact lap splice detail would, however, require that the reinforcement be offset in opposite beam ends to create a 3-inch stagger and avoid conflict of the reinforcement. The UHPC diaphragm width could be reduced to as small as 8 inches for this detail.

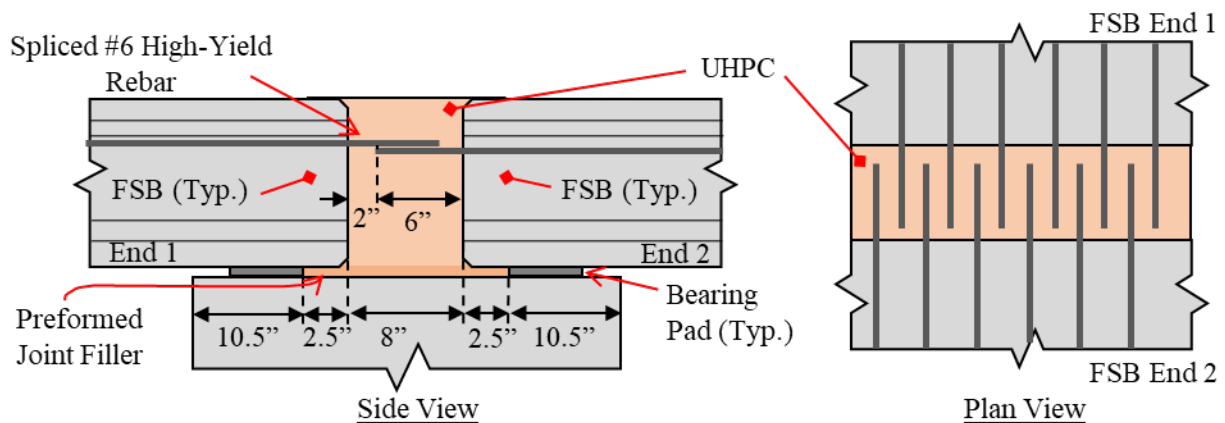


Figure 9.27: Non-contact and lap-spliced high-yield rebar for continuity (adapted from Perry et al., [101])

3. **Spliced, hooked prestressing strands (Figure 9.28):** This detail would involve the splicing of hooked top strands, like what is typically done for the positive moment reinforcement. A similar joint width and hook detail to what is used for the positive moment reinforcement can be used here. As mentioned above, there is no research related to the development of hooked prestressing strands in UHPC.

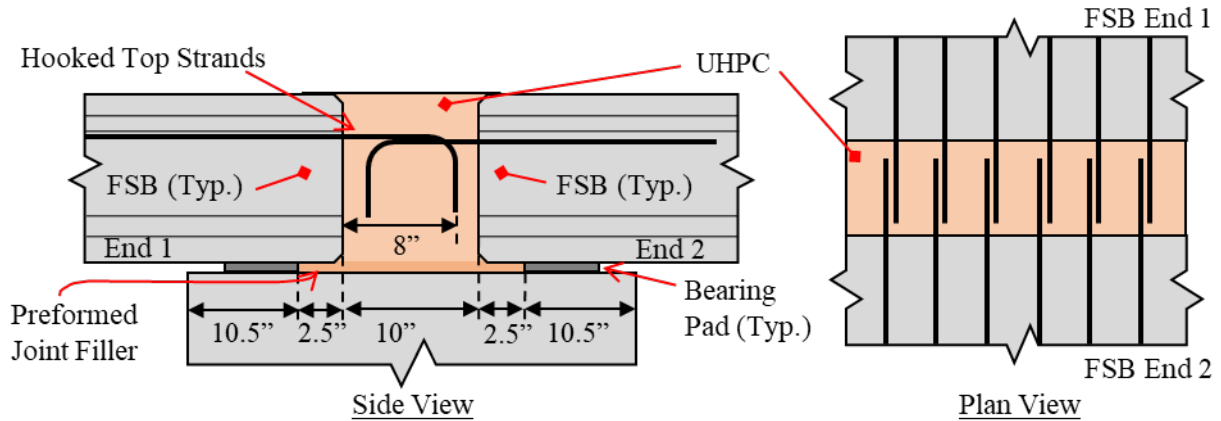


Figure 9.28: Lap-spliced, hooked strands for continuity (adapted from Freyermuth [93])

These preliminary design options were considered when designing the proposed SDCL connection detail for the modified FSB with UHPC joints system.

9.3.2. Preliminary Input and Analysis Assumptions

The design parameters used for the preliminary analysis are shown below. The design was based on a two-lane, two-span bridge with six 12x48 modified FSBs; the six-beam configuration was the same as that conducted to design the modified FSBs for the full-scale testing. The span length was based on the maximum span lengths for the modified FSB sections (without a cast-in-place topping) found earlier in the project, summarized in Table 9.2.

Table 9.2: Maximum span lengths for FSB depths

FSB Depth	Max Span Lengths (L_{span})	Corresponding Beam Length (L_{beam})
12"	32'	33.08'
15"	44'	45.08'
18"	55'	56.08'

The span length and beam length for this initial analysis are shown below.

$$L_{beam} = 33.08 \text{ ft.}$$

$$L_{span} = 32 \text{ ft.}$$

The material and section properties used for the beam and UHPC joints were based on the modified FSB design and UHPC joint detail. These properties are summarized below.

$$f'_{ci_{beam}} = 6 \text{ ksi}$$

$$f'_{c_{beam}} = 8.5 \text{ ksi}$$

$$f'_{c_{joint}} = 21 \text{ ksi}$$

$$E_{ci} = 4,557 \text{ ksi}$$

$$E_c = 5,112 \text{ ksi}$$

$$A_g = 522.42 \text{ in.}^2$$

$$I_g = 6,520.79 \text{ in.}^4$$

$$y_{t_{beam}} = 5.95 \text{ in.}$$

$$y_{b_{beam}} = 6.05 \text{ in.}$$

The assumed construction procedure for the SDCL design and analysis included two main stages:

1. The beams in each span were assumed to be simply supported (without continuity) to carry their self-weight and the weight of the wet concrete for the diaphragms and joints.
2. The hardening of the diaphragm establishes continuity, so the remaining superimposed dead loads (e.g., barriers and future wearing surface) and live loads were assumed to be carried by the continuous structure.

The weight of the beam and weight of the longitudinal joint were determined based on the beam and joint geometry.

$$\text{Self-weight and joint:} \quad w_{beam} = 0.544 \text{ kip/ft.} \quad w_{joint} = 0.058 \text{ kip/ft.}$$

$$w_{noncomposite} = w_{beam} + w_{joint} = 0.602 \text{ kip/ft.}$$

The weight of the barrier and overlay were applied to the continuous structure. The bridge was assumed to have two 36-inch, single-slope barriers, each with a weight of 430 lb/ft. The weight of the barriers was assumed to be evenly distributed amongst all the six beams after continuity was established.

$$\text{Barrier weight per beam:} \quad w_{barrier} = \frac{2(430 \text{ lb/ft.})}{6 \text{ beams}} = 143.3 \text{ lb/ft.} = 0.1433 \text{ kip/ft.}$$

The weight of the future overlay was based on SDG [102] Table 2.2-1 for spans less than 100 feet. The weight of the overlay was applied over the top of the modified FSB shape. No additional weight for utilities was applied.

$$\text{Overlay weight per beam:} \quad q_{overlay} = 0.015 \text{ kip/ft.}^2$$

$$w_{overlay} = \left(0.015 \text{ k/ft}^2\right) \left(\frac{48''}{12''/ft}\right) = 0.060 \text{ kip/ft.}$$

The HL-93 Live Load [82] was applied to the bridge after continuity had been established. The lane load, design tandem, design truck, and dual truck train were all considered in the analysis. Distribution factors were found using the FDOT Mathcad design sheet, Prestressed Beam v6.0 [121], and used to determine the live load demand on each beam.

$$g_{mon} = 0.38$$

$$g_{shear} = 0.62$$

$$g_{mon.fat} = 0.27$$

The continuity diaphragm was designed using the Strength I limit state with the dimensions of the diaphragm assumed equal to the dimensions of the modified FSB section.

$$\begin{aligned}
 h &= 12 \text{ in.} & b &= 48 \text{ in.} \\
 A_{diaphragm} &= 576 \text{ in.}^2 & I_{diaphragm} &= 6,192 \text{ in.}^4 \\
 y_{t_{dia.}} &= 6 \text{ in.} & s_t &= 1,152 \text{ in.}^3 \\
 y_{b_{dia.}} &= 6 \text{ in.} & s_b &= 1,152 \text{ in.}^3
 \end{aligned}$$

The negative moment reinforcement in the continuity diaphragm was designed for the Strength I Limit State based on the moments applied after continuity is achieved.

9.3.3. Structural Analysis

A preliminary structural analysis was performed using QConBridge™ [122] to determine the moment along the length of the beams and over the interior support. Two analysis stages were used to determine the total moments. Each bridge was designed with the same section and material properties described above, including the girder distribution factors [123].

- *Bridge 1* – two-span, simply-supported bridge: only the weight of the beams and joints were considered, as shown in Figure 9.29 (a) and,
- *Bridge 2* – two-span, continuous bridge: weight of beams and joints were deactivated. All live loads and superimposed dead loads (i.e., barriers and overlay) were considered, as shown in Figure 9.29 (b).

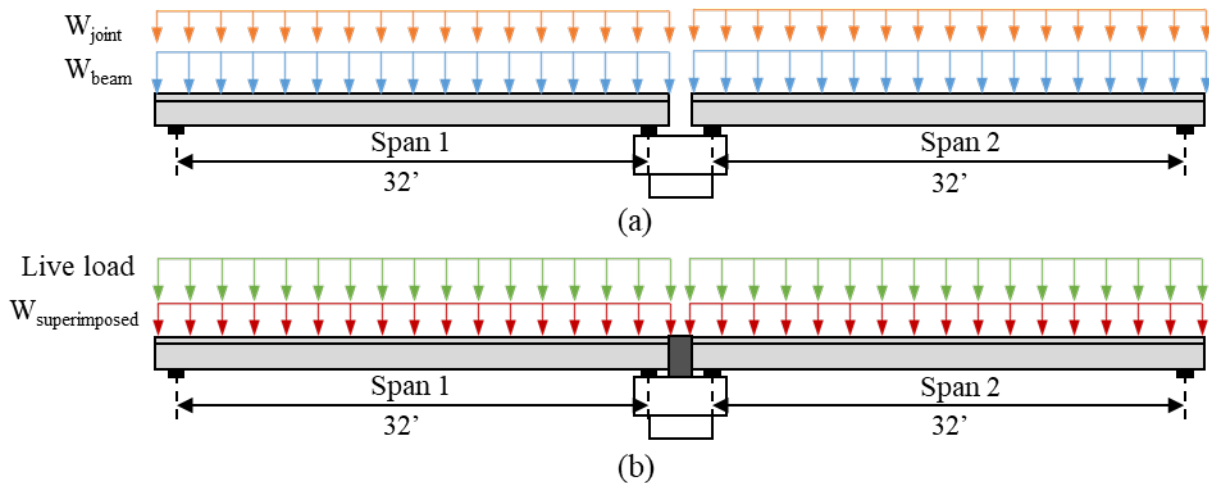


Figure 9.29: Load schematics for (a) Bridge 1 and (b) Bridge 2

The Strength I moment envelopes were determined for each of the bridges. The moment envelopes from Bridge 1 and Bridge 2 were summed to obtain the negative moment to use in the diaphragm design. The model was constructed based on a per-girder (line girder) analysis, so the results shown are for a single girder design. The center support was assumed to be the same for beams in Span 1 and Span 2. A summary of the moment envelope values for Bridge 1, Bridge 2, and the resultant summation is presented in Table 9.3.

Table 9.3: QConBridge™ Strength I Moment envelopes for Bridge 1, Bridge 2, and Summation

Span	L (ft)	Bridge 1 – Simply Supported		Bridge 2 - Continuous		Summation	
		Moment (min.) (ft-kips)	Moment (max.) (ft-kips)	Moment (min.) (ft-kips)	Moment (max.) (ft-kips)	Moment (min.) (ft-kips)	Moment (max.) (ft-kips)
1	0.0	0.0	0.0	0.0	0.0	0.0	0.0
1	3.2	34.7	34.7	-11.1	140.4	23.6	175.1
1	6.4	61.7	61.7	-23.9	234.5	37.7	296.1
1	9.6	80.9	80.9	-38.5	291.8	42.5	372.7
1	12.8	92.5	92.5	-54.7	312.2	37.8	404.7
1	16.0	96.4	96.4	-72.7	304.0	23.7	400.3
1	19.2	92.5	92.5	-92.4	271.1	0.1	363.6
1	22.4	80.9	80.9	-113.8	209.2	-32.9	290.1
1	25.6	61.7	61.7	-139.0	125.4	-77.4	187.0
1	28.8	34.7	34.7	-176.2	38.7	-141.5	73.4
1	32.0	0.0	0.0	-271.3	-21.5	-271.3	-21.5
2	32.0	0.0	0.0	-271.3	-21.5	-271.3	-21.5
2	35.2	34.7	34.7	-176.2	38.7	-141.5	73.4
2	38.4	61.7	61.7	-139.0	125.4	-77.4	187.0
2	41.6	80.9	80.9	-113.8	209.2	-32.9	290.1
2	44.8	92.5	92.5	-92.4	271.1	0.1	363.6
2	48.0	96.4	96.4	-72.7	304.0	23.7	400.3
2	51.2	92.5	92.5	-54.7	312.2	37.8	404.7
2	54.4	80.9	80.9	-38.5	291.8	42.5	372.7
2	57.6	61.7	61.7	-23.9	234.5	37.7	296.1
2	60.8	34.7	34.7	-11.1	140.4	23.6	175.1
2	64.0	0.0	0.0	0.0	0.0	0.0	0.0

Note: Maximum summation Moments are bolded

The resultant summation of the Strength I moment envelope plots are shown in Figure 9.30. Based on the QConBridge™ analysis, the maximum negative moment obtained for the diaphragm design is 280.4 kip-feet per beam.

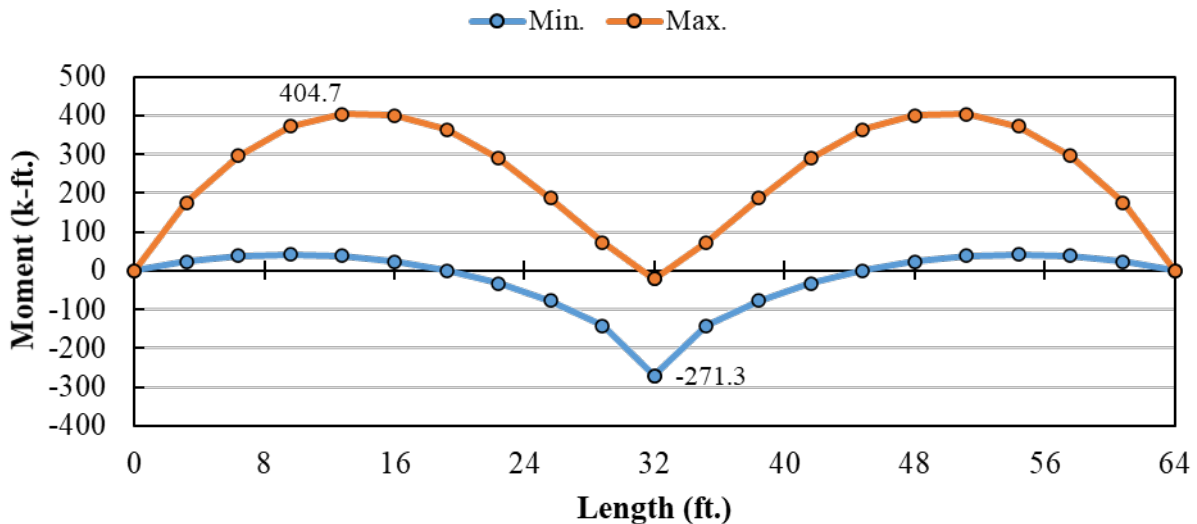


Figure 9.30: Summation of Strength I Moment envelopes for continuous FSB system diaphragm

using non-contact lap-spliced mild steel and (2) using non-prestressed strands extended from the girder ends and hooked in the diaphragm.

9.3.5.1. Mild Steel Reinforcement Option

The entire bottom row of strands (with $d = 9$ inches) is occupied with prestressing strands in the modified FSB design. The mild reinforcement shall be in the next strand layer from the bottom (with $d = 7$ inches) in strand locations where there are not any prestressing strands for the modified FSB design. The initial distance between end of girders in the continuity diaphragm and the vertical location of the positive reinforcement is shown in Figure 9.31.

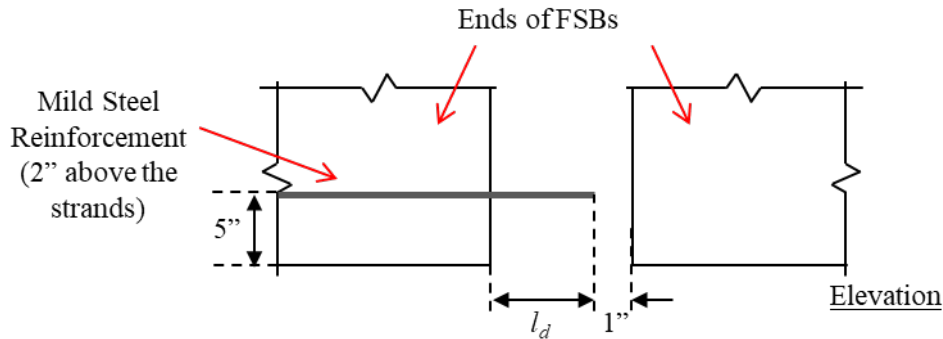


Figure 9.31: Preliminary location of the mild reinforcement for the positive moment design

The amount of reinforcement required is found in this section based on the following input data. A conventional rectangular stress block approach was used to find the nominal moment capacity. The positive moment failure was assumed to occur right at the boundary between the UHPC diaphragm and the precast concrete with crushing of the precast concrete controlling the failure.

Input Data:	$f_y = 60$ ksi	$M_u = 1.2M_{cr} = 80.6$ kip – ft.
	$b = 48$ in.	$h = 12$ in.
	$d = 7$ in.	$f'_c = 8.5$ ksi

$$\beta_1 = 0.85 - 0.05 * (8.5 \text{ ksi} - 4 \text{ ksi}) \leq 0.65$$

$$\beta_1 = 0.65$$

$$\alpha_1 = 0.85$$

Standard #5 bars can be used as the positive moment reinforcement with a non-contact lap splice connection in the UHPC in the diaphragm. The design of the connection and splice in the UHPC diaphragm was based on Graybeal [108]. The following values are for #5 rebar:

#5 Rebar:	$d_b = 0.625$ in.	$A_s = 0.31$ in. ²	$f_y = 60$ ksi
------------------	-------------------	-------------------------------	----------------

For #5 rebar:

Development Length (based on [108]): $l_d = 8d_b = 8(0.625 \text{ in.}) = 5 \text{ in.}$

Minimum rebar cover in UHPC: $1 \text{ in.} \leq c \leq 3d_b = 1.875 \text{ in.}$

Minimum spacing (based on [108]): $s = 1.5(0.5 \text{ in.}) = 0.75 \text{ in.}$

Splice length (based on [108]): $l_s \geq 0.75l_d = 0.75(5 \text{ in.}) = 3.75 \text{ in.}$

The design requirements are satisfied using 9 - #5 bars:

9 - #5 bars: $A_s = (9)(0.31 \text{ in.}^2) = 2.79 \text{ in.}^2$

Neutral axis depth: $c = \frac{(2.79 \text{ in.}^2)(60 \text{ ksi})}{(0.85)(0.65)(8.5 \text{ ksi})(48 \text{ in.})} = 0.743 \text{ in.}$

Rebar strain: $\epsilon_s = 0.003 \left(\frac{d - c}{c} \right) = 0.003 \left(\frac{7'' - 0.743''}{0.743''} \right) = 0.0253 \geq \epsilon_{TC} = 0.005$

For T.C.: $\phi = 0.9$

Nominal moment: $M_n = (2.79 \text{ in.}^2)(60 \text{ ksi}) \left(7 \text{ in.} - \frac{(0.65)(0.743'')}{2} \right)$

$$M_n = 1,131 \text{ kip} - \text{in.} = 94.3 \text{ kip} - \text{ft.}$$

Design check (OK): $\phi M_n = (0.9)(94.3 \text{ kip} - \text{ft.}) = 84.9 \text{ kip} - \text{ft.} \geq 1.2M_{cr} = 80.6 \text{ kip} - \text{ft.}$

A larger size rebar may also be used to satisfy the design requirements. The following values are found for #6 rebar using Graybeal [108].

#6 Rebar: $d_b = 0.75 \text{ in.}$ $A_s = 0.44 \text{ in.}^2$ $f_y = 60 \text{ ksi}$

For #6 rebar:

Development Length (based on [108]): $l_d = 8d_b = 8(0.75 \text{ in.}) = 6 \text{ in.}$

Minimum rebar cover in UHPC: $1 \text{ in.} \leq c \leq 3d_b = 2.25 \text{ in.}$

Minimum spacing (based on [108]): $s = 1.5(0.5 \text{ in.}) = 0.75 \text{ in.}$

Splice length (based on [108]): $l_s \geq 0.75l_d = 0.75(6 \text{ in.}) = 4.5 \text{ in.}$

Seven - #6 bars can be used to meet the design requirement:

7 - #6 bars:

$$A_s = (7)(0.44 \text{ in.}^2) = 3.08 \text{ in.}^2$$

Neutral axis depth:

$$c = \frac{(3.08 \text{ in.}^2)(60 \text{ ksi})}{(0.85)(0.65)(8.5 \text{ ksi})(48 \text{ in.})} = 0.820 \text{ in.}$$

Rebar strain:

$$\varepsilon_s = 0.003 \left(\frac{d - c}{c} \right) = 0.003 \left(\frac{7" - 0.820"}{0.820"} \right) = 0.0226 \geq \varepsilon_{TC} = 0.005$$

For T.C.:

$$\phi = 0.9$$

Nominal moment:

$$M_n = (3.08 \text{ in.}^2)(60 \text{ ksi}) \left(7 \text{ in.} - \frac{(0.65)(0.820")}{2} \right)$$

$$M_n = 1,244 \text{ kip} - \text{in.} = 103.7 \text{ kip} - \text{ft.}$$

Design check (OK):

$$\phi M_n = (0.9)(103.7 \text{ kip} - \text{ft.}) = 93.3 \text{ kip} - \text{ft.} \geq 1.2M_{cr} = 80.6 \text{ kip} - \text{ft.}$$

The rebar must also be developed in the end of the precast girder. The rebar development lengths are found using AASHTO LRFD Bridge Design Specification [82] §5.10.8.2.1a.

Basic development length (#5 bars):

$$l_{db} = 2.4d_b \frac{f_y}{\sqrt{f'_c}} = 2.4(0.625 \text{ in.}) \left(\frac{60 \text{ ksi}}{\sqrt{8.5 \text{ ksi}}} \right) = 30.9 \text{ in.}$$

Modification factors:

$$\lambda_{rl} = \lambda_{cf} = \lambda_{rc} = \lambda_{er} = \lambda = 1.0$$

Tension Development length (#5 bars):

$$l_d = l_{db} \left(\frac{\lambda_{rl} * \lambda_{cf} * \lambda_{rc} * \lambda_{er}}{\lambda} \right) = 30.9 \text{ in.}$$

For #6 bars:

Basic development length (#6 bars):

$$l_{db} = 2.4d_b \frac{f_y}{\sqrt{f'_c}} = 2.4(0.75 \text{ in.}) \left(\frac{60 \text{ ksi}}{\sqrt{8.5 \text{ ksi}}} \right) = 37.0 \text{ in.}$$

Modification factors:

$$\lambda_{rl} = \lambda_{cf} = \lambda_{rc} = \lambda_{er} = \lambda = 1.0$$

Tension Development length (#6 bars):

$$l_d = l_{db} \left(\frac{\lambda_{rl} * \lambda_{cf} * \lambda_{rc} * \lambda_{er}}{\lambda} \right) = 37.0 \text{ in.}$$

An additional check was performed to avoid stress concentrations at rebar ending at same distance, providing two development lengths (l_{d1} and l_{d2}) per rebar size as shown in Figure 9.32. This detailing check is based on Miller et al. [98].

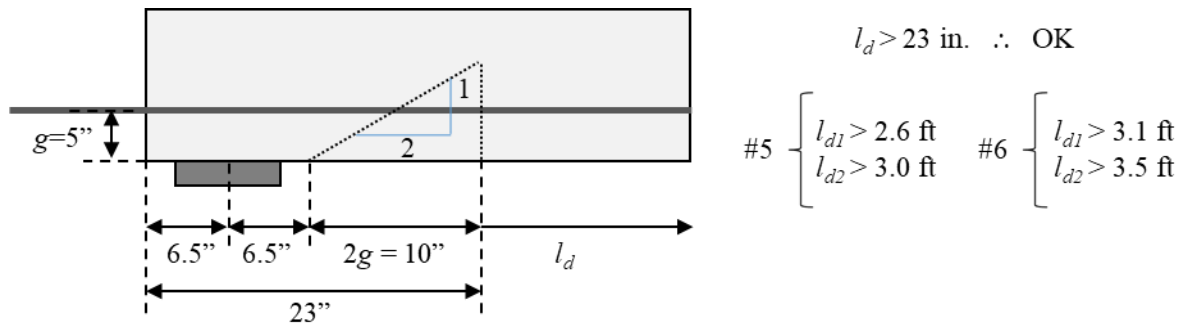


Figure 9.32: Additional detailing check for embedment of reinforcement into the girder, based on Miller et al. [98]

Mild reinforcement should be implemented using a non-contact lap-splice bar configuration. The minimum diaphragm joint width is highlighted in Figure 9.33 (a). The reinforcement would need to be offset between the ends of the members from adjacent spans, like shown in Figure 9.33 (b); 8 bars could extend from one member and 7 from the other to have a symmetrical bar pattern with the bars offset.

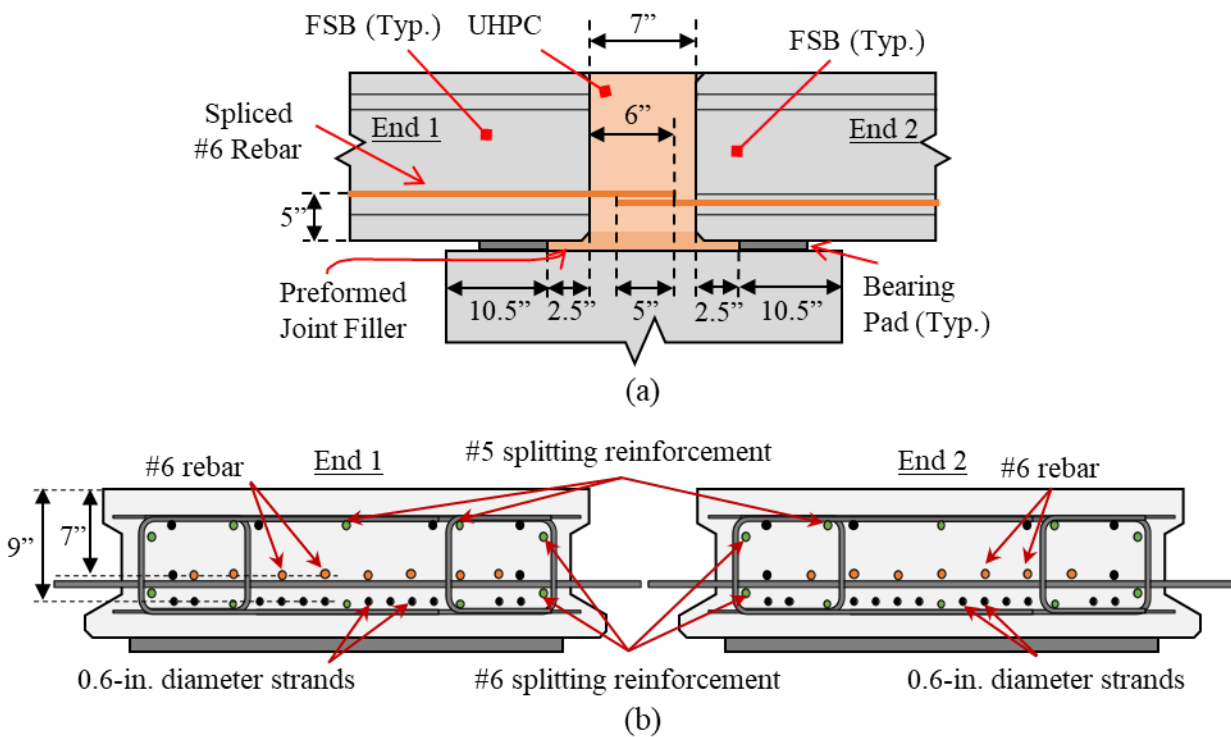


Figure 9.33: Positive moment connection with 8 #6 mild reinforcement: (a) elevation and (b) ends view

9.3.5.2. Non-Prestressed Strands Option

The development length of hooked, non-prestressed strands in UHPC has not been previously tested. Maya and Graybeal [109] conducted testing on straight non-prestressed strands in UHPC. They noted that the development length of non-prestressed strands is longer than prestressed strand due to the absence of Hoyer's effect but found the development length in UHPC to be

significantly shorter than in conventional concrete. Maya and Graybeal [109] suggested a development length as shown in Equation 9.12.

Development length of non-prestressed strand embedded in UHPC: $l_d \geq 40d_s$ Equation 9.12

For 0.6-inch strand: $l_d \geq 40d_s = 40(0.6") = 24"$

A minimum diaphragm joint width of 25 inches would be required for a straight, non-prestressed strand splice using this recommended length, as shown in Figure 9.34.

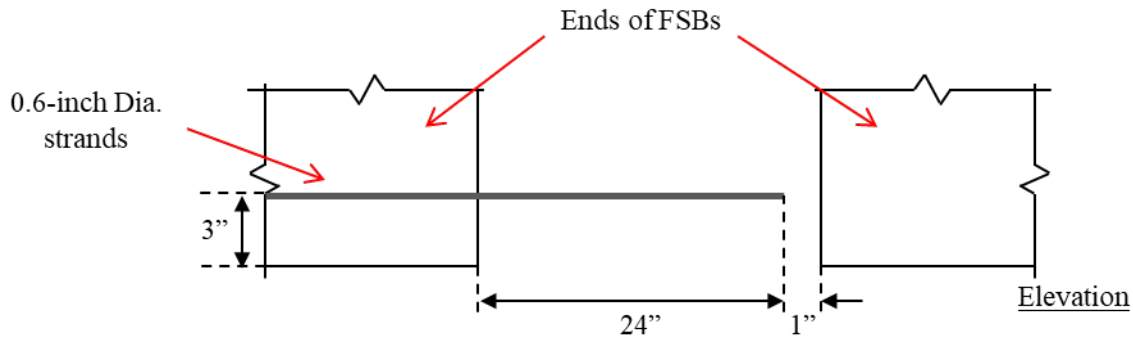


Figure 9.34: Required UHPC diaphragm width for straight, non-prestressed strand splice for positive moment reinforcement

The joint width for a straight strand splice is too wide for the efficient use of UHPC, so a hooked strand splice is recommended. The equation proposed by Noppakunwijai et al. [106] (Equation 9.11) was developed based on 0.6-inch diameter strands embedded in 4,000 psi concrete. The equation assumes 6-inch horizontal embedment length (L_h) and varying vertical embedment length of the hook (L_v), as shown in Figure 9.35. Equation 9.11 can be used to determine the developed stress based on the provided vertical embedment length of the strand.

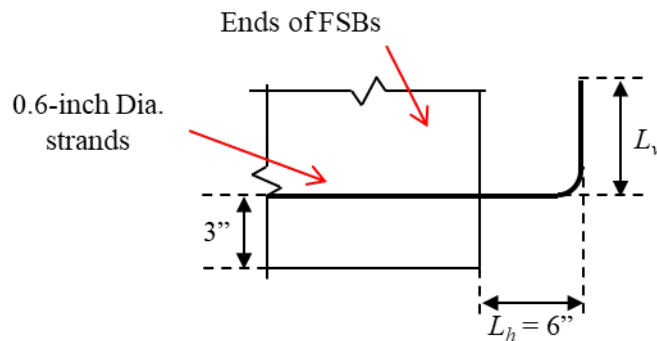


Figure 9.35: Non-prestressed strand hook details at ends of FSB

The maximum vertical embedment length is dependent on the strand location and thickness of the modified FSB section. The vertical distance is the FSB thickness (12 inches) minus the distance from the bottom of the section to the centroid of the strands (3 inches) minus the distance between the top of the strand hook and the top of the diaphragm. The vertical distance

of a hook is typically taken from the outside of the strand, so 0.5 times strand diameter can be added back to the maximum vertical embedment length. This gives a vertical embedment length as shown below.

Vertical embedment length
for a 12-inch-thick FSB:

$$L_v = 12" - 3" + 0.5(0.6") - 2" \text{ (cover)} = 7.3"$$

This vertical embedment length can then be conservatively used with the equation from Noppakunwijai et al. [106] to find the stress in the strand for the nominal moment capacity checks.

Stress in strand at nominal
using Equation 9.11:

$$f_{ps} = 0.017f_{pu} \frac{L_v}{d_b} \leq 0.8f_{pu}$$

$$f_{ps} = 0.017(270 \text{ ksi}) \left(\frac{7.3 \text{ in.}}{0.6 \text{ in.}} \right) = 55.8 \text{ ksi} \leq 0.8(270 \text{ ksi}) = 216 \text{ ksi}$$

This would be a very conservative estimate as the equation from Noppakunwijai et al. [106] was developed using 4 ksi concrete, while the UHPC diaphragm would have 21 ksi concrete.

The current modified FSB would require 12 strands in the bottom layer. Assuming 12 strands with the conservative stress estimate would give us the following:

11 – 0.6-inch strands:

$$A_p = (11)(0.217 \text{ in.}^2) = 2.387 \text{ in.}^2$$

$$f_{ps} = 55.8 \text{ ksi}$$

$$d_p = 12" - 3" = 9"$$

Neutral axis depth:

$$c = \frac{(2.387 \text{ in.}^2)(55.8 \text{ ksi})}{(0.85)(0.65)(8.5 \text{ ksi})(48 \text{ in.})} = 0.591 \text{ in.}$$

Rebar strain:

$$\varepsilon_s = 0.003 \left(\frac{d - c}{c} \right) = 0.003 \left(\frac{9" - 0.591"}{0.591"} \right) = 0.0427 \geq \varepsilon_{TC} = 0.005$$

For T.C.:

$$\phi = 0.9$$

Nominal moment:

$$M_n = (2.387 \text{ in.}^2)(55.8 \text{ ksi}) \left(9 \text{ in.} - \frac{(0.65)(0.591")}{2} \right)$$

$$M_n = 1,174 \text{ kip} - \text{in.} = 97.8 \text{ kip} - \text{ft}$$

Design check (OK):

$$\phi M_n = (0.9)(97.8 \text{ kip} - \text{ft.}) = 88.1 \text{ kip} - \text{ft.} \geq 1.2M_{cr} = 80.6 \text{ k} - \text{in.}$$

The design here will check even with the conservative strand stress used.

The minimum diaphragm width for a hooked strand in UHPC is shown in Figure 9.36. Field-placed, transverse #5 bars can be placed inside the bend radius of the strands to further improve the performance of the splice. The number of spliced strands can likely be decreased, but additional research should be first done on the behavior of hooked, non-prestressed strand splices in UHPC.

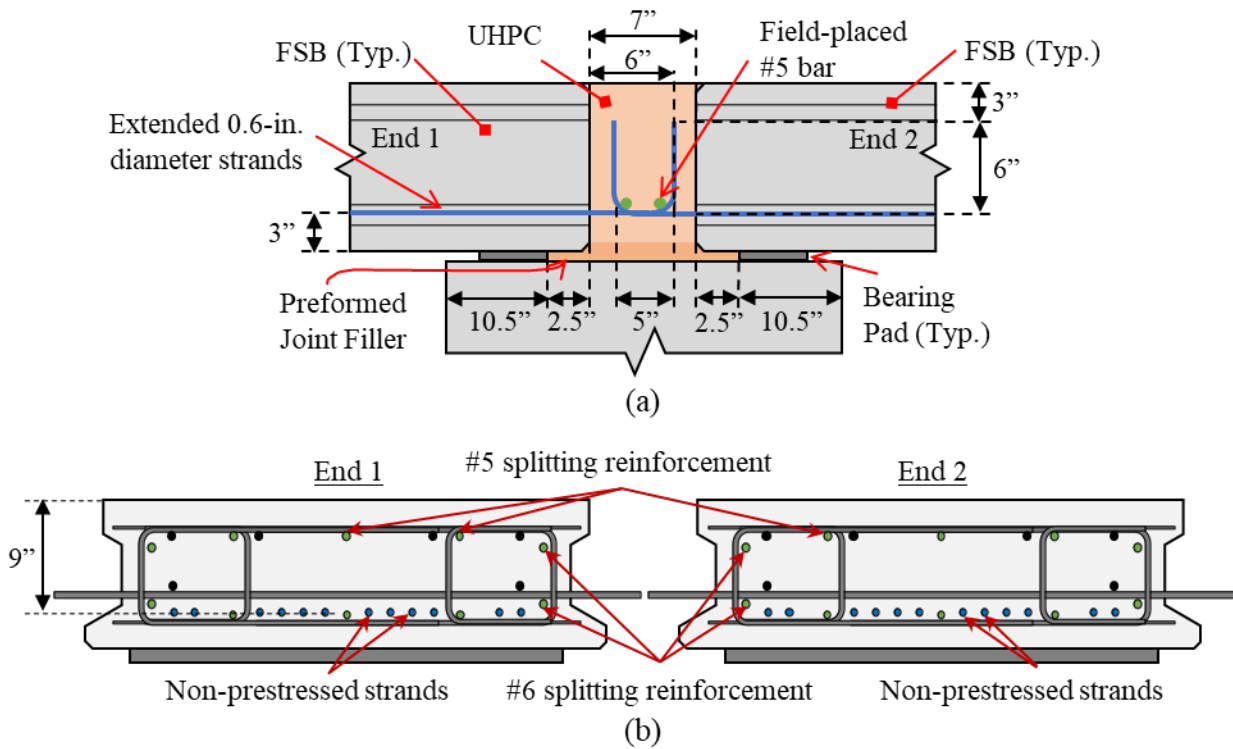


Figure 9.36: Positive moment connection with non-prestressed bent strands: (a) elevation and (b) ends view

9.3.6. Design of Negative Moment Reinforcement

The negative moment reinforcement was designed based on the different options reviewed and discussed in the previous sections of this chapter. The required negative moment reinforcement is based on the maximum negative moment demand found in §9.3.2.

Negative moment demand: $M_u = 271.3 \text{ kip} - \text{ft.}$

The negative moment reinforcement will consist of high-strength ($f_y = 75 \text{ ksi}$) #6 bars. High-strength reinforcement is needed to provide sufficient reinforcement while reducing congestion in the beam ends and diaphragm. A non-contact lap splice is proposed, based on recommendations by Perry et al. [101] to further reduce congestion in the UHPC diaphragm. The non-contact lap splice requirements were found based on Graybeal [108]. These are like those found for #6 bars in the positive moment reinforcement section.

#6 Rebar: $d_b = 0.75$ in. $A_s = 0.44$ in.² $f_y = 60$ ksi

For #6 rebar:

Development Length (based on [108]): $l_d = 8d_b = 8(0.75 \text{ in.}) = 6$ in.

Minimum rebar cover in UHPC: $1 \text{ in.} \leq c \leq 3d_b = 2.25$ in.

Minimum spacing (based on [108]): $s = 1.5(0.5 \text{ in.}) = 0.75$ in.

Splice length (based on [108]): $l_s \geq 0.75l_d = 0.75(6 \text{ in.}) = 4.5$ in.

The proposed reinforcement location would be in the top of the FSB section aligned with the top layer of prestressing strands (3 inches from the top of the section), as shown in Figure 9.37. This would leave a cover as shown below:

Available cover to top of diaphragm: $cover = 3" - 0.5d_b = 3" - 0.5(0.75 \text{ in.}) = 2.625"$

The top cover is still greater than the $3d_b$ limit, so the same development length and splice length can be used.

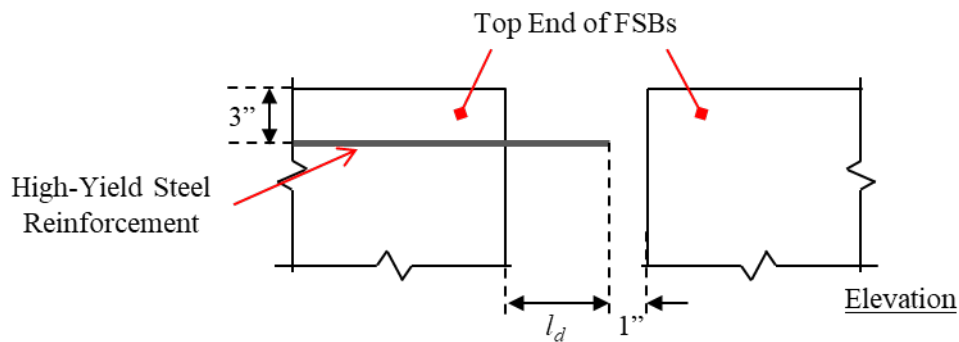


Figure 9.37: Preliminary location of high-strength rebar for the negative moment design

The negative moment capacity was found using a conventional rectangular stress block approach. The negative moment failure was assumed to occur right at the boundary between the UHPC diaphragm and the precast concrete with crushing of the precast concrete controlling the failure.

Input Data: $f_y = 75$ ksi $M_u = 271.3$ kip – ft.
 $b = 48$ in. $h = 12$ in. $d = 9$ in.

If tension-controlled behavior is assumed:

$\phi = 0.90$

$$f'_c = 8.5 \text{ ksi}$$

$$\beta_1 = 0.85 - 0.05(8.5 \text{ ksi} - 4 \text{ ksi}) \leq 0.65$$

$$\beta_1 = 0.65$$

$$\alpha_1 = 0.85$$

There are 12 available positions for high-strength rebar (considering the 4 top strands already present in the precast section) within the precast section. This design cannot be satisfied based on only 12 high-strength #6 bars; the maximum factored negative moment capacity is 250.3 k-ft for this section.

The design requirements are satisfied using 12 high-strength #6 bars and hooking the 4 top strands into the UHPC diaphragm. The stress in the non-prestressed strands at the nominal moment will be taken as the same stress that was found for the positive moment design from Noppakunwijai et al. [106].

12 - #6 bars: $A_{s1} = (12)(0.44 \text{ in.}^2) = 5.28 \text{ in.}^2$

4 - 0.6" strands: $A_{s2} = (4)(0.217 \text{ in.}^2) = 0.868 \text{ in.}^2$

$$f_{ps} = 55.8 \text{ ksi}$$

Neutral axis depth: $c = \frac{(5.28 \text{ in.}^2)(75 \text{ ksi}) + (0.868 \text{ in.}^2)(55.8 \text{ ksi})}{(0.85)(0.65)(8.5 \text{ ksi})(48 \text{ in.})} = 1.972 \text{ in.}$

Rebar strain: $\epsilon_s = 0.003 \left(\frac{d - c}{c} \right) = 0.003 \left(\frac{9" - 1.972"}{1.972"} \right) = 0.0107 \geq \epsilon_{TC} = 0.005$

$$M_n = [(5.28 \text{ in.}^2)(75 \text{ ksi}) + (0.868 \text{ in.}^2)(55.8 \text{ ksi})] \left(9 \text{ in.} - \frac{(0.65)(1.972")}{2} \right)$$

$$M_n = 3,715 \text{ kip} - \text{in.} = 309.6 \text{ kip} - \text{ft.}$$

Design check: $\phi M_n = (0.9)(309.6 \text{ kip} - \text{ft.}) = 278.7 \text{ kip} - \text{ft.} \geq M_u$ **OK**
 $= 271.3 \text{ kip} - \text{ft.}$

The negative moment reinforcement can be satisfied with 12 high-strength #6 bars and hooking the top 4 non-prestressed strands into the UHPC diaphragm. The negative moment reinforcement should be extended 15 feet into each beam, so the bars are extended beyond the inflection points. The high-strength bars in the precast section should be offset by 1 inch to allow for sufficient space for the UHPC to flow.

The preliminary negative moment design with the minimum possible joint width is shown in Figure 9.38.

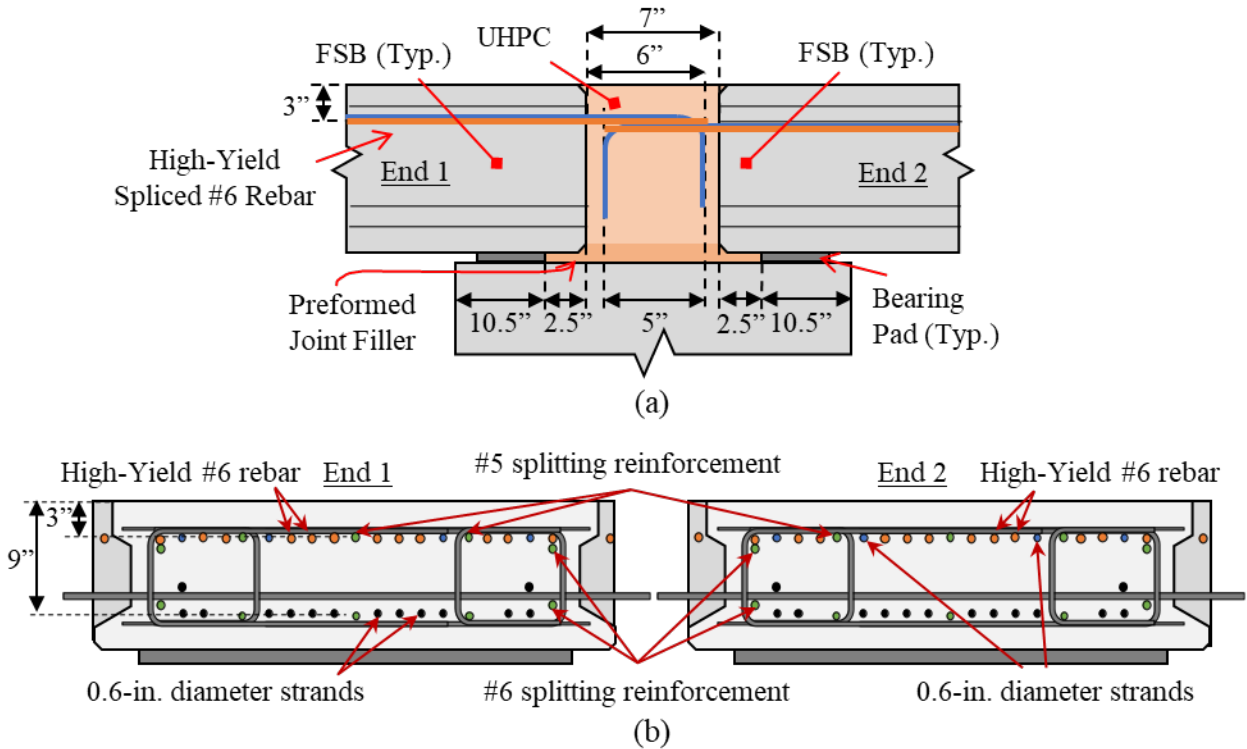


Figure 9.38: Negative moment connection with high-yield reinforcement and non-prestressed hooked strands: (a) elevation and (b) ends view

9.3.7. Stress Checks in Prestressed Concrete Members

The stresses do not need to be checked in the diaphragm region, since it is not a prestressed concrete member. The stresses still should be checked in the prestressed concrete member using the Service III load combination to limit service cracking that will occur in the negative moment region, see AASHTO LRFD Bridge Design Specification [82] §5.12.3.3.6. The tensile stresses in the top of the beam should be found after all prestress losses have occurred and compared to the tensile stress limits from Table 5.9.2.3.1b-1 for other than segmentally constructed bridges where f'_c is used in the equations. This stress limit will be as shown in Equation 9.13.

$$|f_{ct}| \leq 0.24\lambda\sqrt{f'_c} \quad \text{Equation 9.13}$$

There is an additional note:

Alternatively, the top of the precast girders at interior supports may be designed as reinforced concrete members at the strength limit state. In this case, the stress limits for the service limit state shall not apply to the region of the precast girder.

The negative moment reinforcement was already designed for the Strength I limit state as a reinforced concrete member, so this clause would be satisfied.

9.3.8. Proposed Continuity Diaphragm Design (12-inch)

The final proposed UHPC continuity detail for a 12x48 modified FSB span bridge is shown in Figure 9.39. The detail is based on the combined non-prestressed strands for positive moment and high-yield reinforcement and non-prestressed strands for negative moment. The final diaphragm width was chosen as 8 inches to allow for some construction tolerances in the end region.

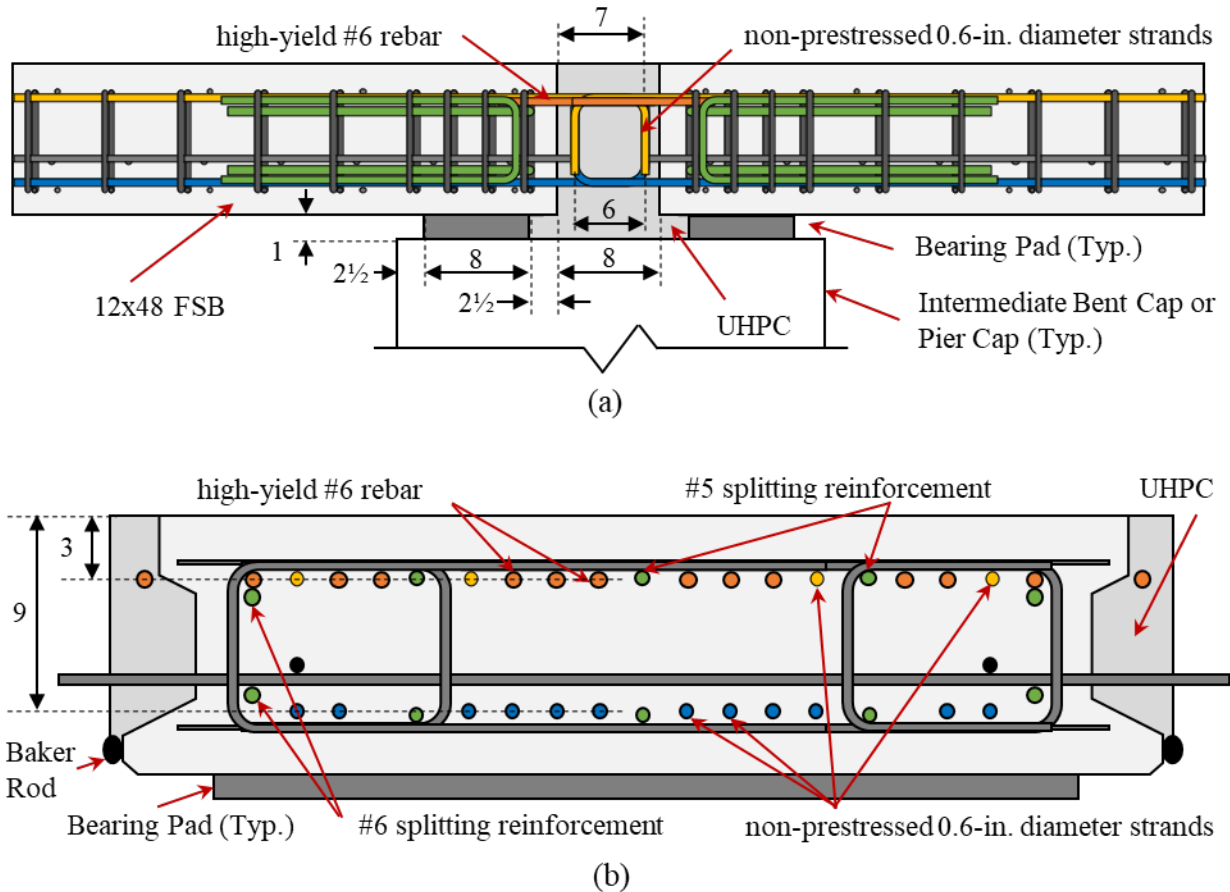


Figure 9.39: Diaphragm connection detail for 12-in. thick FSB system: (a) section through diaphragm connection and (b) FSB end region reinforcement detail. Note: units in inches

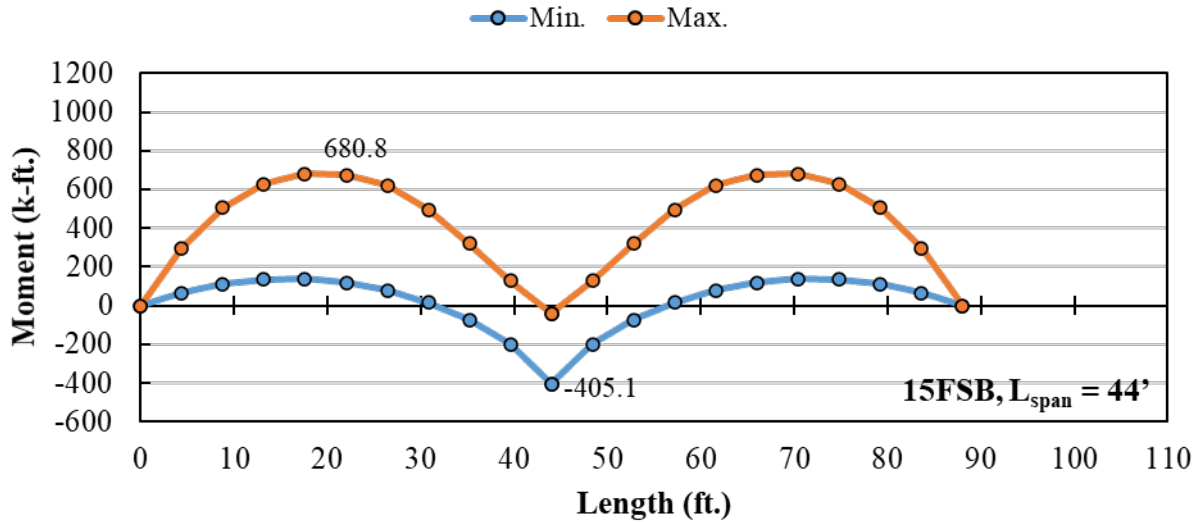
9.3.9. Additional Depths

Additional designs were performed for the 15-inch and 18-inch-deep modified FSB section shape. The span lengths chosen for these designs were based on the maximum span lengths for each of the sections, summarized in Table 9.2. The same design procedure used for the 12-inch-deep modified FSB was used for the 15-inch and 18-inch-deep sections. The same material properties were assumed. The input properties for all three of the analyses are summarized in Table 9.4; input properties are shown for all three section depths for comparison.

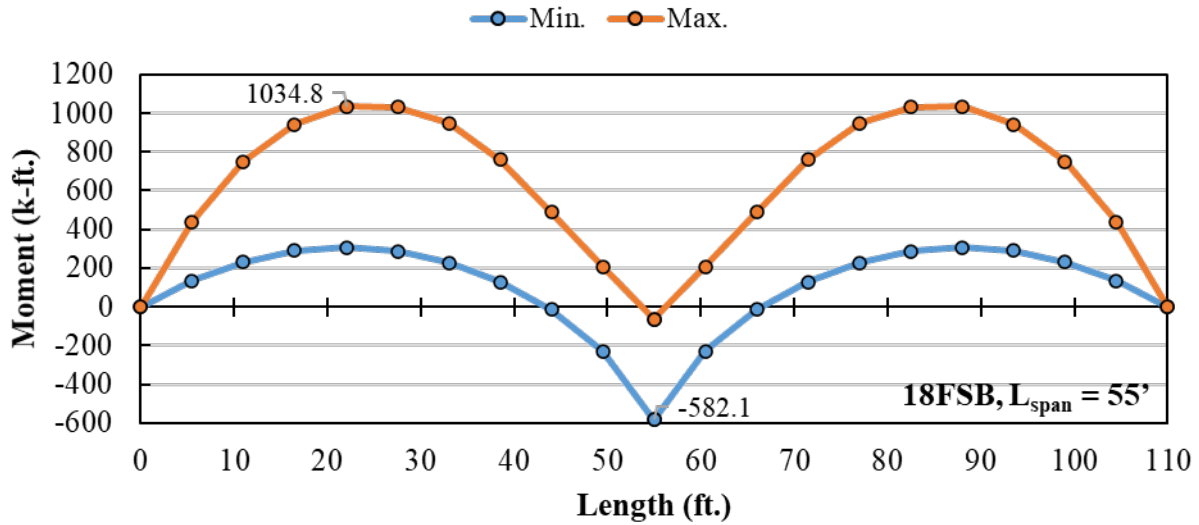
Table 9.4: Summary of inputs for SDCL analyses for all three section depths

Parameter	Modified FSB Section Depth		
	12-inch	15-inch	18-inch
L_{beam} (ft.)	33.08	45.08	56.08
L_{span} (ft.)	32	44	55
$f'_{ci,beam}$ (ksi)	6.0		
$f'_{c,beam}$ (ksi)	8.5		
$f'_{c,joint}$ (ksi)	21		
$E_{ci,beam}$ (ksi)	4,877		
$E_{c,beam}$ (ksi)	5,471		
A_g (in. ²)	522.42	646.4	770.1
I_g (in. ⁴)	6,520.79	12,635.90	21,646.00
$y_{t,beam}$ (in.)	6.1	7.6	9.1
$y_{b,beam}$ (in.)	5.9	7.4	8.9
w_{beam} (k/ft.)	0.544	0.673	0.802
w_{joint} (k/ft.)	0.058	0.077	0.098
w_{nc} (k/ft.)	0.602	0.750	0.900
$w_{barrier}$ (k/ft.)	0.1433		
$q_{overlay}$ (k/ft. ²)	0.015		
$w_{overlay}$ (k/ft)	0.060		
g_{mon}	0.38	0.36	0.34
g_{shear}	0.62	0.60	0.58
$g_{mon,fat}$	0.27	0.23	0.20
h_{dia} (in.)	12	15	18
b_{dia} (in.)	48	48	48
A_{dia} (in. ²)	576	720	864
I_{dia} (in. ⁴)	6,912	13,500	23,328
$y_{t,dia}$ (in.)	6.0	7.5	9.0
$y_{b,dia}$ (in.)	6.0	7.5	9.0
$S_{t,dia}$ (in. ³)	1,152	1,800	2,592
$S_{b,dia}$ (in. ³)	1,152	1,800	2,592

The maximum and minimum moments for the Strength I limit state for the 15-inch and 18-inch-deep modified FSB designs are shown in Figure 9.40.



(a)



(b)

Figure 9.40: Minimum and maximum moments for Strength I for (a) 15-inch-deep FSB with 44-foot spans and (b) 18-inch-deep FSB with 55-foot spans

A summary of the design details for the three different section depths is provided in Table 9.5 and Table 9.6. The design in this table is based on using non-prestressed strands as the positive moment reinforcement and a combination of non-prestressed strands and high-strength ($f_y = 75$ ksi) rebar for the negative moment reinforcement, like the detail shown in Figure 9.39.

Table 9.5: Positive moment design of SDCL connection for 12-, 15-, and 18-inch-deep modified FSB sections with non-prestressed strands

Parameter	Modified FSB Section Depth		
	12-inch	15-inch	18-inch
$M_{cr,beam}$ (k-ft)	67.2	105.0	151.1
$1.2M_{cr,beam}$ (k-ft)	80.6	125.9	181.4
d_{pos} (in.)	9.0	12.0	15.0
L_v (in.)	7.3	10.3	13.3
f_{ps} (ksi)	55.8	78.8	101.7
$n_{strands,pos}$	11	11	11
$\phi M_{n,pos}$ (k-ft)	88.1	165.5	266.8
$M_{u,pos}$ (k-ft)	80.6	125.9	181.4

Table 9.6: Negative moment design of SDCL connection for 12-, 15-, and 18-inch-deep modified FSB sections with high-strength rebar and non-prestressed strands

Parameter	Modified FSB Section Depth		
	12-inch	15-inch	18-inch
d_{neg} (in.)	9	12	15
$BarSize_{neg}$	#6	#6	#6
$n_{bars,neg}$	12	13	14
$n_{strands,neg}$	4	4	4
$\phi M_{n,neg}$ (k-ft)	278.7	420.9	586.4
$M_{u,neg}$ (k-ft)	271.3	405.1	582.1

9.4. NUMERICAL EVALUATION OF FSB JOINT DETAIL FOR CONTINUITY

The proposed continuity detail shown in Figure 9.39 was further evaluated through a numerical analysis using a two-beam configuration. The behavior of the longitudinal and transverse connections was evaluated using ATENA FEM software by modeling the UHPC diaphragm and one longitudinal joint.

9.4.1. Loading Configuration and Protocol

The loading type selected for the model configuration was based on a full FL120 rear axle load as per Chapter 2 of the FDOT Bridge Load Rating Manual [124], as shown in Figure 9.41 (a), with the same wheel patch geometry of a HS20 rear truck axle as per the AASHTO LRFD Bridge Design Specifications (§3.6.1.2.2) [82], as shown in Figure 9.41 (b).

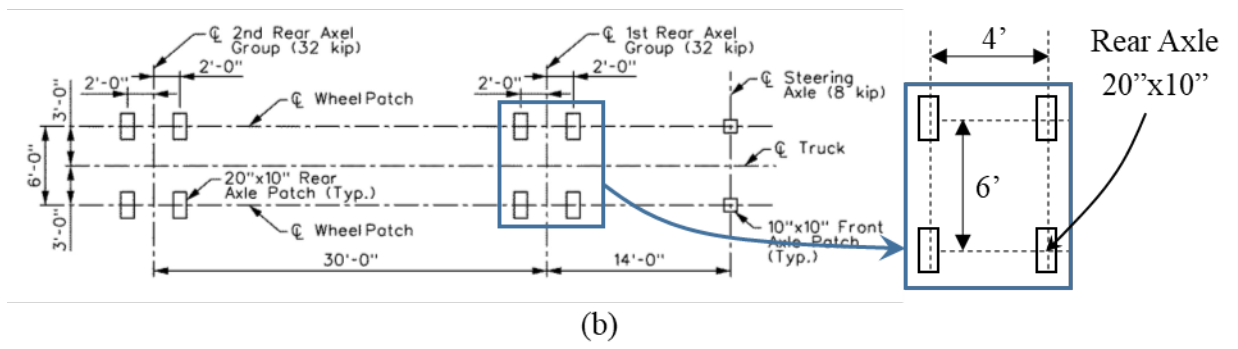
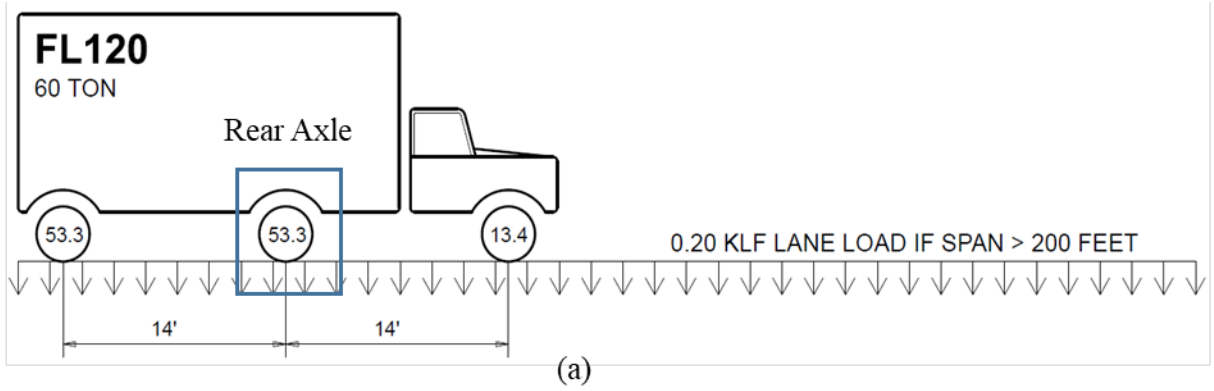


Figure 9.41: Load configuration based on (a) FL120 rear axle [124] load and (b) HS20 rear axle wheel patch geometry [82]

The system was loaded from the unloaded condition (0 kips) to an upper limit of 15.3 kips per patch, as calculated by Equation 9.14, considering a 15 percent dynamic load allowance.

$$P = (1 + IM) * P_{axle} \tag{Equation 9.14}$$

$$P = (1 + 0.15) * 53.3 \text{ kips} = 61.3 \text{ kips}$$

$$P_{wheel} = P/4 = 15.3 \text{ kips}$$

where:

- IM = Dynamic Load Allowance = 0.15 from AASHTO LRFD Bridge Design Specifications (§3.6.2.1) [82]
- P_{axle} = FL120 rear axle load
- P = Load for FL120 with dynamic load allowance
- P_{wheel} = FL120 rear axle wheel load with dynamic load allowance

9.4.2. Model Geometry

The two-beam, two-span continuous model geometry was based two equal 28-foot - 11-inch spans, Figure 9.42 (a), with two 48-inch-wide, 12-inch-thick FSBs joined together using the

longitudinal joint developed earlier in this research effort. The full two-span bridge was modeled as a half bridge on each side to decrease the computational demand required for the analysis, as shown in Figure 9.42 (b). Because the rear axle load (four patches) was applied at midspan of each span, only half of the axle (two patches) were used in the reduced model, as shown in Figure 9.42 (b). The model consisted of a pinned support under the bearings near the diaphragm and a rotational restraint allowing for vertical deflection at each midspan section.

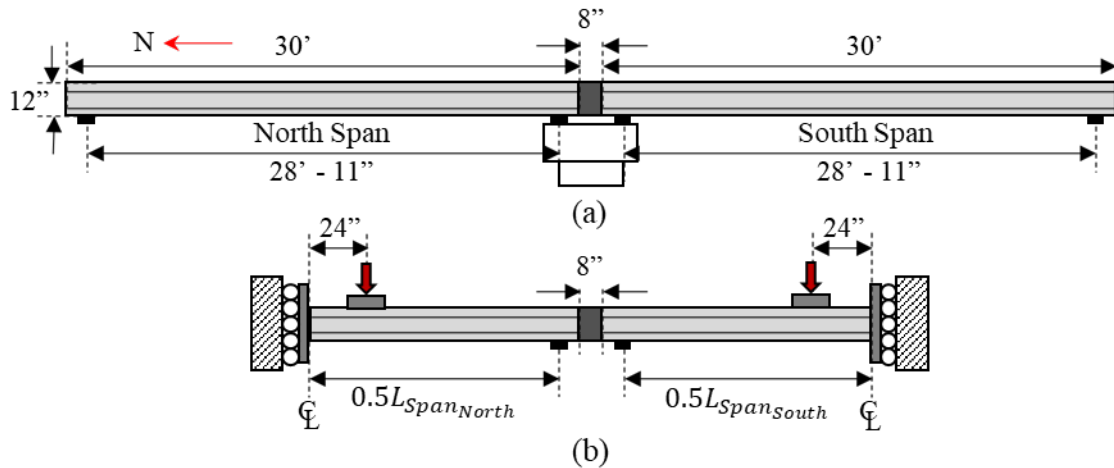


Figure 9.42: Two-span bridge model (not to scale): (a) spans length and (b) half span model restraining rotation at midspan

The design of the FSBs and continuity connection were based on the design discussed in §9.3 and shown in Figure 9.39. The general details for the two-beam system used for the numerical analysis are shown in Figure 9.43 (a).

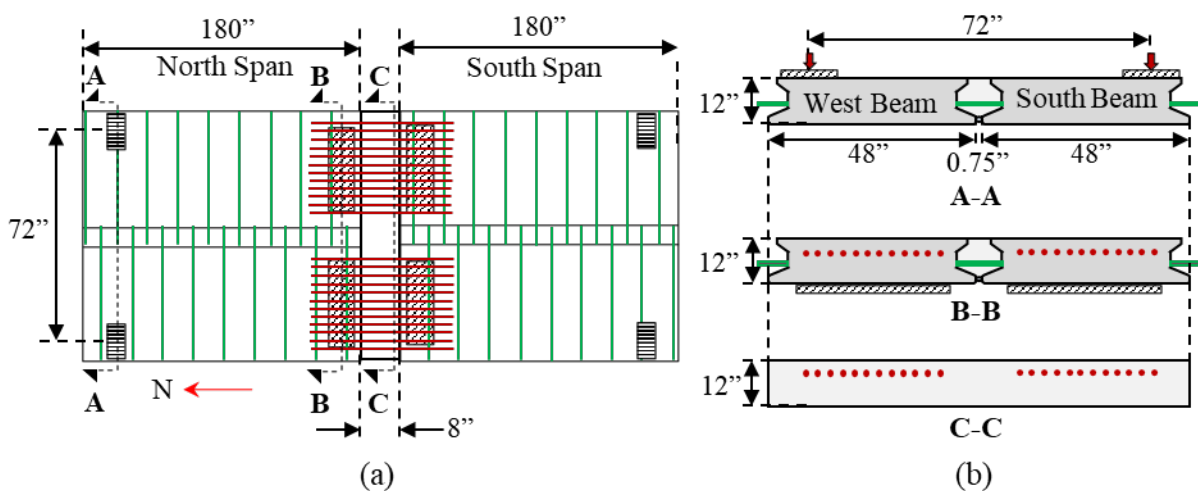


Figure 9.43: Two-beam and longitudinal joint with diaphragm layout (not to scale): (a) longitudinal joint and negative diaphragm reinforcement, and (b) section cuts with reinforcement distribution at load points (A-A), supports (B-B), and diaphragm (C-C)

9.4.3. Material Modeling

The basic material properties used for the ATENA models were based on those used for the beam and continuity connection design discussed in §9.3.6. The material properties required for the numerical analyses are summarized in Table 9.7 through Table 9.9.

Table 9.7: Concrete material definitions

Property		Beams	Joints and Diaphragm
Compressive Strength	f'_c [ksi]	8.50	21.00
Tensile Strength	f'_t [ksi]	0.81	3.00
Young's Modulus	E_c [ksi]	5,024	7,103
Fracture Energy	G_f [lb/in]	0.457	0.714

The precast concrete in the modified FSBs was modeled using a conventional concrete model (CCEDNonLinCementitious2) with the compressive and tensile stresses shown in Table 9.7. The UHPC material was also modeled using CC3DNonLinCementitious2, but with an increased compressive strength (f'_c), tensile strength (f'_t), Young's Modulus (E), and fracture energy (G_f). The UHPC material properties assumption is based on typical material properties utilized for UHPC field-cast connections [108] and recommended values by the software developer [125].

A bilinear relationship was used for the prestressing strands with characteristics defined in Table 9.8. These strand and material properties were used for the prestressed strands in the precast section (with initial stress of 204.4 ksi). The non-prestressed portion of the strands in the continuity diaphragm were not considered in the model.

Table 9.8: Prestressing strand material definitions

Property		Value
Strand Dia.	ϕ	0.600 in
Young's Modulus	E_p	28,500 ksi
Yield Strain	ϵ_2	0.0011
Yield Stress	$f_2 = f_{py}$	243 ksi
Ultimate Strain	ϵ_3	0.043
Ultimate Stress	f_3	270 ksi

A bilinear relationship was also used for the conventional steel rebar used for the longitudinal joints and the high-strength rebar used in the continuity connection, as shown in Table 9.9.

Table 9.9: Joint reinforcement definition

Property		Long. Joint	Trans. Joint
Rebar Dia.	d_b	0.625 in.	0.750 in.
Young's Modulus	E_p	29,000 ksi	29,000 ksi
Yield Strain	ϵ_2	0.00207	0.00259
Yield Stress	$f_2 = f_y$	60 ksi	75 ksi
Ultimate Strain	ϵ_3	0.05	0.05
Ultimate Stress	f_3	71.28	89.10

9.4.4. Loading Protocol and Construction Process

Two main loading stages were used in the numerical analysis based on the typical diaphragm and longitudinal joint construction process:

1. *Prestressing Stage*: Effects of prestressing and self-weight for all FSBs were modeled during this stage. The UHPC joint and diaphragm material were modeled with a very low Young's modulus (i.e., 1 ksi) as they were not yet cast at this point. Also, the diaphragm negative reinforcement was not active because stresses could have developed into the diaphragm volume. The prestressing stage was divided into 20 steps.
2. *System Loading Stage*: The UHPC material properties were changed back to their original hardened properties, and the reinforcement in the diaphragm was activated. No additional prestressing stresses or self-weight increments were added in this stage; however, the effects from the prestressing stage were carried over into this stage. The system was loaded with an equal load applied to all four load patches until the FL120 loading with dynamic load allowance (15.3 kips per patch) was achieved. The system loading stage was divided into 50 steps, which resulted in a total of 70 steps for the complete analysis.

The applied force per load patch and vertical deflection at midspan of each beam were monitored during both stages.

9.4.5. Summary of Results

The load versus deflection response is shown in Figure 9.44 (a) for the beams in the north span and Figure 9.44 (b) for the beams in the south span. The plots remain linear through the loading until a load of 13.4 kips. The first cracks are observed in the top of the precast beams in the negative moment region near the UHPC continuity joint. The load continued to increase after cracking until the final desired load per patch of 15.3 kips was reached.

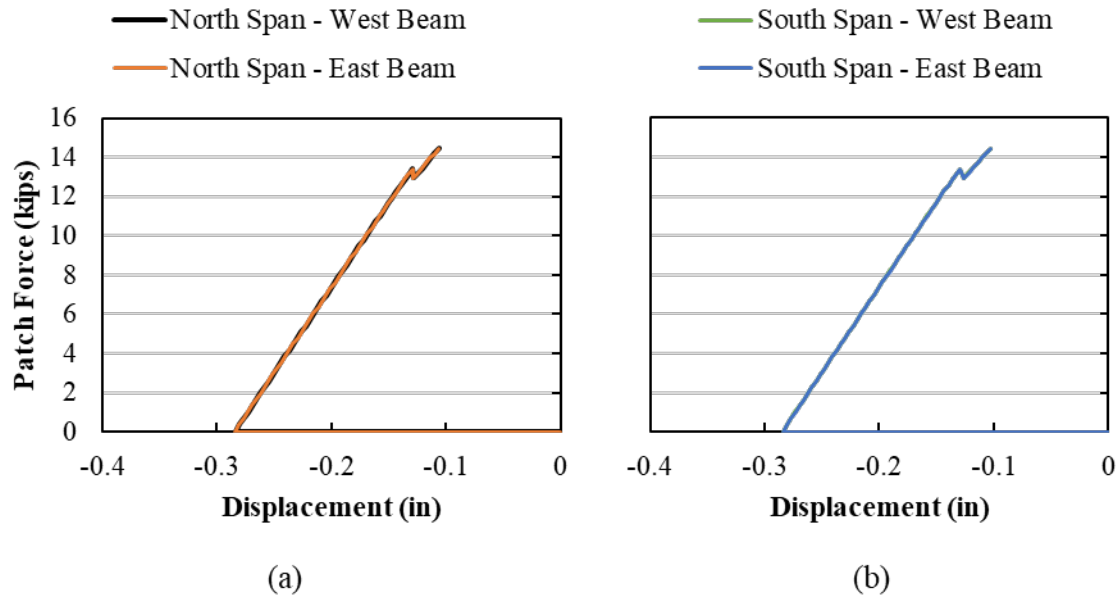


Figure 9.44: Load per patch versus deflection response for: (a) north span and (b) south span

The maximum principal stress maps for the FSBs, longitudinal joint, and diaphragm are shown in Figure 9.45. The maximum tensile stresses in the system developed at the top boundary between the precast FSB and the UHPC diaphragm, with tensile stresses of almost 0.75 ksi, as shown in Figure 9.45 (a). Transverse cracking was observed in the top of the FSB at the boundary with the UHPC diaphragm. Similar longitudinal tensile stresses developed in the UHPC on the top of the diaphragm, as shown in Figure 9.45 (b). There was also a small region of high transverse tensile stresses observed in the longitudinal UHPC joint near the ends of the beams. The highest observed tensile stress in the UHPC joints was 0.73 ksi, which is less than the tensile strength of the UHPC. No cracking was observed at the load application points or underneath the diaphragm and beam supports.

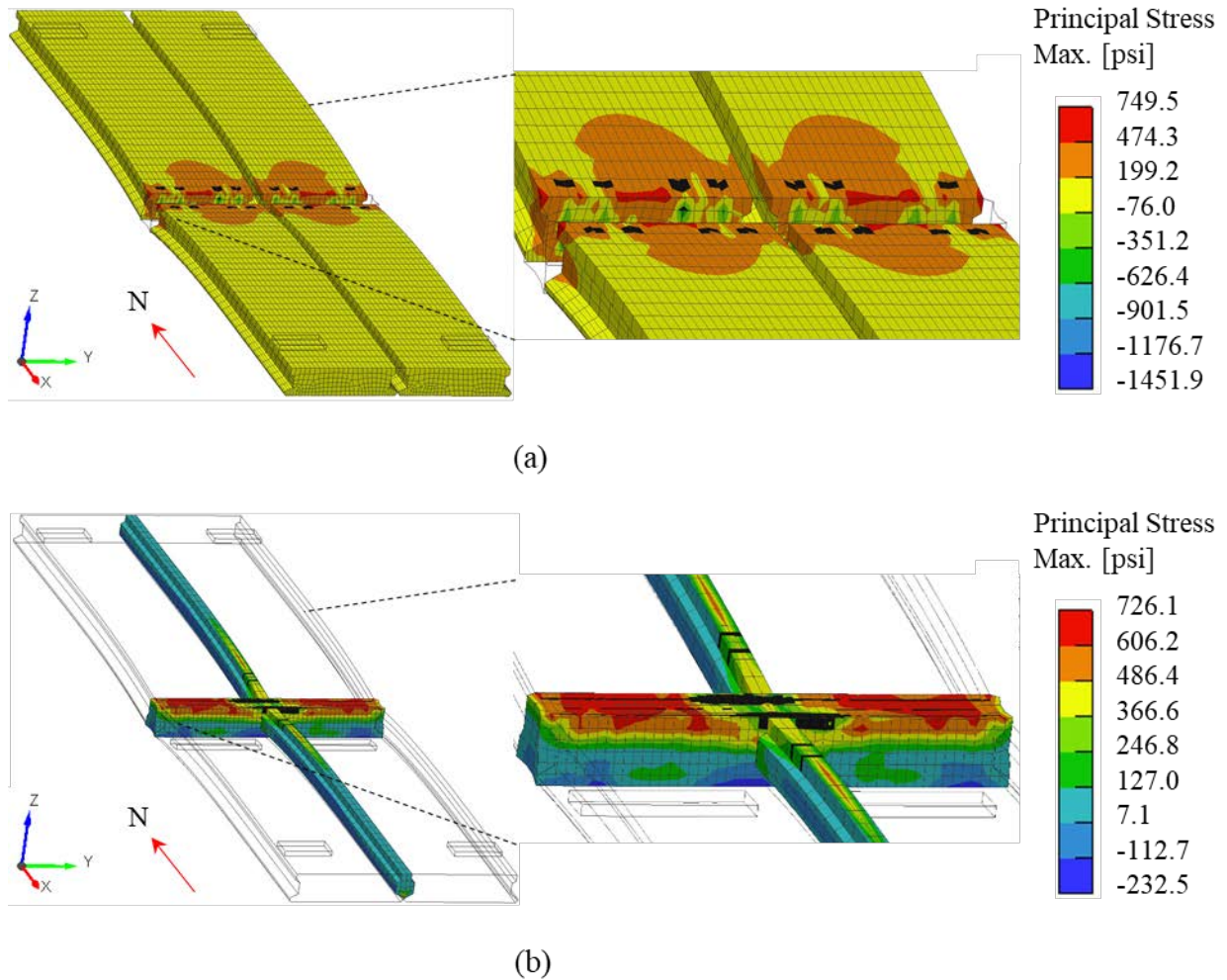


Figure 9.45: Maximum principal stress maps for (a) FSBs and (b) UHPC materials

The maximum principal stress maps of two section cuts made at the FSB-to-UHPC diaphragm boundary and at the center region of the diaphragm are shown in Figure 9.46. The largest tensile stresses of about 0.644 ksi occurred at the top of the FSB regions at the boundary, as shown in Figure 9.46 (a). Stresses do not vary linearly across the depth of the section due to the influence of the prestressing strands and support bearings. Tensile stresses up to 0.692 ksi were observed in the UHPC diaphragm with a linear stress profile between the tensile stress in the top and compression stress in the bottom, shown in Figure 9.46 (b).

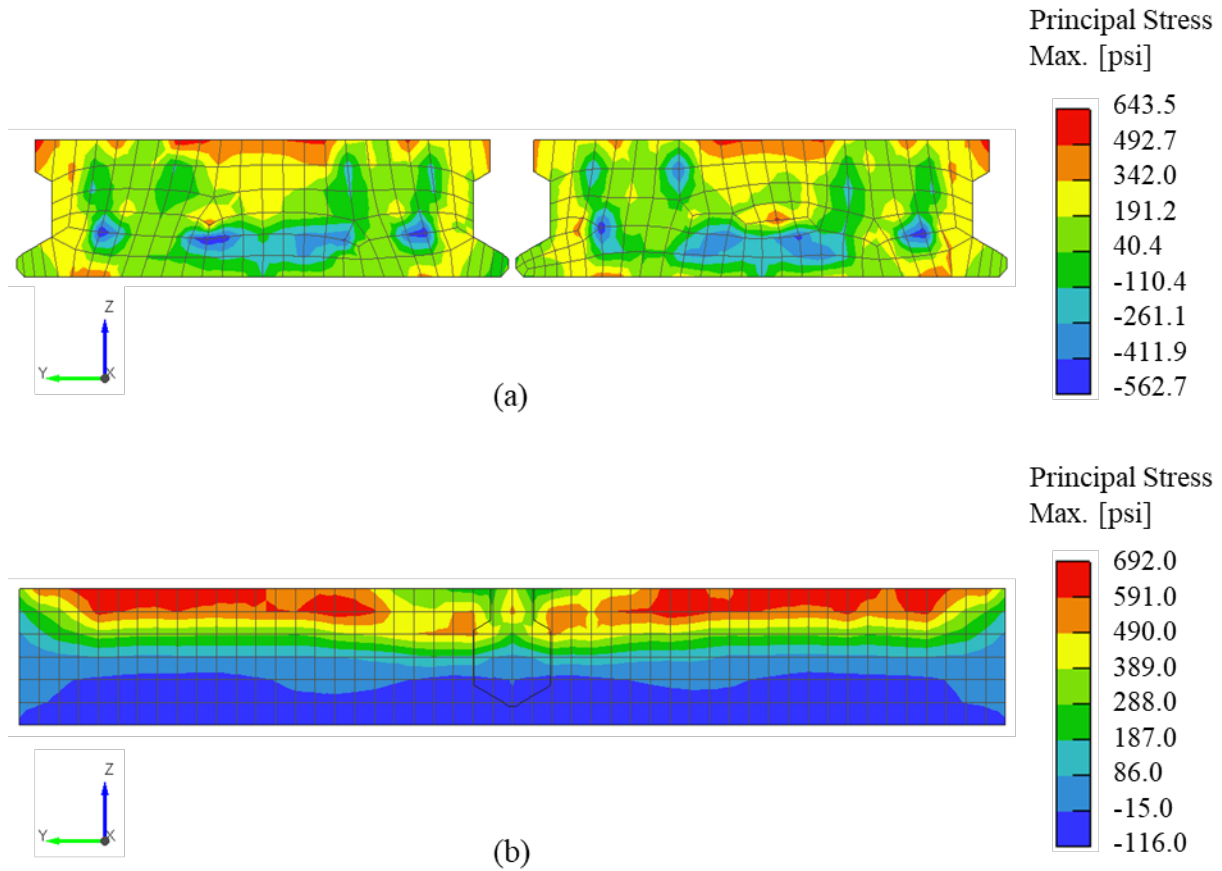


Figure 9.46: Maximum principal stress maps at cuts made at (a) FSB-to-diaphragm boundary and (b) center diaphragm region

The maximum principal stress maps at the joint reinforcement near the supports and the negative reinforcement in the diaphragm are shown in Figure 9.47. Minor engagement of the transverse joint rebar was observed with the largest stresses of about 4.8 ksi, as shown in Figure 9.47 (a). Only minor engagement of the negative moment reinforcement in the SDCL connection was also observed with the largest stresses of about 3.4 ksi, as shown in Figure 9.47 (b).

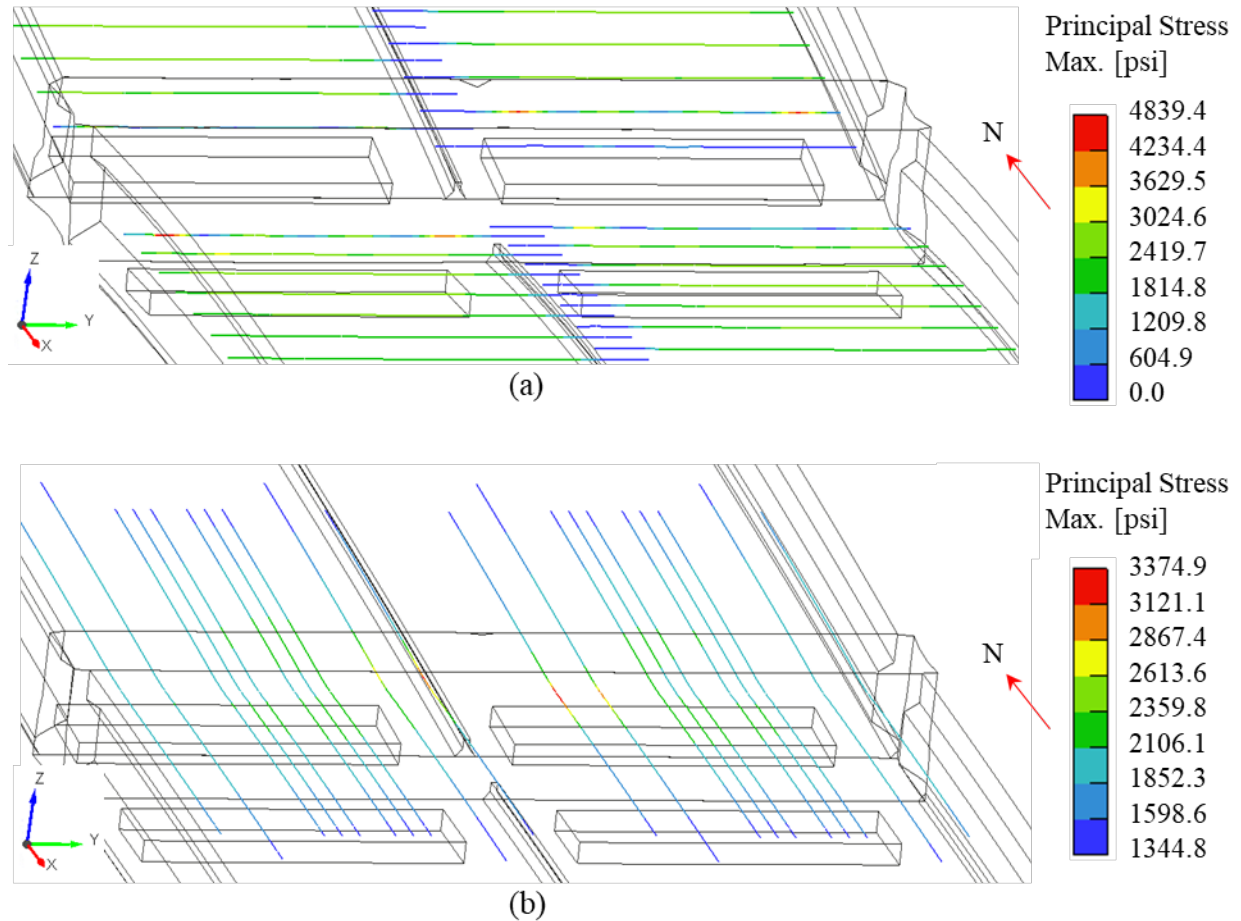


Figure 9.47: Maximum principal stress maps at (a) joint reinforcement near diaphragm region and (b) diaphragm negative reinforcement

9.4.6. Conclusions from FEM study

The following conclusions can be made based on the numerical analysis on the two-beam, two-span-continuous system evaluated in this section:

1. Tensile stresses up to 0.73 ksi developed in the top area of the diaphragm region.
2. Cracking occurred at the FSB-to-diaphragm boundary regions at wheel patch loads of about 13.4 kips. This would represent a truck axle of 53.6 kips applied at the midspan of each span simultaneously and the entire truck axle being carried by only two beams.
3. The transverse joint reinforcement did not significantly engage under the FL120 axle loading, with maximum stresses of 4.8 ksi observed.
4. The stresses in the negative moment reinforcement remained relatively small under the applied service load, with a maximum tensile stress of around 3.4 ksi.

The SDCL joint detail performed well based on these results.

9.5. SUMMARY AND CONCLUSIONS

SDCL connections have been used for decades to eliminate joints, increase possible span lengths for standardized sections, and decrease deflections and demands on the superstructure. A UHPC SDCL connection for use with the modified FSB system was developed based on previous research and previously used SDCL connection. Specific details for this connection were developed for a two-span continuous, six-beam superstructure with 12-, 15-, and 18-inch-deep modified FSB sections with a 48-inch width based on current AASHTO LRFD Bridge Design Specification [82] requirements. The 8-inch-wide diaphragm detail consisted of hooked, non-prestressed strands extended 6 inches into the connection for the positive moment reinforcement and a combination of non-prestressed strands and high-strength (75 ksi) reinforcing bars extended 7 inches into the connection for negative moment reinforcement, shown in Figure 9.39.

The developed UHPC diaphragm detail was evaluated using ATENA FEM software by modeling a two-span bridge with two modified FSBs under service loading. The following conclusions can be made based on the preliminary design and software analysis results:

1. The hooking of the bottom layer of non-prestressed strands provided sufficient positive moment reinforcement for the SDCL connection even with very conservative assumptions on the development of hooked strands in UHPC.
2. Twelve (12) to 14 high-strength ($f_y = 75$ ksi) reinforcing bars and four hooked, non-prestressed strands were sufficient for the negative moment continuity connection between a two-span bridge with maximum possible span lengths for the three different section depths.
3. The developed connection performed well based on FEA results from a two-beam, two-span system with the 12-inch-deep section. The negative moment region remained uncracked up to a single axle load of 53.6 kips applied at midspan of each span simultaneously. Transverse cracking first occurred on top of the precast section adjacent to the UHPC diaphragm.

10.SUMMARY AND CONCLUSIONS

10.1. SUMMARY

A proposed modification to the current Florida Slab Beam (FSB) design standard was developed utilizing ultra-high performance concrete (UHPC) as the joint material based on numerical modeling, small-scale joint testing, and full-scale system testing. The modified FSB design standard (without a composite cast-in-place deck) has possible span ranges of 32 feet for the 12-inch-deep section, 44 feet for the 15-inch-deep section, and 55 feet for the 18-inch-deep section.

Numerical analyses were used to develop options for section and joint geometries and details. Several of the most promising joint details were evaluated through the small-scale joint testing program. Four longitudinal connection details were tested in the small-scale testing protocol: (a) two with straight sides and bottom ledges with varying thicknesses and (b) two with diamond-shape keyways with different transverse joint reinforcement depths and ledge geometries. The small-scale joint testing was performed on 12-inch and 18-inch-deep sections and included both fatigue and ultimate strength testing protocols. The performance of the current FSB design standard was evaluated alongside the proposed joint details in the small-scale testing program. The best performing joint, shown in Figure 8.1, was further evaluated in the full-scale system testing program. Two two-beam systems and one four-beam system with the proposed joint detail were constructed and tested using service, fatigue, and ultimate strength loading protocols.

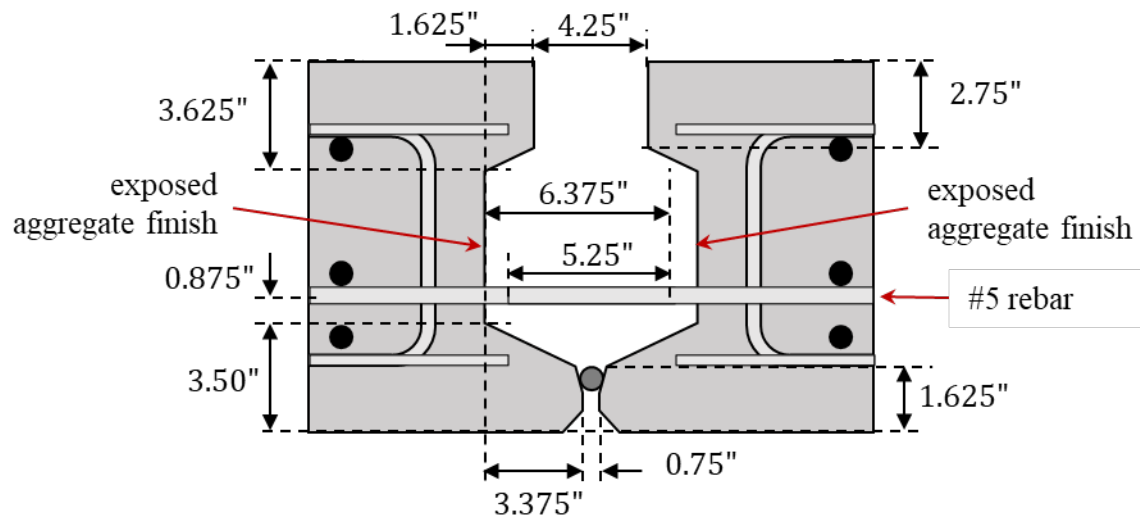


Figure 10.1: Proposed joint geometry based on small-scale joint testing and two-beam system tests

Additionally, a UHPC simple for dead load and continuous for live load (SDCL) detail was developed for the modified FSB system based on previous research and previously used SDCL connection details. The proposed detail, shown in Figure 10.2, has hooked, non-prestressed strands for the positive moment reinforcement and a combination of hooked, non-prestressed strands and high-strength ($f_y = 75$ ksi) rebar for the negative moment reinforcement.

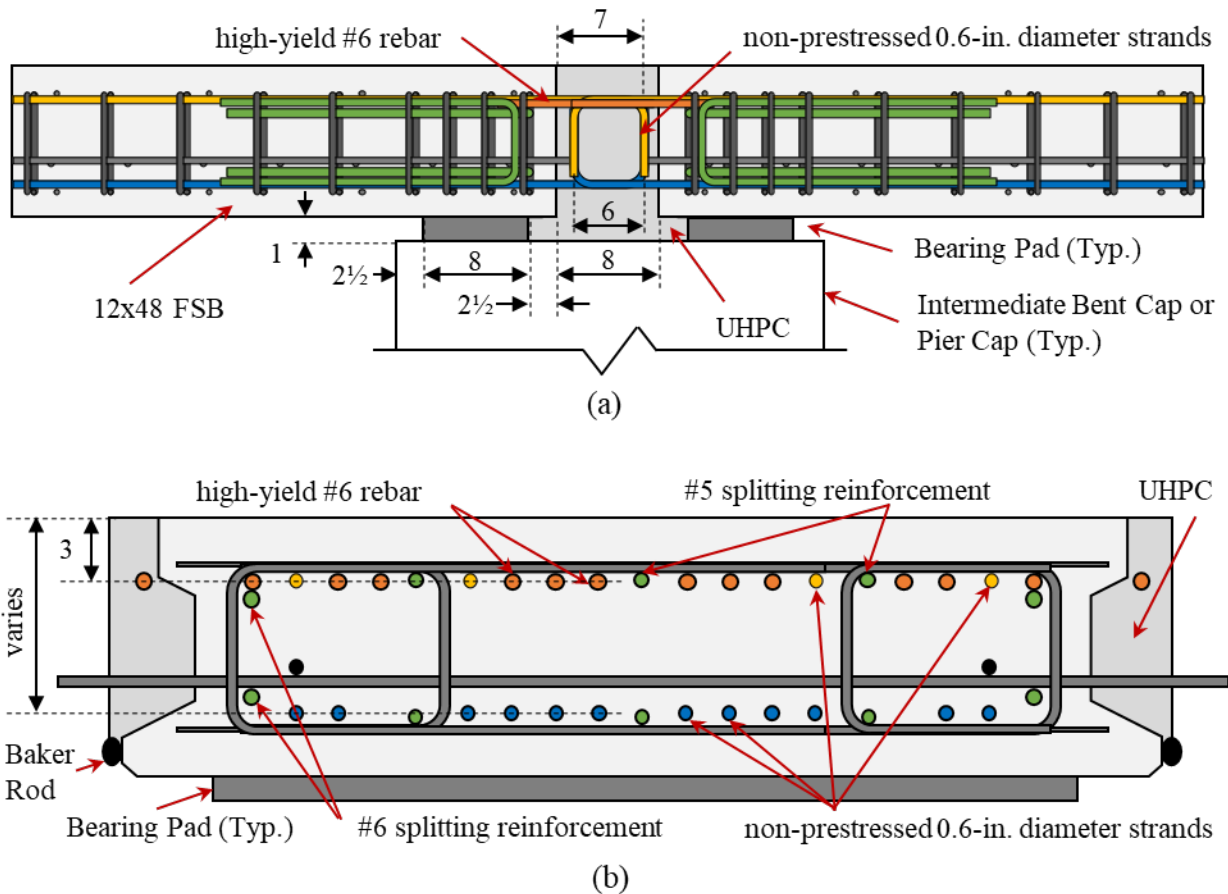


Figure 10.2: Proposed SDCL connection for modified FSB system: (a) section through diaphragm connection and (b) FSB end region reinforcement detail. Note: units in inches

This section summarizes the conclusions from the numerical analyses, specimen construction, small-scale joint testing, full-scale two-beam and four-beam system testing, and SDCL analysis.

10.2. CONCLUSIONS AND RECOMMENDATIONS

The conclusions and recommendations are separated based on small-scale joint testing, full-scale system testing, SDCL, and general construction recommendations.

10.2.1. Small-Scale Testing Protocol

The following conclusions can be made based on the small-scale joint testing:

- The control FSB joint (based on the current FSB Design Standard) did not perform as expected likely due to a larger bend diameter (for both specimens) and the compressive strength of the deck concrete being much lower than specified (for one specimen). These issues caused development failure of the joint reinforcement prior to yield. The results from the numerical analysis were used as the point of comparison for the developed UHPC joints.
- All modified joints with UHPC had similar or greater strength and ductility compared to the current FSB design standard.

- The joints without shear keys with shorter available development and splice lengths for the joint reinforcement typically failed due to development failure of the joint reinforcement. Joints with shear keys and greater available development and splice lengths typically failed due to crushing of the concrete or fracture of the joint reinforcement, which led to more ductile failures.
- The joint finish had a large effect on the behavior of the specimens. The sandblasted joint interface preparation was not sufficient to achieve the desired UHPC-to-precast bond. Debonding was observed in all the specimens with a sandblasted surface finish. A ¼-inch magnitude exposed aggregate finish was required to get satisfactory bond between the precast concrete and UHPC joint material.
- For the specimens that were fatigue loaded, fatigue loading did not cause degradation of specimen performance before or after cracking was intentionally caused. The fatigue loading did not affect the ultimate strength performance of the specimens.

The best performing joint from the small-scale joint testing was used in the full-scale system tests.

10.2.2. Large-Scale Testing Protocol

Service and ultimate strength testing were first performed on one two-beam system (FIU-1/2) and service, fatigue, and ultimate strength testing were performed on a second two-beam system (FIU-4/5). The following conclusions and recommendations can be made based on these two two-beam system tests.

- The joint performed well during service load and ultimate strength testing. No joint debonding or distress was observed in the joint region during any of the service, fatigue, and ultimate load testing. The concrete in the compression block crushed across the entire width of the system (including the UHPC joint), which highlighted the quality of the bond between the UHPC and precast concrete. Additionally, the joint successfully transferred stress between beams; there was only a minor differential displacement between beams when only one beam was loaded.
- FIU-4/5 had similar performance to FIU-1/2 during the ultimate strength testing, which shows that the 4.7 million cycles and other service load and cracking tests did not impact the overall system behavior.
- Transverse tension was measured in the top of the beams (using CSGs) and across the top of the joint (using CDTs) and transverse compression across the bottom of the beams and across the bottom of the joints in all the load and support configurations for FIU-4/5 (LC 2-1, LC 2-4, FC 2-5, FC 2-6, and FC 2-7). Transverse tension was below the estimated tensile cracking strain for the precast concrete for all service tests but exceeded this strain in the ultimate strength test (LC 2-1) at high levels of load (above service levels). Further numerical study should be done on deeper sections (e.g., 15-inch and 18-inch-deep sections) including stresses induced by temperature effects to see if a top layer of reinforcement is needed.
- Transverse cracking of one beam (when the other beam remained uncracked) increased the transverse demand on the top of the adjacent precast beam when interior supports were

provided. The transverse cracking caused a decreased stiffness in the unrestrained beam, which led to the increased transverse strains on the top of the restrained precast beam. However, strains remained less than the expected cracking strain and no longitudinal cracks were observed in the top of the beams. This shows that unequal stiffness between adjacent beams can lead to increased demand in the joint.

- Small compression strains ($< 50 \mu\epsilon$) were generally measured in the joint reinforcement for the service and fatigue load configurations (LC 2-4, FC 2-5, FC 2-6, and FC 2-7). Larger tensile strains ($> 300 \mu\epsilon$) were measured during LC 2-1 in the joint reinforcement with the highest strains measured near the load points. Strains remained under the yield strain for steel. The joint reinforcement also appeared to help inhibit the growth of cracks that developed between the top of the bottom lip and UHPC in the joint.
- There were no signs of bond deterioration between the joint reinforcement and UHPC in the joint during any of the fatigue, service, or strength testing.

Service, fatigue, and ultimate strength testing were also performed on a four-beam system (FIU-6/3/8/7). The following conclusions were made based on these four-beam system tests.

- The camber leveling procedure introduced additional longitudinal tensile stresses in the bottom of FIU-3, which led to a lower cracking load for the beam (35.1 percent less than estimated). The load from the cracked FIU-3 redistributed to the other three beams, which led to a lower cracking load for these beams as well (10.2 percent less than estimated). This could affect the design and load rating for service limit states.
- The camber leveling procedure introduced minor transverse strains (less than $20 \mu\epsilon$ tension and less than $10 \mu\epsilon$ tension) across the precast sections and joints. These locked-in transverse strains did not lead to any adverse joint behavior during any of the service, fatigue, or ultimate strength testing.
- Girder distribution factors (GDFs) were found using longitudinal strain on the top and bottom of the beams and the midspan deflection. GDFs were not influenced by the differential camber and camber leveling procedure performed on FIU-3; symmetrical behavior of the system was observed during all testing stages. GDFs were less than those estimated using AASHTO LRFD.
- The joints performed well during service load, fatigue, and ultimate strength testing. No joint debonding or distress was observed in the joint regions during any of the service, fatigue, and ultimate load testing. The concrete in the compression block crushed across the entire width of the system (including the UHPC joint). Additionally, the joint successfully transferred stress between beams. There were no signs of bond deterioration between the joint reinforcement and UHPC in the joints during any of the fatigue, service, or strength testing.

The modified FSB system performed well during all the service, fatigue, and ultimate load testing on all full-scale system tests.

10.2.3. Simple for Dead Load and Continuous for Live Load (SDCL) Recommendations

The following conclusions were made based on the SDCL analyses:

1. The hooking of the bottom layer of non-prestressed strands provided sufficient positive moment reinforcement for the SDCL connection even with very conservative assumptions on the development of hooked strands in UHPC.
2. Twelve (12) to 14 high-strength ($f_y = 75$ ksi) reinforcing bars and four hooked, non-prestressed strands were sufficient for the negative moment continuity connection between a two-span bridge with maximum possible span lengths for the three different section depths.
3. The developed connection performed well based on FEA results from a two-beam, two-span system with the 12-inch-deep section. The negative moment region remained uncracked up to a single axle load of 53.6 kips applied at midspan of each span simultaneously. Transverse cracking first occurred on top of the precast section adjacent to the UHPC diaphragm.

The proposed detail could be considered for 12-, 15-, and 18-inch-deep systems.

10.2.4. Construction and Design Recommendations

The following construction and design recommendations can be made based on the small-scale joint tests and full-scale system tests:

- *Proper bend diameter for current FSB Design Standard:* The joint reinforcement used in the current FSB Design Standard must have the correct bend diameter to help with the development of the joint reinforcement.
- *Use increased development and splice length of joint reinforcement in UHPC:* Using the currently recommended $8d_b$ embedment length and $0.75l_d$ splice length allowed the reinforcement to develop its yield strength but resulted in pullout or development causing failure. An increased embedment and splice length resulted in fracture of the reinforcement and crushing of the concrete at failure. The proposed joint detail includes this increased available development and splice length.
- *Ensure proper surface finish of joint:* An exposed aggregate finish with ¼-inch magnitude is needed to ensure proper bond between the precast member and UHPC joint. Make sure the proper admixtures are used. An aggregate size of 1 ¼ inch may be needed to achieve the ¼-inch magnitude roughness. Casting mock-ups is recommended to ensure the precaster can provide the proper finish. Additionally, the surface should be pre-wetted to an SSD condition immediately before casting of the UHPC.
- *Minimum bottom flange thickness:* The bottom flange of the beam should have an average thickness greater than 2 inches and contain a #3 transverse reinforcing bar. This will prevent the bottom flange from breaking off during casting, transport, or construction of superstructure. The proposed joint detail includes a bottom flange design sufficient to prevent damage of the flange during casting and construction.
- *Check UHPC materials before casting:* Check that the proper dry pre-mix and compatible admixtures were received. Also check to make sure that the materials are not expired and do not have any large dry clumps.

10.3. RECOMMENDED FUTURE RESEARCH

The following future research needs were identified during this research project:

- The current FSB Design Standard joint detail did not perform as well as expected. This was likely due to issues with the joint construction in the test specimens (e.g., bend diameter of the joint reinforcement, low concrete compressive strength). It is recommended that additional testing or bridge monitoring be done to validate the performance of the current FSB joint detail.
- The camber leveling procedure used to account for the differential camber in the four-beam test configuration led to reduction in the cracking load of 35.1 percent in the beam that was leveled and 10.2 percent in the other beams. The service and strength testing were performed about 2.5 months after the removal of the surcharge load used for camber leveling. Some engineers believe that long-term effects (e.g., creep) will decrease the locked-in stresses caused by camber leveling. Further research, including possible field monitoring, would be beneficial to see if creep decreases locked-in stresses over time, decreasing the impact on the cracking load.
- Temperature-induced stresses may lead to increased stresses in the longitudinal joints and transverse stresses across the top of the system. Additional numerical modeling and possible field monitoring of an in-service bridge would help to determine the magnitude of these stresses and any impact on the design and behavior of the system.
- There has been no previous research on the development and splicing of hooked, non-prestressed strands. Additional testing on this type of connection would allow for reduced positive moment reinforcement and possible improvement of the negative moment reinforcement detail for the developed SDCL connection.
- An expanded parametric study would be useful to investigate the bridge and span configurations where SDCL design would be most beneficial for use with the modified FSB.

REFERENCES

- [1] B. F. Bender and W. G. Kriesel, "Precast, Prestressed Box Beams - A State-of-the-Art Report," *PCI J.*, vol. 14, no. 1, pp. 72–91, 1969.
- [2] A. Avendaño *et al.*, "Pretensioned Box Beams: Prestress Transfer and Shear Behavior," Texas Department of Transportation, Austin, TX, FHWA/TX-13/0-5831-3, 2013.
- [3] K. E. Hanna, G. Morcoux, and M. K. Tadros, "Transverse post-tensioning design and detailing of precast, prestressed concrete adjacent-box-girder bridges," *PCI J.*, vol. 54, no. 4, pp. 160–174, 2009.
- [4] J. Corvin, "Post-Tensioned Box Girders - Design Manual," Federal Highway Administration, Washington, DC, FHWA-HIF-15-016 Sep. 2015.
- [5] Ductal, "Hawk Lake Bridge, Ontario, Canada - Joint Fill," 2010.
<https://www.holcim.com/canada-ductalr-also-a-joint-fill-solution> (accessed Sep. 01, 2016).
- [6] J. Lall, S. Alampalli, and E. DiCocco, "Performance of full-depth shear keys in adjacent prestressed box beam bridges," *PCI J.*, vol. 43, no. 2, pp. 72–79, 1998.
- [7] M. P. Culmo and R. L. Seraderian, "Development of the northeast extreme tee (NEXT) beam for accelerate bridge construction," *PCI J.*, vol. 55, no. 3, pp. 86–101, 2010.
- [8] Precast/Prestressed Concrete Institute Northeast (PCINE), "Northeast Extreme Tee (NEXT) Beam Guide Details." Precast/Prestressed Concrete Institute Northeast (PCINE), 2015.
[Online]. Available:
https://www.pci.org/PCINE/Technical_Resources/Bridge_Resources/Northeast_Extreme_Tee_NEXT_Beam/PCINE/Technical_Resources/Bridge_Resources/NEXT_Beam.aspx?hkey=5dc58288-9dab-4f7d-b23c-55bea7ae9d17
- [9] Matiere, "The principle of Poutre-Dalle beam slab," 2014. <https://www.matiere-tp.com/produit/poutre-dalle/> (accessed Sep. 01, 2016).
- [10] M. S. Mercer, "Transverse Sub-Assemblage Testing of the Inverted-T Bridge System," Virginia Polytechnic Institute and State University, Blacksburg, VA, Dissertation, 2012.
- [11] M. Dimaculangan and T. Lesch, "Minnesota's Precast Composite Slab Span System," *ASPIRE*, vol. Summer, pp. 40–42, 62, 2010.
- [12] C. French, CK. Shield, D. Klaseus, M. Smith, W. Eriksson, ZJ. Ma, P. Zhu, S. Lewis, and C. Chapman, "Cast-in-Place Concrete Connections for Precast Deck Systems (Web-Only Document 173)," National Academies of Sciences, Engineering, and Medicine, Washington DC, 2011. [Online]. Available: <https://doi.org/10.17226/17643>
- [13] R. Piccinin and A. E. Schultz, "The Minnesota inverted-tee system: Parametric studies for preliminary design," *PCI J.*, vol. 57, no. 2, pp. 162–179, 2012.
- [14] F. Menkulasi, M. Mercer, C. Wollmann, and T. Cousins, "Accelerating Bridge Construction Using the Precast Inverted T-Beam Concept," *Precast. Concr. Inst. PCI*, Sep. 2012.

- [15] F. Menkulasi, C. L. Roberts Wollmann, and T. Cousins, “Live-Load Distribution Factors for Composite Bridges with Precast Inverted T-Beams,” *J. Perform. Constr. Facil.*, p. 04016045, 2016.
- [16] B. Goldsberry, “Florida Slab Beam (FSB) - Development and Implementation,” presented at the Design Training Expo, 2015. [Online]. Available: <http://www.dot.state.fl.us/officeofdesign/Training/DesignExpo/2015/presentations/FSBDevelopmentandImplementation-BenGoldsberry.pdf>
- [17] V. Young, “Florida Slab Beam (FSB) - Superstructure Package,” presented at the Design Training Expo, 2016. [Online]. Available: [http://www.dot.state.fl.us/officeofdesign/training/DesignExpo/2016/Presentations/FloridaSlabBeams\(FSB\)SuperstructurePackage-VickieYoung.pdf](http://www.dot.state.fl.us/officeofdesign/training/DesignExpo/2016/Presentations/FloridaSlabBeams(FSB)SuperstructurePackage-VickieYoung.pdf)
- [18] H. T. Bollmann, “Precast Prestressed Slab Units,” Nov. 09, 1984.
- [19] Florida Department of Transportation (FDOT), “Instructions for Developmental Design Standards,” *Index D20450 Ser. Fla. Slab Beam*, Mar. 2016, [Online]. Available: <http://www.dot.state.fl.us/rddesign/DS/Dev/IDDS/IDDS-D20450.pdf>
- [20] R. V. Robertson, “Florida Slab Beam Superstructure System,” 2016. [Online]. Available: <http://www.dot.state.fl.us/officeofdesign/bulletins/SDB16-01.pdf>
- [21] M. Biswas, “Precast bridge deck design systems,” *PCI J.*, vol. 31, no. 2, pp. 40–94, 1986.
- [22] B. A. Graybeal, “Ultra-high-performance concrete connections for precast concrete bridge decks,” *PCI J.*, vol. 59, no. 4, pp. 48–62, Fall 2014.
- [23] D. G. Hieber, J. M. Wacker, M. O. Eberhard, and J. F. Stanton, “State-of-the-art report on precast concrete systems for rapid construction of bridges,” Citeseer, 2005. [Online]. Available: <http://citeseerx.ist.psu.edu/viewdoc/download?doi=10.1.1.369.9839&rep=rep1&type=pdf>
- [24] S. S. Badie and M. K. Tadros, “NCHRP Report 584: Full-Depth, Precast-Concrete Bridge Deck Panel Systems,” National Cooperative Highway Research Program (NCHRP), Report 584, 2008.
- [25] C. M. Bell, C. E. French, and C. K. Shield, “Application of precast decks and other elements to bridge structures,” University of Minnesota, Minneapolis, MN, MN/RC-2006-37, Sep. 2006.
- [26] Federal Highway Administration (FHWA), “MnDOT/FHWA Precast Slab System Workshop Summary Report,” 2015. <https://www.fhwa.dot.gov/bridge/prefab/slab.cfm>
- [27] M. Royce, “Implementing ultra-high-performance concrete for accelerated bridge construction in New York,” *PCI J.*, pp. 38–47, 2014.
- [28] S. Aaleti and S. Sritharan, “Design of Ultrahigh-Performance Concrete Waffle Deck for Accelerated Bridge Construction,” *Transp. Res. Rec. J. Transp. Res. Board*, vol. 2406, pp. 12–22, 2014, doi: 10.3141/2406-02.
- [29] B. Graybeal, “UHPC in the US highway transportation system,” 2008, pp. 11–17.
- [30] S. S. Badie, M. K. Tadros, and R. M. M. Usdan, “Full-depth, precast concrete bridge deck panel systems,” *Concr. Int.*, vol. 31, no. 04, pp. 53–58, 2009.

- [31] Z. Haber, “Ultra-High Performance Concrete (UHPC),” presented at the Design Training Expo, 2016.
- [32] B. Graybeal, “Development of Non-Proprietary Ultra-High Performance Concrete for Use in the Highway Bridge Sector,” 2013.
- [33] E. Brühwiler, ““Structural UHPFRC’: Welcome to the post-concrete era!,” 2016.
- [34] M. A. Saleem, A. Mirmiran, J. Xia, and K. Mackie, “Ultra-high-performance concrete bridge deck reinforced with high-strength steel,” *ACI Struct. J.*, vol. 108, no. 5, p. 601, 2011.
- [35] T. L. Vande Voort, M. T. Suleiman, and S. Sritharan, “Design and performance verification of ultra-high performance concrete piles for deep foundations,” 2008.
- [36] S. Alampalli, J. O’Connor, and A. P. Yannotti, “Fiber reinforced polymer composites for the superstructure of a short-span rural bridge,” *Compos. Struct.*, vol. 58, no. 1, pp. 21–27, 2002.
- [37] B. Graybeal, “Structural Behavior of a Prototype UHPC Pi-Girder,” Federal Highway Administration, McLean, VA, FHWA-HRT-10-027, Nov. 2009.
- [38] Florida Department of Transportation (FDOT), “Structures Design Guidelines - FDOT Structures Manual,” 2017.
- [39] B. A. Graybeal, “Design and construction of field-cast UHPC Connections,” Federal Highway Administration, FHWA-HRT-14-084, Oct. 2014.
- [40] B. A. Graybeal, “Behavior of Ultra-High Performance Concrete Connections between Precast Bridge Deck Elements,” presented at the 2010 Concrete Bridge Conference: Achieving Safe, Smart & Sustainable Bridges, 2010.
- [41] B. Graybeal, “Fatigue response in bridge deck connection composed of field-cast ultra-high-performance concrete,” *Transp. Res. Rec. J. Transp. Res. Board*, no. 2251, pp. 93–100, 2011.
- [42] M. Sayed-Ahmed and K. Sennah, “Development of transverse joints for full-depth precast deck panels incorporating ribbed-surface GFRP bars, HPC and UHPFRC,” presented at the Proceedings of the PCI Convention and National Bridge Conference, 2014.
- [43] Bridgesight Inc., “PGSuper Resource Center,” 2014. <http://www.pgsuper.com/> (accessed Jun. 17, 5AD).
- [44] Texas Department of Transportation (TxDOT), “Bridge Standards.” TxDOT, 2017. [Online]. Available: <http://www.txdot.gov/insdtdot/orgchart/cmd/cserve/standard/bridge-e.htm>
- [45] Precast/Prestressed Concrete Institute (PCI), “Bridge Design Manual,” 2011.
- [46] N. Grace, T. Enomoto, P. Baah, and M. Bebawy, “Flexural Behavior of CFRP Precast Prestressed Decked Bulb T-Beams,” *J. Compos. Constr.*, vol. 16, no. 3, pp. 225–234, 2012, doi: 10.1061/(ASCE)CC.1943-5614.0000266.
- [47] Florida Department of Transportation (FDOT), “SURVEY: FDOT Superstructure Types for Short and Medium Spans,” 2013.

- [48] Florida Department of Transportation (FDOT), “2010 FDOT Design Standards: Inverted-T Beam - Standard Details (Index No. 20320),” 2010.
- [49] Florida Department of Transportation (FDOT), “Prestressed Beam-LRFD v5.1,” 2017.
- [50] D. Garber, J. Gallardo, D. Deschenes, D. Dunkman, and O. Bayrak, “Effect of New Prestress Loss Estimates on Pretensioned Concrete Bridge Girder Design,” Austin, TX, 2012. [Online]. Available: <http://library.ctr.utexas.edu/ctr-publications/0-6374-2.pdf>
- [51] Y. F. Guyon, “Prestressed Concrete,” *Jointly Publ. Contractors Rec. Ltd John Wiley Sons Inc*, vol. 1, p. 239, 1953.
- [52] M. L. Ralls, L. Ybanez, and J. J. Panak, “The New Texas U-Beam Bridges: An Aesthetic and Economical Design Solution,” *PCI J.*, vol. 38, no. 5, pp. 20–29, Sep. 1993.
- [53] W. Podolny and J. M. Muller, *Construction and Design of Prestressed Concrete Segmental Bridges*. New York: John Wiley & Sons, Inc., 1994.
- [54] B. G. Rabbat and H. G. Russell, “Optimized Sections for Precast, Prestressed Bridge Girders,” *PCI J.*, pp. 88–104, Jul. 1982.
- [55] B. A. Graybeal, “Behavior of Field-Cast Ultra-High Performance Concrete Bridge Deck Connections Under Cyclic and Static Structural Loading,” Office of Infrastructure Research & Development, McLean, VA, Final Report FHWA-HRT-11-023, 2010.
- [56] B. A. Graybeal, “Material property characterization of ultra-high performance concrete,” Federal Highway Administration, No. FHWA-HRT-06-103, 2006.
- [57] Florida Department of Transportation (FDOT), “Developmental Design Standards,” *Index No D20450 Ser. Fla. Slab Beam*, Mar. 2016, [Online]. Available: <http://www.dot.state.fl.us/rddesign/DS/Dev/IDDS/IDDS-D20450.pdf>
- [58] Florida Department of Transportation (FDOT), “Portland Cement Concrete - Florida Slab Beam Superstructure System,” Dev346SRA, Jan. 2016. [Online]. Available: <http://www.fdot.gov/programmanagement/OtherFDOTLinks/Developmental/Files/Dev346SRA.pdf>
- [59] Florida Department of Transportation (FDOT), “Standard Specifications for Road and Bridge Construction,” *Sect. 901 Coarse Aggreg.*, Jul. 2018.
- [60] ASTM International, “ASTM C33 / C33M-18, Standard Specification for Concrete Aggregates,” *West Conshohocken Pa*, 2018, doi: 10.1520/C0033_C0033M-18.
- [61] American Society for Testing and Materials (ASTM), “C1437-15 - Standard Test Method for Flow of Hydraulic Cement Mortar,” 2015.
- [62] American Society for Testing and Materials (ASTM), “C39/C39M-15a - Standard Test Method for Compressive Strength of Cylindrical Concrete Specimens,” 2015.
- [63] American Society for Testing and Materials (ASTM), “C1856/C1856M-17 Standard Practice for Fabricating and Testing Specimens of Ultra-High Performance Concrete,” Jun. 2017.

- [64] American Society for Testing and Materials (ASTM), “C1609/C1609M-12 - Standard Test Method for Flexural Performance of Fiber-Reinforced Concrete (Using Beam with Third-Point Loading),” Dec. 2012.
- [65] Z. Haber, “FHWA Representative Discussion,” May 14, 2018.
- [66] BASF Construction Chemicals, “MBT Heat-Cote,” 2018. <https://www.master-builders-solutions.basf.us/en-us/products/masterfinish/masterfinish-hc> (accessed Jun. 24, 2018).
- [67] BASF Construction Chemicals, “MBT MasterFinish HV,” 2018. <https://www.master-builders-solutions.basf.us/en-us/products/masterfinish/masterfinish-hv> (accessed Jun. 24, 2018).
- [68] Architectural Concrete Chemicals, “Altus In-Form Retarder,” 2018. <http://www.acchemicals.com/wp-content/uploads/2010/05/Download-Altus-In-form-Retarders-data-sheet.pdf> (accessed Jun. 24, 2018).
- [69] N. S. Anderson and D. F. Meinheit, “A Review of Headed Stud Design Criteria,” *PCI J.*, vol. 52, no. 1, pp. 82–100, Jan-Feb.
- [70] F. Leonhardt and R. Walther, “The Stuttgart Shear Tests,” *CCA Transl.*, vol. 11, p. 134 pp, 1964.
- [71] W. Hsuimg and G. C. Frantz, “Transverse Stirrup Spacing in R/C Beam,” *ASCE J. Struct. Eng.*, vol. 11, no. 2, pp. 353–362, Feb. 1985.
- [72] American Association of State Highway and Transportation Officials (AASHTO), “AASHTO LRFD Bridge Design Specification, Customary U.S. Units, 7th Edition,” Washington, D. C., 2014.
- [73] Florida Department of Transportation (FDOT), “Plans Preparation Manual, Volume 1.” Roadway Design Office, Jan. 01, 2017. [Online]. Available: <http://www.fdot.gov/roadway/ppmmanual/2017PPM.shtm>
- [74] T. Helgason, J. M. Hanson, N. F. Somes, W. G. Corley, and E. Hognestad, “Fatigue Strength of High-Yield Reinforcing Bars,” *NCHRP Rep.*, no. 164, 1976.
- [75] G. P. Tilly, “Fatigue of Steel Reinforcement Bars in Concrete: A Review,” *Fatigue Fract. Eng. Mater. Struct.*, vol. 2, no. 3, pp. 251–268, 1979.
- [76] American Society for Testing and Materials (ASTM), “C1437-15 - Standard Test Method for Flow of Hydraulic Cement Mortar,” 2015.
- [77] American Association of State Highway and Transportation Officials (AASHTO), “AASHTO LRFD Bridge Design Specification, Customary U.S. Units, 7th Edition,” Washington, D. C., 2015.
- [78] American Association of State Highway and Transportation Officials (AASHTO), “AASHTO LRFD Bridge Design Specification, Customary U.S. Units, 8th Edition,” Washington, D. C., Sep. 2017.
- [79] Precast/Prestressed Concrete Institute (PCI), “Manual for QUALITY CONTROL for Plants and Production of STRUCTURAL PRECAST CONCRETE PRODUCTS,” Precast and Prestressed Concrete Institute (PCI), Chicago, 1999.

- [80] R. Miller, G. Hlavacs, T. Long, and A. Greuel, "Full-Scale Testing of Shear Keys for Adjacent Box Girder Bridges," *PCI J.*, vol. 44, no. 6, pp. 80–90, Dec. 1999.
- [81] N. Grace, E. Jensen, V. Matsagar, and P. Penjendra, "Performance of an AASTHO Beam Bridge Prestressed with CFRP Tendons," *J. Bridge Eng. - ASCE*, vol. 18, no. 2, pp. 110–121, Feb. 2013, doi: 10.1061/(ASCE)BE.1943-5592.0000339.
- [82] American Association of State Highway and Transportation Officials (AASHTO), "AASHTO LRFD Bridge Design Specification, Customary U.S. Units, 8th Edition," Washington, D. C., 2017.
- [83] P. J. Barr and MD. N. Amin, "Shear Live-Load Distribution Factors for I-Girder Bridges," *J. Bridge Eng.*, vol. 11, no. 2, pp. 197–204, 2006.
- [84] P. J. Barr, M. O. Eberhard, and J. F. Stanton, "Live-Load Distribution Factors in Prestressed Concrete Bridges," *J. Bridge Eng.*, vol. 6, no. 5, pp. 298–306, 2001.
- [85] J. Eom and A. S. Nowak, "Live Load Distribution for Steel Girder Bridges," *J. Bridge Eng.*, vol. 6, no. 6, pp. 489–497, 2001.
- [86] K. M. Sennah and J. B. Kennedy, "Load Distribution Factors for Composite Multicell Box Girder Bridges," *J. Bridge Eng. - ASCE*, vol. 4, no. 1, pp. 71–79, Feb. 1999.
- [87] A. Nowak, J. Eom, and D. Ferrand, "Verification of Girder Distribution Factors for Continuous Steel Girder Bridges," Michigan Department of Transportation, Michigan, RC-1429, May 2003.
- [88] X. S. Huo, E. Wasserman, and P. Zhu, "Simplified Method of Lateral Distribution of Live Load Moment," *J. Bridge Eng.*, vol. 9, no. 4, pp. 382–390, 2004.
- [89] T. Zokaie, "AASHTO-LRFD Live Load Distribution Specification," *J. Bridge Eng.*, vol. 5, no. 2, pp. 131–138, 2000.
- [90] M. Ghosn, F. Moses, and J. Gobieski, "Evaluation of Steel Bridges Using In-Service Testing," *Transp. Res. Rec. 1072*, pp. 71–78, 1986.
- [91] J. M. Stallings and C. H. Yoo, "Tests and Ratings of Short-Span Steel Bridges," *J. Struct. Eng.*, vol. 119, no. 7, pp. 2150–2168, 1993.
- [92] T. Ebeido and J. B. Kennedy, "Shear and Reaction Distribution in Continuous Skew Composite Bridges," *J. Bridge Eng.*, vol. 1, no. 4, pp. 155–165, 1996.
- [93] C. L. Freyermuth, "Design of continuous highway bridges with precast, prestressed concrete girders," *PCI J.*, vol. 14, no. 2, pp. 14–39, Apr. 1969, doi: <https://doi.org/10.15554/pcij.04011969.14.39>.
- [94] E. G. Nawy, *Prestressed Concrete: A Fundamental Approach*, Fifth. Prentice Hall, 2010.
- [95] A. Azizinamini, "Simple for Dead Load-Continuous for Live Load Steel Bridge Systems," *Eng. J. Bridge Innov.*, no. Second Quarter, pp. 59–83, 2014.
- [96] S. Walton and T. Bradberry, "Continuous for Live Load: A Texas Historical Perspective," 2011.
- [97] A. Mirmiran, S. Kulkarni, R. Castrodale, R. Miller, and M. Hastak, "Nonlinear Continuity Analysis of Precast, Prestressed Concrete Girders with Cast-in-Place Decks and

- Diaphragms,” *PCI J.*, vol. 46, no. 5, pp. 60–80, Oct. 2001, doi: <https://doi.org/10.15554/pcij.09012001.60.80>.
- [98] R. Miller, R. Castrodale, A. Mirmiran, and M. Hastak, “Connection of Simple-Span Precast Concrete Girders for Continuity,” Transportation Research Board, Washington, D. C., 519, 2004.
- [99] M. K. Tadros, J. A. Ficenec, A. Einea, and S. Holdsworth, “A New Technique to Create Continuity in Prestressed Concrete Members,” *PCI J.*, vol. 58, no. 5, pp. 30–37, Oct. 1993.
- [100] Z. Ma, X. Huo, M. Tadros, and M. Baishya, “Restraint Moments in Precast/Prestressed Concrete Continuous Bridges,” *PCI J.*, vol. 43, no. 6, pp. 40–57, Dec. 1998, doi: <https://doi.org/10.15554/pcij.11011998.40.57>.
- [101] V. Perry, D. Dykstra, P. Murray, and B. Rajlic, “Innovative Field Cast UHPC Joints for Precast Bridge Systems - 3-span Live Load Continuous,” presented at the Annual Conference of the Transportation Association of Canada, Halifax, Nova Scotia, 2010.
- [102] Florida Department of Transportation (FDOT), “Structures Design Guidelines - FDOT Structures Manual,” 2021.
- [103] PCI New England Technical committee, “Prestressed Concrete Girder Continuity Connection,” Precast/Prestressed Concrete Institute New England Region, PCINER-98-PCGCC, May 1998.
- [104] M. Culmo, “Connection Details for Prefabricated Bridge Elements and Systems,” Federal Highway Administration, Office of Bridge Technology, FHWA-IF-09-010, Mar. 2009.
- [105] R. G. Oesterle, J. D. Glikin, and S. C. Larson, “Design of Precast Prestressed Bridge Girders Made Continuous,” National Cooperative Highway Research Program (NCHRP), NCHRP Report 322, Nov. 1989.
- [106] P. Noppakunwijai, N. Jongpitakseel, Z. Ma, S. A. Yehia, and M. Tadros, “Pullout Capacity of Non-Prestressed Bent Strands for Prestressed Concrete Girders,” *PCI J.*, vol. 47, no. 4, pp. 90–103, Aug. 2002, doi: <https://doi.org/10.15554/pcij.07012002.90.103>.
- [107] J. Salmons, “Behavior of Untensioned-Bonded Prestressing Strand,” Missouri Highway & Transportation Department, Columbia, Missouri, FHWA-RD-77-1, Sep. 1980.
- [108] B. A. Graybeal, “Design and construction of field-cast UHPC Connections,” Federal Highway Administration, FHWA-HRT-19-011, Feb. 2019.
- [109] L. F. Maya and B. Graybeal, “Experimental Study of Strand Splice Connections in UHPC for Continuous Precast Prestressed Concrete Bridges,” *Eng. Struct.*, vol. 133, pp. 81–90, 2017, doi: <https://doi.org/10.1016/J.ENGSTRUCT.2016.12.018>.
- [110] B. Graybeal, “Splice Length of Prestressing Strands in Field-Cast UHPC Connections,” *Mater. Struct.*, vol. 48, pp. 1831–1939, Mar. 2014, doi: [10.1617/s11527-014-0277-8](https://doi.org/10.1617/s11527-014-0277-8).
- [111] R. Floyd *et al.*, “Evaluation of Ultra-High-Performance Concrete for Use in Bridge Connections and Repair,” The University of Oklahoma, School of Civil Engineering and Environmental Science, FHWA-OK-21-03, Feb. 2021.

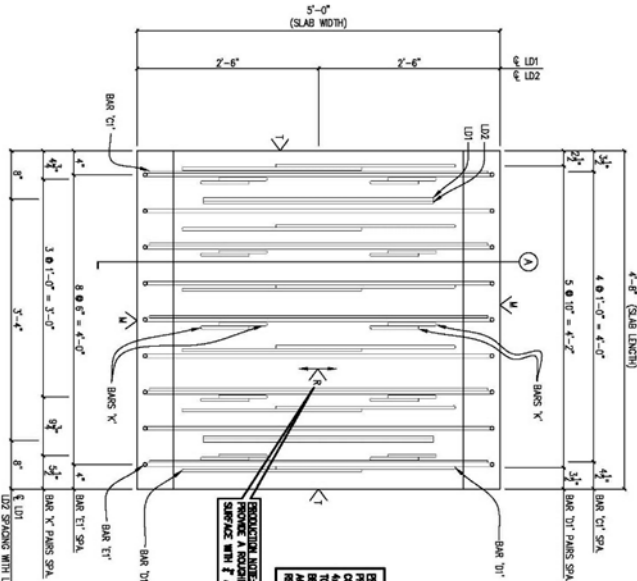
- [112] T. Looney, J. Volz, and R. Floyd, "Behavior of a 3-Span Continuous Bridge Before and After Continuity Joint Replacement Using Ultra-High-Performance Concrete," *J. Perform. Constr. Facil.*, vol. 35, no. 6, p. 12, Sep. 2021.
- [113] J. Benjumea, S. Saïidi, and A. Itani, "Biaxial Seismic Performance of a Two-Span Concrete Bridge Model with Six ABC Connections," *J. Bridge Eng.*, vol. 26, no. 8, p. 15, Jun. 2021.
- [114] R. Floyd *et al.*, "Evaluation of Ultra-High Performance Concrete, Fiber Reinforced Self-Consolidating Concrete, and Malp Concrete for Prestressed Girder Repair," The University of Oklahoma, School of Civil Engineering and Environmental Science, FHWA-OK-21-03, Feb. 2020.
- [115] A. DeJong, W. Shi, B. Shafei, and T. Hosteng, "Integral Abutment Connections with Grouted Reinforcing Bar Couplers and Ultrahigh-Performance Concrete," *J. Bridge Eng.*, vol. 26, no. 8, p. 15, May 2021.
- [116] A. Sadeghnejad, R. Taghinezhadbilondy, and A. Azizinamini, "Seismic Performance of New Connection Detail in an SDCL Steel Bridge System," *J. Bridge Eng.*, vol. 24, no. 10, Jul. 2019, doi: (ASCE)BE.1943-5592.0001460.
- [117] J. Ficenec, S. Kneip, M. Tadros, and L. Fisher, "Prestressed Spliced I-Girders: Tenth Street Viaduct Project, Lincoln, Nebraska," *PCI J.*, vol. 38, no. 5, pp. 38–48, Oct. 1993, doi: <https://doi.org/10.15554/pcij.09011993.38.48>.
- [118] Florida Department of Transportation (FDOT), "Poured Joint with Backer Rod Expansion Joint System," *Index No D21110*, no. FDOT Design Standards, p. 2, 2013.
- [119] F. D. Chitty, C. J. Freeman, and D. B. Garber, "Joint Design Optimization for Accelerated Construction of Slab Beam Bridges," *Journal of Bridge Engineering*, vol. 25, no. 7, p. 04020029, 2020.
- [120] M. K. Tadros and N. Jongpitaksseel, "Anchorage of 0.6" Diameter Strands," SPR-1 (03) P551, Jun. 2003.
- [121] Florida Department of Transportation (FDOT), *Prestressed Beam*. 2021. [Online]. Available: <https://www.fdot.gov/structures/proglib.shtm>
- [122] "QConBridge Reference Manual." Washington State Department of Transportation, May 05, 2005.
- [123] "Bridge Software - QConBridge FAQ's." Washington State Department of Transportation, 2002. [Online]. Available: https://www.wsdot.wa.gov/eesc/bridge/software/index.cfm?fuseaction=FAQs&software_id=48
- [124] Florida Department of Transportation (FDOT), "Bridge Load Rating Manual," *State Load Rat. Eng.*, Jan. 2020, [Online]. Available: <http://www.fdot.gov/maintenance/LoadRating.shtm>
- [125] D. Pryn and J. Cervenka, "ATENA Program Documentation - Troubleshooting Manual," Cervenka Consulting, Oct. 2018.

A. CONSTRUCTION DRAWINGS

The construction drawings for the small-scale and full-scale beam tests are provided in this section.

A.1. CONSTRUCTION PLANS FOR SMALL-SCALE JOINT TEST SPECIMENS

These specimens were cast in two sets. The first set included all specimens other than two specimens with joint A2.



REINFORCING PLAN VIEW

REINFORCING PLAN VIEW

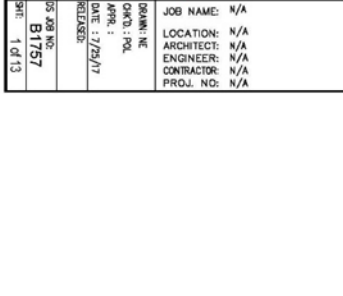
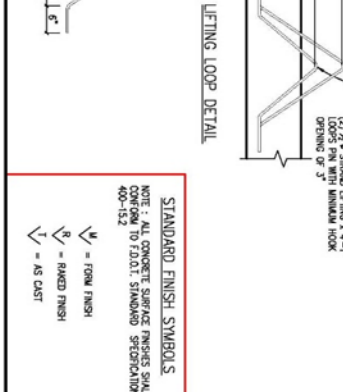
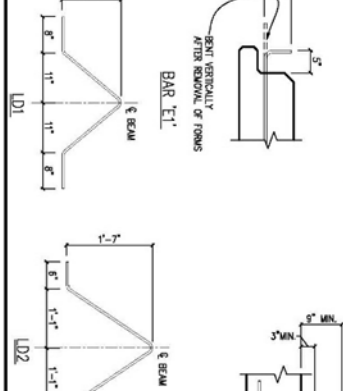
REINFORCING PLAN VIEW

REINFORCING PLAN VIEW

REINFORCING PLAN VIEW

MARK	QTY.	LENGTH @	WEIGHT	DL. VOLS.
PS981	2	4'-0"	3.021 #	0.125 C.Y.

ITEM	QTY.	PART DIA.	SIZE	LENGTH	REMARKS
C1	5	REBAR 3	#3	4'-0"	STRAIGHT BARS
D1	12	REBAR 4	#4	5'-0"	SEE RIGHT
K	20	REBAR 4	#4	2'-0"	SEE RIGHT
E1	9	REBAR 5	#5	5'-10"	SEE RIGHT



REVISIONS

REVISIONS

REVISIONS

REVISIONS

REVISIONS

REVISIONS

REVISIONS

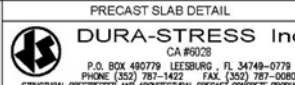
REVISIONS

REVISIONS

REVISIONS

REVISIONS

REVISIONS



PRECAST SLAB DETAIL
DURA-STRESS Inc.
 CA #6028
 P.O. BOX 490779 LEESBURG, FL 34749-0779
 PHONE (352) 787-4422 FAX (352) 787-5880
 SUBORDINATE CONTRACTORS AND APPROVED PRECAST CONCRETE PRODUCTS

REV	DESCRIPTION	DATE	BY	CHK.
1	REVISED AS SHOWN	8/4/17	POL	
2	REVISED AS SHOWN	8/4/17		

JOB NAME:	LOCATION:	ARCHITECT:	ENGINEER:	CONTRACTOR:	PROJ. NO.:
N/A	N/A	N/A	N/A	N/A	N/A

DATE:	BY:	CHK.:
8/4/17	POL	

STANDARD FINISH SYMBOLS

STANDARD FINISH SYMBOLS

STANDARD FINISH SYMBOLS

STANDARD FINISH SYMBOLS

STANDARD FINISH SYMBOLS

STANDARD FINISH SYMBOLS

STANDARD FINISH SYMBOLS

SLAB BEAM SCHEDULE					
MARK	QTY.	LENGTH @	WEIGHT	DL. VOS	DBI. C.V.
PRE2	1	4'-0"	3,295 #		

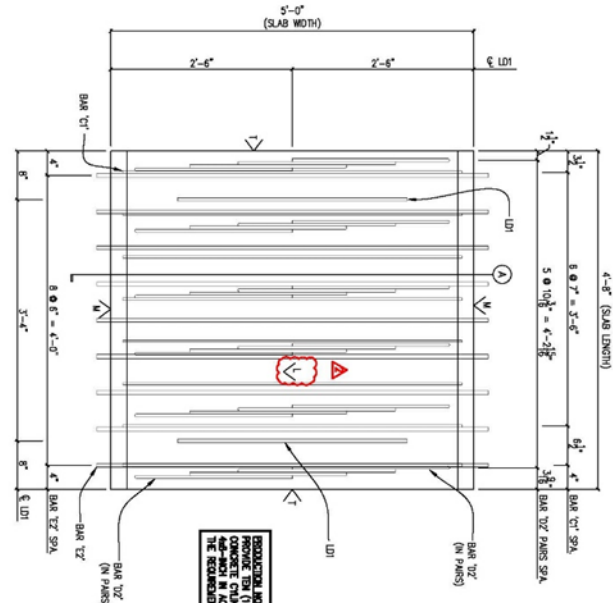
REBAR SCHEDULE (FOR ONE MEMBER ONLY)					
ITEM	QTY.	PART ID.	SIZE	LENGTH	REMARKS
C1	8	REBAR 3	#3	4'-0"	STRAIGHT BARS
D2	24	REBAR 4	#4	5'-0"	SET RIGHT
E2	9	REBAR 5	#5	5'-4"	STRAIGHT BARS

NOTE: ALL BAR DIMENSIONS ARE OUT-TO-OUT.
NOTE: ALL BAR DIMENSIONS ARE OUT-TO-OUT.

LOT	2	STRAND	3/4" STRAND	4'-1"	SET RIGHT
-----	---	--------	-------------	-------	-----------

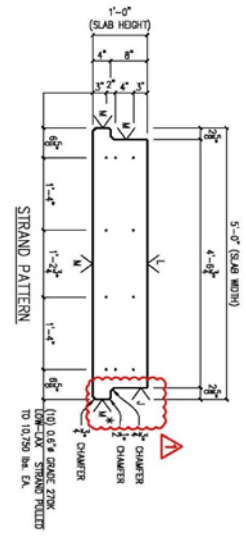
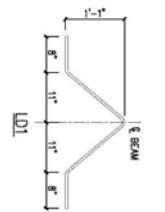
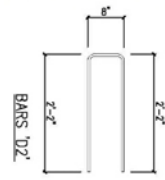
REINFORCING NOTES:
1. SPLIT BAR TOP PARS LONGITUDINALLY AS REQUIRED TO CLEAR BARS E2.
2. SPLIT BAR CT LONGITUDINALLY AS REQUIRED TO CLEAR BAR TZ PARS.

REINFORCING PLAN VIEW



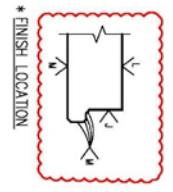
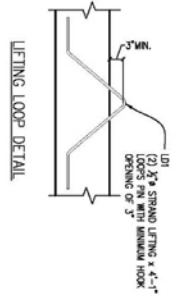
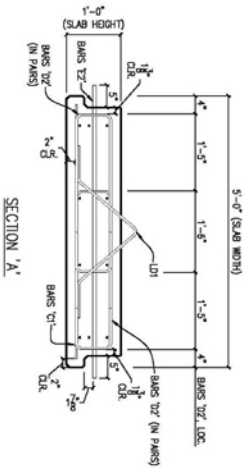
REINFORCING NOTES:
REVISION FOR LOT 101. ADDITIONAL CONCRETE CHAMBERS OF SIZE 4" X 4" X 4" IN ACCORDANCE WITH THE REINFORCING PLAN VIEW.

REVISED DRAWINGS
AUGUST 4, 2017
DESTROY ALL OTHERS



SHIELDING LEGEND
- - - NONE REQUIRED

CONCRETE CLASS VI
F_c (28 DAYS) = 8,500 PSI
F_{cd} (RELEASE) = 6,000 PSI



STANDARD FINISH SYMBOLS
NOTE: ALL CONCRETE SURFACE FINISHES SHALL BE TO THE FOLLOWING TOLERANCES UNLESS OTHERWISE NOTED.
400-152
400-152

M = FORM FINISH
 V = SMOOTH FLOAT
 V = AS CAST

JOB NAME:	N/A
LOCATION:	N/A
ARCHITECT:	N/A
ENGINEER:	N/A
CONTRACTOR:	N/A
PROJ. NO.:	N/A

PRECAST SLAB DETAIL

DURA-STRESS Inc.
CA #5028

P.O. BOX 490779 LEESBURG, FL 34748-0779
888-442-7828 FAX 352-787-3880
PHONE 352-787-3880

STRUCTURAL PROFESSIONAL AND ARCHITECTURAL PRECAST CONCRETE PRODUCTS

REV	DESCRIPTION	DATE	BY	CHK
1	REVISED AS SHOWN	8/4/17	POL	
2	REVISED AS SHOWN	8/4/17		

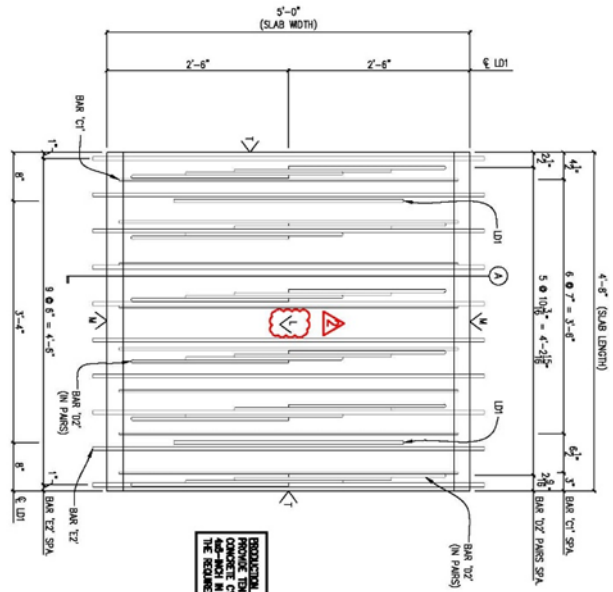


SLAB BEAM SCHEDULE				
MARK	QTY.	LENGTH @	WEIGHT	DL VBS
PSB3	1	4'-6"	3,295 #	CB C.V.

REBAR SCHEDULE (FOR ONE MEMBER ONLY)					
ITEM	QTY.	PART ID.	SIZE	LENGTH	REMARKS
C1	8	REBAR 3	#3	4'-6"	STRAIGHT BARS
D2	24	REBAR 4	#4	5'-0"	SET RIGHT
E2	10	REBAR 5	#5	5'-4"	STRAIGHT BARS

NOTE: ALL BAR DIMENSIONS ARE 001-10-0-OUT
NOTE: LENGTH IS IN FEET, INCHES (F.I., IN.) UNL.D.

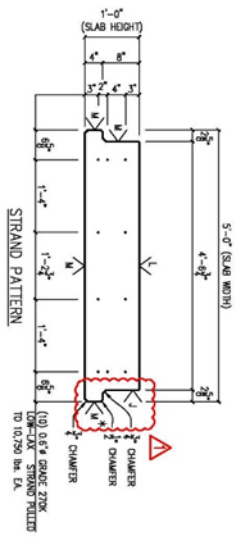
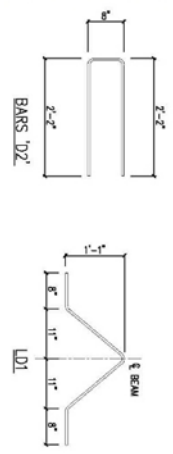
REINFORCING NOTES:
 1. SLAB BEAM TO BE REINFORCED LONGITUDINALLY AS REQUIRED TO CARRY BARS TZ.
 2. SLAB BEAM TO BE REINFORCED TRANSVERSELY AS REQUIRED TO CARRY BARS TZ.
 3. SLAB BEAM TO BE REINFORCED AS REQUIRED TO CARRY BARS TZ.



REINFORCING PLAN VIEW

REVISION NOTE:
 REMOVE THE (10) ANTIWALL CONCRETE CHAMBERS OF SIZE 1'-4\"/>

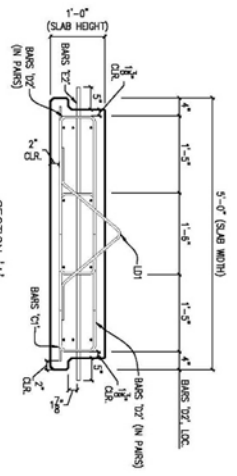
REVISED DRAWINGS
 AUGUST 4, 2017
DESTROY ALL OTHERS



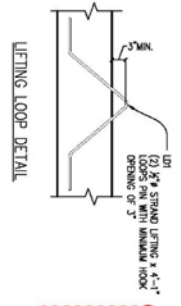
STRAND PATTERN

SHIELDING LEGEND
 * - NONE REQUIRED

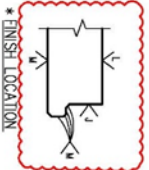
CONCRETE CLASS V
 F_c (28 DAYS) = 6,500 PSI
 F_c (RELEASE) = 6,000 PSI



SECTION 'A-A'



LETTING LOOP DETAIL



* ENGLISH LOCATION

STANDARD ENGLISH SYMBOLS

NOTE: ALL CONCRETE SURFACE FINISHES SHALL CONFORM TO FINISH STANDARD SPECIFICATION 400-152

APP: 1
 DATE: 1/25/17

M = FORM FINISH
 S = SMOOTH FLOAT
 C = AS CAST

JOB NAME:	N/A
LOCATION:	N/A
ARCHITECT:	N/A
ENGINEER:	N/A
CONTRACTOR:	N/A
PROJ. NO.:	N/A

PRECAST SLAB DETAIL

DURA-STRESS Inc.
 CA #9028

P.O. BOX 490779 LEESBURG, FL 34749-0779
 PHONE (352) 787-1422 FAX (352) 787-5880
 STRUCTURAL PRECAST AND ARCHITECTURAL PRECAST CONCRETE PRODUCTS

REV	DESCRIPTION	DATE	BY	CHK
1	REVISED AS SHOWN	8/4/17	POL	
2	REVISED AS SHOWN	8/4/17		

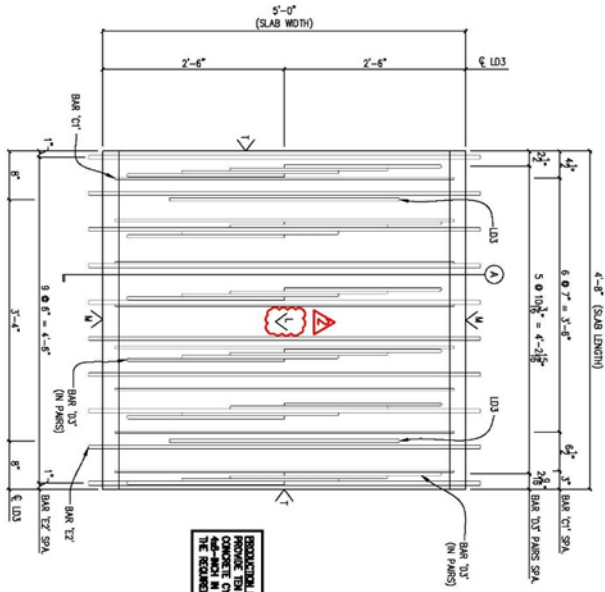


SLAB BEAM SCHEDULE					
MARK	QTY.	LENGTH @	WEIGHT	OL. VOS	OL. VOS
FRS3	1	4'-6"	4.89T #	1.21 C.Y.	

REBAR SCHEDULE (FOR ONE MEMBER ONLY)					
ITEM	QTY.	PART ID	SIZE	LENGTH	REMARKS
C1	8	REBAR 3	#3	4'-6"	STRAIGHT BARS
C3	24	REBAR 4	#4	5'-6"	SET RIGHT
E2	10	REBAR 5	#5	5'-4"	STRAIGHT BARS

NOTE: ALL BAR DIMENSIONS ARE 001-1/2-DIM.
NOTE: LENGTH IS IN FEET, INCHES (F.T., IN.) UNL.S.

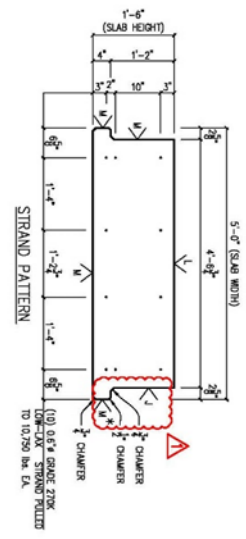
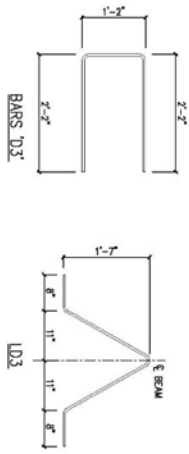
REINFORCING NOTES:
1. SPLIT BAR TOP PANS LONGITUDINALLY AS REQUIRED TO CLEAR BARS E2.
2. SPLIT BAR CT LONGITUDINALLY AS REQUIRED TO CLEAR BAR D3 PANS.



REINFORCING PLAN VIEW

REINFORCING NOTES:
1. SPLIT BAR TOP PANS LONGITUDINALLY AS REQUIRED TO CLEAR BARS E2.
2. SPLIT BAR CT LONGITUDINALLY AS REQUIRED TO CLEAR BAR D3 PANS.

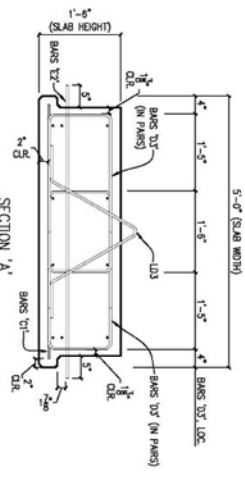
REVISED DRAWINGS
AUGUST 4, 2017
DESTROY ALL OTHERS



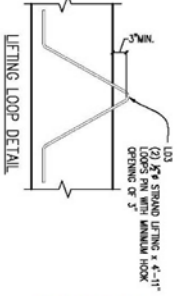
STRAND PATTERN

CONCRETE CLASS VI
F_c (28 DAYS) = 8,500 PSI
F_{ci} (RELEASE) = 6,000 PSI

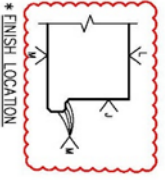
SHIELDING LEGEND
- - - NONE REQUIRED



SECTION 'A-A'



LETTING LOOP DETAIL



* FINISH LOCATION

STANDARD FINISH SYMBOLS
NOTE: ALL CONCRETE SURFACE FINISHES SHALL BE TO THE STANDARD SPECIFICATION FOR PORTLAND CEMENT CONCRETE, SECTION 05100-10.0, PART 1.0, STANDARD SPECIFICATION 400-15.2
DATE: 7/29/17
APP. :
DRAWN: NE
CHKD.: POL
RELEASER:
DATE: 7/29/17
APP. :
DATE: 8/17/17
BY: 5 of 13

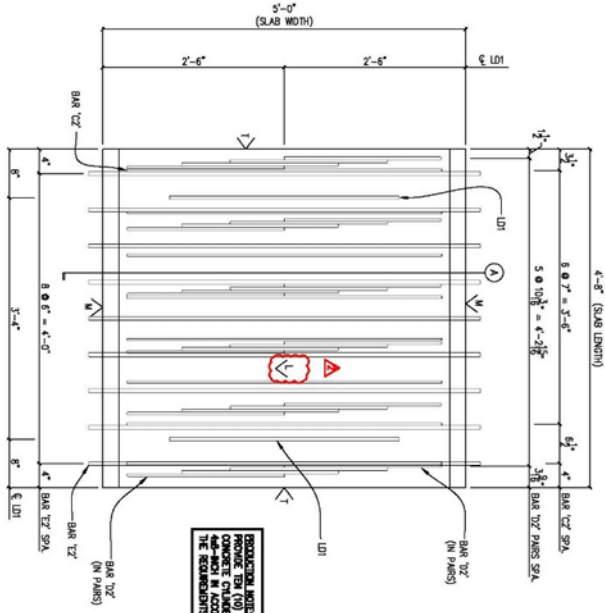
	PRECAST SLAB DETAIL DURA-STRESS Inc. CA #5028 P.O. BOX 490779 LEESBURG, FL 34749-0779 PHONE (352) 782-1422 FAX (352) 782-3880 STRUCTURAL PROFESSIONAL AND ARCHITECTURAL PRECAST CONCRETE PRODUCTS	<table border="1"> <thead> <tr> <th>REV</th> <th>DESCRIPTION</th> <th>DATE</th> <th>BY</th> <th>CHK</th> </tr> </thead> <tbody> <tr> <td>1</td> <td>REVISED AS SHOWN</td> <td>8/4/17</td> <td>POL</td> <td></td> </tr> <tr> <td>2</td> <td>REVISED AS SHOWN</td> <td>8/4/17</td> <td></td> <td></td> </tr> </tbody> </table>	REV	DESCRIPTION	DATE	BY	CHK	1	REVISED AS SHOWN	8/4/17	POL		2	REVISED AS SHOWN	8/4/17			
	REV	DESCRIPTION	DATE	BY	CHK													
1	REVISED AS SHOWN	8/4/17	POL															
2	REVISED AS SHOWN	8/4/17																
JOB NAME: N/A LOCATION: N/A ARCHITECT: N/A ENGINEER: N/A CONTRACTOR: N/A PROJ. NO.: N/A																		

SLAB BEAM SCHEDULE				
MARK	QTY	LENGTH @ E	WEIGHT	DL VSS
PS98	1	4'-5"	3,244 #	0.88 C.V.

REBAR SCHEDULE (FOR ONE MEMBER ONLY)				
ITEM	QTY	PART ID	SIZE	REMARKS
C2	8	REBAR 3	#3	STRAIGHT BARS
D2	24	REBAR 4	#4	SET RIGHT
E2	9	REBAR 3	#5	STRAIGHT BARS

NOTE: ALL BAR DIMENSIONS ARE QTY-TO-CUT
 NOTE: LENGTH IS IN FEET, INCHES (FT., IN.) UNLS.

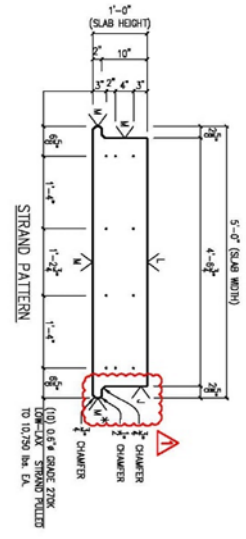
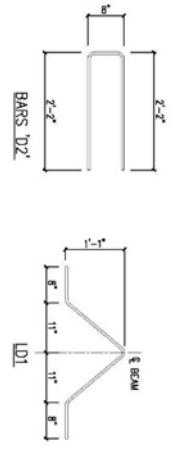
REINFORCING NOTES:
 1. SPLIT BAR T/CZ PARS LONGITUDINALLY AS REQUIRED TO CLEAR BARS T/CZ.
 2. SPLIT BAR T/CZ LONGITUDINALLY AS REQUIRED TO CLEAR BAR T/CZ PARS.



REINFORCING PLAN VIEW

REINFORCING NOTES: ADDITIONAL CONCRETE CHANGERS OF SIZE ARE NOT IN ACCORDANCE WITH THE REQUIREMENTS FOR CON.

REVISED DRAWINGS
 AUGUST 4, 2017
DESTROY ALL OTHERS

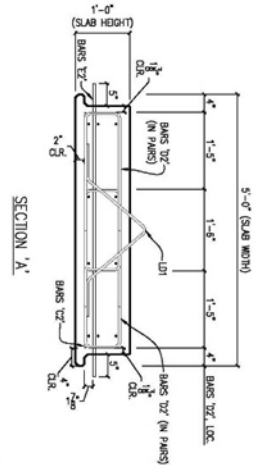


DEINSONING SEQUENCE

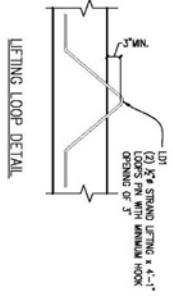
1	2	3	4
4	3	2	1

CONCRETE CLASS VI
 F_c (28 DAYS) = 6,500 PSI
 F_{cd} (RELEASE) = 6,000 PSI

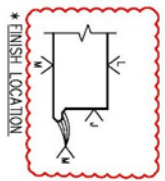
SHIELDING LEGEND
 - - - NONE REQUIRED



SECTION 'A-A'



LIFTING LOOP DETAIL



* ENGLISH LOCATION

STANDARD ENGLISH SYMBOLS
 NOTE: ALL CONCRETE SURFACES FINISHED SHALL BE FINISHED TO 1/8" FINISH, STANDARD SPECIFICATION 400-152
 M = FORM FINISH
 S = SMOOTH FLOAT
 C = AS CAST

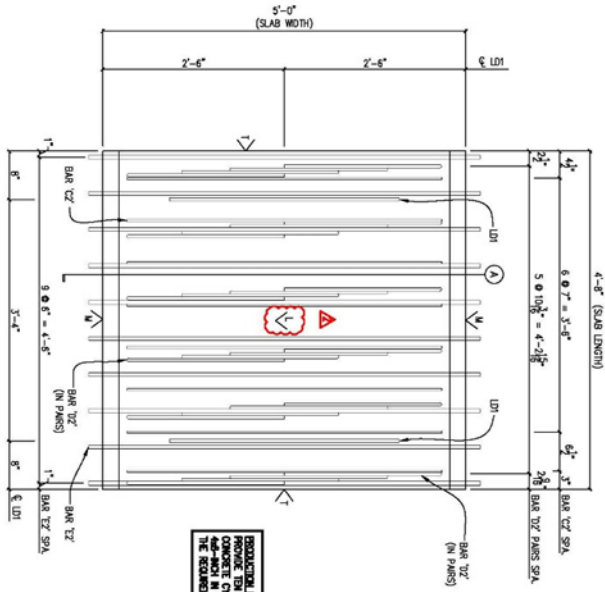
JOB NAME:	N/A
LOCATION:	N/A
ARCHITECT:	N/A
ENGINEER:	N/A
CONTRACTOR:	N/A
PROJ. NO.:	N/A
DRAWING NO.:	05-288-NIS
DATE:	7/25/17
APP'D.:	
REVISED:	
DATE:	8/17/17
BY:	6/07/13

PRECAST SLAB DETAIL

DURA-STRESS Inc.
 CA #5028
 P.O. BOX 480778 DEERBURG, FL 34748-0778
 PHONE (352) 787-1422 FAX (352) 787-0080
 STRUCTURAL PRECASTERS AND ARCHITECTURAL PRECAST CONCRETE PRODUCTS

REV	DESCRIPTION	DATE	BY	CHK
1	REVISED AS SHOWN	8/4/17	POL	
2	REVISED AS SHOWN	8/4/17		





REVISIONS:
 REVISION NO. 1: ADDITIONAL CONCRETE CHAMBERS OF SIZE 1/2" x 1/2" x 1/2" TO BE INSTALLED AT THE REINFORCEMENT FABRICATION.

REINFORCING NOTES:
 1. SPLIT BAR T2Z PARS LONGITUDINALLY AS REQUIRED TO CLEAR BARS B2Z.
 2. SPLIT BAR B2Z LONGITUDINALLY AS REQUIRED TO CLEAR BAR T2Z PARS.

SLAB BEAM SCHEDULE

MARK	QTY.	LENGTH @	WEIGHT	OL. VOS
FR97	1	4'-0"	3.244 #	0.00 C.Y.

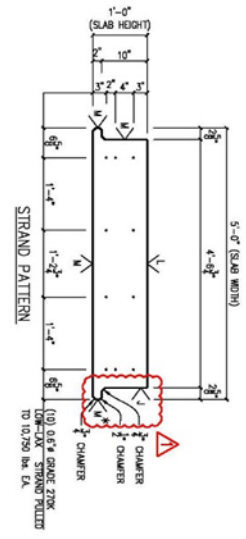
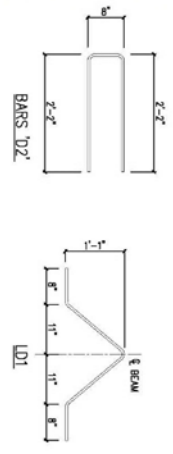
REBAR SCHEDULE (FOR ONE MEMBER ONLY)

NOTE: ALL BAR DIMENSIONS ARE OUT-TO-OUT.
 NOTE: ALL BAR DIMENSIONS ARE OUT-TO-OUT.

ITEM	QTY.	PART ID.	SIZE	LENGTH	REMARKS
CZ	8	REBAR 3	#3	4'-0"	STRAIGHT BARS
DZ	24	REBAR 4	#4	5'-0"	SET RIGHT
EZ	10	REBAR 5	#5	5'-4"	STRAIGHT BARS
LD1	2	STRAND	5/8" STRAND	4'-1"	SET RIGHT

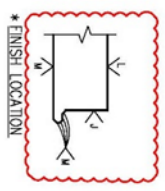
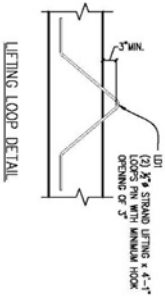
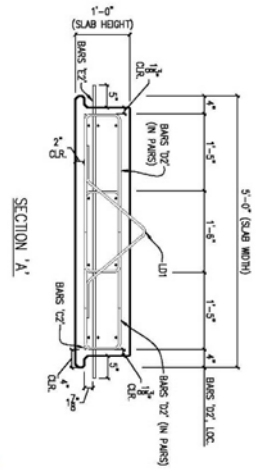
REINFORCING PLAN VIEW

REVISED DRAWINGS
 AUGUST 4, 2017
 DESTROY ALL OTHERS



SHIELDING LEGEND
 - - - NONE REQUIRED

CONCRETE CLASS VI
 F_c (28 DAYS) = 8,500 PSI
 F_{ci} (RELEASE) = 6,000 PSI



STANDARD FINISH SYMBOLS
 NOTE: ALL CONCRETE SURFACE FINISHES SHALL BE TO THE STANDARD SPECIFICATION 400-15.2
 (LD) = FORM FINISH
 (LD) = SMOOTH FLOAT
 (LD) = AS CAST

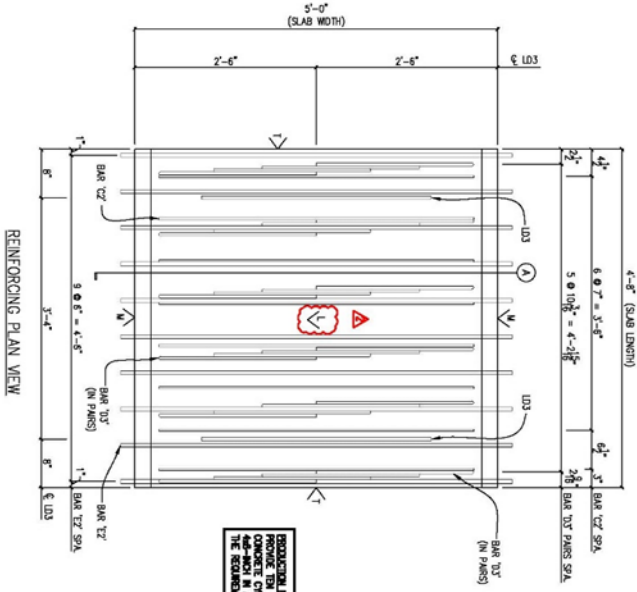
<p>REVISIONS:</p> <table border="1"> <thead> <tr> <th>REV</th> <th>DESCRIPTION</th> <th>DATE</th> <th>BY</th> <th>CHK</th> </tr> </thead> <tbody> <tr> <td>1</td> <td>REVISED AS SHOWN</td> <td>8/4/17</td> <td>POL</td> <td></td> </tr> <tr> <td>2</td> <td>REVISED AS SHOWN</td> <td>8/4/17</td> <td></td> <td></td> </tr> </tbody> </table>	REV	DESCRIPTION	DATE	BY	CHK	1	REVISED AS SHOWN	8/4/17	POL		2	REVISED AS SHOWN	8/4/17			<p>PRECAST SLAB DETAIL</p> <p>DURA-STRESS Inc. CA #50238 P.O. BOX 490779 LEESBURG, FL 34749-0779 PHONE (352) 787-1422 FAX (352) 787-3880 STRUCTURAL PROFESSIONAL AND ARCHITECTURAL PRECAST CONCRETE PRODUCTS</p>	<p>JOB NAME: N/A LOCATION: N/A ARCHITECT: N/A ENGINEER: N/A CONTRACTOR: N/A PROJ. NO.: N/A</p>	<p>DATE: 7/29/17 APPR.: POL DESIGNED: N/A CHECKED: N/A DATE: 7/29/17 APPR.: POL DESIGNED: N/A CHECKED: N/A</p>	<p>DATE: 7/29/17 APPR.: POL DESIGNED: N/A CHECKED: N/A</p>	<p>DATE: 7/29/17 APPR.: POL DESIGNED: N/A CHECKED: N/A</p>
REV	DESCRIPTION	DATE	BY	CHK																
1	REVISED AS SHOWN	8/4/17	POL																	
2	REVISED AS SHOWN	8/4/17																		

SLAB BEAM SCHEDULE				
MARK	QTY	LENGTH @ ϵ	WEIGHT	DL V/S
PS99	1	4'-5"	4,540 #	1/20 C/T

REBAR SCHEDULE (FOR ONE MEMBER ONLY)				
ITEM	QTY	PART ID	SIZE	REMARKS
C2	8	REBAR 3	#3	STRAIGHT BARS
D3	24	REBAR 4	#4	SET RIGHT
E2	10	REBAR 5	#5	STRAIGHT BARS
L03	2	STRAND	2# STRAND	SET RIGHT

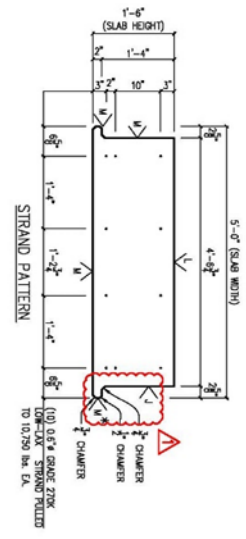
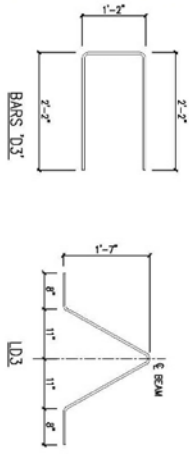
NOTE: ALL BAR DIMENSIONS ARE QTY-TO-QTY LENGTH IS IN FEET, INCHES (FT., IN.) UNL.S.

REINFORCING NOTES:
 1. SPLIT BAR TYP PARS LONGITUDINALLY AS REQUIRED TO CLEAR BARS T2.
 2. SPLIT BAR C2 LONGITUDINALLY AS REQUIRED TO CLEAR BAR D3 PARS.



REINFORCING NOTES:
 PROVIDE BAR TYP ADDITIONAL CONCRETE CHAMBERS OF SETH AND EACH IN ACCORDANCE WITH THE REINFORCEMENT ASH CON.

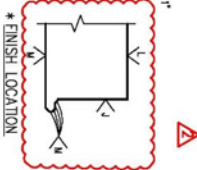
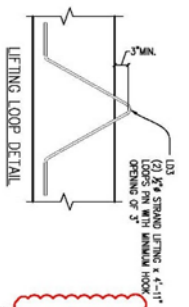
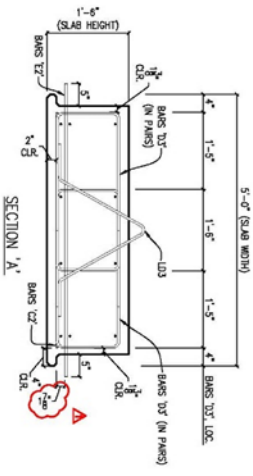
REVISED DRAWINGS
 AUGUST 4, 2017
DESTROY ALL OTHERS



REVISION	DESCRIPTION	DATE	BY	CHK
1	REVISED AS SHOWN	8/4/17	POL	
2	REVISED AS SHOWN	8/4/17		

CONCRETE CLASS VI
 F_c (28 DAYS) = 6,500 PSI
 F_{cd} (RELEASE) = 6,000 PSI

SHIELDING LEGEND
 - - NONE REQUIRED



STANDARD FINISH SYMBOLS
 NOTE: ALL CONCRETE SURFACES FINISHED SHALL BE FINISHED TO THE FOLLOWING SPECIFICATIONS:
 400-152
 FINISH: F = FORM FINISH
 S = SMOOTH FLOAT
 AS = AS CAST

JOB NAME:	N/A
LOCATION:	N/A
ARCHITECT:	N/A
ENGINEER:	N/A
CONTRACTOR:	N/A
PROJ. NO.:	N/A
DRAWING NO.:	05 288 N03
DATE:	7/25/17
APPR.:	B1757
REVISED:	
DATE:	9/1/13

PRECAST SLAB DETAIL

DURA-STRESS Inc.
 CA #5028
 P.O. BOX 480778 DEERBURG, FL 34748-0778
 PHONE (352) 787-1422 FAX (352) 787-0080
 STRUCTURAL PRECASTERS AND ARCHITECTURAL PRECAST CONCRETE PRODUCTS

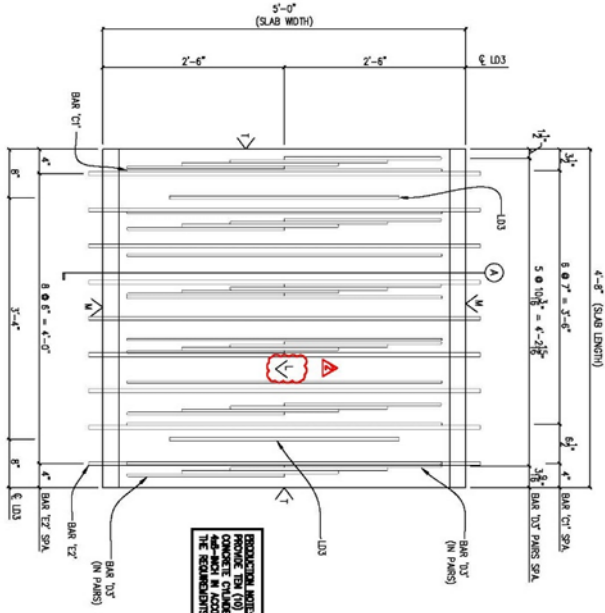


SLAB BEAM SCHEDULE				
MARK	QTY	LENGTH @	WEIGHT	DL. VSS
PSB10	1	4'-5"	3,259 #	0.88 C.V.

REBAR SCHEDULE (FOR ONE MEMBER ONLY)				
ITEM	QTY	PART ID	SIZE	REMARKS
C1	8	REBAR 3	#3	STRAIGHT BARS
C2	24	REBAR 4	#4	SET RIGHT BARS
E2	9	REBAR 3	#5	5'-4" STRAIGHT BARS
L01	2	STRAND	2 1/2" STRAND	SET RIGHT

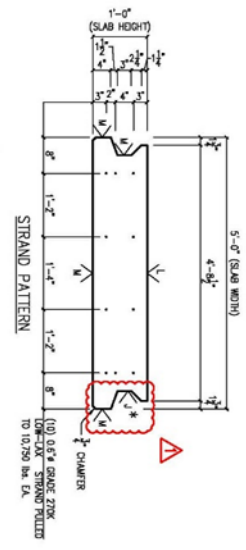
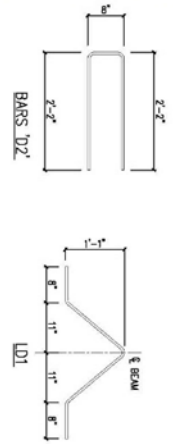
NOTE: ALL BAR DIMENSIONS ARE QTY-TO-CUT
LENGTH IS IN FEET, INCHES (FT. IN.) UNL.S.

REINFORCING NOTES:
1. SPLIT BAR T/C PARS LONGITUDINALLY AS REQUIRED TO CLEAR BARS T2.
2. SPLIT BAR T/C LONGITUDINALLY AS REQUIRED TO CLEAR BAR T/C PARS.

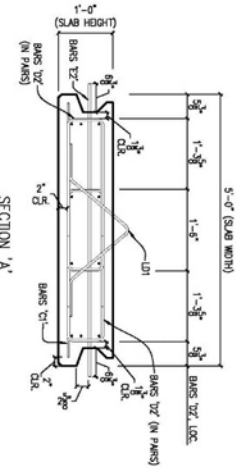


REINFORCING PLAN VIEW

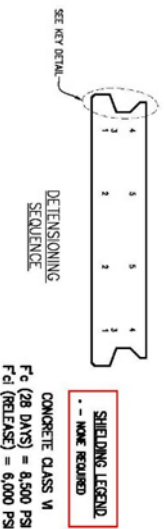
REVISED DRAWINGS
AUGUST 4, 2017
DESTROY ALL OTHERS



STRAND PATTERN

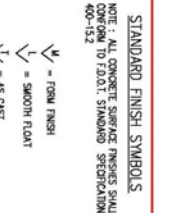
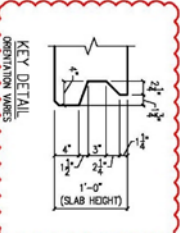


SECTION 'A-A'



LIFTING LOOP DETAIL

FINISH LOCATION



NOTE: ALL CONCRETE SURFACES FINISHED SHALL BE FINISHED TO THE FOLLOWING SPECIFICATIONS
400-152
DATE: 7/25/17
APPR.: POL

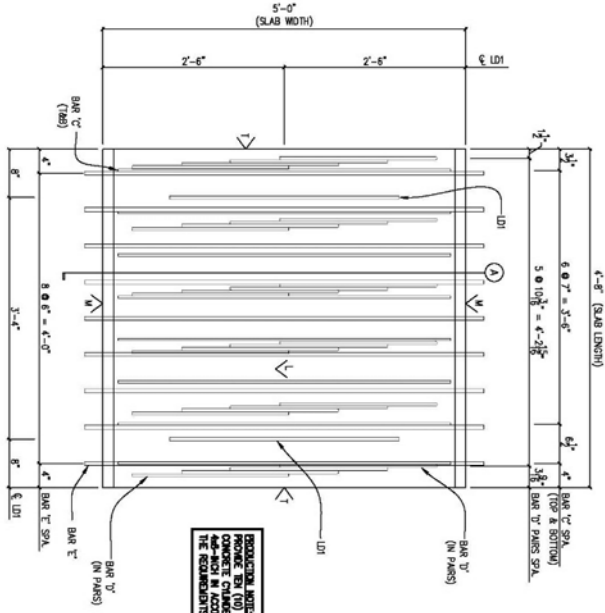
JOB NAME:	N/A
LOCATION:	N/A
ARCHITECT:	N/A
ENGINEER:	N/A
CONTRACTOR:	N/A
PROJ. NO.:	N/A
DRAWING NO.:	05 208 000
DATE:	8/17/17
REVISED:	8/17/17
SHEET:	10 OF 13

PRECAST SLAB DETAIL

DURA-STRESS Inc.
CA #5028
P.O. BOX 480779 DEERBURG, FL 34749-0779
PHONE (352) 787-1422 FAX (352) 787-0080

REV	DESCRIPTION	DATE	BY	CHK
1	REVISED AS SHOWN	8/4/17	POL	
2	REVISED AS SHOWN	8/4/17	POL	





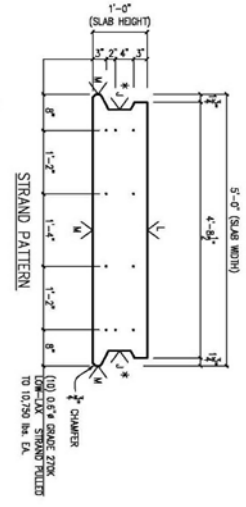
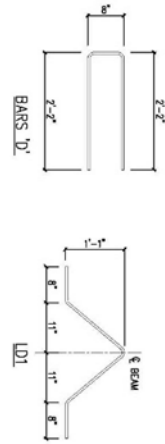
REINFORCING NOTES:
 1. SHEET BAR 'V' PARS LONGITUDINALLY AS REQUIRED TO CLEAR BARS 'E'.
 2. SHEET BAR 'C' LONGITUDINALLY AS REQUIRED TO CLEAR BAR 'V' PARS.

**FOR YOUR
 FEBRUARY 19, 2018
 APPROVAL**

SLAB BEAM SCHEDULE				
MARK	QTY	LENGTH @ E	WEIGHT	DL VSS
PSB1	1	4'-8"	3,240 #	0.88 C.V.

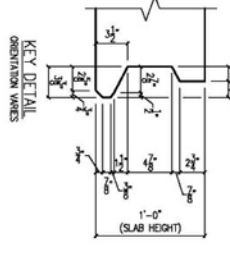
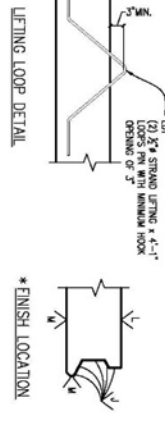
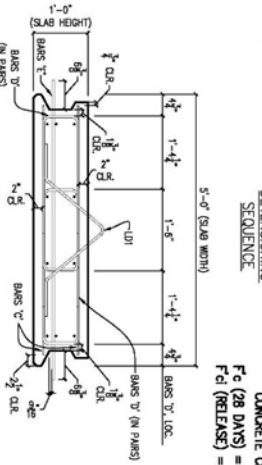
REBAR SCHEDULE (FOR ONE MEMBER ONLY)					
ITEM	QTY	PART ID	SIZE	LENGTH	REMARKS
C	18	REBAR 3	#3	4'-7"	STRAIGHT BARS
D	24	REBAR 4	#4	5'-0"	SET RIGHT BARS
E	9	REBAR 5	#5	5'-0"	STRAIGHT BARS

NOTE: ALL BAR DIMENSIONS ARE OUT-TO-OUT
 LENGTH IS IN FEET, INCHES (FT. IN.) UNLS.



CONCRETE CLASS VI
F_c (28 DAYS) = 6,500 PSI
F_{cd} (RELEASE) = 6,000 PSI

SHIELDING LEGEND
 - - NONE REQUIRED



STANDARD FINISH SYMBOLS
 NOTE: ALL CONCRETE SURFACES FINISHED SHALL BE FINISHED TO FINISH STANDARD SPECIFICATION 400-4.3.2
 - - = HEAVY SANDBLAST
 - - = FORM FINISH
 - - = SMOOTH FLOAT
 - - = AS CAST

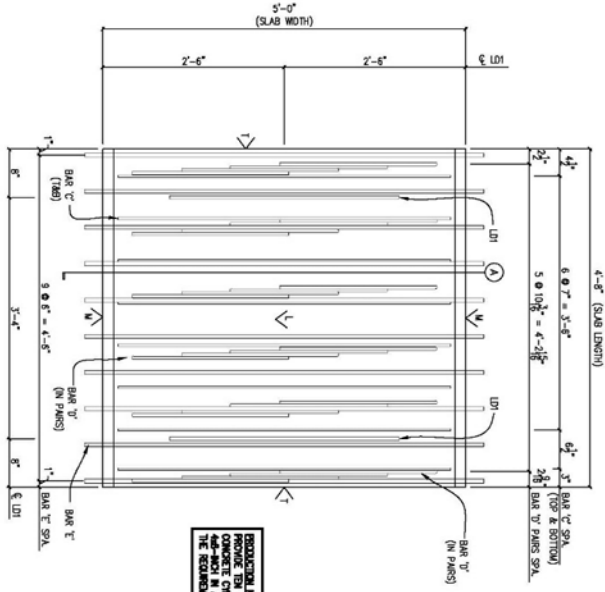
JOB NAME:	N/A
LOCATION:	N/A
ARCHITECT:	N/A
ENGINEER:	N/A
CONTRACTOR:	N/A
PROJ. NO.:	N/A



DURA-STRESS Inc.
 CA #5028
 P.O. BOX 480778 DEERBURG, FL 34748-0778
 PHONE (352) 787-1422 FAX (352) 787-0080
 STRUCTURAL PRECASTERS AND ARCHITECTURAL PRECAST CONCRETE PRODUCTS



REV	DESCRIPTION	DATE	BY	CHK



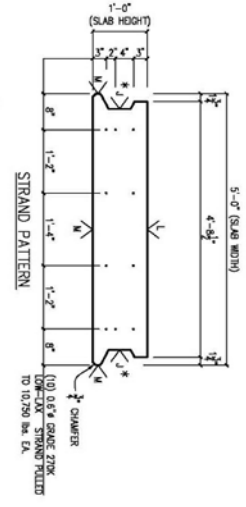
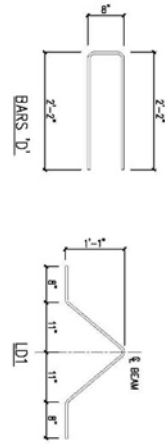
PROVIDER NOTES:
 PROVIDER SHALL VERIFY ALL DIMENSIONS AND CONDITIONS OF SITE PRIOR TO CONSTRUCTION. THE RESPONSIBILITY FOR THE REINFORCEMENT SHALL BE ON THE CONTRACTOR.

**FOR YOUR
 FEBRUARY 19, 2018
 APPROVAL**

SLAB BEAM SCHEDULE				
MARK	QTY	LENGTH @ E	WEIGHT	DL VSS
PSB2	1	4'-8"	3,240 #	0.80 C/T

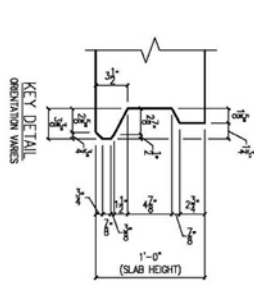
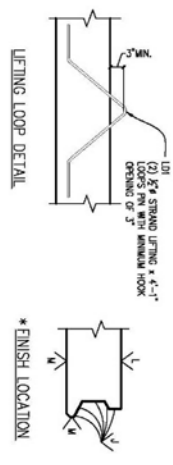
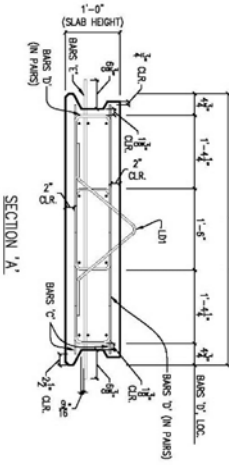
REBAR SCHEDULE (FOR ONE MEMBER ONLY)				
ITEM	QTY	PART ID	SIZE	REMARKS
C	18	REBAR 3	#3	STRAIGHT BARS
D	24	REBAR 4	#4	SET RIGHT BARS
E	10	REBAR 3	#5	STRAIGHT BARS

NOTE: ALL BAR DIMENSIONS ARE OUT-TO-OUT
 LENGTH IS IN FEET, INCHES (FT. IN.) UNLESS OTHERWISE NOTED.



SHIELDING LEGEND
 - - - WORK REQUIRED

CONCRETE CLASS VI
 F_c (28 DAYS) = 8,500 PS
 F_{cd} (RELEASE) = 6,000 PS



STANDARD FINISH SYMBOLS
 NOTE: ALL CONCRETE SURFACES FINISHES SHALL BE TO THE FINISH SHOWN UNLESS OTHERWISE NOTED.
 - - - = FORM FINISH
 - - - = HEAVY SANDBLAST
 - - - = SMOOTH FLOAT
 - - - = AS CAST

JOB NAME:	N/A
LOCATION:	N/A
ARCHITECT:	N/A
ENGINEER:	N/A
CONTRACTOR:	N/A
PROJ. NO.:	N/A

PRECAST SLAB DETAIL
DURA-STRESS Inc.
 CA #5028
 P.O. BOX 490779 LEESBURG, FL 34749-0779
 PHONE (352) 787-1422 FAX (352) 787-0080
 STRUCTURAL PRECASTERS AND ARCHITECTURAL PRECAST CONCRETE PRODUCTS



A.2. CONSTRUCTION PROCEDURE FOR JOINTS OF SMALL-SCALE SPECIMENS

DETAIL AT POCKET

UHPC (Ductal)

FDOT (Typ.)

Steel Shim Plate

1/2\"/>

CONSTRUCTION STEPS

1. Place specimens side by side leaving a gap of $\frac{1}{4}$ of an inch
2. Place form with channel shape and pre-wet before pouring UHPC
3. Cast UHPC (Ductal) in pocket as shown

FDOT (Typ.)

Form (channel shape)

C.I.P UHPC (Ductal)

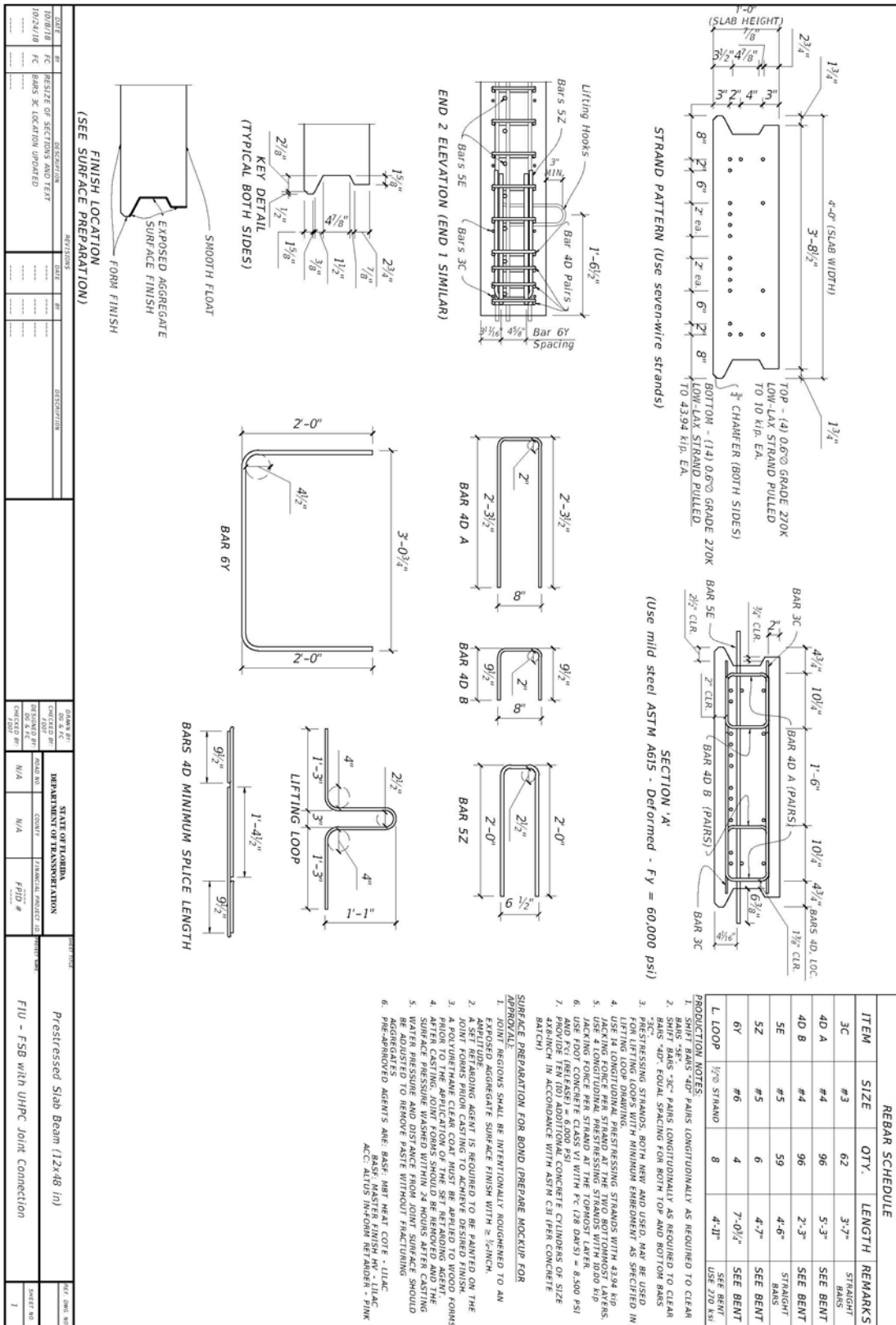
Note: Apply same procedure to all FDOT specimens. Provide five (5) UHPC cylinders of size 3x6-inch per joint.

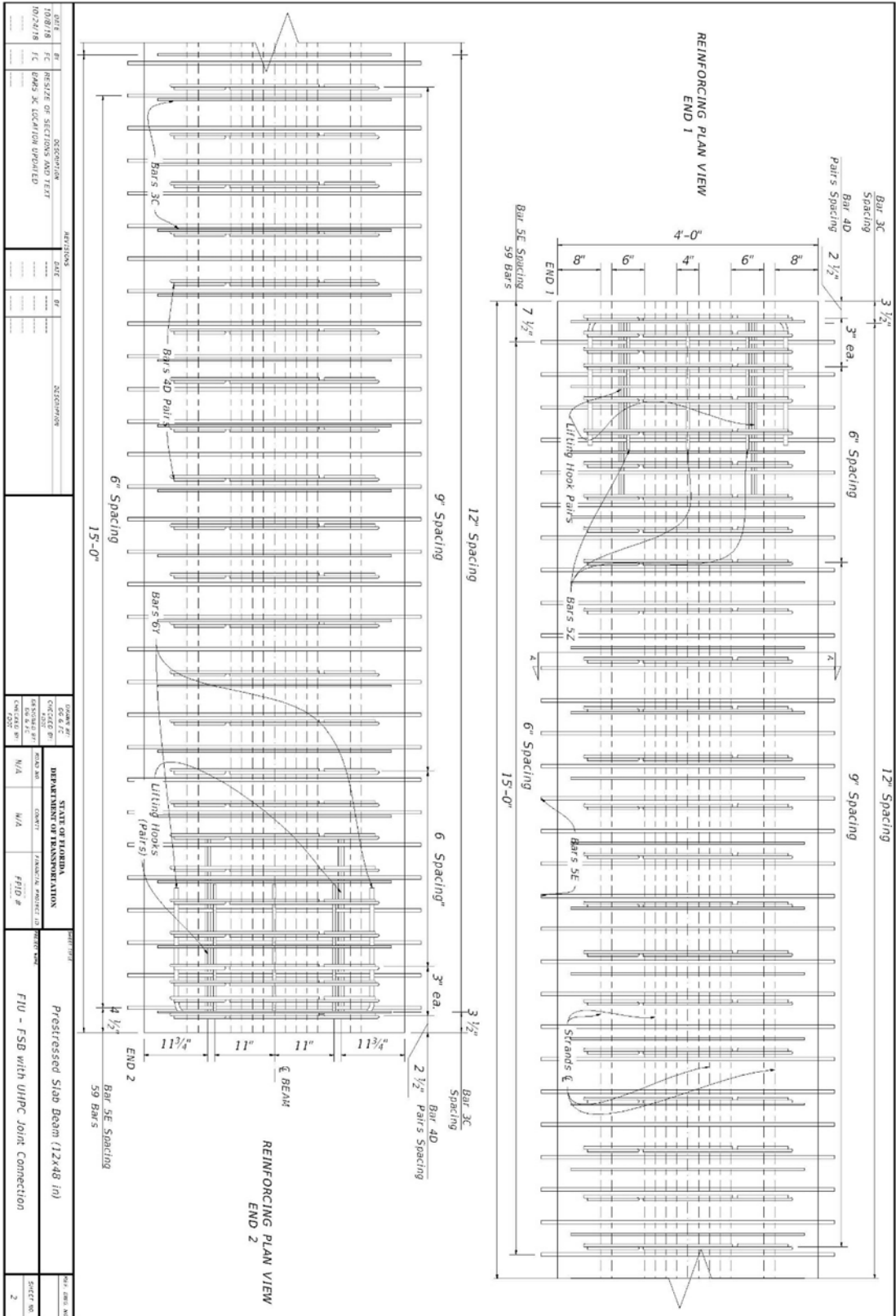
DATE		REVISED		BY		FOR	
REVISION	DESCRIPTION	DATE	BY	FOR	REVISION	DESCRIPTION	DATE
001	NEW SPEC. ADDED						

DESIGNED BY	CHECKED BY	DATE	PROJECT

STATE OF FLORIDA	DEPARTMENT OF TRANSPORTATION	PROJECT TITLE
CONTRACT NO.	CONTRACT	FSB Construction Procedure - FDOT 2 (18 in)
SECTION NO.	CONTRACT	FTU - FSB with UHPC Joint Connection
DATE	CONTRACT	

A.3. CONSTRUCTION PLANS FOR FULL-SCALE BEAMS





DATE	BY	DESCRIPTION	DATE	BY	DESCRIPTION
10/8/18	FC	REVISE OF SECTIONS AND TEXT			
10/24/18	FC	BAR 3C LOCATION UPPLIED			

DATE	BY	DESCRIPTION	DATE	BY	DESCRIPTION

DATE	BY	DESCRIPTION	DATE	BY	DESCRIPTION

DATE	BY	DESCRIPTION	DATE	BY	DESCRIPTION

DATE	BY	DESCRIPTION	DATE	BY	DESCRIPTION

DATE	BY	DESCRIPTION	DATE	BY	DESCRIPTION

DATE	BY	DESCRIPTION	DATE	BY	DESCRIPTION

B. SAMPLE CALCULATIONS FOR 75-FOOT ANALYSES

B.1. SAMPLE CALCULATIONS FOR MODIFIED FSB FOR 75-FOOT SPANS USING FDOT DESIGN PROGRAM

LRFD Prestressed Beam Program

Project = "your project"
 DesignedBy = "your name"
 Date = "today"

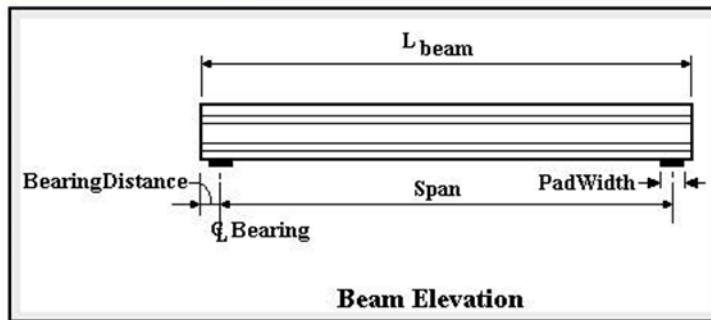
filename = "C:\FDOT Structures\Programs\LRFDBeamV5.1\FSB Data Files\FSBXXx53 75 ft span.dat"

Comment = "FSB15x53 50 ft span"

Legend

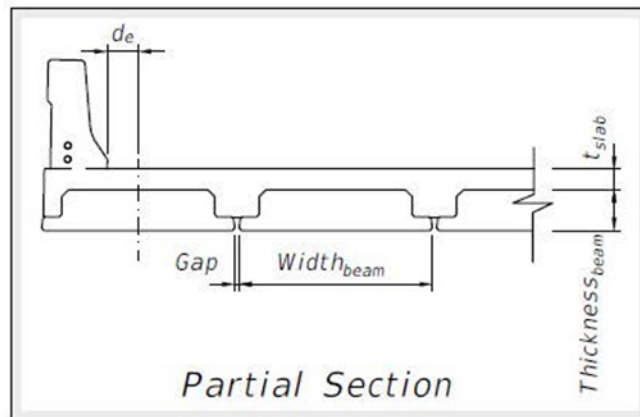
TanHighlight = DataEntry YellowHighlight = CheckValues GreyHighlight = UserComments + Graphs
 BlackText = ProgramEquations MaroonText = CodeReference BlueText = Commentary

Bridge Layout and Dimensions



$L_{beam} = 76.08 \text{ ft}$ $Span = 75 \text{ ft}$ $BearingDistance = 6.5 \text{ in}$ $PadWidth = 8 \text{ in}$

BeamTypeTog = "FSB27x53" *These are typically the FDOT designations found in our standards. The user can also create a coordinate file for a custom shape. In all cases the top of the beam is at the $y=0$ ordinate.*



tendon ultimate tensile strength $f_{pu} = 270 \cdot \text{ksi}$

time in days between jacking and transfer $t_j = 0.75$

tendon modulus of elasticity $E_p = 28500 \cdot \text{ksi}$

ratio of tendon modulus to initial beam concrete modulus $n_{pi} := \frac{E_p}{E_{ci}}$

ratio of tendon modulus to beam concrete modulus $n_p := \frac{E_p}{E_c}$

Mild Steel:

mild steel yield strength $f_y = 60 \cdot \text{ksi}$

mild steel modulus of elasticity $E_s = 29000 \cdot \text{ksi}$

ratio of rebar modulus to initial beam concrete modulus $n_{mi} := \frac{E_s}{E_{ci}}$ $n_{mi} = 6.36$

area per unit width of longitudinal slab reinf. $A_{slab.rebar} = 0.31 \cdot \frac{\text{in}^2}{\text{ft}}$

ratio of rebar modulus to beam concrete modulus $n_m := \frac{E_s}{E_c}$ $n_m = 5.67$

area of mild reinf lumped at centroid of bar locations $A_{s.long} = 0 \cdot \text{in}^2$

d distance from top of slab to centroid of slab reinf. $d_{slab.rebar} = 2.5 \cdot \text{in}$

d distance from top of beam to centroid of mild flexural tension reinf. $d_{long} = 0 \cdot \text{in}$

Size of bar used create used to calculate development length $\text{BarSize} = 5$

Permit Loads

This is the number of wheel loads that comprise the truck, max for DLL is 11 $\text{PermitAxles} = 3$

Indexes used to identify values in the P and d vectors $q := 0 \dots (\text{PermitAxles} - 1)$ $qt := 0 \dots \text{PermitAxles}$

$\text{PermitAxleLoad}^T = (13.33 \ 53.33 \ 53.33) \cdot \text{kip}$

$\text{PermitAxleSpacing}^T = (0 \ 14 \ 14 \ 0) \cdot \text{ft}$

Distribution Factors

$\text{DataMessage} = \text{"This is a FSB27x53 Florida Slab Beam design, AASHTO distribution factors used"}$

calculated values:

$\text{tmp_gmom} = 0.34$

$\text{tmp_gshear} = 0.6$

$\text{tmp_gmom.fatigue} = 0.18$

user value overrides (optional):

$\text{user_gmom} := 0$

$\text{user_gshear} := 0$

$\text{user_gmom.fatigue} := 0$

value check

$\text{gmom} := \text{if}(\text{user_gmom} \neq 0, \text{user_gmom}, \text{tmp_gmom})$

$\text{gmom} = 0.34$

$\text{gshear} := \text{if}(\text{user_gshear} \neq 0, \text{user_gshear}, \text{tmp_gshear})$

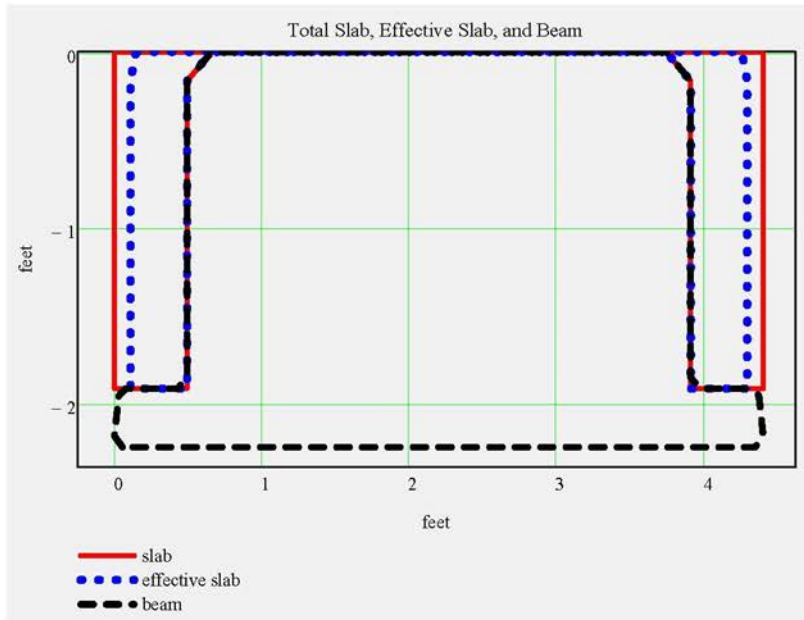
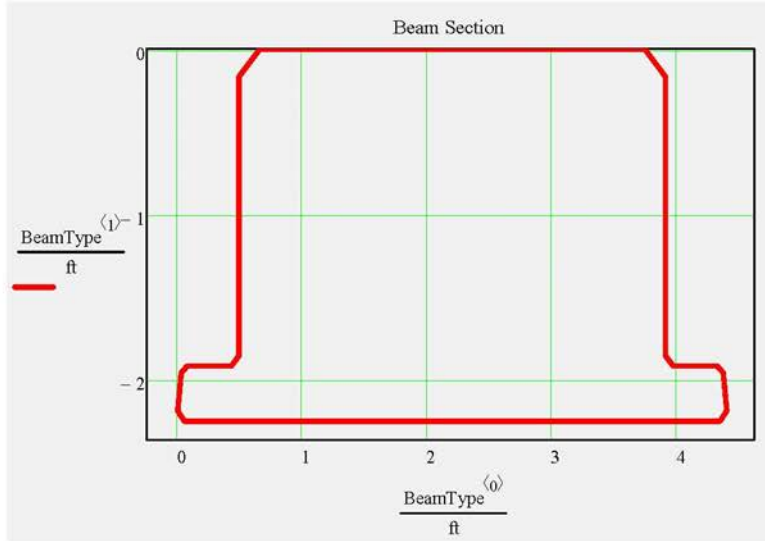
$\text{gshear} = 0.6$

$\text{gmom.fatigue} := \text{if}(\text{user_gmom.fatigue} \neq 0, \text{user_gmom.fatigue}, \text{tmp_gmom.fatigue})$

$\text{gmom.fatigue} = 0.18$



Section Views



Non-Composite Dead Load Input:

$$w_{\text{slab}} = 0.287 \cdot \frac{\text{kip}}{\text{ft}} \quad w_{\text{beam}} = 1.197 \cdot \frac{\text{kip}}{\text{ft}} \quad w_{\text{forms}} = 0 \cdot \frac{\text{kip}}{\text{ft}}$$

$$\text{Add_}w_{\text{noncomp}} := 0.0 \cdot \frac{\text{kip}}{\text{ft}} \quad \textit{additional non composite dead load (positive or negative)}$$

note: not saved to data file, may be saved to Mathcad worksheet.

$$w_{\text{noncomposite}} := w_{\text{slab}} + w_{\text{beam}} + w_{\text{forms}} + \text{Add_}w_{\text{noncomp}} \quad w_{\text{noncomposite}} = 1.484 \cdot \frac{\text{kip}}{\text{ft}}$$

$$w_{\text{bnoncomposite}} := w_{\text{slab}} + w_{\text{forms}} + \text{Add_}w_{\text{noncomp}} \quad w_{\text{bnoncomposite}} = 0.287 \cdot \frac{\text{kip}}{\text{ft}}$$

additional DL due to additional slab thickness over support to accomodate camber
note: maximum at support, zero at mid-span; applicable for flat slab, FSB and double T beams

$$w_{\text{delta.max}} = 0.006 \cdot \frac{\text{kip}}{\text{ft}}$$

Diaphragms/Point Load Input

End Diaphragms or Misc. Point Loads over bearing... included in bearing reaction calculation only

$$\text{EndDiaphragmA} := 0 \cdot \text{kip} \quad \textit{begin bridge}$$

$$\text{EndDiaphragmE} := 0 \cdot \text{kip} \quad \textit{end bridge}$$

Intermediate Diaphragms or Misc. Point Loads... included in shear, moment, and bearing reaction calculations

$$\text{IntDiaphragmB} := 0 \cdot \text{kip} \quad \textit{input load is per beam}$$

$$\text{DistB} := 0 \cdot \text{ft}$$

$$\text{IntDiaphragmC} := 0 \cdot \text{kip}$$

$$\text{DistC} := 0 \cdot \text{ft}$$

Longitudinal Distance B, C, & D - Measured from CL Bearing at begin bridge

$$\text{IntDiaphragmD} := 0 \cdot \text{kip}$$

$$\text{DistD} := 0 \cdot \text{ft}$$

Composite Dead Load Input:

$$w_{\text{future.ws}} = 0.046 \cdot \frac{\text{kip}}{\text{ft}} \quad w_{\text{barrier}} = 0.12 \cdot \frac{\text{kip}}{\text{ft}}$$

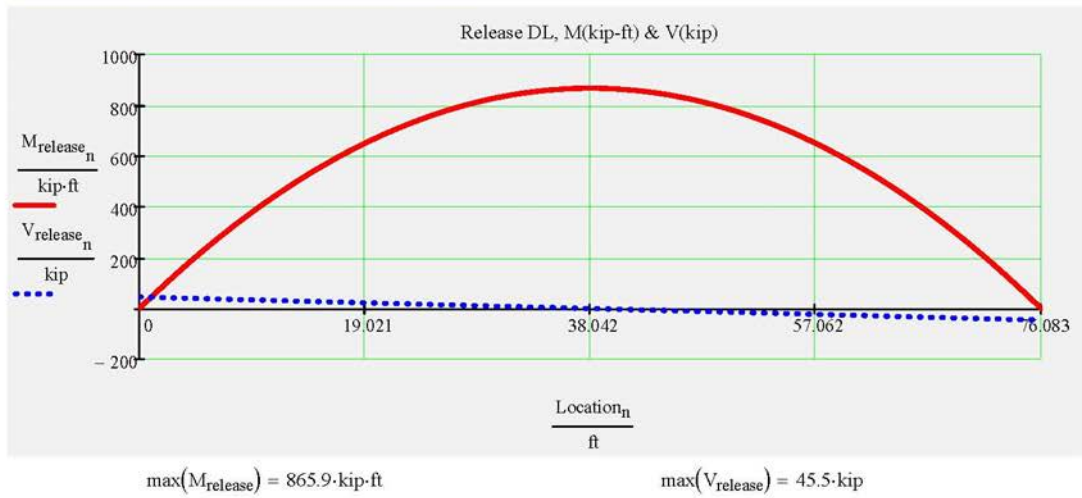
$$\text{Add_}w_{\text{comp}} := 0.0 \cdot \frac{\text{kip}}{\text{ft}} \quad \textit{additional composite dead load (positive or negative)}$$

note: not saved to data file, may be saved to Mathcad worksheet

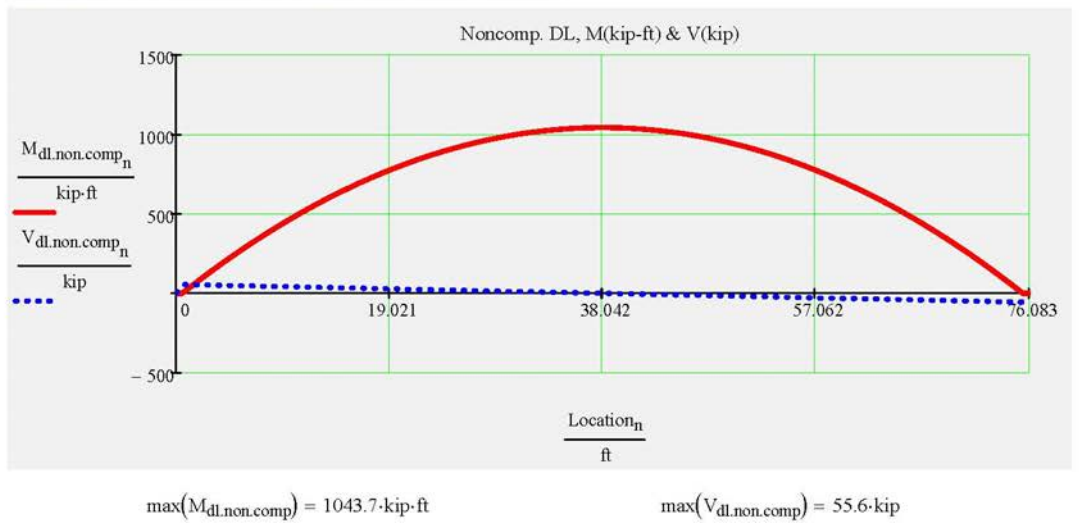
$$w_{\text{composite}} := w_{\text{future.ws}} + w_{\text{barrier}} + \text{Add_}w_{\text{comp}} \quad w_{\text{composite}} = 0.166 \cdot \frac{\text{kip}}{\text{ft}}$$

$$w_{\text{comp.str}} := w_{\text{barrier}} + \text{Add_}w_{\text{comp}} \quad w_{\text{comp.str}} = 0.12 \cdot \frac{\text{kip}}{\text{ft}}$$

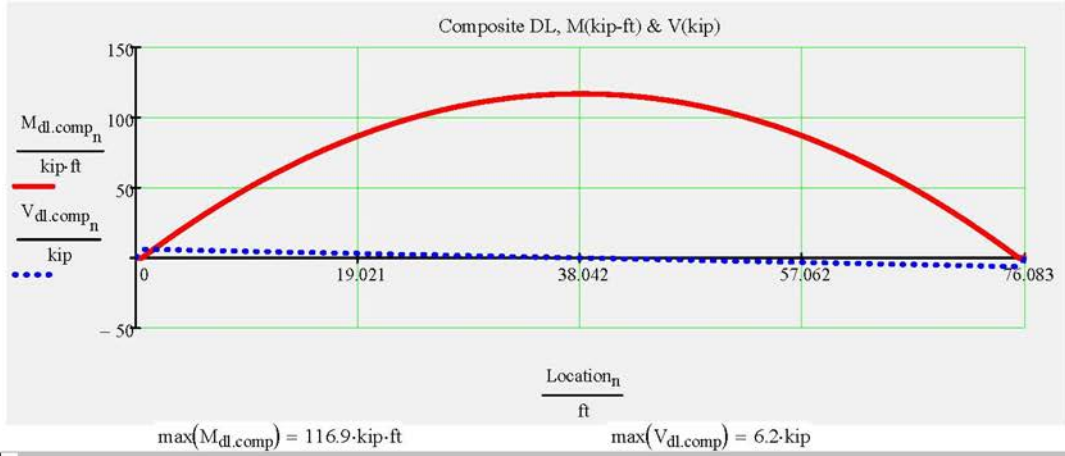
Release Dead Load Moments and Shear



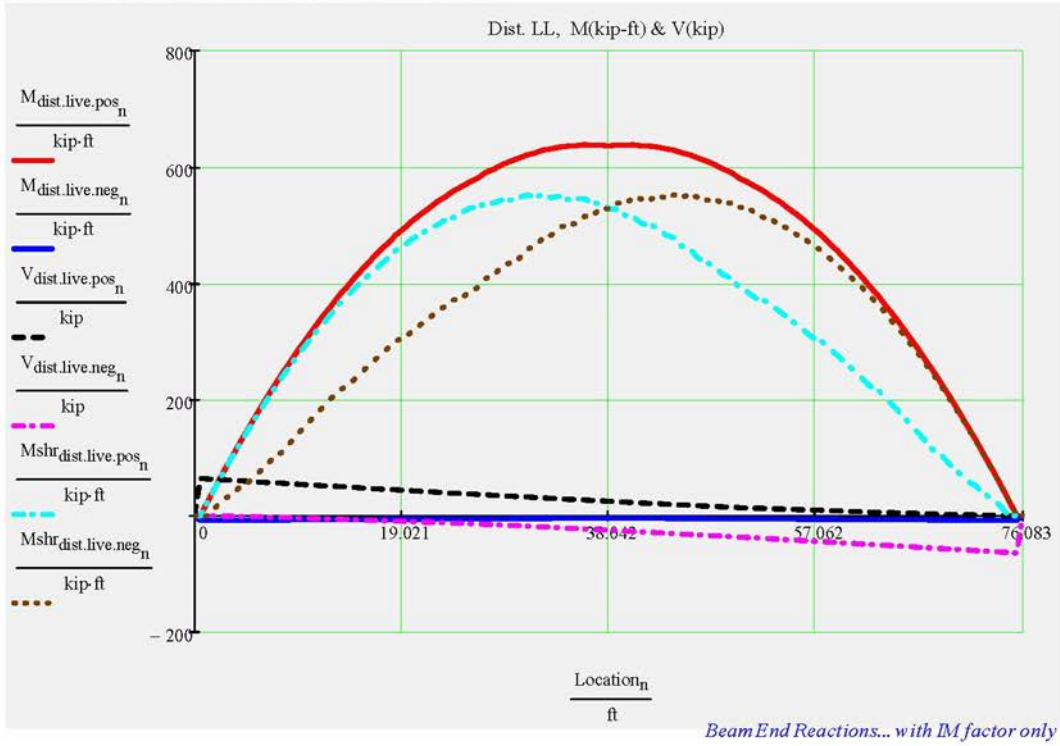
Noncomposite Dead Load Moments and Shear



Composite Dead Load Moments and Shear



Distributed Live Load Moments and Shear



$\max(M_{dist.live.pos}) = 637.6 \cdot kip \cdot ft$

$\min(M_{dist.live.neg}) = -7.9 \cdot kip \cdot ft$

Reaction_{LL} = 65.03 · kip

$\max(V_{dist.live.pos}) = 64.2 \cdot kip$

$\max(Mshr_{dist.live.pos}) = 551.6 \cdot kip \cdot ft$

Reaction_{DL} = 62.77 · kip

Prestress Strand Layout Input

Instructions:

Double click the icon to open the 'Strand Pattern Generator'. Specify the type, location, size, and debonding of strands. When finished, press the 'Continue' button. Then press 'Read Strand Data' button. Then press 'Recalculate Worksheet' button.

Strand Pattern Input Mode:

StrandTemplate :=

- Standard
- Custom

Strand Pattern Generator:

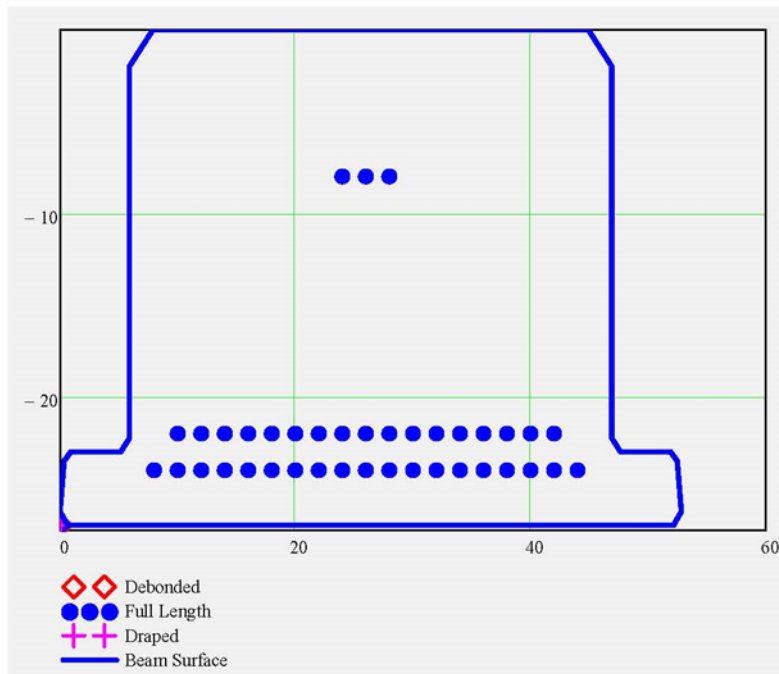


Read Strand Data

Collapsed Region for Custom Strand Sizes..

- ▶ Strand Multiplier
- ▶ Strand Data and Pattern
- ▶ Strand Properties

Tendon Layout



SupportLocation_{release} = 0-ft *distance supports are located from the end of the beam after release; may be used to check lifting points immediately after transfer*

Partially Stressed Tendons ("Strand N")

PartialPS_{force} = 40-kip *partial prestress total force*

PartialPS_{force} := if(BeamTypeTog = "II", 20-kip, PartialPS_{force})

PartialPS_{force} = 40-kip

PartialPS_{location} = 1.4375in *centroid location of partial prestress from the top of the beam*

PartialPS_{location} :=
$$\begin{cases} 2.4375\text{-in} & \text{if BeamTypeTog} = \text{"II"} \\ 3\text{-in} & \text{if substr(BeamTypeTog, 0, 5)} = \text{"FSB12"} \\ 2\text{-in} & \text{if substr(BeamTypeTog, 0, 5)} = \text{"FSB15"} \\ 3\text{-in} & \text{if substr(BeamTypeTog, 0, 5)} = \text{"FSB18"} \\ \text{PartialPS}_{\text{location}} & \text{otherwise} \end{cases}$$

PartialPS_{location} = 1.44-in

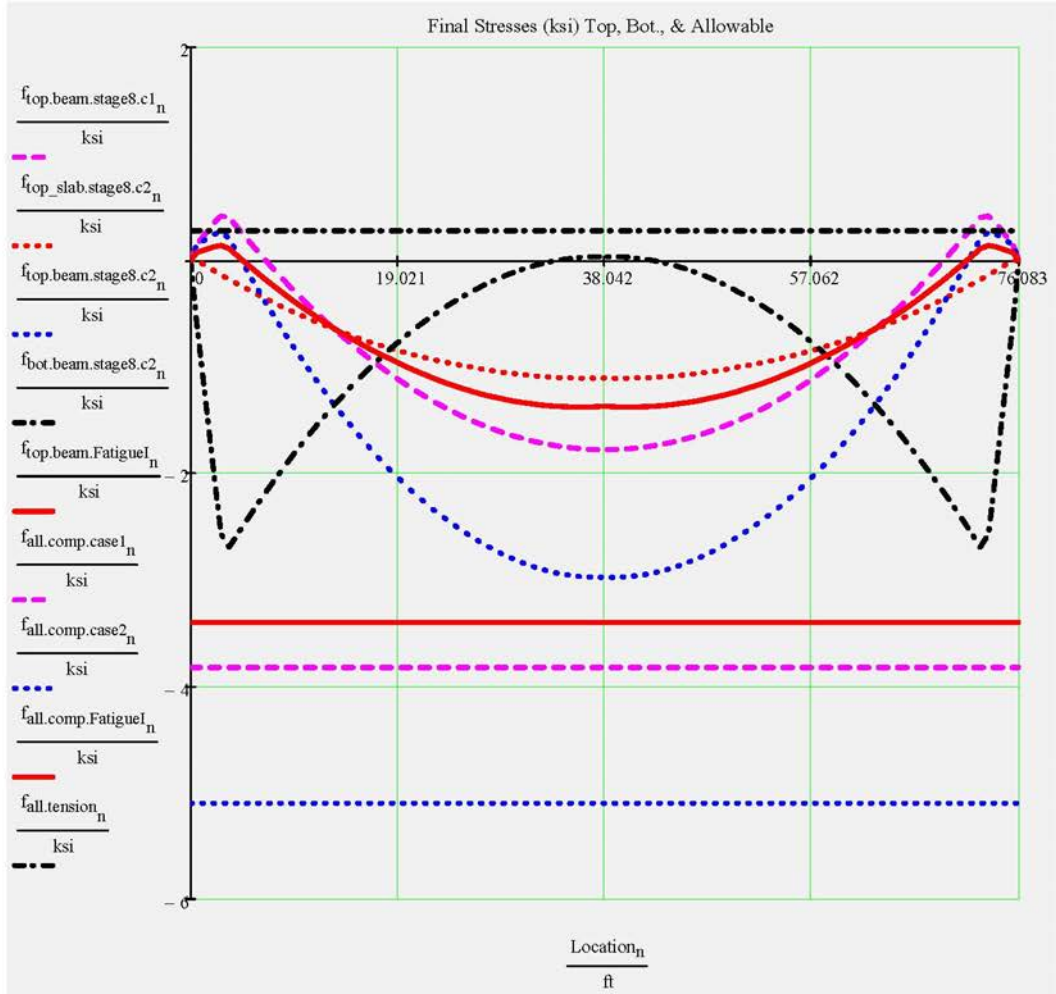
Section Properties & Strand Profile Properties

Release Stresses



Prestress Force

Final Stresses



Release Checks & Final Checks for Capacity Ratio (CR)

Stress Checks

$\min(CR_{f_{tension,rel}}) = 1.09$

Check_f_{tension,rel} = "OK"

[\(Release tension\)](#)

$\min(CR_{f_{comp,rel}}) = 1.2$

Check_f_{comp,rel} = "OK"

[\(Release compression\)](#)

$\min(CR_{f_{tension,stage8}}) = 8.22$

Check_f_{tension,stage8} = "OK"

[\(Service III, PS + DL + LL * 0.8\)](#)

$\min(CR_{f_{comp,stage8.c1}}) = 2.15$

Check_f_{comp,stage8.c1} = "OK"

[\(Service I, PS + DL\)](#)

$\min(CR_{f_{comp,stage8.c2}}) = 1.71$

Check_f_{comp,stage8.c2} = "OK"

[\(Service I, PS + DL + LL\)](#)

$\min(CR_{f_{comp,FatigueI}}) = 2.46$

Check_f_{comp,FatigueI} = "OK"

[\(Fatigue I, \(PS + DL\) * 0.5 + 1.5 Fatigue Truck\)](#)

Strand Pattern Checks

CheckPattern ₀ = "OK"	check 0 - no debonded tendon in outside row	
CheckPattern ₁ = "OK"	check 1 - less than 25% debonded tendons total	<i>*Note: Check 1 may be less than 30% provided that debonding does not occur within the horizontal limits of the web (See SDG 4.3.1)</i>
CheckPattern ₂ = "OK"	check 2 - less than 40% debonded tendons in any row	
CheckPattern ₃ = "OK"	check 3 - less than 40% of debonded tendons terminated at same section	(LRFD 5.11.4.3)
CheckPattern ₄ = "OK"	check 4 - more than half beam depth debond length	(SDG 4.3.1)

Section and Strand Properties Summary

Section and Strand Properties Summary

$A_{beam} = 1148.75 \cdot in^2$	<u>Concrete area of beam</u>	$I_{beam} = 72402.3219 \cdot in^4$	<u>Gross Moment of Inertia of Beam about CG</u>
$y_{comp} = -13.58 \cdot in$	<u>Dist. from top of beam to CG of gross composite section</u>	$I_{comp} = 83383.9395 \cdot in^4$	<u>Gross Moment of Inertia Composite Section about CG</u>
$A_{deck} = 214.98 \cdot in^2$	<u>Concrete area of deck slab</u>	$A_{ps} = 8.5 \cdot in^2$	<u>total area of strands</u>
$d_{b,ps} = 0.6 \cdot in$	<u>diameter of Prestressing strand</u>	$\min(\text{PrestressType}) = 0$	<u>0 - low lax 1 - stress relieved</u>
$f_{py} = 243 \cdot ksi$	<u>tendon yield strength</u>	$f_{pj} = 203 \cdot ksi$	<u>prestress jacking stress</u>

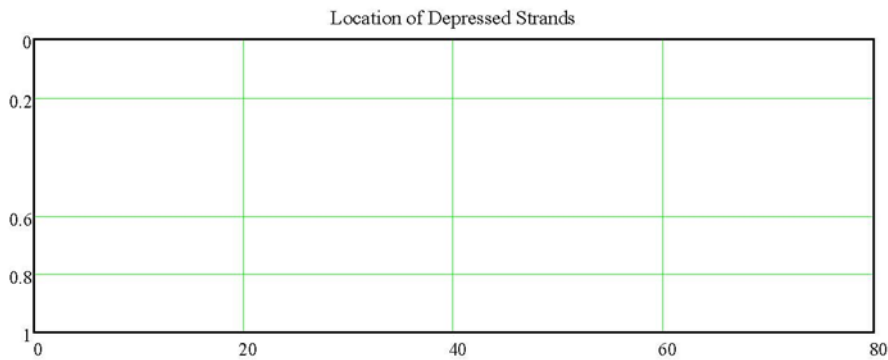
$L_{shielding}^T = (0 \ 0 \ 0 \ 0) \cdot ft$

$A_{ps,row}^T = (4.1 \ 3.7 \ 0.7 \ 0.2) \cdot in^2$

	0	1	2	3	4	5	6	7	8	9		
$d_{ps,row} =$	0	-24	-24	-24	-24	-24	-24	-24	-24	-24	-24	·in
	1	-22	-22	-22	-22	-22	-22	-22	-22	-22	-22	
	2	-8	-8	-8	-8	-8	-8	-8	-8	-8	-8	
	3	-1.44	-1.44	-1.44	-1.44	-1.44	-1.44	-1.44	-1.44	-1.44	-1.44	

TotalNumberOfTendons = 39
 NumberOfDebondedTendons = 0
 NumberOfDrapedTendons = 0

StrandSize = "0.6 in low lax"
 StrandArea = $0.22 \cdot in^2$
 JackingForce_{per.strand} = 43.94·kip



Section and Strand Properties Summary

Prestress Losses Summary

$f_{pj} = 202.5 \cdot \text{ksi}$

Check $f_{pt} = \text{"OK"}$

$\Delta f_{pES} = 0 \cdot \text{ksi}$

Note: Elastic shortening losses are zero in concrete stress calculations when using transformed section properties per LRFD 5.9.5.2.3

$\Delta f_{pT} = -21 \cdot \text{ksi}$

$\frac{\Delta f_{pT}}{f_{pj}} = -10.21 \cdot \%$

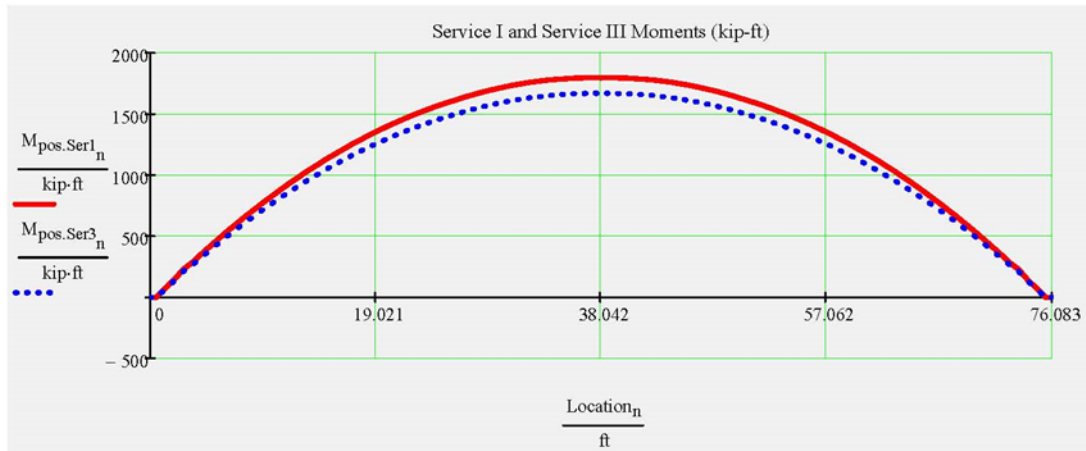
$f_{pe} = 182 \cdot \text{ksi}$

$\frac{f_{pe}}{f_{pj}} = 89.79 \cdot \%$

$0.8 \cdot f_{py} = 194 \cdot \text{ksi}$

Check $f_{pe} = \text{"OK"}$

Service Limit State Moments



$\max(M_{pos.Ser1}) = 1797.4 \cdot \text{kip} \cdot \text{ft}$

$\max(M_{pos.Ser3}) = 1669.9 \cdot \text{kip} \cdot \text{ft}$

Summary of Values at Midspan

$$\text{Stresses} = \begin{pmatrix} \text{"Stage"} & \text{"Top of Beam (ksi)} & \text{"Bott of Beam (ksi)"} \\ 1 & -1.07 & -1.83 \\ 2 & -1.16 & -1.46 \\ 4 & -1.1 & -1.51 \\ 6 & -1.56 & -1.1 \\ 8 & -2.98 & 0.03 \end{pmatrix}$$

$$\text{PrestressForce} = \begin{pmatrix} \text{"Condition"} & \text{"Axial (kip)"} & \text{"Moment (kip*ft)"} \\ \text{"Release"} & -1753.8 & -1093.9 \\ \text{"Final (about composite centroid)"} & -1574.8 & -942.4 \end{pmatrix}$$

$$\text{Properties} = \begin{pmatrix} \text{"Section"} & \text{"Area (in^2)} & \text{"Inertia (in^4)} & \text{"distance to centroid from top of bm (in)"} \\ \text{"Net Beam"} & 1140.09 & 71695.98 & -13.95 \\ \text{"Transformed Beam (initial)"} & 1194.25 & 75998.5 & -14.29 \\ \text{"Transformed Beam"} & 1188.37 & 75544.11 & -14.25 \\ \text{"Composite"} & 1409.72 & 87594.44 & -13.75 \end{pmatrix}$$

$$\text{ServiceMoments} = \begin{pmatrix} \text{"Type"} & \text{"Value (kip*ft)"} \\ \text{"Release"} & 865.9 \\ \text{"Non-composite (includes bm wt.)"} & 1043.7 \\ \text{"Composite"} & 116.9 \\ \text{"Distributed Live Load"} & 635.6 \end{pmatrix}$$

Stage 1 ---> At release with span length equal to length of the beam. Prestress losses are elastic shortening and overnight relax

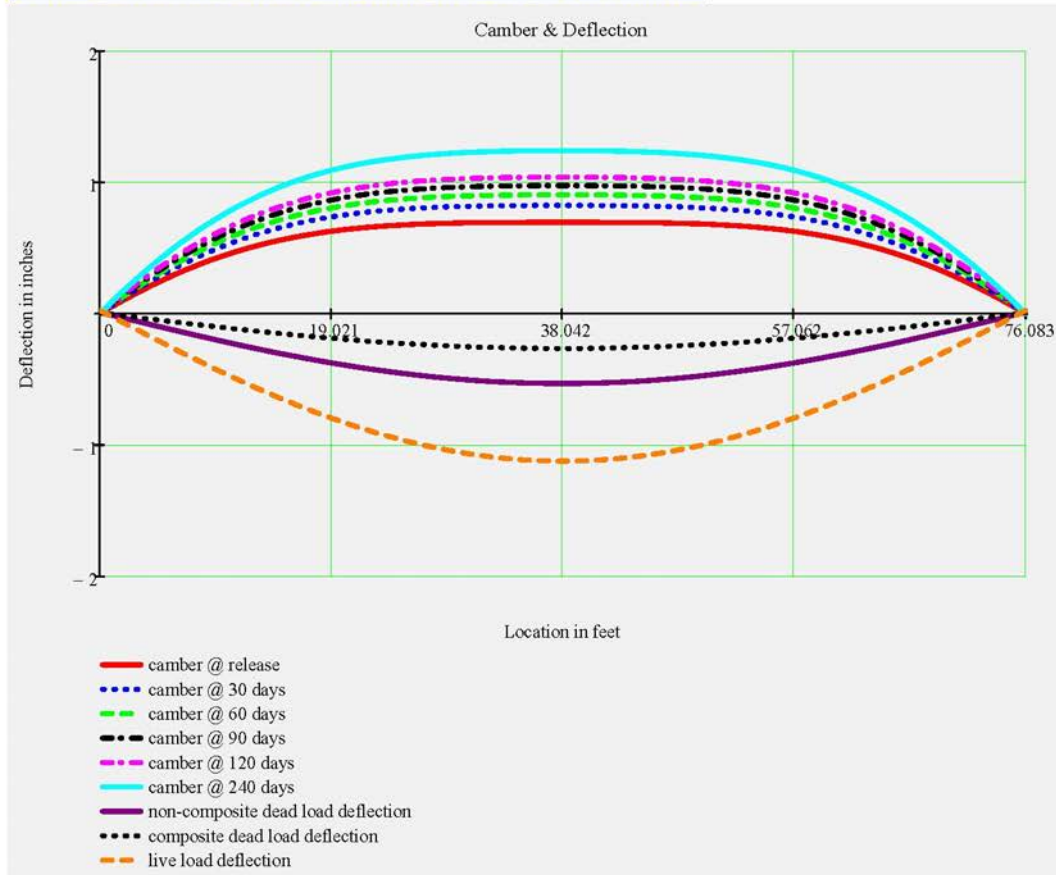
Stage 2 ---> Same as release with the addition of the remaining prestress losses applied to the transformed beam

Stage 4 ---> Same as stage 2 with supports changed from the end of the beam to the bearing locations

Stage 6 ---> Stage 4 with the addition of non-composite dead load excluding beam weight which has been included since Stage 1

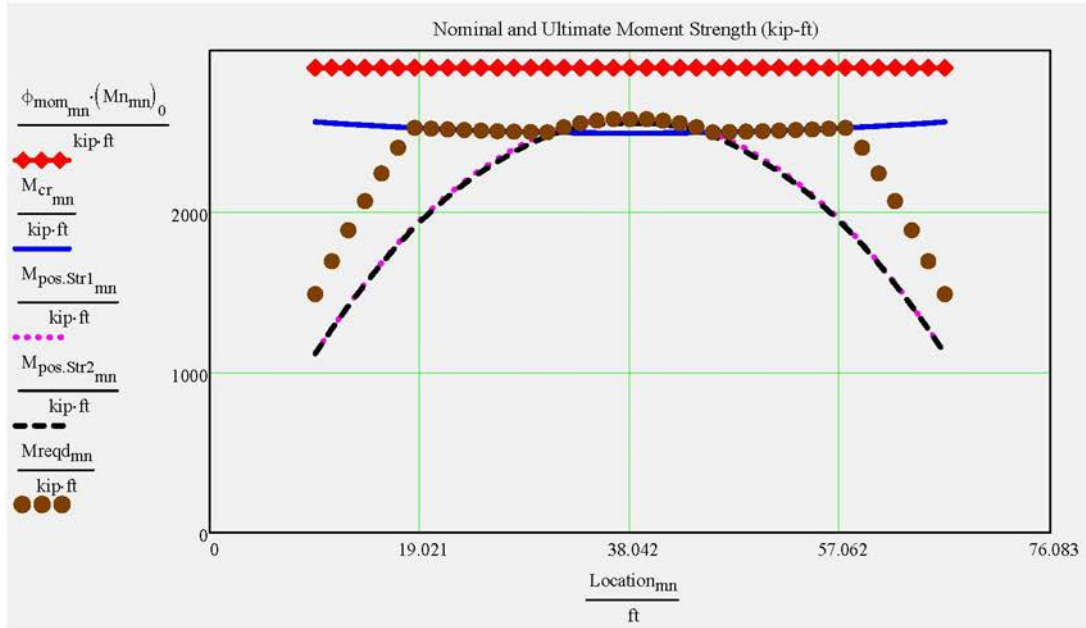
Stage 8 ---> Stage 6 with the addition of composite dead load and live loads applied to the composite section

Camber, Shrinkage, and Dead Load Deflection Components



"Stage"	"Change in L @ Top (in)"	"Change in L @ Bot. (in)"	"Slope at End (deg)"	"midspan defl (in)"
"Release"	-0.0888	-0.4584	0.2715	0.6965
"30 Days"	-0.281	-0.8803	0.4806	0.8253
"60 Days"	-0.3519	-1.036	0.5614	0.9056
"90 Days"	-0.3888	-1.117	0.6035	0.9764
"120 Days"	-0.4114	-1.1666	0.6293	1.0401
"240 Days"	-0.4526	-1.2569	0.6762	1.2425
"non-comp DL"	-0.0538	0.0482	-0.1083	-0.5312
"comp DL"	-0.0258	0.0249	-0.0539	-0.2643
"LL"	-0.1108	0.1067	-0.231	-1.1227

Strength Limit State Moments



$$CR_{Str.mom_n} := 10 \quad CR_{Str.mom_{mn}} := \frac{\phi_{mom_{mn}} \cdot (Mn_{mn})_0}{M_{reqd_{mn}}} \quad (LRFD 5.7.3.3.2) \quad \min(CR_{Str.mom}) = 1.12$$

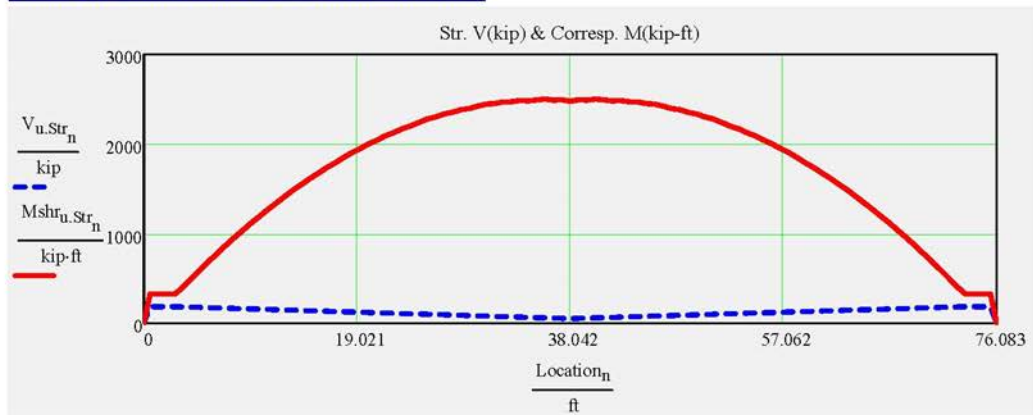
max(Mreqd) = 2571.5-kip-ft CheckMomentCapacity := if(min(CR_{Str.mom}) > 0.99, "OK", "No Good!")

CheckMomentCapacity = "OK"

FSB only - Design Check of Transverse reinforcing Bars E

Shear Analysis

Strength Shear and Associated Moments



max($V_{u.Str}$) = 181.5-kip max($M_{shr_u.Str}$) = 2499.0-kip-ft

Design Shear, Longitudinal, Interface and Anchorage Reinforcement

Stirrup sizes and spacings assigned in input file

Location	spacing	Number of Spaces	area per stirrup
A1 stirrup	$\text{tmp_s} = \begin{pmatrix} 12 \\ 18 \\ 18 \\ 18 \\ 18 \\ 18 \\ 18 \\ 18 \end{pmatrix} \cdot \text{in}$	$\text{tmp_NumberSpaces} = \begin{pmatrix} 4 \\ 1 \\ 1 \\ 1 \\ 1 \\ 1 \\ 1 \\ 0 \end{pmatrix}$	$\text{tmp_A_stirrup} = \begin{pmatrix} 0.8 \\ 0.8 \\ 0.8 \\ 0.8 \\ 0.8 \\ 0.8 \\ 0.8 \\ 0.8 \end{pmatrix} \cdot \text{in}^2$
A2 stirrup			
A3 stirrup			
S1 stirrup			
S2 stirrup			
S3 stirrup			
S4 stirrup			

Locally assigned stirrup sizes and spacings

The interface factor accounts for situations where not all of the shear reinforcing is embedded in the poured in place slab.

To change the values from the input file enter the new values into the vectors below. Input only those that you wish to change. Values less than 0 are ignored.

	user_s_nspacings :=	user_NumberSpaces_nspacings :=	user_A_stirrup_nspacings :=	interface_factor_nspacings :=
A1 stirrup	-1.in	-1	-1.in ²	0.25
A2 stirrup	-1.in	-1	-1.in ²	0.5
A3 stirrup	-1.in	-1	-1.in ²	1
S1 stirrup	-1.in	-1	-1.in ²	1
S2 stirrup	-1.in	-1	-1.in ²	1
S3 stirrup	-1.in	-1	-1.in ²	1
S4 stirrup	-1.in	-1	-1.in ²	1

Recalculate Worksheet

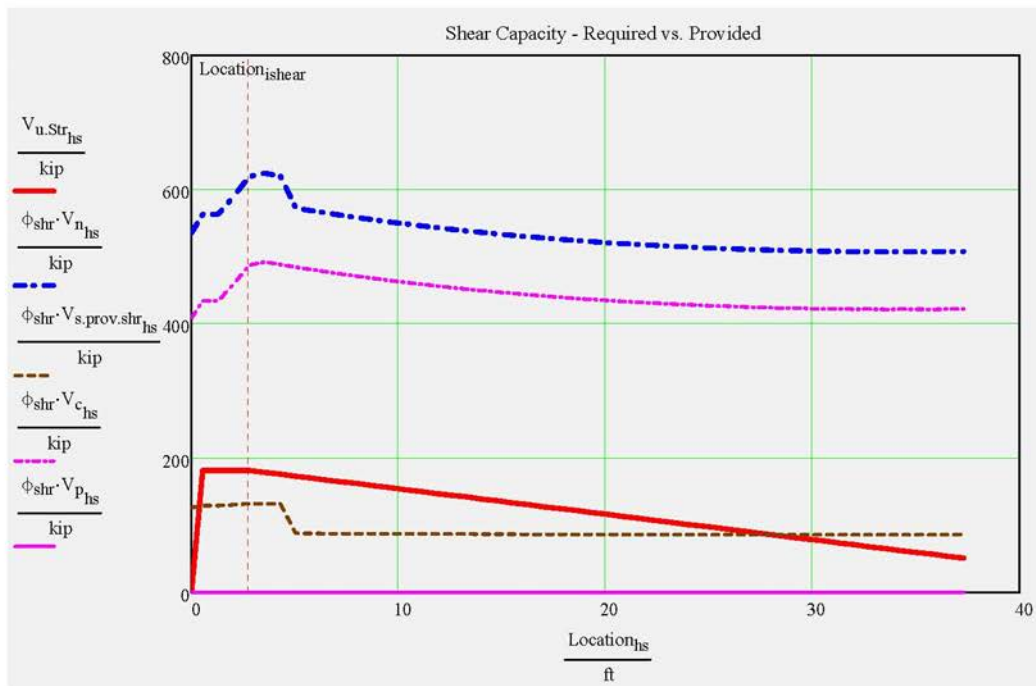
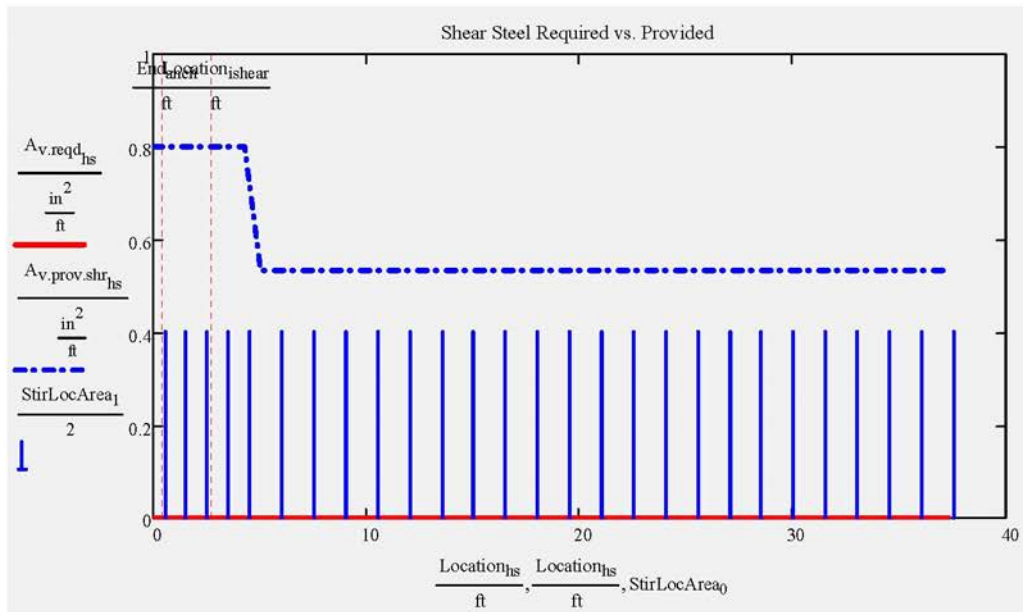
Spacing Computation

Stirrup sizes and spacings used in analysis

The number of spaces for the S4 stirrup is calculated by the program to complete the half beam length.

A1 stirrup	$s = \begin{pmatrix} 12 \\ 18 \\ 18 \\ 18 \\ 18 \\ 18 \\ 18 \\ 18 \end{pmatrix} \cdot \text{in}$	$\text{NumberSpaces} = \begin{pmatrix} 4 \\ 1 \\ 1 \\ 1 \\ 1 \\ 1 \\ 1 \\ 17.33 \end{pmatrix}$	$A_{\text{stirrup}} = \begin{pmatrix} 0.8 \\ 0.8 \\ 0.8 \\ 0.8 \\ 0.8 \\ 0.8 \\ 0.8 \\ 0.8 \end{pmatrix} \cdot \text{in}^2$	$\text{EndCover} = 6.5 \cdot \text{in}$
A2 stirrup				
A3 stirrup				
S1 stirrup				
S2 stirrup				
S3 stirrup				
S4 stirrup				

► Shear Steel Required vs. Provided Computation



► Computation for Checks

CheckShearCapacity = "OK"

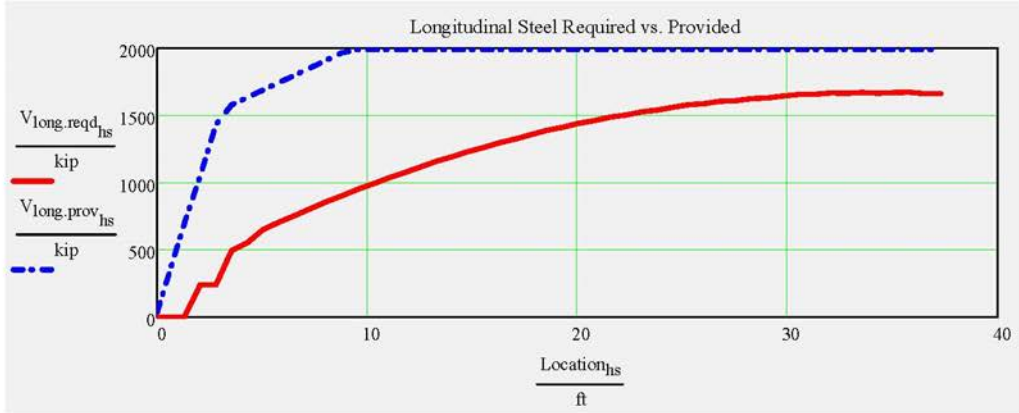
CheckMaxShearStress = "OK"

CheckStirArea = "OK"

CheckMinStirArea = "OK"

CheckMaxStirSpacing = "OK"

► Longitudinal Reinforcement

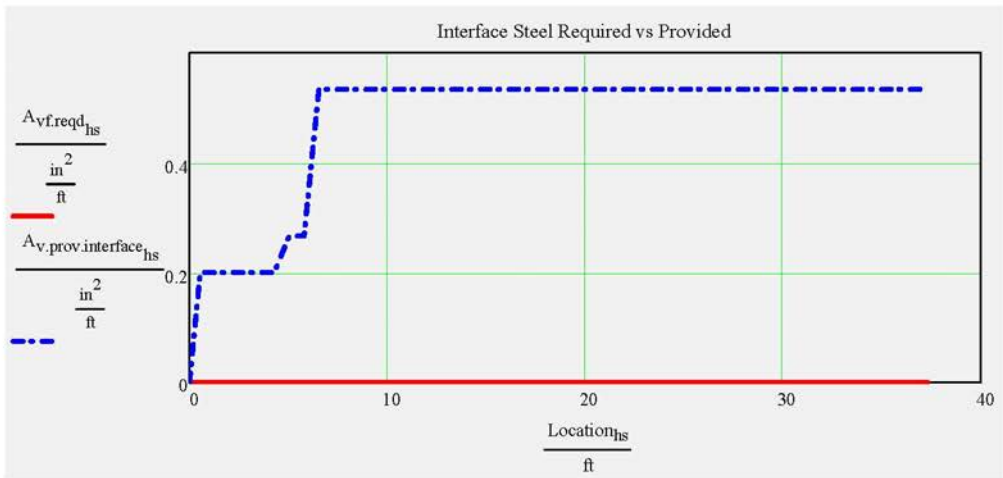


$$CR_{LongSteel}_{hs} := \text{if} \left(V_{long.reqd}_{hs} < .01\text{kip}, 100, \frac{V_{long.prov}_{hs}}{V_{long.reqd}_{hs}} \right) \quad \min(CR_{LongSteel}) = 1.19$$

CheckLongSteel := if (min(CR_{LongSteel}) > 1, "OK", "No Good, add steel!")

CheckLongSteel = "OK"

► Interface Shear Reinforcement



Interface Steel

*Typically shear steel is extended up into the deck slab.
These calculations are based on shear steel functioning as interface reinforcing.
The interface_factor can be used to adjust this assumption.*

$$\max(A_{vf,min}) = 0 \cdot \frac{\text{in}^2}{\text{ft}}$$

$$\max(A_{vf,des}) = 0 \cdot \frac{\text{in}^2}{\text{ft}}$$

If $\max(A_{vf,min})$ or $\max(A_{vf,des})$ is greater than 0 in²/ft, interface steel is required.

CheckInterfaceSpacing = "OK"

$$\text{CheckInterfaceSteel} := \text{if} \left(\frac{\text{TotalInterfaceSteelProvided}}{\text{TotalInterfaceSteelRequired} + 0.001 \cdot \text{in}^2} \geq 1, \text{"OK"}, \text{"No Good"} \right)$$

CheckInterfaceSteel := if (substr(BeamTypeTog, 0, 3) = "FLT", "N.A.", CheckInterfaceSteel)

CheckInterfaceSteel = "OK"

Anchorage Reinforcement and Maximum Prestressing Force

Was FDOT Design Standard splitting reinforcing used? (bars Y, K, & Z)

StandardSplittingReinforcing :=

*if yes-> checks max allowable standard prestress force
if no-> checks stirrup area given input prestress force*

Splitting (Bursting) Resistance

CheckSplittingSteel = "N.A."

CheckMaxPrestressingForce = "OK"

Summary of Design Checks

check₀ := AcceptAASHTO = "OK"

check₂ := AcceptOntario = "N.A."

check₄ := Check_{f_{pe}} = "OK"

check₆ := Check_{f_{comp,rel}} = "OK"

check₈ := Check_{f_{comp,stage8,c1}} = "OK"

check₁₀ := Check_{f_{comp,FatigueI}} = "OK"

check₁₂ := CheckMaxCapacity = "OK"

check₁₄ := CheckShearCapacity = "OK"

check₁₆ := CheckMaxStirSpacing = "OK"

check₁₈ := CheckInterfaceSpacing = "OK"

check₂₀ := CheckMaxPrestressingForce = "OK"

check₂₂ := CheckPattern₁ = "OK"

check₂₄ := CheckPattern₃ = "OK"

check₂₆ := CheckInterfaceSteel = "OK"

check₁ := AcceptSDG = "N.A."

check₃ := Check_{f_{pt}} = "OK"

check₅ := Check_{f_{tension,rel}} = "OK"

check₇ := Check_{f_{tension,stage8}} = "OK"

check₉ := Check_{f_{comp,stage8,c2}} = "OK"

check₁₁ := CheckMomentCapacity = "OK"

check₁₃ := CheckStirArea = "OK"

check₁₅ := CheckMinStirArea = "OK"

check₁₇ := CheckLongSteel = "OK"

check₁₉ := CheckSplittingSteel = "N.A."

check₂₁ := CheckPattern₀ = "OK"

check₂₃ := CheckPattern₂ = "OK"

check₂₅ := CheckPattern₄ = "OK"

check₂₇ := CheckStrandFit = "OK"

check₂₈ := Check_SDG1.2.Display₂ = "OK"

[Link to Note- Checks, 0, 1 & 2](#)

▶					
check ^T =	0	1	2	3	4
0	"OK"	"N.A."	"N.A."	"OK"	...
<i>click table to reveal scroll bar...</i>					TotalCheck = "OK"

LRFR Load Rating Analysis

FDOT Maintenance Office Bridge Load Rating Manual

▶ Load Rating Computations										
Moment (Strength) or Stress (Service)					Shear (Strength)					
LRFR _{loadrating} =	"Limit State"	"DF"	"Rating"	"Tons"	"Dim(ft)"	"DF"	"Rating"	"Tons"	"Dim(ft)"	
	"Strength I(Inv)"	0.34	1.29	"N/A"	36.00	0.60	4.88	"N/A"	4.50	HL-93
	"Strength I(Op)"	0.34	1.67	"N/A"	36.00	0.60	6.33	"N/A"	4.50	HL-93
	"Service III(Inv)"	0.34	1.26	"N/A"	36.75	"N/A"	"N/A"	"N/A"	"N/A"	HL-93
	"Service III(Op)"	0.34	1.71	"N/A"	36.75	"N/A"	"N/A"	"N/A"	"N/A"	HL-93
	"Strength II"	0.34	1.32	78.98	36.00	0.60	4.83	289.88	4.50	*Permit

*note: default permit load is FL120 per input worksheet

Longitudinal Steel Check:

CR_{LongSteel.HL93} = 1.23 CR_{LongSteel.Permit} = 1.19 CheckLongSteel_{loadrating} = "OK"

▶ Write Data Out										
------------------	--	--	--	--	--	--	--	--	--	--

B.2. SAMPLE CALCULATIONS FOR TxDOT TYPE 4B28 FOR 75-FOOT SPANS USING PGSUPER

TxDOT Summary Report (Long Form)

*For
Span 1 Girder A
April 7, 2017 9:34:37 pm*

PGSuper¹ (x64)

Copyright © 2017, WSDOT, All Rights Reserved

Version 3.0.0 - Built on Jan 18 2017



**Washington State
Department of Transportation**



Project Properties

Bridge Name	
Bridge ID	
Company	TxDOT
Engineer	Your Name
Job Number	
Comments	
File	C:\Users\lchit001\Desktop\PGSuper1.pgs

Bridge:

Job:

4/7/2017

Configuration

Configuration Publisher: TxDOT

Configuration Package: ftp://ftp.dot.state.tx.us/pub/txdot-info/brg/pgsuper/version_2.9.2/txdot.pgz

Configuration Date Stamp: May 17, 2016 11:48:51 am

Library	Entry	Source
Girders	Box 4B28	Master Library
Girders	Box 5B28	Master Library
Traffic Barriers	T551	Master Library
Project Criteria	TxDOT 2015	Master Library
Load Rating Criteria	Test	Project Library
Haul Trucks	Old Haul Truck -0	Project Library

Notes

Symbol	Definition
L_r	Span Length of Girder at Release
L_l	Span Length of Girder during Lifting
L_{st}	Span Length of Girder during Storage
L_h	Span Length of Girder during Hauling
L_e	Span Length of Girder after Erection
L_s	Length of Span
Debond	Point where bond begins for a debonded strand
PSXFR	Point of prestress transfer
Diaphragm	Location of a precast or cast in place diaphragm
Bar Cutoff	End of a reinforcing bar in the girder
Deck Bar Cutoff	End of a reinforcing bar in the deck
CS	Critical Section for Shear
SZB	Stirrup Zone Boundary
H	H from end of girder or face of support
1.5H	1.5H from end of girder or face of support
HP	Harp Point
Pick Point	Support point where girder is lifted from form
Bunk Point	Point where girder is supported during transportation

Specification Check Summary

The Specification Check was Successful

Bridge:

Job:

4/7/2017

Girder Summary

TxDOT Girder Schedule

Span	1
Girder	A
Girder Type	Box 4B28
Prestressing Strands	Total
NO. ($N_h + N_s$)	18
Size	0.600 in Dia.
Strength	Grade 270 Low Relaxation
Eccentricity @ CL	11.117 in
Eccentricity @ End	11.117 in
Prestressing Strands Concrete	
Release Strength f'_{ci}	6.000 KSI
Minimum 28 day compressive strength f'_c	8.500 KSI
Optional Design	
Design Load Compressive Stress (Top CL)	3.191 KSI
Design Load Tensile Stress (Bottom CL)	-2.747 KSI
Required minimum ultimate moment capacity	1886.80 kip-ft
Live Load Distribution Factor for Moment (Strength and Service Limit States)	0.30767
Live Load Distribution Factor for Shear (Strength and Service Limit States)	0.54134
Live Load Distribution Factor for Moment (Fatigue Limit States)	0.19540

NOTE: Stresses show in the above table reflect the following sign convention:
Compressive Stress is positive. Tensile Stress is negative

Girder Line Geometry

Girder Type	Box 4B28
Span Length, CL Bearing to CL Bearing	75.000 ft
Girder Length	76.083 ft
Number of Girders	7
Joint Spacing Datum Start of Span	Measured normal to alignment at abutment line
Right Joint Spacing Start of Span	0.625 in
Joint Spacing Datum End of Span	Measured normal to alignment at abutment line
Right Joint Spacing End of Span	0.625 in
Slab Thickness for Design	0.000 in
Slab Thickness for Construction	0.000 in
Slab Offset at Start ("A" Dimension)	0.000 in
Slab Offset at End ("A" Dimension)	0.000 in
Overlay	0.023 KSF
Left Traffic Barrier	T551
Right Traffic Barrier	T551
Traffic Barrier Weight (per girder)	0.127 kip/ft
Connection Geometry at Abutment 1	Bearing Offset: 0.792 ft Measured From and Normal to Abutment Line End Distance: 0.250 ft Measured From and Normal to Abutment Line
Connection Geometry at Abutment 2	Bearing Offset: 0.792 ft Measured From and Normal to Abutment Line End Distance: 0.250 ft Measured From Abutment Line and Along Girder Centerline

Bridge:

Job:

4/7/2017

Loading Details

Uniform Loads Applied Along the Entire Girder

Load Type	w (kip/ft)
Girder	0.707

Distribution of Uniform Barrier, Sidewalk, and Pedestrian Loads to Girder

Load Type	Total Weight (kip/ft)	Fraction to Girder	Girder Load (kip/ft)
Left Ext. Barrier	0.382	0.333	0.127
Right Ext. Barrier	0.382	0.000	0.000

Overlay

Overlay load is uniform along entire girder length.

Load Type	W _{trib} (ft)	w (kip/ft)
Overlay Weight	2.422	0.057

Overlay load is distributed using tributary width.

Shear Key Load

Shear Key Load is uniform along entire girder length

Load Type	w (kip/ft)
Load Within Girder Envelope	0.090
Load Within Joint	0.007
Total Shear Key Weight	0.097

Span 1

Pier Diaphragm Loads

Pier	Location	P (kip)	M (kip-ft)
1	Left Bearing	0.00	0.00
	Right Bearing	0.00	0.00
2	Left Bearing	0.00	0.00
	Right Bearing	0.00	0.00

Live Load Details

Live Loads used for Design

The following live loads were applied to the design (Service and Strength I) limit states:

- AASHTO MBE 6A.4.4.2.1a: Routine Commercial Traffic
- AASHTO LRFD 3.6.1.4: Fatigue Vehicular Live Load
- AASHTO LRFD 3.6.1.2: HL-93 Design Vehicular Live Load
- AASHTO MBE 6A.4.4.2.1b: Specialized Hauling Vehicles (NRL)
- AASHTO MBE 6A.4.4.2.1b: Specialized Hauling Vehicles (SU)

Live Loads Used for Fatigue Limit States

The following live loads were applied to the Fatigue I limit state:

- AASHTO MBE 6A.4.4.2.1a: Routine Commercial Traffic
- AASHTO LRFD 3.6.1.4: Fatigue Vehicular Live Load
- AASHTO LRFD 3.6.1.2: HL-93 Design Vehicular Live Load
- AASHTO MBE 6A.4.4.2.1b: Specialized Hauling Vehicles (NRL)
- AASHTO MBE 6A.4.4.2.1b: Specialized Hauling Vehicles (SU)

Live Loads Used for Design Permit Limit State

The following live loads were applied to the design permit (Strength II) limit state:

- AASHTO MBE 6A.4.4.2.1a: Routine Commercial Traffic
- AASHTO LRFD 3.6.1.4: Fatigue Vehicular Live Load
- AASHTO LRFD 3.6.1.2: HL-93 Design Vehicular Live Load
- AASHTO MBE 6A.4.4.2.1b: Specialized Hauling Vehicles (NRL)

Bridge:

Job:

4/7/2017

AASHTO MBE 6A.4.4.2.1b: Specialized Hauling Vehicles (SU)

User Defined Loads

Locations are measured from left support.
 Point loads were not defined for this girder
 Distributed loads were not defined for this girder
 Moment loads were not defined for this girder

Camber and Deflections

Camber and Deflection for Span 1 Girder A

Design Camber	1.350 in	0.112 ft
Deflection (Prestressing)	2.796 in	0.233 ft
Deflection (Girder)	-1.607 in	-0.134 ft
Deflection (Deck and Diaphragms)	0.000 in	0.000 ft
Deflection (Shear Key)	-0.197 in	-0.016 ft
Deflection (Traffic Barrier)	-0.258 in	-0.021 ft
Deflection (Overlay)	-0.114 in	-0.010 ft
Deflection (User Defined DC)	0.000 in	0.000 ft
Deflection (User Defined DW)	0.000 in	0.000 ft
Screed Camber, C	0.372 in	0.031 ft
Excess Camber (Based on Design Camber)	1.385 in	0.115 ft
Live Load Deflection (HL93 - Per Lane)	-5.075 in	-0.423 ft
Optional Live Load Deflection (LRFD 3.6.1.3.2)	-0.980 in	-0.082 ft

TxDOT Haunch Summary

Span	1
Girder	A
X (in)	0.000
Y (in)	28.125
Z (in)	-1.375
DL Defl Deck @ Pt A {1/4 pt} (ft)	0.000
DL Defl Deck @ Pt B {1/2 pt} (ft)	0.000
DL Defl Shear Key @ Pt A {1/4 pt} (ft)	-0.012
DL Defl Shear Key @ Pt B {1/2 pt} (ft)	-0.016
Haunch Concrete (yd^3)	-0.80

User-input Fillet and Slab Offset dimensions are used to define the geometry of the bottom of haunch for computing the haunch concrete volume.

Prestress Force and Strand Stresses

Effective Prestress at Mid-Span

Loss Stage	Permanent Strand			f _{pe} (KSI)
	Effective Force (kip)	Time-Dependent Effects (KSI)	Instantaneous Effects (KSI)	
At Jacking	790.97	0.000	0.000	202.500
Before Prestress Transfer	790.97	0.000	0.000	202.500
After Prestress Transfer	756.23	0.000	8.892	193.608
At Lifting	756.23	0.000	8.892	193.608
At Shipping	719.72	9.349	8.892	184.259
After Erection	719.72	9.349	8.892	184.259
After Deck Placement	683.20	18.699	8.892	174.910
After Superimposed Dead Loads	683.20	18.699	8.892	174.910
Final	683.20	18.699	8.892	174.910
Final with Live Load (Service I)	683.20	18.699	8.892	174.910
Final with Live Load (Service III)	683.20	18.699	8.892	174.910

Bridge:

Job:

4/7/2017

Stress Checks

Specification = TxDOT 2015

Interval 2: Prestress Release (Casting Yard) : Service I

Service I

For Temporary Stresses before Losses [5.9.4.1]

Compression Stresses [5.9.4.1.1]

Tension Stresses [5.9.4.1.2]

$f'_{ci} = 6.000$ KSI

Allowable compressive stress = $-0.65f'_{ci} = -3.900$ KSI

Allowable tensile stress in areas other than the precompressed tensile zone = $0.2400 \circ f'_{ci} = 0.588$ KSI

Allowable tensile stress in areas with sufficient bonded reinforcement in the precompressed tensile zone = $0.2400 \circ f'_{ci} =$

0.588 KSI if bonded reinforcement sufficient to resist the tensile force in the concrete is provided.

Concrete strength required to satisfy this requirement = 3.992 KSI

Location from End of Girder (ft)	Pre-tension		Service I		Demand		Tensile Capacity		Precompressed Tensile Zone		Tension Status (C/D)	Compression Status (C/D)
	f_t (KSI)	f_b (KSI)	f_t (KSI)	f_b (KSI)	f_t (KSI)	f_b (KSI)	Top (KSI)	Bottom (KSI)	Top	Bottom		
(STRF, 0.0L _r) 0.000	0.000	0.000	0.000	0.000	0.000	0.000	0.588		No	Yes	Pass (○)	Pass (○)
(PSXFR) 3.000	0.645	-2.779	-0.195	0.184	0.450	-2.595	0.588		No	Yes	Pass (1.31)	Pass (1.50)
(0.1L _r) 7.608	0.645	-2.779	-0.462	0.438	0.182	-2.341	0.588		No	Yes	Pass (3.22)	Pass (1.67)
(0.2L _r) 15.217	0.645	-2.779	-0.822	0.778	-0.177	-2.001	0.588		No	Yes	Pass (-)	Pass (1.95)
(0.3L _r) 22.825	0.645	-2.779	-1.079	1.022	-0.434	-1.758	0.588		No	Yes	Pass (-)	Pass (2.22)
(0.4L _r) 30.433	0.645	-2.779	-1.233	1.167	-0.588	-1.612	0.588		No	Yes	Pass (-)	Pass (2.42)
(0.5L _r) 38.041	0.645	-2.779	-1.285	1.216	-0.640	-1.563	0.588		No	Yes	Pass (-)	Pass (2.50)
(0.6L _r) 45.650	0.645	-2.779	-1.233	1.167	-0.588	-1.612	0.588		No	Yes	Pass (-)	Pass (2.42)
(0.7L _r) 53.258	0.645	-2.779	-1.079	1.022	-0.434	-1.758	0.588		No	Yes	Pass (-)	Pass (2.22)
(0.8L _r) 60.866	0.645	-2.779	-0.822	0.778	-0.177	-2.001	0.588		No	Yes	Pass (-)	Pass (1.95)
(0.9L _r) 68.475	0.645	-2.779	-0.462	0.438	0.182	-2.341	0.588		No	Yes	Pass (3.22)	Pass (1.67)
(PSXFR) 73.083	0.645	-2.779	-0.195	0.184	0.450	-2.595	0.588		No	Yes	Pass (1.31)	Pass (1.50)
(STLF, 1.0L _r) 76.083	0.000	0.000	0.000	0.000	0.000	0.000	0.588		No	Yes	Pass (○)	Pass (○)

Interval 9: Cast Deck (Bridge Site 1) : Service I

Service I

Stresses at Service Limit State after Losses [5.9.4.2]

Compression Stresses [5.9.4.2.1]

Tension Stresses [5.9.4.2.2]

$f'_c = 8.500$ KSI

Allowable compressive stress = $-0.6f'_c = -5.100$ KSI

Allowable tensile stress in the precompressed tensile zone = $0.2400 \circ f'_c = 0.700$ KSI

Concrete strength required to satisfy this requirement = 3.901 KSI

Bridge:

Job:

4/7/2017

Location from Left Support (ft)	Pre-tension		Service I		Demand		Tensile Capacity		Precompressed Tensile Zone		Tension Status (C/D)	Compression Status (C/D)
	f_t (KSI)	f_b (KSI)	f_t (KSI)	f_b (KSI)	f_t (KSI)	f_b (KSI)	Top (KSI)	Bottom (KSI)	Top	Bottom		
0.000	0.105	-0.453	0.000	0.000	0.105	-0.453	-	0.700	No	Yes	Pass (-)	Pass (10+)
(0.0L _s) 0.000	0.105	-0.453	0.000	0.000	0.105	-0.453	-	0.700	No	Yes	Pass (-)	Pass (10+)
(PSXFR) 2.458	0.583	-2.511	-0.180	0.170	0.403	-2.340	-	0.700	No	Yes	Pass (-)	Pass (2.18)
(0.1L _s) 7.500	0.583	-2.511	-0.511	0.484	0.072	-2.027	-	0.700	No	Yes	Pass (-)	Pass (2.52)
(0.2L _s) 15.000	0.583	-2.511	-0.909	0.860	-0.326	-1.651	-	0.700	No	Yes	Pass (-)	Pass (3.09)
(0.3L _s) 22.500	0.583	-2.511	-1.192	1.129	-0.610	-1.382	-	0.700	No	Yes	Pass (-)	Pass (3.69)
(0.4L _s) 30.000	0.583	-2.511	-1.363	1.290	-0.780	-1.221	-	0.700	No	Yes	Pass (-)	Pass (4.18)
(0.5L _s) 37.500	0.583	-2.511	-1.420	1.344	-0.837	-1.167	-	0.700	No	Yes	Pass (-)	Pass (4.37)
(0.6L _s) 45.000	0.583	-2.511	-1.363	1.290	-0.780	-1.221	-	0.700	No	Yes	Pass (-)	Pass (4.18)
(0.7L _s) 52.500	0.583	-2.511	-1.192	1.129	-0.610	-1.382	-	0.700	No	Yes	Pass (-)	Pass (3.69)
(0.8L _s) 60.000	0.583	-2.511	-0.909	0.860	-0.326	-1.651	-	0.700	No	Yes	Pass (-)	Pass (3.09)
(0.9L _s) 67.500	0.583	-2.511	-0.511	0.484	0.072	-2.027	-	0.700	No	Yes	Pass (-)	Pass (2.52)
(PSXFR) 72.541	0.583	-2.511	-0.180	0.170	0.403	-2.340	-	0.700	No	Yes	Pass (-)	Pass (2.18)
(1.0L _s) 75.000	0.105	-0.453	0.000	0.000	0.105	-0.453	-	0.700	No	Yes	Pass (-)	Pass (10+)
75.000	0.105	-0.453	0.000	0.000	0.105	-0.453	-	0.700	No	Yes	Pass (-)	Pass (10+)

Interval 11: Composite Deck, Install Railing System and Overlay (Bridge Site 2) : Service I

Service I

Stresses at Service Limit State after Losses [5.9.4.2]

Compression Stresses [5.9.4.2.1]

$f'_c = 8.500$ KSI

Allowable compressive stress = $-0.45f'_c = -3.825$ KSI

Concrete strength required to satisfy this requirement = 5.114 KSI

Location from Left Support (ft)	Pre-tension		Service I		Demand		Precompressed Tensile Zone		Compression Status (C/D)
	f_t (KSI)	f_b (KSI)	f_t (KSI)	f_b (KSI)	f_t (KSI)	f_b (KSI)	Top	Bottom	
0.000	0.105	-0.453	0.000	0.000	0.105	-0.453	No	Yes	Pass (8.44)
(0.0L _s) 0.000	0.105	-0.453	0.000	0.000	0.105	-0.453	No	Yes	Pass (8.44)
(PSXFR) 2.458	0.583	-2.511	-0.221	0.209	0.361	-2.301	No	Yes	Pass (1.66)
(0.1L _s) 7.500	0.583	-2.511	-0.628	0.594	-0.045	-1.916	No	Yes	Pass (2.00)
(0.2L _s) 15.000	0.583	-2.511	-1.116	1.057	-0.534	-1.454	No	Yes	Pass (2.63)
(0.3L _s) 22.500	0.583	-2.511	-1.465	1.387	-0.883	-1.124	No	Yes	Pass (3.40)

Bridge:

Job:

4/7/2017

Location from Left Support (ft)	Pre-tension		Service I		Demand		Precompressed Tensile Zone		Compression Status (C/D)
	f_t (KSI)	f_b (KSI)	f_t (KSI)	f_b (KSI)	f_t (KSI)	f_b (KSI)	Top	Bottom	
(0.4L _g) 30.000	0.583	-2.511	-1.674	1.585	-1.092	-0.926	No	Yes	Pass (3.50)
(0.5L _g) 37.500	0.583	-2.511	-1.744	1.651	-1.162	-0.860	No	Yes	Pass (3.29)
(0.6L _g) 45.000	0.583	-2.511	-1.674	1.585	-1.092	-0.926	No	Yes	Pass (3.50)
(0.7L _g) 52.500	0.583	-2.511	-1.465	1.387	-0.883	-1.124	No	Yes	Pass (3.40)
(0.8L _g) 60.000	0.583	-2.511	-1.116	1.057	-0.534	-1.454	No	Yes	Pass (2.63)
(0.9L _g) 67.500	0.583	-2.511	-0.628	0.594	-0.045	-1.916	No	Yes	Pass (2.00)
(PSXFR) 72.541	0.583	-2.511	-0.221	0.209	0.361	-2.301	No	Yes	Pass (1.66)
(1.0L _g) 75.000	0.105	-0.453	0.000	0.000	0.105	-0.453	No	Yes	Pass (8.44)
75.000	0.105	-0.453	0.000	0.000	0.105	-0.453	No	Yes	Pass (8.44)

Interval 13: Open to Traffic (Bridge Site 3) : Service I

Service I

Stresses at Service Limit State after Losses [5.9.4.2]

Compression Stresses [5.9.4.2.1]

$f'_c = 8.500$ KSI

Allowable compressive stress = $-0.6f'_c = -5.100$ KSI

Concrete strength required to satisfy this requirement = 4.347 KSI

Location from Left Support (ft)	Pre-tension		Service I		Demand		Precompressed Tensile Zone		Compression Status (C/D)
	f_t (KSI)	f_b (KSI)	f_t (KSI)	f_b (KSI)	f_t (KSI)	f_b (KSI)	Top	Bottom	
0.000	0.105	-0.453	0.000	0.000	0.105	-0.453	No	Yes	Pass (10+)
(0.0L _g) 0.000	0.105	-0.453	0.000	0.000	0.105	-0.453	No	Yes	Pass (10+)
(PSXFR) 2.458	0.583	-2.511	-0.419	0.209	0.164	-2.301	No	Yes	Pass (2.22)
(0.1L _g) 7.500	0.583	-2.511	-1.183	0.594	-0.601	-1.916	No	Yes	Pass (2.66)
(0.2L _g) 15.000	0.583	-2.511	-2.088	1.057	-1.506	-1.454	No	Yes	Pass (3.39)
(0.3L _g) 22.500	0.583	-2.511	-2.715	1.387	-2.132	-1.124	No	Yes	Pass (2.39)
(0.4L _g) 30.000	0.583	-2.511	-3.086	1.585	-2.504	-0.926	No	Yes	Pass (2.04)
(0.5L _g) 37.500	0.583	-2.511	-3.191	1.651	-2.608	-0.860	No	Yes	Pass (1.96)
(0.6L _g) 45.000	0.583	-2.511	-3.086	1.585	-2.504	-0.926	No	Yes	Pass (2.04)
(0.7L _g) 52.500	0.583	-2.511	-2.715	1.387	-2.132	-1.124	No	Yes	Pass (2.39)
(0.8L _g) 60.000	0.583	-2.511	-2.088	1.057	-1.506	-1.454	No	Yes	Pass (3.39)
(0.9L _g) 67.500	0.583	-2.511	-1.183	0.594	-0.601	-1.916	No	Yes	Pass (2.66)

Bridge:

Job:

4/7/2017

Location from Left Support (ft)	Pre-tension		Service I		Demand		Precompressed Tensile Zone		Compression Status (C/D)
	f_t (KSI)	f_b (KSI)	f_t (KSI)	f_b (KSI)	f_t (KSI)	f_b (KSI)	Top	Bottom	
(PSXFR) 72.541	0.583	-2.511	-0.419	0.209	0.164	-2.301	No	Yes	Pass (2.22)
(1.0L _s) 75.000	0.105	-0.453	0.000	0.000	0.105	-0.453	No	Yes	Pass (10+)
75.000	0.105	-0.453	0.000	0.000	0.105	-0.453	No	Yes	Pass (10+)

Interval 13: Open to Traffic (Bridge Site 3) : Service III

Service III

Stresses at Service Limit State after Losses [5.9.4.2]

Tension Stresses [5.9.4.2.2]

$f'_c = 8.500$ KSI

Allowable tension stress in the precompressed tensile zone = $0.0948 \cdot f'_c$ but not more than 0.300 KSI = 0.276 KSI

Concrete strength required to satisfy this requirement = 6.209 KSI

Location from Left Support (ft)	Pre-tension		Service III		Demand		Precompressed Tensile Zone		Tension Status (C/D)
	f_t (KSI)	f_b (KSI)	f_t (KSI)	f_b (KSI)	f_t (KSI)	f_b (KSI)	Top	Bottom	
0.000		-0.453	0.000	-0.453	No	Yes	Pass (-)		
(0.0L _s) 0.000		-0.453	0.000	-0.453	No	Yes	Pass (-)		
(PSXFR) 2.458		-2.511	0.359	-2.152	No	Yes	Pass (-)		
(0.1L _s) 7.500		-2.511	1.015	-1.496	No	Yes	Pass (-)		
(0.2L _s) 15.000		-2.511	1.793	-0.718	No	Yes	Pass (-)		
(0.3L _s) 22.500		-2.511	2.334	-0.177	No	Yes	Pass (-)		
(0.4L _s) 30.000		-2.511	2.655	0.144	No	Yes	Pass (1.92)		
(0.5L _s) 37.500		-2.511	2.747	0.236	No	Yes	Pass (1.17)		
(0.6L _s) 45.000		-2.511	2.655	0.144	No	Yes	Pass (1.92)		
(0.7L _s) 52.500		-2.511	2.334	-0.177	No	Yes	Pass (-)		
(0.8L _s) 60.000		-2.511	1.793	-0.718	No	Yes	Pass (-)		
(0.9L _s) 67.500		-2.511	1.015	-1.496	No	Yes	Pass (-)		
(PSXFR) 72.541		-2.511	0.359	-2.152	No	Yes	Pass (-)		
(1.0L _s) 75.000		-0.453	0.000	-0.453	No	Yes	Pass (-)		
75.000		-0.453	0.000	-0.453	No	Yes	Pass (-)		

Interval 13: Open to Traffic (Bridge Site 3) : Fatigue I

Fatigue I

Stresses at Service Limit State after Losses [5.9.4.2]

Compression Stresses [5.9.4.2.1]

$f'_c = 8.500$ KSI

Bridge:

Job:

4/7/2017

Allowable compressive stress = $-0.4f'_c = -3.400$ KSI
 Concrete strength required to satisfy this requirement = 4.544 KSI

Location from Left Support (ft)	Pre-tension		Fatigue I		Demand		Precompressed Tensile Zone		Compression Status (C/D)
	f_t (KSI)	f_b (KSI)	f_t (KSI)	f_b (KSI)	f_t (KSI)	f_b (KSI)	Top	Bottom	
0.000	0.105	-0.453	0.000	0.000	0.053	-0.227	No	Yes	Pass (10+)
(0.0L _s) 0.000	0.105	-0.453	0.000	0.000	0.053	-0.227	No	Yes	Pass (10+)
(PSXFR) 2.458	0.583	-2.511	-0.279	0.105	0.012	-1.151	No	Yes	Pass (2.95)
(0.1L _s) 7.500	0.583	-2.511	-0.788	0.297	-0.496	-0.958	No	Yes	Pass (3.55)
(0.2L _s) 15.000	0.583	-2.511	-1.388	0.528	-1.096	-0.727	No	Yes	Pass (3.10)
(0.3L _s) 22.500	0.583	-2.511	-1.800	0.694	-1.509	-0.562	No	Yes	Pass (2.25)
(0.4L _s) 30.000	0.583	-2.511	-2.043	0.793	-1.752	-0.463	No	Yes	Pass (1.94)
(0.5L _s) 37.500	0.583	-2.511	-2.109	0.826	-1.817	-0.430	No	Yes	Pass (1.87)
(0.6L _s) 45.000	0.583	-2.511	-2.043	0.793	-1.752	-0.463	No	Yes	Pass (1.94)
(0.7L _s) 52.500	0.583	-2.511	-1.800	0.694	-1.509	-0.562	No	Yes	Pass (2.25)
(0.8L _s) 60.000	0.583	-2.511	-1.388	0.528	-1.096	-0.727	No	Yes	Pass (3.10)
(0.9L _s) 67.500	0.583	-2.511	-0.788	0.297	-0.496	-0.958	No	Yes	Pass (3.55)
(PSXFR) 72.541	0.583	-2.511	-0.279	0.105	0.012	-1.151	No	Yes	Pass (2.95)
(1.0L _s) 75.000	0.105	-0.453	0.000	0.000	0.053	-0.227	No	Yes	Pass (10+)
75.000	0.105	-0.453	0.000	0.000	0.053	-0.227	No	Yes	Pass (10+)

Moment Capacity

Positive Moment Capacity for Strength I Limit State [5.7]

Location from Left Support (ft)	M_u (kip-ft)	iM_n (kip-ft)	iM_n Min (kip-ft)	Status	
				iM_n Min / iM_n Min (kip-ft)	M_u / iM_n (kip-ft)
(0.0L _s) 0.000	0.00	264.87	0.00	Pass (∅)	Pass (∅)
(0.1L _s) 7.500	703.31	1796.72	935.40	Pass (1.92)	Pass (2.55)
(0.2L _s) 15.000	1239.63	2061.75	1632.98	Pass (1.26)	Pass (1.66)
(0.3L _s) 22.500	1608.97	2061.75	1632.98	Pass (1.26)	Pass (1.28)
(0.4L _s) 30.000	1827.37	2061.75	1632.98	Pass (1.26)	Pass (1.13)
(0.5L _s) 37.500	1886.80	2061.75	1632.98	Pass (1.26)	Pass (1.09)
(0.6L _s) 45.000	1827.37	2061.75	1632.98	Pass	Pass

Bridge:

Job:

4/7/2017

Location from Left Support (ft)	M_u (kip-ft)	iM_n (kip-ft)	iM_n Min (kip-ft)	Status	
				iM_n Min / iM_n (iM_n/iM_n Min)	M_u / iM_n (M_u/iM_n)
				(1.26)	(1.13)
(0.7L) 52.500	1608.97	2061.75	1632.98	Pass (1.26)	Pass (1.28)
(0.8L) 60.000	1239.63	2061.75	1632.98	Pass (1.26)	Pass (1.66)
(0.9L) 67.500	703.31	1796.72	935.40	Pass (1.92)	Pass (2.55)
(1.0L) 75.000	0.00	264.87	0.00	Pass (0)	Pass (0)

Shear

Ultimate Shears for Strength I Limit State [5.8]

Location from Left Support (ft)	Stirrups Required	Stirrups Provided	$ V_u $ (kip)	iV_n (kip)	Status (iV_n/V_u)
(CS) 2.579	Yes	Yes	141.13	285.22	Pass (2.02)
(H) 2.875	Yes	Yes	140.23	284.40	Pass (2.03)
(1.5H) 4.042	Yes	Yes	136.69	278.92	Pass (2.04)
(0.1L) 7.500	Yes	Yes	126.25	268.37	Pass (2.13)
(0.2L) 15.000	Yes	Yes	103.94	253.62	Pass (2.44)
(0.3L) 22.500	Yes	Yes	82.09	194.26	Pass (2.37)
(0.4L) 30.000	Yes	Yes	60.69	165.54	Pass (2.73)
(SZB) 32.129	Yes	Yes	54.70	101.69	Pass (1.86)
(0.5L) 37.500	Yes	Yes	39.75	102.09	Pass (2.57)
(SZB) 42.871	Yes	Yes	54.70	101.69	Pass (1.86)
(0.6L) 45.000	Yes	Yes	60.69	165.54	Pass (2.73)
(0.7L) 52.500	Yes	Yes	82.09	194.26	Pass (2.37)
(0.8L) 60.000	Yes	Yes	103.94	253.62	Pass (2.44)
(0.9L) 67.500	Yes	Yes	126.25	268.37	Pass (2.13)
(1.5H) 70.958	Yes	Yes	136.69	278.92	Pass (2.04)
(H) 72.125	Yes	Yes	140.23	284.40	Pass (2.03)
(CS) 72.421	Yes	Yes	141.13	285.22	Pass (2.02)

[LRFD 5.8.3.2] The reaction introduces compression into the end of the girder. Load between the CSS and the support is transferred directly to the support by compressive arching action without causing additional stresses in the stirrups. Hence, A_v/S in this region must be equal or greater than A_v/S at the critical section.

Bridge:

Job:

4/7/2017

Ultimate Shears for Strength II Limit State [5.8]

Location from Left Support (ft)	Stirrups Required	Stirrups Provided	$ V_u $ (kip)	ΔV_n (kip)	Status ($\Delta V_n/V_u$)
(H) 2.875	Yes	Yes	103.52	289.21	Pass (2.79)
(1.5H) 4.042	Yes	Yes	100.73	284.23	Pass (2.82)
(0.1L _s) 7.500	Yes	Yes	92.49	275.01	Pass (2.97)
(0.2L _s) 15.000	Yes	Yes	74.88	262.05	Pass (3.50)
(0.3L _s) 22.500	Yes	Yes	57.62	254.91	Pass (4.42)
(0.4L _s) 30.000	No	Yes	40.71	251.28	Pass (6.17)
(SZB) 32.129	No	Yes	35.97	173.15	Pass (4.81)
(0.5L _s) 37.500	No	Yes	24.15	173.15	Pass (7.17)
(SZB) 42.871	No	Yes	35.97	173.15	Pass (4.81)
(0.6L _s) 45.000	No	Yes	40.71	251.28	Pass (6.17)
(0.7L _s) 52.500	Yes	Yes	57.62	254.91	Pass (4.42)
(0.8L _s) 60.000	Yes	Yes	74.88	262.05	Pass (3.50)
(0.9L _s) 67.500	Yes	Yes	92.49	275.01	Pass (2.97)
(1.5H) 70.958	Yes	Yes	100.73	284.23	Pass (2.82)
(H) 72.125	Yes	Yes	103.52	289.21	Pass (2.79)

[LRFD 5.8.3.2] The reaction introduces compression into the end of the girder. Load between the CSS and the support is transferred directly to the support by compressive arching action without causing additional stresses in the stirrups. Hence, $A_v S$ in this region must be equal or greater than $A_v S$ at the critical section.

Longitudinal Reinforcement for Shear Check - Strength I [5.8.3.5]

$$A_s f_y + A_{ps} f_{ps} \geq \left[\frac{M_u}{d_v \phi_f} + 0.5 \frac{N_u}{\phi_a} + \left(\left| \frac{V_u}{\phi_v} - V_p \right| - 0.5 V_s \right) \cot \theta \right] \quad 5.8.3.5 - 1$$

$$A_s f_y + A_{ps} f_{ps} \geq \left(\frac{V_u}{\phi_v} - V_p - 0.5 V_s \right) \cot \theta \quad 5.8.3.5 - 2$$

Location from Left Support (ft)	Capacity (kip)	Demand (kip)	Equation	Status (C/D)
(FoS) 0.542	251.39	146.81	5.8.3.5-2	Pass (1.71)
(SZB) 0.629	271.57	146.81	5.8.3.5-2	Pass (1.85)
(Bar Develop.) 2.031	596.95	146.81	5.8.3.5-2	Pass (4.07)
(CS) 2.579	701.04	274.76	5.8.3.5-1	Pass (2.55)
(H) 2.875	713.00	287.93	5.8.3.5-1	Pass (2.48)

Bridge:

Job:

4/7/2017

Location from Left Support (ft)	Capacity (kip)	Demand (kip)	Equation	Status (C/D)
(1.5H) 4.042	760.15	338.50	5.8.3.5-1	Pass (2.25)
(0.1L _s) 7.500	893.34	478.99	5.8.3.5-1	Pass (1.87)
(0.2L _s) 15.000	1034.98	726.97	5.8.3.5-1	Pass (1.42)
(0.3L _s) 22.500	1034.98	880.37	5.8.3.5-1	Pass (1.18)
(0.4L _s) 30.000	1034.98	965.69	5.8.3.5-1	Pass (1.07)
(SZB) 32.129	1034.98	977.35	5.8.3.5-1	Pass (1.06)
(0.5L _s) 37.500	1034.98	978.51	5.8.3.5-1	Pass (1.06)
(SZB) 42.871	1034.98	977.35	5.8.3.5-1	Pass (1.06)
(0.6L _s) 45.000	1034.98	965.69	5.8.3.5-1	Pass (1.07)
(0.7L _s) 52.500	1034.98	880.37	5.8.3.5-1	Pass (1.18)
(0.8L _s) 60.000	1034.98	726.97	5.8.3.5-1	Pass (1.42)
(0.9L _s) 67.500	893.34	478.99	5.8.3.5-1	Pass (1.87)
(1.5H) 70.958	760.15	338.50	5.8.3.5-1	Pass (2.25)
(H) 72.125	713.00	287.93	5.8.3.5-1	Pass (2.48)
(CS) 72.421	701.04	274.76	5.8.3.5-1	Pass (2.55)
(Bar Develop.) 72.969	596.95	146.81	5.8.3.5-2	Pass (4.07)
(SZB) 74.371	271.57	146.81	5.8.3.5-2	Pass (1.85)
(FoS) 74.458	251.39	146.81	5.8.3.5-2	Pass (1.71)

Longitudinal Reinforcement for Shear Check - Strength II [5.8.3.5]

$$A_s f_y + A_{ps} f_{ps} \geq \left[\frac{M_u}{d_v \phi_f} + 0.5 \frac{N_u}{\phi_a} + \left(\left| \frac{V_u}{\phi_v} - V_p \right| - 0.5 V_s \right) \cot \theta \right] \quad 5.8.3.5 - 1$$

$$A_s f_y + A_{ps} f_{ps} \geq \left(\frac{V_u}{\phi_v} - V_p - 0.5 V_s \right) \cot \theta \quad 5.8.3.5 - 2$$

Location from Left Support (ft)	Capacity (kip)	Demand (kip)	Equation	Status (C/D)
(FoS) 0.542	251.39	109.05	5.8.3.5-2	Pass (2.31)
(SZB) 0.629	271.57	109.05	5.8.3.5-2	Pass (2.49)
(Bar Develop.) 2.031	596.95	109.05	5.8.3.5-2	Pass (5.47)
(H) 2.875	713.00	220.70	5.8.3.5-1	Pass (3.23)
(1.5H) 4.042	760.15	260.89	5.8.3.5-1	Pass (2.91)

Bridge:

Job:

4/7/2017

Location from Left Support (ft)	Capacity (kip)	Demand (kip)	Equation	Status (C/D)
(0.1L _g) 7.500	893.34	372.65	5.8.3.5-1	Pass (2.40)
(0.2L _g) 15.000	1034.98	570.66	5.8.3.5-1	Pass (1.81)
(0.3L _g) 22.500	1034.98	701.71	5.8.3.5-1	Pass (1.47)
(0.4L _g) 30.000	1034.98	773.03	5.8.3.5-1	Pass (1.34)
(SZB) 32.129	1034.98	782.17	5.8.3.5-1	Pass (1.32)
(0.5L _g) 37.500	1034.98	782.04	5.8.3.5-1	Pass (1.32)
(SZB) 42.871	1034.98	782.17	5.8.3.5-1	Pass (1.32)
(0.6L _g) 45.000	1034.98	773.03	5.8.3.5-1	Pass (1.34)
(0.7L _g) 52.500	1034.98	701.71	5.8.3.5-1	Pass (1.47)
(0.8L _g) 60.000	1034.98	570.66	5.8.3.5-1	Pass (1.81)
(0.9L _g) 67.500	893.34	372.65	5.8.3.5-1	Pass (2.40)
(1.5H) 70.958	760.15	260.89	5.8.3.5-1	Pass (2.91)
(H) 72.125	713.00	220.70	5.8.3.5-1	Pass (3.23)
(Bar Develop.) 72.969	596.95	109.05	5.8.3.5-2	Pass (5.47)
(SZB) 74.371	271.57	109.05	5.8.3.5-2	Pass (2.49)
(FoS) 74.458	251.39	109.05	5.8.3.5-2	Pass (2.31)

Stirrup Detailing Check: Strength I [5.8.2.5, 5.8.2.7, 5.10.3.1.2]

Location from Left Support (ft)	Bar Size	S (in)	S _{max} (in)	S _{min} (in)	A _v /S (in ² /ft)	A _v /S _{min} (in ² /ft) ⁺	Status
0.000	#4	4.000	20.229	2.495	1.200	0.000	Pass
(0.0L _g) 0.000	#4	4.000	20.229	2.495	1.200	0.184	Pass
(FoS) 0.542	#4	4.000	20.058	2.495	1.200	0.184	Pass
(SZB) 0.629	#4	6.000	20.031	2.495	0.800	0.184	Pass
(Bar Develop.) 2.031	#4	6.000	19.703	2.495	0.800	0.184	Pass
(CS) 2.579	#4	6.000	19.559	2.495	0.800	0.184	Pass
(H) 2.875	#4	6.000	19.542	2.495	0.800	0.184	Pass
(1.5H) 4.042	#4	6.000	19.471	2.495	0.800	0.184	Pass
(0.1L _g) 7.500	#4	6.000	19.308	2.495	0.800	0.184	Pass
(0.2L _g) 15.000	#4	6.000	19.124	2.495	0.800	0.184	Pass
(0.3L _g) 22.500	#4	6.000	19.124	2.495	0.800	0.184	Pass
(0.4L _g) 30.000	#4	6.000	19.124	2.495	0.800	0.184	Pass
(SZB) 32.129	#4	12.000	19.124	2.495	0.400	0.184	Pass
(0.5L _g) 37.500	#4	12.000	19.124	2.495	0.400	0.184	Pass
(SZB) 42.871	#4	12.000	19.124	2.495	0.400	0.184	Pass

Bridge:

Job:

4/7/2017

Location from Left Support (ft)	Bar Size	S (in)	S _{max} (in)	S _{min} (in)	A _v /S (in ² /ft)	A _v /S _{min} (in ² /ft)*	Status
(0.6L _s) 45.000	#4	6.000	19.124	2.495	0.800	0.184	Pass
(0.7L _s) 52.500	#4	6.000	19.124	2.495	0.800	0.184	Pass
(0.8L _s) 60.000	#4	6.000	19.124	2.495	0.800	0.184	Pass
(0.9L _s) 67.500	#4	6.000	19.308	2.495	0.800	0.184	Pass
(1.5H) 70.958	#4	6.000	19.471	2.495	0.800	0.184	Pass
(H) 72.125	#4	6.000	19.542	2.495	0.800	0.184	Pass
(CS) 72.421	#4	6.000	19.559	2.495	0.800	0.184	Pass
(Bar Develop.) 72.969	#4	6.000	19.703	2.495	0.800	0.184	Pass
(SZB) 74.371	#4	6.000	20.031	2.495	0.800	0.184	Pass
(FoS) 74.458	#4	4.000	20.058	2.495	1.200	0.184	Pass
(1.0L _s) 75.000	#4	4.000	20.229	2.495	1.200	0.184	Pass
75.000	#4	4.000	20.229	2.495	1.200	0.000	Pass

* - Transverse reinforcement not required if $V_u < 0.5i(V_c + V_p)$ [Eqn 5.8.2.4-1]

Stirrup Detailing Check: Strength II [5.8.2.5, 5.8.2.7, 5.10.3.1.2]

Location from Left Support (ft)	Bar Size	S (in)	S _{max} (in)	S _{min} (in)	A _v /S (in ² /ft)	A _v /S _{min} (in ² /ft)*	Status
0.000	#4	4.000	20.229	2.495	1.200	0.000	Pass
(0.0L _s) 0.000	#4	4.000	20.229	2.495	1.200	0.184	Pass
(FoS) 0.542	#4	4.000	20.058	2.495	1.200	0.184	Pass
(SZB) 0.629	#4	6.000	20.031	2.495	0.800	0.184	Pass
(Bar Develop.) 2.031	#4	6.000	19.703	2.495	0.800	0.184	Pass
(H) 2.875	#4	6.000	19.542	2.495	0.800	0.184	Pass
(1.5H) 4.042	#4	6.000	19.471	2.495	0.800	0.184	Pass
(0.1L _s) 7.500	#4	6.000	19.308	2.495	0.800	0.184	Pass
(0.2L _s) 15.000	#4	6.000	19.124	2.495	0.800	0.184	Pass
(0.3L _s) 22.500	#4	6.000	19.124	2.495	0.800	0.184	Pass
(0.4L _s) 30.000	#4	6.000	19.124	2.495	0.800	0.000	Pass
(SZB) 32.129	#4	12.000	19.124	2.495	0.400	0.000	Pass
(0.5L _s) 37.500	#4	12.000	19.124	2.495	0.400	0.000	Pass
(SZB) 42.871	#4	12.000	19.124	2.495	0.400	0.000	Pass
(0.6L _s) 45.000	#4	6.000	19.124	2.495	0.800	0.000	Pass
(0.7L _s) 52.500	#4	6.000	19.124	2.495	0.800	0.184	Pass
(0.8L _s) 60.000	#4	6.000	19.124	2.495	0.800	0.184	Pass
(0.9L _s) 67.500	#4	6.000	19.308	2.495	0.800	0.184	Pass
(1.5H) 70.958	#4	6.000	19.471	2.495	0.800	0.184	Pass
(H) 72.125	#4	6.000	19.542	2.495	0.800	0.184	Pass
(Bar Develop.) 72.969	#4	6.000	19.703	2.495	0.800	0.184	Pass
(SZB) 74.371	#4	6.000	20.031	2.495	0.800	0.184	Pass
(FoS) 74.458	#4	4.000	20.058	2.495	1.200	0.184	Pass
(1.0L _s) 75.000	#4	4.000	20.229	2.495	1.200	0.184	Pass
75.000	#4	4.000	20.229	2.495	1.200	0.000	Pass

* - Transverse reinforcement not required if $V_u < 0.5i(V_c + V_p)$ [Eqn 5.8.2.4-1]

Bridge:

Job:

4/7/2017

C. ESTIMATION OF SMALL-SCALE JOINT STRENGTH

A summary of the estimated strength of the small-scale joints is provided in this appendix. The estimated cracking and ultimate strength and behavior were obtained using ATENA FEM software and hand calculations with simple rectangular stress block assumptions. A summary of all analyses is shown in Table C.1.

Table C.1: Max. forces and displacements computed

Type of Analysis:	Software Analysis	Software Analysis	Software Analysis	Hand Calculation	Hand Calculation
Specimens	Cracking Force [kips]	Max. Force [kips]	Δ @ Max. Force [in]	Cracking Force [kips]	Max. Force [kips]
Control (FSB)	43.85	153.25	-0.477	36.97	88.04
18F1	80.04	149.84	-0.374	54.34	107.12
18F2	86.77	169.36	-0.220	54.34	125.58
18A1	78.13	135.98	-0.185	54.34	100.20
12F1	25.84	68.87	-0.278	24.60	51.74
12F2	33.39	91.90	-0.210	24.60	70.20
12A1	27.92	49.32	-0.423	24.60	44.82
12A2	32.46	104.81	-0.330	24.60	68.47

C.1. MATERIAL DEFINITION AND ANALYSIS PROPERTIES

Basic material properties were defined to perform the numerical simulations. The values were taken from the expected behavior based on manufacturer test results. The basic concrete properties used for the analyses are summarized in Table C.2.

Table C.2: Concrete definition

Property	Variable	Beams	Joints	Slab
Compressive Strength	f'_c [ksi]	10.31	20.00	5.07
Tensile Strength	f'_t [ksi]	0.464	1.16	0.319
Young's Modulus	E_c [ksi]	5,787.68	7,200	4931.28
Fracture Energy	G_F [lb/in]	0.456812	0.588675	0.314058

The joint reinforcement protruding from the concrete face of the beams was used to define the flexure steel in the analyses. A bilinear stress-strain curve was used for the reinforcement in the ATENA model with the important points shown in Table C.3.

Table C.3: Joint reinforcement definition

Property	Variable	Value
Rebar Dia.	ϕ	0.625 in
Yield Strain	ε_1	0.002255
Yield Stress	$f_1 = f_y$	65,400 psi
Ultimate Strain	ε_2	0.05
Ultimate Stress	f_2	96,600 psi

Only the yield stress and strain were used to calculate the moment capacity of the joints based on rectangular stress block assumptions.

Because the beam has less tensile and compressive concrete strength than the joint material (UHPC), the failure was assumed to be controlled by the concrete of the beam at its weakest plane.

The following formulas were used to obtain the cracking moment and ultimate moment capacity for all the specimens.

$$\beta_1 = 0.85 - 0.05(f'_c - 4 \text{ ksi}) \leq 0.65 \quad \text{Equation C-1}$$

Singly reinforced:
$$c = \frac{A_s f_y}{(0.85 f'_c)(\beta_1)(b)} \quad \text{Equation C-2}$$

$$M_n = A_s f_y \left(d - \beta_1 c / 2 \right) \quad \text{Equation C-3}$$

Doubly reinforced:
$$c = \frac{A_s f_y - A'_s f'_s}{(0.85 f'_c)(\beta_1)(b)} \quad \text{Equation C-4}$$

$$M_n = (A_s - A'_s) f_y \left(d - \beta_1 c / 2 \right) + A'_s f'_s (d - d') \quad \text{Equation C-5}$$

$$M_{cr} = \frac{7.5 \sqrt{f'_c} I_g}{d - c} \quad \text{Equation C-6}$$

The expected applied load to cause failure was found using the nominal moment capacity determined from Equation C-3 or Equation C-5. The system was idealized as a simply-supported

beam with uniform load partially distributed as shown in Figure C.1. The distributed load was applied by the loading plate on top of the beam. The distributed load required to cause failure was found by setting the maximum moment (Equation C-8) equal to the nominal moment capacity and solving for w . The distributed load (w) was then multiplied by the length of the plate to get the failure load (P), as shown in Equation C-9.

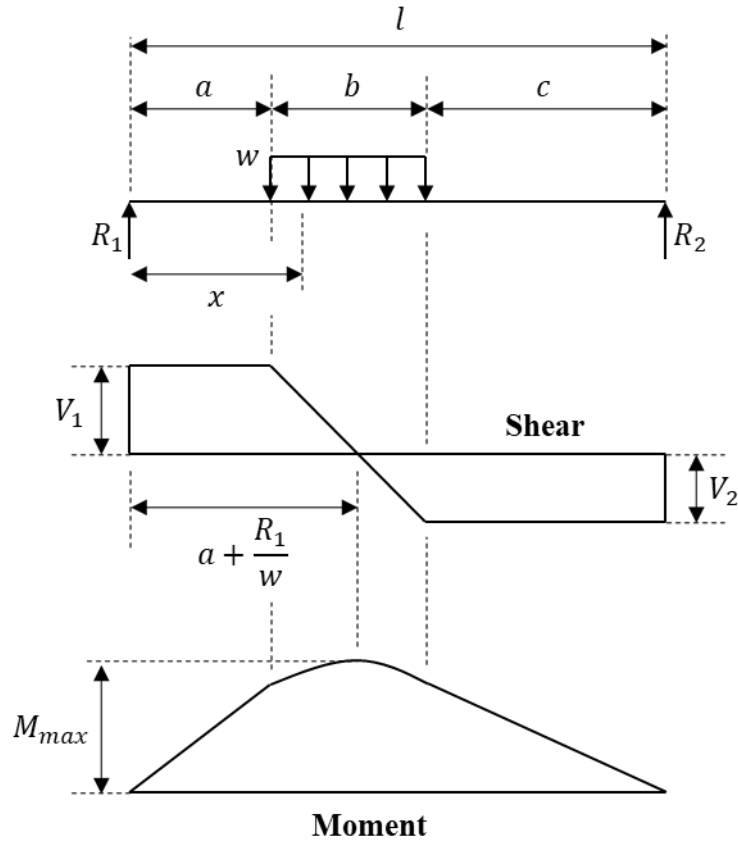


Figure C.1: Simply supported beam with uniform load partially distributed

$$R_1 = \frac{wb}{2l}(2c + b) \quad \text{Equation C-7}$$

$$M_{max} = R_1 \left(a + \frac{R_1}{2w} \right) \quad \text{Equation C-8}$$

$$P = w * \text{Plate length} \quad \text{Equation C-9}$$

C.2. ESTIMATED PERFORMANCE OF EACH SECTION

Results are presented in this section from both numerical models and hand calculation. The numerical model results include the expected load versus displacement response and expected crack pattern from the top and bottom of the beam immediately before failure.

C.2.1. 18-inch-deep FSB System Detail (FSB-Control)

Load-Deflection and Expected Crack Pattern

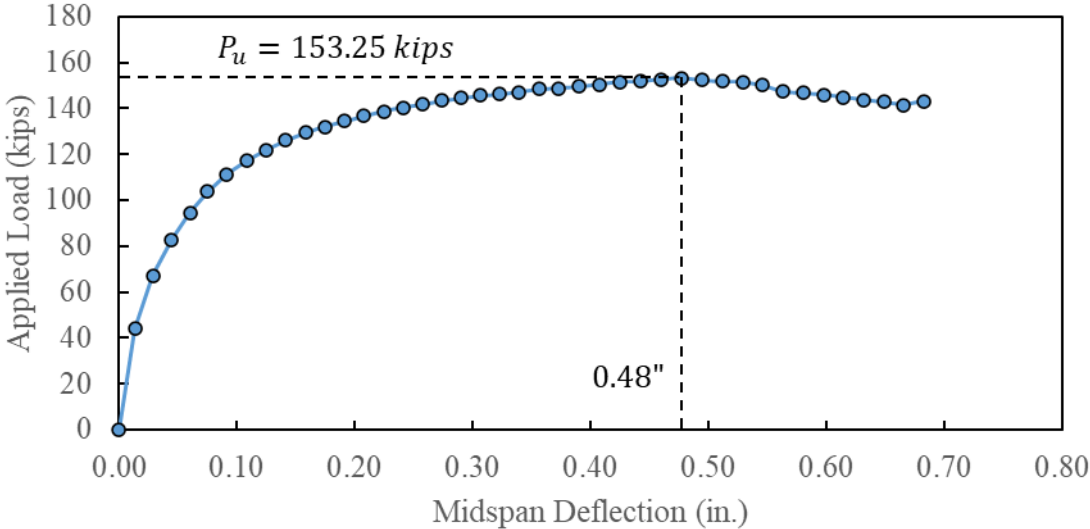


Figure C.2: Estimated load-deflection response for control specimen

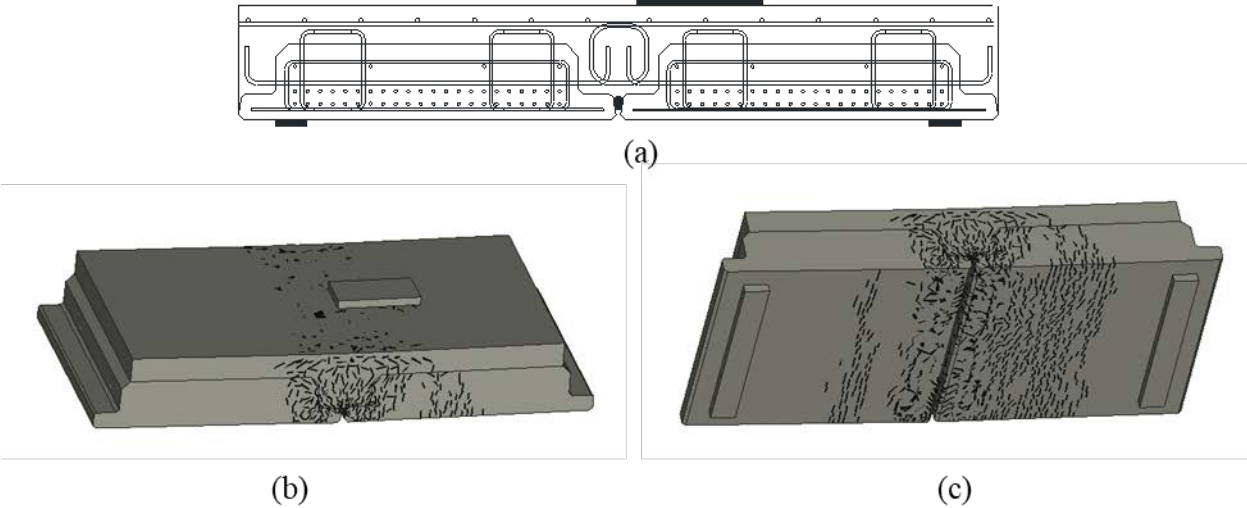
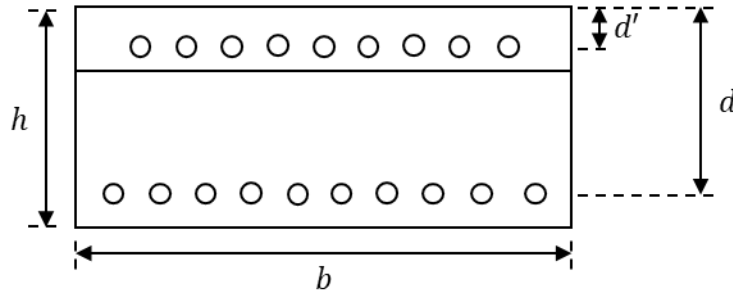


Figure C.3: (a) Specimen testing layout. (b) Top expected cracking pattern before failure and (c) bottom expected cracking pattern before failure for Control

Input Data



$$f'_{c,beam} = 10,310 \text{ psi} \quad f_y = 65,400 \text{ psi} \quad \phi = 0.625 \text{ in} \quad f'_{c,slab} = 5,070 \text{ psi}$$

$$A_s = 3.10 \text{ in}^2 \quad A'_s = 2.79 \text{ in}^2 \quad h = 18 \text{ in} \quad b = 56 \text{ in}$$

$$d = 12.1875 \text{ in} \quad d' = 2.9375 \text{ in} \quad I_g = 27,216 \text{ in}^4$$

Nominal Moment Capacity

$$\beta_1 = 0.85 - 0.05(5.07 \text{ ksi} - 4 \text{ ksi}) = 0.797$$

$$C_c + C_s = T_s$$

$$C_c = 0.85f'_c\beta_1cb = (0.85)(5.07 \text{ ksi})(0.797)c(56") = 192.3c$$

$$C_s = f_sA'_s = (65.4 \text{ ksi})(2.79 \text{ in}^2) = 182.4 \text{ kips}$$

$$T_s = f_sA_s = (65.4 \text{ ksi})(3.1 \text{ in}^2) = 202.7 \text{ kips}$$

$$192.3c + 182.4 \text{ k} = 202.7 \text{ k}$$

$$c = \frac{202.7 \text{ k} - 182.4 \text{ k}}{192.3} = 0.11" \quad a = \beta_1c = 0.084"$$

$$\varepsilon_s = 0.003 \left(\frac{d' - c}{c} \right) = 0.003 \left(\frac{2.9375" - 0.11"}{0.11"} \right) = 0.0835 > \varepsilon_y$$

The first assumption is validated. Compression steel does yield

$$M_n = (3.10 \text{ in}^2 - 2.79 \text{ in}^2)(65.4 \text{ ksi}) \left(12.1875" - (0.797)(0.11") \right) / 2$$

$$+ (2.79 \text{ in}^2)(65.4 \text{ ksi})(12.1875" - 2.9375")$$

$$M_n = 246.2 + 1687.8 = 1,934 \text{ k"}$$

Simple Supported Beam – Uniform Load Partially Distributed

$$a = 54.875 \text{ in} \quad b = 20 \text{ in} \quad c = 28.875 \text{ in} \quad l = 103.75 \text{ in} \quad w = ?$$

$$R_1 = \frac{wb}{2l}(2c + b) \quad \rightarrow \quad R_1 = 7.4940w$$

$$M_{max} = R_1 \left(a + \frac{R_1}{2w} \right) \quad \rightarrow \quad M_{max} = 7.4940w \left(54.875 + \frac{7.4940}{2} \right) = 439.31w$$

$$M_{max} = 439.31w = 1933.94 k'' \rightarrow w = 4.4022 k/in$$

Application load at M_{max}

$$P_{ult} = (4.4022 k/in)(20'') = 88.04 kips$$

The cracking load can be calculated following the same procedure described previously.

Application load at M_{cr}

$$M_{cr} = 812.05 k'' \rightarrow w_{cr} = 1.8485 k/in \rightarrow P_{cr} = 36.97 kips$$

C.2.2. 18-inch-deep FDOT 1 Detail (18F1)

Load-Deflection and Expected Crack Pattern

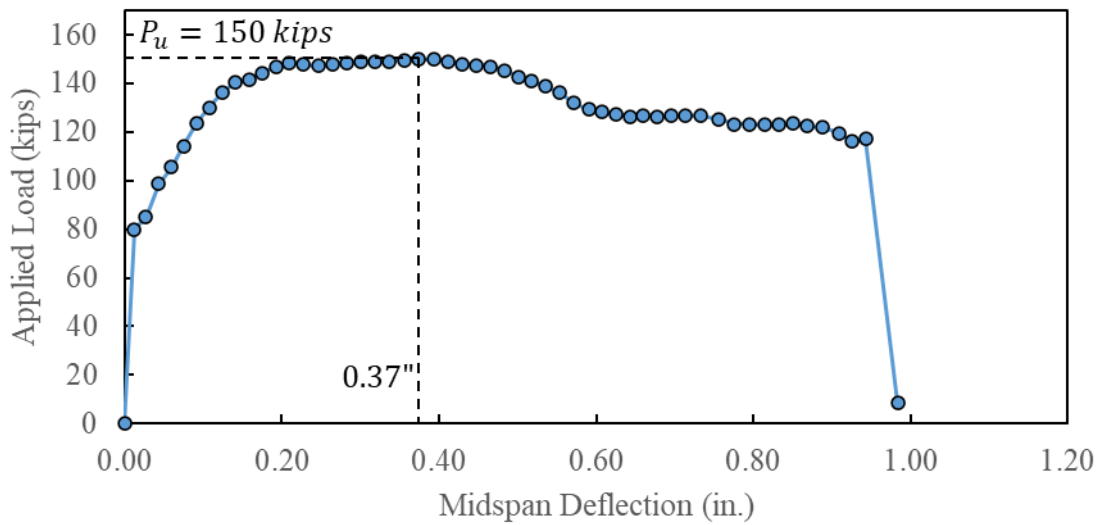


Figure C.4: Estimated load-deflection response for 18F1 specimen

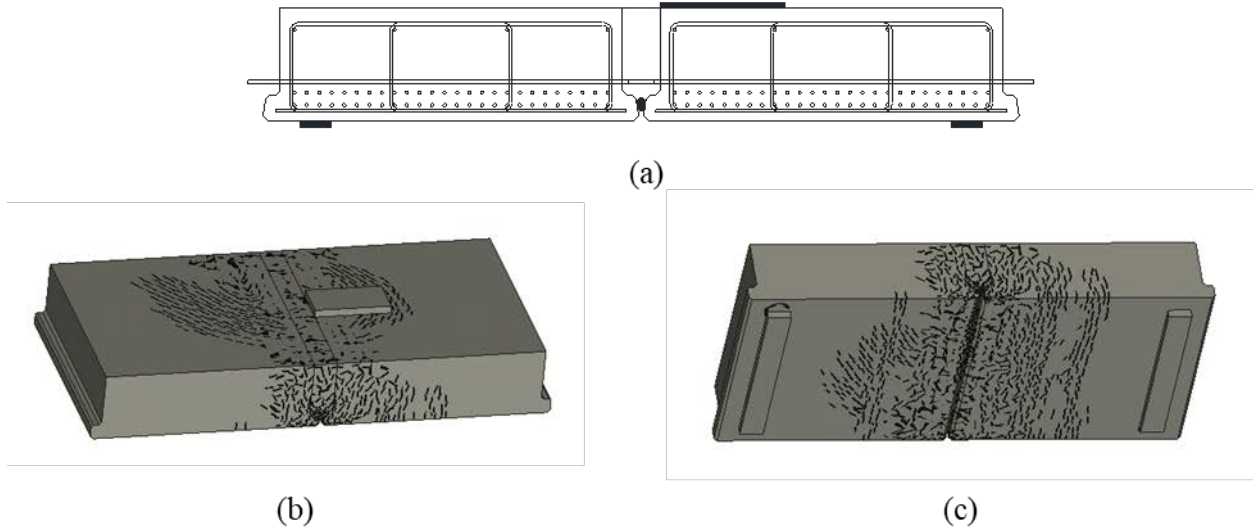
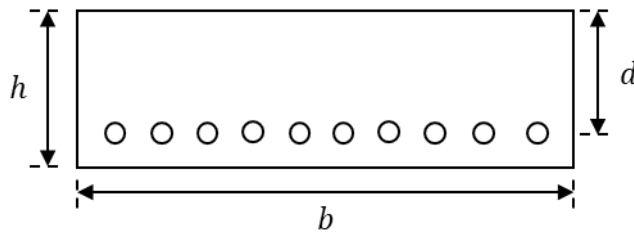


Figure C.5: (a) Specimen testing layout. (b) Top expected cracking pattern before failure and (c) bottom expected cracking pattern before failure for 18F1

Input Data



$$f'_c = 10,310 \text{ psi} \quad f_y = 65,400 \text{ psi} \quad \phi = 0.625 \text{ in} \quad A_s = 0.31 \text{ in}^2$$

$$h = 18 \text{ in} \quad b = 56 \text{ in} \quad d = 11.8125 \text{ in} \quad I_g = 27,216 \text{ in}^4$$

Nominal Moment Capacity

$$\beta_1 = 0.5345 \leq 0.65 \therefore \beta_1 = 0.65$$

$$c = \frac{(10 * 0.31 \text{ in}^2)(65.4 \text{ ksi})}{(0.85)(10.31 \text{ ksi})(0.65)(56 \text{ in})} = 0.636 \text{ in} \quad a = \beta_1 c = 0.4131 \text{ in}$$

$$\epsilon_s = 0.003 \left(\frac{d - c}{c} \right) = 0.003 \left(\frac{11.8125 \text{ in} - 0.636 \text{ in}}{0.636 \text{ in}} \right) = 0.053 > \epsilon_y$$

$$M_n = 10(0.31 \text{ in}^2)(65.4 \text{ ksi}) \left(11.8125 \text{ in} - \frac{(0.65)(0.636 \text{ in})}{2} \right) = 2,352.99 \text{ k-in}$$

Simple Supported Beam – Uniform Load Partially Distributed

$$a = 54.875 \text{ in} \quad b = 20 \text{ in} \quad c = 28.875 \text{ in} \quad l = 103.75 \text{ in} \quad w = ?$$

$$R_1 = \frac{wb}{2l}(2c + b) \rightarrow R_1 = 7.4940w$$

$$M_{max} = R_1 \left(a + \frac{R_1}{2w} \right) \rightarrow M_{max} = 7.4940w \left(54.875 + \frac{7.4940}{2} \right) = 439.31w$$

$$M_{max} = 439.31w = 2,352.99 \text{ k}'' \rightarrow w = 5.3560 \text{ k}/\text{in}$$

Application load at M_{max}

$$P_{ult} = (5.3560 \text{ k}/\text{in})(20'') = 107.12 \text{ kips}$$

The cracking load can be calculated following the same procedure described previously.

Application load at M_{cr}

$$M_{cr} = 1193.59 \text{ k}'' \rightarrow w_{cr} = 2.717 \text{ k}/\text{in} \rightarrow P_{cr} = 54.34 \text{ kips}$$

C.2.3. 18-inch-deep FDOT 2 Detail (18F2)

Load-Deflection and Expected Crack Pattern

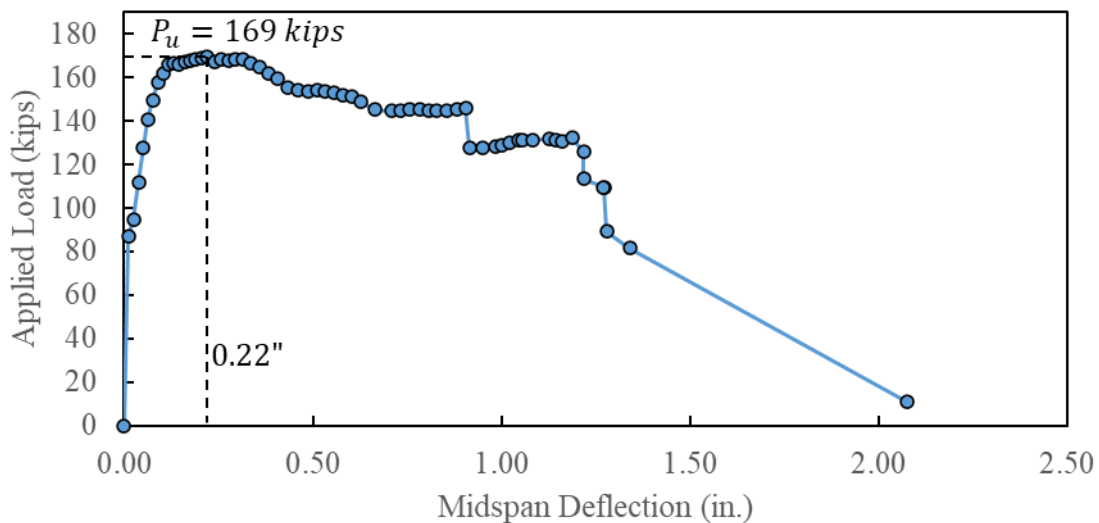


Figure C.6: Estimated load-deflection response for 18F2 specimen

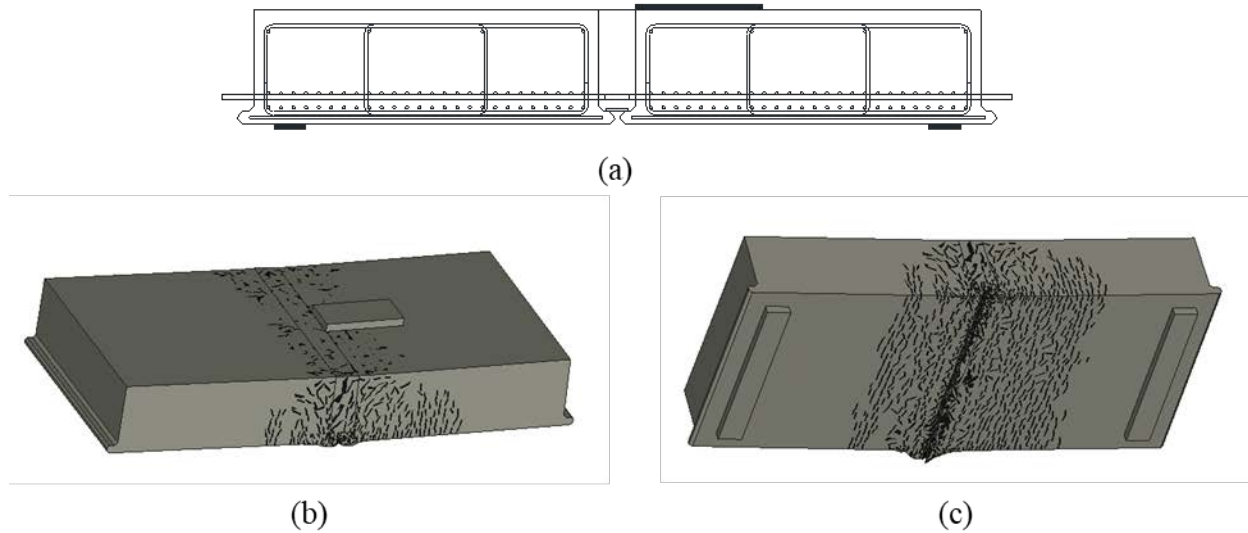
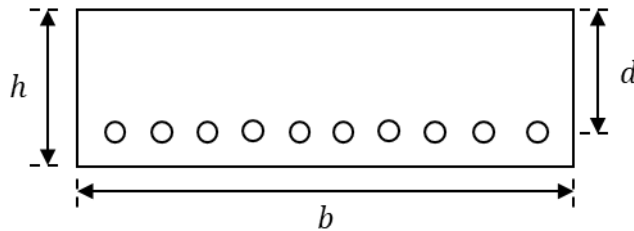


Figure C.7: (a) Specimen testing layout. (b) Top expected cracking pattern before failure and (c) bottom expected cracking pattern before failure for 18F2

Input Data



$$f'c = 10,310 \text{ psi} \quad f_y = 65,400 \text{ psi} \quad \phi = 0.625 \text{ in} \quad A_s = 0.31 \text{ in}^2$$

$$h = 18 \text{ in} \quad b = 56 \text{ in} \quad d = 13.8125 \text{ in} \quad I_g = 27,216 \text{ in}^4$$

Nominal Moment Capacity

$$\beta_1 = 0.5345 \leq 0.65 \therefore \beta_1 = 0.65$$

$$c = \frac{(10 * 0.31 \text{ in}^2)(65.4 \text{ ksi})}{(0.85)(10.31 \text{ ksi})(0.65)(56\text{'})} = 0.636\text{'}$$

$$a = \beta_1 c = 0.4131\text{'}$$

$$\epsilon_s = 0.003 \left(\frac{d - c}{c} \right) = 0.003 \left(\frac{13.8125\text{' } - 0.636\text{'}}{0.636\text{'}} \right) = 0.053 > \epsilon_y$$

$$M_n = 10(0.31 \text{ in.}^2)(65.4 \text{ ksi}) \left(13.8125\text{' } - \frac{(0.65)(0.636\text{'})}{2} \right) = 2,758.47 \text{ k'}$$

Simple Supported Beam – Uniform Load Partially Distributed

$$a = 54.875 \text{ in} \quad b = 20 \text{ in} \quad c = 28.875 \text{ in} \quad l = 103.75 \text{ in} \quad w = ?$$

$$R_1 = \frac{wb}{2l}(2c + b) \rightarrow R_1 = 7.4940w$$

$$M_{max} = R_1 \left(a + \frac{R_1}{2w} \right) \rightarrow M_{max} = 7.4940w \left(54.875 + \frac{7.4940}{2} \right) = 439.31w$$

$$M_{max} = 439.31w = 2,352.99 \text{ k}'' \rightarrow w = 6.279 \text{ k}/\text{in}$$

Application load at M_{max}

$$P_{ult} = (6.279 \text{ k}/\text{in})(20'') = 125.58 \text{ kips}$$

The cracking load can be calculated following the same procedure described previously.

Application load at M_{cr}

$$M_{cr} = 1193.59 \text{ k}'' \rightarrow w_{cr} = 2.717 \text{ k}/\text{in} \rightarrow P_{cr} = 54.34 \text{ kips}$$

C.2.4. 18-inch-deep Alternate 1 Detail (18A1)

Load-Deflection and Expected Crack Pattern

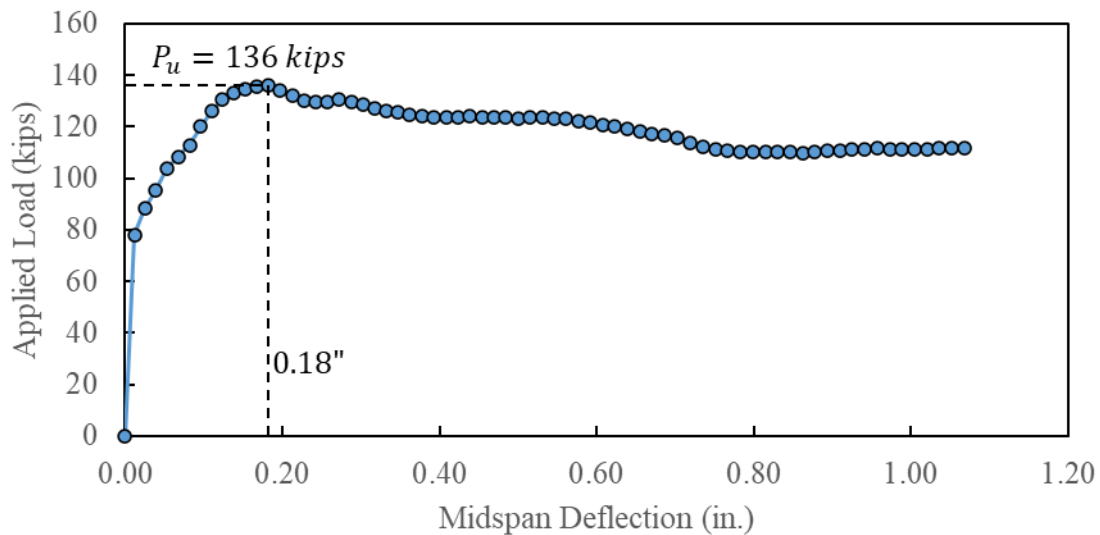


Figure C.8: Estimated load-deflection response for 18A1 specimen

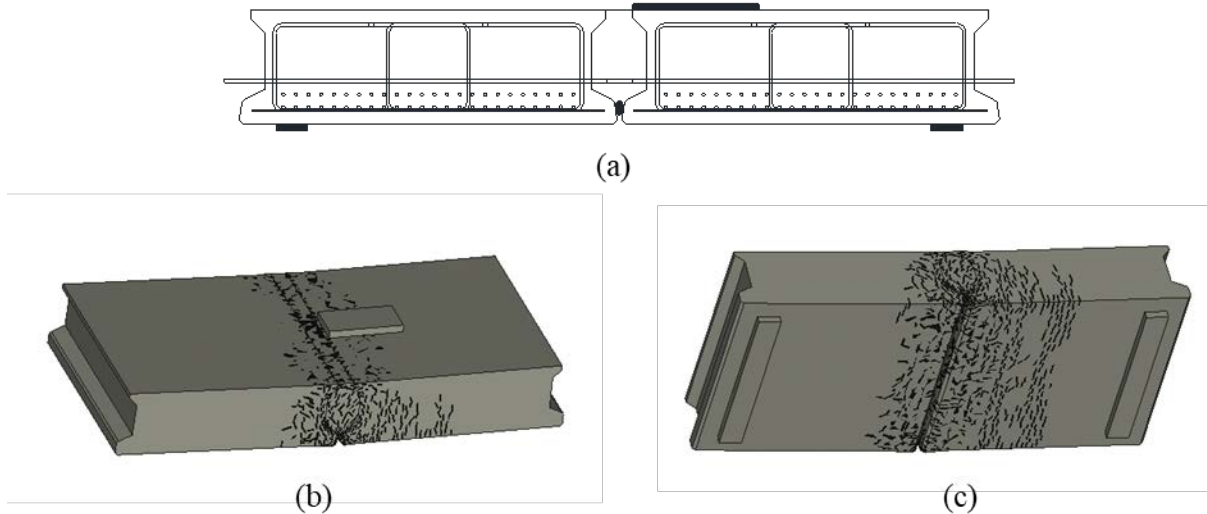
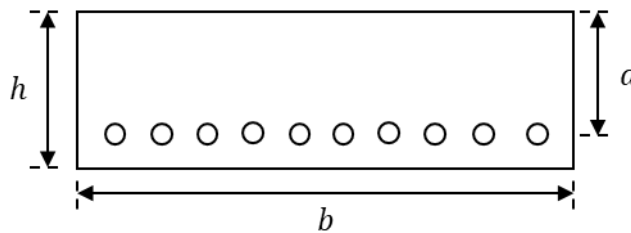


Figure C.9: (a) Specimen testing layout. (b) Top expected cracking pattern before failure and (c) bottom expected cracking pattern before failure for 18A1

Input Data



$$f'_c = 10,310 \text{ psi} \quad f_y = 65,400 \text{ psi} \quad \phi = 0.625 \text{ in} \quad A_s = 0.31 \text{ in}^2$$

$$h = 18 \text{ in} \quad b = 56 \text{ in} \quad d = 11.0625 \text{ in} \quad I_g = 27,216 \text{ in}^4$$

Nominal Moment Capacity

$$\beta_1 = 0.5345 \leq 0.65 \therefore \beta_1 = 0.65$$

$$c = \frac{(10 * 0.31 \text{ in}^2)(65.4 \text{ ksi})}{(0.85)(10.31 \text{ ksi})(0.65)(56'')} = 0.636'' \quad a = \beta_1 c = 0.4131''$$

$$\epsilon_s = 0.003 \left(\frac{d - c}{c} \right) = 0.003 \left(\frac{11.0625'' - 0.636''}{0.636''} \right) = 0.0492 > \epsilon_y$$

$$M_n = 10(0.31 \text{ in}^2)(65.4 \text{ ksi}) \left(11.0625'' - \frac{(0.65)(0.636'')}{2} \right) = 2,200.93 \text{ k''}$$

Simple Supported Beam – Uniform Load Partially Distributed

$$a = 54.875 \text{ in} \quad b = 20 \text{ in} \quad c = 28.875 \text{ in} \quad l = 103.75 \text{ in} \quad w = ?$$

$$R_1 = \frac{wb}{2l}(2c + b) \rightarrow R_1 = 7.4940w$$

$$M_{max} = R_1 \left(a + \frac{R_1}{2w} \right) \rightarrow M_{max} = 7.4940w \left(54.875 + \frac{7.4940}{2} \right) = 439.31w$$

$$M_{max} = 439.31w = 2,200.93 \text{ k}'' \rightarrow w = 5.010 \text{ k}/\text{in}$$

Application load at M_{max}

$$P_{ult} = (5.010 \text{ k}/\text{in})(20'') = 100.20 \text{ kips}$$

The cracking load can be calculated following the same procedure described previously.

Application load at M_{cr}

$$M_{cr} = 1193.59 \text{ k}'' \rightarrow w_{cr} = 2.717 \text{ k}/\text{in} \rightarrow P_{cr} = 54.34 \text{ kips}$$

C.2.5. 12-inch-deep FDOT 1 Detail (12F1)

Load-Deflection and Expected Crack Pattern

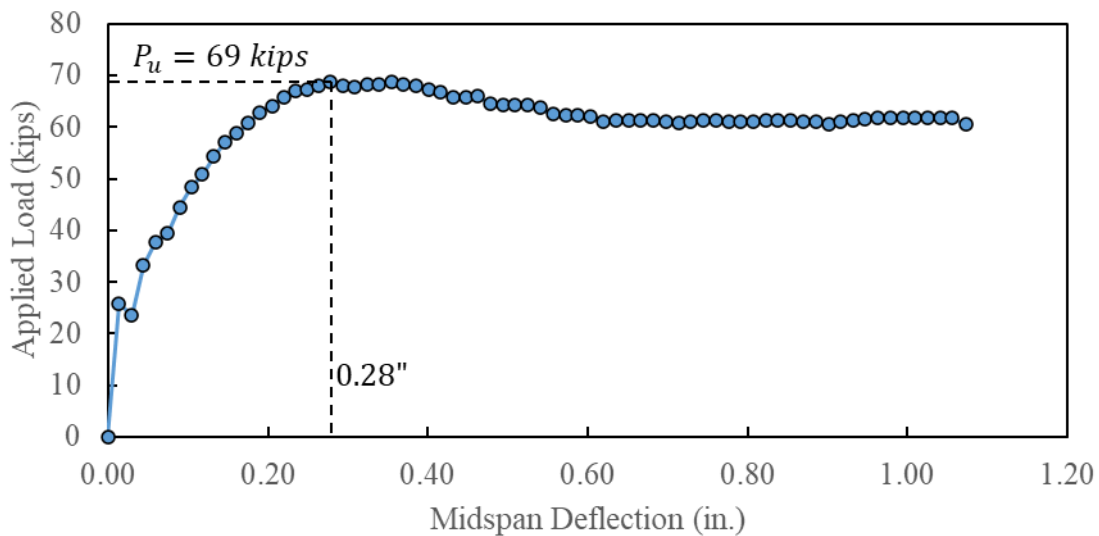


Figure C.10: Estimated load-deflection response for 12F1 specimen

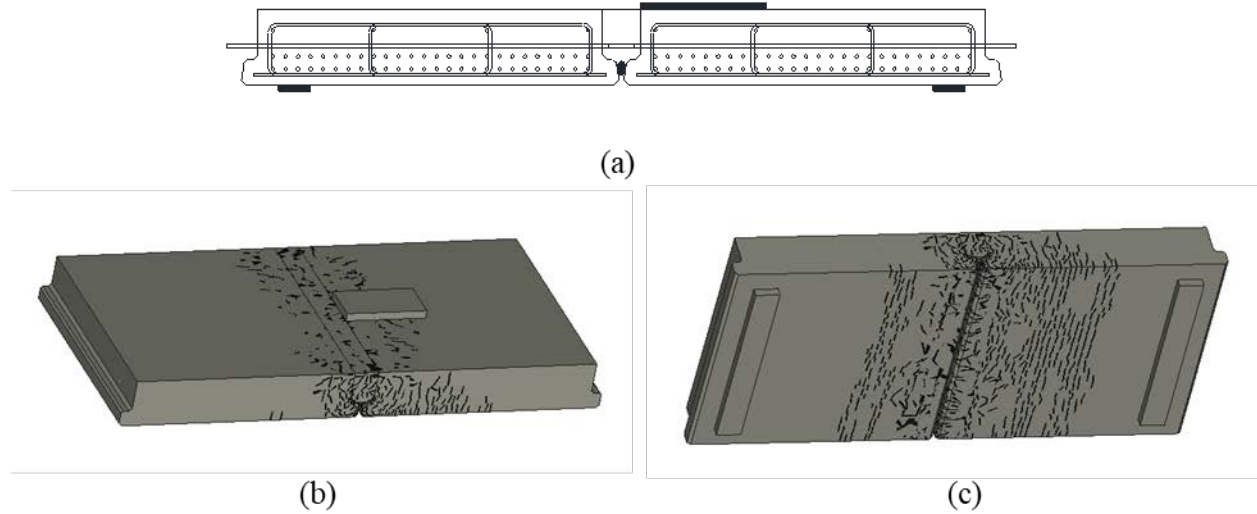
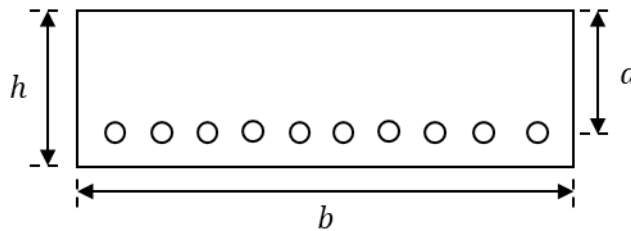


Figure C.11: (a) Specimen testing layout. (b) Top expected cracking pattern before failure and (c) bottom expected cracking pattern before failure for 12F1

Input Data



$$f'_c = 10,310 \text{ psi} \quad f_y = 65,400 \text{ psi} \quad \phi = 0.625 \text{ in} \quad A_s = 0.31 \text{ in}^2$$

$$h = 12 \text{ in} \quad b = 56 \text{ in} \quad d = 5.8125 \text{ in} \quad I_g = 8,064 \text{ in}^4$$

Nominal Moment Capacity

$$\beta_1 = 0.5345 \leq 0.65 \therefore \beta_1 = 0.65$$

$$c = \frac{(10 * 0.31 \text{ in}^2)(65.4 \text{ ksi})}{(0.85)(10.31 \text{ ksi})(0.65)(56\text{'})} = 0.636\text{'}$$

$$a = \beta_1 c = 0.4131\text{'}$$

$$\epsilon_s = 0.003 \left(\frac{d - c}{c} \right) = 0.003 \left(\frac{5.8125\text{'} - 0.636\text{'}}{0.636\text{'}} \right) = 0.0244 > \epsilon_y$$

$$M_n = 10(0.31 \text{ in}^2)(65.4 \text{ ksi}) \left(5.8125\text{'} - \frac{(0.65)(0.636\text{'})}{2} \right) = 1,136.55 \text{ k\text{'}}$$

Simple Supported Beam – Uniform Load Partially Distributed

$$a = 54.875 \text{ in} \quad b = 20 \text{ in} \quad c = 28.875 \text{ in} \quad l = 103.75 \text{ in} \quad w = ?$$

$$R_1 = \frac{wb}{2l}(2c + b) \rightarrow R_1 = 7.4940w$$

$$M_{max} = R_1 \left(a + \frac{R_1}{2w} \right) \rightarrow M_{max} = 7.4940w \left(54.875 + \frac{7.4940}{2} \right) = 439.31w$$

$$M_{max} = 439.31w = 1,136.55 \text{ k}'' \rightarrow w = 2.5871 \text{ k}/\text{in}$$

Application load at M_{max}

$$P_{ult} = (2.5871 \text{ k}/\text{in})(20'') = 51.74 \text{ kips}$$

The cracking load can be calculated following the same procedure described previously.

Application load at M_{cr}

$$M_{cr} = 540.34 \text{ k}'' \rightarrow w_{cr} = 1.230 \text{ k}/\text{in} \rightarrow P_{cr} = 24.60 \text{ kips}$$

C.2.6. 12-inch-deep FDOT 2 Detail (12F2)

Load-Deflection and Expected Crack Pattern

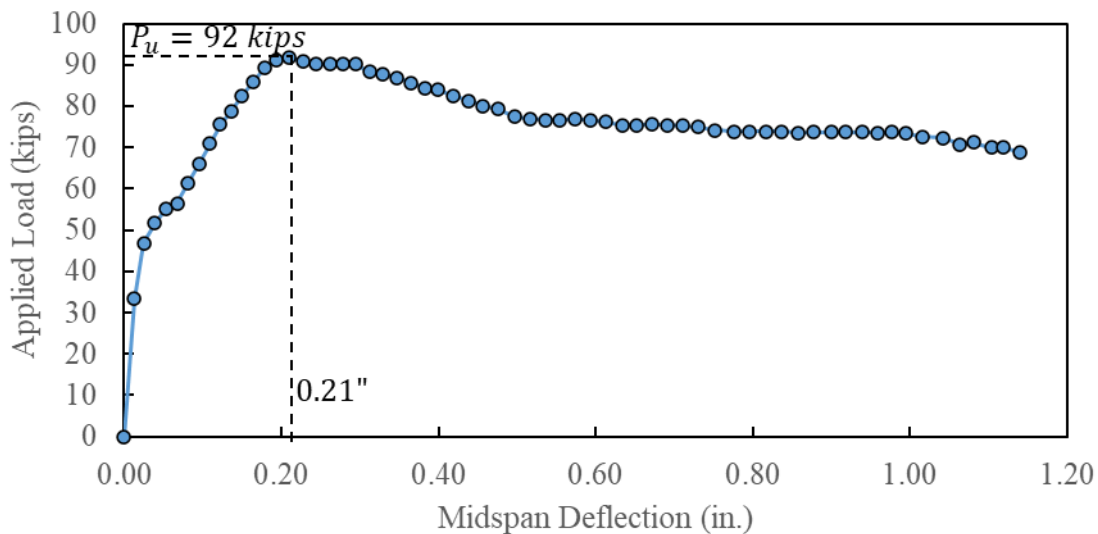
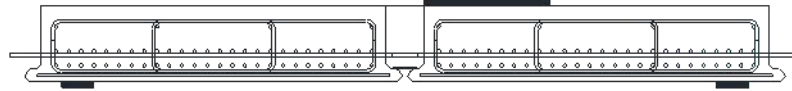
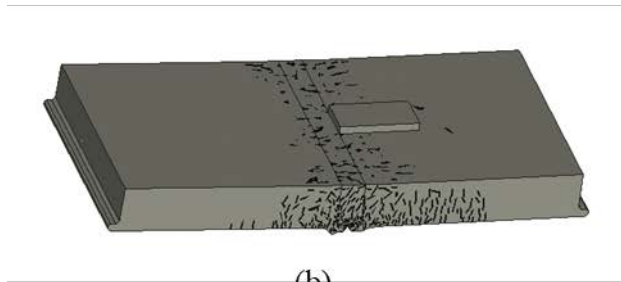


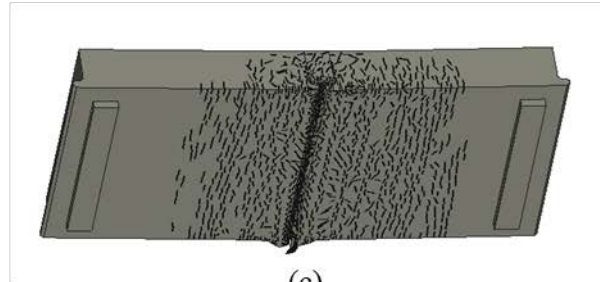
Figure C.12: Estimated load-deflection response for 12F2 specimen



(a)



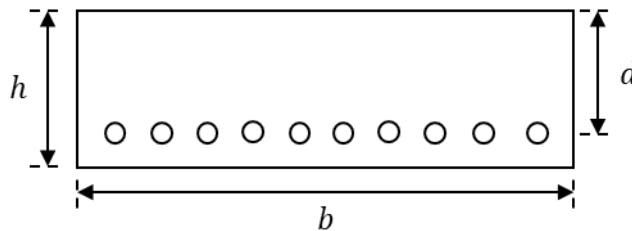
(b)



(c)

Figure C.13: (a) Specimen testing layout. (b) Top expected cracking pattern before failure and (c) bottom expected cracking pattern before failure for 12F2

Input Data



$$f'_c = 10,310 \text{ psi} \quad f_y = 65,400 \text{ psi} \quad \phi = 0.625 \text{ in} \quad A_s = 0.31 \text{ in}^2$$

$$h = 12 \text{ in} \quad b = 56 \text{ in} \quad d = 7.8125 \text{ in} \quad I_g = 8,064 \text{ in}^4$$

Nominal Moment Capacity

$$\beta_1 = 0.5345 \leq 0.65 \therefore \beta_1 = 0.65$$

$$c = \frac{(10 * 0.31 \text{ in}^2)(65.4 \text{ ksi})}{(0.85)(10.31 \text{ ksi})(0.65)(56\text{'})} = 0.636\text{'}$$

$$a = \beta_1 c = 0.4131\text{'}$$

$$\epsilon_s = 0.003 \left(\frac{d - c}{c} \right) = 0.003 \left(\frac{7.8125\text{'} - 0.636\text{'}}{0.636\text{'}} \right) = 0.0339 > \epsilon_y$$

$$M_n = 10(0.31 \text{ in.}^2)(65.4 \text{ ksi}) \left(7.8125\text{'} - \frac{(0.65)(0.636\text{'})}{2} \right) = 1,542.03 \text{ k'}$$

Simple Supported Beam – Uniform Load Partially Distributed

$$a = 54.875 \text{ in} \quad b = 20 \text{ in} \quad c = 28.875 \text{ in} \quad l = 103.75 \text{ in} \quad w = ?$$

$$R_1 = \frac{wb}{2l}(2c + b) \rightarrow R_1 = 7.4940w$$

$$M_{max} = R_1 \left(a + \frac{R_1}{2w} \right) \rightarrow M_{max} = 7.4940w \left(54.875 + \frac{7.4940}{2} \right) = 439.31w$$

$$M_{max} = 439.31w = 1,542.03 \text{ k}'' \rightarrow w = 3.5101 \text{ k}/\text{in}$$

Application load at M_{max}

$$P_{ult} = (3.5101 \text{ k}/\text{in})(20'') = 70.20 \text{ kips}$$

The cracking load can be calculated following the same procedure described previously.

Application load at M_{cr}

$$M_{cr} = 540.34 \text{ k}'' \rightarrow w_{cr} = 1.230 \text{ k}/\text{in} \rightarrow P_{cr} = 24.60 \text{ kips}$$

C.2.7. 12-inch-deep Alternate 1 Detail (12A1)

Load-Deflection and Expected Crack Pattern

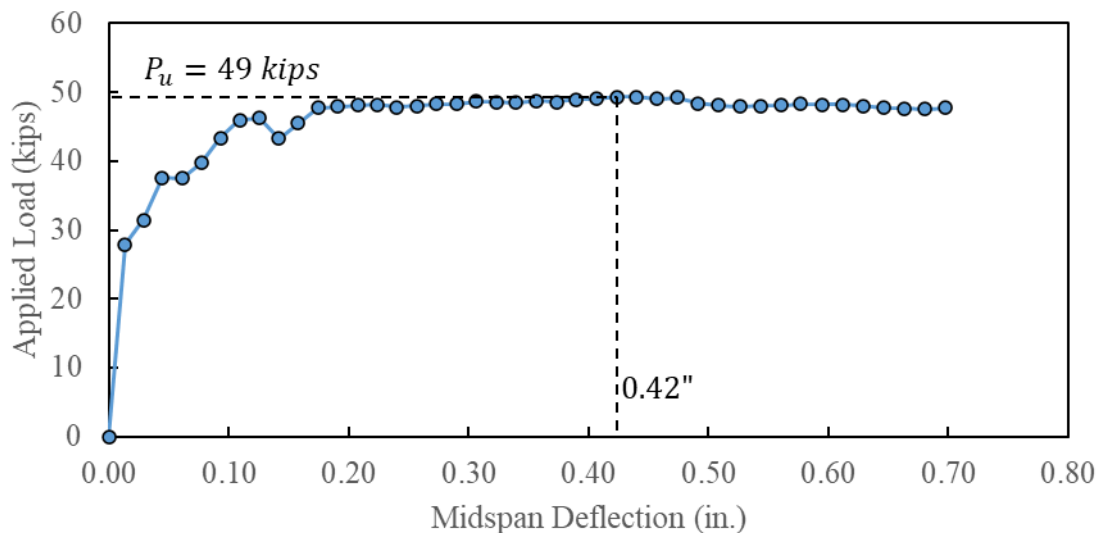


Figure C.14: Estimated load-deflection response for 12A1 specimen

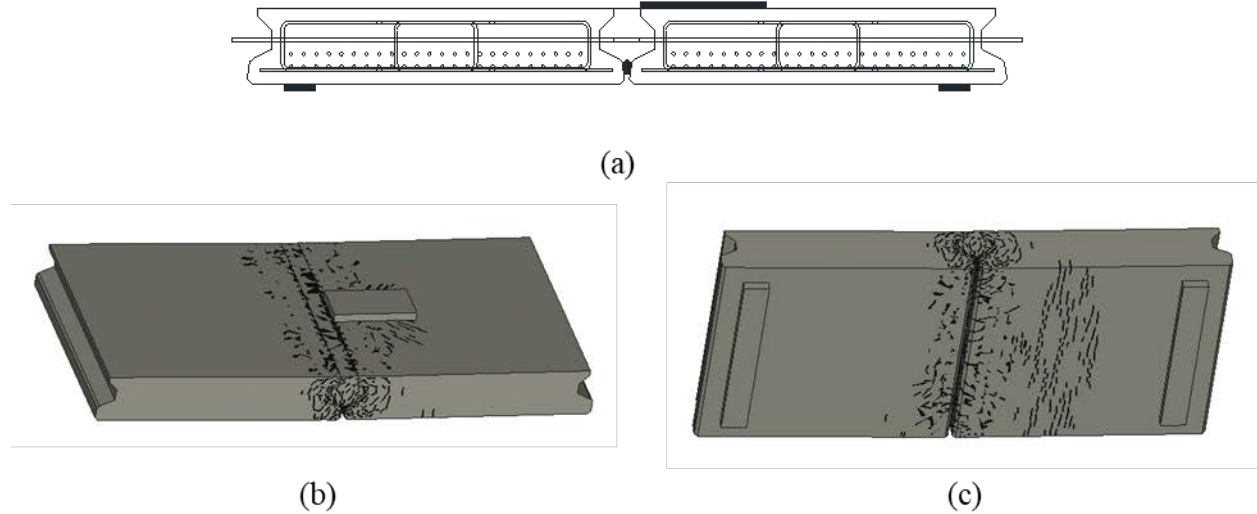
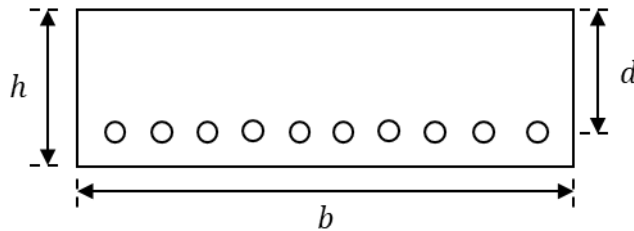


Figure C.15: (a) Specimen testing layout. (b) Top expected cracking pattern before failure and (c) bottom expected cracking pattern before failure for 12A1

Input Data



$$f'_c = 10,310 \text{ psi} \quad f_y = 65,400 \text{ psi} \quad \phi = 0.625 \text{ in} \quad A_s = 0.31 \text{ in}^2$$

$$h = 12 \text{ in} \quad b = 56 \text{ in} \quad d = 5.0625 \text{ in} \quad I_g = 8,064 \text{ in}^4$$

Nominal Moment Capacity

$$\beta_1 = 0.5345 \leq 0.65 \therefore \beta_1 = 0.65$$

$$c = \frac{(10 * 0.31 \text{ in}^2)(65.4 \text{ ksi})}{(0.85)(10.31 \text{ ksi})(0.65)(56'')} = 0.636'' \quad a = \beta_1 c = 0.4131''$$

$$\epsilon_s = 0.003 \left(\frac{d - c}{c} \right) = 0.003 \left(\frac{5.0625'' - 0.636''}{0.636''} \right) = 0.0209 > \epsilon_y$$

$$M_n = 10(0.31 \text{ in.}^2)(65.4 \text{ ksi}) \left(5.0625'' - \frac{(0.65)(0.636'')}{2} \right) = 984.49 \text{ k''}$$

Simple Supported Beam – Uniform Load Partially Distributed

$$a = 54.875 \text{ in} \quad b = 20 \text{ in} \quad c = 28.875 \text{ in} \quad l = 103.75 \text{ in} \quad w = ?$$

$$R_1 = \frac{wb}{2l}(2c + b) \rightarrow R_1 = 7.4940w$$

$$M_{max} = R_1 \left(a + \frac{R_1}{2w} \right) \rightarrow M_{max} = 7.4940w \left(54.875 + \frac{7.4940}{2} \right) = 439.31w$$

$$M_{max} = 439.31w = 984.49 \text{ k}'' \rightarrow w = 2.2410 \text{ k}/\text{in}$$

Application load at M_{max}

$$P_{ult} = (2.2410 \text{ k}/\text{in})(20'') = 44.82 \text{ kips}$$

The cracking load can be calculated following the same procedure described previously.

Application load at M_{cr}

$$M_{cr} = 540.34 \text{ k}'' \rightarrow w_{cr} = 1.230 \text{ k}/\text{in} \rightarrow P_{cr} = 24.60 \text{ kips}$$

C.2.8. 12-inch-deep Alternate 2 Detail (12A2)

Load-Deflection and Expected Crack Pattern

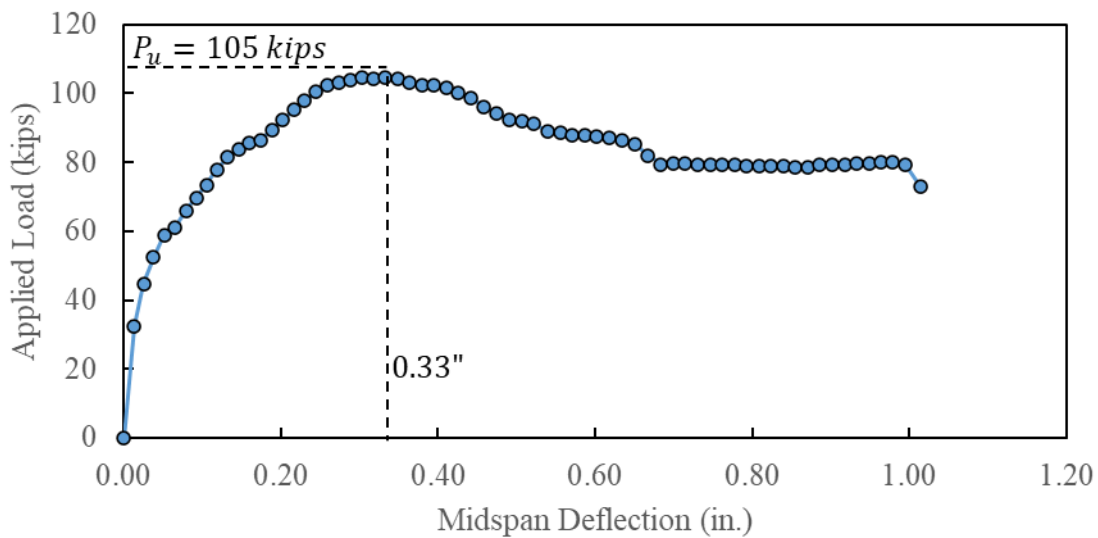
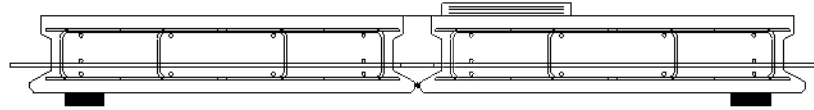
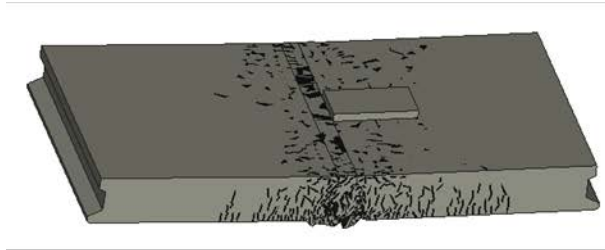


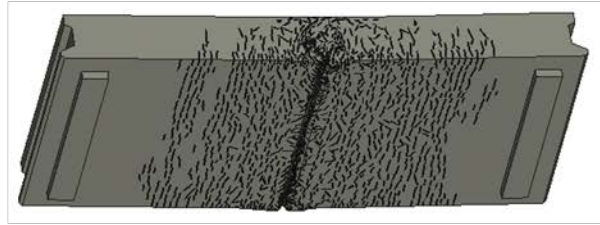
Figure C.16: Estimated load-deflection response for 12A2 specimen



(a)



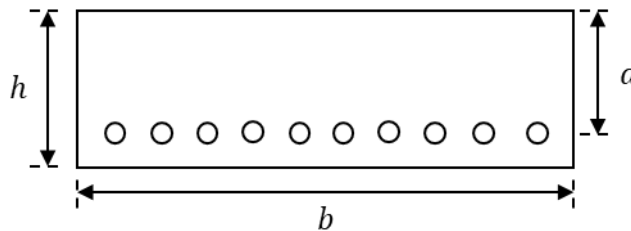
(b)



(c)

Figure C.17: (a) specimen testing layout, (b) top expected cracking pattern before failure, and (c) bottom expected cracking pattern before failure for 12A2

Input Data



$$f'c = 10,310 \text{ psi} \quad f_y = 65,400 \text{ psi} \quad \phi = 0.625 \text{ in} \quad A_s = 0.31 \text{ in}^2$$

$$h = 12 \text{ in} \quad b = 56 \text{ in} \quad d = 7.625 \text{ in} \quad I_g = 8,064 \text{ in}^4$$

Nominal Moment Capacity

$$\beta_1 = 0.5345 \leq 0.65 \therefore \beta_1 = 0.65$$

$$c = \frac{(10 * 0.31 \text{ in}^2)(65.4 \text{ ksi})}{(0.85)(10.31 \text{ ksi})(0.65)(56\text{'})} = 0.636\text{'}$$

$$a = \beta_1 c = 0.4131\text{'}$$

$$\epsilon_s = 0.003 \left(\frac{d - c}{c} \right) = 0.003 \left(\frac{7.625\text{'} - 0.636\text{'}}{0.636\text{'}} \right) = 0.033 > \epsilon_y$$

$$M_n = 10(0.31 \text{ in.}^2)(65.4 \text{ ksi}) \left(7.625\text{'} - \frac{(0.65)(0.636\text{'})}{2} \right) = 1503.99 \text{ k'}$$

Simple Supported Beam – Uniform Load Partially Distributed

$$a = 54.875 \text{ in} \quad b = 20 \text{ in} \quad c = 28.875 \text{ in} \quad l = 103.75 \text{ in} \quad w = ?$$

$$R_1 = \frac{wb}{2l} (2c + b) \rightarrow R_1 = 7.4940w$$

$$M_{max} = R_1 \left(a + \frac{R_1}{2w} \right) \rightarrow M_{max} = 7.4940w \left(54.875 + \frac{7.4940}{2} \right) = 439.31w$$

$$M_{max} = 439.31w = 1503.99 \text{ k}'' \rightarrow w = 3.4235 \text{ k}/\text{in}$$

Application load at M_{max}

$$P_{ult} = (3.4235 \text{ k}/\text{in})(20'') = 68.47 \text{ kips}$$

The cracking load can be calculated following the same procedure described previously.

Application load at M_{cr}

$$M_{cr} = 540.34 \text{ k}'' \rightarrow w_{cr} = 1.230 \text{ k}/\text{in} \rightarrow P_{cr} = 24.60 \text{ kips}$$

D. RESULTS OF SMALL-SCALE SPECIMENS

D.1. INTRODUCTION

All the results from the small-scale specimen testing are summarized in this section. A summary of all the measured cracking loads, ultimate capacities, and deflections at ultimate capacity is provided in Table D.1. Results for each individual specimen are presented. An analysis of these results is presented in the body of the report.

Table D.1: Summary of measured cracking and maximum loads for each specimen

Specimen ID	Cracking Loads					Reported Results		
	$P_{cr,visual}$ (kips)	$P_{cr,P-\Delta}$ (kips)	$P_{cr,RSG}$ (kips)	$P_{cr,CDT}$ (kips)	$P_{cr,CSG}$ (kips)	P_{cr} (kips)	P_{max} (kips)	Δ at P_{max} (in)
FSB-1	45	33.3	33.3	34.2	28.1	28.1	63.4	-1.37
FSB-2	10	22.6	23.1	22.3	22.2	22.2	36.4	-0.63
18F1-1	40	24.5	26.4	24.7	24.3	24.3	149.9	-0.52
18F1-2	40	26.7	28.8	28.2	29.3	29.3	149.5	-0.61
18F2-1	60	33.2	40.5	42.5	24.9	24.9	170.2	-0.58
18F2-2	50	51.1	58.6	55.1	56.9	56.9	177.0	-0.72
18A1-1	30	11.7 ^Δ	15.6 ^Δ	15.4 ^Δ	46.5	46.5	154.4	-1.56
18A1-2	40	29.1	38.6	32.2	26.1	26.1	146.1	-1.01
12F1-1	30	20.8	#	#	21.3	21.3	70.0	-1.36
12F1-2*	--	--	--	--	--	--	66.9	-0.52
12F2-1	45	14.8	15.5	16.1	23.5	23.5	98.1	-1.32
12F2-2	15	20.4	23.9	22.4	27.8	27.8	99.4	-0.96
12A1-1	30	13.4	10.6	10.1	22.1	22.1	61.0	-1.25
12A1-2*	--	--	--	--	--	--	67.5	-2.22
12A2-1	25	12.1	12.1	14.1	22.1	22.1	90.9	-1.67
12A2-2*	--	--	--	--	--	--	100.5	-2.05

* cyclic testing conducted prior to strength testing for this joint; members were cracked during the fatigue testing, so no cracking load is reported here

^Δ small initial drop in stiffness was recorded at a low load; results from CSG were used for cracking load

no immediate change in stiffness could be detected

D.2. INSTRUMENTATION LABELING

Measurements from all the instrumentation is presented in this appendix, so the location and labeling for all the gauges is highlighted in Figure D.1. Note that generally the north beam was loaded during testing.

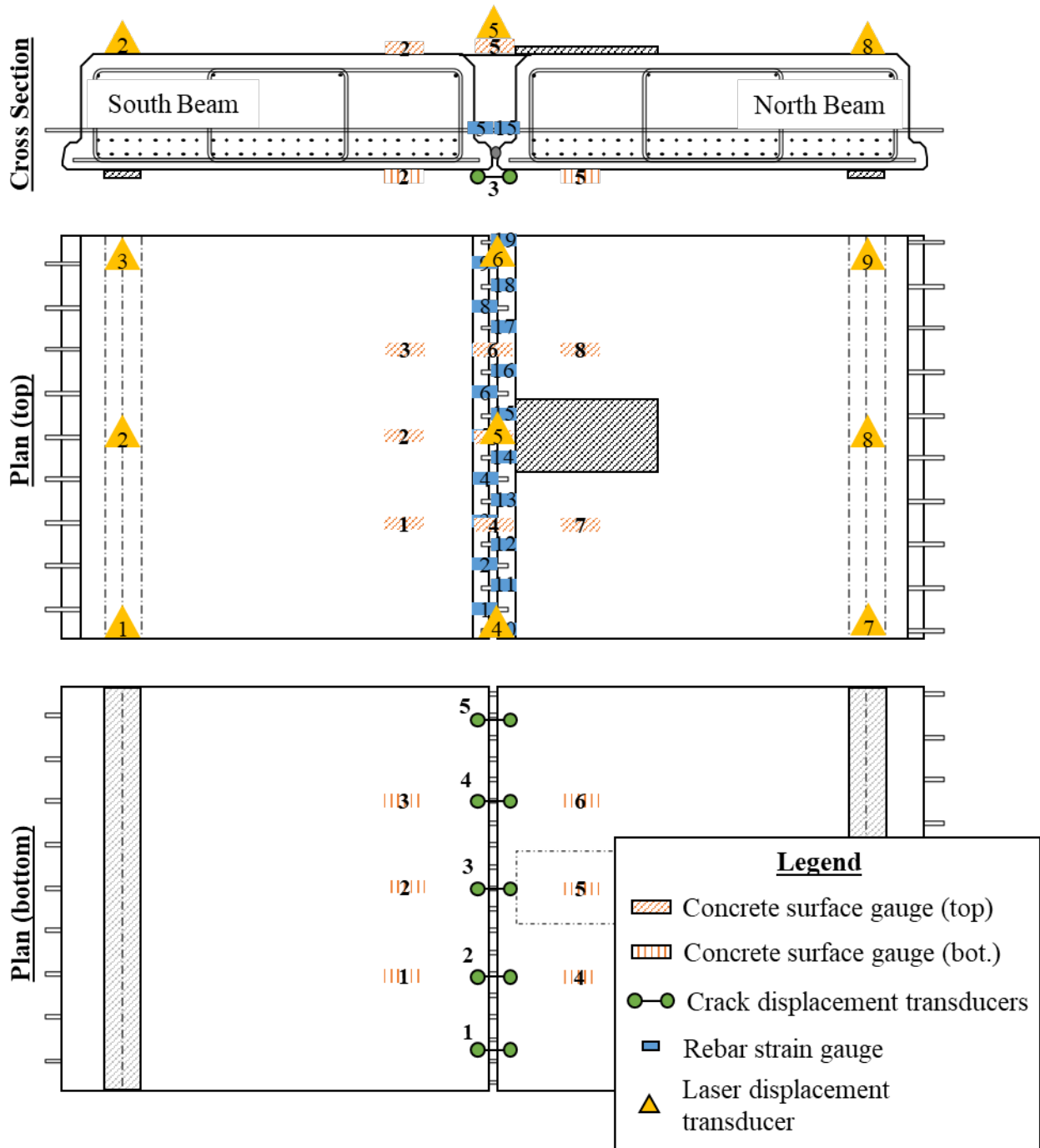


Figure D.1: Instrumentation labels for gauges

D.3. FAILURE MODES

There were two primary failure modes that were observed in the joint specimens:

1. Pull-out failure of joint reinforcement
2. Crushing of concrete along top of joint and fracture of joint reinforcement

D.4. 18-INCH SPECIMENS

The results and observations for each of the experimental static load tests on the 18-inch deep specimens are presented in this section including: the total capacity of each joint specimen, type of failure, comments on UHPC performance (adequate or faulty mix, type of bond achieved, etc.), and comments on joint rebar performance (yielding, breaking, bending, etc.). Figures are provided (including photos from failure) to describe the failure mechanism of each joint geometry.

D.4.1. FSB Control

The strength testing result observations describing the failure forces, type of failures, and concrete and rebar behaviors for the FSB Control specimens are highlighted in Table D.2. Both tests on the control FSB had much lower capacities than expected: due to development of the joint reinforcement controlling the capacity.

Table D.2: FSB Control Strength testing summary

Test	Failure Force [kip]	Type of Failure	Concrete Comments	Rebar Comments
FSB-1	63.4	Development failure of hooked bars	<ul style="list-style-type: none"> • Adequate bond between CIP Deck and precast section • Large crack located at the vertical leg of hook in joint reinforcement • Concrete crushes in the joint as hooked joint reinforcement pulled out 	<ul style="list-style-type: none"> • Transverse joint reinforcement did not break or yield • Longitudinal rebar in joint cage bent as the transverse joint reinforcement pulled out
FSB-2	36.4	Development failure of hooked bars	<ul style="list-style-type: none"> • CIP deck concrete had much lower strength than specified • Large crack located at the vertical leg of hook in joint reinforcement • Joint concrete crumbled apart when specimen failed 	<ul style="list-style-type: none"> • Transverse joint reinforcement did not break or yield • Joint reinforcement could be uncovered after testing by brushing away poor concrete

D.4.1.1. Test 1 (FSB-1)

FSB-1 had a much lower ultimate capacity than expected. The failure of FSB-1 is shown in Figure D.2 and FSB-1 after the beams were removed from the test setup is shown in Figure D.3. A large crack developed in the FSB-1 joint region at the location of the vertical leg of the hooked joint

reinforcement, shown in Figure D.2 (a) and (c). Additionally, there was some spalling of the concrete at the top of the deck when the failure occurred, as shown in Figure D.2 (d).

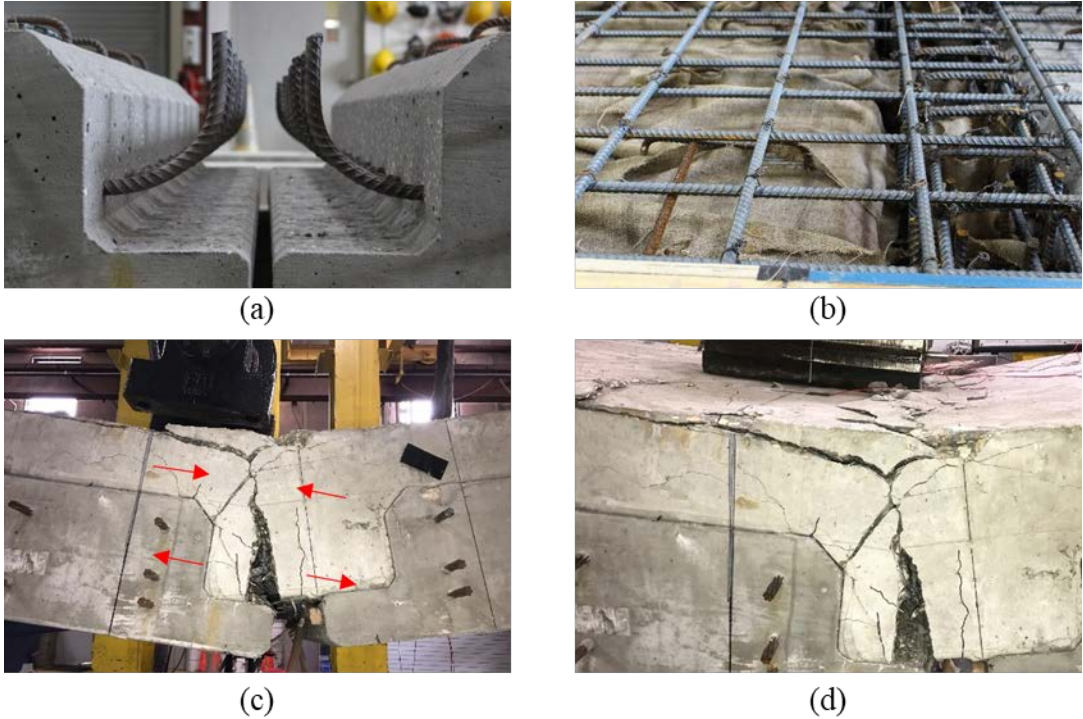


Figure D.2: FSB-1: (a) transverse joint reinforcement, (b) full joint and deck reinforcement before casting, (c) side view of failure, and (d) top view of failure

The failed specimen after it was removed from the test setup is shown in Figure D.3. The specimen split in half at the failure crack when being removed from the test setup. The hooked joint reinforcement all pulled out from the other joint reinforcement. This resulted in the crushing of the concrete in the joint behind the vertical leg of the hook, highlighted in Figure D.3 (b), and the bending of the longitudinal reinforcement in the joint, highlighted in Figure D.3 (c). Finally, some loss of bond was observed in the loaded beam close to the top chamfer, highlighted in Figure D.3 (d).

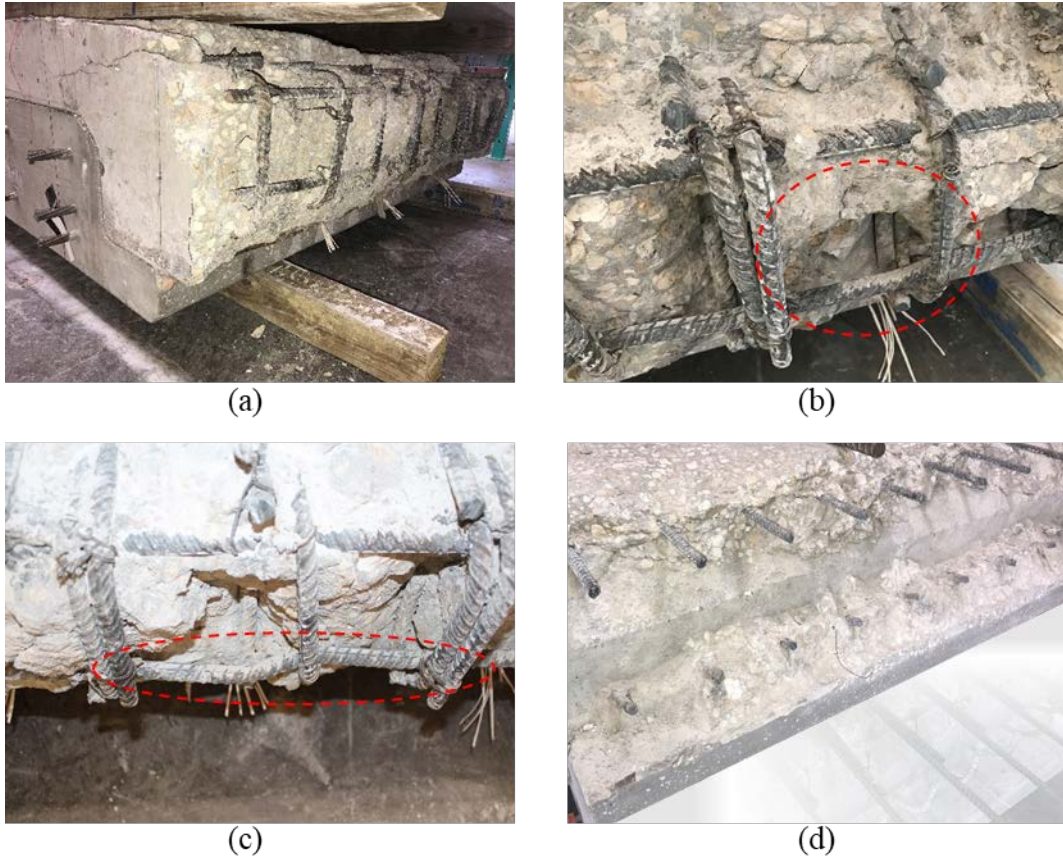


Figure D.3: (a) Unloaded side of control specimen after failure, (b) Concrete rupture inside caged matrix, (c) Longitudinal rebar bend, and (d) Bond loss of CIP deck

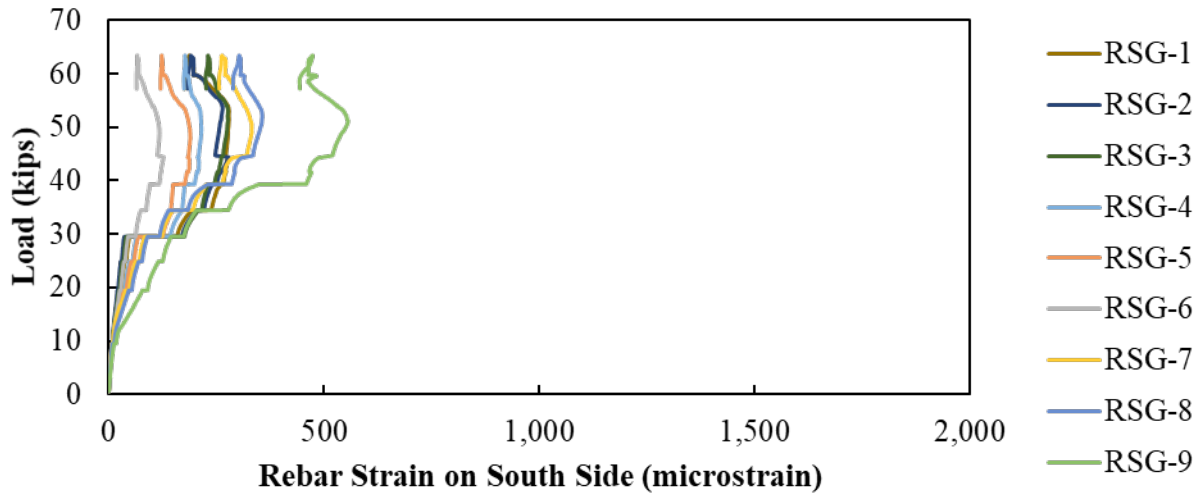
The load versus rebar strain gauge data for all the joint reinforcements are shown in Figure D.4 (a) for the south beam and Figure D.4 (b) for the north beam. The north beam was loaded for FSB-1. The load versus bottom opening data from the CDT is shown in Figure D.4 (c) up until when the gauges were removed. The load versus concrete strain responses are shown in Figure D.5 (a) for bottom gauges, including when the cracking load was observed in Figure D.5 (b), and load versus strain response for the top concrete surface gauges in Figure D.5 (c).

Several observations can be made for these plots:

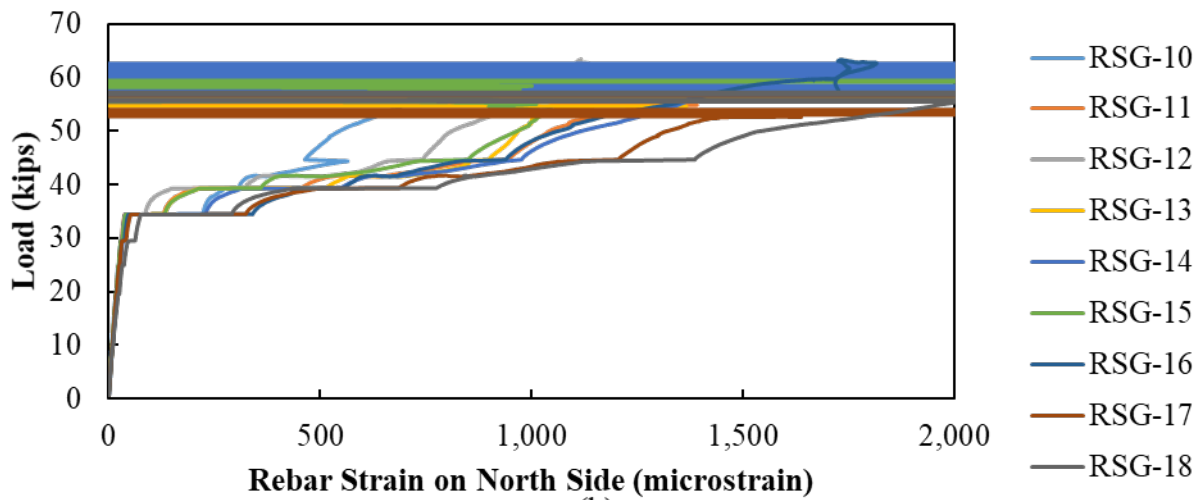
1. **Determining cracking load:** The cracking point can be determined when the load versus strain plots have a change in slope for the reinforcement, Figure D.4 (a) and (b), and bottom opening gauges, Figure D.4 (c). Cracking in the beam will change the stiffness of the joint. It will also result in tensile stress being transferred from the concrete to the joint reinforcement. The cracking load can also be found by looking at when the bottom concrete surface gauges stopped increasing in tensile strain, shown in Figure D.5 (a) and (b). Before cracking, all the bottom fiber concrete will carry tensile stresses. After cracking, tensile stresses will decrease in the concrete surrounding the crack and compressive stress may develop. The decrease in tensile stress signifies cracking.

2. ***Strain concentration at failure crack:*** Because there was one primary failure crack and hinging next the support (highlighted in Figure D.2), the reinforcement on the loaded side of the joint increased in strain at a faster rate than on the unloaded side of the joint. This can be seen by the much larger rebar strains in Figure D.4 (b) compared to Figure D.4 (a).
3. ***Larger concrete strains on loaded side prior to cracking:*** As would be expected, there were larger concrete strains on the loaded side of the beams: CSG-B4, CSG-B5, and CSG-B6 on the loaded side consistently had larger strains than CSG-B1, CSG-B2, and CSG-B3 on the unloaded side, shown in Figure D.5 (b).
4. ***Reasonably even strain distribution across width:*** There was a reasonable distribution of the strains across the entire joint width. All the rebar across the width was equally engaged prior to cracking and then similarly engaged after cracking, shown in Figure D.4 (b). The top concrete strain gauges had similar strains across the width of the specimens, shown in Figure D.5 (c): e.g. CSG-T4, CSG-T5, and CSG-T6 had similar strains.
5. ***Largest concrete strains over joint on top of specimen:*** The largest top concrete strains were observed over the joint, shown in Figure D.5 (c) with CSG-T4, CSG-T5, and CSG-T6 having the largest strains. This is likely a result of the joint concrete being weaker than the concrete in the precast section. This can be confirmed by comparing the same gauges for the UHPC joints where the joint concrete is stronger than the precast concrete.

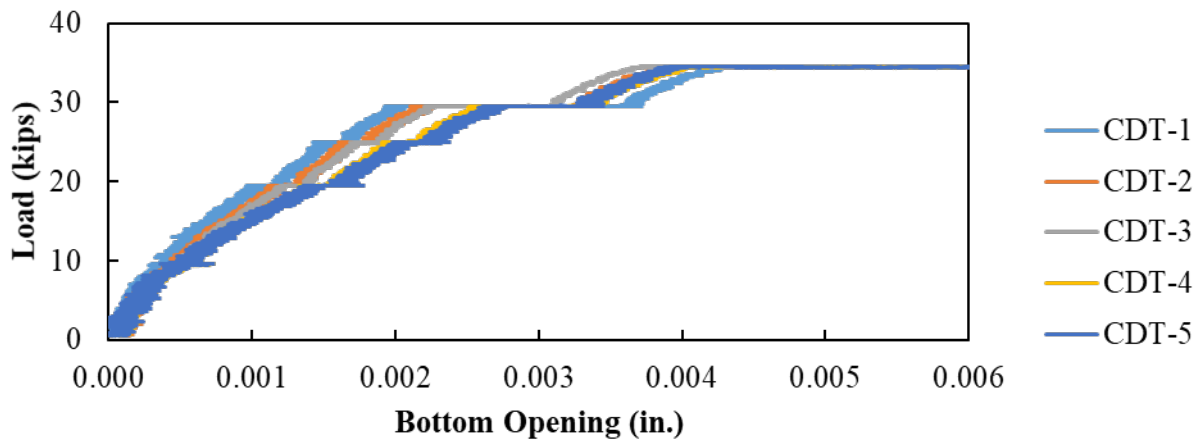
Some of these observations will be the same for future specimens; these observations will be highlighted for future specimens but may not be discussed in as much detail.



(a)

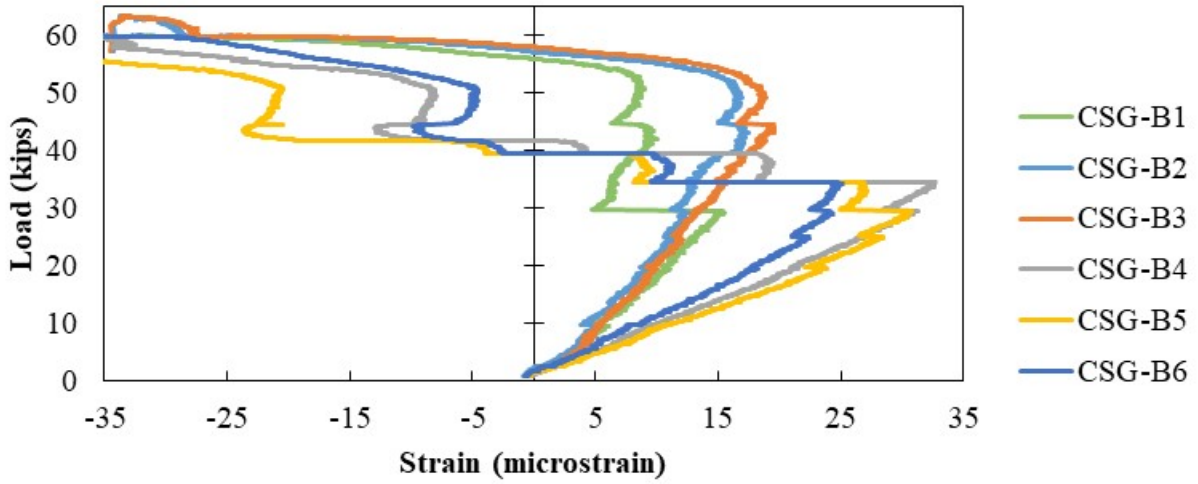


(b)

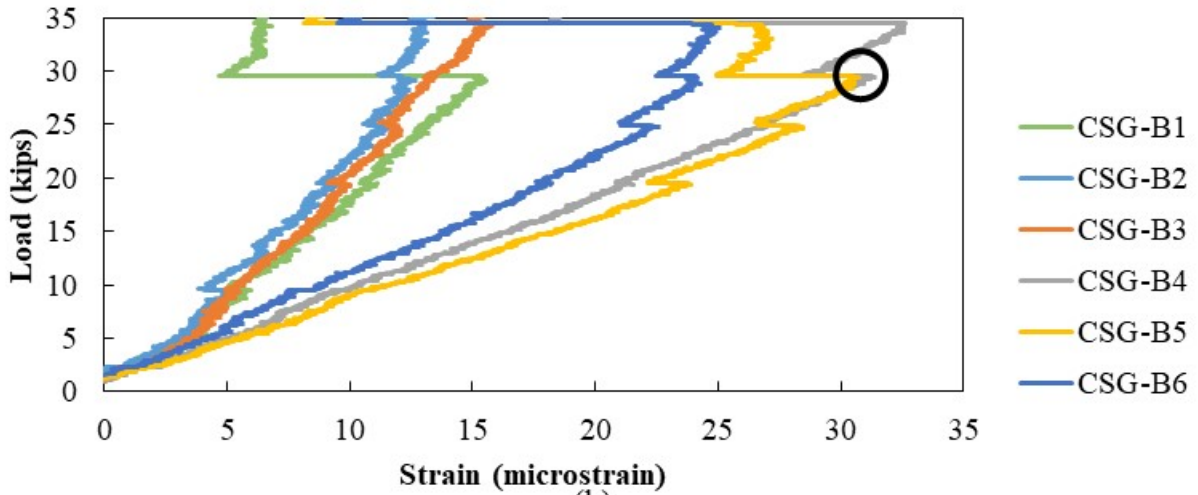


(c)

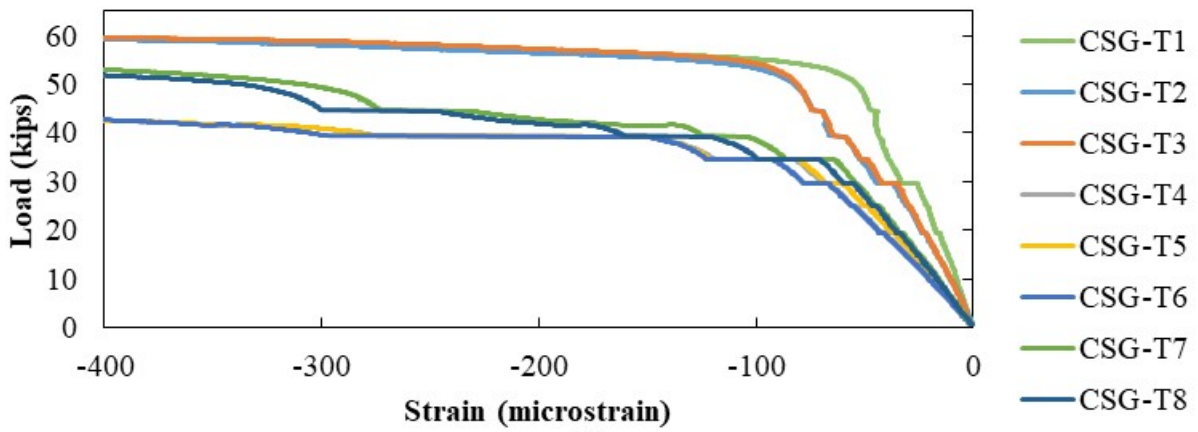
Figure D.4: FSB-1 response: (a) load versus rebar strain on south side, (b) load versus rebar strain on north side, and (c) load versus central bottom opening



(a)



(b)



(c)

Figure D.5: FSB-1 response: (a) load versus bottom concrete strain, (b) cracking load determination based on load versus bottom concrete strain response, and (c) load versus top concrete strain

D.4.1.2. Test 2 (FSB-2)

A larger longitudinal bar (#6 instead of #5) was used in the joint to try and increase the joint capacity. However, the second test on the control FSB (FSB-2) resulted in a lower capacity than FSB-1. A similar failure mechanism occurred in FSB-2, but the deck and joint concrete was a much lower strength than in FSB-1. The failure crack for FSB-2 also developed at the location of the vertical leg of the hooked joint reinforcement, as shown in Figure D.6 (a) and (b). The joint reinforcement was of such poor quality, shown in Figure D.6 (c), that the joint reinforcement pulled out without significant deformation, shown in Figure D.6 (d).

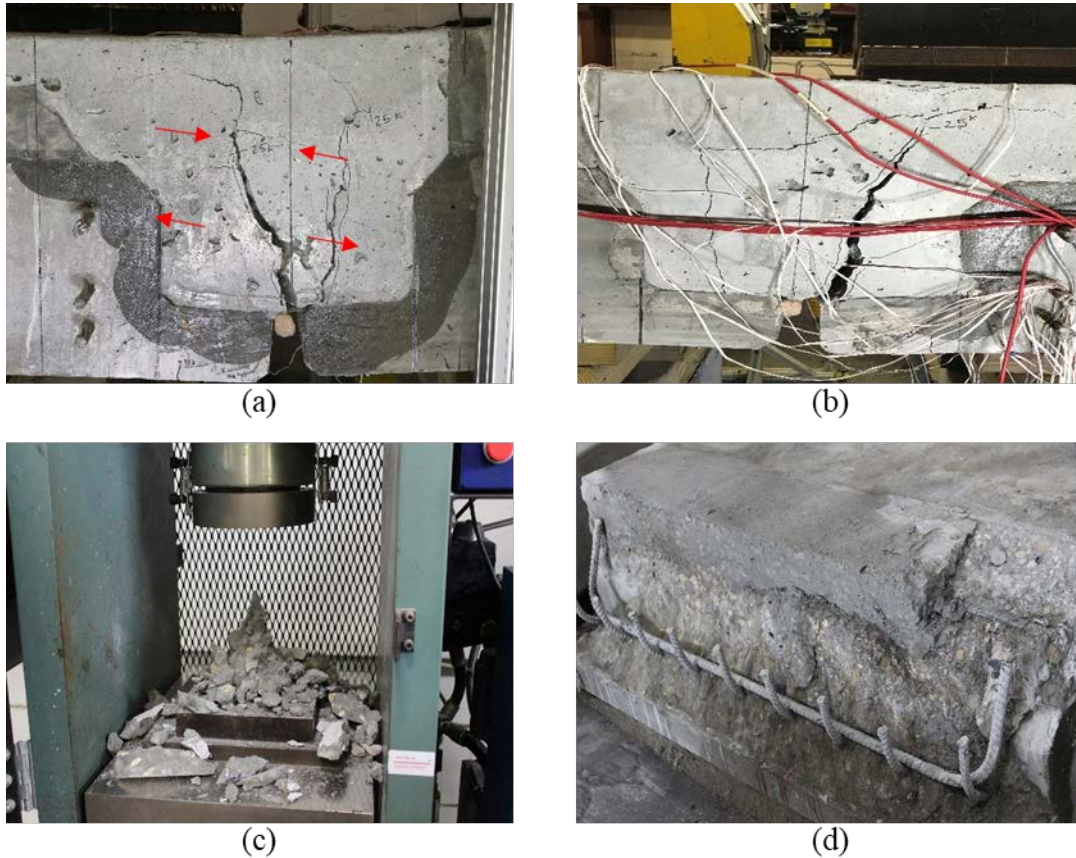
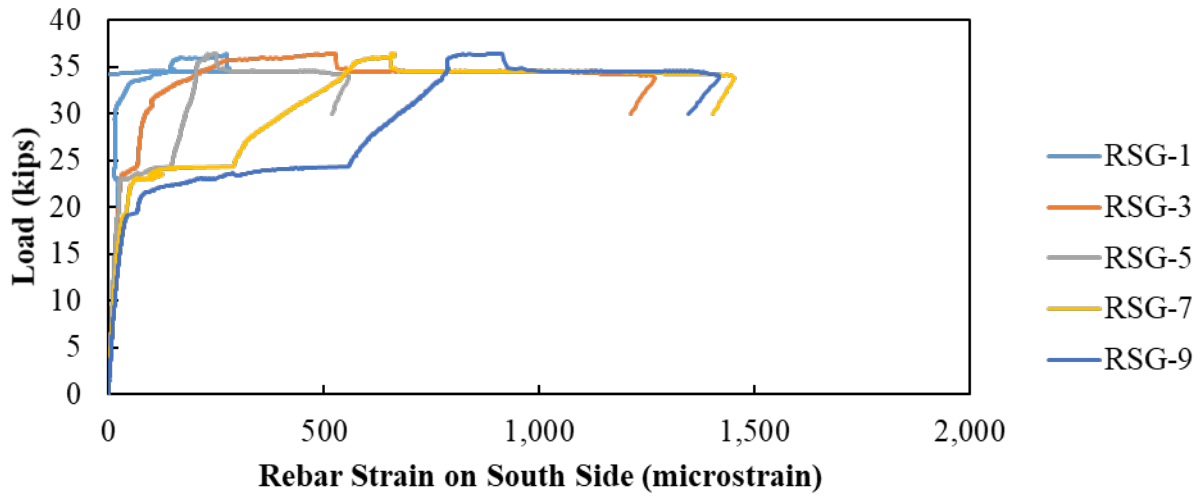
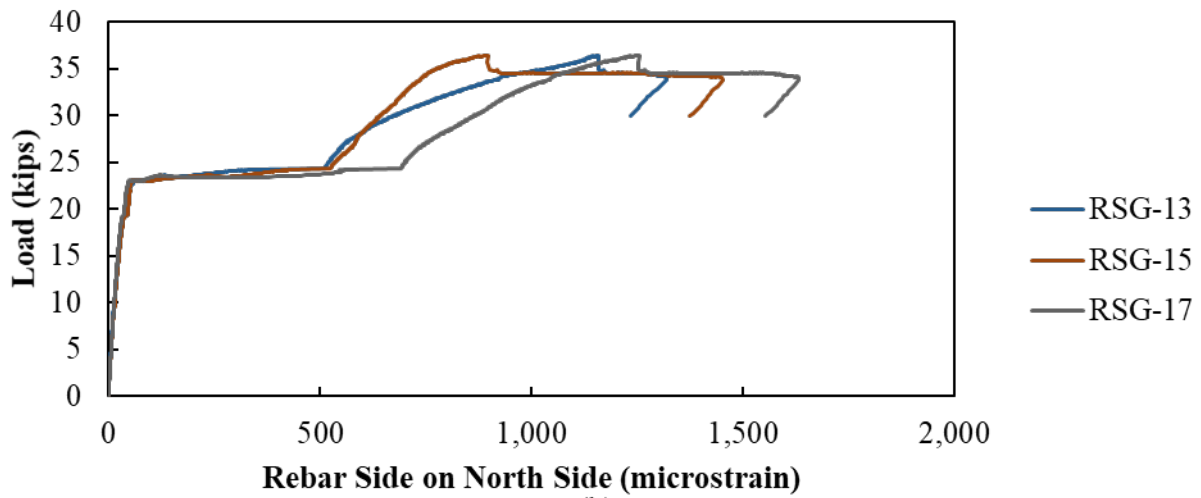


Figure D.6: FSB-2: (a) crack pattern in CIP deck concrete failure, (b) greater crack pattern in CIP deck concrete failure, (c) CIP deck concrete cylinder failure, and (d) exposed joint reinforcement after failure

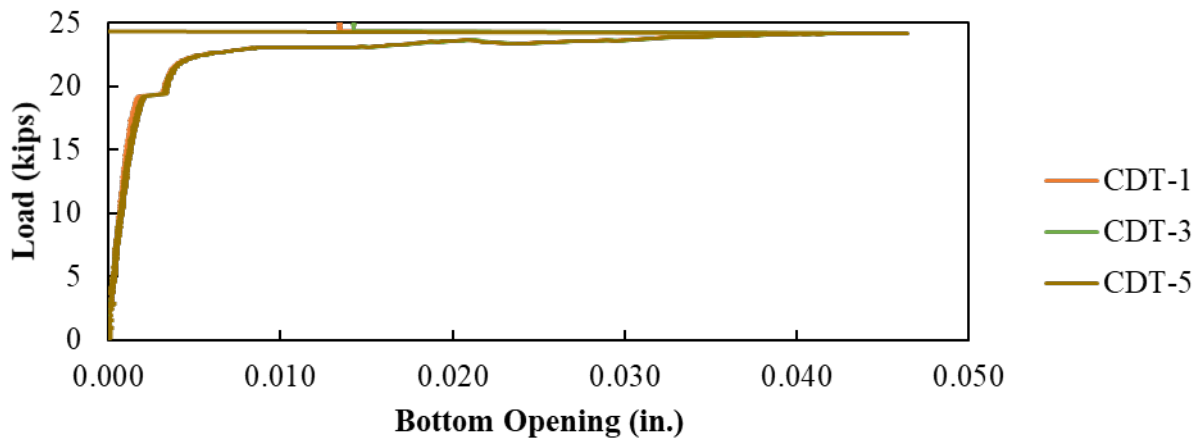
The load versus rebar strain gauge data for all the joint reinforcements is presented in Figure D.7 (a) for the south beam and Figure D.7 (b) for the north beam. The load versus bottom opening data from the CDT gauges is shown in Figure D.7 (c) up until when the gauges were removed. The load versus concrete strain responses are shown in Figure D.8 (a) for bottom gauges, including when the cracking load was observed in Figure D.8 (b), and load versus top gauge response in Figure D.8 (c). The FSB-2 response was similar to FSB-1.



(a)

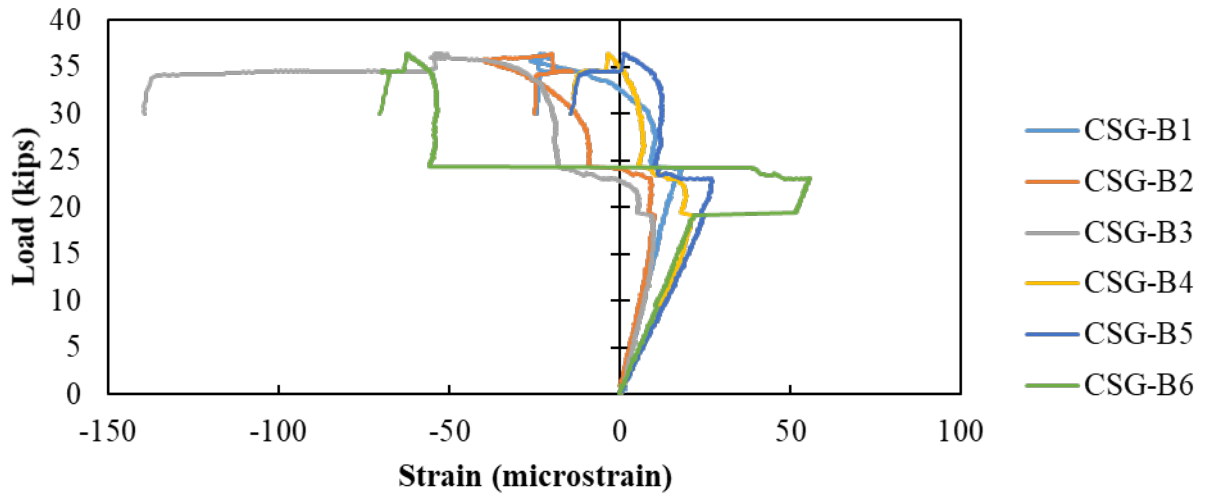


(b)

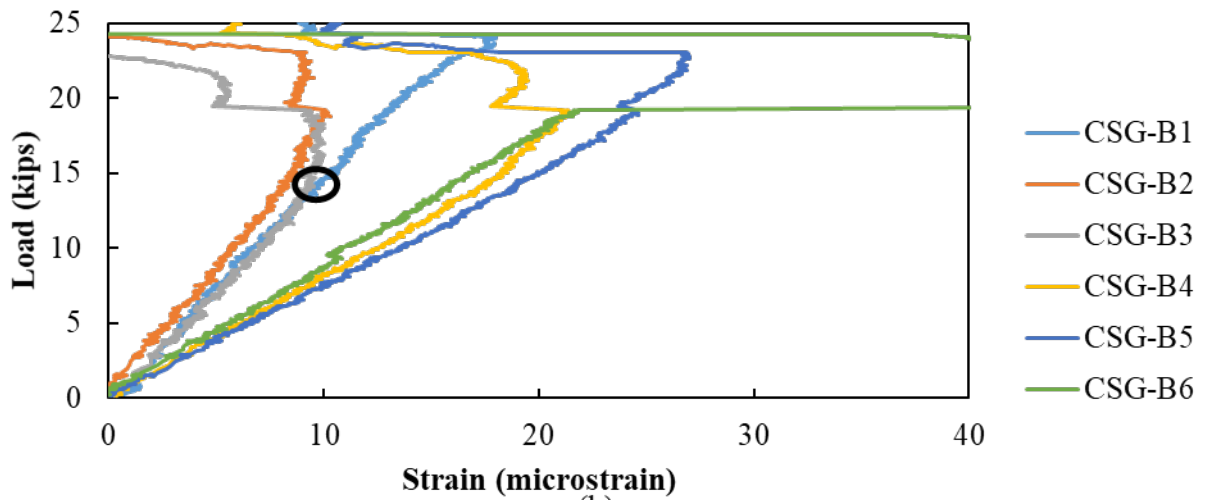


(c)

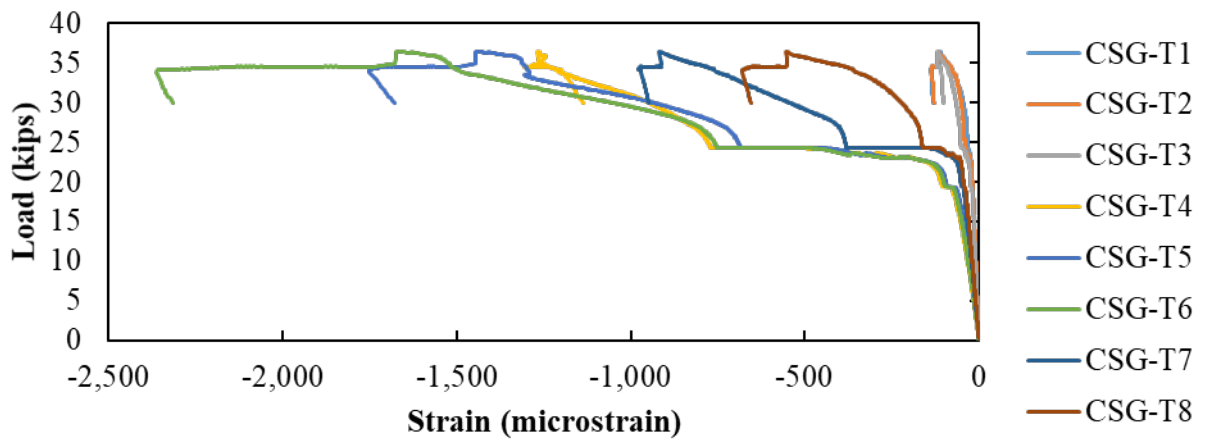
Figure D.7: FSB-2 response: (a) load versus rebar strain on south side, (b) load versus rebar strain on north side, and (c) load versus central bottom opening



(a)



(b)



(c)

Figure D.8: FSB-2 response: (a) load versus bottom concrete strain, (b) cracking load determination based on load versus bottom concrete strain response, and (c) load versus top concrete strain

D.4.2. 18F1 (FDOT 1)

The strength testing result observations describing the failure forces, type of failures, and concrete and rebar behaviors for the 18F1 specimens are highlighted in Table D.3.

Table D.3: 18F1 Strength testing summary

Test	Failure Force [kip]	Type of Failure	Concrete Comments	Rebar Comments
18F1-1	149.9	Pull-out failure	<ul style="list-style-type: none"> Poor bond between UHPC and precast beam Rupture of UHPC at the level of steel 	<ul style="list-style-type: none"> Reinforcement reached yielding plateau on loaded side Slippage observed in almost every rebar from the loaded side
18F1-2	149.5	Pull-out failure	<ul style="list-style-type: none"> Better bond achieved between UHPC and precast beam (best of the 18-inch specimens) Crack developed at failure in precast concrete immediately next to joint Vertical crack also developed in UHPC at failure 	<ul style="list-style-type: none"> Reinforcement reached yielding plateau on loaded side with larger tensile strain Slippage observed in just one rebar from the loaded side

D.4.2.1. Test 1 (18F1-1)

The cracking pattern at failure for 18F1-1 is shown in Figure D.9. A splitting failure in the UHPC at the level of the joint reinforcement appears to have occurred causing a pullout failure of the reinforcement. The poor bond between the UHPC and the precast concrete section resulted in the interface being the primary failure crack. This caused a similar hinge and failure mechanism to occur as illustrated in Figure D.2 above.



Figure D.9: 18F1-1: (a) failed specimen and (b) close-up of hinge developing in top corner of precast member next to UHPC joint

The failed beam after it was removed from the test setup is shown in Figure D.10. The UHPC did appear to have some bond with the precast section toward the center of the section in the compression region, but little bond was achieved toward the outsides of the joint. Some internal cracking in the UHPC can be seen in Figure D.10 (b); this cracking may be a result of shrinkage in the UHPC caused by the rapid setting time and insufficient prewetting of the joint. Some UHPC around the reinforcement pulled out with the reinforcement at failure, shown in Figure D.10 (d).

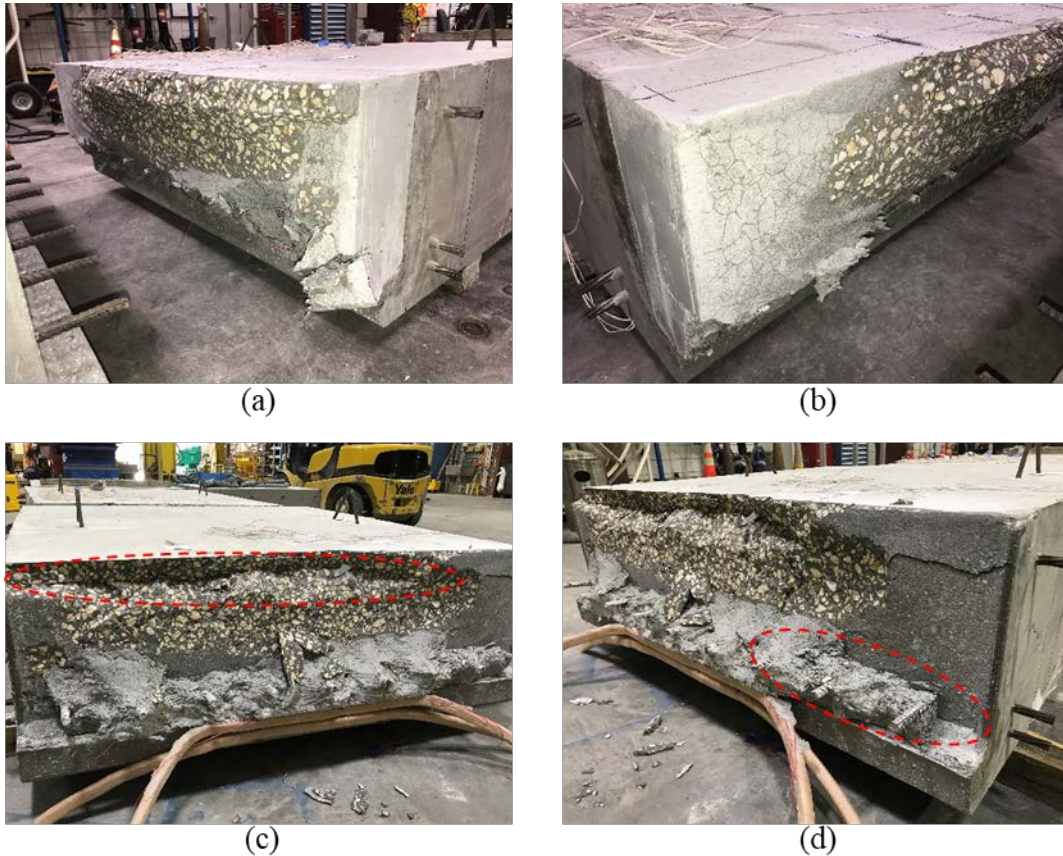
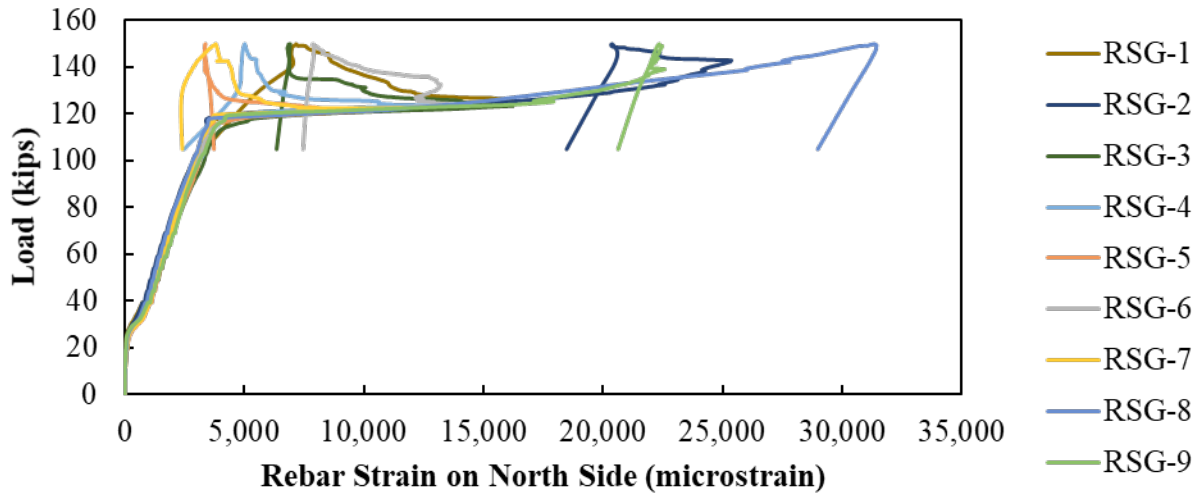


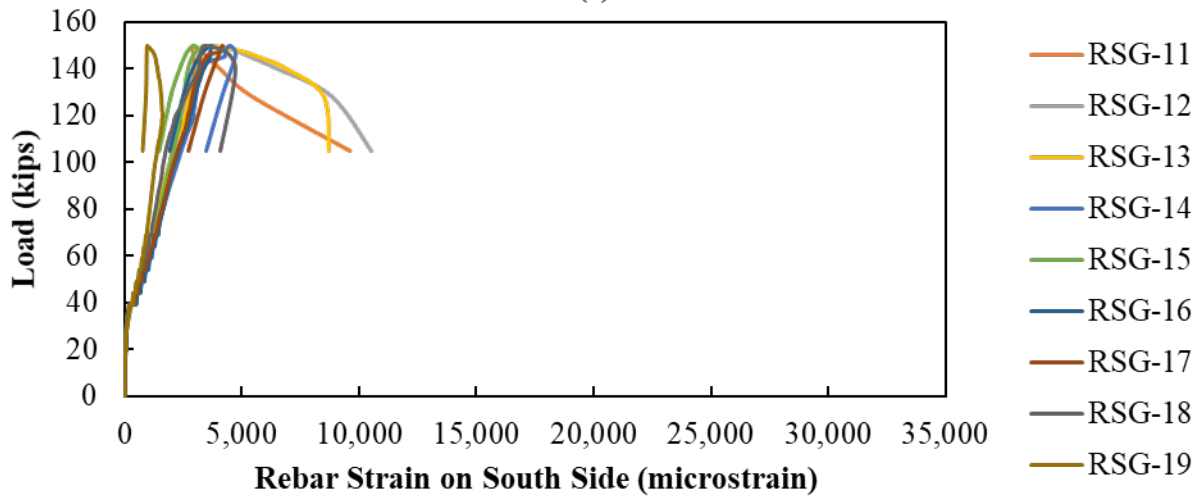
Figure D.10: 18F1-1: (a) south beam with UHPC matrix, (b) poor bond due to unaffected UHPC matrix on south beam, (c) north beam with dent at the top, and (d) poor UHPC bond at the rebar level in north beam

The load versus rebar strain gauge data for all the joint reinforcements are presented in Figure D.11 (a) for the north beam and Figure D.11 (b) for the south beam. The load versus bottom aperture data from the CDT is shown in Figure D.11 (c) up until when the gauges were removed. The load versus concrete strain responses are shown in Figure D.12 (a) for bottom gauges, including when the cracking load was observed in Figure D.12 (b), and load versus top gauge response in Figure D.12 (c).

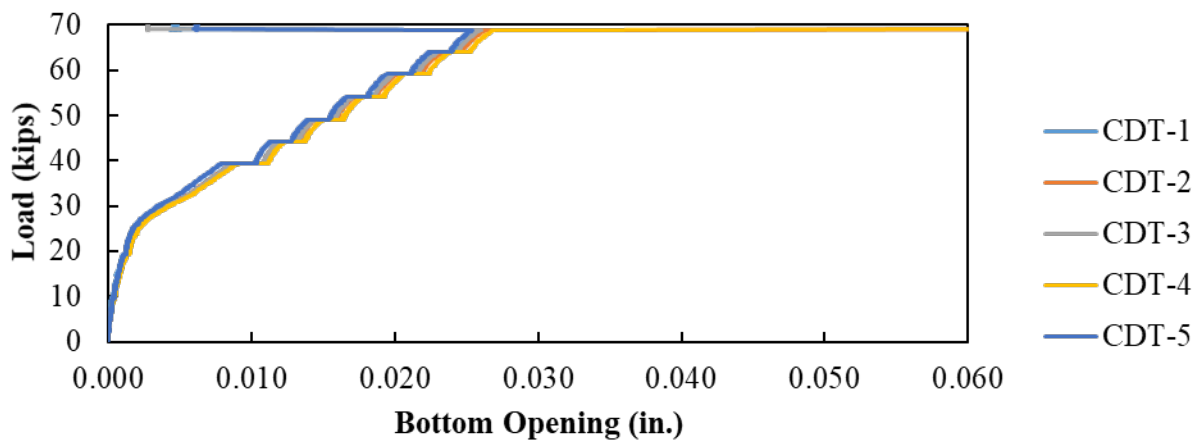
As previously mentioned, the strain on the top of the precast section near the load is greater than the strain on top of the UHPC joint, Figure D.12 (c). This is likely due to a combination of increased local stresses under the load and due to the UHPC having a much higher stiffness than the precast section. Other observations are similar to those made above for FSB-1.



(a)

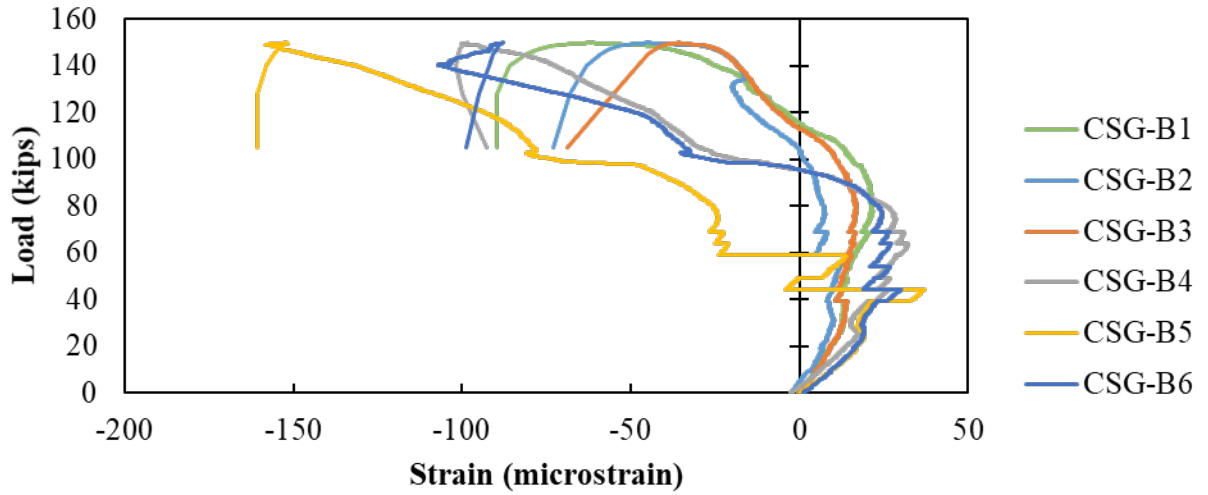


(b)

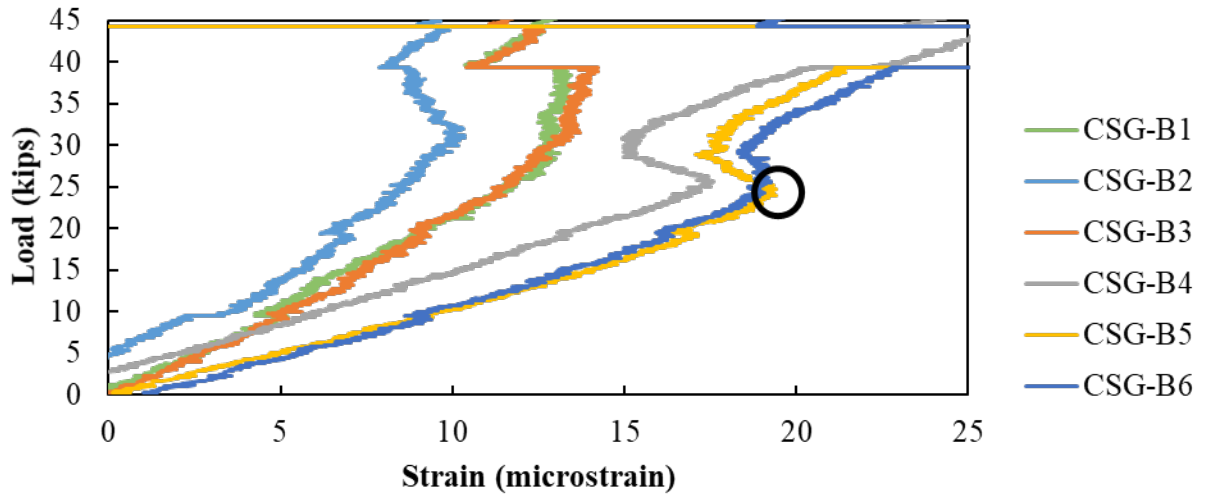


(c)

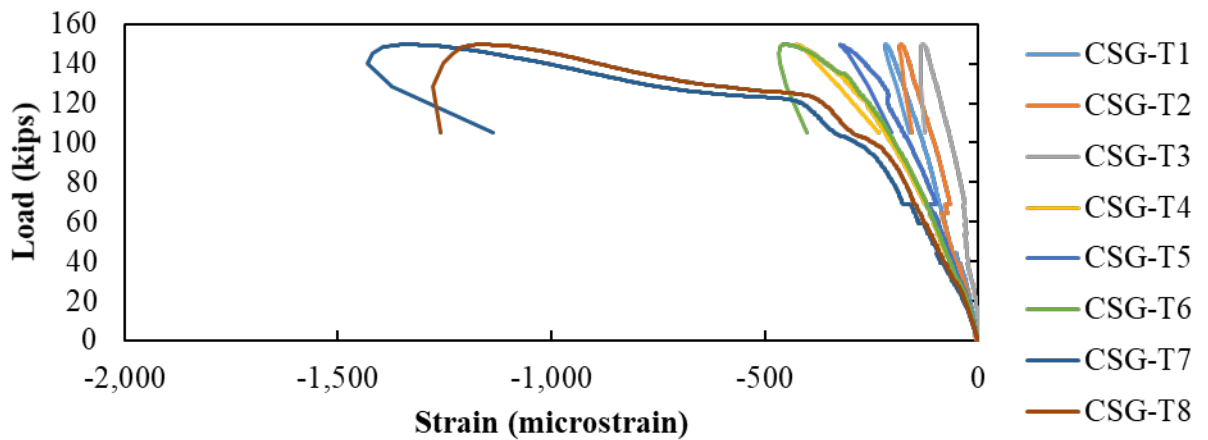
Figure D.11: 18F1-1 response: (a) load versus rebar strain on north side, (b) load versus rebar strain on south side, and (c) load versus central bottom opening



(a)



(b)



(c)

Figure D.12: 18F1-1 response: (a) Load versus bottom concrete strain, (b) cracking load determination based on load versus bottom concrete strain response, and (c) load versus top concrete strain

D.4.2.2. Test 2 (18F1-2)

Although the failure load was like 18F1-1, the overall performance of 18F1-2 was generally better. There was an improved bond between the UHPC and precast section, shown in Figure D.13 (a). A pullout failure of the joint reinforcement still controlled the failure, shown in Figure D.13 (b) and Figure D.14.

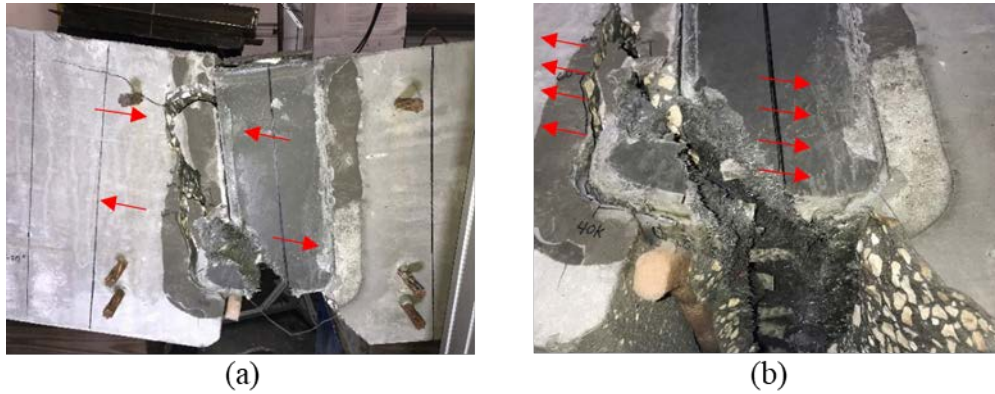


Figure D.13: 18F1-2: (a) fractured joint specimen from west side and (b) bottom view of joint failure from west side

As mentioned earlier, a better bond was observed between the UHPC and precast section for 18F1-2. The UHPC bond caused the cover concrete in the joint to detach from the precast section, shown in Figure D.14. The joint reinforcement pulled out on the loaded side of the joint with some UHPC next to the reinforcement also being pulled out.

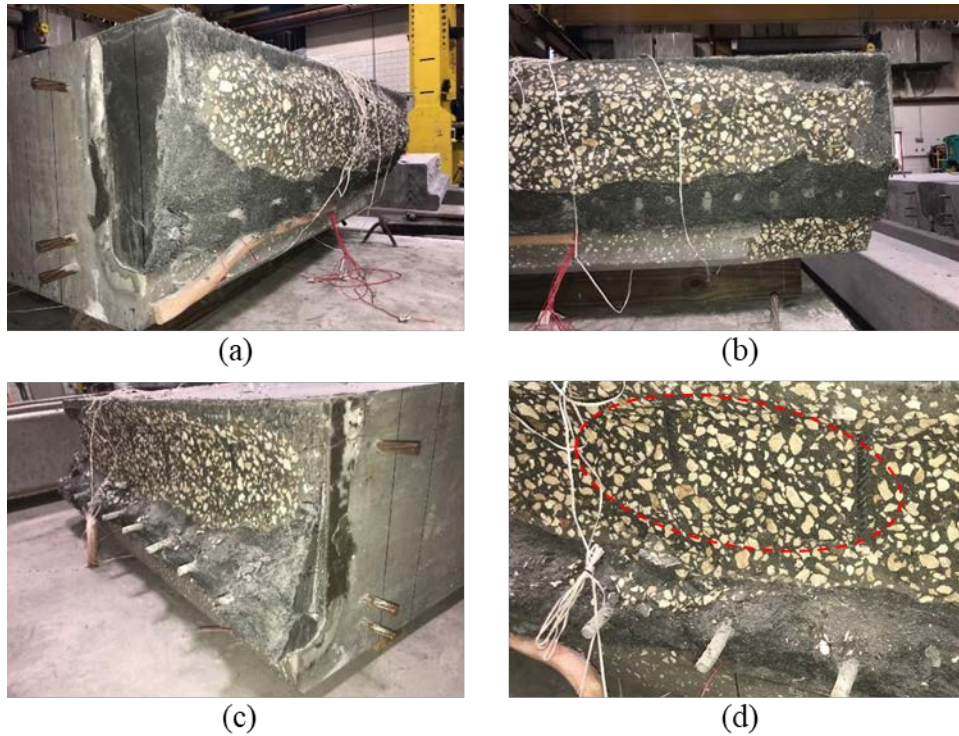
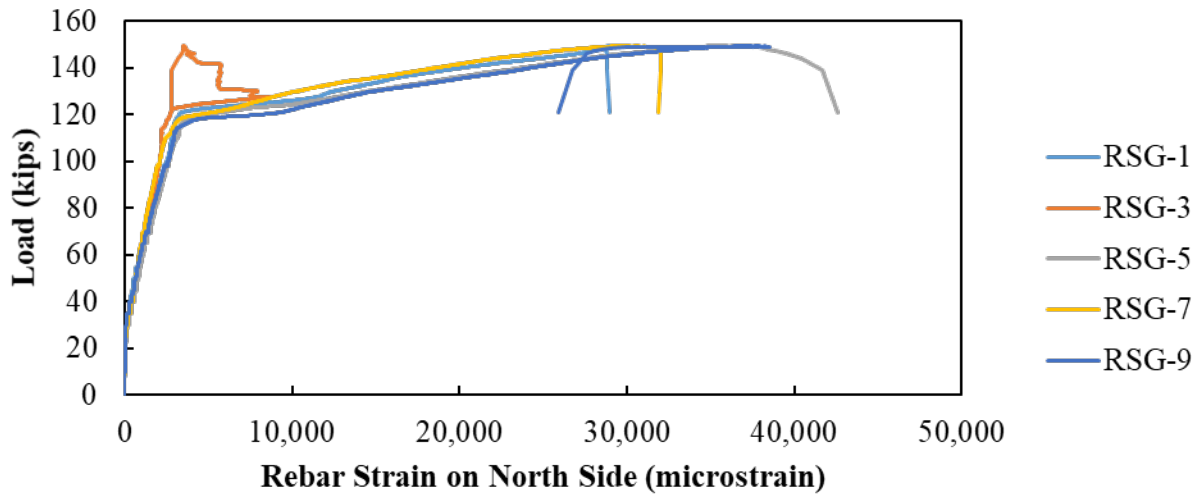
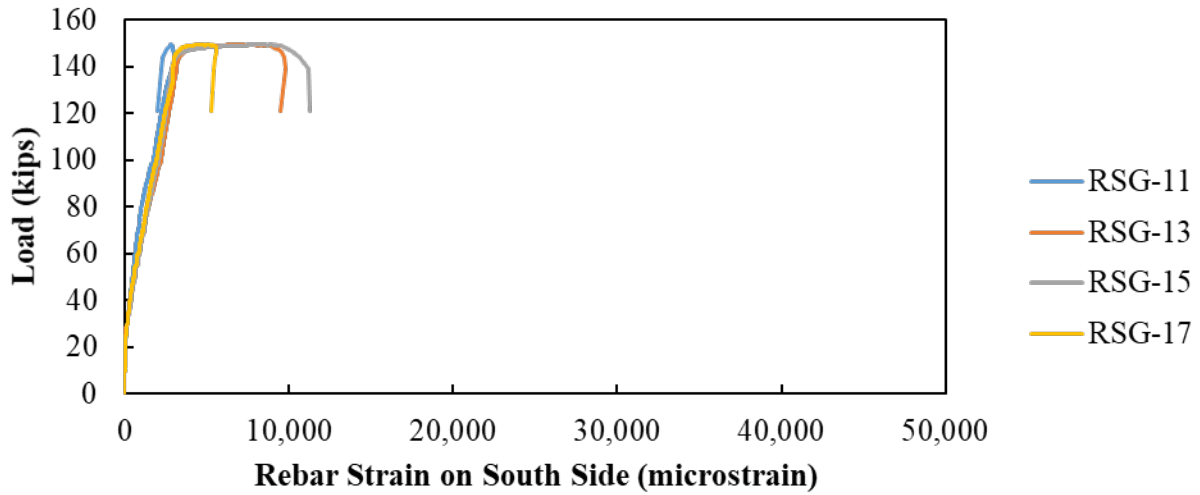


Figure D.14: 18F1-2 after failure (a) failed south beam from the east side, (b) side of failed joint in south beam, (c) failed north beam, and (d) imprints in failed joint of shear reinforcement from precast section

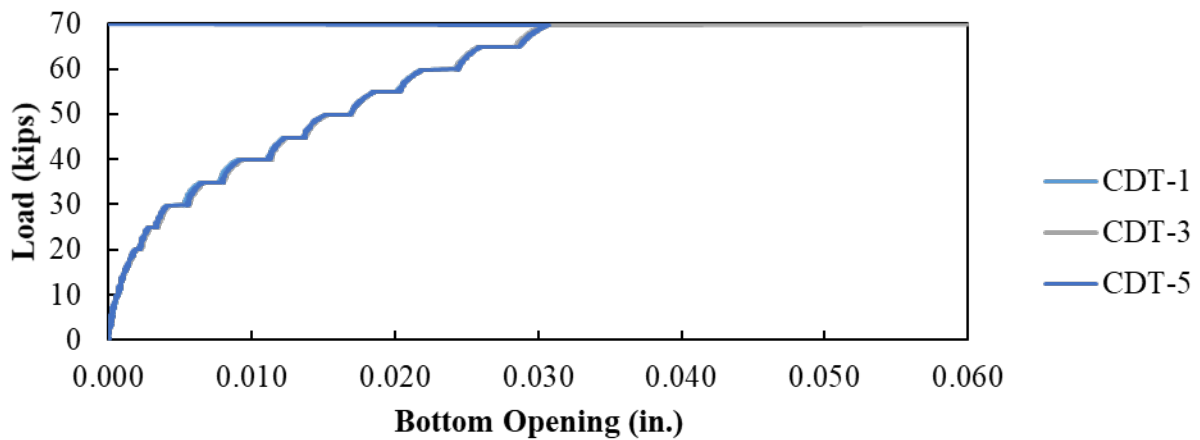
The load versus rebar strain gauge data for all the joint reinforcements are presented in Figure D.15 (a) for the north beam and Figure D.15 (b) for the south beam. The load versus bottom aperture data from the CDT is shown in Figure D.15 (c) up until when the gauges were removed. The load versus concrete strain responses are shown in Figure D.16 (a) for bottom gauges, including when the cracking load was observed in Figure D.16 (b), and load versus top gauge response in Figure D.16 (c).



(a)

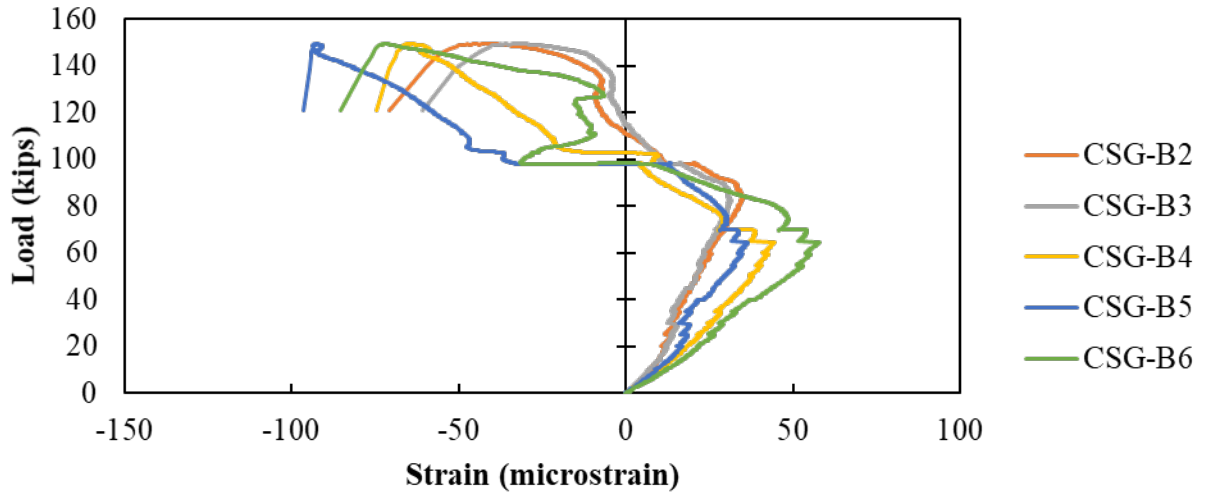


(b)

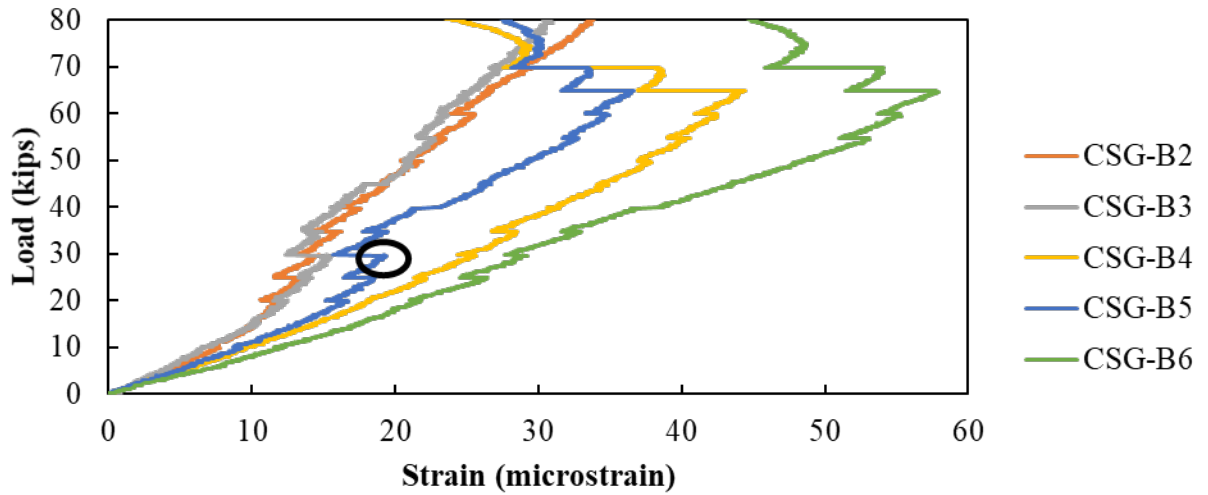


(c)

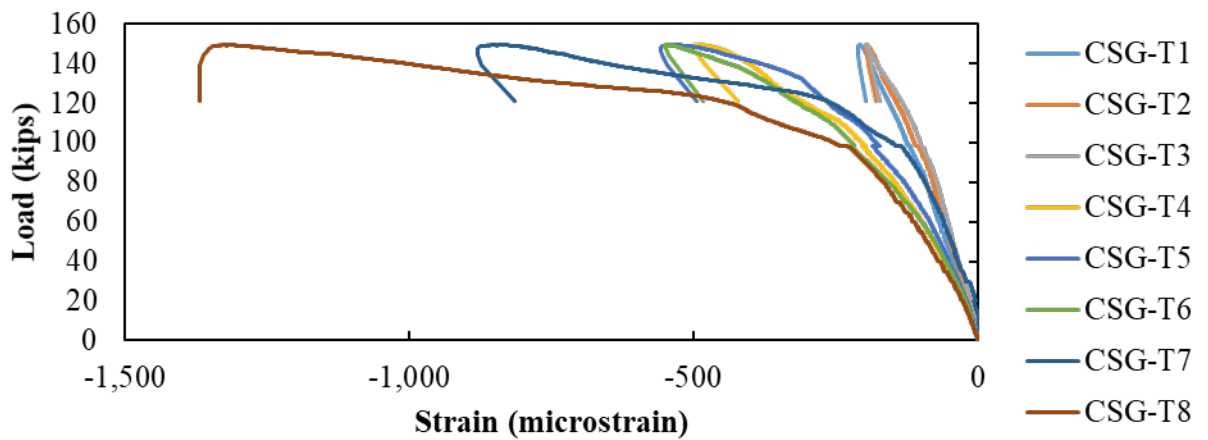
Figure D.15: 18F1-2 response: (a) load versus rebar strain on north side, (b) load versus rebar strain on south side, and (c) load versus central bottom opening



(a)



(b)



(c)

Figure D.16: 18F1-2 response: (a) load versus bottom concrete strain, (b) cracking load determination based on load versus bottom concrete strain response, and (c) load versus top concrete strain

D.4.3. 18F2 (FDOT 2)

The strength testing result observations describing the failure forces, type of failures, and concrete and rebar behaviors for the 18F2 specimens are highlighted in Table D.4.

Table D.4: 18F2 Strength testing summary

Test	Failure Force [kip]	Type of Failure	Concrete Comments	Rebar Comments
18F2-1	170.2	Pull-out failure	<ul style="list-style-type: none"> • Good bond between UHPC and precast section on one end of joint but not the other • Rupture of bottom precast ledge • Map cracking in UHPC on side that debonded 	<ul style="list-style-type: none"> • Most joint reinforcement pulled out of joint • Two of the joint reinforcement fractured at failure
18F2-2	177.0	Pull-out failure	<ul style="list-style-type: none"> • Good bond between UHPC and precast concrete • Rupture of bottom ledges was observed 	<ul style="list-style-type: none"> • All joint reinforcement pulled out of joint

D.4.3.1. Test 1 (18F2-1)

Cracking at failure for 18F2-1 is shown in Figure D.17. There was poor bond between the UHPC and the precast concrete at one of the ends, shown in Figure D.17 (a). Similar to other beams, a hinge formed at the top of the precast section next to the UHPC joint.

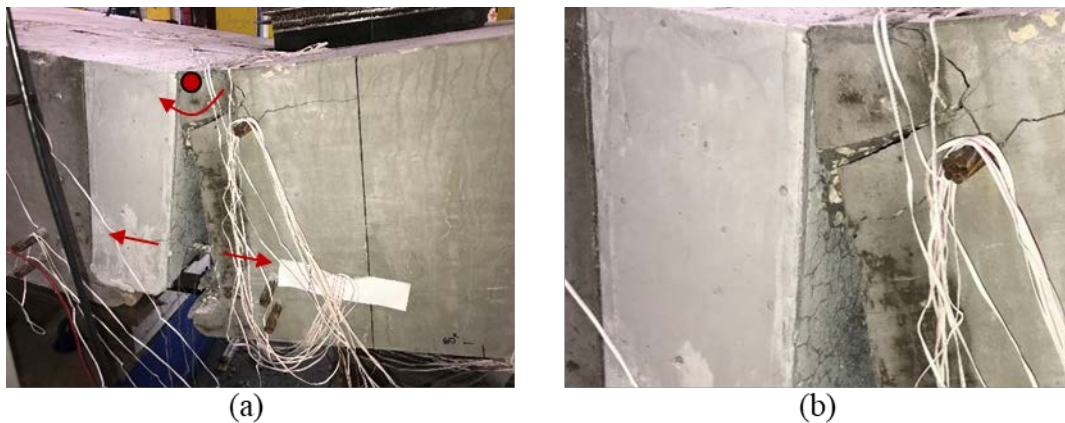


Figure D.17: 18F2-1: (a) failed specimen and (b) possible stress concentration pattern at the top on east side

There was one region on the east side of the joint where the UHPC did not bond with the precast beam, shown in Figure D.18 (a) and (b). The cover concrete from the precast beam detached in the compression region of the rest of the joint. The hinge that formed in the precast section is highlighted in Figure D.18 (c). Two pieces of the joint reinforcement fractured, highlighted in Figure D.18 (d), the rest of the joint reinforcement pulled out from the joint at failure.

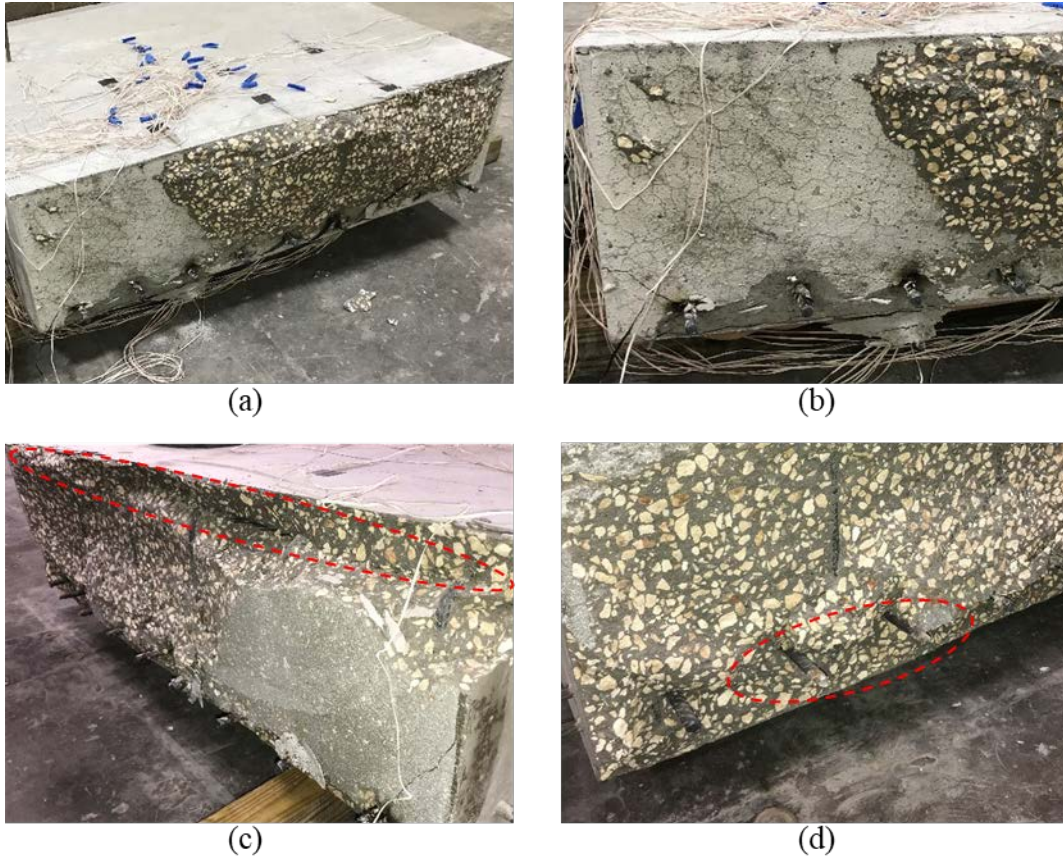
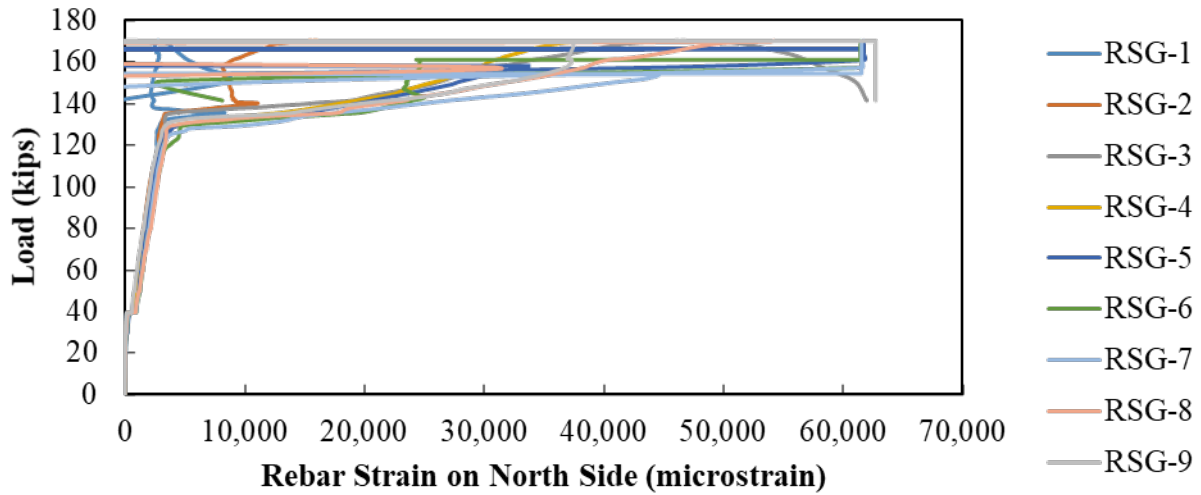
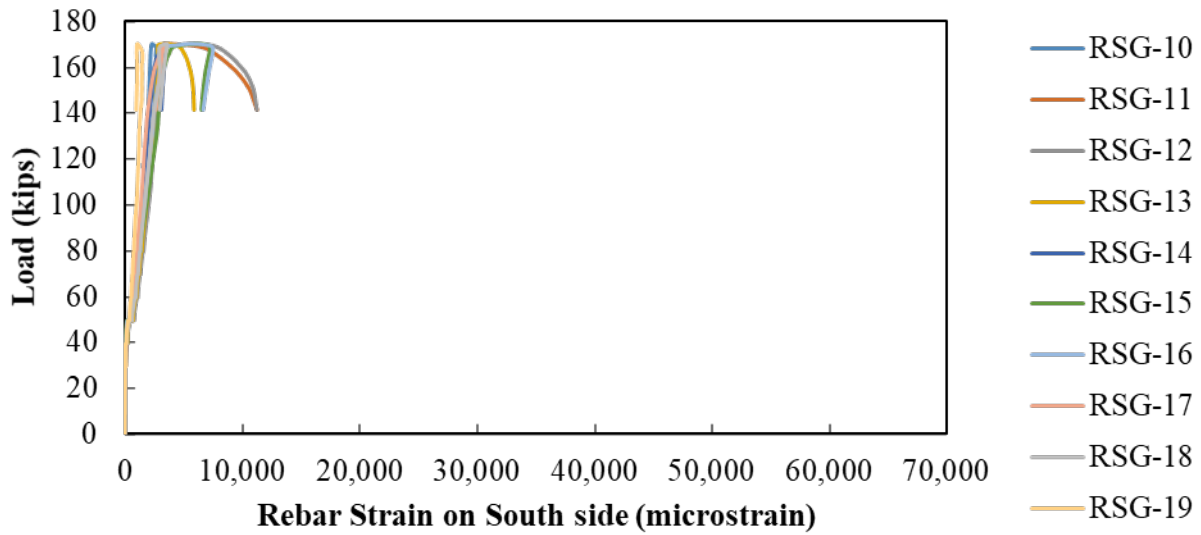


Figure D.18: 18F2-1: (a) south beam with unbonded and bonded UHPC matrix, (b) unbonded UHPC matrix showing shrinkage cracks in south beam, (c) north beam showing precast concrete failure, and (d) failed reinforcement in north beam

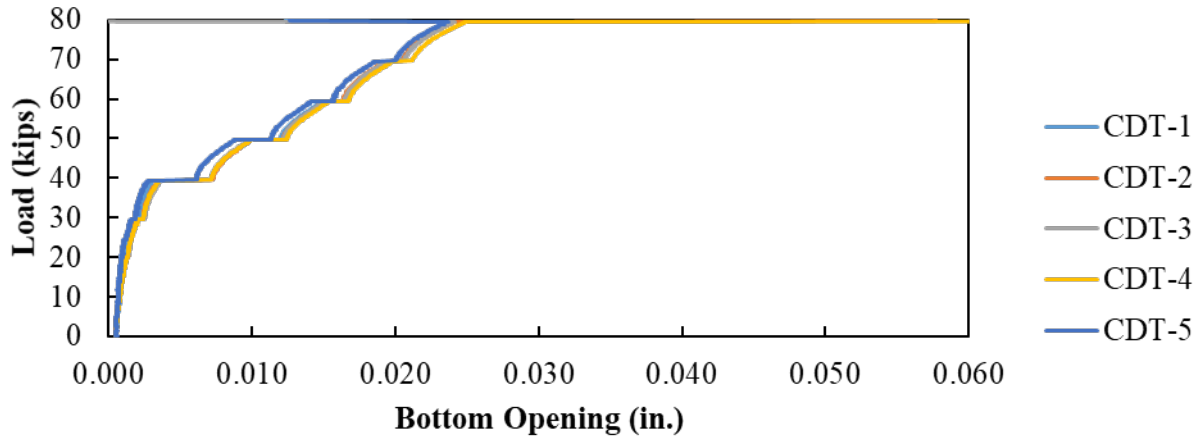
The load versus rebar strain gauge data for all the joint reinforcements are presented in Figure D.19 (a) for the north beam and Figure D.19 (b) for the south beam. The load versus bottom aperture data from the CDT is shown in Figure D.19 (c) up until when the gauges were removed. The load versus concrete strain responses are shown in Figure D.20 (a) for bottom gauges, including when the cracking load was observed in Figure D.20 (b), and load versus top gauge response in Figure D.20 (c).



(a)



(b)



(c)

Figure D.19: 18F2-1 response: (a) load versus rebar strain on north side, (b) load versus rebar strain on south side, and (c) load versus central bottom opening

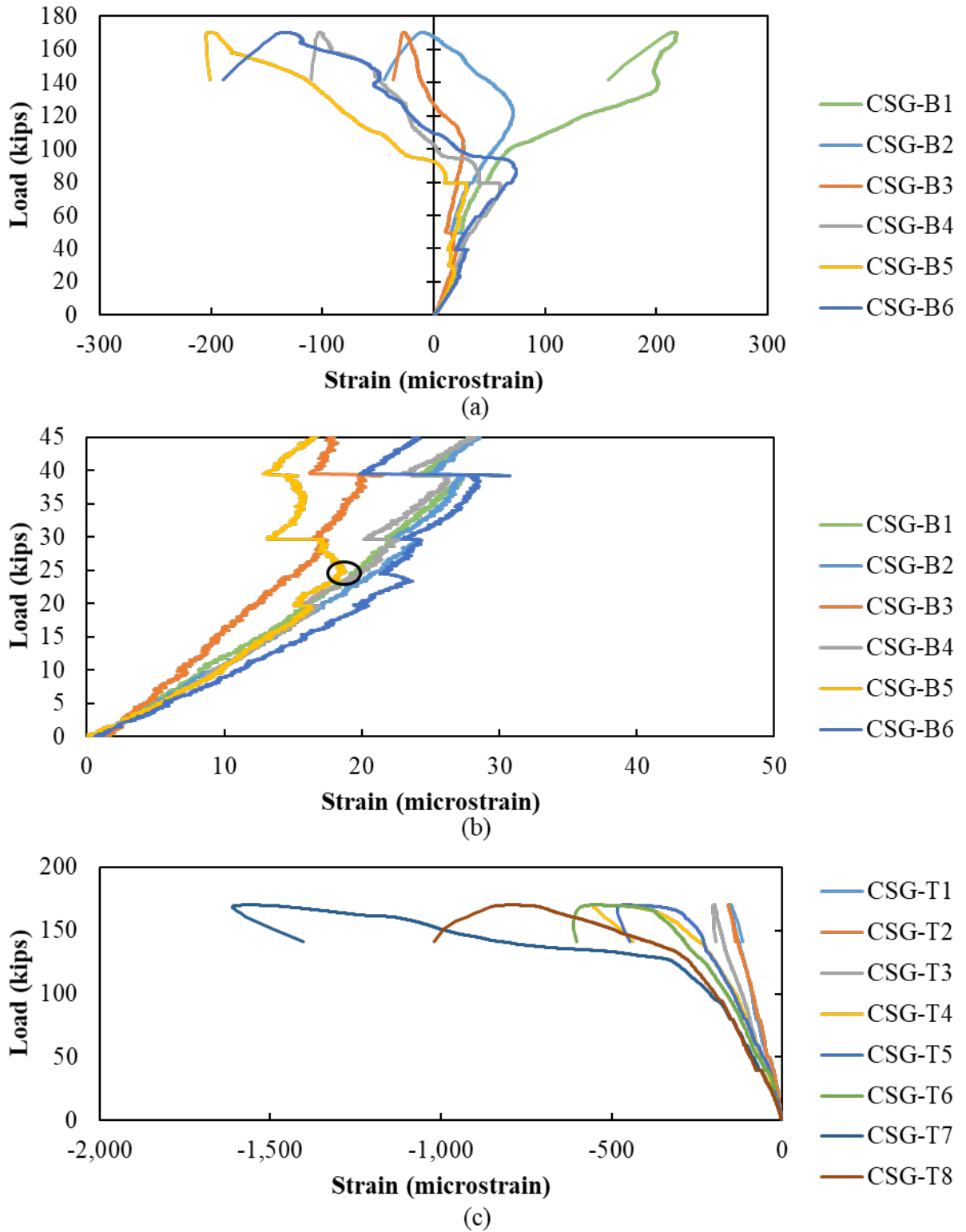


Figure D.20: 18F2-1 response: (a) load versus bottom concrete strain, (b) cracking load determination based on load versus bottom concrete strain response, and (c) load versus top concrete strain

D.4.3.2. Test 2 (18F2-2)

Cracking at failure for 18F2-2 is shown in Figure D.21. There was much better bond between the UHPC and precast concrete but hinging still appeared to occur at the corner of the precast section, highlighted in Figure D.21 (a).



Figure D.21: 18F2-2: (a) possible tension and compression zones and (b) possible compressive stress concentration at the top in west side view

The failed 18F2-2 after it was removed from the test setup is shown in Figure D.22. The strong bond between the UHPC and precast concrete resulted in the cover concrete being broken from the precast section in the compression region, shown in Figure D.22 (a) and (b). The hinge at the top of the precast section next to the UHPC joint can be seen along the length of the joint in Figure D.22 (c). The cover concrete being broken from the precast section left the shear reinforcement exposed after failure, shown in Figure D.22 (d).

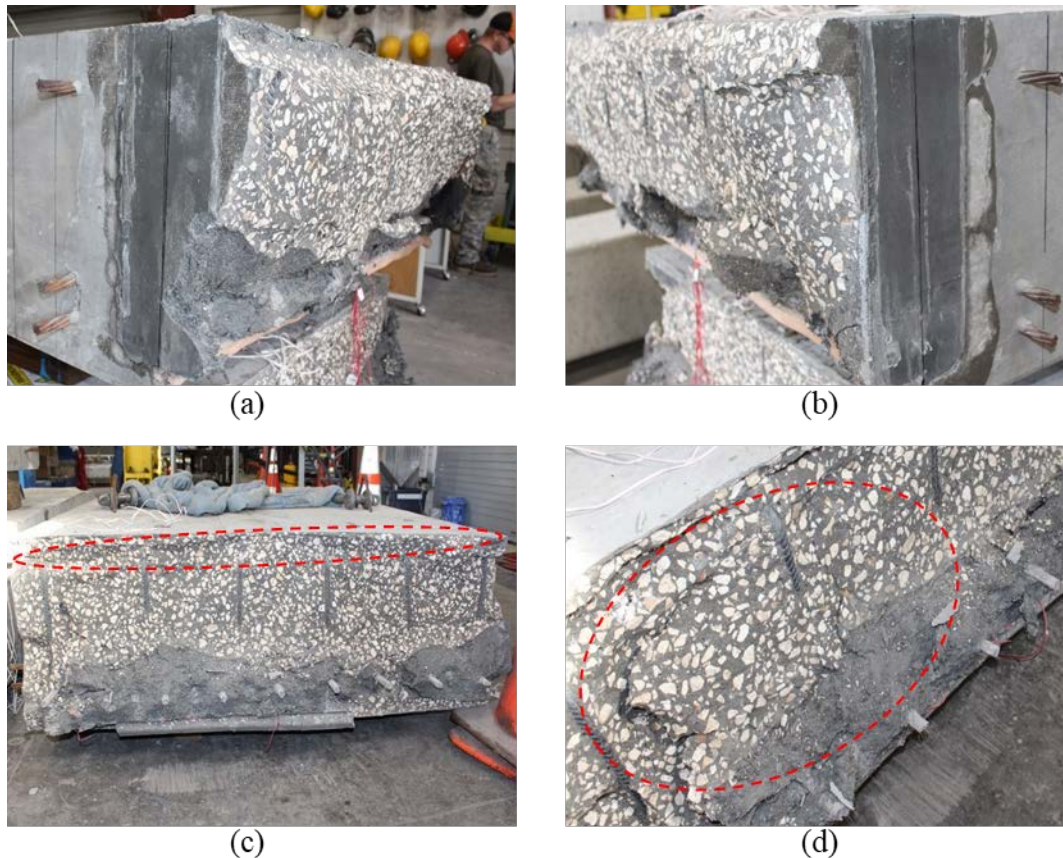
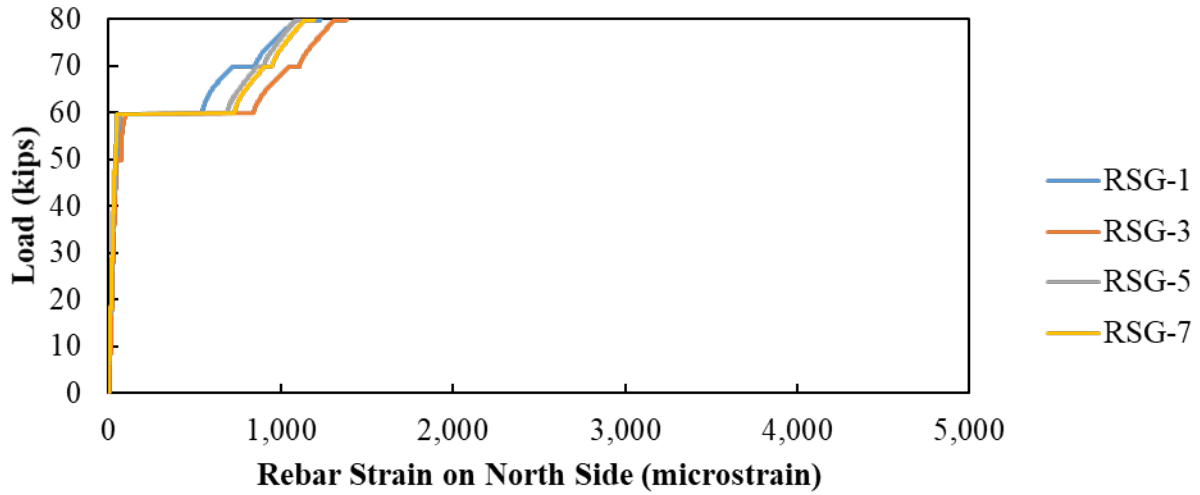
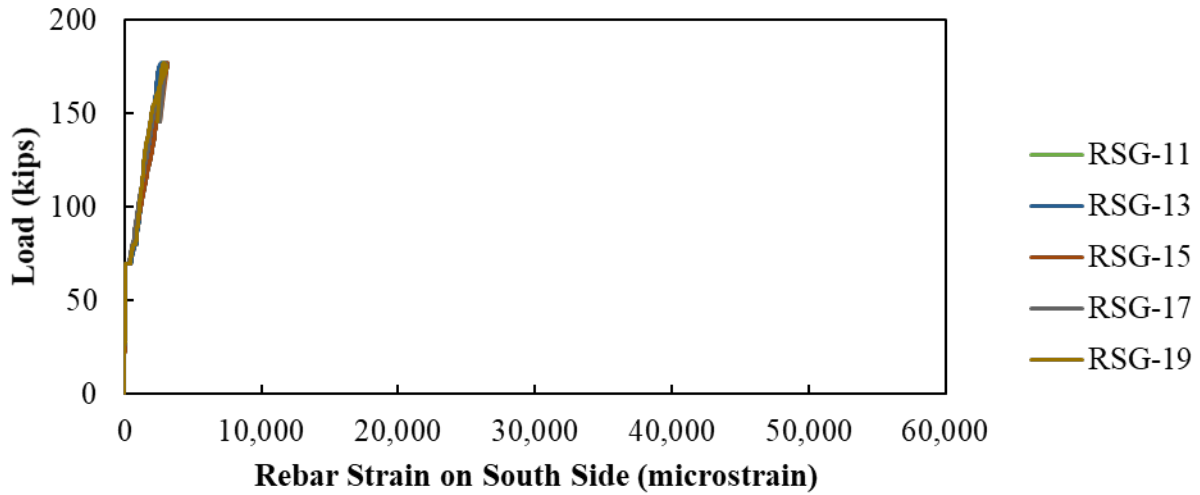


Figure D.22: 18F2-2: (a) UHPC matrix from south beam showing better bond and possible linear strain distribution, (b) UHPC matrix from south beam showing better UHPC-to-beam bond, (c) cover spalled from north beam and top dent, and (d) exposed shear reinforcement due to concrete cover removal on north beam

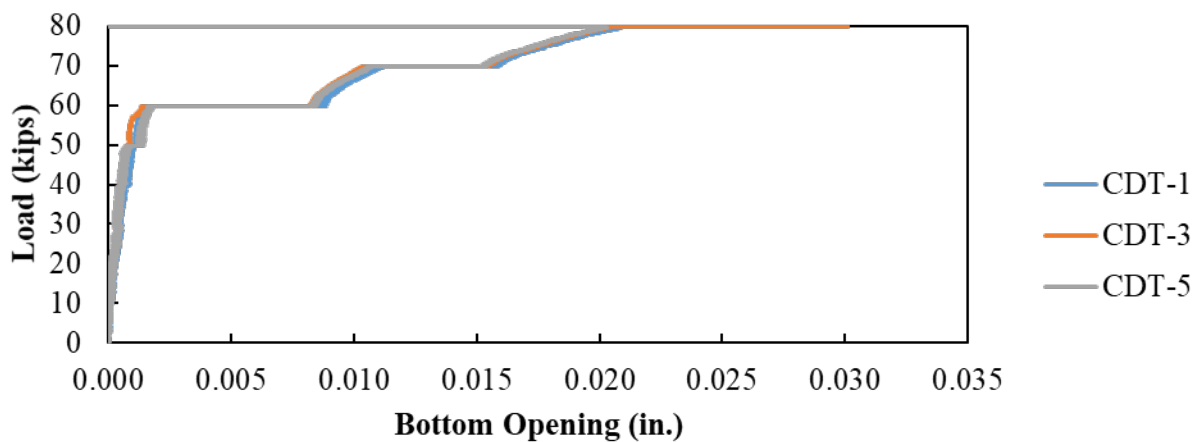
The load versus rebar strain gauge data for all the joint reinforcements are presented in Figure D.23 (a) for the north beam and Figure D.23 (b) for the south beam. The load versus bottom aperture data from the CDT is shown in Figure D.23 (c) up until when the gauges were removed. The load versus concrete strain responses are shown in Figure D.24 (a) for bottom gauges, including when the cracking load was observed in Figure D.24 (b), and load versus top gauge response in Figure D.24 (c). Note that concrete strain gauges CSG-B4 and CSG-B6 were not included in Figure D.24 (a) because their response was irregular after cracking and made it difficult to view the response of the other gauges.



(a)



(b)



(c)

Figure D.23: 12F2-2 response: (a) load versus rebar strain on north side, (b) load versus rebar strain on south side, and (c) load versus central bottom opening

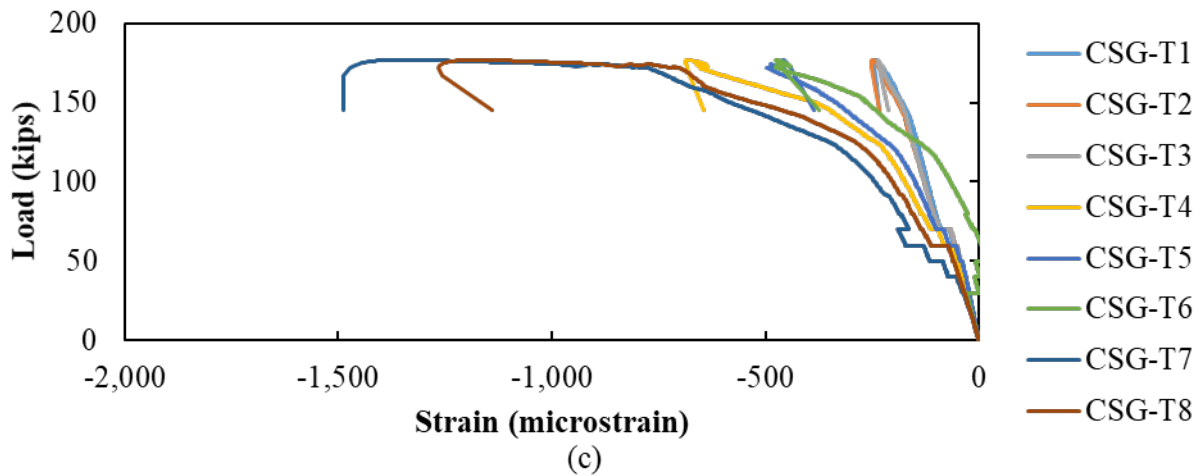
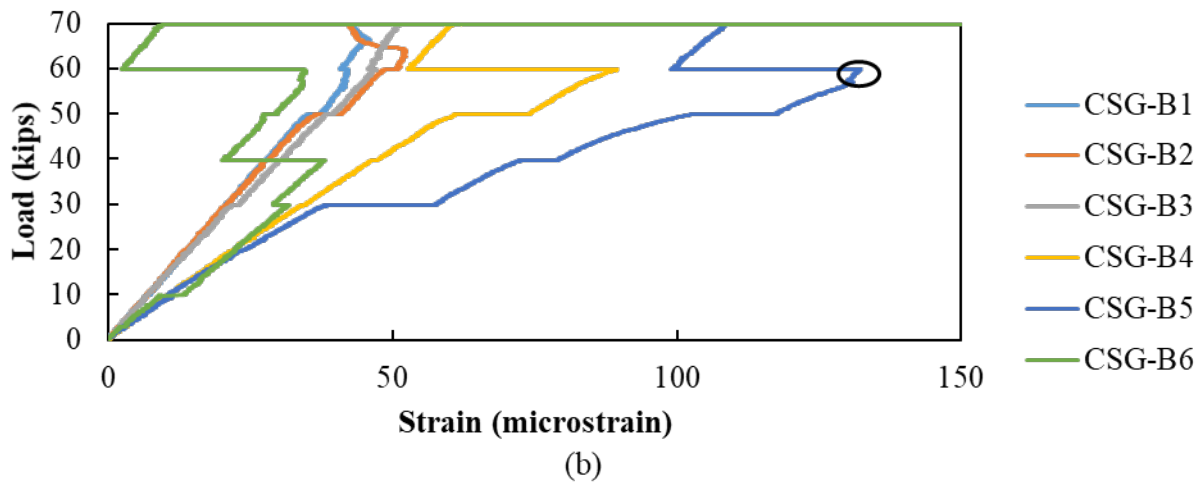
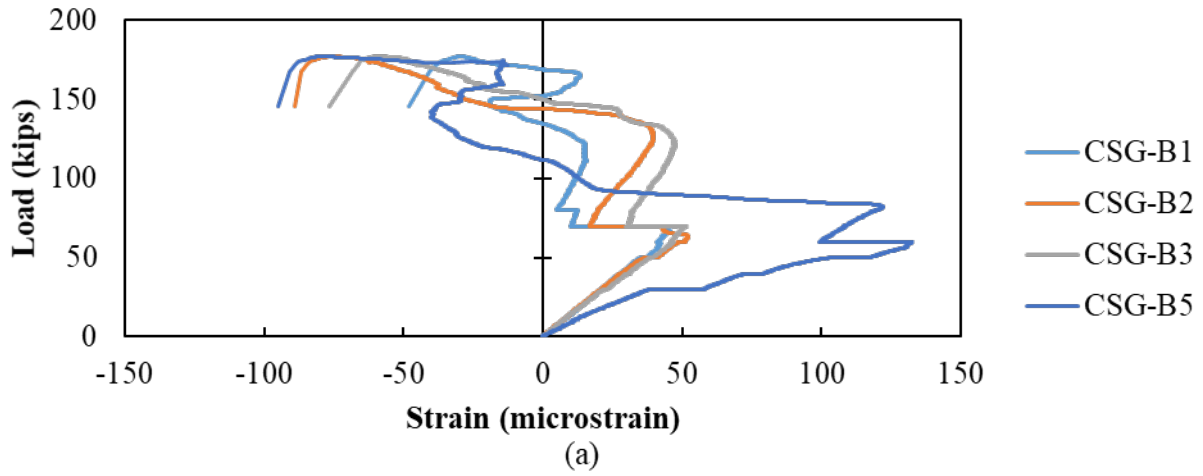


Figure D.24: 12F2-2 response: (a) load versus bottom concrete strain, (b) cracking load determination based on load versus bottom concrete strain response, and (c) load versus top concrete strain

D.4.4. 18A1 (Alternate 1)

The strength testing result observations describing the failure forces, type of failures, and concrete and rebar behaviors for the 18A1 specimens are highlighted in Table D.5.

Table D.5: 18A1 Strength testing summary

Test	Failure Force [kip]	Type of Failure	Concrete Comments	Rebar Comments
18A1-1	154.4	Concrete crushing and rebar fracture	<ul style="list-style-type: none"> Poor bond between UHPC and precast section Map cracking observed on unbonded UHPC side Concrete under load crushed right before failure 	<ul style="list-style-type: none"> All the rebar ruptured
18A1-2	146.1	Concrete crushing and rebar fracture	<ul style="list-style-type: none"> Greatly improved bond between UHPC and precast section Concrete under load crushed right before failure 	<ul style="list-style-type: none"> All the rebar ruptured

D.4.4.1. Test 1 (18A1-1)

The 18A1-1 had the worst bond performance between the UHPC and precast concrete, as shown in Figure D.25 (a); the UHPC completely detached from the precast concrete. Failure in this joint was caused by crushing of the concrete along the length of the specimen under the load and then rupture of the joint reinforcement. The crushing of the concrete under the load is shown in Figure D.25 (b).



Figure D.25: 18A1-1: (a) failed specimen with complete UHPC matrix detachment, (b) Failure of top lip due to compressive stress concentration from west side

Although the sample had poor bond between the UHPC and precast concrete (Figure D.26 (a)), all the joint reinforcement ruptured in tension due, a result of a larger development length. There was some bond between UHPC and precast concrete in the top flange, shown in Figure D.26 (b). This specimen showed larger ductility than the other 18-inch-deep specimens because all the joint

reinforcement developed and fractured, as shown in Figure D.26 (c). A hinge seemed to form in the same location as the other 18-inch-deep specimens, shown in Figure D.25 (a) and Figure D.26 (c) and (d).

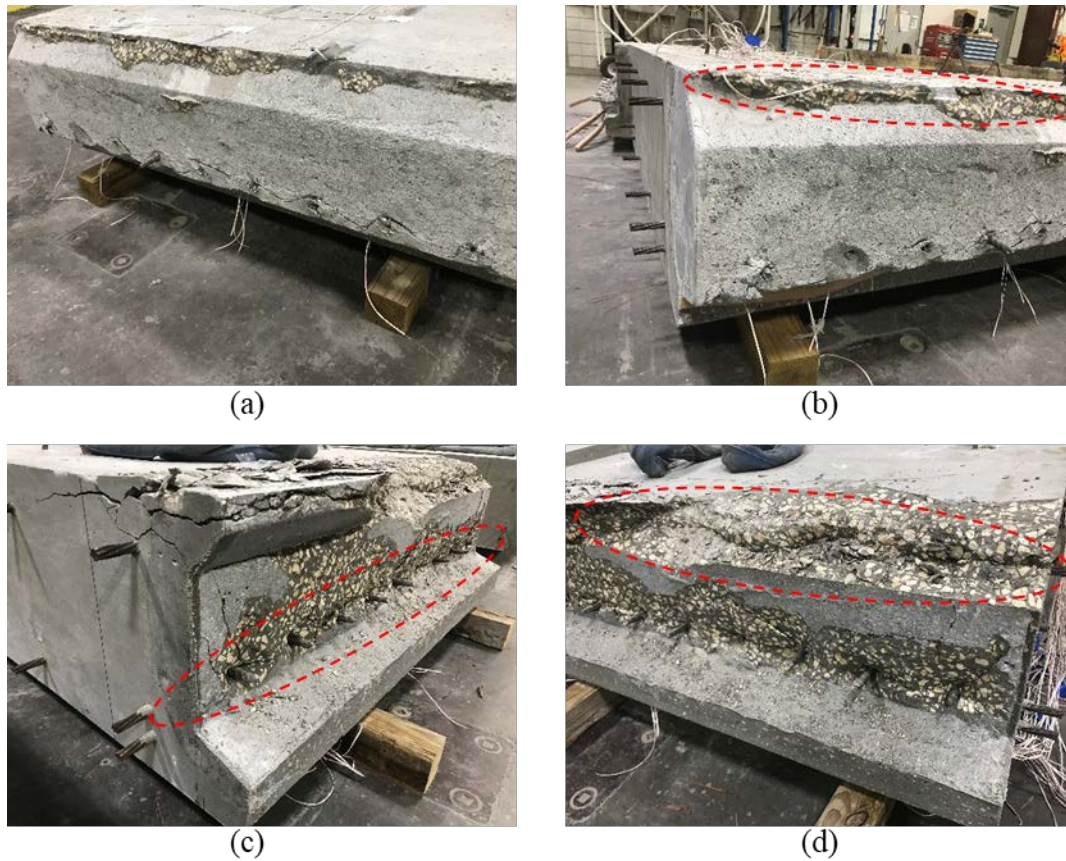
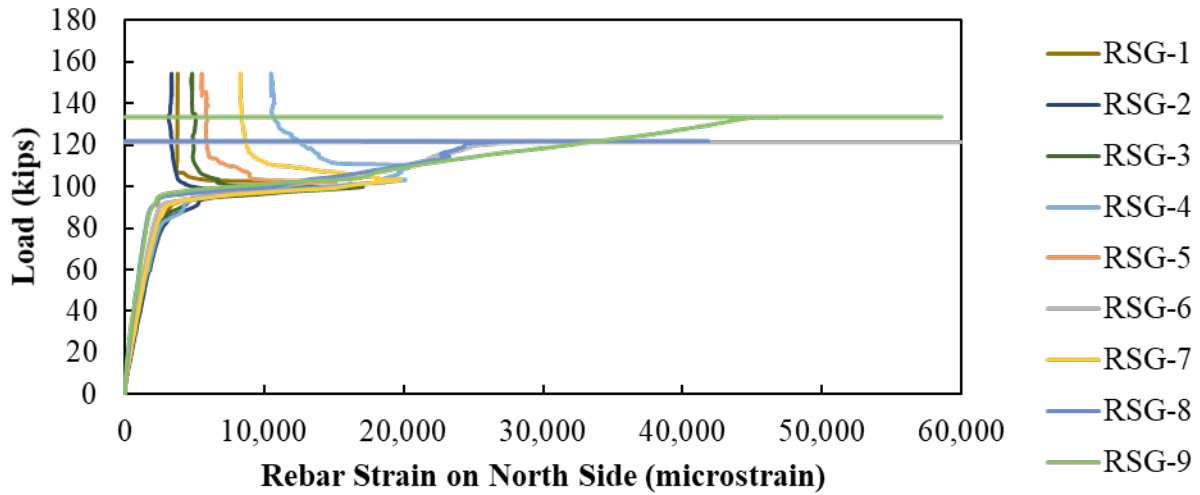
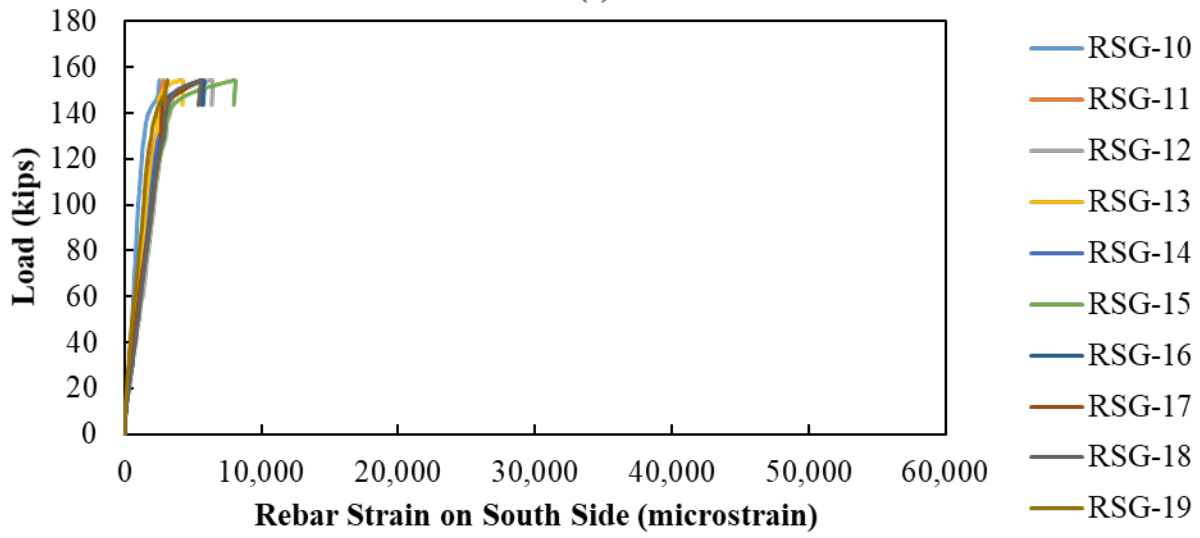


Figure D.26: 18A1-1: (a) UHPC matrix with lack of bond in south beam, (b) poor bond shown at the top UHPC matrix in south beam, (c) development and fracture of transverse rebar in north beam, and (d) top ledge failure due to high compressive stress accumulation in north beam

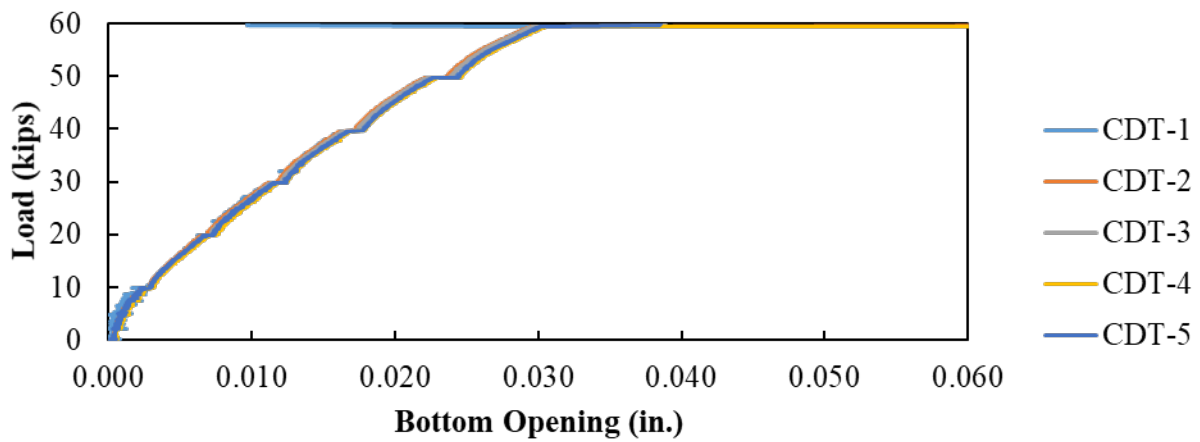
The load versus rebar strain gauge data for all the joint reinforcements are presented in Figure D.27 (a) for the north beam and Figure D.27 (b) for the south beam. The load versus bottom aperture data from the CDT is shown in Figure D.27 (c) up until when the gauges were removed. The load versus concrete strain responses are shown in Figure D.28 (a) for bottom gauges, including when the cracking load was observed in Figure D.28 (b), and load versus top gauge response in Figure D.28 (c).



(a)

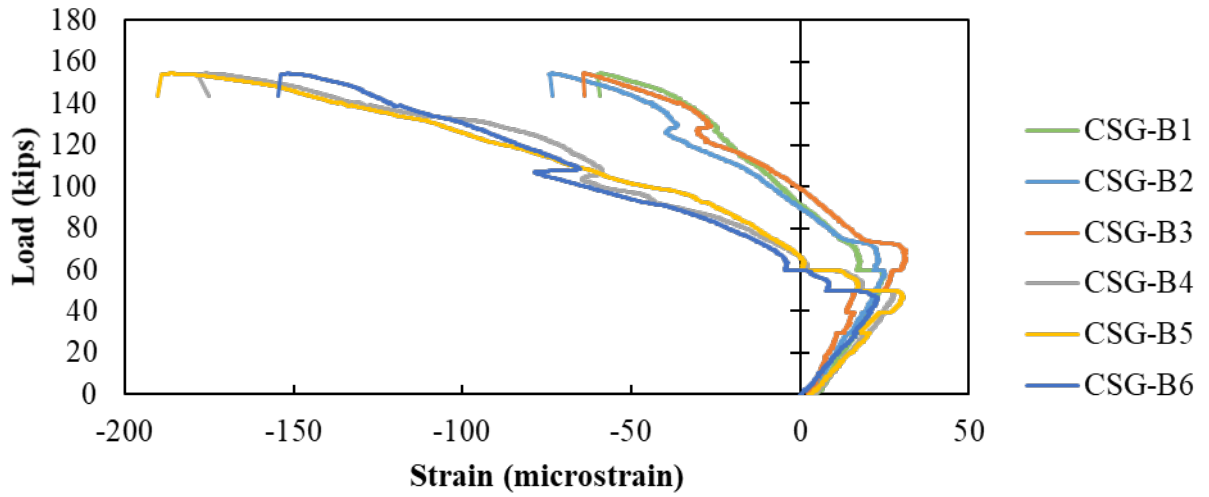


(b)

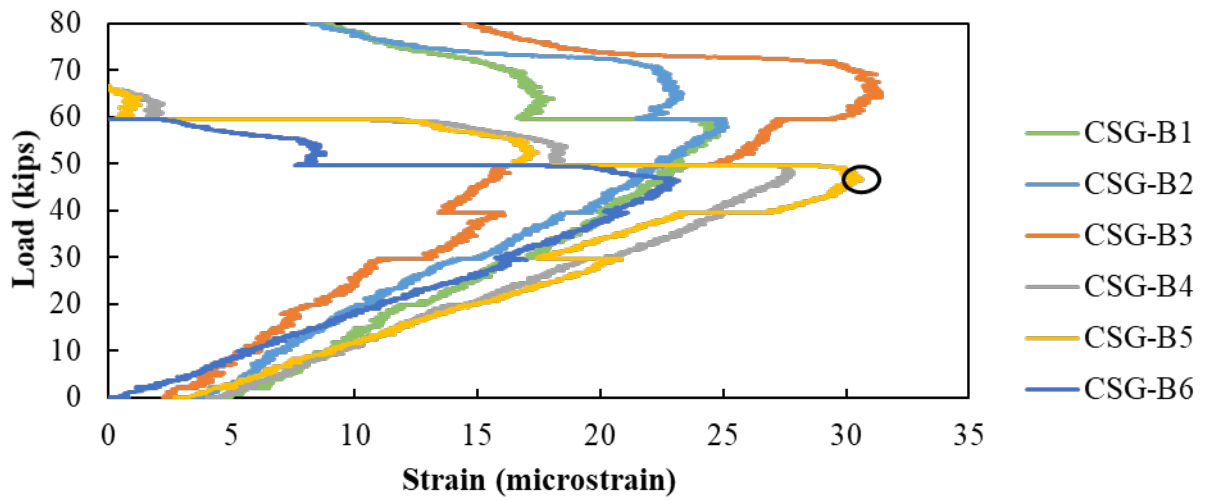


(c)

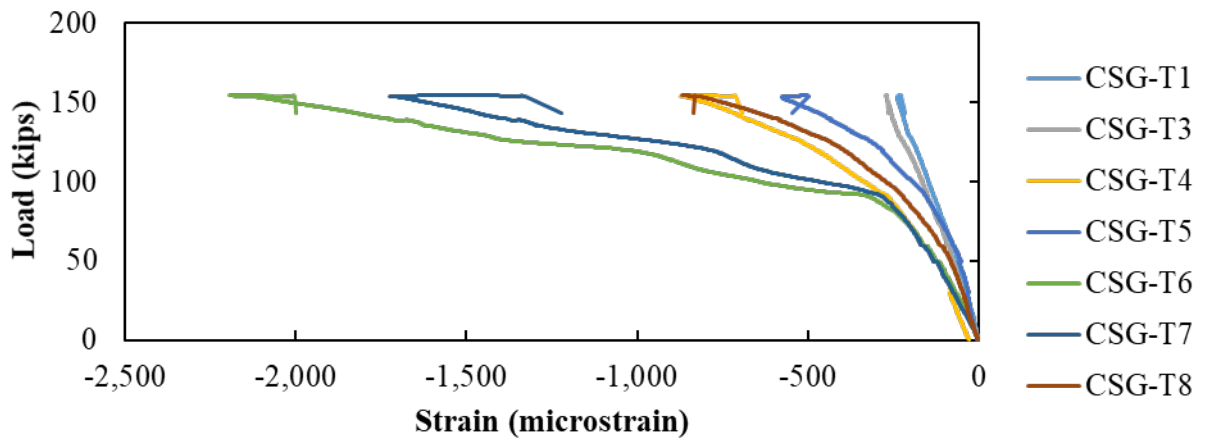
Figure D.27: 18A1-1 response: (a) load versus rebar strain on north side, (b) load versus rebar strain on south side, and (c) load versus central bottom opening



(a)



(b)



(c)

Figure D.28: 18A1-1 response: (a) load versus bottom concrete strain, (b) cracking load determination based on load versus bottom concrete strain response, and (c) load versus top concrete strain

D.4.4.2. Test 2 (18A1-2)

The crack pattern at failure is shown in Figure D.29. Failure of the joint was initiated by the crushing of the concrete along the length of the joint under the load and fracture of the joint reinforcement. A crack developed at failure extending from the corner of the top flange horizontally, shown in Figure D.29 (b). A much better bond was observed between the UHPC joint and precast section.

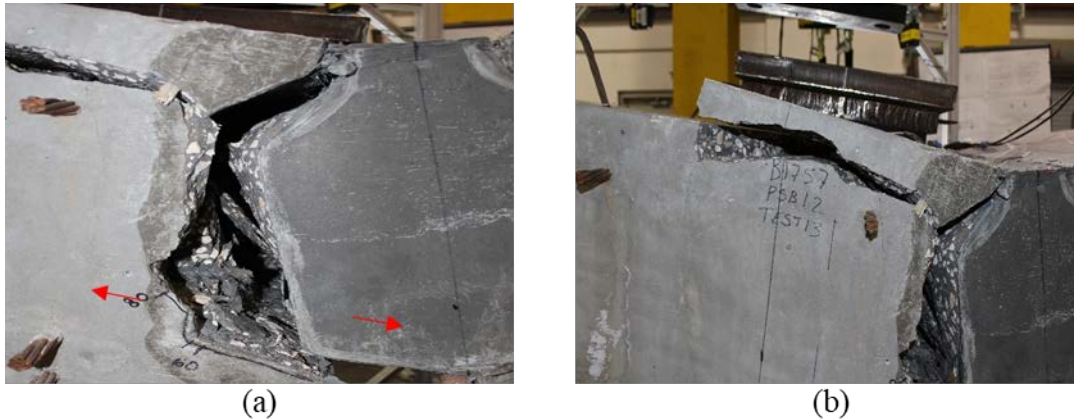
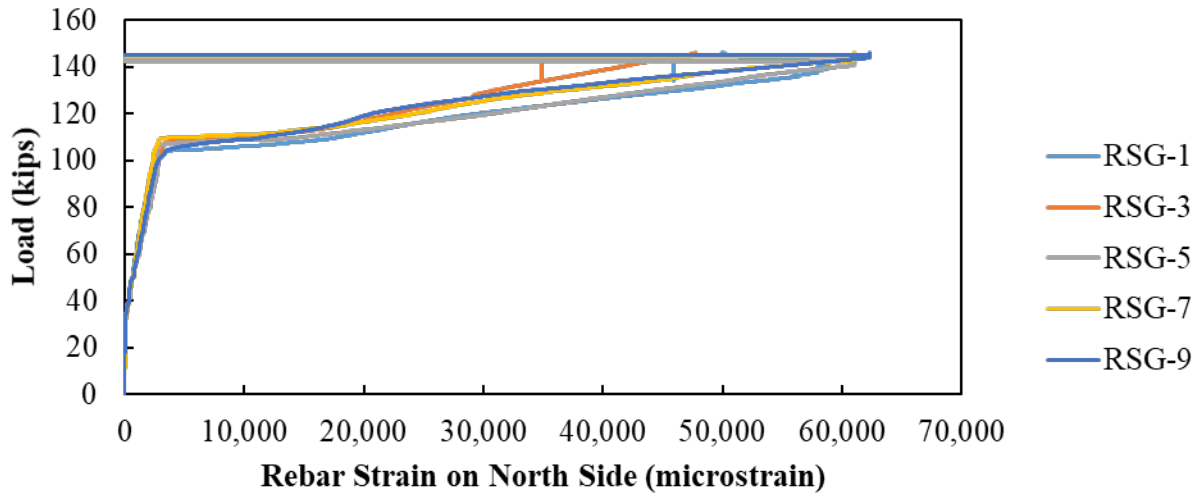
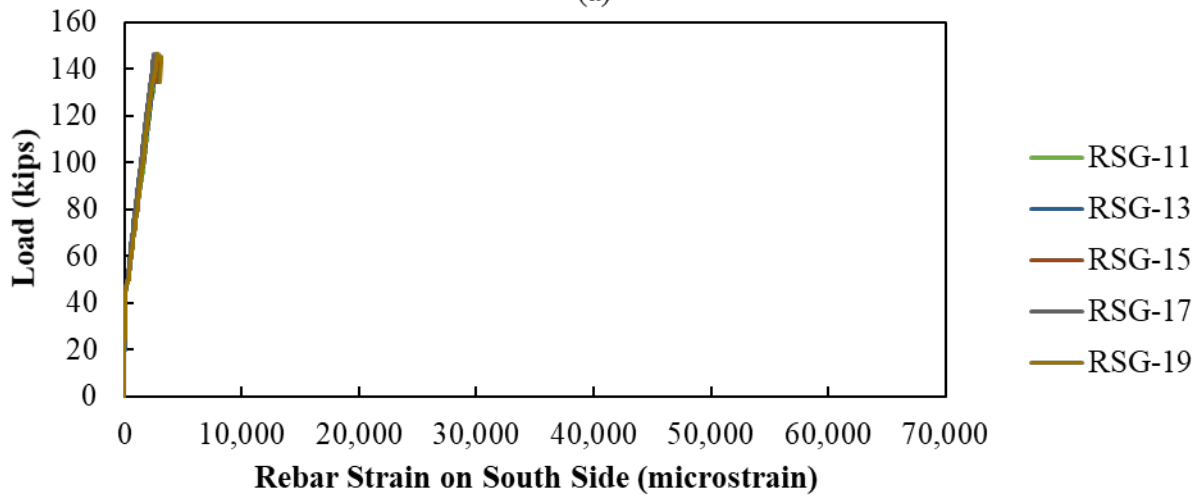


Figure D.29: 18A1-2: (a) failed specimen with probable force distribution and (b) spalling of top lip due to potential shear plane.

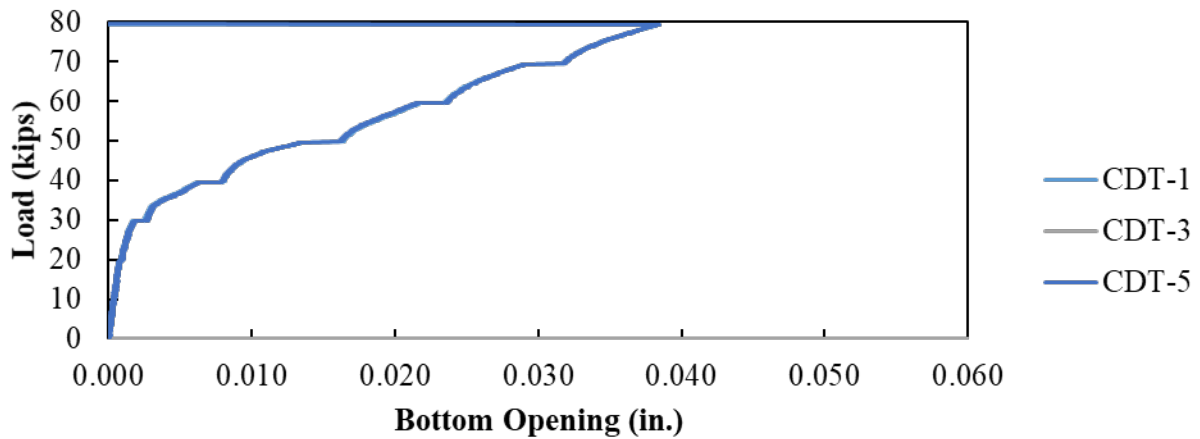
The load versus rebar strain gauge data for all the joint reinforcements are presented in Figure D.30 (a) for the north beam and Figure D.30 (b) for the south beam. The load versus bottom aperture data from the CDT is shown in Figure D.30 (c) up until when the gauges were removed. The load versus concrete strain responses are shown in Figure D.31 (a) for bottom gauges, including when the cracking load was observed in Figure D.31 (b), and load versus top gauge response in Figure D.31 (c).



(a)

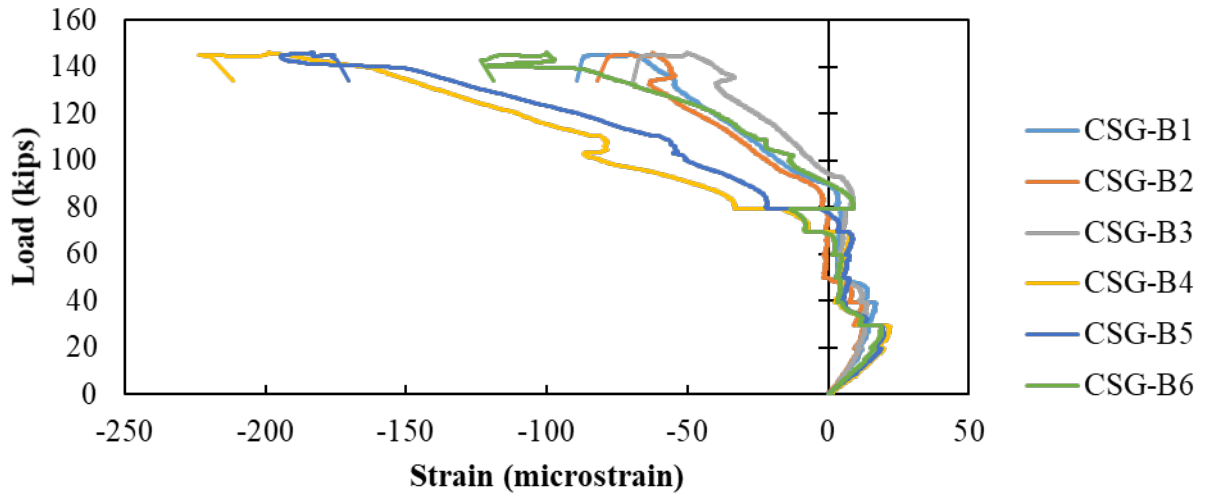


(b)

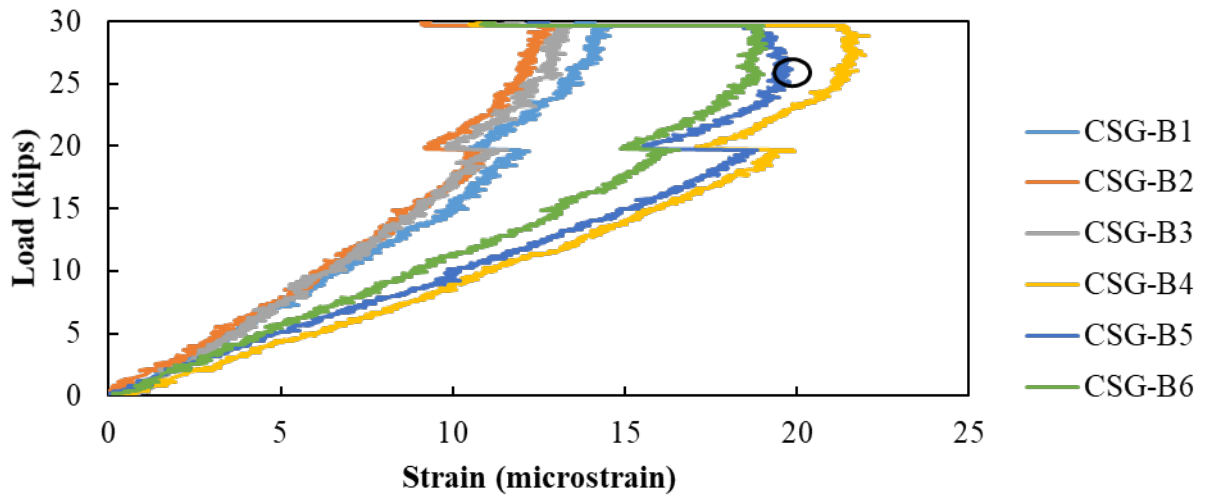


(c)

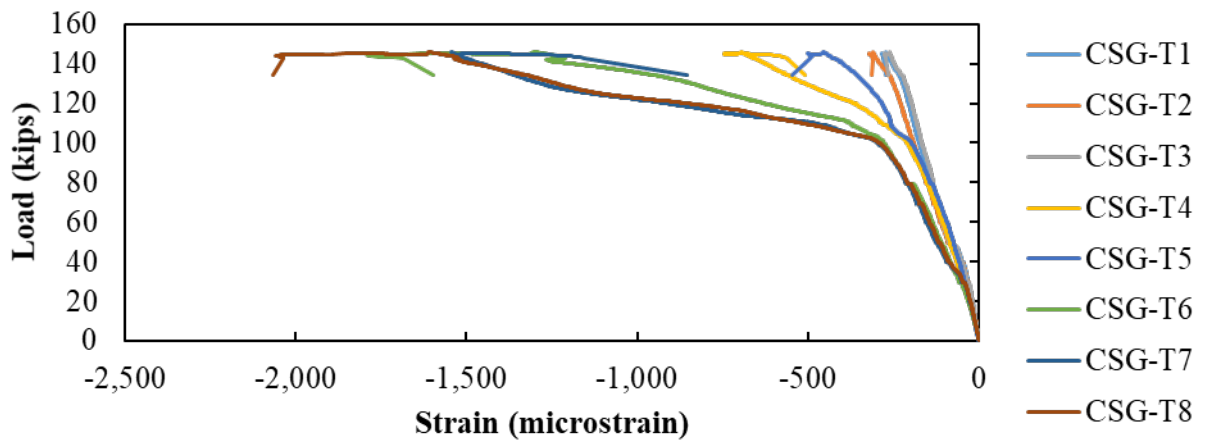
Figure D.30: 18A1-2 response: (a) load versus rebar strain on north side, (b) load versus rebar strain on south side, and (c) load versus central bottom opening



(a)



(b)



(c)

Figure D.31: 18A1-2 response: (a) load versus bottom concrete strain, (b) cracking load determination based on load versus bottom concrete strain response, and (c) load versus top concrete strain

D.5. 12-INCH SPECIMENS

The following section describes the main behaviors observed for each test performed on the 12-inch-thick specimens, including: the total capacity of each joint specimen, type of failure, comments on concrete performance (adequate or faulty mix, type of bond achieved, etc.), and comments on joint reinforcement performance (yielding, breaking, bending, etc.). Some figures will also help to describe the failure mechanism of each joint geometry.

There were some specimens where the first joint test was done under monotonic loading and then the second joint test involved fatigue testing followed by a monotonic load test. Results from static tests that were performed after the fatigue testing are highlighted. Fatigue test results will be presented elsewhere.

There were two primary cracking patterns at failure observed in the 12-inch-deep specimens, shown in Figure D.32 and Figure D.33. The first common failure mechanism began with a diagonal crack forming in the joint region, shown in Figure D.32. This diagonal crack then extended into the top corner of the precast section on the loaded side and through the bottom flange of the precast section on the unloaded side. Failure of these specimens occurred either with crushing of the concrete along the length of the joint under the load point, which was accompanied by fracture or pullout of the reinforcement, or by pullout of the reinforcement before crushing of the concrete occurred.

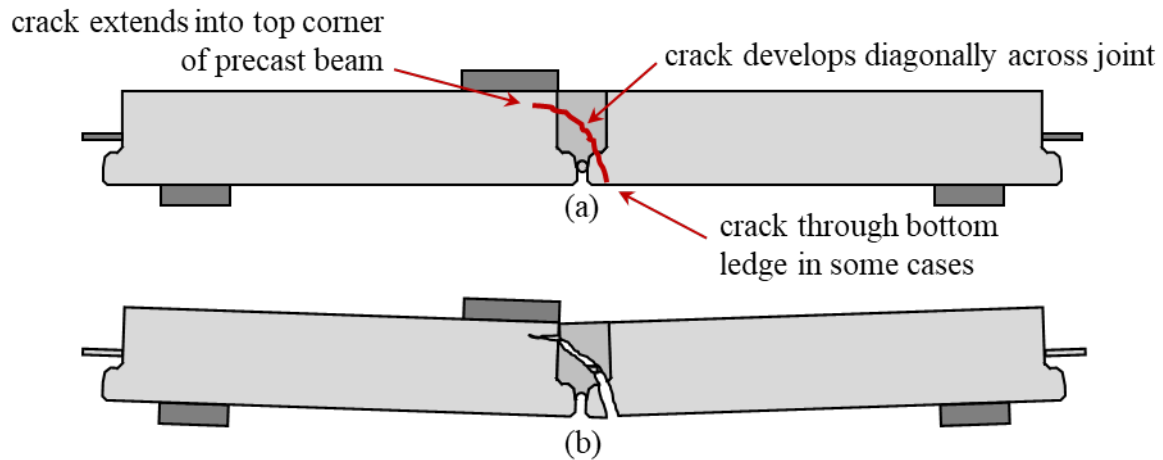


Figure D.32: Typical failure in 12-inch-deep specimens with diagonal crack through joint: (a) cracking at failure and (b) after failure

The second common failure mechanism began with debonding of the UHPC from the precast section or a crack forming parallel to the joint in cases where sufficient bond was achieved. A second crack then would form at the level of the joint reinforcement in the joint and in some cases extending into the precast section. Failure would then be triggered by either crushing of the concrete, which was typically accompanied by fracture of the reinforcement, or splitting of the UHPC at the level of the reinforcement triggering a pullout failure.

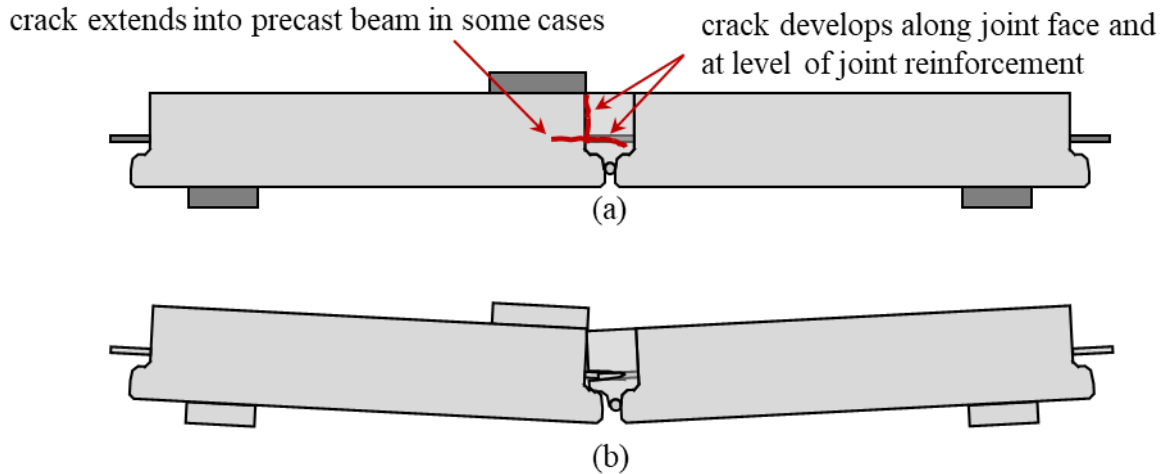


Figure D.33: Typical failure in 12-inch-deep specimens with cracking along joint face and at level of reinforcement: (a) cracking at failure and (b) after failure

D.5.1. 12F1 (FDOT 1)

The strength testing result observations describing the failure forces, type of failures, and concrete and rebar behaviors for the 12F1 specimens are highlighted in Table D.6.

Table D.6: 12F1 Strength testing summary

Test	Failure Force [kip]	Type of Failure	Concrete Comments	Rebar Comments
12F1-1	70.0	Pull-out failure	<ul style="list-style-type: none"> Poor bond between UHPC and precast section Diagonal crack in UHPC matrix at failure Partial rupture of bottom ledge 	<ul style="list-style-type: none"> All joint reinforcement pulled out of joint
12F1-2	66.9*	Pull-out failure	<ul style="list-style-type: none"> Improved bond between UHPC and precast section Cone of UHPC pulled out with the joint reinforcement 	<ul style="list-style-type: none"> All joint reinforcement pulled out of joint

* After cyclic test

D.5.1.1. Test 1 (12F1-1)

The crack pattern at failure for 12F1-1 is shown in Figure D.34. A clear diagonal crack occurred in the UHPC at failure, shown in Figure D.34 (a). This crack started in the UHPC, but then expanded into the top portion of the precast section and down through the bottom ledge, as highlighted in Figure D.34 (b).

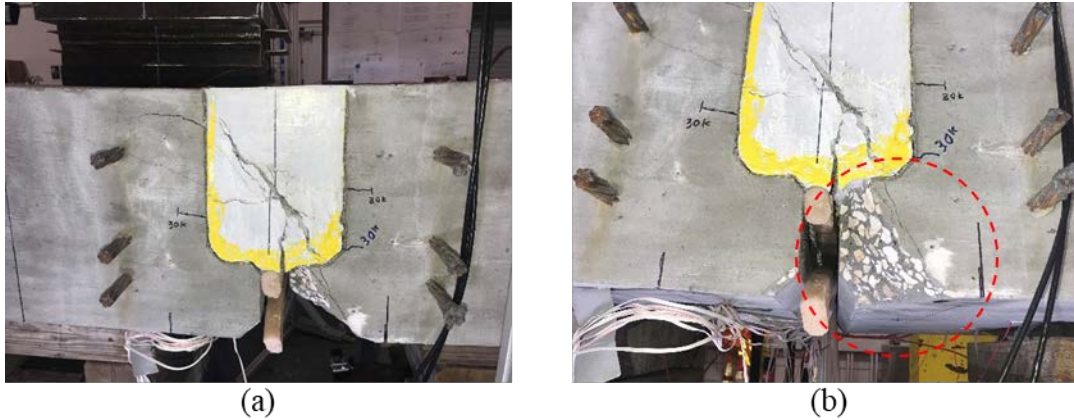
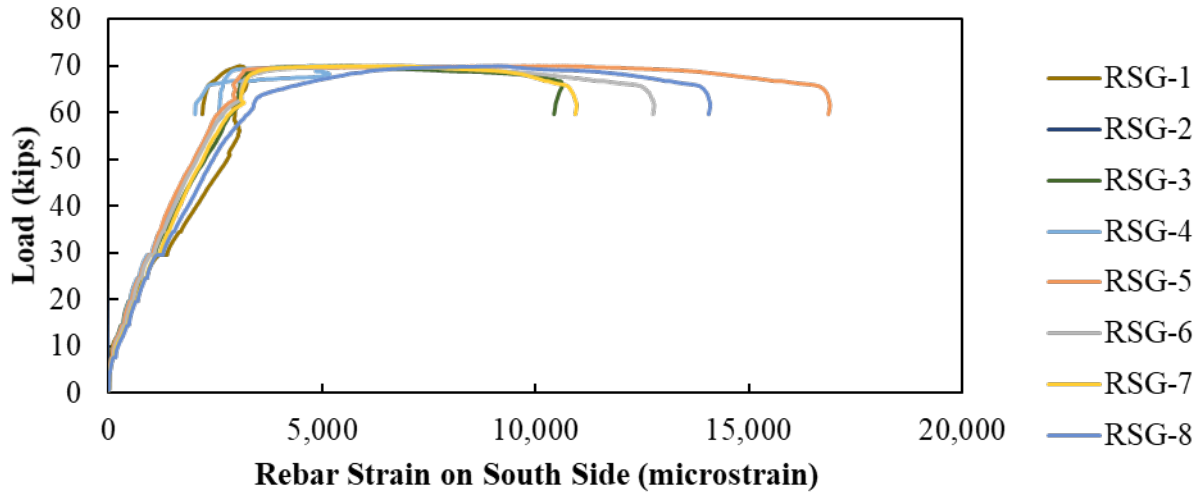


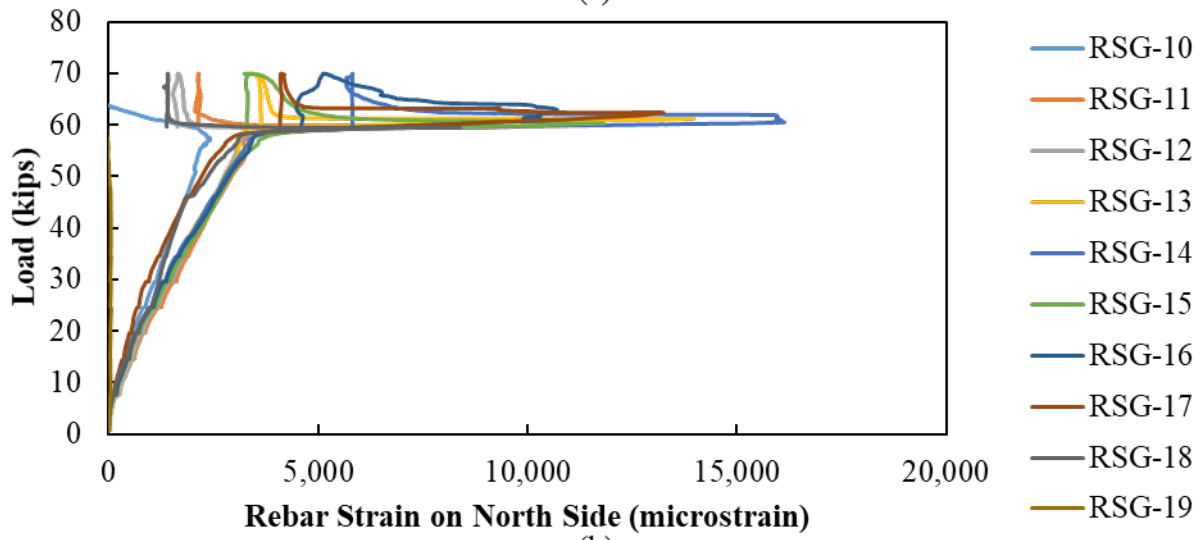
Figure D.34: 12F1-1: (a) failed joint specimen and (b) bottom lip failure

No crushing of the concrete in the compression block occurred. The failure was caused by pullout of the joint reinforcement. However, testing was stopped immediately after the load began to fall, so the specimens had to be cut in half to reposition them for the second test. Because the specimen was cut in half, no photographs could be taken of the fracture plane.

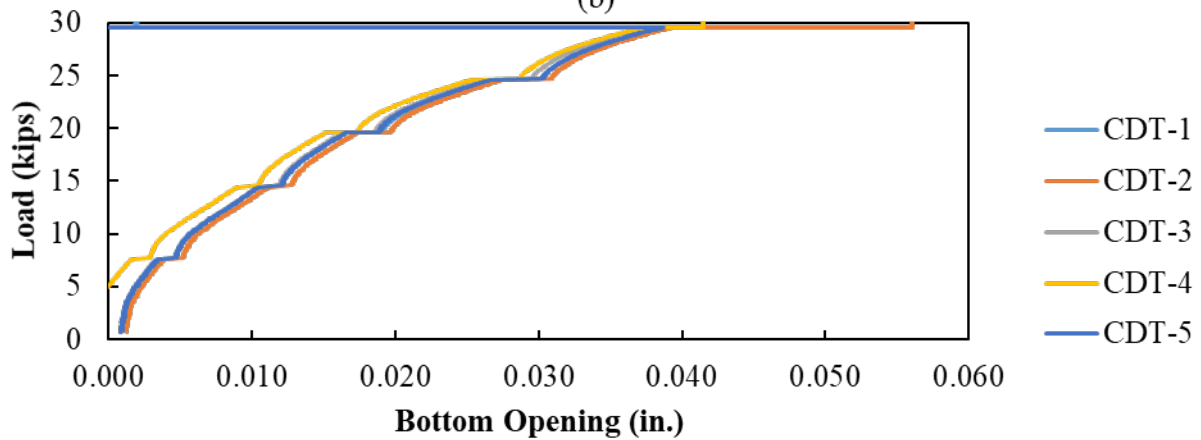
The load versus rebar strain gauge data for all the joint reinforcements are presented in Figure D.35 (a) for the south beam and Figure D.35 (b) for the north beam. The load versus bottom aperture data from the CDT is shown in Figure D.35 (c) up until when the gauges were removed. The load versus concrete strain responses are shown in Figure D.36 (a) for bottom gauges, including when the cracking load was observed in Figure D.36 (b), and load versus top gauge response in Figure D.36 (c).



(a)

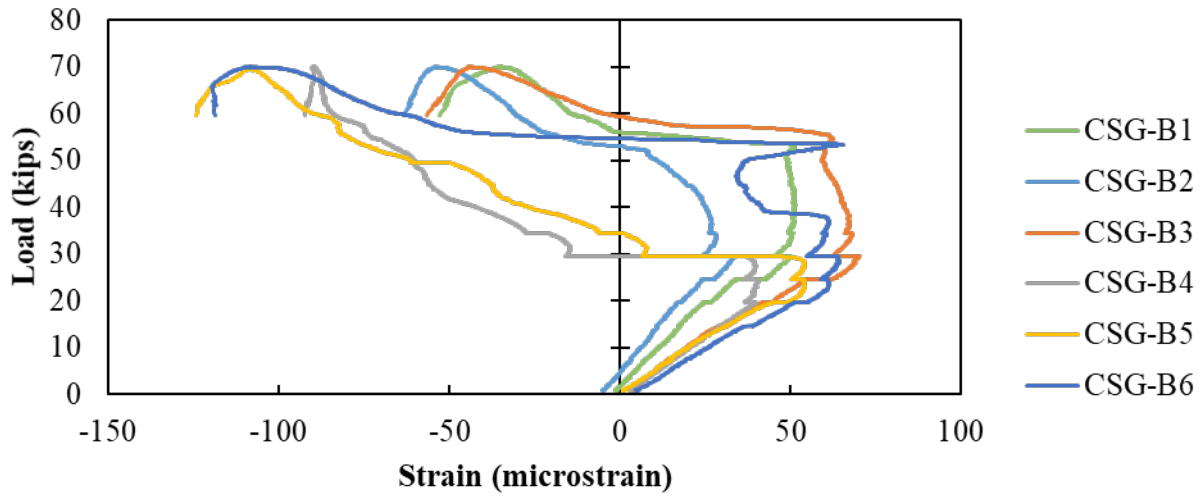


(b)

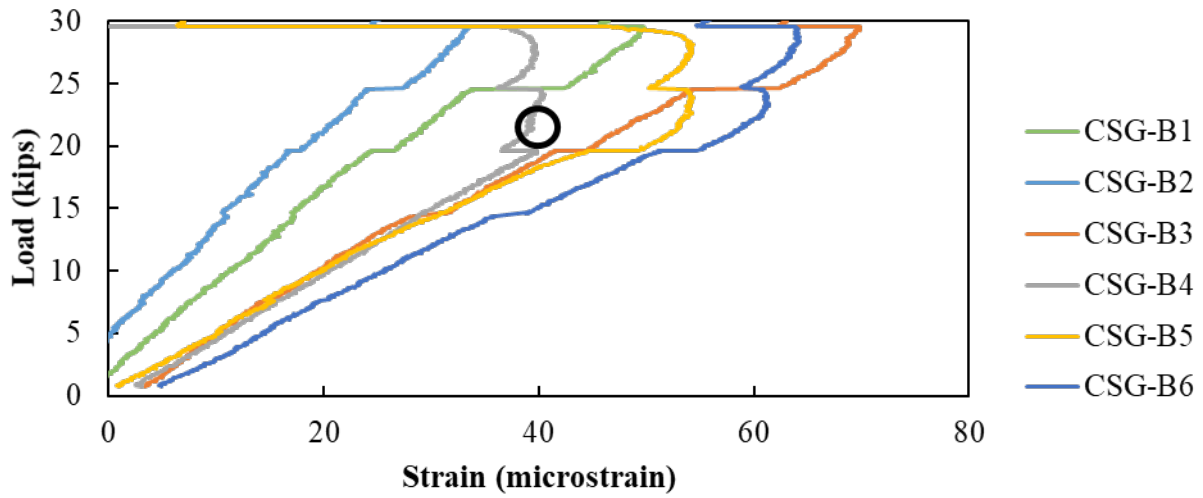


(c)

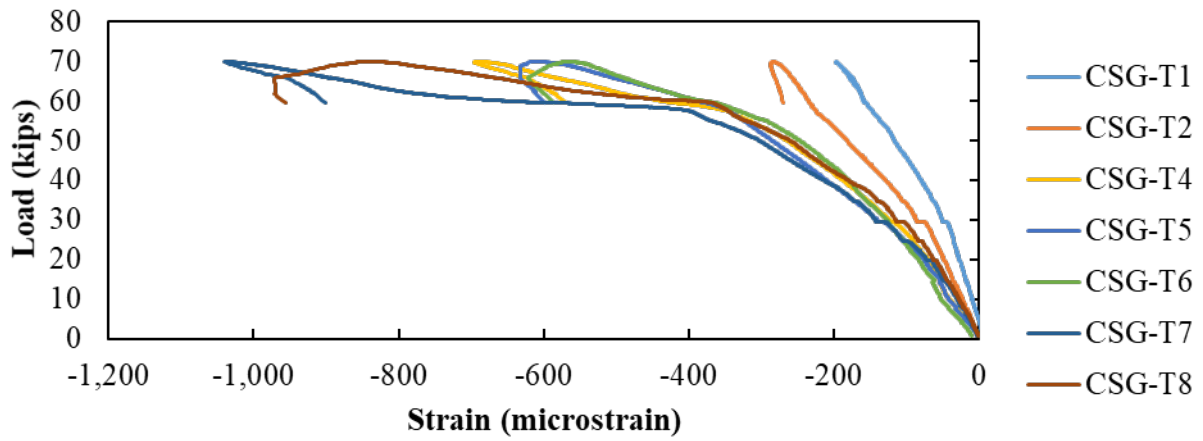
Figure D.35: 12F1-1 response: (a) load versus rebar strain on south side, (b) load versus rebar strain on north side, and (c) load versus central bottom opening



(a)



(b)



(c)

Figure D.36: 12F1-1 response: (a) load versus bottom concrete strain, (b) cracking load determination based on load versus bottom concrete strain response, and (c) load versus top concrete strain

D.5.1.2. Test 2 (12F1-2)

The static test for 12F1-2 was performed after fatigue testing of 2 million cyclic loads. Photographs of the failed specimen are shown in Figure D.37. There was better bond between the UHPC and precast section, but the failure crack still developed at the joint. Additionally, a splitting crack developed at the level of the joint reinforcement, shown in Figure D.37 (a). Failure of the joint was caused by pullout of all the joint reinforcement. Cones of UHPC pulled out with some of the reinforcement, as shown in Figure D.37 (c) and (d), while other reinforcement pulled out without any UHPC attached.

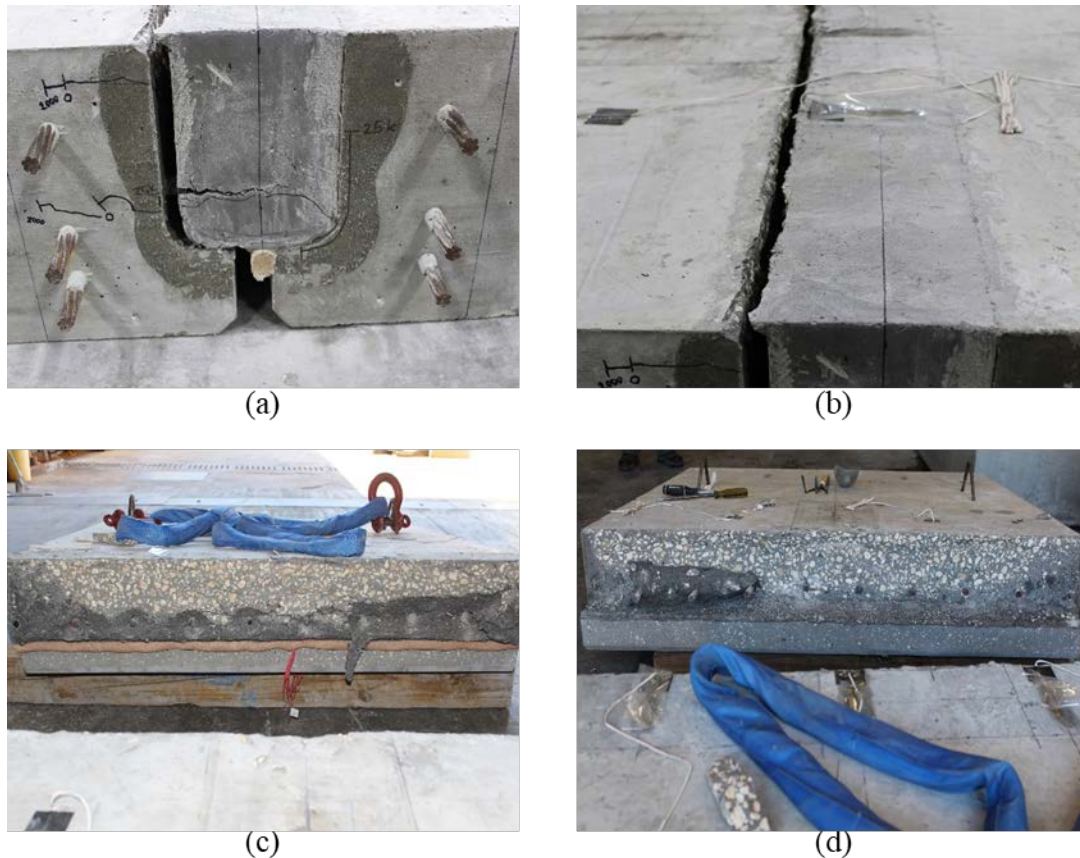
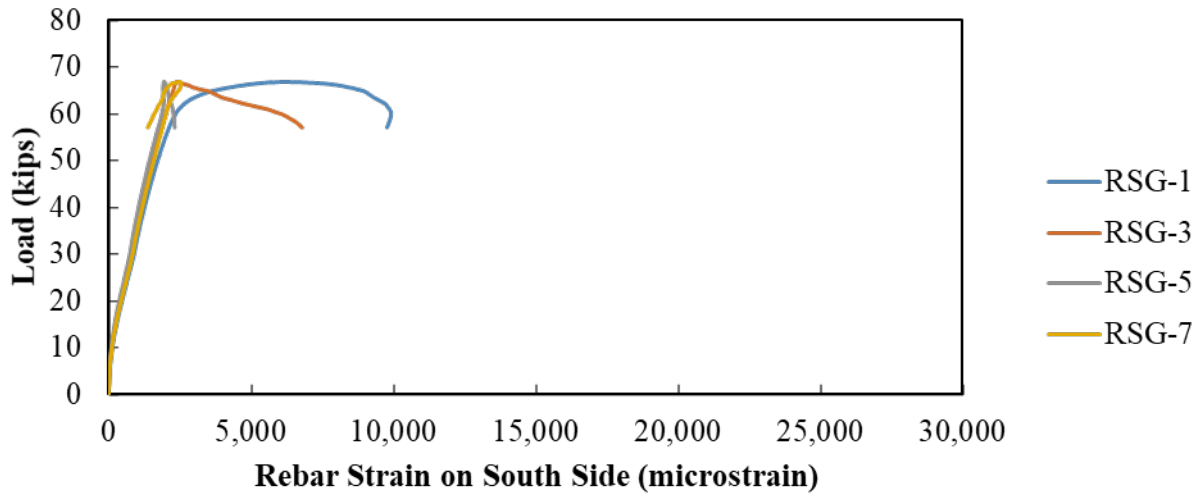
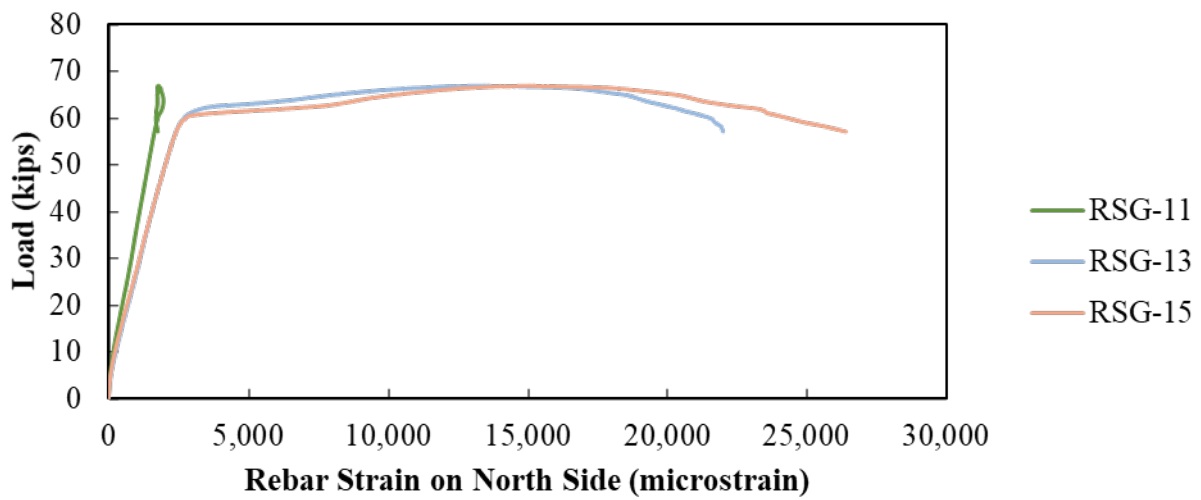


Figure D.37: 12F1-2: (a) failed joint specimen after overload performance, (b) continuous failure line along the UHPC-to-precast boundary, (c) pull-out cone shapes observed in UHPC matrix, and (d) cavity left by UHPC cover detachment

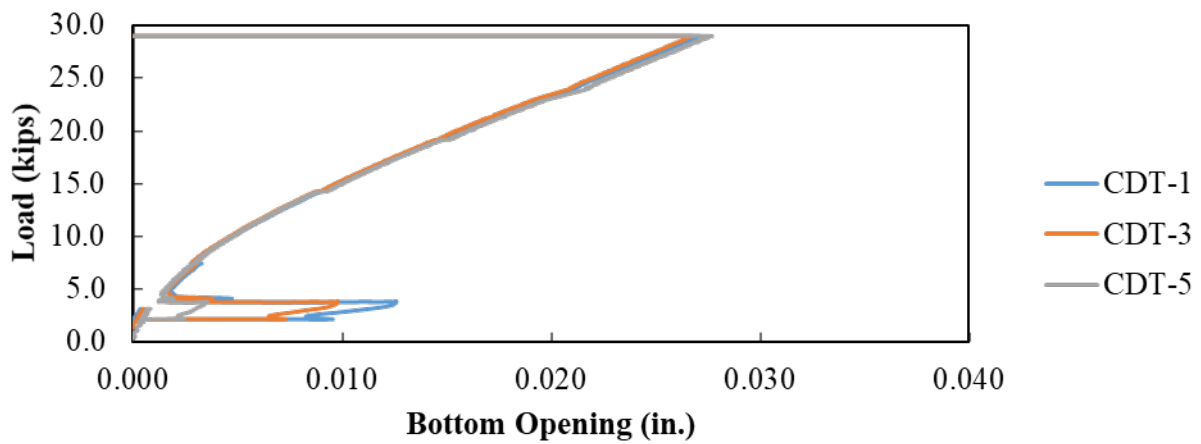
The load versus rebar strain gauge data for all the joint reinforcements are presented in Figure D.38 (a) for the south beam and Figure D.38 (b) for the north beam. The load versus bottom aperture data from the CDT is shown in Figure D.38 (c) up until when the gauges were removed. The load versus concrete strain responses are shown in Figure D.39 (a) for the bottom gauges. Cracking had already occurred in this specimen during the fatigue testing, so the cracking load plot and top concrete strain gauges were not included for this testing instance.



(a)



(b)



(c)

Figure D.38: 12F1-2 response: (a) load versus rebar strain on south side, (b) load versus rebar strain on north side, and (c) load versus central bottom opening

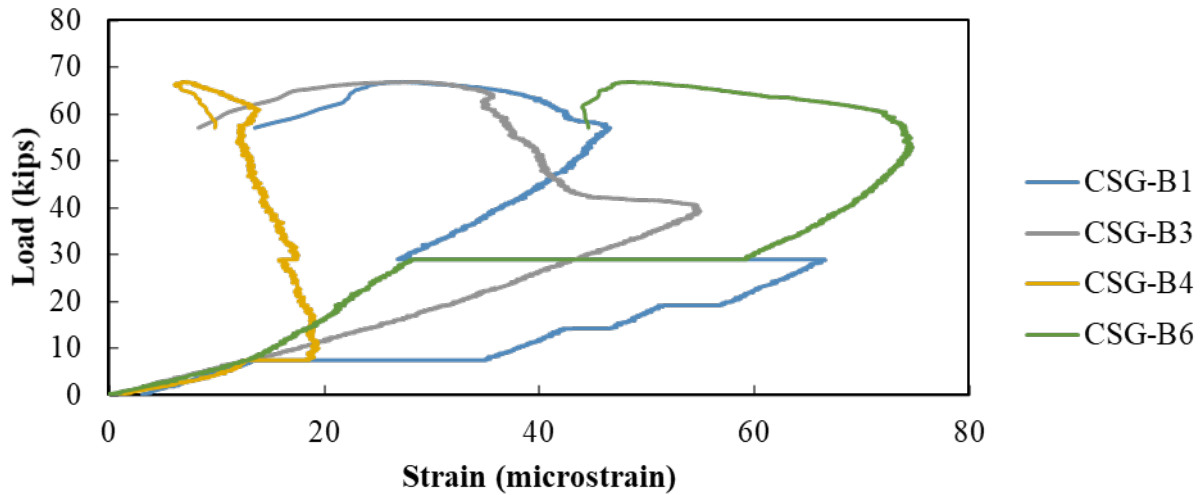


Figure D.39: Load versus bottom concrete strain response for 12F1-2 response

D.5.2. 12F2 (FDOT 2)

The strength testing result observations describing the failure forces, type of failures, and concrete and rebar behaviors for the 12F2 specimens are highlighted in Table D.7.

Table D.7: 12F2 Strength testing summary

Test	Failure Force [kip]	Type of Failure	Concrete Comments	Rebar Comments
12F2-1	98.1	Pull-out failure	<ul style="list-style-type: none"> Poor bond between UHPC and precast section Splitting crack at the level of the reinforcement Rupture of bottom ledge on unloaded beam Crushing of concrete in compression block seemed to cause failure 	<ul style="list-style-type: none"> No reinforcement fractured Reinforcement appears to have begun slipping, but testing was stopped prior to pullout failure
12F2-2	99.4	Pull-out failure	<ul style="list-style-type: none"> Better bond between UHPC and precast section Cone of UHPC pulled out with the joint reinforcement Crack developed in top corner of precast section next to the UHPC joint Rupture of the bottom ledge on the loaded beam 	<ul style="list-style-type: none"> All joint reinforcement pulled out of joint

D.5.2.1. Test 1 (12F2-1)

The cracking pattern at failure for 12F2-1 is shown in Figure D.40. Crushing of the concrete in the compression block under the load, highlighted in Figure D.40 (a), appears to have triggered the failure. Debonding between the UHPC and precast section occurred on the side of the joint toward the load. A splitting crack occurred at the level of the reinforcement and the reinforcement appears to have begun slipping, see Figure D.41 (b), but load application was stopped immediately after a drop in the applied load was detected.

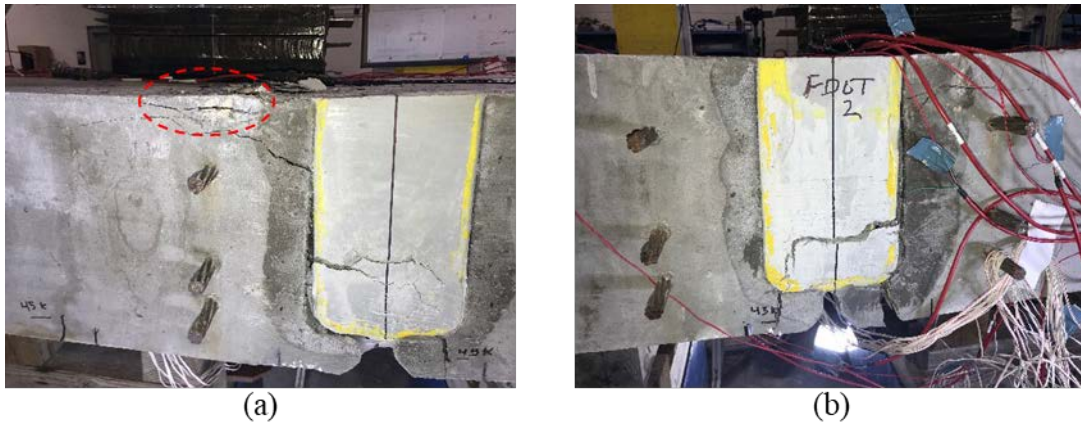
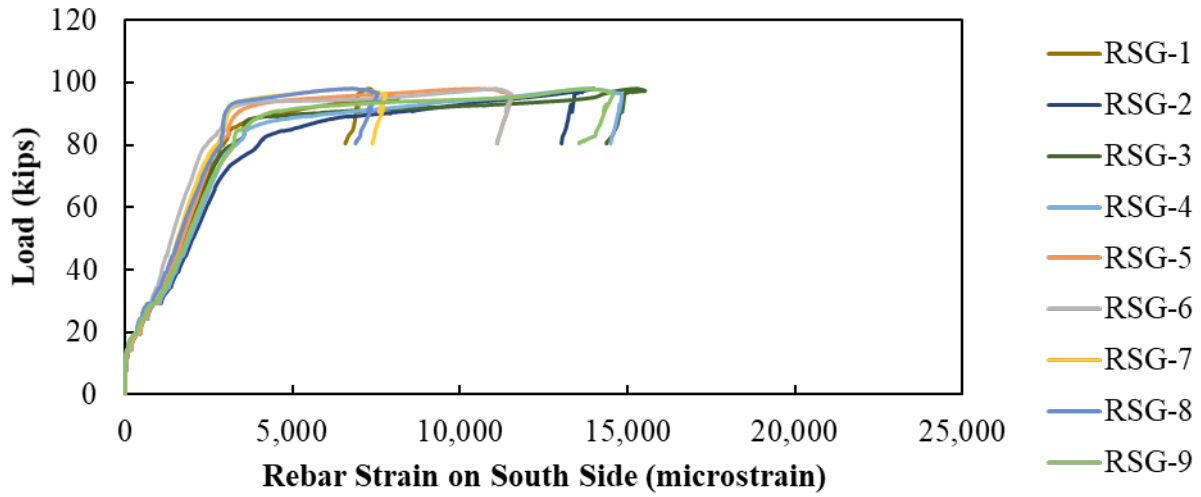


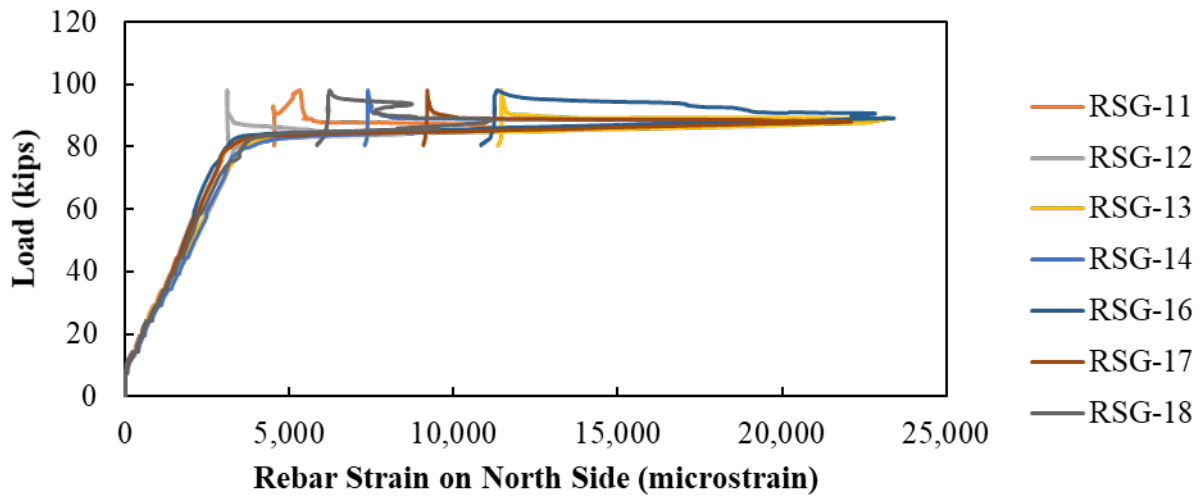
Figure D.40: 12F2-1: (a) failed specimen with similar failure cracks to 18F2 and (b) east side failed specimen

The specimen was not broken apart during testing and needed to be cut in half to prepare it for the second joint test. Because the specimen was cut in half, no photographs could be taken of the fracture plane.

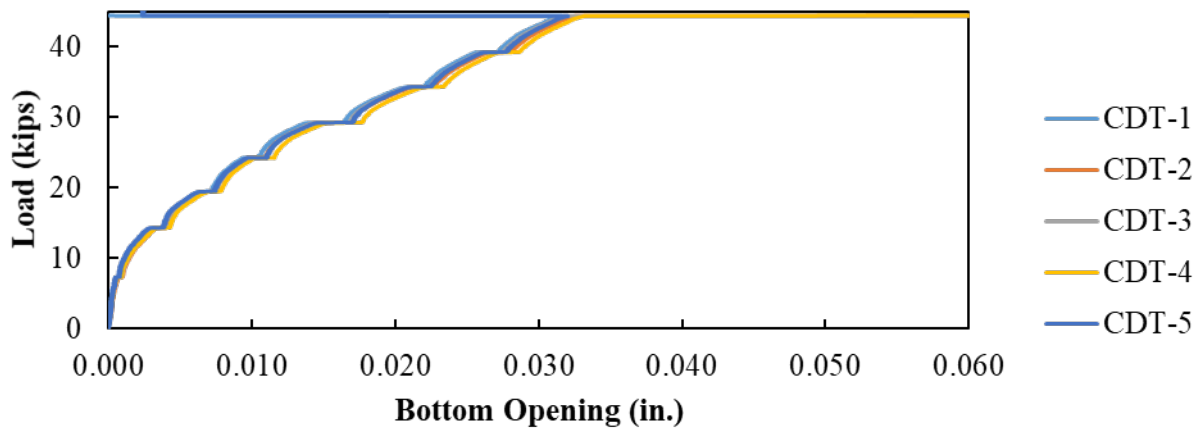
The load versus rebar strain gauge data for all the joint reinforcements are presented in Figure D.41 (a) for the south beam and Figure D.41 (b) for the north beam. The load versus bottom aperture data from the CDT is shown in Figure D.41 (c) up until when the gauges were removed. The load versus concrete strain responses are shown in Figure D.42 (a) for bottom gauges, including when the cracking load was observed in Figure D.42 (b), and load versus top gauge response in Figure D.42 (c).



(a)

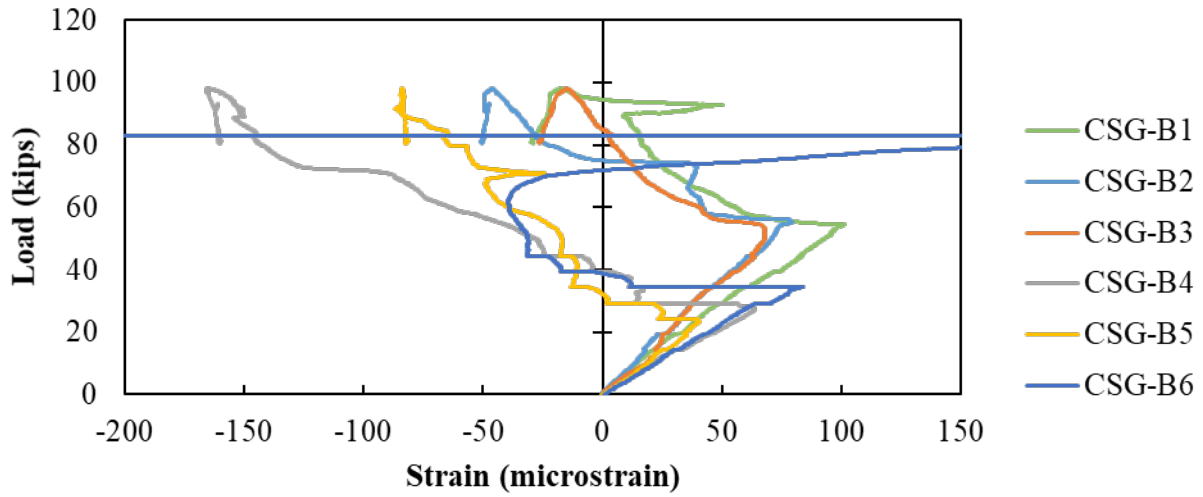


(b)

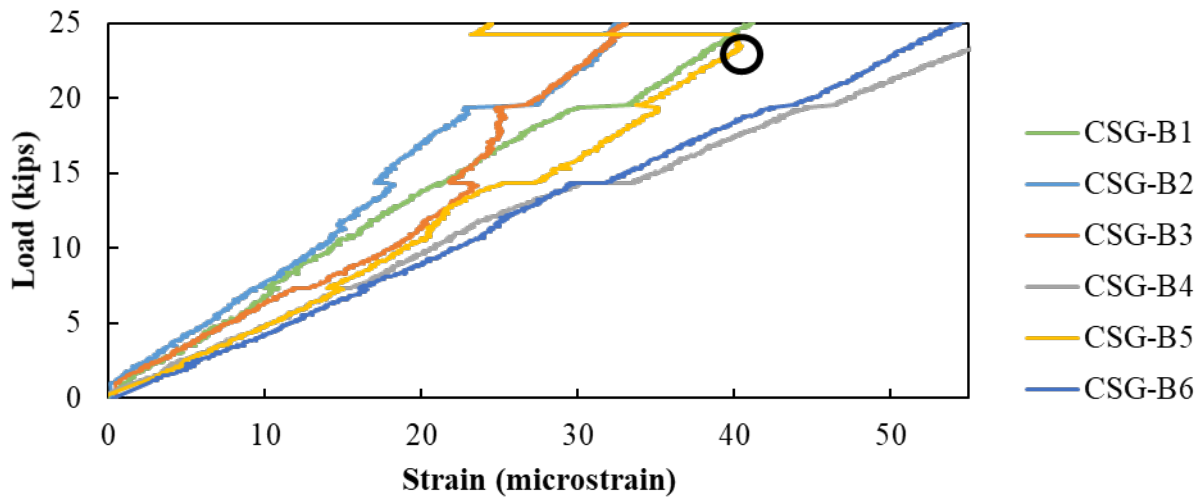


(c)

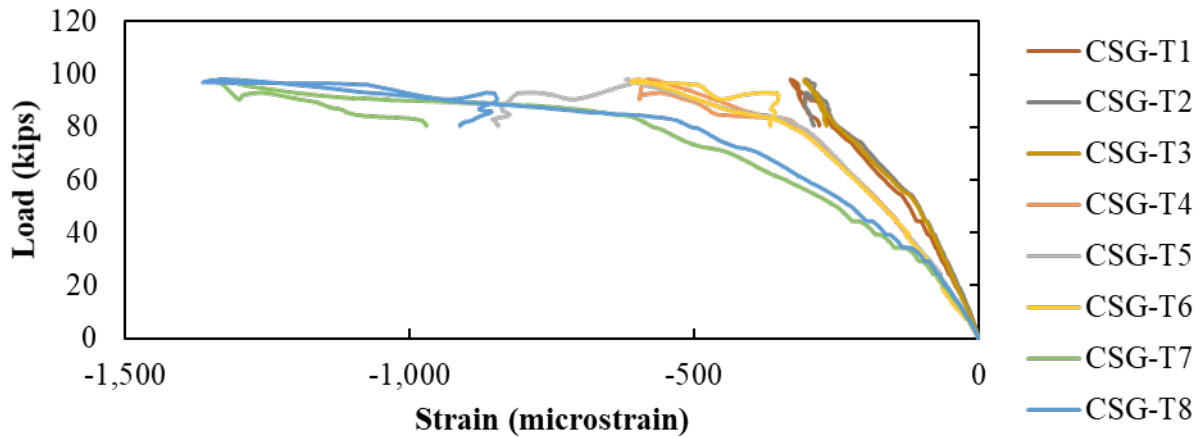
Figure D.41: 12F2-1 response: (a) load versus rebar strain on south side, (b) load versus rebar strain on north side, and (c) load versus central bottom opening



(a)



(b)



(c)

Figure D.42: 12F2-1 response: (a) load versus bottom concrete strain, (b) cracking load determination based on load versus bottom concrete strain response, and (c) load versus top concrete strain

D.5.2.2. Test 2 (12F2-2)

Cracking at failure for 12F2-2 is shown in Figure D.43. No crushing of the concrete in the compression block occurred. Failure was initiated by pullout of the joint reinforcement. A cone of UHPC pulled out with some of the reinforcement, shown in Figure D.43 (a). There was a much better bond between the UHPC and precast section. This improved bond caused the hinge to develop further into the precast section (a few inches from the joint face), highlighted in Figure D.43 (a). Close-up photographs of the hinge caused by bending and the good UHPC bond are shown in Figure D.43 (c) and (d). The bottom lip of the joint cracked before failure and ruptured at ultimate load.

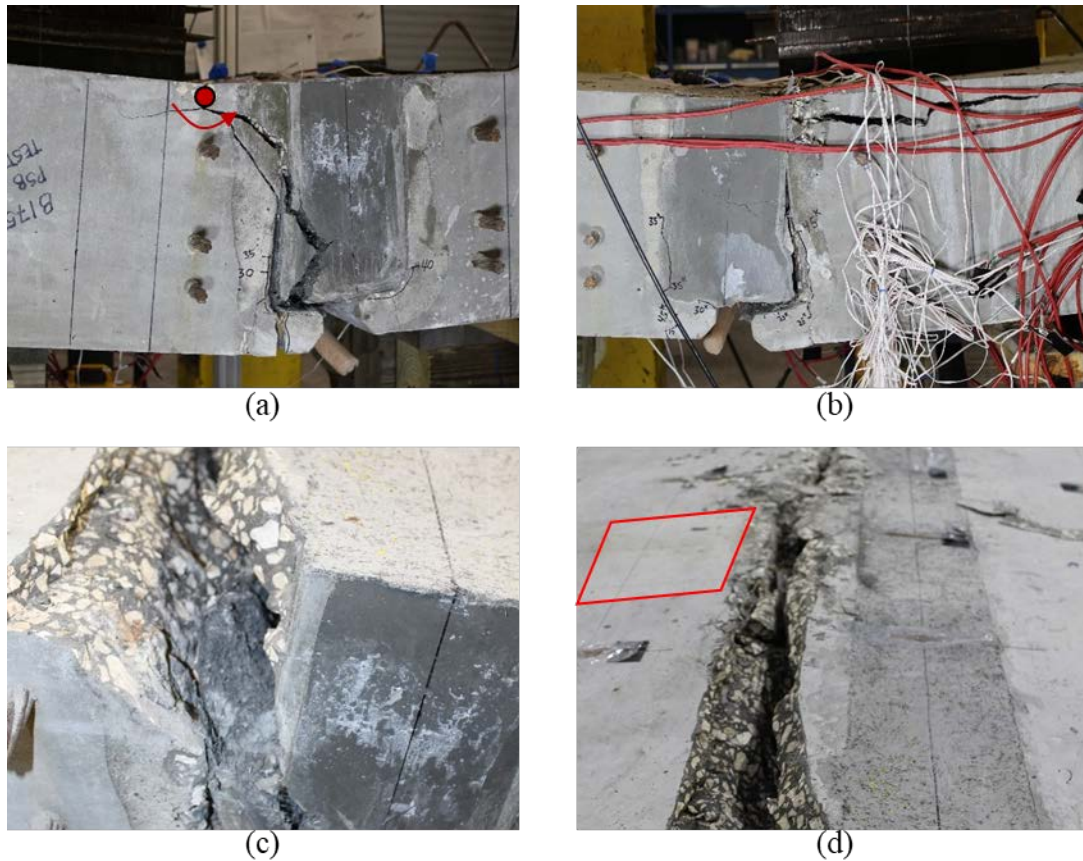
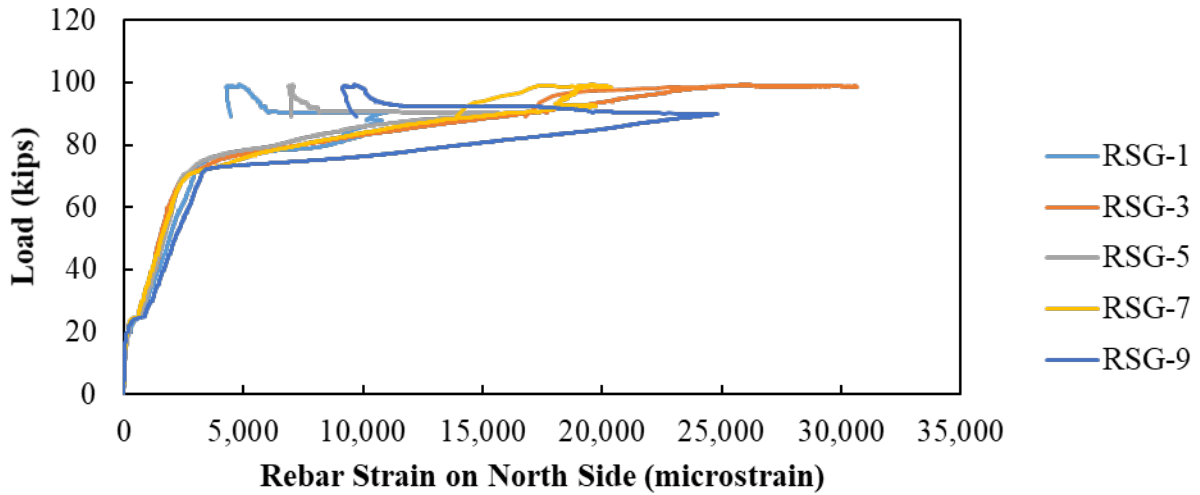
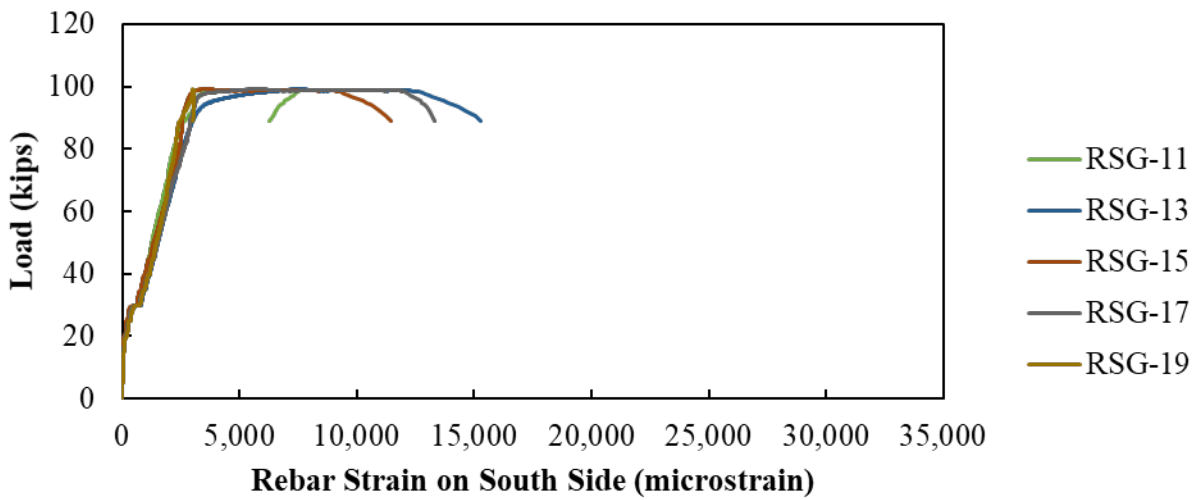


Figure D.43: 12F2-2: (a) failed beam – west side, (b) failed joint – east side, (c) concrete failure at the cover region, and (d) extension of concrete crack (load application point shown)

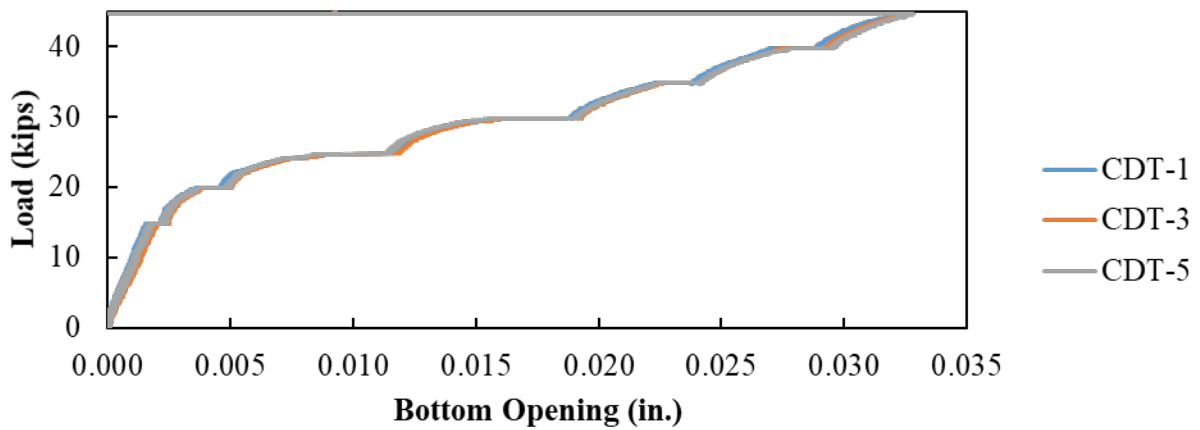
The load versus rebar strain gauge data for all the joint reinforcements are presented in Figure D.44 (a) for the north beam and Figure D.44 (b) for the south beam. The load versus bottom aperture data from the CDT is shown in Figure D.44 (c) up until when the gauges were removed. The load versus concrete strain responses are shown in Figure D.45 (a) for bottom gauges, including when the cracking load was observed in Figure D.45 (b). The top concrete gauges were not included in this testing instance.



(a)

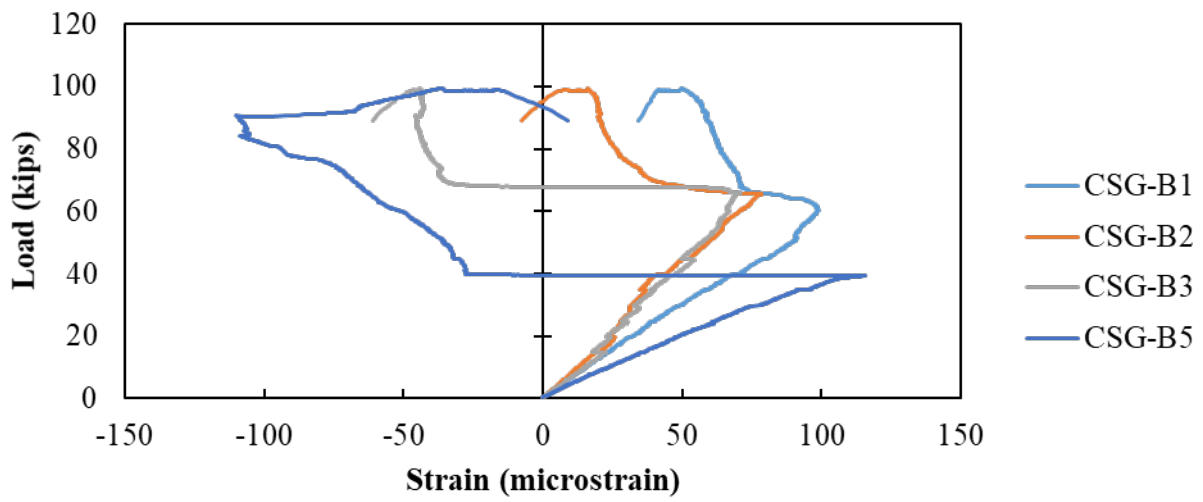


(b)

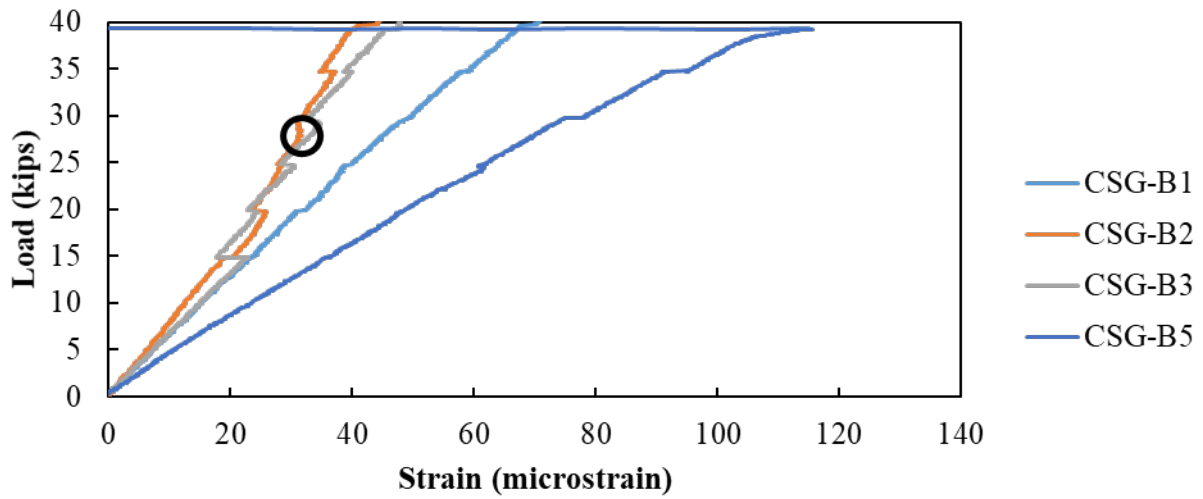


(c)

Figure D.44: 12F2-2 response: (a) load versus rebar strain on north side, (b) load versus rebar strain on south side, and (c) load versus central bottom opening



(a)



(b)

Figure D.45: 12F2-2 response: (a) load versus bottom concrete strain, and (b) cracking load determination based on load versus bottom concrete strain response

D.5.3. 12A1 (Alternate 1)

The strength testing result observations describing the failure forces, type of failures, and concrete and rebar behaviors for the 12A1 specimens are highlighted in Table D.8.

Table D.8: 12A1 Strength testing summary

Test	Failure Force [kip]	Type of Failure	Concrete Comments	Rebar Comments
12A1-1	61.0	Vertical splitting of UHPC in joint	<ul style="list-style-type: none"> • UHPC developed large diagonal crack at failure • No significant debonding observed between UHPC and precast section 	<ul style="list-style-type: none"> • No joint reinforcement fractured
12A1-2	67.5*	Concrete crushing	<ul style="list-style-type: none"> • Only minor cracking occurred in UHPC joint • Crack developed at level of joint reinforcement in precast section next to joint • Debonding observed between UHPC and top of bottom flange 	<ul style="list-style-type: none"> • No joint reinforcement fractured

* After cyclic test – Overload Performance

D.5.3.1. Test 1 (12A1-1)

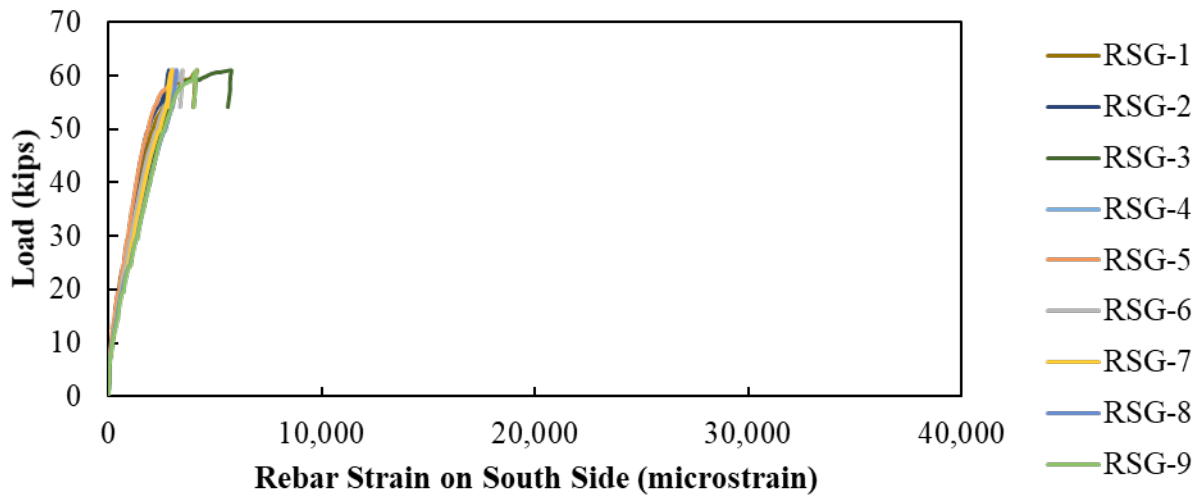
The cracking pattern at failure for 12A1-1 is shown in Figure D.46. A diagonal crack developed in the UHPC joint from the load point to the bottom ledge of the unloaded precast beam, as shown in Figure D.46 (b). A crack also developed in the precast section on the loaded side extending from the top inside corner of the joint to under the middle of the load point, shown in Figure D.46 (a). There was no clear sign of a pullout failure or fractured reinforcement. There may have been a failure of the splicing of the joint reinforcement likely caused failure.



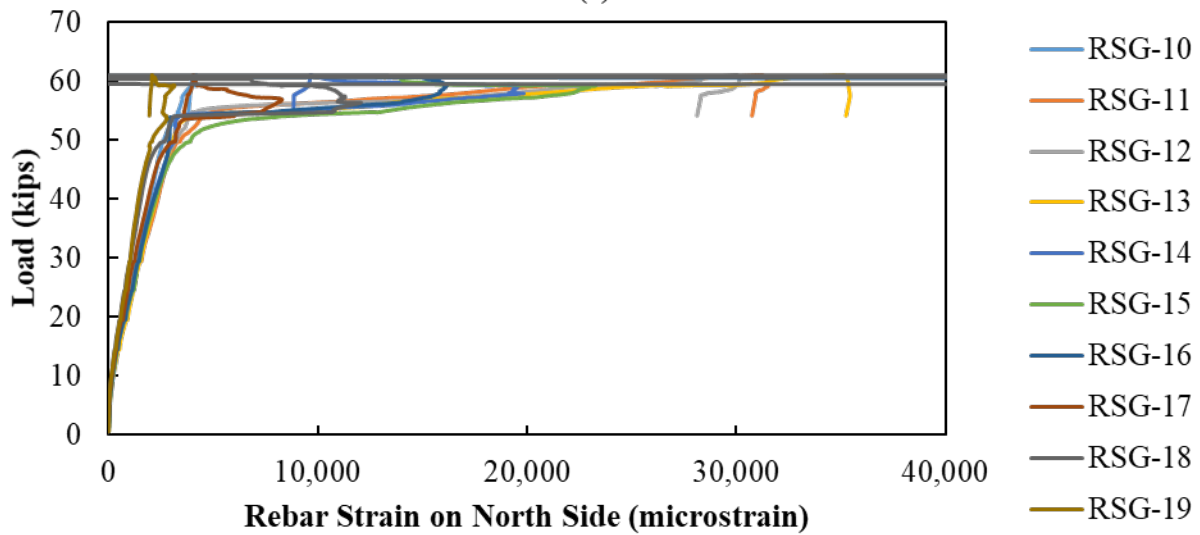
Figure D.46: 12A1-1: (a) failure cracks and (b) diagonal crack in UHPC matrix

The specimen was not broken apart during testing and needed to be cut in half to prepare it for the second joint test. Because the specimen was cut in half, no photographs could be taken of the fracture plane.

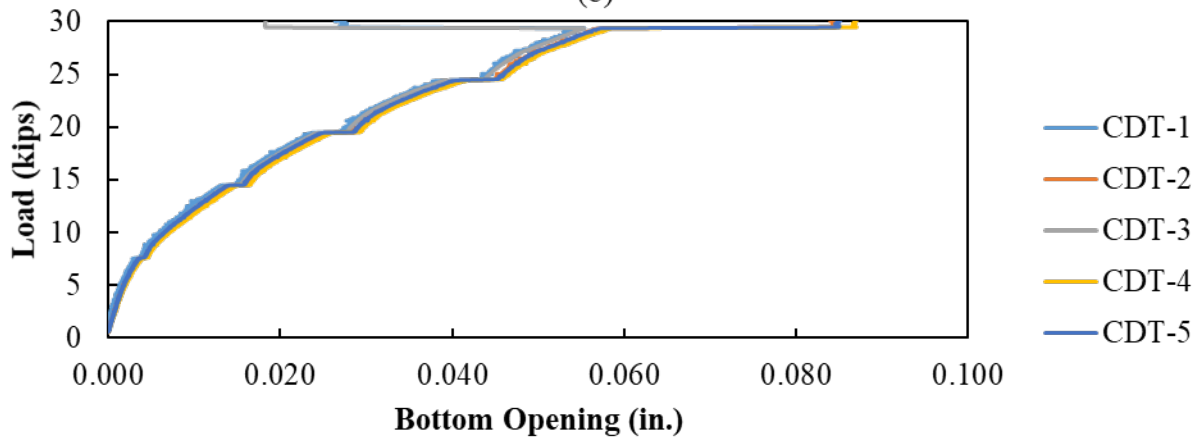
The load versus rebar strain gauge data for all the joint reinforcements are presented in Figure D.47 (a) for the south beam and Figure D.47 (b) for the north beam. The load versus bottom aperture data from the CDT is shown in Figure D.47 (c) up until when the gauges were removed. The load versus concrete strain responses are shown in Figure D.48 (a) for bottom gauges, including when the cracking load was observed in Figure D.48 (b), and load versus top gauge response in Figure D.48 (c).



(a)



(b)



(c)

Figure D.47: 12A1-1 response: (a) load versus rebar strain on south side, (b) load versus rebar strain on north side, and (c) load versus central bottom opening

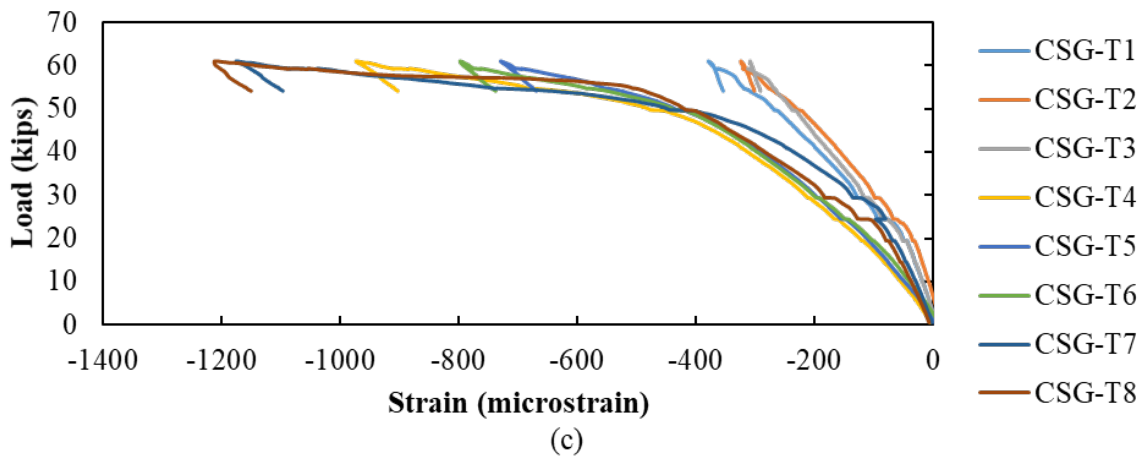
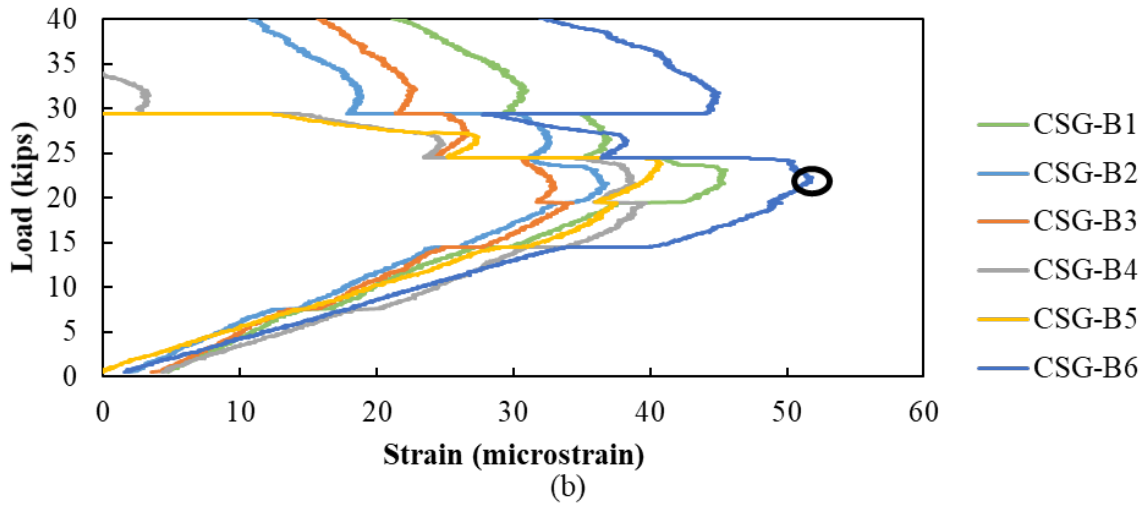
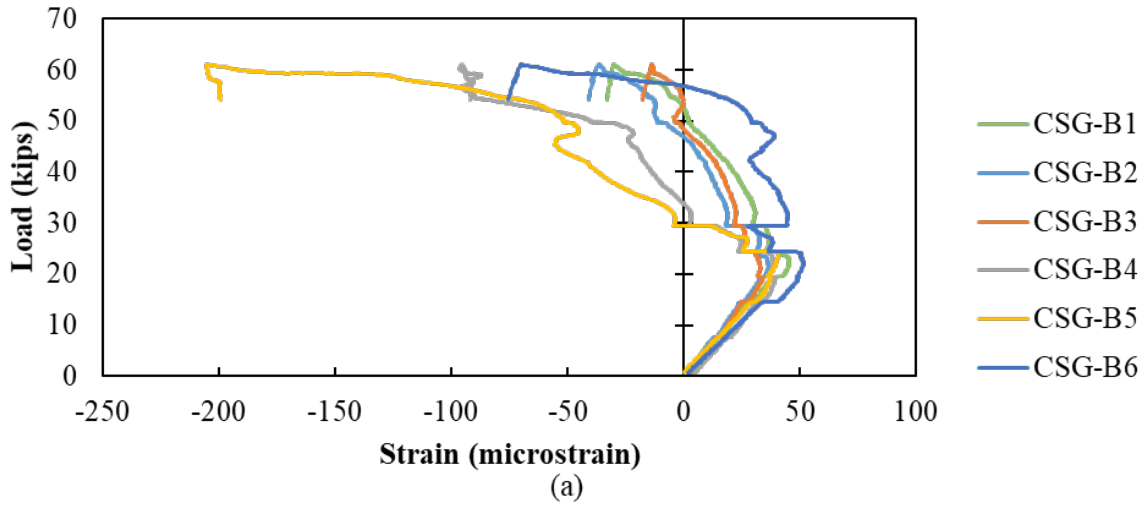


Figure D.48: 12A1-1 response: (a) Load versus bottom concrete strain, (b) cracking load determination based on load versus bottom concrete strain response, and (c) load versus top concrete strain

D.5.3.2. Test 2 (12A1-2)

The cracking at failure for 12A1-2 is shown in Figure D.49. The failure of 12A1-2 was triggered by crushing of the concrete in the compression block under the load, shown in Figure D.49 (b). A large crack developed in the precast section and a small crack in the UHPC at the level of the joint reinforcement, highlighted in Figure D.49 (c). However, there was no pullout or splice failure of the joint reinforcement. The UHPC mixture was greatly improved compared to the mixture used for 12A1-1. The better UHPC mixture resulted in no significant cracking occurring in the joint region and generally good bond between the UHPC and precast section. There was debonding between the top of the bottom flange in the precast section and the UHPC. Finally, some cracking occurred in the top of the precast section parallel to the top face under the load.

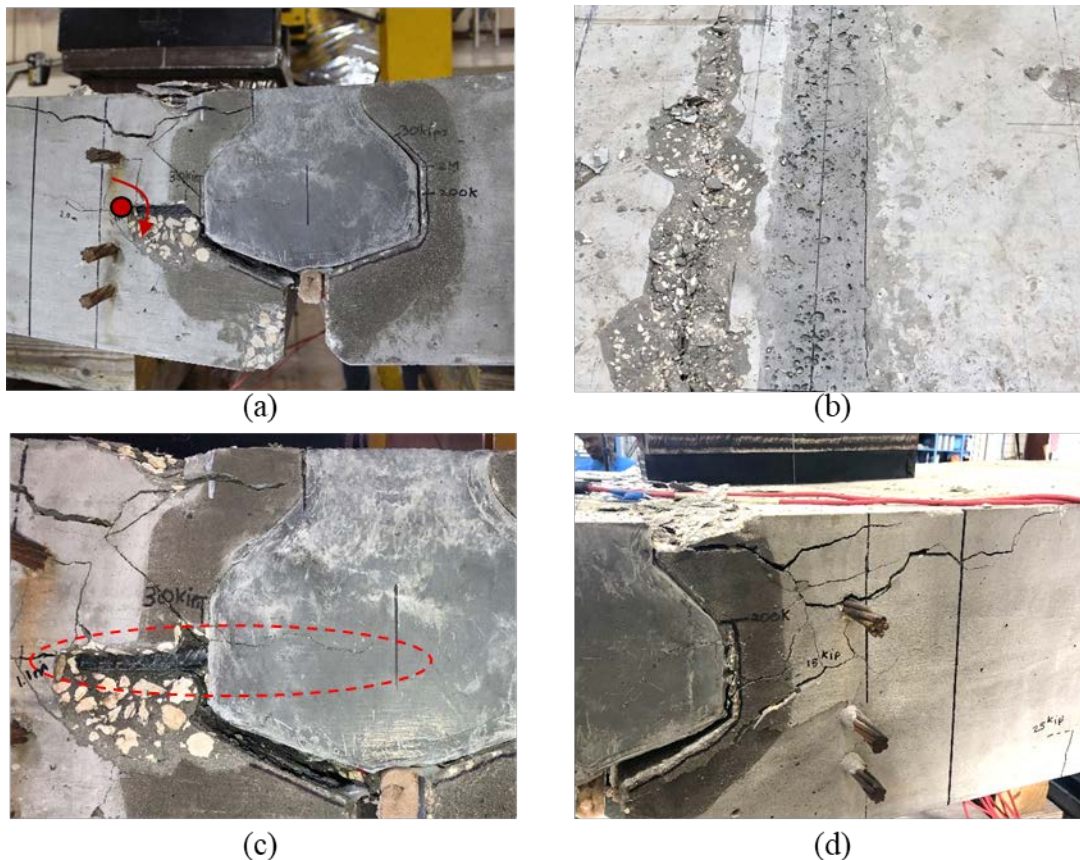
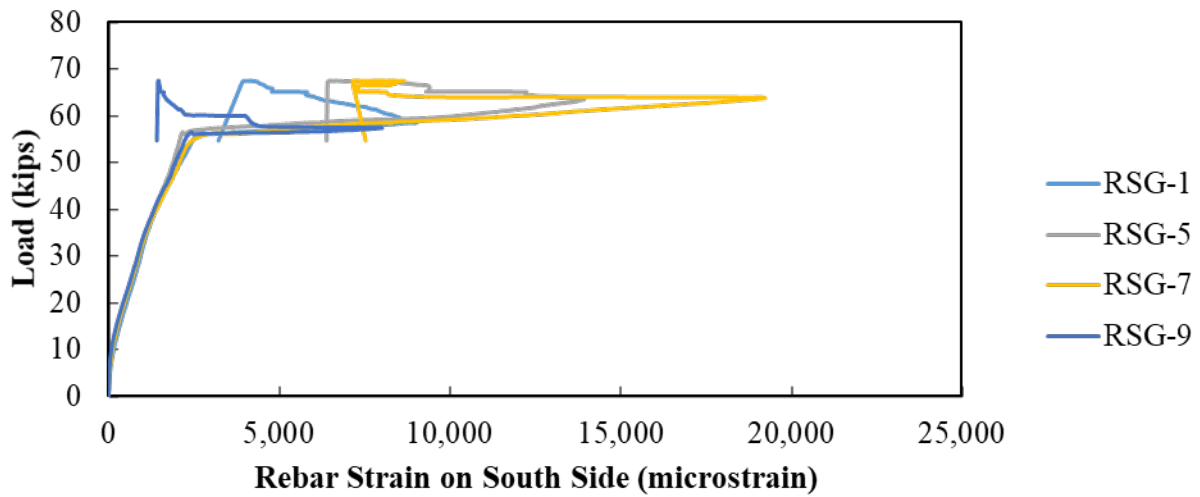
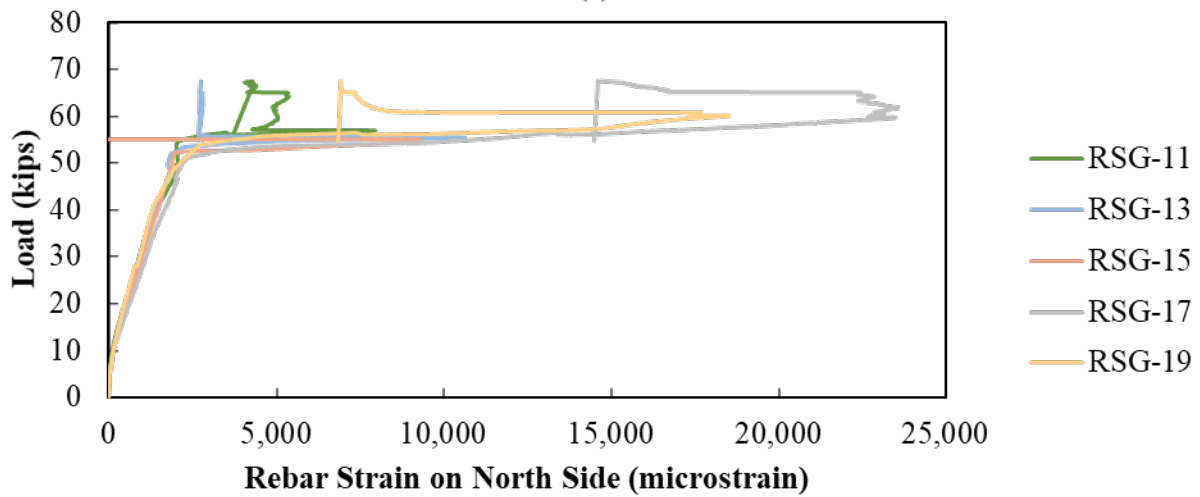


Figure D.49: 12A1-2: (a) failed specimen with hinge location highlighted, (b) longitudinal cracks observed on top of the specimen, (c) transverse crack at level of reinforcement in precast section, and (d) cracks extending into beam from joint

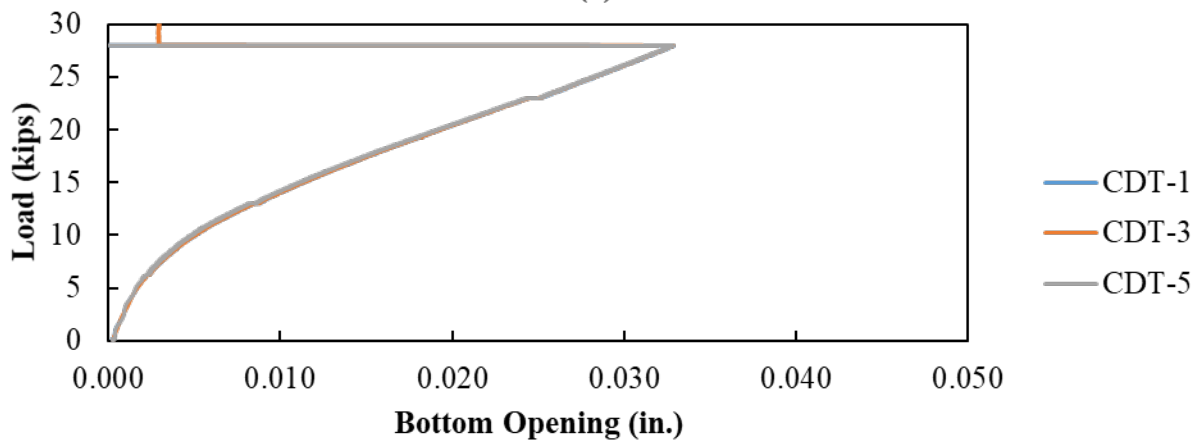
The load versus rebar strain gauge data for all the joint reinforcements are presented in Figure D.44 (a) for the south beam and Figure D.44 (b) for the north beam. The load versus bottom aperture data from the CDT is shown in Figure D.44 (c) up until when the gauges were removed. The load versus concrete strain responses are shown in Figure D.45 for bottom gauges. Cracking had already occurred in this specimen during the fatigue testing, so the cracking load plot and top concrete strain gauges were not included for this testing instance.



(a)



(b)



(c)

Figure D.50: 12A1-2 response: (a) load versus rebar strain on south side, (b) load versus rebar strain on north side, and (c) load versus central bottom opening

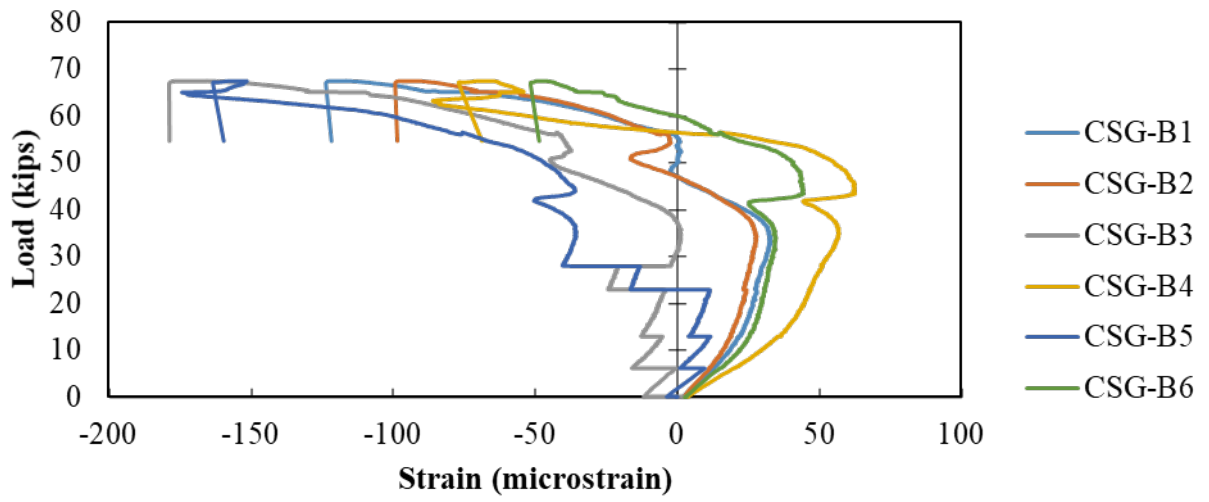


Figure D.51: Load versus bottom concrete strain for 12A1-2

D.5.4. 12A2 (Alternate 2)

This specimen was created based on observations from the testing performed on the other three joint configurations. This joint configuration included the following characteristics:

- Maximized lever arm of joint reinforcement for improved strength
- Thicker bottom flange than 12F2 to improve constructability and decrease early flange cracking
- Better exposed aggregate finish using paste retarder
- Larger available development length of joint reinforcement
- Larger non-contact lap splice length of joint reinforcement
- Smaller top flange to decrease stress concentrations

Additional details on this joint can be found in the body.

The strength testing result observations describing the failure forces, type of failures, and concrete and rebar behaviors for the 12A2 specimens are highlighted in Table D.9.

Table D.9: 12A2 Strength testing summary

Test	Failure Force [kip]	Type of Failure	Concrete Comments	Rebar Comments
12A2-1	90.9	Concrete crushing	<ul style="list-style-type: none"> • Good bond observed between UHPC and precast section • Crushing of concrete in compression block under load triggered failure • Crack formed right at joint interface 	<ul style="list-style-type: none"> • No joint reinforcement fractured
12A2-2	100.5*	Concrete crushing	<ul style="list-style-type: none"> • Good bond observed between UHPC and precast section • Crushing of concrete in compression block under load triggered failure • Crack formed right at joint interface 	<ul style="list-style-type: none"> • No joint reinforcement fractured

* After cyclic test – Overload Performance

D.5.4.1. Test 1 (12A2-1)

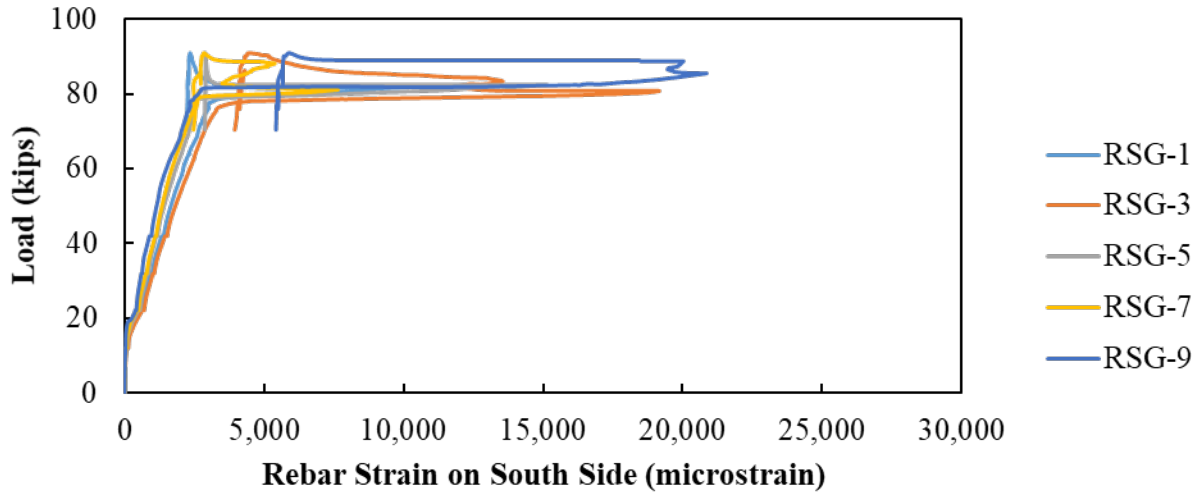
The failure of 12A2-1 is shown in Figure D.52. Cracking began at the interface between the UHPC and precast section and continued in the precast section. The interface crack continued to open followed by a horizontal crack in the UHPC and precast section at the level of the joint

reinforcement. Crushing of the concrete in the compression block triggered failure of the joint. The joint reinforcement did not rupture or experience a development or splice failure.

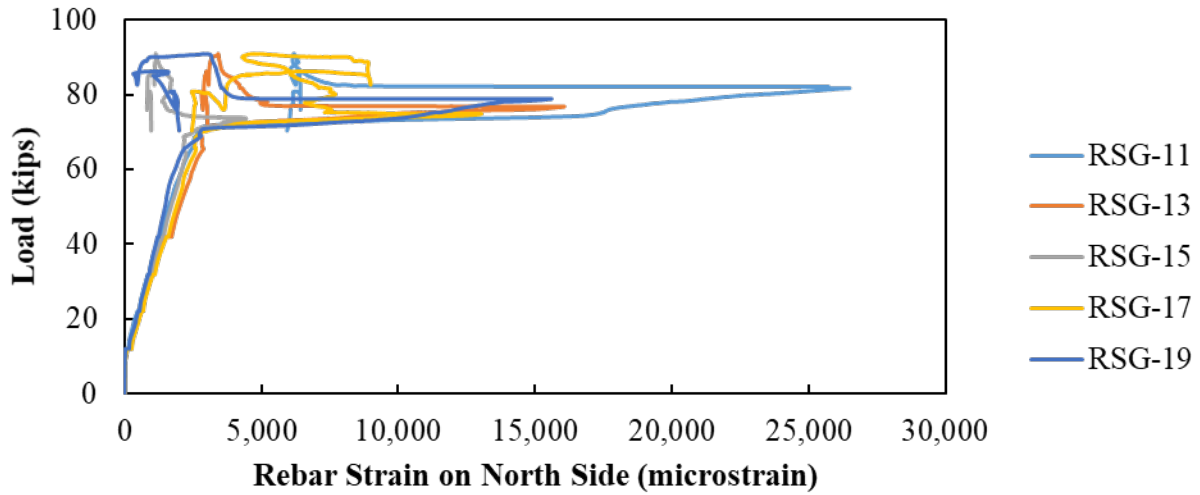


Figure D.52: 12A2-1: (a) failed specimen and (b) east side joint face showing similar rupture pattern with less amount of cracks

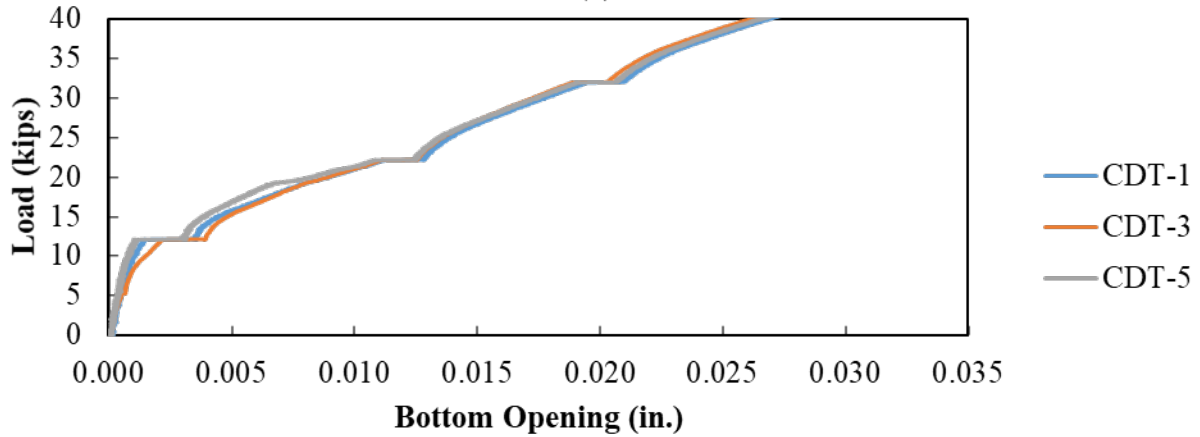
The load versus rebar strain gauge data for all the joint reinforcements are presented in Figure D.53 (a) for the south beam and Figure D.53 (b) for the north beam. The load versus bottom aperture data from the CDT is shown in Figure D.53 (c) up until when the gauges were removed. The load versus concrete strain responses are shown in Figure D.54 (a) for bottom gauges, including when the cracking load was observed in Figure D.54 (b). The top concrete gauges were not included in this testing instance.



(a)



(b)



(c)

Figure D.53: 12A2-1 response: (a) load versus rebar strain on south side, (b) load versus rebar strain on north side, and (c) load versus central bottom opening

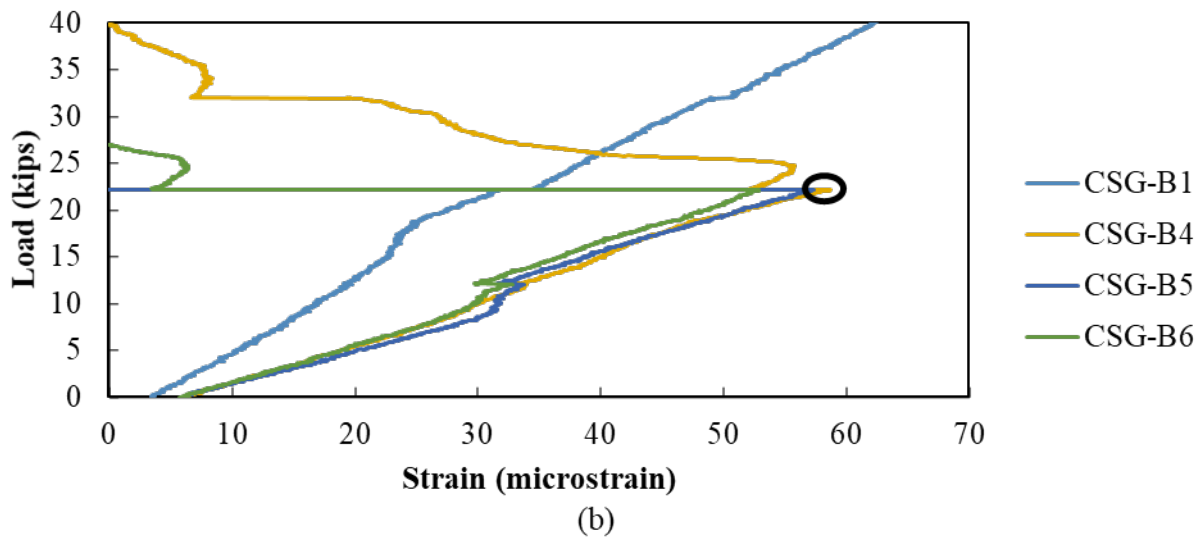
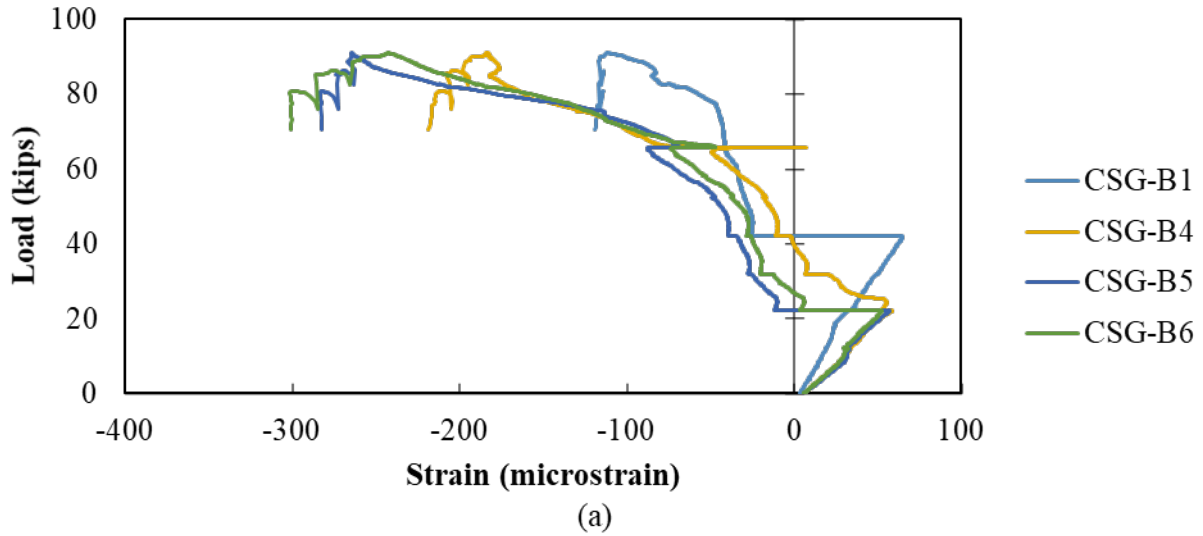


Figure D.54: 12A2-1 response: (a) load versus bottom concrete strain, and (b) cracking load determination based on load versus bottom concrete strain response

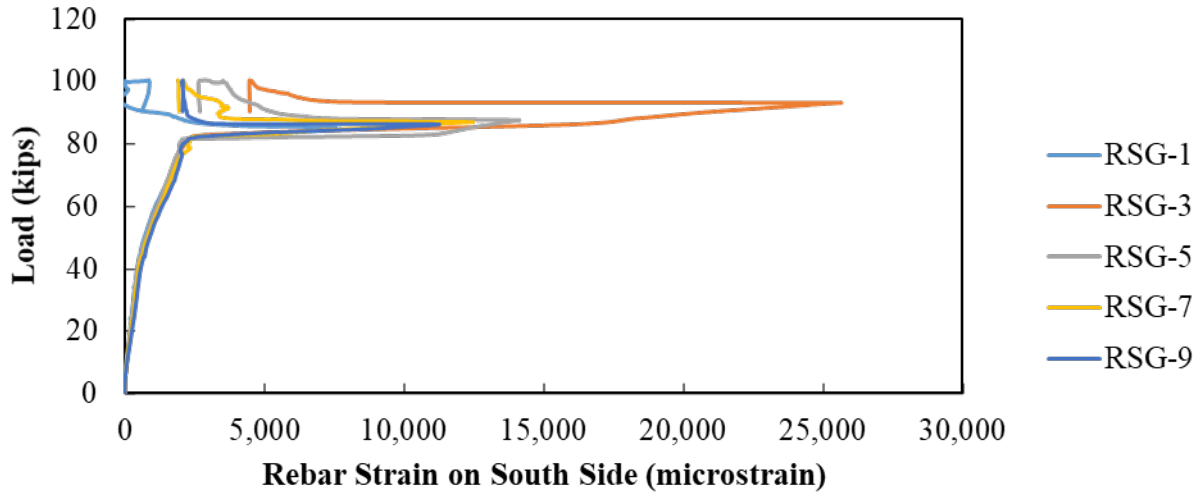
D.5.4.2. Test 2 (12A2-2)

The failure of 12A2-2 is shown in Figure D.55. Similar to the Test 1, cracking began at the interface between the UHPC and precast section and continued in the precast section. The interface crack continued to open with a less predominant crack formed horizontally in the UHPC at the level of reinforcement. Test 2 followed a similar failure mechanism of concrete crushing in the compression block that triggered the failure of the joint. The joint reinforcement did not rupture or experience a development or splice failure.

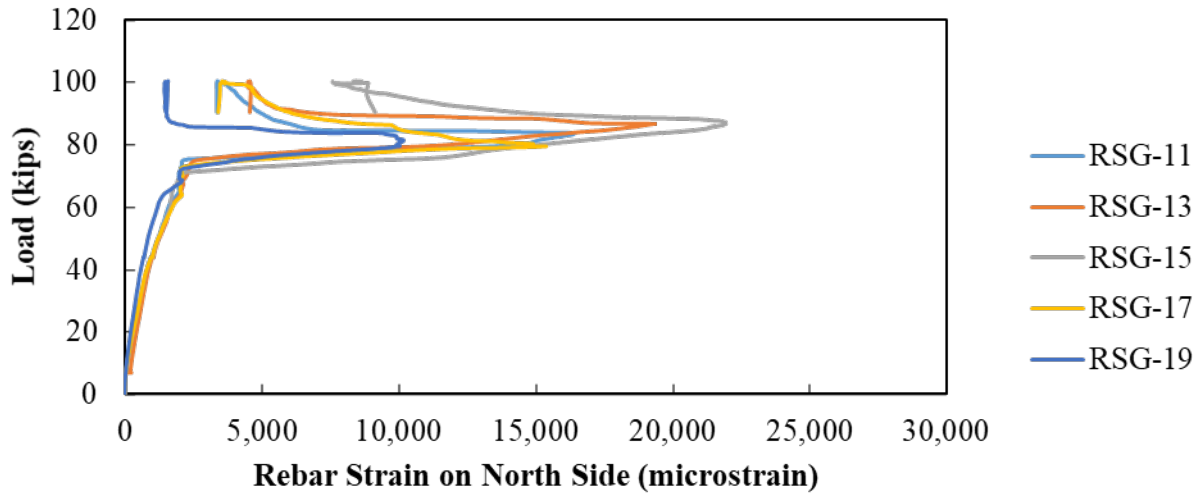


Figure D.55: 12A2-2: (a) west side failed specimen and (b) east side joint face showing similar rupture pattern with more amount of cracks

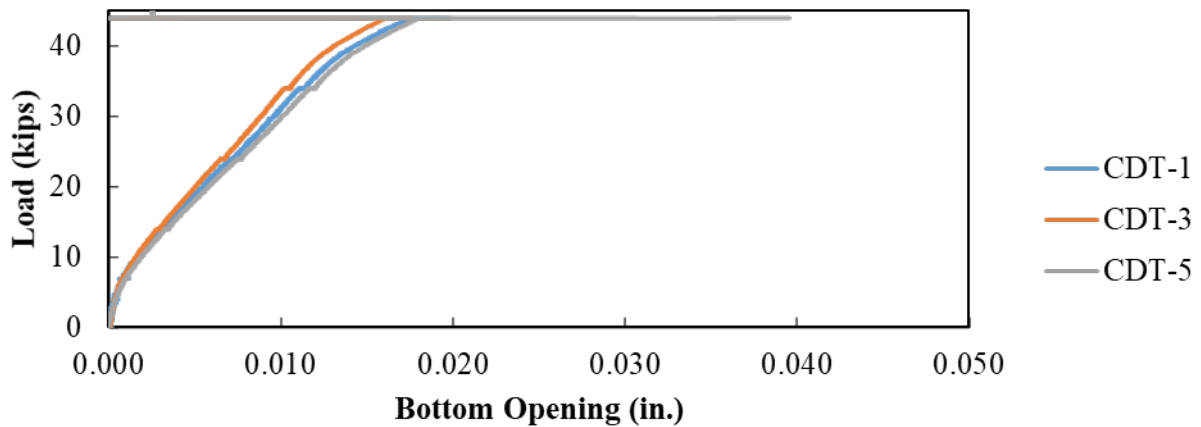
The load versus rebar strain gauge data for all the joint protruding reinforcements are presented in Figure D.56 (a) for the south beam and Figure D.56 (b) for the north beam. The load versus bottom aperture data from the CDT is shown in Figure D.56 (c) up until the when the gauges were removed. The load versus concrete strain responses are shown in Figure D.57 for bottom gauges. The cracking load is not shown because the specimen was already cracked during Test 1. The top concrete gauges were not included in this testing instance.



(a)



(b)



(c)

Figure D.56: 12A2-2 response (a) load versus rebar strain on south side, (b) load versus rebar strain on north side, and (c) load versus central bottom opening

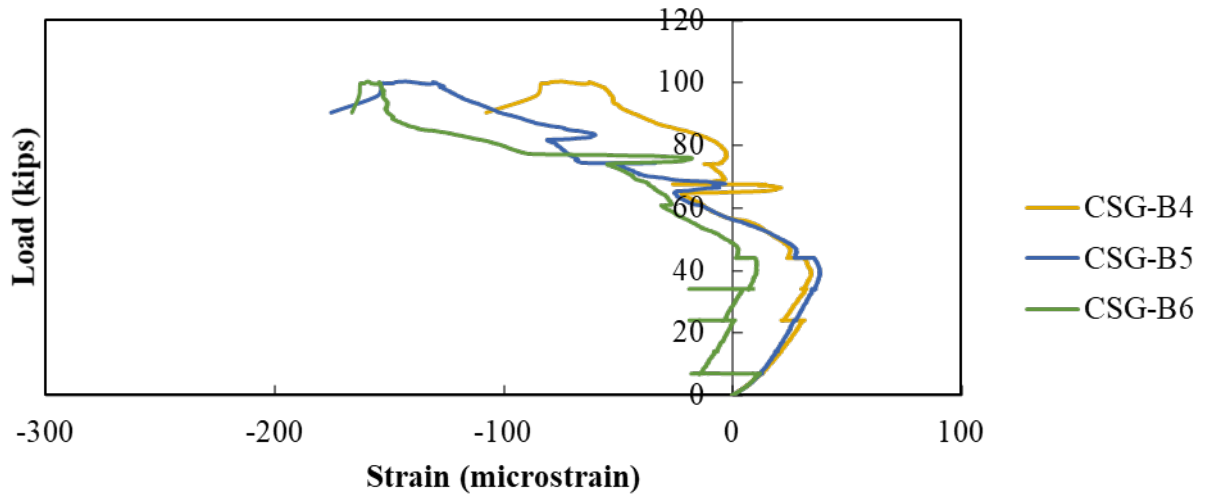


Figure D.57: 12A2-2 response: load versus bottom concrete strain (CSG 1 to 3 malfunctioned)

E. FATIGUE TESTING OF SMALL-SCALE SPECIMENS

E.1. INTRODUCTION

The results from the fatigue testing on the small-scale joint specimens are summarized in this section. The instrumentation labeling, fatigue response, and post-fatigue static response for each individual specimen are presented. An analysis of these results is presented in the body of the report. The ultimate loads for strength and post-fatigue testing strength are also summarized in Table E.1.

Table E.1: Summary of strength and post-fatigue testing strength results

Joint	Strength (Test 1)	Post-Fatigue Strength (Test 2)
12F1	70.0 kips	66.9 kips
12A1	61.0 kips	67.5 kips
12A2	90.9 kips	100.5 kips

A discussion of these test results is presented in Chapter 6.

E.2. INSTRUMENTATION LABELING

Measurements from all the instrumentation is presented in this appendix, so the location and labeling for all the gauges are highlighted in Figure E.1. Note that generally the north beam was loaded during testing.

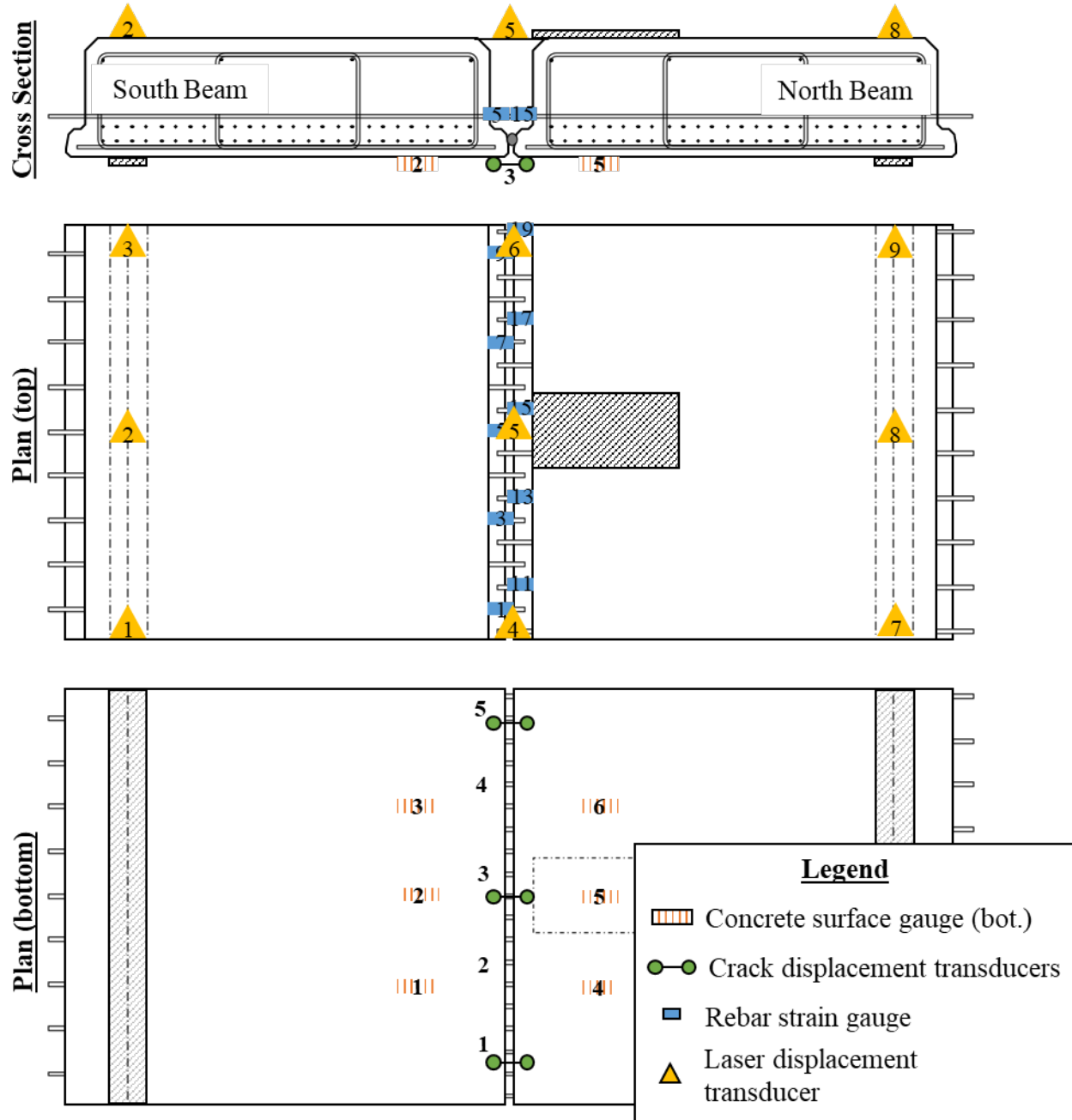


Figure E.1: Instrumentation labels for gauges on the specimens

Note that the results from LDT-1 to LDT-3 and LDT-7 to LDT-9 are not shown in this section. However, these displacements were used to find the actual midspan displacement in Chapter 5.

E.3. RESULTS FOR 12F1-2

The fatigue response for 12F1 is presented in this section. This joint, shown in Figure E.2, has no shear key, an embedment length of 5 inches and a splice length of 4 inches. This specimen had a sandblasted finish in the joint region with no significant surface roughness.

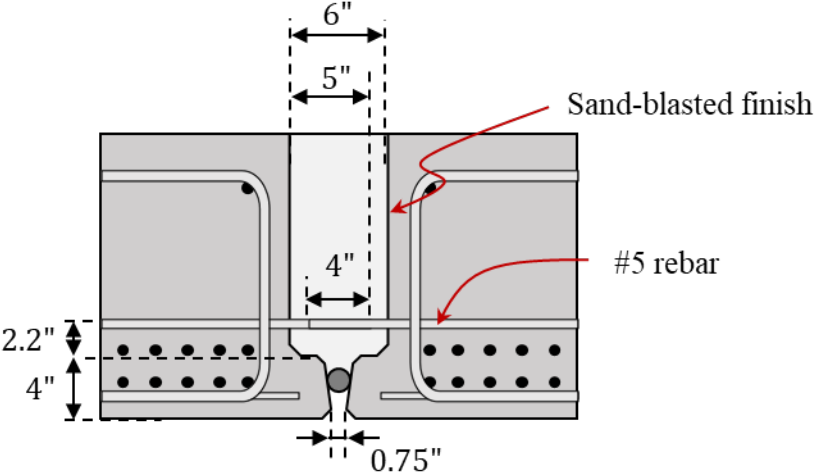


Figure E.2: Joint details for joint 12F1

E.3.1. Fatigue Response

E.3.1.1. Stiffness of System

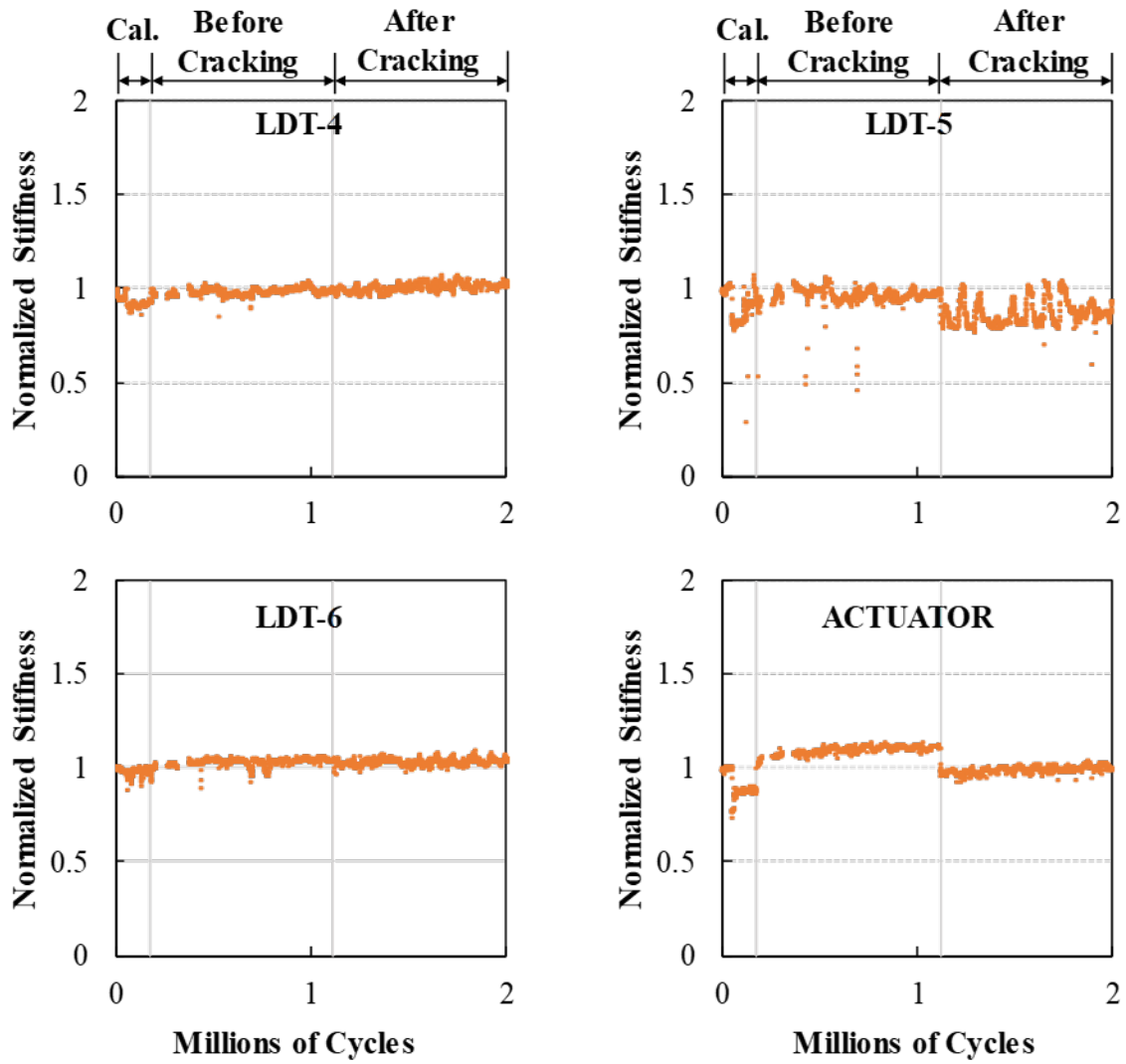


Figure E.3: Normalized cycle stiffness for 12F1-2

E.3.1.2. Reinforcement Strain Gauges

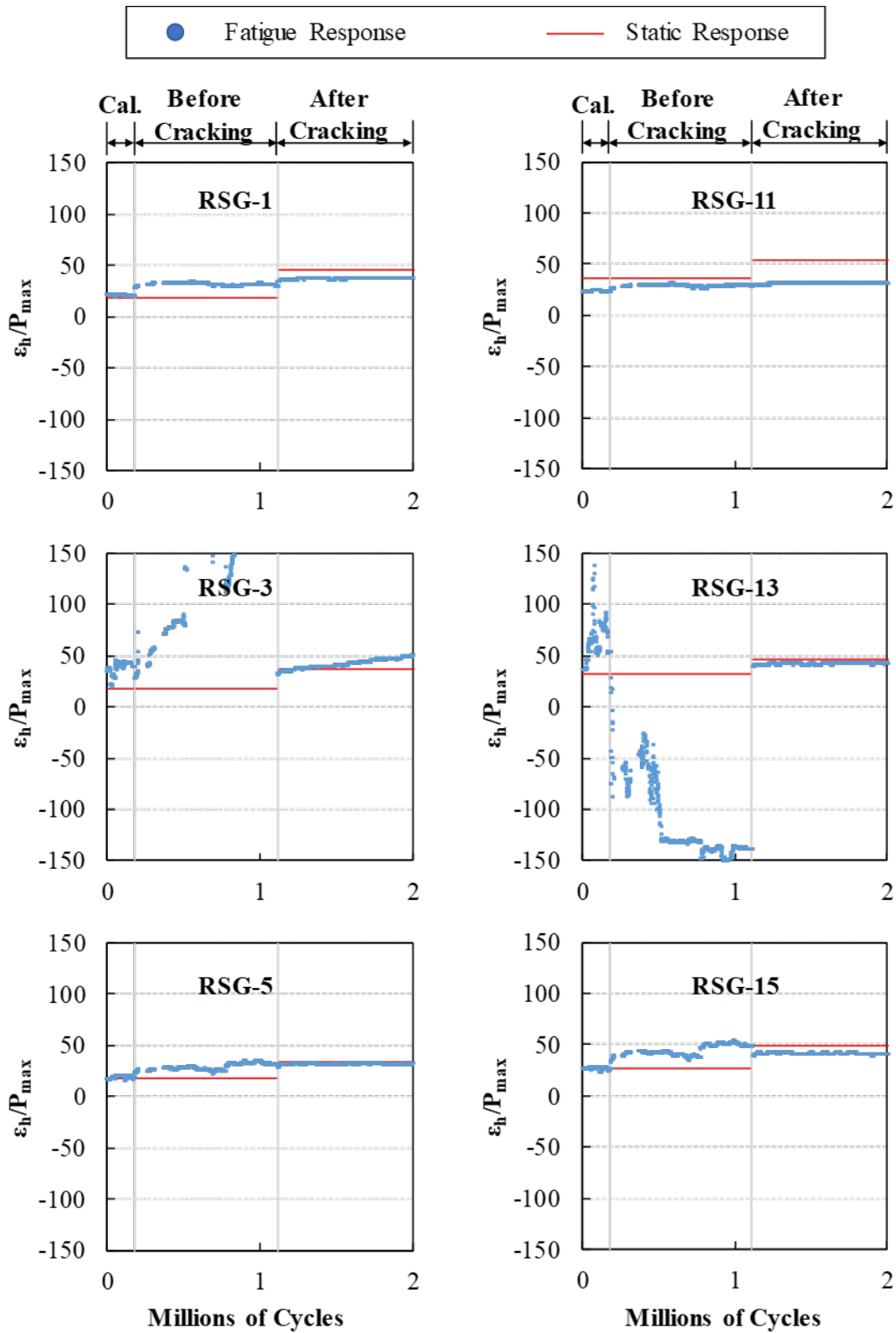


Figure E.4: High reinforcement strain over force for each cycle for 12F1-2 (1 of 2)

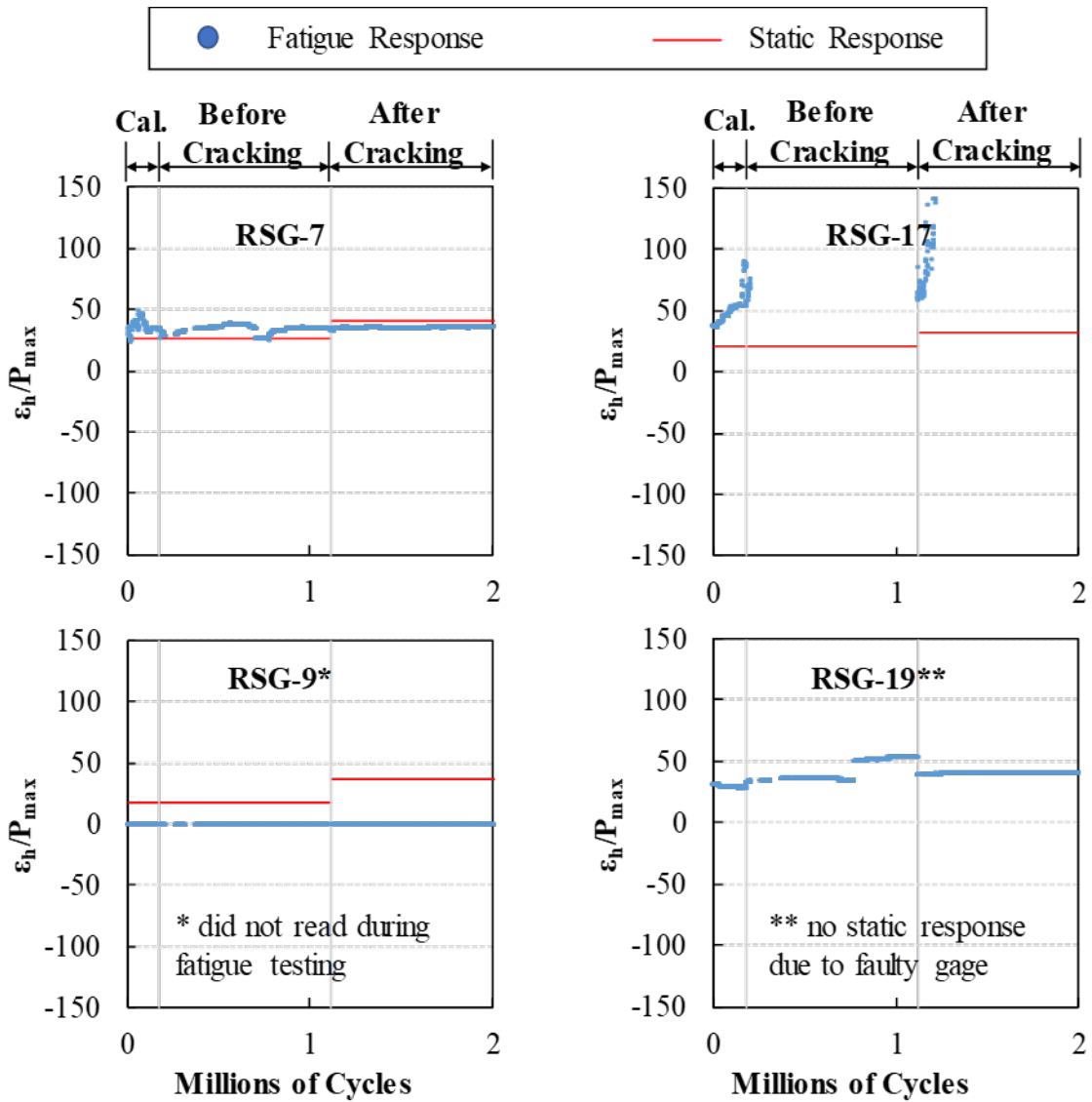


Figure E.5: High reinforcement strain over force for each cycle for 12F1-2 (2 of 2)

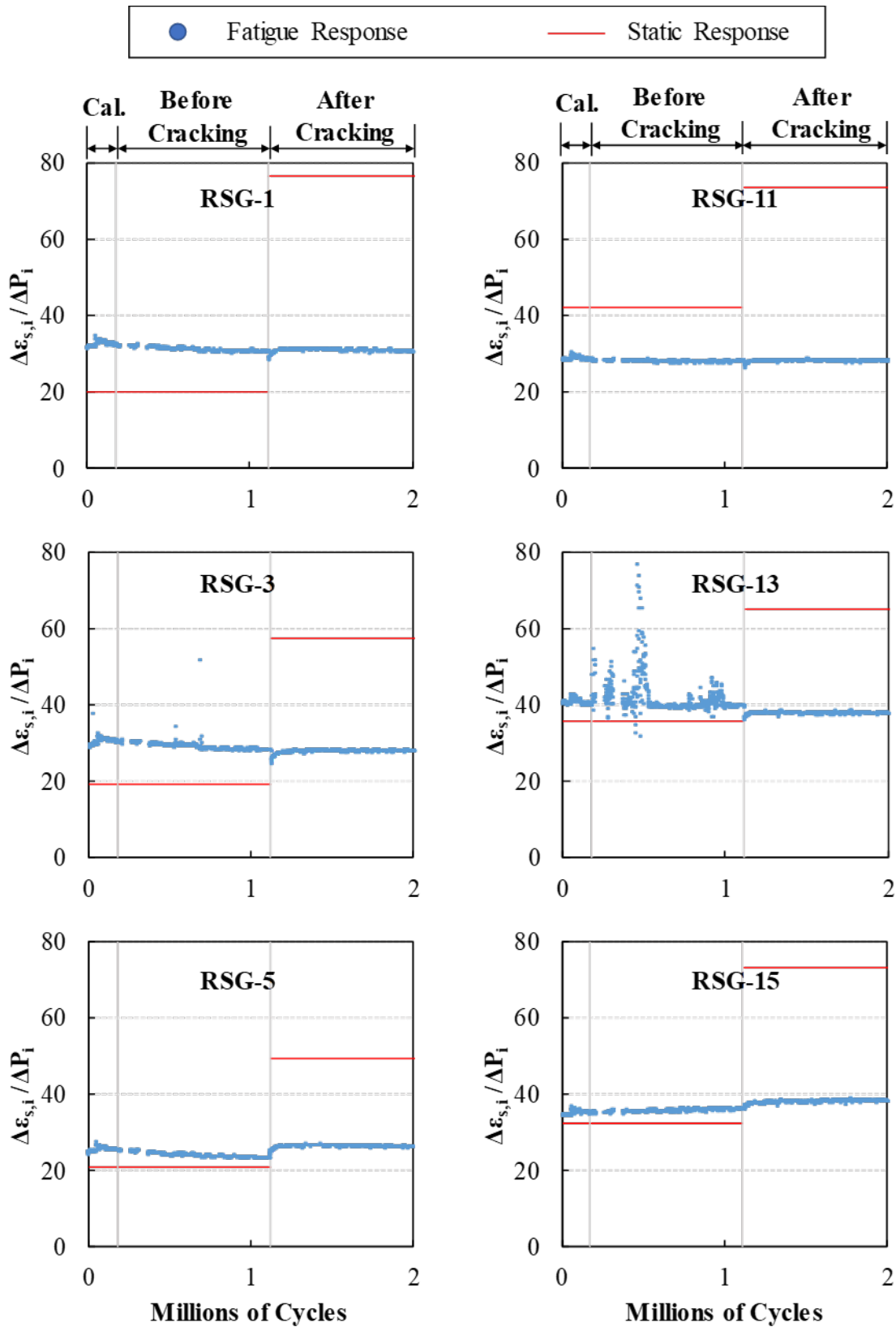


Figure E.6: Reinforcement strain change over force change for each cycle for 12F1-2 (1 of 2)

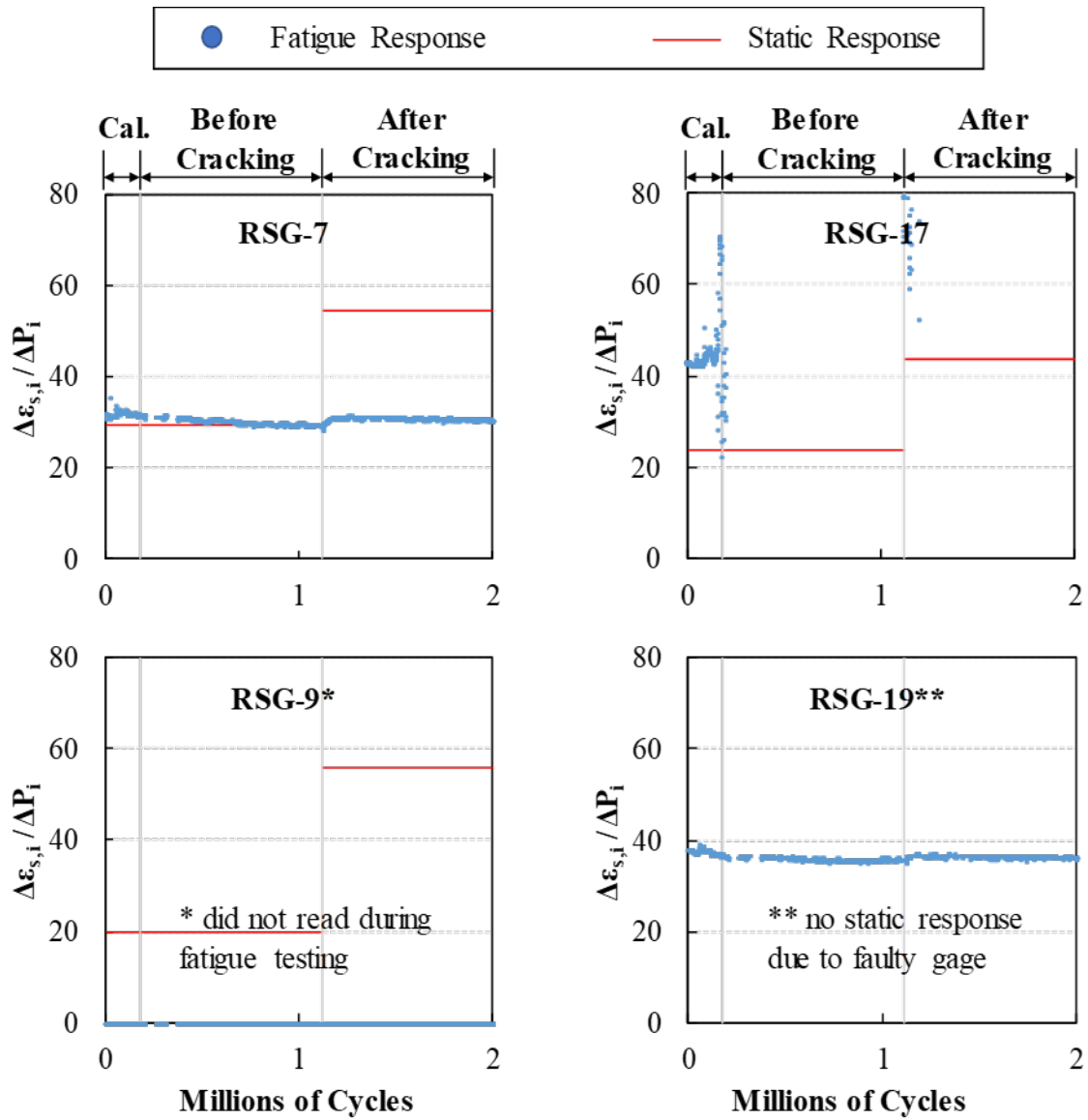


Figure E.7: Reinforcement strain change over force change for each cycle for 12F1-2 (2 of 2)

E.3.1.3. Concrete Strain Gauges

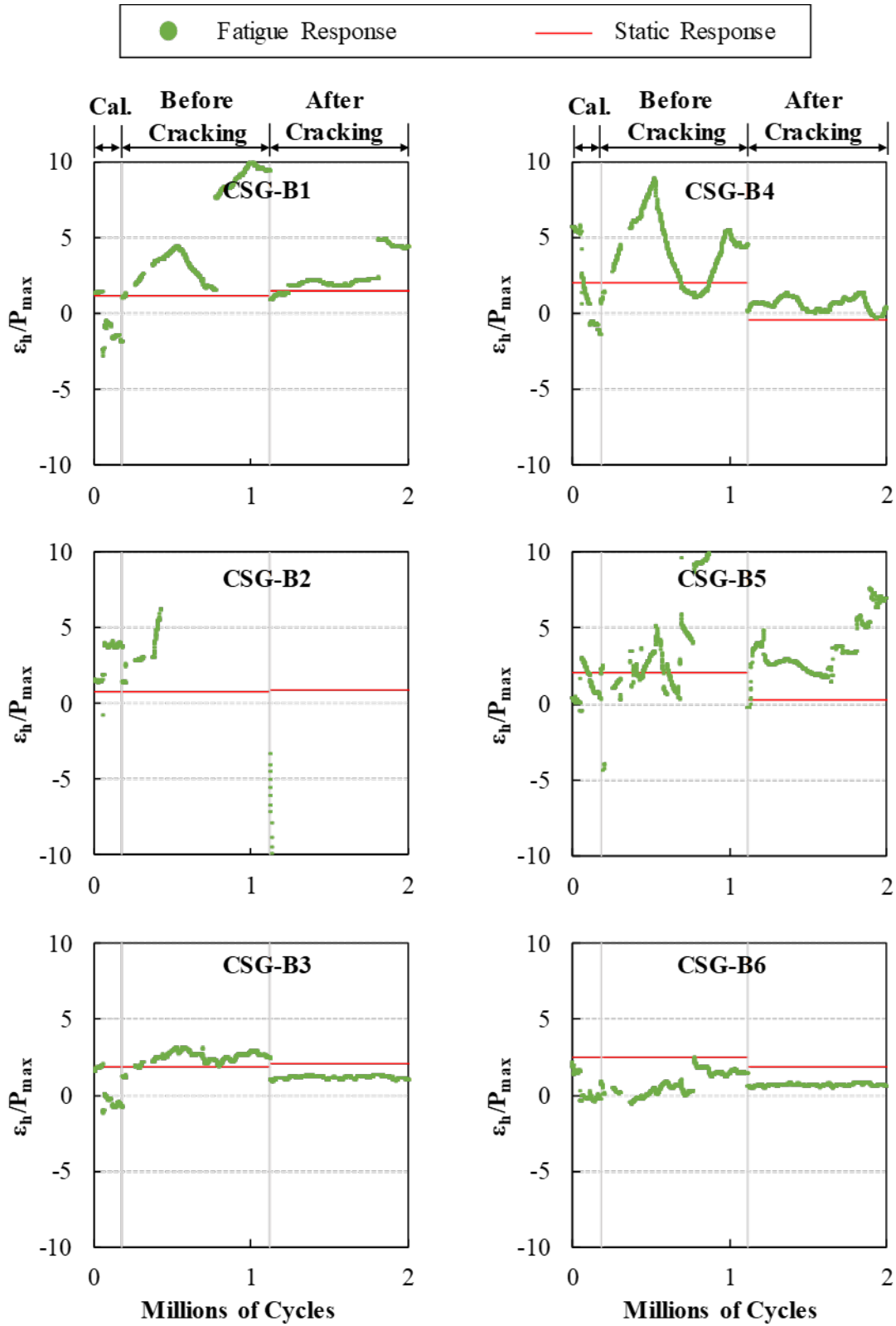


Figure E.8: High concrete strain over force for each cycle for 12F1-2

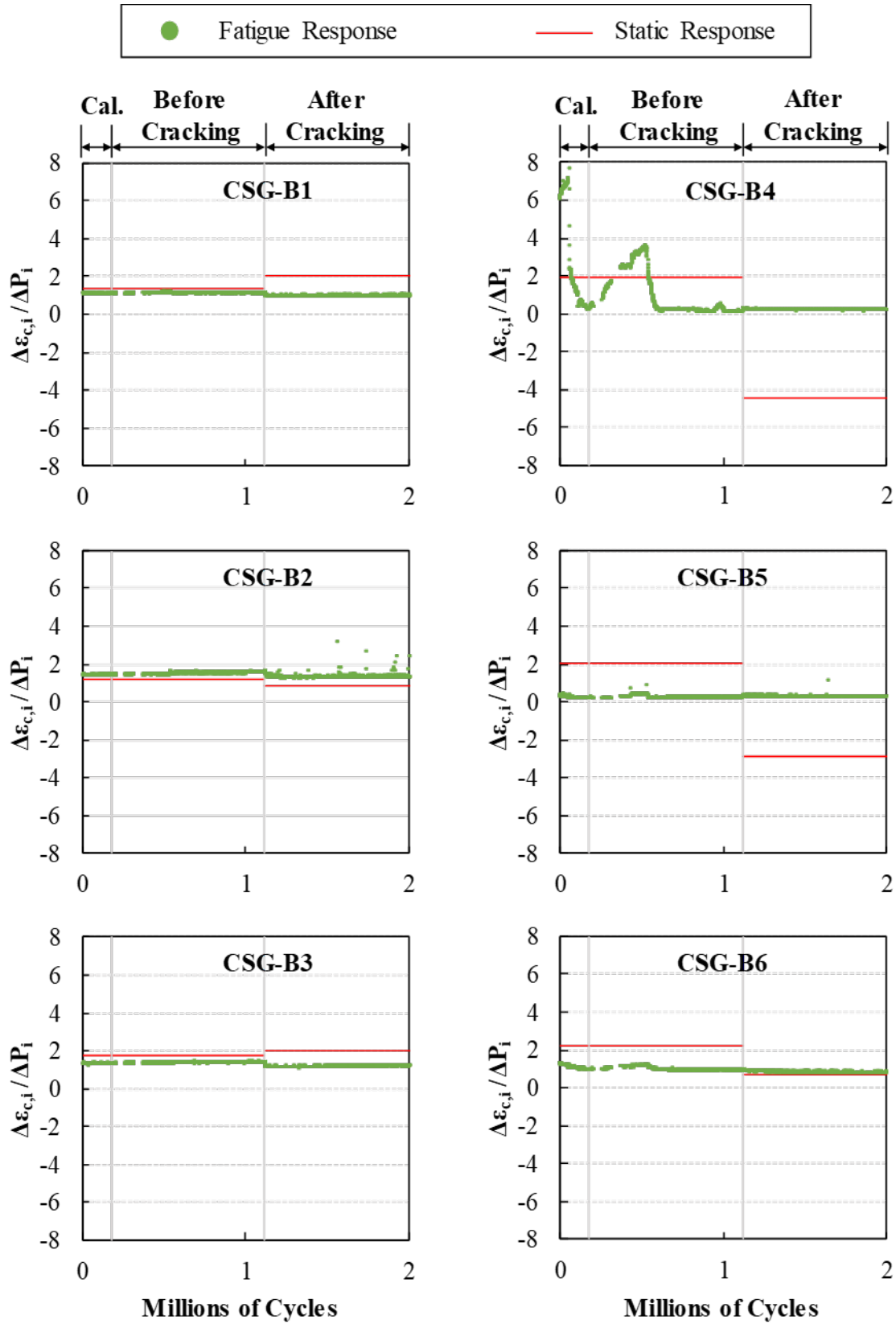


Figure E.9: Concrete strain change over force change for each cycle for 12F1-2

E.3.1.4. Crack Gages

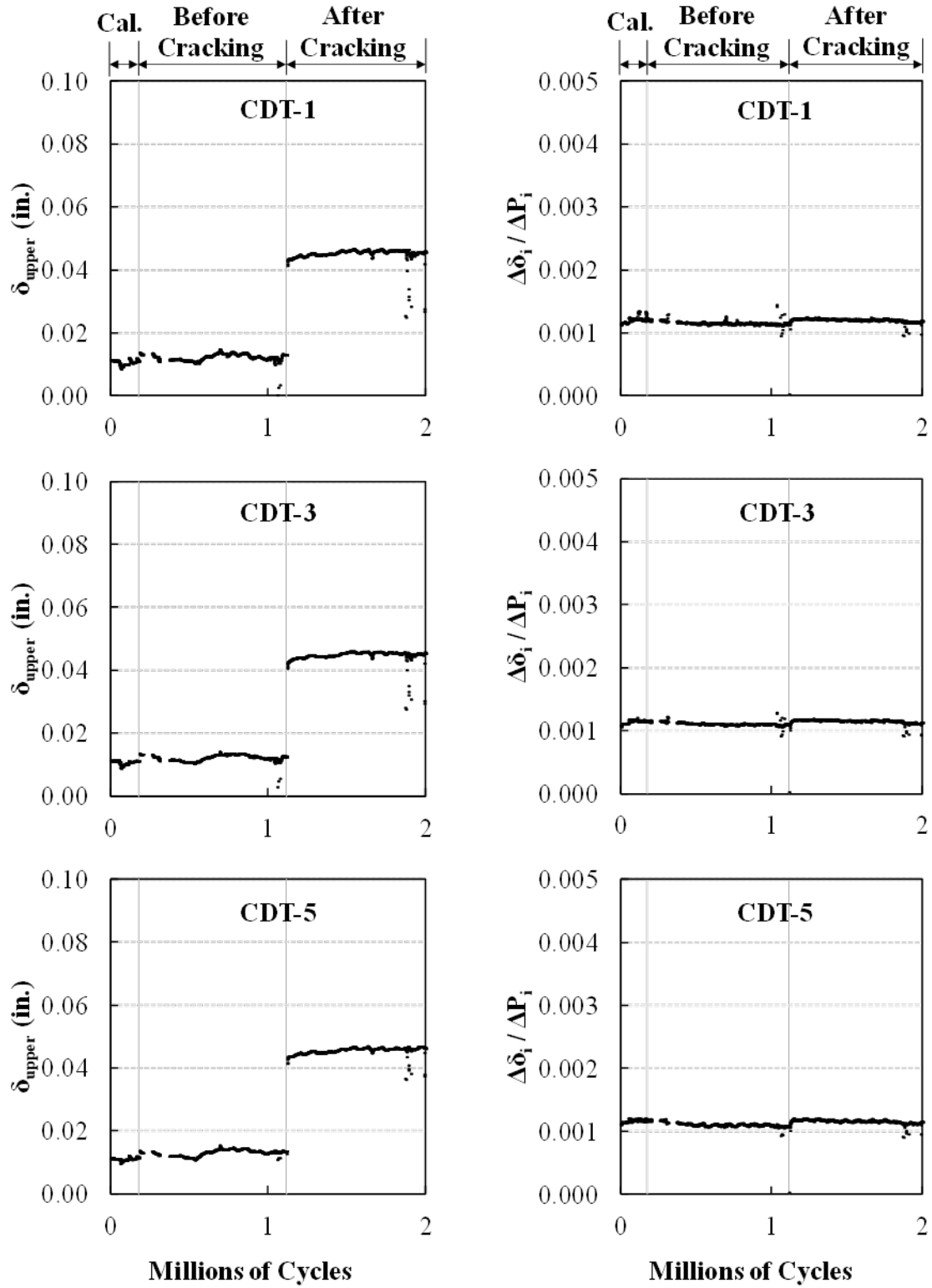


Figure E.10: Crack gage results for each cycle for 12F1-2

E.3.2. Post-Fatigue Static Response

The post-fatigue testing static response for 12F1 (12F1-2) is presented in this section. The load versus deflection plots for the strength response without any fatigue loading (12F1-1) and after the fatigue loading (12F1-2) are shown in Figure E.11. The fatigue loading caused a slight decrease in strength and ductility in the 12F1 joint specimens.

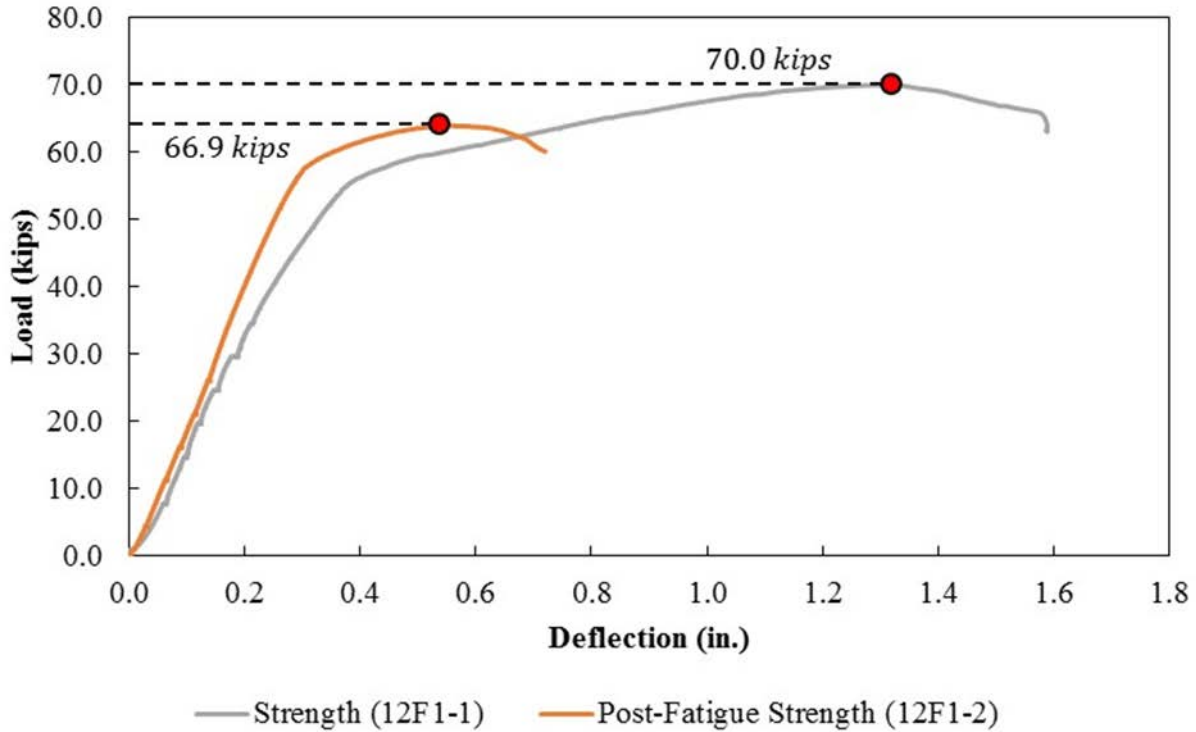


Figure E.11: Load versus displacement plot for strength testing of 12F1 (a) without any fatigue load applied, 12F1-1, and (b) after fatigue loading, 12F1-2

E.4. RESULTS FOR 12A1-2

The fatigue response for 12A1 is presented in this section. This joint, shown in Figure E.12, has a shear key, an embedment length of 6.375 inches and a splice length of 4 inches. This specimen had a sandblasted finish in the joint region with no significant surface roughness.

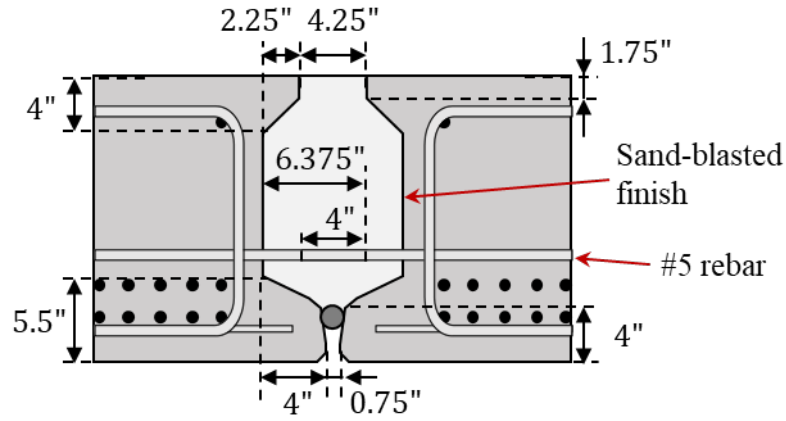


Figure E.12: Joint details for joint 12A1

E.4.1. Fatigue Response

E.4.1.1. Stiffness of System

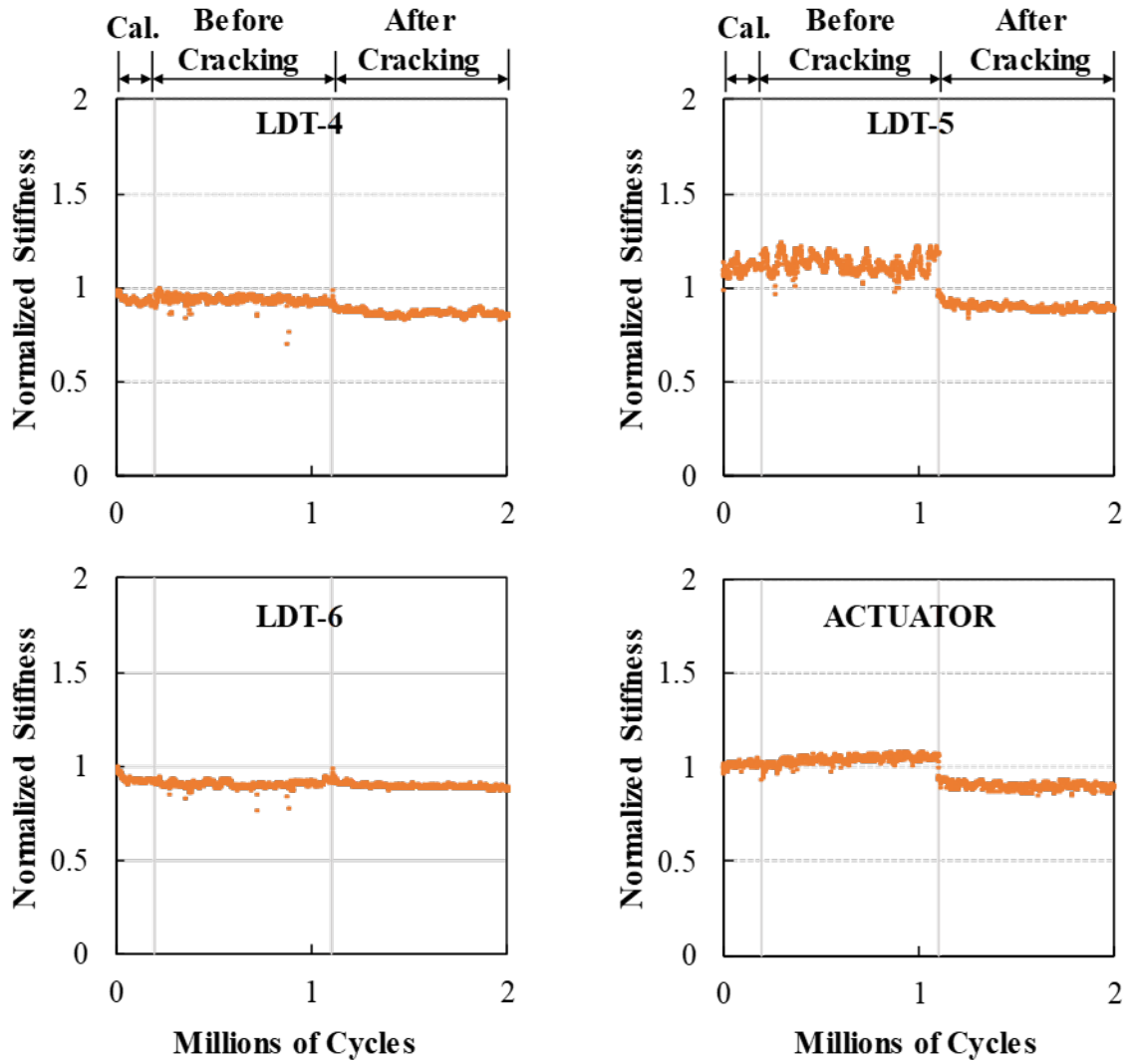


Figure E.13: Normalized cycle stiffness for 12A1-2

E.4.1.2. Reinforcement Strain Gauges

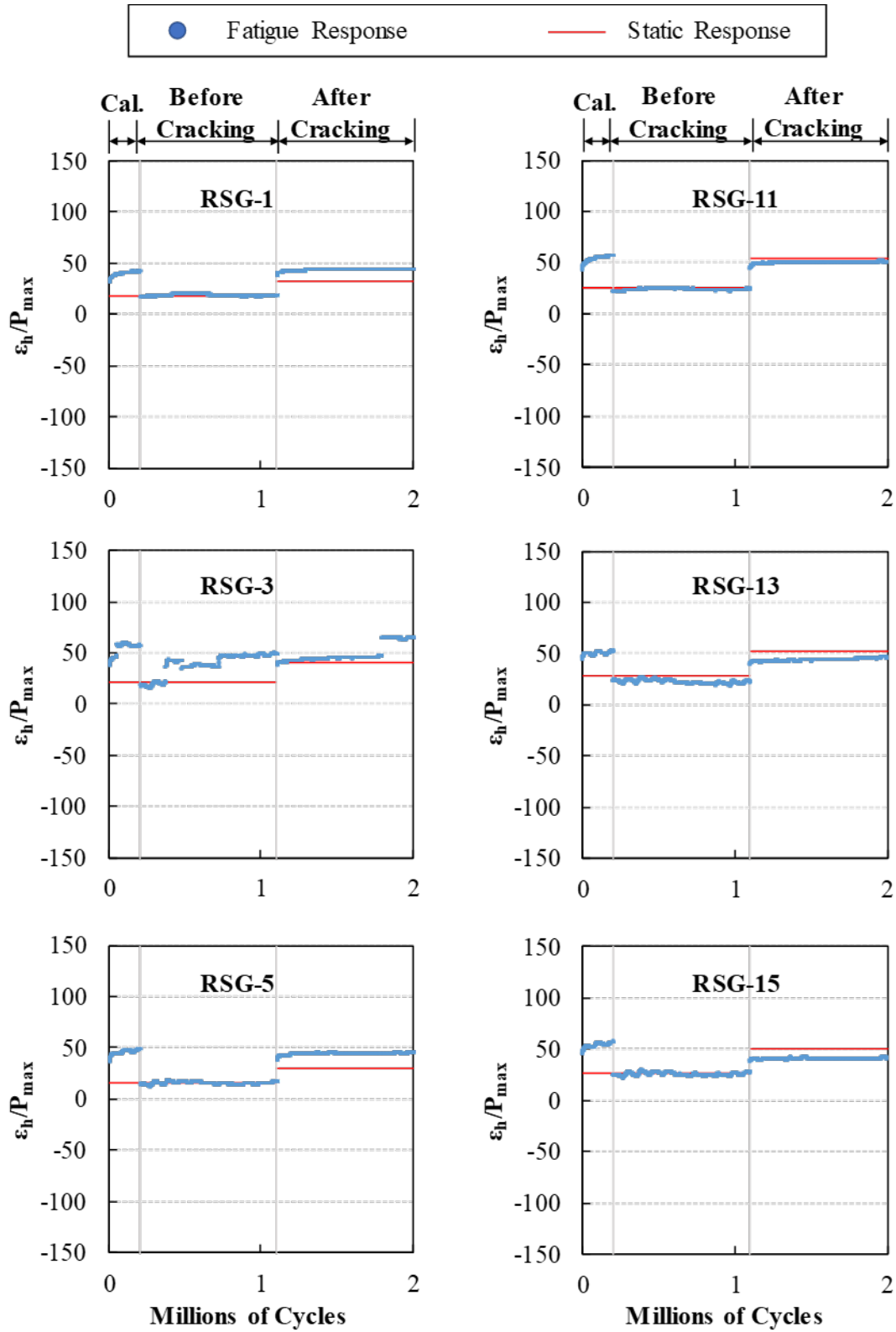


Figure E.14: High reinforcement strain over force for each cycle for 12A1-2 (1 of 2)

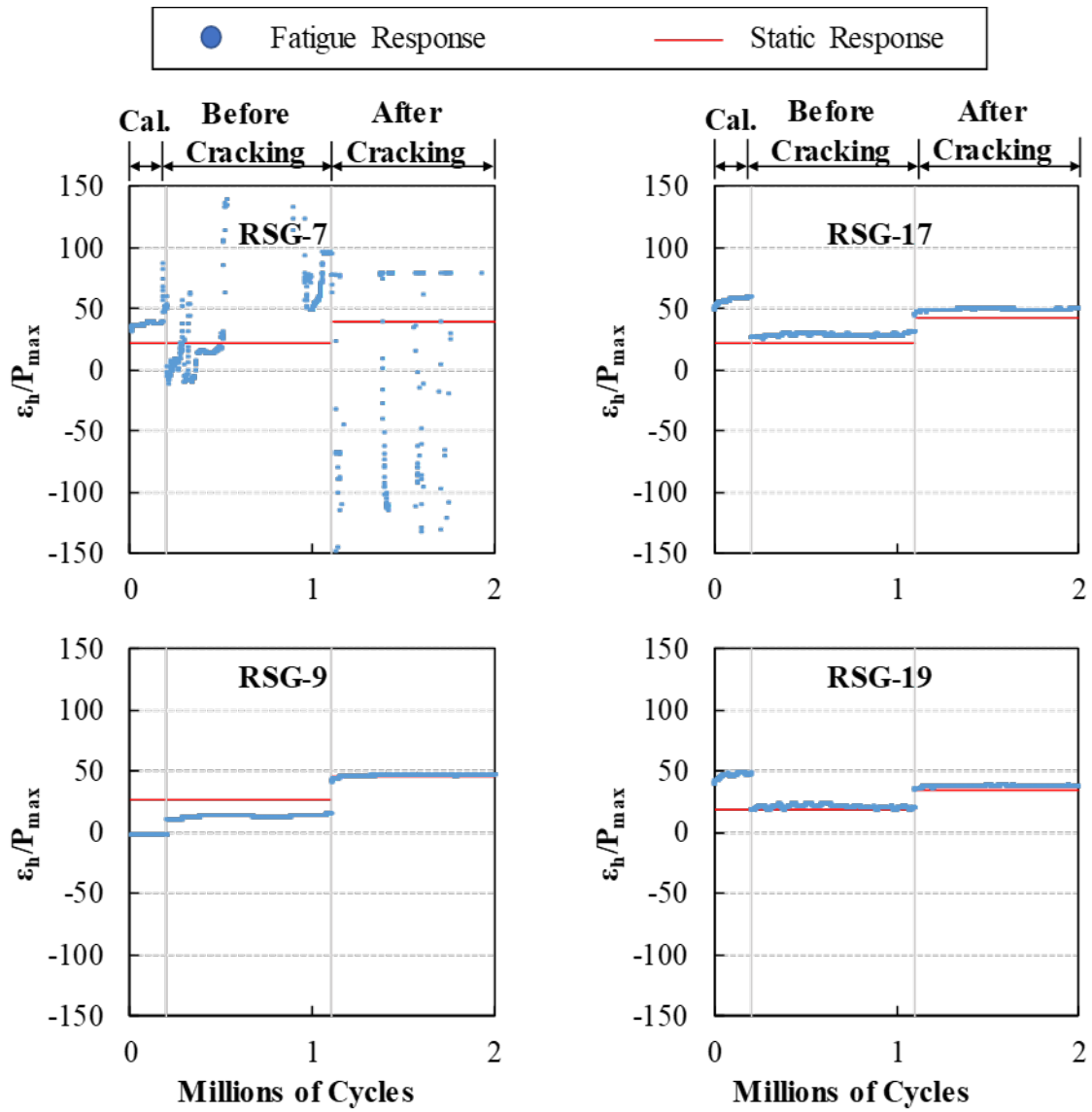


Figure E.15: High reinforcement strain over force for each cycle for 12A1-2 (2 of 2)

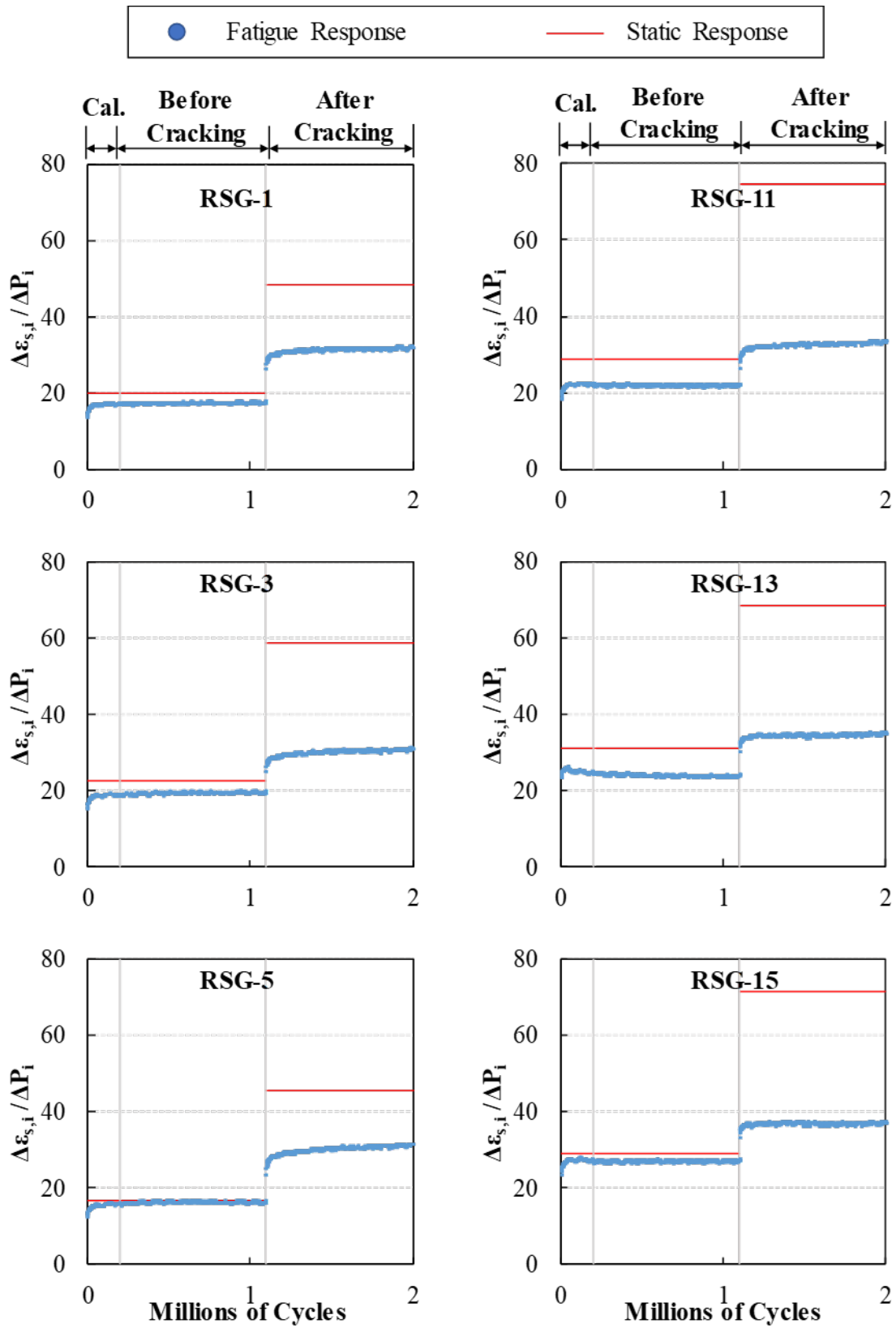


Figure E.16: Reinforcement strain change over force change for each cycle for 12A1-2 (1 of 2)

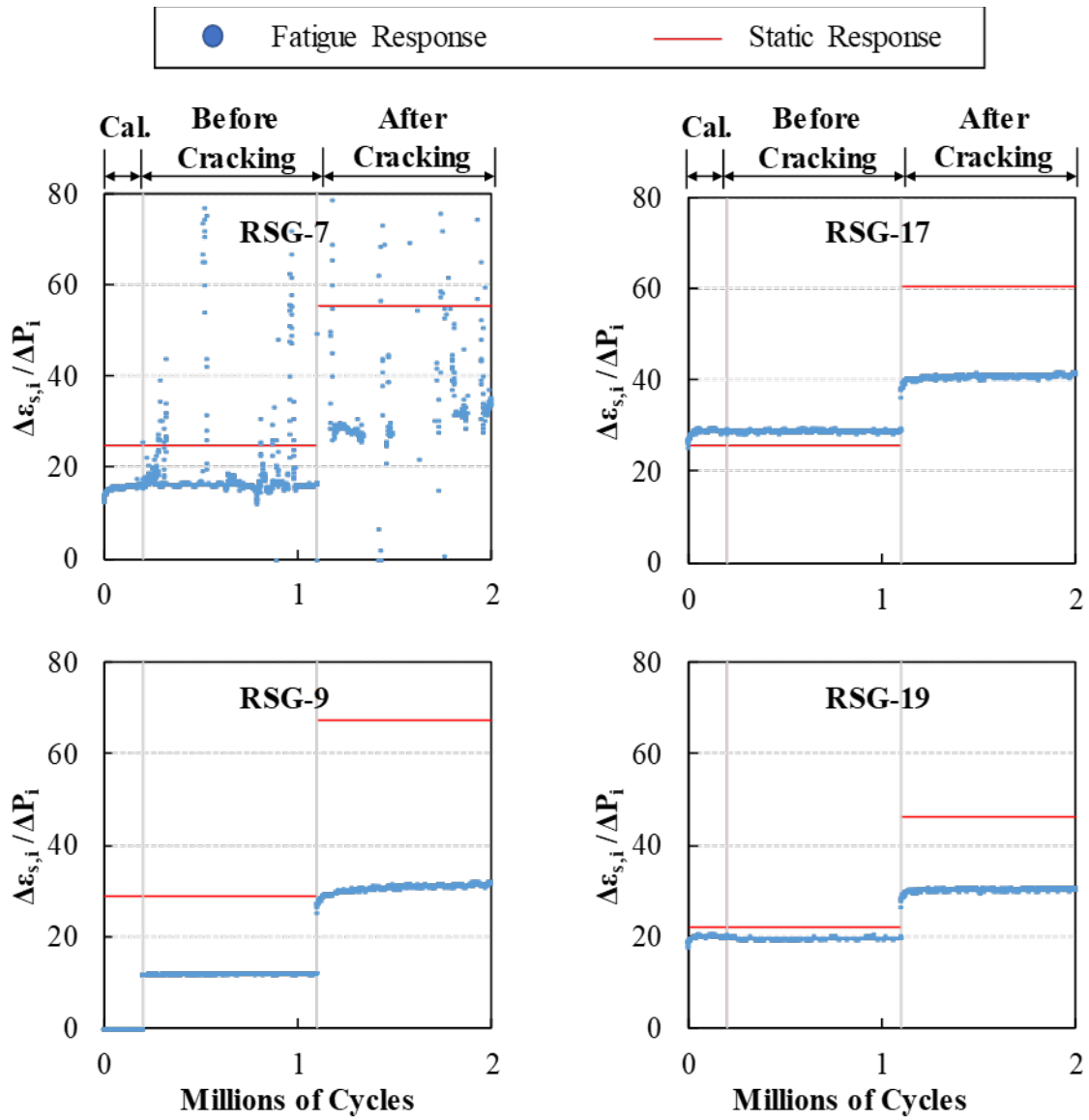


Figure E.17: Reinforcement strain change over force change for each cycle for 12A1-2 (2 of 2)

E.4.1.3. Concrete Strain Gauges

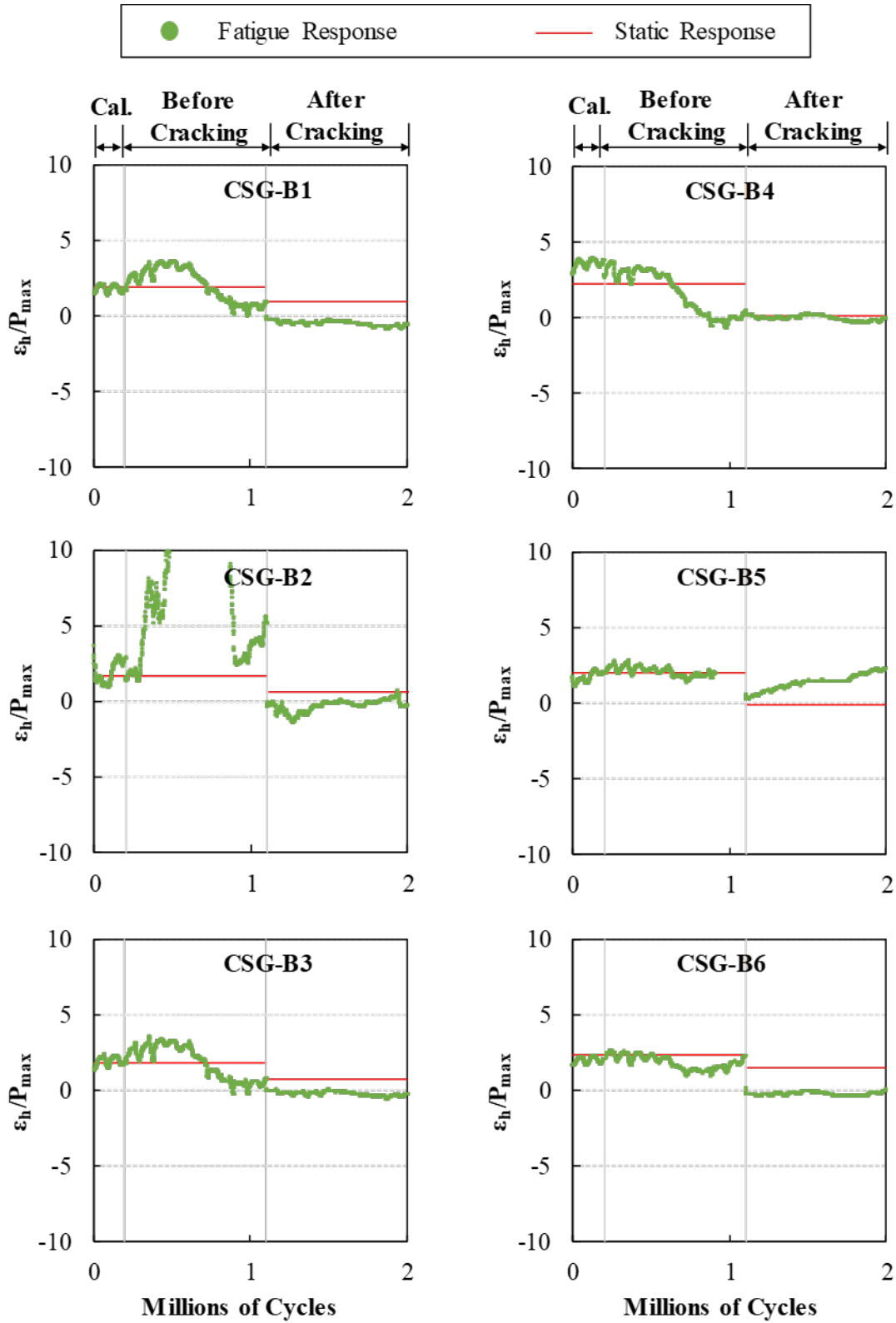


Figure E.18: High concrete strain over force for each cycle for 12A1-2

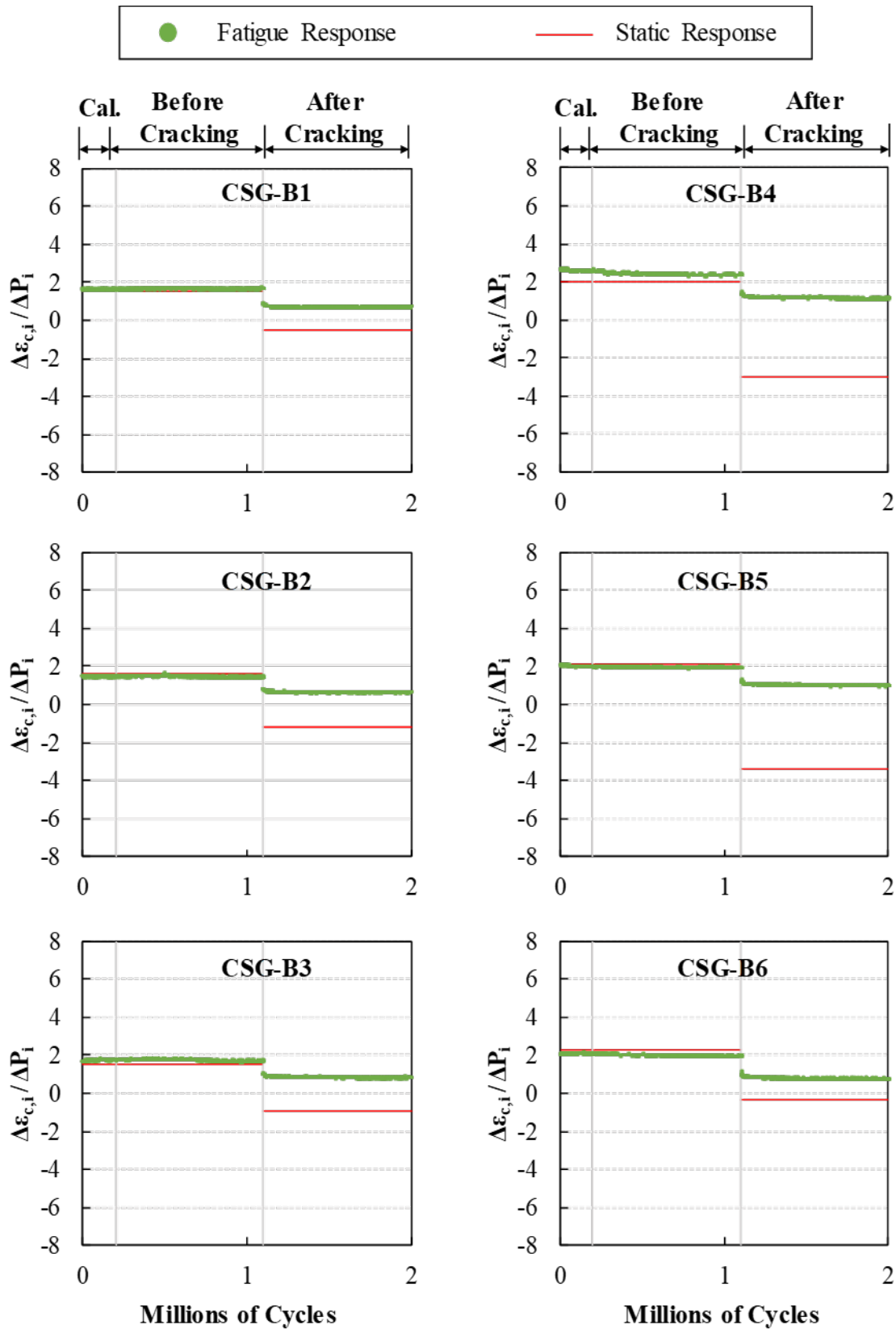


Figure E.19: Concrete strain change over force change for each cycle for 12A1-2

E.4.1.4. Crack Gages

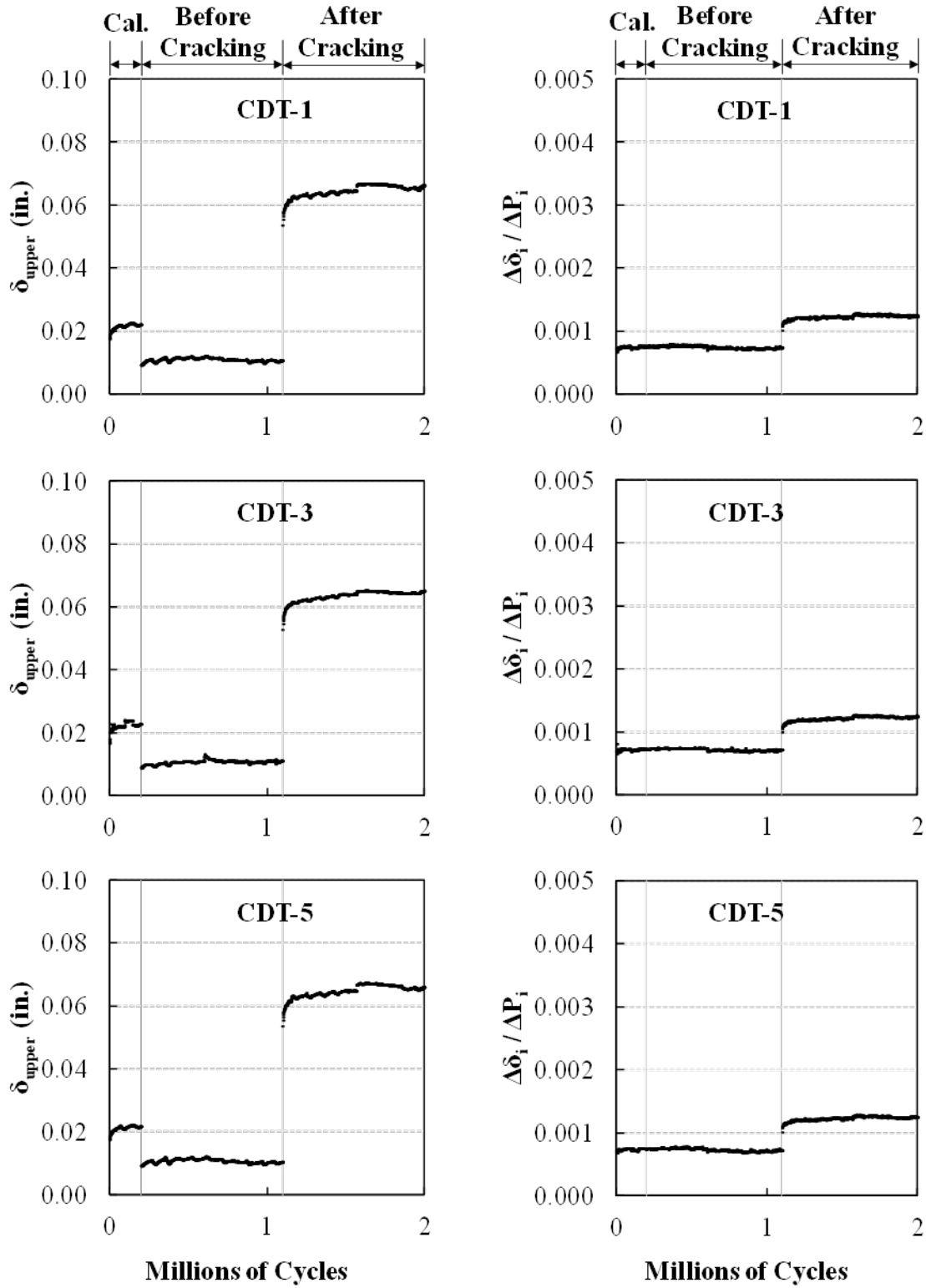


Figure E.20: Crack gage results for each cycle for 12A1-2

E.4.2. Post-Fatigue Static Response

The post-fatigue testing static response for 12A1 (12A1-2) is presented in this section. The load versus deflection plots for the strength response without any fatigue loading (12A1-1) and after the fatigue loading (12A1-2) are shown in Figure E.21. The fatigue loading caused a slight increase in strength and ductility in the 12A1 joint specimens.

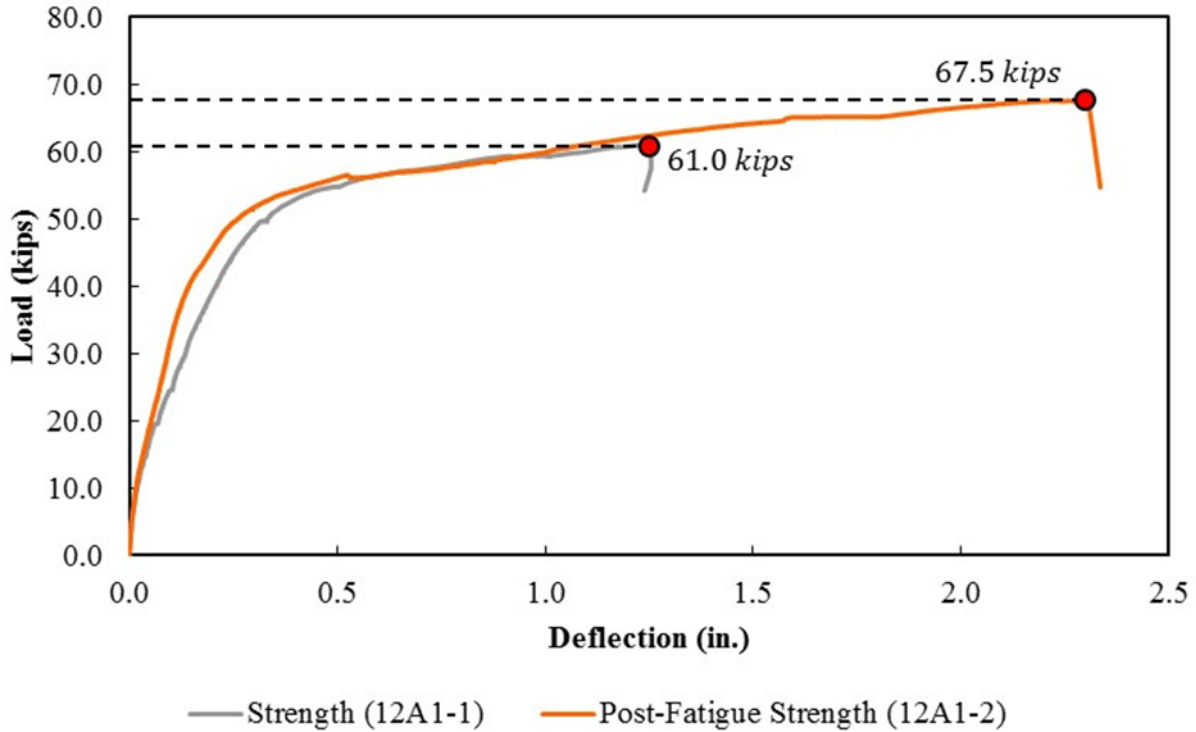


Figure E.21: Load versus displacement plot for strength testing of 12A1 (a) without any fatigue load applied, 12A1-1, and (b) after fatigue loading, 12A1-2

E.5. RESULTS FOR 12A2-2

The fatigue response for 12A2 is presented in this section. This joint, shown in Figure E.22, has a shear key, an embedment length of 6.375 inches and a splice length of 5.25 inches. This specimen had a joint surface roughened using a paste retarding agent, with a surface roughness of 1/8-inch achieved.

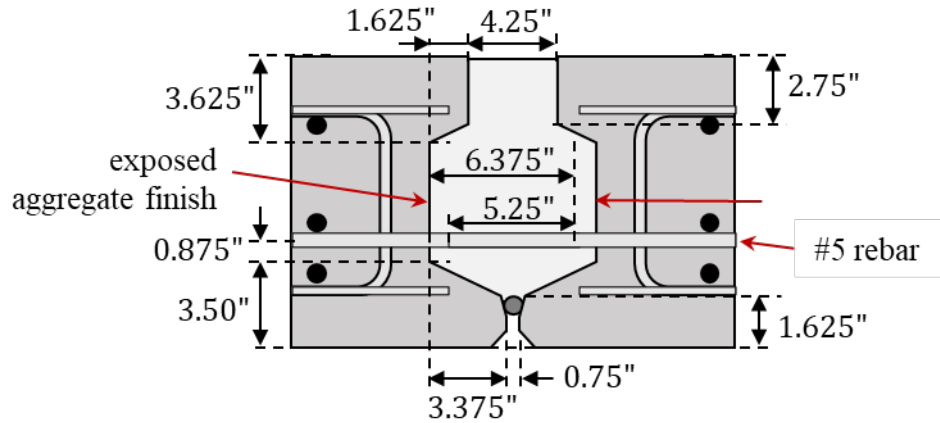


Figure E.22: Joint details for joint 12A2

E.5.1. Fatigue Response

E.5.1.1. Stiffness of System

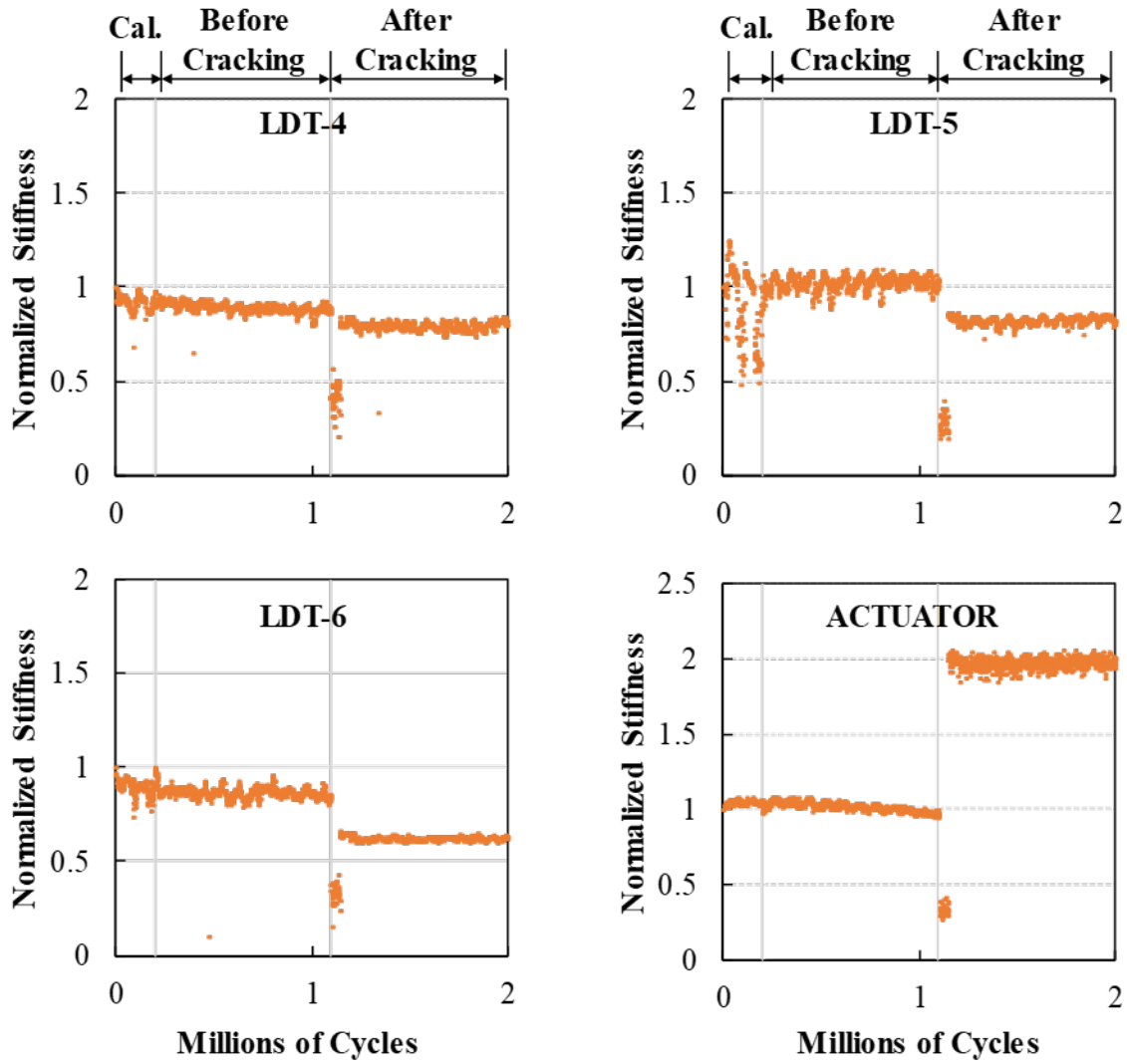


Figure E.23: Normalized cycle stiffness for 12A2-2

E.5.1.2. Reinforcement Strain Gauges

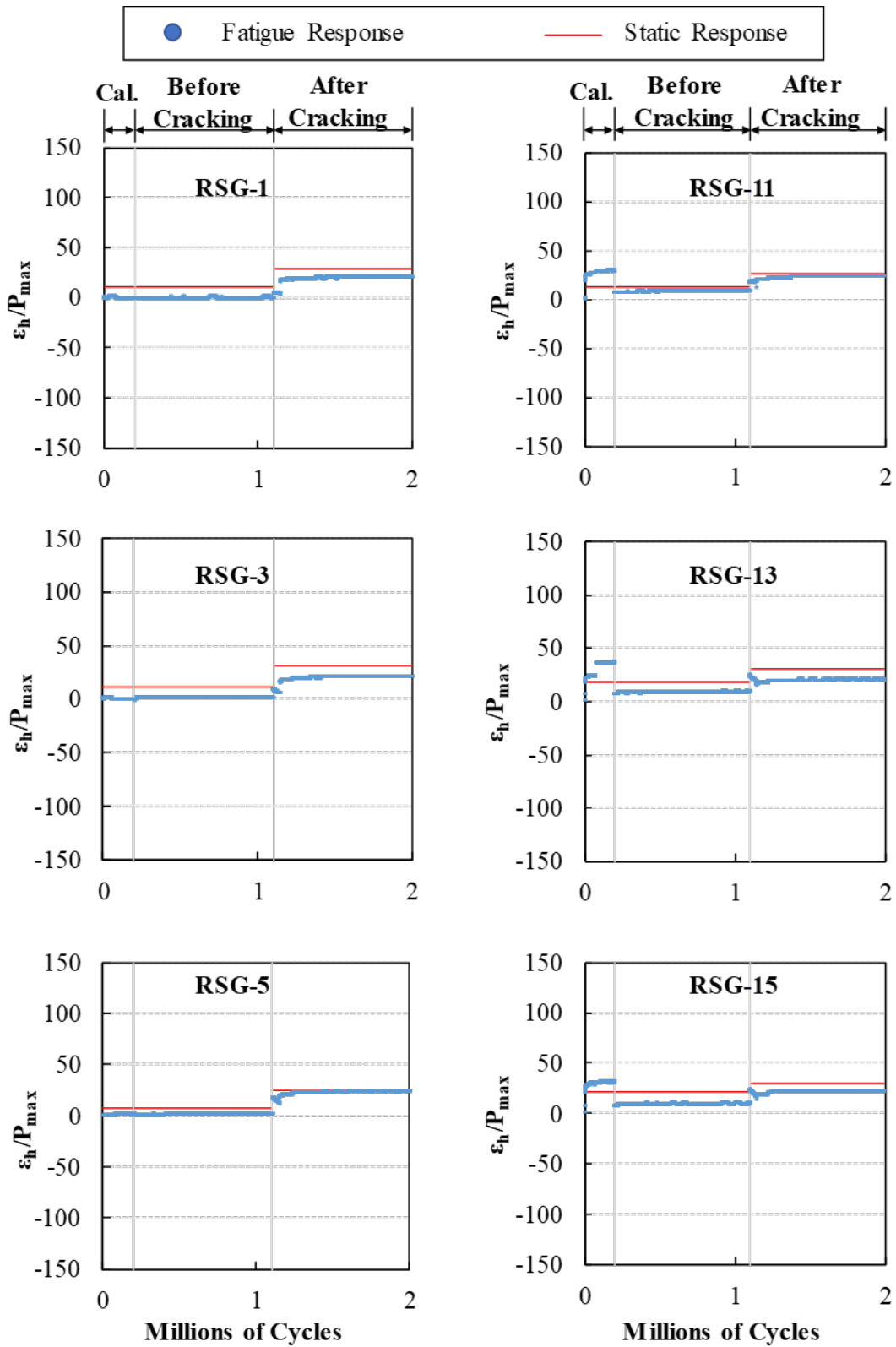


Figure E.24: High reinforcement strain over force for each cycle for 12A2-2 (1 of 2)

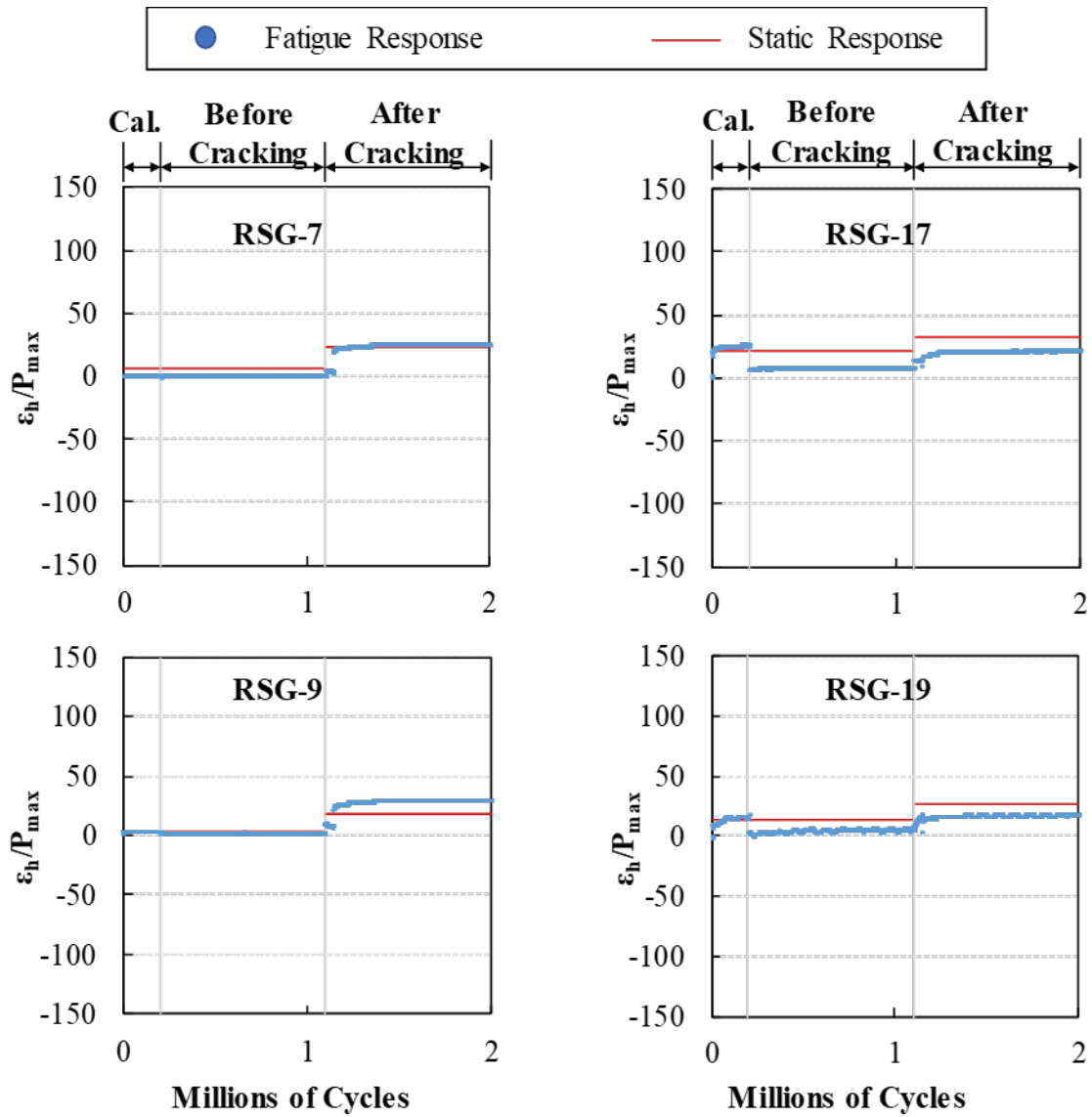


Figure E.25: High reinforcement strain over force for each cycle for 12A2-2 (2 of 2)

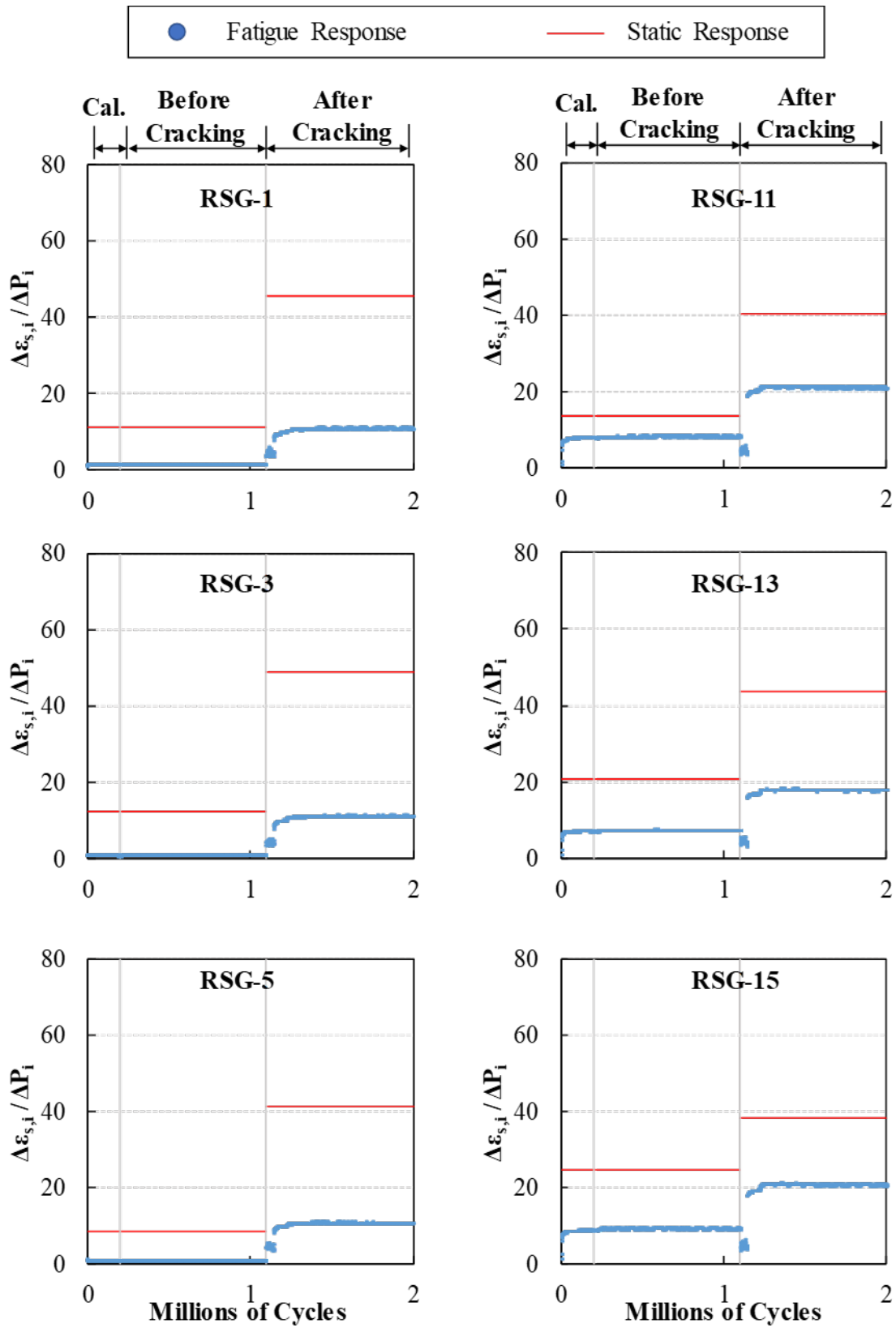


Figure E.26: Reinforcement strain change over force change for each cycle for 12A2-2 (1 of 2)

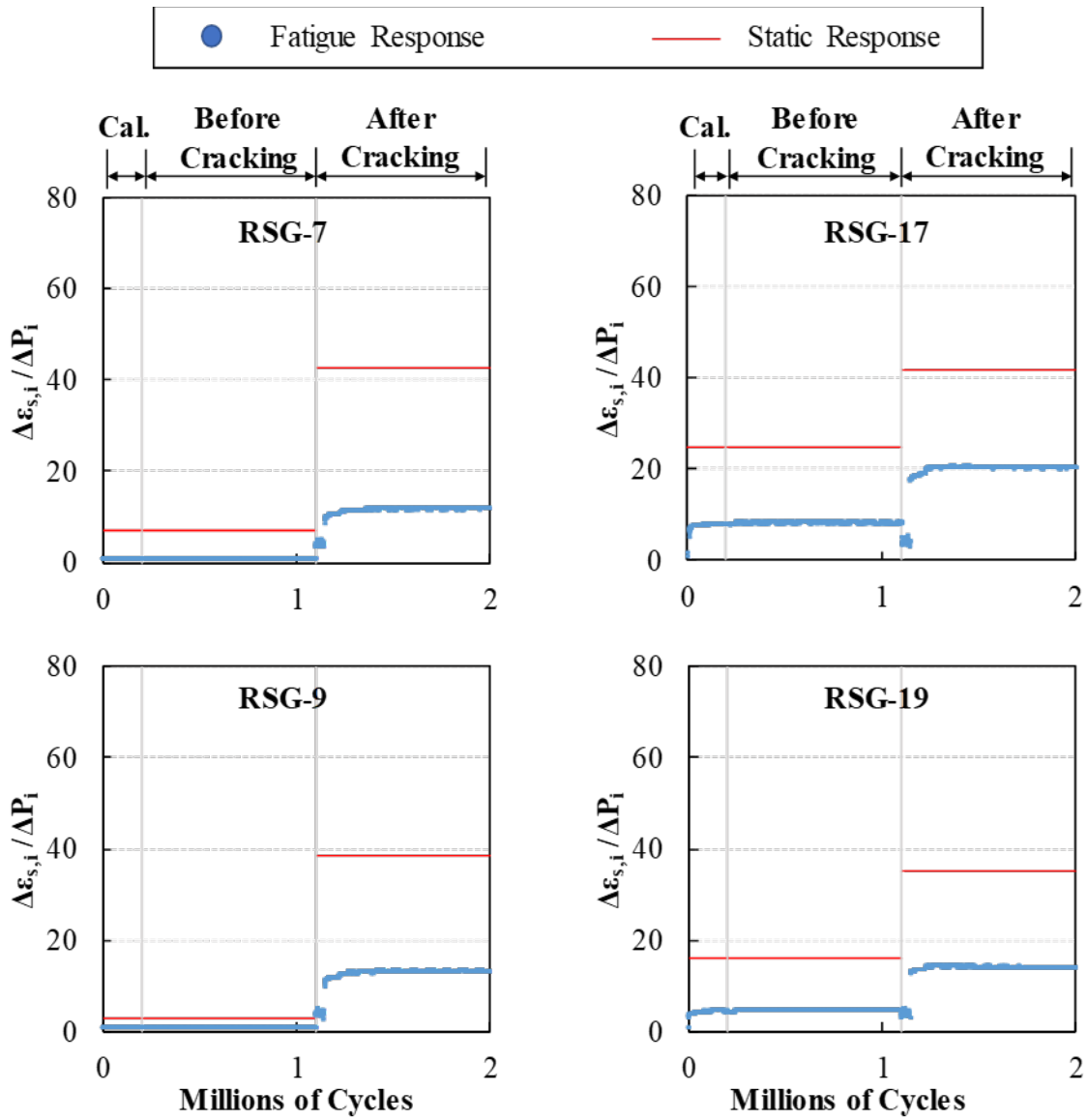


Figure E.27: Reinforcement strain change over force change for each cycle for 12A2-2 (2 of 2)

E.5.1.3. Concrete Strain Gauges

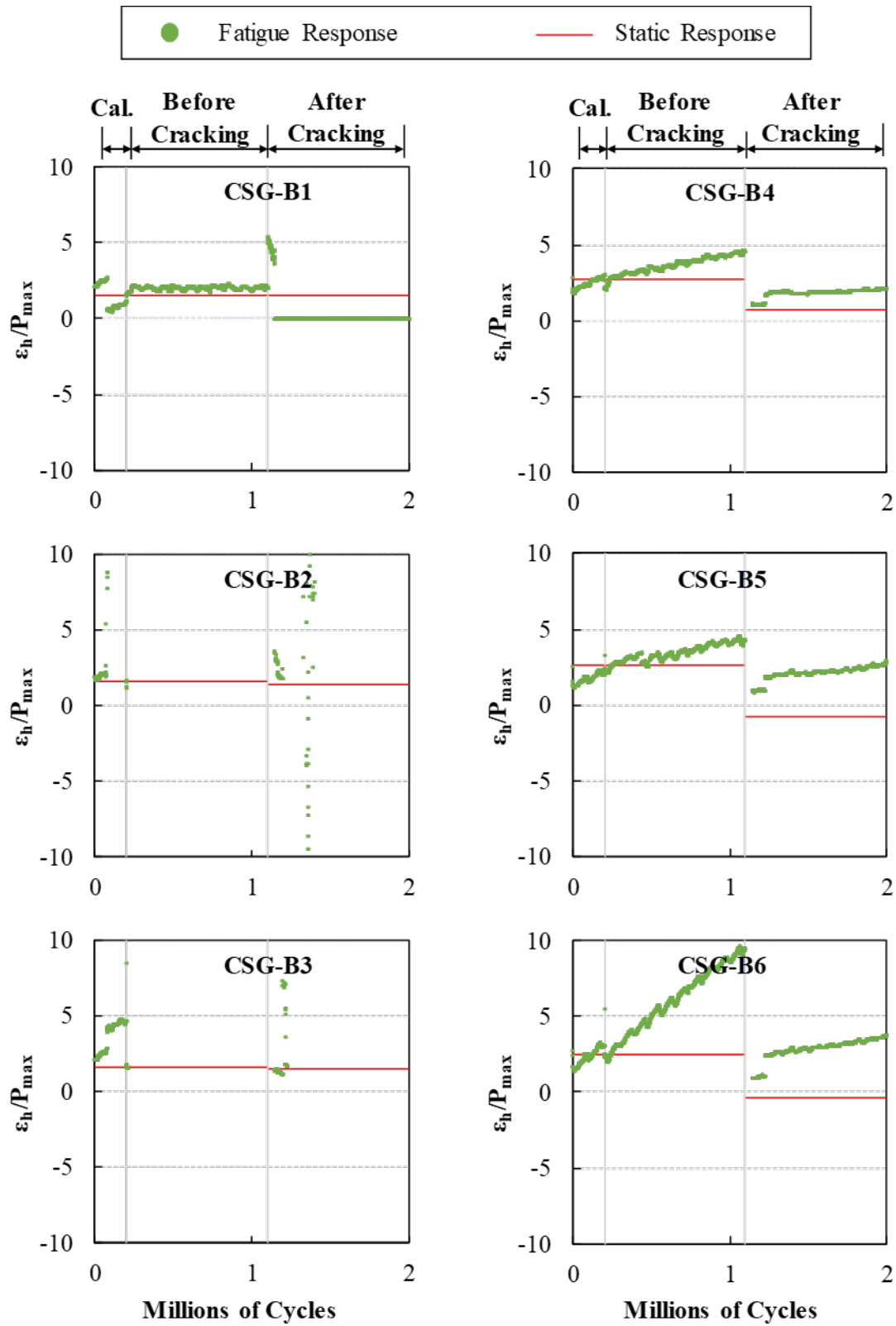


Figure E.28: High concrete strain over force for each cycle for 12A2-2

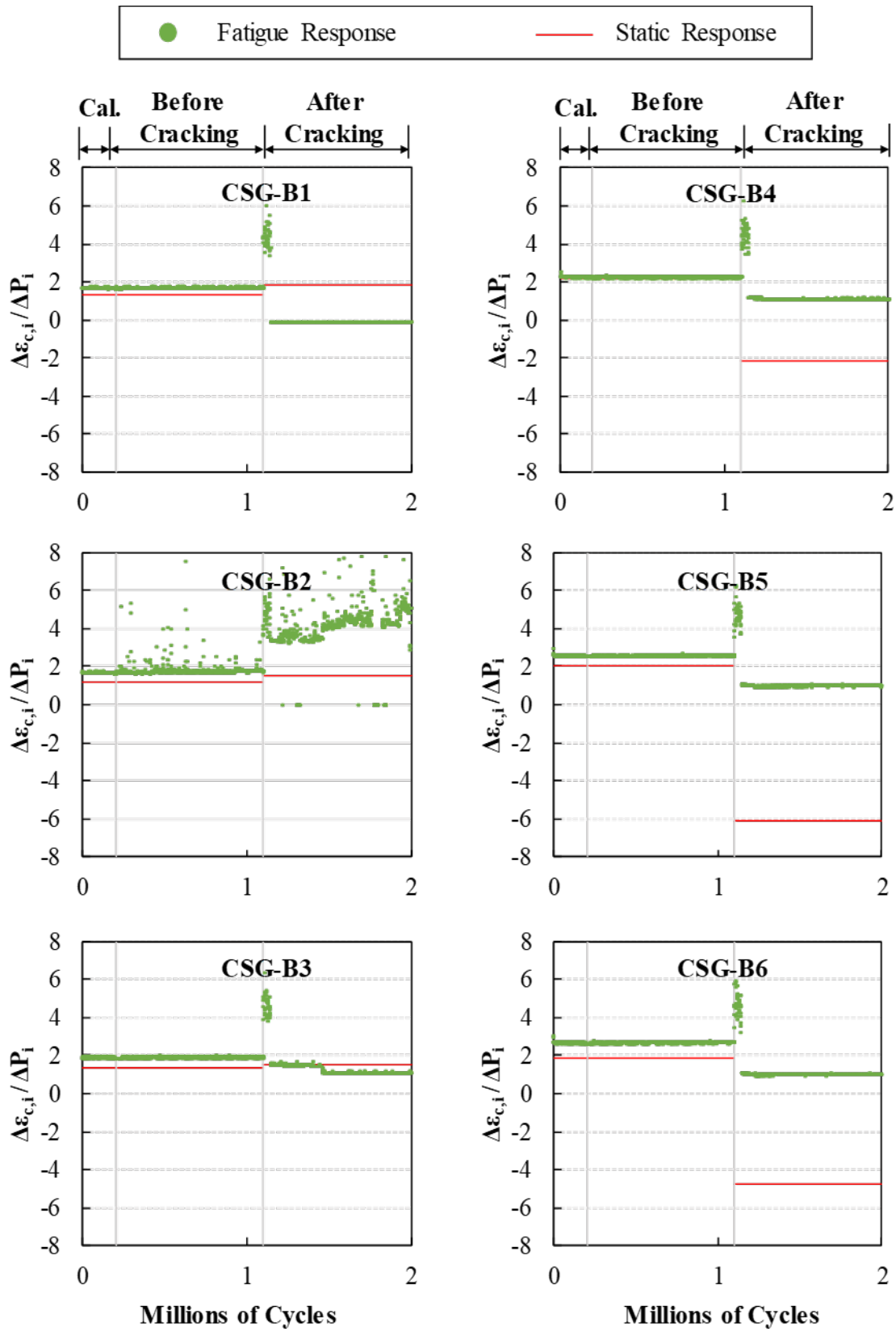


Figure E.29: Concrete strain change over force change for each cycle for 12A2-2

E.5.1.4. Crack Gauges

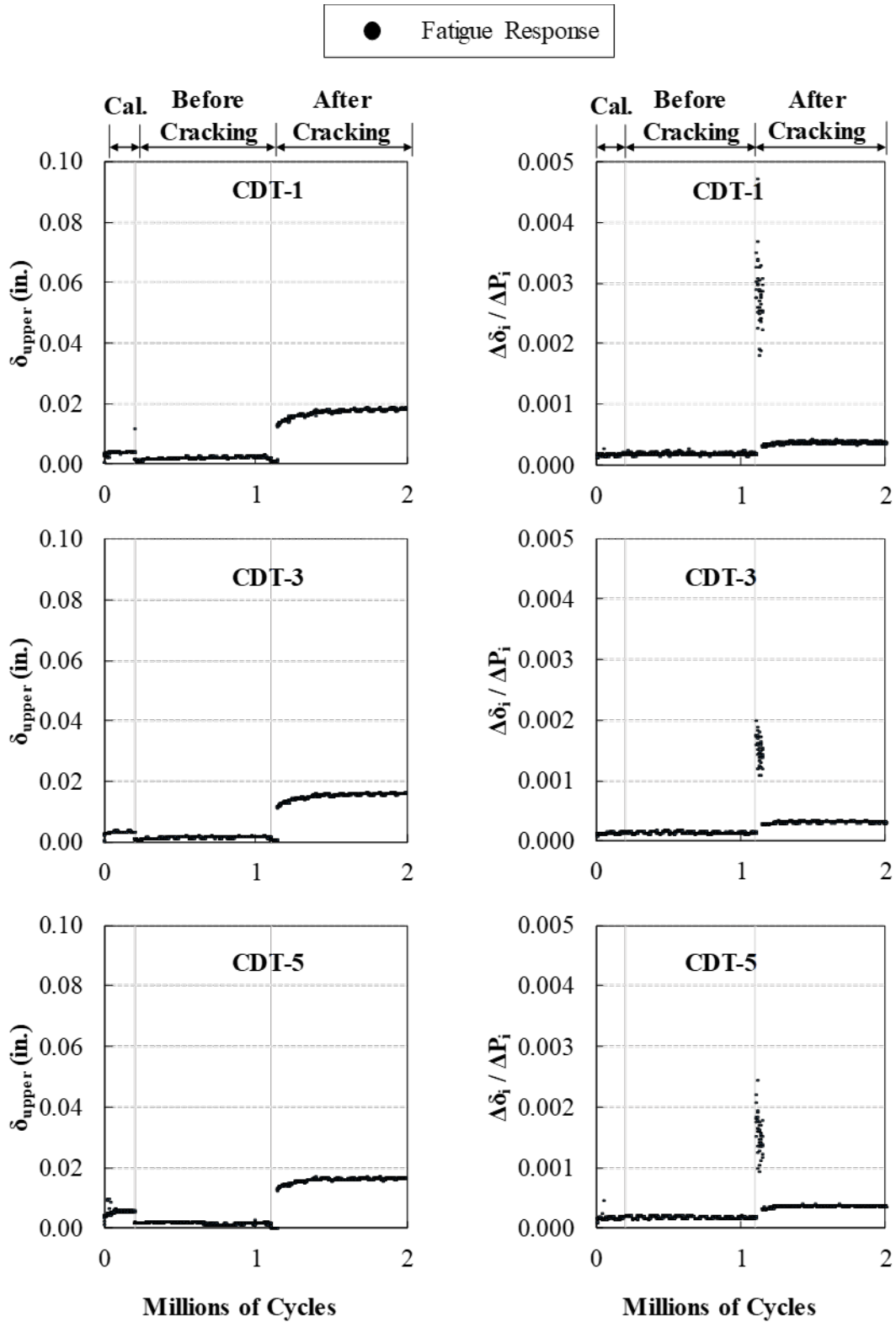


Figure E.30: Crack gage results for each cycle for 12A2-2

E.5.2. Post-Fatigue Static Response

The post-fatigue testing static response for 12A2 (12A2-2) is presented in this section. The load versus deflection plots for the strength response without any fatigue loading (12A2-1) and after the fatigue loading (12A2-2) are shown in Figure E.31. The fatigue loading caused about a 10-percent increase in strength and a 22-percent higher deflection at ultimate strength in the 12A2 joint specimens.

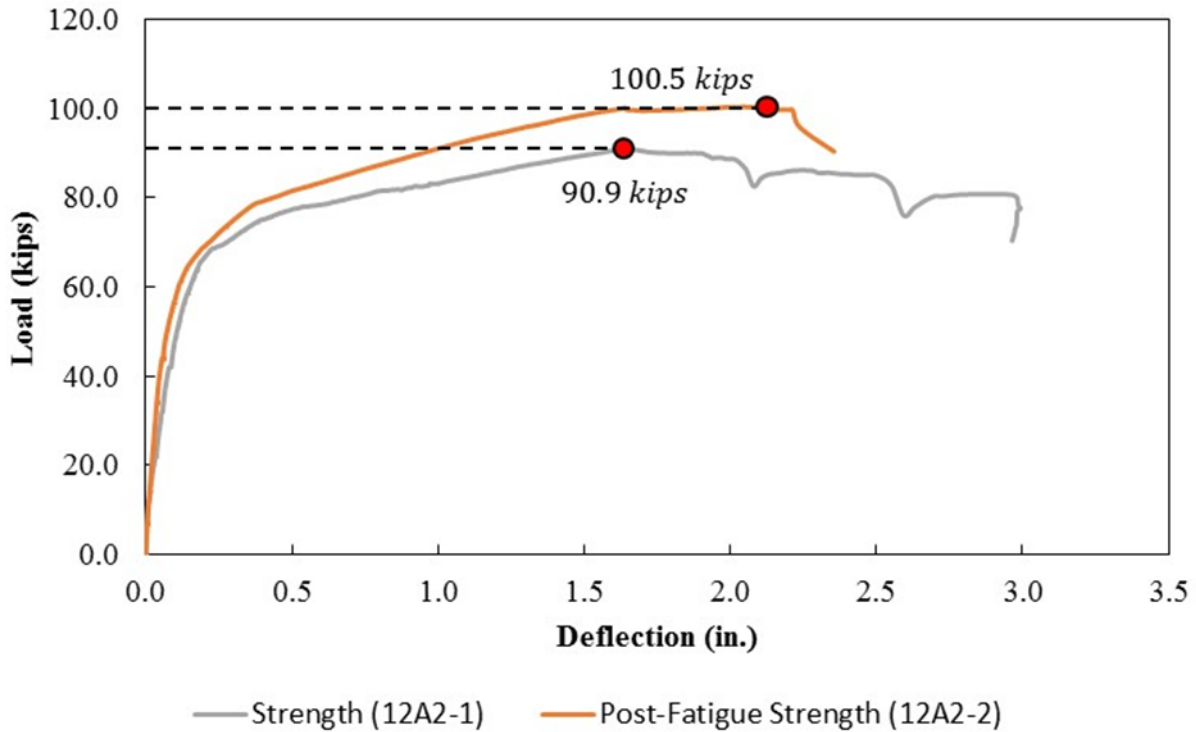


Figure E.31: Load versus displacement plot for strength testing of 12A2 (a) without any fatigue load applied, 12A2-1, and (b) after fatigue loading, 12A2-2

F. RESULTS OF FOUR-BEAM TEST CONFIGURATION

F.1. INTRODUCTION

The test results in this section are organized based on the load stages and load configurations discussed in the body of this report and shown in Table F.1.

Table F.1: Four-beam service, fatigue, and strength loading scheme

Stage	Description	Lower Limit Load ^{(1),(2)} (Δ)	Upper Limit Load ^{(1),(2)} (Δ)	Load Conditions	# Cycles	Testing Days
1.1	FIU-6 Stiffness	0 kip (0.00 in.)	20 kip ⁽³⁾ (0.37 in.)	Service SC 4-1	2	0.5
1.2	FIU-3 Stiffness	0 kip (0.00 in.)	20 kip ⁽³⁾ (0.39 in.)	Service SC 4-2	2	0.5
1.3	FIU-8 Stiffness	0 kip (0.00 in.)	20 kip ⁽³⁾ (0.36 in.)	Service SC 4-3	2	0.5
1.4	FIU-7 Stiffness	0 kip (0.00 in.)	20 kip ⁽³⁾ (0.37 in.)	Service SC 4-4	2	0.5
1.5	FIU-3 Surcharge Application	0 kip (0.00 in.)	19.25 kip ⁽⁴⁾ (0.37 in.)	CL 4-2	1	1
	UHPC joint pour ⁽⁵⁾					
1.6	FIU-3 Surcharge Removal	19.25 kip ⁽⁴⁾ (0.37 in.)	0 kip (0.00 in.)	CL 4-2	1	1
2	Static Elastic–FL120	0 kip (0.00 in.)	30.6 kip ⁽³⁾ (0.00 in.)	Service (LC 4-1 to LC 4-4)	4	4
3	Fatigue Calibration	5 kip (0.00 in.)	23.4 kip ⁽⁶⁾ (0.00 in.)	Fatigue FC 4-6	200,000	2
4	HS20 Truck Load	5 kip (0.00 in.)	23.4 kip ⁽⁶⁾ (0.00 in.)	Service FC 4-6	1,800,000	11
5	Static Elastic–FL120	0 kip (0.00 in.)	30.6 kip ⁽³⁾ (0.00 in.)	Service (LC 4-1, LC 4-3, LC 4-4)	3	2
6	Fatigue Calibration	5 kip (0.00 in.)	23.4 kip ⁽⁶⁾ (0.00 in.)	Fatigue FC 4-7	200,000	2

Stage	Description	Lower Limit Load ^{(1),(2)} (Δ)	Upper Limit Load ^{(1),(2)} (Δ)	Load Conditions	# Cycles	Testing Days
7	HS20 Truck Load	5 kip (0.00 in.)	23.4 kip ⁽⁶⁾ (0.00 in.)	Service FC 4-7	1,800,000	11
8	Static Elastic–FL120	0 kip (0.00 in.)	30.6 kip ⁽³⁾ (0.00 in.)	Service (LC 4-1 to LC 4-4)	4	2
	Longitudinal cracking ⁽⁷⁾					
9	Static Elastic–FL120	0 kip (0.00 in.)	30.6 kip (0.00 in.)	Service (LC 4-1cr to LC 4-4cr)	4	2
10	Ultimate Strength Test			LC 4-5	1	1

⁽¹⁾ Loads/displacements listed are for each actuator (not total)

⁽²⁾ Acceptable load/displacement range for loading is starting load/displacement $\pm 5\%$.

⁽³⁾ Two load ramps applied per beam without casting the joints

⁽⁴⁾ Total surcharge generated by heavy weights (10 load blocks)

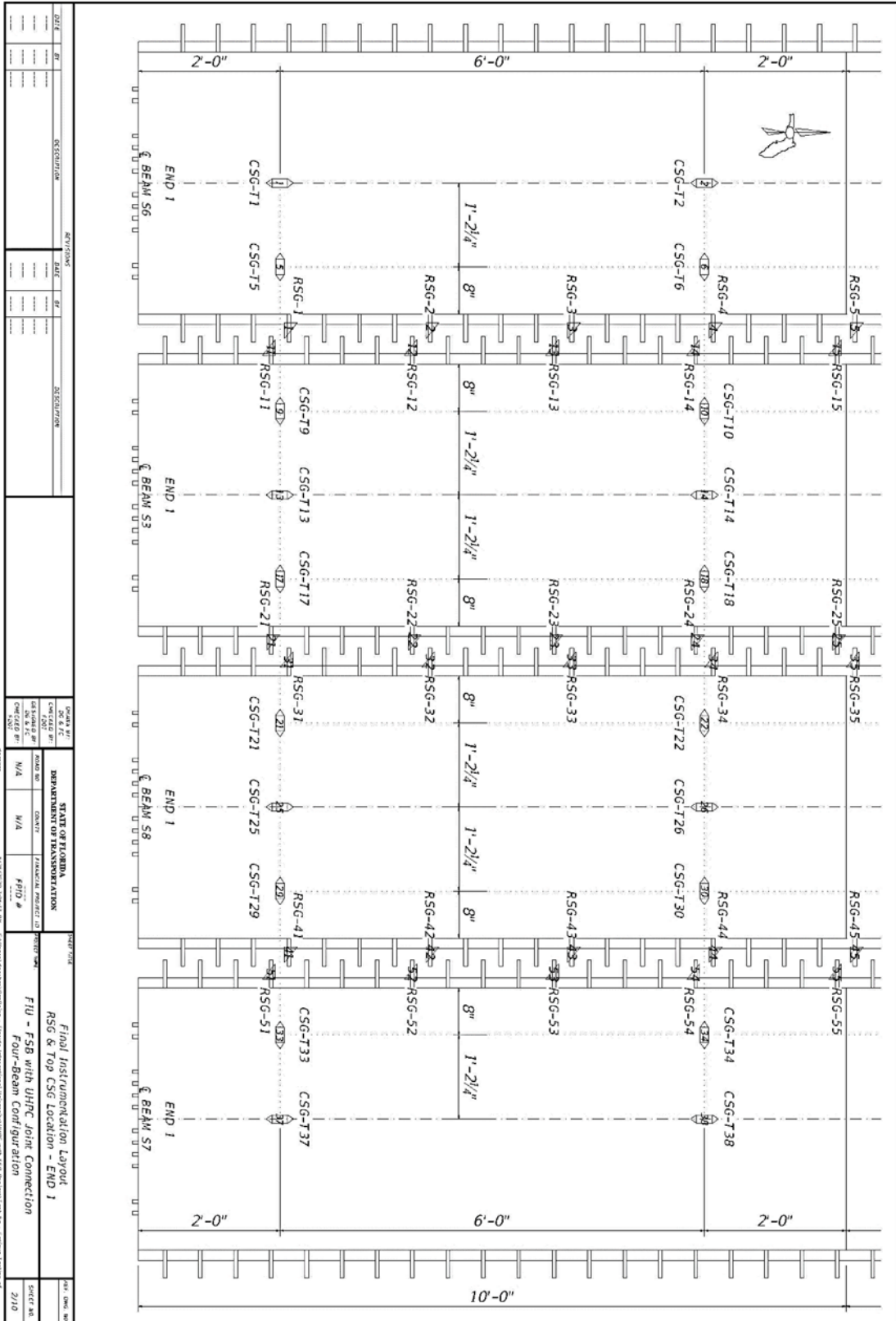
⁽⁵⁾ UHPC joint pour and grind with surcharge (the beams are joined)

⁽⁶⁾ Upper load range determined from lower load range plus 18.4 kips (fatigue)

⁽⁷⁾ Longitudinal crack procedure

F.2. INSTRUMENTATION LAYOUT FOR FOUR-BEAM TEST CONFIGURATION

NAME	UNIT	DESCRIPTION	LOCATION	TYPE	STATUS	DATE	BY	CHECKED	APPROVED																																																																																																																																																																																																								
<div style="display: flex; justify-content: space-between;"> <div style="width: 45%;"> <p>NAME CONVENTION</p> <p> Sensor Type Joint/Beam Section Top/Bottom Location Sensor Number </p> <p> J1-CDT-71 </p> </div> <div style="width: 45%; text-align: right;"> <p>SENSOR DIRECTION/LOCATION</p> <p> Transverse Top Longitudinal Top Longitudinal Bottom Transverse Bottom </p> <p> Transverse Top Longitudinal Top Longitudinal Bottom Transverse Bottom </p> </div> </div>																																																																																																																																																																																																																	
<p>LEGEND</p> <p>56: Beam Specimen 6 (FSB-6)</p> <p>53: Beam Specimen 3 (FSB-3)</p> <p>58: Beam Specimen 8 (FSB-8)</p> <p>57: Beam Specimen 7 (FSB-7)</p> <p>J1: Joint Between 56 and 53</p> <p>J2: Joint Between 53 and 58</p> <p>J3: Joint Between 58 and 57</p> <p>CSG: Concrete Strain Gauge</p> <p>CDT: Crack Displacement Transducer</p> <p>LDT: Laser Displacement Transducer</p> <p>RSG: Rear Strain Gauge</p> <p>T: Top</p> <p>B: Bottom</p>																																																																																																																																																																																																																	
<p>GAUGES LIST</p> <table style="width: 100%; border-collapse: collapse;"> <tr> <td style="width: 15%;">① 56-LDT-1</td> <td style="width: 15%;">↕ 56-C5G-T1</td> <td style="width: 15%;">↗ 56-C5G-B1</td> <td style="width: 15%;">↘ 56-R5G-1</td> <td style="width: 15%;">↖ 58-R5G-41</td> </tr> <tr> <td>② 56-LDT-2</td> <td>↕ 56-C5G-T2</td> <td>↗ 56-C5G-B2</td> <td>↘ 56-R5G-2</td> <td>↖ 58-R5G-42</td> </tr> <tr> <td>③ 56-LDT-3</td> <td>↕ 56-C5G-T3</td> <td>↗ 56-C5G-B3</td> <td>↘ 56-R5G-3</td> <td>↖ 58-R5G-43</td> </tr> <tr> <td>④ 56-LDT-4</td> <td>↕ 56-C5G-T4</td> <td>↗ 56-C5G-B4</td> <td>↘ 56-R5G-4</td> <td>↖ 58-R5G-44</td> </tr> <tr> <td>⑤ 56-LDT-5</td> <td>↕ 56-C5G-T5</td> <td>↗ 56-C5G-B5</td> <td>↘ 56-R5G-5</td> <td>↖ 58-R5G-45</td> </tr> <tr> <td>⑥ 53-LDT-6</td> <td>↕ 56-C5G-T6</td> <td>↗ 56-C5G-B6</td> <td>↘ 56-R5G-6</td> <td>↖ 58-R5G-46</td> </tr> <tr> <td>⑦ 53-LDT-7</td> <td>↕ 56-C5G-T7</td> <td>↗ 56-C5G-B7</td> <td>↘ 56-R5G-7</td> <td>↖ 58-R5G-47</td> </tr> <tr> <td>⑧ 53-LDT-8</td> <td>↕ 56-C5G-T8</td> <td>↗ 56-C5G-B8</td> <td>↘ 56-R5G-8</td> <td>↖ 58-R5G-48</td> </tr> <tr> <td>⑨ 53-LDT-9</td> <td>↕ 53-C5G-T9</td> <td>↗ 53-C5G-B9</td> <td>↘ 56-R5G-9</td> <td>↖ 58-R5G-49</td> </tr> <tr> <td>⑩ 58-LDT-10</td> <td>↕ 53-C5G-T10</td> <td>↗ 53-C5G-B10</td> <td>↘ 56-R5G-10</td> <td>↖ 58-R5G-50</td> </tr> <tr> <td>⑪ 58-LDT-11</td> <td>↕ 53-C5G-T11</td> <td>↗ 53-C5G-B11</td> <td>↘ 53-R5G-11</td> <td>↖ 57-R5G-51</td> </tr> <tr> <td>⑫ 58-LDT-12</td> <td>↕ 53-C5G-T12</td> <td>↗ 53-C5G-B12</td> <td>↘ 53-R5G-12</td> <td>↖ 57-R5G-52</td> </tr> <tr> <td>⑬ 58-LDT-13</td> <td>↕ 53-C5G-T13</td> <td>↗ 53-C5G-B13</td> <td>↘ 53-R5G-13</td> <td>↖ 57-R5G-53</td> </tr> <tr> <td>⑭ 57-LDT-14</td> <td>↕ 53-C5G-T14</td> <td>↗ 53-C5G-B14</td> <td>↘ 53-R5G-14</td> <td>↖ 57-R5G-54</td> </tr> <tr> <td>⑮ 57-LDT-15</td> <td>↕ 53-C5G-T15</td> <td>↗ 53-C5G-B15</td> <td>↘ 53-R5G-15</td> <td>↖ 57-R5G-55</td> </tr> <tr> <td>⑯ 57-LDT-16</td> <td>↕ 53-C5G-T16</td> <td>↗ 53-C5G-B16</td> <td>↘ 53-R5G-16</td> <td>↖ 57-R5G-56</td> </tr> <tr> <td>⑰ 57-LDT-17</td> <td>↕ 53-C5G-T17</td> <td>↗ 53-C5G-B17</td> <td>↘ 53-R5G-17</td> <td>↖ 57-R5G-57</td> </tr> <tr> <td>⑱ 57-LDT-18</td> <td>↕ 53-C5G-T18</td> <td>↗ 53-C5G-B18</td> <td>↘ 53-R5G-18</td> <td>↖ 57-R5G-58</td> </tr> <tr> <td>⑲ J1-CDT-19</td> <td>↕ 53-C5G-T19</td> <td>↗ 53-C5G-B19</td> <td>↘ 53-R5G-19</td> <td>↖ 57-R5G-59</td> </tr> <tr> <td>⑳ J1-CDT-20</td> <td>↕ 53-C5G-T20</td> <td>↗ 53-C5G-B20</td> <td>↘ 53-R5G-20</td> <td>↖ 57-R5G-60</td> </tr> <tr> <td>㉑ J1-CDT-21</td> <td>↕ 58-C5G-T21</td> <td>↗ 58-C5G-B21</td> <td>↘ 53-R5G-21</td> <td></td> </tr> <tr> <td>㉒ J2-CDT-71</td> <td>↕ 58-C5G-T22</td> <td>↗ 58-C5G-B22</td> <td>↘ 53-R5G-22</td> <td></td> </tr> <tr> <td>㉓ J2-CDT-72</td> <td>↕ 58-C5G-T23</td> <td>↗ 58-C5G-B23</td> <td>↘ 53-R5G-23</td> <td></td> </tr> <tr> <td>㉔ J2-CDT-73</td> <td>↕ 58-C5G-T24</td> <td>↗ 58-C5G-B24</td> <td>↘ 53-R5G-24</td> <td></td> </tr> <tr> <td>㉕ J3-CDT-76</td> <td>↕ 58-C5G-T25</td> <td>↗ 58-C5G-B25</td> <td>↘ 53-R5G-25</td> <td></td> </tr> <tr> <td>㉖ J1-CDT-81</td> <td>↕ 58-C5G-T26</td> <td>↗ 58-C5G-B26</td> <td>↘ 53-R5G-26</td> <td></td> </tr> <tr> <td>㉗ J1-CDT-82</td> <td>↕ 58-C5G-T27</td> <td>↗ 58-C5G-B27</td> <td>↘ 53-R5G-27</td> <td></td> </tr> <tr> <td>㉘ J1-CDT-83</td> <td>↕ 58-C5G-T28</td> <td>↗ 58-C5G-B28</td> <td>↘ 53-R5G-28</td> <td></td> </tr> <tr> <td>㉙ J2-CDT-84</td> <td>↕ 58-C5G-T29</td> <td>↗ 58-C5G-B29</td> <td>↘ 53-R5G-29</td> <td></td> </tr> <tr> <td>㉚ J2-CDT-85</td> <td>↕ 58-C5G-T30</td> <td>↗ 58-C5G-B30</td> <td>↘ 53-R5G-30</td> <td></td> </tr> <tr> <td>㉛ J3-CDT-86</td> <td>↕ 58-C5G-T31</td> <td>↗ 58-C5G-B31</td> <td>↘ 58-R5G-31</td> <td></td> </tr> <tr> <td>㉜ J3-CDT-87</td> <td>↕ 58-C5G-T32</td> <td>↗ 58-C5G-B32</td> <td>↘ 58-R5G-32</td> <td></td> </tr> <tr> <td></td> <td>↕ 57-C5G-T33</td> <td>↗ 57-C5G-B33</td> <td>↘ 58-R5G-33</td> <td></td> </tr> <tr> <td></td> <td>↕ 57-C5G-T34</td> <td>↗ 57-C5G-B34</td> <td>↘ 58-R5G-34</td> <td></td> </tr> <tr> <td></td> <td>↕ 57-C5G-T35</td> <td>↗ 57-C5G-B35</td> <td>↘ 58-R5G-35</td> <td></td> </tr> <tr> <td></td> <td>↕ 57-C5G-T36</td> <td>↗ 57-C5G-B36</td> <td>↘ 58-R5G-36</td> <td></td> </tr> <tr> <td></td> <td>↕ 57-C5G-T37</td> <td>↗ 57-C5G-B37</td> <td>↘ 58-R5G-37</td> <td></td> </tr> <tr> <td></td> <td>↕ 57-C5G-T38</td> <td>↗ 57-C5G-B38</td> <td>↘ 58-R5G-38</td> <td></td> </tr> <tr> <td></td> <td>↕ 57-C5G-T39</td> <td>↗ 57-C5G-B39</td> <td>↘ 58-R5G-39</td> <td></td> </tr> <tr> <td></td> <td>↕ 57-C5G-T40</td> <td>↗ 57-C5G-B40</td> <td>↘ 58-R5G-40</td> <td></td> </tr> </table>										① 56-LDT-1	↕ 56-C5G-T1	↗ 56-C5G-B1	↘ 56-R5G-1	↖ 58-R5G-41	② 56-LDT-2	↕ 56-C5G-T2	↗ 56-C5G-B2	↘ 56-R5G-2	↖ 58-R5G-42	③ 56-LDT-3	↕ 56-C5G-T3	↗ 56-C5G-B3	↘ 56-R5G-3	↖ 58-R5G-43	④ 56-LDT-4	↕ 56-C5G-T4	↗ 56-C5G-B4	↘ 56-R5G-4	↖ 58-R5G-44	⑤ 56-LDT-5	↕ 56-C5G-T5	↗ 56-C5G-B5	↘ 56-R5G-5	↖ 58-R5G-45	⑥ 53-LDT-6	↕ 56-C5G-T6	↗ 56-C5G-B6	↘ 56-R5G-6	↖ 58-R5G-46	⑦ 53-LDT-7	↕ 56-C5G-T7	↗ 56-C5G-B7	↘ 56-R5G-7	↖ 58-R5G-47	⑧ 53-LDT-8	↕ 56-C5G-T8	↗ 56-C5G-B8	↘ 56-R5G-8	↖ 58-R5G-48	⑨ 53-LDT-9	↕ 53-C5G-T9	↗ 53-C5G-B9	↘ 56-R5G-9	↖ 58-R5G-49	⑩ 58-LDT-10	↕ 53-C5G-T10	↗ 53-C5G-B10	↘ 56-R5G-10	↖ 58-R5G-50	⑪ 58-LDT-11	↕ 53-C5G-T11	↗ 53-C5G-B11	↘ 53-R5G-11	↖ 57-R5G-51	⑫ 58-LDT-12	↕ 53-C5G-T12	↗ 53-C5G-B12	↘ 53-R5G-12	↖ 57-R5G-52	⑬ 58-LDT-13	↕ 53-C5G-T13	↗ 53-C5G-B13	↘ 53-R5G-13	↖ 57-R5G-53	⑭ 57-LDT-14	↕ 53-C5G-T14	↗ 53-C5G-B14	↘ 53-R5G-14	↖ 57-R5G-54	⑮ 57-LDT-15	↕ 53-C5G-T15	↗ 53-C5G-B15	↘ 53-R5G-15	↖ 57-R5G-55	⑯ 57-LDT-16	↕ 53-C5G-T16	↗ 53-C5G-B16	↘ 53-R5G-16	↖ 57-R5G-56	⑰ 57-LDT-17	↕ 53-C5G-T17	↗ 53-C5G-B17	↘ 53-R5G-17	↖ 57-R5G-57	⑱ 57-LDT-18	↕ 53-C5G-T18	↗ 53-C5G-B18	↘ 53-R5G-18	↖ 57-R5G-58	⑲ J1-CDT-19	↕ 53-C5G-T19	↗ 53-C5G-B19	↘ 53-R5G-19	↖ 57-R5G-59	⑳ J1-CDT-20	↕ 53-C5G-T20	↗ 53-C5G-B20	↘ 53-R5G-20	↖ 57-R5G-60	㉑ J1-CDT-21	↕ 58-C5G-T21	↗ 58-C5G-B21	↘ 53-R5G-21		㉒ J2-CDT-71	↕ 58-C5G-T22	↗ 58-C5G-B22	↘ 53-R5G-22		㉓ J2-CDT-72	↕ 58-C5G-T23	↗ 58-C5G-B23	↘ 53-R5G-23		㉔ J2-CDT-73	↕ 58-C5G-T24	↗ 58-C5G-B24	↘ 53-R5G-24		㉕ J3-CDT-76	↕ 58-C5G-T25	↗ 58-C5G-B25	↘ 53-R5G-25		㉖ J1-CDT-81	↕ 58-C5G-T26	↗ 58-C5G-B26	↘ 53-R5G-26		㉗ J1-CDT-82	↕ 58-C5G-T27	↗ 58-C5G-B27	↘ 53-R5G-27		㉘ J1-CDT-83	↕ 58-C5G-T28	↗ 58-C5G-B28	↘ 53-R5G-28		㉙ J2-CDT-84	↕ 58-C5G-T29	↗ 58-C5G-B29	↘ 53-R5G-29		㉚ J2-CDT-85	↕ 58-C5G-T30	↗ 58-C5G-B30	↘ 53-R5G-30		㉛ J3-CDT-86	↕ 58-C5G-T31	↗ 58-C5G-B31	↘ 58-R5G-31		㉜ J3-CDT-87	↕ 58-C5G-T32	↗ 58-C5G-B32	↘ 58-R5G-32			↕ 57-C5G-T33	↗ 57-C5G-B33	↘ 58-R5G-33			↕ 57-C5G-T34	↗ 57-C5G-B34	↘ 58-R5G-34			↕ 57-C5G-T35	↗ 57-C5G-B35	↘ 58-R5G-35			↕ 57-C5G-T36	↗ 57-C5G-B36	↘ 58-R5G-36			↕ 57-C5G-T37	↗ 57-C5G-B37	↘ 58-R5G-37			↕ 57-C5G-T38	↗ 57-C5G-B38	↘ 58-R5G-38			↕ 57-C5G-T39	↗ 57-C5G-B39	↘ 58-R5G-39			↕ 57-C5G-T40	↗ 57-C5G-B40	↘ 58-R5G-40	
① 56-LDT-1	↕ 56-C5G-T1	↗ 56-C5G-B1	↘ 56-R5G-1	↖ 58-R5G-41																																																																																																																																																																																																													
② 56-LDT-2	↕ 56-C5G-T2	↗ 56-C5G-B2	↘ 56-R5G-2	↖ 58-R5G-42																																																																																																																																																																																																													
③ 56-LDT-3	↕ 56-C5G-T3	↗ 56-C5G-B3	↘ 56-R5G-3	↖ 58-R5G-43																																																																																																																																																																																																													
④ 56-LDT-4	↕ 56-C5G-T4	↗ 56-C5G-B4	↘ 56-R5G-4	↖ 58-R5G-44																																																																																																																																																																																																													
⑤ 56-LDT-5	↕ 56-C5G-T5	↗ 56-C5G-B5	↘ 56-R5G-5	↖ 58-R5G-45																																																																																																																																																																																																													
⑥ 53-LDT-6	↕ 56-C5G-T6	↗ 56-C5G-B6	↘ 56-R5G-6	↖ 58-R5G-46																																																																																																																																																																																																													
⑦ 53-LDT-7	↕ 56-C5G-T7	↗ 56-C5G-B7	↘ 56-R5G-7	↖ 58-R5G-47																																																																																																																																																																																																													
⑧ 53-LDT-8	↕ 56-C5G-T8	↗ 56-C5G-B8	↘ 56-R5G-8	↖ 58-R5G-48																																																																																																																																																																																																													
⑨ 53-LDT-9	↕ 53-C5G-T9	↗ 53-C5G-B9	↘ 56-R5G-9	↖ 58-R5G-49																																																																																																																																																																																																													
⑩ 58-LDT-10	↕ 53-C5G-T10	↗ 53-C5G-B10	↘ 56-R5G-10	↖ 58-R5G-50																																																																																																																																																																																																													
⑪ 58-LDT-11	↕ 53-C5G-T11	↗ 53-C5G-B11	↘ 53-R5G-11	↖ 57-R5G-51																																																																																																																																																																																																													
⑫ 58-LDT-12	↕ 53-C5G-T12	↗ 53-C5G-B12	↘ 53-R5G-12	↖ 57-R5G-52																																																																																																																																																																																																													
⑬ 58-LDT-13	↕ 53-C5G-T13	↗ 53-C5G-B13	↘ 53-R5G-13	↖ 57-R5G-53																																																																																																																																																																																																													
⑭ 57-LDT-14	↕ 53-C5G-T14	↗ 53-C5G-B14	↘ 53-R5G-14	↖ 57-R5G-54																																																																																																																																																																																																													
⑮ 57-LDT-15	↕ 53-C5G-T15	↗ 53-C5G-B15	↘ 53-R5G-15	↖ 57-R5G-55																																																																																																																																																																																																													
⑯ 57-LDT-16	↕ 53-C5G-T16	↗ 53-C5G-B16	↘ 53-R5G-16	↖ 57-R5G-56																																																																																																																																																																																																													
⑰ 57-LDT-17	↕ 53-C5G-T17	↗ 53-C5G-B17	↘ 53-R5G-17	↖ 57-R5G-57																																																																																																																																																																																																													
⑱ 57-LDT-18	↕ 53-C5G-T18	↗ 53-C5G-B18	↘ 53-R5G-18	↖ 57-R5G-58																																																																																																																																																																																																													
⑲ J1-CDT-19	↕ 53-C5G-T19	↗ 53-C5G-B19	↘ 53-R5G-19	↖ 57-R5G-59																																																																																																																																																																																																													
⑳ J1-CDT-20	↕ 53-C5G-T20	↗ 53-C5G-B20	↘ 53-R5G-20	↖ 57-R5G-60																																																																																																																																																																																																													
㉑ J1-CDT-21	↕ 58-C5G-T21	↗ 58-C5G-B21	↘ 53-R5G-21																																																																																																																																																																																																														
㉒ J2-CDT-71	↕ 58-C5G-T22	↗ 58-C5G-B22	↘ 53-R5G-22																																																																																																																																																																																																														
㉓ J2-CDT-72	↕ 58-C5G-T23	↗ 58-C5G-B23	↘ 53-R5G-23																																																																																																																																																																																																														
㉔ J2-CDT-73	↕ 58-C5G-T24	↗ 58-C5G-B24	↘ 53-R5G-24																																																																																																																																																																																																														
㉕ J3-CDT-76	↕ 58-C5G-T25	↗ 58-C5G-B25	↘ 53-R5G-25																																																																																																																																																																																																														
㉖ J1-CDT-81	↕ 58-C5G-T26	↗ 58-C5G-B26	↘ 53-R5G-26																																																																																																																																																																																																														
㉗ J1-CDT-82	↕ 58-C5G-T27	↗ 58-C5G-B27	↘ 53-R5G-27																																																																																																																																																																																																														
㉘ J1-CDT-83	↕ 58-C5G-T28	↗ 58-C5G-B28	↘ 53-R5G-28																																																																																																																																																																																																														
㉙ J2-CDT-84	↕ 58-C5G-T29	↗ 58-C5G-B29	↘ 53-R5G-29																																																																																																																																																																																																														
㉚ J2-CDT-85	↕ 58-C5G-T30	↗ 58-C5G-B30	↘ 53-R5G-30																																																																																																																																																																																																														
㉛ J3-CDT-86	↕ 58-C5G-T31	↗ 58-C5G-B31	↘ 58-R5G-31																																																																																																																																																																																																														
㉜ J3-CDT-87	↕ 58-C5G-T32	↗ 58-C5G-B32	↘ 58-R5G-32																																																																																																																																																																																																														
	↕ 57-C5G-T33	↗ 57-C5G-B33	↘ 58-R5G-33																																																																																																																																																																																																														
	↕ 57-C5G-T34	↗ 57-C5G-B34	↘ 58-R5G-34																																																																																																																																																																																																														
	↕ 57-C5G-T35	↗ 57-C5G-B35	↘ 58-R5G-35																																																																																																																																																																																																														
	↕ 57-C5G-T36	↗ 57-C5G-B36	↘ 58-R5G-36																																																																																																																																																																																																														
	↕ 57-C5G-T37	↗ 57-C5G-B37	↘ 58-R5G-37																																																																																																																																																																																																														
	↕ 57-C5G-T38	↗ 57-C5G-B38	↘ 58-R5G-38																																																																																																																																																																																																														
	↕ 57-C5G-T39	↗ 57-C5G-B39	↘ 58-R5G-39																																																																																																																																																																																																														
	↕ 57-C5G-T40	↗ 57-C5G-B40	↘ 58-R5G-40																																																																																																																																																																																																														
<p>Final Instrumentation Layout</p> <p>GAUGES LIST and Legend</p> <p>FU - F58 with UHPV Joint Connection</p> <p>Four-Beam Configuration</p>																																																																																																																																																																																																																	



DATE		DESCRIPTION		REVISIONS		SCALE		DATE		DESCRIPTION		SCALE		DATE		DESCRIPTION	

DATE	BY	DESCRIPTION	SCALE	DATE	BY	DESCRIPTION	SCALE	DATE	BY	DESCRIPTION	SCALE

DATE	BY	DESCRIPTION	SCALE	DATE	BY	DESCRIPTION	SCALE

DATE	BY	DESCRIPTION	SCALE	DATE	BY	DESCRIPTION	SCALE

DATE	BY	DESCRIPTION	SCALE	DATE	BY	DESCRIPTION	SCALE

DATE	BY	DESCRIPTION	SCALE	DATE	BY	DESCRIPTION	SCALE

DATE	BY	DESCRIPTION	SCALE	DATE	BY	DESCRIPTION	SCALE

DATE	BY	DESCRIPTION	SCALE	DATE	BY	DESCRIPTION	SCALE

DATE	BY	DESCRIPTION	SCALE	DATE	BY	DESCRIPTION	SCALE

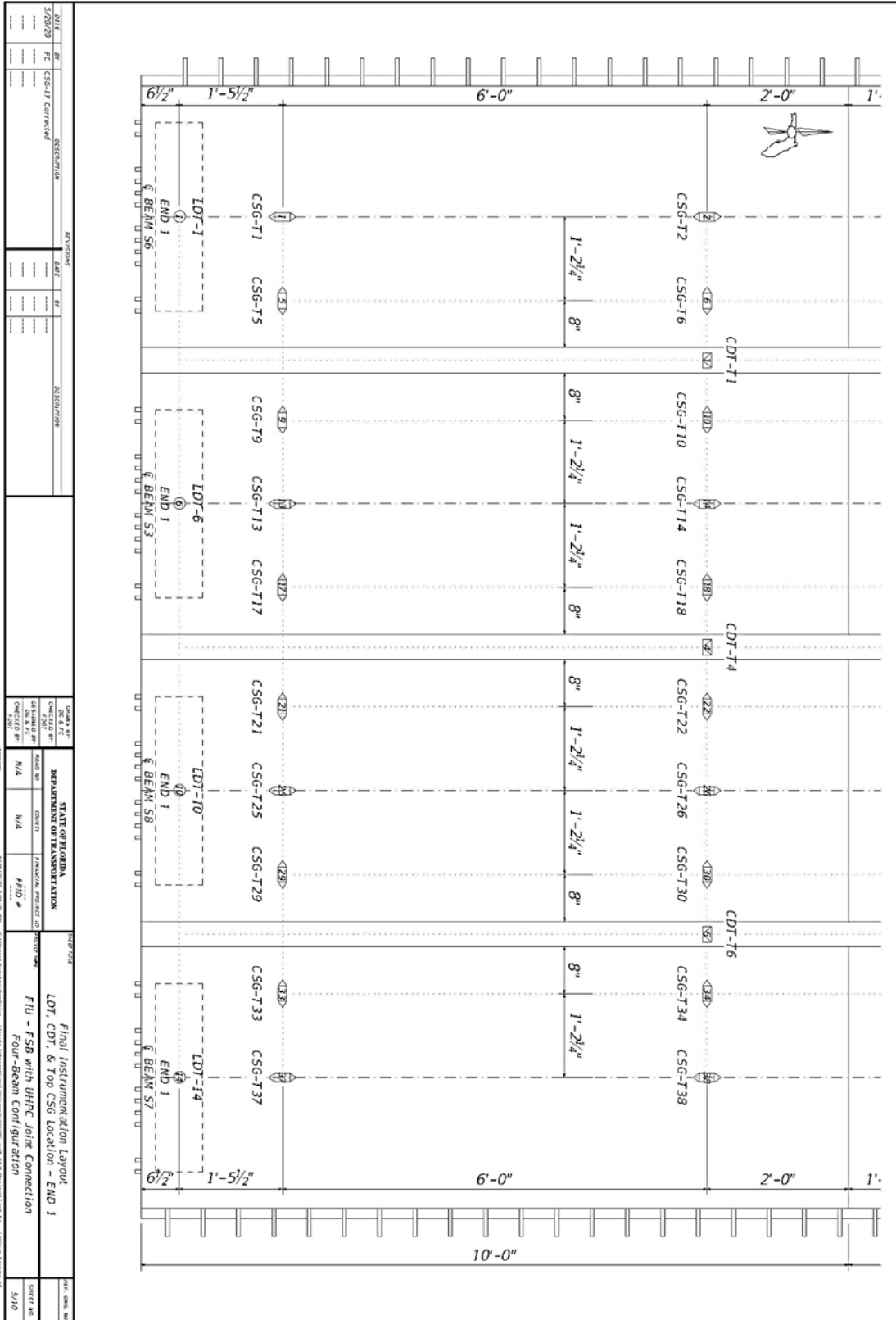
DATE	BY	DESCRIPTION	SCALE	DATE	BY	DESCRIPTION	SCALE

DATE	BY	DESCRIPTION	SCALE	DATE	BY	DESCRIPTION	SCALE

DATE	BY	DESCRIPTION	SCALE	DATE	BY	DESCRIPTION	SCALE

DATE	BY	DESCRIPTION	SCALE	DATE	BY	DESCRIPTION	SCALE

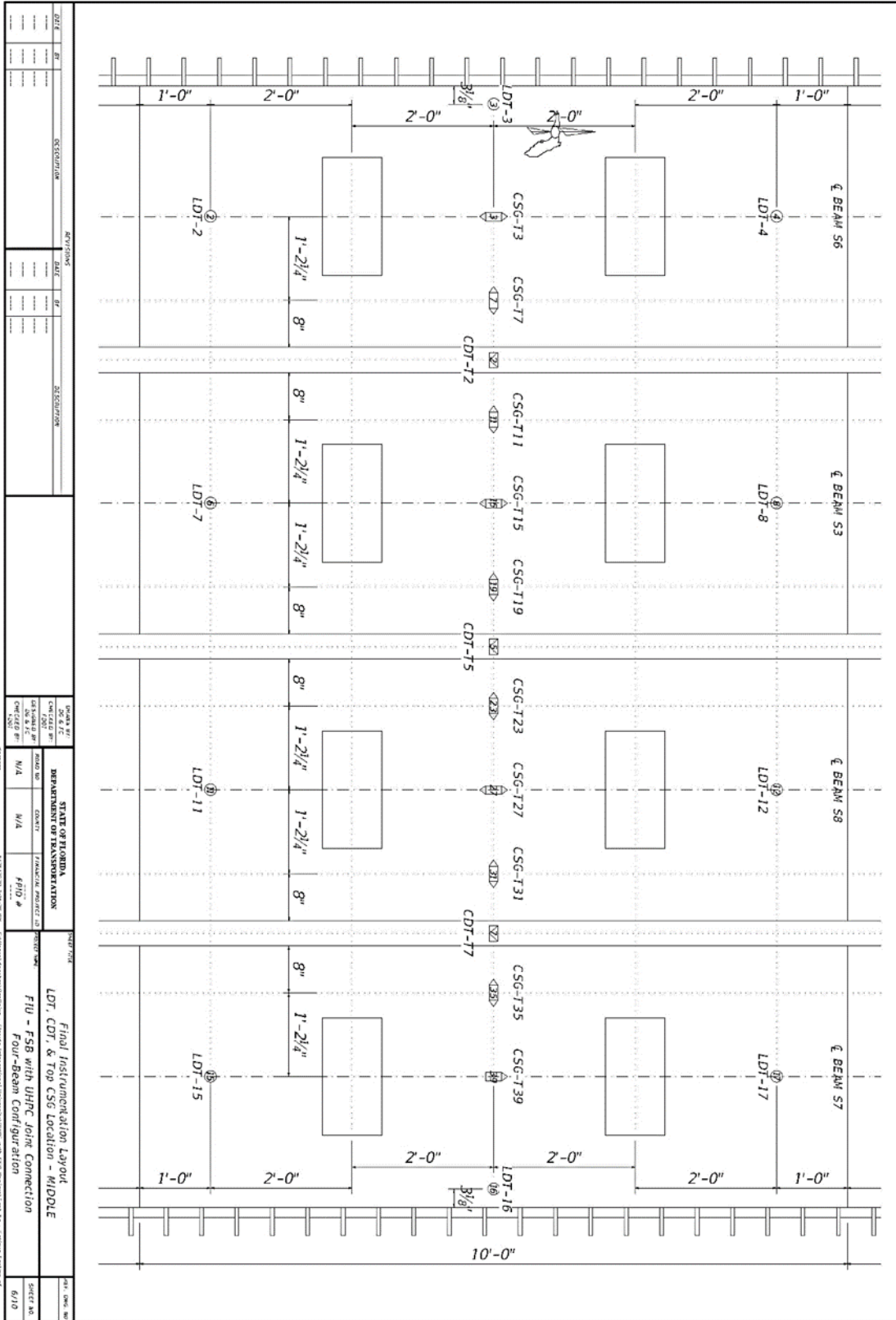
DATE	BY	DESCRIPTION	SCALE	DATE	BY	DESCRIPTION	SCALE



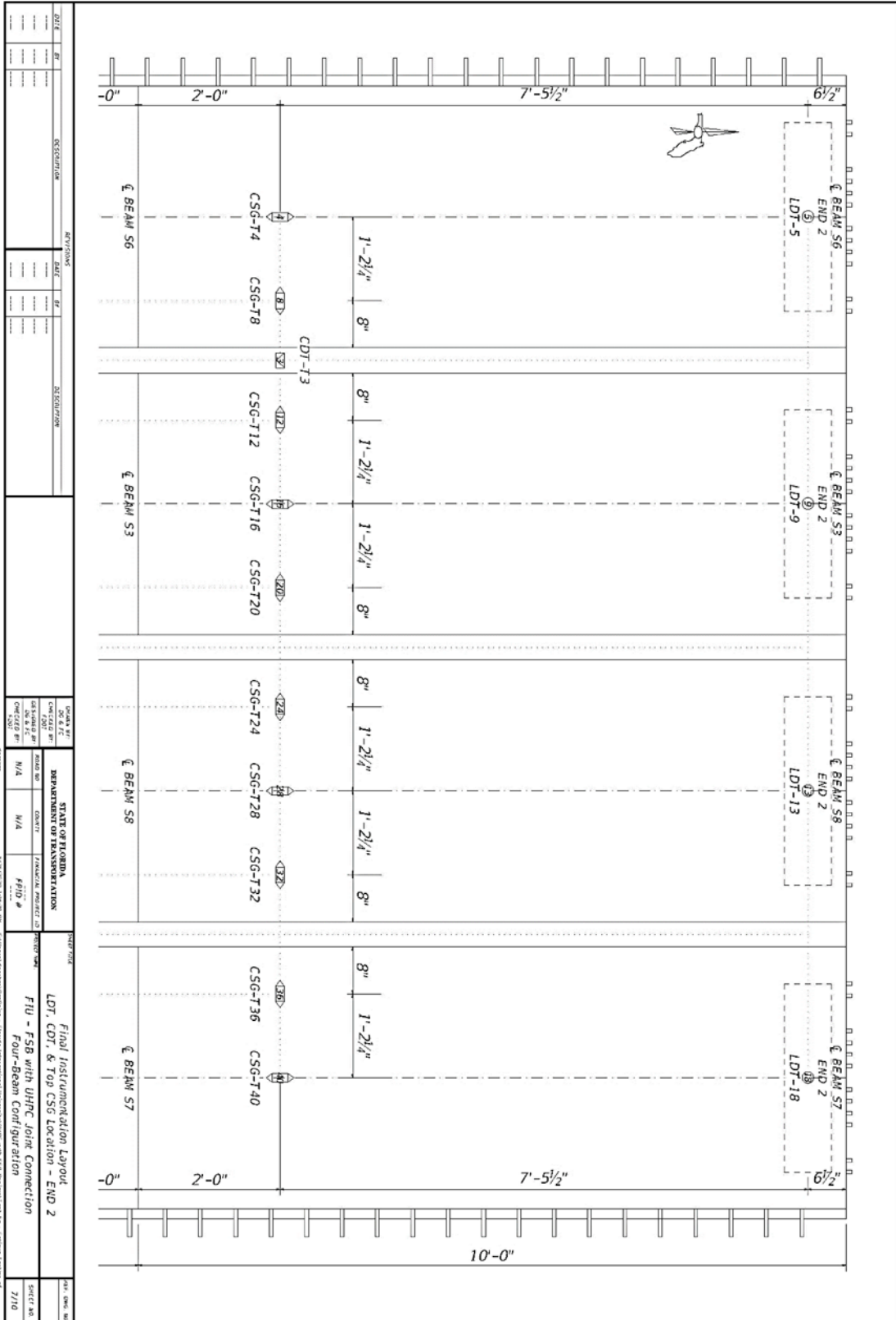
DATE	BY	DESCRIPTION	DATE	BY	DESCRIPTION
5/20/20	FC	CSG-T7 Correction			

UNITS	STATE OF FLORIDA	DEPARTMENT OF TRANSPORTATION	PROJECT NO.	PROJECT NAME
CSG-T1				FTU - FSB with UHPC Joint Connection
CSG-T2				Four-Beam Configuration
CSG-T3				
CSG-T4				
CSG-T5				
CSG-T6				
CSG-T7				
CSG-T8				
CSG-T9				
CSG-T10				
CSG-T11				
CSG-T12				
CSG-T13				
CSG-T14				
CSG-T15				
CSG-T16				
CSG-T17				
CSG-T18				
CSG-T19				
CSG-T20				
CSG-T21				
CSG-T22				
CSG-T23				
CSG-T24				
CSG-T25				
CSG-T26				
CSG-T27				
CSG-T28				
CSG-T29				
CSG-T30				
CSG-T31				
CSG-T32				
CSG-T33				
CSG-T34				
CSG-T35				
CSG-T36				
CSG-T37				
CSG-T38				

DATE	BY	DESCRIPTION
5/10		



DATE		DESCRIPTION		REVISIONS		APPROVED BY		CHECKED BY		STATE OF FLORIDA		PROJECT TITLE	
DATE	BY	DATE	DESCRIPTION	DATE	BY	DATE	BY	DATE	BY	DATE	BY	DATE	BY
				DEPARTMENT OF TRANSPORTATION FLORIDA TURNPIKE AUTHORITY STATE ROAD 94 TALLAHASSEE, FLORIDA				PROJECT NO. 17000000000000000000 CONTRACT NO. 17000000000000000000 FID # 17000000000000000000					
Final Instrumentation Layout LDT, CDT, & Top CSG Location - MIDDLE FIU - FS8 with JHPC Joint Connection Four-Beam Configuration													
SHEET NO. 6/10													

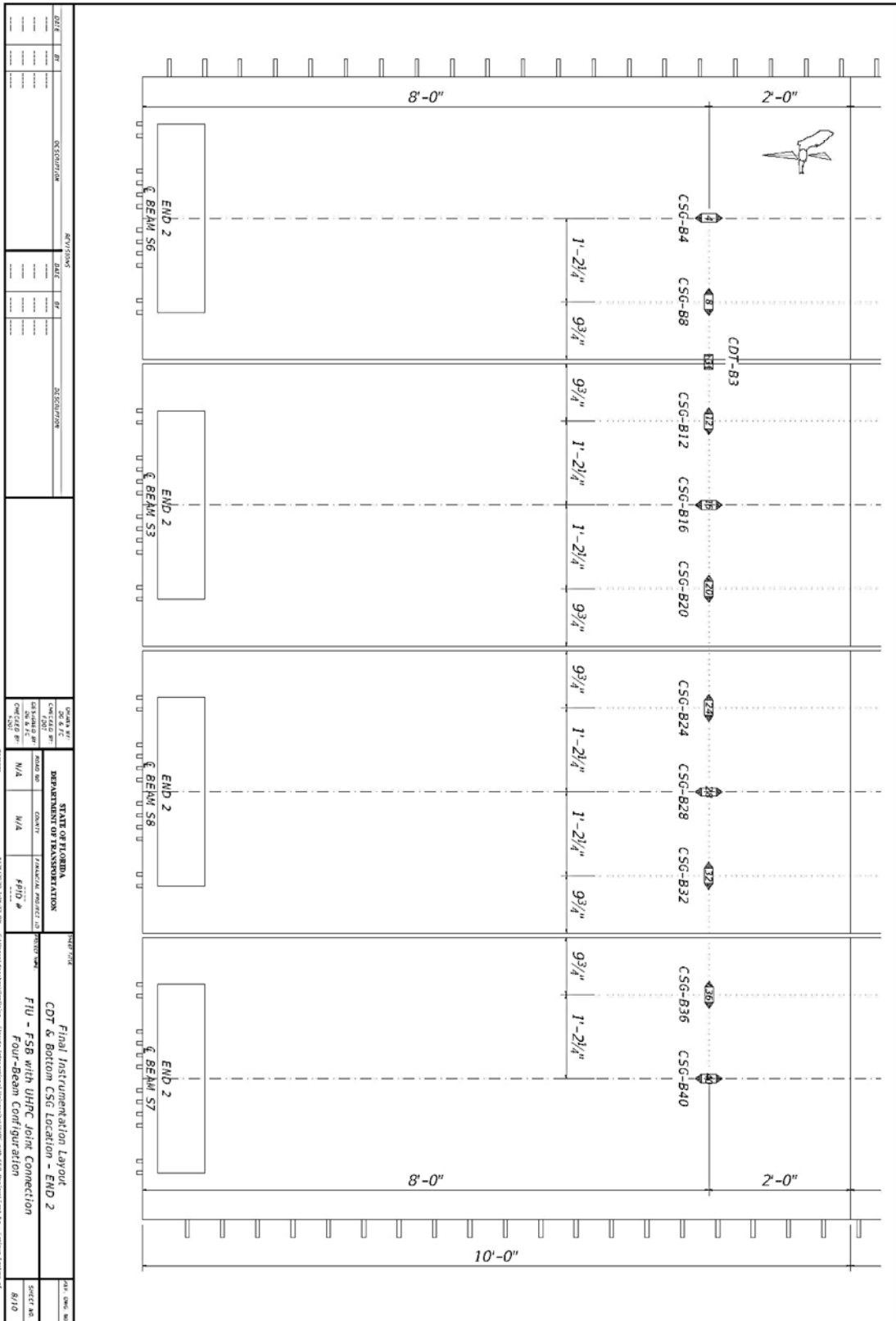


REVISIONS		REVISIONS		REVISIONS		REVISIONS		REVISIONS			
DATE	BY	DESCRIPTION	DATE	BY	DESCRIPTION	DATE	BY	DESCRIPTION	DATE	BY	DESCRIPTION

UNITS		STATE OF FLORIDA		DEPARTMENT OF TRANSPORTATION		PROJECT		DRAWING	
UNIT	CONVERSION	STATE	DEPARTMENT	PROJECT	CONTRACT	PROJECT	CONTRACT	PROJECT	CONTRACT

PROJECT		DRAWING		REVISIONS	
PROJECT	CONTRACT	PROJECT	CONTRACT	PROJECT	CONTRACT

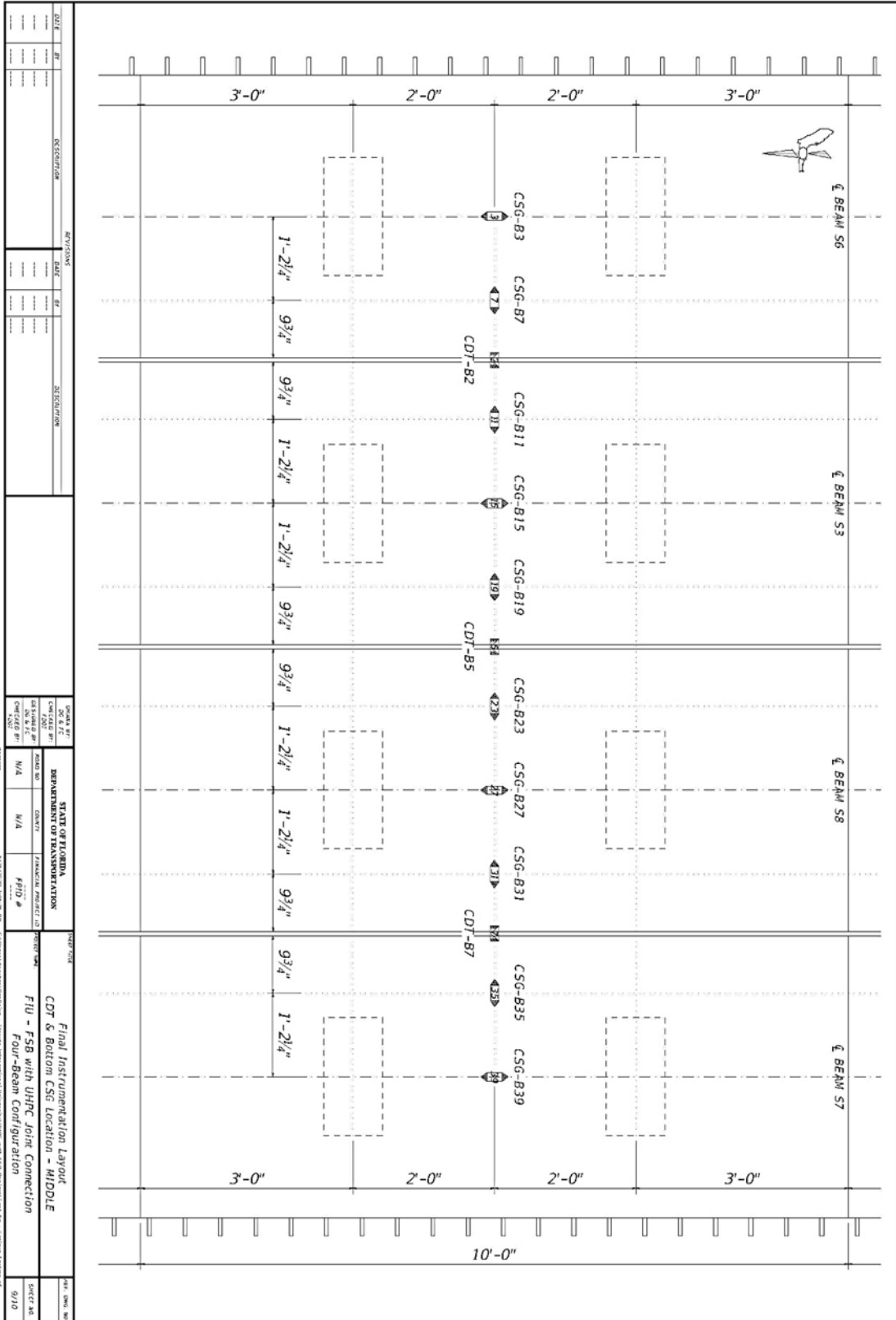
PROJECT		DRAWING		REVISIONS	
PROJECT	CONTRACT	PROJECT	CONTRACT	PROJECT	CONTRACT



DATE	BY	DESCRIPTION	DATE	BY	DESCRIPTION

UNIVERSITY OF FLORIDA	DEPARTMENT OF CIVIL ENGINEERING	STATE OF FLORIDA	DEPARTMENT OF TRANSPORTATION
PROJECT #	PROJECT #	PROJECT #	PROJECT #
CONTRACT #	CONTRACT #	CONTRACT #	CONTRACT #
DATE	DATE	DATE	DATE

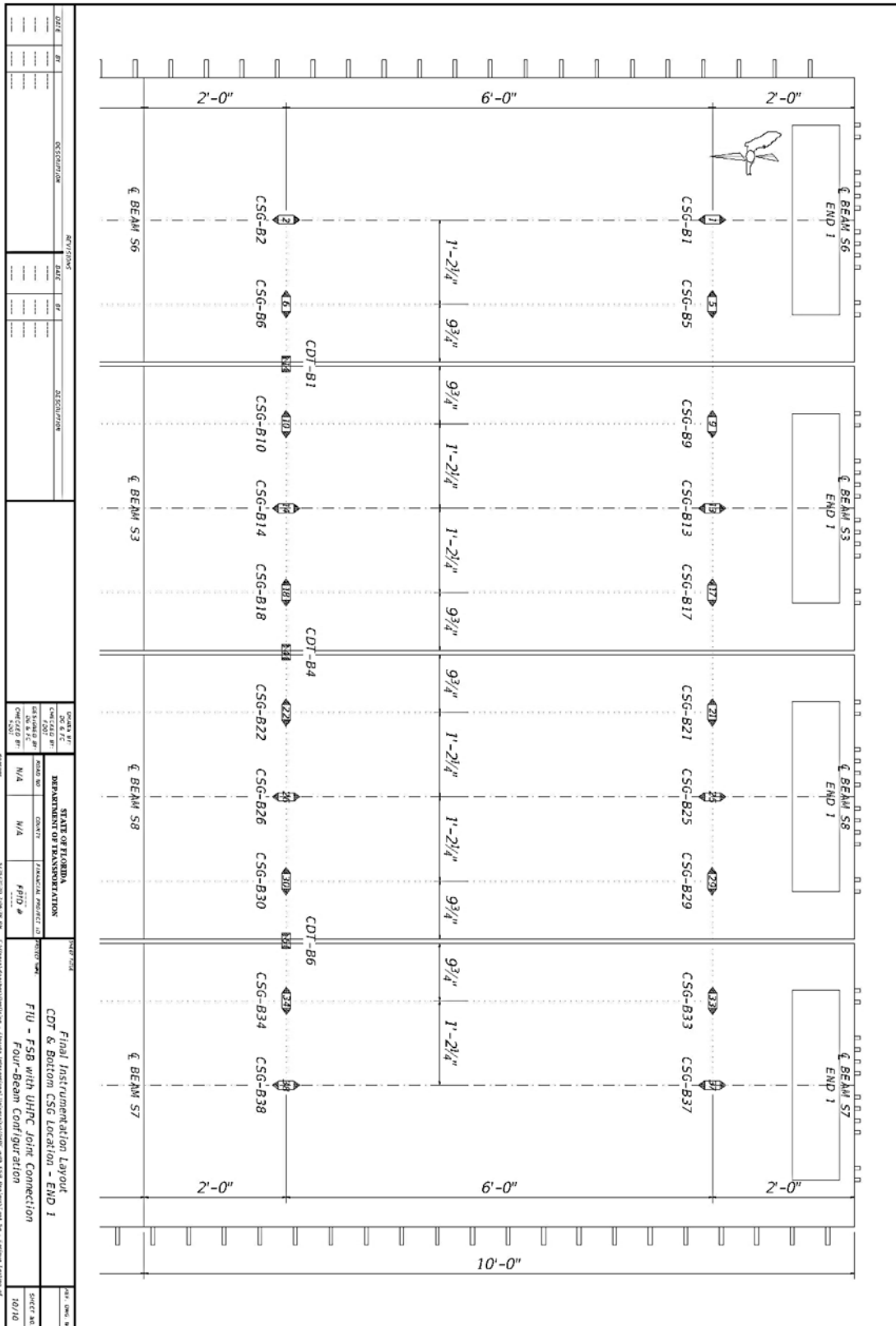
PROJECT TITLE	SHEET NO.	TOTAL SHEETS
Final Instrumentation Layout COT & Bottom CSG Location - END 2 FIU - FSB with UHPC Joint Connection Four-Beam Configuration	8/10	



DATE		DESCRIPTION		REVISIONS		STATE OF ILLINOIS		DEPARTMENT OF TRANSPORTATION		PROJECT INFORMATION		DRAWING INFORMATION		SHEET INFORMATION	
DATE	BY	DESCRIPTION	BY	DATE	DESCRIPTION	DATE	BY	PROJECT NO.	CONTRACT NO.	PROJECT NAME	DRAWING NO.	SHEET NO.	TOTAL SHEETS	SCALE	DATE

Final Instrumentation Layout
 CDT & Bottom CSG Location - MIDDLE
 FIU - FSB with UHPC Joint Connection
 Four-Beam Configuration

DRAWING NO. 9/10
 SHEET NO. 9/10



F.3. LOAD STAGE 1.6 (SURCHARGE REMOVAL)

The response from all instrumentation for Load Stage 1.6, when the load blocks were removed from FIU-3, are shown in this section.

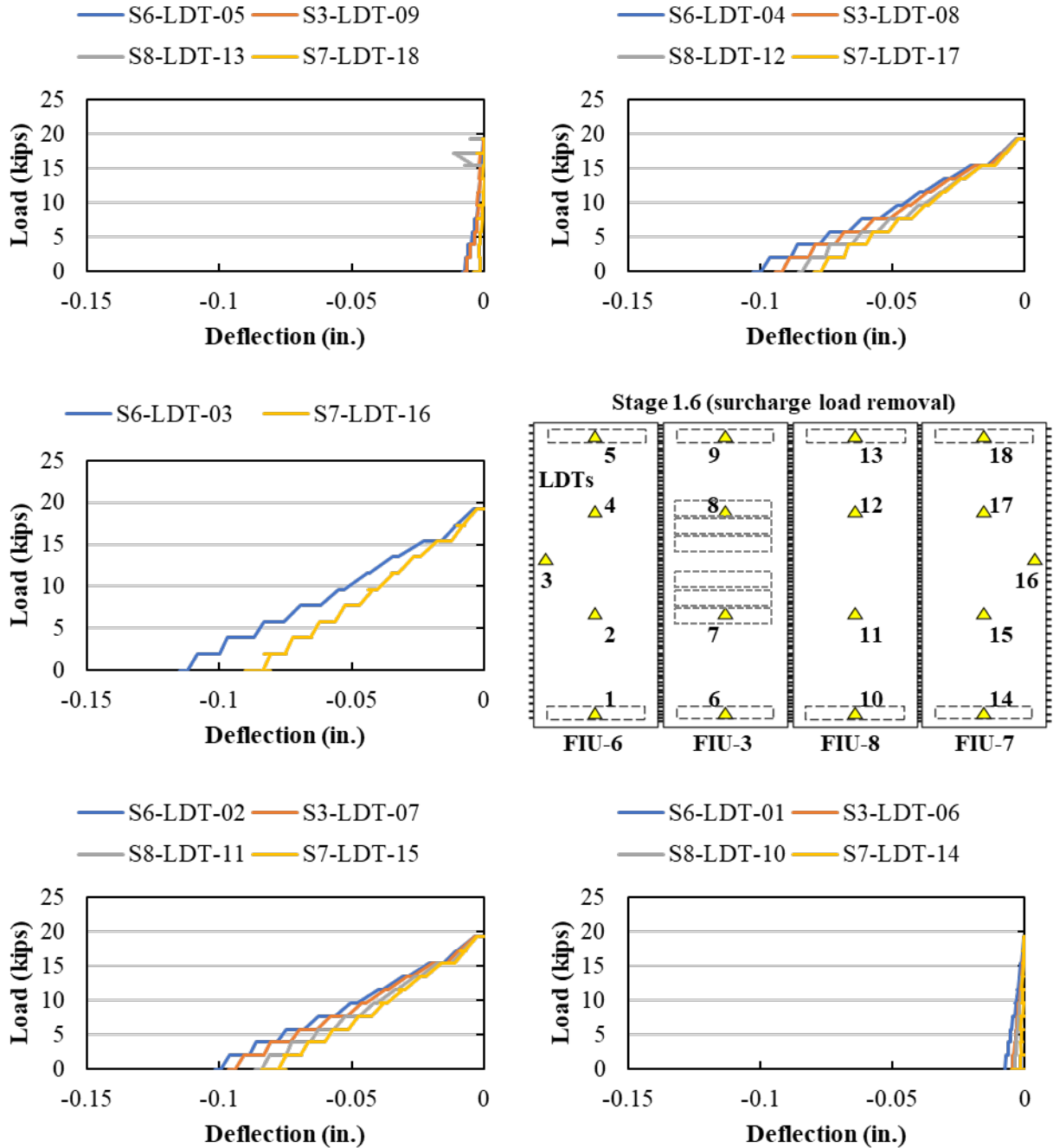


Figure F.1: Load versus displacement measured using LDTs for Load Stage 1.6 (surcharge removal)

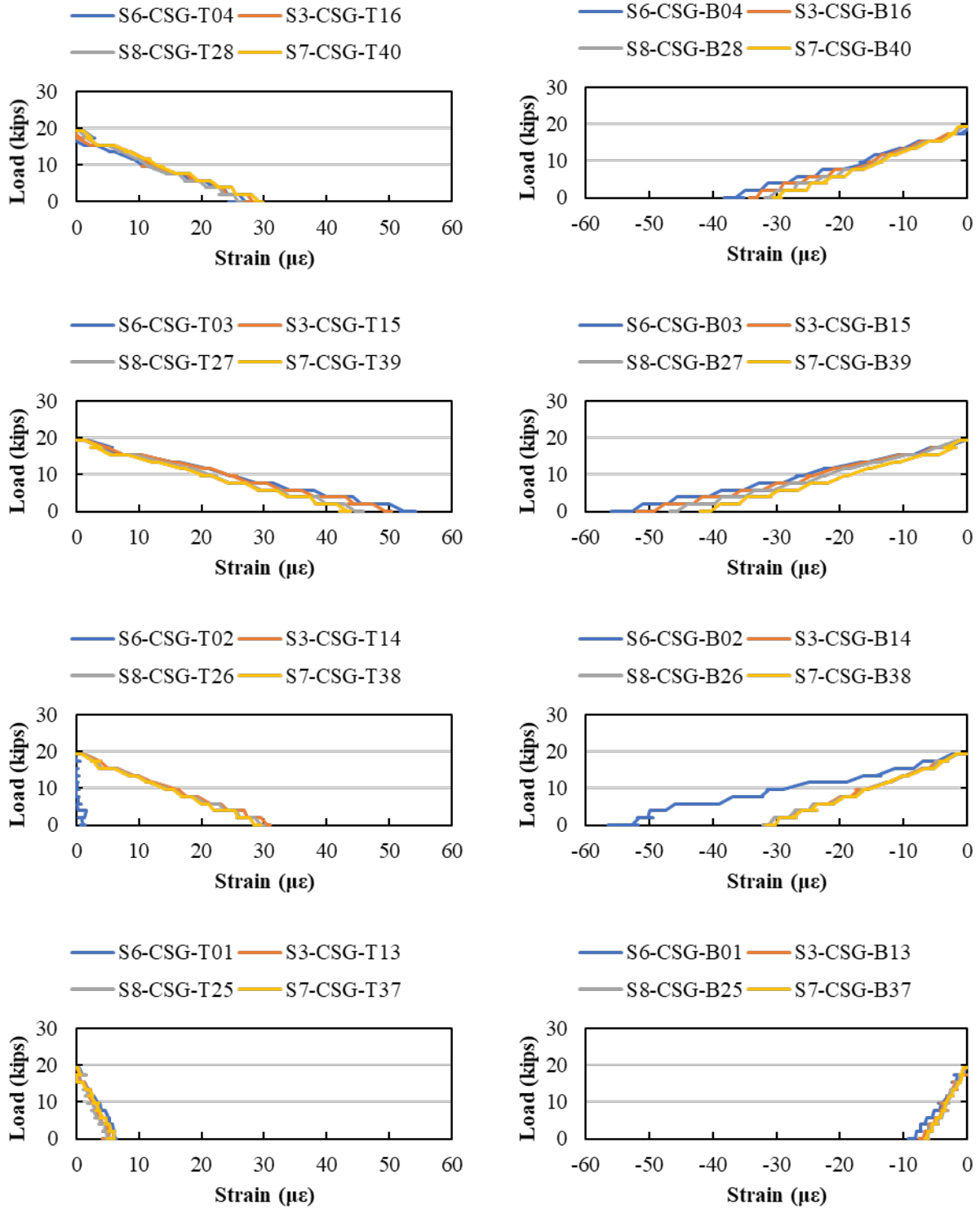


Figure F.2: Load versus longitudinal strain (measured by CSGs) for Load Stage 1.6 (surcharge removal)

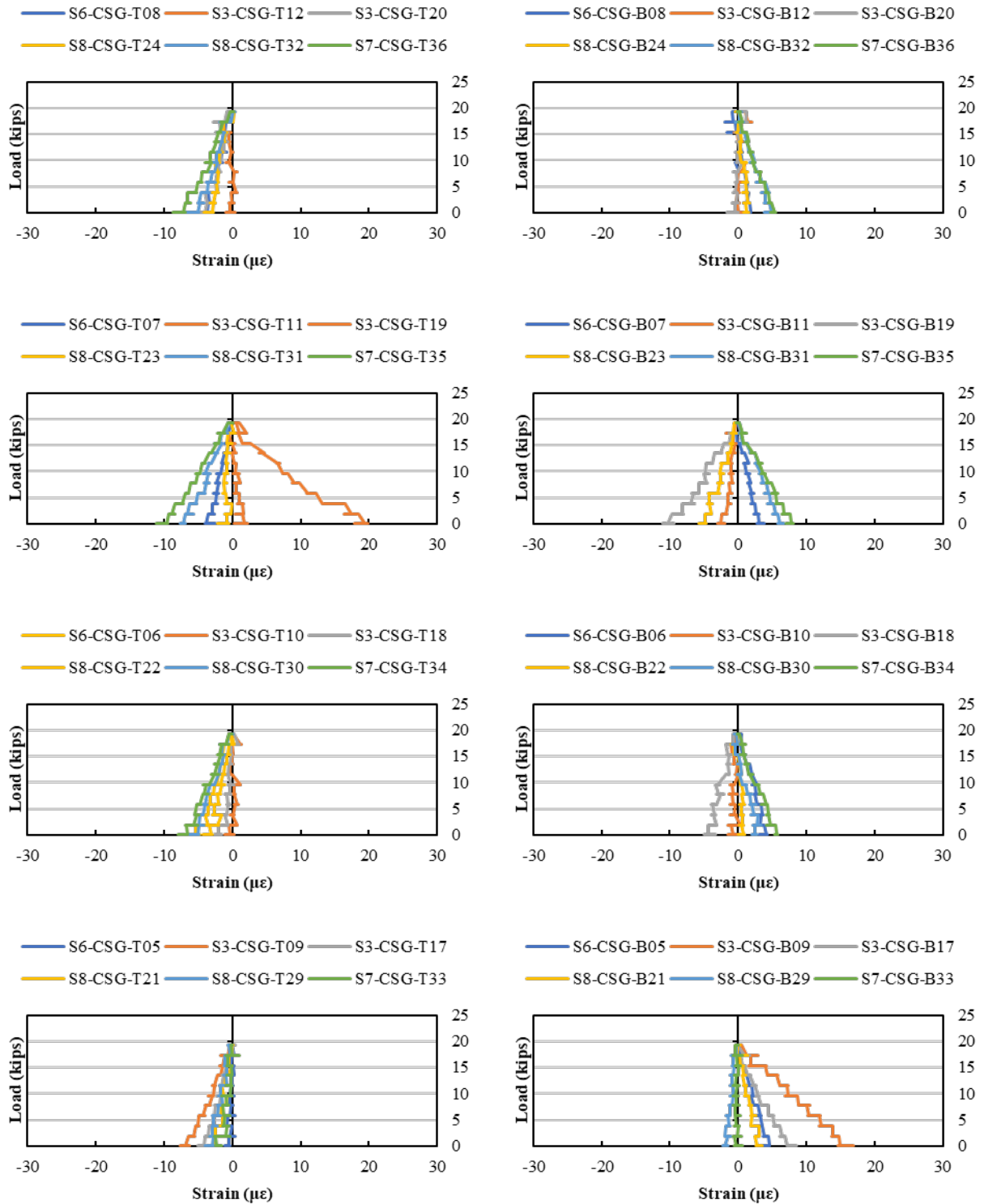


Figure F.3: Load versus transverse strain (measured by CSGs) for Load Stage 1.6 (surcharge removal)

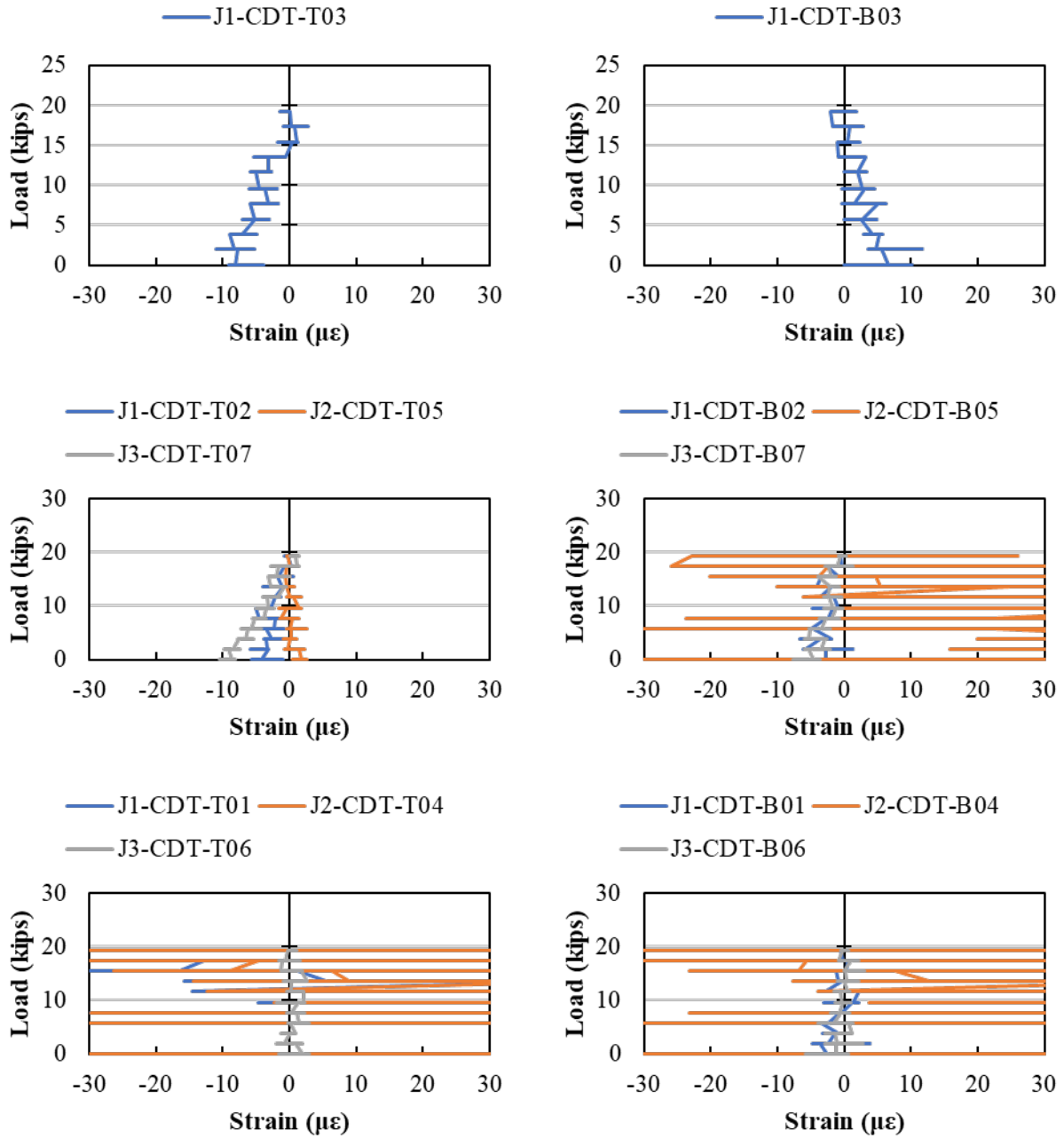


Figure F.4: Load versus average strain across the joints (measured by CDTs) for Load Stage 1.6 (surcharge removal)

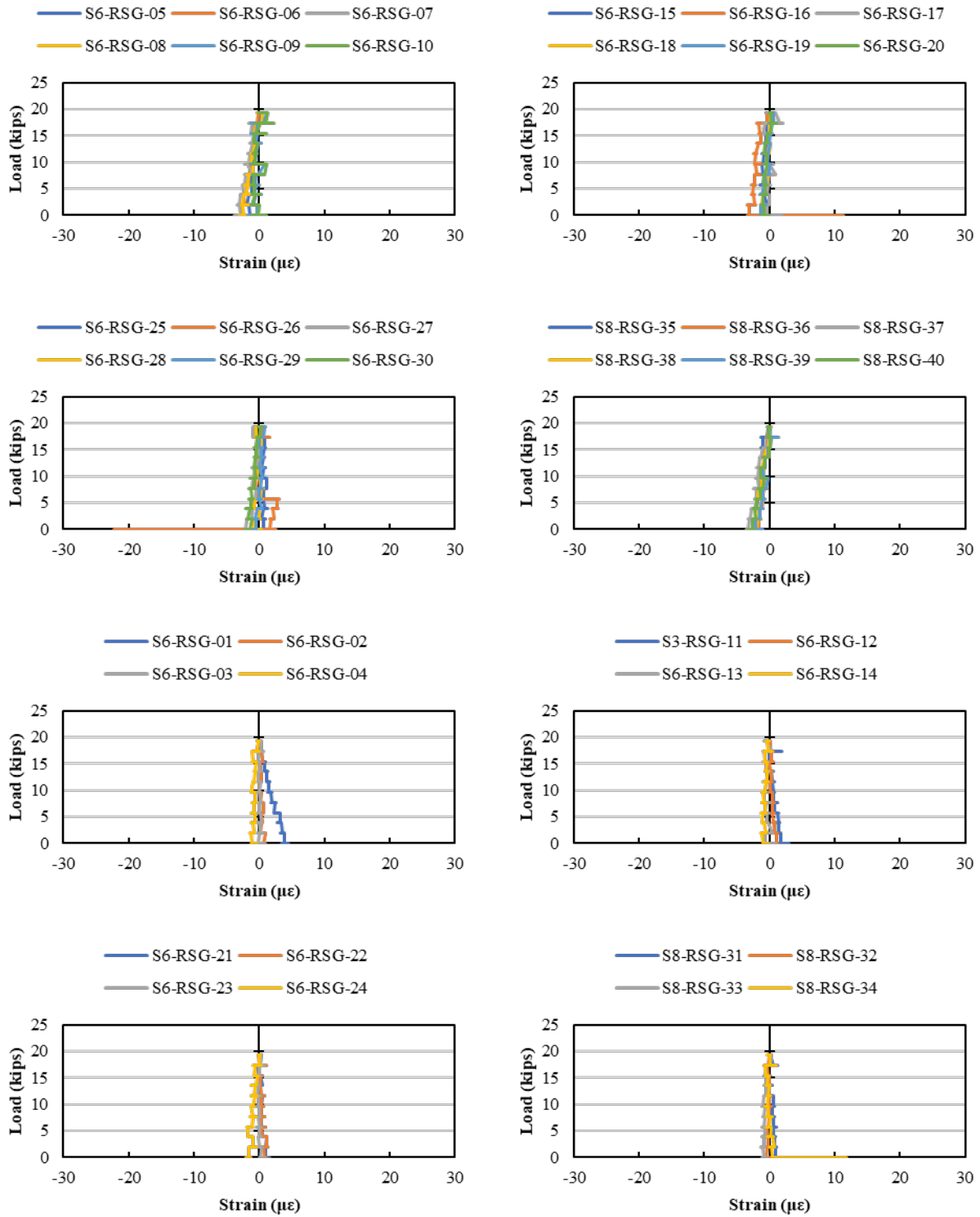


Figure F.5: Load versus rebar strain (measured by RSGs) for Load Stage 1.6 (surcharge removal)

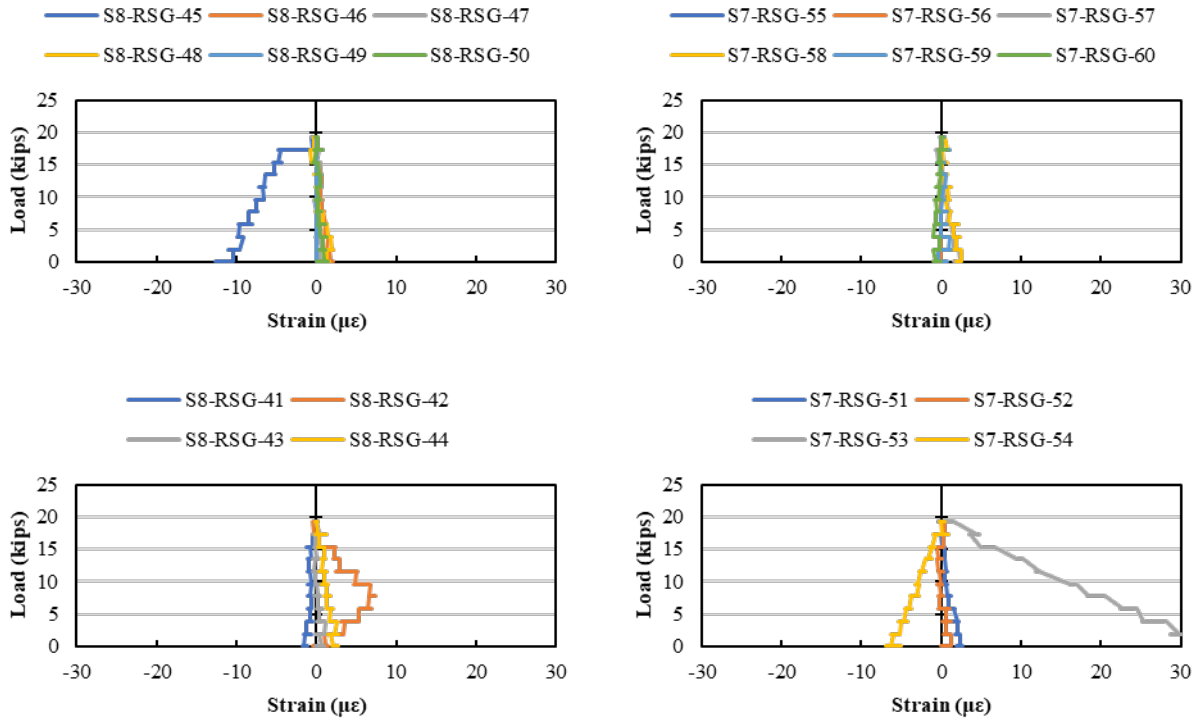


Figure F.6: Load versus rebar strain (measured by RSGs) for Load Stage 1.6 (surcharge removal) (cont.)

F.4. LOAD STAGE 2 – LOAD CONFIGURATION 4-1

The response from all instrumentation for Load Stage 2 with Load Configuration 4-1 are shown in this section.

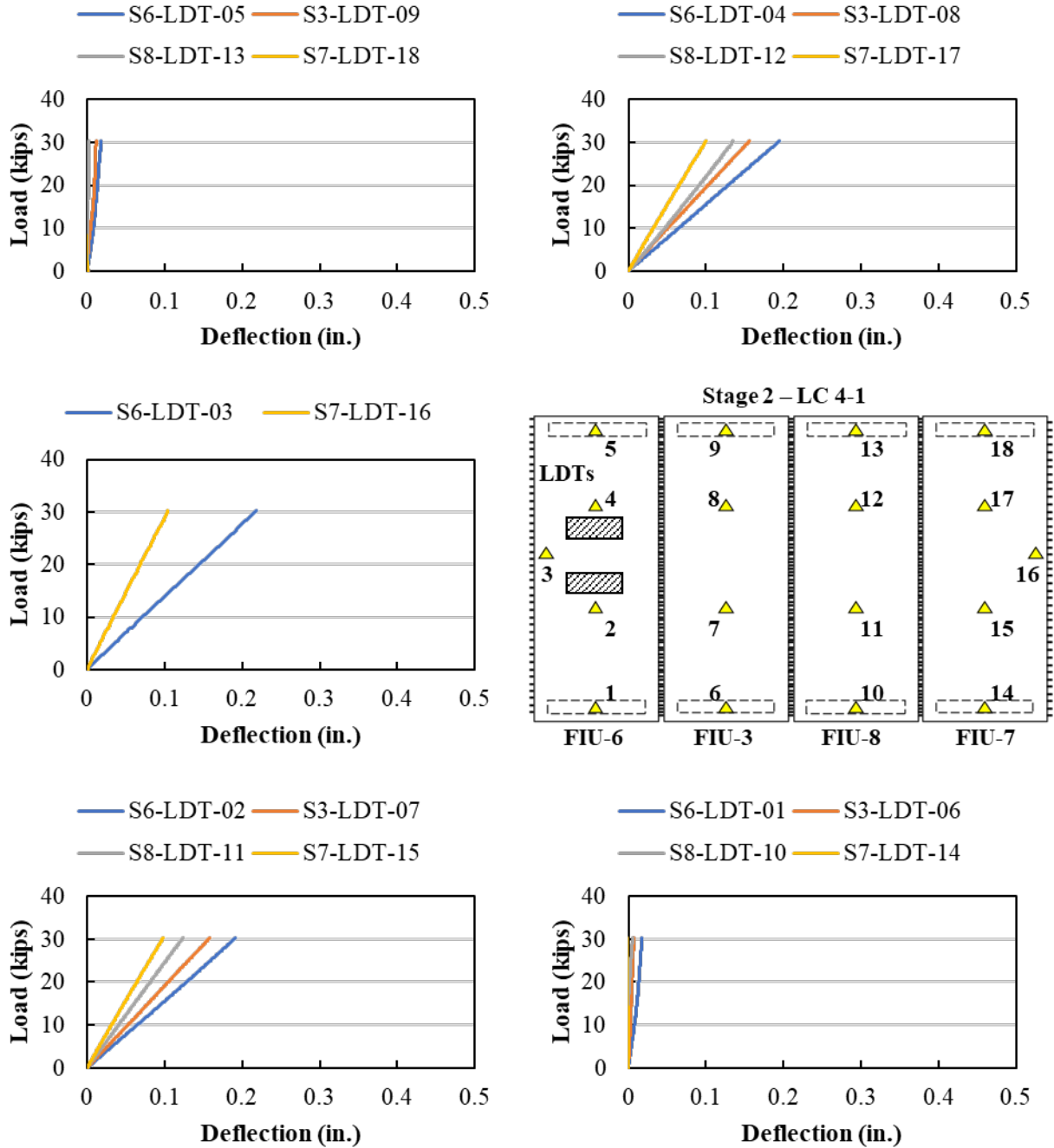


Figure F.7: Load versus displacement measured using LDTs for Load Stage 2, LC 4-1

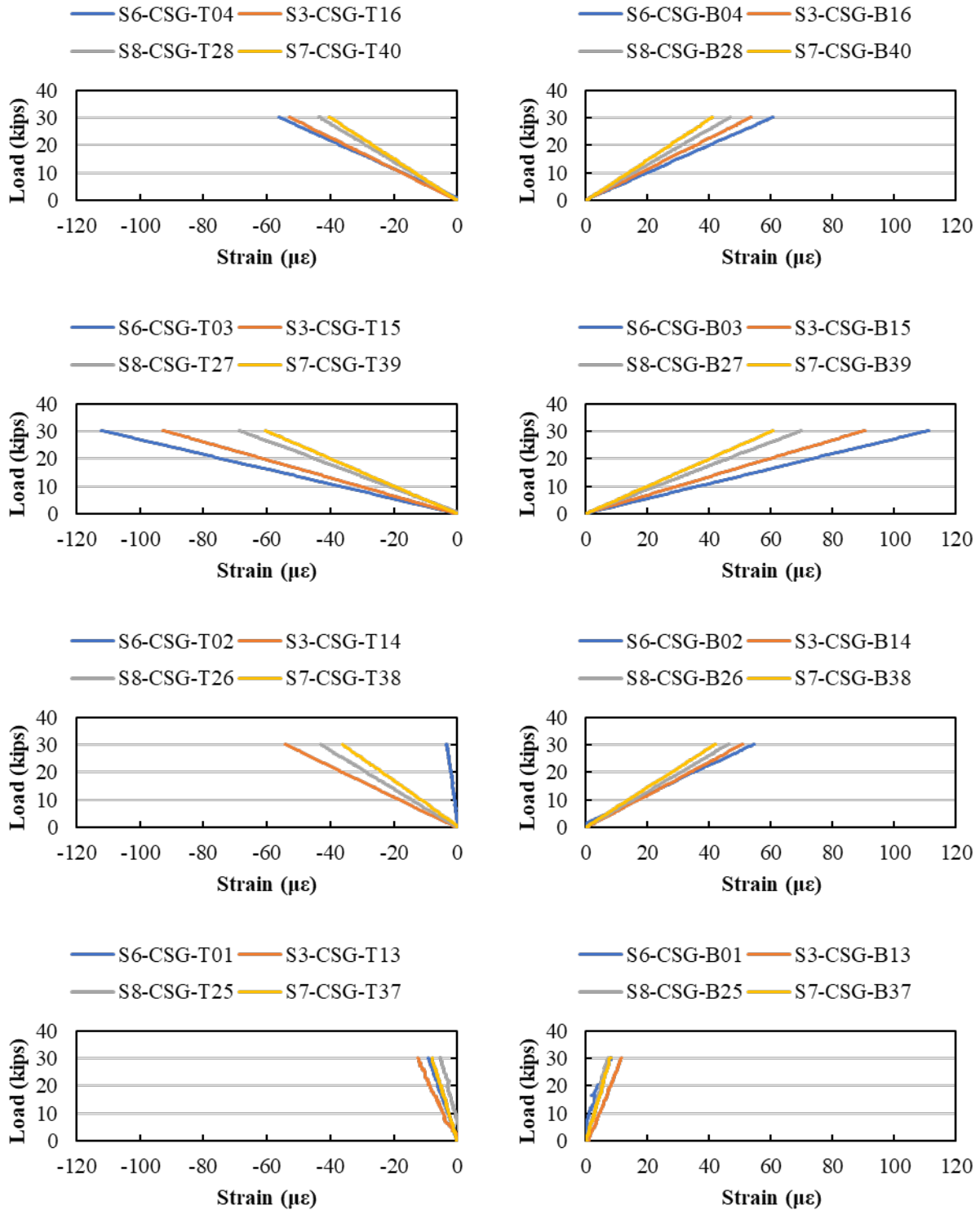


Figure F.8: Load versus longitudinal strain (measured by CSGs) for Load Stage 2, LC 4-1

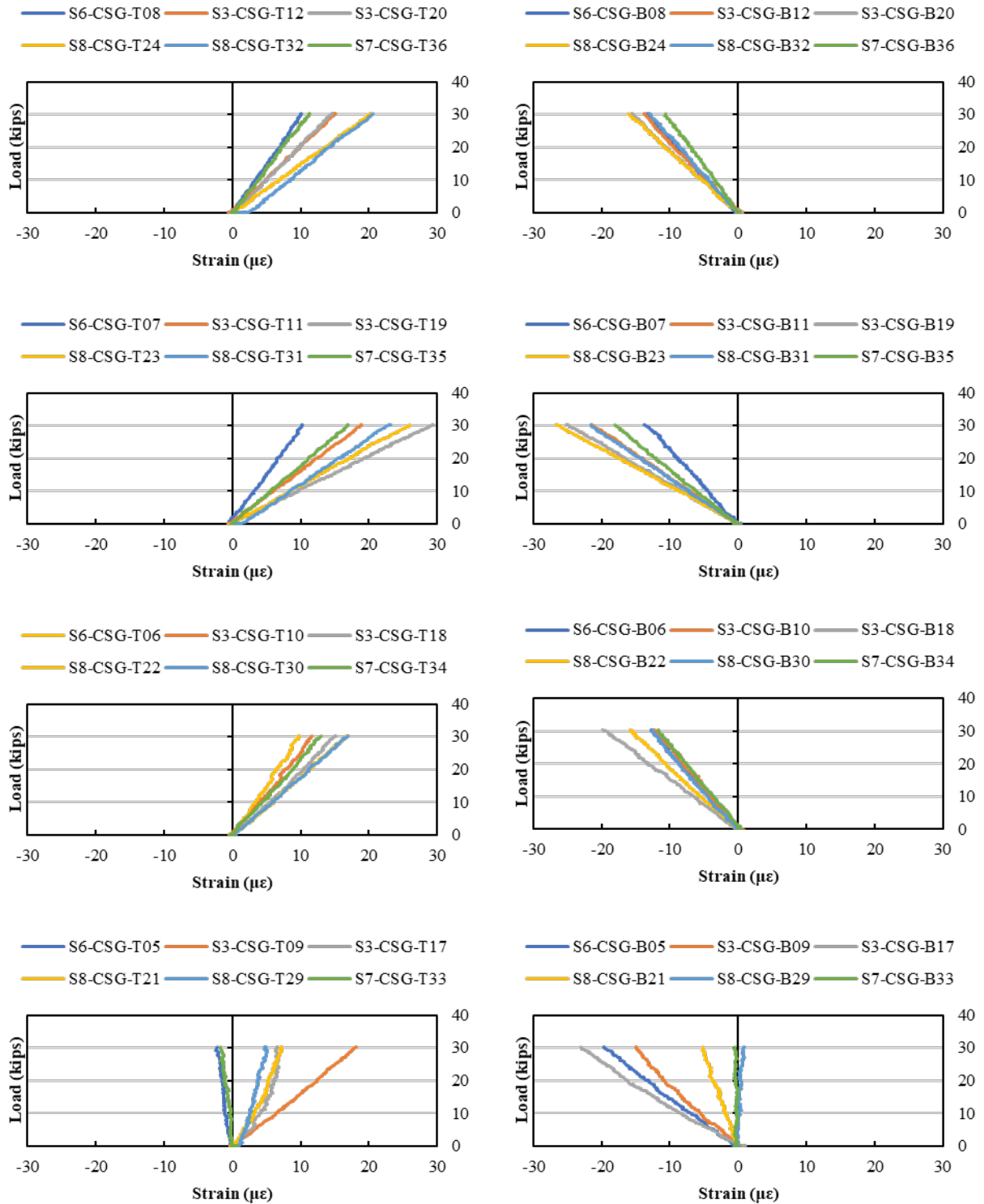


Figure F.9: Load versus transverse strain (measured by CSGs) for Load Stage 2, LC 4-1

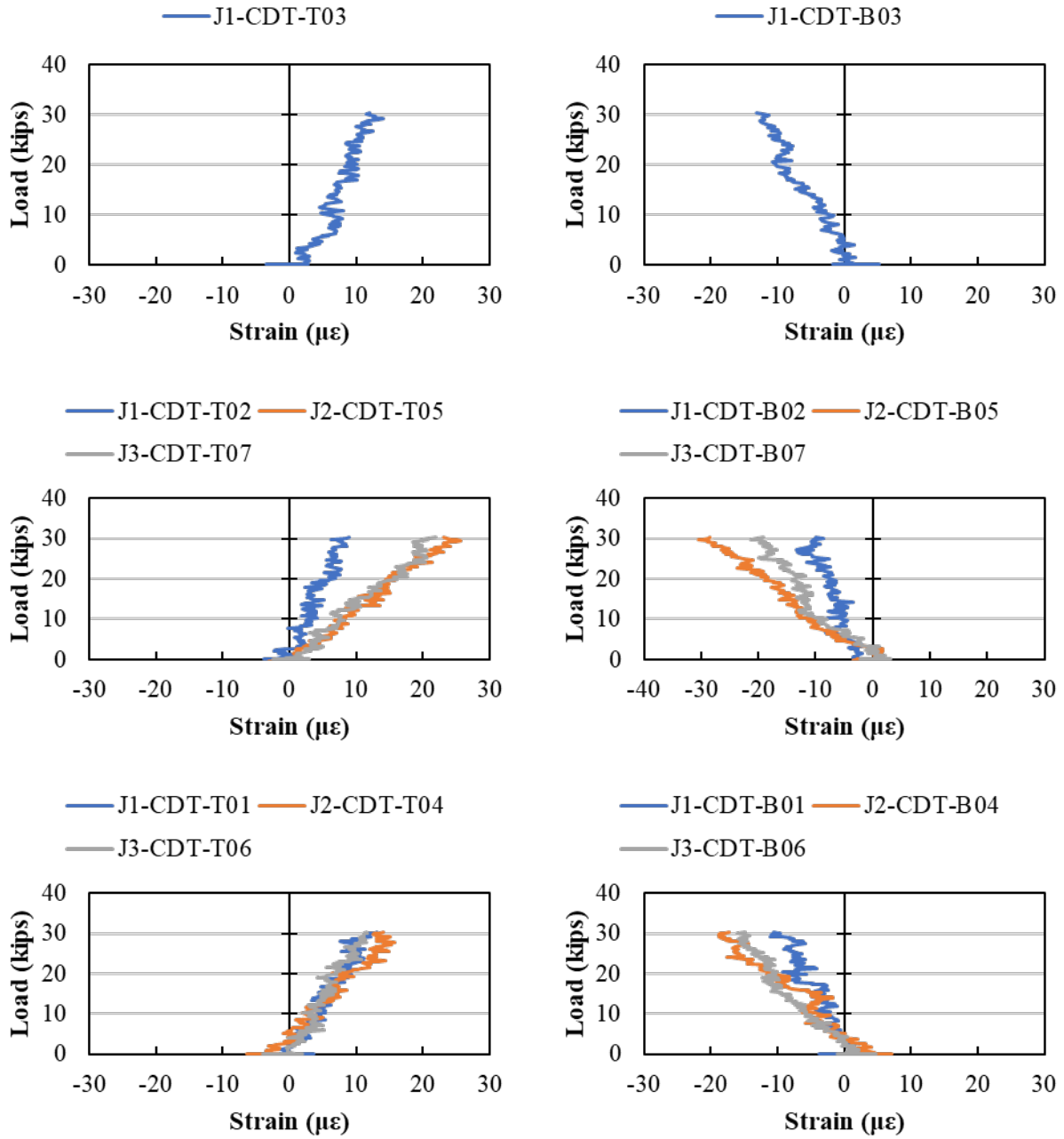


Figure F.10: Load versus average strain across the joints (measured by CDTs) for Load Stage 2, LC 4-1

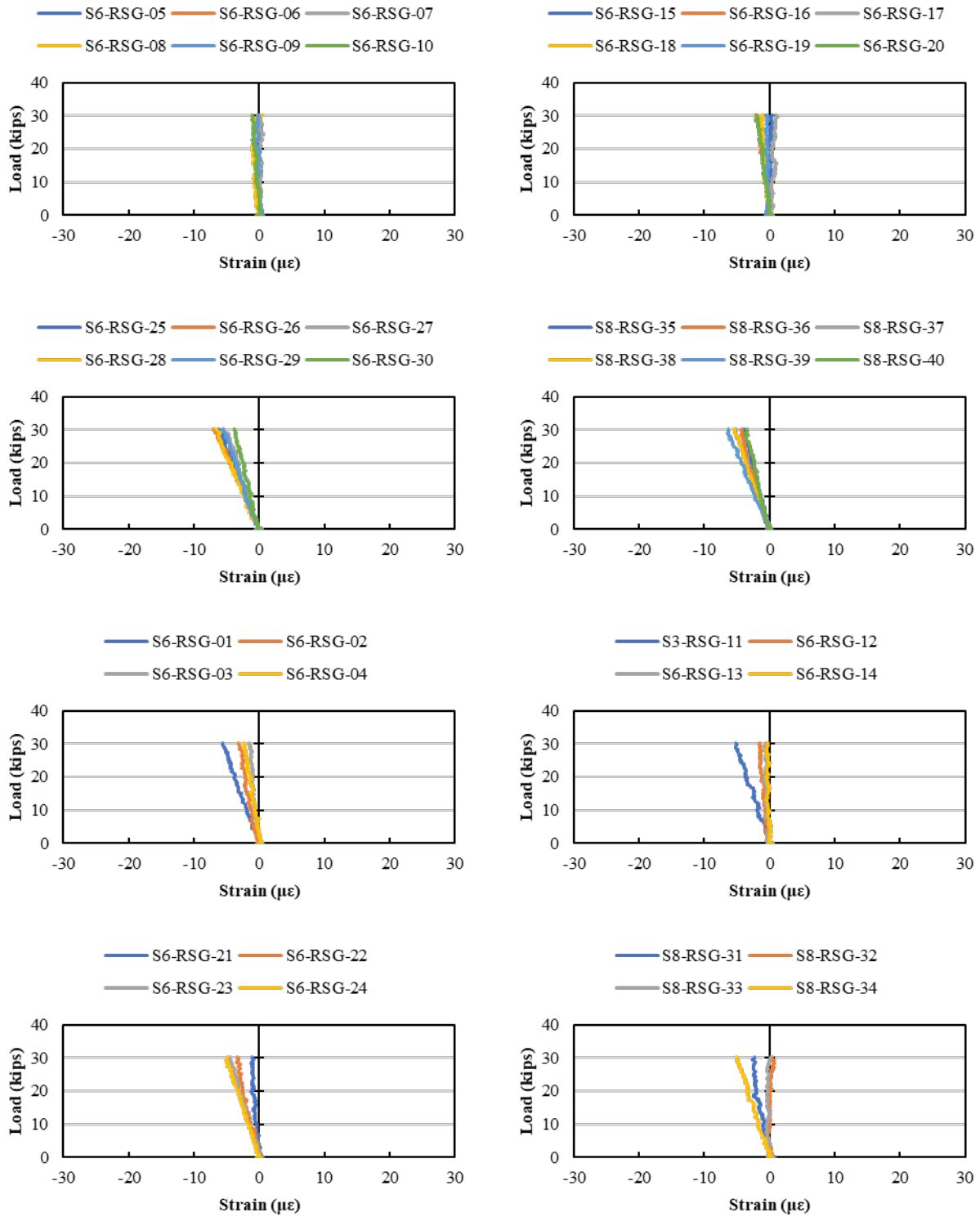


Figure F.11: Load versus rebar strain (measured by RSGs) for Load Stage 2, LC 4-1

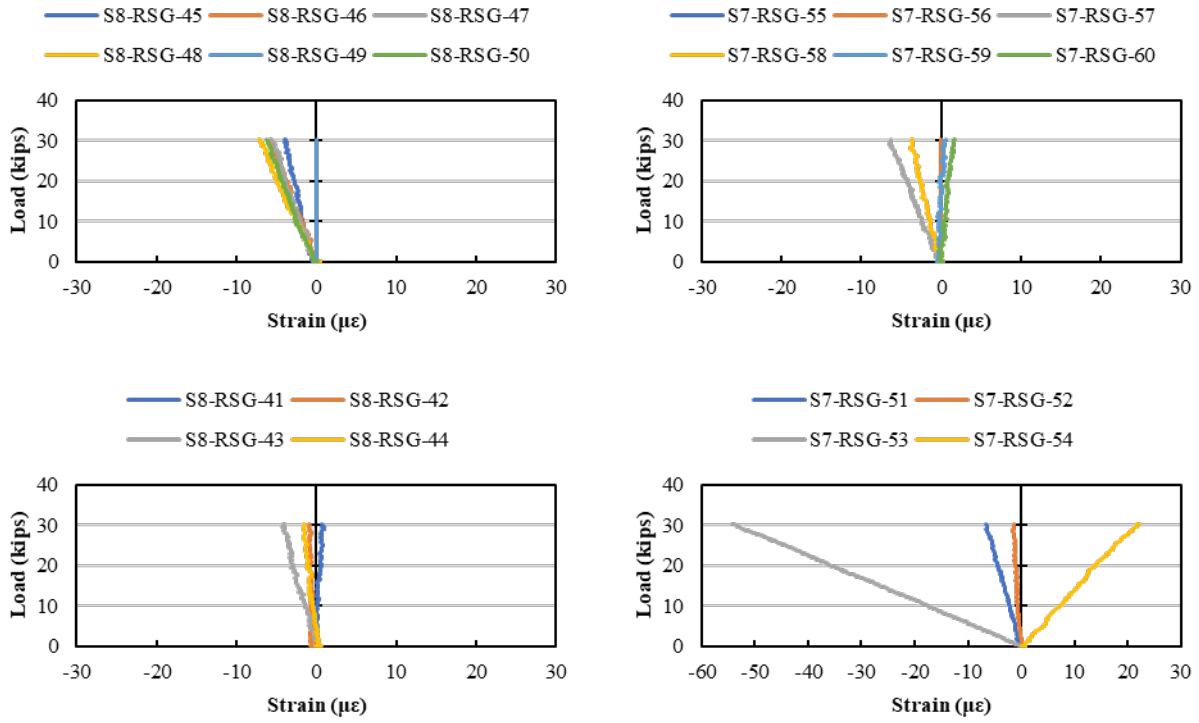


Figure F.12: Load versus rebar strain (measured by RSGs) for Load Stage 2, LC 4-1 (cont.)

F.5. LOAD STAGE 2 – LOAD CONFIGURATION 4-2

The response from all instrumentation for Load Stage 2 with Load Configuration 4-2 are shown in this section.

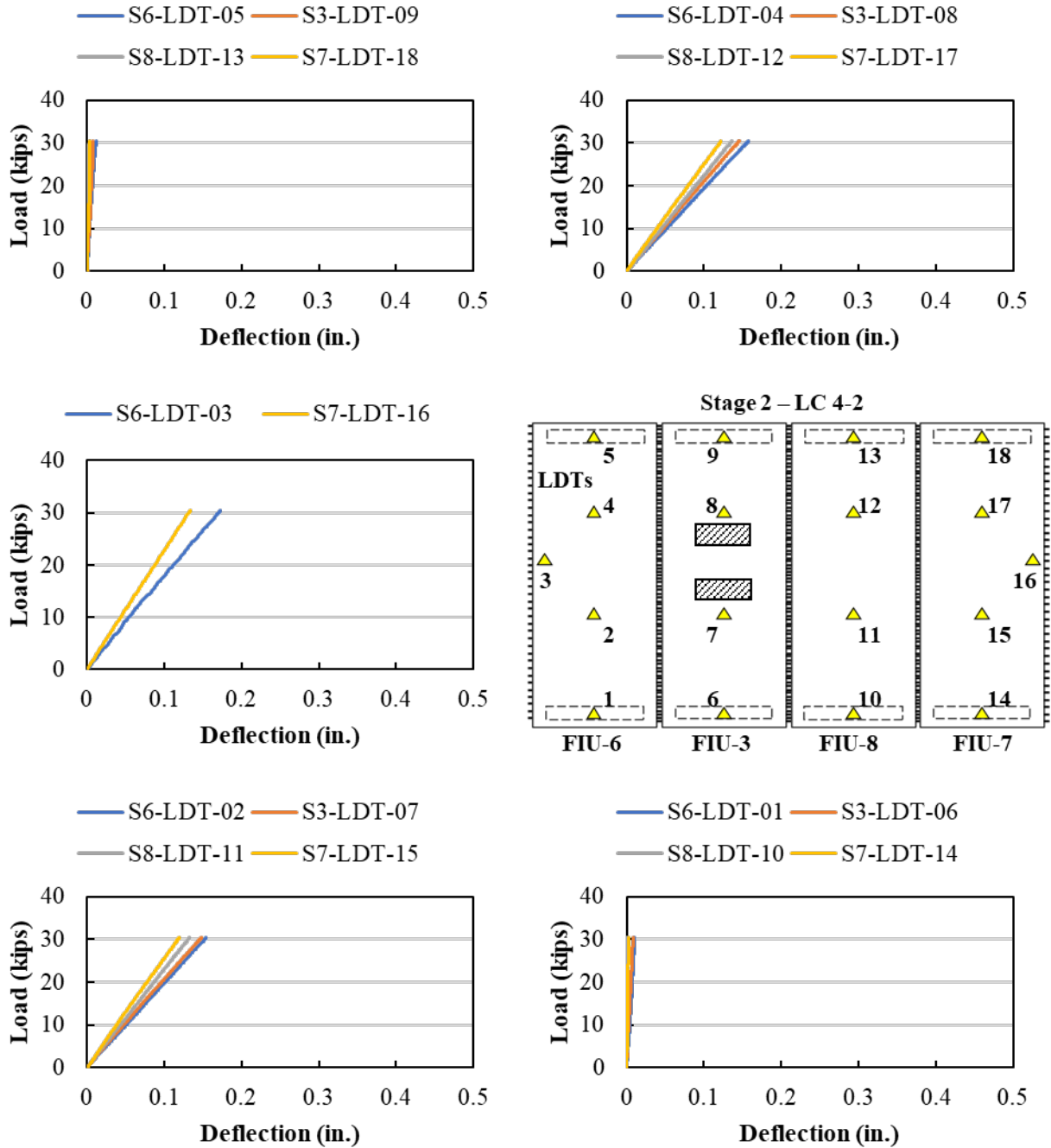


Figure F.13: Load versus displacement measured using LDTs for Load Stage 2, LC 4-2

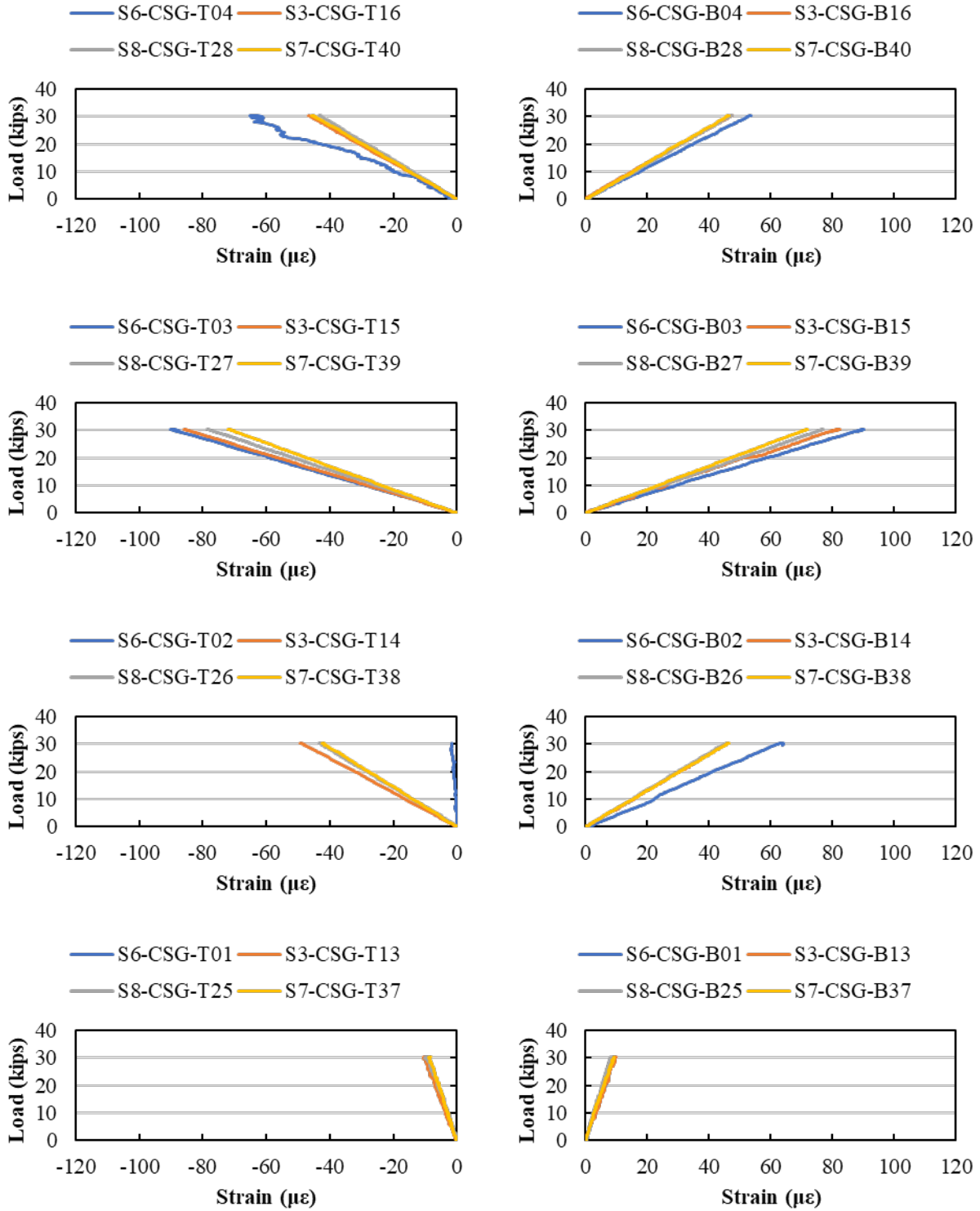


Figure F.14: Load versus longitudinal strain (measured by CSGs) for Load Stage 2, LC 4-2

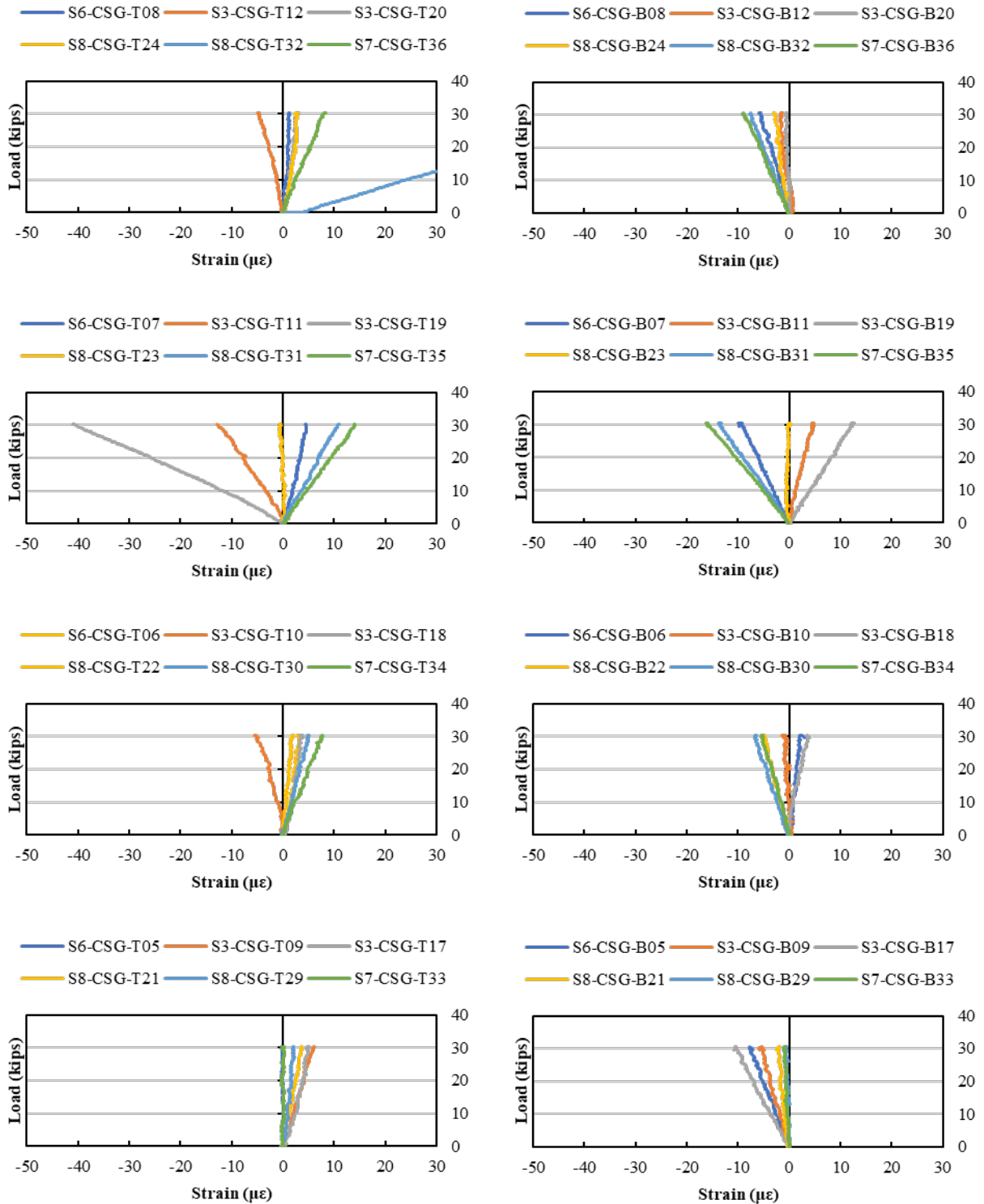


Figure F.15: Load versus transverse strain (measured by CSGs) for Load Stage 2, LC 4-2

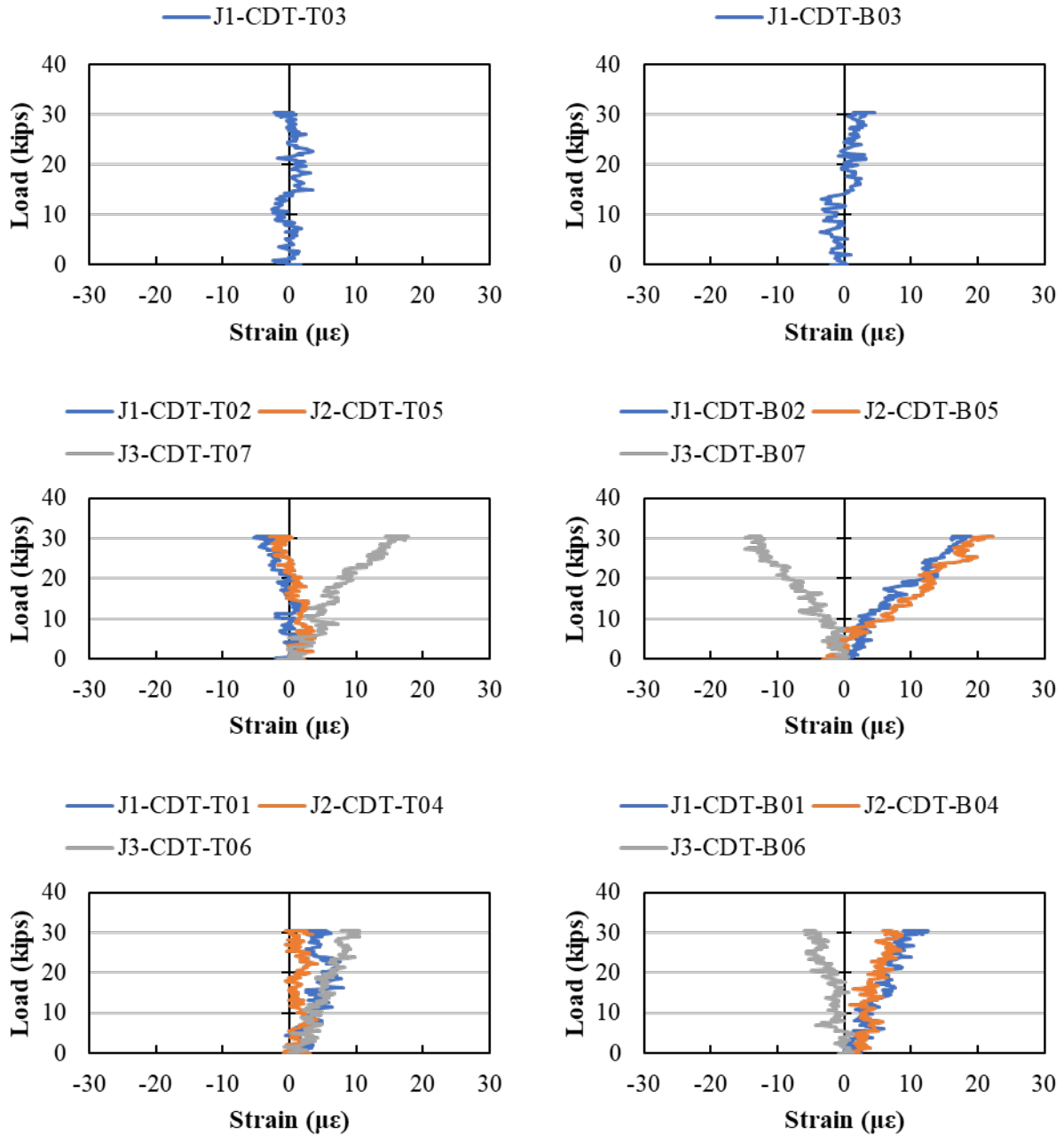


Figure F.16: Load versus average strain across the joints (measured by CDTs) for Load Stage 2, LC 4-2

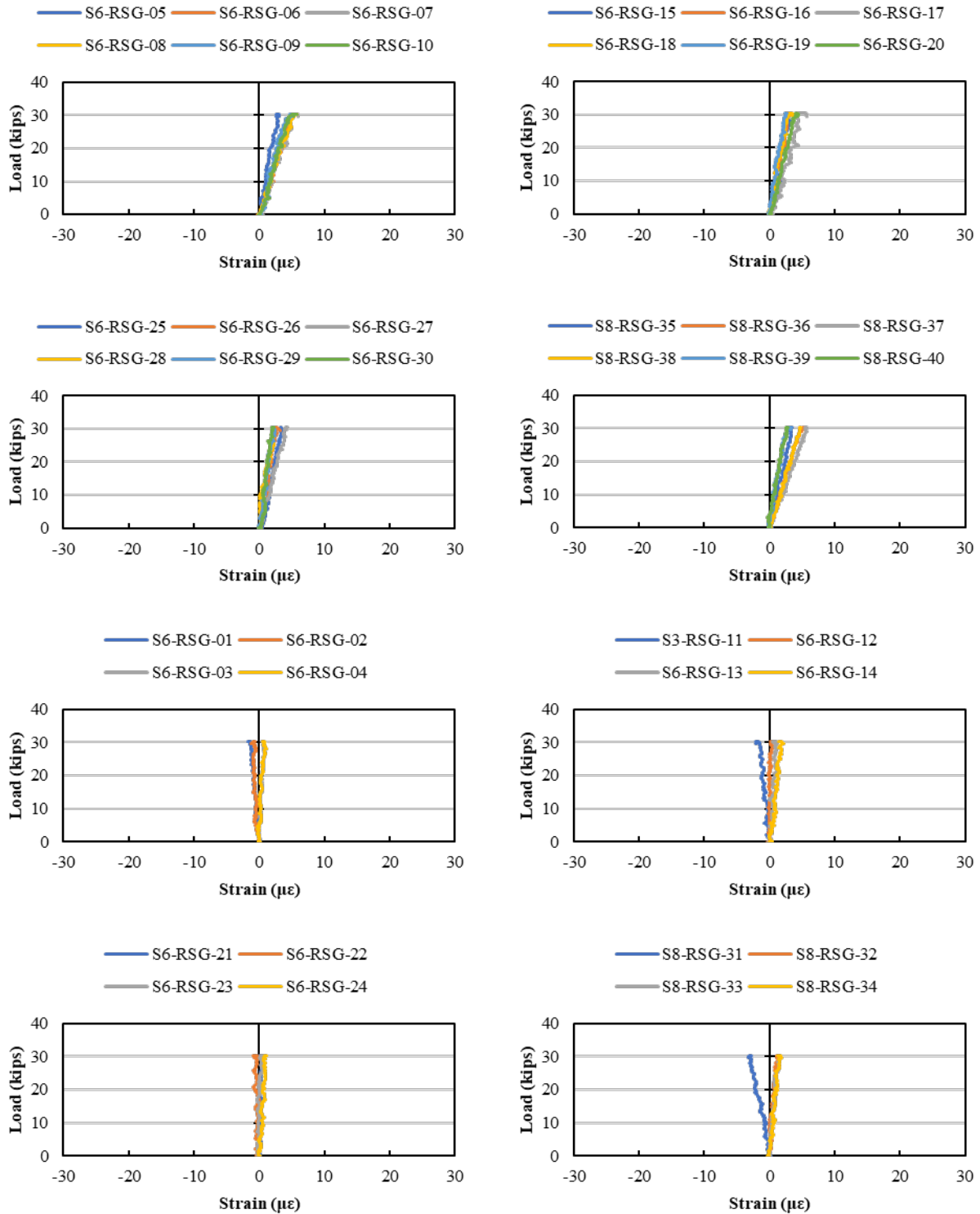


Figure F.17: Load versus rebar strain (measured by RSGs) for Load Stage 2, LC 4-2

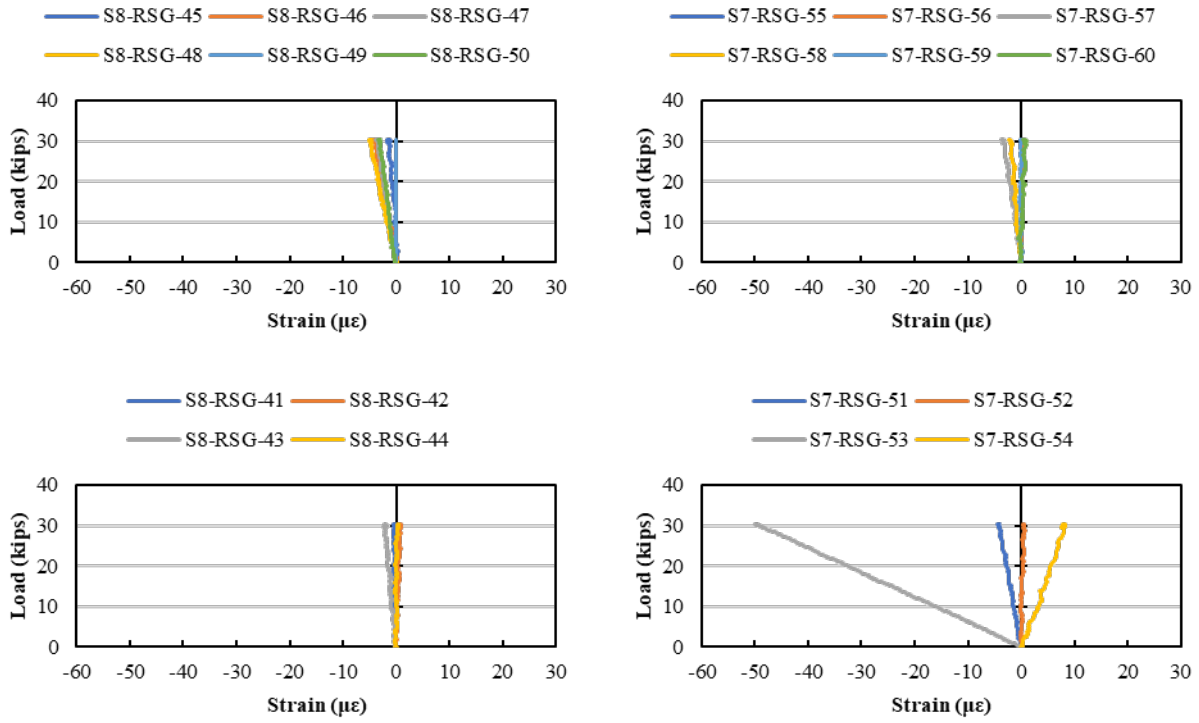


Figure F.18: Load versus rebar strain (measured by RSGs) for Load Stage 2, LC 4-2 (cont.)

F.6. LOAD STAGE 2 – LOAD CONFIGURATION 4-3

The response from all instrumentation for Load Stage 2 with Load Configuration 4-3 are shown in this section.

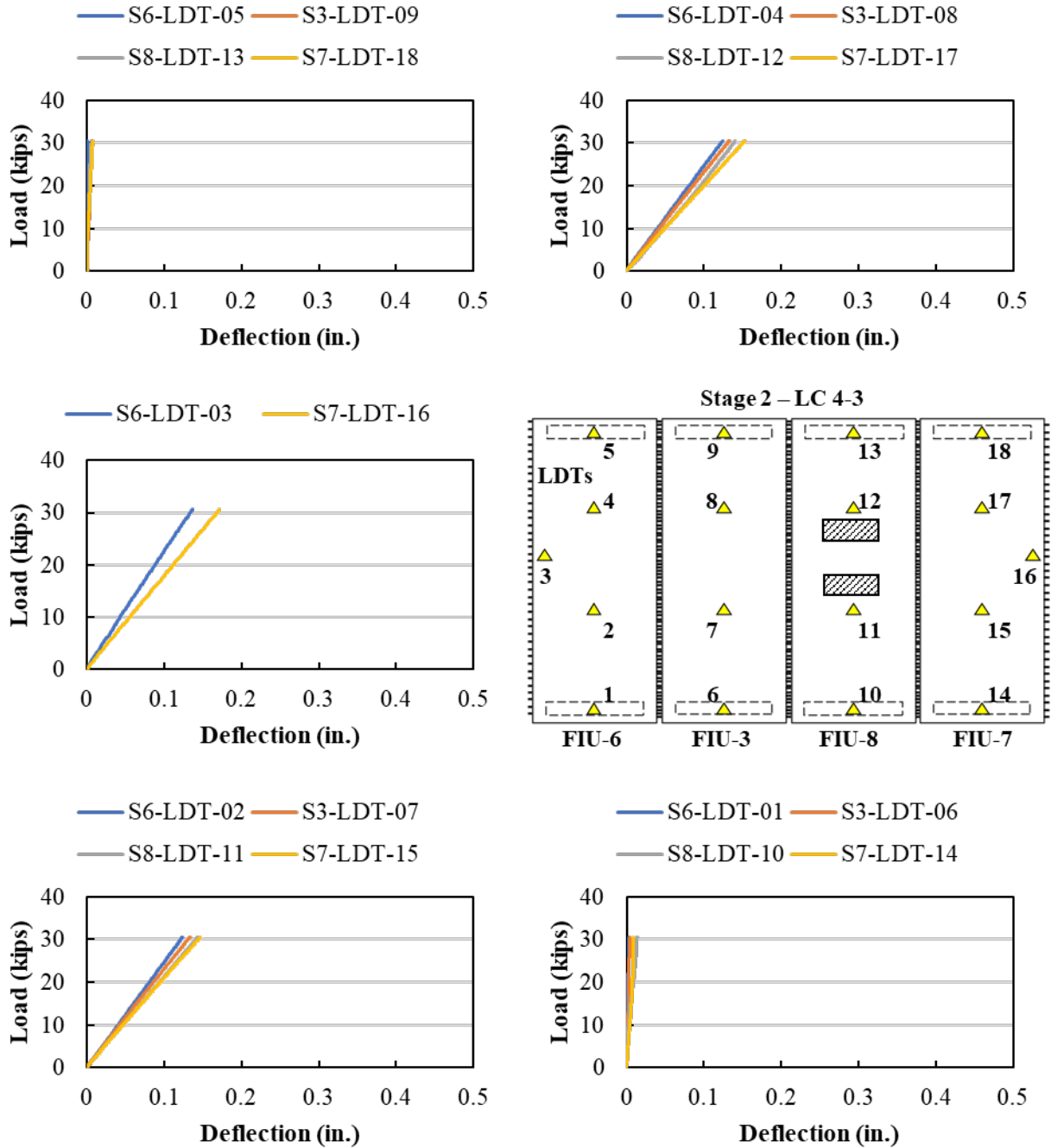


Figure F.19: Load versus displacement measured using LDTs for Load Stage 2, LC 4-3

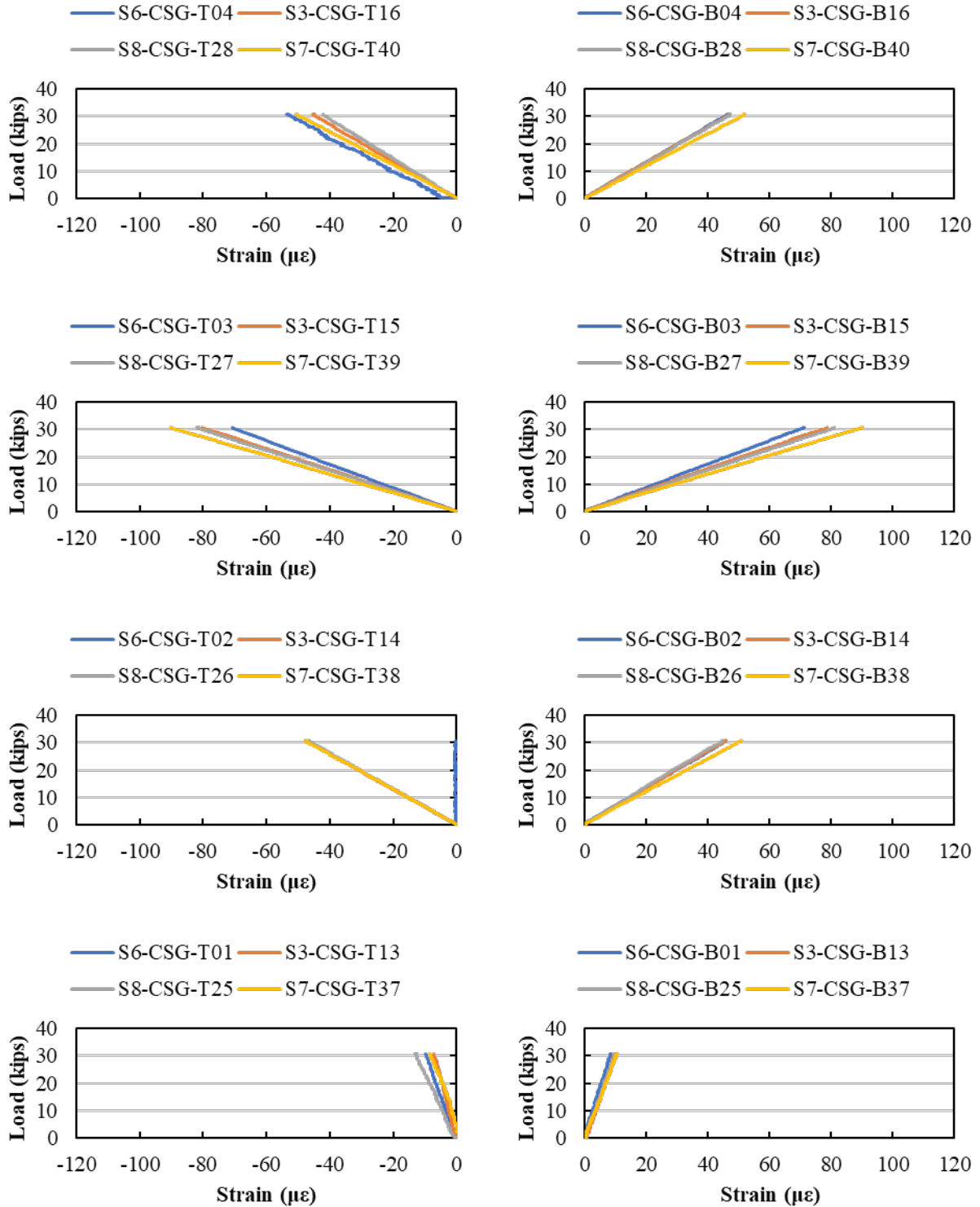


Figure F.20: Load versus longitudinal strain (measured by CSGs) for Load Stage 2, LC 4-3

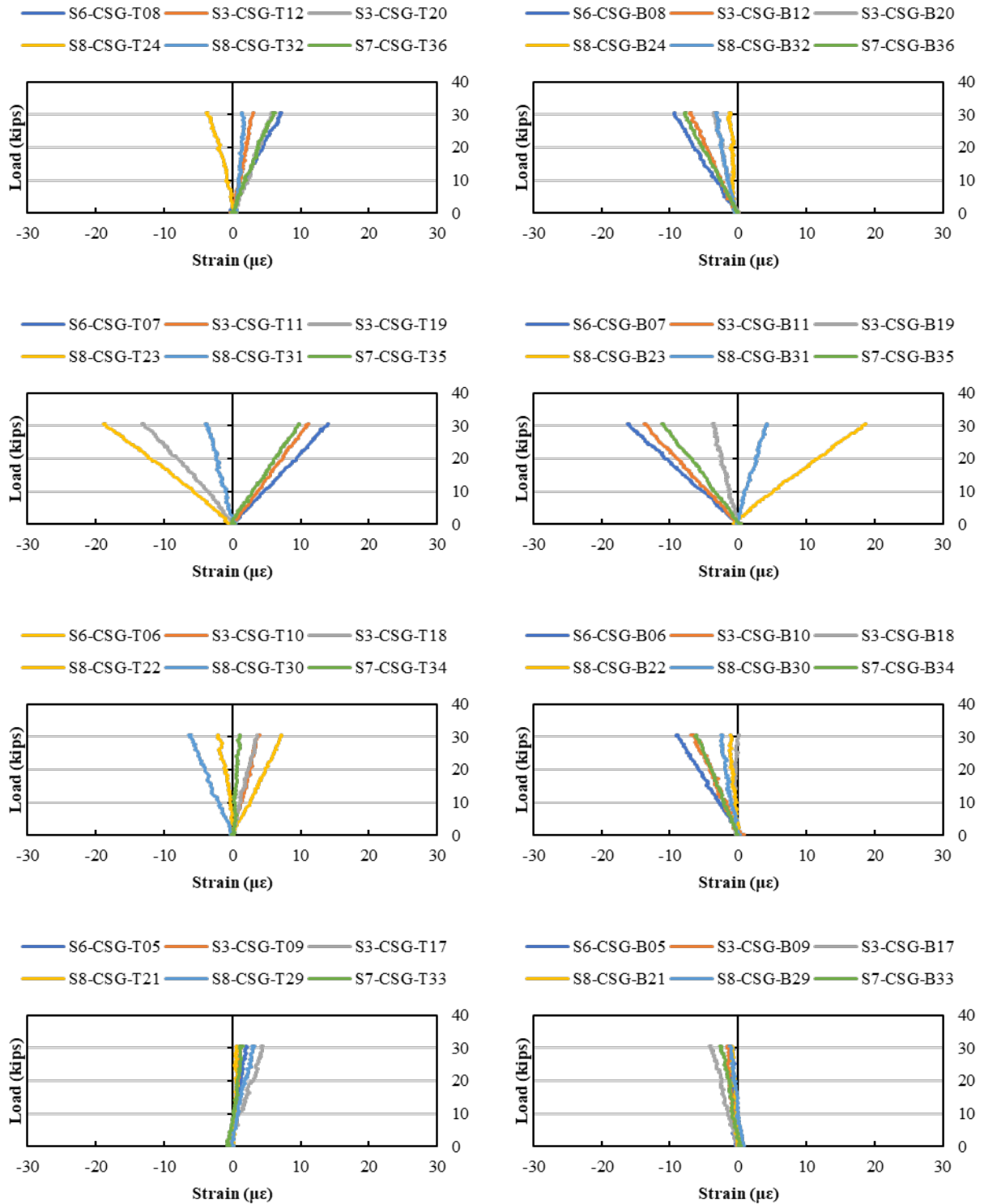


Figure F.21: Load versus transverse strain (measured by CSGs) for Load Stage 2, LC 4-3

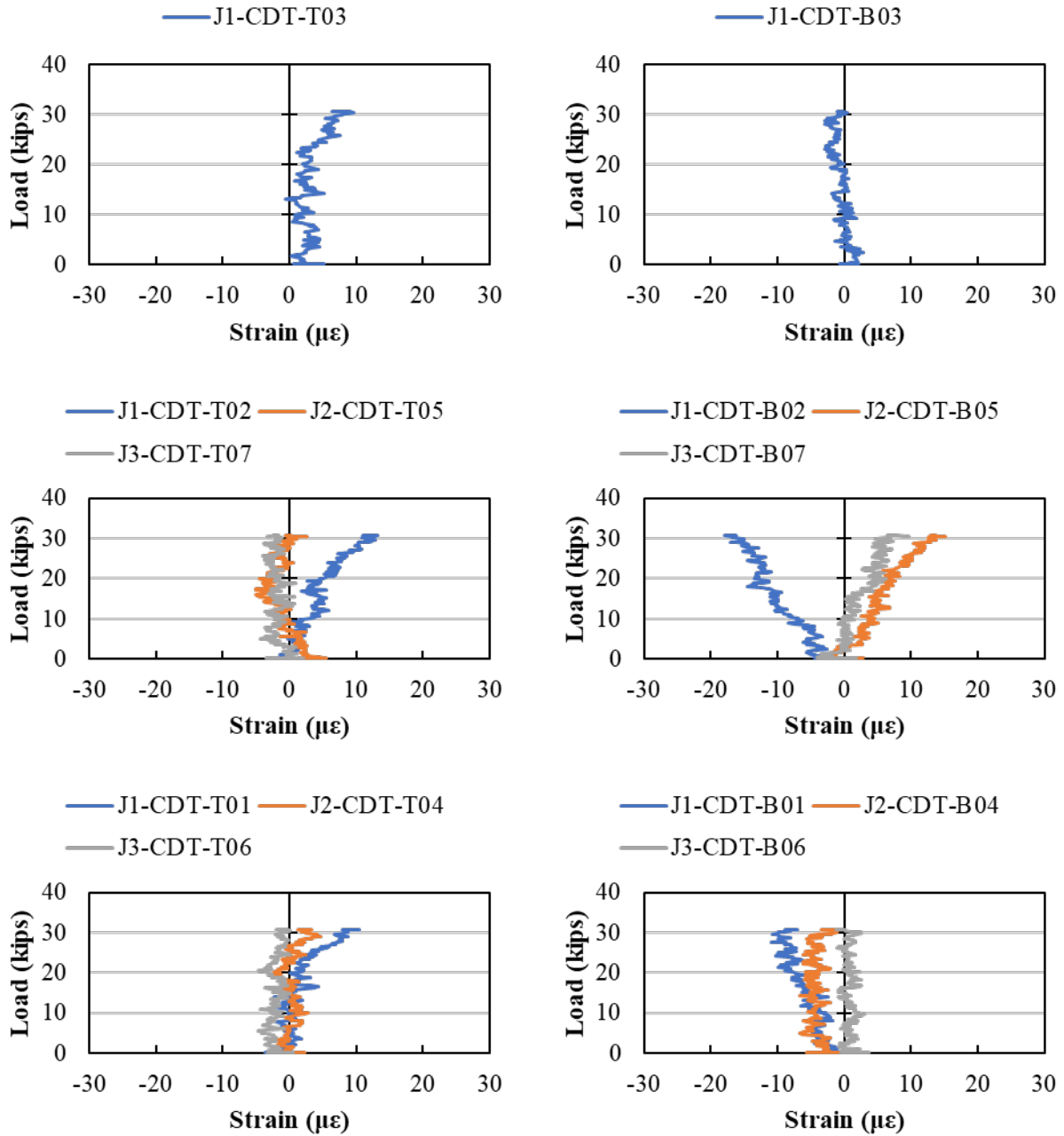


Figure F.22: Load versus average strain across the joints (measured by CDTs) for Load Stage 2, LC 4-3

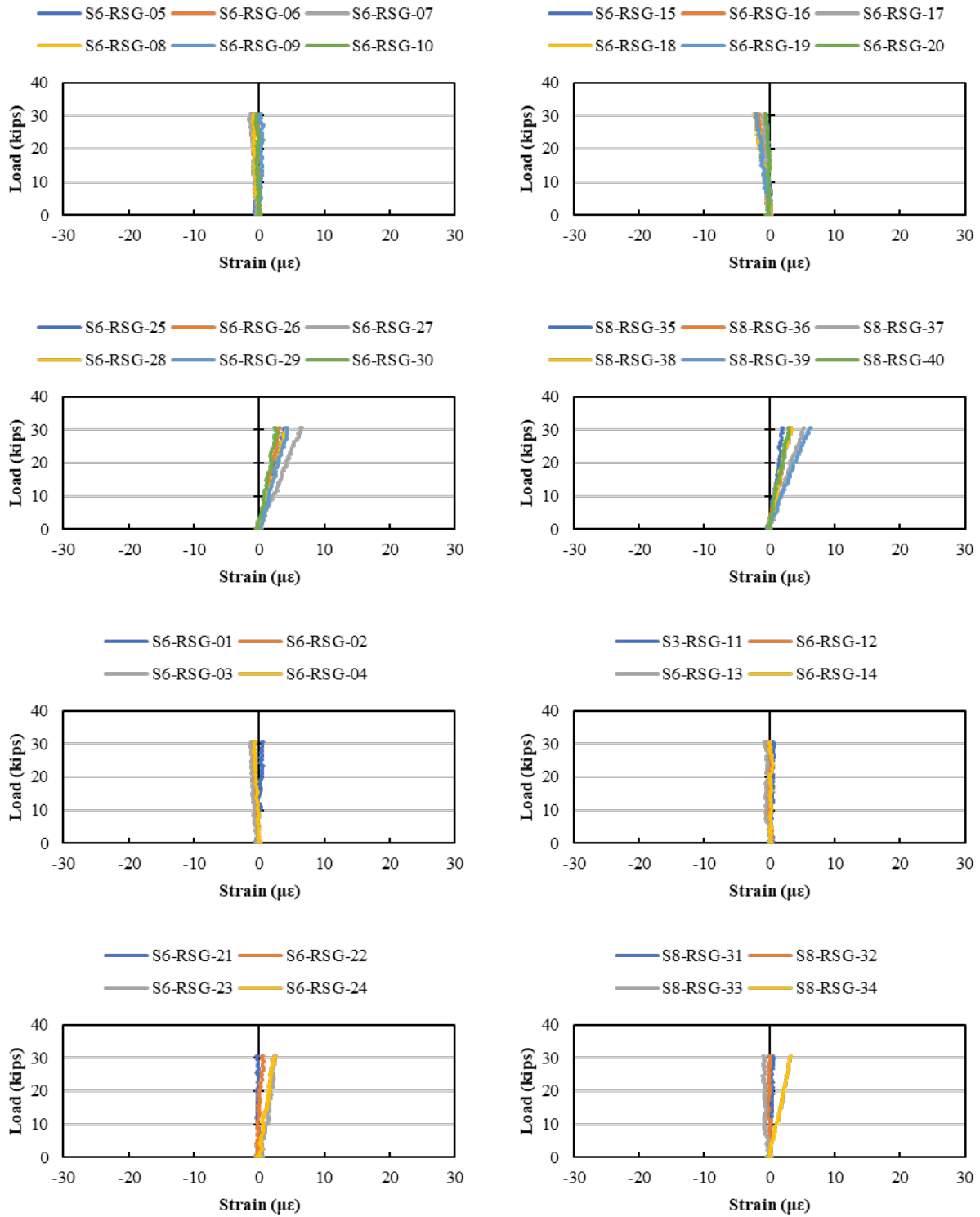


Figure F.23: Load versus rebar strain (measured by RSGs) for Load Stage 2, LC 4-3

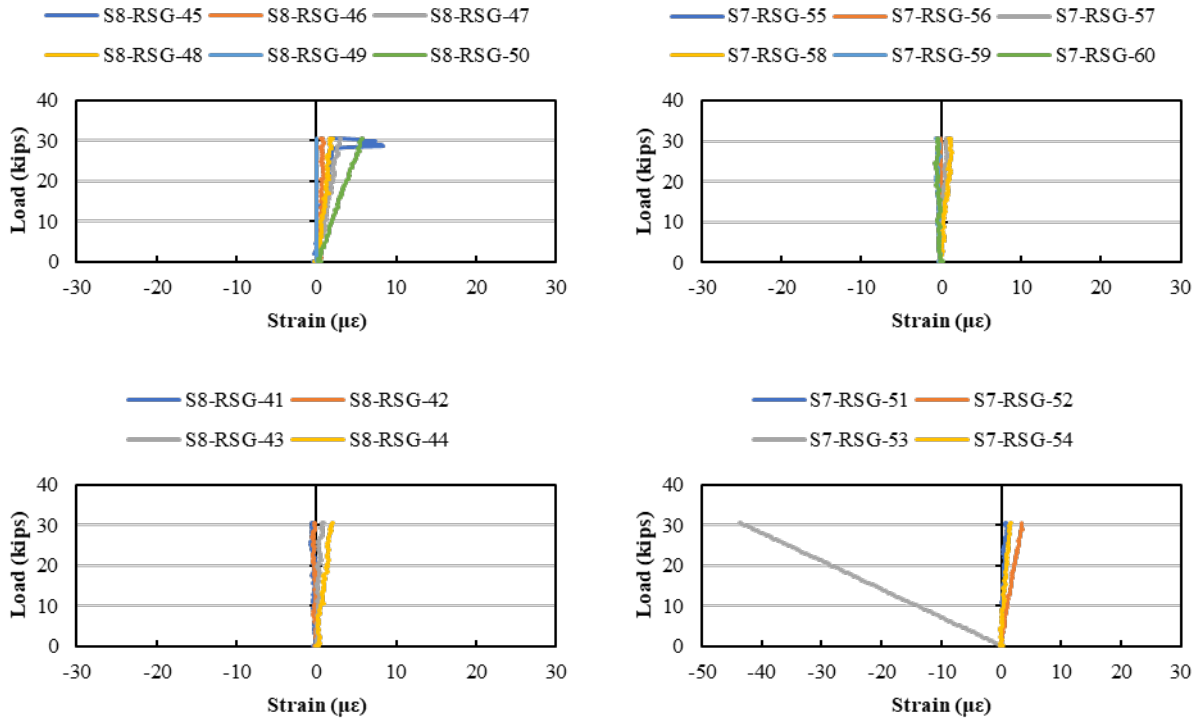


Figure F.24: Load versus rebar strain (measured by RSGs) for Load Stage 2, LC 4-3 (cont.)

F.7. LOAD STAGE 2 – LOAD CONFIGURATION 4-4

The response from all instrumentation for Load Stage 2 with Load Configuration 4-4 are shown in this section.

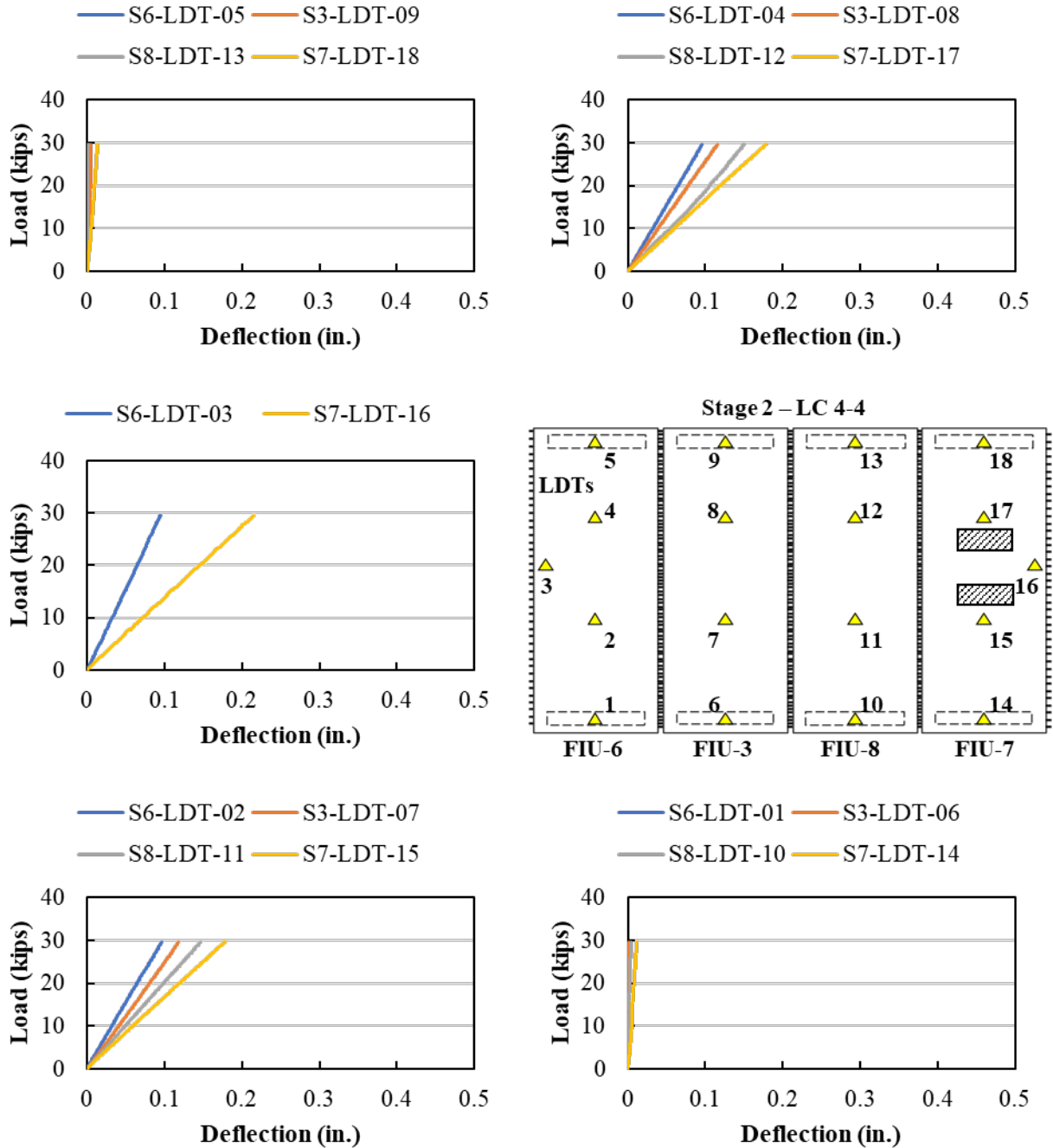


Figure F.25: Load versus displacement measured using LDTs for Load Stage 2, LC 4-4

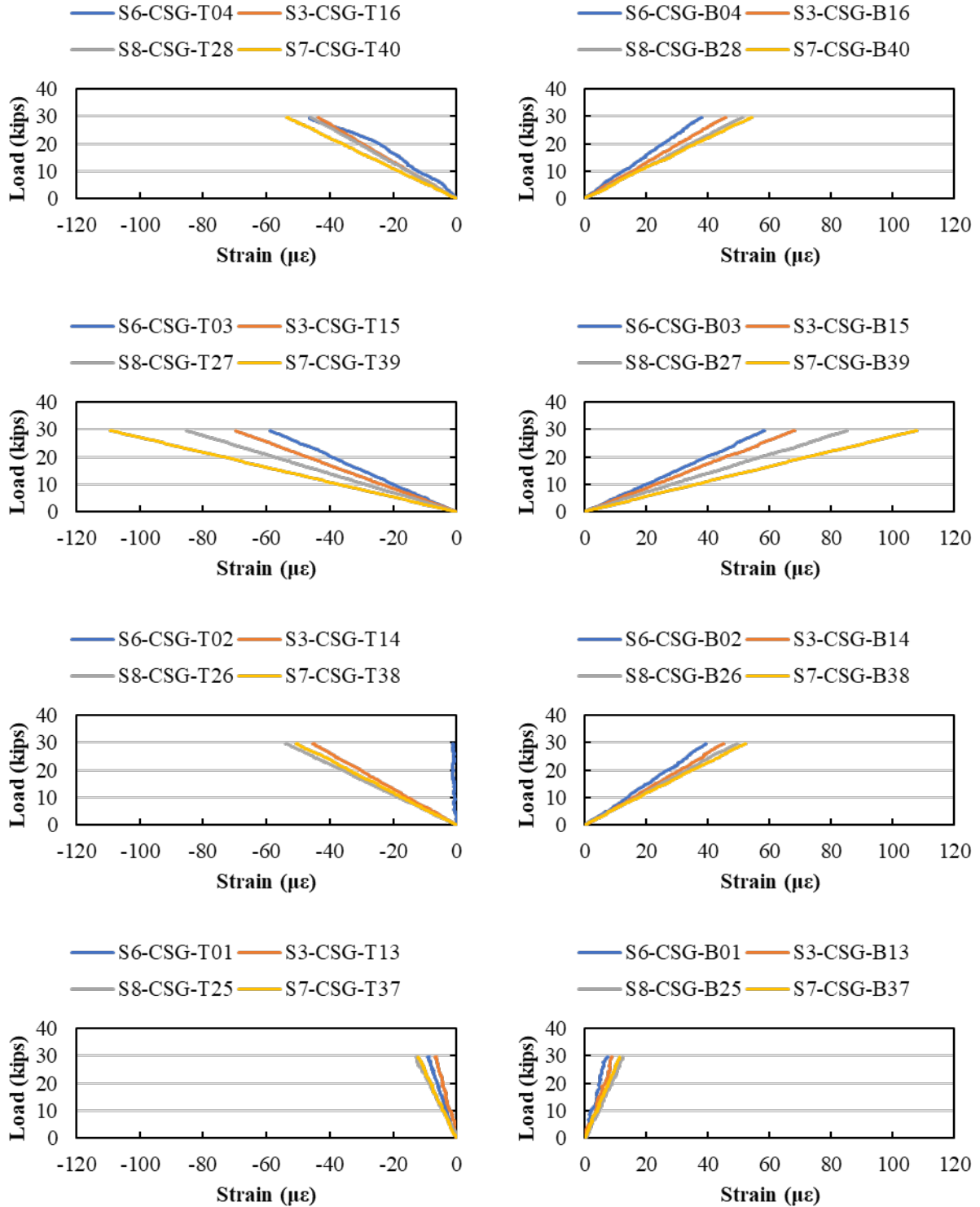


Figure F.26: Load versus longitudinal strain (measured by CSGs) for Load Stage 2, LC 4-4

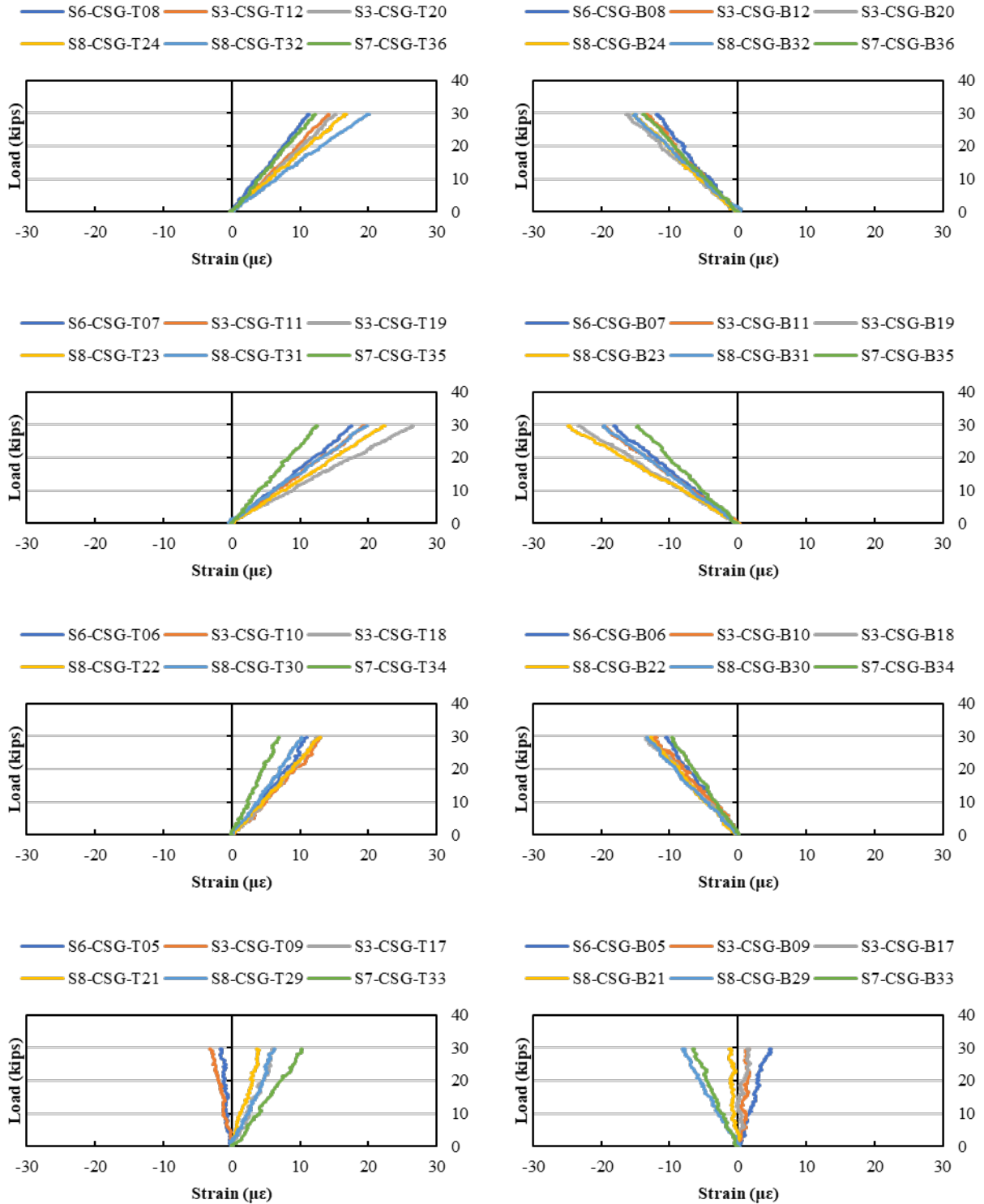


Figure F.27: Load versus transverse strain (measured by CSGs) for Load Stage 2, LC 4-4

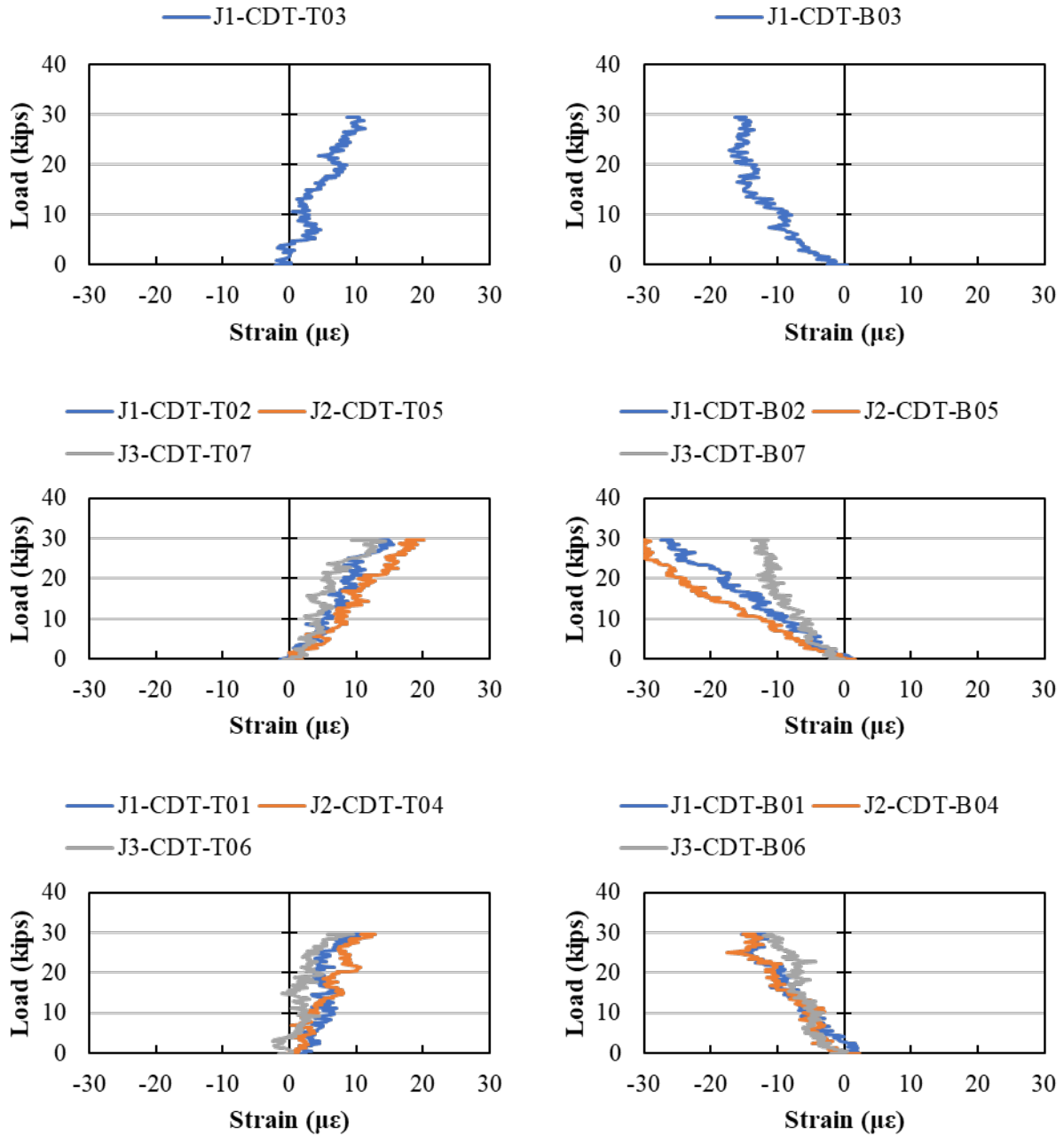


Figure F.28: Load versus average strain across the joints (measured by CDTs) for Load Stage 2, LC 4-4

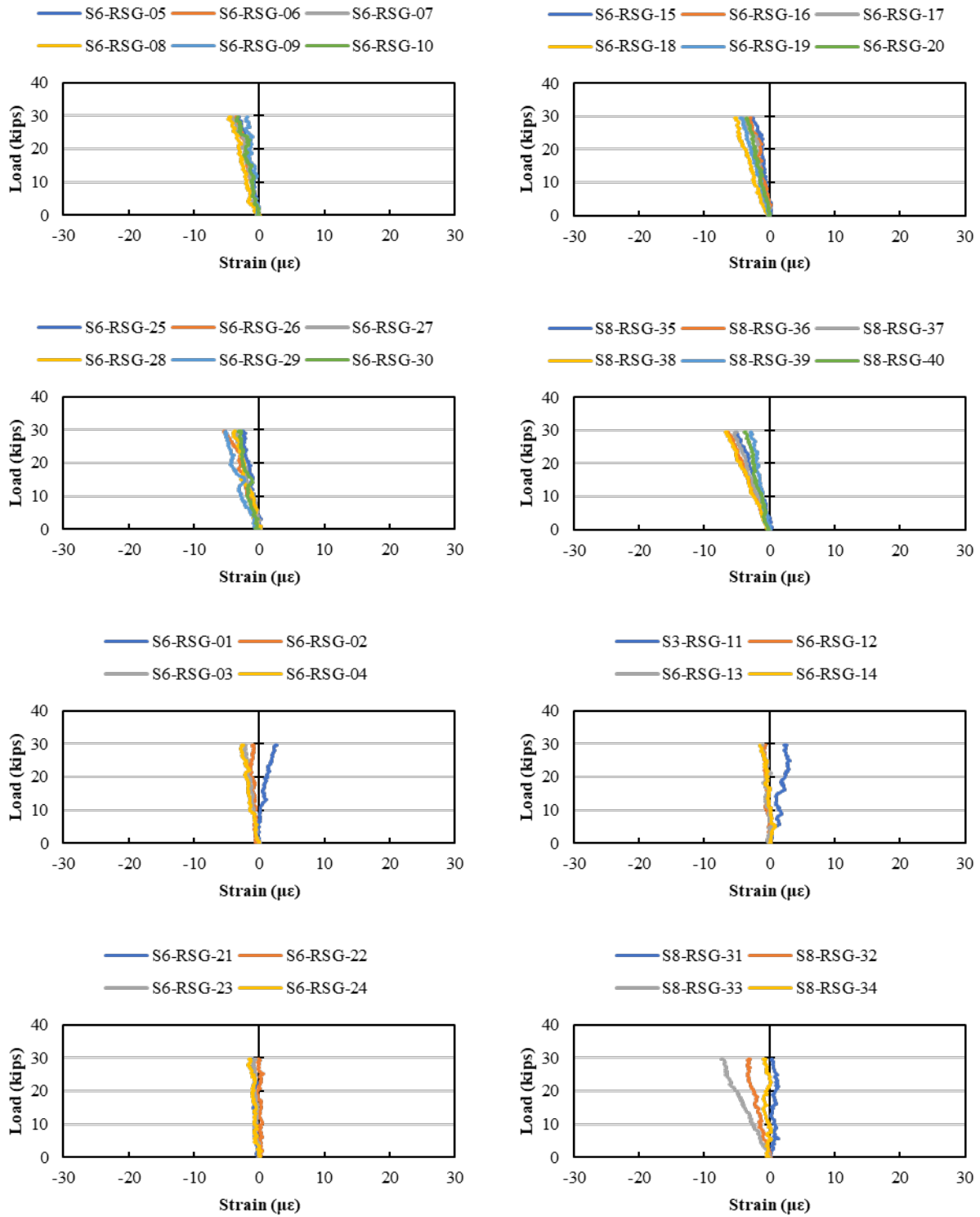


Figure F.29: Load versus rebar strain (measured by RSGs) for Load Stage 2, LC 4-4

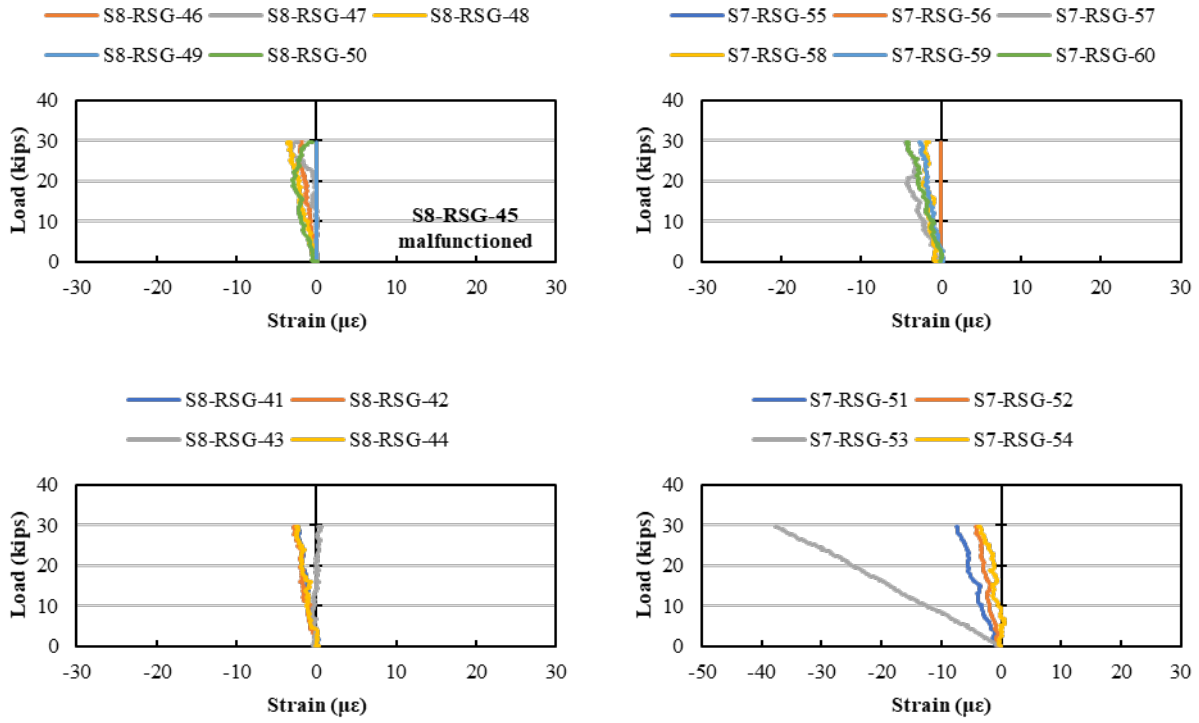


Figure F.30: Load versus rebar strain (measured by RSGs) for Load Stage 2, LC 4-4 (cont.)

F.8. LOAD STAGE 3 AND 4

The data from all the fatigue testing is summarized in §F.12.

F.9. LOAD STAGE 5 – LOAD CONFIGURATION 4-1

The response from all instrumentation for Load Stage 5 with Load Configuration 4-1 are shown in this section.

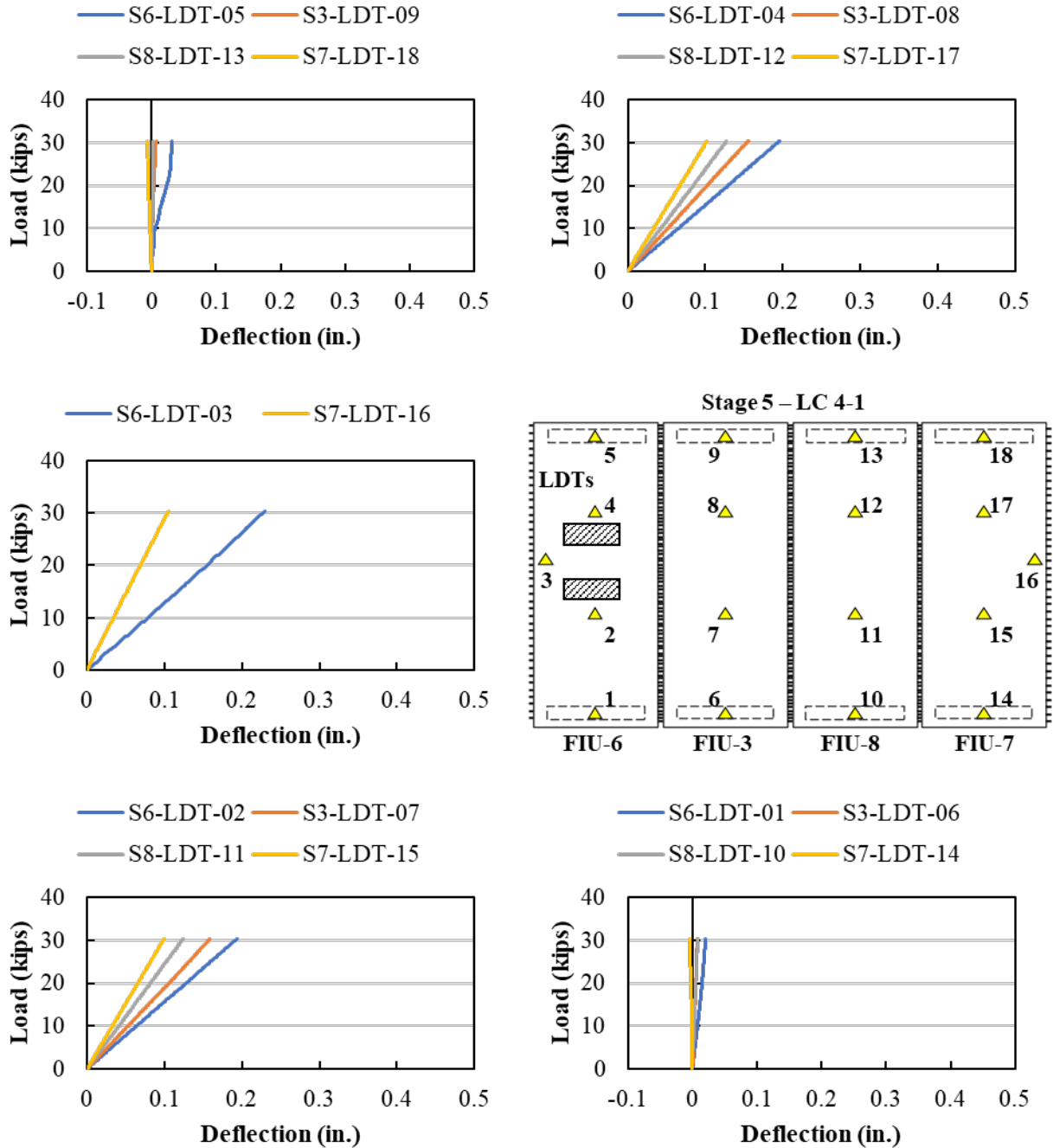


Figure F.31: Load versus displacement measured using LDTs for Load Stage 5, LC 4-1

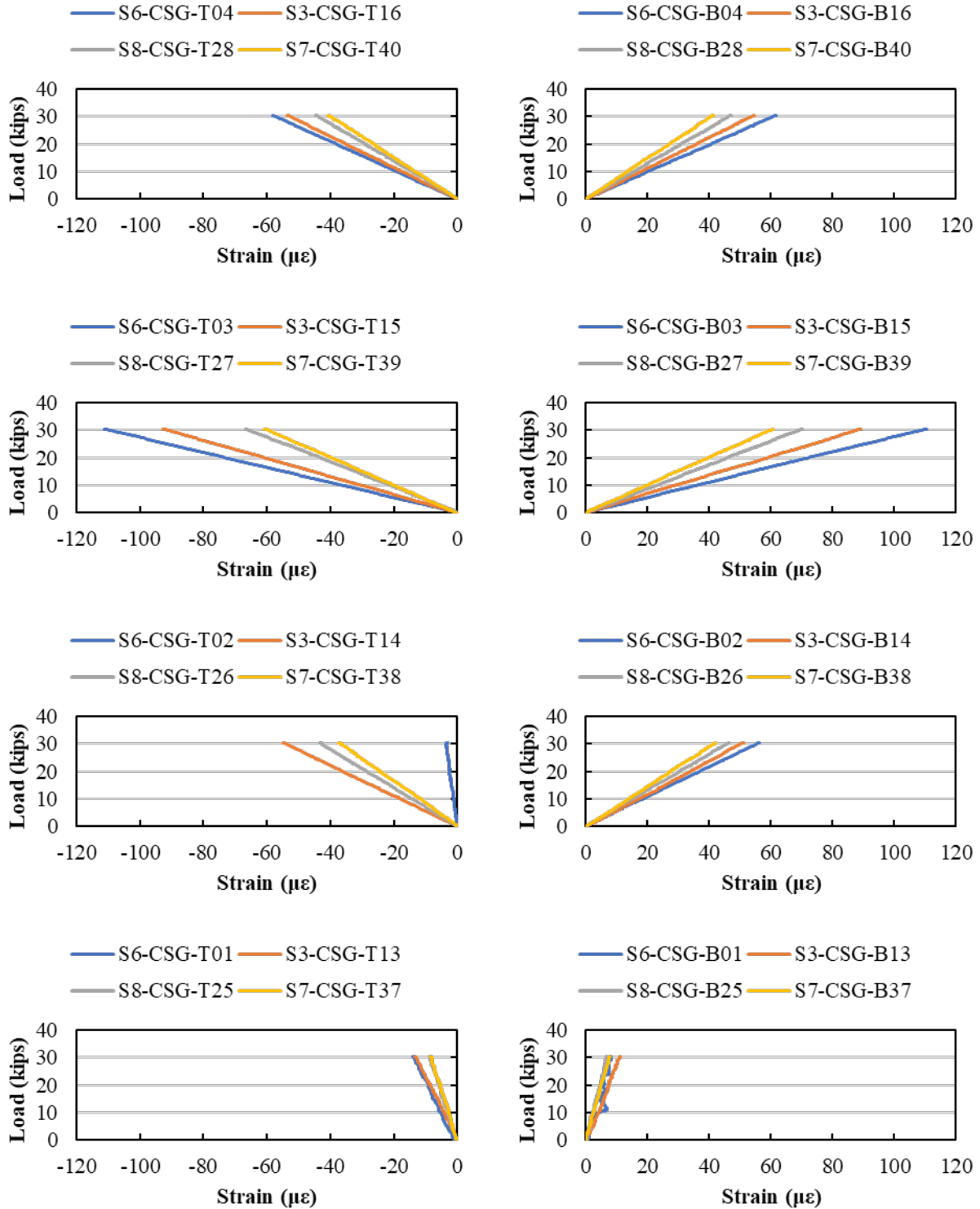


Figure F.32: Load versus longitudinal strain (measured by CSGs) for Load Stage 5, LC 4-1

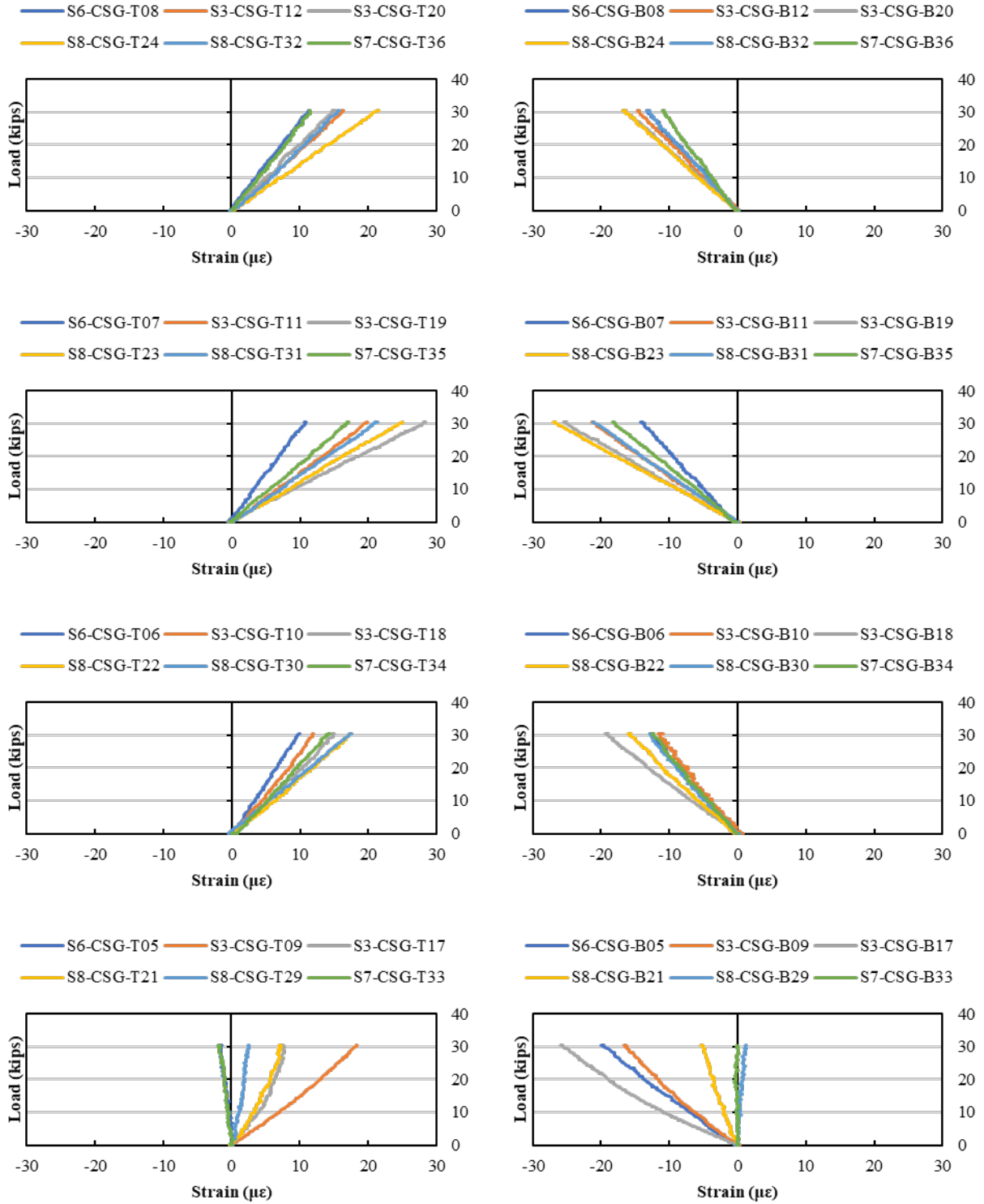


Figure F.33: Load versus transverse strain (measured by CSGs) for Load Stage 5, LC 4-1

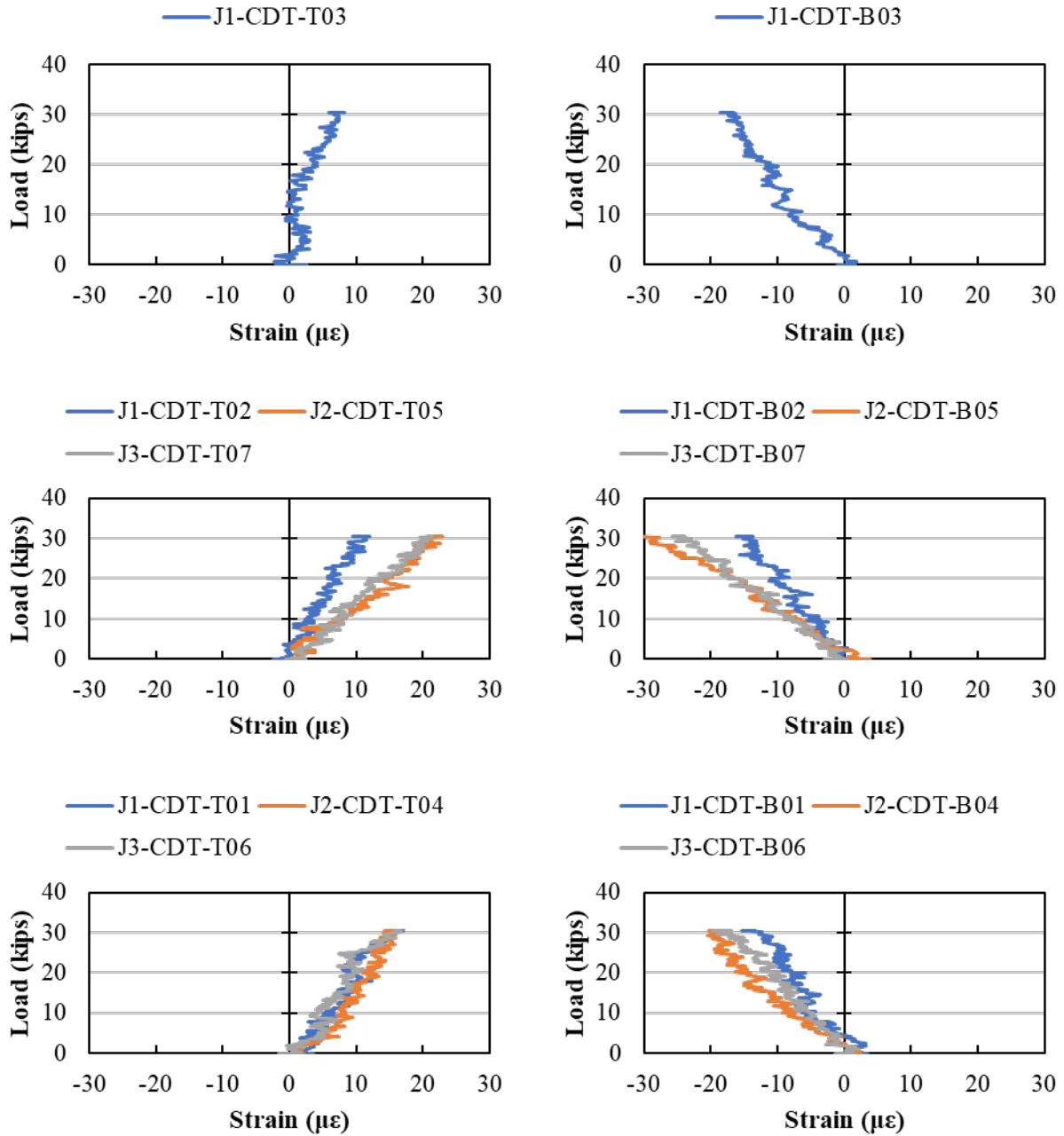


Figure F.34: Load versus average strain across the joints (measured by CDTs) for Load Stage 5, LC 4-1

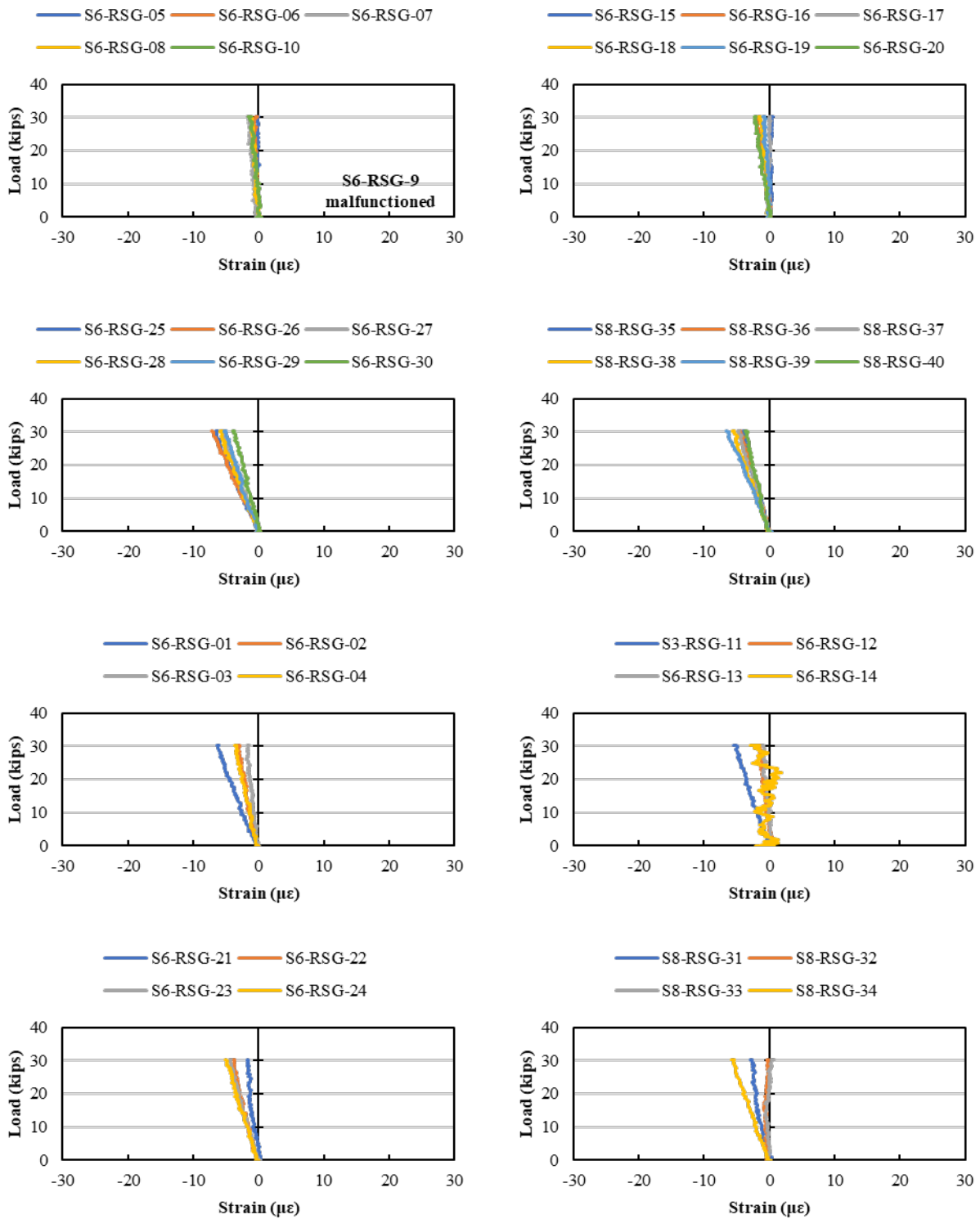


Figure F.35: Load versus rebar strain (measured by RSGs) for Load Stage 5, LC 4-1

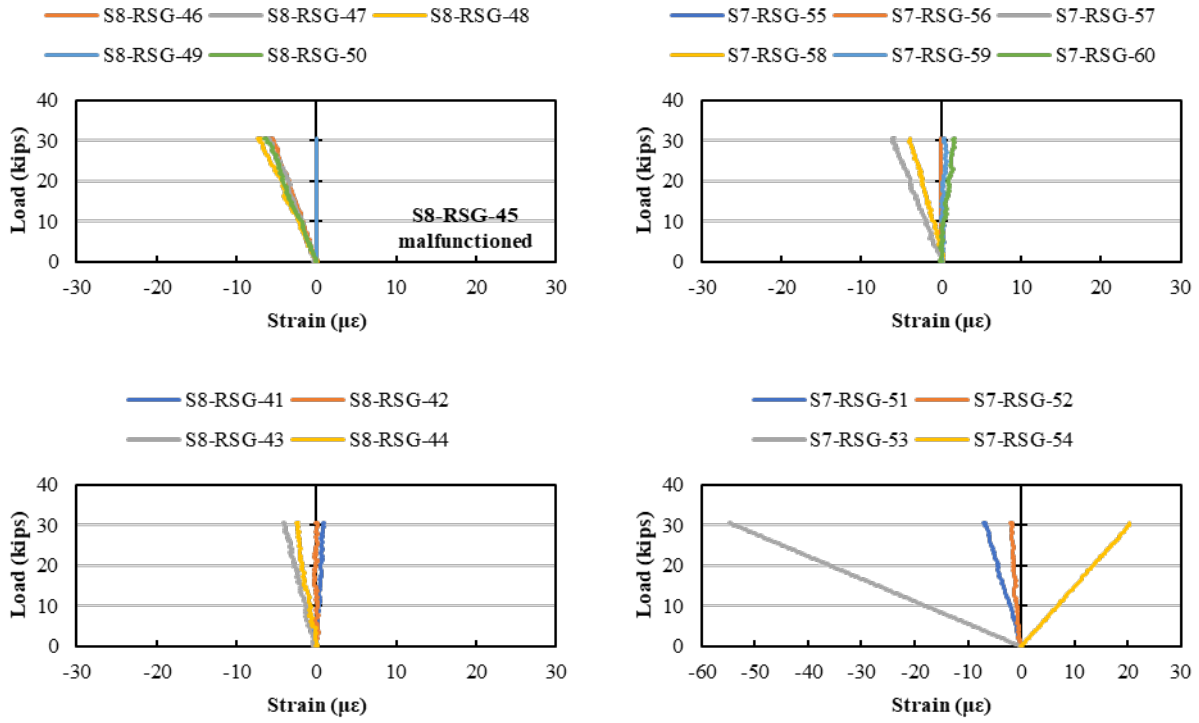


Figure F.36: Load versus rebar strain (measured by RSGs) for Load Stage 5, LC 4-1 (cont.)

F.10. LOAD STAGE 5 – LOAD CONFIGURATION 4-3

The response from all instrumentation for Load Stage 5 with Load Configuration 4-3 are shown in this section.

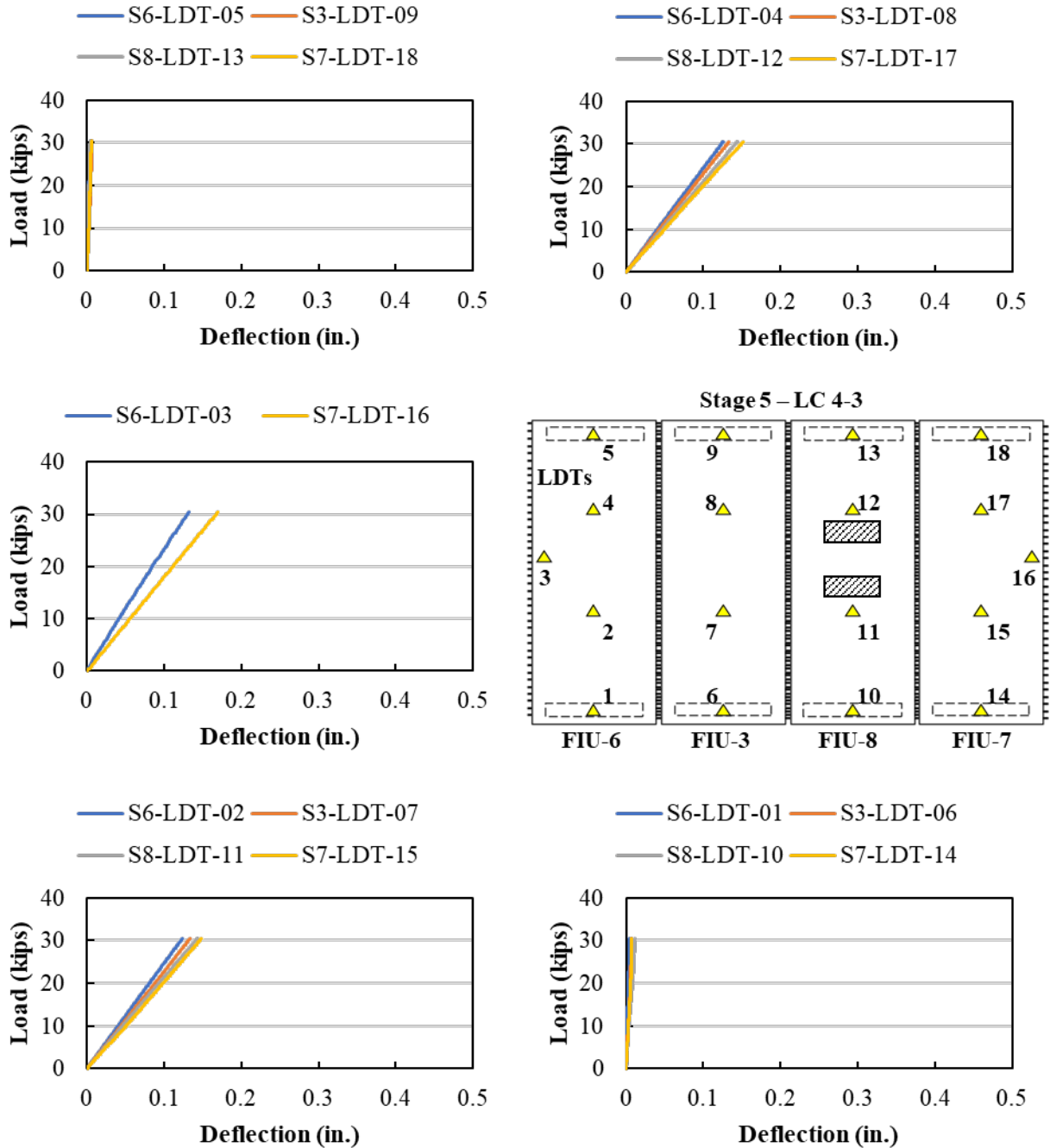


Figure F.37: Load versus displacement measured using LDTs for Load Stage 5, LC 4-3

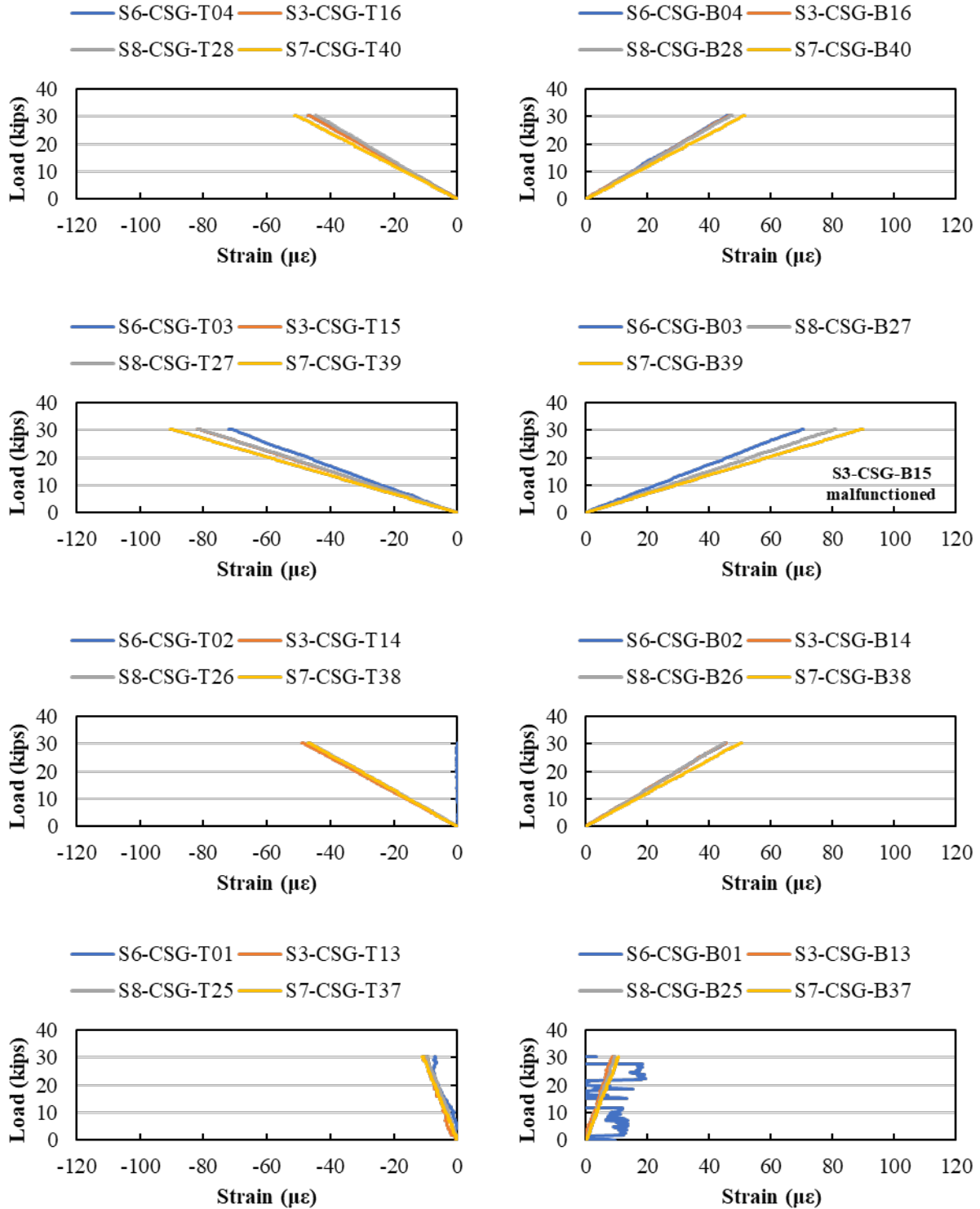


Figure F.38: Load versus longitudinal strain (measured by CSGs) for Load Stage 5, LC 4-3

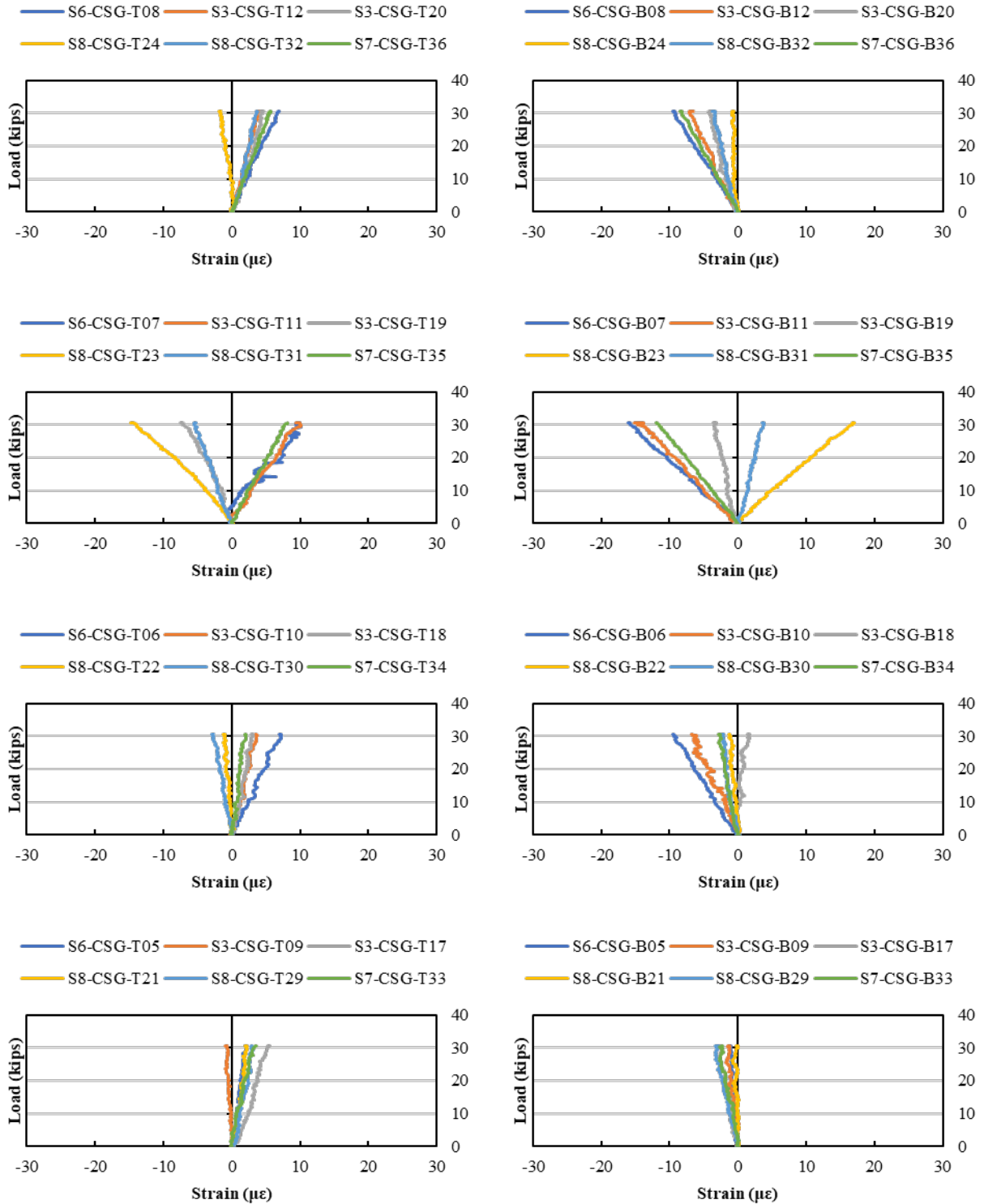


Figure F.39: Load versus transverse strain (measured by CSGs) for Load Stage 5, LC 4-3

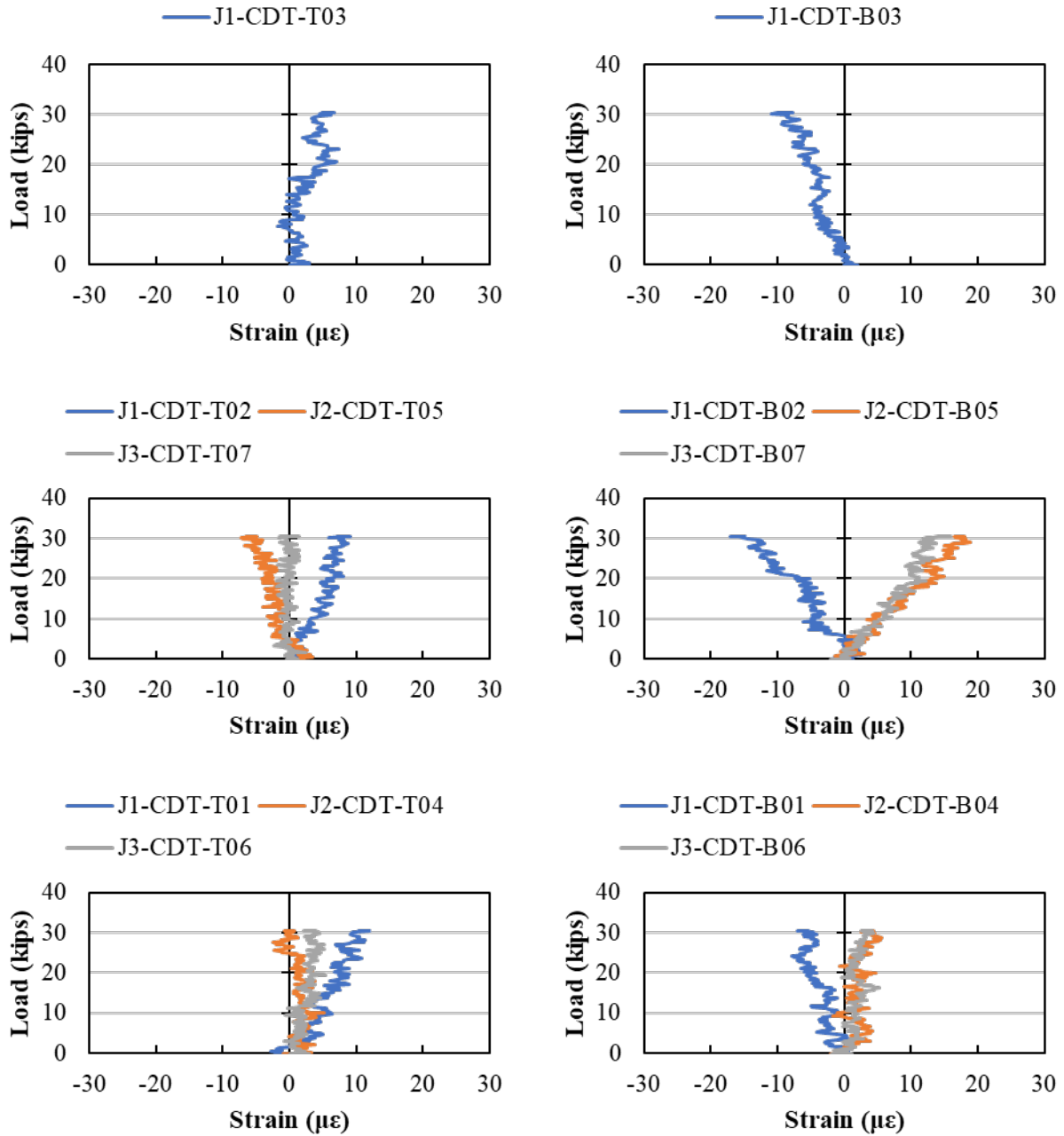


Figure F.40: Load versus average strain across the joints (measured by CDTs) for Load Stage 5, LC 4-3

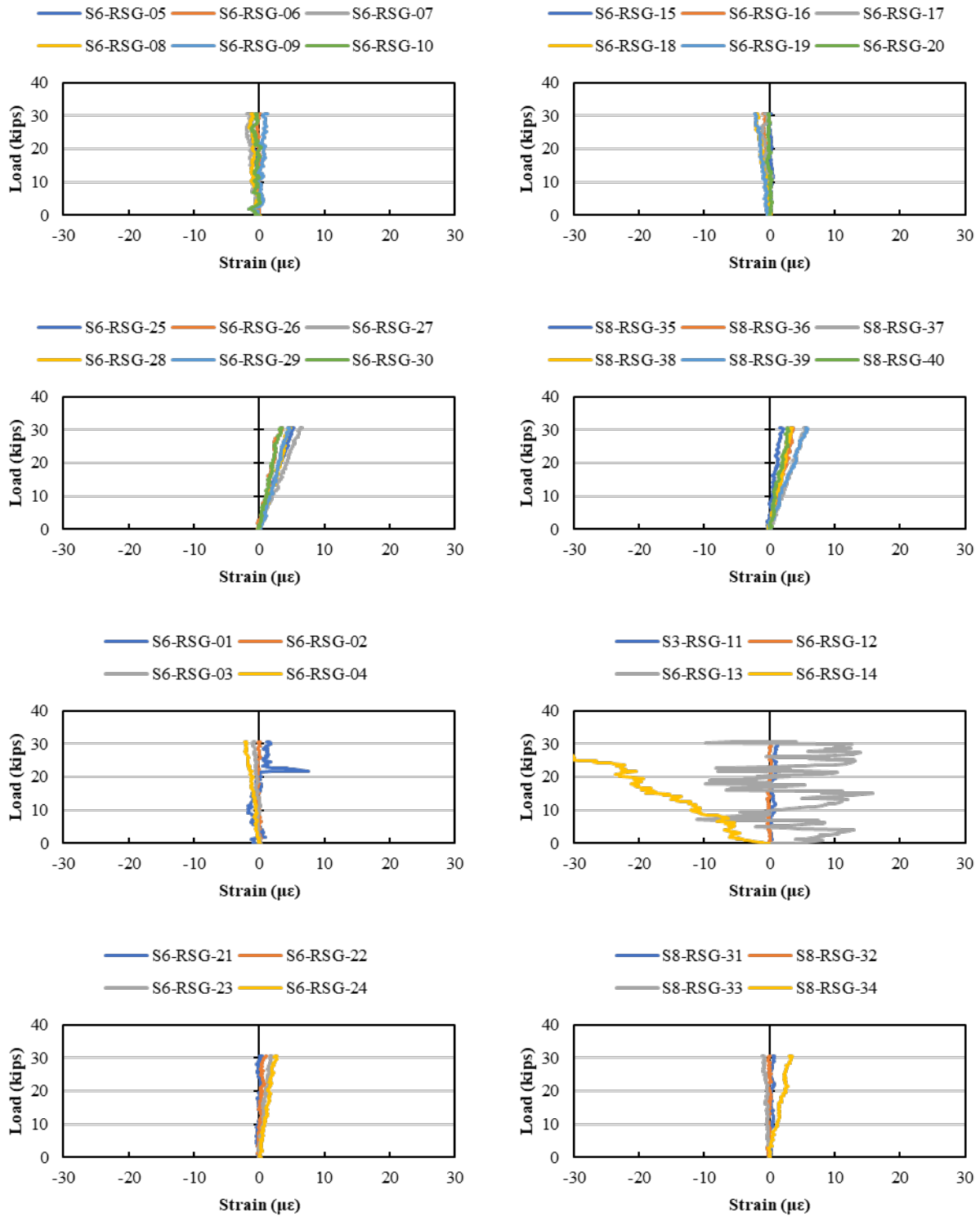


Figure F.41: Load versus rebar strain (measured by RSGs) for Load Stage 5, LC 4-3

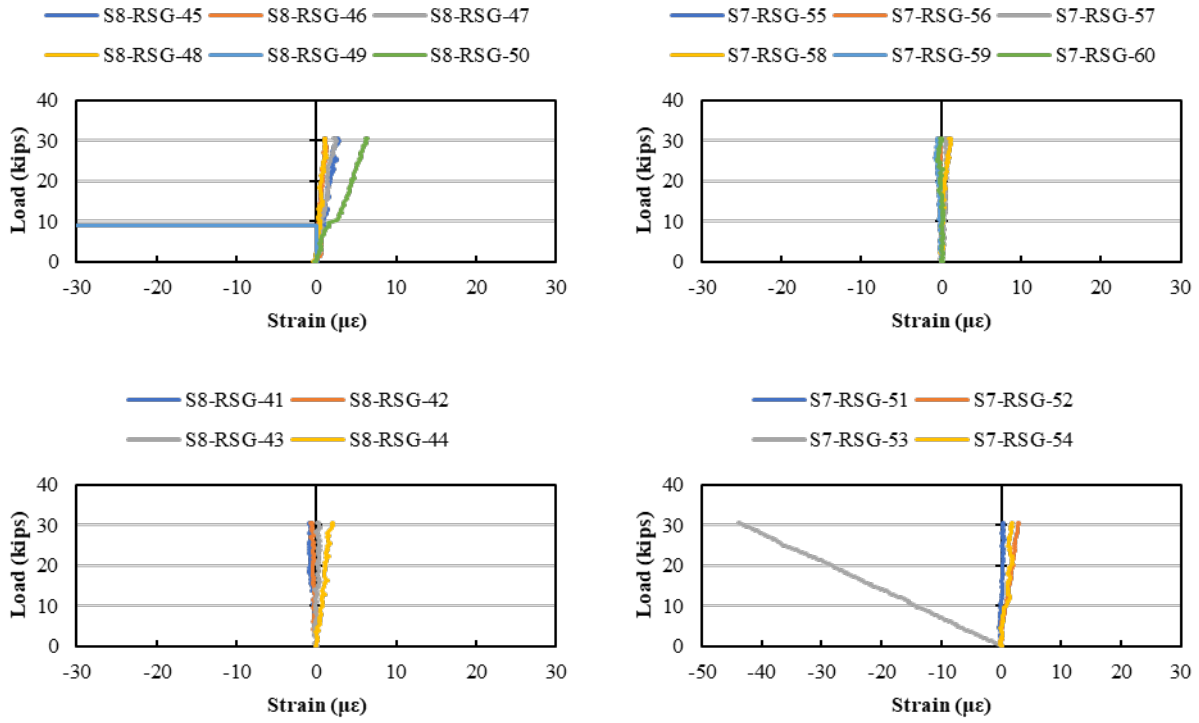


Figure F.42: Load versus rebar strain (measured by RSGs) for Load Stage 5, LC 4-3 (cont.)

F.11. LOAD STAGE 5 – LOAD CONFIGURATION 4-4

The response from all instrumentation for Load Stage 5 with Load Configuration 4-4 are shown in this section.

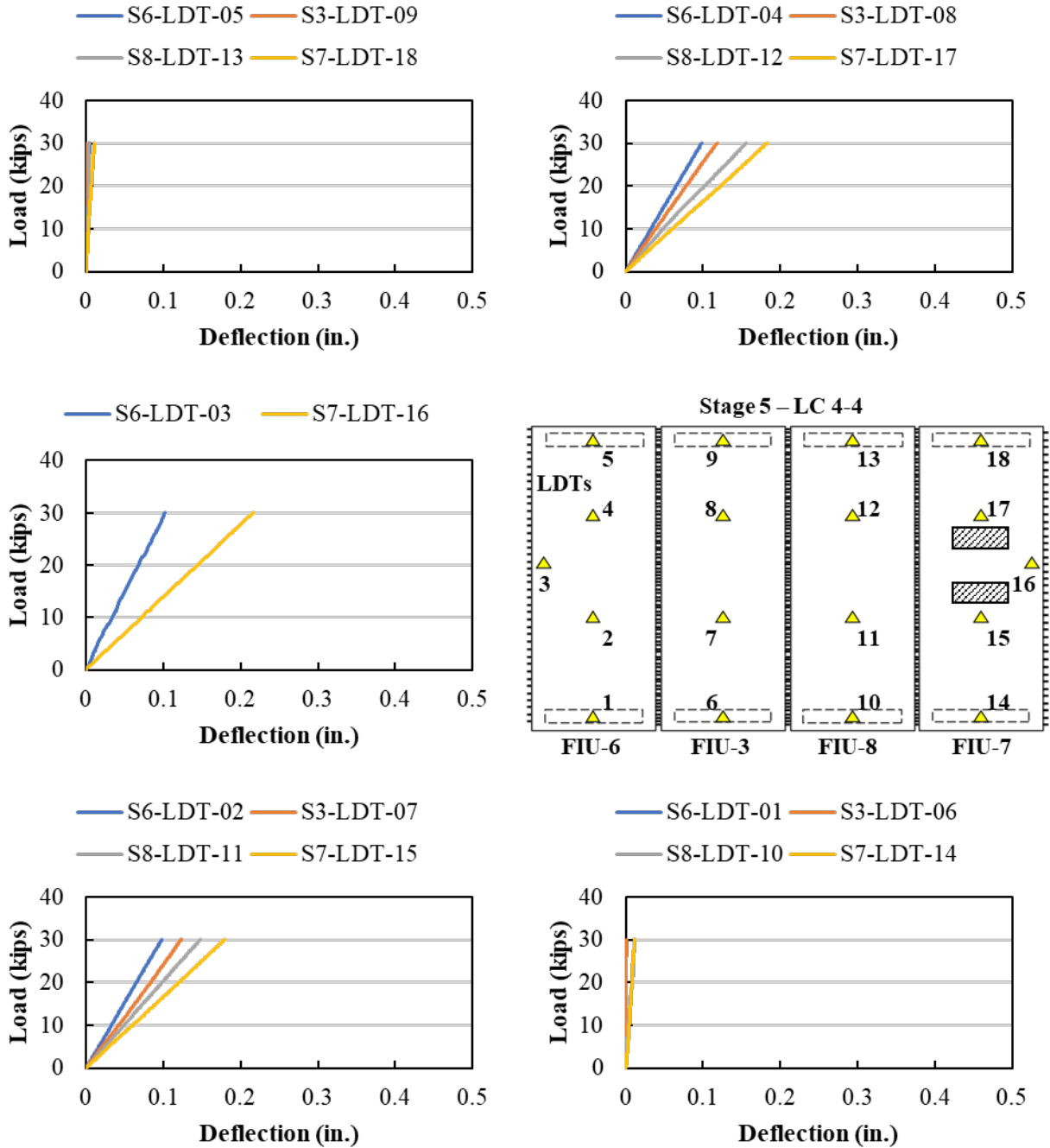


Figure F.43: Load versus displacement measured using LDTs for Load Stage 5, LC 4-4

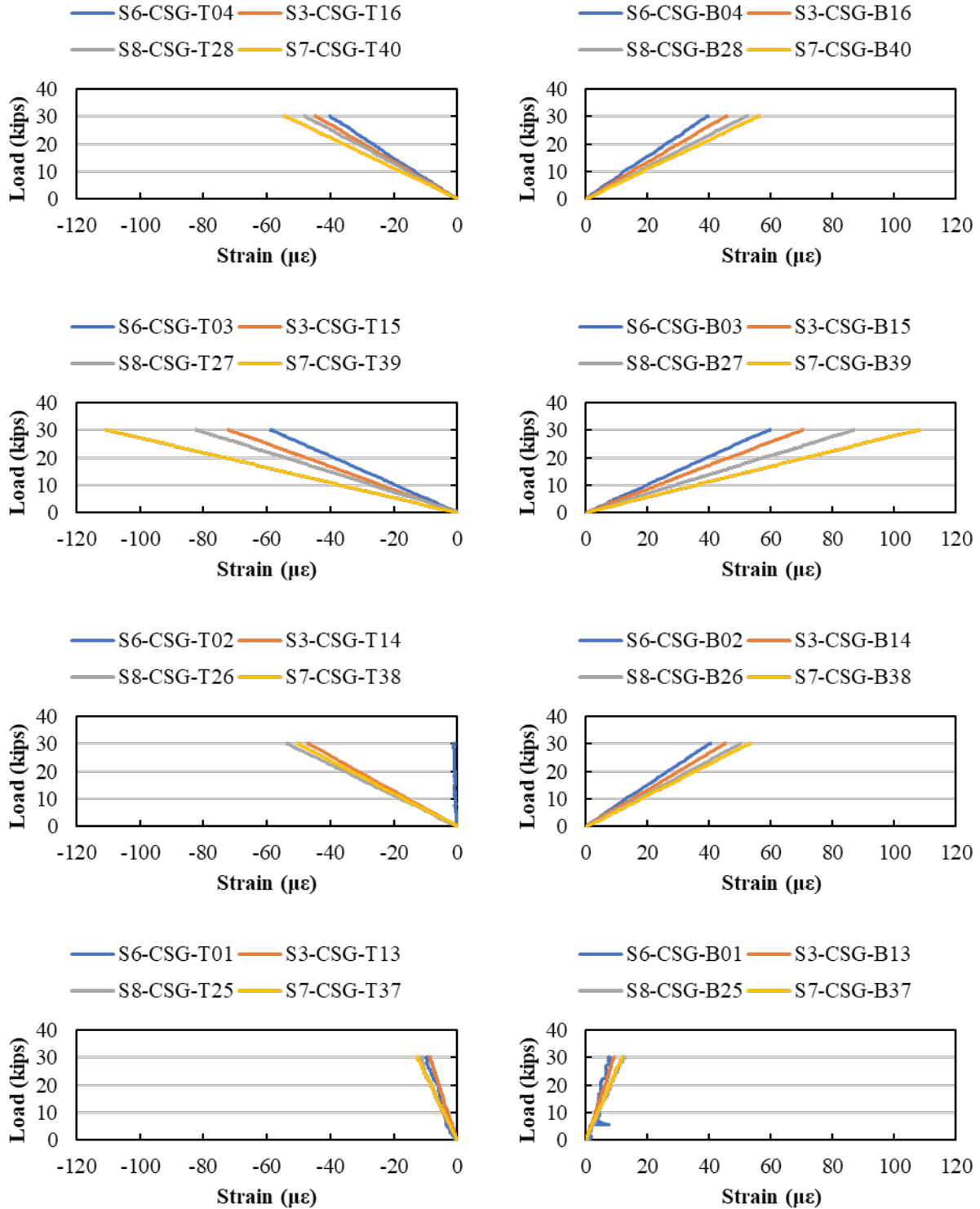


Figure F.44: Load versus longitudinal strain (measured by CSGs) for Load Stage 5, LC 4-4

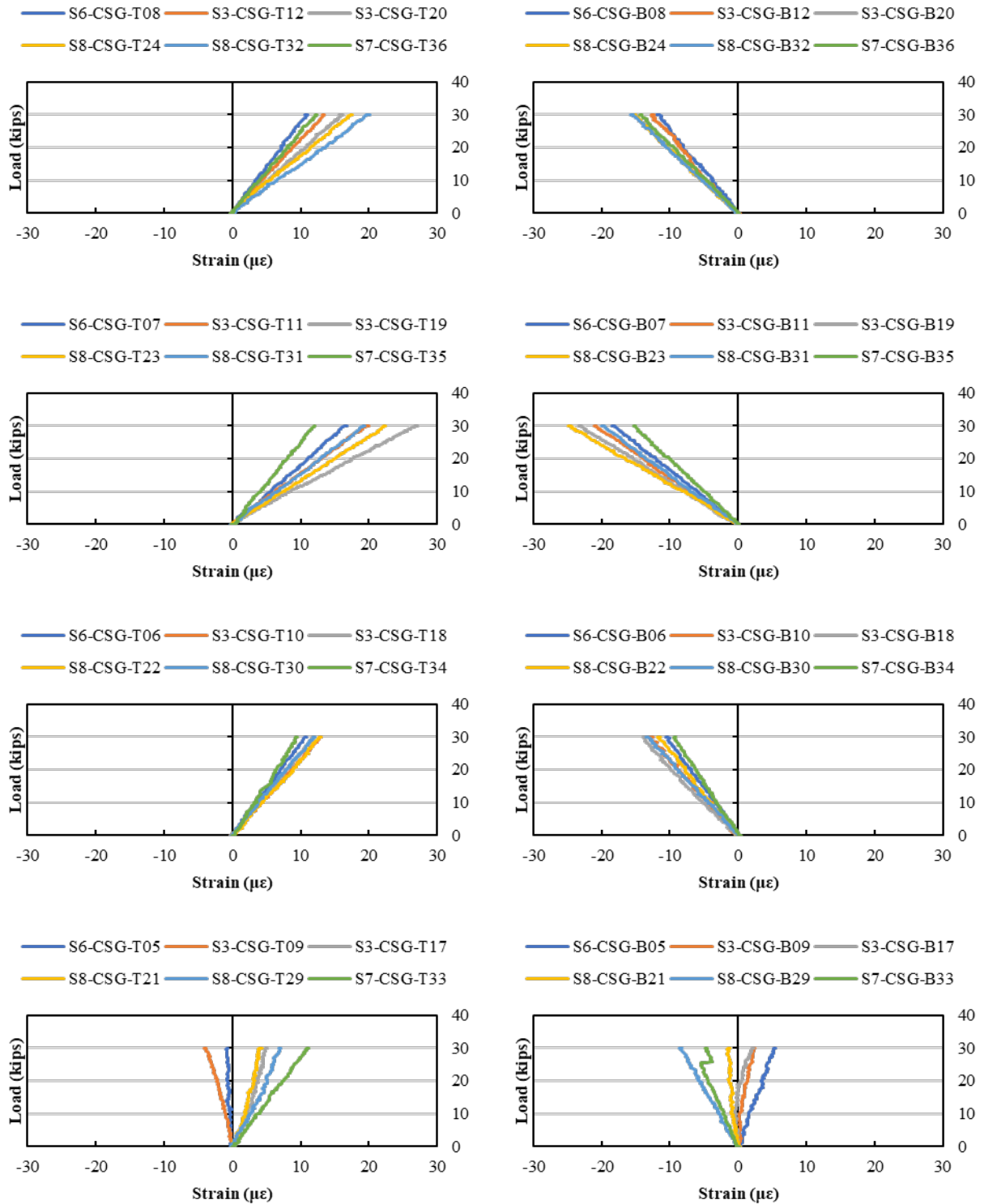


Figure F.45: Load versus transverse strain (measured by CSGs) for Load Stage 5, LC 4-4

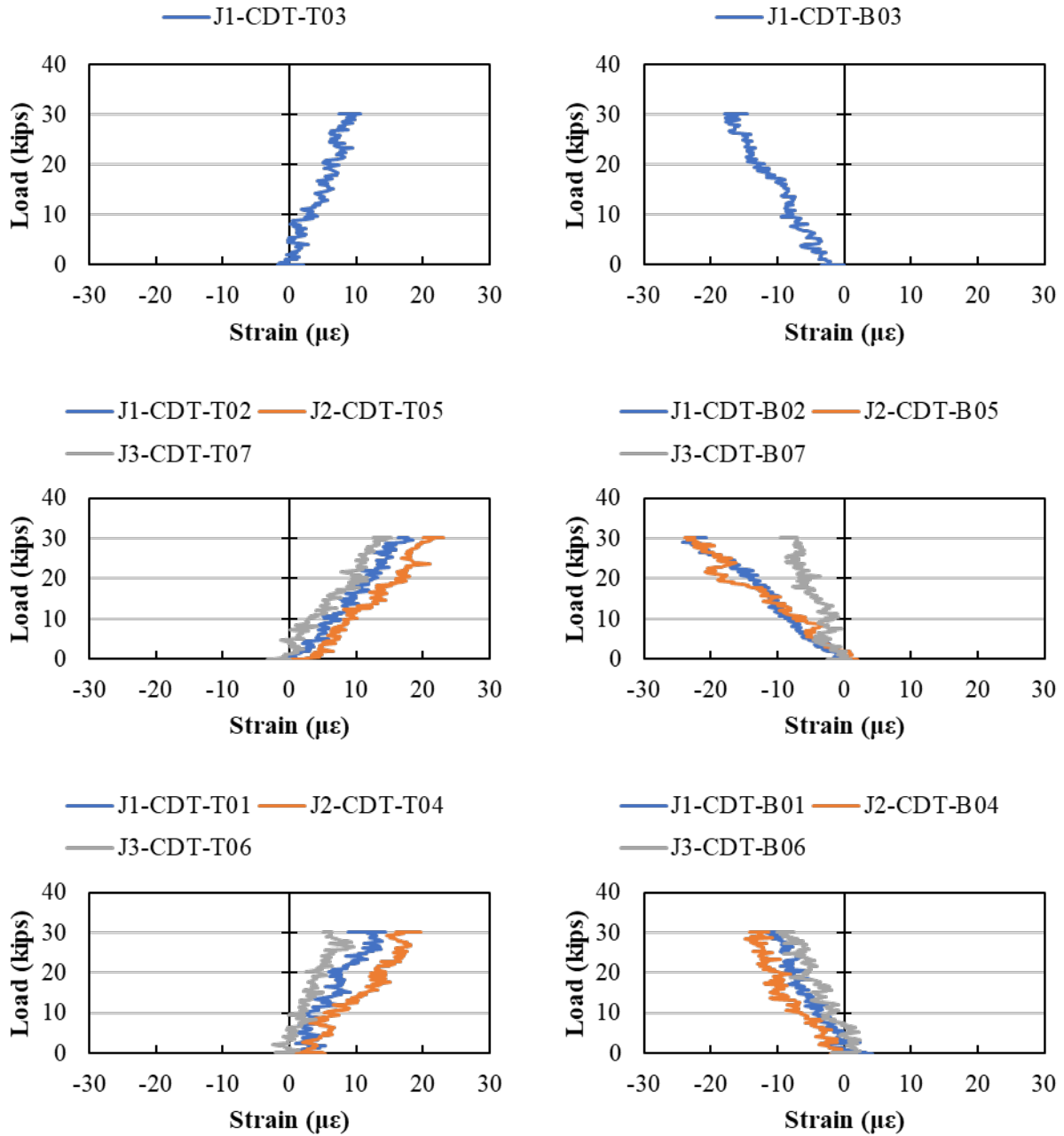


Figure F.46: Load versus average strain across the joints (measured by CDTs) for Load Stage 5, LC 4-4

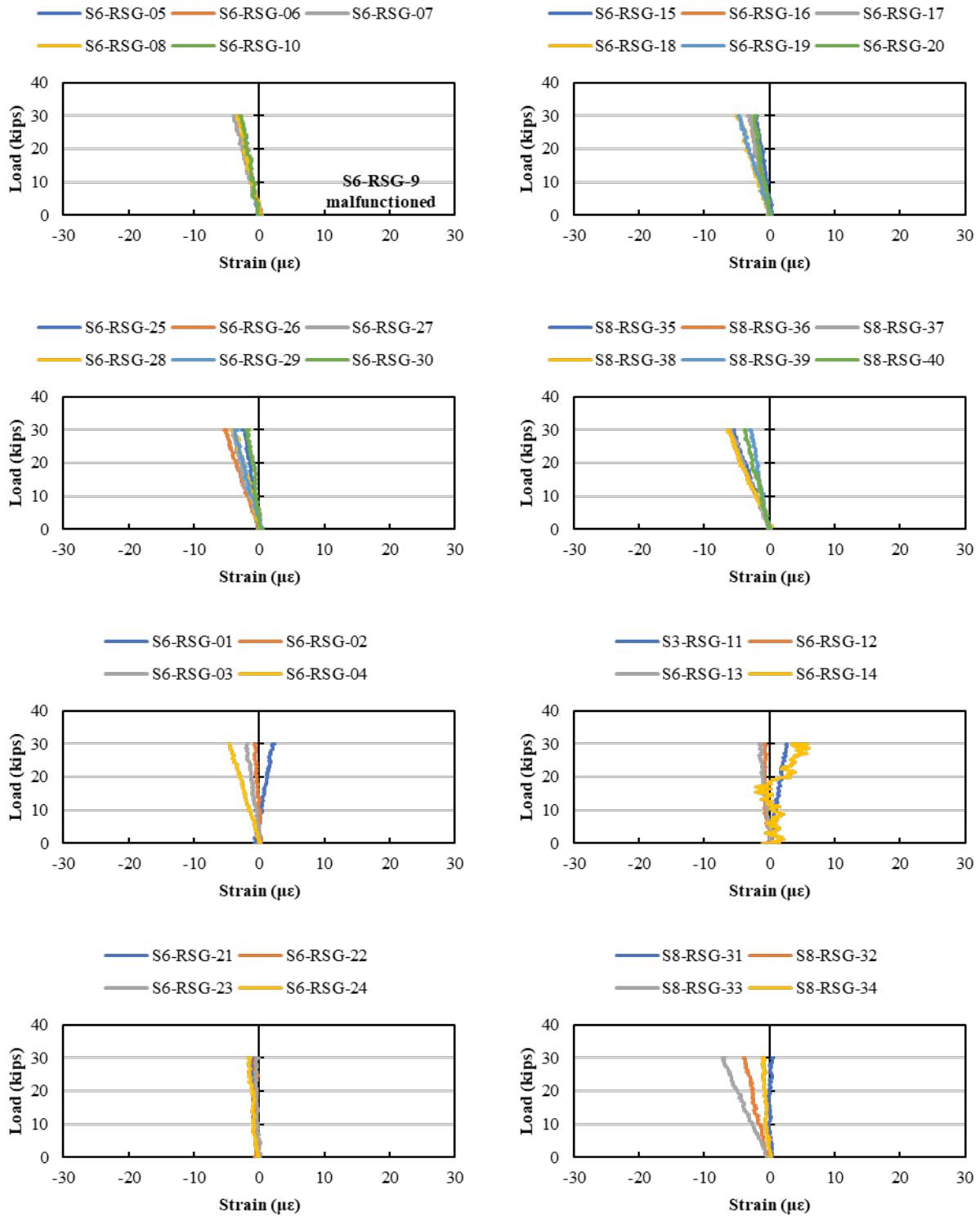


Figure F.47: Load versus rebar strain (measured by RSGs) for Load Stage 5, LC 4-4

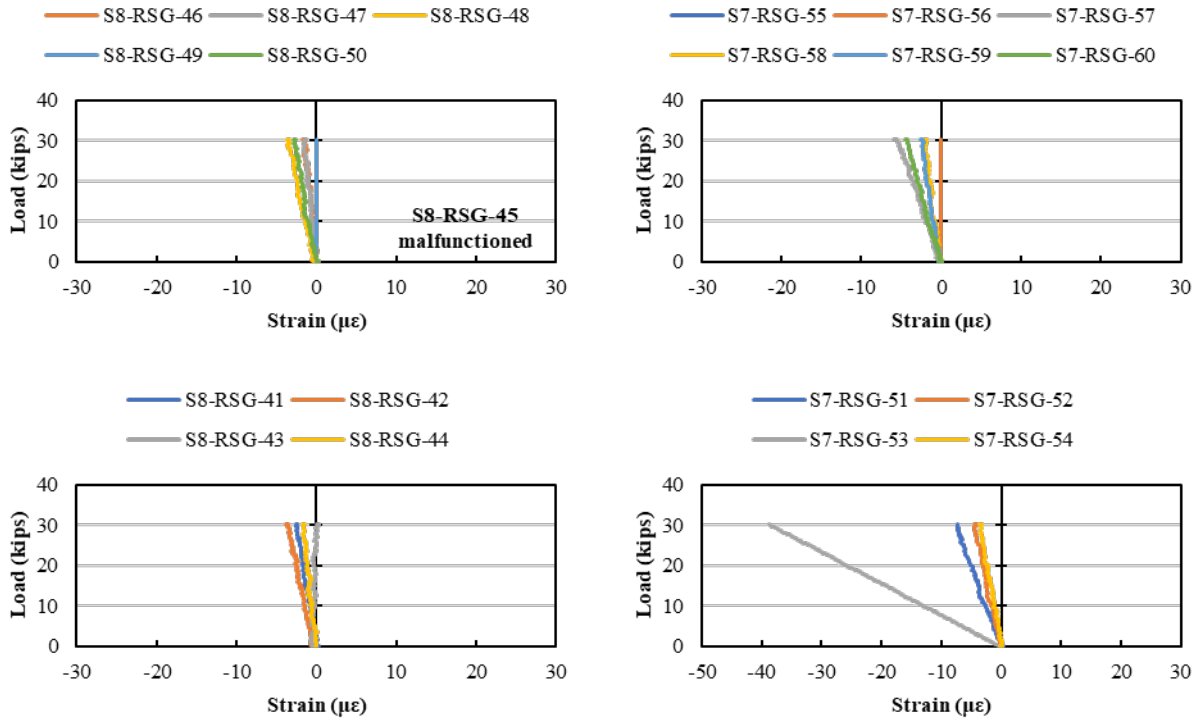


Figure F.48: Load versus rebar strain (measured by RSGs) for Load Stage 5, LC 4-4 (cont.)

F.12. LOAD STAGE 6 AND 7

The fatigue response from all sensors is summarized in this section.

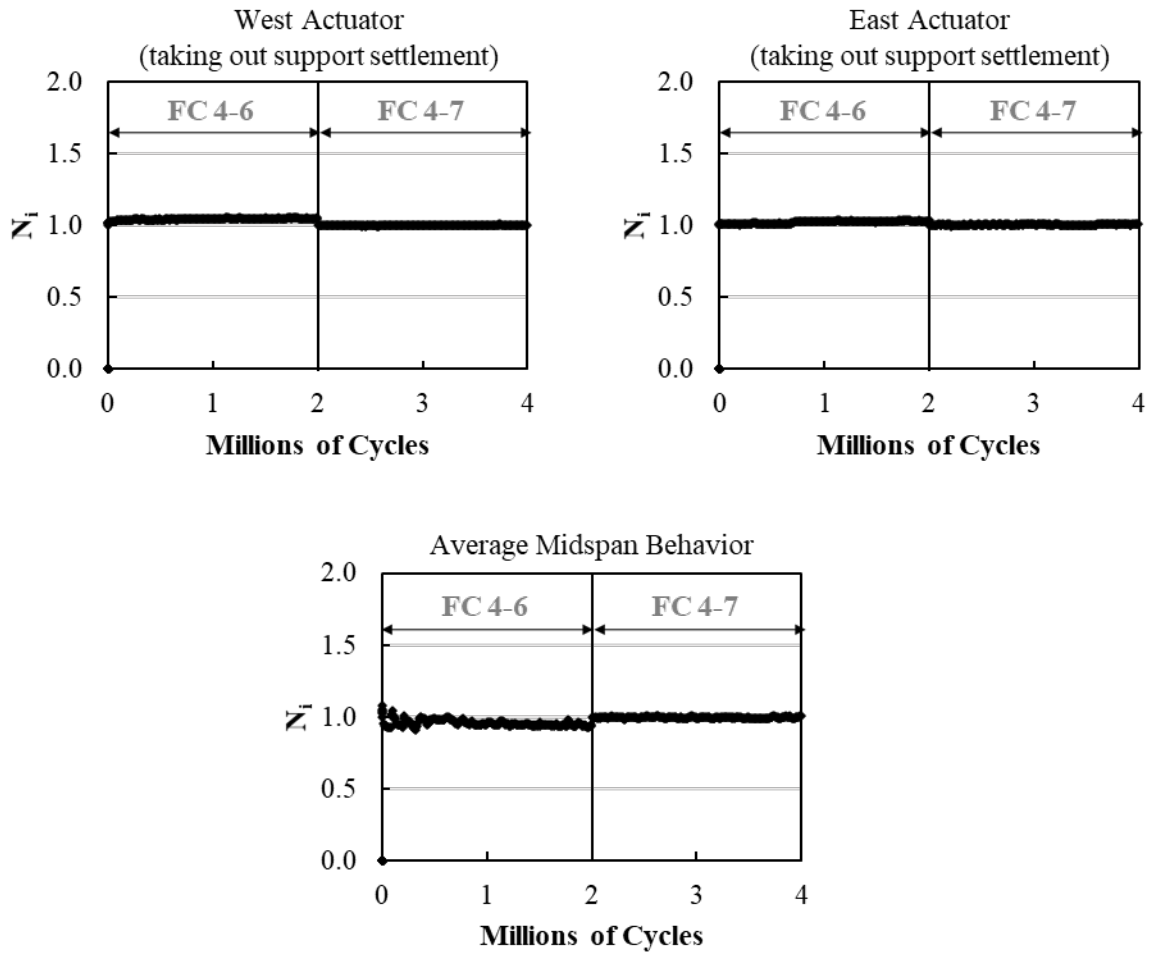


Figure F.49: Normalized Stiffness at midspan for west and east actuators and average system response for FC 4-6 and FC 4-7

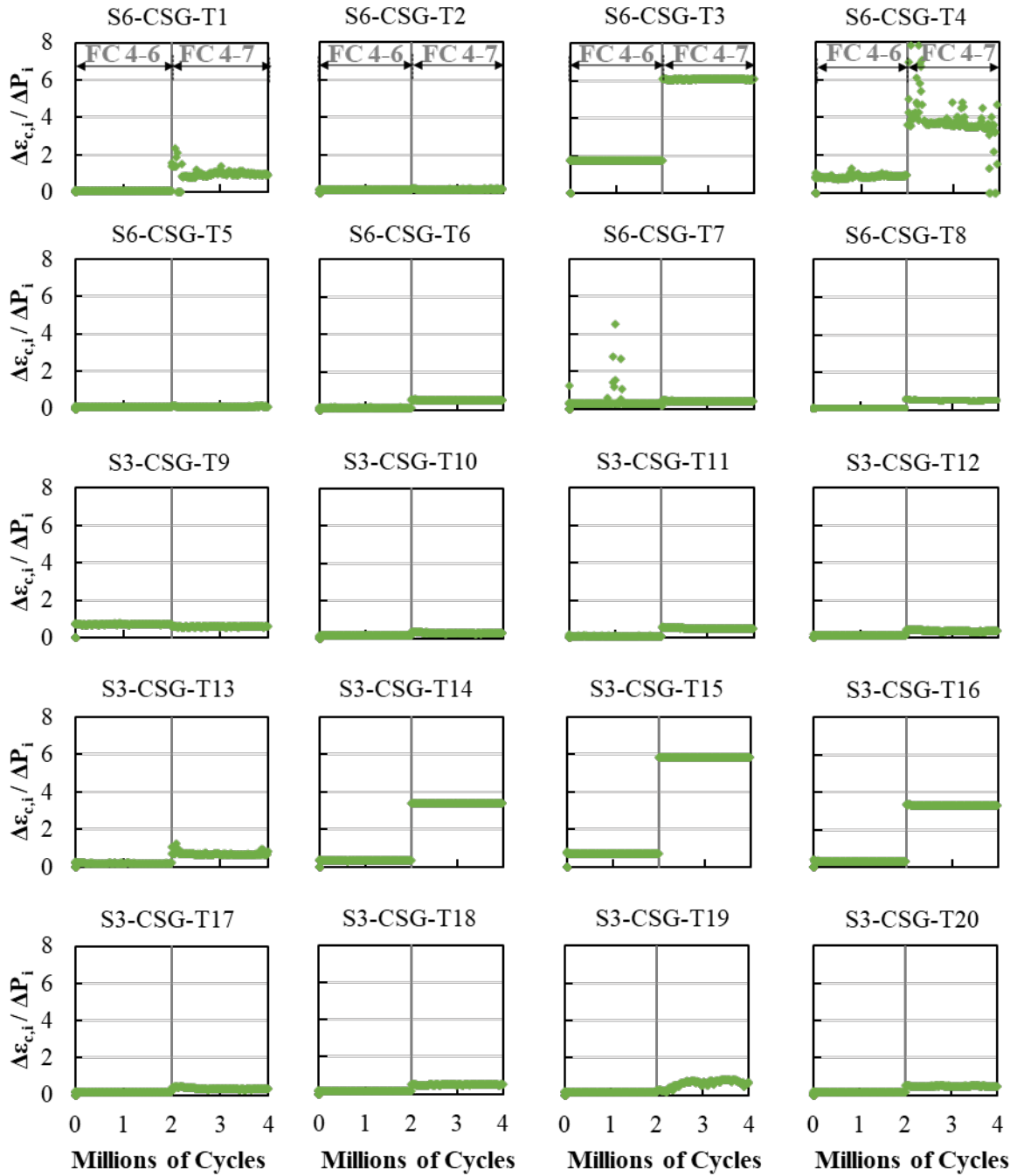


Figure F.50: Top concrete strain change per change in load versus number of cycles

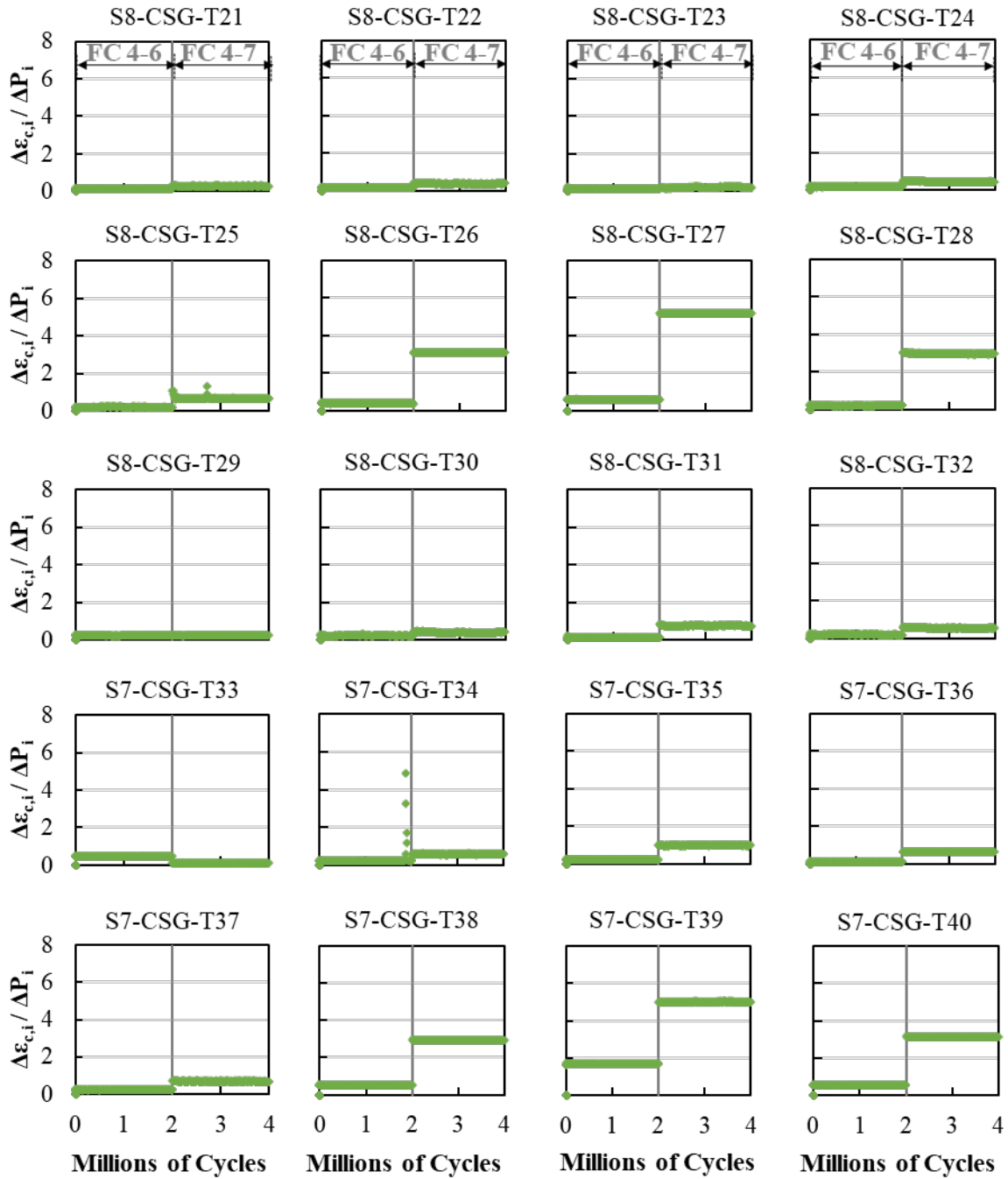


Figure F.51: Top concrete strain change per change in load versus number of cycles (cont.)

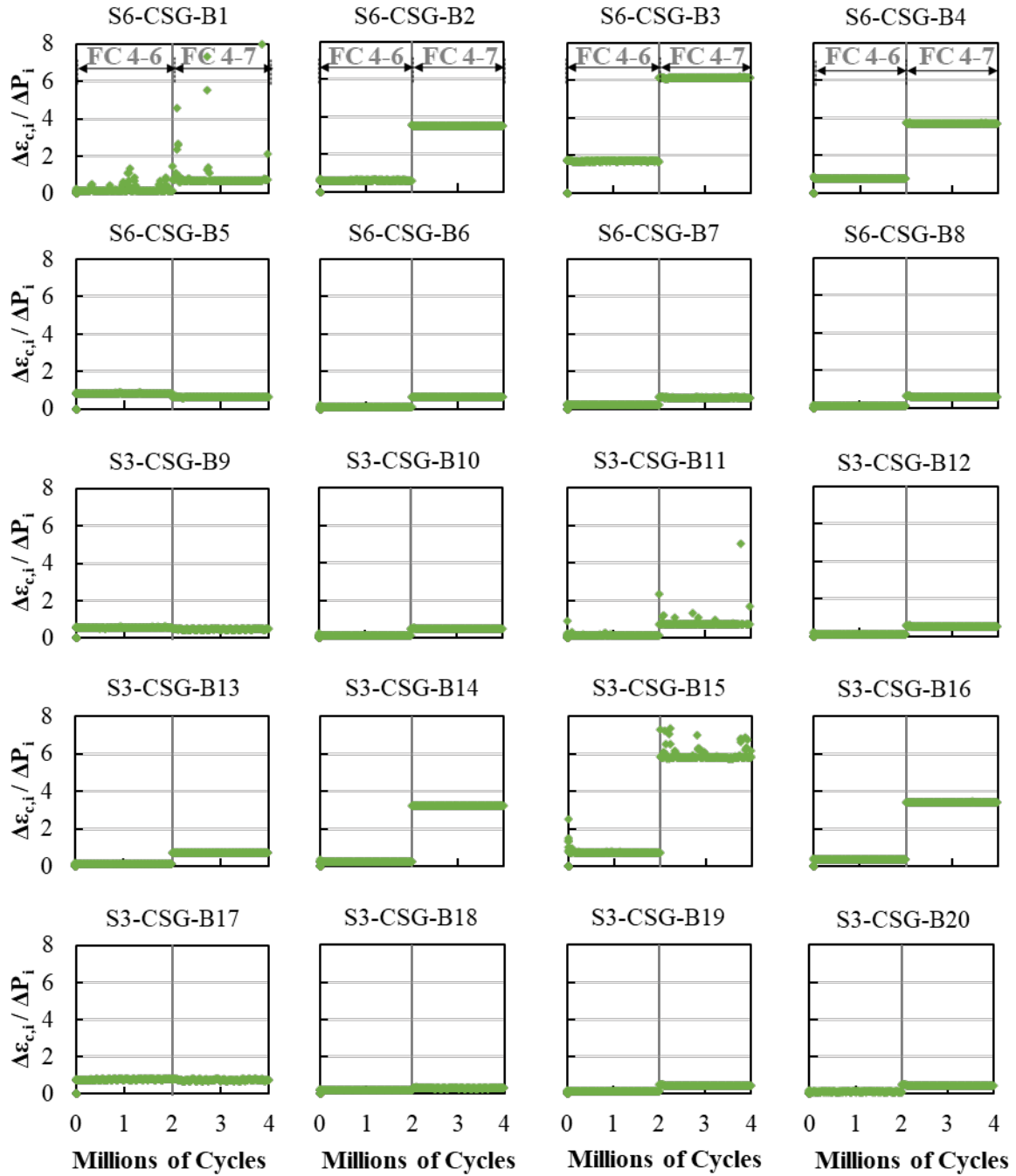


Figure F.52: Bottom concrete strain change per change in load versus number of cycles

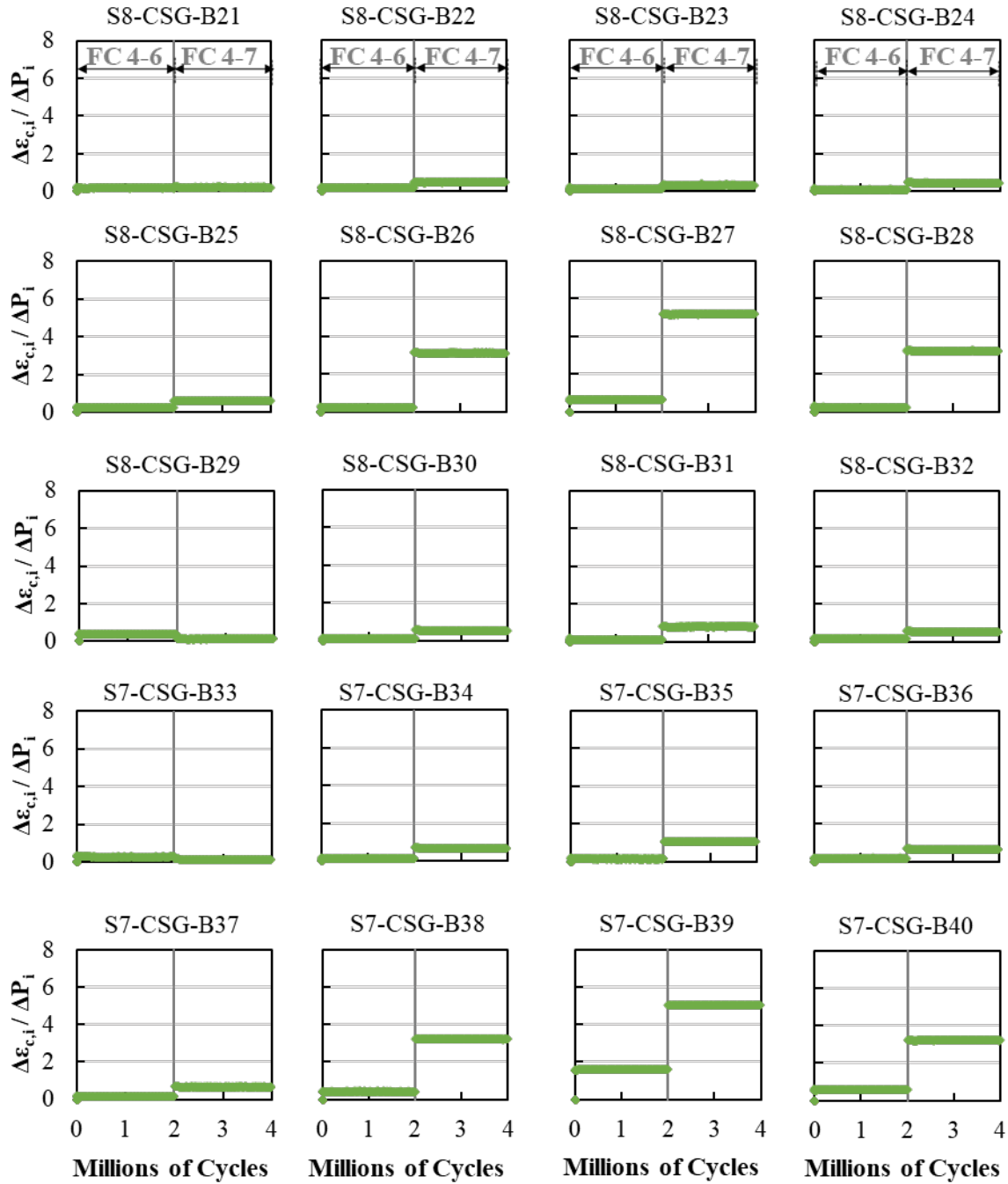


Figure F.53: Bottom concrete strain change per change in load versus number of cycles (cont.)

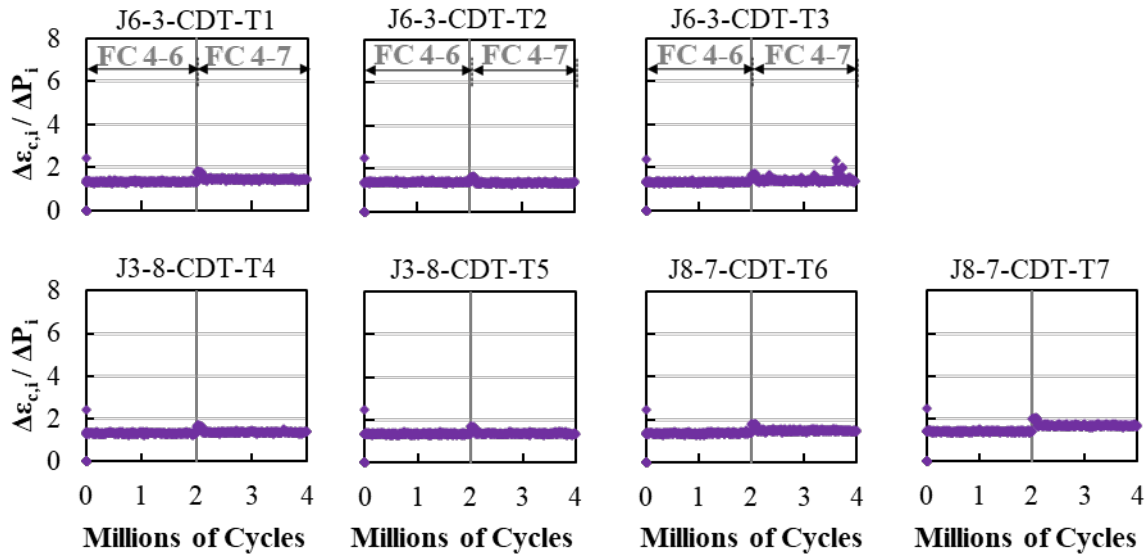


Figure F.54: Top crack gage strain change per change in load versus number of cycles

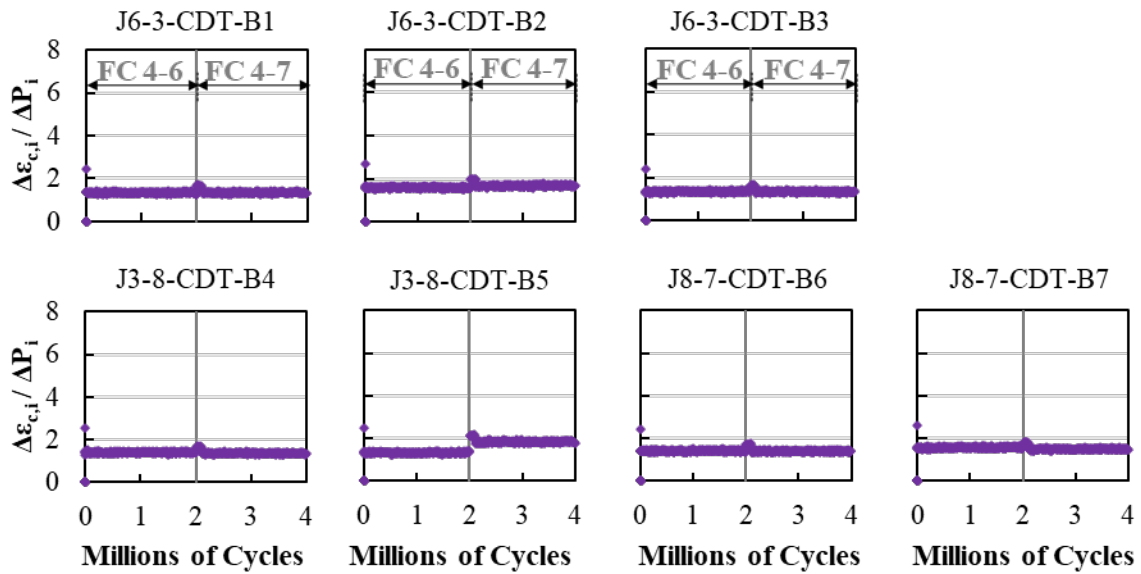


Figure F.55: Bottom crack gage strain change per change in load versus number of cycles

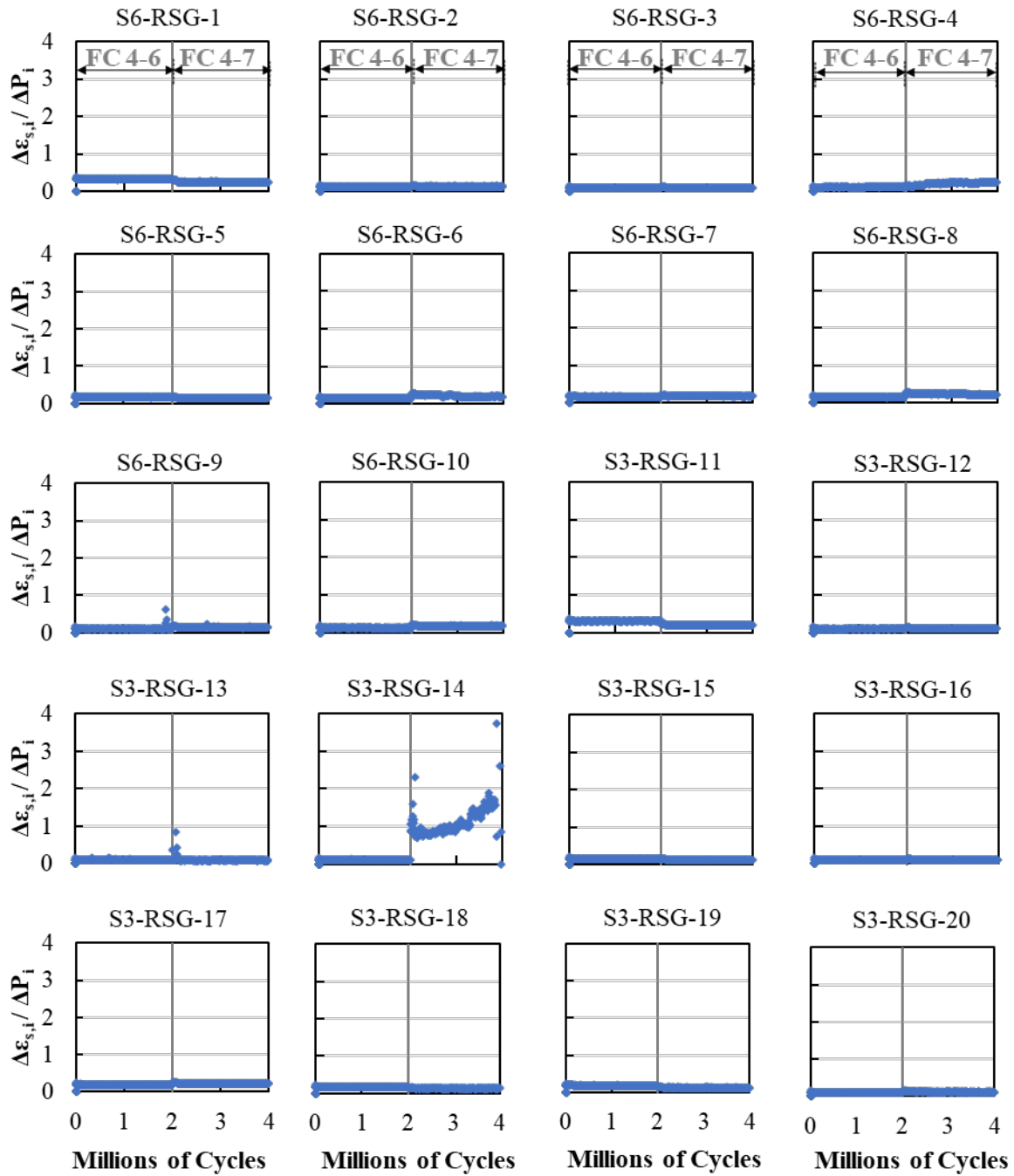


Figure F.56: Rebar strain change per change in load versus number of cycles for Joint 6-3 reinforcement

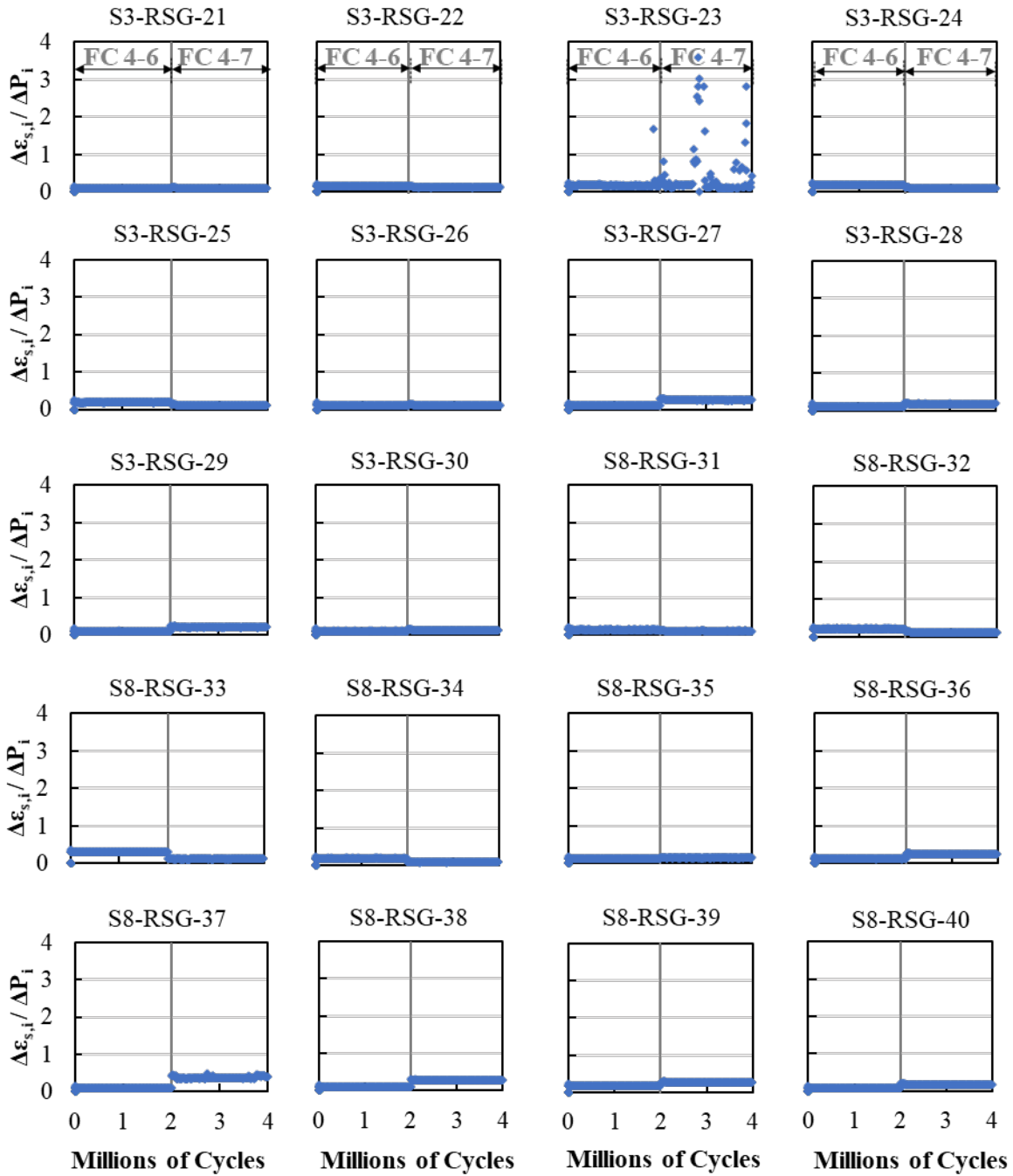


Figure F.57: Rebar strain change per change in load versus number of cycles for Joint 3-8 reinforcement

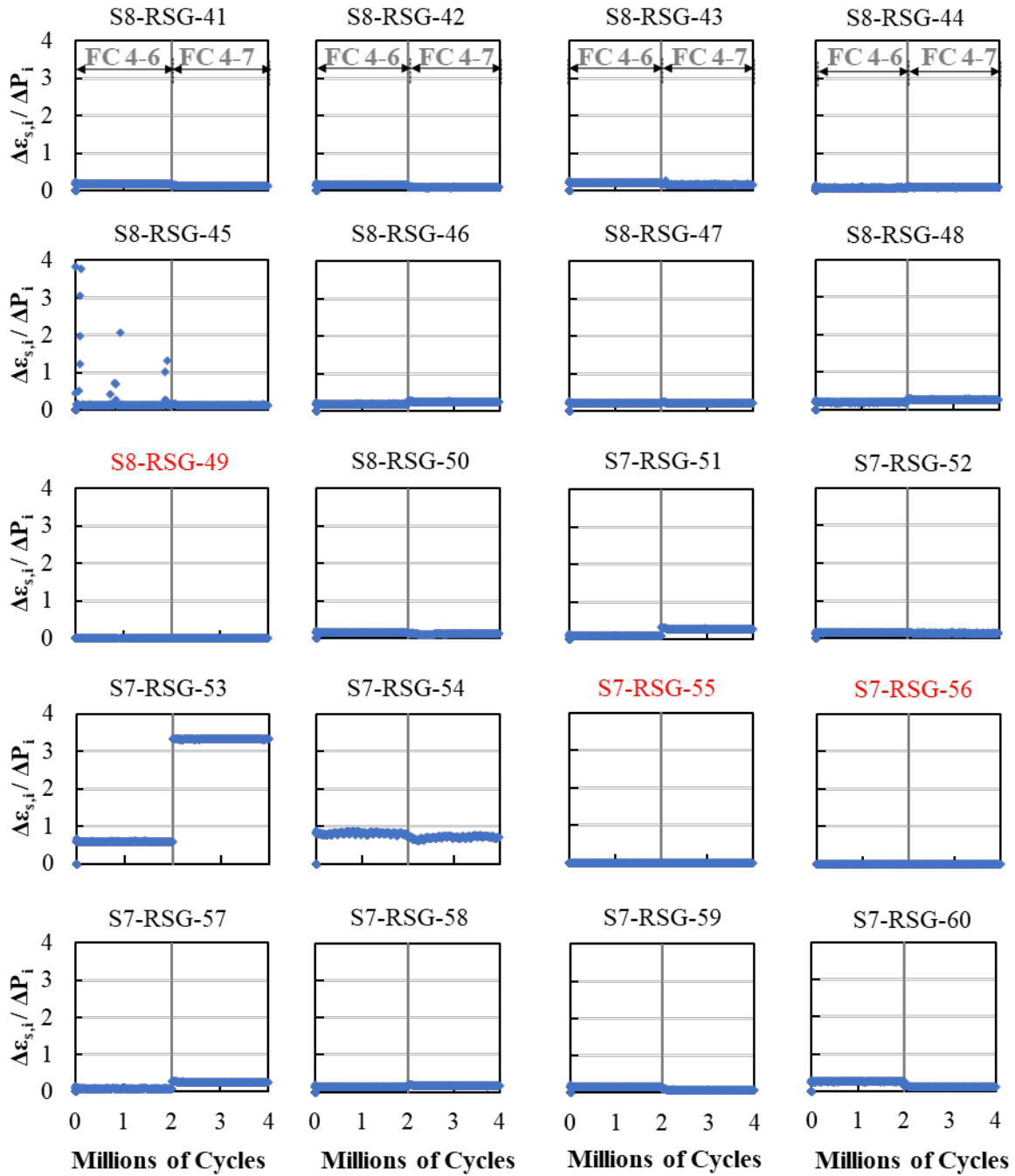


Figure F.58: Rebar strain change per change in load versus number of cycles for Joint 8-7 reinforcement (RSG-49, RSG-55, and RSG-56 malfunctioned)

F.13. LOAD STAGE 8 – LOAD CONFIGURATION 4-1

The response from all instrumentation for Load Stage 8 with Load Configuration 4-1 are shown in this section.

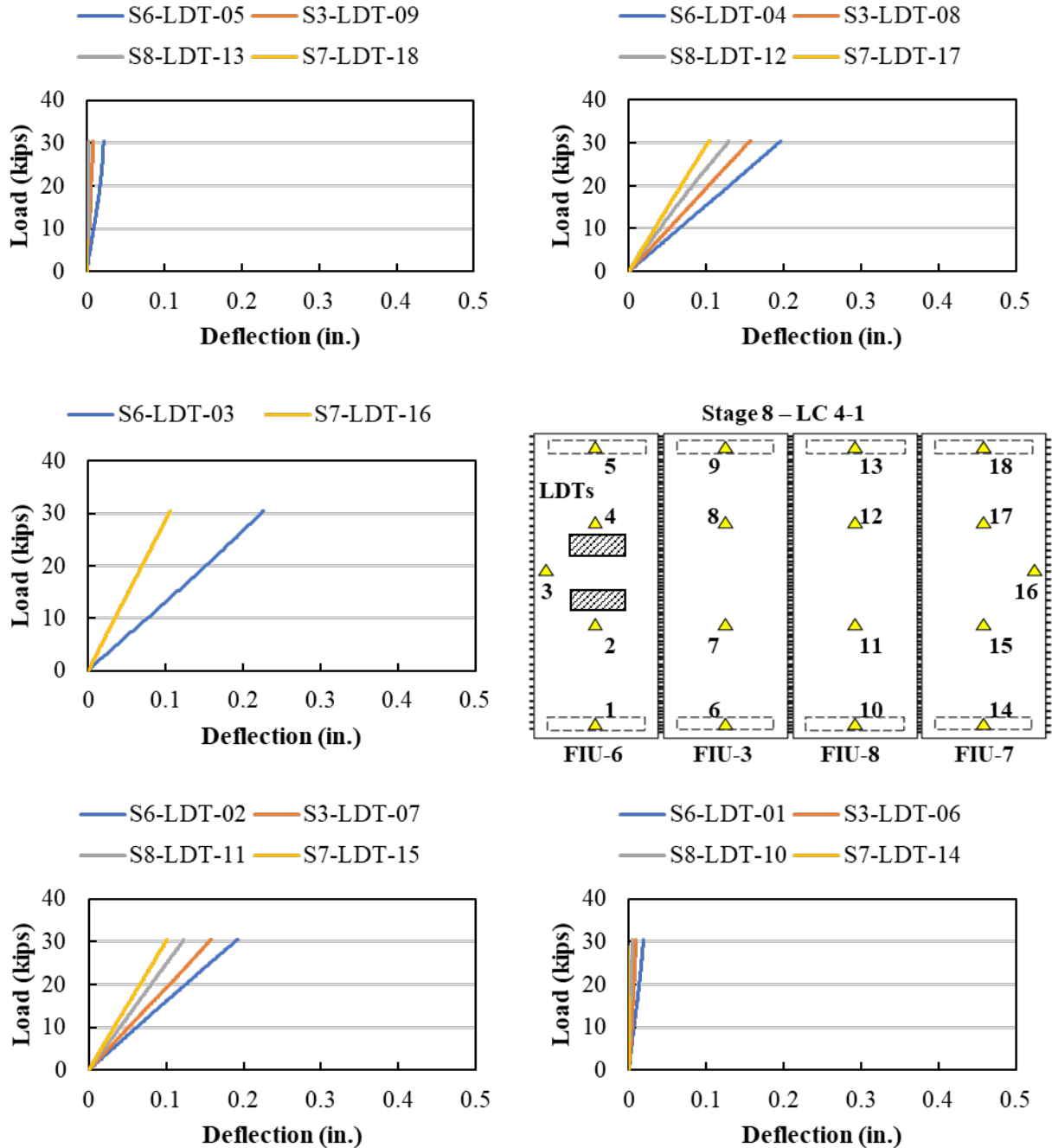


Figure F.59: Load versus displacement measured using LDTs for Load Stage 8, LC 4-1

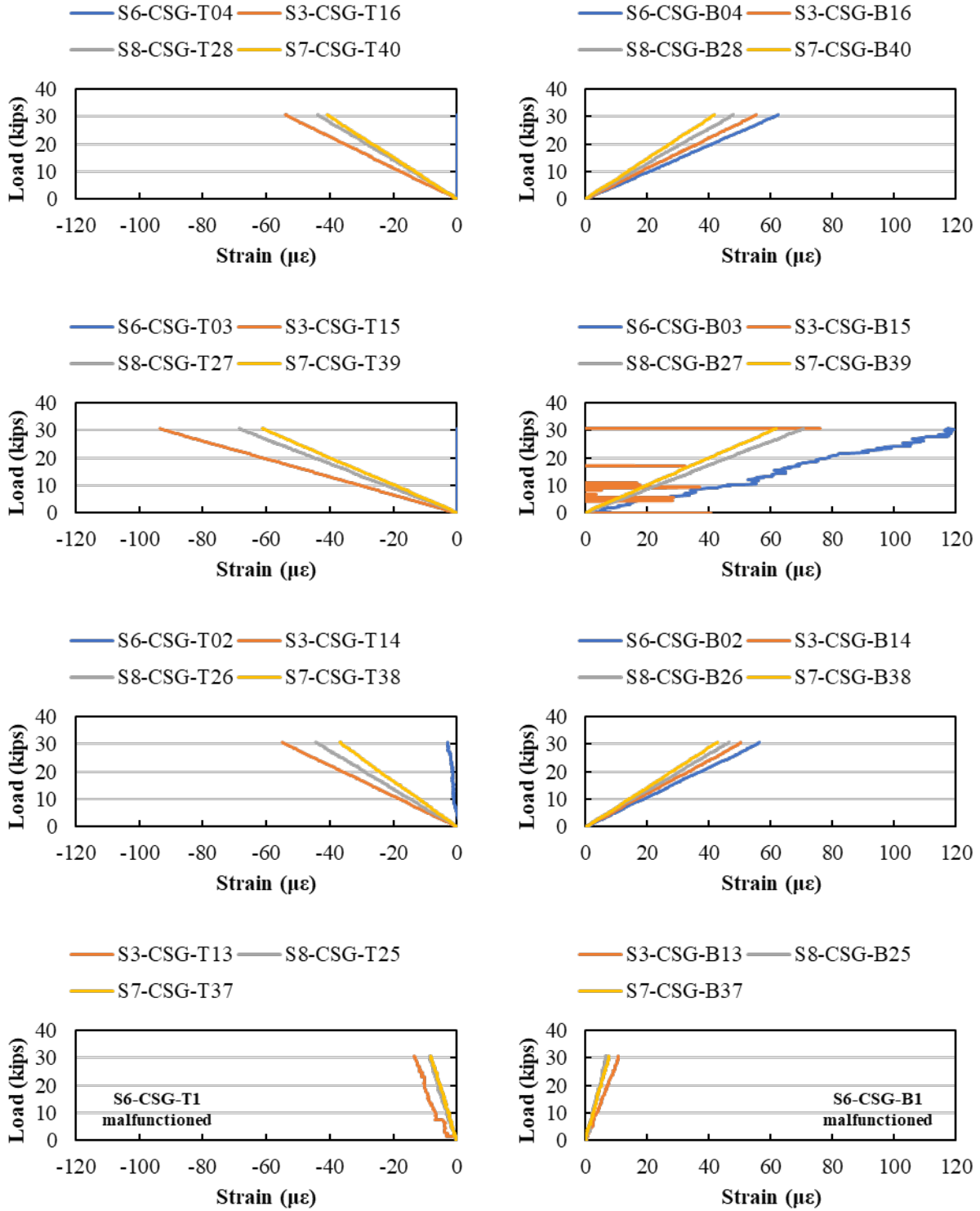


Figure F.60: Load versus longitudinal strain (measured by CSGs) for Load Stage 8, LC 4-1

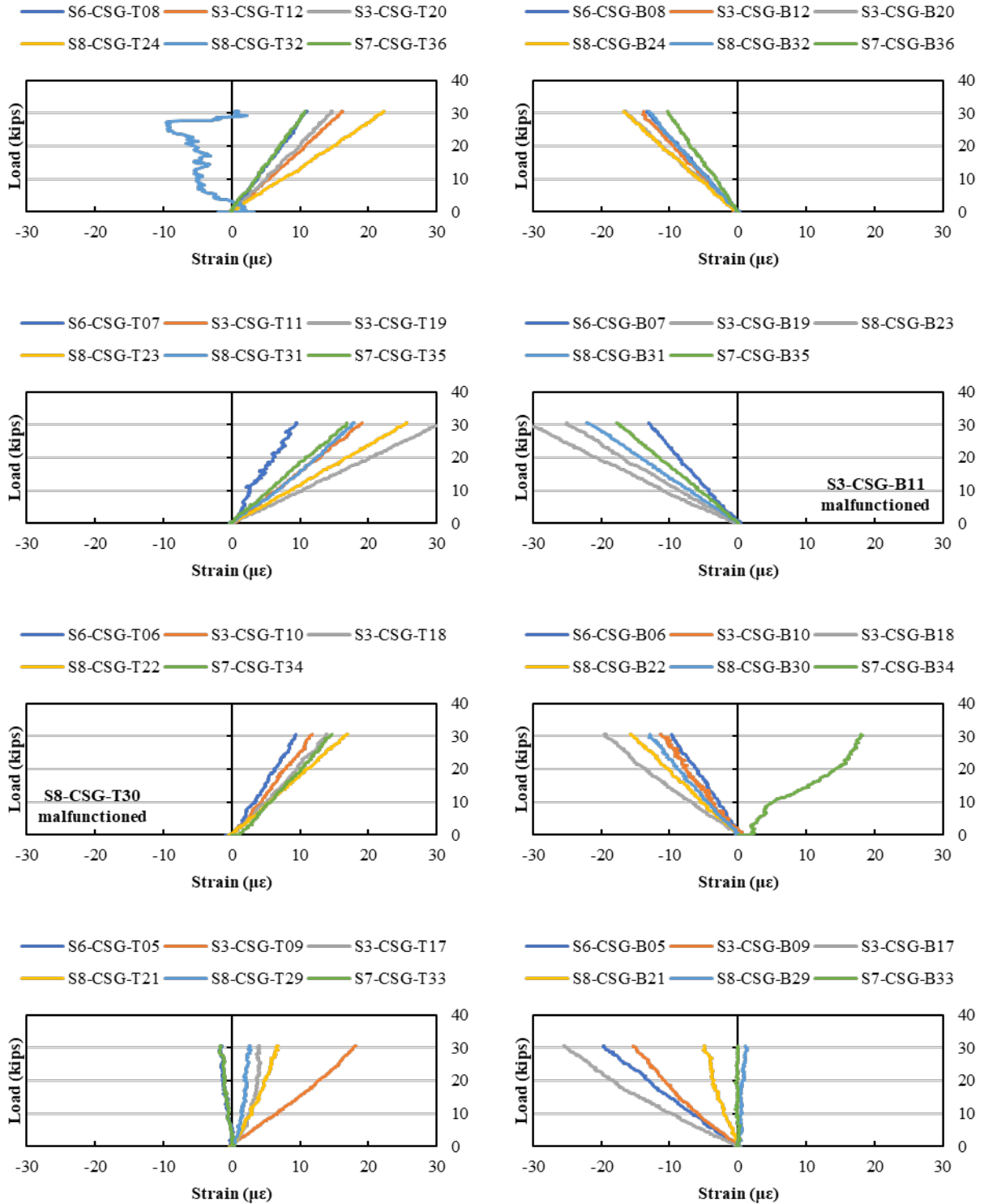


Figure F.61: Load versus transverse strain (measured by CSGs) for Load Stage 8, LC 4-1

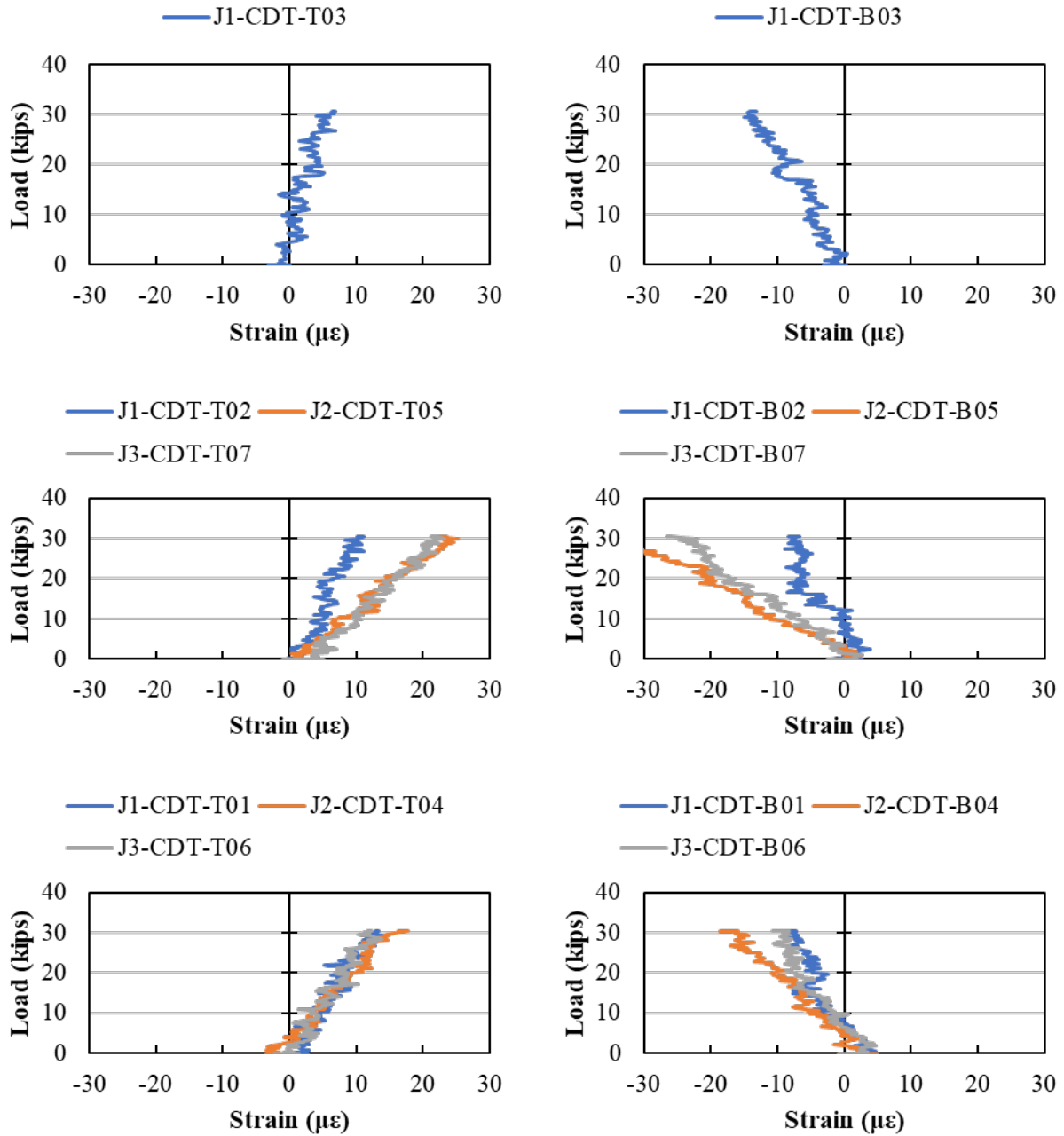


Figure F.62: Load versus average strain across the joints (measured by CDTs) for Load Stage 8, LC 4-1

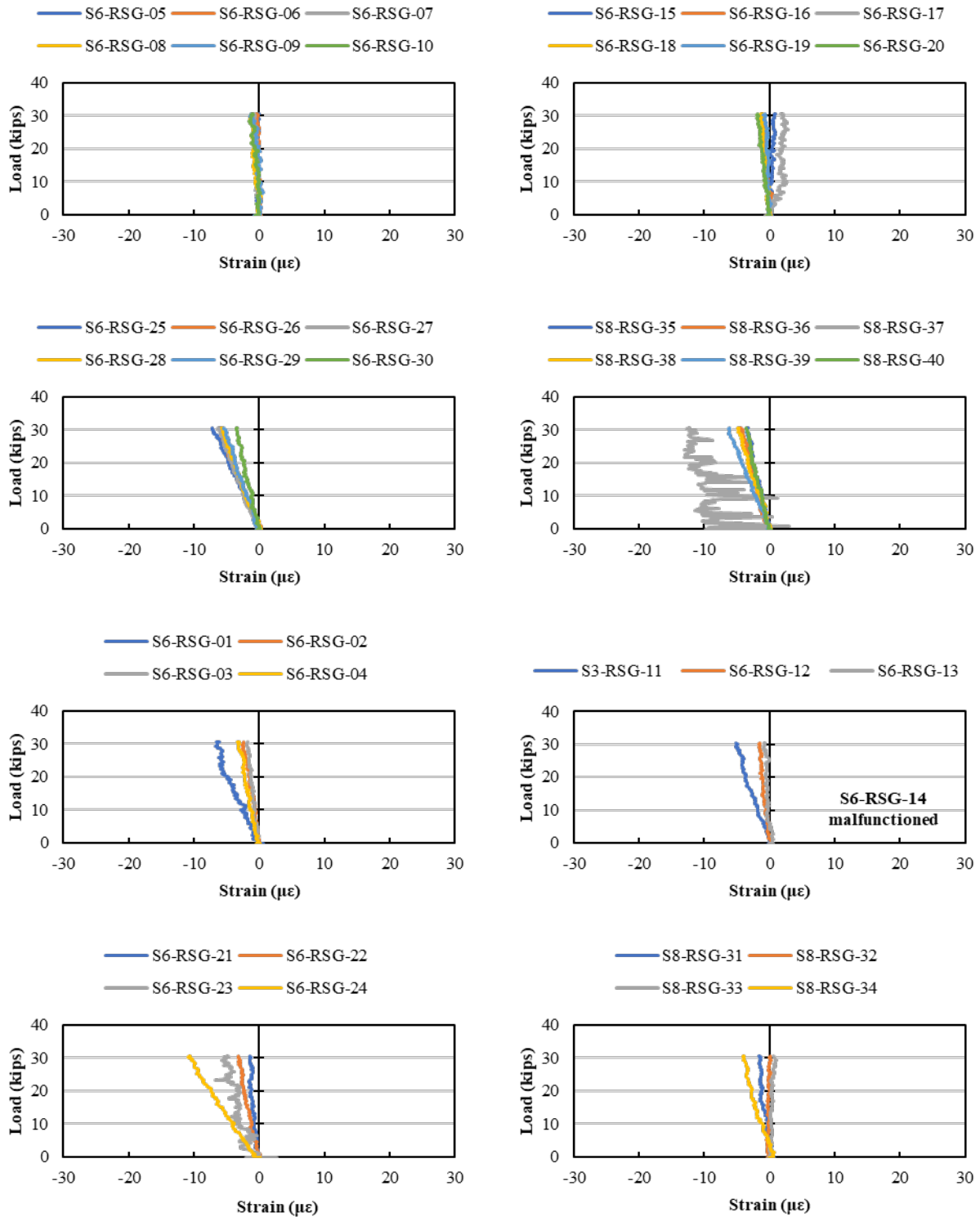


Figure F.63: Load versus rebar strain (measured by RSGs) for Load Stage 8, LC 4-1

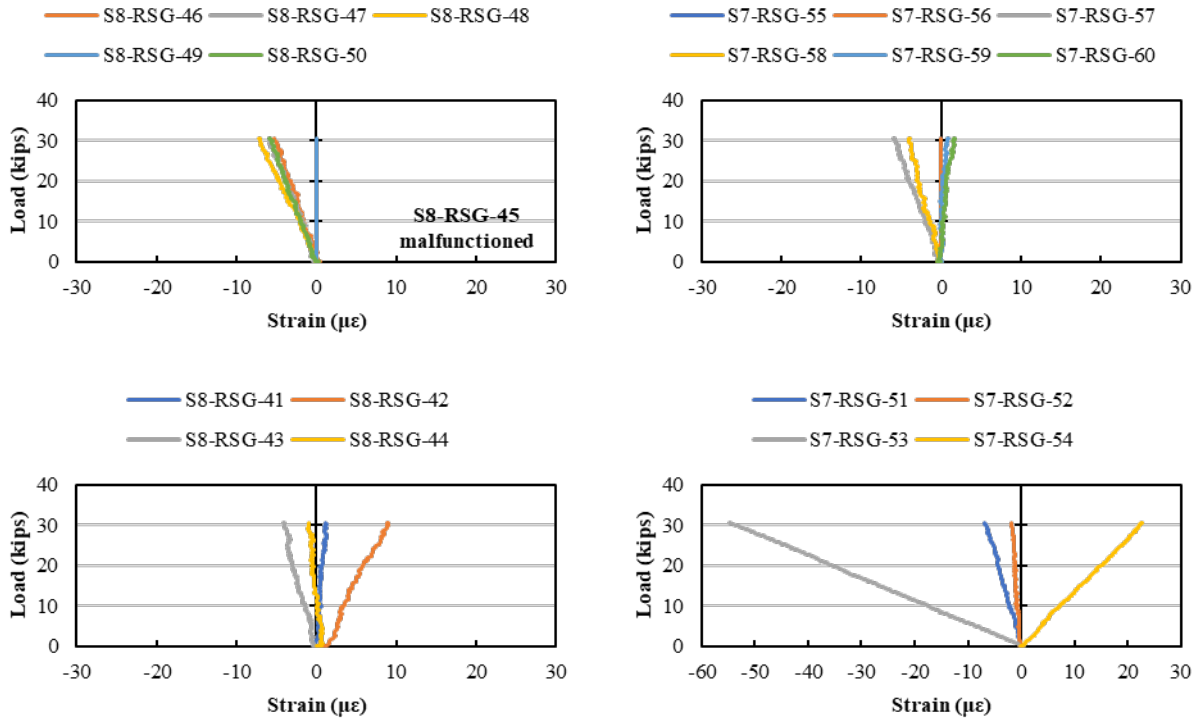


Figure F.64: Load versus rebar strain (measured by RSGs) for Load Stage 8, LC 4-1 (cont.)

F.14. LOAD STAGE 8 – LOAD CONFIGURATION 4-2

The response from all instrumentation for Load Stage 8 with Load Configuration 4-2 are shown in this section.

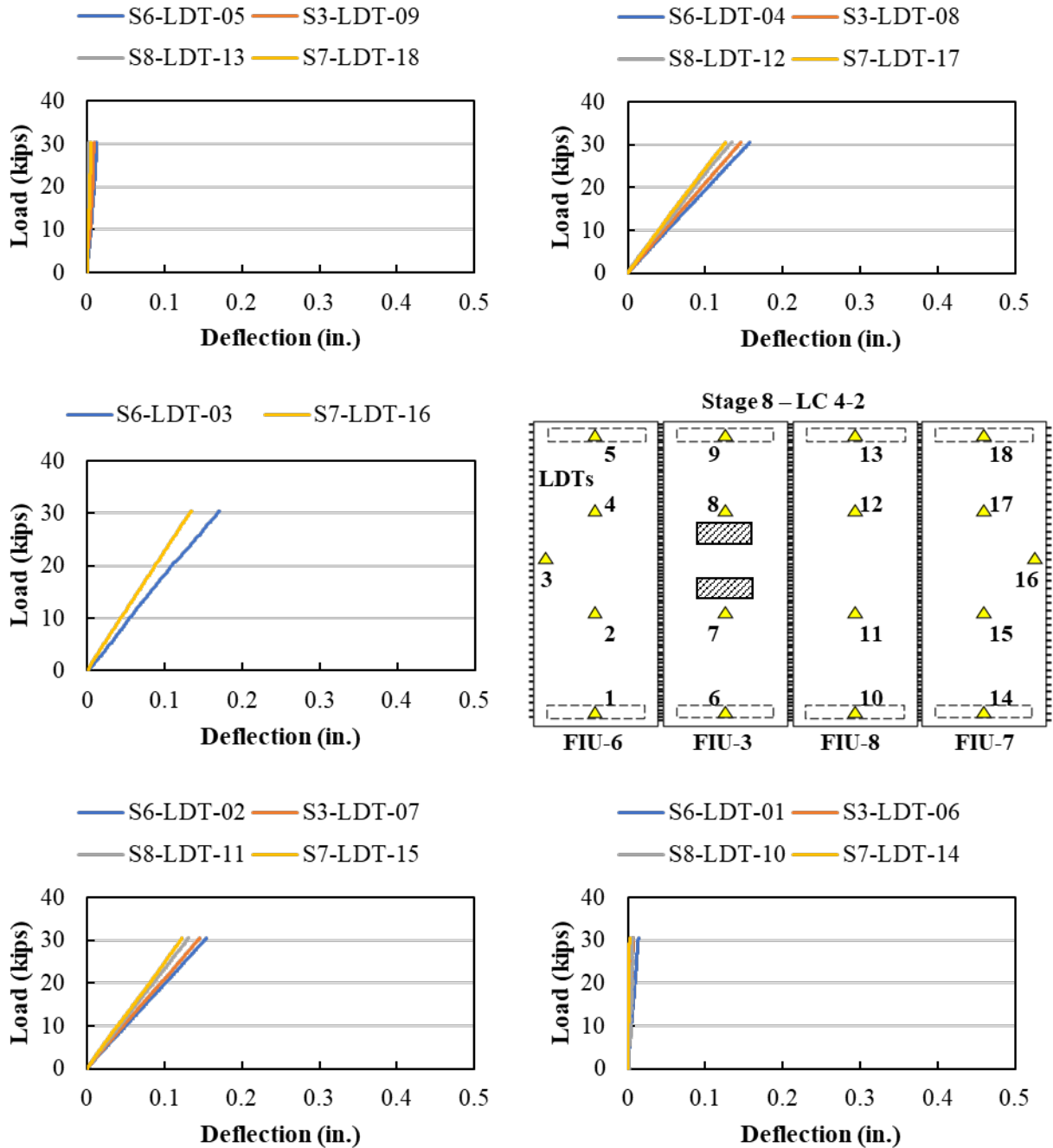


Figure F.65: Load versus displacement measured using LDTs for Load Stage 8, LC 4-2

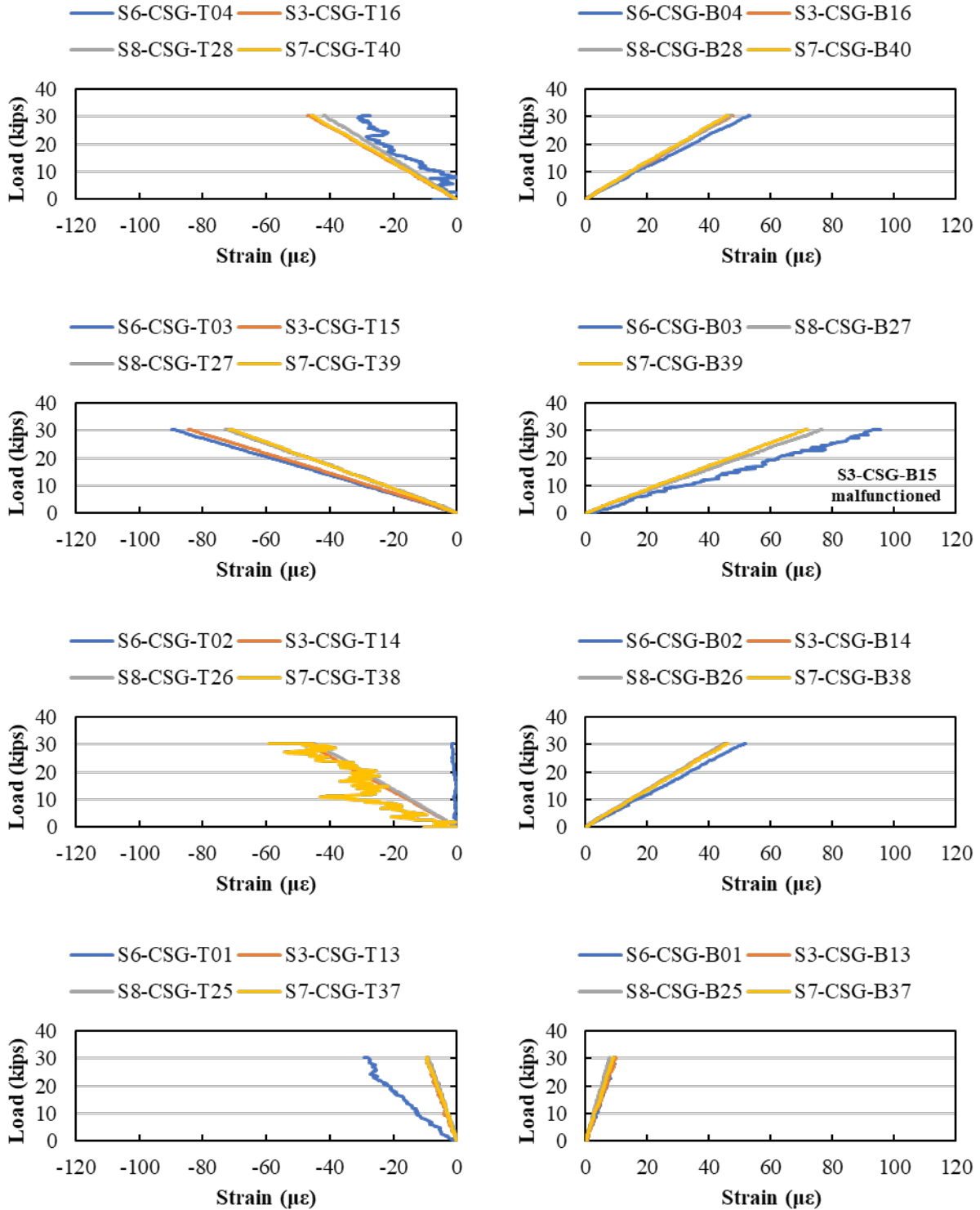


Figure F.66: Load versus longitudinal strain (measured by CSGs) for Load Stage 8, LC 4-2

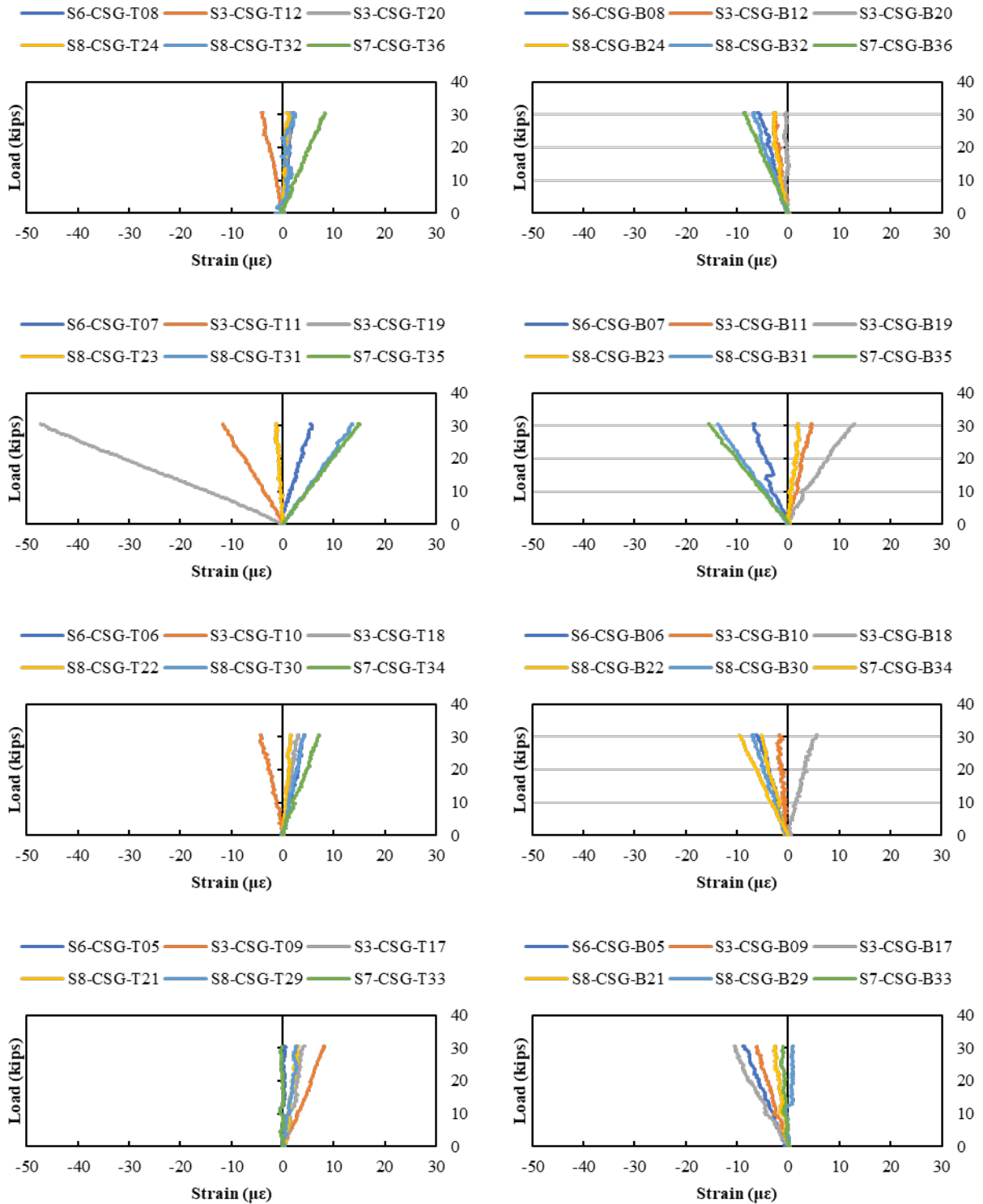


Figure F.67: Load versus transverse strain (measured by CSGs) for Load Stage 8, LC 4-2

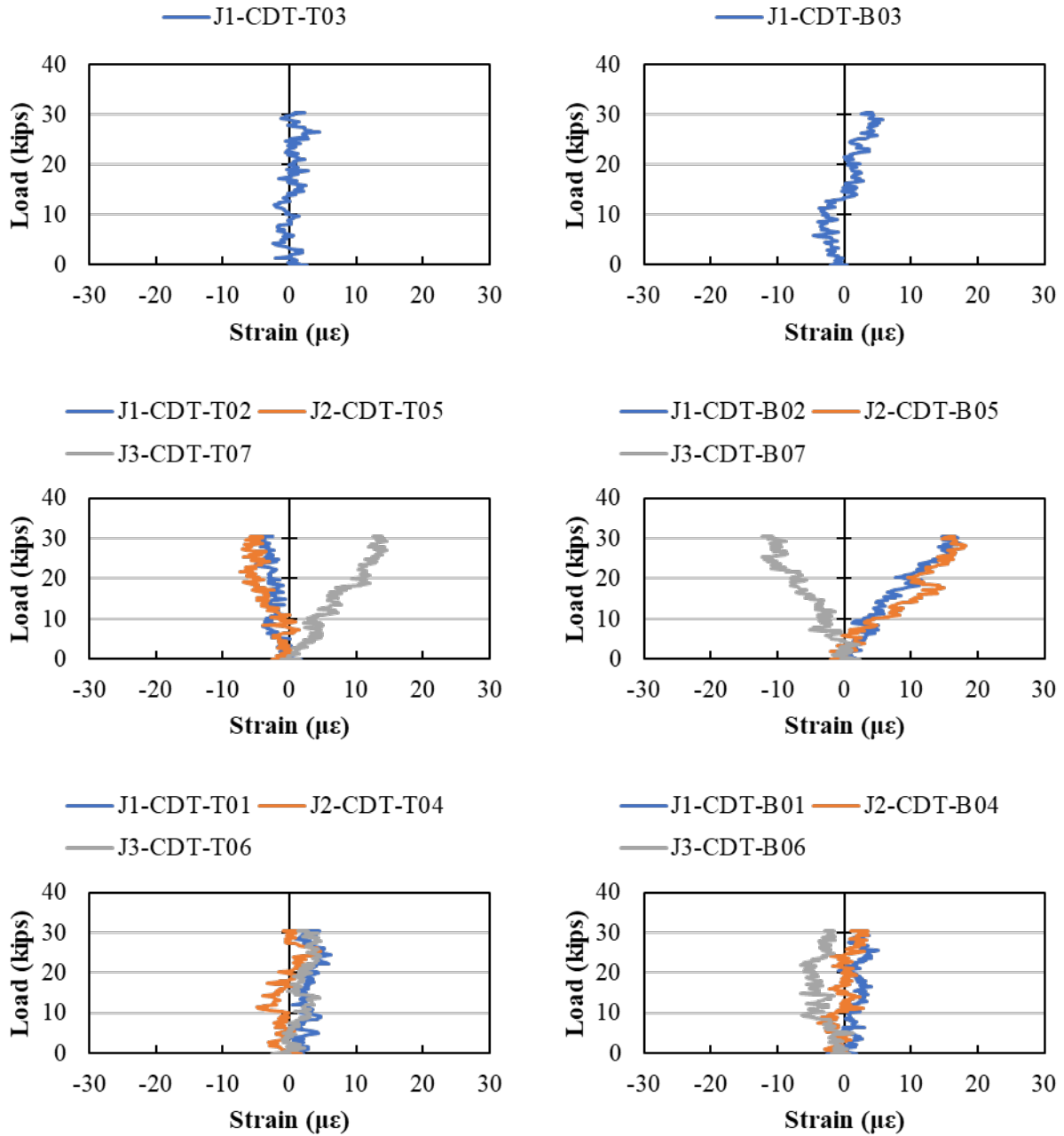


Figure F.68: Load versus average strain across the joints (measured by CDTs) for Load Stage 8, LC 4-2

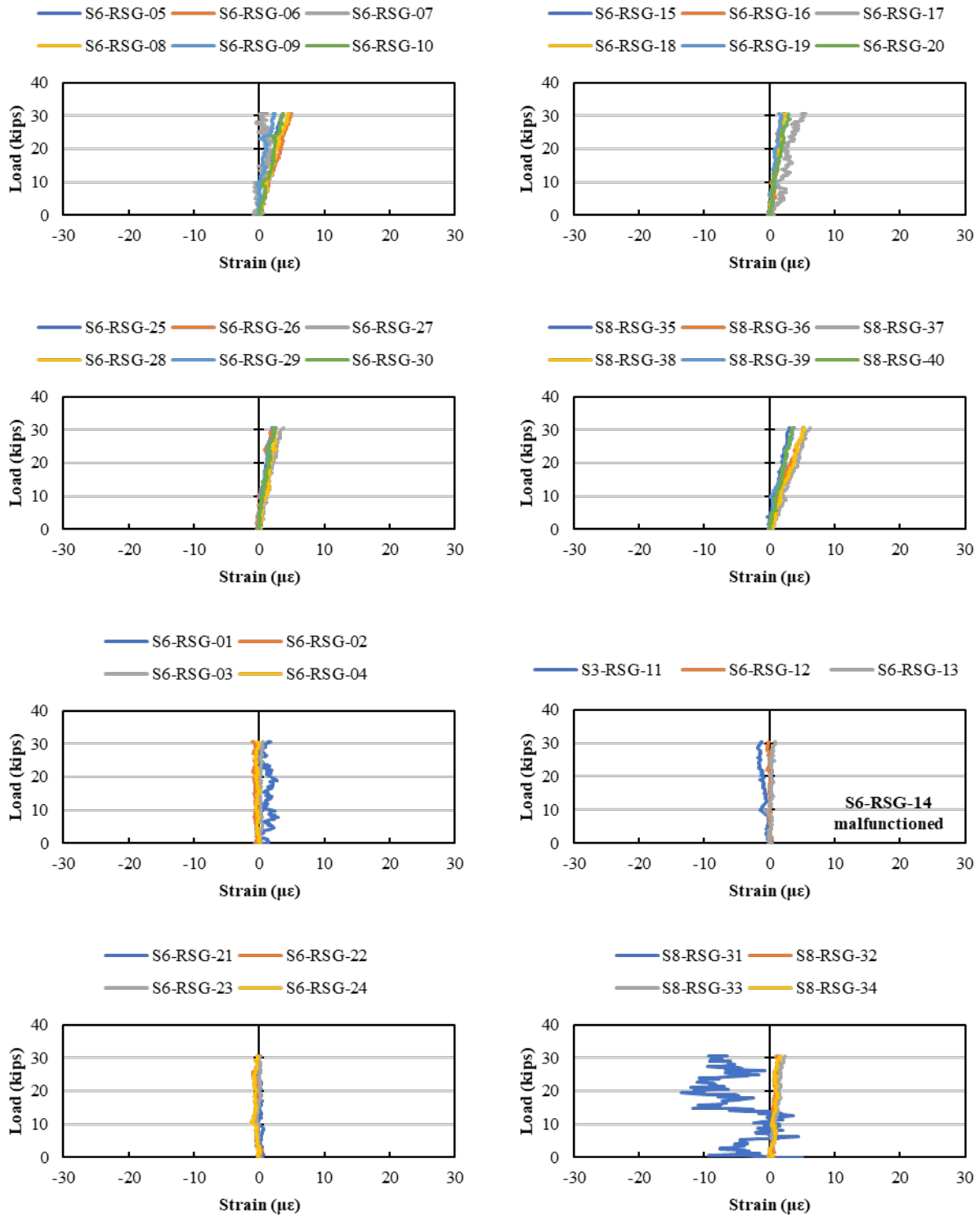


Figure F.69: Load versus rebar strain (measured by RSGs) for Load Stage 8, LC 4-2

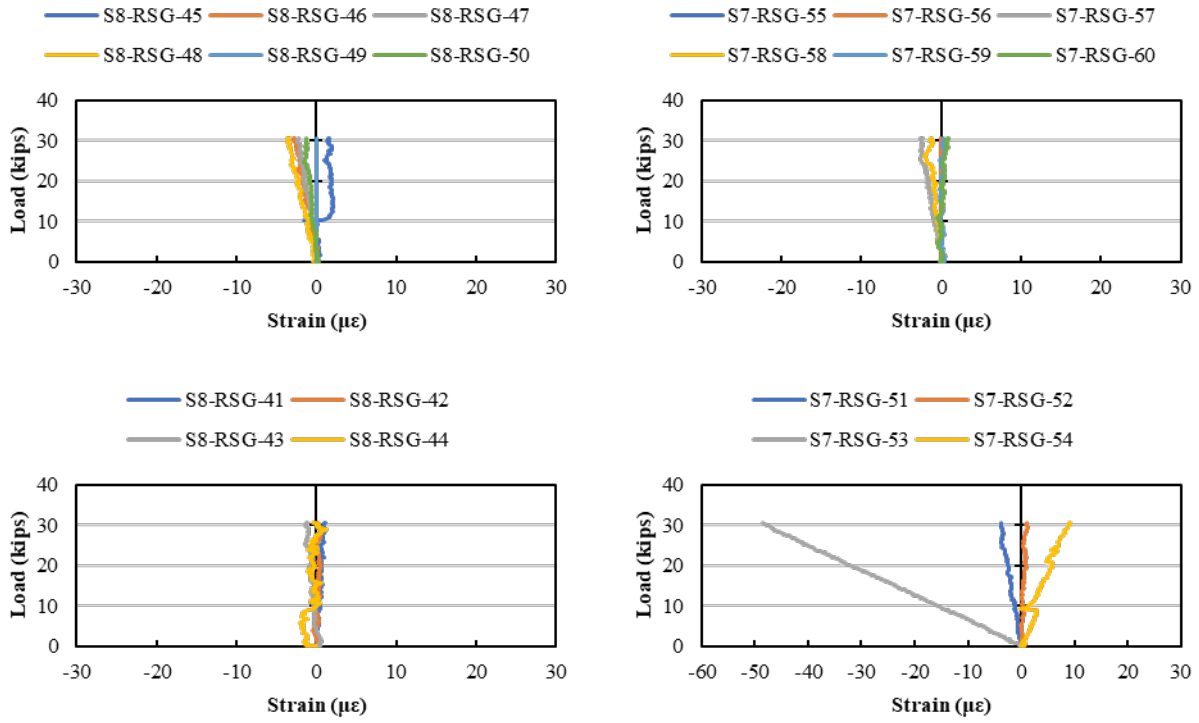


Figure F.70: Load versus rebar strain (measured by RSGs) for Load Stage 8, LC 4-2 (cont.)

F.15. LOAD STAGE 8 – LOAD CONFIGURATION 4-3

The response from all instrumentation for Load Stage 8 with Load Configuration 4-3 are shown in this section.

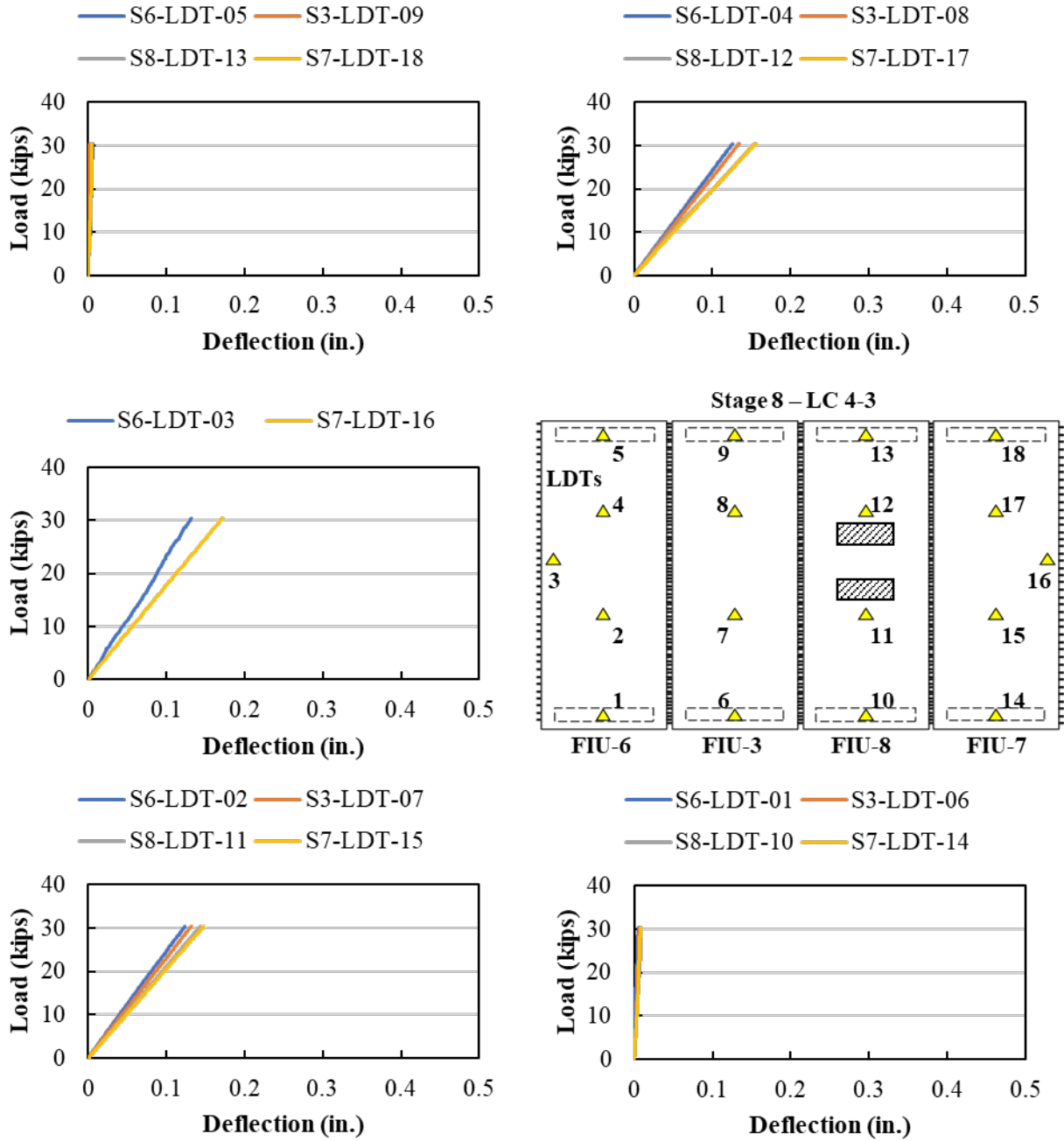


Figure F.71: Load versus displacement measured using LDTs for Load Stage 8, LC 4-3

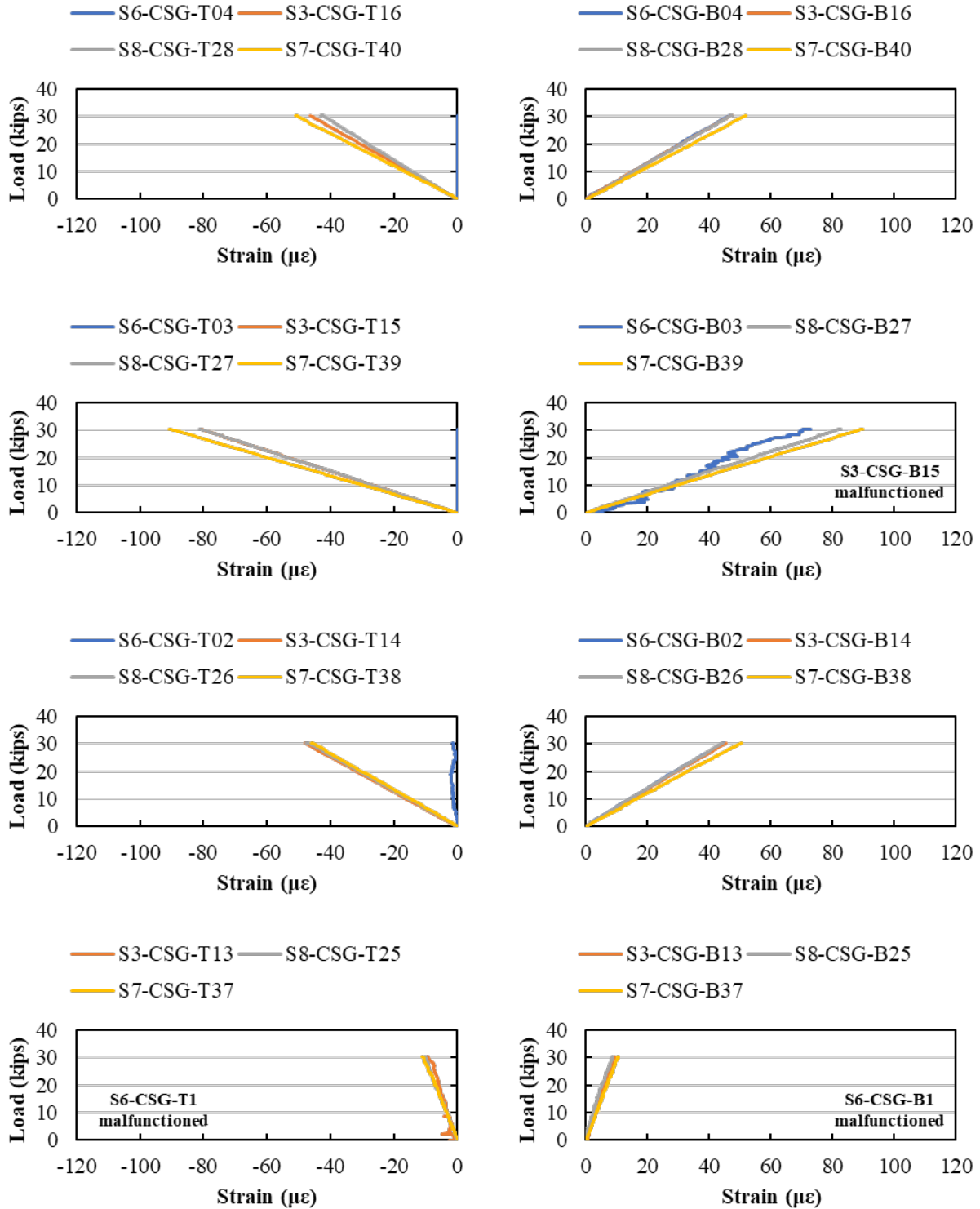


Figure F.72: Load versus longitudinal strain (measured by CSGs) for Load Stage 8, LC 4-3

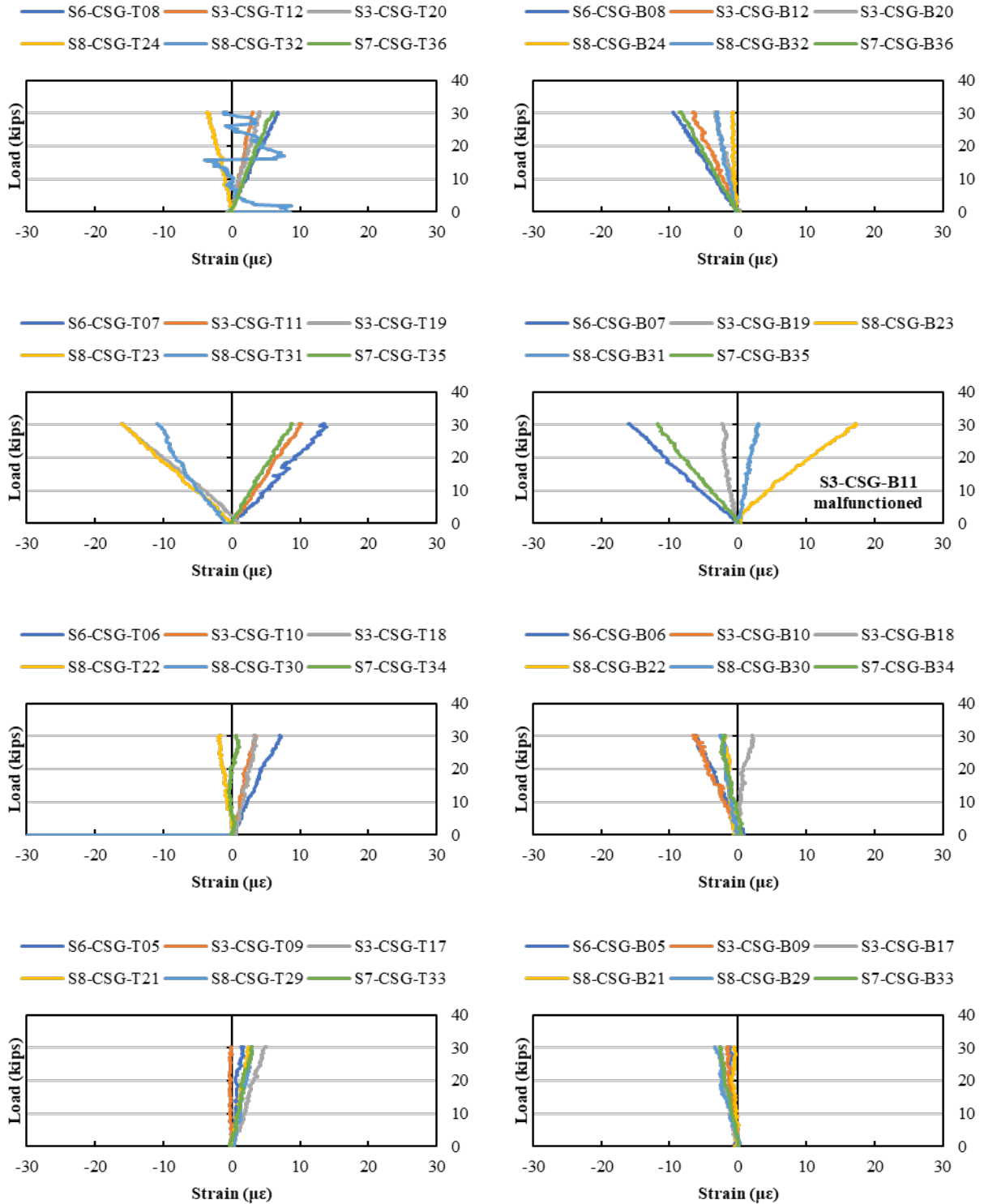


Figure F.73: Load versus transverse strain (measured by CSGs) for Load Stage 8, LC 4-3

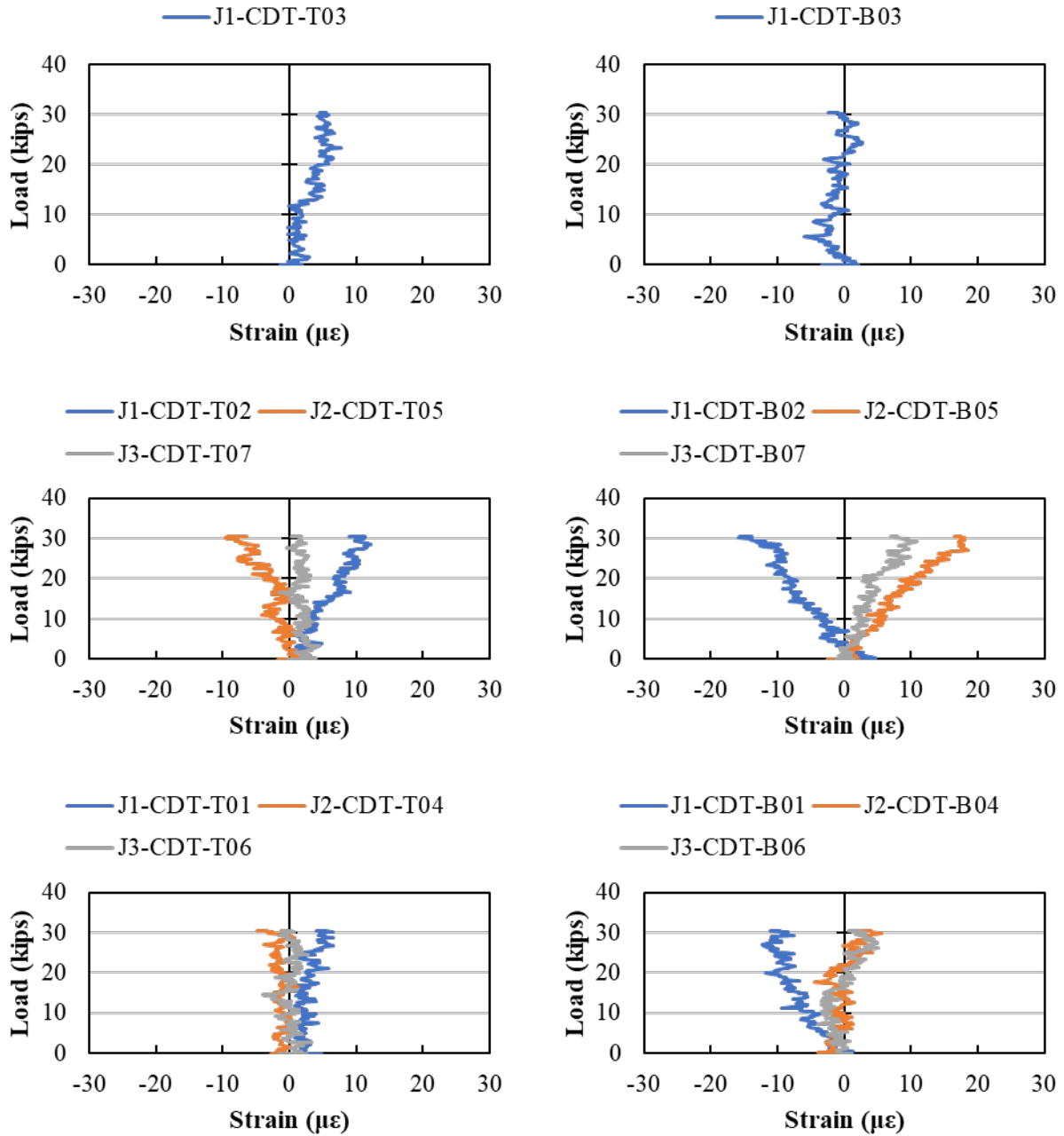


Figure F.74: Load versus average strain across the joints (measured by CDTs) for Load Stage 8, LC 4-3

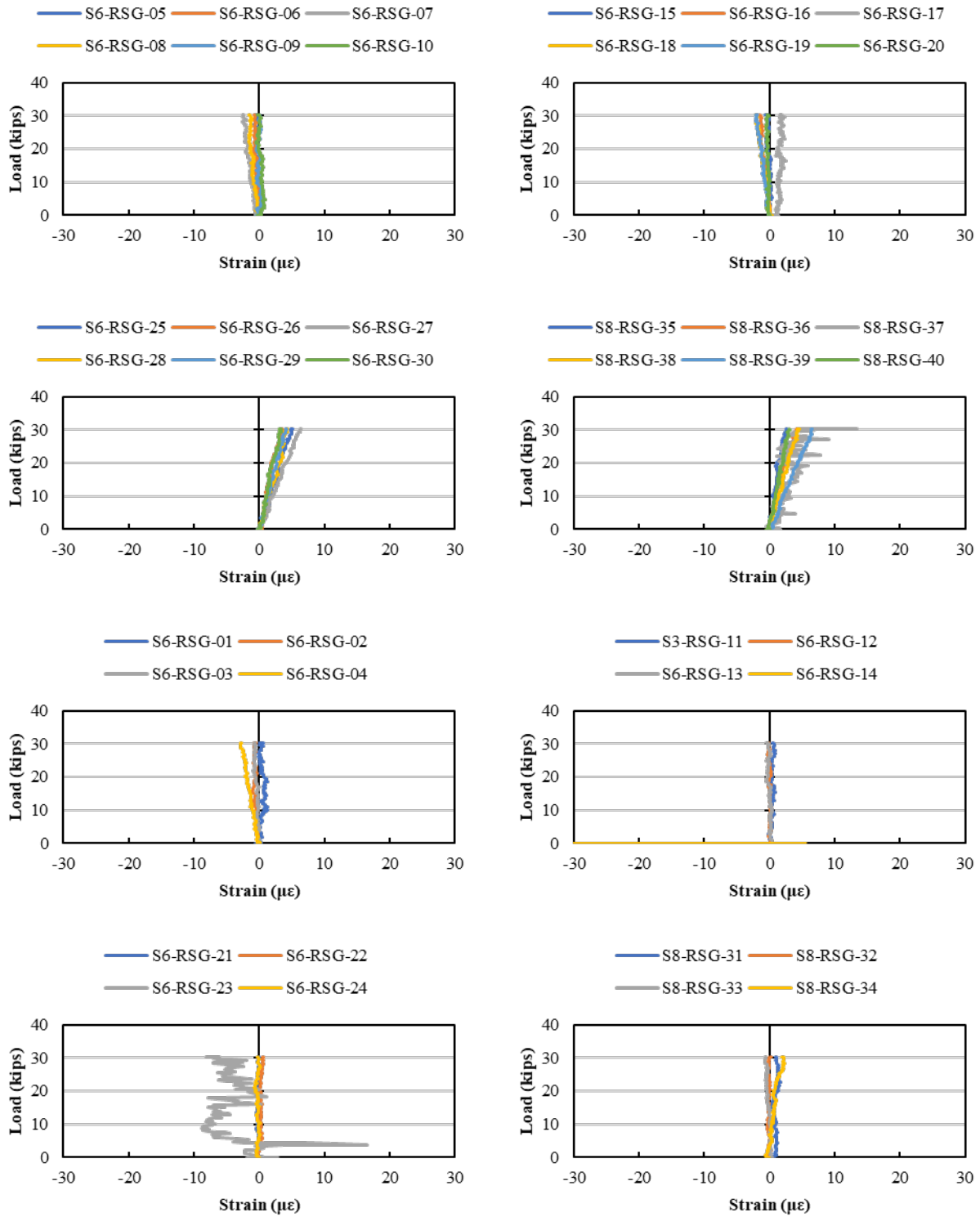


Figure F.75: Load versus rebar strain (measured by RSGs) for Load Stage 8, LC 4-3

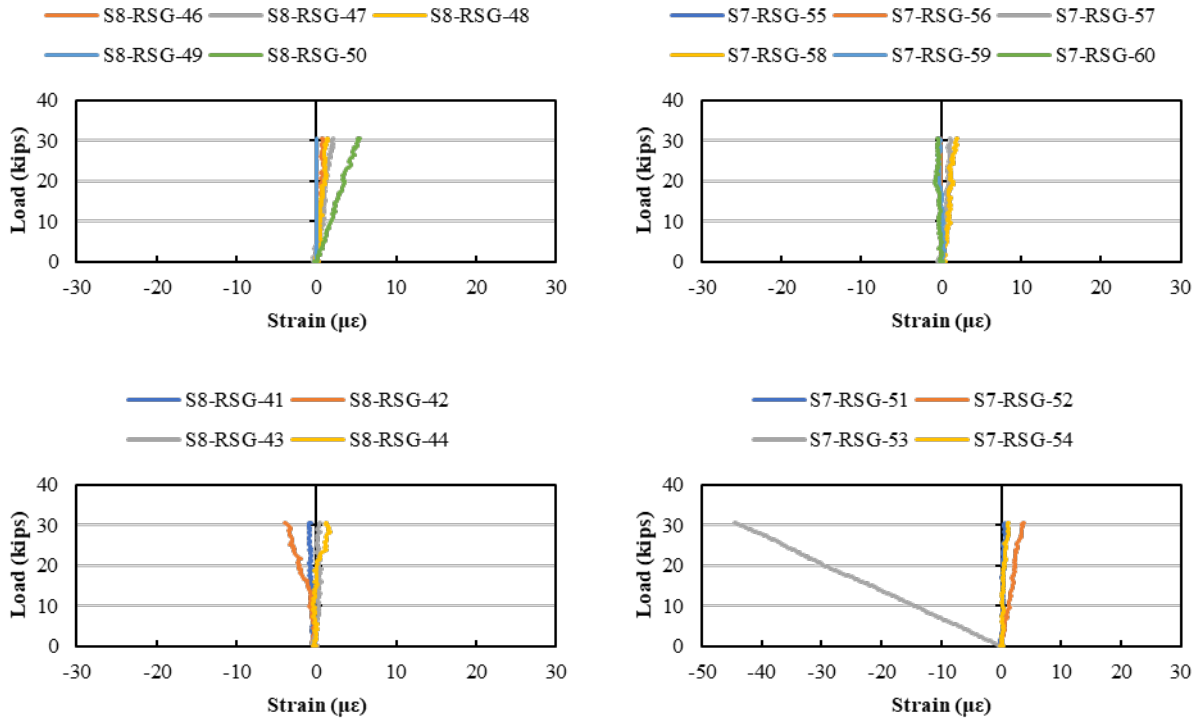


Figure F.76: Load versus rebar strain (measured by RSGs) for Load Stage 8, LC 4-3 (cont.)

F.16. LOAD STAGE 8 – LOAD CONFIGURATION 4-4

The response from all instrumentation for Load Stage 8 with Load Configuration 4-4 are shown in this section.

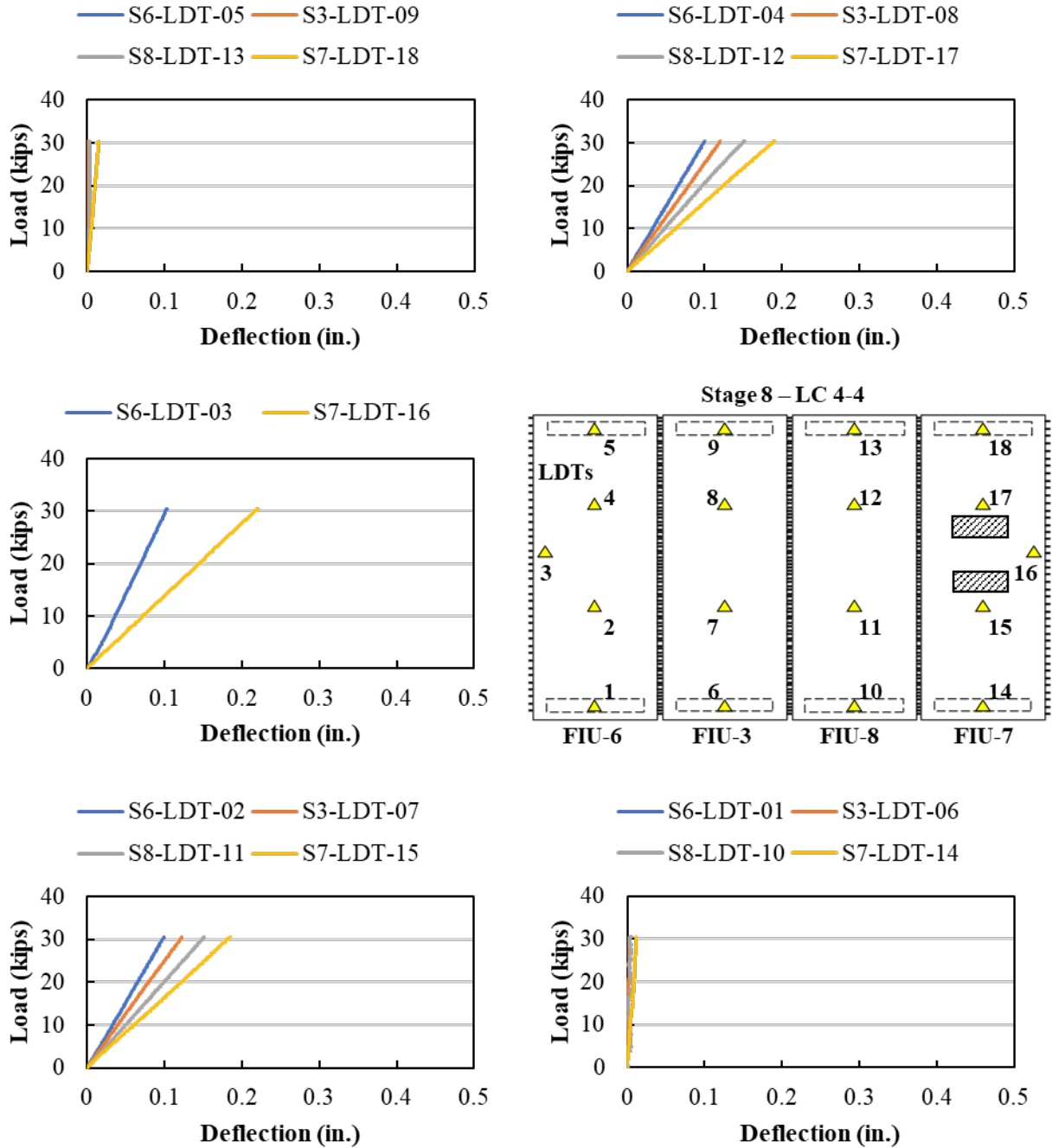


Figure F.77: Load versus displacement measured using LDTs for Load Stage 8, LC 4-4

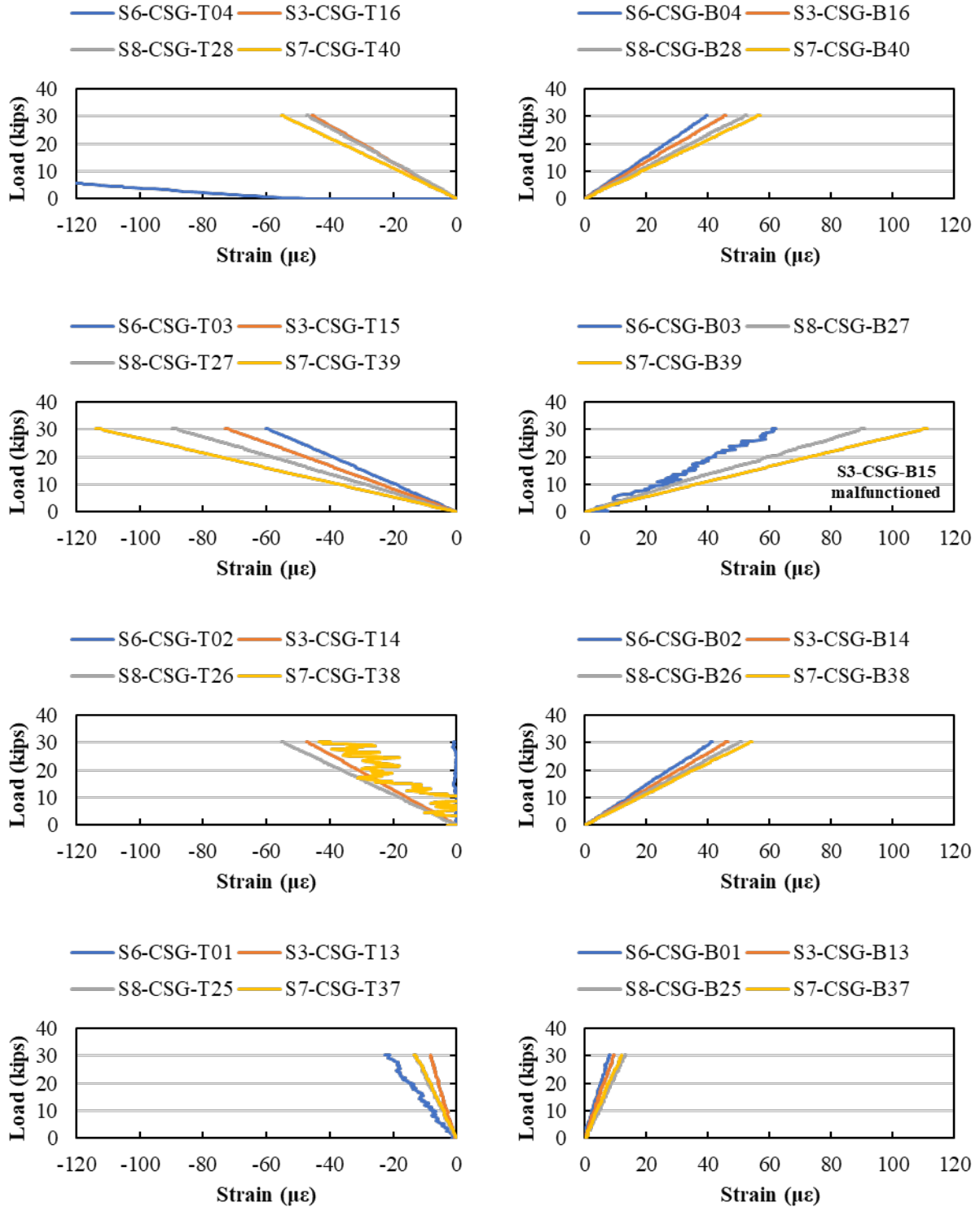


Figure F.78: Load versus longitudinal strain (measured by CSGs) for Load Stage 8, LC 4-4

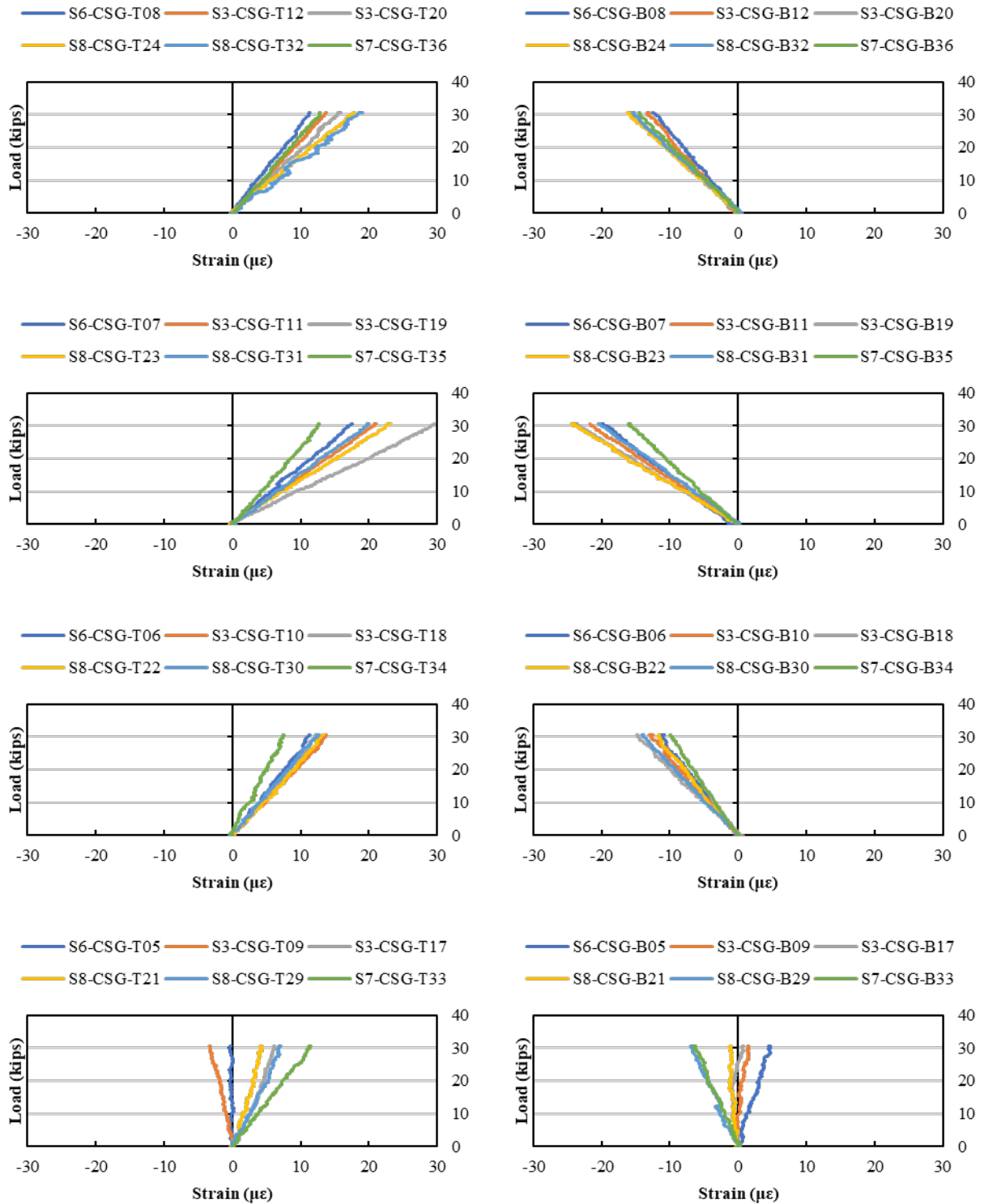


Figure F.79: Load versus transverse strain (measured by CSGs) for Load Stage 8, LC 4-4

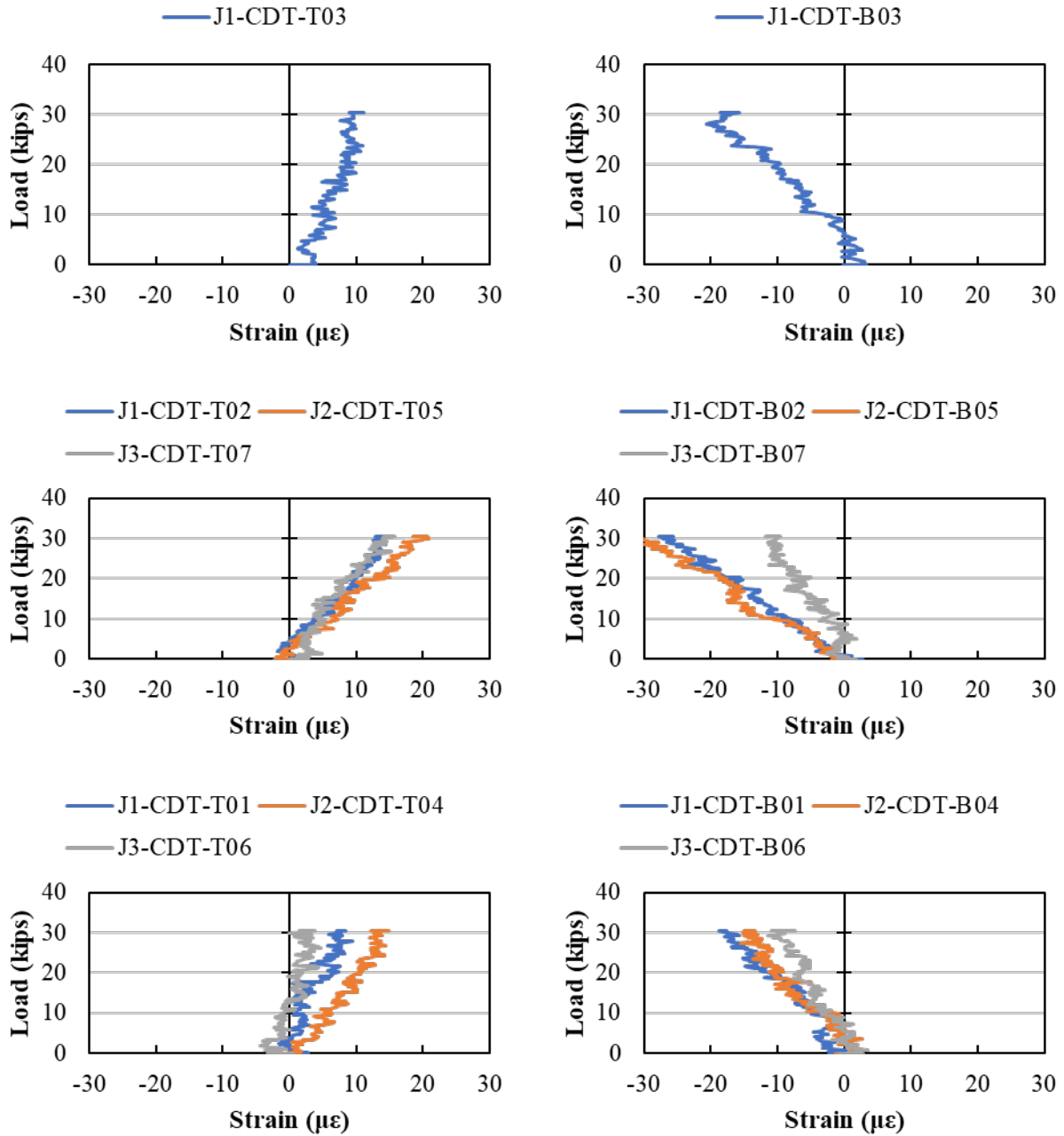


Figure F.80: Load versus average strain across the joints (measured by CDTs) for Load Stage 8, LC 4-4

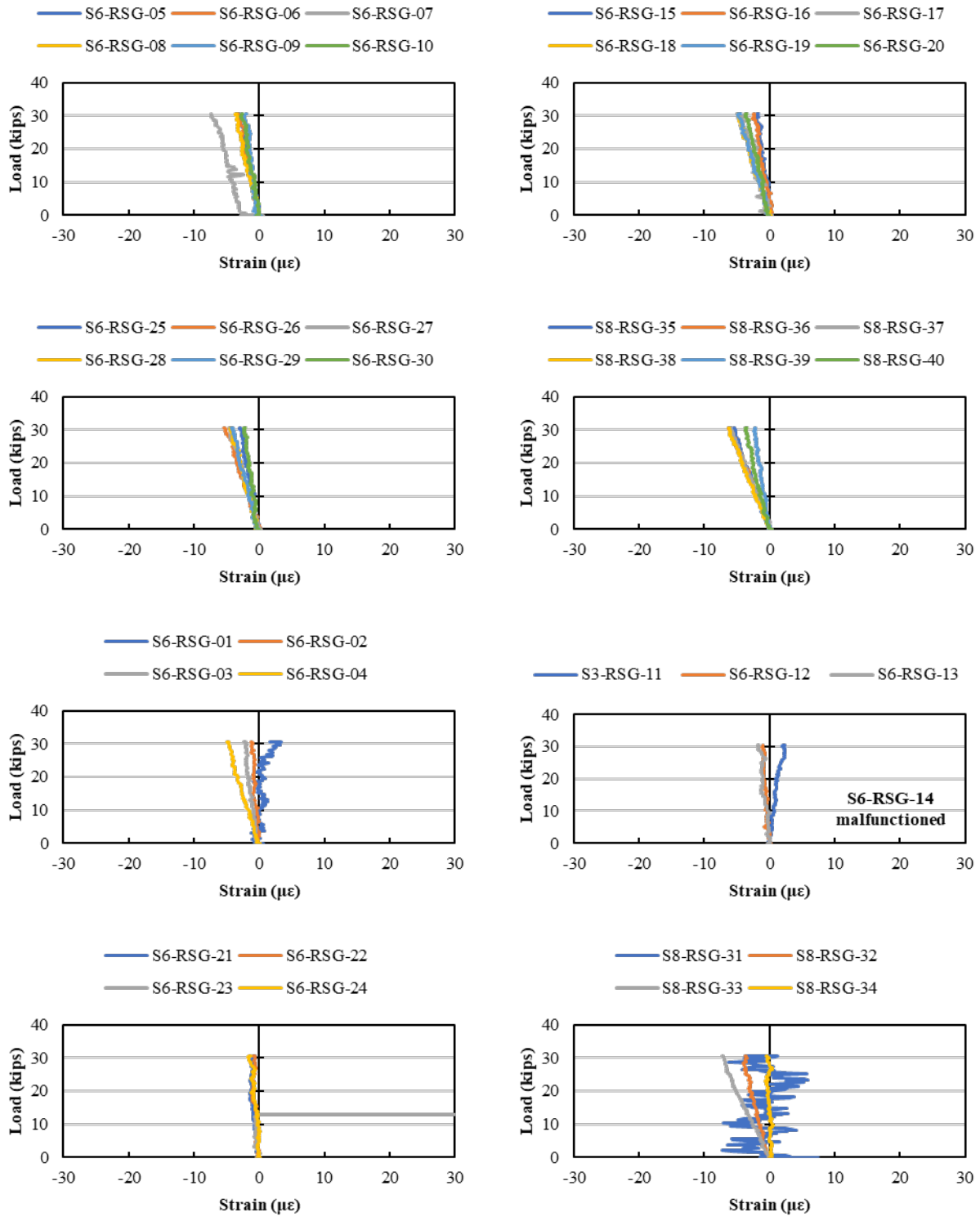


Figure F.81: Load versus rebar strain (measured by RSGs) for Load Stage 8, LC 4-4

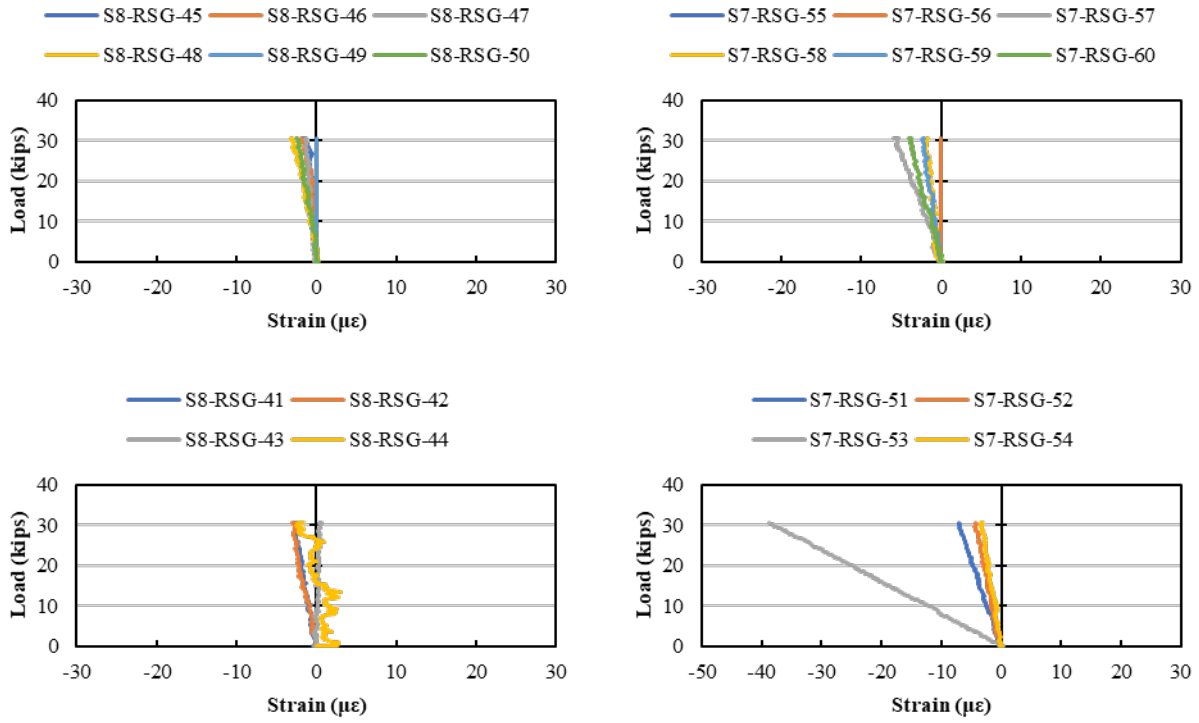


Figure F.82: Load versus rebar strain (measured by RSGs) for Load Stage 8, LC 4-4 (cont.)

F.17. LOAD STAGE 9 – LOAD CONFIGURATION 4-1

The response from all instrumentation for Load Stage 9 with Load Configuration 4-1 are shown in this section.

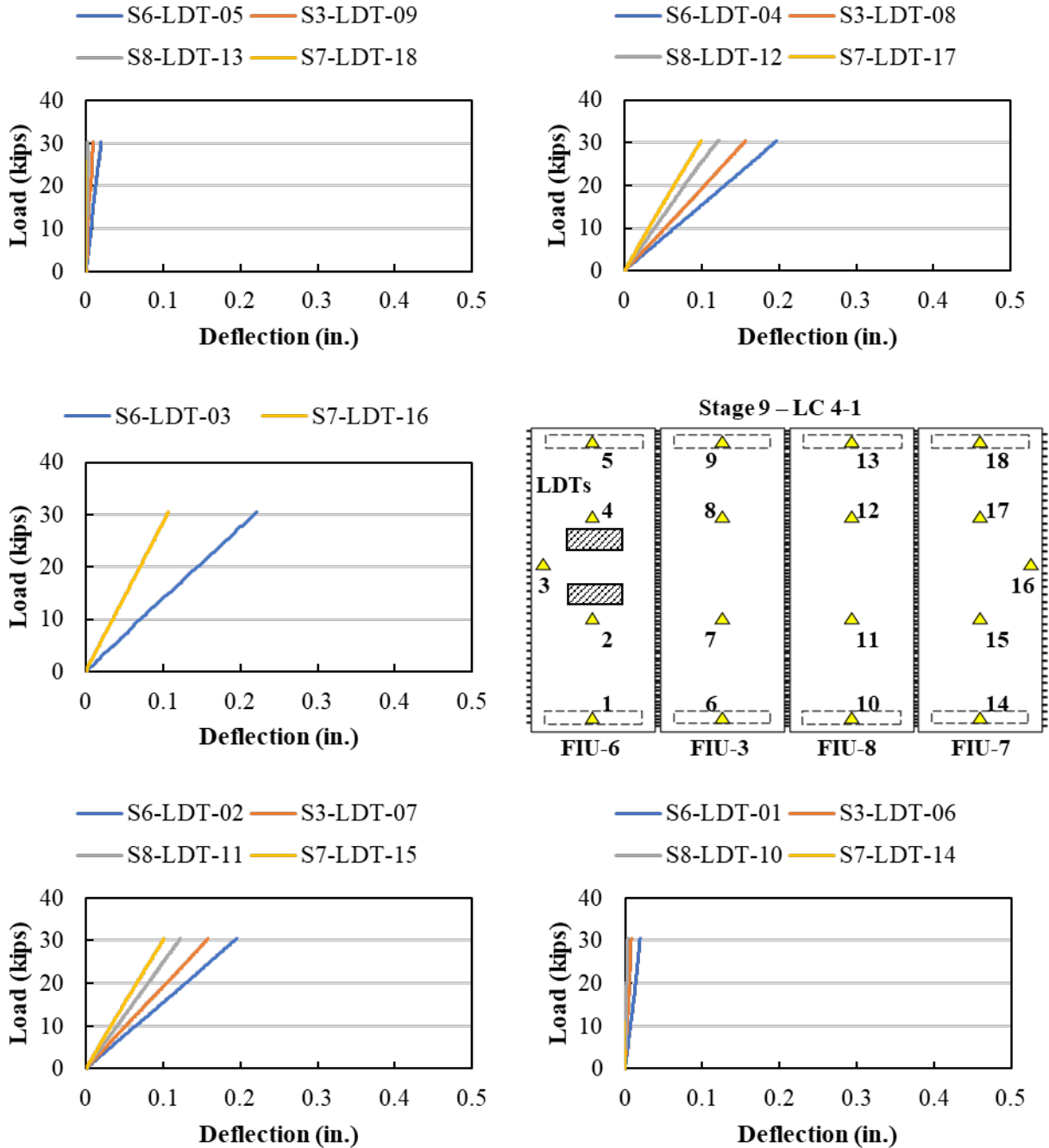


Figure F.83: Load versus displacement measured using LDTs for Load Stage 9, LC 4-1

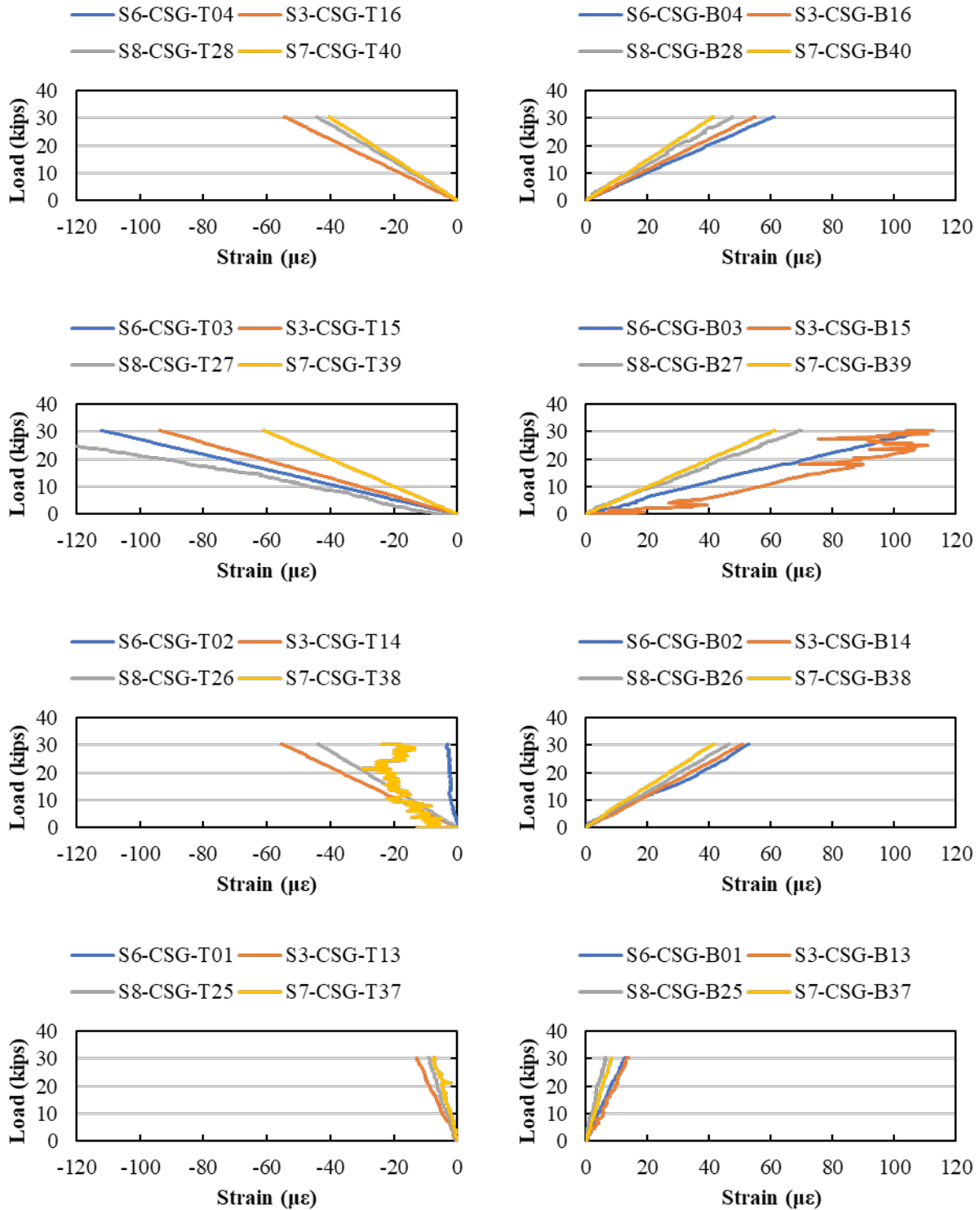


Figure F.84: Load versus longitudinal strain (measured by CSGs) for Load Stage 9, LC 4-1

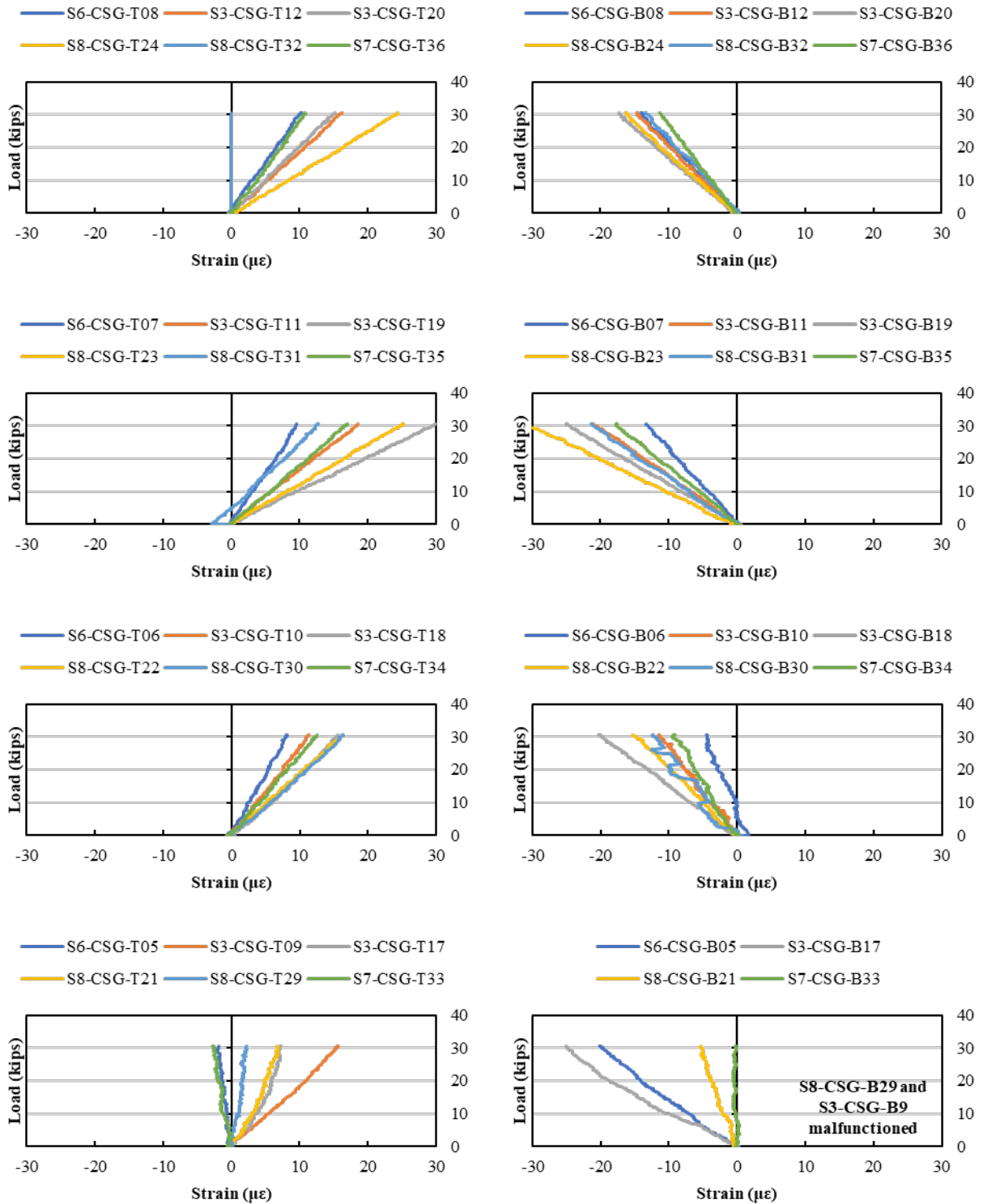


Figure F.85: Load versus transverse strain (measured by CSGs) for Load Stage 9, LC 4-1

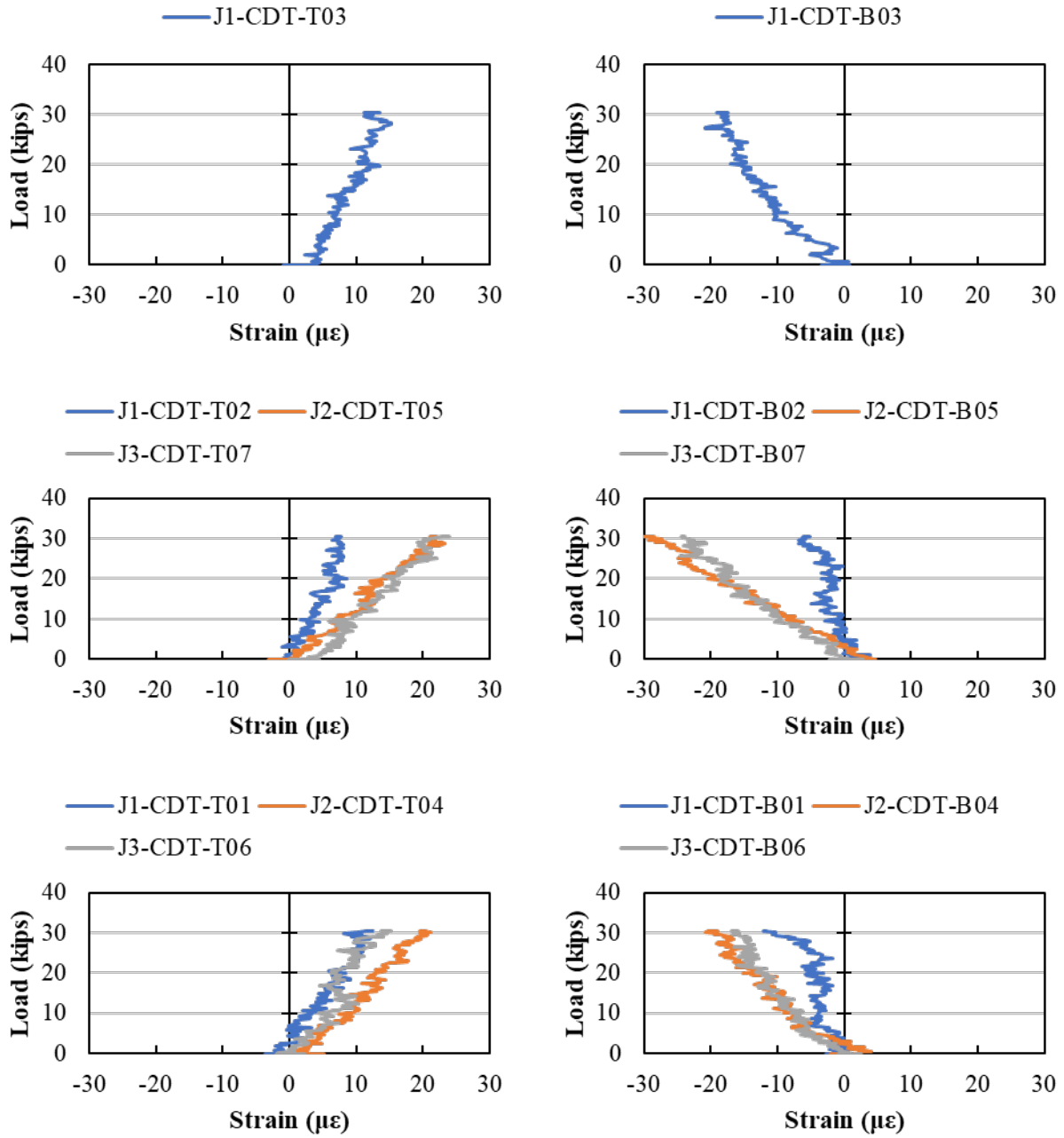


Figure F.86: Load versus average strain across the joints (measured by CDTs) for Load Stage 9, LC 4-1

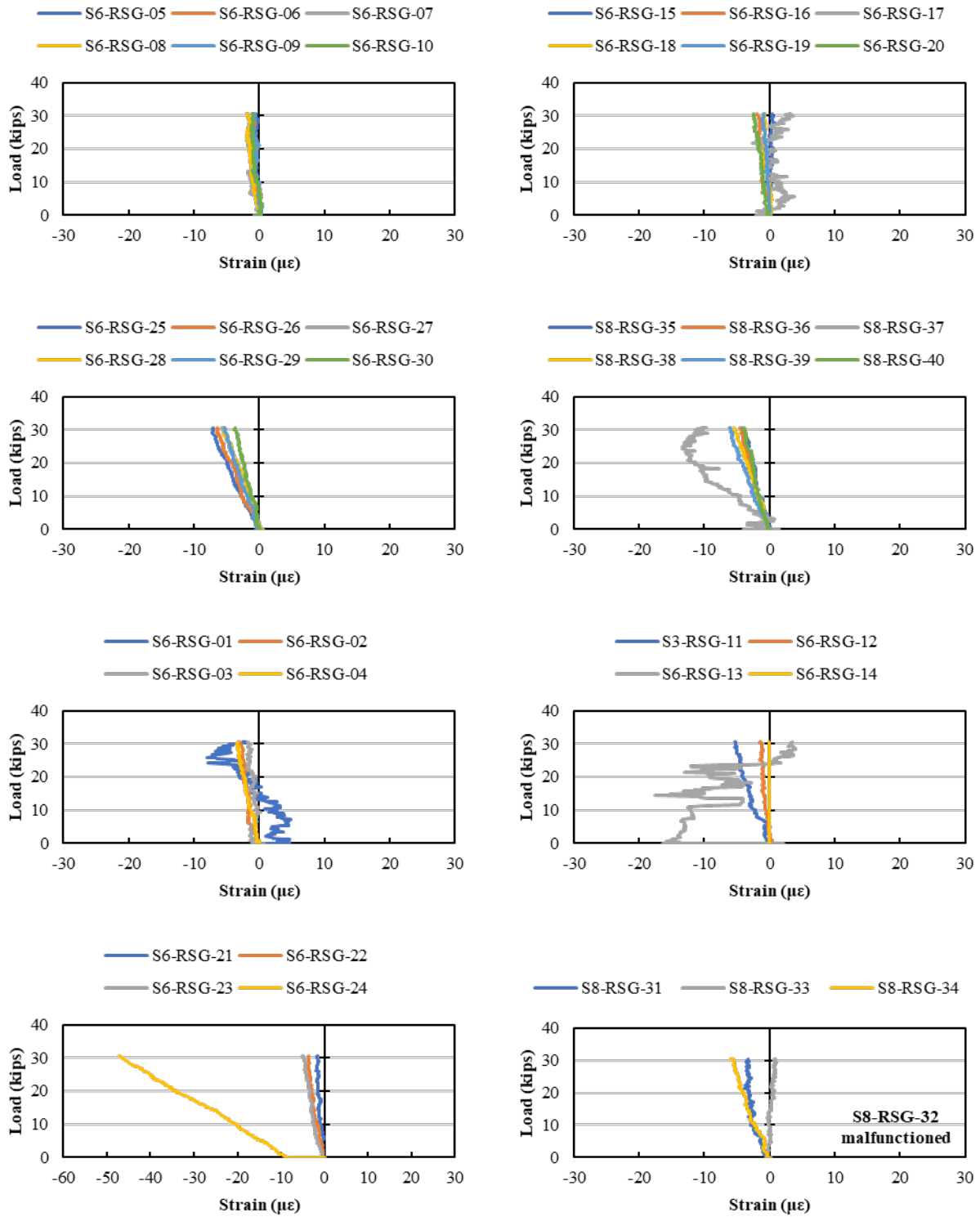


Figure F.87: Load versus rebar strain (measured by RSGs) for Load Stage 9, LC 4-1

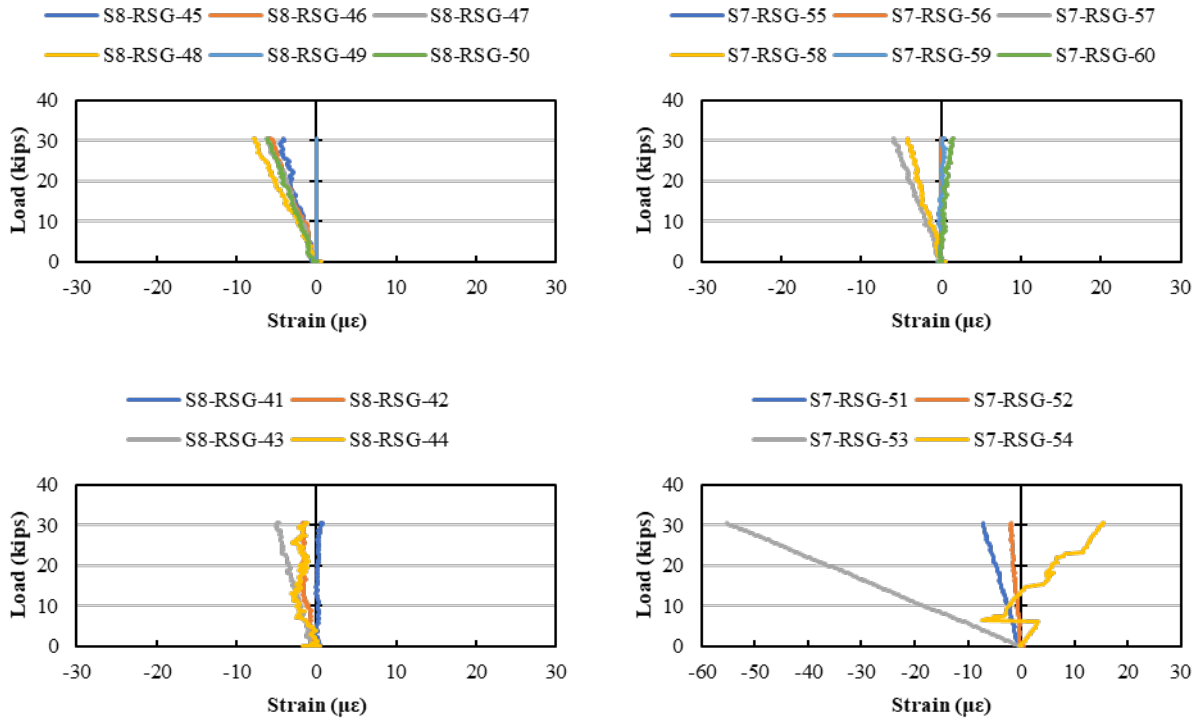


Figure F.88: Load versus rebar strain (measured by RSGs) for Load Stage 9, LC 4-1 (cont.)

F.18. LOAD STAGE 9 – LOAD CONFIGURATION 4-2

The response from all instrumentation for Load Stage 9 with Load Configuration 4-2 are shown in this section.

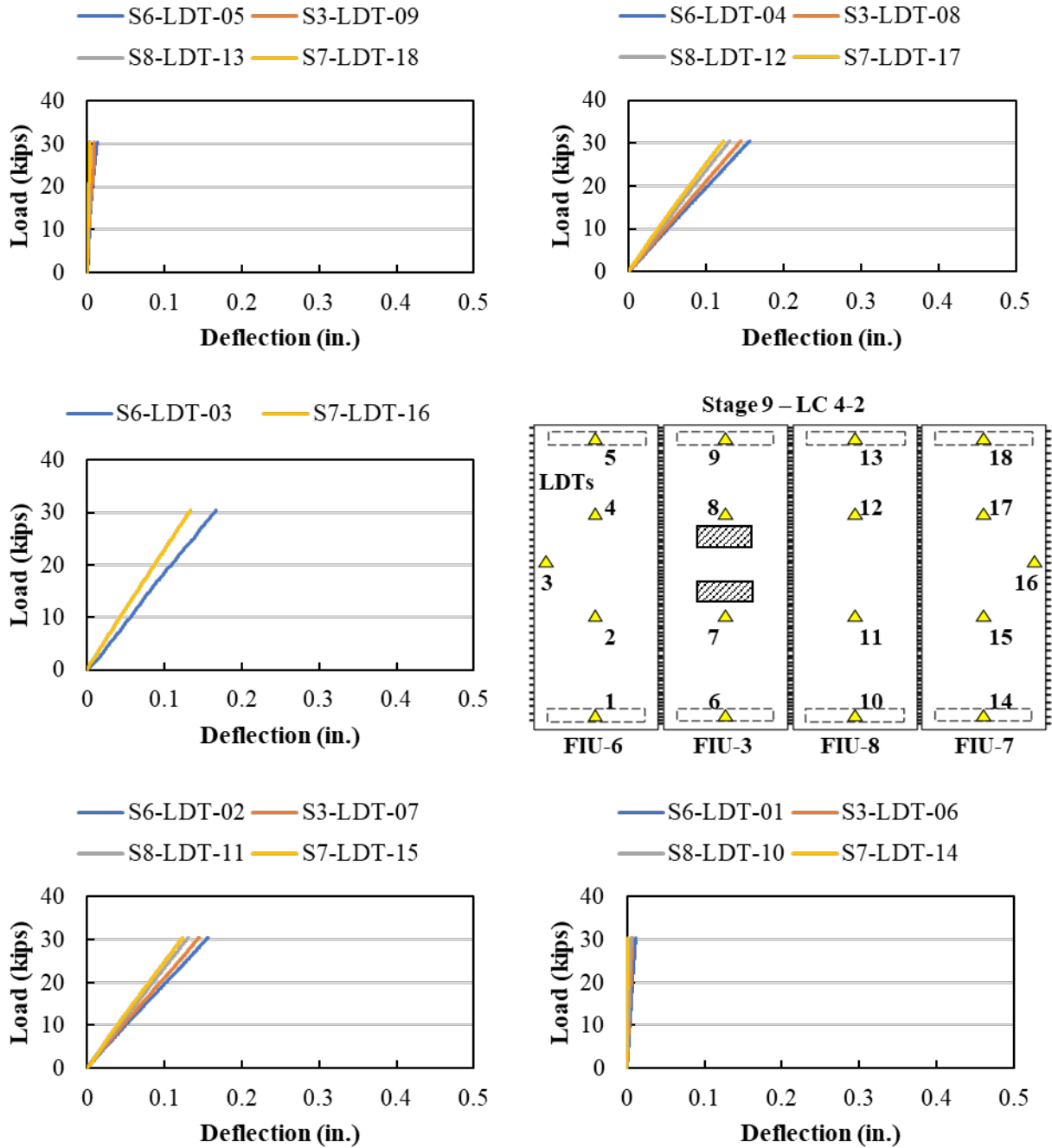


Figure F.89: Load versus displacement measured using LDTs for Load Stage 9, LC 4-2

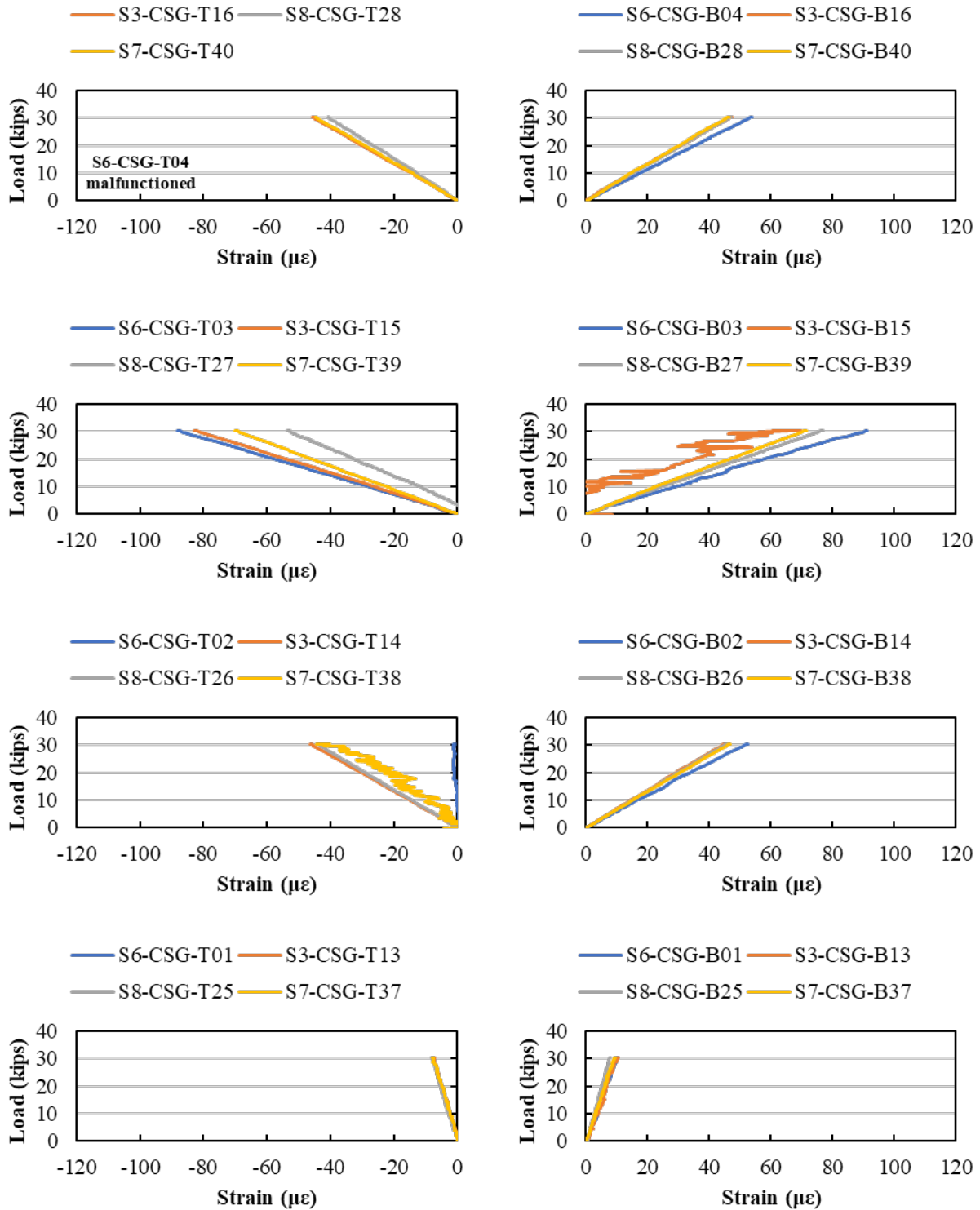


Figure F.90: Load versus longitudinal strain (measured by CSGs) for Load Stage 9, LC 4-2

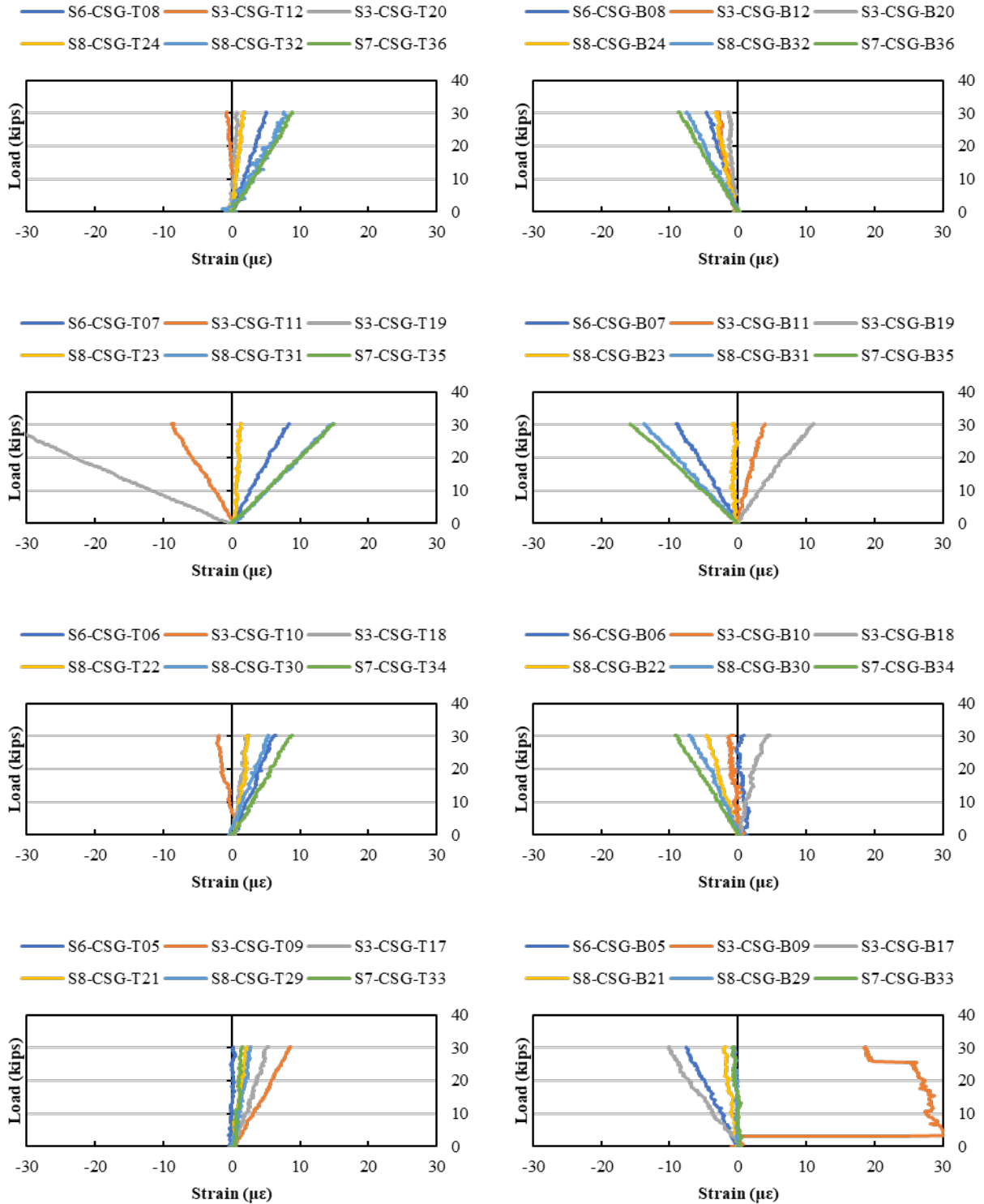


Figure F.91: Load versus transverse strain (measured by CSGs) for Load Stage 9, LC 4-2

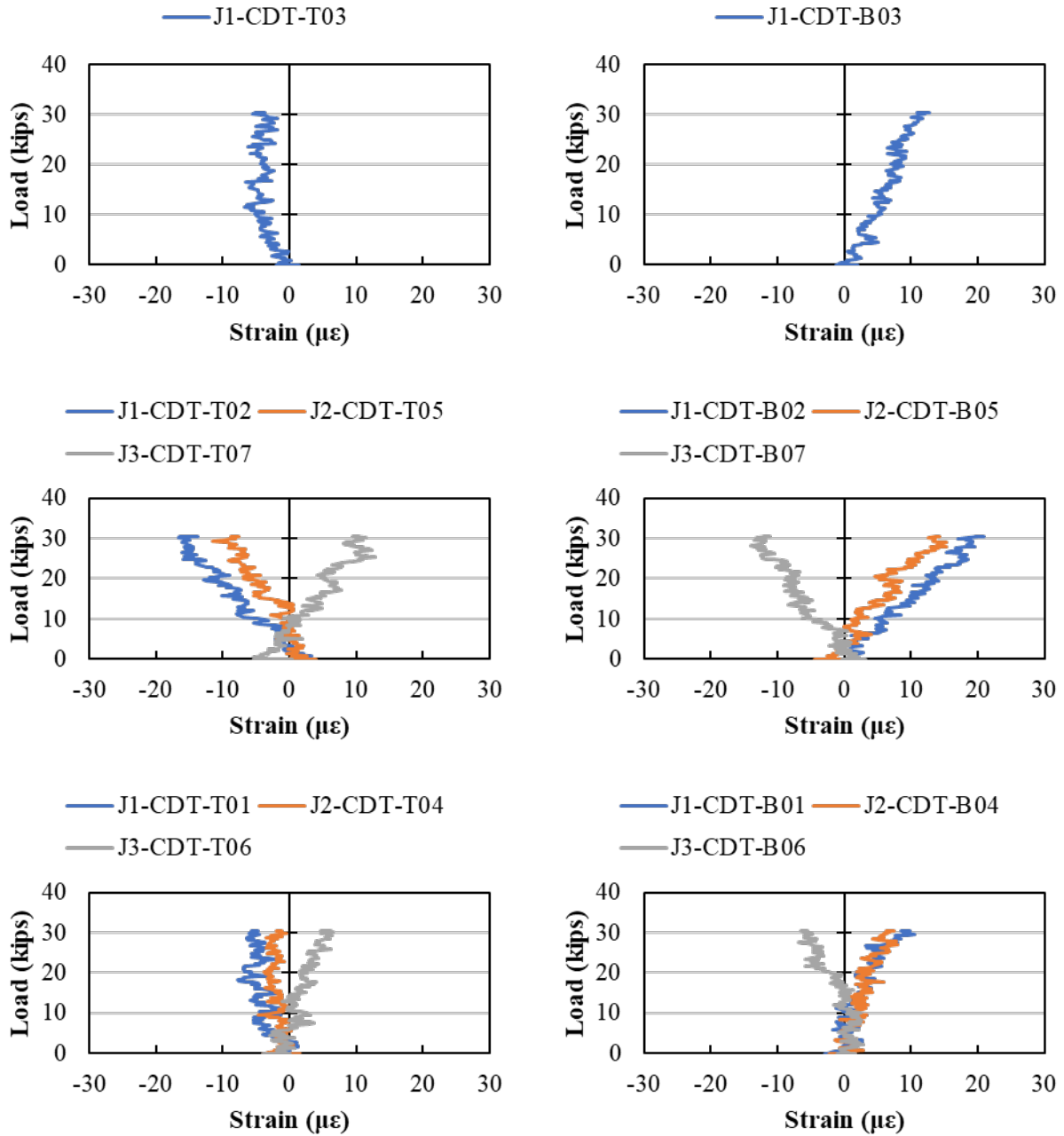


Figure F.92: Load versus average strain across the joints (measured by CDTs) for Load Stage 9, LC 4-2

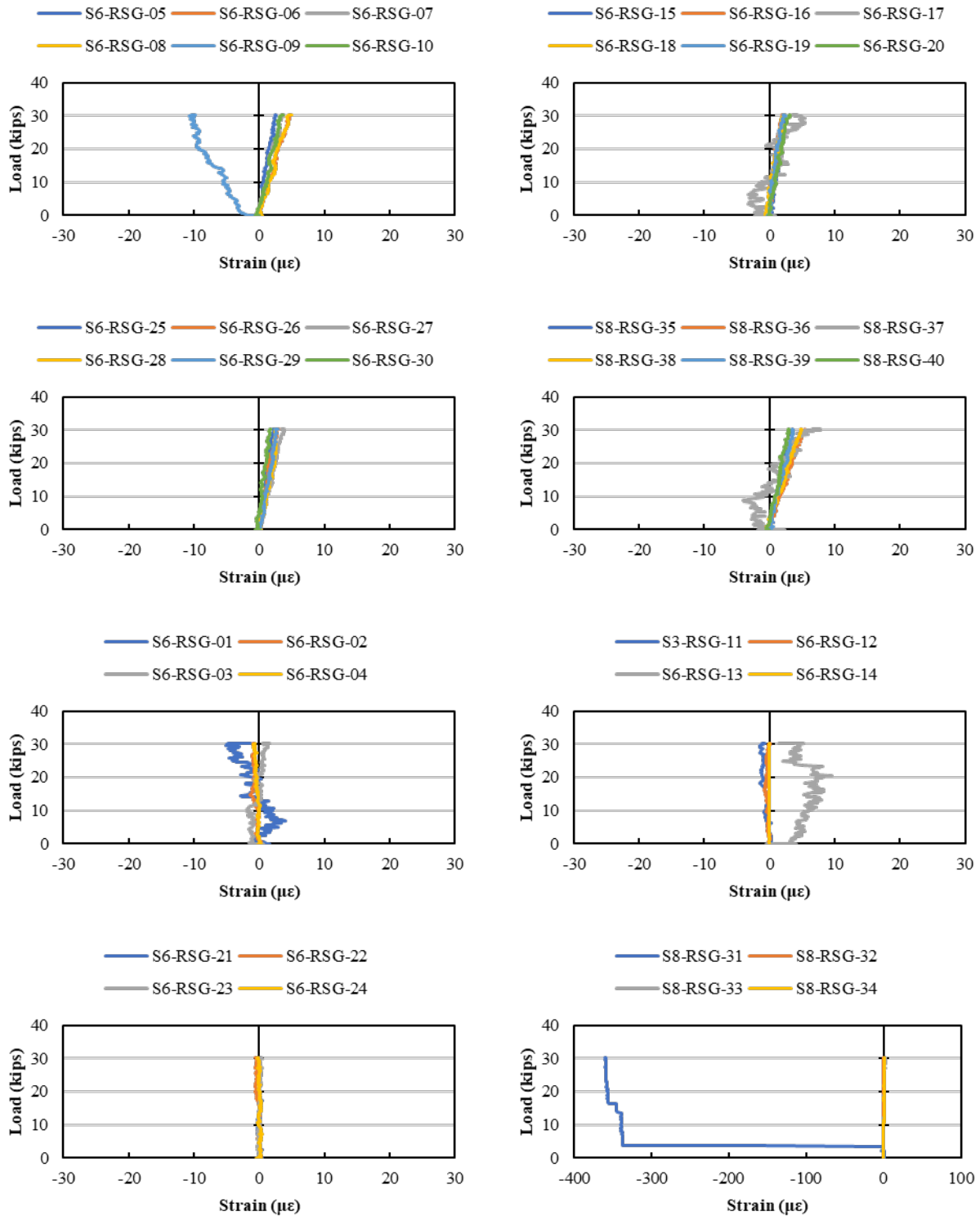


Figure F.93: Load versus rebar strain (measured by RSGs) for Load Stage 9, LC 4-2

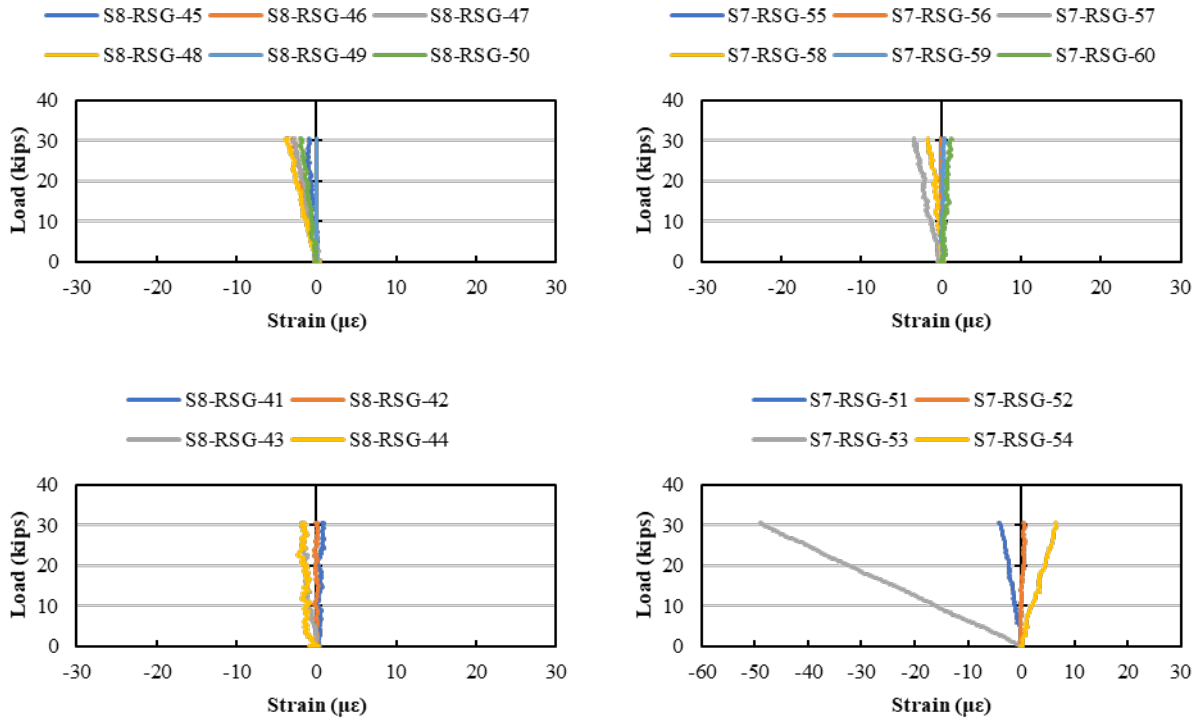


Figure F.94: Load versus rebar strain (measured by RSGs) for Load Stage 9, LC 4-2 (cont.)

F.19. LOAD STAGE 9 – LOAD CONFIGURATION 4-3

The response from all instrumentation for Load Stage 9 with Load Configuration 4-3 are shown in this section.

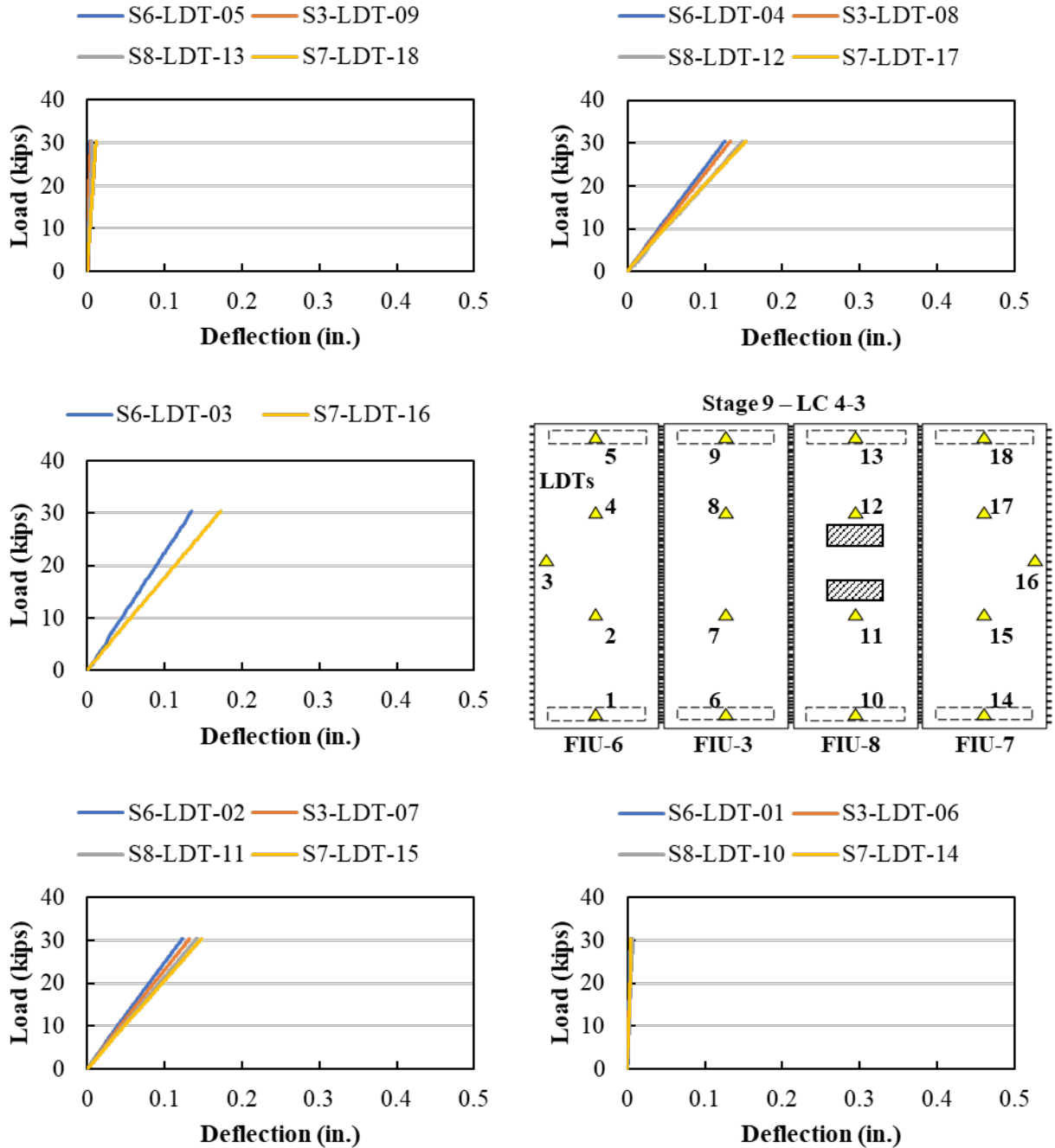


Figure F.95: Load versus displacement measured using LDTs for Load Stage 9, LC 4-3

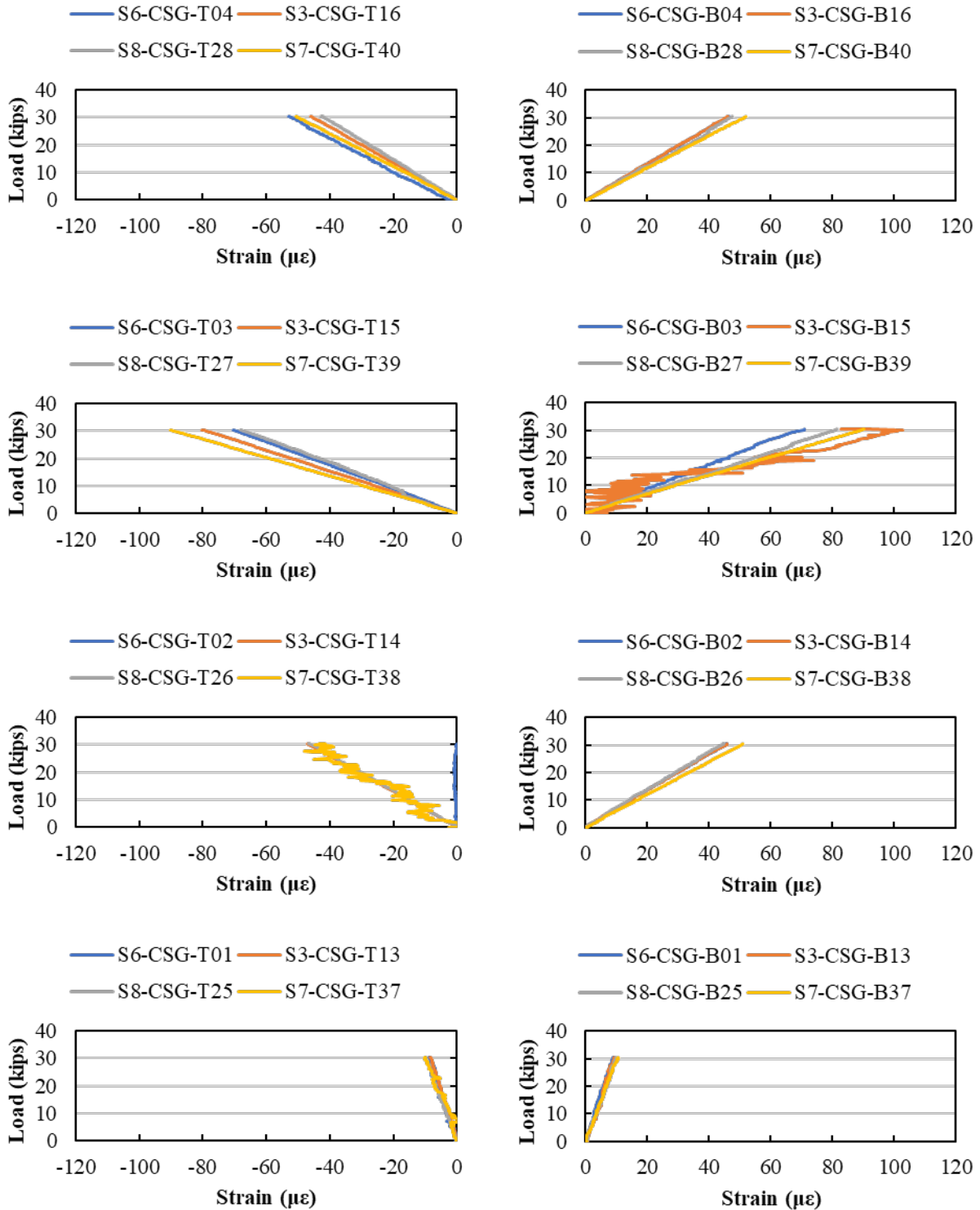


Figure F.96: Load versus longitudinal strain (measured by CSGs) for Load Stage 9, LC 4-3

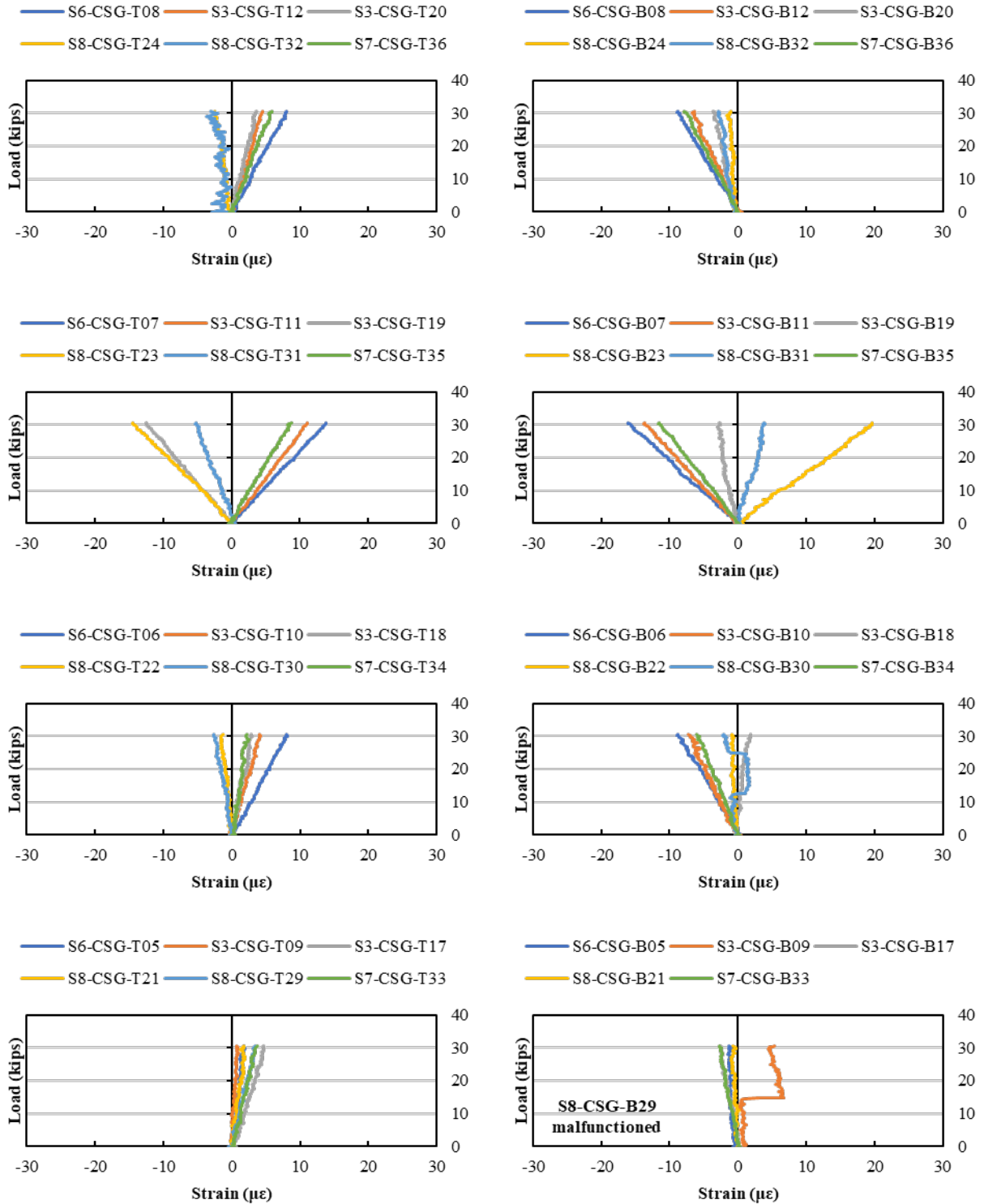


Figure F.97: Load versus transverse strain (measured by CSGs) for Load Stage 9, LC 4-3

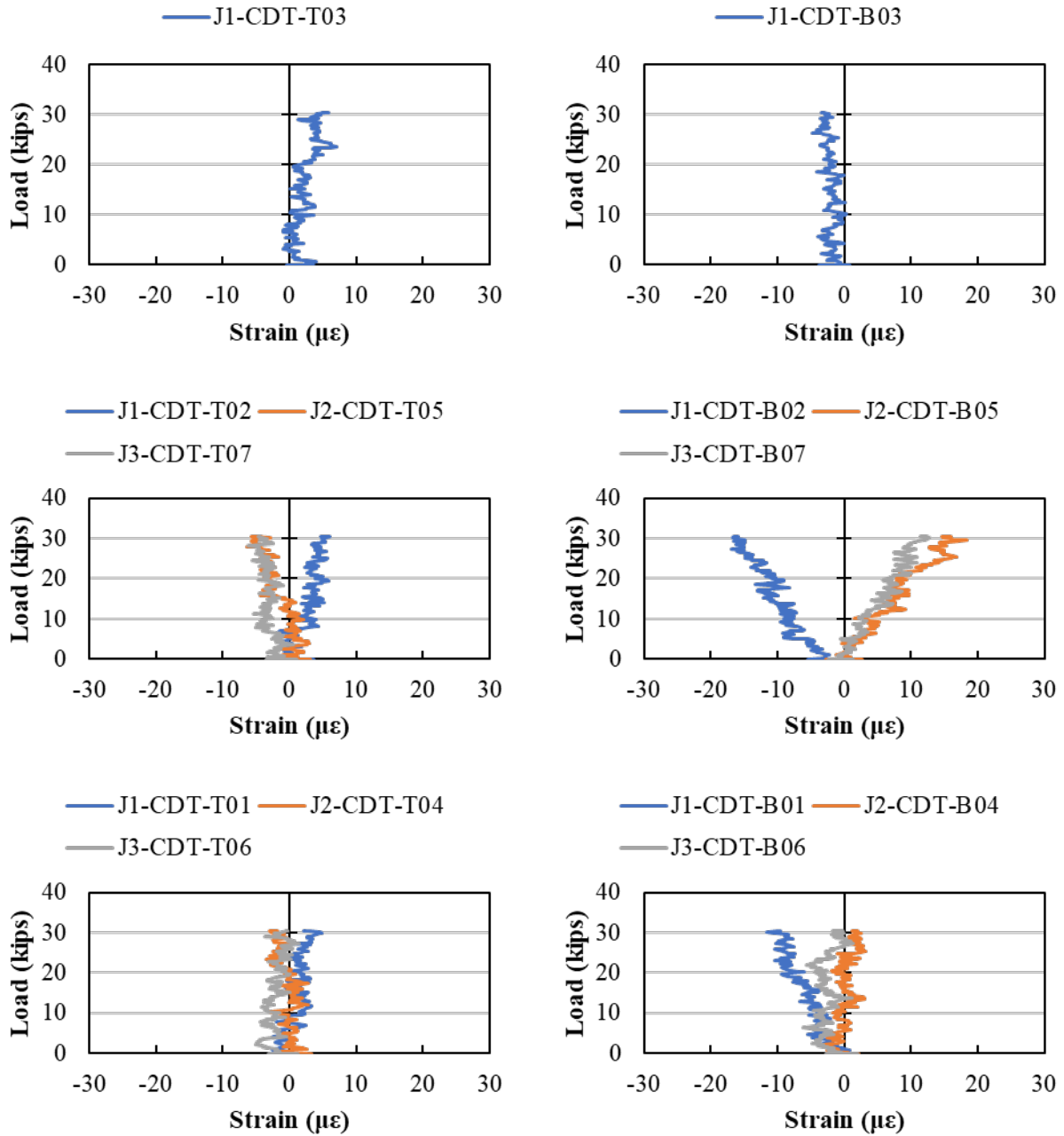


Figure F.98: Load versus average strain across the joints (measured by CDTs) for Load Stage 9, LC 4-3

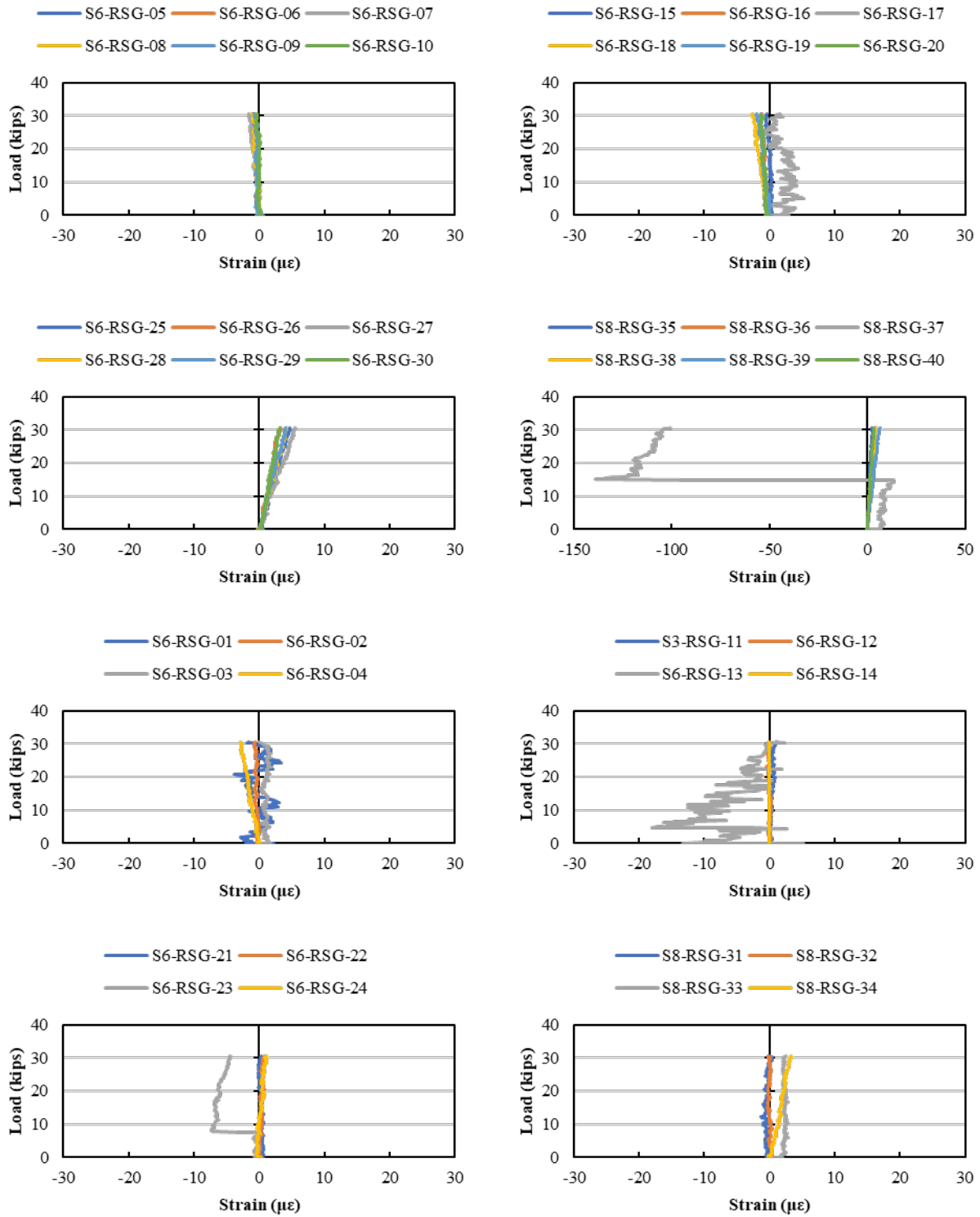


Figure F.99: Load versus rebar strain (measured by RSGs) for Load Stage 9, LC 4-3

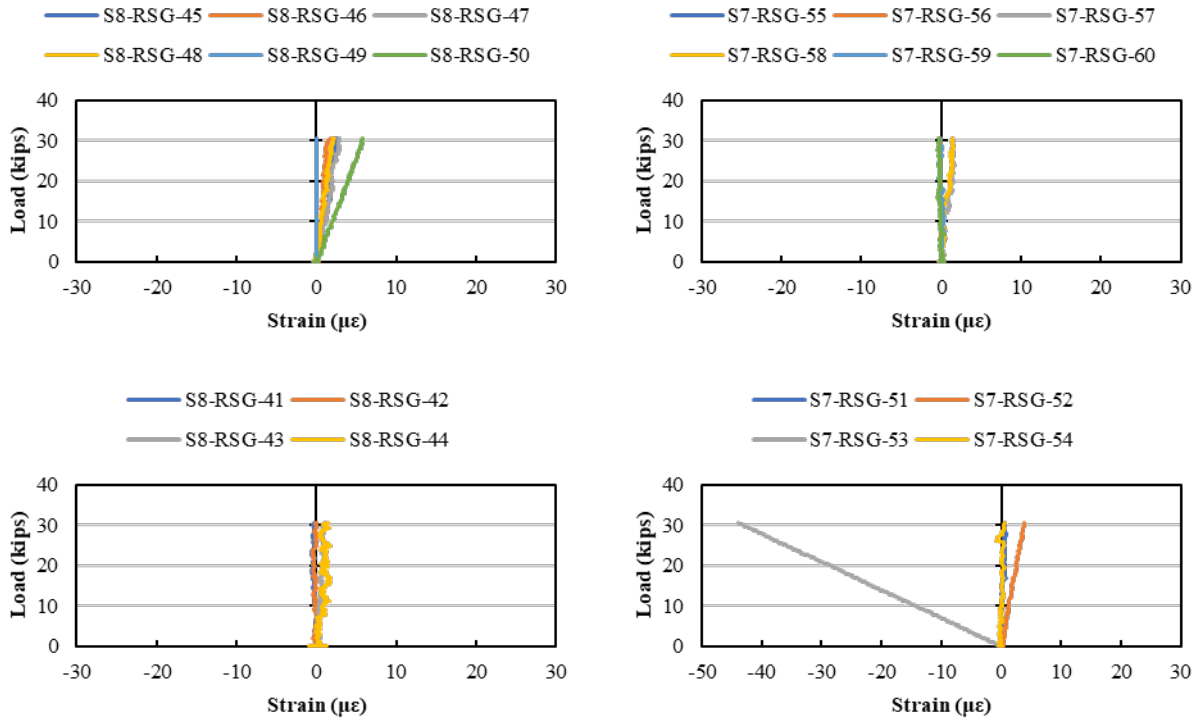


Figure F.100: Load versus rebar strain (measured by RSGs) for Load Stage 9, LC 4-3

F.20. LOAD STAGE 9 – LOAD CONFIGURATION 4-4

The response from all instrumentation for Load Stage 9 with Load Configuration 4-4 are shown in this section.

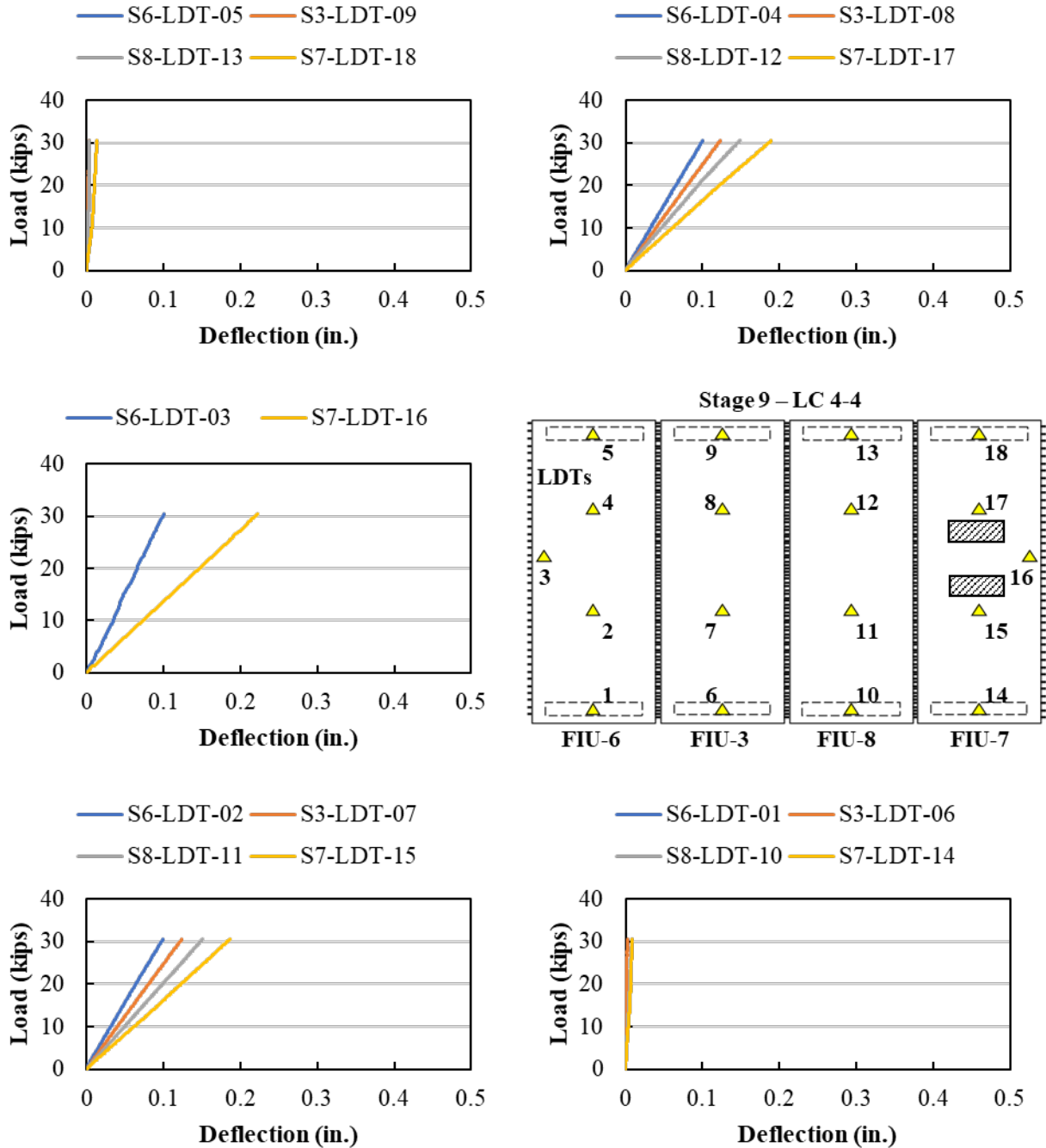


Figure F.101: Load versus displacement measured using LDTs for Load Stage 9, LC 4-4

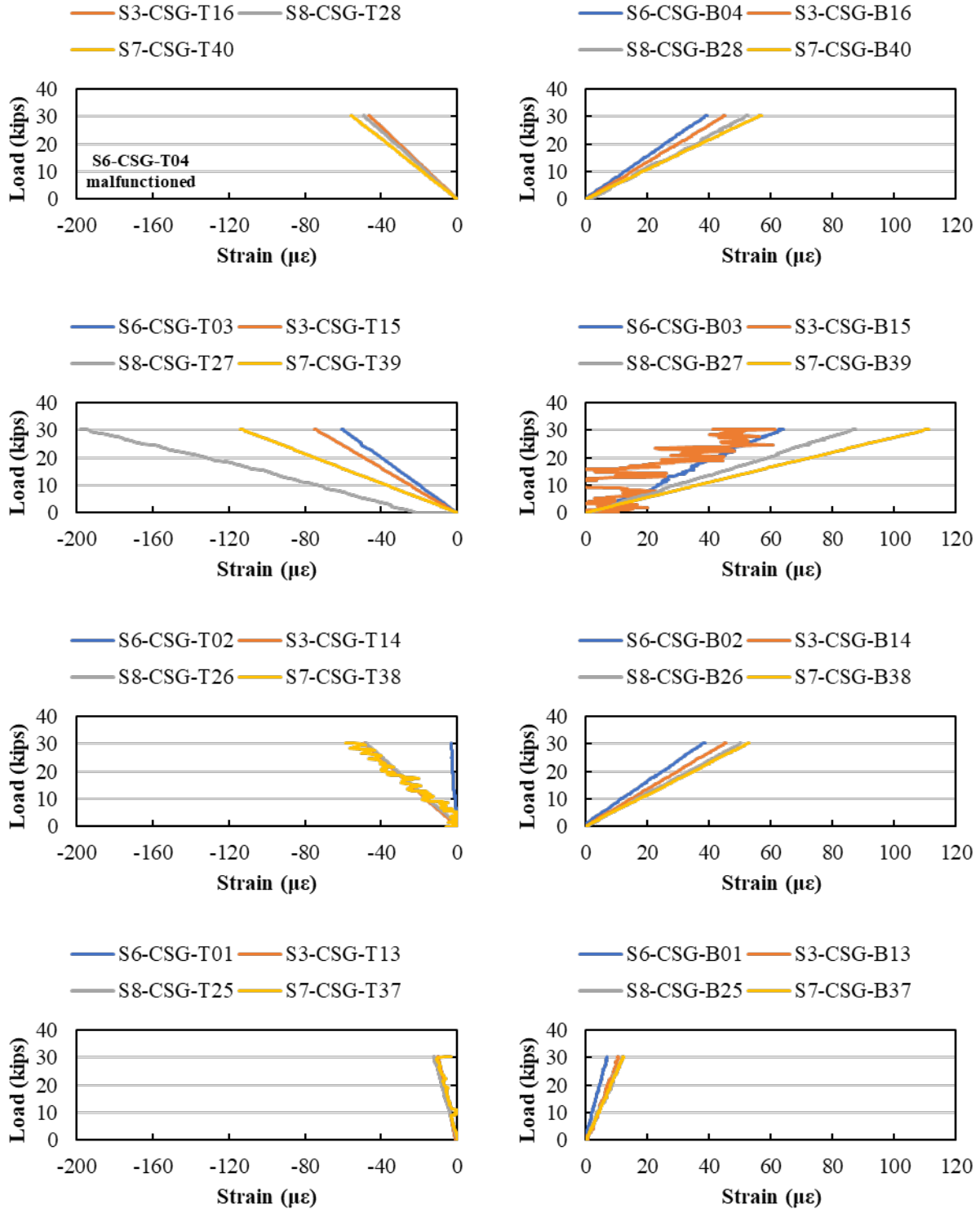


Figure F.102: Load versus longitudinal strain (measured by CSGs) for Load Stage 9, LC 4-4

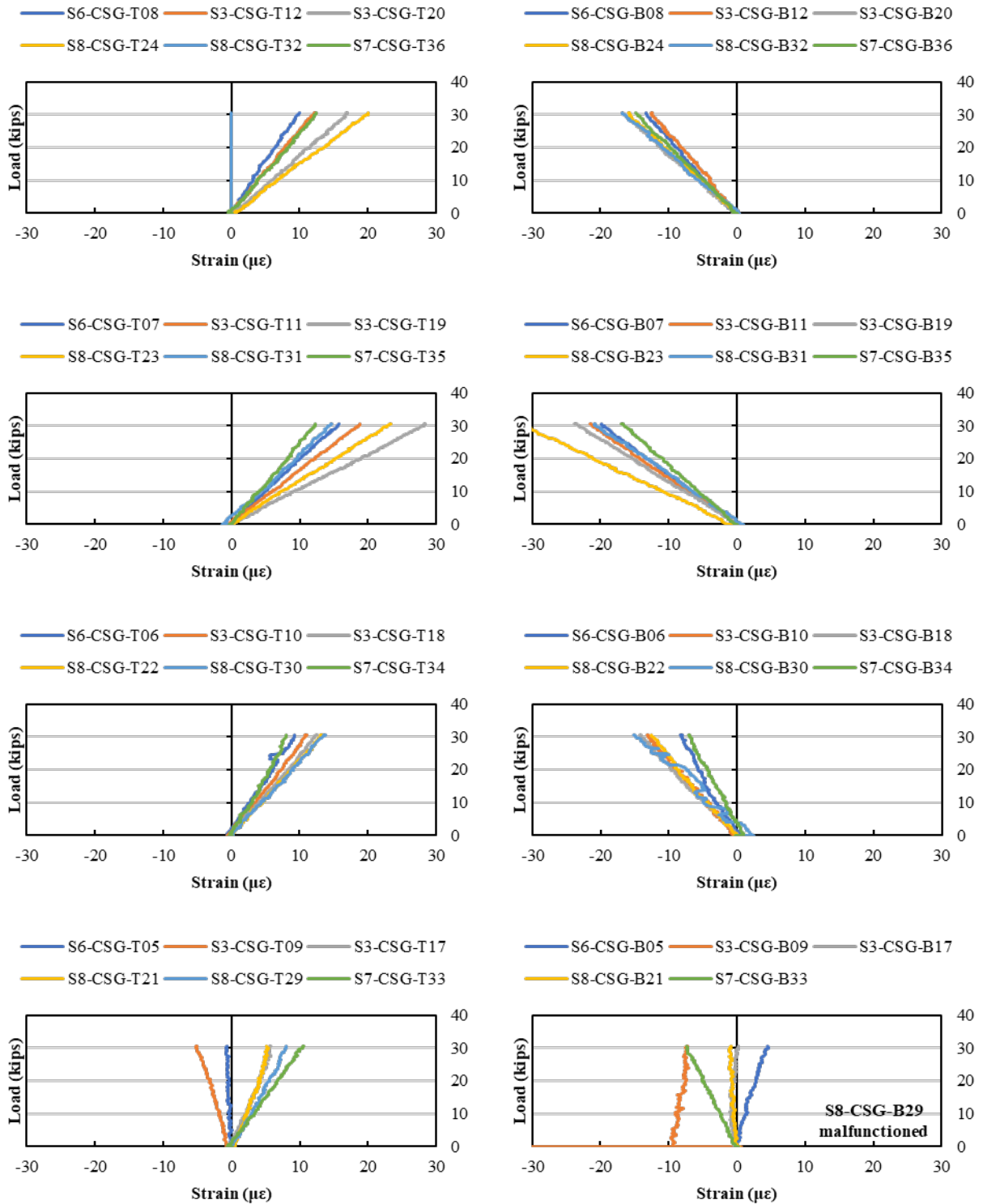


Figure F.103: Load versus transverse strain (measured by CSGs) for Load Stage 9, LC 4-4

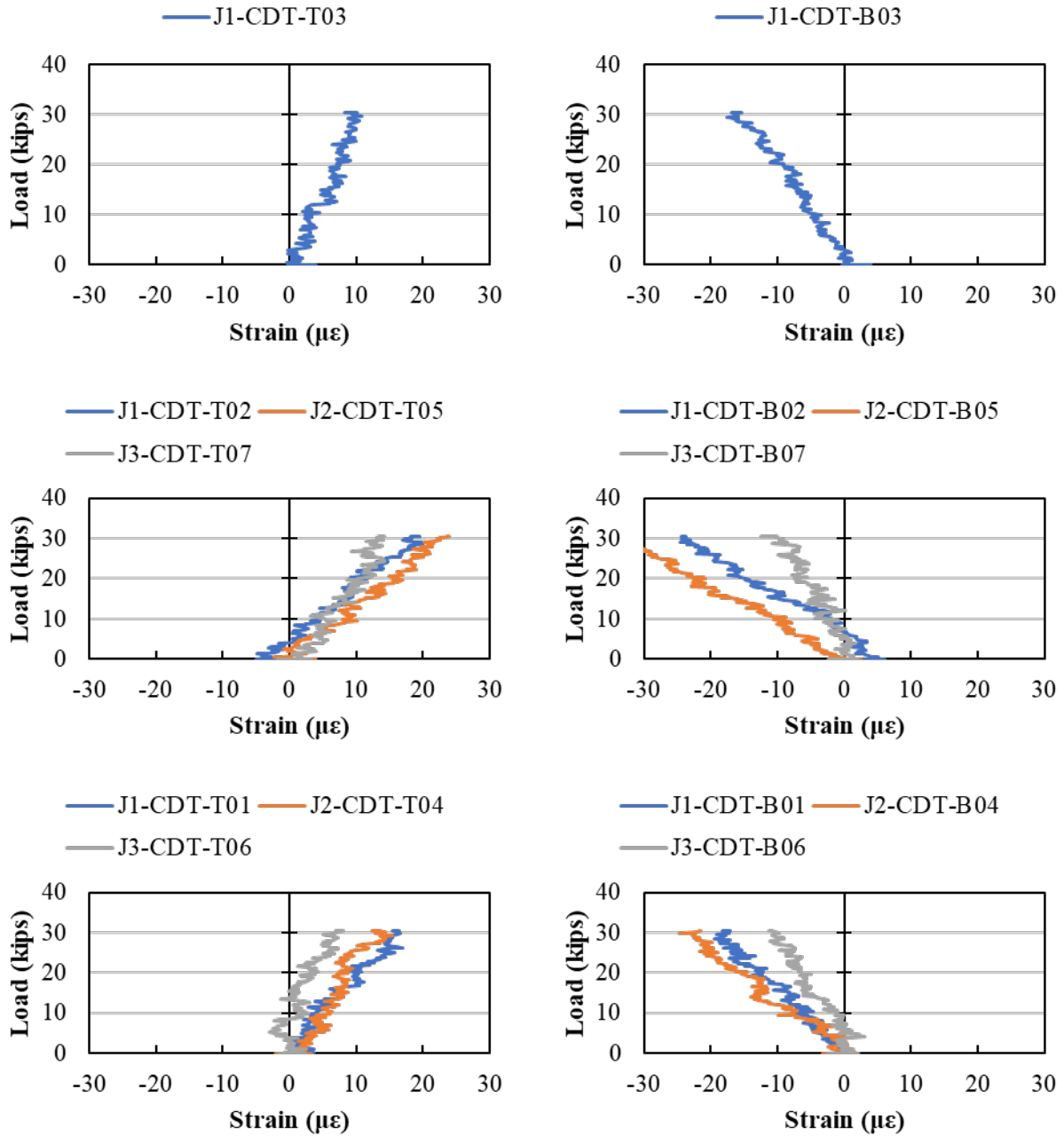


Figure F.104: Load versus average strain across the joints (measured by CDTs) for Load Stage 9, LC 4-4

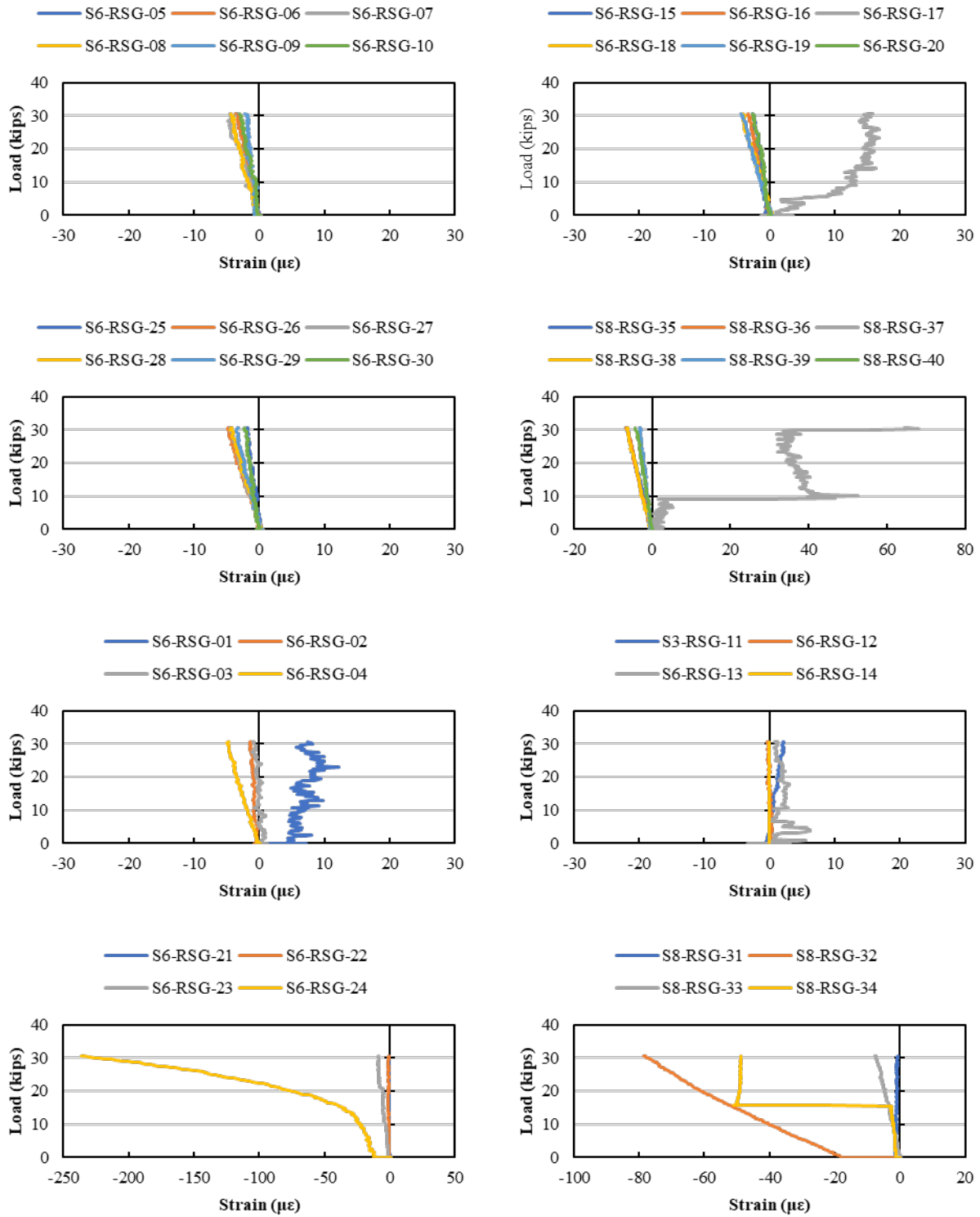


Figure F.105: Load versus rebar strain (measured by RSGs) for Load Stage 9, LC 4-4

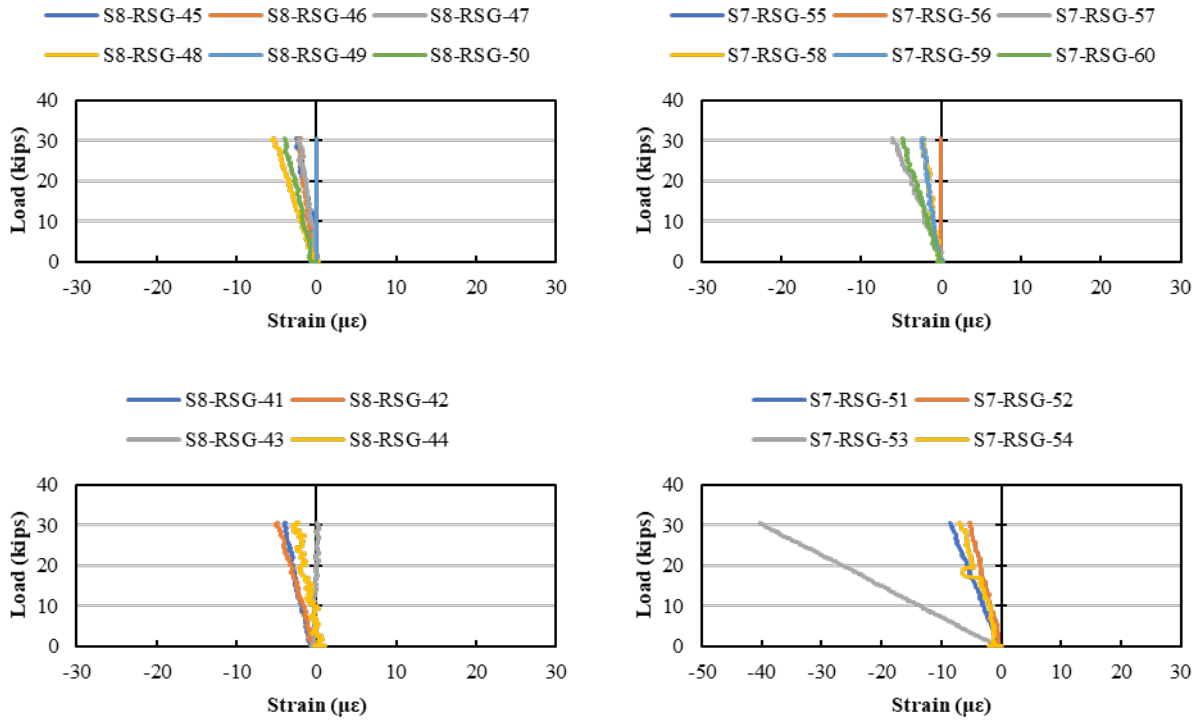


Figure F.106: Load versus rebar strain (measured by RSGs) for Load Stage 9, LC 4-4 (cont.)

F.21. LOAD STAGE 10 – LOAD CONFIGURATION 4-5

The response from all instrumentation for Load Stage 10 with Load Configuration 4-5 are shown in this section.

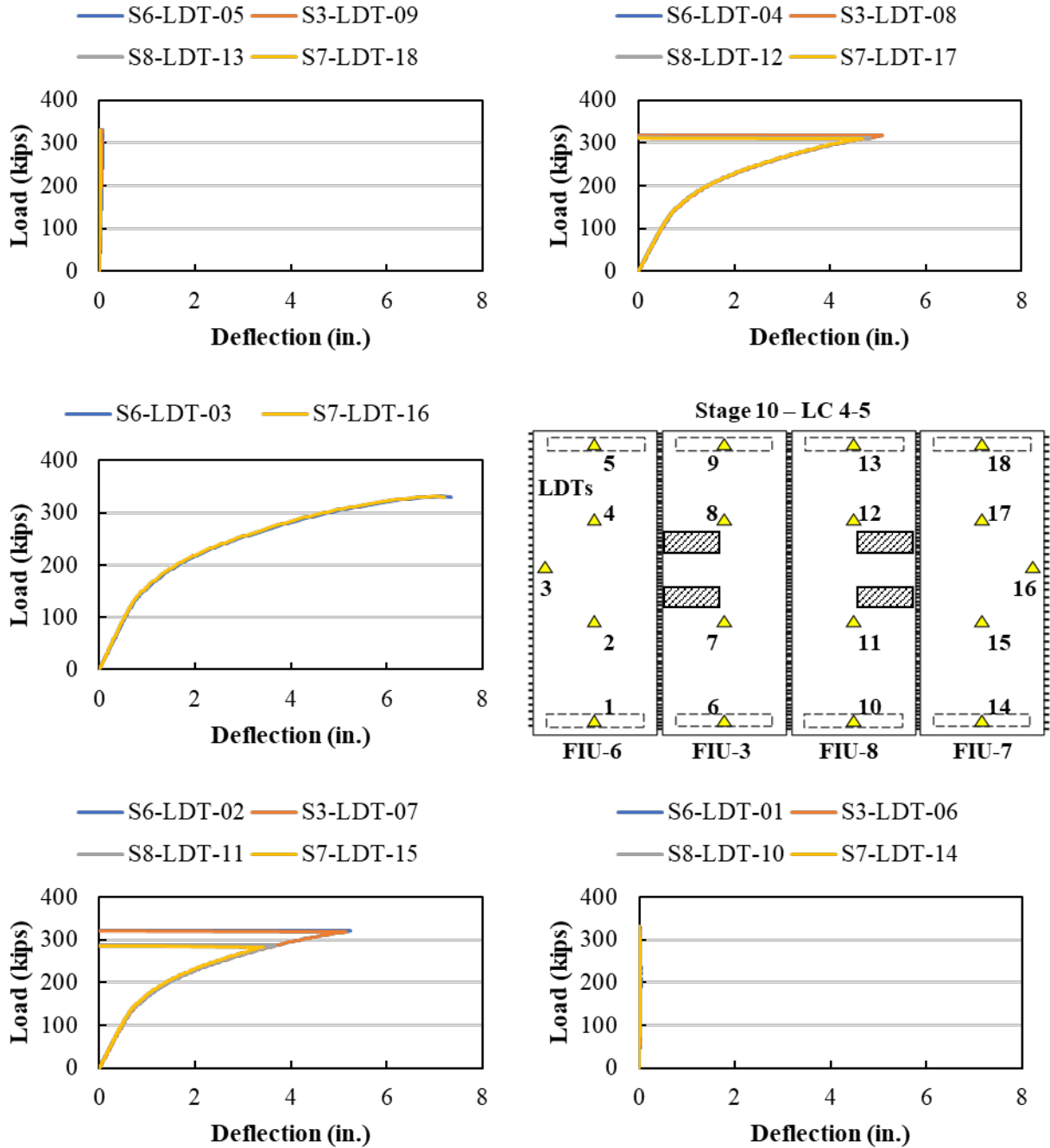


Figure F.107: Load versus displacement measured using LDTs for Load Stage 10, LC 4-5

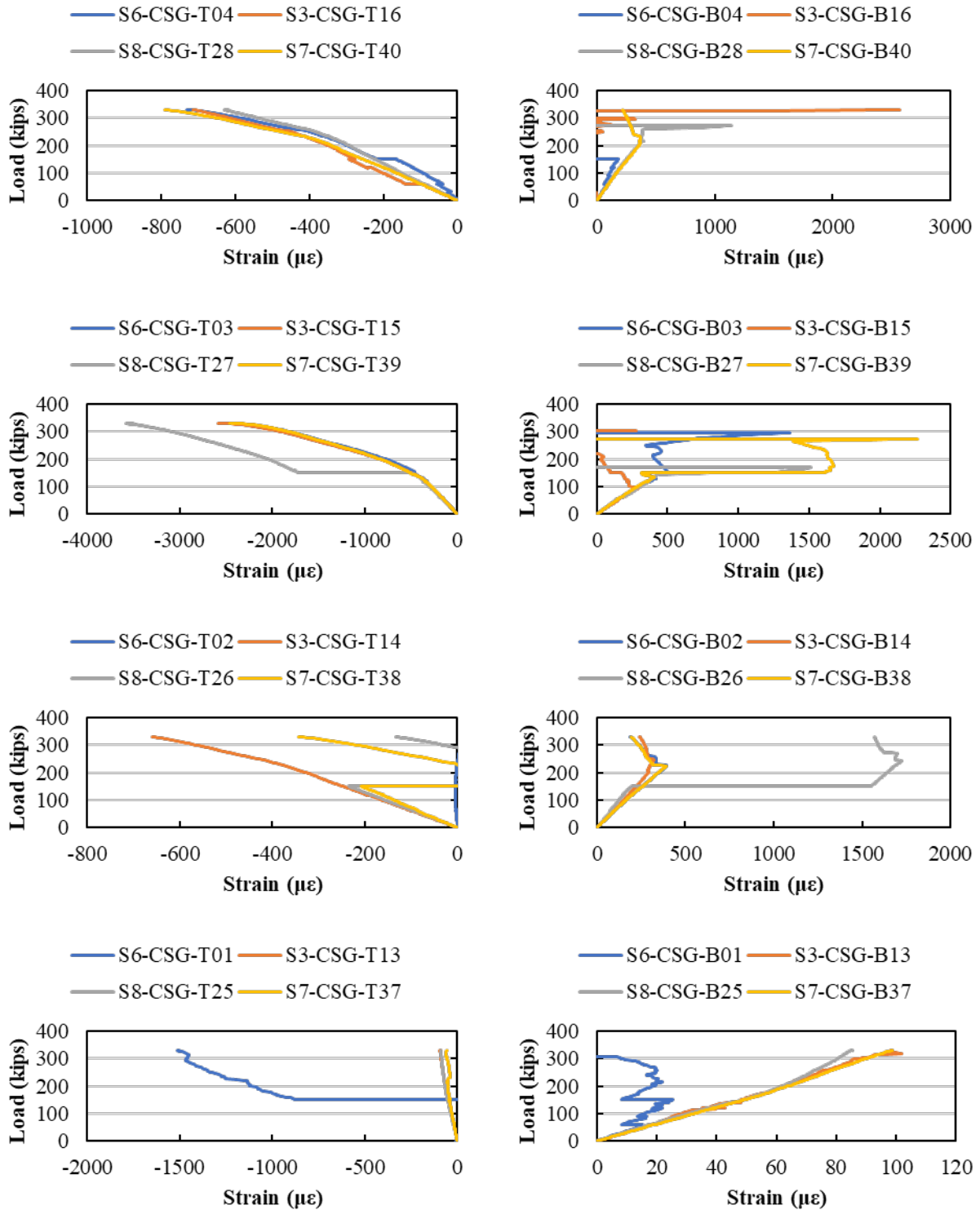


Figure F.108: Load versus longitudinal strain (measured by CSGs) for Load Stage 10, LC 4-5

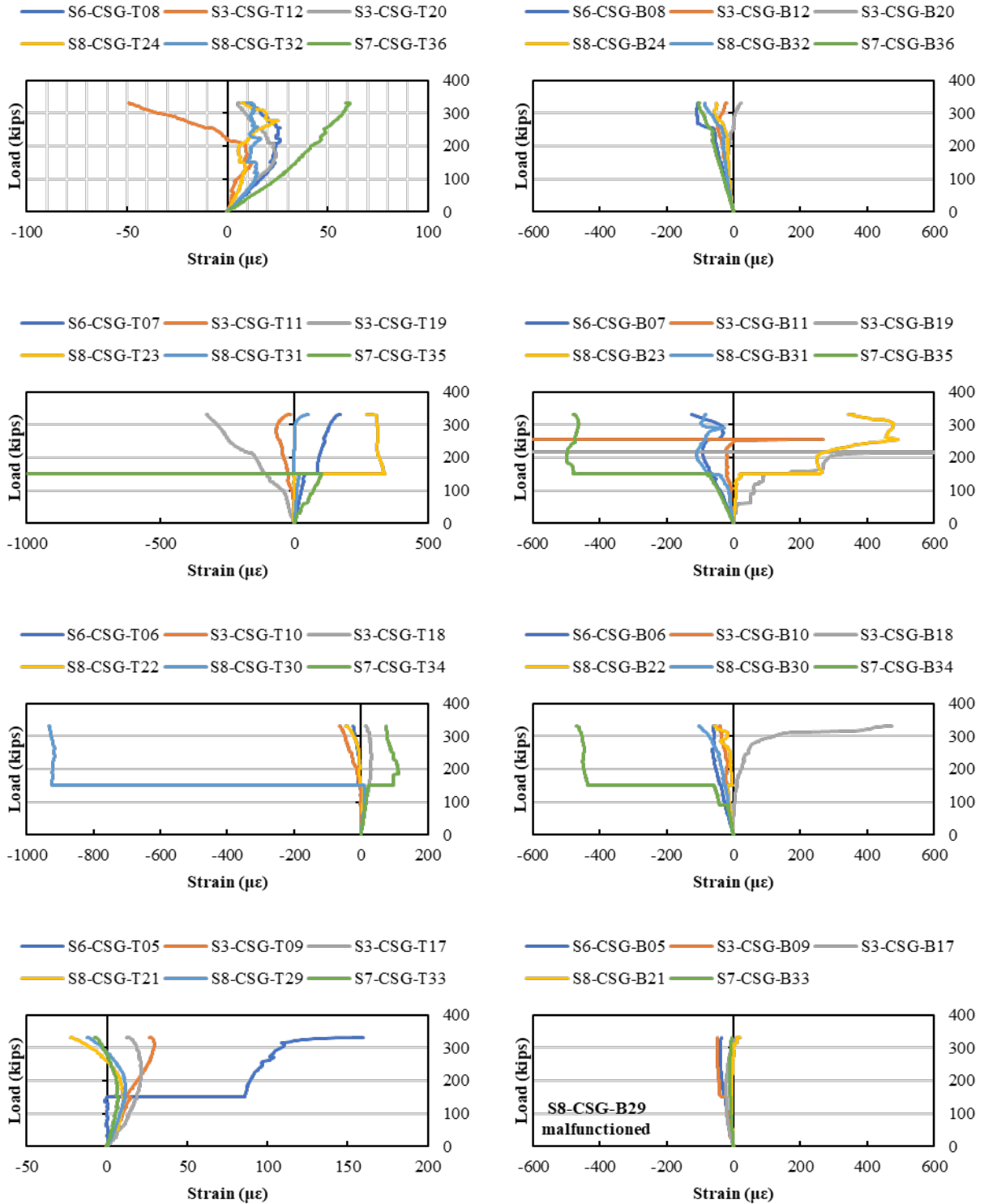


Figure F.109: Load versus transverse strain (measured by CSGs) for Load Stage 10, LC 4-5

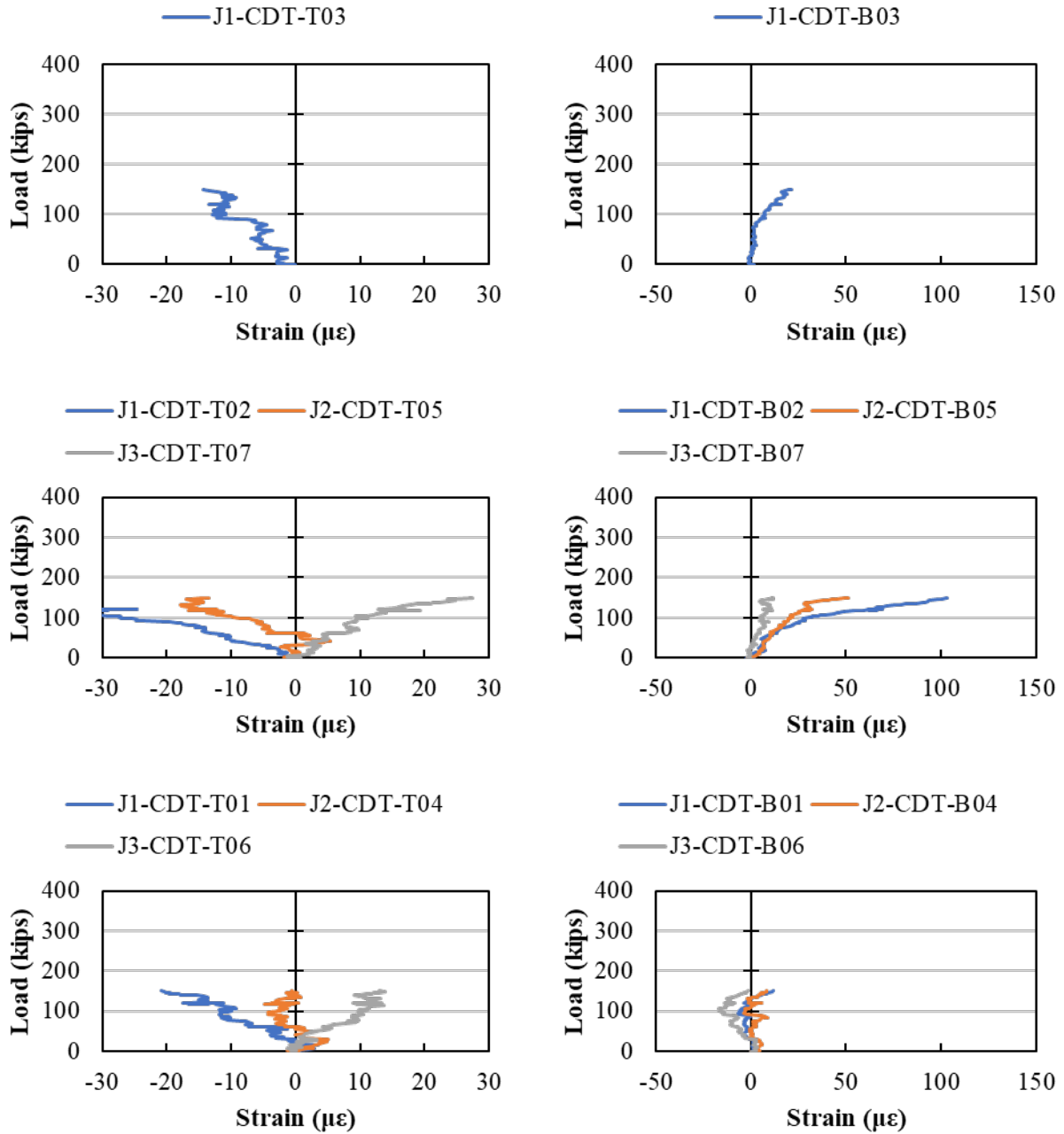


Figure F.110: Load versus average strain across the joints (measured by CDTs) for Load Stage 10, LC 4-5

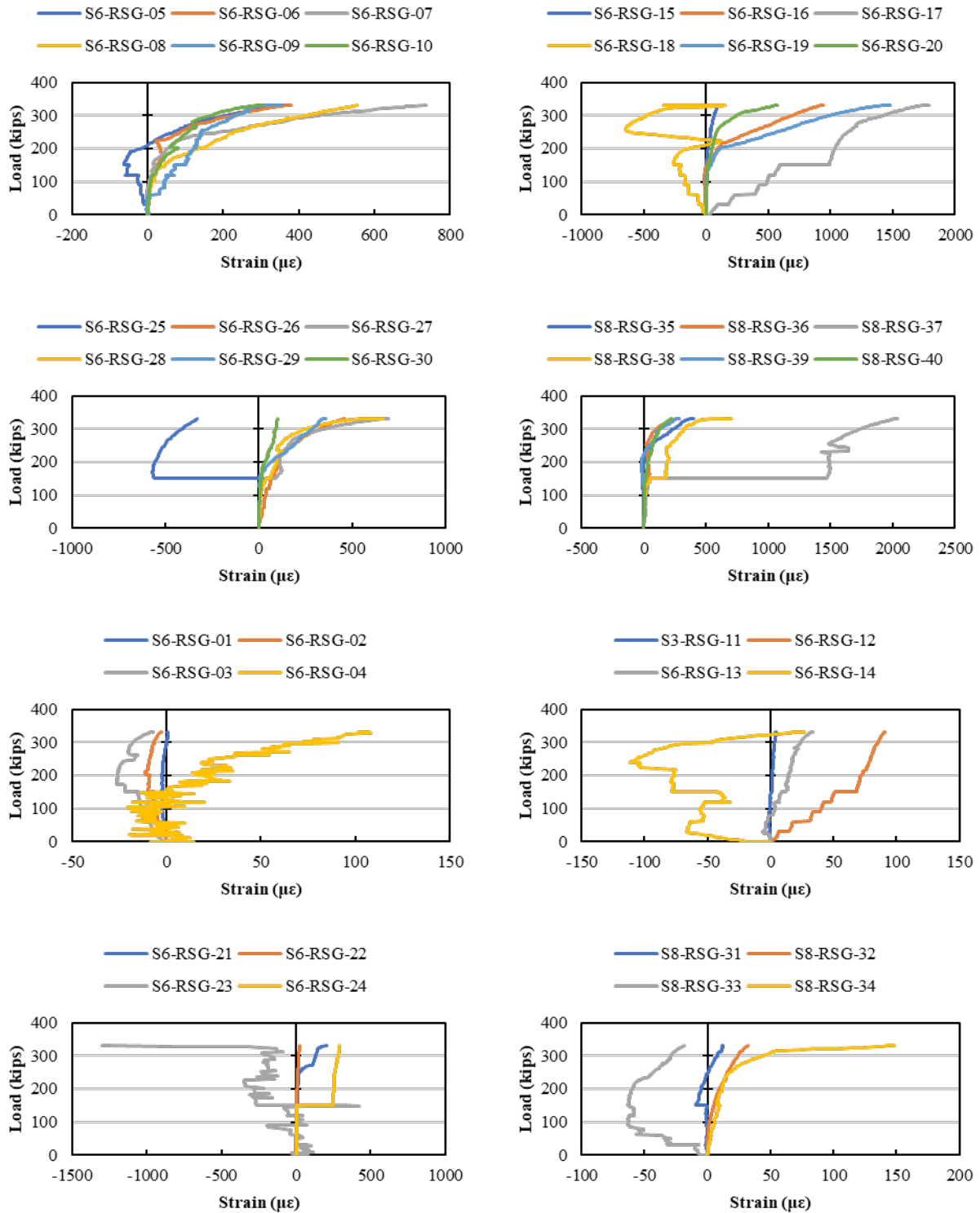


Figure F.111: Load versus rebar strain (measured by RSGs) for Load Stage 10, LC 4-5

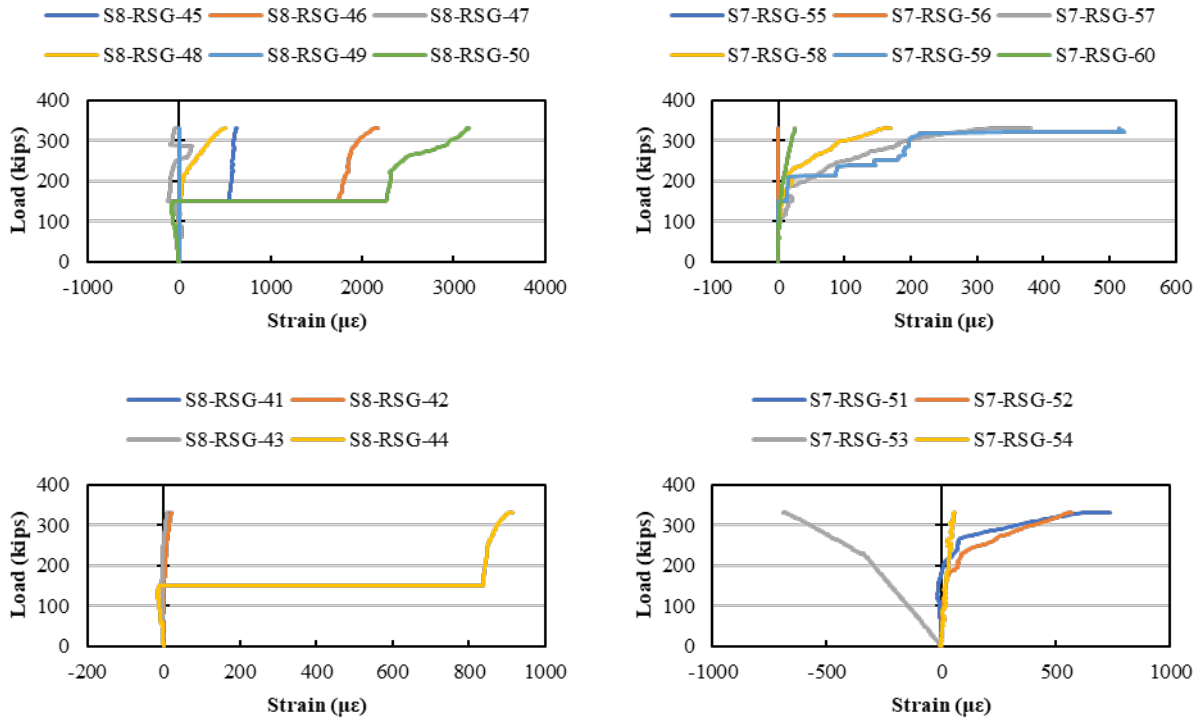


Figure F.112: Load versus rebar strain (measured by RSGs) for Load Stage 10, LC 4-5 (cont.)